

**Copper-Catalyzed Benzylic C–H Cross Couplings: Methodology
Development and Applications in Medicinal Chemistry**

By

Si-Jie (SJ) Chen

A dissertation submitted in partial fulfillment
of the requirements for the degree of

Doctor of Philosophy
(Chemistry)

at the

University of Wisconsin – Madison

2021

Date of Final Oral Examination: 07/27/2021

The dissertation is approved by the following members of the Final Oral Committee:

Shannon S. Stahl, Professor, Chemistry

Tehshik P. Yoon, Professor, Chemistry

Daniel J. Weix, Professor, Chemistry

Weiping Tang, Professor, Pharmacy

Copper-Catalyzed Benzylic C–H Cross Couplings: Methodology

Development and Applications in Medicinal Chemistry

Si-Jie (SJ) Chen

Under the supervision of Professor Shannon S. Stahl

At the University of Wisconsin-Madison

Abstract

Cross coupling methods are among the most synthetically useful and widely applied reaction classes in constructing architecturally complex molecules. Among these reactions, methods that employ sp^2 -hybridized coupling partners have found broad applications in organic syntheses and streamlined the preparation of pharmaceutically relevant compounds. Despite such advances, the prevalence of sp^2 -hybridized coupling partners has resulted in a massive collection of planar compounds, which could contribute to undesirable physicochemical properties for drug discovery. The past decade has witnessed an increasing demand of more topologically diverse libraries for drug discovery. Recent development of C(sp^3)–H functionalization has created opportunities for organic chemists to enrich molecular libraries and incorporate three-dimensionality construction. This thesis discloses our recent development of Cu-catalyzed cross couplings of benzylic C(sp^3)–H bonds and diverse nucleophilic reagents, enabled by a "redox buffering" strategy, and application of these methods in medicinal chemistry research.

Chapter 2 discussed our recent development of a copper-catalyzed benzylic C–H cross coupling with alcohols and the identification of the "redox buffering" strategy. Recent radical relay cyanation and arylation of benzylic C(sp^3)–H bonds precedents prompted us to develop a etherification method. However, direct application of standard cyanation or arylation conditions

failed to afford productive catalysis. Mechanistic interrogation revealed that cyanides and arylboronic acids can induce reduction of Cu^{II} to Cu^{I} , the catalytically reactive form, whereas nucleophiles like alcohols do not reduce Cu^{II} under the same conditions. We identified dialkylphosphite as a sacrificial reductant, or a "redox buffer", that allows continuous generation of Cu^{I} species in a controlled manner, which enabled effective etherification of the diverse (hetero)benzylic C–H substrates. Evaluation of the alcohol scope as well as the cross-coupling reactivity validated the utility of this method for library synthesis.

Chapter 3 disclosed our development of a *N*-site selective copper-catalyzed benzylic C–H cross couplings with azoles. We demonstrated that good coupling reactivity can be achieved with the "redox buffering" strategy, and modification of the reaction conditions allowed *N*-site-selective coupling with azoles. This reactivity proved effective with diverse *N*-H heterocycles and cross coupling of an array of benzylic C–H substrate and azoles was also successful, which should find broad application in pharmaceutical research.

Chapter 4 detailed our recent investigation into the 3D diversity introduced by benzylic C–H cross coupling methods. A cheminformatic approach was taken to virtually enumerate a collection of ethers and ureas with benzylic C–H etherification and isocyanation/amine coupling sequence. Analyses of these products proved benzylic cross couplings reliable methods to deliver 3D structures, in comparison to existing bioactive molecules and selected $\text{C}(sp^2)$ -derived coupling products. Examination of the physicochemical properties of these benzylic coupling products found them highly relevant to a drug-like chemical space. We successfully synthesized and isolated representative drug-like 3D benzylic ethers and ureas and validated the utility of this cheminformatic-guided approach. Further intake of this approach should transform how future synthetic methodologies are developed.

Chapter 5 covered our recent development of a site-selective benzylic C–H azidation method. Employment of the copper radical relay catalysis enabled highly benzylic-selective C–H azidation of a diverse collection (hetero)benzylic C–H substrates. Experimental and density functional theory identified a radical-polar crossover pathway for the reaction of a benzyl radical and a Cu^{II}-azide complex. Conversions of benzyl azide products to various functional groups benchmarked the broad utility of this method for target compound synthesis and medicinal chemistry.

Collectively, Cu-catalyzed cross couplings of benzylic C(*sp*³)–H bonds contributed to a growing library of medicinally relevant compounds and represented a unique opportunity to explore chemical space for drug discovery. Analyses of the physicochemical and topological properties of these benzylic derivatives revealed their "drug-likeness" as well as outstanding three-dimensional features comparing to existing bioactive molecules. Broad applications of these benzylic coupling methods, guided by cheminformatics, should complement the existing synthetic tools, and allow medicinal chemists to assemble compound libraries with higher diversity and complexity.

Acknowledgements

It has been almost nine years since I officially started my journey in Chemistry. Looking back at it, I realized that my exceptional experience from a [2+2] undergraduate program indeed laid a solid foundation for my doctoral research. Under the supervision of Prof. Michael Wing-Yiu Yu, the final year project equipped me with the experimental skills and research mindset for organic chemistry and organometallic catalysis. Such experience helped me prepare myself mentally for the struggles that I later faced as a graduate student. I was fortunate to work with Dr. Fo-Ning Ng and Dr. Pui-Yiu Lee as well, both of whom were cordial mentors and co-workers.

My research experience in the Stahl group at UW-Madison has been formative and inspiring. Prof. Shannon Stahl mentored me in a multifaceted manner, and I was able to hone my skills in many perspectives, including writing and presentation skills, research mindset and project management. I was delighted to witness my growth in the Stahl group, from a student majoring in chemistry to a scientist with expertise in methodology development and catalysis. Dr. Scott McCann and Dr. Shane Krska are two other great scientists and gracious individuals that I followed closely and learnt a lot from as a novice chemist. Scott helped me get through the muddy beginning period as a young graduate student, which served as the crucial basis for any of my later career development. Shane has been consistently giving me guidance in any medicinal chemistry and pharmaceutical industry perspective that I could possibly have. I really appreciate the time and efforts that they have invested in me, which significantly shaped my scientific approach. Additionally, a few other individuals have also contributed significantly to my training over the past few years: Dr. Spring Knapp, Prof. Huayou Hu, Prof. Sung-Eun Suh, Prof. Joshua Buss, Dr. Mandal Mukunda, Dr. Shishi Lin, Dr. Cyndi Qinxi He, Bing Li, Prof. Christopher Cramer. Each of them has not only imparted me knowledge from all different fields that I am personally not

familiar with, but also advised me on how to become a decent scientist, co-worker, and person. I also highly appreciate my committee for their guidance through my Ph.D. Many useful discussions with Prof. Tehshik Yoon and Prof. Daniel Weix at crucial timings during my stay here helped me overcome difficulties in my research and make key decisions in my career development.

I do not think I would make as much progress without massive helpful conversations and collaborations with my co-workers. I have always enjoyed working with Dr. Michael Ryan, Dr. Fei Wang, Prof. Chaofeng Zhang, Dr. Manar Alherech, Dr. Soham Maity and Kristine Golden. Departmental staff including Dr. Martha Vestling in the Mass Spectrometer center, Dr. Charlie Fry, Dr. Heike Hofstetter and Dr. Lingchao Zhu in the NMR facility, the former organic path coordinator Karen Stephens and others also provided much notable assistance in my research here. Lastly, I have to thank my friends I met here, who helped me get through all the difficult times, especially during the pandemic in 2020. Yicheng Hu, Yaqing Wu, Shannon Goes and Xiao Dong are some of my best friends. I am not a highly sociable person, yet they remained important individuals that engage actively in my daily life and people that I turn to when I have troubles. Drinking cocktails, swimming and having fun together with them were some of my unforgettable experiences here and they really sweetened up the bitter part of my graduate school life.

I would like to thank my families as well, who have strongly supported me to pursue my research interests for all these years. Even though I did not have many opportunities to visit my mom and grandparents in the past few years, they have always cared about me and I always have felt accompanied. Finally, I would like to thank my ever-supportive significant other Claudia Yujie Gao. 2020 has been an extremely challenging year, given that all the normal daily activities became so restricted and without her support, my life would have been a lot more excruciating.

I dedicate this thesis to my mother, Hairong Chen.

Table of Contents

Copper-Catalyzed Benzylic C–H Cross Couplings: Methodology Development and Applications in Medicinal Chemistry

| | |
|--|-----------|
| Abstract | i |
| Acknowledgements | iv |
| Table of Contents | vi |
| List of Figures | xi |
| List of Schemes | xviii |
| List of Tables..... | xix |
| Abbreviations and Acronyms..... | xxii |
| Chapter 1. Copper-Catalyzed Benzylic C–H Cross Couplings: Overview..... | 1 |
| 1.1. Introduction..... | 1 |
| 1.2. Discovery of the Redox Buffering Strategy..... | 2 |
| 1.3. Direct Benzylic C–H Cross Couplings | 5 |
| 1.3.1. Benzylic C–H Cross Coupling with Alcohols..... | 5 |
| 1.3.2. Benzylic C–H Cross Coupling with <i>N</i> –H Azoles..... | 7 |
| 1.4. Benzylic C–H Functionalizations/Diversifications..... | 9 |
| 1.4.1. Benzylic C–H Fluorination/Diversification Sequence | 9 |
| 1.4.2. Benzylic C–H Chlorination/Diversification Sequence..... | 11 |
| 1.4.3. Benzylic C–H Isocyanation/Amine Coupling Sequence..... | 12 |
| 1.5. Functionalization of Benzylic Radicals: Mechanistic Investigation..... | 15 |
| 1.6. Benzylic C–H Cross Coupling Improves 3D Structural Diversity | 17 |
| 1.7. Thesis Scope | 20 |
| 1.8. Reference..... | 21 |
| Chapter 2. Copper-Catalyzed Benzylic C–H Coupling with Alcohols via Radical Relay Enabled by Redox Buffering..... | 32 |

| | |
|---|-----------|
| 2.1. Abstract | 33 |
| 2.2. Introduction | 33 |
| 2.3. Results and Discussion..... | 37 |
| 2.4. Conclusion | 50 |
| 2.5. Acknowledgements | 50 |
| 2.6. Author Contributions | 51 |
| 2.7. References..... | 51 |
| Chapter 3. Copper-Catalyzed Cross Coupling of Benzylic C–H Bonds and Azoles with Controlled N-Site Selectivity | 57 |
| 3.1. Abstract | 58 |
| 3.2. Introduction | 58 |
| 3.3. Results and Discussion..... | 60 |
| 3.4. Conclusion | 68 |
| 3.5. Acknowledgements | 68 |
| 3.6. Author Contributions | 68 |
| 3.7. References | 69 |
| Chapter 4. Benzylic C–H Cross Coupling Improves 3D Structural Diversity | 77 |
| 4.1. Abstract | 78 |
| 4.2. Introduction | 79 |
| 4.3. Results and Discussion..... | 81 |
| 4.4. Conclusion | 89 |
| 4.5. Acknowledgements | 89 |
| 4.6. Author Contributions | 89 |
| 4.7. References | 90 |
| Chapter 5. Site-Selective Copper-Catalyzed Azidation of Benzylic C–H Bonds | 94 |
| 5.1. Abstract | 95 |

| | |
|--|------------|
| 5.2. Introduction | 95 |
| 5.3. Results and Discussion..... | 97 |
| 5.4. Conclusion | 105 |
| 5.5. Acknowledgements..... | 105 |
| 5.6. Author Contributions | 106 |
| 5.7. References | 106 |
| Appendix A: Supporting Information Chapter 2 | 113 |
| 2A.I. General Considerations..... | 113 |
| 2A.II. General Procedure (I) for Methoxylation of Benzylic C–H Substrates (pressure tube) | 113 |
| 2A.III. General Procedure (II) for Methoxylation of Benzylic C–H Substrates (glass vial) | 114 |
| 2A.IV. Experimental Procedures for Preparations of Compounds | 114 |
| 2A.V. Optimization of the Reaction Conditions..... | 117 |
| 2A.VI. Effects of Phosphite (Time course experiments, UV-Vis and EPR) | 121 |
| 2A.VII. The Fate of the Dialkyl Phosphites (³¹ P- ¹ H coupled NMR)..... | 123 |
| 2A.VIII. Radical trap experiments..... | 124 |
| 2A.IX. Control experiments with various alcohols | 125 |
| 2A.X. Further analyses of reaction outcomes of benzylic C–H etherification reactions. . | 126 |
| 2A.XI. KIE Experiments..... | 128 |
| 2A.XII. Methods for HPLC/SFC Chiral Separation | 130 |
| 2A.XIII. Characterization of Compounds..... | 130 |
| 2A.XIV. Details of DFT Calculations..... | 153 |
| 2A.XV. References | 154 |
| Appendix B: Supporting Information Chapter 3 | 156 |
| 3B.I. General Considerations | 156 |

| | |
|--|------------|
| 3B.II. Experimental Procedures for Cross-Coupling Reactions | 157 |
| 3B.III. Optimization of the Reaction Conditions | 158 |
| 3B.V. Additional Screening Data with Benzylic C–H Substrates and Azoles | 162 |
| 3B.VI. Additional Screening Data with Benzylic C–H Substrates and Azoles..... | 164 |
| 3B.VII. Crystallization and Crystallographic Data for [(C ₆ H ₅)N(CH ₃) ₃] ₂ [CuBr ₄] and 2a | 165 |
| 3B.VIII. Reactivity Assessment of Benzylic C–H Bonds..... | 172 |
| 3B.IX. Isomerization of 3aa to 3aa' in HFIP | 172 |
| 3B.X. Radical Trap Experiments..... | 173 |
| 3B.XI. KIE Experiments | 173 |
| 3B. XII. Characterization of Compounds..... | 174 |
| 3B. XIII. Reference | 205 |
| 3B.XIV. NMR Spectroscopic Data | 206 |
| Appendix C: Supporting Information Chapter 4 | 334 |
| 4C.I. General Considerations | 334 |
| 4C.II. Experimental Procedures for Preparations of Compounds..... | 334 |
| 4C.III. Procedure for Cheminformatic Study | 336 |
| 4C.IV. Selection and Analysis of the 160-compound subset of P01-20 | 337 |
| 4C.V. Comparison of <i>sp</i> ² and <i>sp</i> ³ functionalization product derived from A10 | 339 |
| 4C.VI. Loading Coefficients for PCA Plots | 339 |
| 4C.VII. Analysis of Benzylic Cross Coupling Products in PCA and PMI Plots | 340 |
| 4C.VIII. Crystallographic Data for A16-1a..... | 344 |
| 4C.IX. Characterization of Compounds..... | 353 |
| 4C.X. Reference | 365 |
| 4C.XI. NMR Spectroscopic Data | 366 |
| Appendix D: Supporting Information Chapter 5 | 416 |

| | |
|---|------------|
| 5D.I. General Considerations | 416 |
| 5D.II. General Procedure for Cu-Catalyzed Benzylic C-H Azidation | 418 |
| 5D.III. Screening Tables for Reaction Optimization | 419 |
| 5D.IV. Racemization Experiments | 430 |
| 5D.V. Comparative Experiments and Results with Known C-H Azidation Methods | 432 |
| 5D.VI. Reactivity Assessment | 434 |
| 5D.VII. Preparation, Crystallization and Reaction of [(BPhen)Cu^{II}(N₃)(μ-N₃)₂] | 438 |
| 5D.VIII. Crystallographic Data for [(BPhen)Cu^{II}(N₃)(μ-N₃)₂]·PhCl. | 439 |
| 5D.IX. Experimental and Computational Redox Potentials and Reaction Energetics | 442 |
| 5D.X. Characterization of Compounds..... | 451 |
| 5D.XI. Reference | 476 |

List of Figures

- Figure 1.1.** (A) Cu-catalyzed benzylic C–H functionalization reactions. (B) Modified radical relay mechanism to account for quenching of the \bullet NSI by Cu^{I} and regeneration of Cu^{I} by a reducing substrate or additive. (C) Calculated reaction pathways and energy landscape for reaction of \bullet NSI with (bio)Cu^ICl and ethylbenzene. (D) Reaction time course for benzylic etherification conducted in the absence (red) and presence of 0.5 equiv. of dimethyl phosphite (blue). (E) Reaction time course for benzylic fluorination conducted in the absence (red) and presence of 2.0 equiv. of methylboronic acid (blue).
..... 4
- Figure 1.2.** (A) Selected substrate scope of benzylic C–H methoxylation. (B) Benzylic C–H etherification of a canagliflozin precursor with various alcohols. (C) Cross-coupling examples of medicinally relevant benzylic C–H substrates and alcohols. 6
- Figure 1.3.** (A) Cross coupling of benzylic C–H cross and azoles with TBACl as the additive for N^2 selectivity and with TMSOTf or $\text{BF}_3 \cdot \text{OEt}_2$ for N^1 selectivity. (B) Cross-coupling examples medicinally relevant benzylic C–H substrates and N–H heterocycles. (C) Mechanistic origin of regioselectivity. 8
- Figure 1.4.** Benzylic C(sp³)–H Fluorination/Diversification Sequence. (A) Switch from C–N to C–F bond formation with Cu/NFSI (B) Benzylic C(sp³)–H Cross Couplings to C–O, C–N and C–C Bonds via benzylic fluorides..... 10
- Figure 1.5.** Selected substrate scope for Cu-catalyzed benzylic C–H chlorination/diversification sequence. (A) Comparison of C–H site-selectivity between radical relay Cu/NFSI benzylic C–H chlorination strategy and other existing C–H chlorination methods. (B) Selected substrate scope of Cu/NFSI benzylic C–H chlorination reaction. (C) Representative examples for diversification of benzylic chlorides with phenols, thiophenols and amines..... 12
- Figure 1.6.** (A) Selective substrate scope for benzylic C–H isocyanation. (B) Representative benzylic ureas synthesized via benzylic C–H isocyanation/amine coupling sequence.
..... 14
- Figure 1.7.** Mechanistic investigation into reaction pathways for benzylic C–H methoxylation and azidation. (A) Calculation reaction pathways for methoxylation of benzylic radical. (B) Synthesis and crystal structure of $[(\text{BPhen})\text{CuII}(\text{N}_3)(\mu\text{-N}_3)]_2$ (hydrogen atoms and chlorobenzene molecule omitted for clarity). (C) Three proposed pathways for azidation of the benzyl radical. (D) Simplified energy diagrams comparing the three azidation pathways..... 16
- Figure 1.8.** Benzylic C(sp³)–H cross couplings improve 3D diversity. (A) PMI analysis of bioactive molecules. (B) Virtual enumeration of benzylic C(sp³)–H ethers and ureas. (C) PMI comparison between C(sp²)- and C(sp³)-derived cross coupling products. (D) PCA comparison between bioactive molecules and benzylic coupling products,

and representative pairs of drugs and benzylic ethers and ureas. (E) Selected examples of synthetically accessed benzylic ethers and ureas. 18

Figure 2.1. Cu-Catalyzed Cross Coupling of Benzylic C–H Etherification Summarization of Reactivity 33

Figure 2.2. Cross-coupling reactions of benzylic C–H bonds and alcohols via a radical relay pathway. (A) Conceptual similarity between traditional cross-coupling reactions of aryl halides and the targeted benzylic C–H functionalization reactions. (B) Important examples of existing drug molecules containing benzylic ether moieties. (C) Proposed radical relay mechanism for benzylic C–H etherification enabling the coupling of two diverse pools of substrates. 35

Figure 2.3. Cu-catalyzed benzylic C–H functionalization with NFSI as the oxidant. (A) Cu-catalyzed benzylic C–H functionalization reactions^{14,34}. (B) Changes in the Cu redox state between +1 (brown) and +2 (blue-green) upon addition of NFSI to a solution of the CuI catalyst precursor, followed by addition of cross-coupling partners. (C) Modified radical relay mechanism (cf. **Figure 2.2C**) to account for quenching of the •NSI by CuI and regeneration of CuI by a reducing substrate or additive. (D) Reaction time course for benzylic etherification conducted in the absence (red) and presence of 0.5 equiv of dimethylphosphite (blue). Reaction conditions: 4-ethylbiphenyl (0.2 mmol), NFSI (0.4 mmol), MeOH (1.0 mmol), CuCl (0.02 mmol), 2,2'-bioxazoline (0.02 mmol), DCM (1 mL), room temperature. 38

Figure 2.4. Electronic effects and site selectivity observed in the oxidative coupling of ethylarenes and methanol. (A) Results observed from the reaction under standard (red) and individually optimized (blue) conditions (¹H NMR yields with CH₂Br₂ as the internal standard. Modified conditions: X = OMe: 20 mol % Cu/biox in DCM at r.t.; X = Br: 5 mol % Cu/biox; X = OAc: 20 mol % Cu/biox at 50 °C. (B) Analysis of benzylic versus tertiary site selectivity observed in etherification of isobutylbenzene and ibuprofen methyl ester (see Figure 2.5 for reaction conditions). 40

Figure 2.5. Calculated reaction pathways and energy landscape for (biox)CuI/NFSI-mediated methoxylation of ethylbenzene. (Gibbs free energies at 313.15 K; computed at M06-L/basis-II/SMD(ε = 10.6)//B3LYP-D3(BJ)/basis-I/SMD(ε = 10.6) level of theory). 42

Figure 2.6. Assessment of different benzylic C–H substrates in oxidative cross-coupling reactions with methanol. Isolated yields unless otherwise noted. ^a ¹H NMR yield; isolated yield unavailable due to compound volatility. ^b See **Figure 2.4A** for optimized conditions. ^c 15 mol % Cu/biox. ^d Reaction yield at 4 h. ^e At room temperature. ^f DCM as the solvent. ^g 20 mol % Cu/biox. ^h Only one regioisomer was observed. ⁱ At 30 °C. ^j 30 mol % Cu/biox. ^k Two regioisomers were observed with a ratio of 9:1. 46

Figure 2.7. Assessment of different alcohols and C–H/alcohol coupling partners in benzylic C–H etherification reactions. (A) Benzylic C–H etherification of a canagliflozin precursor with various alcohols. (B) Cross coupling of medicinally relevant benzylic C–H substrates and alcohols. Isolated yields are reported. ^a ¹H NMR yield with 30 mol %

- Cu/biox. ^b Conducted with 3.0 equiv. alcohol. ^c Conducted with 1.1 equiv. alcohol. ^d 50 °C. e r.t. in DCM..... 49
- Figure 3.1.** Cu-Catalyzed Cross Coupling of Benzylic C–H Bonds and Azoles Summarization of Reactivity..... 58
- Figure 3.2.** (A) Importance of benzylic N-azoles in drug discovery. (B) Impact of regioselectivity of heterocyclic compounds in medicinal chemistry. (C) Copper-catalyzed regioselective cross couplings of benzylic C–H bonds and N–H heterocycles enabled by various additives. 60
- Figure 3.3.** Evaluation of effects of various solvents and additives on the regioselectivity. (A) Effects of solvents on benzylic C–N cross coupling reaction. (B) Regioselectivity switch observed in cross coupling of 1a and 2a with different additives. Conditions identical to those shown in part A, using 10 mol% additive instead of TBABr, 10 mol % CuBr₂ instead of CuCl, and DCM:HFIP (7:3) solvent. a Monitored by ¹H NMR spectroscopy, yield determined using 0.2 mmol mesitylene as internal standard. TBA, tetrabutylammonium; DCM, dichloromethane; HFIP, hexafluoroisopropanol. b Reaction run with TBA+Cl[–] instead of TBABr. c Reaction run at 60 °C. 62
- Figure 3.4.** Mechanistic origin of pyrazole regioselectivity. (A) N¹/N²-isomerization test, implicating the the N¹. (B) Proposed mechanism rationalizing the influence of TMSOTf (and other Lewis acids) on the N²/N¹ regioselectivity..... 63
- Figure 3.5.** Assessment of various benzylic C–H substrates in cross coupling reactions with N–H heterocycles with (A) TBACl as the additive for N² regioselectivity and (B) with TMSOTf as the additive for N¹ regioselectivity. Regioisomers >5% were isolated and reported. ^aConducted in 0.5 mL DCM:HFIP (7:3). ^bConducted with 10 mol % CuBr₂ and 30 mol % TBABr. ^c Conducted with 10 mol % TBACl. ^dConducted at 40 °C. ^eConducted at 60 °C. ^fConducted in DCM. ^gConducted at 30 °C. ^hConducted with 10 mol % BF₃•OEt₂. 64
- Figure 3.6.** Assessment of various N–H heterocycles in cross coupling reactions. Substrate scope with diverse N–H heterocycles and indane under kinetically controlled TBACl conditions (A) and in the presence of BF₃•OEt₂ as a Lewis acid cocatalyst (B). Exploration of cross-coupling reactions of diverse N–H heterocycles and (hetero)benzylic C–H scaffolds under the TBACl conditions of Figure 5A, unless noted otherwise. Regioisomers formed in >5% yield were isolated. ^aConducted in DCM. ^bConducted at 50 °C. ^cConducted at 30 °C. ^dTrace amount of the other benzylic regioisomer was observed. ^eConducted at 40 °C. ^fConducted with 10 mol % BF₃•OEt₂. 66
- Figure 4.1.** Benzylic C–H cross coupling improves 3D structural diversity and affords diverse drug-like molecules. 78
- Figure 4.2.** Cross-coupling reactions of benzylic C–H bonds and alcohols via a radical relay pathway. (A) Known bioactive compounds are topologically diverse, including planar

structures like flurbiprofen (**1**) and 3D structures like JHW-007 (**2**). (B) PMI of **1** and **2** with reference to a reported population analysis of selected compounds from ChEMBL database². C, Benzylic C(sp³)-H cross coupling reactions offer opportunities in introducing more three-dimensionality in contrast to C(sp²)-focused functionalization methods..... 79

Figure 4.3. Enumeration of P01-20 and topological comparison between P01-20 and BC. (A) Display of selected benzylic C(sp³)-H scaffolds for cross coupling product enumeration. (B) Enumeration of P01-20 via etherification with alcohols and isocyanation/urea formation sequence with amines. C, Comparison of 3D scores between BC and P01-20 compounds by parent scaffold. D, Comparison of PMI and 3D scores (Box-Whisker plot, outliers omitted) between sp² and sp³ functionalization products derived from A11..... 82

Figure 4.4. Principal components analysis (PCA) comparing P01-20 and BC compounds. (A) Physicochemical features depicted by PC1 and PC2. (B) Physicochemical features depicted by PC3 and PC4. Libraries are visualized in density heatmaps, where BC (n = 12,611) and P01-20 (n = 368,948) compounds were analyzed by 100 × 100 bins and the color of each bin was determined by the number of compounds in it. Selected pairs of BC and P01-20 compounds with similar coordinates were showcased..... 86

Figure 4.5. Synthesis of medicinally relevant benzylic C-H cross coupling products and comparison with bioactive molecules. (A) Assessment of benzylic ethers and ureas that sample the chemical space generated from virtual enumeration. (B) Comparison of selected P01-20 products (including all isolated regio- and stereoisomers) with BC space in PCA, PMI and Box-Whisker (3D scores) plots. ^aReaction run with 15 mol % CuCl/biox. ^bReaction run at room temperature. ^cReaction run with 20 mol % CuCl/biox. ^dReaction run at 30°C. ^eReaction run in DCM. ^fIsocyanation reaction run at 40°C. ^gIsocyanation reaction run at room temperature. 88

Figure 5.1. Cu-Catalyzed Azidation Benzylic C-H Bonds Summarization of Reactivity 95

Figure 5.2. Azides are important intermediates in organic syntheses (A) and medicinal chemistry (B) and are ideally prepared by direct azidation of sp³ C-H bonds (C). NFSI, N-fluorobenzenesulfonimide. Mes-Acr, 9-mesityl-10-alkylacridinium catalyst. 96

Figure 5.3. (A) Synthesis and crystal structure of [(BPhen)Cu^{II}(N₃)(μ-N₃)]₂ (hydrogen atoms and chlorobenzene molecule omitted for clarity). (B) Reaction of [(BPhen)Cu^{II}(N₃)(μ-N₃)]₂ with Gomberg's dimer (6 mol% Cu(OAc)₂/BPhen, 3.6 equiv. TMSN₃, 2.5 equiv. NFSI). 98

Figure 5.4. Three proposed pathways for azidation of the benzyl radical (A), and simplified energy diagrams comparing the three pathways (B) (see text and Appendix D for details). 99

Figure 5.5. Azidation site selectivity with different catalytic methods (see Section V in the Appendix D for details). Standard condition for method I; substrate (0.4 mmol),

| | |
|---|-----|
| Cu(OAc) ₂ (2.0 mol%), BiO _x (4.0 mol%), TMSN ₃ (3.6 equiv.), NFSI (2.5 equiv.), 0.2 M MeNO ₂ , 30 °C, 24 h for 3b , 48 h for 3c and 3d | 101 |
| Figure 5.6. Azidation site selectivity with different catalytic methods (see Section V in the Appendix D for details). Standard condition for method I; substrate (0.4 mmol), Cu(OAc) ₂ (2.0 mol%), BiO _x (4.0 mol%), TMSN ₃ (3.6 equiv.), NFSI (2.5 equiv.), 0.2 M MeNO ₂ , 30 °C, 24 h for 3b , 48 h for 3c and 3d | 104 |
| Figure 2A.1. Investigation of the reactivities and chemo-selectivity of primary, secondary and tertiary benzylic C–H substrate | 120 |
| Figure 2A.2. Reaction time course for benzylic etherification conducted in the absence (red) and presence of 0.5 equiv. dimethyl phosphite (blue) as well as when 0.5 equiv. dimethyl phosphite was added at the 4 th hour (purple). Reaction conditions: ethylbenzene (0.2 mmol), NFSI (0.4 mmol), MeOH (1.0 mmol), CuCl (0.02 mmol), 2,2'-bioxazoline (0.02 mmol), DCM:HFIP = 4:1 (1 mL), 40 °C | 121 |
| Figure 2A.3. UV-Vis and EPR Experiments to probe the effect of additives on copper speciation. a , UV-Vis traces monitoring the reaction of Cu ^{II} with dimethyl phosphite and methanol. b , EPR experiments investigating the effect of dimethyl phosphite and methanol on Cu ^{II} | 122 |
| Figure 2A.4. ³¹ P- ¹ H coupled NMR spectrum of the reaction mixture of the benzylic C–H methoxylation with 0.2 mmol Ph ₃ P(O) as the internal standard. | 123 |
| Figure 2A.5. Intermolecular Competition Kinetic Isotopic Effect | 128 |
| Figure 2A.6. Independent Kinetic Isotopic Effect | 129 |
| Figure 3B.1. Screening data with additional benzylic C–H substrates and azoles..... | 162 |
| Figure 3B.2. Further analyses of reaction outcomes of cross couplings of benzylic C–H bonds and azoles | 163 |
| Figure 3B.3. Evidence for regioisomer assignment of benzylic C–H cross coupling products with 2a | 164 |
| Figure 3B.4. Proof of regioisomer assignment for benzylic C–H cross coupling products with other ambidentate azoles..... | 164 |
| Figure 3B.5. A molecular drawing of [(C ₆ H ₅)N(CH ₃) ₃] ₂ [CuBr ₄]. The N,N,N-trimethylanilinium cations containing atoms N2 and N3 are 50% occupied. All atoms are shown with 50% probability ellipsoids. All H atoms and minor disorder components are omitted. .. | 167 |
| Figure 3B.6. A molecular drawing of 2a shown with 50% probability ellipsoids for non-hydrogen atoms. [Symmetry code: (i) x, 3/2 – y, z.]..... | 170 |

| | |
|--|-----|
| Figure 3B.6 Investigation of the reactivities and chemo-selectivity of primary, secondary, and tertiary benzylic C–H substrate | 172 |
| Figure 3B.7. Control experiments with radical traps | 173 |
| Figure 3B.8. Intermolecular Competition Kinetic Isotopic Effect..... | 173 |
| Figure 4C.1. Hydrolysis of P01-20 compounds. | 337 |
| Figure 4C.2. Scaffolds and monomers selected to assemble the 160-compound subset of P01-20 library..... | 337 |
| Figure 4C.3. Analysis of 3D scores of the 160-compound subset of P01-20 library. a, Comparison of 3D scores between BC molecules, P01-20 molecules and the 160-compound subset of P01-20 . b, Comparison of 3D scores between BC molecules and the 160-compound subset of P01-20 (160-P01-20) by monomer categories..... | 338 |
| Figure 4C.4. Comparison of PCA between BC, P01-20 and the 160-compound subset of P01-20. PCA depicted for a, BC ; b, P01-20 and c, a 160-compound subset of P01-20 . Libraries are visualized in density heatmaps, where BC (n = 12,611), P01-20 (n = 368,948) and a subset of P01-20 (n = 160) compounds were analyzed by 100 × 100 bins and the color of each bin was determined by the number of compounds in it. | 338 |
| Figure 4C.5. Comparison of PMI and 3D scores (Box-Whisker plot) between sp ² and sp ³ functionalization products derived from A10 | 339 |
| Figure 4C.6. A molecular drawing of the molecule in A16-1 shown with 50% probability ellipsoids. All minor disorder components and H atoms (except for those bound to chiral centers or the N atom) are omitted. The conformations of the chiral atoms C7, C12, and C13 are R, S, and R but the crystal contains a racemate..... | 345 |
| Figure 4C.7. A molecular drawing highlighting the disordered tertbutyl group in A16-1 shown with select atom labels and 50% probability ellipsoids. All H atoms are omitted except for those bound to chiral centers or a N atom. The conformations of the chiral atoms C7, C12, and C13 are R, S, and R but the crystal contains a racemate. | 345 |
| Figure 5D. 1. Supercritical fluid chromatography data. | 430 |
| Figure 5D. 2. Independent comparison and competition experiments of p-methoxy and p-cyanoethylbenzene. Reaction conditions for screening were adopted from General Procedure A. | 434 |
| Figure 5D. 3. Independent comparison and competition experiments of primary, secondary, and tertiary benzylic C–H substrate. Reaction conditions for screening were adopted from General Procedure A..... | 435 |
| Figure 5D. 4. Investigation of vicinal diazide formation. Reaction conditions for screening were adopted from General Procedure A. | 436 |

- Figure 5D.5.** A molecular drawing of the entire complex in $[(\text{BPhen})\text{Cu}^{\text{II}}(\text{N}_3)(\mu\text{-N}_3)]_2 \cdot \text{PhCl}$ shown with 50% probability ellipsoids. All H atoms and solvent molecule are omitted. [Symmetry code: (i) $2-x, 2-y, 1-z$.] 440
- Figure 5D.6.** A molecular drawing of the symmetry independent portion of the complex in $[(\text{BPhen})\text{Cu}^{\text{II}}(\text{N}_3)(\mu\text{-N}_3)]_2 \cdot \text{PhCl}$ shown with 50% probability ellipsoids. All H atoms and solvent molecule are omitted. 440
- Figure 5D.7.** A molecular drawing of $[(\text{BPhen})\text{Cu}^{\text{II}}(\text{N}_3)(\mu\text{-N}_3)]_2 \cdot \text{PhCl}$ shown with 50% probability ellipsoids. All H atoms are omitted. [Symmetry code: (i) $2-x, 2-y, 1-z$.] 441
- Figure 5D.8.** Cyclic voltammogram of $[(\text{BPhen})\text{Cu}^{\text{II}}(\text{N}_3)(\mu\text{-N}_3)]_2$ 442
- Figure 5D.9.** Gibbs free energy change (kcal/mol) due to dimerization. Calculations done at 298.15 K at M06-L/basis-II/SMD(MeNO₂)/B3LYP-D3(BJ)/basis-I level of theory. 443
- Figure 5D.10.** Possible pathways leading to the benzylic azide formation. 449
- Figure 5D.11.** Energetics of pathways leading to the benzylic azide formation using the BiOx (**L4**) ligand. Gibbs free energies are in kcal/mol computed at 298.15 K at M06-L/basis-II/SMD(MeNO₂)/B3LYP-D3(BJ)/basis-I level of theory. Free energy of **Int-3** was determined according to Scheme 5D.1. 449
- Figure 5D.12.** Optimized transition-state (TS) structures leading to product formation via reductive elimination (RE) and direct radical addition to the azide ligand (RAL) for both pro-R and pro-S faces of the benzylic radical derived from 1-ethylnaphthalene. Gibbs free energies of activation (ΔG^\ddagger ; kcal/mol) of the respective TS structures are included in parenthesis. Gibbs free energies are reported at 298.15 K calculated at M06-L/basis-II/SMD(MeNO₂)/B3LYP-D3(BJ)/basis-I level of theory. “RE” implies reductive elimination (Path-I). The prefix “B3–” implies that the reaction is happening at the distal N-atom of the bridging azide group. Similarly, “T1–” prefix means that it is the proximal N-atom of the terminal azide group. 450

List of Schemes

- Scheme 5D.1.** Derivation of Gibbs free energy change (ΔG°) for the oxidation of the 1-Naph-CH(\bullet)Me radical by the Cu^{II}-dimer yielding the corresponding benzylic cation. Reduction potentials were obtained from Table 5D.16. 448

List of Tables

| | |
|---|-----|
| Table 5.1. Reaction Optimization ^a | 97 |
| Table 5.2. Scope of Alkylarene Benzylic C–H Azidation ^{a,b} | 103 |
| Table 2A.1. Investigation of various reductants with ethylbenzene as the substrate..... | 117 |
| Table 2A.2. Investigation of dimethylphosphite with 4-ethylbiphenyl as the substrate | 117 |
| Table 2A.3a. Ligand Optimization | 118 |
| Table 2A.3b. Unsuccessful Ligand Testing for Enantioselective Methoxylation | 118 |
| Table 2A.4a. Optimization of the Reaction Conditions with Various Solvents, Cu Salts and Temperature..... | 119 |
| Table 2A.4b. Control Experiments with Various Amounts of Methanol | 119 |
| Table 2A.5. Investigation of various radical initiators/oxidants | 120 |
| Table 2A.6. Energetics of Cu ^{II} reduction to Cu ^I by (MeO) ₂ P(O)H..... | 124 |
| Table 2A.7. Investigation of various phosphites with a canagliflozin precursor..... | 124 |
| Table 2A.8. Control Experiments with Radical Traps | 124 |
| Table 2A.9. Investigation of ethylbenzene cross-coupling with various alcohols..... | 125 |
| Table 2A.10. Competition experiments in ethylbenzene etherification..... | 125 |
| Table 2A.11. Analyses of mass balances of benzylic C–H etherification reactions..... | 126 |
| Table 2A.12. Unsuccessful substrates in benzylic C-H methoxylation | 127 |
| Table 3B.1a. Assessment of Ancillary Ligands..... | 158 |
| Table 3B.1b. Ligand Comparison with Selected Nucleophiles | 158 |
| Table 3B.2. Effect of Different Additives in Controlling the Regioselectivity ^a | 159 |
| Table 3B.3. Optimization of the Reaction Conditions with Various Solvents, Cu Salts and Temperature ^a | 160 |
| Table 3B.4. Investigation of various reductants with ethylbenzene as the substrate | 160 |
| Table 3B.5. Crystal data and structure refinement for [(C ₆ H ₅)N(CH ₃) ₃] ₂ [CuBr ₄]..... | 168 |

| | |
|--|-----|
| Table 3B.6. Crystal data and structure refinement for 2a | 171 |
| Table 4C.1. Loading coefficients for PC1-PC4 in PCA plots. | 339 |
| Table 4C.2. Compounds synthesized and compounds enumerated and analyzed in cheminformatic study..... | 340 |
| Table 4C.3. Crystal data and structure refinement for A16-1 | 346 |
| Table 4C.4. Fractional Atomic Coordinates ($\times 10^4$) and Equivalent Isotropic Displacement Parameters ($\text{\AA}^2 \times 10^3$) for A16-1. U_{eq} is defined as 1/3 of the trace of the orthogonalized U_{ij} tensor..... | 346 |
| Table 4C.5 Anisotropic Displacement Parameters ($\text{\AA}^2 \times 10^3$) for A16-1. The Anisotropic displacement factor exponent takes the form: $-2\pi^2[h^2a^{*2}U_{11}+2hka^{*}b^{*}U_{12}+\dots]$ | 347 |
| Table 4C.6. Bond Lengths for A16-1. | 348 |
| Table 4C.7. Bond Angles for A16-1 | 349 |
| Table 4C.7. Hydrogen Bonds for A16-1 | 350 |
| Table 4C.8. Torsion Angles for A16-1 | 350 |
| Table 4C.9. Hydrogen Atom Coordinates ($\text{\AA} \times 10^4$) and Isotropic Displacement Parameters ($\text{\AA}^2 \times 10^3$) for A16-1 | 351 |
| Table 4C.10. Atomic Occupancy for A16-1 | 352 |
| Table 5D.1. Optimization of the Reaction Conditions with Various Solvents ^a | 419 |
| Table 5D.2. Optimization of Reaction Conditions with Various Temperatures and Additives ^a | 420 |
| Table 5D.3. Optimization of Reaction Conditions with Various Copper Salts ^a | 421 |
| Table 5D.4. Optimization of Reaction Conditions with Various Ligands and Copper Salts ^a ... | 422 |
| Table 5D.5. Investigation of various radical initiators/oxidants | 423 |
| Table 5D.6. Optimization of Reaction Conditions with Various Equivalents of NFSI/Temperature ^a | 424 |
| Table 5D.7. Optimization of Reaction Conditions with Various Equivalents of TMS-N ₃ ^a | 425 |
| Table 5D.8. Optimization of Reaction Conditions with Various Concentration ^a | 426 |
| Table 5D.9. Optimization of Reaction Conditions with Various Reaction Time ^a | 427 |

| | |
|--|-----|
| Table 5D.10. Optimization of Benzylic C–H Site-Selectivity with Various Solvents and Temperatures ^a | 428 |
| Table 5D.11. Optimization of Benzylic C–H Site-Selectivity with Various Length of Reaction Time ^a | 429 |
| Table 5D.12. Tabulated Summary of Yield of Benzylic and Tertiary Azido Products ^a | 432 |
| Table 5D.13. Unsuccessful C–H Substrates | 437 |
| Table 5D.14. Crystal Data and Structure Refinement for [(BPhen)Cu ^{II} (N ₃)(μ-N ₃)] ₂ ·PhCl | 441 |
| Table 5D.15. Solution phase electronic energies, E(sol)/hartree, spin-projected electronic energies, E'(sol)/hartree, thermal contribution to Gibbs free energy/hartree and absolute solution-phase Gibbs free energies, G(sol)/hartree (at 298.15 K) computed at M06-L/basis-II/SMD(nitromethane) //B3LYP-D3(BJ)/basis-I level of theory | 444 |
| Table 5D.16. Calculated (vs Fc ^{0/+}), and experimental (vs Fc ^{0/+}) reduction potentials (V) of various species at 298.15 K using reaction schemes (eqs S3 and S4) | 447 |

Abbreviations and Acronyms

| | |
|-------------------|---|
| HAT | hydrogen atom transfer |
| NFSI | <i>N</i> -fluorobenzenesulfonimide |
| •NSI | benzenesulfonimidyl radical |
| biox | 2,2'-bis(2-oxazoline) |
| TBACl | tetrabutylammonium chloride |
| TMSOTf | trimethylsilyl triflate |
| TMS | trimethylsilyl (cation) |
| HFIP | 1,1,1,3,3,3-hexafluoroisopropanol |
| BisOx | bisoxazoline ligand |
| HTE | high-throughput experimentation |
| bRO5 | oral druggable space beyond Rule of 5 |
| PMI | principal moments of inertia |
| PCA | principal components analysis |
| DDQ | 2,3-dichloro-5,6-dicyano-1,4-benzoquinone |
| TMSCN | trimethylsilyl cyanide |
| DCM | dichloromethane |
| DFT | density functional theory |
| KIE | kinetic isotope effect |
| Boc | <i>tert</i> -butyloxycarbonyl |
| TBA | tetrabutylammonium |
| Mes-Acr | 9-mesityl-10-alkylacridinium catalyst |
| TMSN ₃ | trimethylsilyl azide |

| | |
|--------|--|
| BiOx | 2,2'-bis(2-oxazoline)-derived ligands |
| Bphen | 4,7-diphenyl-1,10-phenanthroline |
| DCE | 1,2-dichloroethane |
| DMC | dimethyl carbonate |
| IMes | 1,3-bis(2,4,6-trimethylphenyl)-1,3-dihydro-2H-imidazol-2-ylidene |
| RSM | remaining starting material |
| Conv. | percent conversion of the C–H substrate |
| ee | enantiomeric excess |
| d.r. | diastereomeric ratio |
| r.r. | regioisomeric ratio |
| ACN | acetonitrile |
| DME | 1,2-dimethoxyethane |
| THF | tetrahydrofuran |
| DMF | <i>N,N</i> -dimethylformamide |
| DMAc | <i>N,N</i> -dimethylacetamide |
| W.E. | working electrode |
| C.E. | counter electrode |
| R.E. | reference electrode |
| TBAHFP | tetrabutylammonium hexafluorophosphate |

Chapter 1.

Copper-Catalyzed Benzylic C–H Cross Couplings: Overview

1.1. Introduction

Past few decades have witnessed wide applications of cross coupling reactions in syntheses of novel compounds. Coupling reactions that connect versatile building blocks, such as amide coupling and palladium-catalyzed cross coupling reactions,^{1, 2} have emerged to be prominent synthetic tools for medicinal chemists and contributed to success in drug discovery and development. However, historical reliance on use of sp^2 coupling partners has led to limited sampling of topological diversity and, in many cases, suboptimal physical chemical properties.³ Such limitations contribute to emerging needs of $C(sp^3)$ -focused functionalization strategies, which should provide accesses to more three-dimensional characters.⁴ $C(sp^3)$ –H bonds adjacent to aromatic and heteroaromatic rings are prevalent in medicinally relevant building blocks.^{5,6} These benzylic $C(sp^3)$ –H bonds are intrinsically reactive due to their comparatively low bond strength,⁷ and represent opportunities for rapid, *site*-selective elaboration. Benzylic sites are also considered as metabolic "hot spot" and selective functionalization at such sites have profound implications in medicinal chemistry.⁸

Recent development of intermolecular $C(sp^3)$ –H functionalization strategies has allowed site-selective small functional group installation, such as oxygenation,^{9,10} amination,¹¹⁻¹³ carbene insertion¹⁴, halogenation^{15,16-20}, and various pseudohalogenation reactions.²¹⁻²⁵ On the other hand, complementary success was achieved with selective functionalization of low-cost feedstock chemicals like alkylarenes,²⁶⁻²⁸ tetrahydrofurans^{29,30} or simple hydrocarbons^{31,32}. Cross coupling of diverse benzylic C–H and other substrate partners remains underdeveloped³³⁻⁴⁰. Collectively, these precedents do not fully capture the traits associated with cross-coupling

methods: employ two diverse pools of coupling partners, with the more valuable one used as the limiting reagent and show tolerance of substrates with various functional groups as well as diverse electronic and steric profiles. In this account, we demonstrate Cu-catalyzed radical relay benzylic C(*sp*³)-H functionalization methods to allow coupling of building blocks from two diverse pools. This approach, enabled by a "redox buffering" strategy that continuously regenerates the active Cu^I catalyst, affords exquisite benzylic *site*-selectivity with the C-H substrate as the limiting reagent. Synthetic utility of these methods was explored in library synthesis via cross coupling of benzylic C(*sp*³)-H scaffolds and diverse classes of nucleophiles, either in a direct coupling manner or a functionalization/diversification sequence. Mechanistic investigation into the bond-forming steps identified a radical-polar crossover pathway for these reactions and distinguished them from the previously proposed reductive elimination mechanism. Cheminformatic study identified benzylic cross coupling products with drug-like physicochemical properties and diverse topological features and promised the broad applications of these benzylic cross coupling strategies in pharmaceutical research.

1.2. Discovery of the Redox Buffering Strategy

Oxidative coupling methods that employ benzylic C(*sp*³)-H substrates as the limiting reagent often proceed via cationic intermediates generated from hydride^{41, 42} or electron transfer^{37,43}, which limits the scope to electron-rich substrates. Recent advances on Cu-catalyzed radical-relay functionalization methods prompted us to evaluate hydrogen atom transfer (HAT) as the enabling strategy, a radical-mediated C-H activation mechanism that is less sensitive to the electronic nature of the aromatic ring.⁴⁴ We aimed to extend a general method for benzylic C-H cross couplings with versatile coupling partners, for example, alcohols, from our recent success in

benzylic C–H cyanation²¹ as well as arylation from Liu and coworkers^{33,35}. However, when methanol was used as the coupling partner, only negligible yield of the desirable methyl ether was afforded, with little conversion of the substrate and N-fluorobenzenesulfonimide (NFSI) under the cyanation- and arylation-related conditions (Figure 1.1A).⁴⁵ Such results suggested that the previously identified conditions was not general but rather dependent on the choice of coupling partners. We hypothesized that the coupling partner plays a role in modifying the reactive form of the Cu catalyst. Stoichiometric reactions between Cu^{II} and various coupling partners revealed that reduction of Cu^{II} to Cu^I was rapidly induced by TMSCN and ArB(OH)₂, whereas no reaction was observed with MeOH.⁴⁵

Reconsideration of the reaction mechanism suggested a possible pathway that might stall the productive catalytic cycle: the potent hydrogen abstractor, an N-centered radical, •NSI, maybe captured by another equivalent of Cu^I (Figure 1.1B). Computational study revealed that following the activation of NFSI by Cu^I, reaction of •NSI with a second equivalent of Cu^I proved highly thermodynamically favorable ($\Delta G^\circ = -27.5$ kcal/mol, Figure 1.1C), while reaction of •NSI with ethylbenzene, though thermodynamically downhill ($\Delta G^\circ = -17.0$ kcal/mol), did encounter an activation free energy (ΔG^\ddagger , +9.6 kcal mol⁻¹). Since Cu^{II} does not react with NFSI to initiate productive catalysis under these conditions, we postulated that a mild reductant that reduces Cu^{II} to Cu^I can be identified as a "redox buffer", which does not directly react with the oxidant NFSI, but induces reduction of Cu^{II} to Cu^I in a controlled manner. Through screening with various reducing agents, dialkylphosphite stood out with promising reactivity, improving both conversion of the substrate and yield of the desirable methyl ether (Figure 1.1D). This redox buffering strategy provides the basis to expand the scope of coupling partners. In a separate study, MeB(OH)₂ in the presence of Li₂CO₃ also proved effective as a redox buffer for benzylic C–H fluorination reaction

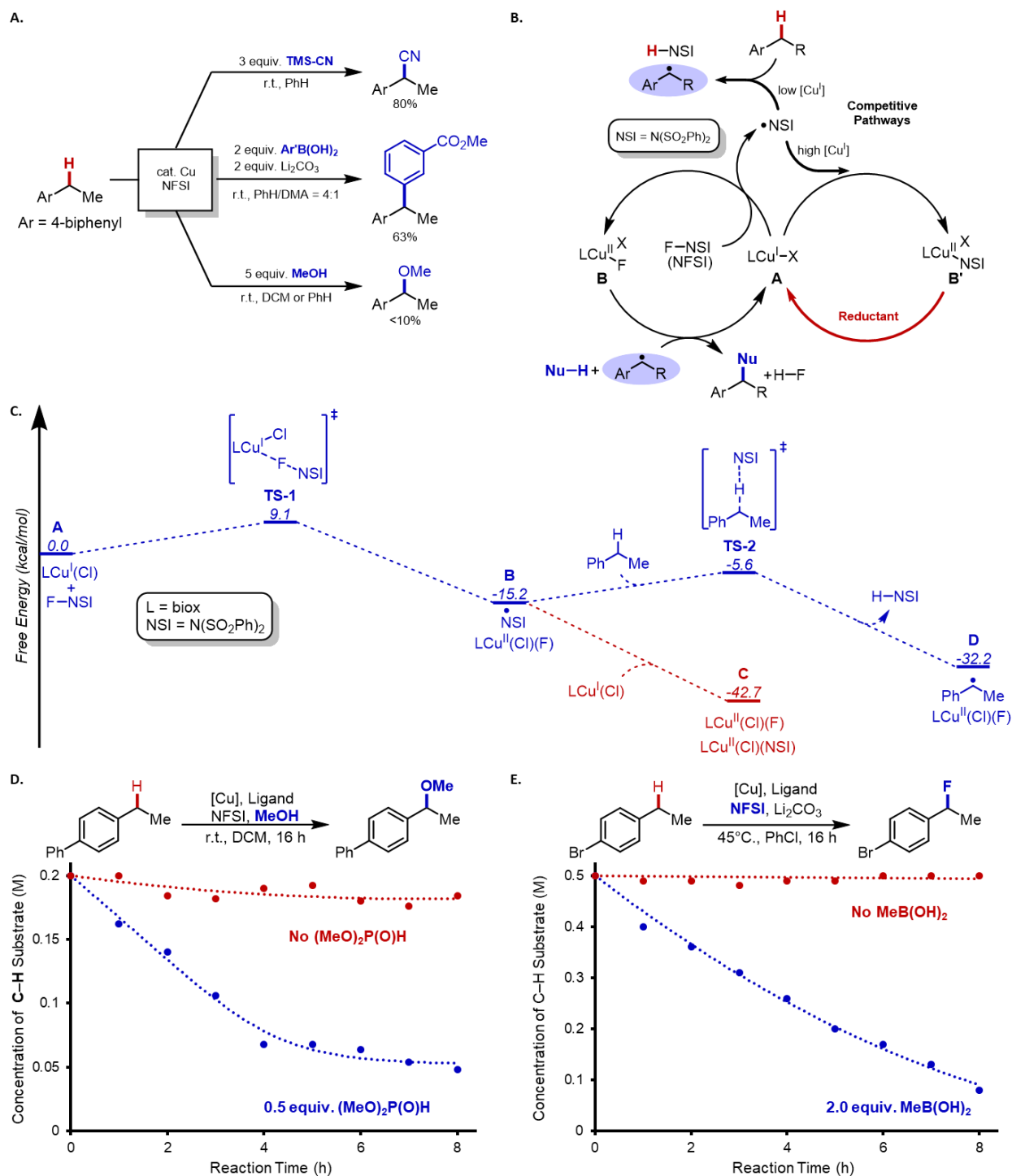


Figure 1.1. (A) Cu-catalyzed benzylic C–H functionalization reactions. (B) Modified radical relay mechanism to account for quenching of the $\bullet\text{NSI}$ by Cu^{I} and regeneration of Cu^{I} by a reducing substrate or additive. (C) Calculated reaction pathways and energy landscape for reaction of $\bullet\text{NSI}$ with $(\text{biox})\text{Cu}^{\text{I}}\text{Cl}$ and ethylbenzene. (D) Reaction time course for benzylic etherification conducted in the absence (red) and presence of 0.5 equiv. of dimethyl phosphite (blue). (E) Reaction time course for benzylic fluorination conducted in the absence (red) and presence of 2.0 equiv. of methylboronic acid (blue).

(Figure 1.1E), where little conversion of the benzylic C–H was found in the absence of the redox buffer. This "redox buffering" concept sheds new mechanistic insights into the Cu-catalyzed radical relay chemistry, which promises efficient benzylic C(*sp*³)–H functionalization, and potentially enables the underdeveloped cross coupling reactivity.

1.3. Direct Benzylic C–H Cross Couplings

1.3.1. Benzylic C–H Cross Coupling with Alcohols

Benzylic ethers are prevalent motifs in drug molecules and medicinally relevant compounds. Alcohols are building blocks widely employed in both classical synthetic methods, such as Williamson ether synthesis⁴⁶, and modern catalytic strategies⁴⁷⁻⁴⁹. Late-stage benzylic methoxylation is particularly valued in strategic modification of lead compounds and drug molecules, where the methoxy group has been found to improve potency with little perturbation on lipophilicity and steric hindrance^{50,51}. Existing oxidative couplings of benzylic C–H bonds and alcohols are largely mediated by direct electron transfer^{37,43} or hydride transfer^{41,42}, which limit the substrate scope to electron-rich arenes. We conceived that a radical relay strategy that activates the C–H bonds via HAT should promise better tolerance of the electronic features of the arenes⁴⁴ and allow more efficient cross couplings of benzylic C–H bonds and alcohols, using benzylic C–H substrates as the limiting reagents.

The desired reactivity was achieved by using CuCl as the catalyst, 2,2'-bis(2-oxazoline) (biox) as the ligand, NFSI as the oxidant and methanol as the coupling partner, enabled by the redox buffering strategy (Figure 1.2A). The reaction showed broad scope with benzylic C–H substrates, including alkylbenzenes, benzhydryl derivatives and benzylic C–H scaffolds that contain heterocycles like thiophene, chroman, benzothiazole and indazole. This methoxylation method

was successfully applied to a number of pharmaceuticals and bioactive molecules with moderate to high yields. The utility of this $C(sp^3)$ -O coupling approach was further demonstrated with diversification of a canagliflozin precursor, where good reactivities were observed with an array of medicinally relevant and structurally diverse alcohols and highlighted in the gram-scale synthesis of a complicated benzylic ether (Figure 1.2B). Cross coupling of pairs of benzylic C-H scaffolds and alcohols also proved fruitful with moderate to good yields of the benzylic ethers (Figure 1.2C).

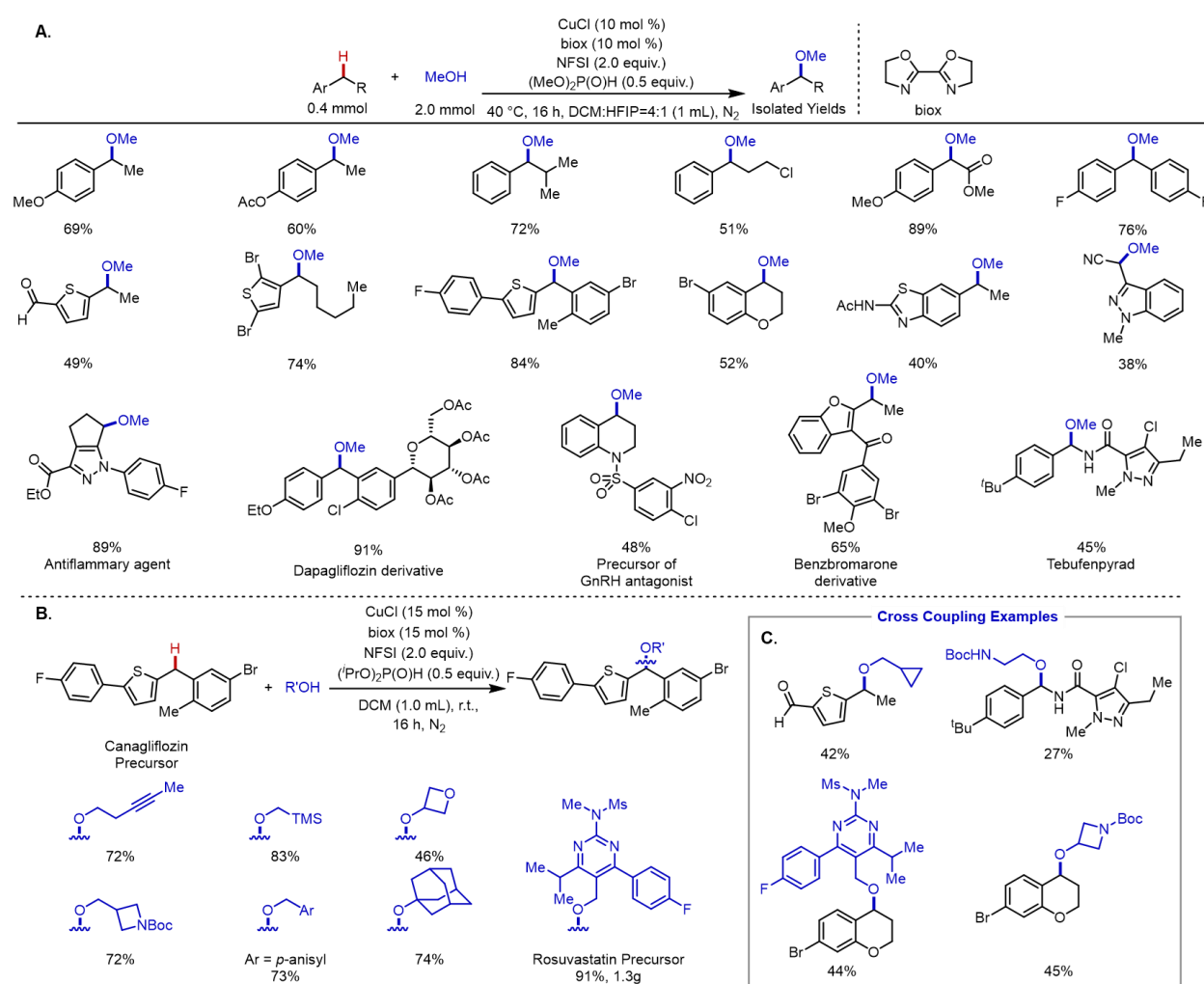


Figure 1.2. (A) Selected substrate scope of benzylic C-H methoxylation. (B) Benzylic C-H etherification of a canagliflozin precursor with various alcohols. (C) Cross-coupling examples of medicinally relevant benzylic C-H substrates and alcohols.

1.3.2. Benzylic C–H Cross Coupling with N–H Azoles

Pd-⁵² and Cu-catalyzed^{53,54} C(*sp*²)-N cross coupling reactions are some of the widely applied methods for syntheses of pharmaceuticals.^{1,2} Recent efforts in C(*sp*³)-N coupling reactions have started to complement these methods in pursuit of topological diversity and physicochemical properties.⁵⁵ Direct amination of C(*sp*³)-H bonds with ammonia surrogates via nitrenes^{11,12} and azides^{22-24,38,56} has allowed rapid access to a collection of alkylamines, while direct C–H/N–H cross-coupling strategies, for example, with secondary sulfonamides/amides or azoles remain constrained^{43,57-59} and often require excess C–H substrates^{60,61}.

N-benzylic azoles constitute an important class of pharmacophores and find broad applications in drug discovery.^{6,62} The ambident reactivity of many azoles, however, presents significant selectivity challenges.⁶³ We developed a copper-catalyzed method that achieves *site*-selective cross coupling pyrazoles and other N–H heterocycles with substrates bearing (hetero)benzylic C–H bonds.⁶⁴ Excellent *N*-site selectivity is achieved, with the preferred site controlled by the additives like tetrabutylammonium chloride (TBACl) or Lewis acids like trimethylsilyl triflate (TMSOTf) or BF₃•OEt₂ (Figure 1.3A). This cross-coupling strategy exhibits broad scope of (hetero)benzylic C–H scaffolds and features high *N*-site selectivity with an array of N–H heterocycle, including pyrazoles, purines, triazoles and tetrazoles. Cross coupling of complicated C–H scaffolds and N–H heterocycles also proved successful (Figure 1.3B). Coupling with N–H heterocycles beyond azoles, like β -lactams or sultams, also proceeded in moderate-to-good yields and *N*-site selectivity switch was effective despite the scaffold complexity. We postulated that the origin of the unique selectivity switch observed could arise from kinetic versus thermodynamic control (Figure 1.3C, top). The structure of the pyrazole under the base-free reaction conditions supported the observed reactivity with *N*² lone pair, in contrast to the preferred reactivity at the *N*¹

site in deprotonated pyrazolide^{65, 66}. Isomerization of the N^2 kinetic product to the N^1 thermodynamic product could be promoted by a strong Lewis acid, such as a trimethylsilyl (TMS) cation. Collectively, we anticipate this benzylic $C(sp^3)$ -N coupling, along with the mechanistic insights about N -site selectivity switch, to feature broad applications in synthesis of medically relevant compounds for drug discovery.

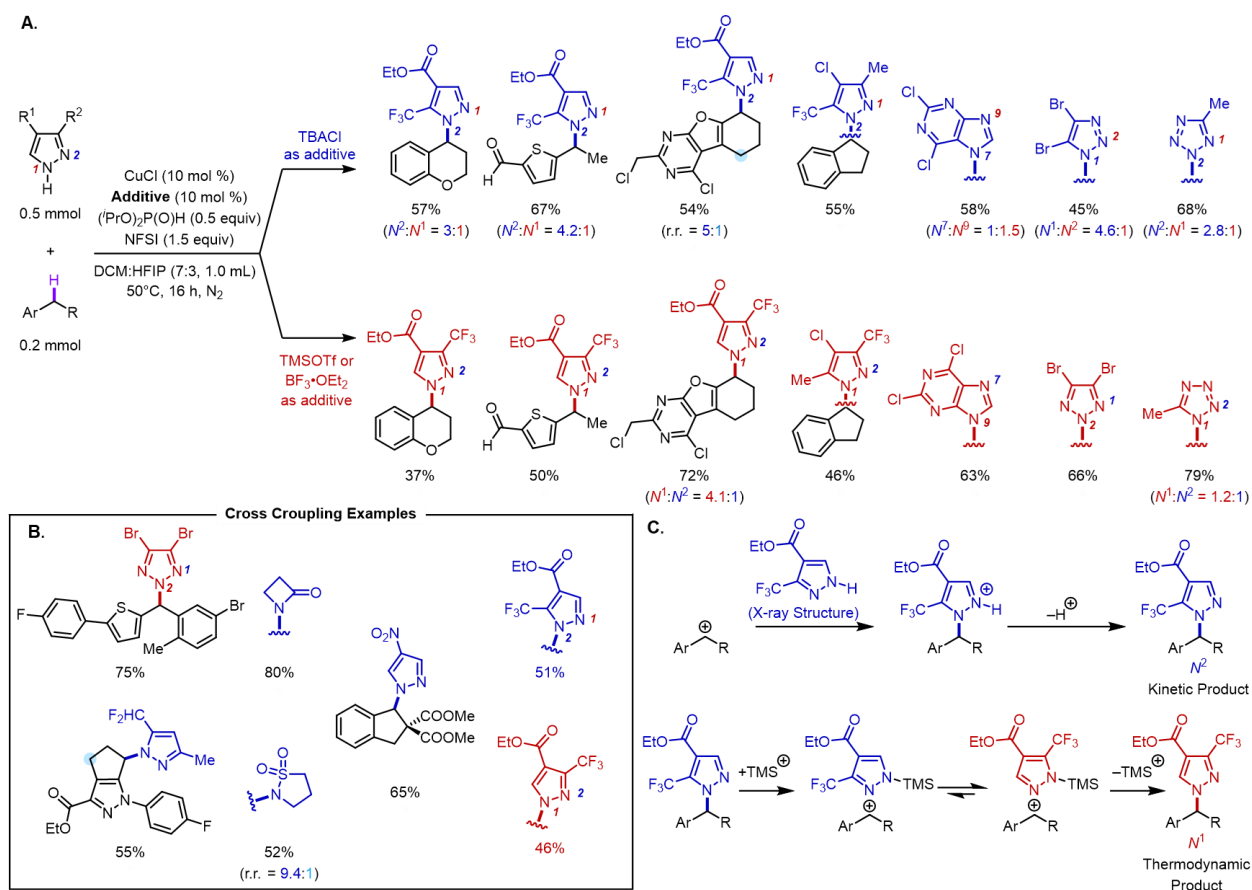


Figure 1.3. (A) Cross coupling of benzylic C–H cross and azoles with TBACl as the additive for N^2 selectivity and with TMSOTf or $\text{BF}_3 \cdot \text{OEt}_2$ for N^1 selectivity. (B) Cross-coupling examples medically relevant benzylic C–H substrates and N–H heterocycles. (C) Mechanistic origin of regioselectivity.

1.4. Benzylic C–H Functionalizations/Diversifications

Direct cross couplings of benzylic C–H bonds and various nucleophilicities have enabled rapid elaboration of building blocks. The C(*sp*³)–O⁴⁵ and C(*sp*³)–N⁶⁴ cross coupling examples described in section 1.3 streamlined syntheses of benzylic ethers and *N*-benzylic heterocycles efficiently via one-step protocols. However, oxidatively sensitive or strongly nucleophilic coupling partners, for example, carboxylic acids⁶⁷, phenols⁶⁸, amines⁶⁸ etc., would interfere with the desirable transformation in a direct coupling manner. In complementary efforts, we have explored sequential benzylic C–H functionalization/diversification protocols, where functional handles are installed at the benzylic sites first, followed by reaction with versatile coupling partners. These sequential approaches allow the use of much broader scope of coupling partners and further expand the synthetic utility of benzylic C–H cross coupling reactions.

1.4.1. Benzylic C–H Fluorination/Diversification Sequence

While fluorination of C(*sp*³)–H has long been a sought-after tool for metabolic stability improvement⁶⁹, the lability of benzylic fluorides suggest that they are prone to undergo substitution and unlikely ideal surrogates to protect metabolically vulnerable sites^{70,71}. This labile feature renders benzylic fluorides valuable as functional handles for rapid elaboration, which promises the access to diverse analogs of pharmaceutically relevant building blocks.

Cu-catalyzed radical relay chemistry, with NFSI as the oxidant, has enabled many site-selective benzylic C–H functionalization strategies, and the earliest precedent featured a direct transfer of a sulfonimide group from NFSI to the benzylic position.⁷² We recently discovered MeB(OH)₂ can serve as a redox buffer and modifications of reaction conditions switched the previously reported C–N coupling reactivity to C–F bond formation (Figure 1.4A).⁷³ Addition of

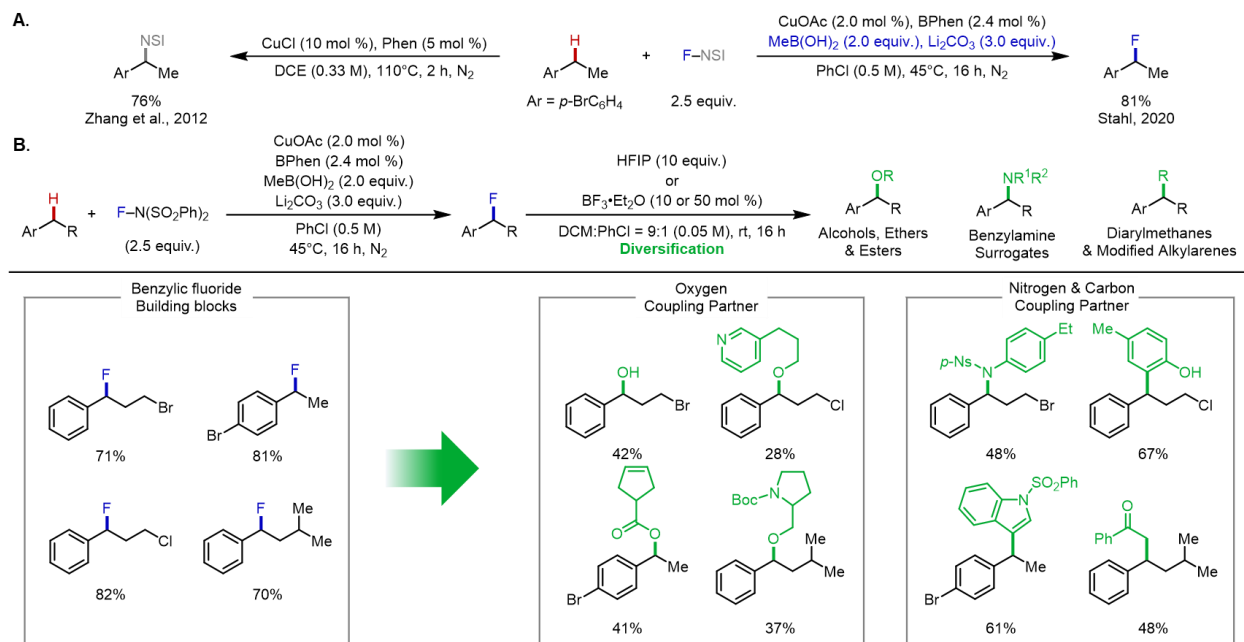


Figure 1.4. Benzylic C(sp³)-H Fluorination/Diversification Sequence. (A) Switch from C-N to C-F bond formation with Cu/NFSI (B) Benzylic C(sp³)-H Cross Couplings to C-O, C-N and C-C Bonds via benzylic fluorides.

MeB(OH)₂ significantly improved the conversion of benzylic C-H substrates, consistent with our earlier observation with dialkyl phosphites. The use of Li₂CO₃ as a Brønsted base sequestered the byproduct HN(SO₂Ph)₂ and circumvented the undesired fluoride acidolysis or C-N coupling reactivity. Employing PhCl as the solvent and lower catalyst loading also helped boost the formation of benzylic fluorides.

Upon reaction condition optimization, good to high yields of the benzylic fluorides were generally afforded. In an effort to leverage benzylic fluorides as a functional handle, we developed a fluorination/diversification sequence (Figure 1.4B).⁷⁴ Activation of benzylic fluorides by a hydrogen bond donor like HFIP or a Lewis acid like BF₃·Et₂O allowed the rapid displacement of them and contributed to a collection of elaborated building blocks. Selected oxygen-, nitrogen- and carbon-based coupling partners underwent effective couplings through displacement of

benzylic fluorides. This approach allowed incorporation of many challenging moieties like hydroxyl, alkene, indole, phenol and pyrrolidine, which proved oxidatively sensitive in the direct coupling manner. Collectively, this benzylic C–H functionalization/diversification sequence provided a convenient alternative to direct coupling protocols and enabled the use of difficult coupling partners.

1.4.2. Benzylic C–H Chlorination/Diversification Sequence

C(*sp*³)–Cl units are important functional handles in building blocks. Strategic activation of such alkyl chlorides allowed rapid diversification of these building blocks via C–C, C–N, C–O and C–S bond formation.⁷⁵ Preparation of alkyl chlorides typically involved ring-opening chlorination strategies,^{76,77} addition to alkenes^{78,79} or interconversion of pre-installed functional handles⁸⁰. Direct chlorination of C(*sp*³)–H bonds represents a convenient and efficient approach to prepare alkyl chlorides, yet existing catalytic methods are limited to excessive use of C–H substrates¹⁵ and tend to exhibit promiscuous reactivity in the myriad of C–H bonds^{16,18,81–83}.

We developed a radical relay Cu-catalyzed benzylic C–H chlorination method that is enabled by the redox buffering strategy and allowed the use of benzylic C–H substrate as the limiting reagent,⁸⁴ with excellent benzylic *site*-selectivity comparing to selected existing method^{79–86} (Figure 1.5A). Evaluation of the benzylic C–H substrate scope found good tolerance of highly electron-deficient substrate and heterocycle fragments (Figure 1.5B). Representative benzylic chlorides of drug-relevant synthetic intermediates were transformed to an array of benzylic ethers, thioethers and amines (Figure 1.5C). The promising reactivity shown with these oxidatively sensitive, highly nucleophilic coupling partners demonstrated the potential of this chlorination/diversification sequence to further broaden the scope of benzylic cross coupling products.

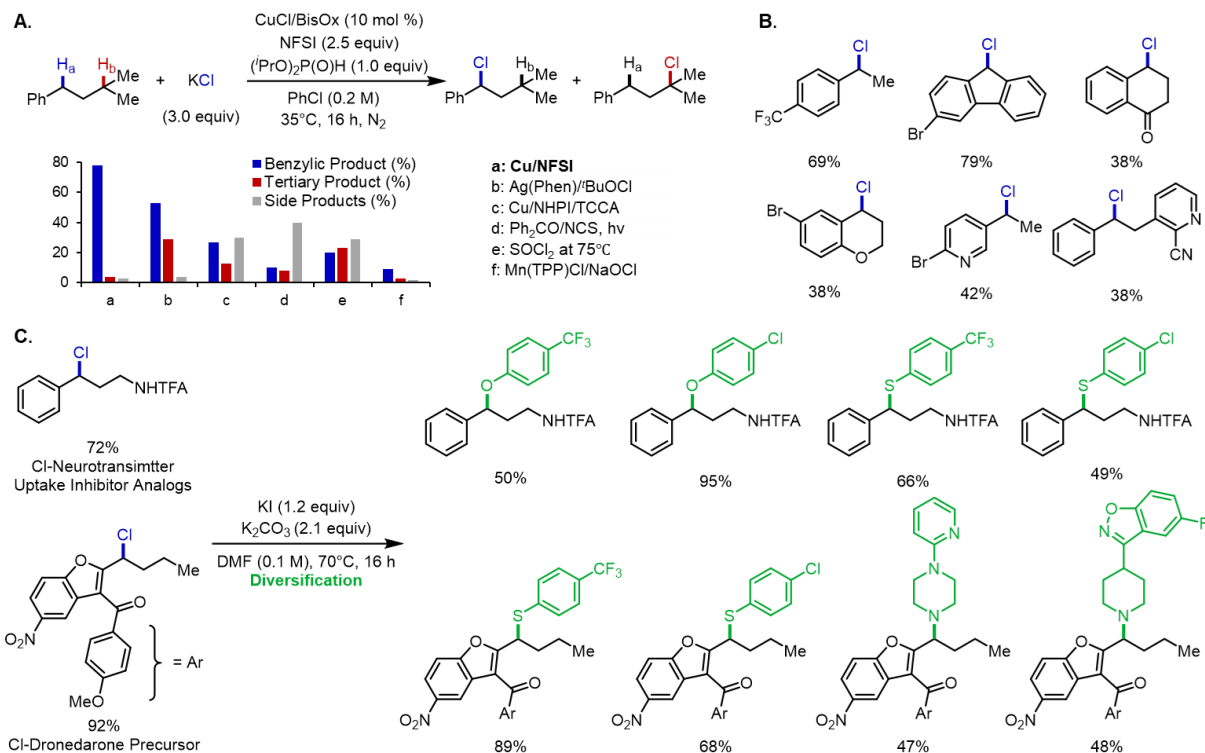


Figure 1.5. Selected substrate scope for Cu-catalyzed benzylic C–H chlorination/diversification sequence. (A) Comparison of C–H site-selectivity between radical relay Cu/NFSI benzylic C–H chlorination strategy and other existing C–H chlorination methods. (B) Selected substrate scope of Cu/NFSI benzylic C–H chlorination reaction. (C) Representative examples for diversification of benzylic chlorides with phenols, thiophenols and amines.

1.4.3. Benzylic C–H Isocyanation/Amine Coupling Sequence

Benzylic ureas are important moieties that have found broad applications in medicinal chemistry⁸⁷⁻⁸⁹. (Hetero)benzylic C–H bonds are ubiquitous in medically relevant building blocks and represent unique opportunities to directly construct benzylic ureas. Conventional routes to access ureas involve cross coupling of isocyanates and amines and therefore two benzylic C–H functionalization/diversification sequences can be envisioned: benzylic C–H amination/isocyanate coupling sequence and benzylic C–H isocyanation/amine coupling sequence. The former approach employs benzylic C–H amination strategies with use of ammonia surrogates like azides,^{17,22,23,38}

sulfamates,^{11,12} and sulfonamides¹³, where a deprotection step is likely needed before coupling with isocyanates; moreover, insufficient supply of purchasable isocyanates limits the number of ureas synthetically accessible.⁹⁰ In comparison, the benzylic C–H isocyanation/amine coupling sequence benefits from the readily available amines and promises access to vast number of benzylic ureas in only two steps⁹⁰. However, existing benzylic C–H isocyanation precedents prove operationally complicated and lack of synthetic utility due to the use of excess C–H substrates.^{91,92}

We developed a benzylic C–H isocyanation that features the use of benzylic C–H substrates as the limiting reagent and commercially available catalysts and reagents, as well as operational simplicity and compatibility with high-throughput experimentation (HTE).⁹³ This Cu/NFSI-mediated C–H isocyanation approach, enabled by the redox buffering strategy with (ⁱPrO)₂P(O)H as the sacrificial reductant, exhibited exquisite benzylic site-selectivity under mild conditions and afforded moderate to good yields of the (hetero)benzylic isocyanates (Figure 1.6A). Without further work-up, addition of the reaction mixture to the amine coupling partners led to the efficient formation of benzylic ureas.

The synthetic utility of this urea synthesis protocol in medicinal chemistry was further demonstrated with HTE. Three benzylic isocyanates derived from bioactive molecules or drug precursors were evaluated in this amine coupling approach with a collection of 96 amines, including 43 aromatic and 53 aliphatic amines. Selected benzylic ureas were highlighted in Figure 1.6B with moderate to good yields. Analyses of the physicochemical properties for these 3 × 96 benzylic ureas revealed that these products would fit in the "oral druggable space beyond Rule of 5 (bRO5)".⁹⁴ Collectively, this benzylic C–H isocyanation/amine coupling sequence enabled rapid access to a diverse array of benzylic ureas with drug-like physicochemical properties and promises broad applications in bioactive compound syntheses for drug discovery.

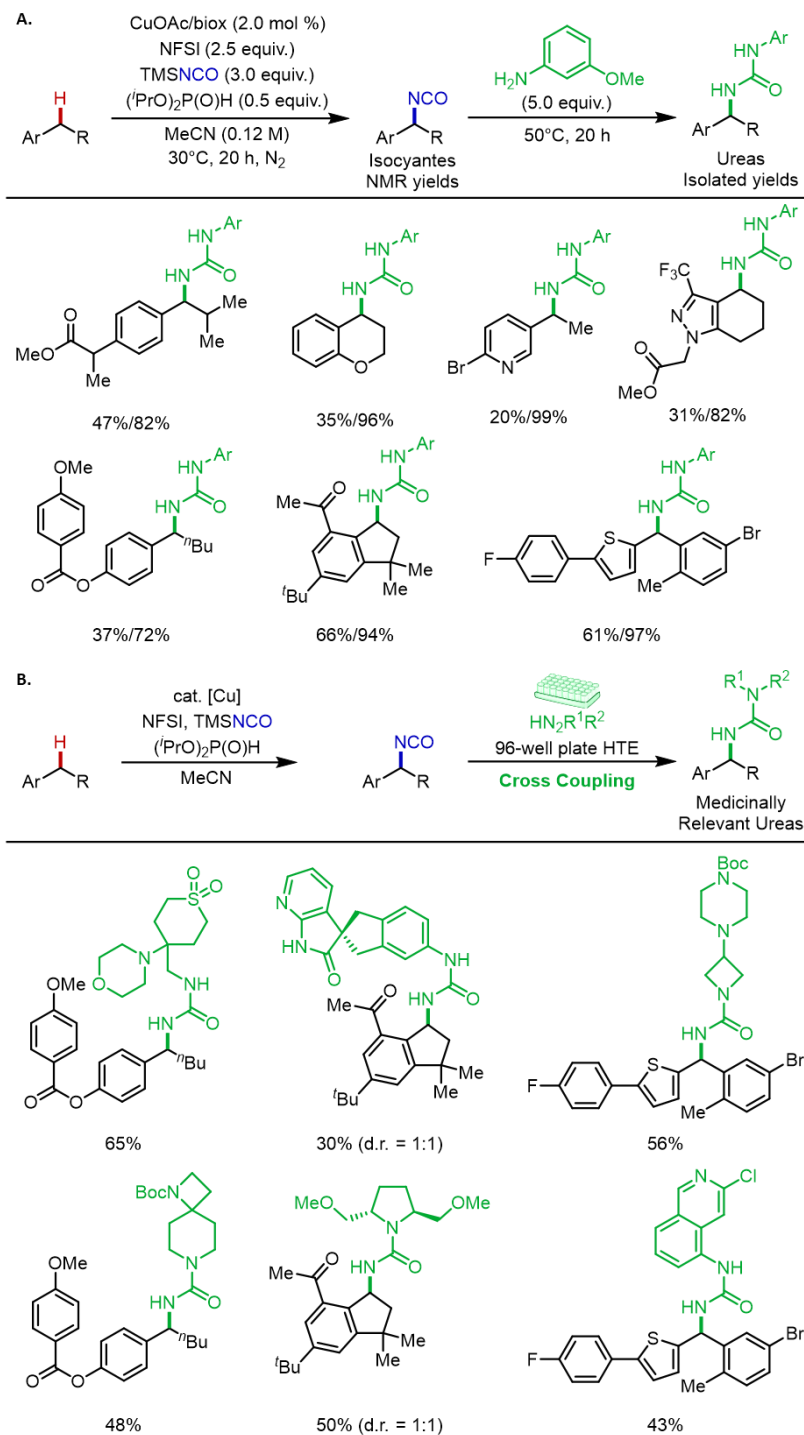


Figure 1.6. (A) Selective substrate scope for benzylic C–H isocyanation. (B) Representative benzylic ureas synthesized via benzylic C–H isocyanation/amine coupling sequence.

1.5. Functionalization of Benzylic Radicals: Mechanistic Investigation

Functionalization of the benzylic radicals represents the last step of the radical relay Cu-catalyzed benzylic C–H functionalization reactions. Understanding this bond-forming step is of paramount importance since the mechanism involved here dictates whether enantioselectivity could be induced. The radical functionalization step appeared to be highly sensitive to the nature of the nucleophiles as well as the electronic profiles of the copper catalyst: high enantioselectivity was observed with benzylic C–H cyanation,²¹ yet only racemic products were afforded with benzylic C–H methoxylation⁴⁵ and azidation reactions³⁸.

Computational study revealed that ligand exchange of a (biox)Cu^{II}(Cl)(F) species with MeOH proved highly energetically uphill (**A'**, $\Delta G^\circ = +10.9$ kcal/mol, Figure 1.7A), followed by another activation energy barrier to form the benzylcopper(III) species (**TS-1**, $\Delta G^\ddagger = +5.1$ kcal/mol, Figure 1.7A). The subsequent C–O reductive elimination proceeded via the highest energy species (**TS-2**, $\Delta G^\ddagger = +18.6$ kcal/mol, Figure 1.7A) along this pathway. The alternative pathway featured a radical-polar crossover mechanism, where the benzylic radical was oxidized by (biox)Cu^{II}(Cl)(NSI) to afford a benzylic cation, which is only moderately uphill (**B**, $\Delta G^\ddagger = +6.2$ kcal/mol). The resulting benzylic cation can then be trapped by an outer-sphere methanol, a highly thermodynamically favorable event (**C**, $\Delta G^\circ = -29.8$ kcal/mol), to afford the methoxylated product. The more favorable radical-polar crossover pathway identified here accounted for the lack of enantioselectivity for methoxylation and contrasted with the organocopper(III) pathway proposed for the enantioselective cyanation reaction.²¹

A separate study on benzylic C–H azidation also found the radical-crossover mechanism as the most favorable pathway.³⁸ Distinguished from the MeOH case, ligand exchange of copper(II) species with TMS–N₃ appeared to be favorable, as suggested by the formation of the Cu^{II}–N₃

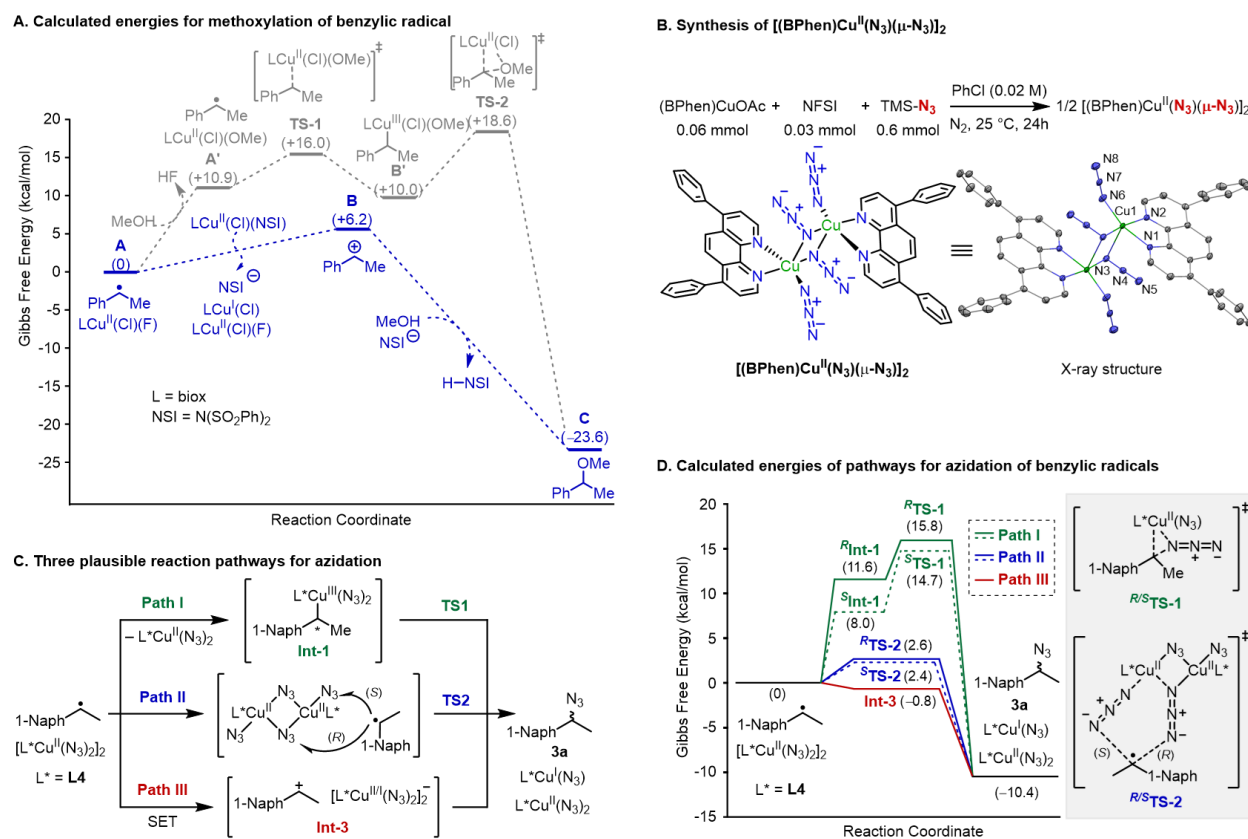


Figure 1.7. Mechanistic investigation into reaction pathways for benzylic C–H methoxylation and azidation. (A) Calculation reaction pathways for methoxylation of benzylic radical. (B) Synthesis and crystal structure of $[(\text{BPhen})\text{Cu}^{\text{II}}(\text{N}_3)(\mu\text{-N}_3)]_2$ (hydrogen atoms and chlorobenzene molecule omitted for clarity). (C) Three proposed pathways for azidation of the benzyl radical. (D) Simplified energy diagrams comparing the three azidation pathways.

dimeric complex under simulated catalytic conditions (Figure 1.7B). In addition to the aforementioned organocopper(III) pathway (**Path I**, Figure 1.7C) and radical-polar crossover pathway (**Path III**, Figure 1.7C), a direct radical addition to N_3 ligand was also considered (**Path II**, Figure 1.7C).^{95–97} The overall energetic profile showed that reductive elimination from organocopper(III) has the highest energies among all pathways calculated ($R/S\text{TS-1}$, $\Delta G^\ddagger = +15.8$ and $+14.7$ kcal/mol, Figure 1.7D), followed by radical addition pathway ($R/S\text{TS-2}$, $\Delta G^\circ = +2.6$ and $+2.4$ kcal/mol, Figure 1.7D). The radical-polar crossover mechanism represented the lowest energy pathway and is thermodynamically favorable (**Int-3**, $\Delta G^\circ = +0.8$ kcal/mol, Figure 1.7D).

Collectively, these results suggest that nucleophiles that struggle to transmetalate like MeOH, and those that do not suppress the oxidation power of Cu^{II} like TMS–N₃, would likely functionalize radicals via cations. Further efforts should focus on how other nucleophiles, like cyanides, aryls and alkynyls influenced the nature of the copper species and favored the reductive elimination pathway, which enabled enantioselective induction.

1.6. Benzylic C–H Cross Coupling Improves 3D Structural Diversity

Compound collections of diverse structures are highly valued in medicinal chemistry, which promise successful identification of a hit in screening processes. To this end, synthetic methods that join complicated fragments, like palladium-catalyzed cross-coupling reactions and amide couplings, have enabled syntheses of many novel molecules.^{1,2} However, prevalent use of C(*sp*²)-based coupling partners in these reaction classes have led to limitation in topology.³ A collection of bioactive compounds was analyzed in a principal moments of inertia (PMI) plot, where molecules with diverse topology could be mapped on a triangular plot and vertices are occupied by molecules with "rod", "disc", and "sphere" shape, respectively (Fig 1.8A).⁹⁸ These bioactive molecules densely populate the "rod-disc" region, and such bias can contribute to suboptimal physicochemical properties like low water solubility and eventually undesirable outcomes in drug development like high attrition rates.³ Application of the underexplored C(*sp*³)-focused cross-coupling methods can potentially complement the existing collection of compounds and open the gate for more topological diversity.

Recently, C(*sp*³)-H functionalization methodologies have emerged to be enabling tools for medicinal chemists to quickly access compound libraries with diversity.⁵¹ Among these methods, radical relay Cu/NFSI-mediated catalysis stood out with exquisite benzylic *site*-selectivity and

proved powerful in cross coupling reactions, enabled by the redox buffering strategy.^{45,64,73,74,84,93}

These benzylic $C(sp^3)$ -H cross coupling reactions create opportunities to assemble 3D libraries that complement the existing "flat" compounds.

To scrutinize the molecular profiles of benzylic C–H cross coupling product, a cheminformatic approach was taken to systematically compare these compounds with bioactive molecules and $C(sp^2)$ -derived coupling products.⁹⁹ A benzylic C–H cross coupling products library was virtually

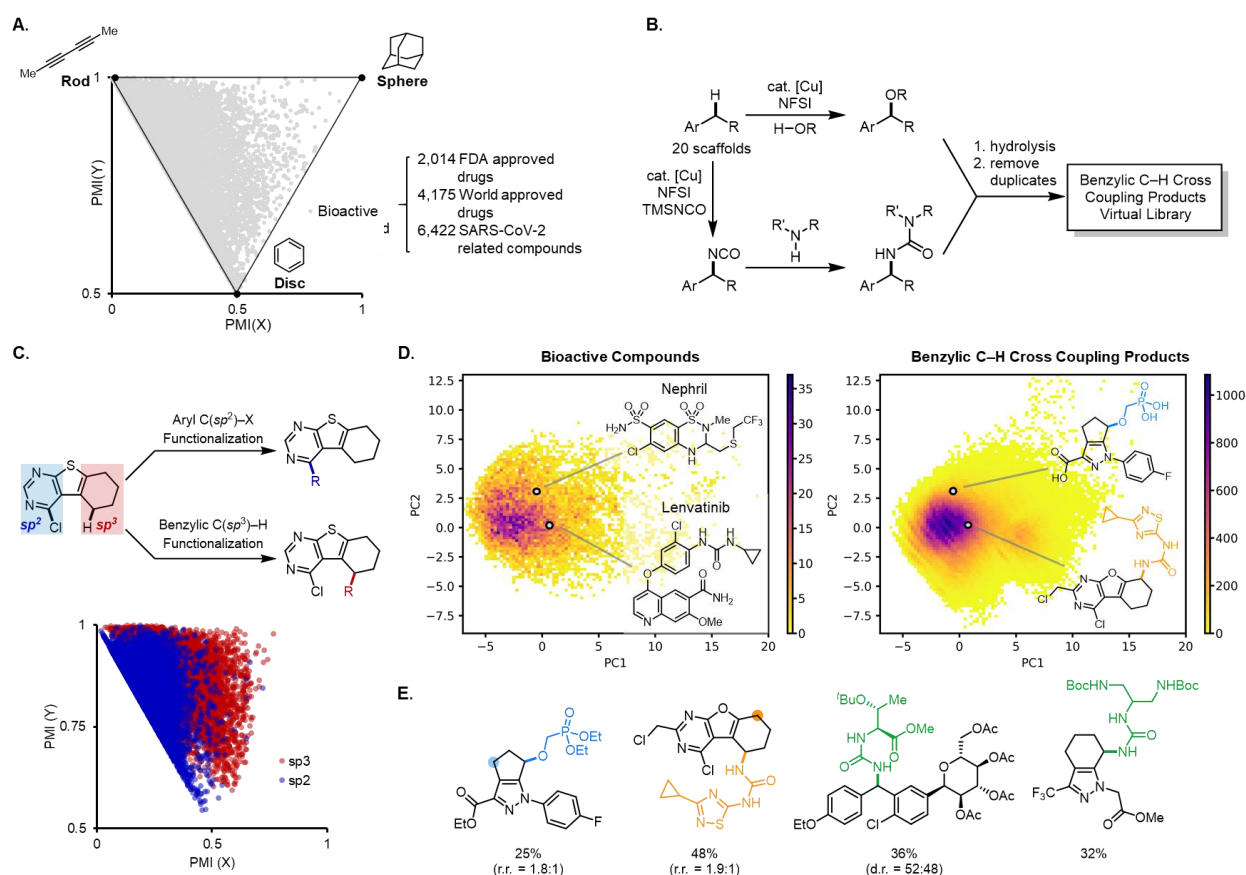


Figure 1.8. Benzylic $C(sp^3)$ -H cross couplings improve 3D diversity. (A) PMI analysis of bioactive molecules. (B) Virtual enumeration of benzylic $C(sp^3)$ -H ethers and ureas. (C) PMI comparison between $C(sp^2)$ - and $C(sp^3)$ -derived cross coupling products. (D) PCA comparison between bioactive molecules and benzylic coupling products, and representative pairs of drugs and benzylic ethers and ureas. (E) Selected examples of synthetically accessed benzylic ethers and ureas.

enumerated with etherification⁴⁵ and isocyanation/amine coupling sequence⁹³ (Fig 1.8B). Overall, benzylic coupling products exhibited higher three-dimensionality and this observation is especially evident when comparison is made between C(*sp*²) and C(*sp*³) functionalization products, where C(*sp*²)-derived products roughly fell into the "rod-disc" region and C(*sp*³)-derived products, however, moved to populate the less explored 3D chemical space (Fig 1.8C).

Analysis and comparison of the physicochemical properties between benzylic cross coupling products and bioactive molecules demonstrated the relevance of the benzylic products in a drug-like chemical space. The assessment was conducted with principal components analysis (PCA), an informative tool that deconvolutes multidimensional chemical space and visualize compounds in lower dimensions by maximizing variance of the projected data. The significant overlap between these PCA plots clearly showed the resemblance of the benzylic coupling products to the bioactive molecules, and selected pairs of these compounds manifested the potential of benzylic coupling methods to supply drug-like molecules (Fig 1.8D). We finally evaluated the synthetic accessibility of a selection of these drug-like molecules (Fig 1.8E). Moderate to good yields of these drug-like compounds were achieved, which validate benzylic C(*sp*³)-H cross coupling methods as powerful tools to synthesize medicinally relevant products. Collectively, these results demonstrated benzylic C(*sp*³)-H cross coupling reactions to reliably enable access to 3D, drug-like structure. Broader application of this informatics-guided synthesis approach should transform the way methodologies are developed and drive the field to afford compounds of more desirable and diverse molecular properties.

1.7. Thesis Scope

The enclosed thesis research describes two radical relay Cu-catalyzed benzylic C–H cross coupling reactions, a cheminformatic study of the coupling products and a Cu-catalyzed benzylic C–H azidation reaction. The first benzylic C–H cross coupling reaction was the cross couplings with alcohols (Chapter 2). A "redox buffering" strategy through the development of this etherification method, which sheds mechanistic insight into the radical relay chemistry and sets the stage for other benzylic cross coupling reactions. Enabled by "redox buffering", the second reaction described was the benzylic C–H cross couplings with N–H azoles (Chapter 3), where a *N*-site selectivity control was made possible by switching reaction conditions. To systematically evaluate the molecular properties of benzylic cross coupling products, a cheminformatics-synthesis approach was taken to study the physicochemical and topological features of benzylic ethers and ureas via virtual enumeration (Chapter 4). In that study, benzylic C(*sp*³)–H cross coupling products were found significantly more three-dimensional than existing bioactive compounds and C(*sp*²)-derived coupling products. The final chapter (Chapter 5) details the development of a Cu-catalyzed benzylic C–H azidation reaction, where the utility of azides was demonstrated, and mechanistic insights were gained through experimental and density functional theory studies of the C–N bond formation step. Overall, the enclosed study embodies the radical relay Cu-catalyzed benzylic C–H cross coupling reactions that were discussed in this introductory section.

1.8. Reference

1. Brown, D. G.; Boström, J. Analysis of Past and Present Synthetic Methodologies on Medicinal Chemistry: Where Have All the New Reactions Gone?: Miniperspective. *J. Med. Chem.* **2016**, *59*, 4443–4458.
2. Boström, J.; Brown, D. G.; Young, R. J.; Keserü, G. M. Expanding the Medicinal Chemistry Synthetic Toolbox. *Nat Rev Drug Discov* **2018**, *17*, 709–727.
3. Lovering, F.; Bikker, J.; Humblet, C. Escape from Flatland: Increasing Saturation as an Approach to Improving Clinical Success. *J. Med. Chem.* **2009**, *52*, 6752–6756.
4. Choi, J.; Fu, G. C. Transition Metal–Catalyzed Alkyl–Alkyl Bond Formation: Another Dimension in Cross-Coupling Chemistry. *Science* **2017**, *356*, eaaf7230.
5. Ritchie, T. J.; Macdonald, S. J. F. The Impact of Aromatic Ring Count on Compound Developability – Are Too Many Aromatic Rings a Liability in Drug Design? *Drug Discovery Today* **2009**, *14*, 1011–1020.
6. Taylor, R. D.; MacCoss, M.; Lawson, A. D. G. Rings in Drugs: Miniperspective. *J. Med. Chem.* **2014**, *57*, 5845–5859.
7. Xue, X.-S.; Ji, P.; Zhou, B.; Cheng, J.-P. The Essential Role of Bond Energetics in C–H Activation/Functionalization. *Chem. Rev.* **2017**, *117*, 8622–8648.
8. Thompson, T. N. Optimization of Metabolic Stability as a Goal of Modern Drug Design. *Med. Res. Rev.* **2001**, *21*, 412–449.
9. White, M. C., Zhao, J. Aliphatic C–H oxidations for late-stage functionalization. *J. Am. Chem. Soc.* **2018**, *140*, 13988–14009.

10. Tanwar, L.; Börgel, J.; Ritter, T. Synthesis of Benzylic Alcohols by C–H Oxidation. *J. Am. Chem. Soc.* **2019**, *141*, 17983–17988.
11. Clark, J. R., Feng, K., Sookezian, A. & White, M. C. Manganese-catalysed benzylic C(sp³)–H amination for late-stage functionalization. *Nat. Chem.* **2018**, *10*, 583–591.
12. Chiappini, N., Mack, J. & Du Bois, J. Intermolecular C(sp³)–H amination of complex molecules. *Angew. Chem. Int. Ed.* **2018**, *57*, 4956–4959.
13. Muniz, K. & Bosnidou, A. E. Intermolecular radical C(sp³)–H amination under iodine catalysis. *Angew. Chem. Int. Ed.* **2019**, *58*, 7485–7489.
14. Davies, H. M. L. & Morton, D. Guiding principles for site selective and stereoselective intermolecular C–H functionalization by donor/acceptor rhodium carbenes. *Chem. Soc. Rev.* **2011**, *40*, 1857.
15. Liu, W., Groves, J. T. Manganese catalyzed C–H halogenation. *Acc. Chem. Res.* **48**, 1727–1735 (2015).
16. Quinn, R. K.; Könst, Z. A.; Michalak, S. E.; Schmidt, Y.; Szklarski, A. R.; Flores, A. R.; Nam, S.; Horne, D. A.; Vanderwal, C. D.; Alexanian, E. J. Site-Selective Aliphatic C–H Chlorination Using *N*-Chloroamides Enables a Synthesis of Chlorolissoclimide. *J. Am. Chem. Soc.* **2016**, *138*, 696–702.
17. Margrey, K. A., Czaplyski, W. L., Nicewicz, D. A. & Alexanian, E. J. A general strategy for aliphatic C–H functionalization enabled by organic photoredox catalysis. *J. Am. Chem. Soc.* **140**, 4213–4217 (2018).
18. McMillan, A. J.; Sieńkowska, M.; Di Lorenzo, P.; Gransbury, G. K.; Chilton, N. F.; Salamone, M.; Ruffoni, A.; Bietti, M.; Leonori, D. Practical and Selective sp³ C–H Bond Chlorination via Aminium Radicals. *Angew. Chem. Int. Ed.* **2021**, *60*, 7132–7139.

19. Fawcett, A.; Keller, M. J.; Herrera, Z.; Hartwig, J. F. Site Selective Chlorination of C(sp^3)–H Bonds Suitable for Late-Stage Functionalization. *Angew. Chem. Int. Ed.* **2021**, *60*, 8276–8283.
20. Jin, J.; Zhao, Y.; Kyne, S. H.; Farshadfar, K.; Ariaifard, A.; Chan, P. W. H. Copper(I)-Catalysed Site-Selective C(sp^3)–H Bond Chlorination of Ketones, (E)-Enones and Alkylbenzenes by Dichloramine-T. *Nat Commun* **2021**, *12*, 4065.
21. Zhang, W. et al. Enantioselective cyanation of benzylic C–H bonds via copper-catalyzed radical relay. *Science* **2016**, *353*, 1014–1018.
22. Sharma, A. & Hartwig, J. F. Metal-catalysed azidation of tertiary C–H bonds suitable for late-stage functionalization. *Nature* **2015**, *517*, 600–604.
23. Huang, X. & Groves, J. T. Taming azide radicals for catalytic C–H azidation. *ACS Catal.* **2016**, *6*, 751–759.
24. Czaplyski, W. L., Na, C. G. & Alexanian, E. J. C–H xanthylation: A synthetic platform for alkane functionalization. *J. Am. Chem. Soc.* **2016**, *138*, 13854–13857.
25. Sarver, P. J.; Bacauanu, V.; Schultz, D. M.; DiRocco, D. A.; Lam, Y.; Sherer, E. C.; MacMillan, D. W. C. The Merger of Decatungstate and Copper Catalysis to Enable Aliphatic C(sp^3)–H Trifluoromethylation. *Nat. Chem.* **2020**, *12*, 459–467.
26. Vasilopoulos, A.; Zultanski, S. L.; Stahl, S. S. Feedstocks to Pharmacophores: Cu-Catalyzed Oxidative Arylation of Inexpensive Alkylarenes Enabling Direct Access to Diarylalkanes. *J. Am. Chem. Soc.* **2017**, *139* (23), 7705–7708.
27. Wang, Z.; Zheng, Z.; Xu, X.; Mao, J.; Walsh, P. J. One-Pot Aminobenylation of Aldehydes with Toluene. *Nat Commun* **2018**, *9*, 3365.
28. Cheng, X.; Lu, H.; Lu, Z. Enantioselective Benzylic C–H Arylation via Photoredox and Nickel Dual Catalysis. *Nat Commun* **2019**, *10*, 3549.

29. Heitz, D. R.; Tellis, J. C.; Molander, G. A. Photochemical Nickel-Catalyzed C–H Arylation: Synthetic Scope and Mechanistic Investigations. *J. Am. Chem. Soc.* **2016**, *138*, 12715–12718.
30. Shields, B. J.; Doyle, A. G. A. Direct C(sp³)–H Cross Coupling Enabled by Catalytic Generation of Chlorine Radicals. *J. Am. Chem. Soc.* **2016**, *138*, 12719–12722.
31. Tran, B. L.; Li, B.; Driess, M.; Hartwig, J. F. Copper-Catalyzed Intermolecular Amidation and Imidation of Unactivated Alkanes. *J. Am. Chem. Soc.* **2014**, *136*, 2555–2563.
32. Perry, I. B.; Brewer, T. F.; Sarver, P. J.; Schultz, D. M.; DiRocco, D. A.; MacMillan, D. W. C. Direct Arylation of Strong Aliphatic C–H Bonds. *Nature* **2018**, *560*, 70–75.
33. Zhang, W., Chen, P. & Liu, G. Copper-catalyzed arylation of benzylic C–H bonds with alkylarenes as the limiting reagents. *J. Am. Chem. Soc.* **2017**, *139*, 7709–7712.
34. Xiao, H.; Liu, Z.; Shen, H.; Zhang, B.; Zhu, L.; Li, C. Copper-Catalyzed Late-Stage Benzylic C(sp³)–H Trifluoromethylation. *Chem* **2019**, *5*, 940–949.
35. Zhang, W., Wu, L., Chen, P. & Liu., G. Enantioselective arylation of benzylic C-H bonds via copper-catalyzed radical relay. *Angew. Chem. Int. Ed.* **2019**, *58*, 6425–6429.
36. Xu, W.; Wang, W.; Liu, T.; Xie, J.; Zhu, C. Late-Stage Trifluoromethylthiolation of Benzylic C-H Bonds. *Nat Commun* **2019**, *10*, 4867.
37. Lee, B. J.; DeGlopper, K. S.; Yoon, T. P. Site-Selective Alkoxylation of Benzylic C–H Bonds by Photoredox Catalysis. *Angew. Chem. Int. Ed.* **2020**, *59*, 197–202.
38. Suh, S.-E.; Chen, S.-J.; Mandal, M.; Guzei, I. A.; Cramer, C. J.; Stahl, S. S. Site-Selective Copper-Catalyzed Azidation of Benzylic C–H Bonds. *J. Am. Chem. Soc.* **2020**, *142*, 11388–11393.
39. Jiang, C.; Chen, P.; Liu, G. Copper-Catalyzed Benzylic C–H Bond Thiocyanation: Enabling Late-Stage Diversifications. *CCS Chem.* **2020**, *2*, 1884–1893.

40. Liu, S.; Achou, R.; Boulanger, C.; Pawar, G.; Kumar, N.; Lusseau, J.; Robert, F.; Landais, Y. Copper-catalyzed oxidative benzylic C(sp³)-H amination: Direct synthesis of benzylic carbamates. *Chem. Commun.* **2020**, *56*, 13013–13016.
41. Maloney, D. J.; Chen, S.; Hecht, S. M. Stereoselective Synthesis of the Atropisomers of Myristinin B/C. *Org. Lett.* **2006**, *8*, 1925–1927.
42. Chapman, L. M.; Beck, J. C.; Wu, L.; Reisman, S. E. Enantioselective Total Synthesis of (+)-Psiguadial B. *J. Am. Chem. Soc.* **2016**, *138*, 9803–9806.
43. Hou, Z.-W.; Liu, D.-J.; Xiong, P.; Lai, X.-L.; Song, J.; Xu, H.-C. Site-Selective Electrochemical Benzylic C–H Amination. *Angew. Chem. Int. Ed.* **2020**, *60*, 2943–2947.
44. Rafiee, M.; Wang, F.; Hruszkewycz, D. P.; Stahl, S. S. *N*-Hydroxyphthalimide-Mediated Electrochemical Iodination of Methylarenes and Comparison to Electron-Transfer-Initiated C–H Functionalization. *J. Am. Chem. Soc.* **2018**, *140*, 22–25.
45. Hu, H.; Chen, S.-J.; Mandal, M.; Pratik, S. M.; Buss, J. A.; Krska, S. W.; Cramer, C. J.; Stahl, S. S. Copper-catalysed benzylic C–H coupling with alcohols via radical relay enabled by redox buffering. *Nat. Catal.* **2020**, *3*, 358–367.
46. Williamson, A. Theory of ætherification. *Philos. Mag.* **1850**, *37*, 350–356.
47. Marcoux, J.-F.; Doye, S.; Buchwald, S. L. A General Copper-Catalyzed Synthesis of Diaryl Ethers. *J. Am. Chem. Soc.* **1997**, *119*, 10539–10540.
48. Hartwig, J. F. Transition Metal Catalyzed Synthesis of Arylamines and Aryl Ethers from Aryl Halides and Triflates: Scope and Mechanism. *Angew. Chem. Int. Ed.* **1998**, *37*, 2046–2067.
49. Enthaler, S.; Company, A. Palladium-Catalysed Hydroxylation and Alkoxylation. *Chem. Soc. Rev.* **2011**, *40*, 4912–4924.

50. Nawrozkij, M. B.; Forgione, M.; Yablokov, A. S.; Lucidi, A.; Tomaselli, D.; Patsilnakos, A.; Panella, C.; Hailu, G. S.; Kirillov, I. A.; Badia, R.; Riveira-Muñoz, E.; Crespan, E.; Armijos Rivera, J. I.; Cirilli, R.; Ragno, R.; Esté, J. A.; Maga, G.; Mai, A.; Rotili, D. Effect of α -Methoxy Substitution on the Anti-HIV Activity of Dihydropyrimidin-4(3H)-Ones. *J. Med. Chem.* **2019**, *62*, 604–621.
51. Cernak, T.; Dykstra, K. D.; Tyagarajan, S.; Vachal, P.; Krska, S. W. The Medicinal Chemist's Toolbox for Late Stage Functionalization of Drug-like Molecules. *Chem. Soc. Rev.* **2016**, *45*, 546–576.
52. Ruiz-Castillo, P.; Buchwald, S. L. Applications of Palladium-Catalyzed C–N Cross-Coupling Reactions. *Chem. Rev.* **2016**, *116*, 12564–12649.
53. West, M. J.; Fyfe, J. W. B.; Vantourout, J. C.; Watson, A. J. B. Mechanistic Development and Recent Applications of the Chan–Lam Amination. *Chem. Rev.* **2019**, *119*, 12491–12523.
54. Qiao, J. X.; Lam, P. Y. S. Copper-Promoted Carbon–Heteroatom Bond Cross-Coupling with Boronic Acids and Derivatives. *Synthesis.* **2011**, *6*, 829–856.
55. Trowbridge, A.; Walton, S. M.; Gaunt, M. J. New Strategies for the Transition-Metal Catalyzed Synthesis of Aliphatic Amines. *Chem. Rev.* **2020**, *120*, 2613–2692.
56. Niu, L.; Jiang, C.; Liang, Y.; Liu, D.; Bu, F.; Shi, R.; Chen, H.; Chowdhury, A. D.; Lei, A. Manganese-Catalyzed Oxidative Azidation of C(sp³)–H Bonds under Electrophotocatalytic Conditions. *J. Am. Chem. Soc.* **2020**, *142*, 17693–17702.
57. Pandey, G.; Laha, R.; Singh, D. Benzylic C(sp³)–H Functionalization for C–N and C–O Bond Formation via Visible Light Photoredox Catalysis. *J. Org. Chem.* **2016**, *81*, 7161–7171.
58. Yang, Y.-Z.; Song, R.-J.; Li, J.-H. Intermolecular Anodic Oxidative Cross-Dehydrogenative C(sp³)–N Bond-Coupling Reactions of Xanthenes with Azoles. *Org. Lett.* **2019**, *21*, 3228–3231.

59. Hou, Z.-W.; Li, L.; Wang, L. Organocatalytic Electrochemical Amination of Benzylic C–H Bonds. *Org. Chem. Front.* **2021**, DOI: 10.1039/D1QO00746G.
60. Song, C.; Dong, X.; Yi, H.; Chiang, C.-W.; Lei, A. DDQ-Catalyzed Direct C(sp³)–H Amination of Alkylheteroarenes: Synthesis of Biheteroarenes under Aerobic and Metal-Free Conditions. *ACS Catal.* **2018**, *8*, 2195–2199. (b)
61. Ruan, Z.; Huang, Z.; Xu, Z.; Zeng, S.; Feng, P.; Sun, P.-H. Late-stage azolation of benzylic C–H bonds enabled by electrooxidation. *Sci. China. Chem.* **2021**, *64*, 800-807.
62. Eight of top 50 best-selling drugs contain N-benzylic heterocycles: Baumann, M.; Baxendale, I. R.; Ley, S. V.; Nikbin, N. *Beilstein J. Org. Chem.* **2011**, *7*, 442–495.
63. Blakemore, D. C.; Castro, L.; Churcher, I.; Rees, D. C.; Thomas, A. W.; Wilson, D. M.; Wood, A. Organic synthesis provides opportunities to transform drug discovery. *Nat. Chem.* **2018**, *10*, 383–394.
64. Manuscript submitted.
65. Huang, A.; Wo, K.; Lee, S. Y. C.; Kneitschel, N.; Chang, J.; Zhu, K.; Mello, T.; Bancroft, L.; Norman, N. J.; Zheng, S.-L. Regioselective Synthesis, NMR, and Crystallographic Analysis of N1-Substituted Pyrazoles. *J. Org. Chem.* **2017**, *82*, 8864–8872.
66. Hilpert, L. J.; Sieger, S. V.; Haydl, A. M.; Breit, B. Palladium- and Rhodium-Catalyzed Dynamic Kinetic Resolution of Racemic Internal Allenes Towards Chiral Pyrazoles. *Angew. Chem. Int. Ed.* **2019**, *58*, 3378–3381.
67. Fang, Z.; Feng, Y.; Dong, H.; Li, D.; Tang, T. Copper(I)-Catalyzed Radical Decarboxylative Imidation of Carboxylic Acids with N-Fluoroarylsulfonimides. *Chem. Commun.* **2016**, *52*, 11120–11123.

68. Jing, L.; Yu, X.; Guan, M.; Wu, X.; Wang, Q.; Wu, Y. An Efficient Method for Sulfonylation of Amines, Alcohols and Phenols with N-Fluorobenzenesulfonimide Under Mild Conditions. *Chem. Res. Chin. Univ.* **2018**, *34*, 191–196.
69. Szpera, R.; Moseley, D. F. J.; Smith, L. B.; Sterling, A. J.; Gouverneur, V. The Fluorination of C–H Bonds: Developments and Perspectives. *Angew. Chem., Int. Ed.* **2019**, *58*, 14824–14848.
70. Amii, H.; Uneyama, K. C–F Bond Activation in Organic Synthesis. *Chem. Rev.* **2009**, *109*, 2119–2183.
71. Hamel, J.-D.; Paquin, J.-F. Activation of C–F Bonds α to C–C Multiple Bonds. *Chem. Commun.* **2018**, *54*, 10224–10239.
72. Ni, Z.; Zhang, Q.; Xiong, T.; Zheng, Y.; Li, Y.; Zhang, H.; Zhang, J.; Liu, Q. Highly Regioselective Copper-Catalyzed Benzylic C–H Amination by N-Fluorobenzenesulfonimide. *Angew. Chem., Int. Ed.* **2012**, *51*, 1244–1247.
73. Buss, J. A.; Vasilopoulos, A.; Golden, D. L.; Stahl, S. S. Copper-Catalyzed Functionalization of Benzylic C–H Bonds with N-Fluorobenzenesulfonimide: Switch from C–N to C–F Bond Formation Promoted by a Redox Buffer and Brønsted Base. *Org. Lett.* **2020**, *22*, 5749–5752.
74. Vasilopoulos, A.; Golden, D. L.; Buss, J. A.; Stahl, S. S. Copper-Catalyzed C–H Fluorination/Functionalization Sequence Enabling Benzylic C–H Cross Coupling with Diverse Nucleophiles. *Org. Lett.* **2020**, *22*, 5753–5757.
75. *Science of Synthesis: Houben-Weyl Methods of Molecular Transformations Vol. 35: Chlorine, Bromine, and Iodine*; Georg Thieme Verlag, 2014.

76. Huang, F.-Q.; Xie, J.; Sun, J.-G.; Wang, Y.-W.; Dong, X.; Qi, L.-W.; Zhang, B. Regioselective Synthesis of Carbonyl-Containing Alkyl Chlorides via Silver-Catalyzed Ring-Opening Chlorination of Cycloalkanols. *Org. Lett.* **2016**, *18*, 684–687.
77. Pu, X.; Qi, X.; Ready, J. M. Allenes in Asymmetric Catalysis: Asymmetric Ring Opening of Meso-Epoxides Catalyzed by Allene-Containing Phosphine Oxides. *J. Am. Chem. Soc.* **2009**, *131*, 10364–10365.
78. Sauer, G. S.; Lin, S. An Electrocatalytic Approach to the Radical Difunctionalization of Alkenes. *ACS Catal.* **2018**, *8*, 5175–5187.
79. Cresswell, A. J.; Eey, S. T.-C.; Denmark, S. E. Catalytic, Stereoselective Dihalogenation of Alkenes: Challenges and Opportunities. *Angew. Chem. Int. Ed.* **2015**, *54*, 15642–15682.
80. An, J.; Denton, R. M.; Lambert, T. H.; Nacsa, E. D. The Development of Catalytic Nucleophilic Substitution Reactions: Challenges, Progress and Future Directions. *Org. Biomol. Chem.* **2014**, *12*, 2993–3003.
81. Ozawa, J.; Kanai, M. Silver-Catalyzed C(sp³)-H Chlorination. *Org. Lett.* **2017**, *19*, 1430–1433.
82. Combe, S. H.; Hosseini, A.; Parra, A.; Schreiner, P. R. Mild Aliphatic and Benzylic Hydrocarbon C-H Bond Chlorination Using Trichloroisocyanuric Acid. *J. Org. Chem.* **2017**, *82*, 2407–2413.
83. Han, L.; Xia, J.-B.; You, L.; Chen, C. Ketone-Catalyzed Photochemical C(sp³)-H Chlorination. *Tetrahedron* **2017**, *73*, 3696–3701.
84. Manuscript in preparation.
85. Kharasch, M. S.; Brown, H. C. Chlorinations with Sulfuryl Chloride. I. The Peroxide-Catalyzed Chlorination of Hydrocarbons. *J. Am. Chem. Soc.* **1939**, *61*, 2142–2150.

86. Liu, W.; Groves, J. T. Manganese Porphyrins Catalyze Selective C–H Bond Halogenations. *J. Am. Chem. Soc.* **2010**, *132*, 12847–12849.
87. Gomtsyan, A.; Bayburt, E. K.; Schmidt, R. G.; Surowy, C. S.; Honore, P.; Marsh, K. C.; Hannick, S. M.; McDonald, H. A.; Wetter, J. M.; Sullivan, J. P.; Jarvis, M. F.; Faltynek, C. R.; Lee, C.-H. Identification of (R)-1-(5-Tert-Butyl-2,3-Dihydro-1H-Inden-1-Yl)-3-(1H-Indazol-4-Yl)Urea (ABT-102) as a Potent TRPV1 Antagonist for Pain Management. *J. Med. Chem.* **2008**, *51*, 392–395.
88. Bellizzi, M. E.; Bhatia, A. V.; Cullen, S. C.; Gandarilla, J.; Kruger, A. W.; Welch, D. S. Asymmetric Synthesis of a TRPV1 Antagonist via Tert-Butanesulfinamide-Directed Reductive Amination with a Chromanone. *Org. Process Res. Dev.* **2014**, *18*, 303–309.
89. Mikami, S.; Nakamura, S.; Ashizawa, T.; Nomura, I.; Kawasaki, M.; Sasaki, S.; Oki, H.; Kokubo, H.; Hoffman, I. D.; Zou, H.; Uchiyama, N.; Nakashima, K.; Kamiguchi, N.; Imada, H.; Suzuki, N.; Iwashita, H.; Taniguchi, T. Discovery of Clinical Candidate N-((1S)-1-(3-Fluoro-4-(Trifluoromethoxy)Phenyl)-2-Methoxyethyl)-7-Methoxy-2-Oxo-2,3-Dihydropyrido[2,3-b]Pyrazine-4(1H)-Carboxamide (TAK-915): A Highly Potent, Selective, and Brain-Penetrating Phosphodiesterase 2A Inhibitor for the Treatment of Cognitive Disorders. *J. Med. Chem.* **2017**, *60*, 7677–7702.
90. Structure search was performed on Reaxys on December 18, 2020. It was drawn that "Y–NCO" locking N, C, and O atoms for isocyanates or "Y–N(AH)H" locking H atom for amines (AH = any including H). Y was defined as ACY (any acyclic), CBC (carbocyclic), or CHC (heterocyclic). Each search excluded hits of tautomers, mixtures, and isotopes. Availability was limited to "product for purchase" only.

91. Hill, C. L.; Smegal, J. A.; Henly, T. J. Catalytic Replacement of Unactivated Alkane Carbon-Hydrogen Bonds with Carbon-X Bonds (X = Nitrogen, Oxygen, Chlorine, Bromine, or Iodine). Coupling of Intermolecular Hydrocarbon Activation by MnIIITPPX Complexes with Phase-Transfer Catalysis. *J. Org. Chem.* **1983**, *48*, 3277–3281.
92. Huang, X.; Zhuang, T.; Kates, P. A.; Gao, H.; Chen, X.; Groves, J. T. Alkyl Isocyanates via Manganese-Catalyzed C–H Activation for the Preparation of Substituted Ureas. *J. Am. Chem. Soc.* **2017**, *139*, 15407–15413.
93. Suh, S.-E.; Nkulu, L. E.; Lin, S.; Krska, S.; Stahl, S. S. Benzylic C–H Isocyanation/Amine Coupling Sequence Enabling High-Throughput Synthesis of Pharmaceutically Relevant Ureas. *Chem. Sci.* **2021**, DOI: 10.1039/D1SC02049H.
94. Doak, B. C.; Over, B.; Giordanetto, F.; Kihlberg, J. Oral Druggable Space beyond the Rule of 5: Insights from Drugs and Clinical Candidates. *Chemistry & Biology* **2014**, *21*, 1115–1142.
95. Jenkins, C. L.; Kochi, J. K. I. Ligand Transfer of Halides (Chloride, Bromide, Iodide) and Pseudohalides (Thiocyanate, Azide, Cyanide) from Copper(II) to Alkyl Radicals. *J. Org. Chem.* **1971**, *36*, 3095–3102.
96. Jenkins, C. L.; Kochi, J. K. II. Kinetics of Ligand Transfer Oxidation of Alkyl Radicals. Evidence for Carbonium Ion Intermediates. *J. Org. Chem.* **1971**, *36*, 3103–3111.
97. Jenkins, C. L.; Kochi, J. K. Homolytic and Ionic Mechanisms in the Ligand-Transfer Oxidation of Alkyl Radicals by Copper(II) Halides and Pseudohalides. *J. Am. Chem. Soc.* **1972**, *94*, 856–865.
98. Sauer, W. H. B.; Schwarz, M. K. Molecular Shape Diversity of Combinatorial Libraries: A Prerequisite for Broad Bioactivity. *J. Chem. Inf. Comput. Sci.* **2003**, *43*, 987–1003.
99. Manuscript in preparation.

Chapter 2.

Copper-Catalyzed Benzylic C–H Coupling with Alcohols via Radical Relay Enabled by Redox Buffering

Reproduced with permission from: Huayou Hu, **Si-Jie Chen**, Mukunda Mandal, Saied Md Pratik, Joshua A. Buss, Shane W. Krska, Christopher J. Cramer, Shannon S. Stahl. Copper-catalyzed benzylic C–H coupling with alcohols via radical relay enabled by redox buffering. *Nat. Catal.* **2020**, 3, 358-367. Copyright 2020 Nature Portfolio.

2.1. Abstract

Cross-coupling reactions enable rapid, convergent synthesis of diverse molecules and provide the foundation for modern chemical synthesis. The most widely used methods employ sp^2 -hybridized coupling partners, such as aryl halides or related pre-functionalized substrates. Here, we demonstrate copper-catalyzed oxidative cross coupling of benzylic C–H bonds with alcohols to afford benzyl ethers, enabled by a novel redox-buffering strategy that maintains the activity of the copper catalyst throughout the reaction. The reactions employ the C–H substrate as the limiting reagent and exhibit broad scope with respect to both coupling partners. This approach to direct site-selective functionalization of $C(sp^3)$ –H bonds provides the basis for efficient three-dimensional diversification of organic molecules and should find widespread utility in organic synthesis, particularly for medicinal chemistry applications.

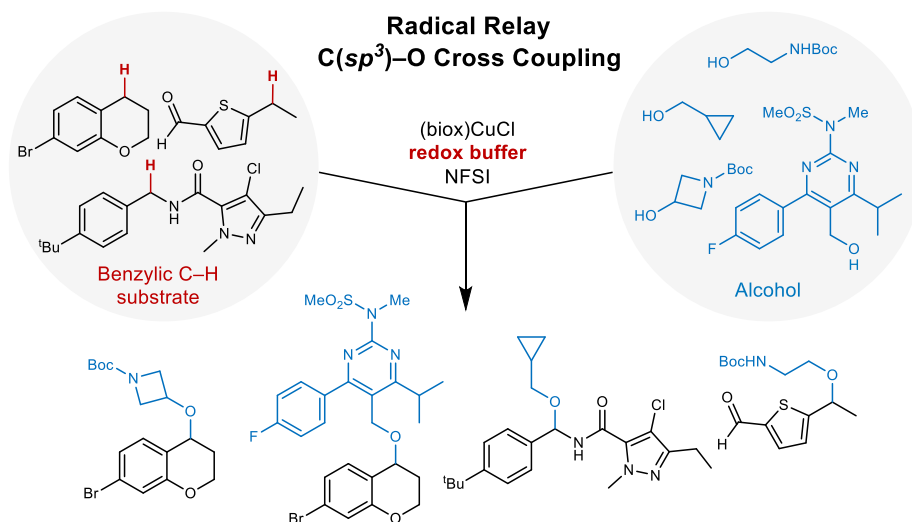


Figure 2.1. Cu-Catalyzed Cross Coupling of Benzylic C–H Etherification Summarization of Reactivity

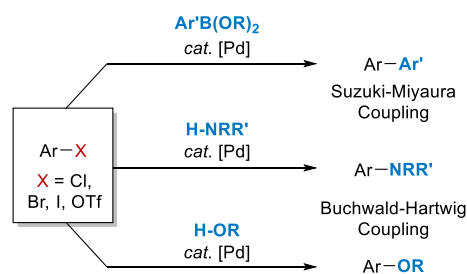
2.2. Introduction

Medicinal chemistry efforts in the pharmaceutical industry rely on efficient synthetic methods to prepare molecules with diverse chemical structures and compositions. Coupling methods that

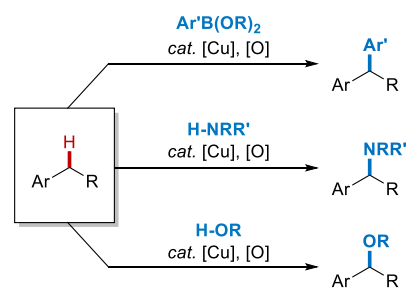
unite molecular fragments from two large pools of substrates, such as amide coupling and palladium-catalyzed cross coupling, are among the most important and widely used reaction classes in this domain^{1,2}. The prevalent use of sp^2 -hybridized coupling partners (i.e., aryl, vinyl, acyl electrophiles), however, constrains the topological diversity of molecules that may be accessed and, in many cases, leads to molecules with less desirable physicochemical and other pharmaceutical properties. These limitations have contributed to a growing demand for cross-coupling methods involving sp^3 -hybridized carbon atoms to access molecules with more three-dimensional character^{3,4}. $C(sp^3)$ -H bonds adjacent to aromatic and heteroaromatic rings are ubiquitous in key pharmacophores, and methods for selective cross coupling of benzylic C-H bonds and other versatile substrate partners (e.g., arylboronic acids, amines, alcohols, Figure 2.2A) could have a transformative influence on drug discovery. Such reactions would present a wealth of opportunities for elaboration of simple building blocks and pharmaceutical intermediates, as well as late-stage functionalization of drug molecules⁵. The comparatively low bond strength of benzylic C-H bonds makes them intrinsically reactive and provides a potential basis for high site selectivity in complex molecules bearing many other C-H bonds. Benzylic sites are also notorious metabolic "hot spots" in pharmaceuticals, and their selective substitution has important pharmacological implications⁶. Here, we report a method for the preparation of benzyl ethers, a prominent motif in pharmaceuticals and bioactive molecules (Figure 2.2B), via direct oxidative cross coupling of benzylic C-H bonds with alcohols. A unique strategy for in situ reductive activation of the catalyst provides the basis for successful reactivity in the present reactions and sets the stage for development of other benzylic C-H cross-coupling methods.

Cross-coupling reactions

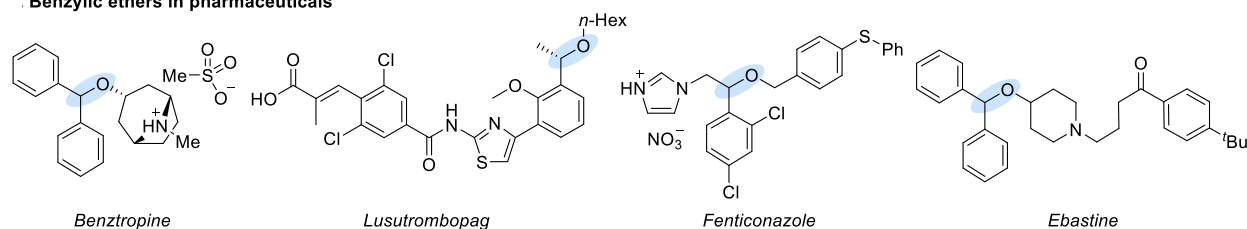
Existing methods, e.g., aryl halides



Target: Benzylic C-H substrates



Benzylic ethers in pharmaceuticals



Radical relay strategy for cross-coupling of alcohols and benzylic C-H substrates

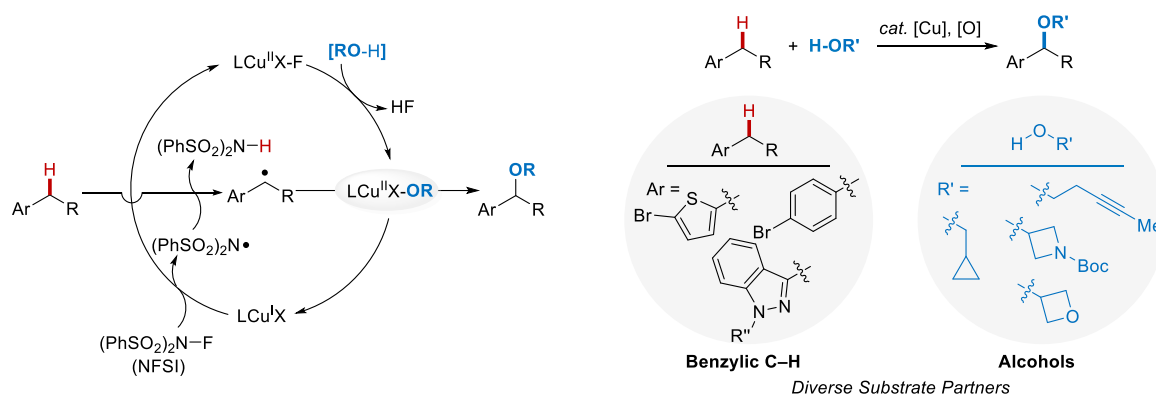


Figure 2.2. Cross-coupling reactions of benzylic C–H bonds and alcohols via a radical relay pathway. (A) Conceptual similarity between traditional cross-coupling reactions of aryl halides and the targeted benzylic C–H functionalization reactions. (B) Important examples of existing drug molecules containing benzylic ether moieties. (C) Proposed radical relay mechanism for benzylic C–H etherification enabling the coupling of two diverse pools of substrates.

In recent years, a number of methods have been developed for intermolecular functionalization of $\text{C}(\text{sp}^3)\text{-H}$ bonds that show good site-selectivity, even in the absence of a directing group. Some of the most effective are those that replace the hydrogen atom of a C–H bond with a small fragment, for example, oxygenation⁷, amination^{8–10}, carbene insertion¹¹, halogenation^{12,13}, and various pseudohalogenation reactions^{14–17}. Complementary advances have been made in methods

for site-selective functionalization of low-cost feedstock molecules, such as alkylarenes^{18,19}, tetrahydrofuran^{20,21}, or simple hydrocarbons²²⁻²⁴ that use excess C–H substrate relative to the oxidant and/or functionalization reagent. Collectively, these precedents do not incorporate the characteristics typically associated with "cross coupling" reactions. The most effective cross-coupling methods, such as the Suzuki-Miyaura²⁵ and Buchwald-Hartwig^{26,27} reactions, have a number of common traits: (a) the most valuable coupling partner is used as the limiting reagent, in ideal cases approaching a 1:1 stoichiometry of the two coupling partners, (b) both coupling partners draw from a diverse pool of readily (ideally commercially) available reagents, and (c) the reactions exhibit broad tolerance of the steric, electronic and functional-group properties of both coupling partners.

Alcohols represent an abundant class of building blocks that are widely used as partners in other coupling reactions, including classical methods, such as the Williamson ether synthesis²⁸, in addition to modern catalytic methods^{26,29}. Precedents for the direct oxidative coupling of benzylic C–H bonds and alcohols, however, are confined to electron-rich arenes³⁰⁻³² such as those capable of undergoing hydride transfer to DDQ (2,3-dichloro-5,6-dicyano-1,4-benzoquinone). C–H cleavage via hydrogen-atom transfer (HAT) should be much less sensitive to electronic effects relative to pathways initiated by electron or hydride transfer³³, which directly generate cationic intermediates. Thus, we postulated that a "radical relay" strategy¹⁴ could provide the basis for selective, broad-scope cross coupling of benzylic C–H bonds and alcohols, using the C–H substrate as the limiting reagent (Figure 1c). This reaction could be initiated by Cu^I-mediated activation of an oxidant, such as *N*-fluorobenzenesulfonimide (NFSI), which generates an N-centered radical capable of promoting HAT from the benzylic C–H bond. The resulting Cu^{II} species is then

available to mediate coupling of the benzylic radical with the alcohol coupling partner (Figure 2.2C).

2.3. Results and Discussion

Identifying the "redox buffer" effect. Recent examples of radical relay cyanation¹⁴, arylation³⁴, and related functionalization of benzylic C–H bonds^{35–37} provided a starting point for this investigation. We anticipated that reaction conditions similar to these precedents could lead to effective benzylic etherification (Figure 2.3A). Attempted coupling of 4-ethylbiphenyl and methanol, however, led to negligible yield of the benzylic ether **4** with little conversion of the substrate or NFSI (Figure 2.3B). The good product yields observed from analogous cyanation and arylation reactions indicate that the coupling partner can have a major influence on the reaction outcome. We postulated that the coupling partner could influence the reactive form of the Cu catalyst. Stoichiometric experiments probing the reaction of Cu^{II} with the different coupling partners revealed that TMSCN and ArB(OH)₂ induce rapid reduction of Cu^{II} to Cu^I, resulting in the formation of cyanogen³⁸ and biaryl³⁹. In contrast, MeOH does not reduce Cu^{II} under these conditions (Figure 2.3B).

These observations indicate that the mechanism in Figure 1c is overly simplified and needs to be modified to explain successful reaction with certain coupling partners, but not with others. The modified mechanism in Figure 2c retains reaction of Cu^I (**A**) with NFSI to initiate catalysis. This step generates Cu^{II} (**B**) and a nitrogen-centered radical, •NSI (Fig 2c, left cycle). The latter species can either undergo a productive reaction with the benzylic C–H bond, or it can react with a second equivalent of Cu^I, quenching the radical and forming a second Cu^{II} species (**B'**; Fig 2c, right cycle). Experimental observations suggest that NFSI rapidly oxidizes all of the Cu^I to Cu^{II} when the

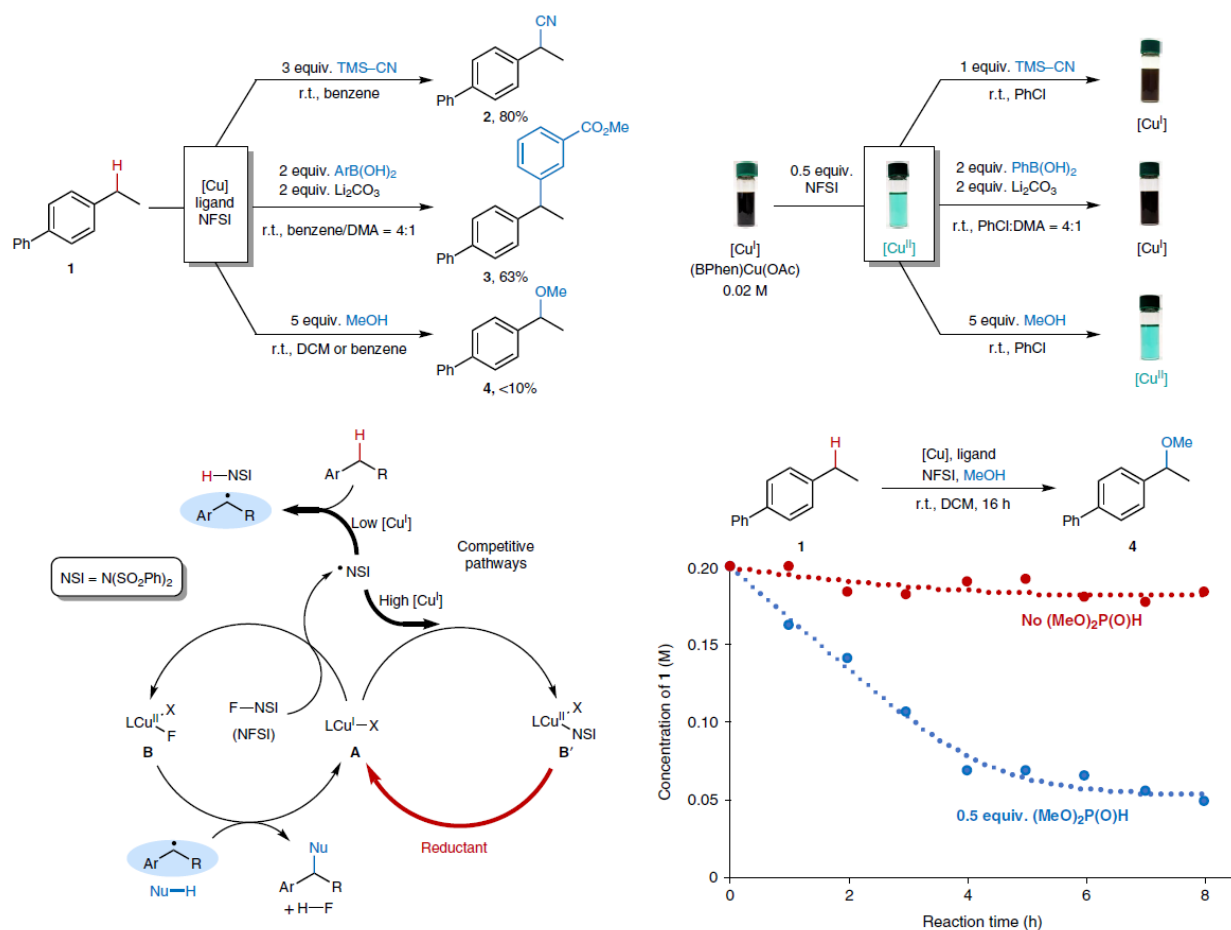


Figure 2.3. Cu-catalyzed benzylic C–H functionalization with NFSI as the oxidant. (A) Cu-catalyzed benzylic C–H functionalization reactions^{14,34}. (B) Changes in the Cu redox state between +1 (brown) and +2 (blue-green) upon addition of NFSI to a solution of the Cu^I catalyst precursor, followed by addition of cross-coupling partners. (C) Modified radical relay mechanism (cf. **Figure 2.2C**) to account for quenching of the •NSI by Cu^I and regeneration of Cu^I by a reducing substrate or additive. (D) Reaction time course for benzylic etherification conducted in the absence (red) and presence of 0.5 equiv of dimethylphosphite (blue). Reaction conditions: 4-ethylbiphenyl (0.2 mmol), NFSI (0.4 mmol), MeOH (1.0 mmol), CuCl (0.02 mmol), 2,2'-bioxazoline (0.02 mmol), DCM (1 mL), room temperature.

reaction is initiated, but that certain coupling partners, such as TMS-CN or ArB(OH)₂, are capable of reducing Cu^{II} to regenerate Cu^I during the course of the reaction (right cycle, red arrow). The Cu^I generated in this manner will react with NFSI to generate •NSI in the absence of a large pool of Cu^I, thereby supporting productive HAT from the benzylic substrate. MeOH does not readily reduce Cu^{II}, and the Cu catalyst will accumulate as a Cu^{II} species, such as **B** or **B'**. The inability

of Cu^{II} to react with NFSI under such conditions will cause the reaction to stall. These mechanistic considerations suggested that a reductant could be identified as a "redox buffer", leading to controlled regeneration of Cu^I during the reaction. To test this hypothesis, several reductants were investigated as additives in the etherification reaction with MeOH, including phosphites, silanes, hydrazines, and sodium ascorbate (see Appendix A Table A2.1 and A2.2 for details). Promising reactivity was observed with dimethylphosphite [(MeO)₂P(O)H], and a representative time course of the reaction in Figure 2d illustrates the effect of this additive. In the absence of phosphite, the reaction proceeds to <10% conversion of 4-ethylbiphenyl, while inclusion of 0.5 equiv of (MeO)₂P(O)H leads to high conversion within 5 h at room temperature, generating the benzyl methyl ether in 52% yield (unoptimized). The latter reaction mixture exhibits a blue-green color (cf. Figure 2.3B), implicating a Cu^{II} catalyst resting state; however, the results are consistent with the ability of phosphite to serve as a redox buffer (Figure 2.3C).⁴⁰ This hypothesis was probed further with a series of UV-visible and EPR experiments, in which reduction of Cu^{II} to Cu^I by dimethyl phosphite was clearly indicated (see Appendix A Figure A2.2 and A2.3 for details).

Reaction development. These preliminary results provided the basis for further reaction optimization, and the oxidative coupling of ethylbenzene and methanol was tested with different solvents, ancillary ligands, Cu sources, and reaction temperatures (see the Appendix A Tables 2A.3 and 2A.4 for details). A number of monodentate and bidentate ligands were evaluated, and the unsubstituted 2,2'-bioxazoline (biox) ligand led to the best product yields. Use of chiral ligand derivatives did not lead to enantioselectivity under these conditions (see below for further discussion)^{14,41}. Inclusion of hexafluoroisopropanol (HFIP) as a co-solvent with dichloromethane (DCM:HFIP = 4:1) led to higher yields and significantly increased the reaction rate, allowing the

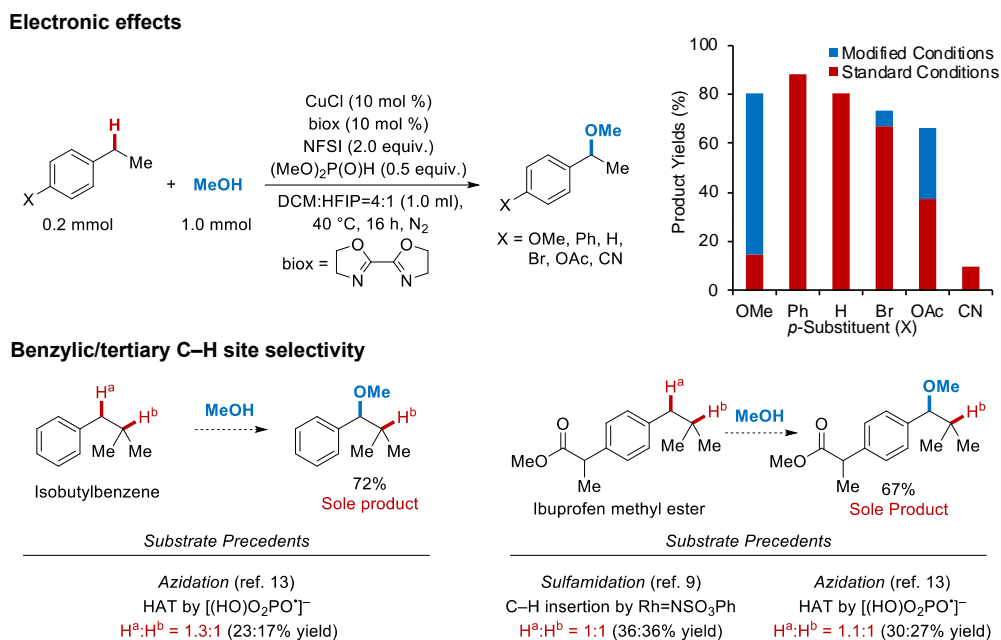


Figure 2.4. Electronic effects and site selectivity observed in the oxidative coupling of ethylarenes and methanol. (A) Results observed from the reaction under standard (red) and individually optimized (blue) conditions (¹H NMR yields with CH₂Br₂ as the internal standard). Modified conditions: X = OMe: 20 mol % Cu/biox in DCM at r.t.; X = Br: 5 mol % Cu/biox; X = OAc: 20 mol % Cu/biox at 50 °C. (B) Analysis of benzylic versus tertiary site selectivity observed in etherification of isobutylbenzene and ibuprofen methyl ester (see Figure 2.5 for reaction conditions).

reaction to proceed at lower temperature (40 °C). The activating effect of HFIP suggests that it may enhance the reactivity of the •NSI radical, for example, by hydrogen-bonding to the sulfonyl groups⁴². Under these conditions, reactions of ethylbenzene and 4-ethylbiphenyl, which are electronically similar, generated the 1-methoxyethylbenzene and 4-(1-methoxyethyl)biphenyl in 80% and 88% yield, respectively (Figure 2.4). Use of ethylarenes bearing electron-donating versus electron-withdrawing substituents exhibited variable results, with yields ranging from 10–67% (Figure 2.4A, red bars); however, the modular nature of the reaction conditions enabled straightforward optimization of these yields by applying intuitive principles. For example, the electron-rich 4-methoxyethylbenzene is more reactive under the standard conditions and undergoes full conversion with the generation of considerable unidentified side products. Use of

milder conditions, including removing the co-solvent HFIP (which enhances reactivity) and lowering the temperature from 40 °C to room temperature, led to formation of the desired product in 80% yield. Substrates bearing electron-withdrawing substituents are somewhat less reactive, as evident from incomplete conversion of the starting material under the original conditions. In these cases, the product yield was improved by raising the reaction temperature to 50 °C and/or increasing the Cu catalyst loading to 20 mol %. After applying these variations, the product yields ranged from 66–88%. Only the 4-cyano derivative, which is very electron deficient, retained a low yield (10%) after attempted optimization.

The good results obtained here with electronically differentiated substrates may be rationalized by the HAT C–H activation mechanism. Previous reports of benzylic etherification initiated by hydride or single-electron transfer directly generate cationic intermediates and are typically only effective for electron-rich substrates³⁰⁻³². Loss of a neutral hydrogen atom is much less susceptible to electronic effects³³.

The broad tolerance of arene electronic properties is complemented by nearly exclusive site selectivity for benzylic over tertiary C–H bonds. Isobutylbenzene and ibuprofen methyl ester have been used previously to probe selectivity for benzylic versus tertiary C–H activation in photoredox-based azidation¹³ and nitrene insertion^{9,43} reactions. Approximately 1:1 product ratios were observed in the reported reactions with these substrates (Figure 2.4B). Recognizing that the selectivity depends on the mechanism and reagent involved in the C–H cleavage step, we tested these substrates in the present oxidative coupling conditions with methanol. Exclusive reaction at the benzylic position was observed with both substrates (Figure 2.4B), affording 72% and 67% yield of the two methyl ethers, respectively. Complementary experiments with toluene,

ethylbenzene, and cumene reveal preferential reactivity at secondary benzylic positions (see Appendix A Figure 2A.1 for details).

Computational analysis of the proposed mechanism. The catalytic mechanism proposed in Figure 2.3 was analyzed by density functional theory (DFT) methods to probe the energetics of individual reaction steps, with a particular focus on the competing pathways involving the \bullet NSI and benzylic radical intermediates, and to gain further insights into C–O bond formation (Figure 4). The following computation methods were employed in this effort: M06-L/basis-II/SMD($\epsilon = 10.6$)/B3LYP-D3(BJ)/basis-I/SMD($\epsilon = 10.6$) level of theory (basis-I = 6-31G(d,p) for non-

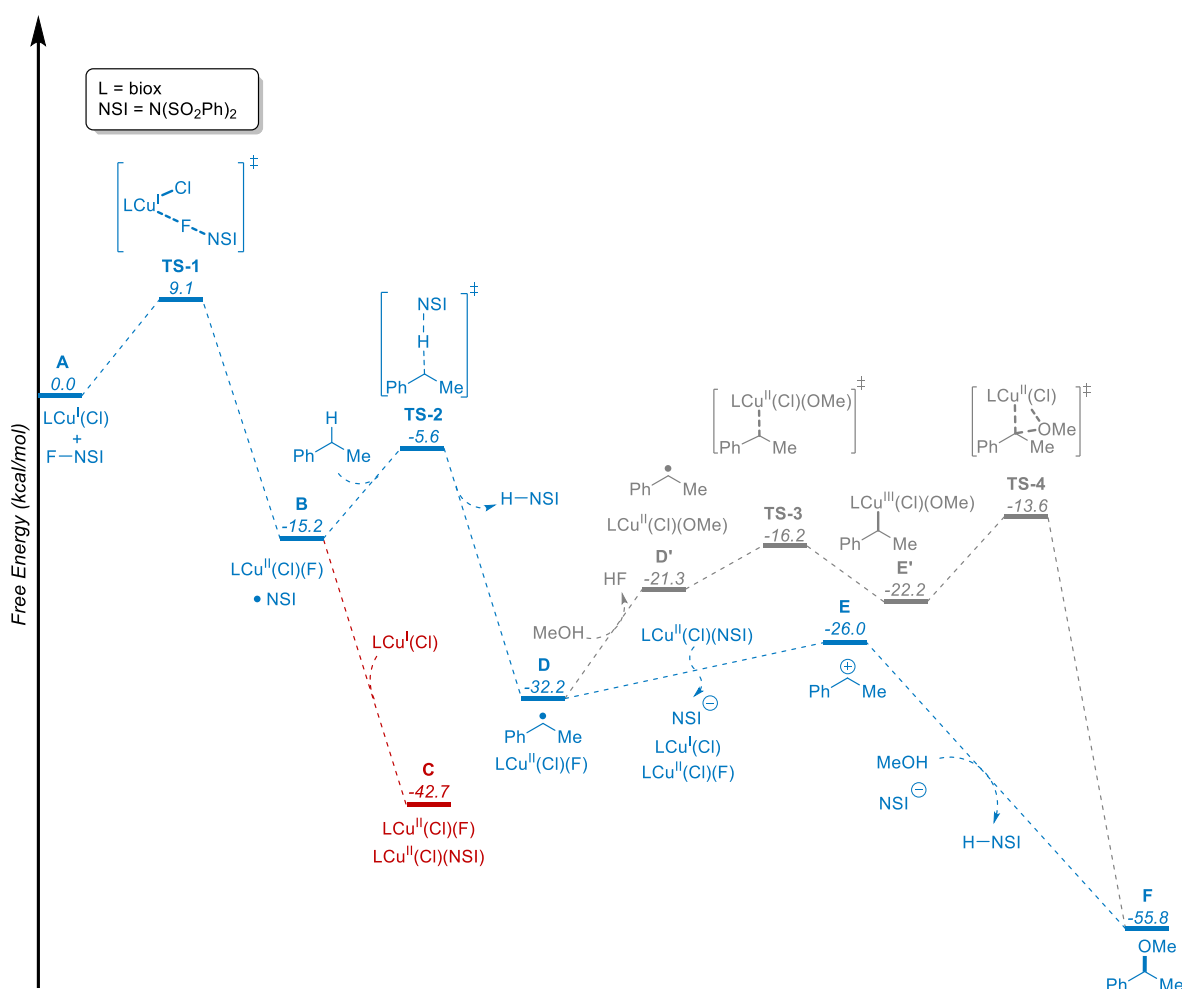


Figure 2.5. Calculated reaction pathways and energy landscape for (biox)CuI/NFSI-mediated methoxylation of ethylbenzene. (Gibbs free energies at 313.15 K; computed at M06-L/basis-II/SMD($\epsilon = 10.6$)/B3LYP-D3(BJ)/basis-I/SMD($\epsilon = 10.6$) level of theory).

metals and SDD basis and pseudopotential for Cu; basis-II = def2-TZVP for non-metals, def2-TZVP basis and SDD pseudopotential for Cu. (See Appendix A for full computational details).

The reaction of NFSI with (biox)Cu^I(Cl) is computed to be highly favorable ($\Delta G^\circ = -15.2$ kcal/mol), generating •NSI and (biox)Cu^{II}(Cl)(F)⁴⁴. Subsequent reaction of •NSI with a second equivalent of Cu^I is even more favorable ($\Delta G^\circ = -27.5$ kcal/mol), generating (biox)Cu^{II}(Cl)(NSI) (Figure 2.5, red pathway). This sequence is consistent with the experimental observations in Figure 2.3B which show rapid formation of Cu^{II} species upon addition of NFSI to solutions of Cu^I. We then evaluated the energetics of •NSI reactivity with the benzylic C–H bond of ethylbenzene. This HAT reaction, which forms a benzylic radical and H–NSI is also strongly favored ($\Delta G^\circ = -17.0$ kcal/mol) and exhibits an activation free energy (ΔG^\ddagger ; cf. **TS-2**) of +9.6 kcal/mol.

Two possible pathways were considered for product formation. The first features benzylic radical addition to Cu^{II} and C–O bond formation via reductive elimination from an organocopper(III) intermediate (Figure 4, grey pathway), while the second features a radical-polar crossover pathway^{45,46} in which C–O bond formation involves reaction of the alcohol with a benzylic cation (Figure 4, blue pathway). The former pathway requires incorporation of a methoxide ligand into the Cu^{II} coordination sphere, and the calculations indicate that substitution of fluoride is favored over chloride. The resulting process, which affords (biox)Cu^{II}(Cl)(OMe) and HF, is endergonic ($\Delta G^\circ = +10.9$ kcal/mol). Addition of the benzylic radical to the Cu^{II} species proceeds with a small kinetic barrier (**TS-3**, $\Delta G^\ddagger = +5.1$ kcal/mol) to form the benzylcopper(III) species **E'** in a nearly ergoneutral process ($\Delta G^\circ = -0.9$ kcal/mol). Subsequent C–O reductive elimination yields the methoxylated product via **TS-4**, which represents the highest energy species along this pathway (+18.6 kcal/mol relative to **D**). The alternative pathway for C–O bond formation involves one-electron oxidation of the benzylic radical by (biox)Cu^{II}(Cl)(NSI) to afford

a benzylic cation. This electron-transfer step is only moderately uphill (**E**, $\Delta G^\circ = +6.2$ kcal/mol), and the resulting cation can undergo a highly favorable reaction with methanol to produce the methoxylated product (**F**, $\Delta G^\circ = -29.8$ kcal/mol).

The organocopper(III) pathway aligns with the pathway proposed for Cu/NFSI-mediated cyanation of benzylic C–H bonds, which proceeds with high enantioselectivity¹⁴. The computational results in Figure 4, however, favor the radical-polar crossover pathway for the etherification reaction, and this conclusion is further supported by several additional observations. The methoxylation reaction generates racemic products, even when chiral biox ligands are used. Deuterium kinetic isotope effect experiments conducted with PhEt and PhEt-*d*₁₀ reveal the presence of a small, but significant, primary KIE (competition experiment: KIE = 2.1; independent rate measurement: KIE = 1.7; see Appendix A Figures. 2A.5 and 2A.6). These results are consistent with the radical-polar crossover pathway, which shows that the HAT step has the highest barrier. In contrast, C–O reductive elimination is calculated to be the rate-limiting step in the organocopper(III) pathway, and a negligible KIE is expected for this step.

Synthetic scope and utility. Benzylic methoxylation is a valuable transformation in medicinal chemistry, particularly in late-stage functionalization applications, because the introduction of small molecular fragments can significantly influence the activity and pharmacological properties of pharmaceuticals^{4,5}. For example, these groups can modulate the physicochemical characteristics and conformational dynamics of the molecule, introduce hydrogen bond donors/acceptors that can lead to enhanced ligand-target binding interactions, and block reactive sites to slow metabolism and excretion. The methoxy group is an appealing fragment because it has minimal impact on the mass or lipophilicity (i.e., LogP) of the molecule and introduces a potential hydrogen bond acceptor site⁵.

Examination of the substrate scope for benzylic methoxylation began with a number of small molecules and pharmaceutical building blocks as coupling partners (Figure 2.6). Longer alkyl chains, including those bearing primary alkyl halide substituents are tolerated by the reaction conditions (**10-12, 14**), and good reactivity was also observed with a phenylacetic ester derivative (**13**). Tetralin (**14**), a substructure present in numerous drugs such as sertraline, treprostinil and rotigotine, underwent effective methoxylation at room temperature. Benzhydryl ethers, including benztropine and ebastine (cf. Figure 2.2A) represent an important class of antihistamines⁴⁷. Methyl ethers were obtained in good yield with a series of benzhydryls (**15-19**) via oxidative cross coupling with methanol. Substrates included the benzhydryl fragment present in dapagliflozin, an approved drug for treatment of type 2 diabetes (cf. **19**). This promising reactivity was extended to C-H bonds adjacent to medicinally relevant sulfur-, oxygen- and nitrogen-containing heterocycles (**20-29**). Noteworthy features among these examples include tolerance of (hetero)aryl bromides (**20, 23, 24**) and a formyl group (**22**), which are versatile functional groups that permit further elaboration of the products. The thiophenylarylmethane core in **24** is a key fragment in canagliflozin, another commercial drug for type 2 diabetes. Chromans and azoles, which represent important pharmacophores⁴⁸ undergo effective coupling with methanol (**25-29**). These studies also showed that certain functional groups, such as amines and carboxylic acids required modification (e.g., via acetylation or methyl ester formation, cf. **27** and **28**, respectively) to attain the desired reactivity. Other substrates, such as those with pyridine and indole heterocycles, led to lower yields or failed to afford the desired product (see summary provided in Appendix A Table 2A.12).

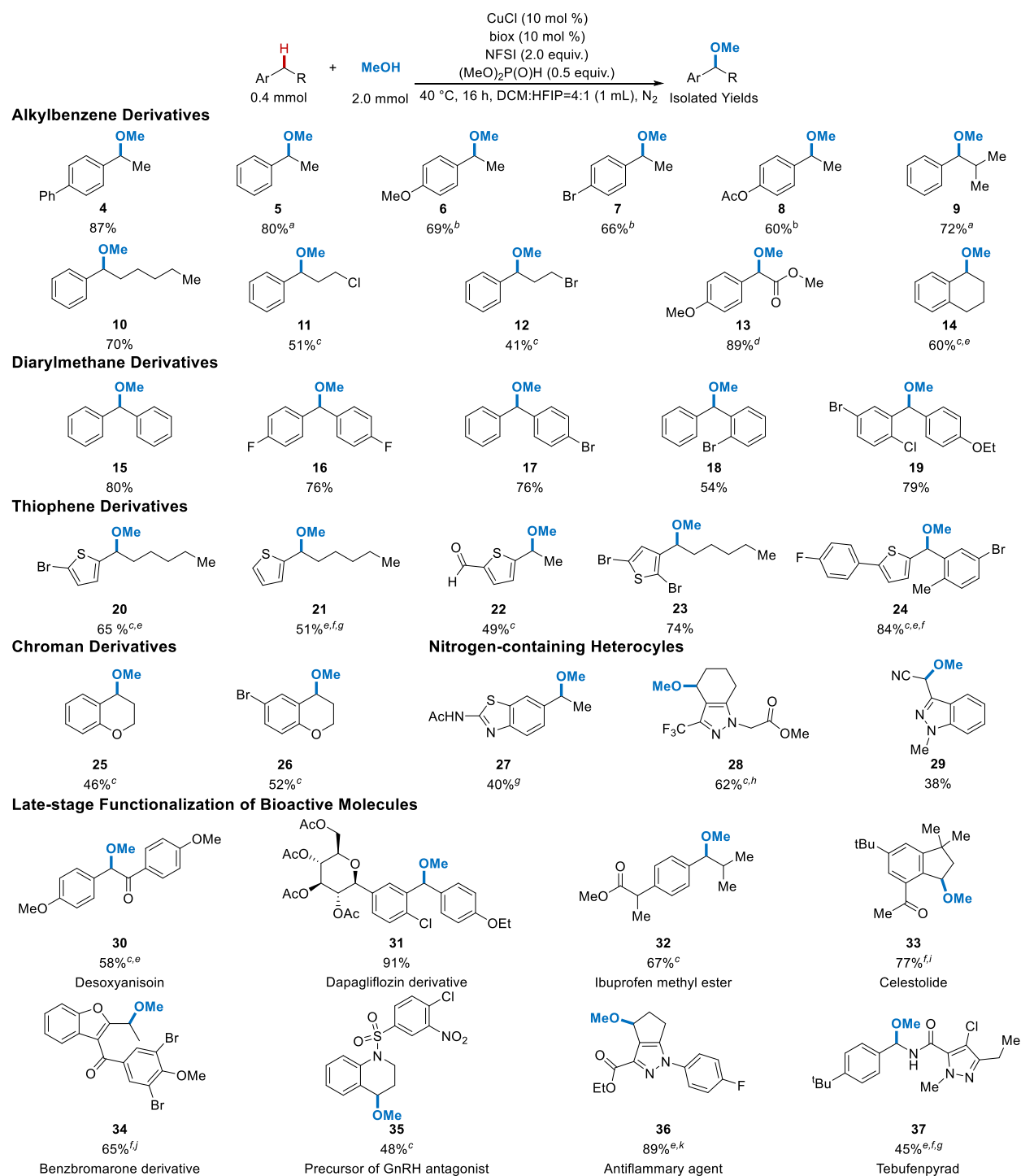


Figure 2.6. Assessment of different benzylic C–H substrates in oxidative cross-coupling reactions with methanol. Isolated yields unless otherwise noted. ^a ¹H NMR yield; isolated yield unavailable due to compound volatility. ^b See **Figure 2.4A** for optimized conditions. ^c 15 mol % Cu/biox. ^d Reaction yield at 4 h. ^e At room temperature. ^f DCM as the solvent. ^g 20 mol % Cu/biox. ^h Only one regioisomer was observed. ⁱ At 30 °C. ^j 30 mol % Cu/biox. ^k Two regioisomers were observed with a ratio of 9:1.

The methoxylation reaction also proceeded effectively in the late-stage functionalization of a number of pharmaceuticals and related bioactive molecules, including the immunosuppressant desoxyanisoin (**30**)⁴⁹; the natural product celestolide (**33**); a precursor to a GnRH antagonist (**35**)⁵⁰; a cyclopentapyrazolyl anti-inflammatory and anti-allergy agent (**36**)⁵¹; and the insecticide, tebufenpyrad (**37**). Each of these underwent effective coupling with methanol and exhibited excellent selectivity for reaction at the benzylic position. For example, no products were obtained from methoxylation of the aliphatic C–H bond next to the nitrogen atom in **35** or adjacent to the alkoxy oxygen atoms in **30**. Good selectivity was also observed between the two similar cyclopentyl C–H positions in **36**. The 9:1 ratio favoring the product shown over the alternate regioisomer probably arises from higher reactivity at the more electron-rich site. Free -OH groups, such as those present in a sugar fragment of dapagliflozin (anti-diabetic), a carboxylic acid of ibuprofen (anti-inflammatory), and a phenol in benzbromarone (xanthine oxidase inhibitor⁵²) interfere with the etherification reaction, but successful reactivity proceeds when these groups are suitably protected (**31**, **32**, **34**).

The potential utility of this method for medicinal chemistry library synthesis is especially evident from assessment of the C–H cross-coupling reaction with diverse alcohols. The thiophene-containing fragment of canagliflozin was selected as a representative, moderately complex core structure for these studies (Figure 2.7A). Initial tests employing 2-chloroethanol as the coupling partner led to two products, the desired 2-chloroethyl ether in addition to the methyl ether product in 64% and 18% yields, respectively. The latter product derives from participation of the methoxy group from the (MeO)₂P(O)H reductant in the reaction. Reevaluation of other phosphites showed that this side product formation could be nearly eliminated (<2%) by using diisopropyl phosphite (see Appendix A Table 2A.7 for details). This insight was then implemented in reactions with

numerous alcohol coupling partners. Several 2-substituted ethanol derivatives, including those bearing chloro, methoxy, BocNH (Boc = *tert*-butyloxycarbonyl), alkynyl, vinyl, naphthyl, and benzyl ether substituents (**38–44**), were effective in the reaction, in most cases affording product in good-to- excellent yields. Only the alkene-containing substrate **42** led to a relatively low yield, possibly reflecting competitive reaction with the allylic C–H bonds. The presence of benzylic C–H bonds in the alcohols **43** and **44** did not interfere with successful reactivity. Both afforded the desired product in good yield. Expanding on this compatibility, a series of *ortho*-, *meta*-, and *para*-substituted benzyl alcohols with different electronic and steric properties proved to be excellent coupling partners in these reactions (**45–49**, 73-91% yields), with only small amounts of benzaldehyde by-product observed.

Other aliphatic alcohols were also successful, including trimethylsilylmethanol, cyclopropylmethanol (**50**, **51**), and several oxetane and azetidine analogs (**52–54**). Small groups such as these are increasingly featured in preclinical and clinical drug candidates^{53,54}, and the cross coupling of benzylic C–H bonds and alcohols provides a compelling strategy to introduce these units. The effectiveness of adamantanol and (–)-borneol (**55**, **56**) showed that sterically hindered alcohols can serve as effective coupling partners. The method also proved effective with complex alcohols, including cholesterol (**57**) and a pyrimidinylmethanol precursor to rosuvastatin (**58**). The latter reaction was demonstrated on >1 g scale (91% yield, 1.3 g) and was also successful with only 1.1 equiv of **58** (88% yield). In a final assessment of the method, six substrate pairs were selected from three representative heterocyclic substrates containing benzylic C–H bonds and four alcohol coupling partners. Moderate to good yields of benzylic ethers were obtained in each of these cross-coupling examples (Figure 2.7B).

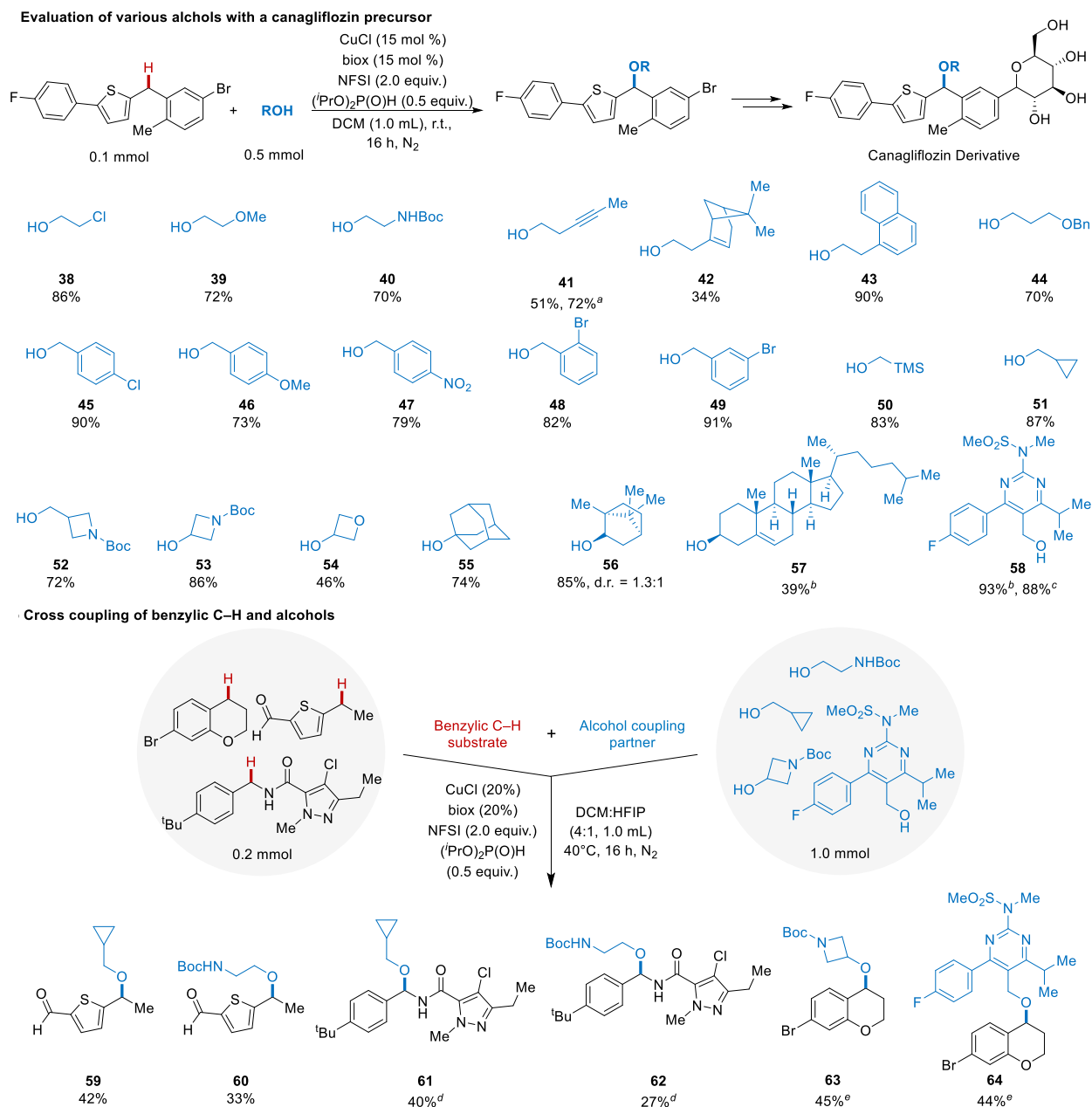


Figure 2.7. Assessment of different alcohols and C–H/alcohol coupling partners in benzylic C–H etherification reactions. (A) Benzylic C–H etherification of a canagliflozin precursor with various alcohols. (B) Cross coupling of medically relevant benzylic C–H substrates and alcohols. Isolated yields are reported. ^a ¹H NMR yield with 30 mol % Cu/biox. ^b Conducted with 3.0 equiv. alcohol. ^c Conducted with 1.1 equiv. alcohol. ^d 50 °C. ^e r.t. in DCM.

2.4. Conclusion

Collectively, these results demonstrate a new class of highly selective, non-directed C–H cross coupling reactions that create opportunities for efficient synthesis of novel molecules and diversification of chemical structures, ranging from simple aromatic and heteroaromatic building blocks to complex pharmacophores and existing drug molecules. Prominent features of these reactions include good product yields, the ability to use the benzylic substrate as the limiting reagent, high benzylic site selectivity, and access to a broad substrate scope with respect to both reaction partners. Mechanistic insights set the stage for these results by revealing that traditional reaction conditions lead to accumulation of the catalyst in an inactive Cu^{II} state, and the key breakthrough arose from identification of dialkylphosphites as effective in situ reductants that convert Cu^{II} into catalytically active Cu^{I} during the course of the reaction. Further mechanistic studies support a catalytic pathway involving radical-polar crossover initiated by HAT from the benzylic C–H site. This pathway is noteworthy because HAT exhibits a weak dependence on substrate electronic properties that allows for broad substrate scope, and the subsequent trapping of the benzylic cation by alcohols is similarly promiscuous, allowing for broad scope among alcohol coupling partners. Overall, it is likely that the "redox buffering" strategy will not be unique to this reaction class and allow for the discovery and development of other radical relay C–H cross-coupling methods with widespread impact and utility in medicinal chemistry and organic synthesis.

2.5. Acknowledgements

We thank Bing Li (Merck & Co., Inc., Kenilworth, NJ, USA) for technical assistance. This work was supported by the NIH (R01 GM126832, to S.S.S. and F32 GM129909, to J.A.B.);

Jiangsu Province (BK20161307 and “333” Talents Project, to H.H.) and Huaiyin Normal University (JSKC18014, to H.H.); Merck & Co., Inc., Kenilworth, NJ, USA (S.W.K.; travel funds to S.-J.C.); and M.M. acknowledges a doctoral dissertation fellowship from the University of Minnesota. Spectroscopic instrumentation was supported by a gift from Paul. J. Bender, the NSF (CHE-1048642), and the NIH (1S10 OD020022-1).

2.6. Author Contributions

H.H. and S.-J.C. performed the experimental work and led the data interpretation and analysis. S.-J.C. and J.A.B. designed and implemented the mechanistic experiments. M.M and S.M.P conducted the computational studies. All work was done in consultation with S.S.S., S.W.K. and C.J.C. All authors contributed to preparation of the manuscript.

2.7. References

1. Brown, D. G. & Boström, J. Analysis of past and present synthetic methodologies on medicinal chemistry: where have all the new reactions gone?: miniperspective. *J. Med. Chem.* **59**, 4443–4458 (2016).
2. Boström, J., Brown, D. G., Young, R. J. & Keserü, G. M. Expanding the medicinal chemistry synthetic toolbox. *Nat. Rev. Drug Disc.* **17**, 709–727 (2018).
3. Lovering, F., Bikker, J. & Humblet, C. Escape from flatland: increasing saturation as an approach to improving clinical success. *J. Med. Chem.* **52**, 6752–6756 (2009).
4. Blakemore, D. C. *et al.* Organic synthesis provides opportunities to transform drug discovery. *Nat. Chem.* **10**, 383–394 (2018).

5. Cernak, T., Dykstra, K. D., Tyagarajan, S., Vachal, P. & Krska, S. W. The medicinal chemist's toolbox for late stage functionalization of drug-like molecules. *Chem. Soc. Rev.* **45**, 546–576 (2016).
6. Thompson, T. N. Optimization of metabolic stability as a goal of modern drug design. *Med. Res. Rev.* **21**, 412-449 (2001).
7. White, M. C., Zhao, J. Aliphatic C–H oxidations for late-stage functionalization. *J. Am. Chem. Soc.* **140**, 13988-14009 (2018).
8. Muniz, K. & Bosnidou, A. E. Intermolecular radical C(sp³)–H amination under iodine catalysis. *Angew. Chem. Int. Ed.* **58**, 7485-7489 (2019).
9. Chiappini, N., Mack, J. & Du Bois, J. Intermolecular C(sp³)–H amination of complex molecules. *Angew. Chem. Int. Ed.* **57**, 4956-4959 (2018).
10. Clark, J. R., Feng, K., Sookezian, A. & White, M. C. Manganese-catalysed benzylic C(sp³)–H amination for late-stage functionalization. *Nat. Chem.* **10**, 583–591 (2018).
11. Davies, H. M. L. & Morton, D. Guiding principles for site selective and stereoselective intermolecular C–H functionalization by donor/acceptor rhodium carbenes. *Chem. Soc. Rev.* **40**, 1857 (2011).
12. Liu, W., Groves, J. T. Manganese catalyzed C–H halogenation. *Acc. Chem. Res.* **48**, 1727-1735 (2015).
13. Margrey, K. A., Czaplowski, W. L., Nicewicz, D. A. & Alexanian, E. J. A general strategy for aliphatic C–H functionalization enabled by organic photoredox catalysis. *J. Am. Chem. Soc.* **140**, 4213–4217 (2018).
14. Zhang, W. et al. Enantioselective cyanation of benzylic C–H bonds via copper-catalyzed radical relay. *Science* **353**, 1014-1018 (2016).

15. Sharma, A. & Hartwig, J. F. Metal-catalysed azidation of tertiary C–H bonds suitable for late-stage functionalization. *Nature* **517**, 600–604 (2015).
16. Huang, X. & Groves, J. T. Taming azide radicals for catalytic C–H azidation. *ACS Catal.* **6**, 751–759 (2016).
17. Czaplyski, W. L., Na, C. G. & Alexanian, E. J. C–H xanthylation: A synthetic platform for alkane functionalization. *J. Am. Chem. Soc.* **138**, 13854–13857 (2016).
18. Vasilopoulos, A., Zultanski, S. L. & Stahl, S. S. Feedstocks to pharmacophores: Cu-catalyzed oxidative arylation of inexpensive alkylarenes enabling direct access to diarylalkanes. *J. Am. Chem. Soc.* **139**, 7705–7708 (2017).
19. Wang, Z., Zheng, Z., Xu, X., Mao, J. & Walsh, P. J. One-pot aminobenylation of aldehydes with toluenes. *Nat. Commun.* **9**, (2018).
20. Shield, B. J., Doyle, A. G. Direct C(sp³)–H cross coupling enabled by catalytic generation of chlorine radicals. *J. Am. Chem. Soc.* **138**, 12719–12722 (2016).
21. Heitz, D. R., Tellis, J. C. & Molander, G. A. Photochemical nickel-catalyzed C–H arylation: synthetic scope and mechanistic investigations. *J. Am. Chem. Soc.* **138**, 12715–12718 (2016).
22. Perry, I. B. *et al.* Direct arylation of strong aliphatic C–H bonds. *Nature* **560**, 70–75 (2018).
23. Liu, D. *et al.* Nickel-catalyzed selective oxidative radical cross-coupling: an effective strategy for inert Csp³–H functionalization. *Org. Lett.* **17**, 998–1001 (2015).
24. Tran, B. L., Li, B., Driess, M. & Hartwig, J. F. Copper-catalyzed intermolecular amidation and imidation of unactivated alkanes. *J. Am. Chem. Soc.* **136**, 2555–2563 (2014).
25. Miyaura, N. & Suzuki, A. Palladium-catalyzed cross-coupling reactions of organoboron compounds. *Chem. Rev.* **95**, 2457–2483 (1995).

26. Ruiz-Castillo, P. & Buchwald, S. L. Applications of palladium-catalyzed C–N cross-coupling reactions. *Chem. Rev.* **116**, 12564–12649 (2016).
27. Hartwig, J. F. Transition metal catalyzed synthesis of arylamines and aryl ethers from aryl halides and triflates: scope and mechanism. *Angew. Chem. Int. Ed.* **37**, 2046-2067 (1998).
28. Williamson, A. Theory of ætherification. *Philos. Mag.* **37**, 350-356 (1850).
29. Enthaler, S. & Company, A. Palladium-catalysed hydroxylation and alkoxylation. *Chem. Soc. Rev.* **40**, 4912-4924 (2011).
30. Chapman, L. M., Beck, J. C., Wu, L. & Reisman, S. E. Enantioselective total synthesis of (+)-psiguadial B. *J. Am. Chem. Soc.* **138**, 9803–9806 (2016).
31. Maloney, D. J., Chen, S. & Hecht, S. M. Stereoselective synthesis of the atropisomers of myristinin B/C. *Org. Lett.* **8**, 1925–1927 (2006).
32. Lee, B. J., Deglopper, K. S. & Yoon, T. P. Site-Selective Alkoxylation of Benzylic C–H Bonds via Photoredox Catalysis. *Angew. Chem. Int. Ed.* **59**, 197-202 (2019).
33. Rafiee, M., Wang, F., Hruszkewycz, D. P. & Stahl S. S. N-Hydroxyphthalimide-mediated electrochemical iodination of methylarenes and comparison to electron-transfer-initiated C–H Functionalization. *J. Am. Chem. Soc.* **140**, 22–25 (2018).
34. Zhang, W., Chen, P. & Liu, G. Copper-catalyzed arylation of benzylic C–H bonds with alkylarenes as the limiting reagents. *J. Am. Chem. Soc.* **139**, 7709–7712 (2017).
35. Ni, Z. et al. Highly Regioselective copper-catalyzed benzylic C-H amination by N-Fluorosulfonimide. *Angew. Chem. Int. Ed.* **51**, 1244-1247 (2012).
36. Yang, H. et al. Silver-promoted oxidative benzylic C–H trifluoromethoxylation. *Angew. Chem. Int. Ed.* **57**, 13266–13270 (2018).

37. Xiao, H. *et al.* Copper-catalyzed late-stage benzylic C(sp³)-H trifluoromethylation. *Chem* **5**, 940-949 (2019).
38. Janz, G. J. Cyanogen. *Inorg. Synth.* **5**, 43-48 (1957).
39. Demir, A. S., Reis, Ö. & Emrullahoglu, M. Role of copper species in the oxidative dimerization of arylboronic acids: synthesis of symmetrical biaryls. *J. Org. Chem.* **68**, 10130–10134 (2003).
40. Hong, Y., Yang, D., Luo, Y., Pao, C.-W., Lee, J.-F. & Lei, A. Direct observation of reduction of Cu(II) to Cu(I) by P-H compounds using XAS and EPR spectroscopy. *Organometallics* **35**, 1426-1429 (2016).
41. Zhang, W., Wu, L., Chen, P. & Liu., G. Enantioselective arylation of benzylic C-H bonds via copper-catalyzed radical relay. *Angew. Chem. Int. Ed.* **58**, 6425-6429 (2019).
42. Colomer, I., Chamberlain, A. E. R., Donohoe, T. J. Hexafluoroisopropanol as a highly versatile solvent. *Nat. Rev. Chem.* **1**, 0088 (2017).
43. Bess, E. N. *et al.* Analyzing site selectivity in Rh₂(esp)₂-catalyzed intermolecular C-H amination reactions. *J. Am. Chem. Soc.* **136**, 5783-5789 (2014).
44. Haines, B. E. *et al.* Cu-Catalyzed aromatic C-H imidation with N-fluorobenzenesulfonimide: mechanistic details and predictive models. *Chem. Sci.* **8**, 988–1001 (2017).
45. Murphy, J. A. The Radical-Polar Crossover Reaction. In *Radicals in Organic Synthesis* (eds. P. Renaud & M. P. Sibi) 298-315 (Wiley, 2001).
46. Banerjee, S., Sathyamoorthi, S., Du Bois, J. & Zare, R. N. Mechanistic analysis of a copper-catalyzed C-H oxidative cyclization of carboxylic acids. *Chem. Sci.* **8**, 7003–7008 (2017).

47. Loew, E. R., MacMillan, R. & Kaiser, M. E. The anti-histamine properties of benadryl, β -dimethylaminoethyl benzhydryl ether hydrochloride. *J. Pharmacol. Exp. Ther.* **86**, 229 (1946).
48. Du, L. *et al.* Molecular hybridization, synthesis, and biological evaluation of novel chroman IKr and IKs dual blockers. *Bioorg. Med. Chem. Lett.* **19**, 1477–1480 (2009).
49. Rhodes, J. R. Immunopotentiatory agents and physiologically acceptable salts thereof. US Patent US5508310A (1996).
50. Fushimi, N., Yonekubo, S., Ohno, K., Miyagi, T. Nitrogen-containing fused ring derivatives, pharmaceutical compositions containing them and their pharmaceutical use. JP Patent 5308342B2 (2008).
51. Upjohn Co. Cyclopentapyrazole and tetrahydroindazole compounds. WO Patent Appl. 8607357 (1986).
52. Schepers, G. Benzbromarone therapy in hyperuricaemia; comparison with allopurinol and probenecid. *J. Int. Med. Res.* **9**, 511-515 (1981).
53. Talele, T. T. The ‘cyclopropyl fragment’ is a versatile player that frequently appears in preclinical/clinical drug molecules. *J. Med. Chem.* **59**, 8712–8756 (2016).
54. Wuitschik, G. *et al.* Oxetanes in drug discovery: structural and synthetic insights. *J. Med. Chem.* **53**, 3227–3246 (2010).

Chapter 3.
**Copper-Catalyzed Cross Coupling of Benzylic C–H Bonds and Azoles with
Controlled *N*-Site Selectivity**

Reproduced with permission from: Joshua A. Buss, **Aristidis Vasilopoulos**, Dung L. Golden, Shannon S. Stahl. Copper-Catalyzed Functionalization of Benzylic C–H Bonds with *N*-Fluorobenzenesulfonimide: Switch from C–N to C–F Bond Formation Promoted by a Redox Buffer and Brønsted Base. *Org. Lett.* **2020**, *22*, 5749-5752. Copyright 2020 American Chemical Society.

3.1. Abstract

Azoles are important motifs in medicinal chemistry, and elaboration of their structures via direct N–H/C–H coupling could have broad utility in drug discovery. The ambident reactivity of many azoles, however, presents significant selectivity challenges. Here, we report a copper-catalyzed method that achieves site-selective cross coupling pyrazoles and other N–H heterocycles with substrates bearing (hetero)benzylic C–H bonds. Excellent *N*-site selectivity is achieved, with the preferred site controlled by the identity of co-catalytic additives. This cross-coupling strategy features broad scope for both the N–H heterocycle and benzylic C–H coupling partners, enabling application of this method to complex molecule synthesis and medicinal chemistry.

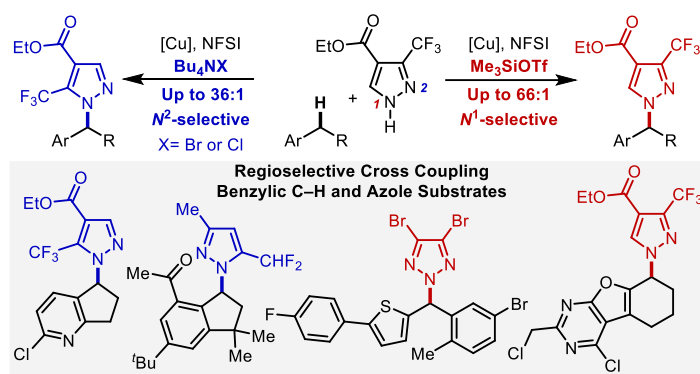


Figure 3.1. Cu-Catalyzed Cross Coupling of Benzylic C–H Bonds and Azoles Summarization of Reactivity

3.2. Introduction

Pd¹ and Cu-catalyzed² C(*sp*²)-N cross coupling reactions are some of the most widely used methods for pharmaceutical synthesis.³ Recent efforts have begun prioritizing complementary methods for C(*sp*³)-N coupling⁴ as a means to expand the topological diversity and physiochemical properties of the resulting molecules.^{3,5} C–N coupling methods that directly functionalize C(*sp*³)-H bonds bypass the need for pre-functionalized alkyl electrophiles and represent important targets for medicinal chemistry.⁶ Significant progress has been made in

C(*sp*³)-H amination reactions that install ammonia surrogates via nitrene transfer⁷ or azidation,⁸ while C-H/N-H cross-coupling reactions, for example, with secondary amines/amides or N-H heterocycles, are more limited⁹ and often require excess C-H substrate.¹⁰ Here, we report a copper-catalyzed method for selective cross-coupling of azoles with (hetero)benzylic C-H substrates as the limiting reagent, affording *N*-benzylic heterocycles featured in pharmaceutical and agrochemical compounds (Figure 3.2A).¹¹⁻¹⁴ In addition to the challenge of C-H site selectivity, these reactions feature a second selectivity challenge arising from azoles that incorporate two (or more) nucleophilic nitrogen atoms.¹⁵ This issue has important implications for medicinal chemistry because regioisomeric *N*-substituted azoles can have very different properties and/or bioactivity (Figure 3.2B).¹⁶ The method described herein achieves excellent C-H site selectivity via hydrogen-atom transfer (HAT) from (hetero)benzylic C-H bonds. Reaction with the azole coupling partners via Cu^{II}-mediated radical-polar crossover exhibits excellent *N*¹/*N*² site-selectivity (e.g., with pyrazoles), and variation of the reaction conditions lead to selective formation of either regioisomeric *N*-benzyl product with many coupling partners (Figure 3.2C).

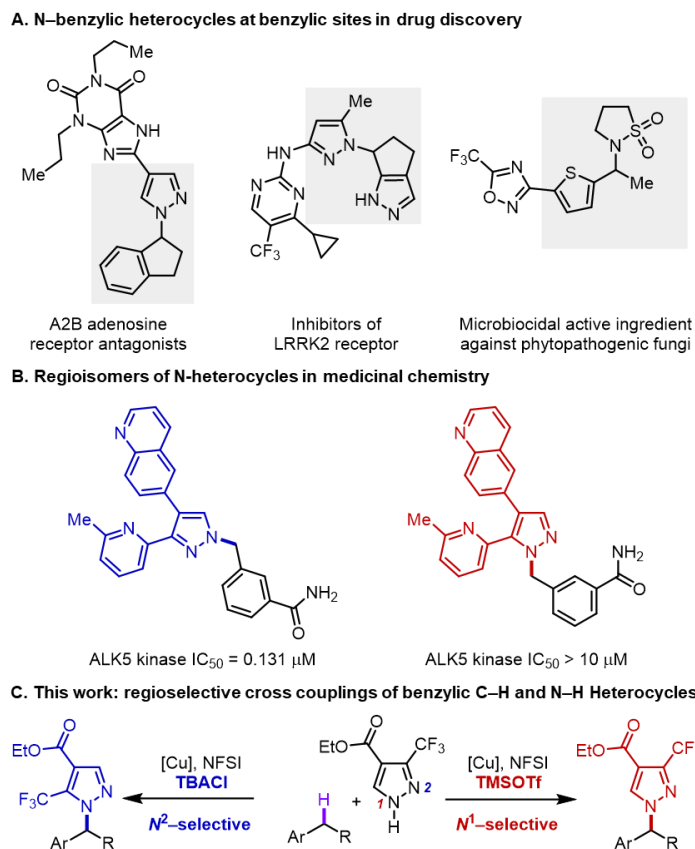


Figure 3.2. (A) Importance of benzylic N-azoles in drug discovery. (B) Impact of regioselectivity of heterocyclic compounds in medicinal chemistry. (C) Copper-catalyzed regioselective cross couplings of benzylic C–H bonds and N–H heterocycles enabled by various additives.

3.3. Results and Discussion

Investigation of oxidative cross coupling of benzylic C–H substrates and N–H azoles started with ethylbenzene (**1a**) and ethyl 3-(trifluoromethyl)-1H-pyrazole-4-carboxylate (**2a**), a pyrazole featured in previous drug discovery efforts.¹⁷ Potential reaction conditions were inspired by recent studies involving the use of copper catalysts in combination with *N*-fluorobenzenesulfonimide (NFSI) as the oxidant. Diverse nucleophilic coupling partners have been used in these reactions, including (pseudo)halides (cyanide,¹⁸ azide,^{8d} isocyanate¹⁹), alcohols,²⁰ carbamates,²¹ and carbon-based nucleophiles ($Zn(CF_3)_2$,²² $ArB(OH)_2$,²³ alkynes²⁴). Cu^I -mediated activation of NFSI generates an *N*-centered radical that promotes selective HAT from benzylic C–H bonds, and

subsequent coupling with heteroatom nucleophiles appears to favor a radical-polar crossover pathway leading to formation of a benzylic cation.^{8d,19,20} Complementary studies have shown that mild reductants, such as dialkylphosphites, can promote these reactions by buffering the redox state of the Cu catalyst and ensuring that both Cu^I and Cu^{II} are present in the reaction.^{19,20,25}

The above mechanistic considerations guided a survey of reaction conditions. Initial screening data showed that Cu/NFSI-catalyzed oxidative coupling of **1a** and **2a** favors the *N*² isomeric product **3aa** when the reaction is conducted in chlorinated solvents PhCl and dichloromethane (DCM) (Figure 3.3A, entries 1-2; see Appendix C for full screening details). Use of more polar solvents [hexafluoroisopropanol (HFIP) and MeNO₂] led to a switch in selectivity, favoring the *N*¹ isomer **3aa'** (entries 3-4). Tetrabutylammonium (TBA) bromide helped to solubilize the Cu catalyst and improved the reactivity and selectivity. Conventional ancillary ligands, such as phenanthroline or bioxazolines, led to lower yields (see Appendix B Table 3B.1 and 3B.2 for detailed information). A mixture of DCM:HFIP (7:3) enhanced the conversion of **1a** and improved the product yield to 71% (**3aa** + **3aa'**, entry 5). Increasing the loading of TBABr to 0.3 equiv further improved the reaction yield and increased the *N*²:*N*¹ selectivity to 36:1 (entry 6). Optimal results were obtained upon replacing TBABr with TBACl, affording **3aa** in 75% yield (entry 7). Further screening experiments revealed that the *N*²/*N*¹ regioselectivity could be switched to favor the *N*¹ product **3aa'** with certain additives (Figure 3.3B, see Appendix B Table 3B.2 for additional data). The initial entries in Figure 3.3B show that additives with halide anions favor formation of the *N*² regioisomer **3aa**. In contrast, additives with triflate anion or Lewis acids, such as silyl triflates or BF₃•OEt₂, favor formation of the *N*¹ regioisomer **3aa'**. Optimal results for the formation of **3aa'** were achieved with trimethylsilyl triflate (TMSOTf) as the additive at 60 °C (67% yield; *N*²:*N*¹ = 1:66).

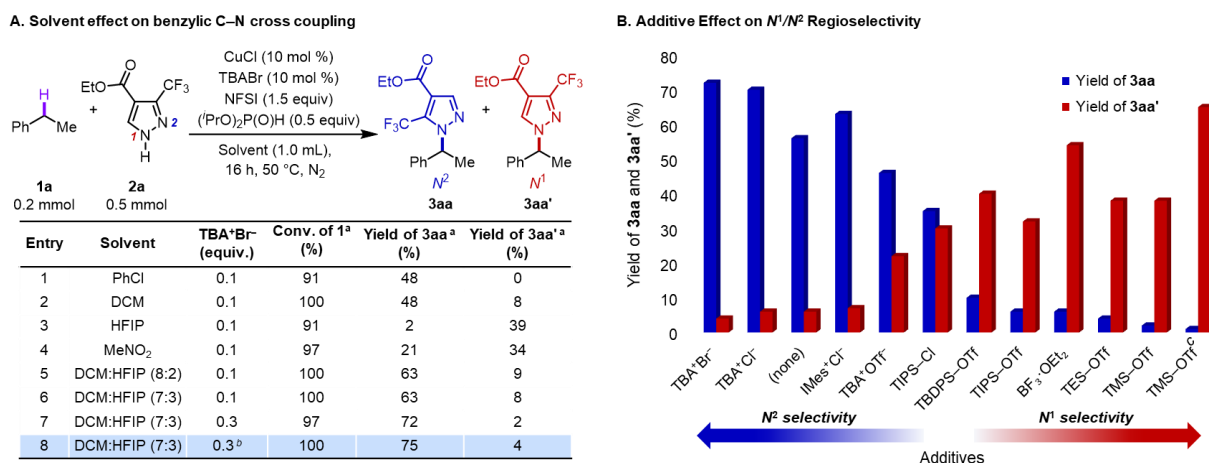


Figure 3.3. Evaluation of effects of various solvents and additives on the regioselectivity. (A) Effects of solvents on benzylic C–N cross coupling reaction. (B) Regioselectivity switch observed in cross coupling of 1a and 2a with different additives. Conditions identical to those shown in part A, using 10 mol% additive instead of TBABr, 10 mol % CuBr₂ instead of CuCl, and DCM:HFIP (7:3) solvent. ^a Monitored by ¹H NMR spectroscopy, yield determined using 0.2 mmol mesitylene as internal standard. TBA, tetrabutylammonium; DCM, dichloromethane; HFIP, hexafluoroisopropanol. ^b Reaction run with TBA+Cl⁻ instead of TBABr. ^c Reaction run at 60 °C.

The pyrazole reagent **2a** has an N–H bond at the N¹ position, as revealed by X-ray crystallography and depicted in Figure 3.3A (see Appendix B Section 7 in the Supporting Information for details). This structure is consistent with previous reports for other electron-deficient, 3-substituted pyrazoles.²⁶ We postulated that the switch in pyrazole regioselectivity could arise from kinetic versus thermodynamic control over the C–N bond-forming step. Experimental data supported this hypothesis: addition of TMSOTf to **3aa** induced isomerization of **3aa'**, whereas no isomerization of **3aa'** was observed in the presence of TBABr. These results suggest **3aa** is the kinetic product, and they are rationalized by the non-basic reaction conditions. The observed reactivity with the pyrazole N² lone pair (Figure 3.4B, top), contrasts previously reported reactivity with deprotonated pyrazolide reagents which react preferentially at the N¹ site.^{26b, 27} The isomerization data in Figure 3A suggests that strong Lewis acids, such as trimethylsilyl (TMS) cation, can promote isomerization via the benzylic cation and N²-TMS species, to the thermodynamically favored N¹ product.^{26b, 28} The data in Figure 3.3A, entries 1–4

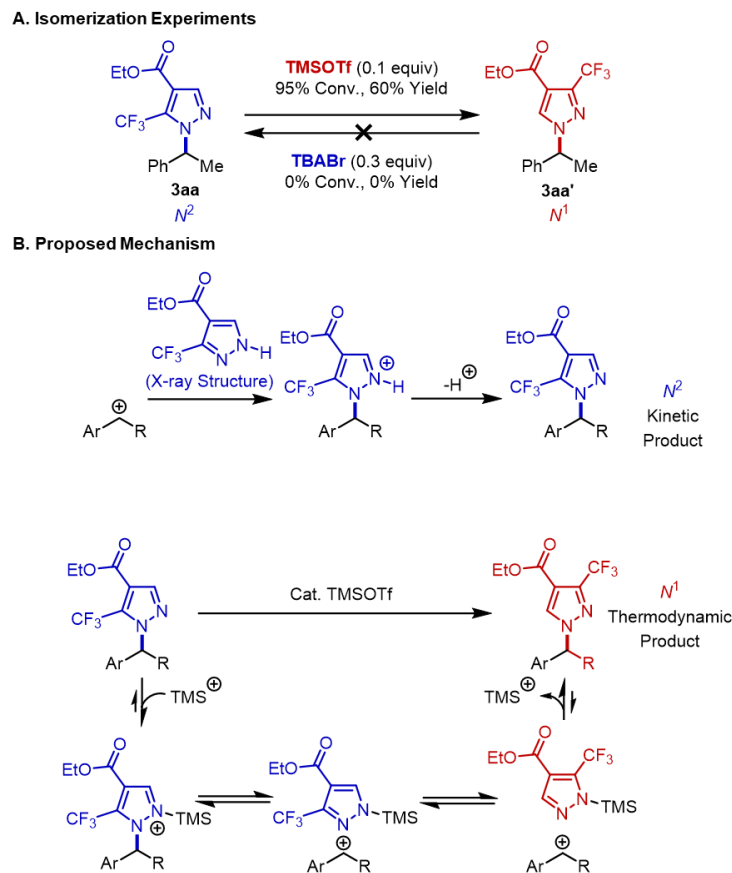


Figure 3.4. Mechanistic origin of pyrazole regioselectivity. (A) N^1/N^2 -isomerization test, implicating the the N^1 . (B) Proposed mechanism rationalizing the influence of TMSOTf (and other Lewis acids) on the N^2/N^1 regioselectivity.

suggest that solvents capable of stabilizing charged intermediates also favor the thermodynamic product.

Access to both isomeric pyrazole coupling products is noteworthy because most coupling reactions with pyrazoles employ a base and access only the thermodynamic products.^{27,29} For example, reaction of (1-bromoethyl)benzene with pyrazole **2a** affords exclusively the N^1 isomer **3aa'** (see Appendix B Section 4 in the Supporting Information for details). To explore the scope of this reactivity, we evaluated numerous other C–H/N–H cross-coupling reactions with (hetero)benzylic and azole coupling partners (Figures 3.5 and 3.6). Reactions with (hetero)benzylic C–H substrates were initially tested using the TBACl conditions, which tend to

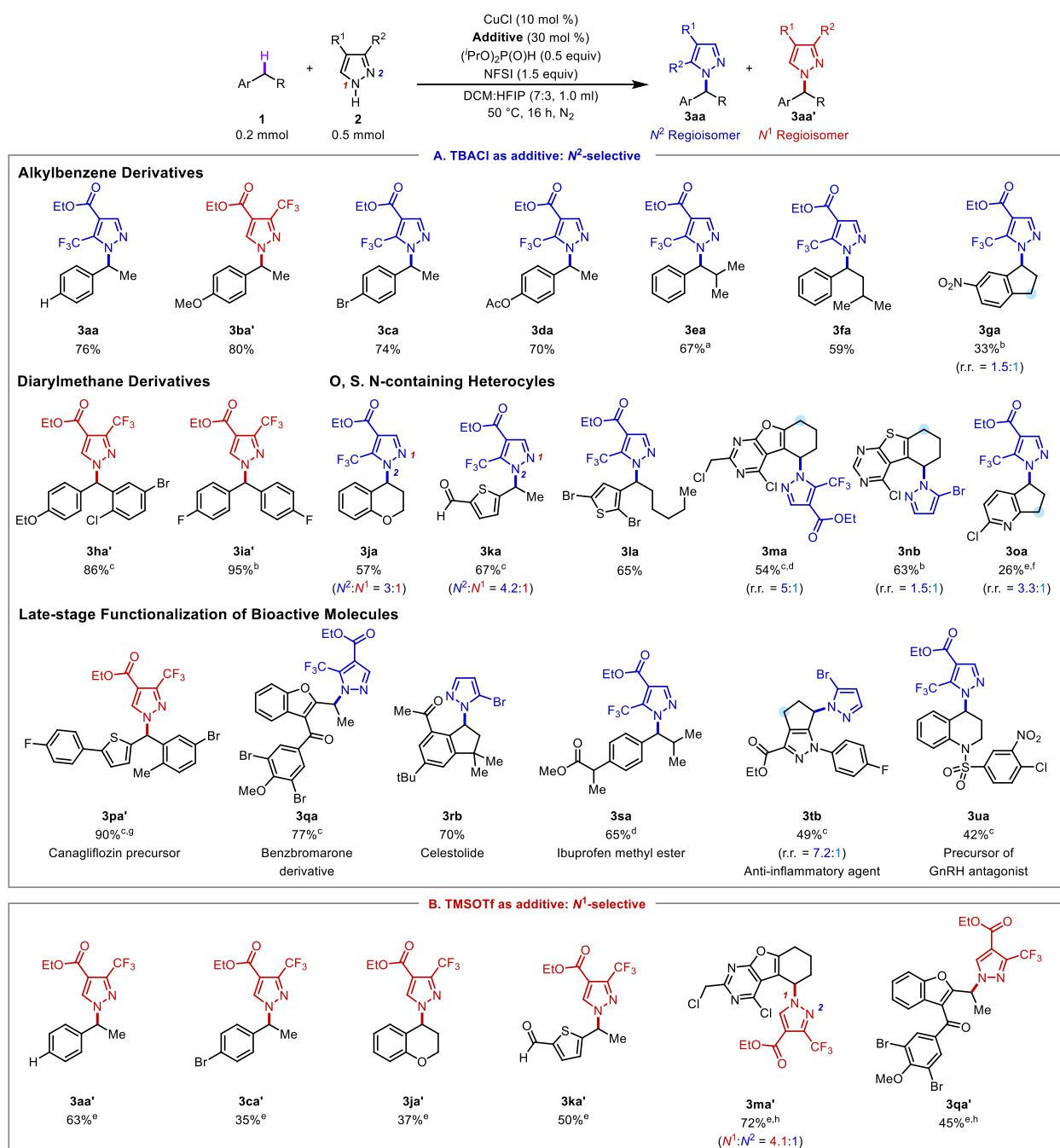


Figure 3.5. Assessment of various benzylic C–H substrates in cross coupling reactions with N–H heterocycles with (A) TBACl as the additive for N² regioselectivity and (B) with TMSOTf as the additive for N¹ regioselectivity. Regioisomers >5% were isolated and reported. ^aConducted in 0.5 mL DCM:HFIP (7:3). ^bConducted with 10 mol % CuBr₂ and 30 mol % TBABr. ^cConducted with 10 mol % TBACl. ^dConducted at 40 °C. ^eConducted at 60 °C. ^fConducted in DCM. ^gConducted at 30 °C. ^hConducted with 10 mol % BF₃•OEt₂.

be more robust and promote formation of the unique N^2 -pyrazolyl product (Figure 3.5A). Ethylbenzene derivatives with different p -substituents are well tolerated (70-86%, **3aa-3da**). While the N^2 product is typically observed under these conditions, only the N^1 product **3ba'** is observed with p -MeO-ethylbenzene (**1b**). This result is rationalized by the stability of the benzylic carbocation, which facilitates isomerization to the thermodynamic product (cf. Figure 3.4). The lack of C–N coupling at tertiary C–H sites in reactions with isobutyl- and isopentylbenzene (**3ea**, **3fa**) highlights the exquisite site-selectivity of the HAT steps with the NFSI-derived imidyl radical.^{8d,20} The strongly electron-withdrawing nitro group in the indane substrate **1g** reduces the product yield (33%, **3ga**). Benzhydryl N -azoles, a class of compounds that exhibit aromatase inhibitory activity,³⁰ exhibit good reactivity (86%, **3ha**; 95%, **3ia**) and form only the N^1 regioisomers, again rationalized by the benzylic cation stability.

Benzylic pyrazoles of chromans,³¹ thiophene,^{14,32} and other substrates bearing oxygen-, sulfur- and nitrogen-containing heterocycles react successfully (**1j-1u**). These reactions demonstrate a tolerance for a formyl group (**3ka**), heteroaryl bromides (**3la**), and pyrimidines (**3ma**, **3nb**).³³ The pyridine substrate **1o** reacts in lower yield (26%, **3oa**). Substrates with two possible (hetero)benzylic sites (**1g**, **1m**, **1n**, and **1o**) generate a mixture of products, with moderate to good regioisomeric ratios (r.r.).

Pyrazoles **2a** and 3-bromopyrazole (**2b**) undergo successful late-stage reactivity with bioactive molecules. Examples include an antidiabetic intermediate **1p**, which affords only the N^1 coupling product (90%, **3pa'**); benzbromarone methyl ether (77%, **3qa**), a derivative of a xanthine oxidase inhibitor;³⁴ celestolide (70%, **3rb**); ibuprofen methyl ester (65%, **3sa**); an anti-inflammatory anti-allergy agent³⁵ (49%, **3tb**, r.r. = 7.2:1) and a precursor to a GnRH antagonist³⁶ (42%, **3ua**). These results were complemented with a focused assessment of the Lewis acid co-catalytic conditions

(Figure 3.5B). These reactions lead to exclusive or high N^1 pyrazole site-selectivity in the C–N coupling reactions.

Different pyrazoles and other azole coupling partners were then tested in reactions with indane, motivated by the relevance of *N*-indanyl azoles in medicinal chemistry (Figure 3.6A).³⁷ Symmetrical 4-substituted pyrazoles, bearing fluoro, chloro, iodo, formyl, trifluoromethyl and nitro substituents, undergo coupling in good-to-excellent yields (60–82%, **3vc–3vh**). Other di- and trisubstituted pyrazoles with di- and trifluoromethyl (**2i**, **2j**)^{17a} and sulfonyl chloride (**2k**)

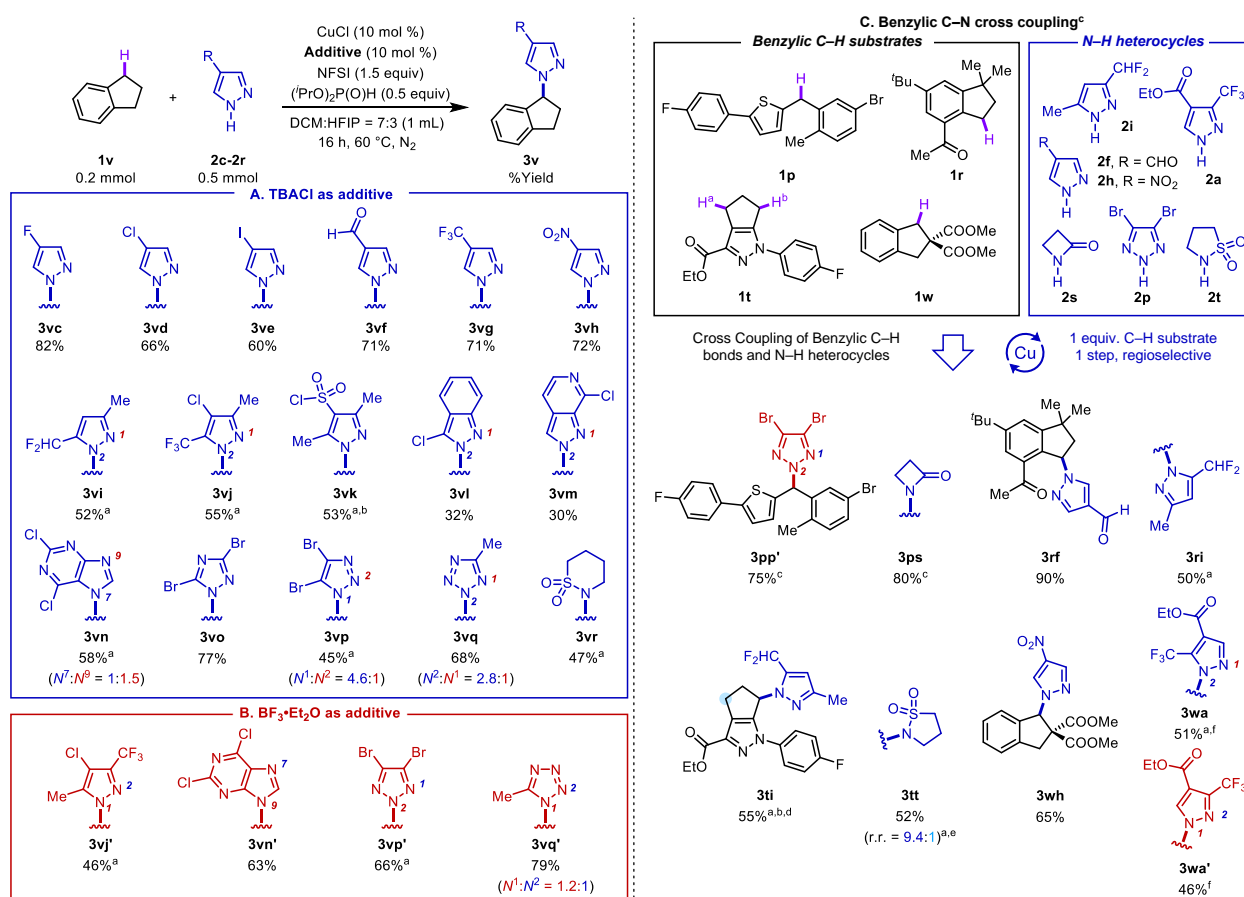


Figure 3.6. Assessment of various N–H heterocycles in cross coupling reactions. Substrate scope with diverse N–H heterocycles and indane under kinetically controlled TBACl conditions (A) and in the presence of $\text{BF}_3 \cdot \text{OEt}_2$ as a Lewis acid cocatalyst (B). Exploration of cross-coupling reactions of diverse N–H heterocycles and (hetero)benzylic C–H scaffolds under the TBACl conditions of Figure 5A, unless noted otherwise. Regioisomers formed in >5% yield were isolated. ^aConducted in DCM. ^bConducted at 50 °C. ^cConducted at 30 °C. ^dTrace amount of the other benzylic regioisomer was observed. ^eConducted at 40 °C. ^fConducted with 10 mol % $\text{BF}_3 \cdot \text{OEt}_2$.

substituents react effectively (52-55% yields, **3vi-3vk**). Successful reactivity, but lower yields are observed with indazole coupling partners **2l** and **2m** (32%, **3vl**; 30%, **3vm**).^{38,39} The dichloropurine derivative **2n** generates both N^9 and N^7 regioisomeric products (58% yield, $N^7:N^9 = 1:1.5$, **3vn**). Triazoles, including 1,2,4- and 1,2,3-isomers **2o** and **2p** and a tetrazole **2q** undergo successful reactivity (77%, **3vo**; 45%, **3vp**; 68%, **3vq**). The reaction with **2p** favors formation of the less common N^1 regioisomer ($N^1:N^2 = 4.6:1$),⁴⁰ consistent with the mechanistic rationale above.

Inclusion of $\text{BF}_3 \cdot \text{OEt}_2$ in these reactions enabled modulation of the azole regioselectivity (results with $\text{BF}_3 \cdot \text{OEt}_2$ were slightly better than with TMSOTf). In each of the four cases shown in Figure 5B, the favored regioisomer is different from that observed in the TBACl conditions. For example, the reaction with **2j** completely switches from N^2 to N^1 selectivity (46%, **3vj'**). In other cases, use of $\text{BF}_3 \cdot \text{OEt}_2$ ensures only a single isomer is formed (63%, **3vn'**; 66%, **3vp'**).

In a final assessment of the method, we explored C–N cross coupling reaction with different (hetero)benzylic and *N*-heterocyclic partners (Figure 3.6C). These reactions proceed in moderate-to-excellent yields. The reaction conditions show promise for heterocyclic coupling partners beyond azoles, including the beta-lactam **2s** (80%, **3ps**) and sultams **2r** and **2t** (47%, **3vr**, Figure 3.6A; 52%, **3tt**, Figure 3.6C). Reactions of the azoles **2a**, **2i**, and **2p** react with the regioselectivity expected from the observation elaborated above. For example, **1p** affords the thermodynamically favored coupling product upon reaction with **2p**, reflecting the stability of benzylic cation. On the other hand, the reaction of **1w** and **2a** afforded the kinetically favored the N^2 regioisomer even with $\text{BF}_3 \cdot \text{OEt}_2$ as a cocatalyst (51%, **3wa**). The combined effect of $\text{BF}_3 \cdot \text{OEt}_2$ cocatalyst and HFIP as a cosolvent, however, supported a switch in the observed regioselectivity (46%, **3wa'**). The reaction of **1t** and **2i** affords only one of the four possible C–N coupling products (55%, **3ti**), demonstrating both C–H and N-nucleophile selectivity.

3.4. Conclusion

In summary, the results outlined herein introduce a unique synthetic method for direct C(sp³)-H/N-H coupling of (hetero)benzylic substrates and azoles. Multiple features contribute to the potential impact of these methods. Perhaps the most notable feature is the ability to control the azole *N*-site selectivity, often enabling access to either regioisomeric product. Other highlights include the high-to-exclusive (hetero)benzylic C-H site selectivity, use of the C-H substrate as the limiting reagent, excellent scope for both coupling partners, and broad functional group compatibility. Overall, these C(sp³)-N coupling methods provide efficient access to complex, pharmaceutically relevant structures, and they should find widespread utility for library synthesis and exploration of chemical space in medicinal chemistry and related disciplines.⁴¹

3.5. Acknowledgements

The authors thank Iliia A. Guzei and Amelia M. Wheaton for assistance with the X-ray crystallographic characterization of **2a** and [PhN(CH₃)₃]₂[CuBr₄]. This work was supported by funding from the NIH (R35 GM134929). Spectroscopic instrumentation was supported by a gift from Paul. J. Bender, the NSF (CHE-1048642), and the NIH (S10 OD020022).

3.6. Author Contributions

Chen, S.-J.: leading experimental work and manuscript preparation

Golden, D. L: experimental work and manuscript preparation

3.7. References

1. Ruiz-Castillo, P.; Buchwald, S. L. Applications of Palladium-Catalyzed C–N Cross-Coupling Reactions. *Chem. Rev.* **2016**, *116*, 12564–12649.
2. (a) West, M. J.; Fyfe, J. W. B.; Vantourout, J. C.; Watson, A. J. B. Mechanistic Development and Recent Applications of the Chan–Lam Amination. *Chem. Rev.* **2019**, *119*, 12491–12523.
(b) Qiao, J. X.; Lam, P. Y. S. Copper-Promoted Carbon–Heteroatom Bond Cross-Coupling with Boronic Acids and Derivatives. *Synthesis*. **2011**, *6*, 829-856.
3. Brown, D. G.; Boström, J. Analysis of Past and Present Synthetic Methodologies on Medicinal Chemistry: Where Have All the New Reactions Gone? *J. Med. Chem.* **2016**, *59*, 4443–4458.
4. Trowbridge, A.; Walton, S. M.; Gaunt, M. J. New Strategies for the Transition-Metal Catalyzed Synthesis of Aliphatic Amines. *Chem. Rev.* **2020**, *120*, 2613–2692.
5. (a) Lovering, F.; Bikker, J.; Humblet, C. Escape from Flatland: Increasing Saturation as an Approach to Improving Clinical Success. *J. Med. Chem.* **2009**, *52*, 6752–6756. (b) Morley, A. D.; Pugliese, A.; Birchall, K.; Bower, J.; Brennan, P.; Brown, N.; Chapman, T.; Drysdale, M.; Gilbert, I. H.; Hoelder, S.; Jordan, A.; Ley, S. V.; Merritt, A.; Miller, D.; Swarbrick, M. E.; Wyatt, P. G. Fragment-based hit identification: thinking in 3D. *Drug Discov. Today* **2013**, *18*, 1221–1227.
6. Cernak, T.; Dykstra, K. D.; Tyagarajan, S.; Vachal, P.; Krska, S. W. The medicinal chemist's toolbox for late stage functionalization of drug-like molecules. *Chem. Soc. Rev.* **2016**, *45*, 546-576.
7. (a) Clark, J. R.; Feng, K.; Sookezian, A.; White, M. C. Manganese-Catalysed Benzylic C(sp³)–H Amination for Late-Stage Functionalization. *Nat. Chem.* **2018**, *10*, 583-591. (b) Chiappini,

- N. D.; Mack, J. B. C.; Du Bois, J. Intermolecular C(sp³)–H Amination of Complex Molecules. *Angew. Chem. Int. Ed.* **2018**, *57*, 4956-4959.
8. (a) Sharma, A.; Hartwig, J. F. Metal-Catalysed Azidation of Tertiary C–H Bonds Suitable for Late-Stage Functionalization. *Nature* **2015**, *517*, 600–604. (b) Huang, X.; Bergsten, T. M.; Groves, J. T. Manganese-Catalyzed Late-Stage Aliphatic C–H Azidation. *J. Am. Chem. Soc.* **2015**, *137*, 5300–5303. (c) Margrey, K. A.; Czaplyski, W. L.; Nicewicz, D. A.; Alexanian, E. J. A General Strategy for Aliphatic C–H Functionalization Enabled by Organic Photoredox Catalysis. *J. Am. Chem. Soc.* **2018**, *140*, 4213–4217. (d) Suh, S.-E.; Chen, S.-J.; Mandal, M.; Guzei, I. A.; Cramer, C. J.; Stahl, S. S. Site-Selective Copper-Catalyzed Azidation of Benzylic C–H Bonds. *J. Am. Chem. Soc.* **2020**, *142*, 11388-11393. (e) Niu, L.; Jiang, C.; Liang, Y.; Liu, D.; Bu, F.; Shi, R.; Chen, H.; Chowdhury, A. D.; Lei, A. Manganese-Catalyzed Oxidative Azidation of C(sp³)–H Bonds under Electrophotocatalytic Conditions. *J. Am. Chem. Soc.* **2020**, *142*, 17693-17702.
9. (a) Pandey, G.; Laha, R.; Singh, D. Benzylic C(sp³)–H Functionalization for C–N and C–O Bond Formation via Visible Light Photoredox Catalysis. *J. Org. Chem.* **2016**, *81*, 7161-7171. (b) Yang, Y.-Z.; Song, R.-J.; Li, J.-H. Intermolecular Anodic Oxidative Cross-Dehydrogenative C(sp³)–N Bond-Coupling Reactions of Xanthenes with Azoles. *Org. Lett.* **2019**, *21*, 3228–3231. (c) Hou, Z.-W.; Liu, D.-J.; Xiong, P.; Lai, X.-L.; Song, J.; Xu, H.-C. Site-Selective Electrochemical Benzylic C–H Amination. *Angew. Chem. Int. Ed.* **2020**, *60*, 2943-2947. (d) Hou, Z.-W.; Li, L.; Wang, L. Organocatalytic Electrochemical Amination of Benzylic C–H Bonds. *Org. Chem. Front.* **2021**, DOI: 10.1039/D1QO00746G.
10. (a) Song, C.; Dong, X.; Yi, H.; Chiang, C.-W.; Lei, A. DDQ-Catalyzed Direct C(sp³)–H Amination of Alkylheteroarenes: Synthesis of Biheteroarenes under Aerobic and Metal-Free

- Conditions. *ACS Catal.* **2018**, *8*, 2195–2199. (b) Ruan, Z.; Huang, Z.; Xu, Z.; Zeng, S.; Feng, P.; Sun, P.-H. Late-stage azolation of benzylic C–H bonds enabled by electrooxidation. *Sci. China. Chem.* **2021**, *64*, 800–807.
11. Eight of top 50 best-selling drugs contain N-benzylic heterocycles: Baumann, M.; Baxendale, I. R.; Ley, S. V.; Nikbin, N. *Beilstein J. Org. Chem.* **2011**, *7*, 442–495.
12. Taylor, R. D.; MacCoss, M.; Lawson, A. D. G. Rings in Drugs. *J. Med. Chem.* **2014**, *57*, 5845–5859.
13. Estrada, A. A.; Feng, J. A.; Lyssikatos, J. P.; Sweeney, Z. K. Compounds, compositions, and methods. Worldwide patent, WO2017087905 A1, May 26, 2017.
14. Hoffman, T. J.; Stierli, D.; Pitterna, T.; Rajan, R. Microbiocidal oxadiazole derivatives. Worldwide patent 2018158365 A1, September 07, 2018.
15. Blakemore, D. C.; Castro, L.; Churcher, I.; Rees, D. C.; Thomas, A. W.; Wilson, D. M.; Wood, A. Organic synthesis provides opportunities to transform drug discovery. *Nat. Chem.* **2018**, *10*, 383–394.
16. Adams, N. D.; Adams, J. L.; Burgess, J. L.; Chaudhari, A. M.; Copeland, R. A.; Donatelli, C. A.; Drewry, D. H.; Fisher, K. E.; Hamajima, T.; Hardwicke, M. A.; Huffman, W. F.; Koretke-Brown, K. K.; Lai, Z. V.; McDonald, O. B.; Nakamura, H.; Newlander, K. A.; Oleykowski, C. A.; Parrish, C. A.; Patrick, D. R.; Plant, R.; Sarpong, M. A.; Sasaki, K.; Schmidt, S. J.; Silva, D. J.; Sutton, D.; Tang, J.; Thompson, C. S.; Tummino, P. J.; Wang, J. C.; Xiang, H.; Yang, J.; Dhanak, D. Discovery of GSK1070916, a Potent and Selective Inhibitor of Aurora B/C Kinase. *J. Med. Chem.* **2010**, *53*, 3973–4001.
17. (a) Mykhailiuk, P. K. Fluorinated Pyrazoles: From Synthesis to Applications. *Chem. Rev.* **2021**, *121*, 1670–1715. (b) Davie, R. L.; Edwards, H. J.; Evans, D. M.; Hodgson, S. T.; Miller, I.;

- Novak, A. R.; Smith, A. J.; Stocks, M. J. Heterocyclic derivatives. Worldwide Patent 2014188211 A1, November 27, 2014.
18. Zhang, W.; Wang, F.; McCann, S. D.; Wang, D.; Chen, P.; Stahl, S. S.; Liu, G. Enantioselective Cyanation of Benzylic C–H Bonds via Copper-Catalyzed Radical Relay. *Science* **2016**, *353*, 1014–1018..
19. Suh, S.-E.; Nkulu, L. E.; Lin, S.; Krska, S.; Stahl, S. S. Benzylic C–H Isocyanation/Amine Coupling Sequence Enabling High-Throughput Synthesis of Pharmaceutically Relevant Ureas. *Chem. Sci.* **2021**, DOI: 10.1039/D1SC02049H.
20. Hu, H.; Chen, S.-J.; Mandal, M.; Pratik, S. M.; Buss, J. A.; Krska, S. W.; Cramer, C. J.; Stahl, S. S. Copper-catalysed benzylic C–H coupling with alcohols via radical relay enabled by redox buffering. *Nat. Catal.* **2020**, *3*, 358–367.
21. Liu, S.; Achou, R.; Boulanger, C.; Pawar, G.; Kumar, N.; Lusseau, J.; Robert, F.; Landais, Y. Copper-catalyzed oxidative benzylic C(sp³)–H amination: Direct synthesis of benzylic carbamates. *Chem. Commun.* **2020**, *56*, 13013–13016.
22. Xiao, H.; Liu, Z.; Shen, H.; Zhang, B.; Zhu, L.; Li, C. Copper-Catalyzed Late-Stage Benzylic C(Sp³)–H Trifluoromethylation. *Chem* **2019**, *5*, 940–949.
23. (a) Zhang, W.; Chen, P.; Liu, G. Copper-Catalyzed Arylation of Benzylic C–H bonds with Alkylarenes as the Limiting Reagents. *J. Am. Chem. Soc.* **2017**, *139*, 7709–7712. (b) Zhang, W.; Wu, L.; Chen, P.; Liu, G. Enantioselective Arylation of Benzylic C–H Bonds by Copper-Catalyzed Radical Relay. *Angew. Chem. Int. Ed.* **2019**, *58*, 6425–6429.
24. Fu, L.; Zhang, Z.; Chen, P.; Lin, Z.; Liu, G. Enantioselective Copper-Catalyzed Alkynylation of Benzylic C–H Bonds via Radical Relay. *J. Am. Chem. Soc.* **2020**, *142*, 12493–12500.

25. (a) Vasilopoulos, A.; Golden, D. L.; Buss, J. A.; Stahl, S. S. Copper-Catalyzed C–H Fluorination/Functionalization Sequence Enabling Benzylic C–H Cross Coupling with Diverse Nucleophiles. *Org. Lett.* **2020**, *22*, 5753–5757. (b) Buss, J. A.; Vasilopoulos, A.; Golden, D. L.; Stahl, S. S. Copper-Catalyzed Functionalization of Benzylic C–H Bonds with *N*-Fluorobenzenesulfonimide: Switch from C–N to C–F Bond Formation Promoted by a Redox Buffer and Brønsted Base. *Org. Lett.* **2020**, *22*, 5749–5752.
26. (a) Stanovnik, B.; Svete, J. Product Class 1: Pyrazoles. *Science of Synthesis*; Neier, R.; Bellus, D., Eds.; Thieme: Stuttgart, 2002; Vol. 12, pp 15–225. (b) Ivanova, A. E.; Burgart, Y. V.; Saloutin, V. I.; Slepukhin, P. A.; Borisevich, S. S.; Khursan, S. L. Ambident polyfluoroalkyl-substituted pyrazoles in the methylation reactions. *J. Fluor. Chem.* **2017**, *195*, 47–56.
27. Huang, A.; Wo, K.; Lee, S. Y. C.; Kneitschel, N.; Chang, J.; Zhu, K.; Mello, T.; Bancroft, L.; Norman, N. J.; Zheng, S.-L. Regioselective Synthesis, NMR, and Crystallographic Analysis of N1-Substituted Pyrazoles. *J. Org. Chem.* **2017**, *82*, 8864–8872.
28. For selected examples where cations have been used to influence *N*-regioselectivity, see: (a) Goikhman, R.; Jacques, T. L.; Sames, D. C-H Bonds as Ubiquitous Functionality: A General Approach to Complex Arylated Pyrazoles via Sequential Regioselective *C*-Arylation and *N*-Alkylation Enabled by SEM-Group Transposition. *J. Am. Chem. Soc.* **2009**, *131*, 3042–3048. (b) Wang, X.; Wang, Q.; Xue, Y.; Sun, K.; Wu, L.; Zhang, B. An organoselenium-catalyzed N¹- and N²-selective aza-Wacker reaction of alkenes with benzotriazoles. *Chem. Commun.* **2020**, *56*, 4436–4439.
29. Hilpert, L. J.; Sieger, S. V.; Haydl, A. M.; Breit, B. Palladium- and Rhodium-Catalyzed Dynamic Kinetic Resolution of Racemic Internal Allenes Towards Chiral Pyrazoles. *Angew. Chem. Int. Ed.* **2019**, *58*, 3378–3381.

30. Jones, C. D.; Winter, M. A.; Hirsch, K. S.; Stamm, N.; Taylor, H. M.; Holden, H. E.; Davenport, J. D.; Krumkalns, E. V.; Suhr, R. G. Estrogen Synthetase Inhibitors. 2. Comparison of the in Vitro Aromatase Inhibitory Activity for a Variety of Nitrogen Heterocycles Substituted with Diarylmethane or Diarylmethanol Groups. *J. Med. Chem.* **1990**, *33*, 416–429.
31. Wang, L.; Doherty, G.; Wang, X.; Tao, Z.-F.; Brunko, M.; Kunzer, A. R.; Wendt, M. D.; Song, X.; Frey, R.; Hansen, T. M.; Sullivan, G. M.; Judd, A.; Souers, A. Apoptosis-inducing agents for the treatment of cancer and immune and autoimmune diseases. Worldwide patent 2013055895 A1, April 18, 2013.
32. (a) Zhi, L.; Grote, M.; Reddy, R. K.; Li, W.; Craigo, W. Glucagon Receptor Antagonists. Worldwide patent 2018035172 A1, February 22, 2018.
33. (a) Gangjee, A. Tricyclic Compounds Having Antimitotic and/or Antitumor Activity and Method of Use Thereof. Worldwide patent 2010006032A1, January 14, 2010. (b) Aponte, J. C.; Vaisberg, A. J.; Castillo, D.; Gonzalez, G.; Estevez, Y.; Arevalo, J.; Quiliano, M.; Zimic, M.; Verástegui, M.; Málaga, E.; Gilman, R. H.; Bustamante, J. M.; Tarleton, R. L.; Wang, Y.; Franzblau, S. G.; Pauli, G. F.; Sauvain, M.; Hammond, G. B. Trypanoside, anti-tuberculosis, leishmanicidal, and cytotoxic activities of tetrahydrobenzothienopyrimidines. *Bioorg. & Med. Chem.* **2010**, *18*, 2880–2886.
34. Schepers, G. Benzbromarone therapy in hyperuricaemia; comparison with allopurinol and probenecid. *J. Int. Med. Res.* **1981**, *9*, 511–515.
35. Smith, H. W. Cyclopentapyrazole and tetrahydroindazole compounds. Worldwide patent 8607357, December 18, 1986.

36. Fushimi, N.; Yonekubo, S.; Ohno, K.; Miyagi, T. Nitrogen-containing fused ring derivatives, pharmaceutical compositions containing them and their pharmaceutical use. Japan patent 5308342B2, October 9, 2013.
37. Shu, S.; Cai, X.; Li, J.; Feng, Y.; Dai, A.; Wang, J.; Yang, D.; Wang, M.-W.; Liu, H. Design, synthesis, structure–activity relationships, and docking studies of pyrazole-containing derivatives as a novel series of potent glucagon receptor antagonists. *Bioorg. & Med. Chem.* **2016**, *24*, 2852–2863.
38. Indazoles tend to exist as 1*H*-tautomers: Minkin, V. I.; Garnovskii, A. D.; Elguero, J.; Katritzky, A. R.; Denisko, O. V. The Tautomerism of Heterocycles: Five-Membered Rings with Two or More Heteroatoms. In *Advances in Heterocyclic Chemistry*; Elsevier, 2000; Vol. 76, pp 157–323.
39. Selected methods that achieved indazole *N*²-alkylations: (a) Cheung, M.; Bloor, A.; Stafford, J. A. Efficient and Regioselective Synthesis of 2-Alkyl-2*H*-indazoles. *J. Org. Chem.* **2003**, *68*, 4093–4095. (b) Luo, G.; Chen, L.; Dubowchik, G. Regioselective Protection at *N*-2 and Derivatization at *C*-3 of Indazoles. *J. Org. Chem.* **2006**, *71*, 5392–5395. (c) Slade, D. J.; Pelz, N. F.; Bodnar, W.; Lampe, J. W.; Watson, P. S. Indazoles: Regioselective Protection and Subsequent Amine Coupling Reactions. *J. Org. Chem.* **2009**, *74*, 6331–6334.
40. Wang, X.; Zhang, L.; Krishnamurthy, D.; Senanayake, C. H.; Wipf, P. General Solution to the Synthesis of *N*-2-Substituted 1,2,3-Triazoles *Org. Lett.* **2010**, *12*, 4632–4635.
41. (a) Gordon, E. M.; Barrett, R. W.; Dower, W. J.; Fodor, S. P. A.; Gallop, M. A. Applications of Combinatorial Technologies to Drug Discovery. 2. Combinatorial Organic Synthesis, Library Screening Strategies, and Future Directions. *J. Med. Chem.* **1994**, *37*, 1385–1401. (b)

Thompson, L. A.; Ellman, J. A. Synthesis and Applications of Small Molecule Libraries.
Chem. Rev. **1996**, *96*, 555–600.

Chapter 4.

Benzylic C–H Cross Coupling Improves 3D Structural Diversity

4.1. Abstract

Easy access to a large collection of structurally diverse, three-dimensional (3D) compounds has been steadily but rapidly gaining importance in drug discovery. Most of the established and commonly utilized cross-coupling methodologies have been largely focused on $C(sp^2)$ centers, limiting the physicochemical and topological properties that can be accessed^{1,2}. Here, we demonstrate benzylic $C(sp^3)$ -H cross-coupling strategies to reliably afford three-dimensional structures via informatics-guided selection of C-H scaffolds, in contrast to existing $C(sp^2)$ -focused methods. Efficient exploration of the drug-like chemical space was enabled by virtual enumeration of diverse benzylic ethers and ureas, with distinctively higher three-dimensionality. Synthetic access to these coupling products were validated by sampling of the chemical space. These results highlight benzylic cross-coupling reactions as enabling tools to afford structurally diverse and drug-like molecules and promise future applications of these methods in pursuit of novel biological targets.

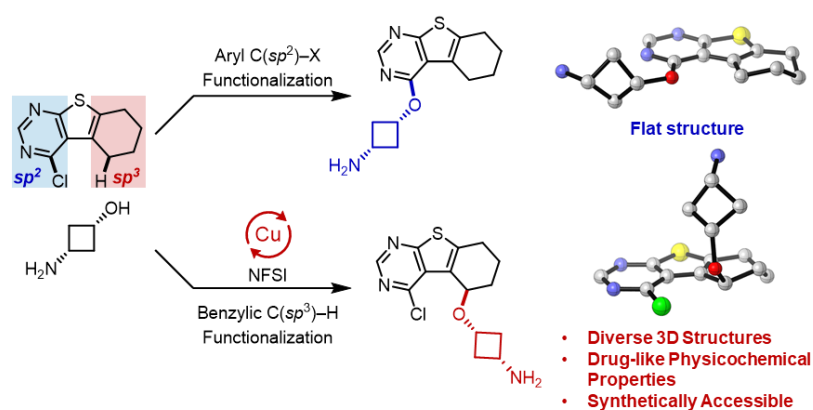


Figure 4.1. Benzylic C-H cross coupling improves 3D structural diversity and affords diverse drug-like molecules.

4.2. Introduction

Efficient access to libraries containing structurally diverse compounds is of paramount importance to the success of drug discovery^{3,4}. Since its debut, Lipinski's "Rule of 5" has formed the baseline for medicinal chemistry library design, which helped supply lead candidates with tailored properties and streamline the compound screening processes⁵. Libraries of high quality often comprise diverse compounds with drug-like characteristics, where structural diversity promises broad chemical space coverage and drug-likeness establishes foundation for subsequent lead optimization⁶. To this end, $C(sp^2)$ -focused coupling strategies that connects versatile building blocks, for example, palladium-catalyzed cross-coupling reactions and amide couplings, represent powerful tools for medicinal chemists to rapidly assemble compound libraries^{2,4}. For instance, the anti-inflammatory drug flurbiprofen (**1**) features a biaryl structure that can be conveniently constructed via Suzuki-Miyaura coupling (Figure 4.2A)⁷.

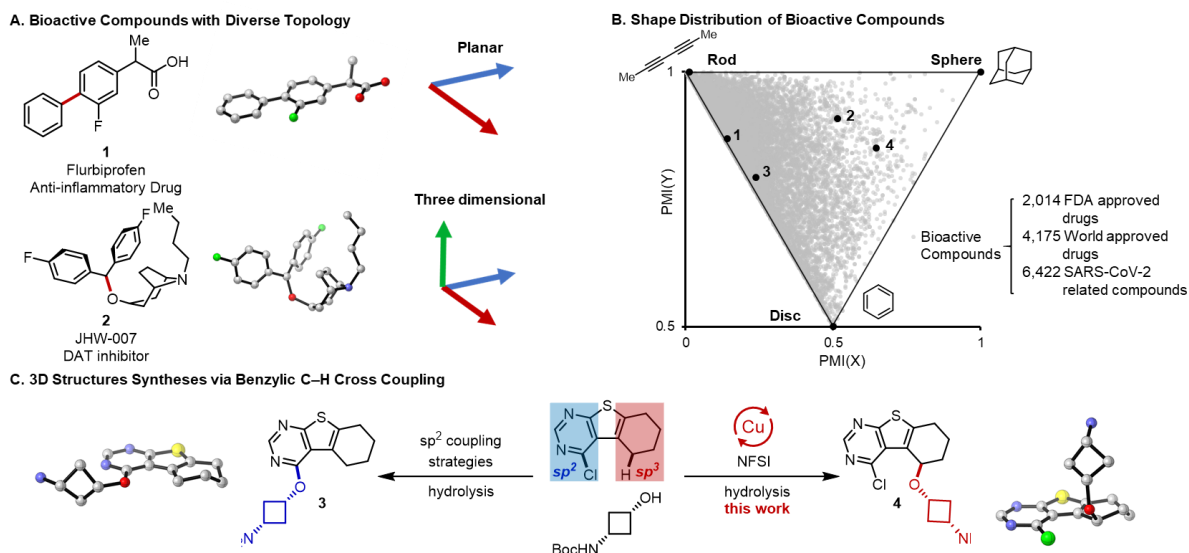


Figure 4.2. Cross-coupling reactions of benzylic C–H bonds and alcohols via a radical relay pathway. (A) Known bioactive compounds are topologically diverse, including planar structures like flurbiprofen (**1**) and 3D structures like JHW-007 (**2**). (B) PMI of **1** and **2** with reference to a reported population analysis of selected compounds from ChEMBL database². (C) Benzylic $C(sp^3)$ –H cross coupling reactions offer opportunities in introducing more three-dimensionality in contrast to $C(sp^2)$ -focused functionalization methods.

Recent medicinal chemistry efforts have sought to explore the topological diversity of libraries, where principal moments of inertia (PMI) were introduced as a reliable metrics⁸. PMI determine the torque needed for a given angular acceleration along three orthogonal principal axes ($I_1 \leq I_2 \leq I_3$). Normalization of these values ($\text{PMI}(X) = I_1/I_3$, $\text{PMI}(Y) = I_2/I_3$) allows comparison of molecules with diverse topological features in a triangular region. Mapping a collection of 12,611 bioactive molecules (**BC**, see Appendix C Section 4C.III for additional details) on a PMI plot found them topologically similar to **1** and heavily condensed in the "linear" or "flat" region (Figure 4.2B). Such bias in topology, related to suboptimal pharmacological properties like low water solubilities and consequently high attrition rates¹, could be attributed to overreliance on C(sp^2)-focused synthetic approaches². Application of the newly developed yet underutilized C(sp^3)-focused cross-coupling strategies could offer efficient access to the largely underexplored 3D chemical space and complement the existing collection of compounds. As an example, the dopamine transporter (DAT) inhibitor JHW-007 (**2**)⁹, constructed around a C(sp^3) center, presents a highly three-dimensional geometry.

Recent emergence of C(sp^3)-H functionalization strategies has created a wealth of opportunities to rapidly assemble libraries of diverse compounds.¹⁰ C(sp^3)-H bonds adjacent to (hetero)aromatic rings are ubiquitous in medicinally relevant building blocks¹¹, and development of Cu-catalyzed radical-relay catalysis has enabled efficient *site*-selective benzylic C(sp^3)-H cross-coupling reactions with diverse coupling partners. Prominent examples include direct couplings with readily available coupling partners like arylboronic acids^{12,13}, alcohols¹⁴, and azoles¹⁵, as well as functionalization/diversification sequence like halogenation/substitution reactions^{16,17} and urea synthesis via isocyanation/amine addition¹⁸. These reactions employ benzylic C(sp^3)-H substrates as the limiting reagent, conserving precious synthetic intermediates often resulting from

multistep synthesis, and exhibited broad utility for library syntheses in medicinal chemistry. Collectively, efficient, selective cross coupling strategies that connect benzylic C(sp^3)-H sites and versatile coupling partners should promise rapid access to libraries of 3D molecules, which complement the existing collection of C(sp^2)-derived compounds for medicinal research. Herein, we demonstrated that benzylic C(sp^3)-H cross coupling reactions, guided by cheminformatics, can reliably afford 3D structures with diversity in physicochemical properties. Cheminformatic studies shed new insights into how choices of benzylic C(sp^3)-H scaffolds can help distinguish benzylic cross coupling products from the C(sp^2)-derivatives (**3** and **4** in Figure 4.2B and 4.2C) with much higher three-dimensionality. Virtual enumeration of benzylic ethers and ureas with a diverse array of alcohols and amines broadly covered the drug-like chemical space. Synthetic accesses to these ethers and ureas were validated via strategic sampling of the virtual benzylic cross-coupling product library.

4.3. Results and Discussion

Enumeration of benzylic cross coupling product library. Investigation started with selection of 20 (hetero)benzylic C(sp^3)-H scaffolds (**A01-A20**, Figure 4.3A), most of which have exhibited reasonable reactivity in Cu-catalyzed radical relay chemistry¹²⁻¹⁸. Such an array featured diversity in the benzylic C(sp^3)-H sites via inclusion of acyclic and cyclic backbones, benzenoid and heterocycles, various aryl substitution patterns as well as achiral and chiral environments. On the other hand, alcohols and amines, two of the most abundant building block classes, were chosen for benzylic ether and urea syntheses (Figure 4.3B). These coupling partners have found broad applications in coupling reactions, such as Ullmann reactions¹⁹, Buchwald-Hartwig amination²⁰ and amide couplings²¹, and played key roles in syntheses of novel compounds for drug discovery.

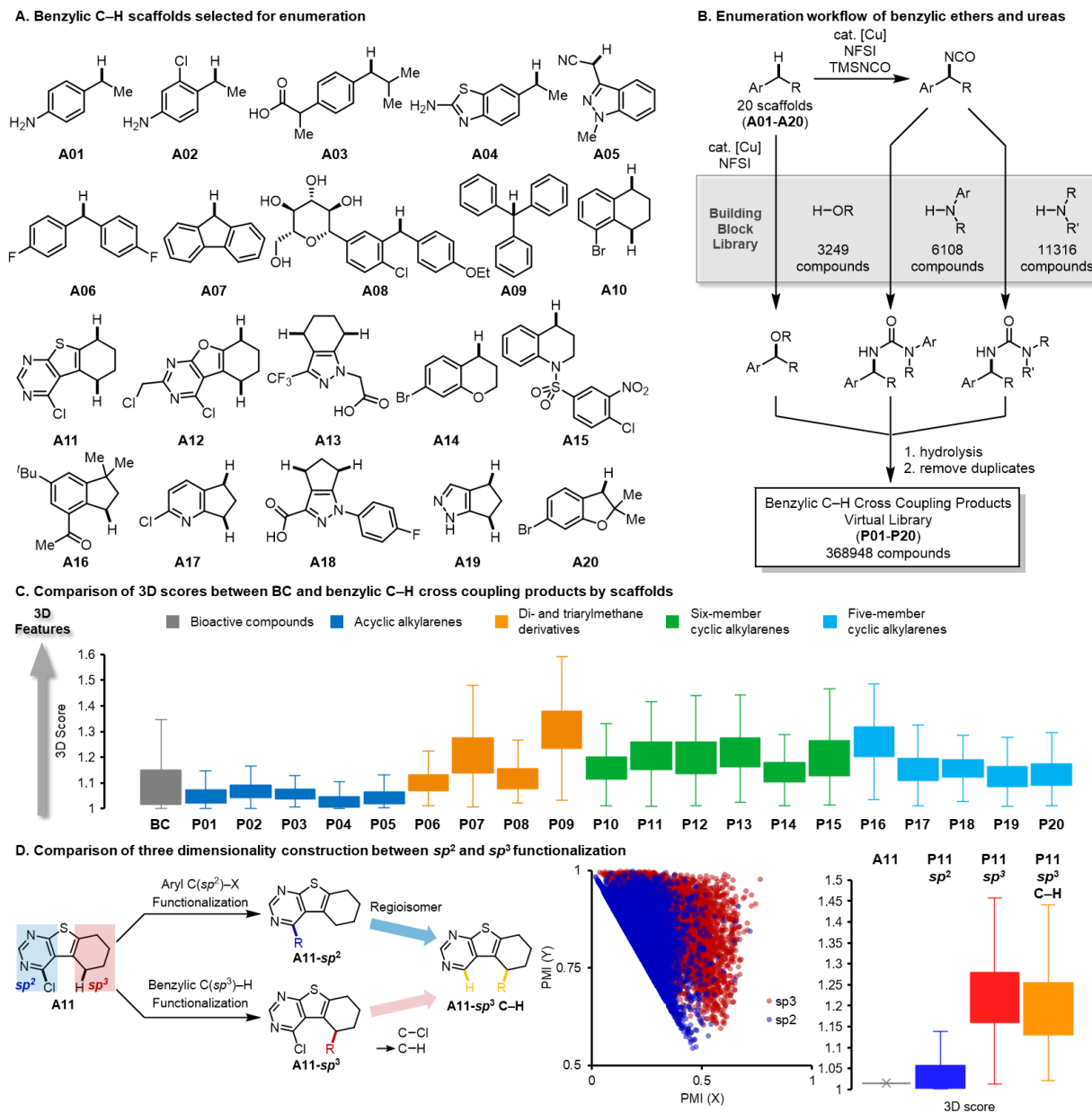


Figure 4.3. Enumeration of P01-20 and topological comparison between P01-20 and BC. (A) Display of selected benzylic C(sp^3)–H scaffolds for cross coupling product enumeration. (B) Enumeration of P01-20 via etherification with alcohols and isocyanation/urea formation sequence with amines. (C), Comparison of 3D scores between BC and P01-20 compounds by parent scaffold. (D), Comparison of PMI and 3D scores (Box-Whisker plot, outliers omitted) between sp^2 and sp^3 functionalization products derived from A11.

Three pools of coupling partners: 3,249 alcohols, 6,108 anilines and 11,316 alkylamines, were collected for combinatorial enumeration of benzylic ethers and ureas (See Appendix C section

4C.III for additional details). Common protecting groups the benzylic cross coupling products were removed via hydrolysis following the enumeration to retrieve drug-relevant physicochemical features and duplicated structures were discarded thereafter (See Appendix C Fig 4C.1 for additional details). These enumeration steps amounted to 368,948 coupling products that constituted a virtual benzylic cross coupling product library (**P01-P20**). To assess these compounds in a drug-relevant context, we compared them with the bioactive molecule collection **BC**.

Topological analyses. Comparison between **P01-20** and **BC** began with their topological features. Both libraries were evaluated in PMI plots or the numeric sum of normalized PMI values, $3D\ score = PMI(X) + PMI(Y)^2$, with the higher score being considered more 3D in character.

Most structures from **BC** fell in the range of 3D score < 1.2, exhibiting largely linear and planar geometries (Figure 4.3C). Mining compounds from **P01-20** by scaffolds revealed that the benzylic C(*sp*³)-H scaffolds had decisive influence on the topology of the cross-coupling products. Acyclic alkylarenes (**A01-A05**) mostly afforded products with 3D scores < 1.2 and no improvement in three-dimensionality comparing to **BC** molecules. Di-, and triarylmethane derivatives exhibited slightly more three-dimensionality in the coupling products, where substitution pattern on arenes showed negligible effect (**A06, A08**), while rigidity of the backbone significantly shifted the mass to possess more spheric topology (**A07, A09**). The beneficial effect from scaffold rigidity was also observed when six-member (**A10-A15**) and five-member (**A16-A20**) cyclic alkylarenes were employed, where the 3D scores substantially increase. Moreover, wider distribution in the 3D score span was consistently observed with scaffold classes other than acyclic alkylarenes, indicating diversity in the topology of the benzylic cross coupling products. In order to validate the influence of the scaffold rigidity, 5 cyclic benzylic C-H scaffolds (**A11, A12, A15, A18, A20**),

7 alcohols and 13 amines (from the building block library, cf. Figure 4.3B) were selected to couple and assemble a 160-compound subset of **P01-20** for comparison (**160-P01-20**, See Supplementary Figs. 2 and 3 for additional details). Although limited in library size, **160-P01-20** achieved apparently higher 3D scores than **P01-20** itself, highlighting the outstanding importance of the benzylic C–H scaffold in defining molecular topology⁸.

Further analyses focused on **A11**, a scaffold featuring C(*sp*²)–Cl adjacent to one of the benzylic C(*sp*³)–H sites, which allowed direct comparison of topological changes introduced via *sp*² and *sp*³ functionalization (Figure 4.3D). Virtual combinatorial cross couplings at C(*sp*²)–Cl of **A11** were performed with the same set of coupling alcohols and amines for **P01-20** to generate the aryl equivalent of the benzylic ethers and ureas. The scaffold **A11** is structurally flat (3D scores = 1.02) and roughly located along the rod-disc axis (cf. Figure 4.2B) and aryl functionalization of **A11** barely induced three-dimensionality, populating most structures of **A11-*sp*²** in the 3D score < 1.1 region. In stark contrast, **A11-*sp*³** spanned widely in the 3D score > 1.15 region, with some scoring as high as 1.45. Displacing C(*sp*²)–Cl with C(*sp*²)–H in **A11-*sp*³** afforded **A11-*sp*³ C–H** with only minimal drop in the 3D scores, indicating that the improvement in three-dimensionality was mainly contributed by benzylic C(*sp*³)–H substitution and the proximal C(*sp*²)–Cl had minor influence. Notably, **A11-*sp*³ C–H** represent the benzylic regioisomers to **A11-*sp*²** with identical molecular formulas and fsp³, yet **A11-*sp*³ C–H** featured much higher sphericity and diversity in topology, indicated by overall higher and broader coverage of 3D scores. Comparison of 3D scores was also conducted between **A10-*sp*³** and **A10-*sp*²** (via displacement of C(*sp*²)–Br), and a similar but not as significant improvement in three-dimensionality and topological diversity was observed (See Appendix C section 4C.V for additional details). Such results suggest that simple incorporation of *sp*³-rich cores proved insufficient to improve three-dimensionality of the library

and it is pivotal to construct chemical bonds and attach fragments around such sp^3 carbon centers. In this realm, benzylic $C(sp^3)$ -H cross coupling strategies, paired with judicious selection of $C(sp^3)$ -H scaffolds, reliably afford 3D molecules and promise more efficient exploration of structurally diverse chemical space.

Principal components analysis. Drug discovery is a multiparameter optimization process and high-profile drugs often strike a good balance of various characteristics, such as efficacy, toxicology profile, ADME properties (absorption, distribution, metabolism, and elimination) and physicochemical properties²³. Among these characteristics, physicochemical properties represent key criteria in evaluation of compounds' relevance to pharmaceutical research⁵. To evaluate **P01-20** compounds within the drug-like chemical space, we mapped **P01-20** and **BC** compounds with principal components analysis (PCA) to deconvolute multidimensional chemical space and visualize compounds in lower dimensions by maximizing variance of the projected data²⁴. This analysis aggregates entities with similar properties and has demonstrated utility in assessing relationship between sets of compounds^{25,26}.

We performed PCA with 21 molecular descriptors, including molecular weight, number of charged atoms, number of stereo atoms, number of hydrogen bond donors/acceptors, AlogP, fractional molecular polar surface area, quantitative estimate of drug-likeness (QED)²⁷, 3D scores, fraction of sp^3 carbon atoms (F sp^3) and plane of best fit (PBF)²⁸. **P01-20** and **BC** compounds were combined for PCA and subsequently plotted in density heatmaps respectively with the first four principal components (72% cumulative variance explained) in a pairwise manner (Figure 4.4A and 4.4B, see Appendix C section 4C.VI for additional details). The PC1-PC2 plot clustered both sets of compounds largely by molecule size, polar surface area and number of hydrogen bond donors/acceptors, while compounds aggregated in PC3-PC4 plot shared similarities in the number

of charged and stereo atoms. Representative **BC** molecules, *e.g.*, Levantinib, a kinase inhibitor, and fenofibrate, a drug used to control blood lipid levels, can find their counterparts in the **P01-20** chemical space with similar physicochemical properties but substantially higher three dimensionality, as suggested by their 3D scores. The significant overlap in shared chemical space (shown in purple color, more densely populated regions on PCA plots) validated the relevance of **P01-20** compounds to the drug-like chemical space and contextualized benzylic cross coupling methods as enabling strategies to elaborate pharmaceutically relevant structures.

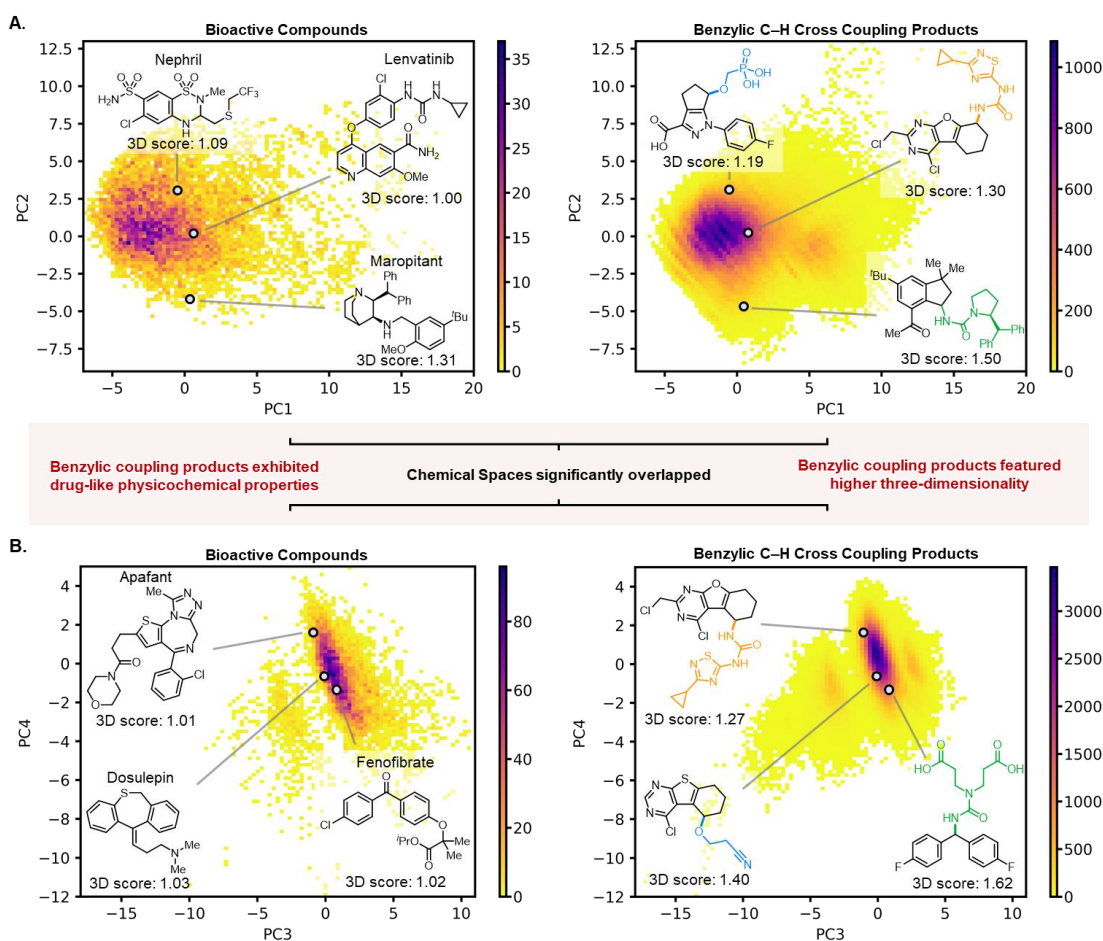


Figure 4.4. Principal components analysis (PCA) comparing P01-20 and BC compounds. (A) Physicochemical features depicted by PC1 and PC2. (B) Physicochemical features depicted by PC3 and PC4. Libraries are visualized in density heatmaps, where **BC** ($n = 12,611$) and **P01-20** ($n = 368,948$) compounds were analyzed by 100×100 bins and the color of each bin was determined by the number of compounds in it. Selected pairs of **BC** and **P01-20** compounds with similar coordinates were showcased.

Synthetic accessibility benchmarking. Benzylic C–H cross coupling strategies represent powerful tools to prepare diverse molecules¹⁴⁻¹⁸ and proved amenable to high-throughput experimentation for library synthesis¹⁸. Guided by the PCA maps (cf. Figure 4.4), we selected 16 benzylic ethers and ureas to sample the drug-like chemical space and evaluate their synthetic accessibility (Figure 4.5A). Reactions, conducted with conditions adapted from previously developed protocols^{14,18}, afforded moderate to good yields of these cross coupling products. These benzylic ethers and ureas featured some highly valued structural motifs in medicinal chemistry applications, including sugar fragments (**A08-1**, **A15-1**)²⁹, phosphonate (**A18-1**)³⁰, spirocyclic (**A08-2**)³¹ and heteroaryl ureas (**A12-2**, **A12-3**)³², piperidine core (**A06-1**)³³, amino acid fragments (**A06-2**, **A08-3**) and polyamine derivative (**A13-1**)³⁴. Overall, these benzylic cross coupling products captured a wide range of physicochemical features that qualify compounds for drug development purposes (PC1 vs. PC2 and PC3 vs. PC4, Figure 4.5B). On the other hand, these drug-like benzylic functionalized compounds readily shifted from the heavily exploited "rod-disc" territory and populated the more three-dimensional chemical space (PMI and the box-whisker plots, Figure 4.5B), entailing potential applications of benzylic C–H cross couplings to drug discovery campaigns in a 3D chemical space.

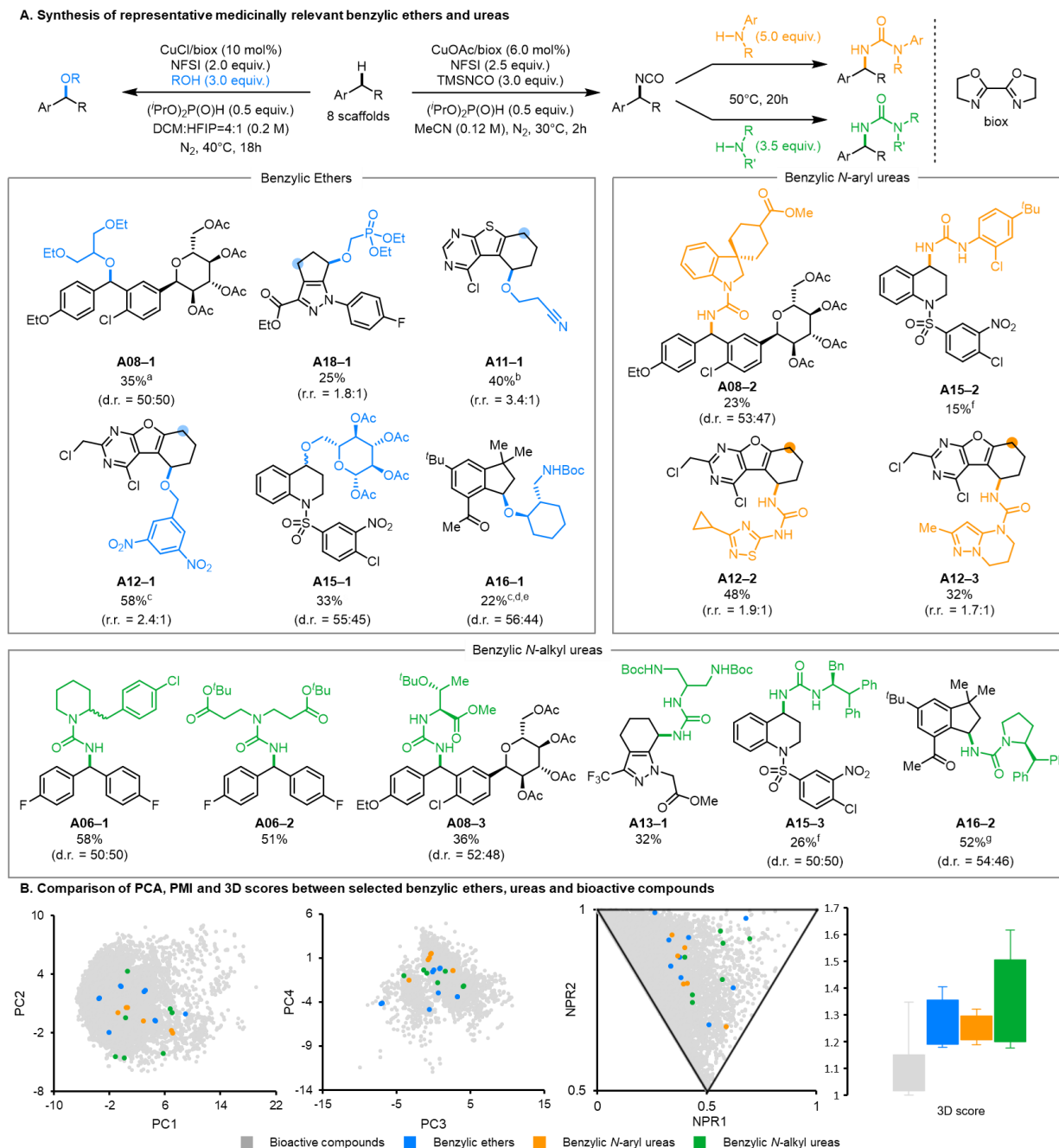


Figure 4.5. Synthesis of medicinally relevant benzylic C–H cross coupling products and comparison with bioactive molecules. (A) Assessment of benzylic ethers and ureas that sample the chemical space generated from virtual enumeration. (B) Comparison of selected P01–20 products (including all isolated regio- and stereoisomers) with BC space in PCA, PMI and Box-Whisker (3D scores) plots. ^aReaction run with 15 mol % CuCl/biox. ^bReaction run at room temperature. ^cReaction run with 20 mol % CuCl/biox. ^dReaction run at 30°C. ^eReaction run in DCM. ^fIsocyanation reaction run at 40°C. ^gIsocyanation reaction run at room temperature.

4.4. Conclusion

Collectively, these results demonstrate that benzylic C(sp^3)-H cross-coupling reactions, in contrast to existing C(sp^2)-focused functionalization methods, create opportunities for efficient access to three-dimensional structures in the drug-like space. Combination of cheminformatic tools and synthetic lab efforts benchmarked the utility of the benzylic cross-coupling strategies and effectively sampled the chemical space for potential medicinal chemistry application. Further intake of this informatics-synthesis approach should drive the field to develop synthetic methods that supply structurally diverse compounds with drug-relevant physicochemical properties and promise exploration of uncharted chemical space.

4.5. Acknowledgements

We thank Ilia A. Guzei and Kyana M. Sanders for assistance with the X-ray crystallographic characterization of **A16-1**. This work was supported by funding from the NIH (R35 GM134929). Spectroscopic instrumentation was supported by a gift from Paul. J. Bender, the NSF (CHE-1048642), and the NIH (S10 OD020022).

4.6. Author Contributions

Chen, S.-J.: monomer selection, reaction ideation, leading experimental work, computational protocol design and manuscript preparation

He, C. Q.: computational protocol design and manuscript preparation

Lin, S.: monomer selection and manuscript preparation

4.7. References

1. Lovering, F., Bikker, J. & Humblet, C. Escape from Flatland: Increasing Saturation as an Approach to Improving Clinical Success. *J. Med. Chem.* **52**, 6752–6756 (2009).
2. Brown, D. G. & Boström, J. Analysis of Past and Present Synthetic Methodologies on Medicinal Chemistry: Where Have All the New Reactions Gone?: Miniperspective. *J. Med. Chem.* **59**, 4443–4458 (2016).
3. Blakemore, D. C. *et al.* Organic synthesis provides opportunities to transform drug discovery. *Nat. Chem.* **10**, 383–394 (2018).
4. Boström, J., Brown, D. G., Young, R. J. & Keserü, G. M. Expanding the medicinal chemistry synthetic toolbox. *Nat. Rev. Drug Discov.* **17**, 709–727 (2018).
5. Lipinski, C. A.; Lombardo, F.; Dominy, B. W.; Feeney, P. J. Experimental and computational approaches to estimate solubility and permeability in drug discovery and development settings. *Adv. Drug Deliv. Rev.* **23**, 3–25 (1997).
6. Dolle, R. E. Historical Overview of Chemical Library Design. in *Chemical Library Design* (ed. Zhou, J. Z.) 3–25 (Humana Press, 2011).
7. Quasdorf, K. W., Riener, M., Petrova, K. V. & Garg, N. K. Suzuki–Miyaura Coupling of Aryl Carbamates, Carbonates, and Sulfamates. *J. Am. Chem. Soc.* **131**, 17748–17749 (2009).
8. Sauer, W. H. B. & Schwarz, M. K. Molecular Shape Diversity of Combinatorial Libraries: A Prerequisite for Broad Bioactivity †. *J. Chem. Inf. Comput. Sci.* **43**, 987–1003 (2003).
9. Agoston, G. E. *et al.* Novel N-Substituted 3 α -[Bis(4'-fluorophenyl)methoxy]tropane Analogues: Selective Ligands for the Dopamine Transporter. *J. Med. Chem.* **40**, 4329–4339 (1997).

10. Cernak, T., Dykstra, K. D., Tyagarajan, S., Vachal, P. & Krska, S. W. The medicinal chemist's toolbox for late stage functionalization of drug-like molecules. *Chem. Soc. Rev.* **45**, 546–576 (2016).
11. Taylor, R. D., MacCoss, M. & Lawson, A. D. G. Rings in Drugs: Miniperspective. *J. Med. Chem.* **57**, 5845–5859 (2014).
12. Zhang, W., Chen, P. & Liu, G. Copper-Catalyzed Arylation of Benzylic C–H bonds with Alkylarenes as the Limiting Reagents. *J. Am. Chem. Soc.* **139**, 7709–7712 (2017).
13. Zhang, W., Wu, L., Chen, P. & Liu, G. Enantioselective Arylation of Benzylic C–H Bonds by Copper-Catalyzed Radical Relay. *Angew. Chem. Int. Ed.* **58**, 6425–6429 (2019).
14. Hu, H. *et al.* Copper-catalysed benzylic C–H coupling with alcohols via radical relay enabled by redox buffering. *Nat Catal* **3**, 358–367 (2020).
15. Manuscript submitted.
16. Buss, J. A., Vasilopoulos, A., Golden, D. L. & Stahl, S. S. Copper-Catalyzed Functionalization of Benzylic C–H Bonds with *N*-Fluorobenzenesulfonimide: Switch from C–N to C–F Bond Formation Promoted by a Redox Buffer and Brønsted Base. *Org. Lett.* **22**, 5749–5752 (2020).
17. Vasilopoulos, A., Golden, D. L., Buss, J. A. & Stahl, S. S. Copper-Catalyzed C–H Fluorination/Functionalization Sequence Enabling Benzylic C–H Cross Coupling with Diverse Nucleophiles. *Org. Lett.* **22**, 5753–5757 (2020).
18. Suh, S.-E., Nkulu, L. E., Lin, S., Krska, S. & Stahl, S. S. Benzylic C–H Isocyanation/Amine Coupling Sequence Enabling High-Throughput Synthesis of Pharmaceutically Relevant Ureas. *Chem. Sci.* (2021) doi:10.1039/D1SC02049H.

19. Sambiaro, C., Marsden, S. P., Blacker, A. J. & McGowan, P. C. Copper catalysed Ullmann type chemistry: from mechanistic aspects to modern development. *Chem. Soc. Rev.* **43**, 3525–3550 (2014).
20. Dorel, R., Grugel, C. P. & Haydl, A. M. The Buchwald–Hartwig Amination After 25 Years. *Angew. Chem. Int. Ed.* **58**, 17118–17129 (2019).
21. Dunetz, J. R., Magano, J. & Weisenburger, G. A. Large-Scale Applications of Amide Coupling Reagents for the Synthesis of Pharmaceuticals. *Org. Process Res. Dev.* **20**, 140–177 (2016).
22. Prosser, K. E., Stokes, R. W. & Cohen, S. M. Evaluation of 3-Dimensionality in Approved and Experimental Drug Space. *ACS Med. Chem. Lett.* **11**, 1292–1298 (2020).
23. Wu, G. *et al.* Overview of Recent Strategic Advances in Medicinal Chemistry. *J. Med. Chem.* **62**, 9375–9414 (2019).
24. Medina-Franco, J., Martinez-Mayorga, K., Giulianotti, M., Houghten, R. & Pinilla, C. Visualization of the Chemical Space in Drug Discovery. *CAD* **4**, 322–333 (2008).
25. Kutchukian, P. S. *et al.* Chemistry informer libraries: a chemoinformatics enabled approach to evaluate and advance synthetic methods. *Chem. Sci.* **7**, 2604–2613 (2016).
26. Greshock, T. J. *et al.* Synthesis of Complex Druglike Molecules by the Use of Highly Functionalized Bench-Stable Organozinc Reagents. *Angew. Chem. Int. Ed.* **55**, 13714–13718 (2016).
27. Bickerton, G. R., Paolini, G. V., Besnard, J., Muresan, S. & Hopkins, A. L. Quantifying the chemical beauty of drugs. *Nat. Chem.* **4**, 90–98 (2012).
28. Firth, N. C., Brown, N. & Blagg, J. Plane of Best Fit: A Novel Method to Characterize the Three-Dimensionality of Molecules. *J. Chem. Inf. Model.* **52**, 2516–2525 (2012).

29. Chen, F., Huang, G. & Huang, H. Sugar ligand-mediated drug delivery. *Future Med. Chem.* **12**, 161–171 (2020).
30. Heidel, K. M. & Dowd, C. S. Phosphonate prodrugs: an overview and recent advances. *Future Med. Chem.* **11**, 1625–1643 (2019).
31. Tice, C. M. *et al.* Spirocyclic ureas: Orally bioavailable 11 β -HSD1 inhibitors identified by computer-aided drug design. *Bioorg. Med. Chem. Lett.* **20**, 881–886 (2010).
32. Tichenor, M. S. *et al.* Heteroaryl urea inhibitors of fatty acid amide hydrolase: Structure–mutagenicity relationships for arylamine metabolites. *Bioorg. Med. Chem. Lett.* **22**, 7357–7362 (2012).
33. Vardanyan, R. 2-Substituted and 1,2-Disubstituted Piperidines. in *Piperidine-Based Drug Discovery* 103–125 (Elsevier, 2017). doi:10.1016/B978-0-12-805157-3.00003-X.
34. Wallace, H. M., Fraser, A. V. & Hughes, A. A perspective of polyamine metabolism. *Biochem. J.* **376**, 1–14 (2003).

Chapter 5.

Site-Selective Copper-Catalyzed Azidation of Benzylic C–H Bonds

Reproduced with permission from: Sung-Eun Suh, **Si-Jie Chen**, Mukunda Mandal, Ilia A. Guzei, Christopher J. Cramer and, Shannon S. Stahl. Site-Selective Copper-Catalyzed Azidation of Benzylic C–H Bonds. *J. Am. Chem. Soc.* **2020**, *142*, 11388-11393. Copyright 2020 American Chemical Society.

5.1. Abstract

Site selectivity represents a key challenge for non-directed C–H functionalization, even when the C–H bond is intrinsically reactive. Here, we report a copper-catalyzed method for benzylic C–H azidation of diverse molecules. Experimental and density functional theory studies suggest the benzyl radical reacts with a Cu^{II}-azide species via a radical-polar crossover pathway. Comparison of this method with other C–H azidation methods highlights the unique site-selectivity of this method, and conversions of the benzyl azide products into amine, triazole, tetrazole, and pyrrole functional groups highlight the broad utility of this method for target molecule synthesis and medicinal chemistry.

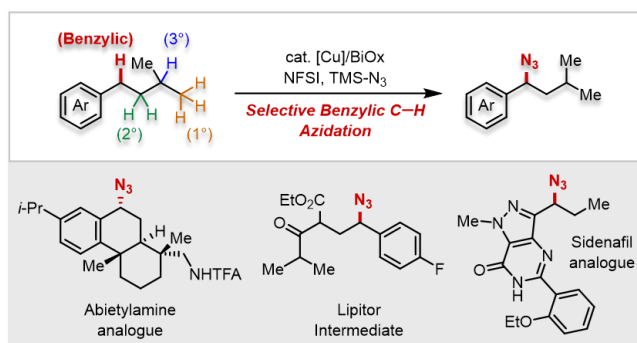


Figure 5.1. Cu-Catalyzed Azidation Benzylic C–H Bonds Summarization of Reactivity

5.2. Introduction

C–H functionalization methods improve the efficiency of target molecule syntheses^{1–3} and expand the scope of accessible structures.⁴ The large number of C–H bonds within individual molecules, however, introduces site-selectivity challenges.^{1, 5, 6} Organic azides are versatile synthetic intermediates.^{7–9} They represent effective ammonia surrogates,¹⁰ are readily converted into *N*-heterocycles,^{11,12} and provide access to important bioactive molecules. (Figures 5.1A and 1B).^{13–15} Recent efforts have demonstrated C(sp³)–H azidation,¹⁶ including iron-^{17, 18} and manganese-catalyzed¹⁹ and photochemical^{20,21} methods that are compatible with diverse C–H

substrates as the limiting reagent. These methods proceed via radical intermediates that show high selectivity for tertiary over primary and secondary aliphatic C–H bonds, but selectivity for benzylic over aliphatic positions is relatively low²⁰ or has not been investigated. Benzylic and heterobenzylic C–H bonds are ubiquitous in bioactive molecules, and site-selective functionalization of such positions could have broad impact. We^{22,23} and others^{24–27} have reported copper catalysts with *N*-fluorobenzenesulfonimide (NFSI) that enable selective functionalization of benzylic C–H bonds.^{28–30} Here, we describe a similar approach for C–H azidation that exhibits unique benzylic site-selectivity relative to other azidation methods (Figure 5.1C). Complementary studies provide mechanistic insights into the reaction and showcase the synthetic utility in the preparation of important target molecules.

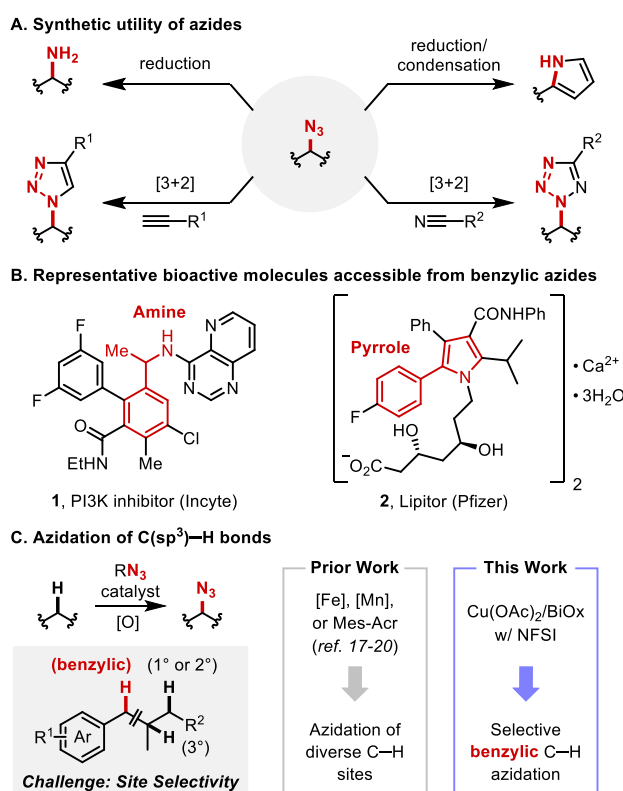


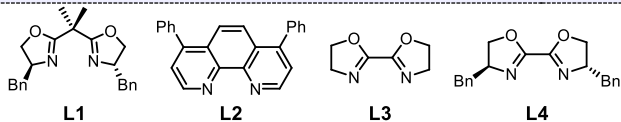
Figure 5.2. Azides are important intermediates in organic syntheses (A) and medicinal chemistry (B) and are ideally prepared by direct azidation of sp³ C–H bonds (C). NFSI, *N*-fluorobenzenesulfonimide. Mes-Acr, 9-mesityl-10-alkylacridinium catalyst.

5.3. Results and Discussion

Initial reaction optimization efforts used 1-ethylnaphthalene **3a** and TMSN_3 as coupling partners. An initial attempt with previous benzylic C–H cyanation conditions²² led to the desired product, but with low conversion and yield (6%, entry 1, Table 1). Increasing the temperature to 50 °C and using nitromethane as the solvent significantly increased the yield of **4a** (entries 2 and 3, Table 1; see Tables 5D.1-5D.9 in Appendix D for full screening data). Cu^{I} and Cu^{II} acetate salts were the most effective catalyst precursors (entries 3 and 6). $\text{Cu}(\text{OAc})_2$ was selected because it led to higher yields, and its air-stability facilitated handling. Testing the reaction without **L1** highlighted the importance of an ancillary ligand (entry 7). Screening other ligands (entries 8-10 and Table S4) showed that improved yields could be obtained with 2,2'-bioxazoline (BiOx) ligands (e.g., 85% yield with **L4**, entry 10). Further screening led to the optimized conditions in entry 11, affording 93% yield of azide **4a**. The lack of enantioselectivity, even with a single enantiomer of the ligand, prompted several efforts to probe the reaction mechanism.

Table 5.1. Reaction Optimization^a

| entry | catalyst (mol%), ligand (mol%) | NFSI (equiv.) | TMS-N ₃ (equiv.) | yield ^b (%) |
|-----------|--|---------------|-----------------------------|------------------------|
| 1 | CuOAc (10), L1 (10), (room temp., solv = benzene) ²² | 1.5 | 3.0 | 6 |
| 2 | CuOAc (10), L1 (10), (solv = benzene) | 1.5 | 3.0 | 51 |
| 3 | CuOAc (10), L1 (10) | 1.5 | 3.0 | 55 |
| 4 | CuI (10), L1 (10) | 1.5 | 3.0 | 31 |
| 5 | Cu(acac) ₂ (10), L1 (10) | 1.5 | 3.0 | 42 |
| 6 | Cu(OAc) ₂ (10), L1 (10) | 1.5 | 3.0 | 62 |
| 7 | Cu(OAc) ₂ (10) (no ligand) | 1.5 | 3.0 | 15 |
| 8 | Cu(OAc) ₂ (10), L2 (10) | 1.5 | 3.0 | 37 |
| 9 | Cu(OAc) ₂ (10), L3 (10) | 1.5 | 3.0 | 69 |
| 10 | Cu(OAc) ₂ (10), L4 (10) | 1.5 | 3.0 | 85 |
| 11 | Cu(OAc)₂ (2.0), L4 (4.0) | 2.5 | 3.6 | 93^c |



^a 0.4 mmol **3a**. ^bNMR yield, ext. std. = mesitylene. ^cIsolated yield.

Cu^I-mediated reductive activation of NFSI will generate an imidyl radical that promotes hydrogen-atom transfer (HAT) from the benzylic C–H bond.²³ The resulting benzyl radical can react with a Cu^{II}-azide species to afford the benzyl azide. Under simulated catalytic conditions lacking the benzylic substrate, Cu^IOAc, **L2**, NFSI, and TMSN₃ generate a dimeric Cu^{II}-azide complex, characterized by X-ray crystallography (Figure 5.2A). Addition of Gomberg's dimer,³¹ which readily dissociates into two trityl radicals, to a solution of this complex generated trityl azide in 91% yield (Figure 5.3B).^{32,33} This stoichiometric reaction was complemented by a catalytic reaction with triphenylmethane, which afforded the benzyl azide in 66% yield.

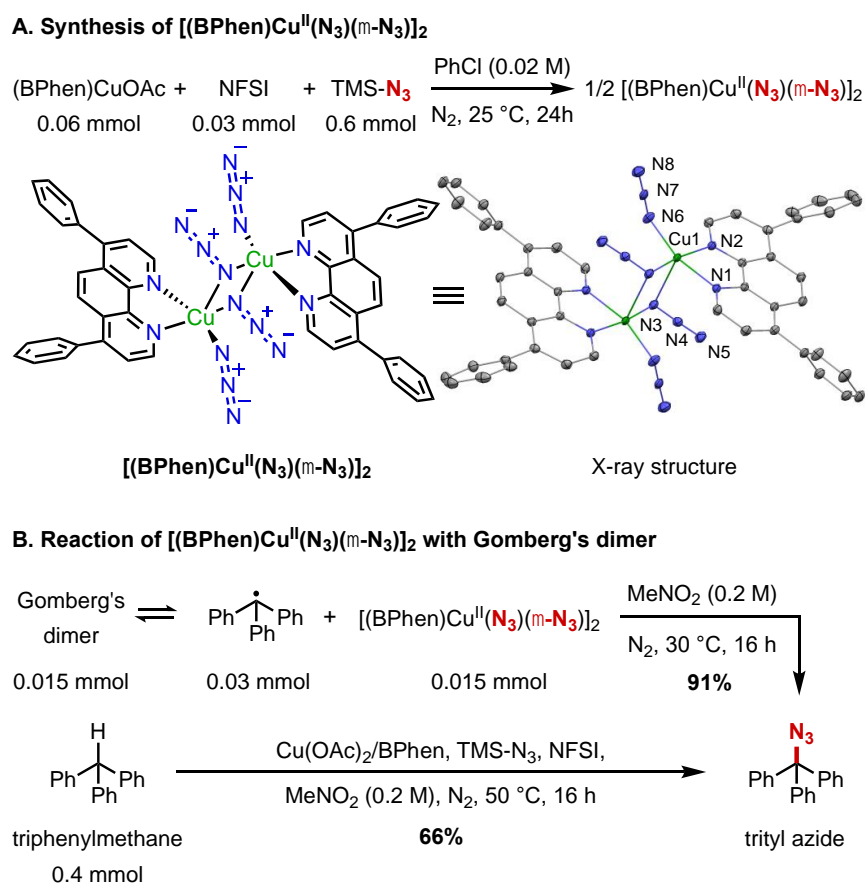


Figure 5.3. (A) Synthesis and crystal structure of [(BPhen)Cu^{II}(N₃)(μ-N₃)₂] (hydrogen atoms and chlorobenzene molecule omitted for clarity). (B) Reaction of [(BPhen)Cu^{II}(N₃)(μ-N₃)₂] with Gomberg's dimer (6 mol% Cu(OAc)₂/BPhen, 3.6 equiv. TMSN₃, 2.5 equiv. NFSI).

Seminal studies by Kochi suggest several possible pathways for C–N bond formation (Figure 5.4A).³⁴⁻³⁹ In Path I, the benzyl radical adds to Cu^{II} to generate a benzyl- Cu^{III} species that can undergo C–N reductive elimination.^{22,34} Path II includes multiple pathways involving radical attack at a terminal or bridging azide ligand, either at the proximal or distal *N*-atom of the azide.³⁵⁻³⁷ Finally, Path III involves one-electron oxidation of the benzyl radical by Cu^{II} to generate a cation, which can react readily with an azide nucleophile.^{23,38,39} Density functional theory calculations were performed to assess relevant structures and the energies of these pathways (M06-L/basis-II/SMD(MeNO₂); B3LYP-D3(BJ)/basis-I level of theory: Basis-I = 6–31G(d,p) for non-metals; SDD basis and pseudopotential for Cu. Basis-II = def2-TZVP for non-metals, def2-TZVP

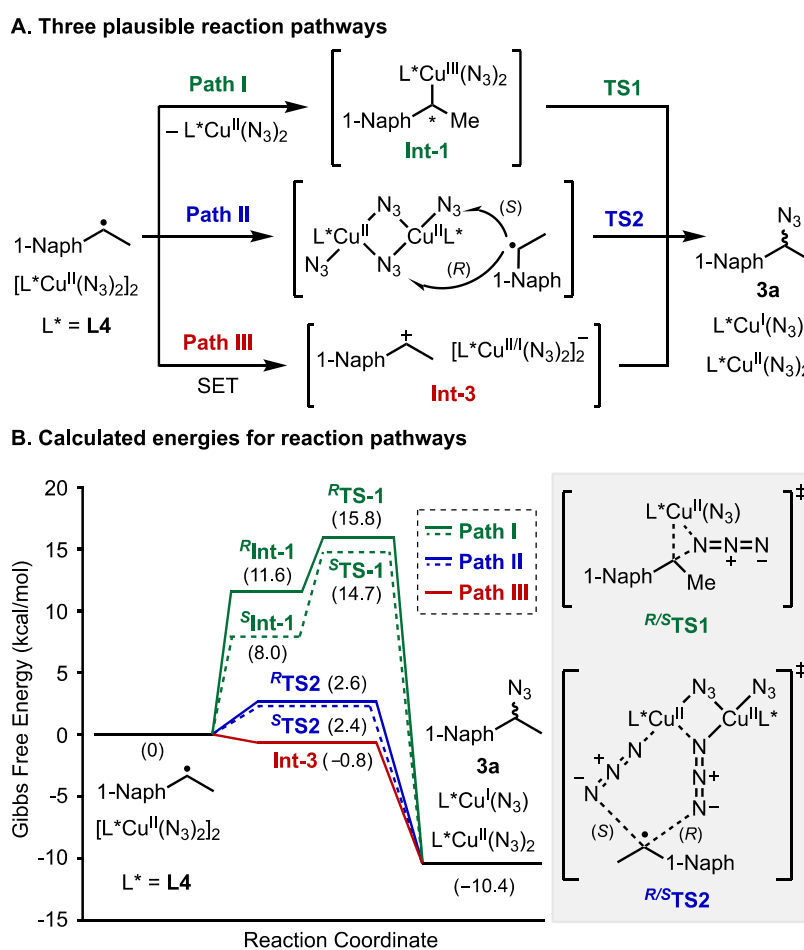


Figure 5.4. Three proposed pathways for azidation of the benzyl radical (A), and simplified energy diagrams comparing the three pathways (B) (see text and Appendix D for details).

basis and SDD pseudopotential for Cu; see Section IX in Appendix D). The energy diagrams in Figure 5.4B highlight the most favorable energies identified for Paths I–III involving reaction of the benzyl radical of 1-ethylnaphthalene and **L4**-ligated Cu^{II}-dimer. The results show that radical addition to Cu^{II}, followed by C–N reductive elimination from **Int-1** has the highest energy among the different mechanisms (Figure 5.4B). Radical addition to an azide ligand proceeds with much lower barrier. The pro-*R* face favors addition to a bridging azide while the pro-*S* favors addition to a terminal azide: $\Delta G^\ddagger = 2.6$ and 2.4 kcal/mol for **^RTS2** and **^STS2**, respectively. In both cases, radical addition is favored at the distal *N*-atom of the azide ligand. Computational analysis of the electron-transfer pathway leveraged the experimental redox potential measured for [(BPhen)Cu^{II}(N₃)(μ-N₃)₂] (−0.16 V vs. Fc^{0/+}; see Appendix D Figure 5D.8) and reported potentials for the benzyl radicals of ethylbenzene and isopropylbenzene ($E_{R^+|R^\bullet}^\circ = -0.01$ and -0.22 V vs. Fc^{0/+}).⁴⁰ Using these values as benchmarks, calculated redox potentials for [(**L4**)Cu^{II}(N₃)(μ-N₃)₂] and the benzyl radical of **3a** reveal that oxidation of the radical by the Cu^{II}-dimer is thermodynamically favorable ($\Delta G^\circ = -0.8$ kcal/mol). The small calculated energy difference between Paths II and III, and the absence of an electron-transfer rate constant, prevent clear distinction between these two paths on the basis of computational studies; however, both are predicted to afford little or no enantioselectivity.⁴¹ Experimental data providing some support for Path III was obtained from catalytic azidation of 4-Ph-cumene. Benzylic azidation was observed in 2:1 ratio with a vicinal diazide byproduct. Control experiments suggest diazidation arises from an α -methylstyrene intermediate (see Appendix D Figures 5D.3 and 5D.4). These results are most consistent with a radical-polar crossover mechanism, in which the benzyl cation is trapped by an

azide nucleophile or loses a proton to generate an alkene, which can undergo subsequent 1,2-diazidation.

Efforts were then made to explore the site-selectivity of this method (Figure 5.5). Three substrates incorporating both secondary benzylic and tertiary aliphatic C–H bonds were selected: isobutylbenzene **3b**, isopentylbenzene **3c**, and ibuprofen methyl ester **3d**. Use of the Cu/NFSI catalytic conditions at 30 °C led to azidation yields of 48%, 71%, and 62%, respectively, with benzylic:tertiary (B:T) selectivity ranging from 11:1–30:1. No azidation was observed at the tertiary benzylic position adjacent to the ester in **3d**. This result probably reflects both steric inhibition and a polarity mismatch in reaction with the sulfonimidyl radical. These results were compared to analogous data from three other C–H azidation methods, including photochemical,²⁰

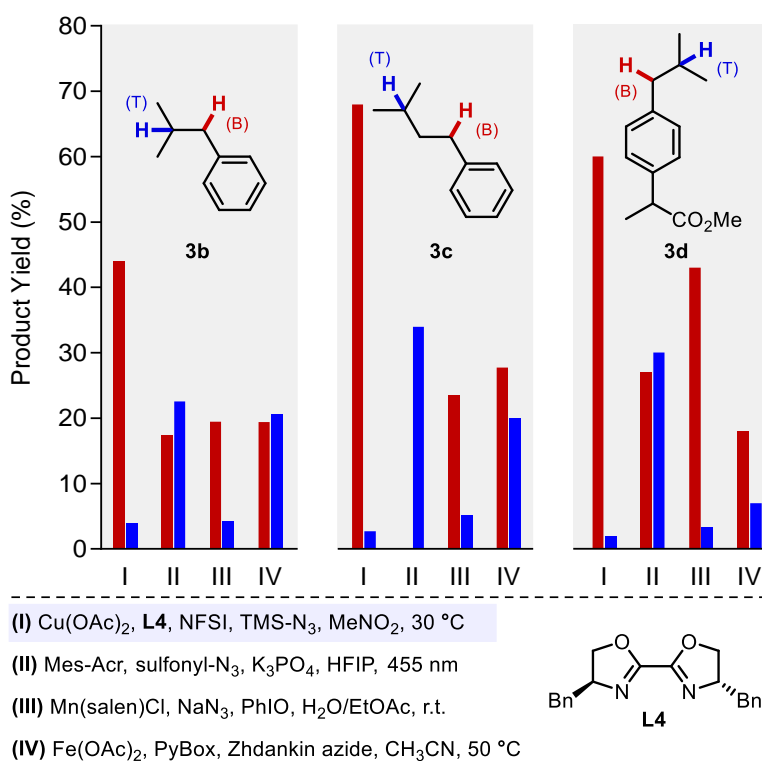
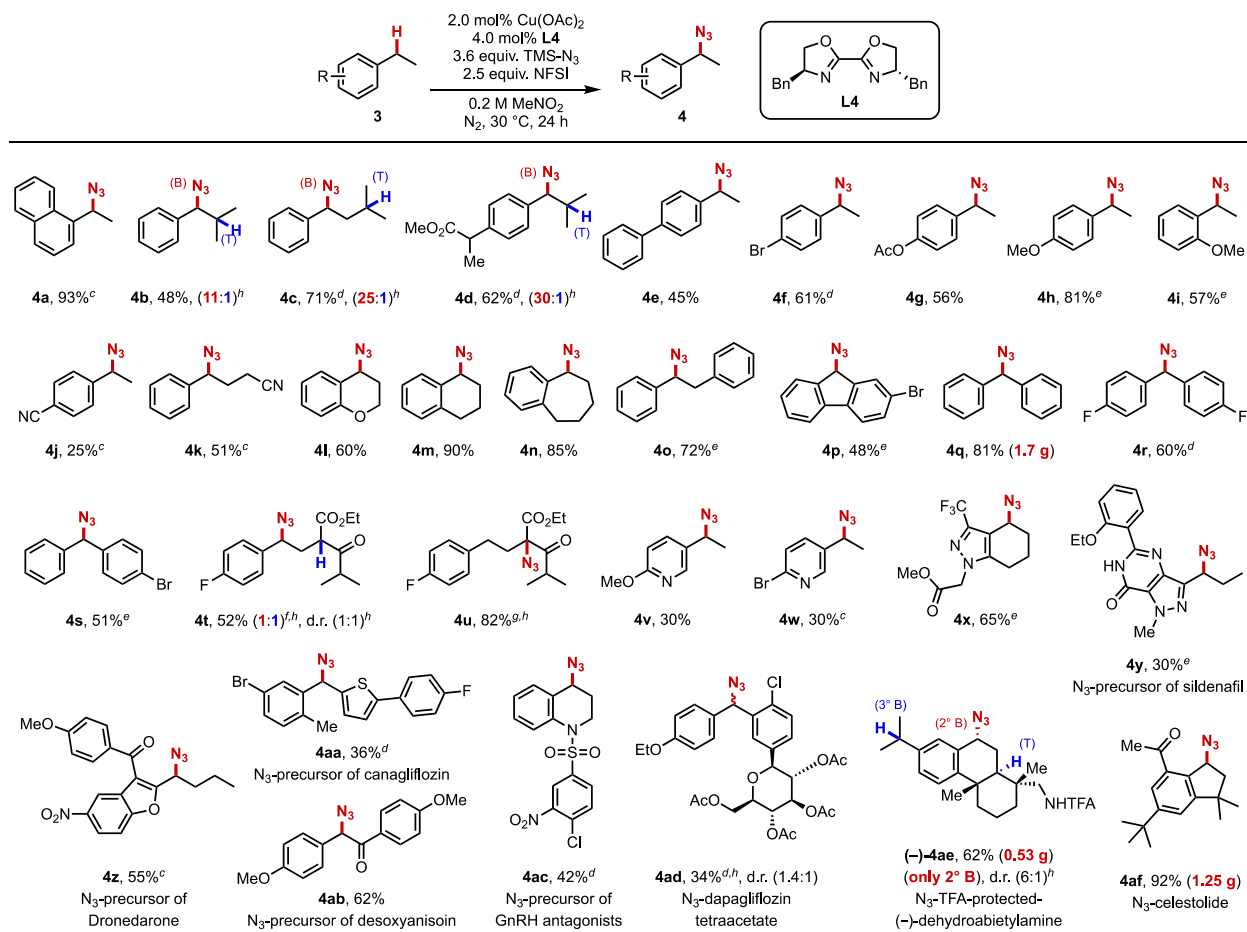


Figure 5.5. Azidation site selectivity with different catalytic methods (see Section V in the Appendix D for details). Standard condition for method I; substrate (0.4 mmol), Cu(OAc)₂ (2.0 mol%), BiOx (4.0 mol%), TMSN₃ (3.6 equiv.), NFSI (2.5 equiv.), 0.2 M MeNO₂, 30 °C, 24 h for **3b**, 48 h for **3c** and **3d**.

Mn-catalyzed,¹⁹ and Fe-catalyzed¹⁷⁻¹⁸ reactions (II–IV, Figure 5.5). The reported site-selectivity for **3b** and **3d** with method II exhibit a B:T ratio of ~ 1:1.²⁰ Independent testing of **3c** revealed tertiary C–H azidation. Mn(salen)Cl with PhIO (method III)¹⁹ also exhibits good selectivity for benzylic azidation: B:T = 4.6:1, 4.6:1, and 14:1, respectively, for **3b**, **3c**, and **3d**, although these reactions were operationally more challenging and led to lower yields (28–48%) than Cu/NFSI. The Fe(OAc)₂/I^{III}-azide system (method IV)¹⁷⁻¹⁸ showed relatively low B:T selectivity with **3b–3d** (1:1–2.5:1). Collectively, the data in Figure 5.4 show that Cu/NFSI exhibits unique benzylic site-selectivity.

Expanding on the results obtained with substrates **3a–3d**, we evaluated the azidation of other benzylic C–H substrates (Table 2). Reactions of various *para*-substituted ethylbenzenes (4-Ph, -Br, -OAc, and -OMe) resulted in moderate-to-good yields (45-81%, **4e–4h**). An exception was the electron-deficient 4-CN derivative **4j** (25%), while an aliphatic nitrile was better tolerated (**4k**, 51%). The common pharmacophore chroman⁴² underwent azidation in 60% yield (**4l**), and tetralin and benzosuberan, containing 6- and 7-membered rings, afforded good yields of **4m** (90%) or **4n** (85%). In contrast, indane led to only 12% yield of the azide, together with various byproducts (see Table S13 for a summary of this and other unsuccessful substrates). Bibenzyl underwent selective mono-azidation (72%, **4o**), and a series of diarylmethane derivatives, which are common pharmaceutical core structures, accessed moderate-to-good azide product yields (**4p–4s**).⁴³ Substrate **3t** underwent azidation at two sites: adjacent to the carbonyls of the ketoester and at the benzylic position (**4t/4u**). Increasing the temperature to 60 °C led to exclusive azidation at the α -C–H of the ketoester. Heterobenzylic substrates with pyridine and pyrazole units afforded the desired azides **4v–4x** in moderate yield (30-65%), demonstrating tolerance to pharmaceutically relevant heterocycles.

Table 5.2. Scope of Alkylarene Benzylic C–H Azidation^{a,b}

^aSubstrate (0.4 mmol). ^bIsolated yield. ^cStandard condition at 50 °C for 16 h. ^dStandard condition for 48 h. ^eSubstrate (0.2 mmol), Cu(OAc)₂ (6.0 mol%), BiOx (12 mol%). ^fSubstrate (0.2 mmol), Cu(OAc)₂ (1.0 mol%), BiOx (2.0 mol%), 24 °C. ^g60 °C for 48 h. ^h¹H NMR analysis.

The azidation reaction was also used in late-stage functionalization of drug molecules and derivatives. Examples include azidation of precursors to sildenafil⁴⁴ with a nitrogen heterocycle (**4y**); dronedarone⁴⁵ with a benzofuran (**4z**); canagliflozin⁴⁶ with a thiophene (**4aa**), and the natural product desoxyanisoin (**4ab**).⁴⁷ The tetrahydroquinoline of a GnRH antagonist precursor led to reaction at the benzylic position (**4ac**), with no byproduct observed from reaction adjacent to nitrogen. The tetraacetate derivative of dapagliflozin⁴⁸ reacted at the benzhydryl position, rather than the benzyl ether (**4ad**). Dehydroabietylamine derivative **3ae** features three potential sites for

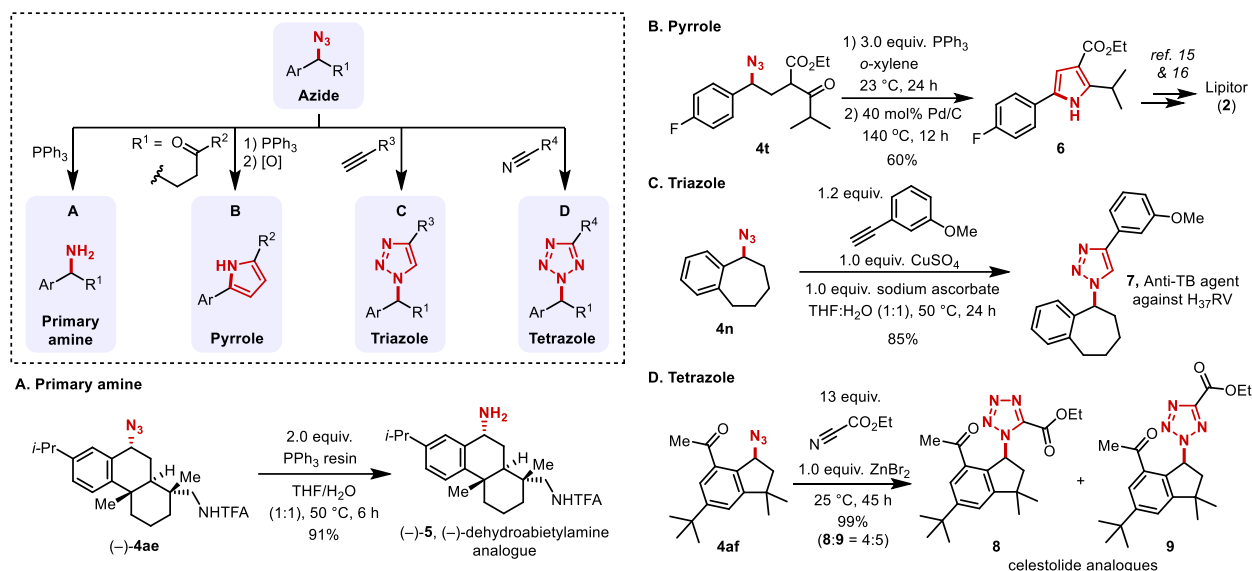


Figure 5.6. Azidation site selectivity with different catalytic methods (see Section V in the Appendix D for details). Standard condition for method I; substrate (0.4 mmol), $\text{Cu}(\text{OAc})_2$ (2.0 mol%), BiOx (4.0 mol%), TMSN_3 (3.6 equiv.), NFSI (2.5 equiv.), 0.2 M MeNO_2 , 30 °C, 24 h for **3b**, 48 h for **3c** and **3d**.

functionalization, a tertiary aliphatic and secondary and tertiary benzylic C–H bonds. Only the secondary benzylic azide (–)-**4ae** was observed (62% yield, 0.5 g). Finally, azidation of celestolide⁴⁹ proceeded in excellent yield to **4af** (92%, 1.25 g).

The appeal of the benzylic C–H azidation reactions in Table 2 is amplified by opportunities for further elaboration of the azide unit. For example, azides are highly effective ammonia surrogates. A Staudinger reduction of the azide in (–)-**4ae** proceeded efficiently to (–)-**5** in 91% yield with a phosphine resin that facilitates product isolation (Figure 5.6A). This route to (–)-**5** is an appealing alternative to a recently reported route involving Mn-catalyzed C–H amidation of **3ae** with a sulfamate ester, followed by reductive deprotection of the sulfamate to afford (–)-**5** in 43% overall yield.²⁹ Azides are also versatile precursors to pharmaceutically important heterocycles. The formal synthesis of Lipitor, **2**, a lipid-lowering drug,⁵⁰ was achieved via conversion of azido compound **4t** into the pyrrole precursor to Lipitor (**6**, Figure 5.6B; cf. Figure

5.1).^{14,15} The anti-tuberculosis agent **7**, used against mycobacterium tuberculosis strain H₃₇RV, was synthesized via copper-catalyzed alkyne-azide cycloaddition of **4n** with *m*-methoxyphenylacetylene (Figure 5.6C).⁵¹ The related [3+2]-cycloaddition of **4af** with ethyl cyanofornate gave two regioisomeric celestolide analogues (**8** and **9**) in quantitative yield (Figure 5.6D).

5.4. Conclusion

The results described herein demonstrate that a copper-based catalyst system composed entirely of commercially available components enables selective benzylic C–H azidation with broad scope. The reaction is initiated by hydrogen-atom transfer, followed by reaction of the benzylic radical with a Cu^{II}-azide intermediate. Experimental and computational data support a radical-polar crossover pathway involving a benzylic cation. The unique combination of good yields, diverse functional group compatibility, and high benzylic site-selectivity make this method well-suited for the incorporation of primary amines and azide-derived heterocycles (pyrroles, triazoles, and tetrazoles) into pharmaceutical and agrochemical building blocks, intermediates, and existing bioactive molecules.

5.5. Acknowledgements

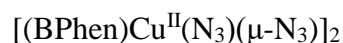
This work was supported by funding from the NIH (R01 GM126832 and R35 GM134929). Spectroscopic instrumentation was supported by a gift from Paul. J. Bender, the NSF (CHE-1048642), and the NIH (1S10 OD020022-1). Mukunda Mandal acknowledges a doctoral dissertation fellowship from the University of Minnesota. The authors thank Dr. Joshua A. Buss

for providing a sample of Gomberg's dimer and Amelia M. Wheaton for X-ray crystallographic assistance.

5.6. Author Contributions

Suh, S.-E.: manuscript preparation and leading experimental work

Chen, S.-J.: preliminary results, manuscript preparation, and synthesis of the



Mandal, M.: computational studies, manuscript preparation

5.7. References

1. Hartwig, J. F. Catalyst-Controlled Site-Selective Bond Activation. *Acc. Chem. Res.* **2017**, *50*, 549–555.
2. Stang, E. M.; White, M. C. Total Synthesis and Study of 6-Deoxyerythronolide B by Late-Stage C–H Oxidation. *Nat. Chem.* **2009**, *1*, 547–551.
3. Rosen, B. R.; Simke, L. R.; Thuy-Boun, P. S.; Dixon, D. D.; Yu, J.-Q.; Baran, P. S. C–H Functionalization Logic Enables Synthesis of (+)-Hongoquercin A and Related Compounds *Angew. Chem., Int. Ed.* **2013**, *52*, 7317–7320.
4. Cernak, T.; Dykstra, K. D.; Tyagarajan, S.; Vachal, P.; Krska, S. W. The Medicinal Chemist's Toolbox for Late Stage Functionalization of Drug-Like Molecules. *Chem. Soc. Rev.* **2016**, *45*, 546–576.

5. Newhouse, T.; Baran, P. S. If C–H Bonds Could Talk: Selective C–H Bond Oxidation. *Angew. Chem., Int. Ed.* **2011**, *50*, 3362–3374.
6. Hartwig, J. F.; Larsen, M. A. Undirected, Homogeneous C–H Bond Functionalization: Challenges and Opportunities. *ACS Cent. Sci.* **2016**, *2*, 281–292.
7. Wang, X.; Huang, B.; Liu, X.; Zhan, P. Discovery of Bioactive Molecules from CuAAC Click-Chemistry-Based Combinatorial Libraries. *Drug Discov. Today* **2016**, *21*, 118–132.
8. El-Sagheer, A. H.; Brown, T. Click Nucleic Acid Ligation: Applications in Biology and Nanotechnology. *Acc. Chem. Res.* **2012**, *45*, 1258–1267.
9. Pickens, C. J.; Johnson, S. N.; Pressnall, M. M.; Leon, M. A.; Berkland, C. J. Practical Considerations, Challenges, and Limitations of Bioconjugation via Azide–Alkyne Cycloaddition. *Bioconjugate Chem.* **2018**, *29*, 686–701.
10. Gololobov, Y. G.; Kasukhin, L. F. Recent Advances in the Staudinger Reaction. *Tetrahedron* **1992**, *48*, 1353–1406.
11. Bräse, S.; Gil, C.; Knepper, K.; Zimmermann, V. Organic Azides: An Exploding Diversity of a Unique Class of Compounds. *Angew. Chem. Int. Ed.* **2005**, *44*, 5188–5240.
12. Padwa, A. Aziridines and Azirines: Monocyclic. In *Comprehensive Heterocyclic Chemistry III*; Katritzky, A. R.; Ramsden, C. A.; Scriven, E. F. V.; Taylor, R. J. K., Eds.; Elsevier Science: Oxford, 2008; Vol. 1, Chapter 1.01.6.2, pp 50–64.
13. Li, Y.-L.; Combs, A. P.; Bicyclic Heteroaryl aminoalkyl Phenyl Derivatives as PI3K Inhibitors, International Patent 2015191677A1, Dec 17, 2015.
14. Ivanov, K. L.; Villemson, E. V.; Budynina, E. M.; Ivanova, O. A.; Trushkov, I. V.; Melnikov, M. Y. Ring Opening of Donor-Acceptor Cyclopropanes with the Azide Ion: A Tool for Construction of N-Heterocycles. *Chem. Eur. J.* **2015**, *21*, 4975–4987.

15. Kim, M.-S.; Yoo, M.-H.; Rhee, J.-K.; Kim, Y.-J.; Park, S.-J.; Choi, J.-H.; Sung, S.-Y.; Lim, H.-G.; Cha, D.-W.; Synthetic Intermediates, Process for Preparing Pyrrolylheptanoic Acid Derivatives Therefrom. International Patent 2009084827A3, July 9, 2009.
16. Goswami, M.; de Bruin, B. Metal-Catalysed Azidation of Organic Molecules. *Eur. J. Org. Chem.* **2017**, 2017, 1152–1176.
17. Karimov, R. R.; Sharma, A.; Hartwig, J. F. Late Stage Azidation of Complex Molecules. *ACS Cent. Sci.* **2016**, 2, 715–724.
18. Sharma, A.; Hartwig, J. F. Metal-Catalysed Azidation of Tertiary C–H Bonds Suitable for Late-Stage Functionalization. *Nature* **2015**, 517, 600–604.
19. Huang, X.; Bergsten, T. M.; Groves, J. T. Manganese-Catalyzed Late-Stage Aliphatic C–H Azidation. *J. Am. Chem. Soc.* **2015**, 137, 5300–5303.
20. Margrey, K. A.; Czaplyski, W. L.; Nicewicz, D. A.; Alexanian, E. J. A General Strategy for Aliphatic C–H Functionalization Enabled by Organic Photoredox Catalysis. *J. Am. Chem. Soc.* **2018**, 140, 4213–4217.
21. Wang, Y.; Li, G.-X.; Yang, G.; He, G.; Chen, G. A Visible-Light-Promoted Radical Reaction System for Azidation and Halogenation of Tertiary Aliphatic C–H Bonds. *Chem. Sci.* **2016**, 7, 2679–2683.
22. Zhang, W.; Wang, F.; McCann, S. D.; Wang, D.; Chen, P.; Stahl, S. S.; Liu, G. Enantioselective Cyanation of Benzylic C–H Bonds via Copper-Catalyzed Radical Relay. *Science* **2016**, 353, 1014–1018.
23. Hu, H.; Chen, S.-J.; Mandal, M.; Pratik, S. M.; Buss, J. A.; Krska, S. W.; Cramer, C. J.; Stahl, S. S. Copper-Catalyzed Benzylic C–H Coupling with Alcohols via Radical Relay Enabled by Redox Buffering. *Nat. Catal.* **2020**, 3, 358–367.

24. Ni, Z.; Zhang, Q.; Xiong, T.; Zheng, Y.; Li, Y.; Zhang, H.; Zhang, J.; Liu, Q. Highly Regioselective Copper-Catalyzed Benzylic C–H Amination by *N*-Fluorobenzenesulfonimide. *Angew. Chem., Int. Ed.* **2012**, *51*, 1244–1247.
25. Zhang, W.; Chen, P.; Liu, G. Copper-Catalyzed Arylation of Benzylic C–H Bonds with Alkylarenes as the Limiting Reagents. *J. Am. Chem. Soc.* **2017**, *139*, 7709–7712.
26. Zhang, W.; Wu, L.; Chen, P.; Liu, G. Enantioselective Arylation of Benzylic C–H Bonds by Copper-Catalyzed Radical Relay. *Angew. Chem. Int. Ed.* **2019**, *58*, 6425–6429.
27. Xiao, H.; Liu, Z.; Shen, H.; Zhang, B.; Zhu, L.; Li, C. Copper-Catalyzed Late-Stage Benzylic C(sp³)–H Trifluoromethylation. *Chem* **2019**, *5*, 940–949.
28. Complementary C–H functionalization methods showing high benzylic site selectivity have been reported recently. See refs. 29 and 30.
29. Clark, J. R.; Feng, K.; Sookezian, A.; White, M. C. Manganese-Catalysed Benzylic C(sp³)–H Amination for Late-Stage Functionalization. *Nat. Chem.* **2018**, *10*, 583–591.
30. Tanwar, L.; Börgel, J.; Ritter, T. Synthesis of Benzylic Alcohols by C–H Oxidation. *J. Am. Chem. Soc.* **2019**, *141*, 17983–17988.
31. Gomberg, M. An instance of Trivalent Carbon: Triphenylmethyl. *J. Am. Chem. Soc.* **1900**, *22*, 757–771.
32. Jang, E. S.; McMullin, C. L.; Käß, M.; Meyer, K.; Cundari, T. R.; Warren, T. H. Copper(II) Anilides in sp³ C–H Amination. *J. Am. Chem. Soc.* **2014**, *136*, 10930–10940.
33. Bower, J. K.; Cypcar, A. D.; Henriquez, B.; Stieber, S. C. E.; Zhang, S. C(sp³)–H Fluorination with a Copper(II)/(III) Redox Couple. *J. Am. Chem. Soc.* **2020**, *142*, 8514–8521.
34. Kochi, J. K. Electron-Transfer Mechanisms for Organometallic Intermediates in Catalytic Reactions. *Acc. Chem. Res.* **1974**, *7*, 351–360.

35. Jenkins, C. L.; Kochi, J. K. I. Ligand Transfer of Halides (Chloride, Bromide, Iodide) and Pseudohalides (Thiocyanate, Azide, Cyanide) from Copper(II) to Alkyl Radicals. *J. Org. Chem.* **1971**, *36*, 3095–3102.
36. Jenkins, C. L.; Kochi, J. K. II. Kinetics of Ligand Transfer Oxidation of Alkyl Radicals. Evidence for Carbonium Ion Intermediates. *J. Org. Chem.* **1971**, *36*, 3103–3111.
37. Jenkins, C. L.; Kochi, J. K. Homolytic and Ionic Mechanisms in the Ligand-Transfer Oxidation of Alkyl Radicals by Copper(II) Halides and Pseudohalides. *J. Am. Chem. Soc.* **1972**, *94*, 856–865.
38. Kochi, J. K.; Bemis, A. Carbonium Ions from Alkyl Radicals by Electron Transfer. *J. Am. Chem. Soc.* **1968**, *90*, 4038–4051.
39. Kochi, J. K.; Bemis, A.; Jenkins, C. L. Mechanism of Electron Transfer Oxidation of Alkyl Radicals by Copper(II) Complexes. *J. Am. Chem. Soc.* **1968**, *90*, 4616–4625.
40. Wayner, D. D. M.; McPhee, D. J.; Griller, D. Oxidation and Reduction Potentials of Transient Free Radicals. *J. Am. Chem. Soc.* **1988**, *110*, 132–137.
41. Control experiments show that benzyl azides can racemize under the reaction conditions. See section IV of Appendix D for details, in addition to the following reference: Ott, A. A.; Topczewski, J. J. Catalytic Racemization of Activated Organic Azides *Org. Lett.* **2018**, *20*, 7253–7256.
42. Ellis, G. P.; Lockhart, I. M.; Meeder-Nycz, D.; Schweizer, E. E. Chromenes, Chromanones, and Chromones. In *The Chemistry of Heterocyclic Compounds*; Ellis, G. P., Ed.; John Wiley and Sons, Inc.: New York, 1977; Vol. 31, pp 1-1196.
43. Herzon, S. B.; Woo, C. M. The Diazofluorene Antitumor Antibiotics: Structural Elucidation, Biosynthetic, Synthetic, and Chemical Biological Studies. *Nat. Prod. Rep.* **2012**, *29*, 87–118.

44. Galiè, N.; Ghofrani, H. A.; Torbicki, A.; Barst, R. J.; Rubin, L. J.; Badesch, D.; Fleming, T.; Parpia, T.; Burgess, G.; Branzi, A.; Grimminger, F.; Kurzyna, M.; Simonneau, G. Sildenafil Citrate Therapy for Pulmonary Arterial Hypertension. *N. Engl. J. Med.* **2005**, *353*, 2148–2157.
45. Hohnloser, S. H.; Crijns, H. J. G. M.; van Eickels, M.; Gaudin, C.; Page, R. L.; Torp-Pedersen, C.; Connolly, S. J. Effect of Dronedarone on Cardiovascular Events in Atrial Fibrillation. *N. Engl. J. Med.* **2009**, *360*, 668–678.
46. Perkovic, V.; Jardine, M. J.; Neal, B.; Bompoint, S.; Heerspink, H. J. L.; Charytan, D. M.; Edwards, R.; Agarwal, R.; Bakris, G.; Bull, S.; Cannon, C. P.; Capuano, G.; Chu, P.-L.; de Zeeuw, D.; Greene, T.; Levin, A.; Pollock, C.; Wheeler, D. C.; Yavin, Y.; Zhang, H.; Zinman, B.; Meininger, G.; Brenner, B. M.; Mahaffey, K. W. Canagliflozin and Renal Outcomes in Type 2 Diabetes and Nephropathy. *N. Engl. J. Med.* **2019**, *380*, 2295–2306.
47. Rhodes, J. R. Immunopotentiatory Agents and Physiologically Acceptable Salts Thereof. U.S. Patent 5508310A, Apr 16, 1996.
48. Plosker, G. L. Dapagliflozin: A Review of Its Use in Patients with Type 2 Diabetes. *Drugs* **2014**, *74*, 2191–2209.
49. Peck, A. M.; Kucklick, J. R.; Schantz, M. M. Synthetic Musk Fragrances in Environmental Standard Reference Materials. *Anal. Bioanal. Chem.* **2007**, *387*, 2381–2388.
50. LaRosa, J. C.; Grundy, S. M.; Waters, D. D.; Shear, C.; Barter, P.; Fruchart, J.-C.; Gotto, A. M.; Greten, H.; Kastelein, J. J. P.; Shepherd, J.; Wenger, N. K. Intensive Lipid Lowering with Atorvastatin in Patients with Stable Coronary Disease. *N. Engl. J. Med.* **2005**, *352*, 1425–1435.
51. Sajja, Y.; Vanguru, S.; Jilla, L.; Vulupala, H. R.; Bantu, R.; Yogeswari, P.; Sriram, D.; Nagarapu, L. A Convenient Synthesis and Screening of Benzosuberone Bearing 1,2,3-

Triazoles against Mycobacterium Tuberculosis. *Bioorg. Med. Chem. Lett.* **2016**, *26*, 4292–4295.

Appendix A: Supporting Information Chapter 2

2A.I. General Considerations

All reagents were purchased and used as received unless otherwise noted. Cu salts were purchased from Aldrich. Benzylic C–H substrates were purchased from Oakwood Chemicals, Combi-Blocks, Chem-Impex, Alfa Aesar, TCI America, Ark Pharm, Enamine, AstaTech or Aldrich. With the exception of ligand L8 (cf. Table 2A.3a), which was prepared by a literature protocol¹, ligands were purchased from Aldrich or TCI America. N-Fluorobenzenesulfonimide (NFSI) was purchased from Combi-Blocks and Ark Pharm. Methanol was purchased from Aldrich and Macron Fine Chemicals. Dialkyl phosphites were purchased from Aldrich, TCI America, Alfa Aesar and Oakwood Chemicals.

¹H and ¹³C NMR spectra were recorded on Bruker 400 MHz or Bruker 500 MHz spectrometers and chemical shifts are reported in parts per million (ppm). ¹H NMR spectra were referenced to tetramethylsilane at 0.00 ppm and ¹³C NMR spectra were referenced to CDCl₃ at 77.16 ppm. Chromatography was performed using either a Combi-flash® with reusable 24 g or 12 g Combi-flash gold® cartridges, or a Biotage Isolera One® with reusable 25 g SNAP Ultra® cartridges or standard silica cartridges unless otherwise noted. Enantiomeric separation was conducted with supercritical fluid chromatography (SFC, Waters ACQUITY UPC) or chiral HPLC (Waters Alliance). UV-Vis experiments were performed with a Cary 60 UV-Vis Spectrophotometer from Agilent in quartz cuvettes. Electron paramagnetic resonance (EPR) spectra were acquired on a Bruker ELEXSYS E500 EPR spectrometer. High-resolution mass spectra were obtained using a Thermo Q Exactive™ Plus (ESI or ASAP-MS) by the mass spectrometry facility at the University of Wisconsin (funded by NIH grant: 1S10OD020022-1).

Note that the reported benzylic C–H etherification reactions involve generation of (RO)₂P(O)F and/or HF, which are hazardous and have safety concerns. Appropriate standard operation procedures should be followed when handling these reactions.

2A.II. General Procedure (I) for Methoxylation of Benzylic C–H Substrates (pressure tube)

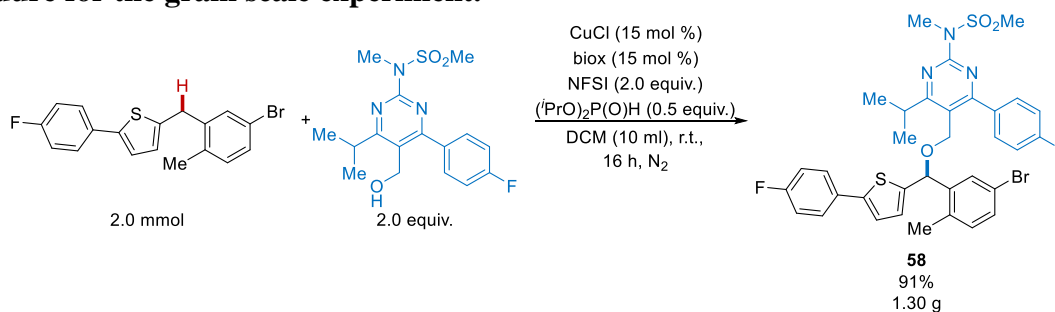
Copper(I) chloride (2.0 mg, 0.020 mmol, 10 mol%), 4,4',5,5'-tetrahydro-2,2'-bioxazole (2.8 mg, 0.020 mmol, 10 mol%), NFSI (126.1 mg, 0.40 mmol, 2.0 equiv.) and benzylic substrate (if solid, 0.20 mmol, 1.0 equiv.) were added to a pressure tube under air, and then the tube was moved to a glove box. Solvent (1.0 mL), benzylic substrate (if liquid, 0.20 mmol, 1.0 equiv.), methanol (42 μL, 1.0 mmol, 5.0 equiv.) and dimethyl phosphonate (9.5 μL, 0.10 mmol, 0.5 equiv.) were added to the tube. The tube was sealed in the glove box and taken out to a hot plate. The sealed tube was heated at 40 °C with stirring for 16 h. When the reaction finished, the mixture was cooled down to room temperature, poured into water and extracted with CHCl₃ (10 mL × 3). The organic layers were combined and washed sequentially with saturated sodium bicarbonate and brine, then dried with Na₂SO₄ and filtered. The mixture was evaporated under vacuum and the crude mixture was purified by automated flash chromatography (silica gel, eluted by pentane:ethyl acetate = 20:1 to 4:1).

2A.III. General Procedure (II) for Methoxylation of Benzylic C–H Substrates (glass vial)

Copper(I) chloride (2.0 mg, 0.020 mmol, 10 mol%), 4,4',5,5'-tetrahydro-2,2'-bioxazole (2.8 mg, 0.020 mmol, 10 mol%), NFSI (126.1 mg, 0.40 mmol, 2.0 equiv.) and benzylic substrate (if solid, 0.20 mmol, 1.0 equiv.) were added under air to a 4 mL vial containing a magnetic stir bar. Then the vial was capped with a pierceable Teflon cap. A needle was pierced through the cap to facilitate exchange of the vial headspace with the atmosphere. The vial was moved into a glove box, through three vacuum-nitrogen-backfill cycles. The needle was removed, and the vial was taken out of the glove box (now sealed under an inert gas). Solvent (1.0 mL), benzylic substrate (if liquid, 0.20 mmol, 1.0 equiv.), methanol (42 μ L, 1.0 mmol, 5.0 equiv.) and dimethyl phosphonate (9.5 μ L, 0.10 mmol, 0.5 equiv.) were added into the vial via injection through the cap. The sealed vial was heated at 40 °C and stirred for 16 h. When the reaction finished, the mixture was cooled down to room temperature and triethylamine (140 μ L, 1.0 mmol, 5.0 equiv.) was added to quench any unreacted NFSI. Then the mixture was evaporated under vacuum and the crude mixture was purified by automated flash chromatography (silica gel, eluted by pentane:ethyl acetate = 20:1 to 4:1).

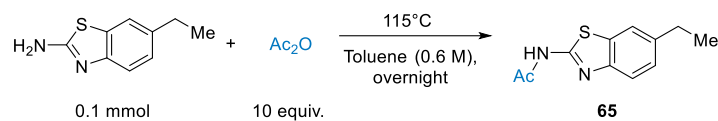
2A.IV. Experimental Procedures for Preparations of Compounds

Procedure for the gram scale experiment.



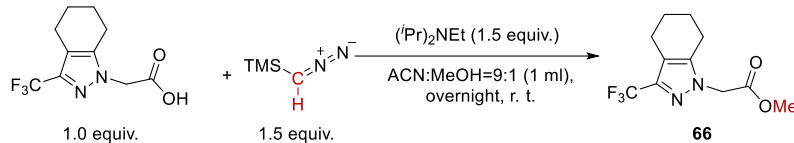
Copper(I) chloride (15 mg, 0.30 mmol), 4,4',5,5'-tetrahydro-2,2'-bioxazole (42 mg, 0.30 mmol), 4-(4-Fluorophenyl)-6-isopropyl-2-[(N-methyl-N-methylsulfonyl)amino]pyrimidine-5-yl-methanol (1414 mg, 4.0 mmol), 2-(5-Bromo-2-methylbenzyl)-5-(4-fluorophenyl)thiophene (723 mg, 2.0 mmol) and NFSI (1261 mg, 4.0 mmol) were added under air to a 24 mL vial containing a magnetic stir bar. Then the vial was capped with a pierceable Teflon cap. A needle was pierced through the cap and kept in the cap to facilitate the exchange of the vial headspace with the atmosphere. The vial was transferred to a glove box, through three vacuum-nitrogen-backfill cycles. The needle was removed. Dichloromethane (10 mL) and diisopropyl phosphite (163 μ L, 1.0 mmol) were added into the vial. The vial was capped, taken out of the glove box and stirred at room temperature for 16 h. When the reaction finished, triethylamine (1.4 mL, 10 mmol) was added. Then the mixture was evaporated under vacuum and the crude mixture was purified by flash chromatography (silica gel, eluted by pentane/ethyl acetate = 9:1). 1.30 g (91%) of pale-yellow liquid was obtained.

Procedure for the preparation of the substrate 65.



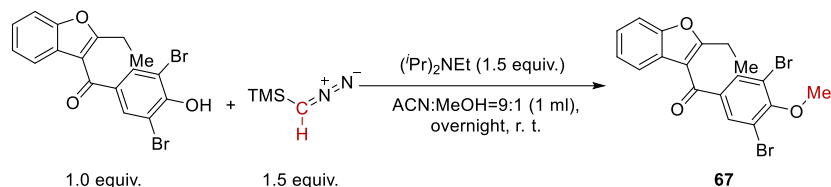
The synthetic protocol for the preparation of **59** was adapted from a literature procedure². 6-ethyl-1,3-benzothiazol-2-amine (446 mg, 2.5 mmol) was weighed into 15 mL glass vial containing a Teflon coated magnetic stir bar. Toluene (15 ml) and acetic anhydride (94.5 μ L, 10.0 equiv.) were added into the flask in sequence. The vial was then capped with a pierceable Teflon cap and the reaction mixture was stirred at 115 °C overnight. The reaction was concentrated under vacuum and the residue was triturated with 5 mL of ethyl acetate and 50 mL of pentane. The product was filtered out and dried. Trituration and filtration were repeated three times and 473 mg off-white non-crystalline powder (86% isolated yield) of **59** (the substrate of **27**) was collected.

Procedure for the preparation of the substrate 66.



The synthetic protocol for the preparation of **62** was adapted from a literature procedure³. 2-[3-(trifluoromethyl)-4,5,6,7-tetrahydro-1H-indazol-1-yl]acetic acid (298 mg, 1.2 mmol) was weighed into 15 mL vial containing a Teflon coated magnetic stir bar. A mixture of acetonitrile and MeOH (9:1, 4.8 mL), followed diisopropylethylamine (0.43 mL, 1.5 equiv.) were added into the vial and the mixture was stirred for 10 min, at which time trimethylsilyldizaomethane (2.0 M Hexane solution, 0.9 mL, 1.5 equiv.) was added dropwise into the reaction mixture. When no obvious bubbling was observed, the vial was capped with a pierceable Teflon cap and the reaction mixture was stirred at room temperature overnight. The reaction mixture was concentrated under vacuum and the residue was purified by column chromatography (pentane:ethyl acetate = 4:1). 255 mg white non-crystalline powder (82% isolated yield) of **60** (the substrate of **28**) was collected.

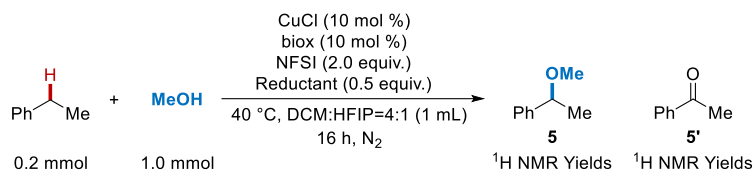
Procedure for the preparation of the substrate 67.



The synthetic protocol for the preparation of **61** was adapted from a literature procedure³. Benzbromarone (1.70 g, 4.0 mmol) was weighed into a 50 mL round bottom flask containing a Teflon coated magnetic stir bar. A mixture of acetonitrile and MeOH (9:1, 16 mL), followed diisopropylethylamine (1.44 mL, 1.5 equiv.) was added into the flask and the mixture was stirred for 10 min, at which time trimethylsilyldizaomethane (2.0 M Hexane solution, 3 mL, 1.5 equiv.) was added dropwise into the reaction mixture. A funnel was placed upside down on top of the flask to minimize the evaporation of the solvent and the reaction mixture was stirred at room temperature overnight. The reaction mixture was concentrated under vacuum and the residue was purified by column chromatography (pentane:ethyl acetate = 4:1). 1.67 g white non-crystalline powder (95% isolated yield) of **61** (the substrate of **34**) was collected.

2A.V. Optimization of the Reaction Conditions

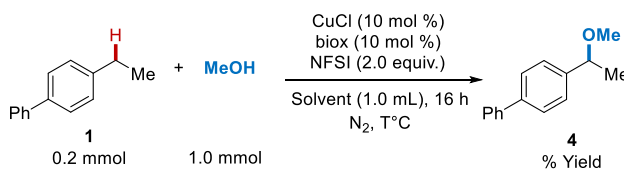
Table 2A.1. Investigation of various reductants with ethylbenzene as the substrate



| Entry | Reductant | Conv. of EtPh (%) | Yield of 3 (%) |
|----------|--|-------------------|-----------------------|
| 1 | (MeO)₂P(O)H | 97 | 80 |
| 2 | (EtO) ₂ P(O)H | 91 | 77 |
| 3 | (ⁱ PrO) ₂ P(O)H | 88 | 73 |
| 4 | (^t BuO) ₂ P(O)H | 34 | 28 |
| 5 | (ⁿ BuO) ₂ P(O)H | 94 | 75 |
| 6 | (MeO) ₂ MeSiH | 79 | 70 |
| 7 | (EtO) ₂ MeSiH | 100 | 62 |
| 8 | PhNHNHPh | 7 | 0 |
| 9 | EtCO ₂ NHNHCO ₂ E t | 94 | 62 |
| 10 | P(ⁿ Bu) ₃ | 37 | 22 |
| 11 | Sodium Ascorbate | 100 | 62 |

^aReaction yields monitored by ¹H NMR spectroscopy with 0.2 mmol mesitylene as the external standard. Conv., conversion.

Table 2A.2. Investigation of dimethylphosphite with 4-ethylbiphenyl as the substrate



| Entry | Additive (0.5 equiv.) | Solvent | T (°C) | Conv. of EtPh (%) | Yield (%) ^a |
|-------|------------------------|--------------------|--------|-------------------|------------------------|
| 1 | — | Benzene | r. t. | 5 | 4 |
| 2 | — | DCM | r. t. | 9 | 9 |
| 3 | (MeO) ₂ POH | DCM | r. t. | 88 | 57 |
| 4 | — | DCM | 40 | 52 | 26 |
| 5 | (MeO) ₂ POH | DCM | 40 | 100 | 70 |
| 6 | — | DCM : HFIP = 4 : 1 | r. t. | 4 | 5 |
| 7 | (MeO) ₂ POH | DCM : HFIP = 4 : 1 | r. t. | 49 | 45 |
| 8 | — | DCM : HFIP = 4 : 1 | 40 | 25 | 23 |
| 9 | (MeO) ₂ POH | DCM : HFIP = 4 : 1 | 40 | 85 | 77 |

^aReaction yields monitored by ¹H NMR spectroscopy with 0.2 mmol mesitylene as the external standard. T, temperature; Conv., conversion.

Table 2A.3a. Ligand Optimization

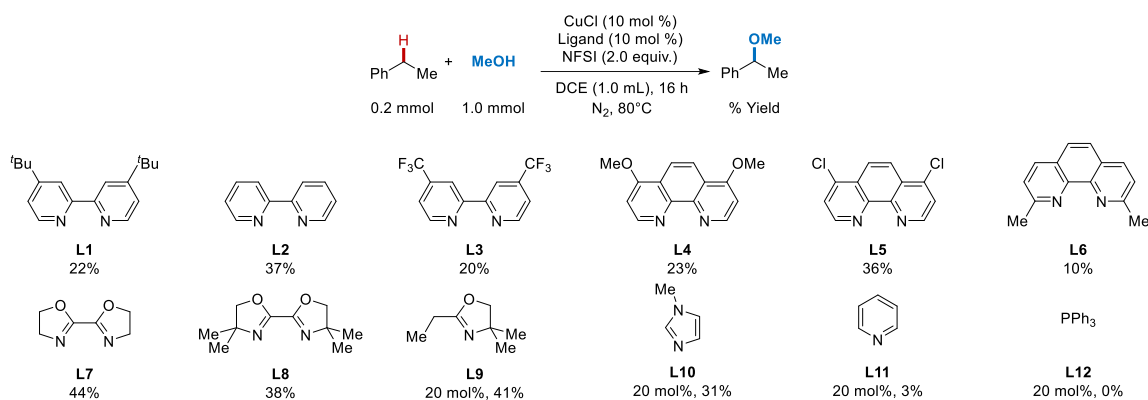


Table 2A.3b. Unsuccessful Ligand Testing for Enantioselective Methoxylation

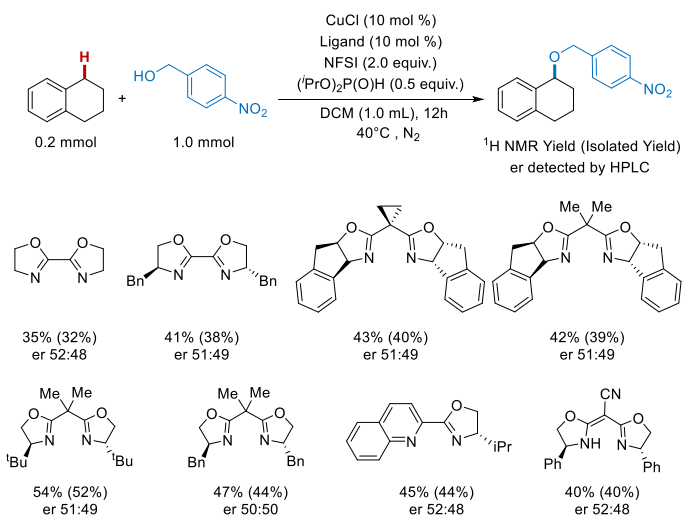
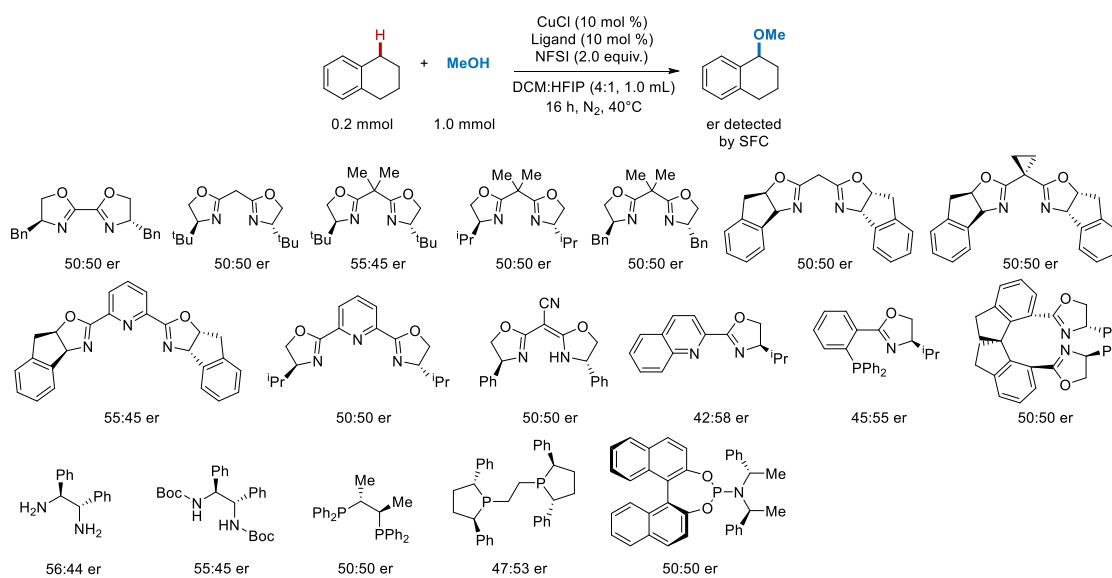
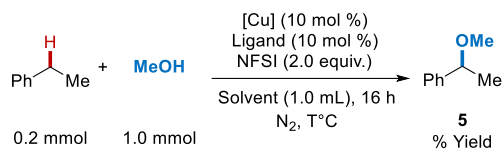
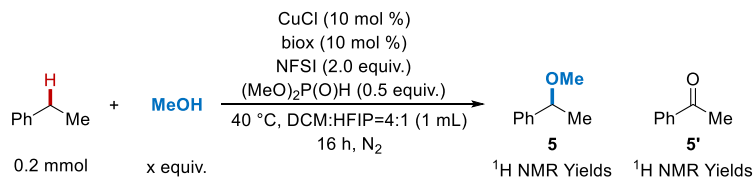


Table 2A.4a. Optimization of the Reaction Conditions with Various Solvents, Cu Salts and Temperature

| Entry | Cu Source | Solvent | T (°C) | Conv. of EtPh (%) | Yield of 5 (%) ^a |
|-----------------------|---|---------------------|-----------|-------------------|------------------------------------|
| 1 | CuCl | DCE | 80 | 56 | 44 |
| 2 | CuBr | DCE | 80 | 64 | 41 |
| 3 | CuCl ₂ | DCE | 80 | 59 | 42 |
| 4 | [Cu(MeCN) ₄]BF ₄ | DCE | 80 | 69 | 40 |
| 5 | CuCl | DMC | 80 | 56 | 33 |
| 6 | CuCl | Benzene | 80 | 59 | 35 |
| 7 | CuCl | EtOAc | 80 | 30 | 17 |
| 8 | CuCl | DCM | 80 | 67 | 49 |
| 9 | CuCl | MeOH | 80 | 16 | 16 |
| 10 | CuCl | HFIP | 80 | 85 | 2 |
| 11 | CuCl | DCM:HFIP=4:1 | 40 | 81 | 72 |
| 12 | CuCl | DCM | 40 | 23 | 23 |
| 13^b | CuCl | DCM:HFIP=4:1 | 40 | 97 | 80 |

^aReaction yields monitored by ¹H NMR spectroscopy with 0.2 mmol mesitylene as the external standard.

^b50 mol % of (MeO)₂P(O)H was added. DCE, 1,2-dichloroethane; DMC, dimethyl carbonate; DCM, dichloromethane; HFIP, hexafluoroisopropanol; T, temperature; Conv., conversion.

Table 2A.4b. Control Experiments with Various Amounts of Methanol

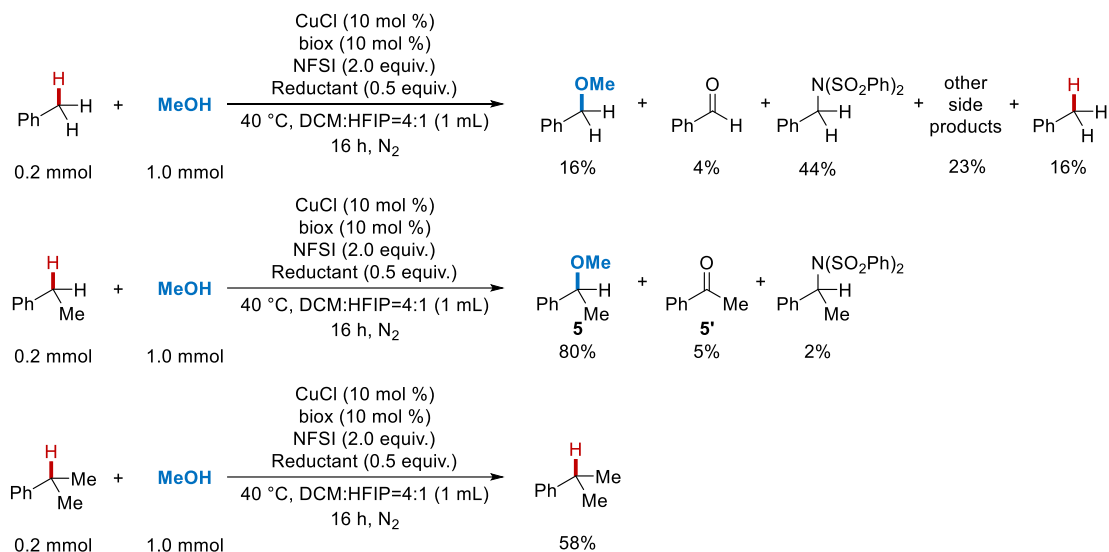
| Entry | Equivalents (X) | Conv. of EtPh (%) | Yield of 5' (%) | Yield of 5 (%) ^a |
|-------|-----------------|-------------------|------------------------|------------------------------------|
| 1 | 5.0 | 100 | 5 | 80 |
| 2 | 3.0 | 94 | 4 | 68 |
| 3 | 2.0 | 79 | 3 | 60 |
| 4 | 1.0 | 100 | 22 | 43 |

^aReaction yields monitored by ¹H NMR spectroscopy with 0.2 mmol mesitylene as the external standard. Conv., conversion.

Table 2A.5. Investigation of various radical initiators/oxidants

| Entry | [O] | Solvent | Temperature (°C) | Conv. of EtPh (%) | Yield of 5 (%) ^a |
|-------|--|----------------|------------------|-------------------|------------------------------------|
| 1 | NFSI | DCM:HFIP = 4:1 | 40 | 97 | 80 |
| 2 | ^t BuOO ^t Bu | DCM:HFIP = 4:1 | 40 | 0 | 0 |
| 3 | ^t BuOOH | DCM:HFIP = 4:1 | 40 | 30 | 0 |
| 4 | ^t BuOOBz | DCM:HFIP = 4:1 | 40 | 15 | 5 |
| 5 | BzOOBz | DCM:HFIP = 4:1 | 40 | 14 | 7 |
| 6 | K ₂ S ₂ O ₈ | DCM:HFIP = 4:1 | 40 | 7 | 2 |
| 7 | Oxone | DCM:HFIP = 4:1 | 40 | 0 | 0 |
| 8 | PhI(OAc) ₂ | DCM:HFIP = 4:1 | 40 | 12 | 5 |
| 9 | PhI(OTFA) ₂ | DCM:HFIP = 4:1 | 40 | 24 | 3 |
| 10 | Selectfluor | DCM:HFIP = 4:1 | 40 | 23 | 11 |
| 11 | NFSI | DCE | 80 | 56 | 44 |
| 12 | ^t BuOO ^t Bu | DCE | 80 | 1 | 1 |
| 13 | ^t BuOOH | DCE | 80 | 37 | 0 |
| 14 | ^t BuOOBz | DCE | 80 | 16 | 0 |
| 15 | BzOOBz | DCE | 80 | 27 | 4 |
| 16 | K ₂ S ₂ O ₈ | DCE | 80 | 5 | 0 |
| 17 | Oxone | DCE | 80 | 6 | 1 |
| 18 | PhI(OAc) ₂ | DCE | 80 | 32 | 2 |
| 19 | PhI(OTFA) ₂ | DCE | 80 | 31 | 5 |
| 20 | Selectfluor | DCE | 80 | 3 | 0 |

^aReaction yields monitored by ¹H NMR spectroscopy with 0.2 mmol mesitylene as the external standard. Conv. conversion.

**Figure 2A.1.** Investigation of the reactivities and chemo-selectivity of primary, secondary and tertiary benzylic C–H substrate

Reaction yields were determined by ^1H NMR spectroscopy with 0.2 mmol mesitylene as the external standard. Toluene shows good reactivity, but poor selectivity. The major product is the coupling product of toluene and $(\text{PhSO}_2)_2\text{N}$ fragment from NFSI, while several other side products were observed. Ethylbenzene shows good reactivity and selectivity. Cumene is much less reactive and the conversion is much lower comparing to toluene and ethylbenzene.

2A.VI. Effects of Phosphite (Time course experiments, UV-Vis and EPR)

The data in Tables 2A.1, 2A.2, and 2A.4a show that phosphite can have a beneficial effect on the reaction yield; however, the magnitude of the effect appears to be substrate dependent. A moderate improvement in yield was observed with ethylbenzene (cf. Table 2A.4a, entries 11 and 13), while a significant improvement was observed upon adding phosphite to the reaction of 4-ethylbiphenyl (e.g., entries 8 and 9, Table 2A.2). In spite of the relatively modest yield improvement with ethylbenzene in the 16 h reaction, monitoring of the reaction time course clearly shows the beneficial effect of added phosphite (Supplementary Fig. 2).

To further corroborate our "redox buffering" hypothesis, we performed a series of UV-Vis and EPR experiments to investigate the copper speciation under catalysis-relevant conditions (Fig. 3). When NFSI is added to a (biox)Cu(Cl) solution, a characteristic absorption at 270 nm was observed in the UV-Vis trace (red trace, Supplementary Fig. 3a), indicating the formation of Cu^{II} species, corroborated by a Cu^{II} signal in the EPR spectrum of the same mixture (red trace, Fig. 3b). Addition of dimethyl phosphite significantly attenuates the UV absorption at 270 nm as well as the observed EPR signal after heating the mixture at 40 °C for 4 h (black and grey traces, Fig. 3a and 3b), suggesting a slow reduction of Cu^{II} to Cu^{I} . These observations in UV-Vis and EPR experiments support that dimethyl phosphite slowly reduces Cu^{II} to Cu^{I} .

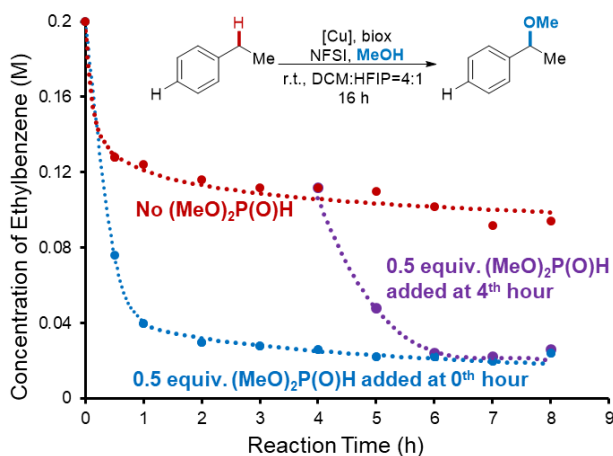


Figure 2A.2. Reaction time course for benzylic etherification conducted in the absence (red) and presence of 0.5 equiv. dimethyl phosphite (blue) as well as when 0.5 equiv. dimethyl phosphite was added at the 4th hour (purple). Reaction conditions: ethylbenzene (0.2 mmol), NFSI (0.4 mmol), MeOH (1.0 mmol), CuCl (0.02 mmol), 2,2'-bioxazoline (0.02 mmol), DCM:HFIP = 4:1 (1 mL), 40°C.

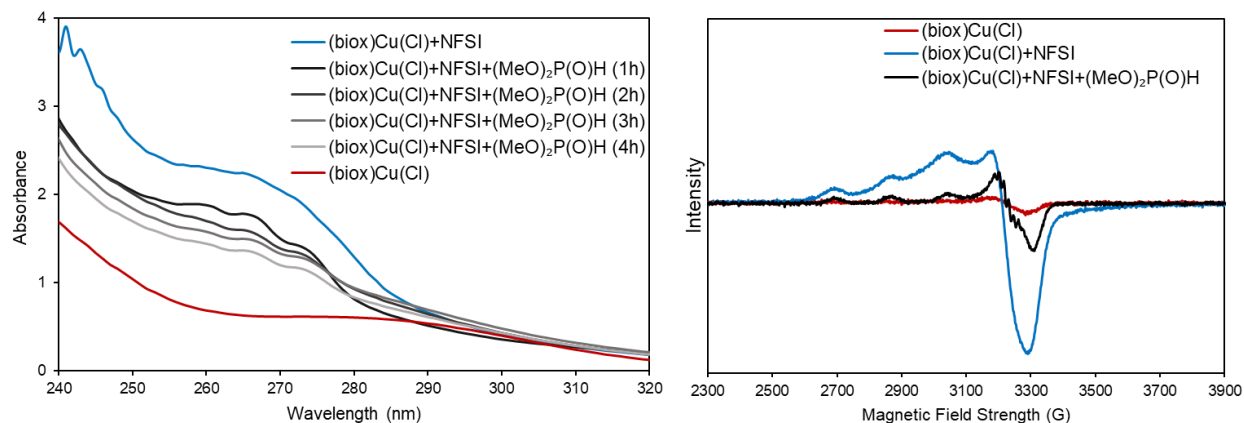


Figure 2A.3. UV-Vis and EPR Experiments to probe the effect of additives on copper speciation. **a**, UV-Vis traces monitoring the reaction of Cu^{II} with dimethyl phosphite and methanol. **b**, EPR experiments investigating the effect of dimethyl phosphite and methanol on Cu^{II} .

Procedure for EPR experiments

Copper(I) chloride (20.0 mg, 0.20 mmol), 4,4',5,5'-tetrahydro-2,2'-bioxazole (28.0 mg, 0.20 mmol,) were weighed into a 10 mL volumetric flask. Then DCM:HFIP = 4:1 as a solvent mixture was added to the graduation marking, followed by the addition of a magnetic stir bar to assist stirring. 1 mL of this stock solution was transferred into 4 mL glass vials containing NFSI (126.1 mg, 0.40 mmol), $(\text{MeO})_2\text{P}(\text{O})\text{H}$ (9.5 μL , 0.10 mmol, 0.5 equiv.), methanol (42 μL , 1.0 mmol, 5.0 equiv.) and an empty vial respectively in the glove box. Magnetic stir bars were added into each one of these four vials and the reaction mixtures were sealed, stirred and heated at 40 °C for 16 h. After that, an aliquot of each solution was transferred into a quartz EPR tube for analysis. All the EPR spectra were acquired with the following parameters: Center: 3100 G; Sweeping width: 3000 G; Attenuation: 30 dB; Number of scans: 4; Number of points: 2048; Conversion time: 10 ms; Temperature: 105 K.

Procedure for UV-Vis experiments

Copper(I) chloride (20.0 mg, 0.20 mmol), 4,4',5,5'-tetrahydro-2,2'-bioxazole (28.0 mg, 0.20 mmol,) were weighed into a 10 mL volumetric flask. Then DCM:HFIP = 4:1 as a solvent mixture was added to the graduation marking, followed by the addition of a magnetic stir bar to assist stirring. 1 mL of this stock solution was transferred into six 4 mL glass vials containing NFSI (126.1 mg, 0.40 mmol) as well as an empty one. $(\text{MeO})_2\text{P}(\text{O})\text{H}$ (9.5 μL , 0.10 mmol, 0.5 equiv.) were added into five of the vials and methanol (42 μL , 1.0 mmol, 5.0 equiv.) was added to the final vial, all in the glove box. Magnetic stir bars were added into each one of these six vials and the reaction mixtures were sealed, stirred and heated at 40 °C for 1-4 h (indicated in the figures). After that, 50 μL of each solution was transferred into a quartz UV-Vis cuvette and diluted with 2.5 mL of DCM:HFIP = 4:1 solvent mixture for analysis.

2A.VII. The Fate of the Dialkyl Phosphites (^{31}P - ^1H coupled NMR)

Dialkyl phosphites are reported to serve as single-electron reductants of Cu^{II} . Chlorinated, fluorinated and methoxylated products were observed in ^{31}P NMR spectrum from a reaction mixture run under standard conditions and worked up via filtration through a silica plug (Supplementary Fig. 4). Only 35% of the starting dimethyl phosphite was converted, consistent with the slow reduction of Cu^{II} observed in the experiments described above. Controlled experiment without ethylbenzene afforded similar product yields and distribution. The loss of P-based material(s) is attributed to retention of polar dimethyl phosphite derivatives in the silica gel. Attempts to characterize the phosphite speciation of reaction mixtures containing paramagnetic Cu salts proved unfruitful

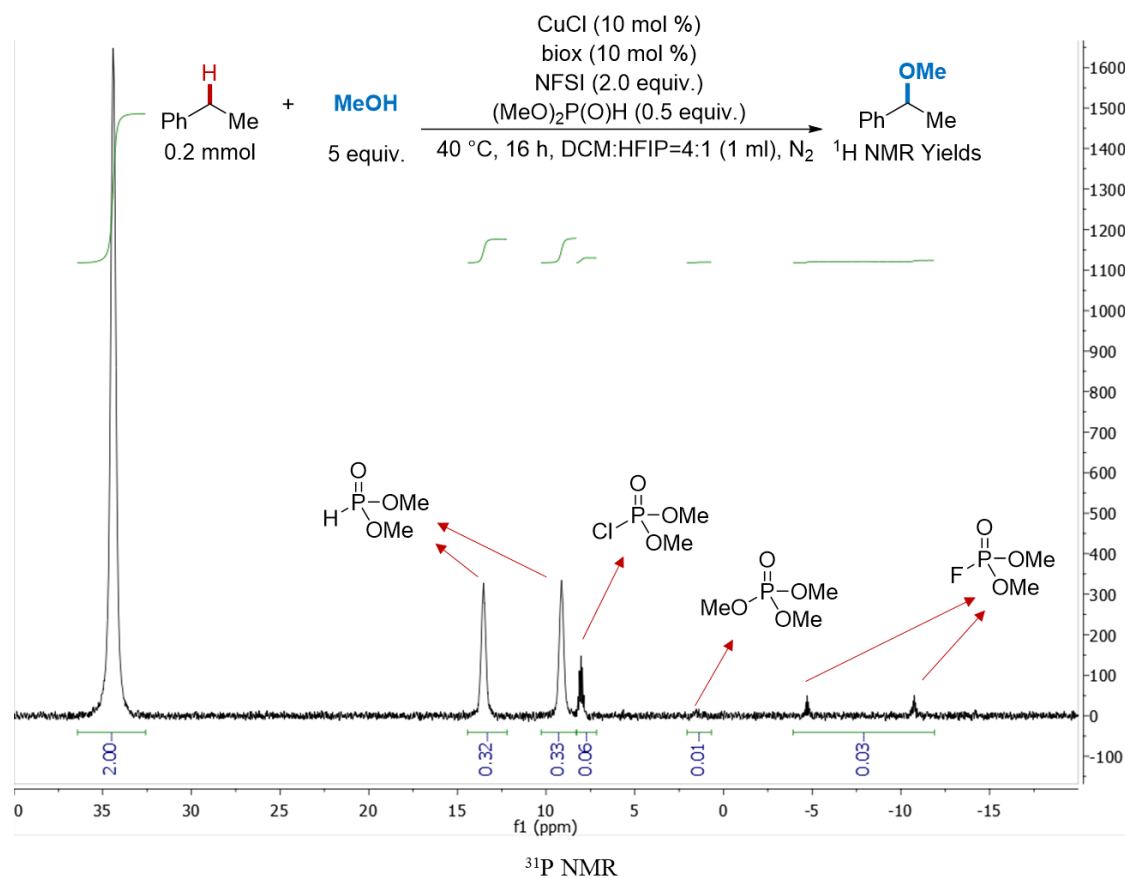
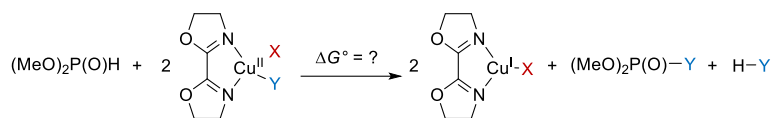
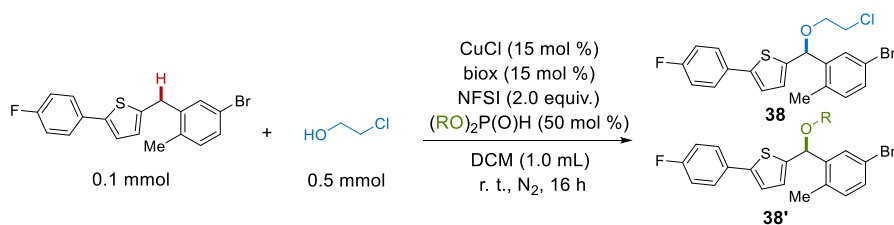


Figure 2A.4. ^{31}P - ^1H coupled NMR spectrum of the reaction mixture of the benzylic C–H methoxylation with 0.2 mmol $\text{Ph}_3\text{P}(\text{O})$ as the internal standard.

DFT calculations suggest that oxidation of $(\text{MeO})_2\text{P}(\text{O})\text{H}$ by $(\text{biox})\text{Cu}^{\text{II}}(\text{Cl})(\text{F})$ is the most thermodynamically favorable, forming a strong P–F bond (Table 2A.6). Thermodynamics remains favorable when $(\text{MeO})_2\text{P}(\text{O})\text{H}$ reduces $(\text{biox})\text{Cu}^{\text{II}}(\text{Cl})(\text{NSI})$ to form either P–N or P–Cl bonds.

Table 2A.6. Energetics of Cu^{II} reduction to Cu^I by (MeO)₂P(O)H

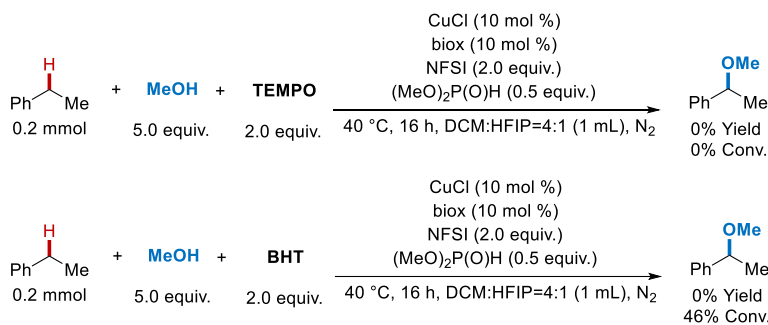
| Entry | (biox)CuXY | X | Y | ΔG° (kcal/mol) |
|-------|------------|-----|-----|-----------------------------|
| 1 | | Cl | F | -45.2 |
| 2 | | F | Cl | +1.5 |
| 3 | | Cl | NSI | -24.5 |
| 4 | | NSI | Cl | -11.0 |

Table 2A.7. Investigation of various phosphites with a canagliflozin precursor

| Entry | Additive | Conv. of the substrate (%) ^a | Yield of 38' (%) ^a | Yield of 38 (%) ^a |
|-------|--|---|--------------------------------------|-------------------------------------|
| 1 | (MeO) ₂ P(O)H | 83 | 18 | 64 |
| 2 | (EtO) ₂ P(O)H | 92 | 8 | 81 |
| 3 | (ⁱ PrO) ₂ P(O)H | 95 | 2 | 92 |
| 4 | (^t BuO) ₂ P(O)H | 94 | 8 | 84 |
| 5 | (BnO) ₂ P(O)H | 92 | 13 | 76 |
| 6 | (CF ₃ CH ₂ O) ₂ P(O)H | 69 | 3 | 59 |
| 7 | (^t BuO) ₂ P(O)H | 68 | 3 | 65 |
| 8 | - | 23 | - | 23 |

^aCalibrated ¹H NMR yields using dibromomethane as the internal standard. Conv., conversion.

2A.VIII. Radical trap experiments

Table 2A.8. Control Experiments with Radical Traps

The reactions were set up following the standard procedure, with TEMPO (62.4 mg, 0.4 mmol) and BHT (88.1 mg, 0.4 mmol) weighed into the glass vials respectively before the vials were charged with nitrogen.

2A.IX. Control experiments with various alcohols

Table 2A.9. Investigation of ethylbenzene cross-coupling with various alcohols

| Entry | R | Conv. of EtPh (%) | Yield of 3' (%) | Yield of C-O'Pr (%) | Yield of C-OH (%) | Yield of C-NSI (%) | Yield of C-OR (%) |
|-------|------------------------------------|-------------------|-----------------|---------------------|-------------------|--------------------|-------------------|
| 1 | Me | 88 | 5 | 3 | 0 | 3 | 73 |
| 2 | Et | 82 | 4 | 3 | 0 | 3 | 47 |
| 3 | <i>i</i> Pr | 82 | 5 | - | 0 | 9 | 54 |
| 4 | <i>t</i> Bu | 95 | 6 | 5 | 14 | 22 | 0 |
| 5 | (CF ₃) ₂ CH | 70 | 3 | 0 | 11 | 12 | 0 |

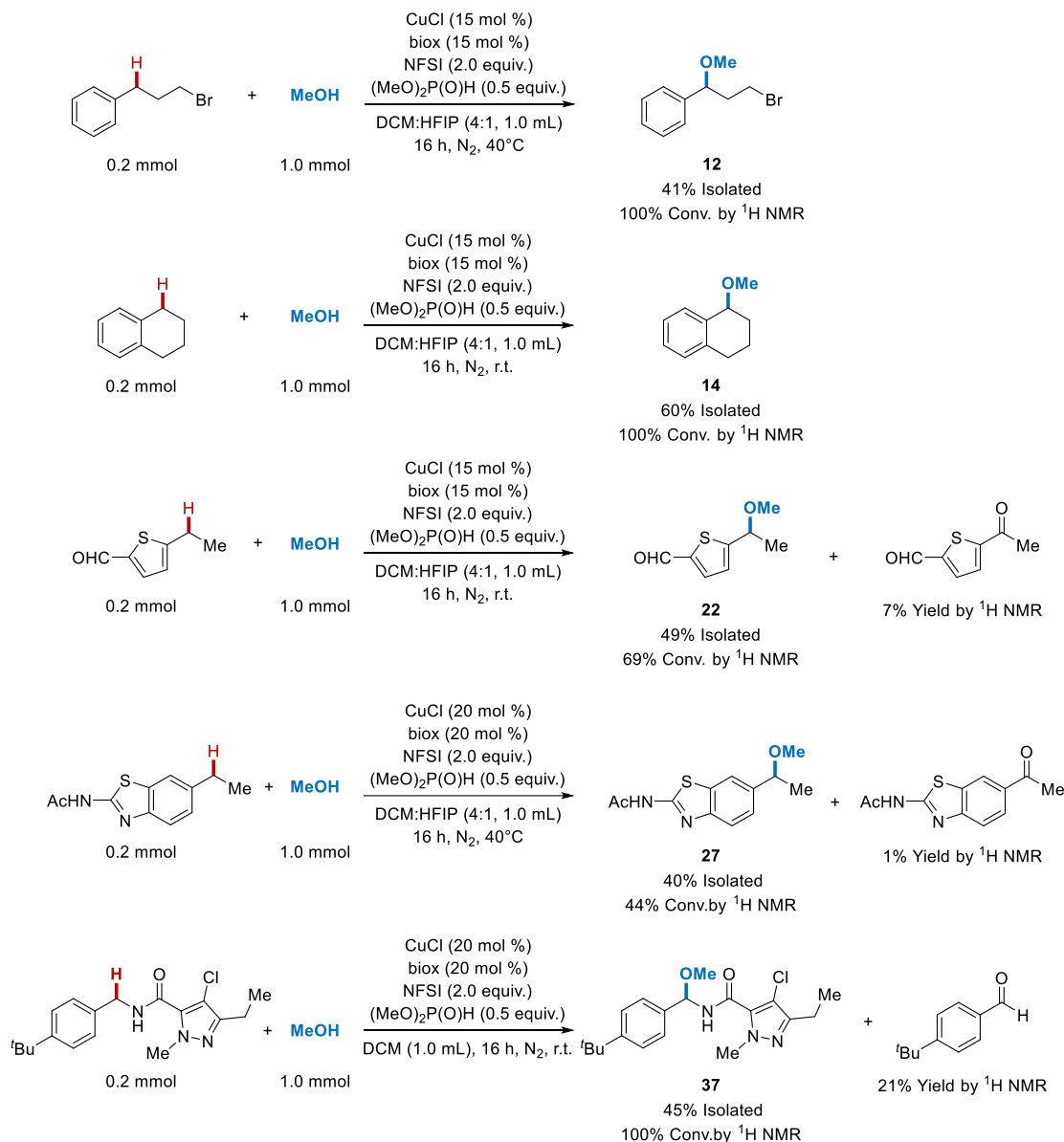
Table 2A.10. Competition experiments in ethylbenzene etherification

| Entry | R ¹ | R ² | Conv. of EtPh (%) | Yield of C-NSI (%) | Yield of C-OR ¹ (%) | Yield of C-OR ² (%) |
|-------|---------------------------------|---------------------------------|-------------------|--------------------|--------------------------------|--------------------------------|
| 1 | Me | Et | 84 | 4 | 25 | 30 |
| 2 | Me | <i>i</i> Pr | 73 | 6 | 28 | 19 |
| 3 | Et | <i>i</i> Pr | 67 | 16 | 30 | 17 |
| 4 | Et | CF ₃ CH ₂ | 86 | 2 | 39 | 31 |
| 5 | Et | <i>i</i> PrCH ₂ | 80 | 4 | 30 | 25 |
| 6 | CF ₃ CH ₂ | <i>i</i> PrCH ₂ | 91 | 2 | 39 | 39 |

Alcohols with various steric bulk and electronic profiles were evaluated with ethylbenzene as the benzylic C–H substrate to probe the nature of the bond-forming step. In independent reactions, both ethanol and isopropanol gave moderate yields of the benzyl ethers, whereas *tert*-butanol failed to undergo effective coupling. Formation of sulfonimidated product becomes increasingly favorable with increased steric bulk of the alcohol coupling partner. Competitions between methanol, ethanol and isopropanol afforded similar yields of the corresponding ethers in each reaction. On the other hand, trifluoroethanol and isobutanol, with similar steric bulk but drastically different electronics, showed comparable yields. These data support a radical/polar crossover mechanism, where benzylic cations are generated via the oxidation of benzylic radicals.

2A.X. Further analyses of reaction outcomes of benzylic C–H etherification reactions

Table 2A.11. Analyses of mass balances of benzylic C–H etherification reactions

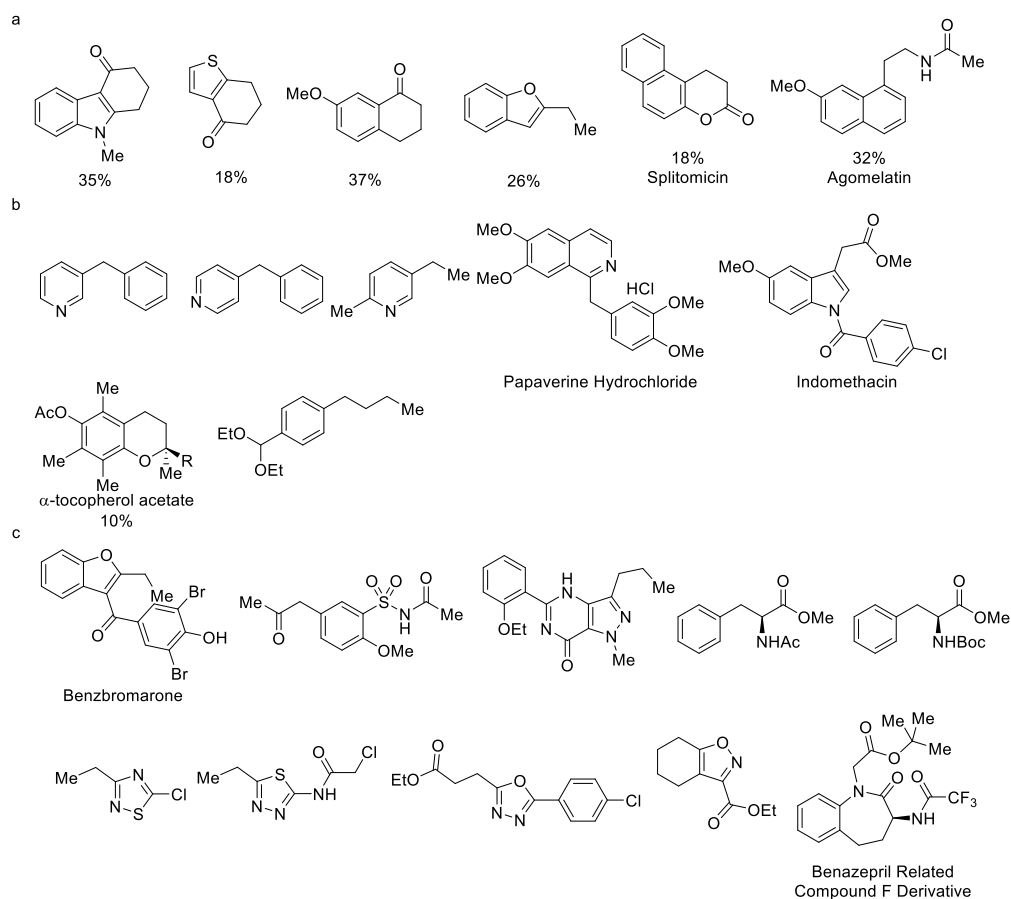


A selection of benzylic substrates were further analyzed to insight the mass balance of this benzylic C–H etherification. No undesired substitution at Br was observed with **12**. Bis-methoxylation product has not been detected with any substrate that has more than one benzylic C–H sites, for example, **14**. In the cases of **22** and **27**, significant amounts of starting materials were observed after the reactions were terminated. More forcing conditions only led to the formation of more side products, for example, ketones in the case of **22** and **27** as well as the aldehyde in the case of **37**, but not higher yields of the desired products.

Unsuccessful Substrates.

Not all substrates tested were effective in the benzylic etherification reaction. The substrates in Table 2A.12 afford methyl ethers in < 40% yield, based on analysis of the crude reaction mixture by ^1H NMR spectroscopy (Supplementary Table 12a). An elimination product was observed in the case of splitomicin. Substrates in Table 2A.12b generally underwent high conversion but led to low-to-negligible yields of the desired products. Pyridines, quinoline and pyrimidine derivatives have been reported to react directly with NFSI⁴ and no desirable methoxylated product was observed under all the reaction conditions tested. Substrates in Table 2A.12c are rather inactive, giving low conversions and low yields. Substrates with free phenols or acidic N–H groups suffered from low conversion, possibly reflecting inhibition by coordination to Cu or quenching of reactive radicals (in the case of phenols). Free carboxylic acids and amines are known to undergo side reactions⁵⁻⁶⁷ and are therefore incompatible with this reaction unless suitably modified. Sites adjacent to electron-deficient heterocycles were generally unreactive, and unreacted starting material was observed with the substrates in Table 2A.12c.

Table 2A.12. Unsuccessful substrates in benzylic C-H methoxylation



2A.XI. KIE Experiments

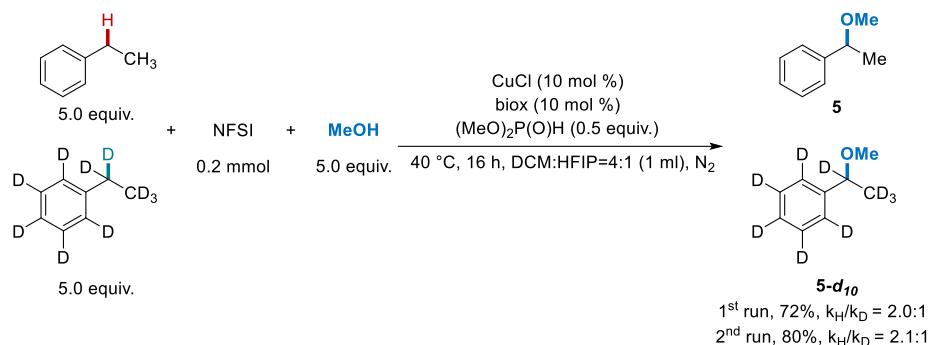


Figure 2A.5. Intermolecular Competition Kinetic Isotopic Effect

Procedure: Copper(I) chloride (2.0 mg, 0.020 mmol, 10 mol%), 4,4',5,5'-tetrahydro-2,2'-bioxazole (2.8 mg, 0.020 mmol, 10 mol%) and NFSI (63.6 mg, 0.20 mmol, 1.0 equiv.) were weighed into a 4 mL glass vial containing a magnetic stir bar. Then the vial was capped with a pierceable Teflon cap. A needle was pierced through the cap to facilitate exchange of the vial headspace with the atmosphere. The vial was moved into a glove box, through three vacuum-nitrogen-backfill cycles. The needle was removed, and the vial was taken out of the glove box (now sealed under an inert gas). DCM (0.8 mL), HFIP (0.2 mL), ethylbenzene-*d*₁₀ (122.5 μ L, 1.0 mmol, 5.0 equiv.), ethylbenzene (122.5 μ L, 1.0 mmol, 5.0 equiv.), methanol (42 μ L, 1.0 mmol, 5.0 equiv.) and dimethyl phosphonate (9.5 μ L, 0.10 mmol, 0.5 equiv.) were added into the vial by injection through the cap. The sealed vial was heated at 40 °C and stirred for 16 h. When the reaction finished, the mixture was cooled down to room temperature. The mixture was quenched by a silica plug and an aliquot was taken into an NMR tube, which was diluted to the volume suitable for crude ¹H NMR analysis.

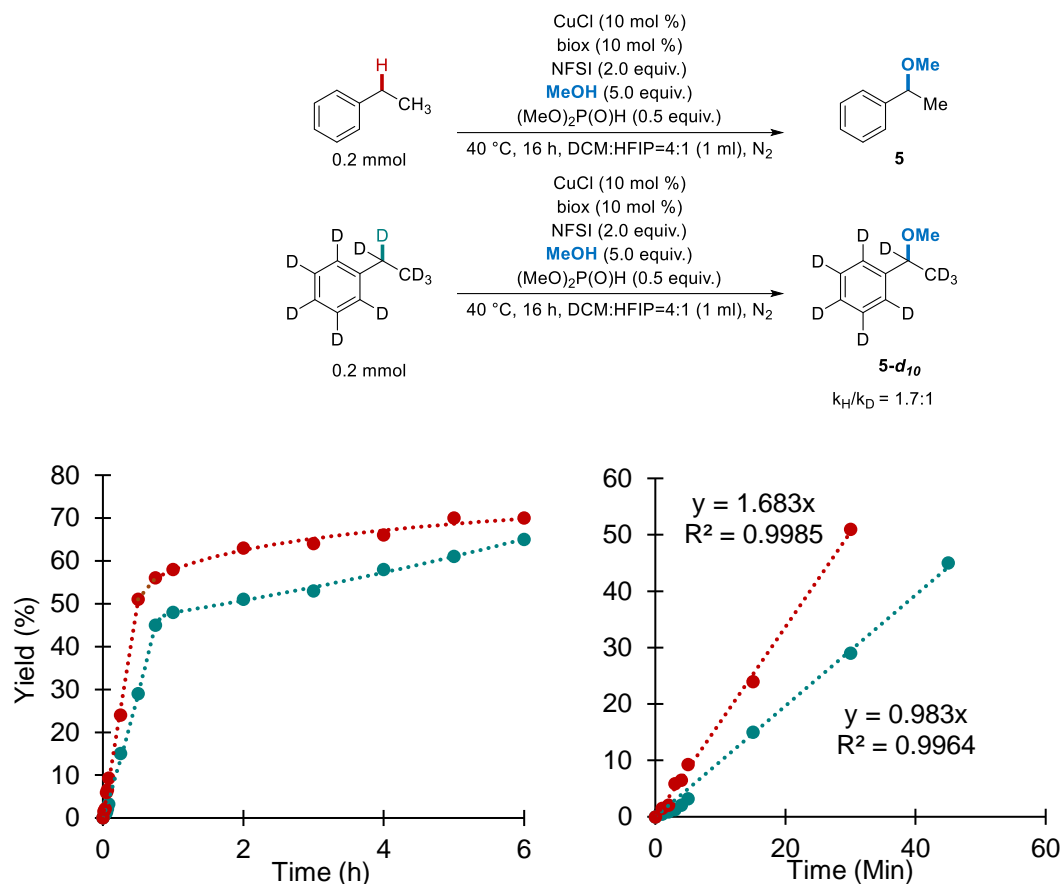


Figure 2A.6. Independent Kinetic Isotopic Effect

Procedure: Copper(I) chloride (2.0 mg, 0.020 mmol, 10 mol%), 4,4',5,5'-tetrahydro-2,2'-bioxazole (2.8 mg, 0.020 mmol, 10 mol%) and NFSI (126.1 mg, 0.40 mmol, 2.0 equiv.) were weighed into a 4 mL glass vial containing a magnetic stir bar. Then the vial was capped with a pierceable Teflon cap. A needle was pierced through the cap to facilitate exchange of the vial headspace with the atmosphere. The vial was moved into a glove box, through three vacuum-nitrogen-backfill cycles. The needle was removed, and the vial was taken out of the glove box (now sealed under an inert gas). The vials were kept at 40 °C in the heating block on a hot plate. A stock solution of ethylbenzene (24.5 μ L, 0.2 mmol, 1.0 equiv.), methanol (42 μ L, 1.0 mmol, 5.0 equiv.) and dimethyl phosphonate (9.5 μ L, 0.10 mmol, 0.5 equiv.) in DCM:HFIP = 4:1 was prepared and maintained at 40 °C in a water bath. 1 mL of the stock solution was added into each reaction vial by injection through the cap. The sealed vial was heated at 40 °C and stirred. The reaction mixture was cooled in a dry ice-isopropanol bath after the reaction has been run for a certain amount of time. The mixture was then through a silica plug and an aliquot was taken into an NMR tube, which was diluted to the volume suitable for crude ¹H NMR analysis. Reactions were stopped at 1, 2, 3, 4, 5, 15, 30 and 45 minutes to study the initial rates of the methoxylation of ethylbenzene and ethylbenzene-*d*₁₀.

2A.XII. Methods for HPLC/SFC Chiral Separation

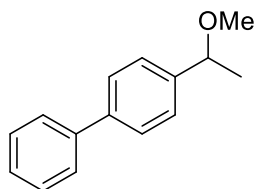
HPLC

A Daicel CHIRALPAK® AS-H column (4.6 mm × 250 mm, 5 μm PS) was used for separations. The eluent was a mixture (gradient, 95:5 to 50:50 hexanes/*i*PrOH, 20 min) with a flow rate of 1 mL/min at 25 °C.

SFC

A Daicel CHIRALPAK® IA column (3 mm ID × 150 mm, 3 μm PS) was used for separations. The eluent was a mixture (99:1 CO₂/*i*PrOH) with a flow rate of 2 mL/min at 40 °C with ABPR at 1500 psi.

2A.XIII. Characterization of Compounds

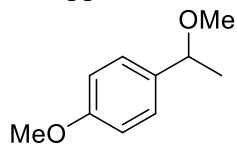


4-(1-methoxyethyl)-1,1'-biphenyl, **4**. Characterization data matched those previously reported⁸.

Reaction run at 0.4 mmol scale and 73.8 mg (87%) of colorless liquid isolated.

¹H NMR (CDCl₃, 400 MHz): 7.62 – 7.55 (m, 4H), 7.44 (t, *J* = 7.5 Hz, 2H), 7.38 (d, *J* = 8.0 Hz, 2H), 7.34 (t, *J* = 7.4 Hz, 1H), 4.35 (q, *J* = 6.5 Hz, 1H), 3.26 (s, 3H), 1.48 (d, *J* = 6.4 Hz, 3H) ppm.

¹³C NMR (CDCl₃, 100 MHz): 142.6, 141.0, 140.4, 128.8, 127.2 (2C), 127.1, 126.6, 79.4, 56.5, 23.9 ppm.

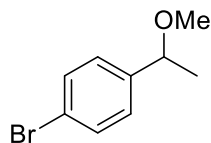


1-methoxy-4-(1-methoxyethyl)benzene, **6**. Characterization data matched those previously reported⁹.

Reaction run at 0.4 mmol scale and 45.9 mg (69%) of colorless liquid isolated.

¹H NMR (CDCl₃, 400 MHz): 7.23 (d, *J* = 8.5 Hz, 1H), 6.89 (d, *J* = 8.6 Hz, 1H), 4.25 (q, *J* = 6.4 Hz, 1H), 3.80 (s, 3H), 3.19 (s, 3H), 1.42 (d, *J* = 6.4 Hz, 3H) ppm.

¹³C NMR (CDCl₃, 100 MHz): 159.0, 135.5, 127.4, 113.8, 79.1, 56.2, 55.3, 23.8 ppm.

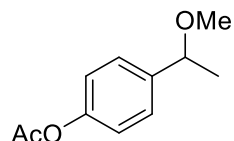


1-bromo-4-(1-methoxyethyl)benzene, **7**. Characterization data matched those previously reported⁵.

Reaction run at 0.2 mmol scale and 28.4 mg (66%) of colorless liquid isolated.

¹H NMR (CDCl₃, 400 MHz): 7.47 (d, *J* = 8.4 Hz, 2H), 7.19 (d, *J* = 8.5 Hz, 2H), 4.26 (q, *J* = 6.5 Hz, 1H), 3.21 (s, 3H), 1.40 (t, *J* = 6.5 Hz, 3H) ppm.

¹³C NMR (CDCl₃, 100 MHz): 142.6, 131.6, 127.9, 121.2, 79.0, 56.5, 23.8 ppm.



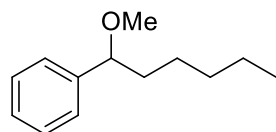
4-(1-methoxyethyl)phenyl acetate, **8**.

Reaction run at 0.4 mmol scale and 46.6 mg (60%) of colorless liquid isolated.

^1H NMR (CDCl_3 , 400 MHz): 7.31 (d, $J = 8.4$ Hz, 2H), 7.06 (d, $J = 8.5$ Hz, 2H), 4.29 (q, $J = 6.5$ Hz, 1H), 3.22 (s, 3H), 2.30 (s, 3H), 1.42 (d, $J = 6.4$ Hz, 3H) ppm.

^{13}C NMR (CDCl_3 , 100 MHz): 169.5, 149.9, 141.1, 127.2, 121.5, 79.1, 56.5, 23.9, 21.2 ppm.

HRMS Calculated for $[\text{C}_{11}\text{H}_{14}\text{O}_3 + \text{NH}_4]^+$: 212.1281, Found: 212.1278.



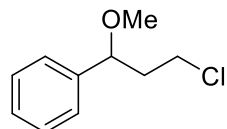
(1-methoxyhexyl)benzene, **10**.

Reaction run at 0.4 mmol scale and 53.8 mg (70%) of colorless liquid isolated.

^1H NMR (CDCl_3 , 400 MHz): 7.38 – 7.31 (m, 2H), 7.31 – 7.24 (m, 3H), 4.07 (dd, $J = 7.3, 6.0$ Hz, 1H), 3.20 (s, 3H), 1.86 – 1.72 (m, 1H), 1.67 – 1.55 (m, 1H), 1.46 – 1.33 (m, 1H), 1.32 – 1.16 (m, 5H), 0.86 (t, $J = 6.9$ Hz, 3H) ppm.

^{13}C NMR (CDCl_3 , 100 MHz): 142.6, 128.3, 127.4, 126.7, 84.2, 56.6, 38.2, 31.8, 25.5, 22.6, 14.1 ppm.

HRMS (ASAP-MS) Calculated for $[\text{C}_{13}\text{H}_{20}\text{O} - \text{OMe}]^+$: 161.1325, Found: 161.1323.

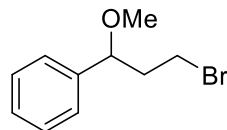


(3-chloro-1-methoxypropyl)benzene, **11**.

Reaction run at 0.4 mmol scale and 37.7 mg (51%) of colorless liquid isolated. Characterization data matched those previously reported¹⁰.

^1H NMR (CDCl_3 , 400 MHz): 7.40 – 7.34 (m, 2H), 7.33 – 7.27 (m, 3H), 4.37 (dd, $J = 8.5, 4.8$, 1H), 3.71 (ddd, $J = 10.8, 8.1, 5.6$, 1H), 3.50 (ddd, $J = 10.8, 5.9$, 1H), 3.23 (s, 3H), 2.23 (ddt, $J = 14.2, 8.4, 5.7$ Hz, 1H), 2.01 (dddd, $J = 14.3, 8.1, 6.0, 4.9$ Hz, 1H) ppm.

^{13}C NMR (CDCl_3 , 100 MHz): 141.2, 128.6, 127.9, 126.6, 80.4, 56.8, 41.7, 40.9 ppm.

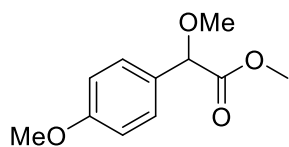


(3-bromo-1-methoxypropyl)benzene, **12**. Characterization data matched those previously reported¹¹.

Reaction run at 0.4 mmol scale and 37.7 mg (41%) of colorless liquid isolated.

^1H NMR (CDCl_3 , 400 MHz): 7.40 – 7.34 (m, 2H), 7.33 – 7.27 (m, 3H), 4.35 (dd, $J = 8.4, 4.8$ Hz, 1H), 3.61 – 3.52 (m, 1H), 3.41 – 3.33 (m, 1H), 3.24 (s, 3H), 2.36 – 2.26 (m, 1H), 2.15 – 2.04 (m, 1H) ppm.

^{13}C NMR (CDCl_3 , 100 MHz): 141.1, 128.6, 127.9, 126.6, 81.4, 56.9, 41.1, 30.3 ppm.

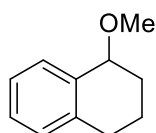


methyl 2-methoxy-2-(4-methoxyphenyl)acetate, **13**. Characterization data matched those previously reported¹².

Reaction run at 0.4 mmol scale and 74.8 mg (89%) of colorless liquid isolated.

¹H NMR (CDCl₃, 400 MHz): 7.36 (d, *J* = 8.6 Hz, 2H), 6.90 (d, *J* = 8.8 Hz, 2H), 4.72 (s, 1H), 3.80 (s, 3H), 3.72 (s, 3H), 3.38 (s, 3H) ppm.

¹³C NMR (CDCl₃, 100 MHz): 171.4, 160.0, 128.6, 128.2, 114.1, 82.1, 57.1, 55.3, 52.3 ppm.

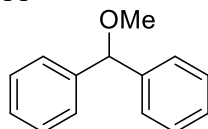


1-methoxy-1,2,3,4-tetrahydronaphthalene, **14**. Characterization data matched those previously reported¹³.

Reaction run at 0.4 mmol scale and 38.9 mg (60%) of colorless liquid isolated.

¹H NMR (CDCl₃, 400 MHz): 7.38 – 7.31 (m, 1H), 7.22 – 7.14 (m, 1H), 7.12 – 7.06 (m, 1H), 4.31 (t, *J* = 4.7 Hz, 1H), 2.83 (dt, *J* = 16.8, 5.7 Hz, 1H), 2.71 (ddd, *J* = 16.7, 8.3, 6.0 Hz, 1H), 2.07 – 1.93 (m, 2H), 1.93 – 1.83 (m, 1H), 1.79 – 1.67 (m, 1H) ppm.

¹³C NMR (CDCl₃, 100 MHz): 137.5, 136.6, 129.3, 129.0, 127.5, 125.7, 76.8, 56.2, 29.1, 27.4, 18.7 ppm.

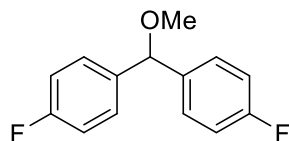


(methoxymethylene)dibenzene, **15**. Characterization data matched those previously reported¹⁴.

Reaction run at 0.4 mmol scale and 63.4 mg (80%) of colorless liquid isolated.

¹H NMR (CDCl₃, 400 MHz): 7.37–7.28 (m, 8H), 7.26 – 7.21 (m, 2H), 5.24 (s, 1H), 3.38 (s, 3H) ppm.

¹³C NMR (CDCl₃, 100 MHz): 142.1, 128.4, 127.5, 126.9, 85.5, 57.1 ppm.



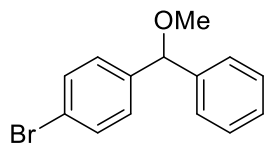
4,4'-(methoxymethylene)bis(fluorobenzene), **16**. Characterization data matched those previously reported¹⁵.

Reaction run at 0.4 mmol scale and 71.2 mg (76%) of colorless liquid isolated.

¹H NMR (CDCl₃, 400 MHz): 7.31 – 7.24 (m, 4H), 7.05 – 6.97 (m, 4H), 5.20 (s, 1H), 3.35 (s, 3H) ppm.

¹³C NMR (CDCl₃, 100 MHz): 162.2 (d, *J* = 244.3 Hz), 137.7 (d, *J* = 3.2 Hz), 128.5 (d, *J* = 8.1 Hz), 115.3 (d, *J* = 21.3 Hz), 84.0, 56.9 ppm.

¹⁹F NMR (377 MHz, CDCl₃): -114.9 ppm.

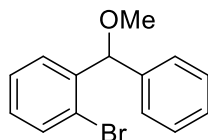


1-bromo-4-(methoxy(phenyl)methyl)benzene, **17**. Characterization data matched those previously reported¹⁶.

Reaction run at 0.4 mmol scale and 84.3 mg (76%) of colorless liquid isolated.

¹H NMR (CDCl₃, 400 MHz): 7.44 (d, *J* = 8.4 Hz, 2H), 7.35 – 7.24 (m, 5H), 7.22 (dd, *J* = 8.6, 0.6 Hz, 2H), 5.19 (s, 1H), 3.36 (s, 3H) ppm.

¹³C NMR (CDCl₃, 100 MHz): 141.5, 141.3, 131.5, 128.6, 128.6, 127.8, 126.9, 121.4, 84.7, 57.0 ppm.

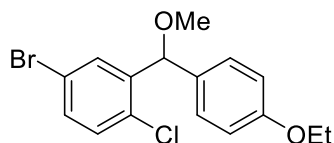


1-bromo-2-(methoxy(phenyl)methyl)benzene, **18**. Characterization data matched those previously reported¹⁷.

Reaction run at 0.4 mmol scale and 59.9 mg (54%) of colorless liquid isolated.

¹H NMR (CDCl₃, 400 MHz): 7.56 – 7.50 (m, 2H), 7.42 – 7.37 (m, 2H), 7.35 – 7.29 (m, 3H), 7.28 – 7.22 (m, 1H), 7.12 (td, *J* = 7.6, 1.7 Hz, 1H), 5.67 (s, 1H), 3.39 (s, 3H) ppm.

¹³C NMR (CDCl₃, 100 MHz): 141.0, 140.5, 132.8, 129.0, 128.5, 128.4, 127.8, 127.7, 127.4, 123.6, 83.5, 57.2 ppm.



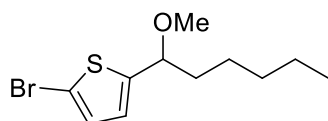
4-bromo-1-chloro-2-((4-ethoxyphenyl)(methoxy)methyl)benzene, **19**.

Reaction run at 0.2 mmol scale and 112 mg (79%) of colorless liquid isolated.

¹H NMR (CDCl₃, 400 MHz): 7.75 (d, *J* = 2.4 Hz, 1H), 7.31 (dd, *J* = 8.5, 2.5 Hz, 1H), 7.25 (d, *J* = 8.7 Hz, 2H), 7.18 (d, *J* = 8.5 Hz, 1H), 6.85 (d, *J* = 8.7 Hz, 2H), 5.52 (s, 1H), 4.01 (q, *J* = 7.0 Hz, 2H), 3.36 (s, 3H), 1.39 (t, *J* = 7.0 Hz, 3H) ppm.

¹³C NMR (CDCl₃, 100 MHz): 158.7, 142.0, 131.7, 131.5, 131.5, 130.9, 130.6, 128.8, 121.0, 114.4, 80.8, 63.4, 57.0, 14.8 ppm.

HRMS (ASAP-MS) Calculated for [C₁₆H₁₆BrClO₂-OMe]⁺: 322.9833, Found: 322.9832.



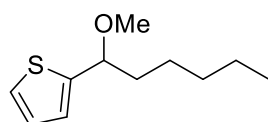
2-bromo-5-(1-methoxyhexyl)thiophene, **20**.

Reaction run at 0.4 mmol scale and 72.1 mg (65%) of colorless liquid isolated.

^1H NMR (CDCl_3 , 400 MHz): 6.90 (d, $J = 3.7$ Hz, 1H), 6.70 (d, $J = 3.7$ Hz, 1H), 4.25 (t, $J = 6.8$ Hz, 1H), 3.26 (s, 3H), 1.91 – 1.78 (m, 1H), 1.67 (m, 1H), 1.46 – 1.17 (m, 6H), 0.87 (t, $J = 6.9$ Hz, 3H) ppm.

^{13}C NMR (CDCl_3 , 100 MHz): 148.3, 129.0, 125.6, 111.6, 79.8, 56.5, 38.1, 31.6, 25.4, 22.5, 14.0 ppm.

HRMS Calculated for $[\text{C}_{11}\text{H}_{17}\text{BrOS}+\text{Na}]^+$: 299.0076, Found: 299.0074.



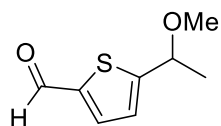
2-(1-methoxyhexyl)thiophene, **21**.

Reaction run at 0.4 mmol scale and 40.5 mg (51%) of colorless liquid isolated.

^1H NMR (CDCl_3 , 400 MHz): 7.30 – 7.23 (m, 1H), 7.01 – 6.92 (m, 2H), 4.35 (t, $J = 6.8$ Hz, 1H), 3.25 (s, 3H), 1.99 – 1.84 (m, 1H), 1.72 (m, 1H), 1.49 – 1.34 (m, 1H), 1.33 – 1.23 (m, 5H), 0.87 (t, $J = 6.7$ Hz, 3H) ppm.

^{13}C NMR (CDCl_3 , 100 MHz): 146.4, 126.2, 125.2, 124.8, 79.5, 56.4, 38.3, 31.6, 25.5, 22.6, 14.0 ppm.

HRMS Calculated for $[\text{C}_{11}\text{H}_{18}\text{OS}+\text{Na}]^+$: 221.0971, Found: 221.0969.



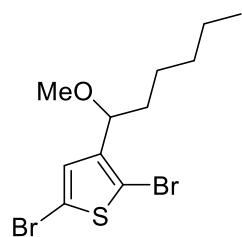
5-(1-methoxyethyl)thiophene-2-carbaldehyde, **22**.

Reaction run at 0.4 mmol scale and 33.4 mg (49%) of yellow liquid isolated.

^1H NMR (CDCl_3 , 400 MHz): 9.88 (s, 1H), 7.66 (d, $J = 3.8$ Hz, 1H), 7.07 (dd, $J = 3.8, 0.7$ Hz, 1H), 4.59 (qd, $J = 6.5, 0.7$ Hz, 1H), 3.33 (s, 3H), 1.55 (d, $J = 6.5$ Hz, 3H) ppm.

^{13}C NMR (CDCl_3 , 100 MHz): 183.0, 158.0, 142.7, 136.3, 125.1, 75.2, 56.8, 23.6 ppm.

HRMS Calculated for $[\text{C}_8\text{H}_{10}\text{O}_2\text{S}+\text{H}]^+$: 171.0474, Found: 171.0473.



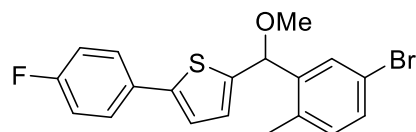
2,5-dibromo-3-(1-methoxyhexyl)thiophene, **23**.

Reaction run at 0.2 mmol scale and 52.6 mg (74%) of colorless liquid isolated.

^1H NMR (CDCl_3 , 400 MHz): 8.43 (d, $J = 7.8$ Hz, 1H), 8.24 (s, 1H), 6.88 (s, 1H), 4.23 (dd, $J = 7.2$, 6.4 Hz, 1H), 3.20 (s, 3H), 1.76 (dddd, $J = 13.4$, 9.8, 7.2, 5.2 Hz, 1H), 1.57 (dddd, $J = 13.4$, 10.0, 6.4, 5.3 Hz, 1H), 1.42 – 1.19 (m, 6H), 0.87 (t, $J = 6.8$ Hz, 3H) ppm.

^{13}C NMR (CDCl_3 , 100 MHz): 143.4, 128.8, 111.5, 109.4, 78.2, 56.8, 36.2, 31.6, 25.1, 22.6, 14.1 ppm.

HRMS Calculated for $[\text{C}_{11}\text{H}_{16}\text{Br}_2\text{OS}+\text{Na}]^+$: 376.9181, Found: 376.9180.



2-((5-bromo-2-methylphenyl)(methoxy)methyl)-5-(4-fluorophenyl)thiophene, **24**.

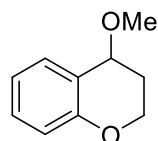
Reaction run at 0.4 mmol scale and 65.7 mg (84%) of white non-crystalline powder isolated.

^1H NMR (CDCl_3 , 400 MHz): 7.72 (d, $J = 2.2$ Hz, 1H), 7.53 – 7.46 (m, 2H), 7.34 (dd, $J = 8.1$, 2.2 Hz, 1H), 7.07 – 6.99 (m, 4H), 6.75 (dd, $J = 3.6$, 0.8 Hz, 1H), 5.51 (s, 1H), 3.41 (s, 3H), 2.24 (s, 3H) ppm.

^{13}C NMR (CDCl_3 , 100 MHz): 162.3 (d, $J = 245.7$ Hz), 143.8, 143.7, 141.2, 134.5, 132.3, 130.8, 130.5 (d, $J = 3.4$ Hz), 129.1, 127.4 (d, $J = 8.0$ Hz), 126.9, 122.3 (d, $J = 1.2$ Hz), 120.1, 115.8 (d, $J = 21.7$ Hz), 78.0, 57.0, 18.8 ppm.

^{19}F NMR (377 MHz, CDCl_3): -114.5 ppm.

HRMS Calculated for $[\text{C}_{19}\text{H}_{16}\text{BrFOS}+\text{Na}]^+$: 412.9982, Found: 412.9980.



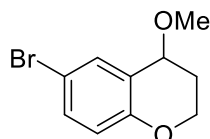
4-methoxychromane, **25**.

Reaction run at 0.4 mmol scale and 30.2 mg (46%) of colorless liquid isolated.

^1H NMR (CDCl_3 , 400 MHz): 7.24 (dd, $J = 7.7$, 1.7 Hz, 1H), 7.28 (td, $J = 7.7$, 1.7 Hz, 1H), 6.89 (td, $J = 7.4$, 1.2 Hz, 1H), 6.84 (dd, $J = 8.2$, 1.2 Hz, 1H), 4.32 – 4.21 (m, 3H), 3.44 (s, 3H), 2.18 – 2.10 (m, 1H), 2.09 – 1.98 (m, 1H) ppm.

^{13}C NMR (CDCl_3 , 100 MHz): 154.8, 130.6, 129.7, 121.6, 119.9, 117.0, 71.8, 62.0, 55.8, 27.2 ppm.

HRMS (ASAP-MS) Calculated for $[\text{C}_{10}\text{H}_{12}\text{O}_2-\text{OMe}]^+$: 133.0648, Found: 133.0646.

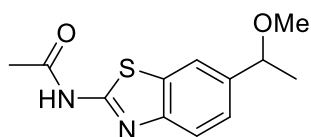


6-bromo-4-methoxychromane, **26**.

Reaction run at 0.4 mmol scale and 50.6 mg (52%) of colorless liquid isolated.

^1H NMR (CDCl_3 , 400 MHz): 7.37 (d, $J = 2.4$ Hz, 1H), 7.28 (dd, $J = 8.8, 3.2$ Hz, 1H), 6.72 (d, $J = 8.7$ Hz, 1H), 4.29 – 4.19 (m, 3H), 3.44 (s, 3H), 2.16 – 2.08 (m, 1H), 2.01 (dddd, $J = 14.2, 9.6, 5.4, 3.8$ Hz, 1H) ppm.

^{13}C NMR (CDCl_3 , 100 MHz): 153.9, 132.9, 132.5, 123.7, 118.9, 111.9, 71.5, 62.3, 56.0, 26.8 ppm.
HRMS (ASAP-MS) Calculated for $[\text{C}_{10}\text{H}_{11}\text{BrO}_2\text{-OMe}]^+$: 210.9753, Found: 210.9752.



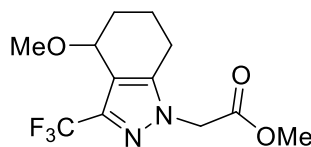
N-[6-(1-methoxyethyl)-1,3-benzothiazol-2-yl]acetamide, **27**.

Reaction run at 0.4 mmol scale and 40.3 mg (40%) of white non-crystalline powder isolated.

^1H NMR (CDCl_3 , 400 MHz): 11.77 (s, 1H), 7.80 (d, $J = 1.7$ Hz, 2H), 7.74 (d, $J = 8.3$ Hz, 1H), 7.41 (dd, $J = 8.4$ Hz, $J = 1.7$ Hz, 1H), 4.43 (q, $J = 6.4$ Hz, 1H), 3.27 (s, 3H), 2.30 (s, 3H), 1.50 (d, $J = 6.4$ Hz, 3H) ppm.

^{13}C NMR (CDCl_3 , 100 MHz): 168.89, 159.91, 147.17, 139.91, 132.07, 124.80, 120.28, 119.22, 79.52, 56.59, 24.00, 23.57 ppm.

HRMS Calculated for $[\text{C}_{12}\text{H}_{14}\text{N}_2\text{O}_2\text{S+H}]^+$: 251.0849, Found: 251.0846



N-[6-(1-methoxyethyl)-1,3-benzothiazol-2-yl]acetamide, **28**.

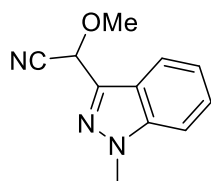
Reaction run at 0.4 mmol scale and 72.9 mg (62%) of yellow liquid isolated.

^1H NMR (CDCl_3 , 400 MHz): 4.88 (d, $J = 17.5$ Hz, 1H), 4.78 (d, $J = 17.5$ Hz, 1H), 4.43 (t, $J = 3.4$ Hz, 1H), 3.77 (s, 3H), 3.42 (s, 3H), 2.61 (ddd, $J = 16.3$ Hz, $J = 5.8$ Hz, $J = 3.0$ Hz, 1H), 2.46 (ddd, $J = 16.5$ Hz, $J = 10.7$ Hz, $J = 6.1$ Hz, 1H), 2.14 (ddd, $J = 14.1$ Hz, $J = 5.4$ Hz, $J = 2.8$ Hz, 1H), 2.00 (tdd, $J = 10.5$ Hz, $J = 8.1$ Hz, $J = 5.3$ Hz, 1H), 1.95-1.79 (m, 1H), 1.68-1.54 (m, 1H) ppm.

^{13}C NMR (CDCl_3 , 100 MHz): 167.3, 142.7, 140.0 (q, $J = 37.3$ Hz), 121.6 (q, $J = 269.4$ Hz), 116.2, 69.3, 56.5, 52.8, 50.5, 26.5, 21.0, 17.0 ppm.

^{19}F NMR (377 MHz, CDCl_3): -61.5 ppm.

HRMS Calculated for $[\text{C}_{12}\text{H}_{15}\text{F}_3\text{N}_2\text{O}_3\text{+H}]^+$: 293.1108, Found: 293.1102



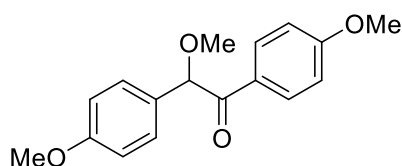
methoxy(1-methyl-1H-indazol-3-yl)acetonitrile, **29**.

Reaction run at 0.4 mmol scale and 30.5 mg (38%) of orange to green liquid isolated.

^1H NMR (CDCl_3 , 400 MHz): 7.90 (d, $J = 8.2$ Hz, 1H), 7.43 (m, 2H), 7.24 (m, 1H), 5.63 (s, 1H), 4.08 (s, 3H), 3.57 (s, 3H) ppm.

^{13}C NMR (CDCl_3 , 100 MHz): 141.3, 136.5, 127.1, 121.7, 121.3, 120.2, 116.2, 189.5, 66.6, 57.1, 35.8 ppm.

HRMS Calculated for $[\text{C}_{11}\text{H}_{11}\text{N}_3\text{O}_2+\text{H}]^+$: 202.0975, Found: 202.0975



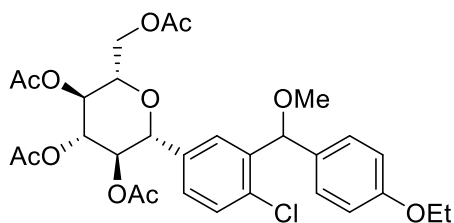
{2-methoxy-1, 2-bis(4-methoxyphenyl) ethenone}, **30**. Characterization data matched those previously reported¹⁸.

Reaction run at 0.4 mmol scale and 66.6 mg (58%) of colorless liquid isolated.

^1H NMR (CDCl_3 , 400 MHz): 7.99 (d, $J = 8.96$ Hz, 2H), 7.38 (d, $J = 8.62$ Hz, 2H), 6.87 (d, $J = 2.85$ Hz, 2H), 6.85 (d, $J = 3.03$ Hz, 2H), 5.45 (s, 1H), 3.81 (s, 3H), 3.76 (s, 3H), 3.42 (s, 3H) ppm.

^{13}C NMR (CDCl_3 , 100 MHz): 195.5, 163.5, 159.7, 131.3, 129.0, 128.5, 127.9, 114.3, 113.7, 85.8, 57.2, 55.4, 55.2 ppm.

HRMS Calculated for $[\text{C}_{17}\text{H}_{18}\text{O}_4+\text{Na}]^+$: 309.1097, Found: 309.1092.



(2*R*,3*R*,4*R*,5*S*,6*S*)-2-(acetoxymethyl)-6-(4-chloro-3-((4-ethoxyphenyl)(methoxy)methyl)phenyl) tetrahydro-2*H*-pyran-3,4,5-triyl triacetate, **31**.

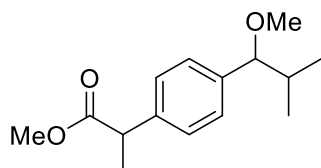
Reaction run at 0.4 mmol scale and 233 mg (91%) of white non-crystalline powder was isolated. (a mixture of two diastereomers): d. r. = 1.1:1 (by ^1H NMR spectroscopy. Reported spectral values are of the mixture).

Major diastereomer: ^1H NMR (CDCl_3 , 400 MHz): 7.54 (d, $J = 2.1$ Hz, 1H, major diastereomer), 7.48 (d, $J = 2.1$ Hz, 1H, minor diastereomer), 7.34 (dd, $J = 10.1$, 1H, minor diastereomer), 7.32 (dd, $J = 10.1$, 1H, major diastereomer), 7.28 – 7.17 (m, 3H), 6.88 – 6.77 (m, 2H), 5.61 (s, 1H, minor diastereomer), 5.55 (s, 1H, major diastereomer), 5.32 (t, $J = 9.3$ Hz, 1H, minor diastereomer), 5.31 (t, $J = 9.3$ Hz, 1H, major diastereomer), 5.23 (t, $J = 9.7$, 1H), 5.11 (t, 9.6 Hz, 1H, major diastereomer), 5.06 (t, 9.6 Hz, 1H), 4.40 (d, $J = 9.8$ Hz, 1H), 4.27 (dd, $J = 12.4$, 4.9, 1H), 4.18 (dd, $J = 12.4$, 2.4 Hz, 1H), 4.00 (q, $J = 7.0$ Hz, 2H, major diastereomer), 3.98 (q, $J = 7.0$ Hz, 2H), 3.82 (ddd, $J = 9.9$, 4.8, 2.1 Hz, 1H), 3.37 (s, 3H, minor diastereomer), 3.32 (s, 3H, major diastereomer),

2.09 (s, 3H), 2.06 (s, 3H), 2.01 (s, 3H, minor diastereomer), 1.99 (s, 3H, major diastereomer), 1.87 (s, 3H, major diastereomer), 1.61 (s, 3H, minor diastereomer), 1.38 (t, $J = 7.0$, 3H).

^{13}C NMR (CDCl_3 , 100 MHz): 170.73, 170.36, 170.34, 169.51, 168.90, 168.81, 158.53, 158.47, 139.85, 139.61, 135.57, 135.37, 133.43, 133.20, 132.42, 131.94, 129.90, 129.79, 128.81, 128.33, 126.95, 126.79, 126.72, 126.68, 114.50, 114.30, 114.24, 80.81, 80.63, 79.43, 76.15, 76.11, 74.17, 74.14, 72.66, 72.56, 68.54, 63.40, 63.38, 62.29, 57.12, 56.74, 20.79, 20.67, 20.66, 20.43, 20.19, 14.84, 14.81.

HRMS Calculated for $[\text{C}_{30}\text{H}_{35}\text{ClO}_{11}+\text{NH}_4]^+$: 624.2206, Found: 624.2203.



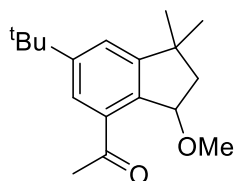
Methyl 2-[4-(1-methoxy-2-methylpropyl)phenyl]propanoate, **32**.

Reaction run at 0.4 mmol scale and 33.5 mg (67%) of colorless liquid was isolated.

^1H NMR (CDCl_3 , 400 MHz): 7.26 (d, $J = 8.3$ Hz, 2H), 7.19 (d, $J = 8.2$ Hz, 2H), 3.73 (m, 2H), 3.67 (s, 3H), 3.18 (s, 3H), 1.89 (doublet of septets, $J = 6.8$ Hz, 1H), 1.50 (d, $J = 7.2$ Hz, 3H), 0.98 (d, $J = 6.7$ Hz, 3H), 0.73 (d, $J = 6.8$ Hz, 3H) ppm.

^{13}C NMR (CDCl_3 , 100 MHz): 175.1, 140.0, 139.4, 127.7, 127.1, 89.4, 57.0, 52.0, 45.1, 34.7, 19.0, 18.9, 18.6 ppm.

HRMS Calculated for $[\text{C}_{15}\text{H}_{22}\text{O}_3+\text{NH}_4]^+$: 268.1907, Found: 268.1904.



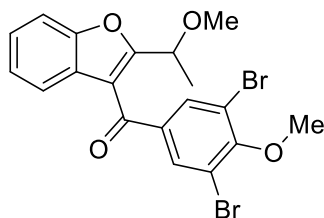
1-(6-tert-butyl-3-methoxy-1,1-dimethyl-2,3-dihydro-1H-inden-4-yl)ethan-1-one, **33**.

Reaction run at 0.4 mmol scale and 84.1 mg (77%) of colorless liquid isolated.

^1H NMR (CDCl_3 , 400 MHz): 7.66 (d, $J = 1.8$ Hz, 1H), 7.36 (d, $J = 1.8$ Hz, 1H), 5.21 (dd, $J = 5.7$, 3.1 Hz, 1H), 3.42 (s, 3H), 2.62 (s, 3H), 2.18 – 1.99 (m, 2H), 1.34 (s, 9H), 1.35 (s, 3H), 1.30 (s, 3H) ppm.

^{13}C NMR (CDCl_3 , 100 MHz): 200.77, 154.23, 152.59, 137.84, 135.24, 125.05, 123.18, 81.61, 57.16, 46.12, 42.63, 34.94, 31.42, 31.19, 29.77, 28.77 ppm.

HRMS Calculated for $[\text{C}_{17}\text{H}_{23}\text{O}_2-\text{OCH}_3]^+$: 243.1743, Found: 243.1740.



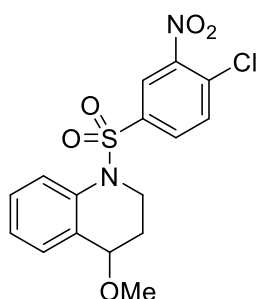
1-(6-tert-butyl-3-methoxy-1,1-dimethyl-2,3-dihydro-1H-inden-4-yl)ethan-1-one, **34**.

Reaction run at 0.4 mmol scale and 61.0 mg (65%) of white non-crystalline powder isolated.

^1H NMR (CDCl_3 , 400 MHz): 8.03 (s, 2H), 7.71-7.48 (m, 1H), 7.43-7.33 (m, 2H), 7.32-7.24 (m, 1H), 4.73 (q, $J = 6.6$ Hz, 1H), 3.99 (s, 3H), 3.29 (s, 3H), 1.63 (d, $J = 6.6$ Hz, 3H) ppm.

^{13}C NMR (CDCl_3 , 100 MHz): 187.6, 162.5, 158.1, 154.0, 136.6, 133.8, 125.7, 125.67, 124.1, 121.3, 118.7, 117.6, 111.9, 71.3, 60.9, 57.0, 19.4 ppm.

HRMS Calculated for $[\text{C}_{19}\text{H}_{16}\text{Br}_2\text{O}_4+\text{H}]^+$: 466.9488, Found: 466.9484.



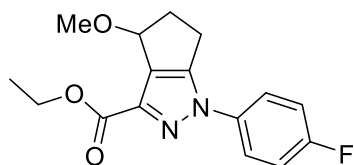
1-(4-chloro-3-nitrobenzene-1-sulfonyl)-4-methoxy-1,2,3,4-tetrahydroquinoline, **35**.

Reaction run at 0.4 mmol scale and 36.8 mg (48%) of white solid isolated.

^1H NMR (CDCl_3 , 400 MHz): 8.02 (d, $J = 2.1$ Hz, 2H), 7.89 (d, $J = 8.3$ Hz, 2H), 7.65 (dd, $J = 8.5$ Hz, $J = 2.1$ Hz, 2H), 7.56 (d, $J = 8.5$ Hz, 2H), 7.36 (ddd, $J = 8.4$ Hz, $J = 5.6$ Hz, $J = 2.8$ Hz, 3H), 7.16 (m, 2H), 4.04 (t, $J = 6.8$ Hz, 1H), 3.96 (ddd, $J = 12.3$ Hz, $J = 5.9$ Hz, $J = 3.0$ Hz, 1H), 3.72 (td, $J = 12.3$ Hz, $J = 4.9$ Hz, 1H), 2.94 (s, 3H), 2.16 (m, 1H), 1.75 (dddd, $J = 14.0$ Hz, $J = 12.3$ Hz, $J = 5.9$ Hz, $J = 2.9$ Hz, 1H) ppm.

^{13}C NMR (CDCl_3 , 100 MHz): 147.6, 138.1, 135.3, 132.3, 131.4, 131.2, 129.9, 129.6, 129.5, 125.2, 124.4, 124.3, 73.8, 55.7, 42.3, 27.9 ppm.

HRMS Calculated for $[\text{C}_{16}\text{H}_{15}\text{ClN}_2\text{O}_5\text{S}+\text{NH}_4]^+$: 400.0729, Found: 400.0721.



Ethyl-1-(4-fluorophenyl)-4-methoxy-1,3a,4,5,6,6a-hexahydrocyclopenta[c]pyrazole-3-carboxylate, **36a**.

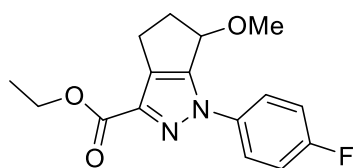
Reaction run at 0.4 mmol scale and 97.7 mg (80%) of white solid isolated.

^1H NMR (CDCl_3 , 400 MHz): 7.65 (dd, $J = 8.4$ Hz, $J = 4.3$ Hz, 2H), 7.14 (t, $J = 8.2$ Hz, 2H), 4.84 (d, $J = 5.7$ Hz, 1H), 4.43 (q, $J = 7.1$ Hz, 2H), 3.22 (m, 1H), 2.83 (m, 2H), 2.63 (m, 1H), 1.40 (t, $J = 7.0$ Hz, 3H) ppm.

^{13}C NMR (CDCl_3 , 100 MHz): 162.1, 161.5 (d, $J = 247.4$ Hz), 152.2, 138.8, 135.7 (d, $J = 3.0$ Hz), 131.3, 122.3 (d, $J = 8.5$ Hz), 116.2 (d, $J = 23.1$ Hz), 76.1, 61.1, 56.6, 38.9, 24.6, 14.3 ppm.

^{19}F NMR (377 MHz, CDCl_3): -114.3 ppm.

HRMS Calculated for $[\text{C}_{16}\text{H}_{17}\text{FN}_2\text{O}_3+\text{H}]^+$: 305.1296, Found: 305.1290.



Ethyl-1-(4-fluorophenyl)-6-methoxy-1,3a,4,5,6,6a-hexahydrocyclopenta[c]pyrazole-3-carboxylate, **36b**.

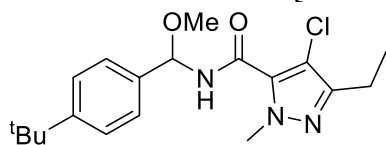
Reaction run at 0.4 mmol scale and 11.0 mg (9%) of white solid isolated.

^1H NMR (CDCl_3 , 400 MHz): 7.84 (m, 2H), 7.14 (m, 2H), 4.95 (m, 1H), 4.41 (q, $J = 7.1$ Hz, 2H), 3.00 (m, 1H), 2.82 (m, 2H), 2.63 (m, 1H), 1.40 (t, $J = 7.1$ Hz, 3H) ppm.

^{13}C NMR (CDCl_3 , 100 MHz): 162.3, 161.6 (d, $J = 247.0$ Hz), 148.5, 138.0, 135.9 (d, $J = 3.0$ Hz), 134.7, 122.5 (d, $J = 8.4$ Hz), 116.1 (d, $J = 22.9$ Hz), 75.7, 61.0, 54.6, 36.9, 22.4, 14.4 ppm.

^{19}F NMR (377 MHz, CDCl_3): -114.7 ppm.

HRMS Calculated for $[\text{C}_{16}\text{H}_{17}\text{FN}_2\text{O}_3+\text{H}]^+$: 305.1296, Found: 305.1291.



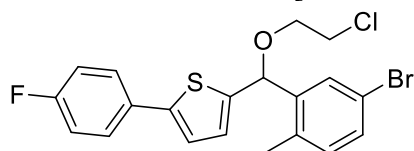
4-chloro-3-ethyl-N-[methoxy(4-tert-butylphenyl)methyl]-1-methyl-1H-pyrazole-5-carboxamide, **37**.

Reaction run at 0.2 mmol scale and 32.7 mg (45%) of white solid isolated.

^1H NMR (CDCl_3 , 500 MHz) δ 7.42 (s, 4H), 7.22 (d, $J = 9.0$ Hz, 1H), 6.28 (d, $J = 9.1$ Hz, 1H), 4.15 (s, 3H), 3.53 (s, 3H), 2.63 (q, $J = 7.6$ Hz, 2H), 1.32 (s, 9H), 1.23 (t, $J = 7.6$ Hz, 3H) ppm.

^{13}C NMR (CDCl_3 , 125 MHz): 158.55, 151.86, 149.71, 135.66, 130.52, 125.75, 125.70, 125.62, 125.58, 108.16, 81.63, 56.21, 40.79, 34.65, 31.30, 19.23, 12.84 ppm.

HRMS Calculated for $[\text{C}_{19}\text{H}_{26}\text{ClN}_3\text{O}_2+\text{H}]^+$: 364.1786, Found: 364.1782.



2-((5-bromo-2-methylphenyl)(2-chloroethoxy)methyl)-5-(4-fluorophenyl)thiophene, **38**.

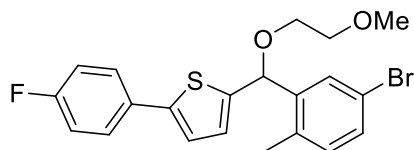
Reaction run at 0.2 mmol scale and 75.6 mg (86%) of colorless liquid isolated.

^1H NMR (CDCl_3 , 400 MHz): 7.74 (d, $J = 2.2$ Hz, 1H), 7.53 – 7.46 (m, 2H), 7.35 (dd, $J = 8.0$, 2.2 Hz, 1H), 7.07 – 6.99 (m, 4H), 6.77 (dd, $J = 3.8$, 0.8 Hz, 1H), 5.71 (s, 1H), 3.81 – 3.72 (m, 2H), 3.69 (td, $J = 5.8$, 1.0 Hz, 1H), 2.24 (s, 3H) ppm.

^{13}C NMR (CDCl_3 , 100 MHz): 162.4 (d, $J = 245.8$ Hz), 144.1, 143.2, 140.9, 134.5, 132.3, 131.0, 130.5 (d, $J = 3.4$ Hz), 129.3, 127.4 (d, $J = 8.0$ Hz), 127.1, 122.4 (d, $J = 1.2$ Hz), 120.2, 115.8 (d, $J = 21.7$ Hz), 76.9, 69.2, 42.8, 18.8 ppm.

^{19}F NMR (377 MHz, CDCl_3): -114.3 ppm.

HRMS Calculated for $[\text{C}_{20}\text{H}_{18}\text{BrClFOS}+\text{Na}]^+$: 460.9748, Found: 460.9744.



2-((5-bromo-2-methylphenyl)(2-methoxyethoxy)methyl)-5-(4-fluorophenyl)thiophene, **39**.

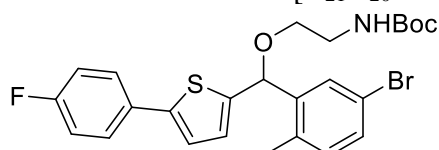
Reaction run at 0.2 mmol scale and 62.7 mg (72%) of colorless liquid isolated.

$^1\text{H NMR}$ (CDCl_3 , 400 MHz): 7.75 (d, $J = 2.2$ Hz, 1H), 7.53 – 7.46 (m, 2H), 7.34 (dd, $J = 8.1, 2.2$ Hz, 1H), 7.07 – 6.99 (m, 4H), 6.76 (dd, $J = 3.7, 0.8$ Hz, 1H), 5.72 (s, 1H), 3.73 – 3.59 (m, 4H), 3.40 (s, 3H), 2.24 (s, 3H) ppm.

$^{13}\text{C NMR}$ (CDCl_3 , 100 MHz): 162.3 (d, $J = 245.7$ Hz), 143.8, 141.4, 134.5, 132.2, 130.8, 130.6 (d, $J = 3.4$ Hz), 129.3, 127.4 (d, $J = 8.0$ Hz), 127.0, 122.32, 122.30, 120.1, 115.8 (d, $J = 21.7$ Hz), 76.6, 72.1, 68.5, 59.1, 18.8 ppm.

$^{19}\text{F NMR}$ (377 MHz, CDCl_3): -114.6 ppm.

HRMS Calculated for $[\text{C}_{21}\text{H}_{20}\text{BrFNO}_2\text{S}+\text{Na}]^+$: 457.0244, Found: 457.0242.



tert-butyl(2-((5-bromo-2-methylphenyl)(5-(4-fluorophenyl)thiophen-2-yl)methoxy)ethyl)carbamate, **40**.

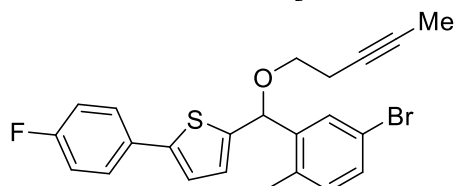
Reaction run at 0.2 mmol scale and 72.7 mg (70%) of yellow liquid isolated.

$^1\text{H NMR}$ (CDCl_3 , 400 MHz): 7.70 (d, $J = 2.2$ Hz, 1H), 7.53 – 7.46 (m, 2H), 7.35 (dd, $J = 8.1, 2.2$ Hz, 1H), 7.08 – 6.99 (m, 4H), 6.76 (dd, $J = 3.6, 0.8$ Hz, 1H), 5.63 (s, 1H), 5.03 – 4.83 (m, 1H), 3.60 (dt, $J = 9.5, 5.1$ Hz, 1H), 3.55 (dt, $J = 9.5, 4.9$ Hz, 1H), 3.40 (d, $J = 5.5$ Hz, 1H), 3.38 (d, $J = 5.5$ Hz, 1H), 2.24 (s, 3H), 1.43 (s, 9H) ppm.

$^{13}\text{C NMR}$ (CDCl_3 , 100 MHz): 162.4 (d, $J = 245.8$ Hz), 156.0, 144.0, 143.6, 141.2, 134.4, 132.3, 130.9, 130.5 (d, $J = 3.4$ Hz), 129.0, 127.4 (d, $J = 8.0$ Hz), 127.0, 122.3 (d, $J = 1.2$ Hz), 120.1, 115.8 (d, $J = 21.6$ Hz), 79.4, 76.5, 68.5, 40.5, 28.4, 18.8 ppm.

$^{19}\text{F NMR}$ (377 MHz, CDCl_3): -114.4 ppm.

HRMS Calculated for $[\text{C}_{25}\text{H}_{27}\text{BrFNO}_3\text{S}+\text{Na}]^+$: 542.0771, Found: 542.0768.



2-((5-bromo-2-methylphenyl)(pent-3-yn-1-yloxy)methyl)-5-(4-fluorophenyl)thiophene, **41**.

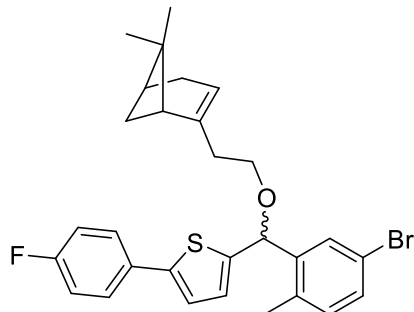
Reaction run at 0.2 mmol scale and 45.2 mg (51%) of colorless liquid isolated.

$^1\text{H NMR}$ (CDCl_3 , 400 MHz): 7.75 (d, $J = 2.2$ Hz, 1H), 7.53 – 7.46 (m, 2H), 7.34 (dd, $J = 8.0, 2.2$ Hz, 1H), 7.07 – 6.99 (m, 4H), 6.73 (dd, $J = 3.6, 0.9$ Hz, 1H), 5.69 (s, 1H), 3.60 (qt, $J = 9.0, 6.9$ Hz, 1H), 2.50 (tq, $J = 7.2, 2.5$ Hz, 1H), 2.24 (s, 3H), 1.79 (t, $J = 2.5$ Hz, 3H) ppm.

$^{13}\text{C NMR}$ (CDCl_3 , 100 MHz): 162.3 (d, $J = 245.8$ Hz), 143.8, 143.8, 141.2, 134.5, 132.2, 130.8, 130.6 (d, $J = 3.3$ Hz), 129.3, 127.4 (d, $J = 8.0$ Hz), 126.9, 122.3 (d, $J = 1.2$ Hz), 120.1, 115.8 (d, $J = 21.7$ Hz), 77.0, 76.4, 75.7, 67.9, 20.3, 18.8, 3.6 ppm.

$^{19}\text{F NMR}$ (377 MHz, CDCl_3): -114.5 ppm.

HRMS Calculated for $[\text{C}_{23}\text{H}_{20}\text{BrFOS}+\text{Na}]^+$: 465.0295, Found: 465.0294.



2-((5-bromo-2-methylphenyl)(2-((1*R*,5*S*)-6,6-dimethylbicyclo[3.1.1]hept-2-en-2-yl)ethoxy)methyl)-5-(4-fluorophenyl)thiophene, **42**.

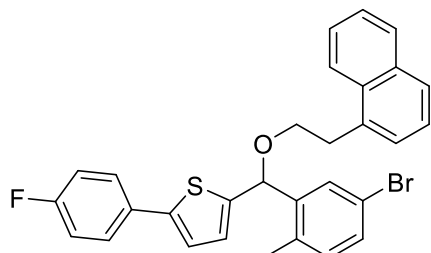
Reaction run at 0.2 mmol scale and 35.7 mg (34%) of colorless liquid isolated.

¹H NMR (CDCl₃, 400 MHz): 7.73 (d, *J* = 2.2 Hz, 1H), 7.53 – 7.46 (m, 2H), 7.34 (dd, *J* = 8.1, 2.2 Hz, 1H), 7.07 – 6.99 (m, 4H), 6.71 (dd, *J* = 3.6, 0.8 Hz, 1H), 5.60 (d, *J* = 2.0 Hz, 1H), 5.27 (ddq, *J* = 4.7, 3.2, 1.6 Hz, 1H), 3.58 – 3.45 (m, 2H), 2.42 – 2.14 (m, 8H), 2.10 – 2.02 (m, 2H), 1.26 (d, *J* = 3.7 Hz, 3H), 1.17 (d, *J* = 8.5 Hz, 1H), 0.82 (d, *J* = 1.5 Hz, 3H) ppm.

¹³C NMR (CDCl₃, 100 MHz): 162.3 (d, *J* = 245.5 Hz), 144.9, 144.3, 143.6, 141.7, 134.4, 132.2, 130.7, 130.6 (d, *J* = 3.4 Hz), 129.3, 127.3 (d, *J* = 8.0 Hz), 126.6, 122.3, 120.1, 118.1, 115.8 (d, *J* = 21.6 Hz), 76.3, 67.9, 46.0, 40.8, 38.0, 37.2, 31.7, 31.4, 26.3, 21.2, 18.8 ppm.

¹⁹F NMR (377 MHz, CDCl₃): -114.6 ppm.

HRMS Calculated for [C₂₉H₃₀BrFOS+Na]⁺: 547.1077, Found: 547.1071.



2-((5-bromo-2-methylphenyl)(2-(naphthalen-1-yl)ethoxy)methyl)-5-(4-fluorophenyl)thiophene, **43**.

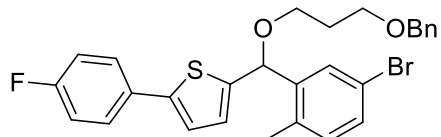
Reaction run at 0.2 mmol scale and 95.7 mg (90%) of colorless liquid isolated.

¹H NMR (CDCl₃, 400 MHz): 8.02 (d, *J* = 8.6 Hz, 1H), 7.84 (dd, *J* = 7.8, 1.8 Hz, 1H), 7.75 – 7.70 (m, 2H), 7.53 – 7.43 (m, 4H), 7.43 – 7.36 (m, 2H), 7.32 (dd, *J* = 8.1, 2.2 Hz, 1H), 7.08 – 6.95 (m, 4H), 6.67 (dd, *J* = 3.7, 0.8 Hz, 1H), 5.58 (s, 1H), 3.90 – 3.78 (m, 2H), 3.46 (t, *J* = 7.3 Hz, 2H), 2.14 (s, 3H) ppm.

¹³C NMR (CDCl₃, 100 MHz): 162.4 (d, *J* = 245.7 Hz), 144.0, 143.7, 141.5, 134.7, 134.4, 133.9, 132.2, 132.1, 130.8, 130.6 (d, *J* = 3.4 Hz), 129.2, 128.8, 127.4 (d, *J* = 8.0 Hz), 127.2, 127.1, 126.8, 126.1, 125.6 (d, *J* = 1.5 Hz), 123.8, 122.3, 122.3, 120.1, 115.8 (d, *J* = 21.6 Hz), 76.5, 69.5, 33.6, 18.7 ppm.

¹⁹F NMR (377 MHz, CDCl₃): -114.4 ppm.

HRMS Calculated for [C₃₀H₂₄BrFOS+Na]⁺: 553.0608, Found: 553.0606.



2-((3-(benzyloxy)propoxy)(5-bromo-2-methylphenyl)methyl)-5-(4-fluorophenyl)thiophene, **44**.

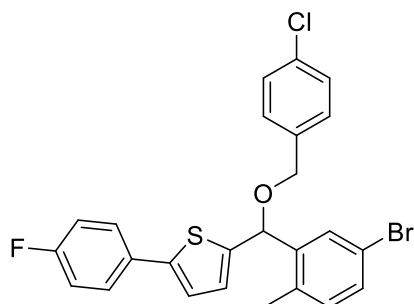
Reaction run at 0.2 mmol scale and 73.7 mg (70%) of colorless liquid isolated.

^1H NMR (CDCl_3 , 400 MHz): 7.71 (d, $J = 2.1$ Hz, 1H), 7.51 – 7.45 (m, 2H), 7.33 (dd, $J = 8.0$, 2.2 Hz, 1H), 7.32 – 7.22 (m, 5H), 7.06 – 6.99 (m, 4H), 6.70 (dd, $J = 3.7$, 0.9 Hz, 1H), 5.60 (s, 1H), 4.51 (d, $J = 11.8$ Hz, 1H), 4.49 (d, $J = 11.8$ Hz, 1H), 3.69 – 3.55 (m, 4H), 2.23 (s, 3H), 1.96 (p, $J = 6.2$ Hz, 2H) ppm.

^{13}C NMR (CDCl_3 , 100 MHz): 162.3 (d, $J = 245.5$ Hz), 144.3, 143.6, 141.6, 138.5, 134.5, 132.2, 130.8, 130.6 (d, $J = 3.4$ Hz), 129.3, 128.4, 127.7, 127.6, 127.4 (d, $J = 8.0$ Hz), 126.7, 122.3 (d, $J = 1.2$ Hz), 120.1, 115.8 (d, $J = 21.6$ Hz), 76.5, 73.1, 67.2, 66.3, 30.2, 18.8 ppm.

^{19}F NMR (377 MHz, CDCl_3): -114.5 ppm.

HRMS Calculated for $[\text{C}_{28}\text{H}_{26}\text{BrFO}_2\text{S}+\text{Na}]^+$: 547.0713, Found: 547.0709.



2-((5-bromo-2-methylphenyl)((4-chlorobenzyl)oxy)methyl)-5-(4-fluorophenyl)thiophene, **45**.

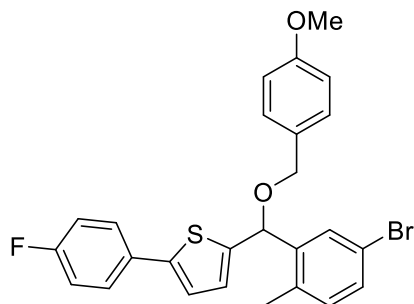
Reaction run at 0.2 mmol scale and 90.3 mg (90%) of colorless liquid isolated.

^1H NMR (CDCl_3 , 400 MHz): 7.77 (d, $J = 2.2$ Hz, 1H), 7.54 – 7.46 (m, 2H), 7.39 – 7.27 (m, 5H), 7.07 – 6.99 (m, 4H), 6.72 (dd, $J = 3.8$, 0.9 Hz, 1H), 5.67 (s, 1H), 4.57 (d, $J = 12.1$ Hz, 1H), 4.51 (d, $J = 12.1$ Hz, 1H), 2.18 (s, 3H) ppm.

^{13}C NMR (CDCl_3 , 100 MHz): 162.4 (d, $J = 245.8$ Hz), 144.0, 143.7, 140.9, 136.2, 134.6, 133.6, 132.4, 131.0, 130.9, 130.5 (d, $J = 3.4$ Hz), 129.5, 129.4, 129.2, 128.7, 127.4 (d, $J = 8.0$ Hz), 127.0, 122.4 (d, $J = 1.2$ Hz), 120.2, 115.8 (d, $J = 21.7$ Hz), 75.2, 69.9, 18.8 ppm.

^{19}F NMR (377 MHz, CDCl_3): -114.3 ppm.

HRMS Calculated for $[\text{C}_{25}\text{H}_{19}\text{BrClFOS}+\text{Na}]^+$: 522.9905, Found: 522.9899.



2-((5-bromo-2-methylphenyl)((4-methoxybenzyl)oxy)methyl)-5-(4-fluorophenyl)thiophene, **46**.

Reaction run at 0.2 mmol scale and 72.6 mg (73%) of yellow liquid isolated.

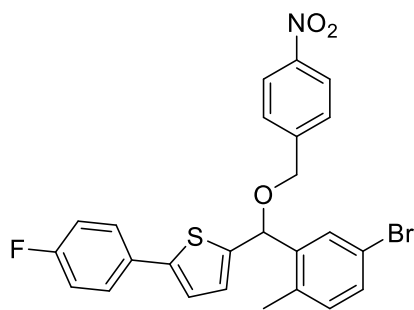
^1H NMR (CDCl_3 , 400 MHz): 7.78 (d, $J = 2.2$ Hz, 1H), 7.53 – 7.46 (m, 2H), 7.35 (dd, $J = 8.1$, 2.2

Hz, 1H), 7.29 (d, $J = 8.6$ Hz, 2H), 7.07 – 6.98 (m, 4H), 6.69 (dd, $J = 3.6, 0.9$ Hz, 1H), 5.66 (s, 1H), 4.56 (d, $J = 11.6$ Hz, 1H), 4.46 (d, $J = 11.6$ Hz, 1H), 3.81 (s, 3H), 2.17 (s, 3H) ppm.

^{13}C NMR (CDCl_3 , 100 MHz): 162.3 (d, $J = 245.7$ Hz), 159.4, 144.1, 143.7, 141.2, 134.7, 132.3, 130.9, 130.6 (d, $J = 3.4$ Hz), 129.7, 129.6, 129.6, 127.4 (d, $J = 8.0$ Hz), 126.8, 122.3 (d, $J = 1.2$ Hz), 120.1, 115.8 (d, $J = 21.6$ Hz), 113.9, 74.5, 70.3, 55.3, 18.8 ppm.

^{19}F NMR (377 MHz, CDCl_3): -114.5 ppm.

HRMS Calculated for $[\text{C}_{26}\text{H}_{22}\text{BrFO}_2\text{S}+\text{Na}]^+$: 519.0400, Found: 519.0397.



2-((5-bromo-2-methylphenyl)((4-nitrobenzyl)oxy)methyl)-5-(4-fluorophenyl)thiophene, **47**.

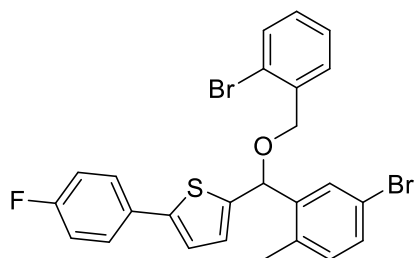
Reaction run at 0.2 mmol scale and 81.9 mg (79%) of yellow liquid isolated.

^1H NMR (CDCl_3 , 400 MHz): 8.23 (d, $J = 8.7$ Hz, 2H), 7.78 (d, $J = 2.2$ Hz, 1H), 7.55 (d, $J = 8.6$ Hz, 2H), 7.54 – 7.48 (m, 2H), 7.38 (dd, $J = 8.1, 2.2$ Hz, 1H), 7.09 – 7.01 (m, 4H), 6.77 (dd, $J = 3.6, 0.9$ Hz, 1H), 5.73 (s, 1H), 4.69 (d, $J = 13.1$ Hz, 1H), 4.67 (d, $J = 13.1$ Hz, 1H), 2.21 (s, 3H) ppm.

^{13}C NMR (CDCl_3 , 100 MHz): 162.4 (d, $J = 245.7$ Hz), 147.5, 145.3, 144.2, 143.1, 140.6, 134.6, 132.5, 131.2, 130.4 (d, $J = 3.4$ Hz), 129.2, 127.9, 127.4 (d, $J = 8.0$ Hz), 127.2, 123.8, 122.4 (d, $J = 1.2$ Hz), 120.2, 115.9 (d, $J = 21.7$ Hz), 76.2, 69.6, 18.8 ppm.

^{19}F NMR (377 MHz, CDCl_3): -114.1 ppm.

HRMS Calculated for $[\text{C}_{25}\text{H}_{19}\text{BrFNO}_3\text{S}+\text{Na}]^+$: 534.0145, Found: 534.0144.



2-((5-bromo-2-methylphenyl)((2-bromobenzyl)oxy)methyl)-5-(4-fluorophenyl)thiophene, **48**.

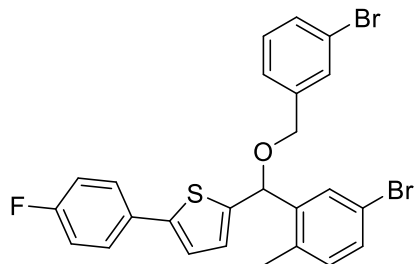
Reaction run at 0.2 mmol scale and 89.6 mg (82%) of white solid isolated.

^1H NMR (CDCl_3 , 400 MHz): 7.81 (d, $J = 2.2$ Hz, 1H), 7.59 – 7.46 (m, 4H), 7.39 – 7.31 (m, 2H), 7.16 (td, $J = 7.7, 1.7$ Hz, 1H), 7.06 – 6.99 (m, 4H), 6.75 (dd, $J = 3.8, 0.9$ Hz, 1H), 5.76 (s, 1H), 4.642 (d, $J = 13.3$ Hz, 1H), 4.639 (d, $J = 13.3$ Hz, 1H), 2.22 (s, 3H) ppm.

^{13}C NMR (CDCl_3 , 100 MHz): 162.4 (d, $J = 245.8$ Hz), 144.0, 143.7, 141.0, 137.1, 134.7, 132.6, 132.4, 131.0, 130.6 (d, $J = 3.4$ Hz), 129.5, 129.4, 129.2, 127.6, 127.4 (d, $J = 8.0$ Hz), 127.0, 122.9, 122.4 (d, $J = 1.2$ Hz), 120.2, 115.8 (d, $J = 21.6$ Hz), 76.1, 70.4, 18.8 ppm.

^{19}F NMR (377 MHz, CDCl_3): -114.4 ppm.

HRMS Calculated for $[\text{C}_{25}\text{H}_{19}\text{Br}_2\text{FOS}+\text{Na}]^+$: 566.9400, Found: 566.9396.



2-((5-bromo-2-methylphenyl)((3-bromobenzyl)oxy)methyl)-5-(4-fluorophenyl)thiophene, **49**.

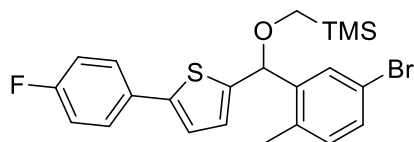
Reaction run at 0.2 mmol scale and 99.4 mg (91%) of colorless liquid isolated.

^1H NMR (CDCl_3 , 400 MHz): 7.77 (d, $J = 2.2$ Hz, 1H), 7.54 – 7.48 (m, 3H), 7.44 (dt, $J = 7.9$, 1.6 Hz, 1H), 7.36 (dd, $J = 8.1$, 2.2 Hz, 1H), 7.30 (dt, $J = 7.7$, 1.4 Hz, 1H), 7.24 (t, $J = 7.7$ Hz, 1H), 7.08 – 7.00 (m, 4H), 6.73 (dd, $J = 3.7$, 0.9 Hz, 1H), 5.68 (s, 1H), 4.57 (d, $J = 12.2$ Hz, 1H), 4.51 (d, $J = 12.2$ Hz, 1H), 2.19 (s, 3H) ppm.

^{13}C NMR (CDCl_3 , 100 MHz): 162.4 (d, $J = 245.9$ Hz), 144.0, 143.5, 140.8, 140.0, 134.6, 132.4, 131.0, 130.9, 130.8, 130.5 (d, $J = 3.4$ Hz), 130.1, 129.4, 127.4 (d, $J = 8.0$ Hz), 127.0, 126.3, 122.6, 122.4 (d, $J = 1.2$ Hz), 120.2, 115.8 (d, $J = 21.7$ Hz), 75.5, 69.9, 18.8 ppm.

^{19}F NMR (377 MHz, CDCl_3): -114.4 ppm.

HRMS Calculated for $[\text{C}_{25}\text{H}_{19}\text{Br}_2\text{FNOS}+\text{Na}]^+$: 566.9400, Found: 566.9399.



(((5-bromo-2-methylphenyl)(5-(4-fluorophenyl)thiophen-2-yl)methoxy)methyl)trimethylsilane, **50**.

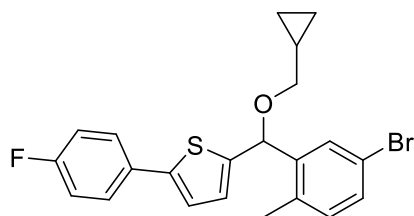
Reaction run at 0.2 mmol scale and 76.9 mg (83%) of colorless liquid isolated.

^1H NMR (CDCl_3 , 400 MHz): 7.63 (d, $J = 2.1$ Hz, 1H), 7.55 – 7.48 (m, 2H), 7.34 (dd, $J = 8.1$, 2.2 Hz, 1H), 7.08 – 6.99 (m, 4H), 6.66 (dd, $J = 3.6$, 1.0 Hz, 1H), 5.45 (s, 1H), 3.17 (d, $J = 12.4$ Hz, 1H), 3.10 (d, $J = 12.4$ Hz, 1H), 2.24 (s, 3H), 0.10 (s, 9H) ppm.

^{13}C NMR (CDCl_3 , 100 MHz): 162.2 (d, $J = 245.5$ Hz), 144.8, 143.4, 141.7, 134.9, 132.2, 130.7 (d, $J = 3.3$ Hz), 130.6, 129.7, 127.4 (d, $J = 8.0$ Hz), 126.3, 122.2 (d, $J = 1.2$ Hz), 119.9, 115.7 (d, $J = 21.6$ Hz), 80.4, 63.0, 18.7, -3.0 ppm.

^{19}F NMR (377 MHz, CDCl_3): -114.7 ppm.

HRMS Calculated for $[\text{C}_{22}\text{H}_{24}\text{BrFOSSi}+\text{Na}]^+$: 485.0377, Found: 485.0377.



2-((5-bromo-2-methylphenyl)(cyclopropylmethoxy)methyl)-5-(4-fluorophenyl)thiophene, **51**.

Reaction run at 0.2 mmol scale and 75.1 mg (87%) of colorless liquid isolated.

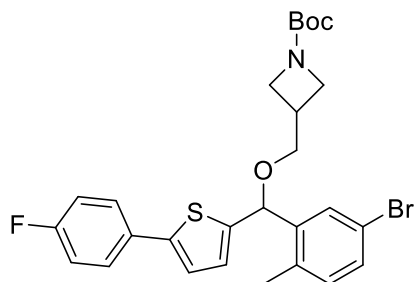
^1H NMR (CDCl_3 , 400 MHz): 7.76 (d, $J = 2.2$ Hz, 1H), 7.55 – 7.48 (m, 2H), 7.35 (dd, $J = 8.1$, 2.2 Hz, 1H), 7.08 – 7.00 (m, 4H), 6.74 (dd, $J = 3.7$, 0.8 Hz, 1H), 5.71 (s, 1H), 3.42 (dd, $J = 10.1$, 6.8 Hz, 1H), 3.34 (dd, $J = 10.1$, 6.9 Hz, 1H), 2.27 (s, 3H), 1.15 (dddd, $J = 13.2$, 6.8, 5.0, 2.6 Hz, 1H),

0.65 – 0.51 (m, 2H), 0.30 – 0.17 (m, 2H) ppm.

^{13}C NMR (CDCl_3 , 100 MHz): 162.3 (d, $J = 245.6$ Hz), 144.2, 143.6, 141.5, 134.6, 132.2, 130.7, 130.6 (d, $J = 3.3$ Hz), 129.4, 127.4 (d, $J = 8.0$ Hz), 126.7, 122.3 (d, $J = 1.2$ Hz), 120.1, 115.8 (d, $J = 21.6$ Hz), 75.7, 73.9, 18.8, 10.7, 3.25, 3.24 ppm.

^{19}F NMR (377 MHz, CDCl_3): -114.6 ppm.

HRMS Calculated for $[\text{C}_{22}\text{H}_{20}\text{BrFOS}+\text{Na}]^+$: 453.0295, Found: 453.0288.



tert-butyl 3-(((5-bromo-2-methylphenyl)(5-(4-fluorophenyl)thiophen-2-yl)methoxy)methyl)azetidine-1-carboxylate, **52**.

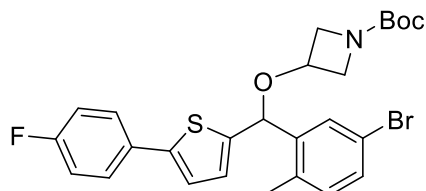
Reaction run at 0.2 mmol scale and 78.7 mg (72%) of yellow liquid isolated.

^1H NMR (CDCl_3 , 400 MHz): 7.67 (d, $J = 2.1$ Hz, 1H), 7.54 – 7.47 (m, 2H), 7.36 (dd, $J = 8.1$, 2.2 Hz, 1H), 7.08 – 7.01 (m, 4H), 6.73 (dd, $J = 3.7$, 0.8 Hz, 1H), 5.62 (s, 1H), 4.02 (td, $J = 8.5$, 2.1 Hz, 2H), 3.75 – 3.58 (m, 4H), 2.89 – 2.77 (m, 1H), 2.24 (s, 3H), 1.43 (s, 9H) ppm.

^{13}C NMR (CDCl_3 , 100 MHz): 162.3 (d, $J = 197.0$ Hz), 156.4, 143.9, 143.6, 141.1, 134.5, 132.3, 132.2, 130.4 (d, $J = 3.0$ Hz), 129.2, 127.4 (d, $J = 12.0$ Hz), 126.8, 122.3 (d, $J = 2.0$ Hz), 120.1, 115.8 (d, $J = 17.0$ Hz), 79.4, 77.2, 76.9, 71.2, 64.6, 64.8, 28.4, 18.8 ppm.

^{19}F NMR (377 MHz, CDCl_3): -114.4 ppm.

HRMS Calculated for $[\text{C}_{27}\text{H}_{29}\text{BrFO}_3\text{S}+\text{Na}]^+$: 568.0928, Found: 568.0921.



tert-butyl 3-(((5-bromo-2-methylphenyl)(5-(4-fluorophenyl)thiophen-2-yl)methoxy)azetidine-1-carboxylate, **53**.

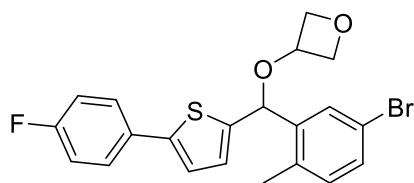
Reaction run at 0.2 mmol scale and 91.6 mg (86%) of colorless liquid isolated.

^1H NMR (CDCl_3 , 400 MHz): 7.76 (d, $J = 2.1$ Hz, 1H), 7.53 – 7.46 (m, 2H), 7.36 (dd, $J = 8.1$, 2.2 Hz, 1H), 7.08 – 7.00 (m, 4H), 6.78 (dd, $J = 3.7$, 0.8 Hz, 1H), 5.59 (s, 1H), 4.37 (tt, $J = 6.6$, 4.5 Hz, 1H), 4.04 (dddd, $J = 14.3$, 9.4, 6.6, 1.0 Hz, 2H), 3.92 (ddd, $J = 14.3$, 9.3, 4.6 Hz, 2H), 2.20 (s, 3H), 1.43 (s, 9H) ppm.

^{13}C NMR (CDCl_3 , 100 MHz): 162.4 (d, $J = 246.1$ Hz), 156.3, 144.5, 142.8, 140.7, 134.2, 132.3, 131.1, 130.3 (d, $J = 3.5$ Hz), 129.1, 127.4 (d, $J = 8.0$ Hz), 127.3, 122.4 (d, $J = 1.2$ Hz), 120.1, 115.9 (d, $J = 21.7$ Hz), 79.7, 75.0, 66.4, 57.2 – 56.3 (m), 28.4, 18.8 ppm.

^{19}F NMR (377 MHz, CDCl_3): -114.2 ppm.

HRMS Calculated for $[\text{C}_{26}\text{H}_{27}\text{BrFO}_3\text{S}+\text{Na}]^+$: 554.0771, Found: 554.0767.



3-(((5-bromo-2-methylphenyl)(5-(4-fluorophenyl)thiophen-2-yl)methoxy)oxetane, **54**.

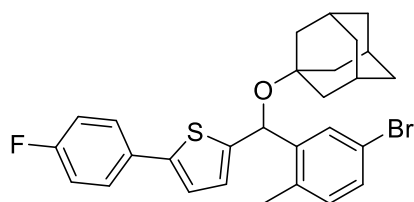
Reaction run at 0.2 mmol scale and 39.9 mg (46%) of colorless liquid isolated.

^1H NMR (CDCl_3 , 400 MHz): 7.78 (d, $J = 2.1$ Hz, 1H), 7.53 – 7.46 (m, 2H), 7.36 (dd, $J = 8.1$, 2.2 Hz, 1H), 7.08 – 6.99 (m, 4H), 6.77 (dd, $J = 3.6$, 0.8 Hz, 1H), 5.58 (s, 1H), 4.76 – 4.62 (m, 5H), 2.20 (s, 3H) ppm.

^{13}C NMR (CDCl_3 , 100 MHz): 162.4 (d, $J = 246.2$ Hz), 144.4, 143.0, 140.8, 134.1, 132.3, 131.1, 130.3 (d, $J = 3.4$ Hz), 129.1, 127.4 (d, $J = 8.0$ Hz), 127.3, 122.4 (d, $J = 1.2$ Hz), 120.1, 115.9 (d, $J = 21.8$ Hz), 79.1, 75.3, 71.2, 18.8 ppm.

^{19}F NMR (377 MHz, CDCl_3): -114.1 ppm.

HRMS Calculated for $[\text{C}_{21}\text{H}_{18}\text{BrFO}_2\text{S}+\text{Na}]^+$: 455.0087, Found: 455.0083.



2-(((3*S*,5*S*,7*S*)-adamantan-1-yl)oxy)(5-bromo-2-methylphenyl)methyl)-5-(4-fluorophenyl)thiophene, **55**.

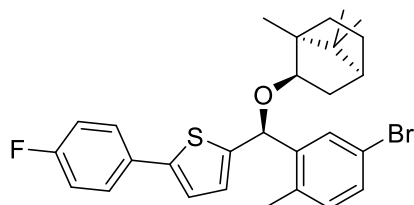
Reaction run at 0.2 mmol scale and 75.7 mg (74%) of white solid isolated.

^1H NMR (CDCl_3 , 400 MHz): 7.83 (d, $J = 2.2$ Hz, 1H), 7.53 – 7.46 (m, 2H), 7.32 (dd, $J = 8.1$, 2.2 Hz, 1H), 7.07 – 6.98 (m, 3H), 6.95 (d, $J = 3.6$ Hz, 1H), 6.42 (dd, $J = 3.7$, 1.0 Hz, 1H), 5.96 (s, 1H), 2.27 (s, 3H), 2.14 (q, $J = 3.2$ Hz, 3H), 1.83 (d, $J = 11.3$ Hz, 3H), 1.76 (d, $J = 11.3$ Hz, 3H), 1.63 (d, $J = 13.9$ Hz, 3H), 1.60 (d, $J = 13.9$ Hz, 3H) ppm.

^{13}C NMR (CDCl_3 , 100 MHz): 162.2 (d, $J = 245.4$ Hz), 147.3, 144.5, 143.1, 133.2, 131.9, 130.4 (d, $J = 3.4$ Hz), 130.3, 130.2, 127.3 (d, $J = 8.0$ Hz), 125.8, 122.4 (d, $J = 0.9$ Hz), 119.8, 115.7 (d, $J = 21.6$ Hz), 75.0, 66.8, 42.6, 36.3, 30.7, 18.9 ppm.

^{19}F NMR (377 MHz, CDCl_3): -114.9 ppm.

HRMS Calculated for $[\text{C}_{28}\text{H}_{28}\text{BrFNOS}+\text{Na}]^+$: 533.0921, Found: 533.0916.



2-(((*S*)-5-bromo-2-methylphenyl)((1*S*,2*R*,4*S*)-1,7,7-trimethylbicyclo[2.2.1]heptan-2-yl)oxy)methyl)-5-(4-fluorophenyl)thiophene, **56a**.

Reaction run at 0.2 mmol scale and 49.3 mg (48%) of white solid isolated.

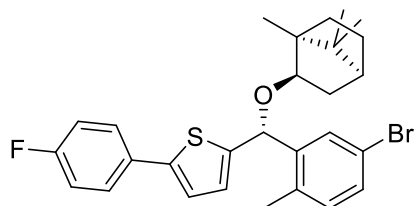
^1H NMR (CDCl_3 , 400 MHz): 7.69 (d, $J = 2.2$ Hz, 1H), 7.55 – 7.47 (m, 2H), 7.35 (dd, $J = 8.0$, 2.2 Hz, 1H), 7.08 – 7.01 (m, 3H), 6.99 (d, $J = 3.6$ Hz, 1H), 6.50 (dd, $J = 3.7$, 1.1 Hz, 1H), 5.62 (d, $J = 1.1$ Hz, 1H), 3.64 (ddd, $J = 9.1$, 3.3, 1.8 Hz, 1H), 2.29 – 2.20 (m, 4H), 2.17 – 2.07 (m, 1H), 1.78

(tq, $J = 11.8, 4.1$ Hz, 1H), 1.70 (t, $J = 4.6$ Hz, 1H), 1.38 (ddd, $J = 11.9, 9.4, 4.4$ Hz, 1H), 1.34 – 1.25 (m, 1H), 1.22 (dd, $J = 12.8, 3.2$ Hz, 1H), 0.86 (s, 3H), 0.85 (s, 3H), 0.76 (s, 3H) ppm.

^{13}C NMR (CDCl_3 , 100 MHz): 162.2 (d, $J = 245.3$ Hz), 146.2, 143.1, 141.5, 134.9, 132.2, 130.8 (d, $J = 3.4$ Hz), 130.7, 130.2, 127.4 (d, $J = 7.9$ Hz), 125.5, 122.3 (d, $J = 1.2$ Hz), 119.9, 115.7 (d, $J = 21.7$ Hz), 82.5, 74.6, 49.4, 47.9, 45.2, 36.0, 28.3, 26.9, 19.8, 19.0, 18.8, 13.7 ppm.

^{19}F NMR (377 MHz, CDCl_3): -114.8 ppm.

HRMS Calculated for $[\text{C}_{28}\text{H}_{30}\text{BrFNOS}+\text{Na}]^+$: 535.1077, Found: 535.1081.



2-((*R*)-(5-bromo-2-methylphenyl)(((1*S*,2*R*,4*S*)-1,7,7-trimethylbicyclo[2.2.1]heptan-2-yl)oxy)methyl)-5-(4-fluorophenyl)thiophene, **56b**.

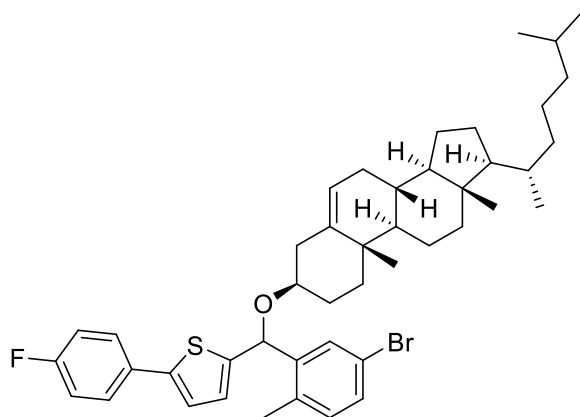
Reaction run at 0.2 mmol scale and 38.0 mg (37%) of white solid isolated.

^1H NMR (CDCl_3 , 400 MHz): 7.76 (d, $J = 2.2$ Hz, 1H), 7.54 – 7.48 (m, 2H), 7.33 (dd, $J = 8.1, 2.2$ Hz, 1H), 7.07 – 6.98 (m, 4H), 6.64 (dd, $J = 3.7, 0.9$ Hz, 1H), 5.61 (s, 1H), 3.79 (ddd, $J = 9.5, 3.5, 1.8$ Hz, 1H), 2.23 (s, 3H), 2.22 – 2.16 (m, 1H), 2.02 (ddd, $J = 13.1, 9.3, 4.1$ Hz, 1H), 1.71 (tt, $J = 12.2, 4.1$ Hz, 1H), 1.61 (t, $J = 4.6$ Hz, 1H), 1.36 – 1.19 (m, 1H), 1.03 (dd, $J = 13.1, 3.4$ Hz, 1H), 0.95 (s, 3H), 0.85 (s, 3H), 0.79 (s, 3H) ppm.

^{13}C NMR (CDCl_3 , 100 MHz): 162.3 (d, $J = 196.5$ Hz), 145.2, 143.4, 142.8, 134.2, 132.1, 130.7 (d, $J = 2.7$ Hz), 130.5, 129.8, 127.3 (d, $J = 6.4$ Hz), 126.2 (d, $J = 1.4$ Hz), 122.1 (d, $J = 2.4$ Hz), 119.8, 115.7 (d, $J = 17.3$ Hz), 83.6, 76.0, 49.7, 47.7, 45.1, 35.9, 28.2, 27.1, 19.8, 19.0, 18.9, 14.1 ppm.

^{19}F NMR (377 MHz, CDCl_3): -114.8 ppm.

HRMS Calculated for $[\text{C}_{28}\text{H}_{30}\text{BrFNOS}+\text{Na}]^+$: 535.1077, Found: 535.1077.



2-((5-bromo-2-methylphenyl)(((3*S*,8*S*,9*S*,10*R*,13*R*,14*S*,17*R*)-10,13-dimethyl-17-((*R*)-6-methylheptan-2-yl)-2,3,4,7,8,9,10,11,12,13,14,15,16,17-tetradecahydro-1*H*-cyclopenta[*a*]phenanthren-3-yl)oxy)methyl)-5-(4-fluorophenyl)thiophene, **57**.

Reaction run at 0.2 mmol scale and 58.2 mg (39%) of pale-yellow liquid isolated.

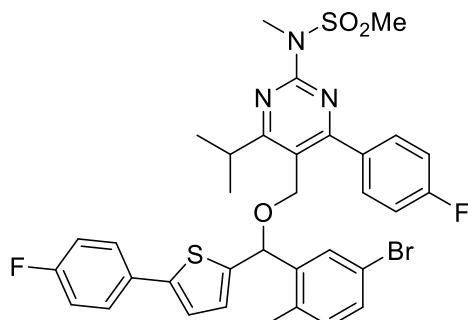
^1H NMR (CDCl_3 , 400 MHz): 7.77 (d, $J = 2.2$ Hz, 1H), 7.53 – 7.46 (m, 2H), 7.33 (dd, $J = 8.1, 2.2$ Hz, 1H), 7.07 – 6.98 (m, 4H), 6.66 (dd, $J = 4.6, 0.8$ Hz, 1H), 5.81 (s, 1H), 5.33 (dd, $J = 12.1, 5.0$ Hz, 1H), 3.31 (td, $J = 10.2, 5.0$ Hz, 1H), 2.50 – 2.30 (m, 2H), 2.25 (s, 3H), 2.05 – 1.75 (m, 4H),

1.70 – 0.93 (m, 22H), 1.02 (s, 3H), 0.91 (d, $J = 6.5$ Hz, 3H), 0.862 (d, $J = 6.6$ Hz, 3H), 0.857 (d, $J = 6.6$ Hz, 3H), 0.67 (s, 3H) ppm.

^{13}C NMR (CDCl_3 , 100 MHz): 163.3 (d, $J = 245.4$ Hz), 145.0, 143.5, 142.2, 140.7, 134.3, 132.2, 130.6 (d, $J = 3.2$ Hz), 129.6, 127.4 (d, $J = 7.9$ Hz), 126.4, 122.3, 121.88, 121.86, 120.1, 115.7 (d, $J = 21.6$ Hz), 73.1, 56.8, 56.1, 50.2, 42.3, 39.8, 39.5, 39.4, 39.2, 37.2, 36.9, 36.2, 35.8, 31.9, 28.8, 28.5, 28.2, 28.0, 24.3, 23.8, 22.8, 22.6, 21.1, 19.4, 18.9, 18.7, 11.9 ppm.

^{19}F NMR (377 MHz, CDCl_3): -114.6 ppm.

HRMS Calculated for $[\text{C}_{45}\text{H}_{58}\text{BrFOS-OC}_{27}\text{H}_{45}]^+$ (ASAP-MS): 358.9900, Found: 358.9895.



N-(5-(((5-bromo-2-methylphenyl)(5-(4-fluorophenyl)thiophen-2-yl)methoxy)methyl)-4-(4-fluorophenyl)-6-isopropylpyrimidin-2-yl)-*N*-methylmethanesulfonamide, **58**.

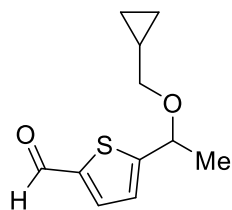
Reaction run at 0.2 mmol scale and 133 mg (93%) of pale-yellow liquid isolated.

^1H NMR (CDCl_3 , 400 MHz): 7.83 (d, $J = 2.1$ Hz, 1H), 7.77 – 7.70 (m, 2H), 7.54 – 7.47 (m, 2H), 7.39 (dd, $J = 8.1, 2.2$ Hz, 1H), 7.11 – 7.02 (m, 6H), 6.74 (dd, $J = 3.6, 0.8$ Hz, 1H), 5.68 (s, 1H), 4.46 (d, $J = 10.2$ Hz, 1H), 4.41 (d, $J = 10.2$ Hz, 1H), 3.58 (s, 3H), 3.51 (s, 3H), 3.34 (sept., $J = 6.6$ Hz, 1H), 2.22 (s, 3H), 1.34 (d, $J = 6.6$ Hz, 3H), 1.31 (d, $J = 6.6$ Hz, 3H) ppm.

^{13}C NMR (CDCl_3 , 100 MHz): 178.3, 166.6, 163.7 (d, $J = 248.4$ Hz), 162.5 (d, $J = 246.1$ Hz), 158.2, 144.3, 143.1, 140.8, 134.3, 134.0 (d, $J = 3.2$ Hz), 132.4, 131.4 (d, $J = 8.4$ Hz), 131.2, 130.3 (d, $J = 3.4$ Hz), 129.2, 127.44 (d, $J = 8.0$ Hz), 127.37, 122.5 (d, $J = 1.2$ Hz), 120.1, 118.3, 115.9 (d, $J = 21.7$ Hz), 115.4 (d, $J = 21.5$ Hz), 76.6, 64.6, 42.4, 33.1, 31.7, 22.4, 22.2, 18.9 ppm.

^{19}F NMR (377 MHz, CDCl_3): -111.1, -114.0 ppm.

HRMS Calculated for $[\text{C}_{34}\text{H}_{32}\text{BrF}_2\text{O}_3\text{S}_2+\text{Na}]^+$: 712.1109, Found: 712.1112.



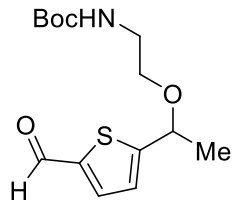
5-[1-(cyclopropylmethoxy)ethyl]thiophene-2-carbaldehyde, **59**

Reaction run at 0.4 mmol scale and 34.9 mg (42%) of pale-yellow liquid was isolated.

^1H NMR (CDCl_3 , 400 MHz) δ 9.87 (s, 1H), 7.65 (d, $J = 3.8$ Hz, 1H), 7.04 (d, $J = 3.8$ Hz, 1H), 4.73 (q, $J = 6.5$ Hz, 1H), 3.31 (dd, $J = 9.9, 6.7$ Hz, 1H), 3.22 (dd, $J = 10.0, 7.1$ Hz, 1H), 1.56 (d, $J = 6.5$ Hz, 3H), 1.06 (ddt, $J = 10.8, 7.6, 3.8$ Hz, 1H), 0.56 – 0.44 (m, 2H), 0.18 (dd, $J = 4.7, 1.6$ Hz, 2H).

^{13}C NMR (CDCl_3 , 101 MHz) δ 183.0, 159.8, 142.5, 136.4, 124.9, 73.9, 73.3, 24.2, 10.7, 3.2, 3.0.

HRMS Calculated for $[\text{C}_{11}\text{H}_{14}\text{O}_2\text{S}+\text{H}]^+$: 211.0787, Found: 211.0786.



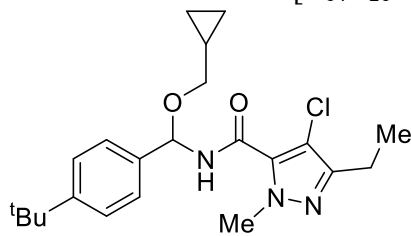
tert-butyl {2-[1-(5-formylthiophen-2-yl)ethoxy]ethyl} carbamate, **60**

Reaction run at 0.4 mmol and 36.7 mg (31%) of pale-yellow liquid was isolated.

$^1\text{H NMR}$ (CDCl_3 , 500 MHz) δ 9.87 (s, 1H), 7.64 (d, $J = 3.8$ Hz, 1H), 7.04 (d, $J = 3.8$ Hz, 1H), 4.87 (b, 1H), 4.71 (q, $J = 6.4$ Hz, 1H), 3.49 (t, $J = 5.1$ Hz, 2H), 3.31 (q, $J = 5.1$ Hz, 2H), 1.55 (d, $J = 6.4$ Hz, 3H), 1.44 (s, 9H).

$^{13}\text{C NMR}$ (CDCl_3 , 126 MHz) δ 182.9, 158.8, 155.9, 142.8, 136.3, 125.1, 79.4, 74.0, 68.2, 40.5, 28.4, 23.8.

HRMS Calculated for $[\text{C}_{14}\text{H}_{21}\text{NO}_4\text{S}+\text{Na}]^+$: 322.1084, Found: 322.1078.



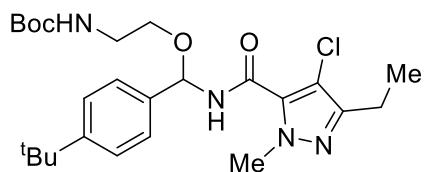
4-chloro-3-ethyl-N-[cyclopropylmethoxy(4-tert-butylphenyl)methyl]-1-methyl-1H-pyrazole-5-carboxamide, **61**

Reaction run at 0.2 mmol and 39.0 mg (40%) of pale yellow liquid was isolated.

$^1\text{H NMR}$ (CDCl_3 , 500 MHz) δ 7.45 (d, $J = 8.5$ Hz, 2H), 7.41 (d, $J = 8.6$ Hz, 2H), 7.24 (d, $J = 9.1$ Hz, 1H), 6.42 (d, $J = 9.1$ Hz, 1H), 4.14 (s, 3H), 3.57 (dd, $J = 10.2, 7.0$ Hz, 1H), 3.51 (dd, $J = 10.3, 6.9$ Hz, 1H), 2.63 (q, $J = 7.6$ Hz, 2H), 1.32 (s, 9H), 1.23 (t, $J = 7.6$ Hz, 3H), 0.55 (dq, $J = 7.8, 2.6$ Hz, 2H), 0.36 – 0.19 (m, 2H).

$^{13}\text{C NMR}$ (CDCl_3 , 126 MHz) δ 158.4, 151.7, 149.7, 136.1, 130.6, 129.1, 128.8, 125.7, 125.6, 108.1, 80.0, 73.4, 40.8, 34.6, 31.3, 19.2, 12.8, 10.6, 3.3, 3.0.

HRMS Calculated for $[\text{C}_{22}\text{H}_{30}\text{ClN}_3\text{O}_2+\text{Na}]^+$: 426.1919, Found: 426.1913.



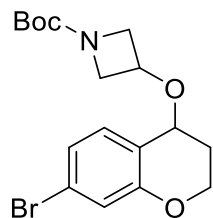
4-chloro-3-ethyl-N-[cyclopropylmethoxy(4-tert-butylphenyl)methyl]-1-methyl-1H-pyrazole-5-carboxamide, **62**

Reaction run at 0.4 mmol and 52.3 mg (27%) of pale-yellow semisolid was isolated by reverse phase column chromatography using Biotage Isolera One® with reusable 60 g SNAP C18® cartridges with $\text{H}_2\text{O}:\text{MeCN}$ as the eluents.

$^1\text{H NMR}$ (CDCl_3 , 500 MHz) δ 7.44 – 7.29 (m, 4H), 7.21 (d, $J = 9.2$ Hz, 1H), 6.27 (d, $J = 8.9$ Hz, 1H), 4.99 (br, 1H), 4.08 (s, 3H), 3.72 (dt, $J = 10.4, 5.3$ Hz, 1H), 3.63 (dt, $J = 9.9, 5.0$ Hz, 1H), 3.33 (d, $J = 5.4$ Hz, 2H), 2.55 (q, $J = 7.6$ Hz, 2H), 1.36 (s, 9H), 1.26 (s, 9H), 1.16 (t, $J = 7.6$ Hz, 3H).

$^{13}\text{C NMR}$ (CDCl_3 , 126 MHz) δ 157.6, 154.9, 151.0, 148.7, 134.4, 129.4, 124.7, 124.7, 112.9, 107.2, 79.5, 66.7, 39.8, 39.4, 33.7, 30.7, 28.7, 27.4, 18.2, 11.8.

HRMS Calculated for $[\text{C}_{25}\text{H}_{37}\text{ClN}_4\text{O}_4+\text{NH}_4]^+$: 510.2842, Found: 510.2834.



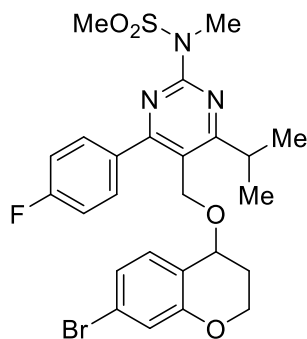
tert-butyl 3-[(7-bromo-3,4-dihydro-2*H*-1-benzopyran-4-yl)oxy]azetidine-1-carboxylate, **63**

Reaction run at 0.4 mmol scale and 68.6 mg (45%) of colorless semisolid was isolated.

^1H NMR (CDCl_3 , 500 MHz) δ 7.30 (dd, $J = 8.7, 2.5$ Hz, 1H), 7.26 (d, $J = 2.6$ Hz, 1H), 6.73 (d, $J = 8.7$ Hz, 1H), 4.45 (tt, $J = 6.6, 4.5$ Hz, 1H), 4.34 (t, $J = 3.8$ Hz, 1H), 4.30 (td, $J = 10.6, 3.8$ Hz, 1H), 4.24 (dt, $J = 11.0, 4.1$ Hz, 1H), 4.15 (dd, $J = 8.9, 7.0$ Hz, 1H), 4.04 (dd, $J = 9.0, 6.7$ Hz, 1H), 3.89 (dd, $J = 9.2, 4.5$ Hz, 1H), 3.74 (dd, $J = 9.3, 4.4$ Hz, 1H), 2.03 (m, 2H), 1.44 (s, 9H) ppm.

^{13}C NMR (126 MHz) δ 156.3, 154.0, 132.9, 132.5, 122.8, 119.1, 112.0, 79.7, 69.4, 65.7, 62.1, 28.4, 27.7 ppm.

HRMS Calculated for $[\text{C}_{17}\text{H}_{22}\text{NO}_4 + \text{H}]^+$: 384.0805, Found: 384.0801.



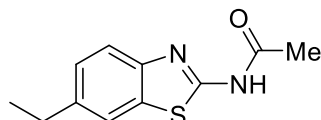
N-(5-((7-bromo-3,4-dihydro-2*H*-1-benzopyran-4-yl)oxy)methyl)-4-(4-fluorophenyl)-6-isopropylpyrimidin-2-yl)-*N*-methylmethanesulfonamide **64**

^1H NMR (CDCl_3 , 400 MHz) δ 7.69 (dd, $J = 8.5, 5.4$ Hz, 2H), 7.33 (dd, $J = 8.7, 2.5$ Hz, 1H), 7.28 (d, $J = 2.4$ Hz, 1H), 7.08 (t, $J = 8.5$ Hz, 2H), 6.79 (d, $J = 8.7$ Hz, 1H), 4.50 (q, $J = 10.0$ Hz, 2H), 4.43 (t, $J = 3.7$ Hz, 1H), 4.32 (m, 2H), 3.56 (s, 3H), 3.50 (s, 3H), 3.31 (hept, $J = 6.7$ Hz, 1H), 2.30 – 2.00 (m, 2H), 1.32 (t, $J = 7.3$ Hz, 6H).

^{13}C NMR (CDCl_3 , 101 MHz) δ 178.0, 166.5, 163.7 (d, $J = 250.2$ Hz), 158.1, 153.9, 133.9, 132.8 (d, $J = 2.4$ Hz), 131.3 (d, $J = 8.4$ Hz), 126.9 (d, $J = 275.4$ Hz), 122.9, 119.2, 118.4, 115.3 (d, $J = 21.6$ Hz), 111.9, 70.6, 63.5, 62.1, 42.4, 33.1, 31.6, 27.5, 22.2, 22.1.

^{19}F NMR (377 MHz, CDCl_3): -110.9 ppm.

HRMS Calculated for $[\text{C}_{25}\text{H}_{27}\text{BrFN}_3\text{O}_4\text{S} + \text{H}]^+$: 564.0962, Found: 564.0964.



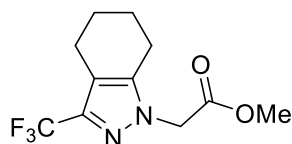
N-(6-ethyl-1,3-benzothiazol-2-yl)acetamide, **65**.

Reaction run at 2.5 mmol scale and 473 mg (86%) of off-white non-crystalline powder was isolated.

^1H NMR (CDCl_3 , 400 MHz): 10.01 (s, 1H), 7.69 (m, 2H), 7.31 (m, 1H), 2.80 (q, $J = 7.5$ Hz, 2H), 2.32 (s, 3H), 1.32 (t, 3H) ppm.

^{13}C NMR (CDCl_3 , 126 MHz): 168.8, 159.4, 145.7, 140.6, 132.0, 126.8, 120.3, 120.0, 28.9, 23.5, 15.9 ppm.

HRMS Calculated for $[\text{C}_{11}\text{H}_{12}\text{N}_2\text{OS}+\text{H}]^+$: 221.0743, Found: 221.0737.



methyl [3-(trifluoromethyl)-4,5,6,7-tetrahydro-1H-indazol-1-yl]acetate, **66**.

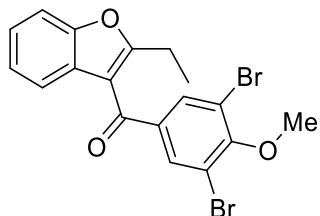
Reaction run at 2.0 mmol scale and 347 mg (66%) of white crystals was isolated.

Mp: 145-148°C. ^1H NMR (CDCl_3 , 400 MHz): 4.82 (s, 2H), 3.76 (s, 3H), 2.56 (m, 4H), 1.80 (m, 4H) ppm.

^{13}C NMR (CDCl_3 , 100 MHz): 167.6, 141.3, 139.2 (q, $J = 36.7$ Hz), 121.9 (q, $J = 269.1$ Hz), 115.5 (q, $J = 1.5$ Hz), 52.7, 50.5, 22.2, 22.0, 21.1, 19.9 ppm.

^{19}F NMR (377 MHz, CDCl_3): -61.7 ppm.

HRMS Calculated for $[\text{C}_{11}\text{H}_{13}\text{F}_3\text{N}_2\text{O}_2+\text{H}]^+$: 263.1002, Found: 263.0999.



(3,5-dibromo-4-methoxyphenyl)(2-ethyl-1-benzofuran-3-yl)methanone, **67**.

Reaction run at 4.0 mmol scale and 1.67 g (95%) of white non-crystalline powder was isolated.

^1H NMR (CDCl_3 , 400 MHz): 8.01 (s, 2H), 7.53 (dt, $J = 8.2$ Hz, $J = 0.9$ Hz, 1H), 7.44 (dt, $J = 7.6$ Hz, $J = 0.9$ Hz, 1H), 7.34 (ddd, $J = 8.3$ Hz, $J = 7.3$ Hz, $J = 1.5$ Hz, 1H), 7.27 (td, $J = 7.5$ Hz, $J = 1.1$ Hz, 1H), 4.01 (s, 3H), 2.92 (q, $J = 7.5$ Hz, 2H), 1.38 (t, $J = 7.5$ Hz, 3H)

^{13}C NMR (CDCl_3 , 100 MHz): 188.1, 166.9, 157.7, 153.7, 137.2, 133.6, 126.4, 124.7, 123.9, 121.0, 118.5, 115.3, 111.2, 60.9, 22.1, 12.2.

HRMS Calculated for $[\text{C}_{19}\text{H}_{16}\text{Br}_2\text{O}_4+\text{H}]^+$: 436.9383, Found: 436.9380.

2A.XIV. Details of DFT Calculations

1. Computational details

All density functional theory (DFT) calculations were performed with the Gaussian 16 (rev. A.03) electronic structure program suite.¹⁹ As noted in the text, geometry optimization and frequency calculations were done at the B3LYP-D3(BJ)/basis-I level of theory,²⁰⁻²³ where basis-I is the 6-31G(d,p)²⁴ basis set for non-metal atoms and the Stuttgart/Dresden effective core potential with its associated basis set (SDD) for Cu.²⁵ An “ultrafine” grid was used for numerical integration in DFT, together with an integral accuracy set to 10^{-12} . The natures of all stationary points were verified by calculating vibrational frequencies at the same level of theory; frequencies below 50 cm^{-1} were replaced with a value of 50 cm^{-1} in the vibrational partition function when computing thermal contributions to free energies ($T = 313.15\text{ K}$). For a best estimate of Gibbs free energies, single-point electronic energies were recomputed for the B3LYP-D3(BJ)/basis-I geometries using the M06-L²⁶ density functional and the def2-TZVP basis set²⁷ for non-metals and def2-TZVP basis/SDD pseudo potential for Cu (basis-II). All geometry optimizations, frequency calculations and single-point electronic energies employed the SMD continuum solvation model.²⁸ To mimic the 4:1 mixture of DCM:HFIP (DCM = Dichloromethane; $\epsilon=8.93$ and HFIP = Hexafluoro-2-propanol; $\epsilon=16.75$ ²⁹) used experimentally, solvent parameters for 5-nonanone having $\epsilon = 10.6 (\approx \frac{4}{5}\epsilon(\text{DCM}) + \frac{1}{5}\epsilon(\text{HFIP}))$ were employed. In some cases, transition-state (TS) geometries were located on the broken-symmetry (BS) singlet surface (e.g., TS1 and TS3, where the substrates pass from two closed-shell singlet species to two open-shell doublet species), and in those instances, the final electronic energies were spin-purified using the scheme proposed by Yamaguchi et al.³⁰

2. Cartesian coordinates of structures

Cartesian coordinates of all DFT-optimized structures are assembled in a separate coordinate file (.xyz).

3. Energetics for reactivity calculations

Single point electronic energies employing SMD solvation effects, $E(\text{sol})$, spin-purified electronic energies for broken-symmetry singlet TS structures, $E^1(\text{sol})$, and the absolute solution-phase Gibbs free energies, $G(\text{sol})$ of all relevant species are presented in Table 2A.13.

2A.XV. References

1. Altenhoff, G.; Goddard, R.; Lehmann, C. W.; Glorius, F. Sterically demanding, bioxazoline-derived N-heterocyclic carbene ligands with restricted flexibility for catalysis. *J. Am. Chem. Soc.*, **126**, 15195-15201 (2004).
2. Wang, H.-L. et al. Novel vanilloid receptor-1 antagonists: 3. the identification of a second-generation clinical candidate with improved physicochemical and pharmacokinetic properties. *J. Med. Chem.* **50**, 3528–3539 (2007).
3. Aoyama, T.; Teraswa, S.; Sudo, K.; Shioiri, New Methods and Reagents in Organic Synthesis. 46. Trimethylsilyldiazomethane: a convenient reagent for the O-methylation of phenols and enols. *Chem. Pharm. Bull.*, **32**, 3759-3760 (1984).
4. Meanwell, M. et al. Direct heterobenzylic fluorination, difluorination and trifluoromethylthiolation with dibenzenesulfonimide derivatives. *Chem. Sci.* **9**, 5608-5613 (2018).
5. Fang, Z., Feng, Y., Dong, H., Li, D. & Tang, T. Copper(i)-catalyzed radical decarboxylative imidation of carboxylic acids with N-fluoroarylsulfonimides. *Chem. Commun.* **52**, 11120–11123 (2016).
6. Yang, D. et al. Copper-catalyzed decarboxylative stereospecific amidation of cinnamic acids with N-fluorobenzenesulfonimide. *RSC Adv.* **6**, 72361–72365 (2016).
7. Jing, L. et al. An Efficient Method for Sulfonylation of Amines, Alcohols and Phenols with N-Fluorobenzenesulfonimide Under Mild Conditions. *Chem. Res. Chin. Univ.* **34**, 191–196 (2018).
8. Barba, I., Chinchilla, R., Gómez, C., Synthesis of phenyl substituted cyclohexa-1,4-dienes and cyclohexa-2,5-dienones by anodic methoxylation of alkylbiphenyls. *Tetrahedron* **46**, 7813-7822 (1990)
9. Sudalai, A., Talluri, S. K. NBS-catalyzed hydroamination and hydroalkoxylation of activated styrenes. *Org. Lett.*, **7**, 855–857 (2005).
10. Sawama, Y. et al. Chemoselective and direct functionalization of methyl benzyl ethers and unsymmetrical dibenzyl ethers by using iron trichloride. *Chem. Eur. J.* **20**, 2631–2636 (2014).
11. LaLonde, R. T., Ferrara, P. B. Reactions of arylcyclopropanes with n-bromosuccinimide in hydroxylic solvents. *J. Org. Chem.*, **37**, 2502-2505 (1972).
12. Guinaudau, H. et al. (+)-Uskudaramine: A novel type aporphine-benzylisoquinoline alkaloid. *J. Org. Chem.* **47**, 5406-5407 (1982).
13. Tokumaru, T.; Nakata, K. InCl₃-promoted intramolecular decarboxylative etherification of benzylic carbonates. *Tetrahedron Lett.*, **56**, 2336-2339 (2015).
14. Min, S., Yoshiki, O. Setsuo, T. Photolysis of tetraarylmethanes and 3-(triarylmethyl)pyridines *Bull. Chem. Soc. Jpn.* **63**, 2731-2733 (1990).
15. Masui, Y., Hattori, T., Onaka, M. Reversible Generation of labile secondary carbocations from alcohols in the nanospace of H-mordenite and their long-lasting preservation at ambient temperature. *J. Am. Chem. Soc.* **139**, 8612-8620, (2017).
16. Kuribayashi, T. et al. Patent Appl. WO 2009131129 A1 20091029 (2009).
17. Bauer, V. J. et al. Synthesis of spiro[isobenzofuran-1(3H),4'-piperidines] as potential central nervous system agents. 1, *J. Med. Chem.*, **19**, 1315-1324 (1976).

18. Kulkarni, G. C., Karmarkar, S. N., Kelkar, S. L., Wadia S. M. Generation of α -acylcarbenium ions : a novel uncatalysed C-C bond formation at room temperature. *Tetrahedron.*, **44** , 5189-5198 (1988).
19. Gaussian 16, Revision A.03, Frisch, M. J.; Trucks, G. W.; Schlegel, H. B.; Scuseria, G. E.; Robb, M. A.; *et al.* Gaussian, Inc., Wallingford CT, 2016.
20. Becke, A. D. Density-Functional Thermochemistry. III. The Role of Exact Exchange. *J. Chem. Phys.* **98**, 5648 (1993).
21. Becke, A. D. Density-functional Thermochemistry. IV. A New Dynamical Correlation Functional and Implications for Exact-exchange Mixing. *J. Chem. Phys.* **104**, 1040 (1996).
22. Grimme, S.; Ehrlich, S.; Goerigk, L. Effect of the Damping Function in Dispersion Corrected Density Functional Theory. *J. Comput. Chem.* **32**, 1456–1465 (2011).
23. Johnson, E. R.; Becke, A. D. A Post-Hartree-Fock Model of Intermolecular Interactions: Inclusion of Higher-Order Corrections. *J. Chem. Phys.* **124**, 174104 (2006).
24. Hehre, W. J.; Ditchfield, R.; Pople, J. A. Self—Consistent Molecular Orbital Methods. XII. Further Extensions of Gaussian—Type Basis Sets for Use in Molecular Orbital Studies of Organic Molecules. *J. Chem. Phys.* **56**, 2257–2261 (1972).
25. Dolg, M.; Wedig, U.; Stoll, H.; Preuss, H. Energy-adjusted Ab Initio Pseudopotentials for the First Row Transition Elements. *J. Chem. Phys.* **86**, 866–872 (1987).
26. Zhao, Y.; Truhlar, D. G. A New Local Density Functional for Main-Group Thermochemistry, Transition Metal Bonding, Thermochemical Kinetics, and Noncovalent Interactions. *J. Chem. Phys.* **125**, 194101 (2006).
27. Weigend, F.; Ahlrichs, R. Balanced Basis Sets of Split Valence, Triple Zeta Valence and Quadruple Zeta Valence Quality for H to Rn: Design and Assessment of Accuracy. *Phys. Chem. Chem. Phys.* **7**, 3297 (2005).
28. Marenich, A. V.; Cramer, C. J.; Truhlar, D. G. Universal Solvation Model Based on Solute Electron Density and on a Continuum Model of the Solvent Defined by the Bulk Dielectric Constant and Atomic Surface Tensions. *J. Phys. Chem. B* **113**, 6378–6396 (2009).
29. Evans, D. F.; Matesich, S. M. A. Ionic Association in Hydrogen-Bonding Solvents. *J. Solution Chem.* **2**, 193–216 (1973).
30. Yamaguchi, K.; Takahara, Y.; Fueno, T.; Houk, K. N. Extended Hartree-Fock (EHF) Theory of Chemical Reactions. *Theor. Chim. Acta* **73**, 337–364 (1988).

Appendix B: Supporting Information Chapter 3

3B.I. General Considerations

All reagents were purchased and used as received unless otherwise noted. Cu salts were purchased from Aldrich. Benzylic C–H substrates were purchased from Alfa Aesar, Ambeed, Ark Pharm, AstaTech, Chem-Impex, Combi-Blocks, Enamine, Matrix Chemicals, Millipore Sigma, Oakwood Chemicals and TCI America. Additives were purchased from Aldrich or TCI America. N-Fluorobenzenesulfonimide (NFSI) was purchased from Ark Pharm and Combi-Blocks. Diisopropyl phosphites were purchased from Aldrich, Oakwood Chemicals, Alfa Aesar and TCI America. All the reagents were used without further purification. Substrate **1q** was prepared with the procedure reported in literature.¹

¹H, ¹³C, ¹⁹F and all the 2D NMR spectra were recorded on Bruker 400 MHz or Bruker 500 MHz spectrometers and chemical shifts are reported in parts per million (ppm). ¹H NMR spectra were referenced to tetramethylsilane at 0.00 ppm and ¹³C NMR spectra were referenced to CDCl₃ at 77.16 ppm. Column chromatography was performed using a Biotage Isolera One® with reusable 25 g SNAP Ultra® cartridges, 25 g Sfär® cartridges or standard silica cartridges. Further purification of impure samples was conducted using preparative thin-layer chromatography with Analtech® Glass-Backed Silica G UNIPLATES®. High-resolution mass spectra were obtained using a Thermo Q Exactive™ Plus (ESI or ASAP-MS) by the mass spectrometry facility at the University of Wisconsin. Melting points were determined using a DigiMelt MPA160 SRS melting point apparatus.

3B.II. Experimental Procedures for Cross-Coupling Reactions

General Procedure (I) for Cross Coupling of N–H Nucleophiles and Benzylic C–H Substrates (pressure tube, temperature ≥ 50 °C)

Copper(I) chloride (2.0 mg, 0.020 mmol, 10 mol%), tetrabutylammonium chloride (2.8 mg, 0.020 mmol, 10 mol% or 16.8 mg, 0.060 mmol, 30 mol%), NFSI (94.6 mg, 0.30 mmol, 1.5 equiv), N–H nucleophile (0.50 mmol, 2.5 equiv) and benzylic substrate (if solid, 0.20 mmol, 1.0 equiv) were added to a glass pressure tube under air. The pressure tube was then moved to a glove box under N₂ atmosphere. Solvent (1.0 mL), benzylic substrate (if liquid, 0.20 mmol, 1.0 equiv) and diisopropyl phosphite (16.3 μ L, 0.10 mmol, 0.5 equiv) were added to the tube. The tube was sealed in the glove box and taken out to a hot plate. The sealed tube was heated at 50 °C with stirring for 16 h. When the reaction finished, the mixture was cooled down to room temperature. Then the mixture was evaporated under vacuum and the crude mixture was purified by column chromatography (silica gel, eluted by pentane:ethyl acetate = 20:1 to 4:1). Trimethylsilyl triflate (3.6 μ L, 0.020 mmol, 10 mol%) or BF₃•OEt₂ (2.5 μ L, 0.020 mmol, 10 mol%) was added in the glove box when they were used as an additive instead of tetrabutylammonium chloride.

General Procedure (II) for Cross Coupling of N–H nucleophiles and Benzylic C–H Substrates (glass vial, temperature ≤ 40 °C)

Copper(I) chloride (2.0 mg, 0.020 mmol, 10 mol%), tetrabutylammonium chloride (5.6 mg, 0.020 mmol, 10 mol% or 16.8 mg, 0.060 mmol, 30 mol%), NFSI (94.6 mg, 0.30 mmol, 1.5 equiv), N–H nucleophile (0.50 mmol, 2.5 equiv) and benzylic substrate (if solid, 0.20 mmol, 1.0 equiv) were added under air to a 4 ml borosilicate glass vial containing a magnetic stir bar. Then the vial was capped with a pierceable Teflon cap. A needle was pierced through the cap to facilitate exchange of the vial headspace with the atmosphere. Then the vial was moved into a glove box, through three vacuum-nitrogen-backfill cycles. The needle was removed, and the vial was taken out of the glove box (now sealed under an inert gas). Solvent (1.0 mL), benzylic substrate (if liquid, 0.20 mmol, 1.0 equiv), and diisopropyl phosphite (16.3 μ L, 0.10 mmol, 0.5 equiv) were added into the vial by injection through the cap. The sealed vial was heated at 30 °C and stirred for 16 h. When the reaction finished, the mixture was cooled down to room temperature. Then the mixture was evaporated under vacuum and the crude mixture was purified by column chromatography (silica gel, eluted by pentane:ethyl acetate = 20:1 to 4:1).

3B.III. Optimization of the Reaction Conditions

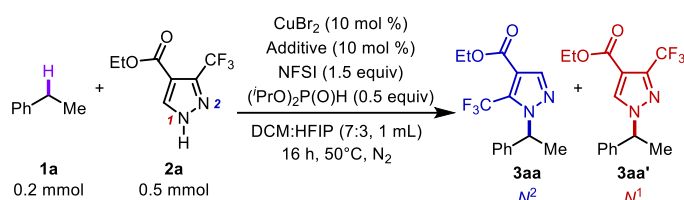
Optimization of reaction conditions were conducted according to general procedure (I) or (II), with variations specified in each table. Reaction yields were monitored by ^1H NMR spectroscopy with 0.2 mmol mesitylene as the internal standard.

Table 3B.1a. Assessment of Ancillary Ligands

| | | | | | |
|---------------------------------|--------------------------------|---------------------------------|-------------------------------|-------------------------------|--------------------------------|
| None | | | | | |
| 37% (18+19%) Yield 58% Conv. | 50% (45+5%) Yield 73% Conv. | 11% (11+0) Yield 25% Conv. | 14% (12+2) Yield 28% Conv. | 18% (16+2) Yield 34% Conv. | 6% (6+0) Yield 25% Conv. |
| | | | | | |
| 10% (10+0) Yield 25% Conv. | 29% (28+1) Yield 43% Conv. | 74% (64+10) Yield 100% Conv. | 51% (48+3) Yield 70% Conv. | 7% (7+0) Yield 16% Conv. | 9% (9+0) Yield 22% Conv. |
| | | | | | |
| 12% (12+0) Yield 25% Conv. | 0% (0+0) Yield 13% Conv. | 19% (18+1) Yield 55% Conv. | 60% (58+2) Yield 79% Conv. | 30% (26+4) Yield 58% Conv. | 68% (56+12) Yield 85% Conv. |

Table 3B.2b. Ligand Comparison with Selected Nucleophiles

| | | |
|---------------------------------|--------------------------------|-------------------------------|
| | | |
| 74% (64+10) Yield 100% Conv. | 68% (56+12) Yield 85% Conv. | 12% (12+0) Yield 25% Conv. |
| | | |
| 0% Yield 4% Conv. | 61% (52+9) Yield 88% Conv. | 25% (20+5) Yield 40% Conv. |

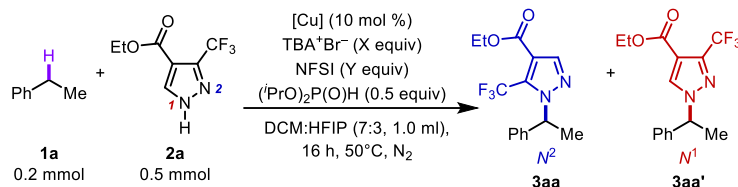
Table 3B.2. Effect of Different Additives in Controlling the Regioselectivity^a

| Entry | Additive | Conv. of 1a (%) | Yield of N-2 (%) | Yield of N-1 (%) | N-2:N-1 |
|-----------------|--|------------------------|-------------------------|-------------------------|----------------|
| 1 | IMes ⁺ Cl ⁻ | 100 | 63 | 7 | 9.0:1 |
| 2 | TBA ⁺ Br ⁻ | 100 | 72 | 4 | 18:1 |
| 3 | TBA ⁺ NO ₃ ⁻ | 91 | 54 | 2 | 13:1 |
| 4 | TBA ⁺ Cl ⁻ | 100 | 70 | 6 | 11.7:1 |
| 5 | (none) | 89 | 57 | 5 | 9.3:1 |
| 6 | TBA ⁺ PF ₆ ⁻ | 91 | 57 | 11 | 5.8:1 |
| 7 | TBA ⁺ HSO ₄ ⁻ | 100 | 57 | 10 | 5.7:1 |
| 8 | TBA ⁺ BH ₂ ⁻ | 88 | 52 | 24 | 2.2:1 |
| 9 | TBA ⁺ OTf ⁻ | 96 | 45 | 23 | 2.1:1 |
| 10 | TBA ⁺ ClO ₄ ⁻ | 100 | 63 | 34 | 1.7:1 |
| 11 | TBDMSCl | 94 | 44 | 27 | 1.6:1 |
| 12 | TMSCN | 91 | 42 | 28 | 1.5:1 |
| 13 | TIPSCl | 91 | 36 | 29 | 1.2:1 |
| 14 | TBA ⁺ BF ₄ ⁻ | 100 | 26 | 34 | 1:1.3 |
| 15 | TEA ⁺ BF ₄ ⁻ | 97 | 35 | 43 | 1:1.2 |
| 16 | (Ph) ₃ SiCl | 97 | 34 | 37 | 1:1.1 |
| 17 | TMSCl | 94 | 30 | 47 | 1:1.8 |
| 18 | BF ₃ •OEt ₂ | 91 | 6 | 60 | 1:10 |
| 19 | TMSOTf | 42 | 2 | 38 | 1:19 |
| 20 ^b | TMSOTf | 100 | 1 | 66 | 1:66 |

^aTBA, tetrabutylammonium; TEA, tetraethylammonium; TMS, trimethylsilyl; TIPS, triisopropylsilyl; TBDMS, *tert*-butyldimethyl; DCM, dichloromethane; HFIP, hexafluoroisopropanol; Conv., conversion.

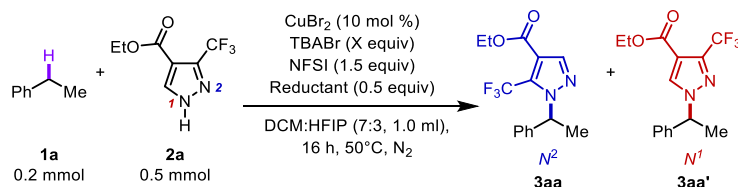
^bReaction conducted at 60 °C.

Note: The screening of salts in this study indicate the imidazolium cation identified in previous screening results does not play an important role in reactivity or *N*¹/*N*² regioselectivity and can be replaced by tetrabutylammonium cation. When the additive contains a Lewis acid, such as TMSCl or BF₃•OEt₂, the regioselectivity switches to favor *N*¹.

Table 3B.3. Optimization of the Reaction Conditions with Various Solvents, Cu Salts and Temperature^a

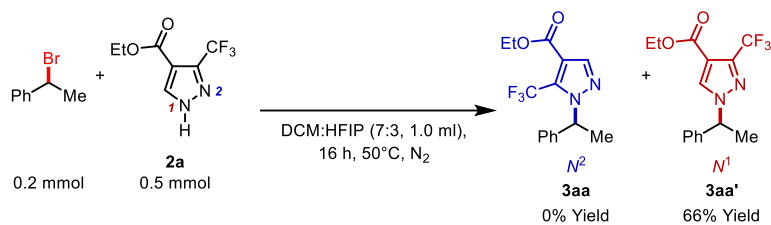
| Entry | [Cu] | Solvent | X | Y | Z | Conv. of 1 (%) | Yield of N-2 (%) | Yield of N-1 (%) | N-2:N-1 |
|-------|-------------------|-------------------|------------------|-----|-----|-----------------------|-------------------------|-------------------------|----------------|
| 1 | CuCl | DCE | 0.1 | 1.5 | 2.5 | 94 | 60 | 3 | 20:1 |
| 2 | CuCl | PhH | 0.1 | 1.5 | 2.5 | 58 | 12 | 0 | – |
| 3 | CuCl | PhCl | 0.1 | 1.5 | 2.5 | 91 | 48 | 0 | – |
| 4 | CuCl | PhCF ₃ | 0.1 | 1.5 | 2.5 | 64 | 24 | 1 | 24:1 |
| 5 | CuCl | PhNO ₂ | 0.1 | 1.5 | 2.5 | 64 | 12 | 1 | 12:1 |
| 6 | CuCl | MeNO ₂ | 0.1 | 1.5 | 2.5 | 97 | 21 | 34 | 1:1.6 |
| 7 | CuCl | DCM | 0.1 | 1.5 | 2.5 | 100 | 48 | 8 | 6:1 |
| 8 | CuCl | HFIP | 0.1 | 1.5 | 2.5 | 91 | 2 | 39 | 1:19.5 |
| 10 | CuCl | DCM:HFIP (8:2) | 0.1 | 1.5 | 2.5 | 100 | 63 | 9 | 7:1 |
| 11 | CuCl | DCM:HFIP (6:4) | 0.1 | 1.5 | 2.5 | 100 | 45 | 16 | 2.8:1 |
| 12 | CuCl | DCM:HFIP (7:3) | 0.1 | 1.5 | 2.5 | 100 | 63 | 8 | 7.9:1 |
| 13 | CuOAc | DCM:HFIP=7:3 | 0.1 | 1.5 | 2.5 | 94 | 66 | 6 | 11:1 |
| 14 | CuI | DCM:HFIP=7:3 | 0.1 | 1.5 | 2.5 | 100 | 57 | 11 | 5.2:1 |
| 15 | CuBr | DCM:HFIP=7:3 | 0.1 | 1.5 | 2.5 | 100 | 57 | 11 | 5.2:1 |
| 16 | CuCl ₂ | DCM:HFIP=7:3 | 0.1 | 1.5 | 2.5 | 100 | 60 | 10 | 6:1 |
| 17 | CuBr ₂ | DCM:HFIP=7:3 | 0.1 | 1.5 | 2.5 | 100 | 63 | 11 | 5.7:1 |
| 18 | CuBr ₂ | DCM:HFIP=7:3 | 0.1 | 1.0 | 2.5 | 94 | 60 | 8 | 7.5:1 |
| 19 | CuBr ₂ | DCM:HFIP=7:3 | 0.1 | 2.0 | 2.5 | 100 | 63 | 8 | 7.9:1 |
| 20 | CuBr ₂ | DCM:HFIP=7:3 | 0.1 | 1.5 | 2.5 | 100 | 69 | 6 | 11.5:1 |
| 21 | CuBr ₂ | DCM:HFIP=7:3 | 0.3 | 1.5 | 2.5 | 97 | 72 | 2 | 36:1 |
| 22 | CuCl | DCM:HFIP=7:3 | 0.3 ^a | 1.5 | 2.5 | 100 | 76 | 4 | 19:1 |
| 23 | CuCl | DCM:HFIP=7:3 | 0.1 ^a | 1.5 | 2.5 | 100 | 75 | 4 | 19:1 |

^aReactions were conducted with TBA⁺Cl⁻ instead of TBA⁺Br⁻. DCE, 1,2-dichloroethane; DCM, DCM; HFIP, hexafluoroisopropanol; T, temperature; Conv., conversion.

Table 3B.4. Investigation of various reductants with ethylbenzene as the substrate

| Entry | Reductant | Conv. of 1 (%) | Yield of N-2 (%) | Yield of N-1 (%) | N-2:N-1 |
|-------|--|-----------------------|-------------------------|-------------------------|----------------|
| 1 | – | 100 | 63 | 5 | 13:1 |
| 2 | (MeO) ₂ P(O)H | 100 | 33 | 5 | 6.6:1 |
| 3 | (EtO) ₂ P(O)H | 100 | 42 | 7 | 6.0:1 |
| 4 | (iPrO) ₂ P(O)H | 100 | 68 | 4 | 17:1 |
| 5 | (^t BuO) ₂ P(O)H | 76 | 45 | 4 | 11:1 |
| 6 | (ⁿ BuO) ₂ P(O)H | 100 | 51 | 7 | 7.3:1 |
| 7 | (MeO) ₂ MeSiH | 91 | 48 | 3 | 16:1 |
| 8 | (EtO) ₂ MeSiH | 94 | 51 | 5 | 10:1 |
| 9 | PhNHNHPh | 28 | 4 | 0 | – |
| 10 | EtCO ₂ NHNHCO ₂ Et | 100 | 51 | 2 | 26:1 |
| 11 | P(ⁿ Bu) ₃ | 88 | 54 | 6 | 9.0:1 |
| 12 | Sodium Ascorbate | 100 | 36 | 11 | 3.3:1 |

3B.IV. Displacement of Benzylic Bromide with 2a



2a (104 mg, 0.50 mmol, 2.5 equiv) was added to a glass pressure tube under air. The pressure tube was then moved to a glove box under N₂ atmosphere. DCM:HFIP (7:3, 1.0 mL) and (1-Bromoethyl)benzene (27.3 μL, 0.20 mmol, 1.0 equiv) and were added to the tube. The tube was sealed in the glove box and taken out to a hot plate. The sealed tube was heated at 50 °C with stirring for 16 h. When the reaction finished, the mixture was cooled down to room temperature. Then an aliquot of the mixture was taken, diluted with CDCl₃. Reaction yield was monitored by ¹H NMR spectroscopy with 0.2 mmol mesitylene as the internal standard.

3B.V. Additional Screening Data with Benzylic C–H Substrates and Azoles

Not all substrates tested afforded good reactivity in the cross-coupling reactions, and a survey of suboptimal results are provided in Figure S1. Ethylbenzene derivatives with electron-deficient *para*-substituents are less reactive toward C–H activation, and lower conversions and yields are observed (Figure 3B.1A and B). Pyridine-containing substrates do afford the desirable products but often with low yield (Figure 3B.1C). More electron-rich azoles appear to inhibit the C–N cross coupling reactivity, possibly reflecting coordination/inhibition of the copper catalyst or because they undergo side reactions with NFSI (Figure 3B.1D). The presence of large substituents near the benzylic C–H site also inhibits the conversion of the starting material (Figure 3B.1E). Reaction yields were monitored by ^1H NMR spectroscopy with 0.2 mmol mesitylene as the internal standard.

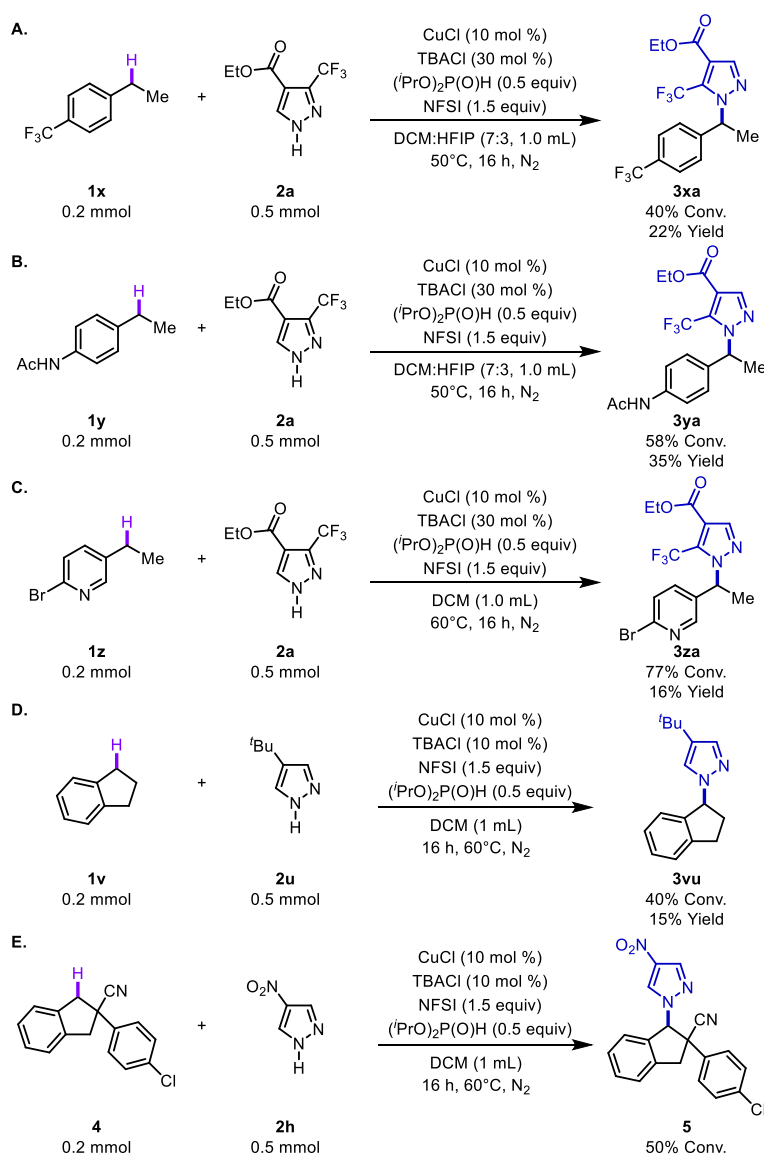


Figure 3B.1. Screening data with additional benzylic C–H substrates and azoles.

A selection of cross coupling reactions of benzylic C–H substrates and azoles were further analyzed to insight the mass balance of this method.

- While TBABr has shown high selectivity for *N*-2 regioisomer in coupling reactions with **2a**, when electron-rich substrates like **1h** were employed, formation of brominated products on the arene were observed. Substituting TBABr with TBACl avoided this side reactivity (Figure 3B.2A).
- Minor side products were observed where the byproduct benzenesulfonimide from NFSI was introduced to the benzylic sites, especially when cyclic substrates were engaged (Figure 3B.2B and 3B.2C).

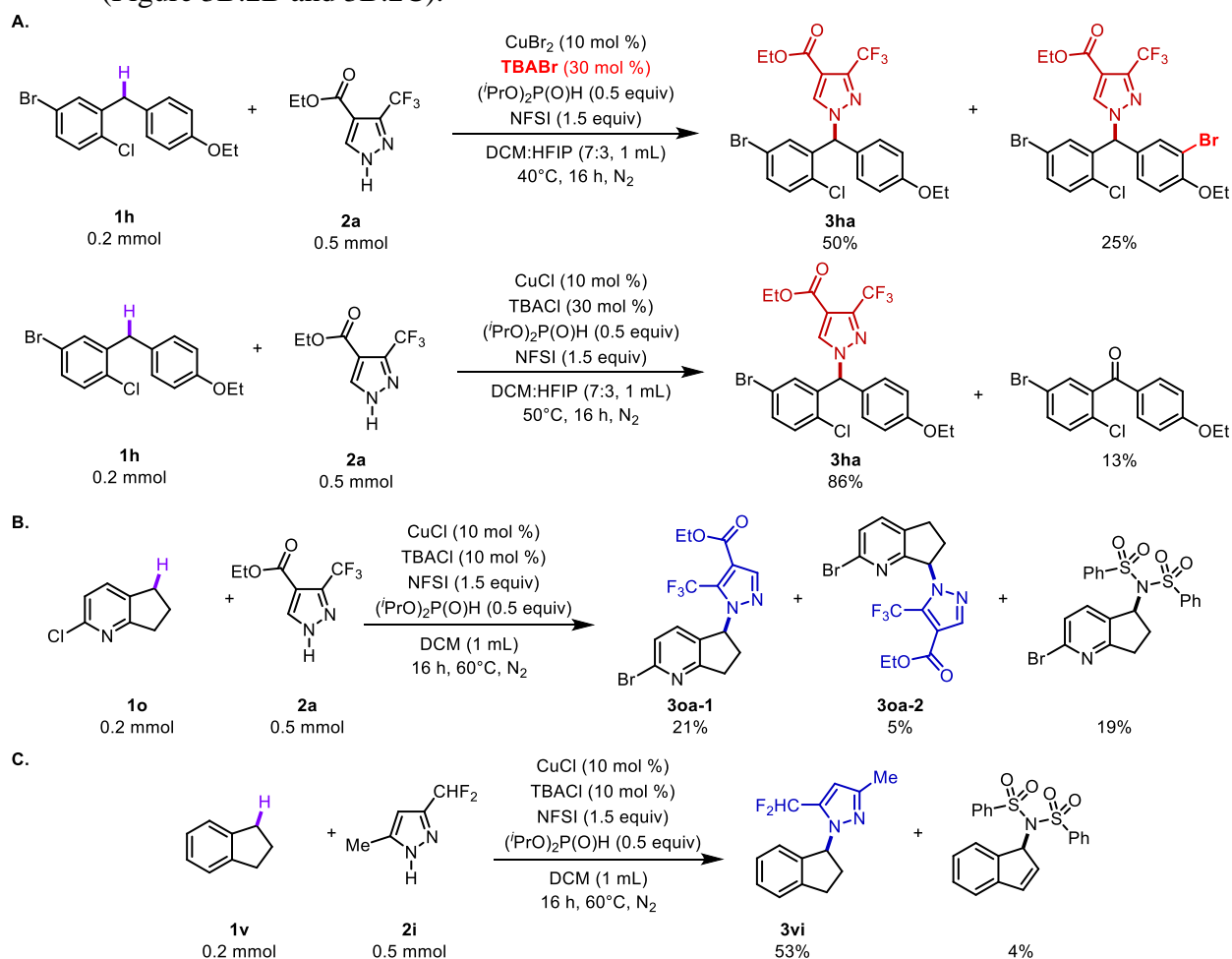


Figure 3B.2. Further analyses of reaction outcomes of cross couplings of benzylic C–H bonds and azoles

3B.VI. Additional Screening Data with Benzylic C–H Substrates and Azoles

A. Benzylic C–H cross coupling products with 2a

All the *N*-1 and *N*-2 regioisomers were assigned based on 2D NMR spectra (HSQC and HMBC), along with additional characteristics in the ^{13}C and ^{19}F NMR spectra.

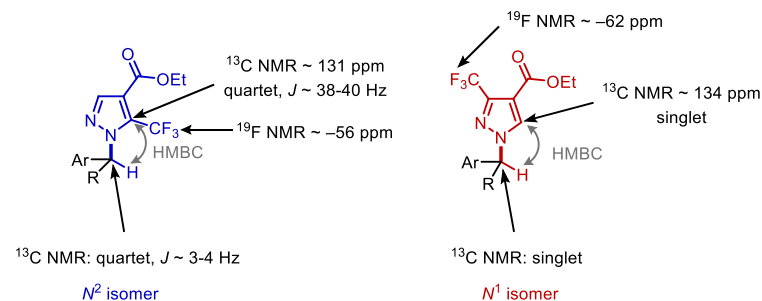


Figure 3B.3. Evidence for regioisomer assignment of benzylic C–H cross coupling products with 2a

B. Benzylic C–H cross coupling products with other ambidentate azoles

Regioisomers with other azoles were assigned based on 2D NMR spectra (HSQC and HMBC), literature values and/or the number of peaks in ^{13}C NMR spectra.

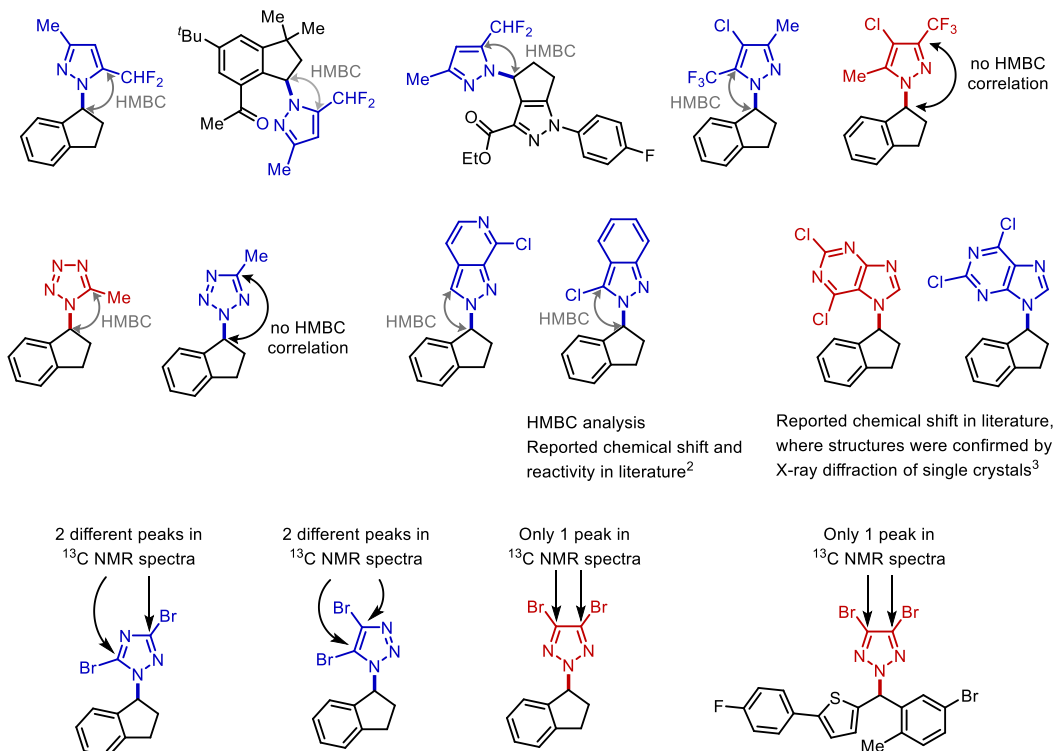


Figure 3B.4. Proof of regioisomer assignment for benzylic C–H cross coupling products with other ambidentate azoles

3B.VII. Crystallization and Crystallographic Data for $[(\text{C}_6\text{H}_5)\text{N}(\text{CH}_3)_3]_2[\text{CuBr}_4]$ and **2a**

Preparation

Copper(I) bromide (28.7 mg, 0.2 mmol, 1.0 equiv) and trimethylphenylammonium bromide (129.7 mg, 0.6 mmol, 3.0 equiv) were weighed into a 4 mL borosilicate glass vial in a glove box under nitrogen atmosphere, followed by the addition of 1 mL 1,1,1,3,3,3-hexafluoroisopropanol. N-fluorobenzenesulfonimide (31.5 mg, 0.1 mmol, 0.5 equiv) was then added into the solution. The vial was then sealed with a Teflon cap and the reaction mixture was then heated at 50°C for 30 min. After that, **2a** (166.5 mg, 0.4 mmol, 4.0 equiv) was added into the solution. The reaction mixture was then removed from the glovebox and heated at 50°C on a hot plate for 16 h before cooling down to room temperature. The 4 mL glass vial was uncapped and placed in a 15 mL borosilicate glass vial containing pentane. The 15 mL glass vial was then sealed with a 15 mL Teflon cap to allow vapor diffusion. Two kinds of crystals were found in the glass vial: blue crystal $[(\text{C}_6\text{H}_5)\text{N}(\text{CH}_3)_3]_2[\text{CuBr}_4]$ and colorless crystal **2a**.

Crystallographic Data for $[(\text{C}_6\text{H}_5)\text{N}(\text{CH}_3)_3]_2[\text{CuBr}_4]$

Data Collection

A blue crystal with approximate dimensions 0.14 x 0.01 x 0.005 mm³ was selected under oil under ambient conditions and attached to the tip of a MiTeGen MicroMount©. The crystal was mounted in a stream of cold nitrogen at 100(1) K and centered in the X-ray beam by using a video camera.

The crystal evaluation and data collection were performed on a Bruker Quazar SMART APEXII diffractometer with Mo K α ($\lambda = 0.71073 \text{ \AA}$) radiation and a diffractometer to crystal distance of 4.96 cm.⁴

The initial cell constants were obtained from three series of ω scans at different starting angles. Each series consisted of 12 frames collected at intervals of 0.5° in a 6° range about ω with the exposure time of 30 seconds per frame. The reflections were successfully indexed by an automated indexing routine built in the APEXII program suite. The final cell constants were calculated from a set of 5662 strong reflections from the actual data collection.

The data were collected by using a full sphere data collection routine to survey reciprocal space to the extent of a full sphere to a resolution of 0.80 Å. A total of 28817 data were harvested by collecting 4 sets of frames with 0.6° scans in ω and ϕ with exposure times of 180 sec per frame. These highly redundant datasets were corrected for Lorentz and polarization effects. The absorption correction was based on fitting a function to the empirical transmission surface as sampled by multiple equivalent measurements.⁵

Structure Solution and Refinement

The systematic absences in the diffraction data were consistent for the space groups Pn and $P2/n$. The E -statistics strongly suggested the centrosymmetric space group $P2/n$ that yielded chemically reasonable and computationally stable results of refinement.⁶⁻¹¹

A successful solution by direct methods provided most non-hydrogen atoms from the E -map. The remaining non-hydrogen atoms were located in an alternating series of least-squares cycles and difference Fourier maps. All non-hydrogen atoms were refined with anisotropic displacement coefficients. All hydrogen atoms were included in the structure factor calculation at idealized positions and were allowed to ride on the neighboring atoms with relative isotropic displacement coefficients.

The structure crystallizes as an inorganic salt with the formula $[(C_6H_5)N(CH_3)_3]_2[CuBr_4]$. Atom Br4 in the $[CuBr_4]^{2-}$ anion is disordered over two positions, with a major component occupancy of 58.5(16) %.

The structure also contains two trimethylaniline cations. One of these cations resides on a crystallographic general position and is fully occupied. The second cation is disordered over two different crystallographic sites. Both of these sites are crystallographic special positions corresponding to two-fold axes. Thus, this cation presents itself in the symmetry-independent unit as being 50% occupied at two different crystallographic sites and is equally disordered across the crystallographic two-fold axis at each site. This cation was refined with 1,2 and 1,3 distance restraints, as well as with atomic displacement parameter restraints and constraints.

The final least-squares refinement of 305 parameters against 4749 data resulted in residuals R (based on F^2 for $I \geq 2\sigma$) and wR (based on F^2 for all data) of 0.0453 and 0.0962, respectively. The final difference Fourier map was featureless.

Summary

Crystal Data for $C_{18}H_{28}Br_4CuN_2$ ($M = 655.60$ g/mol): monoclinic, space group $P2/n$ (no. 13), $a = 9.247(4)$ Å, $b = 8.397(3)$ Å, $c = 29.837(10)$ Å, $\beta = 93.608(11)$ °, $V = 2312.2(14)$ Å³, $Z = 4$, $T = 99.99$ K, $\mu(\text{Mo K}\alpha) = 7.862$ mm⁻¹, $D_{\text{calc}} = 1.883$ g/cm³, 28817 reflections measured ($2.736^\circ \leq 2\theta \leq 52.85^\circ$), 4749 unique ($R_{\text{int}} = 0.0705$, $R_{\text{sigma}} = 0.0545$) which were used in all calculations. The final R_1 was 0.0453 ($I > 2\sigma(I)$) and wR_2 was 0.0962 (all data).

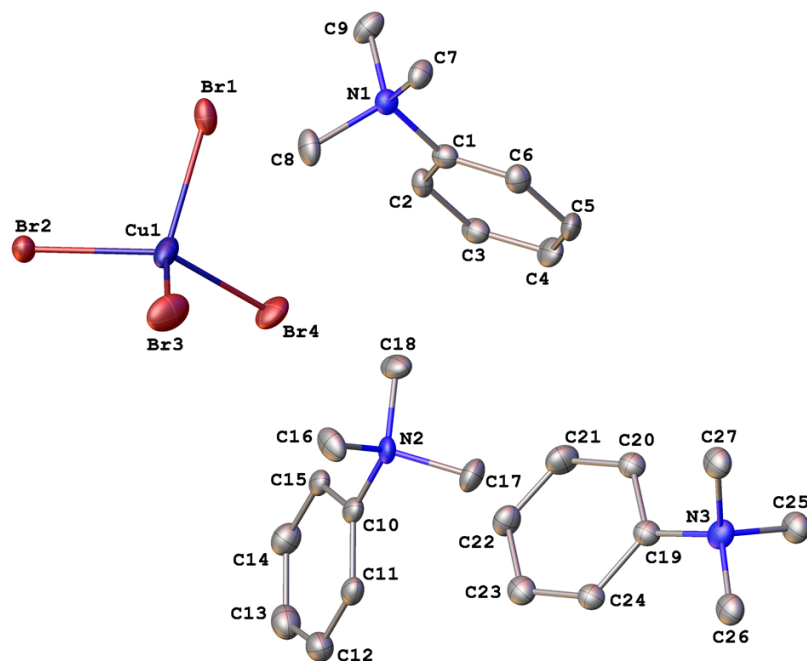


Figure 3B.5. A molecular drawing of $[(C_6H_5)N(CH_3)_3]_2[CuBr_4]$. The *N,N,N*-trimethylanilinium cations containing atoms N2 and N3 are 50% occupied. All atoms are shown with 50% probability ellipsoids. All H atoms and minor disorder components are omitted.

Table 3B.5. Crystal data and structure refinement for [(C₆H₅)N(CH₃)₃]₂[CuBr₄].

| | |
|--|---|
| Empirical formula | [(C ₆ H ₅)N(CH ₃) ₃] ₂ [CuBr ₄] |
| Formula weight | 655.60 |
| Temperature/K | 99.99 |
| Crystal system | monoclinic |
| Space group | <i>P2/n</i> |
| <i>a</i> /Å | 9.247(4) |
| <i>b</i> /Å | 8.397(3) |
| <i>c</i> /Å | 29.837(10) |
| α /° | 90 |
| β /° | 93.608(11) |
| γ /° | 90 |
| Volume/Å ³ | 2312.2(14) |
| <i>Z</i> | 4 |
| ρ_{calc} /cm ³ | 1.883 |
| μ /mm ⁻¹ | 7.862 |
| <i>F</i> (000) | 1276.0 |
| Crystal size/mm ³ | 0.14 × 0.01 × 0.005 |
| Radiation | Mo K α (λ = 0.71073) |
| 2 Θ range for data collection/° | 2.736 to 52.85 |
| Index ranges | -11 ≤ <i>h</i> ≤ 11, -10 ≤ <i>k</i> ≤ 9, -37 ≤ <i>l</i> ≤ 35 |
| Reflections collected | 28817 |
| Independent reflections | 4749 [<i>R</i> _{int} = 0.0705, <i>R</i> _{sigma} = 0.0545] |
| Data/restraints/parameters | 4749/95/305 |
| Goodness-of-fit on <i>F</i> ² | 1.067 |
| Final <i>R</i> indexes [<i>I</i> ≥ 2 σ (<i>I</i>)] | <i>R</i> ₁ = 0.0453, <i>wR</i> ₂ = 0.0879 |
| Final <i>R</i> indexes [all data] | <i>R</i> ₁ = 0.0727, <i>wR</i> ₂ = 0.0962 |
| Largest diff. peak/hole / e Å ⁻³ | 0.70/-1.02 |

Crystallographic Data for 2a

Data Collection

A colorless crystal with approximate dimensions 0.50 x 0.40 x 0.40 mm³ was selected under oil under ambient conditions and attached to the tip of a MiTeGen MicroMount[®]. The crystal was mounted in a stream of cold nitrogen at 100(1) K and centered in the X-ray beam by using a video camera.

The crystal evaluation and data collection were performed on a Bruker SMART APEXII diffractometer with Cu K α ($\lambda = 1.54178 \text{ \AA}$) radiation and the diffractometer to crystal distance of 4.03 cm.⁴

The initial cell constants were obtained from three series of ω scans at different starting angles. Each series consisted of 50 frames collected at intervals of 0.5° in a 25° range about ω with an exposure time of 10 seconds per frame. The reflections were successfully indexed by an automated indexing routine built in the APEX3 program. The final cell constants were calculated from a set of 2234 strong reflections from the actual data collection.

The data were collected by using a full sphere data collection routine to survey reciprocal space to the extent of a full sphere to a resolution of 0.81 Å. A total of 3882 data were harvested by collecting 9 sets of frames with 0.6° scans in ω and ϕ with an exposure time 5-20 sec per frame. These highly redundant datasets were corrected for Lorentz and polarization effects. The absorption correction was based on fitting a function to the empirical transmission surface as sampled by multiple equivalent measurements.⁵

Structure Solution and Refinement

The systematic absences in the diffraction data were consistent for the space groups $P2_1/m$ and $P2_1$. The E -statistics strongly suggested the centrosymmetric space group $P2_1/m$ that yielded chemically reasonable and computationally stable results of refinement.⁶⁻¹¹

A successful solution by direct methods provided most non-hydrogen atoms from the E -map. The remaining non-hydrogen atoms were located in an alternating series of least-squares cycles and difference Fourier maps. All non-hydrogen atoms were refined with anisotropic displacement coefficients.

The molecule resides on a crystallographic mirror plane.

The final least-squares refinement of 99 parameters against 912 data resulted in residuals R (based on F^2 for $I \geq 2\sigma$) and wR (based on F^2 for all data) of 0.0305 and 0.0814, respectively. The final difference Fourier map was featureless.

Summary

Crystal Data for C₇H₇F₃N₂O₂ ($M = 208.15 \text{ g/mol}$): monoclinic, space group $P2_1/m$ (no. 11), $a = 6.7889(11) \text{ \AA}$, $b = 6.6884(5) \text{ \AA}$, $c = 9.9202(8) \text{ \AA}$, $\beta = 105.469(11)^\circ$, $V = 434.13(9) \text{ \AA}^3$, $Z = 2$, $T = 99.97 \text{ K}$, $\mu(\text{Cu K}\alpha) = 1.420 \text{ mm}^{-1}$, $D_{\text{calc}} = 1.592 \text{ g/cm}^3$, 3882 reflections measured ($9.25^\circ \leq 2\Theta \leq 144.162^\circ$), 912 unique ($R_{\text{int}} = 0.0278$, $R_{\text{sigma}} = 0.0202$) which were used in all calculations. The final R_1 was 0.0305 ($I > 2\sigma(I)$) and wR_2 was 0.0814 (all data).

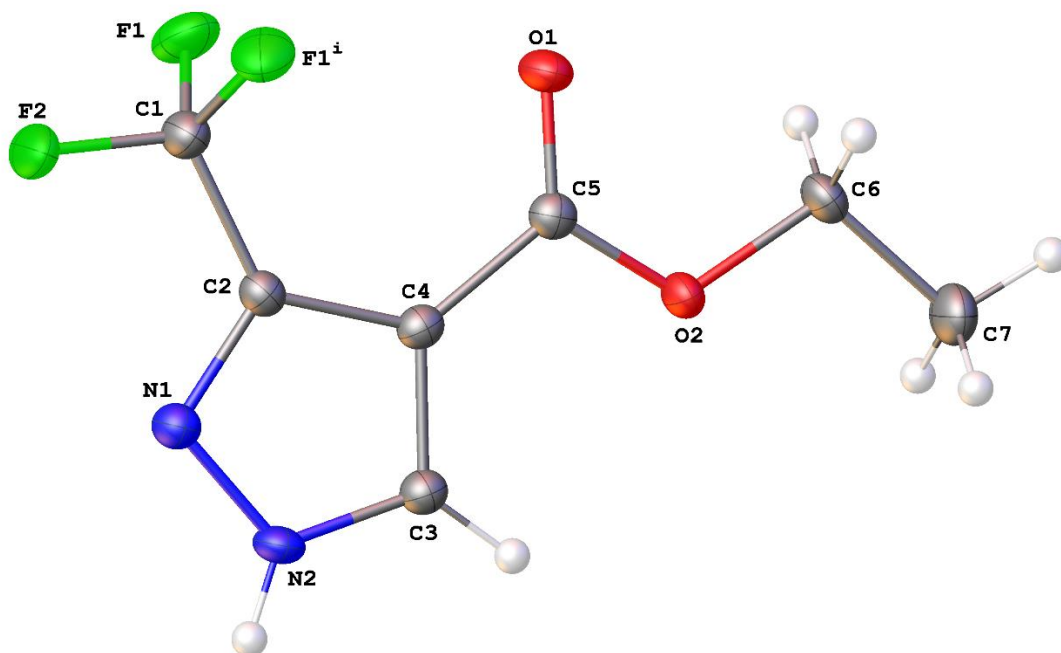


Figure 3B.6. A molecular drawing of **2a** shown with 50% probability ellipsoids for non-hydrogen atoms. [Symmetry code: (i) $x, 3/2 - y, z$.]

Table 3B.6. Crystal data and structure refinement for **2a**.

| | |
|--|---|
| Empirical formula | C ₇ H ₇ F ₃ N ₂ O ₂ |
| Formula weight | 208.15 |
| Temperature/K | 99.97 |
| Crystal system | monoclinic |
| Space group | <i>P</i> 2 ₁ / <i>m</i> |
| <i>a</i> /Å | 6.7889(11) |
| <i>b</i> /Å | 6.6884(5) |
| <i>c</i> /Å | 9.9202(8) |
| α /° | 90 |
| β /° | 105.469(11) |
| γ /° | 90 |
| Volume/Å ³ | 434.13(9) |
| <i>Z</i> | 2 |
| ρ_{calc} /cm ³ | 1.592 |
| μ /mm ⁻¹ | 1.420 |
| <i>F</i> (000) | 212.0 |
| Crystal size/mm ³ | 0.5 × 0.4 × 0.4 |
| Radiation | Cu K α (λ = 1.54178) |
| 2 Θ range for data collection/° | 9.25 to 144.162 |
| Index ranges | -7 ≤ <i>h</i> ≤ 8, -8 ≤ <i>k</i> ≤ 8, -12 ≤ <i>l</i> ≤ 12 |
| Reflections collected | 3882 |
| Independent reflections | 912 [<i>R</i> _{int} = 0.0278, <i>R</i> _{sigma} = 0.0202] |
| Data/restraints/parameters | 912/0/99 |
| Goodness-of-fit on <i>F</i> ² | 1.073 |
| Final <i>R</i> indexes [<i>I</i> ≥ 2 σ (<i>I</i>)] | <i>R</i> ₁ = 0.0305, <i>wR</i> ₂ = 0.0788 |
| Final <i>R</i> indexes [all data] | <i>R</i> ₁ = 0.0343, <i>wR</i> ₂ = 0.0814 |
| Largest diff. peak/hole / e Å ⁻³ | 0.28/-0.27 |

3B.VIII. Reactivity Assessment of Benzylic C–H Bonds

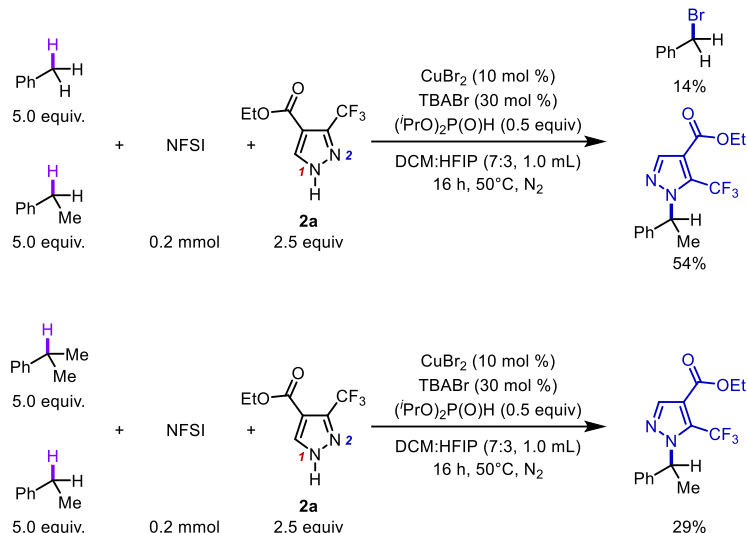
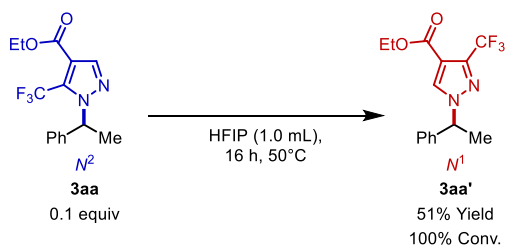


Figure 3B.6 Investigation of the reactivities and chemo-selectivity of primary, secondary, and tertiary benzylic C–H substrate

Reaction yields were determined by ^1H NMR spectroscopy with 0.2 mmol mesitylene as the external standard. Similar to the reactivity observed in our previous publication,¹ the cross coupling of benzylic C–H bonds and N–H heterocycles shows highly selective reactivity for the secondary benzylic C–H site, compared to primary and tertiary benzylic C–H bonds. Toluene proved less reactive than ethylbenzene and only brominated product was observed. Cumene showed comparable conversion and did not lead to the formation of desirable product.

3B.IX. Isomerization of 3aa to 3aa' in HFIP



3aaa (31.2 mg, 0.10 mmol, 1.0 equiv) and HFIP (1.0 mL) were added to a glass pressure tube. The tube was sealed and heated at 50 °C with stirring for 16 h. When the reaction finished, the mixture was cooled down to room temperature. Then an aliquot of the mixture was taken, diluted with CDCl_3 . Reaction yields were determined by ^1H NMR spectroscopy with 0.1 mmol mesitylene as the external standard.

3B.X. Radical Trap Experiments

The reactions were set up following the standard pressure tube procedure, with TEMPO (62.4 mg, 0.4 mmol) or BHT (88.1 mg, 0.4 mmol) weighed into the pressure tubes, respectively, before the tubes were transferred into a glove box under nitrogen.

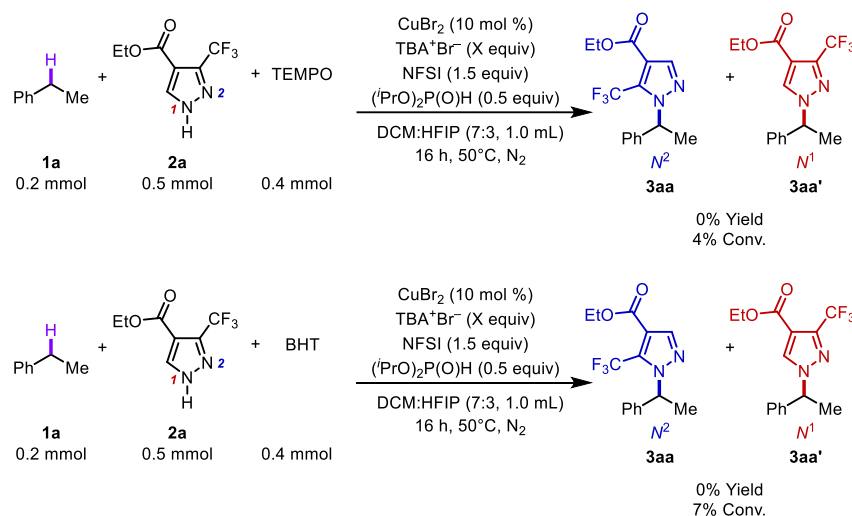


Figure 3B.7. Control experiments with radical traps

3B.XI. KIE Experiments

Procedure: Copper(II) bromide (4.4 mg, 0.020 mmol, 10 mol%), tetrabutylammonium bromide (19.3 mg, 0.060 mmol, 10 mol%) and NFSI (63.6 mg, 0.20 mmol, 1.0 equiv.), **2a** (0.50 mmol, 2.5 equiv.) were added to a pressure tube under air. The pressure tube was then moved into a glove box under N₂ atmosphere. DCM (0.8 mL), HFIP (0.2 mL), ethylbenzene-d₁₀ (122.5 μL, 1.0 mmol, 5.0 equiv.), ethylbenzene (122.5 μL, 1.0 mmol, 5.0 equiv.) and diisopropyl phosphite (16.3 μL, 0.10 mmol, 0.5 equiv.) were added to the tube. The tube was sealed in the glove box and taken out to a hot plate. The sealed tube was heated at 50 °C with stirring for 16 h. When the reaction finished, the mixture was cooled down to room temperature. The mixture was quenched by a silica plug and an aliquot was taken into an NMR tube, which was diluted to the volume suitable for crude ¹H NMR analysis. Yields of the **3aa** and **3aa-D** were determined with mesitylene as the internal standard.

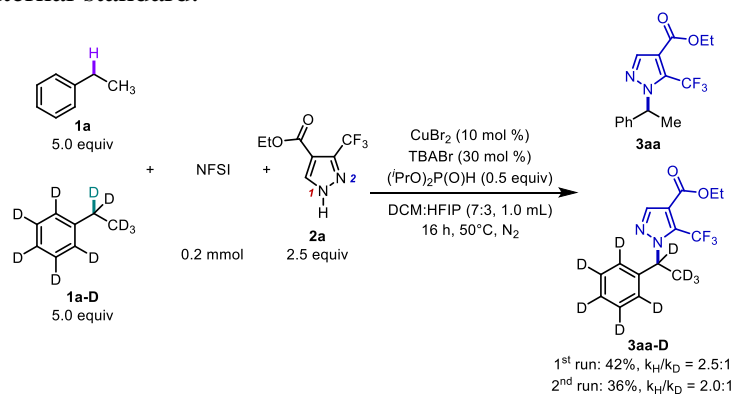
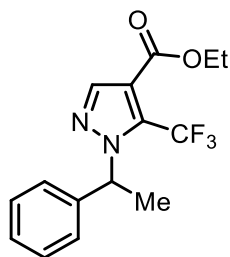


Figure 3B.8. Intermolecular Competition Kinetic Isotopic Effect

3B. XII. Characterization of Compounds



Ethyl 1-(1-phenylethyl)-5-(trifluoromethyl)-1H-pyrazole-4-carboxylate, **3aa**

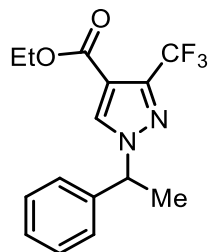
Reaction run using ethylbenzene **1a** (24.5 μ L, 0.2 mmol, 1.0 equiv), ethyl 3-(trifluoromethyl)-1H-pyrazole-4-carboxylate **2a** (104.1 mg, 0.50 mmol, 2.5 equiv), and tetrabutylammonium chloride (5.6 mg, 0.02 mmol, 0.1 equiv) following the general procedure I (pressure tube). Yield = 47.3 mg (76%) of pale-yellow liquid. TLC (Pentane:EtOAc, 9:1 v/v): R_f = 0.71.

^1H NMR (CDCl_3 , 500 MHz): 7.99 (s, 1H), 7.40 – 7.19 (m, 5H), 5.79 (q, J = 6.9 Hz, 1H), 4.31 (q, J = 7.1 Hz, 2H), 1.94 (d, J = 6.9 Hz, 3H), 1.33 (t, J = 7.1 Hz, 3H) ppm.

^{13}C NMR (CDCl_3 , 126 MHz): 161.2, 141.5, 140.5, 131.4 (q, J = 40.1 Hz), 128.7, 128.1, 126.3, 119.7 (q, J = 271.2 Hz), 115.8 (q, J = 1.5 Hz), 61.1, 61.0 (q, J = 3.6 Hz), 22.1, 14.1 ppm.

^{19}F NMR (CDCl_3 , 377 MHz): -55.9 ppm.

HRMS Calculated for $[\text{C}_{15}\text{H}_{15}\text{F}_3\text{N}_2\text{O}_2+\text{H}]^+$: 313.1158, Found: 313.1153.



Ethyl 1-(1-phenylethyl)-3-(trifluoromethyl)-1H-pyrazole-4-carboxylate, **3aa'**

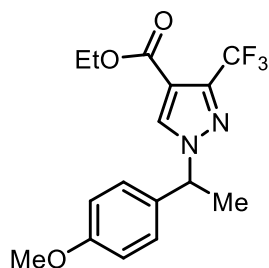
Reaction run using ethylbenzene **1a** (24.5 μ L, 0.2 mmol, 1.0 equiv), ethyl 3-(trifluoromethyl)-1H-pyrazole-4-carboxylate **2a** (104.1 mg, 0.50 mmol, 2.5 equiv), and TMSOTf (3.6 μ L, 0.02 mmol, 0.1 equiv) following the general procedure I (pressure tube). Yield = 39.6 mg (63%) of clear colorless liquid. TLC (pentane:EtOAc, 9:1 v/v): R_f = 0.38.

^1H NMR (CDCl_3 , 500 MHz): 7.91 (s, 1H), 7.42 – 7.32 (m, 3H), 7.28 – 7.26 (m, 2H), 5.56 (q, J = 7.1 Hz, 1H), 4.29 (q, J = 7.1 Hz, 2H), 1.92 (d, J = 7.1 Hz, 3H), 1.32 (t, J = 7.1 Hz, 3H) ppm.

^{13}C NMR (CDCl_3 , 126 MHz): 161.0, 141.2 (q, J = 38.3 Hz), 139.4, 134.1, 129.1, 128.8, 126.7, 120.5 (q, J = 269.6 Hz), 113.2, 62.6, 61.0, 21.1, 14.1 ppm.

^{19}F NMR (CDCl_3 , 377 MHz): -61.9 ppm.

HRMS Calculated for $[\text{C}_{15}\text{H}_{15}\text{F}_3\text{N}_2\text{O}_2+\text{H}]^+$: 313.1158, Found: 313.1157.



Ethyl 1-(1-(4-methoxyphenyl)ethyl)-3-(trifluoromethyl)-1H-pyrazole-4-carboxylate, **3ba'**

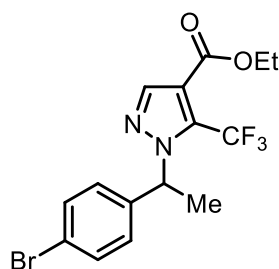
Reaction run using 4-ethylanisole **1b** (29.3 μL , 0.2 mmol, 1.0 equiv), ethyl 3-(trifluoromethyl)-1H-pyrazole-4-carboxylate **2a** (104.1 mg, 0.50 mmol, 2.5 equiv), and trimethylsilyl triflate (3.6 μL , 0.02 mmol, 0.1 equiv) at 60°C following the general procedure I (pressure tube). Yield = 54.7 mg (80%) of clear colorless liquid. TLC (pentane:EtOAc, 9:1 v/v): R_f = 0.42.

^1H NMR (CDCl_3 , 500 MHz): 7.84 (s, 1H), 7.26 – 7.20 (m, 2H), 6.94 – 6.86 (m, 2H), 5.51 (q, J = 7.0 Hz, 1H), 4.28 (q, J = 7.1 Hz, 2H), 3.81 (s, 3H), 1.89 (d, J = 7.0 Hz, 3H), 1.32 (t, J = 7.1 Hz, 3H) ppm.

^{13}C NMR (CDCl_3 , 126 MHz): 161.0, 159.8, 141.1 (q, J = 38.4 Hz), 133.8, 131.1, 128.1, 120.5 (q, J = 269.6 Hz), 114.4, 113.0, 62.1, 60.8, 55.3, 21.1, 14.1 ppm.

^{19}F NMR (CDCl_3 , 377 MHz): -61.9 ppm.

HRMS Calculated for $[\text{C}_{16}\text{H}_{17}\text{F}_3\text{N}_2\text{O}_3+\text{Na}]^+$: 365.1083, Found: 365.1089.



Ethyl 1-(1-(4-bromophenyl)ethyl)-5-(trifluoromethyl)-1H-pyrazole-4-carboxylate, **3ca**

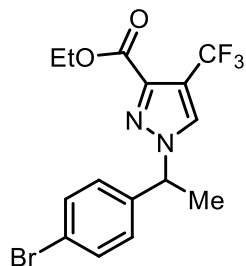
Reaction run using 4-bromoethylbenzene **1c** (27.5 μL , 0.2 mmol, 1.0 equiv), ethyl 3-(trifluoromethyl)-1H-pyrazole-4-carboxylate **2a** (104.1 mg, 0.50 mmol, 2.5 equiv), and tetrabutylammonium chloride (5.6 mg, 0.02 mmol, 0.1 equiv) following the general procedure I (pressure tube). Yield = 57.6 mg (74%) of clear colorless liquid. TLC (pentane:EtOAc, 9:1 v/v): R_f = 0.61.

^1H NMR (CDCl_3 , 500 MHz): 7.98 (s, 1H), 7.52 – 7.39 (m, 2H), 7.24 – 7.05 (m, 2H), 5.73 (q, J = 6.9 Hz, 1H), 4.31 (q, J = 7.1 Hz, 2H), 1.92 (d, J = 6.9 Hz, 3H), 1.34 (t, J = 7.1 Hz, 3H) ppm.

^{13}C NMR (CDCl_3 , 126 MHz): 161.1, 141.7, 139.5, 131.9, 131.4 (q, J = 39.9 Hz), 128.2, 122.3, 119.6 (q, J = 271.3 Hz), 115.9 (q, J = 1.6 Hz), 61.2, 60.5 (q, J = 3.4 Hz), 22.1, 14.1 ppm.

^{19}F NMR (CDCl_3 , 377 MHz): -55.9 ppm.

HRMS Calculated for $[\text{C}_{15}\text{H}_{14}\text{BrF}_3\text{N}_2\text{O}_2+\text{H}]^+$: 391.0264, Found: 391.0257.



Ethyl 1-(1-(4-bromophenyl)ethyl)-5-(trifluoromethyl)-1H-pyrazole-4-carboxylate, **3ca'**

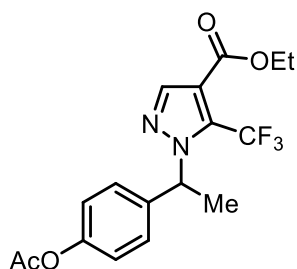
Reaction run using 4-bromoethylbenzene **1c** (27.5 μ L, 0.2 mmol, 1.0 equiv), ethyl 3-(trifluoromethyl)-1H-pyrazole-4-carboxylate **2a** (104.1 mg, 0.50 mmol, 2.5 equiv), and trimethylsilyl triflate (3.6 μ L, 0.02 mmol, 0.1 equiv) at 60°C following the general procedure I (pressure tube). Yield = 78.2 mg (35%) of pale-yellow semisolid. TLC (pentane:EtOAc, 9:1 v/v): R_f = 0.31. Mp: 89-90 °C

^1H NMR (CDCl_3 , 500 MHz): 7.92 (s, 1H), 7.71 – 7.41 (m, 2H), 7.18 – 7.11 (m, 2H), 5.51 (q, J = 7.1 Hz, 1H), 4.30 (q, J = 7.1 Hz, 2H), 1.90 (d, J = 7.1 Hz, 3H), 1.33 (t, J = 7.1 Hz, 3H) ppm.

^{13}C NMR (CDCl_3 , 126 MHz): 160.9, 141.4 (q, J = 38.6 Hz), 138.5, 134.0, 132.3, 128.3, 122.8, 120.4 (q, J = 269.7 Hz), 113.4 (d, J = 1.2 Hz), 62.0, 61.0, 21.0, 14.1 ppm.

^{19}F NMR (CDCl_3 , 377 MHz): -61.94 ppm.

HRMS Calculated for $[\text{C}_{15}\text{H}_{14}\text{BrF}_3\text{N}_2\text{O}_2+\text{Na}]^+$: 413.0083, Found: 413.0083.



Ethyl 1-(1-(4-acetoxyphenyl)ethyl)-5-(trifluoromethyl)-1H-pyrazole-4-carboxylate, **3da**

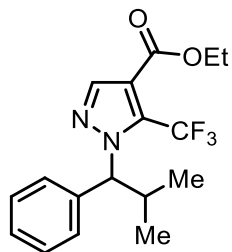
Reaction run using 4-ethylphenyl acetate **1d** (32.0 μ L, 0.2 mmol, 1.0 equiv), ethyl 3-(trifluoromethyl)-1H-pyrazole-4-carboxylate **2a** (104.1 mg, 0.50 mmol, 2.5 equiv), and tetrabutylammonium chloride (5.6 mg, 0.02 mmol, 0.1 equiv) following the general procedure I (pressure tube). Yield = 51.5 mg (70%) of brown solid. TLC (pentane:EtOAc, 9:1 v/v): R_f = 0.33. Mp: 88-90 °C

^1H NMR (CDCl_3 , 500 MHz): 7.98 (s, 1H), 7.34 – 7.28 (m, 2H), 7.10 – 7.01 (m, 2H), 5.77 (q, J = 6.9 Hz, 1H), 4.31 (q, J = 7.1 Hz, 2H), 2.28 (s, 3H), 1.93 (d, J = 6.9 Hz, 3H), 1.34 (t, J = 7.1 Hz, 3H) ppm.

^{13}C NMR (CDCl_3 , 126 MHz): 169.3, 161.1, 150.4, 141.6, 137.9, 131.3 (q, J = 40.0 Hz), 127.7, 121.8, 119.6 (q, J = 271.2 Hz), 115.8 (q, J = 1.6 Hz), 61.1, 60.5 (q, J = 3.4 Hz), 22.2, 21.1, 14.1 ppm.

^{19}F NMR (CDCl_3 , 377 MHz): -55.8 ppm.

HRMS Calculated for $[\text{C}_{17}\text{H}_{17}\text{F}_3\text{N}_2\text{O}_4+\text{H}]^+$: 371.1213, Found: 371.1218.



Ethyl 1-(2-methyl-1-phenylpropyl)-5-(trifluoromethyl)-1H-pyrazole-4-carboxylate, **3ea**

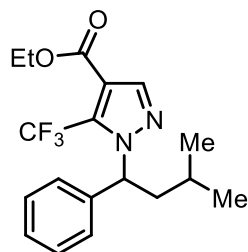
Reaction run using isobutylbenzene **1e** (31.4 μ L, 0.2 mmol, 1.0 equiv), ethyl 3-(trifluoromethyl)-1H-pyrazole-4-carboxylate **2a** (104.1 mg, 0.50 mmol, 2.5 equiv), and tetrabutylammonium chloride (5.6 mg, 0.02 mmol, 0.1 equiv) following the general procedure I (pressure tube). Yield = 45.8 mg (67%) of yellow liquid. TLC (pentane:EtOAc, 9:1 v/v): R_f = 0.47.

^1H NMR (CDCl_3 , 400 MHz): 7.98 (s, 1H), 7.57 – 7.46 (m, 2H), 7.41 – 7.26 (m, 3H), 4.96 (d, J = 10.6 Hz, 1H), 4.29 (q, J = 7.1 Hz, 2H), 2.94 (dh, J = 12.6, 6.4, 5.8 Hz, 1H), 1.33 (t, J = 7.1 Hz, 4H), 0.82 (d, J = 2.3 Hz, 3H), 0.80 (d, J = 2.0 Hz, 3H) ppm.

^{13}C NMR (CDCl_3 , 126 MHz): 161.3, 141.7, 138.1, 131.9 (q, J = 39.6 Hz), 128.5, 128.4, 128.2, 119.7 (q, J = 271.3 Hz), 115.1 (q, J = 1.5 Hz), 72.7 (q, J = 3.0 Hz), 61.1, 33.6, 19.9, 19.7, 14.1 ppm.

^{19}F NMR (CDCl_3 , 377 MHz): -54.9 ppm.

HRMS Calculated for $[\text{C}_{17}\text{H}_{19}\text{F}_3\text{N}_2\text{O}_2+\text{H}]^+$: 341.1471, Found: 341.1470.



Ethyl 1-(3-methyl-1-phenylbutyl)-5-(trifluoromethyl)-1H-pyrazole-4-carboxylate, **3fa**

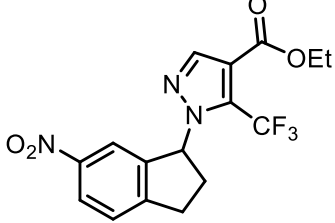
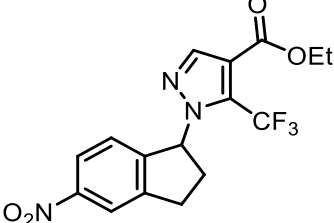
Reaction run using isopentylbenzene **1f** (34.7 μ L, 0.2 mmol, 1.0 equiv), ethyl 3-(trifluoromethyl)-1H-pyrazole-4-carboxylate **2a** (104.1 mg, 0.50 mmol, 2.5 equiv), and tetrabutylammonium chloride (5.6 mg, 0.02 mmol, 0.1 equiv) following the general procedure I (pressure tube). Yield = 42.1 mg (59%) of pale-yellow semisolid. TLC (pentane:EtOAc, 9:1 v/v): R_f = 0.67.

^1H NMR (CDCl_3 , 500 MHz): 7.99 (s, 1H), 7.38 – 7.25 (m, 5H), 5.63 (dd, J = 9.1, 6.0 Hz, 1H), 4.30 (q, J = 7.1 Hz, 2H), 2.50 (ddd, J = 14.5, 9.1, 5.8 Hz, 1H), 2.00 (ddd, J = 14.0, 7.9, 6.0 Hz, 1H), 1.42 – 1.36 (m, 1H), 1.33 (t, J = 7.1 Hz, 3H), 0.95 (d, J = 6.6 Hz, 3H), 0.92 (d, J = 6.6 Hz, 3H) ppm.

^{13}C NMR (CDCl_3 , 126 MHz): 141.5, 139.7, 131.72 (q, J = 39.7 Hz), 128.7, 128.2, 127.0, 119.7 (q, J = 271.3 Hz), 115.6 (q, J = 1.5 Hz), 63.9 (q, J = 3.1 Hz), 61.1, 45.1, 29.7, 24.9, 22.5, 21.9, 14.1 ppm.

^{19}F NMR (CDCl_3 , 377 MHz): -55.6 ppm.

HRMS Calculated for $[\text{C}_{18}\text{H}_{21}\text{F}_3\text{N}_2\text{O}_2+\text{Na}]^+$: 377.1447, Found: 377.1444.

| | |
|--|--|
|  |  |
| Ethyl 1-(6-nitro-2,3-dihydro-1H-inden-1-yl)-5-(trifluoromethyl)-1H-pyrazole-4-carboxylate, 3ga-1 | Ethyl 1-(5-nitro-2,3-dihydro-1H-inden-1-yl)-5-(trifluoromethyl)-1H-pyrazole-4-carboxylate, 3ga-2 |

Reaction run using 5-nitroindane **1g** (32.7 mg, 0.2 mmol, 1.0 equiv), ethyl 3-(trifluoromethyl)-1H-pyrazole-4-carboxylate **2a** (104.1 mg, 0.50 mmol, 2.5 equiv), and tetrabutylammonium chloride (5.6 mg, 0.02 mmol, 0.1 equiv) following the general procedure I (pressure tube) and two regioisomers were isolated.

3ga-1: Yield = 14.5 mg (20%) of pale-yellow semisolid. TLC (pentane:EtOAc, 4:1 v/v): $R_f = 0.47$.

^1H NMR (CDCl_3 , 500 MHz): δ 8.20 (dd, $J = 8.4, 2.2$ Hz, 1H), 7.90 (s, 1H), 7.89 (d, $J = 2.1$ Hz, 1H), 7.49 (d, $J = 8.4$ Hz, 1H), 6.16 (dd, $J = 7.9, 6.0$ Hz, 1H), 4.35 (q, $J = 7.1$ Hz, 2H), 3.40 (ddd, $J = 17.0, 8.9, 5.2$ Hz, 1H), 3.11 (ddd, $J = 16.9, 8.8, 6.2$ Hz, 1H), 2.80 (dtd, $J = 13.6, 8.4, 5.2$ Hz, 1H), 2.61 (ddt, $J = 12.7, 9.0, 6.1$ Hz, 1H), 1.37 (t, $J = 7.1$ Hz, 3H) ppm

^{13}C NMR (CDCl_3 , 126 MHz): δ 160.9, 151.5, 147.7, 142.5, 141.9, 131.9 (q, $J = 40.0$ Hz), 125.8, 124.6, 120.0, 119.7 (q, $J = 271.3$ Hz), 115.9 (q, $J = 1.3$ Hz), 65.4 (q, $J = 3.5$ Hz), 61.3, 33.7, 31.0, 14.1 ppm.

^{19}F NMR (377 MHz, CDCl_3): -55.5 ppm.

HRMS Calculated for $[\text{C}_{16}\text{H}_{14}\text{F}_3\text{N}_3\text{O}_4 + \text{NH}_4]^+$: 387.1275, Found: 387.1271.

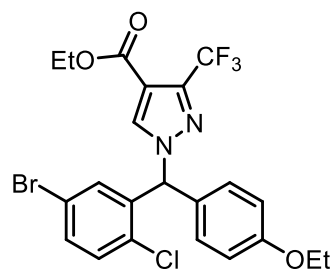
3ga-2: Yield = 9.8 mg (13%) of pale-yellow liquid. TLC (pentane:EtOAc, 4:1 v/v): $R_f = 0.59$.

^1H NMR (CDCl_3 , 500 MHz): δ 8.19 (d, $J = 2.1$ Hz, 1H), 8.09 (dd, $J = 8.4, 2.1$ Hz, 1H), 7.90 (s, 1H), 7.17 (d, $J = 8.3$ Hz, 1H), 6.15 (dd, $J = 8.2, 6.0$ Hz, 1H), 4.35 (q, $J = 7.1$ Hz, 2H), 3.40 (ddd, $J = 16.3, 9.0, 5.0$ Hz, 1H), 3.12 (dt, $J = 15.9, 7.6$ Hz, 1H), 2.81 (dtd, $J = 13.4, 8.4, 5.0$ Hz, 1H), 2.64 (ddt, $J = 13.1, 8.9, 6.3$ Hz, 1H), 1.37 (t, $J = 7.1$ Hz, 3H) ppm.

^{13}C NMR (CDCl_3 , 126 MHz): δ 160.9, 148.8, 147.0, 145.7, 142.4, 131.9 (q, $J = 40.0$ Hz), 125.1, 122.8, 120.5, 119.7 (q, $J = 271.5$ Hz), 115.9 (q, $J = 1.3$ Hz), 65.4 (q, $J = 3.5$ Hz), 61.3, 33.6, 30.7, 14.1 ppm.

^{19}F NMR (377 MHz, CDCl_3): -55.6 ppm.

HRMS Calculated for $[\text{C}_{16}\text{H}_{14}\text{F}_3\text{N}_3\text{O}_4 + \text{NH}_4]^+$: 387.1275, Found: 387.1271.



Ethyl 1-((5-bromo-2-chlorophenyl)(4-ethoxyphenyl)methyl)-3-(trifluoromethyl)-1H-pyrazole-4-carboxylate, **3ha'**

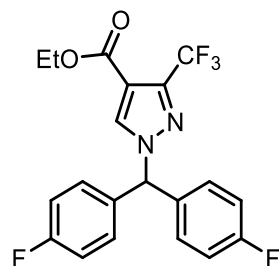
Reaction run using 4-(5-bromo-2-chlorobenzyl)phenyl ethyl ether **1h** (65.1 mg, 0.2 mmol, 1.0 equiv), ethyl 3-(trifluoromethyl)-1H-pyrazole-4-carboxylate **2a** (104.1 mg, 0.50 mmol, 2.5 equiv), and tetrabutylammonium chloride (5.6 mg, 0.02 mmol, 0.1 equiv) following the general procedure I (pressure tube). Yield = 91.5 mg (86%) of yellow solid. TLC (pentane:EtOAc, 9:1 v/v): R_f = 0.44. Mp: 84-87 °C

^1H NMR (CDCl_3 , 500 MHz): 7.74 (s, 1H), 7.44 (dd, J = 8.5, 2.3 Hz, 1H), 7.29 (d, J = 8.5 Hz, 1H), 7.07 – 7.01 (m, 2H), 6.98 (s, 1H), 6.95 – 6.88 (m, 2H), 6.81 (d, J = 2.3 Hz, 1H), 4.31 (q, J = 7.1 Hz, 2H), 4.05 (q, J = 7.0 Hz, 2H), 1.43 (t, J = 7.0 Hz, 3H), 1.34 (t, J = 7.1 Hz, 3H) ppm.

^{13}C NMR (CDCl_3 , 126 MHz): 160.9, 159.7, 142.3 (q, J = 38.5 Hz), 138.0, 136.1, 132.9, 132.5, 131.6, 131.3, 129.9, 126.7, 121.1, 120.2 (q, J = 269.9 Hz), 115.2, 113.2, 67.1, 63.6, 61.1, 14.8, 14.0 ppm.

^{19}F NMR (CDCl_3 , 377 MHz): -62.0 ppm.

HRMS Calculated for $[\text{C}_{22}\text{H}_{19}\text{BrClF}_3\text{N}_2\text{O}_3+\text{Na}]^+$: 553.0112, Found: 553.0112.



Ethyl 1-(bis(4-fluorophenyl)methyl)-3-(trifluoromethyl)-1H-pyrazole-4-carboxylate, **3ia**

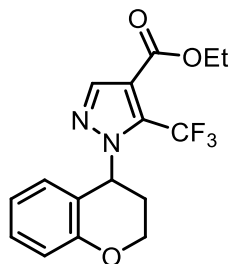
Reaction run using 4,4'-difluorodiphenylmethane **1i** (40.8 mg, 0.2 mmol, 1.0 equiv), ethyl 3-(trifluoromethyl)-1H-pyrazole-4-carboxylate **2a** (104.1 mg, 0.50 mmol, 2.5 equiv), and tetrabutylammonium chloride (5.6 mg, 0.02 mmol, 0.1 equiv) following the general procedure I (pressure tube). Yield = 78.3 mg (95%) of yellow solid. TLC (pentane:EtOAc, 9:1 v/v): R_f = 0.30. Mp: 96-97 °C

^1H NMR (CDCl_3 , 500 MHz): 7.83 – 7.78 (m, 1H), 7.12 – 7.03 (m, 8H), 6.78 (s, 1H), 4.30 (q, J = 7.1 Hz, 2H), 1.33 (t, J = 7.1 Hz, 3H) ppm.

^{13}C NMR (CDCl_3 , 126 MHz): 162.8 (d, J = 249.1 Hz), 161.8, 160.8, 142.0 (q, J = 38.6 Hz), 135.4, 133.3 (d, J = 3.3 Hz), 129.9 (d, J = 8.3 Hz), 120.3 (q, J = 269.8 Hz), 116.2 (d, J = 21.8 Hz), 113.5, 69.3, 61.1, 14.0 ppm.

^{19}F NMR (CDCl_3 , 377 MHz): -61.97, -112.26 ppm.

HRMS Calculated for $[\text{C}_{20}\text{H}_{15}\text{F}_5\text{N}_2\text{O}_2+\text{Na}]^+$: 433.0946, Found: 433.0951.



Ethyl 1-(chroman-4-yl)-5-(trifluoromethyl)-1H-pyrazole-4-carboxylate, **3ja**

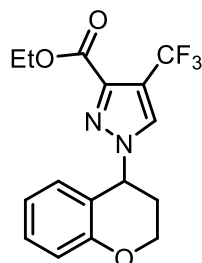
Reaction run using chroman **1j** (25.3 μ L, 0.2 mmol, 1.0 equiv), ethyl 3-(trifluoromethyl)-1H-pyrazole-4-carboxylate **2a** (104.1 mg, 0.50 mmol, 2.5 equiv), and tetrabutylammonium chloride (16.8 mg, 0.06 mmol, 0.3 equiv) following the general procedure I (pressure tube). Yield = 29.4 mg (43%) of yellow semisolid. TLC (pentane:EtOAc, 15:1 v/v): R_f = 0.51. **3ja'** (9.7 mg, 14%) was also isolated in this reaction.

^1H NMR (CDCl_3 , 500 MHz): 7.91 (s, 1H), 7.22 (ddd, J = 8.5, 6.9, 1.5 Hz, 1H), 6.92 (dd, J = 8.3, 1.0 Hz, 1H), 6.85 (td, J = 7.6, 1.1 Hz, 1H), 6.75 (dd, J = 7.9, 0.9 Hz, 1H), 5.82 (t, J = 5.7 Hz, 1H), 4.51 (dt, J = 11.6, 5.7 Hz, 1H), 4.34 (q, J = 7.2 Hz, 2H), 4.28 (dt, J = 10.8, 5.0 Hz, 1H), 2.45 (q, J = 5.6 Hz, 2H), 1.36 (t, J = 7.2 Hz, 3H) ppm.

^{13}C NMR (CDCl_3 , 126 MHz): 161.1, 155.2, 141.9, 132.0 (q, J = 39.9 Hz), 130.0, 128.6, 120.9, 119.8 (q, J = 271.2 Hz), 119.1, 117.6, 115.7 (d, J = 1.6 Hz), 62.8, 61.3, 55.4 (q, J = 3.6 Hz), 30.1, 14.1 ppm.

^{19}F NMR (CDCl_3 , 377 MHz): -55.7 ppm.

HRMS Calculated for $[\text{C}_{16}\text{H}_{15}\text{F}_3\text{N}_2\text{O}_3+\text{Na}]^+$: 363.0927, Found: 363.0918.



Ethyl 1-(chroman-4-yl)-4-(trifluoromethyl)-1H-pyrazole-3-carboxylate, **3ja'**

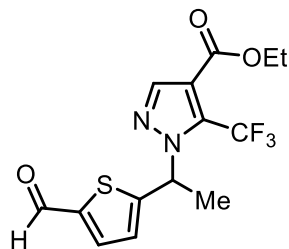
Reaction run using chroman **1j** (25.3 μ L, 0.2 mmol, 1.0 equiv), ethyl 3-(trifluoromethyl)-1H-pyrazole-4-carboxylate **2a** (104.1 mg, 0.50 mmol, 2.5 equiv), and trimethylsilyl triflate (3.6 μ L, 0.02 mmol, 0.1 equiv) at 60°C following the general procedure I (pressure tube). Yield = 25.4 mg (37%) of white solid. TLC (pentane:EtOAc, 9:1 v/v): R_f = 0.94. Mp: 86-88 °C

^1H NMR (CDCl_3 , 500 MHz): 7.71 (s, 1H), 7.33 (ddd, J = 8.6, 7.3, 1.7 Hz, 1H), 7.08 (dd, J = 8.1, 1.8 Hz, 1H), 6.97 (m, 2H), 5.58 (t, J = 4.3 Hz, 1H), 4.34 – 4.23 (m, 3H), 3.92 (td, J = 11.5, 2.5 Hz, 1H), 2.53 (dtd, J = 14.6, 3.9, 2.5 Hz, 1H), 2.43 (ddt, J = 14.7, 11.4, 4.3 Hz, 1H), 1.31 (t, J = 7.1 Hz, 3H) ppm.

^{13}C NMR (CDCl_3 , 126 MHz): 160.9, 155.5, 142.0 (q, J = 38.4 Hz), 135.3, 131.2, 130.5, 121.4, 120.4 (q, J = 269.8 Hz), 118.0, 116.4, 112.9, 61.5, 61.0, 56.7, 28.9, 14.0 ppm.

^{19}F NMR (CDCl_3 , 377 MHz): -62.0 ppm.

HRMS Calculated for $[\text{C}_{16}\text{H}_{15}\text{F}_3\text{N}_2\text{O}_3+\text{Na}]^+$: 363.0927, Found: 363.0922.



Ethyl 1-(1-(5-formylthiophen-2-yl)ethyl)-5-(trifluoromethyl)-1H-pyrazole-4-carboxylate, **3ka**

Reaction run using 5-ethyl-2-thiophenecarboxaldehyde **1k** (25.1 μ L, 0.2 mmol, 1.0 equiv), ethyl 3-(trifluoromethyl)-1H-pyrazole-4-carboxylate **2a** (104.1 mg, 0.50 mmol, 2.5 equiv), and tetrabutylammonium chloride (16.8 mg, 0.06 mmol, 0.3 equiv) following the general procedure I (pressure tube). Yield = 37.7 mg (54%) of pale-yellow liquid. TLC (pentane:EtOAc, 4:1 v/v): R_f = 0.52.

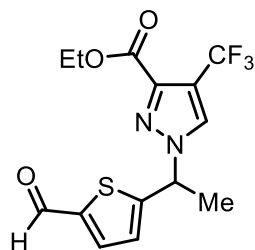
3ka' (13%) was observed in ^1H NMR analysis of the reaction crude, with 0.2 mmol mesitylene as the external standard.

^1H NMR (CDCl_3 , 500 MHz): δ 9.86 (s, 1H), 8.00 (s, 1H), 7.61 (d, J = 3.9 Hz, 1H), 7.05 (d, J = 3.9 Hz, 1H), 6.05 (q, J = 6.8 Hz, 1H), 4.33 (q, J = 7.1 Hz, 2H), 2.03 (d, J = 6.8 Hz, 3H), 1.35 (t, J = 7.1 Hz, 3H) ppm.

^{13}C NMR (CDCl_3 , 126 MHz): δ 182.8, 160.8, 153.1, 143.8, 142.2, 135.7, 131.2 (q, J = 40.2 Hz), 126.5, 116.1 (q, J = 1.3 Hz), 119.5 (q, J = 271.4 Hz), 61.3, 56.8 (q, J = 3.7 Hz), 22.9, 14.1 ppm.

^{19}F NMR (377 MHz, CDCl_3): -55.9 ppm.

HRMS Calculated for $[\text{C}_{14}\text{H}_{13}\text{BF}_3\text{N}_2\text{O}_3\text{S}+\text{Na}]^+$: 369.0491, Found: 369.0485.



Ethyl 1-(1-(5-formylthiophen-2-yl)ethyl)-4-(trifluoromethyl)-1H-pyrazole-3-carboxylate, **3ka'**

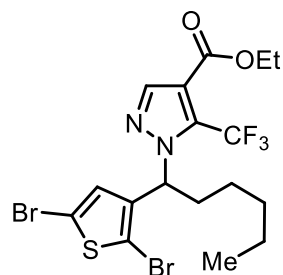
Reaction run using 5-ethyl-2-thiophenecarboxaldehyde **1k** (25.1 μ L, 0.2 mmol, 1.0 equiv), ethyl 3-(trifluoromethyl)-1H-pyrazole-4-carboxylate **2a** (104.1 mg, 0.50 mmol, 2.5 equiv), and trimethylsilyl triflate (3.6 μ L, 0.02 mmol, 0.1 equiv) at 60°C following the general procedure I (pressure tube). Yield = 34.6 mg (50%) of yellow semisolid. TLC (pentane:EtOAc, 9:1 v/v): R_f = 0.91.

^1H NMR (CDCl_3 , 500 MHz): 9.88 (s, 1H), 8.04 (s, 1H), 7.66 (d, J = 3.8 Hz, 1H), 7.11 (d, J = 3.8 Hz, 1H), 5.83 (q, J = 7.0 Hz, 1H), 4.31 (q, J = 7.1 Hz, 2H), 2.02 (d, J = 7.1 Hz, 3H), 1.34 (t, J = 7.1 Hz, 4H) ppm.

^{13}C NMR (CDCl_3 , 126 MHz): 182.8, 160.6, 152.2, 143.9, 141.8 (q, J = 38.7 Hz), 136.1, 133.7, 126.94, 120.2 (q, J = 269.8 Hz), 113.8, 61.1, 58.3, 21.8, 14.0 ppm.

^{19}F NMR (CDCl_3 , 377 MHz): -62.0 ppm.

HRMS Calculated for $[\text{C}_{14}\text{H}_{13}\text{F}_3\text{N}_2\text{O}_3\text{S}+\text{Na}]^+$: 369.0491, Found: 369.0487.



Ethyl 1-(1-(2,5-dibromothiophen-3-yl)hexyl)-5-(trifluoromethyl)-1H-pyrazole-4-carboxylate, **3la**

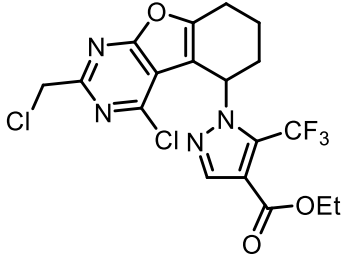
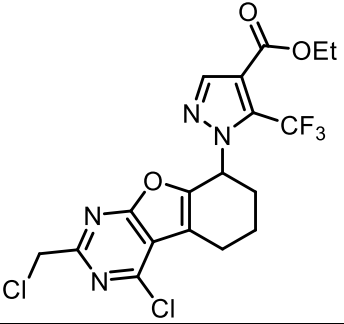
Reaction run using 2,5-dibromo-3-hexylthiophene **11** (42 μ L, 0.2 mmol, 1.0 equiv), ethyl 3-(trifluoromethyl)-1H-pyrazole-4-carboxylate **2a** (104.1 mg, 0.50 mmol, 2.5 equiv), and tetrabutylammonium chloride (16.8 mg, 0.06 mmol, 0.3 equiv) following the general procedure I (pressure tube). Yield = 68.7 mg (65%) of pale-yellow liquid. TLC (pentane:EtOAc, 9:1 v/v): R_f = 0.59.

^1H NMR (CDCl_3 , 500 MHz): 8.00 (s, 1H), 7.14 (s, 1H), 5.69 (dd, J = 8.7, 6.3 Hz, 1H), 4.32 (q, J = 7.1 Hz, 2H), 2.35 (dtd, J = 14.2, 9.2, 5.3 Hz, 1H), 2.03 (ddt, J = 13.5, 9.8, 6.1 Hz, 1H), 1.35 (t, J = 7.1 Hz, 3H), 1.32 – 1.25 (m, 4H), 1.26 – 1.19 (m, 1H), 1.16 – 1.08 (m, 1H), 0.88 – 0.83 (m, 3H) ppm.

^{13}C NMR (CDCl_3 , 126 MHz): 161.1, 142.0, 139.9, 132.0 (q, J = 40.1 Hz), 129.8, 119.5 (q, J = 271.6 Hz), 115.6, 111.7, 110.0, 61.2, 60.1 (q, J = 3.4 Hz), 36.0, 31.0, 25.5, 22.3, 14.1, 13.9 ppm.

^{19}F NMR (CDCl_3 , 377 MHz): -55.7 ppm.

HRMS Calculated for $[\text{C}_{17}\text{H}_{19}\text{BrF}_3\text{N}_2\text{O}_2\text{S}+\text{H}]^+$: 530.9559, Found: 530.9554.

| | |
|--|--|
|  |  |
| Ethyl 1-(4-chloro-2-(chloromethyl)-5,6,7,8-tetrahydrobenzofuro[2,3-d]pyrimidin-5-yl)-5-(trifluoromethyl)-1H-pyrazole-4-carboxylate, 3ma-1 | Ethyl 1-(4-chloro-2-(chloromethyl)-5,6,7,8-tetrahydrobenzofuro[2,3-d]pyrimidin-8-yl)-5-(trifluoromethyl)-1H-pyrazole-4-carboxylate, 3ma-2 |

Reaction run using 3-chloro-5-(chloromethyl)-8-oxa-4,6-diazatricyclo[7.4.0.0{2,7}]trideca-1(9),2,4,6-tetraene **1m** (51.4 mg, 0.2 mmol, 1.0 equiv), ethyl 3-(trifluoromethyl)-1H-pyrazole-4-carboxylate **2a** (104.1 mg, 0.50 mmol, 2.5 equiv), and tetrabutylammonium chloride (16.8 mg, 0.06 mmol, 0.3 equiv) following the general procedure II (glass vial) and two regioisomers were isolated.

3ma-1: Yield = 72.3 mg (45%) of yellow semisolid. TLC (pentane:EtOAc, 9:1 v/v): $R_f = 0.32$.

^1H NMR (CDCl_3 , 500 MHz): 7.89 (s, 1H), 5.87 (t, $J = 5.6$ Hz, 1H), 4.73 (s, 2H), 4.35 (q, $J = 7.1$ Hz, 2H), 3.11 (dtd, $J = 17.0, 5.5, 1.6$ Hz, 1H), 2.92 (dddd, $J = 17.0, 7.3, 5.5, 1.7$ Hz, 1H), 2.43 (q, $J = 5.9$ Hz, 2H), 2.30 – 2.18 (m, 1H), 2.00 (dh, $J = 17.2, 5.6$ Hz, 1H), 1.37 (t, $J = 7.1$ Hz, 3H) ppm.

^{13}C NMR (CDCl_3 , 126 MHz): 167.0, 161.1, 160.7, 153.4, 149.7, 142.0, 132.0 (q, $J = 40.3$ Hz), 119.6 (q, $J = 271.4$ Hz), 117.2, 116.3 (q, $J = 1.6$ Hz), 116.1, 61.3, 54.5 (q, $J = 3.9$ Hz), 46.2, 30.8, 21.0, 19.4, 14.1 ppm.

^{19}F NMR (CDCl_3 , 377 MHz): -55.8 ppm.

HRMS Calculated for $[\text{C}_{18}\text{H}_{15}\text{Cl}_2\text{F}_3\text{N}_4\text{O}_3 + \text{H}]^+$: 463.0546, Found: 463.0543.

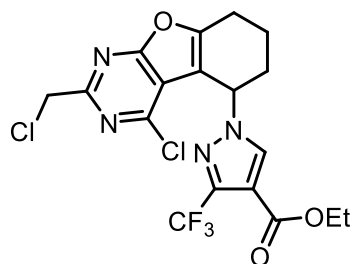
3ma-2: Yield = 8.1 mg (9%) of yellow semisolid. TLC (pentane:EtOAc, 4:1 v/v): $R_f = 0.39$.

^1H NMR (CDCl_3 , 500 MHz): 7.84 (s, 1H), 6.07 (t, $J = 4.5$ Hz, 2H), 4.73 (s, 2H), 4.34 (q, $J = 7.1$ Hz, 2H), 3.05 (dt, $J = 18.1, 5.1$ Hz, 1H), 2.86 (dt, $J = 17.5, 7.2$ Hz, 1H), 2.34 (ddt, $J = 16.8, 8.7, 2.8$ Hz, 1H), 2.26 – 2.09 (m, 2H), 2.08 – 1.95 (m, 2H), 1.36 (t, $J = 7.1$ Hz, 3H) ppm.

^{13}C NMR (CDCl_3 , 126 MHz): 167.1, 160.9, 160.2, 159.7, 151.6, 141.4, 131.4 (q, $J = 40.3$ Hz), 119.8 (q, $J = 271.6$ Hz), 116.7, 115.5, 109.3, 61.3, 54.2 (q, $J = 3.8$ Hz), 46.3, 31.2, 23.1, 18.2, 14.1 ppm.

^{19}F NMR (CDCl_3 , 377 MHz): -56.0 ppm.

HRMS Calculated for $[\text{C}_{18}\text{H}_{15}\text{Cl}_2\text{F}_3\text{N}_4\text{O}_3 + \text{H}]^+$: 463.0546, Found: 463.0545.



Ethyl 1-(4-chloro-2-(chloromethyl)-5,6,7,8-tetrahydrobenzofuro[2,3-d]pyrimidin-5-yl)-3-(trifluoromethyl)-1H-pyrazole-4-carboxylate, **3ma'-1**

Reaction run using 3-chloro-5-(chloromethyl)-8-oxa-4,6-diazatricyclo[7.4.0.0{2,7}]trideca-1(9),2,4,6-tetraene **1m** (51.4 mg, 0.2 mmol, 1.0 equiv), ethyl 3-(trifluoromethyl)-1H-pyrazole-4-carboxylate **2a** (104.1 mg, 0.50 mmol, 2.5 equiv), and $\text{BF}_3 \cdot \text{Et}_2\text{O}$ (2.5 μL , 0.02 mmol, 0.1 equiv) at 60°C following the general procedure I (pressure tube) and two regioisomers were isolated.

3ma'-1: Yield = 52.6 mg (58%) of colorless semisolid. TLC (pentane:Et₂O, 1:1 v/v): $R_f = 0.18$.

¹H NMR (CDCl₃, 400 MHz): 7.93 (s, 1H), 5.65 (t, $J = 5.0$ Hz, 1H), 4.76 (s, 2H), 4.31 (q, $J = 7.2$ Hz, 2H), 3.12 (dt, $J = 17.4, 5.3$ Hz, 1H), 2.97 – 2.82 (m, 1H), 2.57 (dq, $J = 14.3, 4.7$ Hz, 1H), 2.48 – 2.31 (m, 1H), 2.04 (p, $J = 5.2$ Hz, 2H), 1.34 (t, $J = 7.1$ Hz, 3H) ppm.

¹³C NMR (CDCl₃, 126 MHz): 167.3, 161.7, 160.6, 153.9, 148.6, 142.2 (q, $J = 38.8$ Hz), 135.1, 120.2 (q, $J = 269.8$ Hz), 118.4, 115.9, 113.6, 61.1, 55.4, 46.2, 29.9, 21.1, 18.8, 14.1 ppm.

¹⁹F NMR (CDCl₃, 377 MHz): -62.1 ppm.

HRMS Calculated for [C₁₈H₁₅Cl₂F₃N₄O₃+H]⁺: 463.0546, Found: 463.0539.

3ma-1: Yield = 12.9 mg (14%) of yellow semisolid. TLC (pentane:EtOAc, 9:1 v/v): $R_f = 0.32$.

| | |
|---|---|
| | |
| <p>5-(5-bromo-1H-pyrazol-1-yl)-4-chloro-5,6,7,8-tetrahydrobenzo[4,5]thieno[2,3-d]pyrimidine, 3nb-1</p> | <p>8-(5-bromo-1H-pyrazol-1-yl)-4-chloro-5,6,7,8-tetrahydrobenzo[4,5]thieno[2,3-d]pyrimidine, 3nb-2</p> |

Reaction run using 4-chloro-5,6,7,8-tetrahydro[1]benzothieno[2,3-d]pyrimidine **1n** (44.8 mg, 0.2 mmol, 1.0 equiv), 3-bromopyrazole **2b** (73.5 mg, 0.50 mmol, 2.5 equiv), and tetrabutylammonium chloride (5.6 mg, 0.02 mmol, 0.1 equiv) following the general procedure I (pressure tube) and two regioisomers were isolated.

3nb-1: Yield = 28.1 mg (38%) of white solid. (pentane:EtOAc, 2:1 v/v): $R_f = 0.48$.

¹H NMR (CDCl₃, 500 MHz): δ 8.72 (s, 1H), 7.39 (d, $J = 2.0$ Hz, 1H), 6.39 (d, $J = 1.9$ Hz, 1H), 6.18 (t, $J = 2.4$ Hz, 1H), 3.19 (ddd, $J = 17.8, 5.4, 2.1$ Hz, 1H), 3.02 – 2.81 (m, 1H), 2.33 (ddt, $J = 13.8, 5.0, 2.7$ Hz, 1H), 2.15 (tdd, $J = 13.7, 4.5, 2.9$ Hz, 1H), 2.04 (tddd, $J = 13.6, 11.3, 5.3, 2.5$ Hz, 1H), 1.96 – 1.86 (m, 1H) ppm.

^{13}C NMR (CDCl_3 , 126 MHz): 168.8, 152.8, 152.0, 145.6, 139.8, 127.9, 122.7, 112.0, 109.2, 52.7, 29.9, 26.1, 17.0 ppm.

HRMS Calculated for $[\text{C}_{13}\text{H}_{10}\text{BrClN}_4\text{S}+\text{H}]^+$: 368.9571, Found: 368.9570.

3nb-2: Yield = 18.8 mg (25%) of white solid. (pentane:EtOAc, 2:1 v/v): $R_f = 0.06$.

^1H NMR (CDCl_3 , 500 MHz): 8.75 (s, 1H), 7.56 (d, $J = 1.8$ Hz, 1H), 6.40 (d, $J = 1.9$ Hz, 1H), 5.86 (dd, $J = 7.7, 5.4$ Hz, 1H), 3.37 – 3.14 (m, 2H), 2.52 – 2.40 (m, 1H), 2.42 – 2.27 (m, 2H), 2.07 – 1.95 (m, 1H) ppm.

^{13}C NMR (CDCl_3 , 126 MHz): 169.6, 154.5, 152.5, 141.3, 137.7, 131.0, 128.3, 112.8, 109.1, 55.6, 29.9, 26.1, 20.5 ppm.

HRMS Calculated for $[\text{C}_{13}\text{H}_{10}\text{BrClN}_4\text{S}+\text{H}]^+$: 368.9571, Found: 368.9571.

| | |
|---|---|
| | |
| Ethyl 1-(2-chloro-6,7-dihydro-5H-cyclopenta[b]pyridin-5-yl)-5-(trifluoromethyl)-1H-pyrazole-4-carboxylate, 30a-1 | Ethyl 1-(2-chloro-6,7-dihydro-5H-cyclopenta[b]pyridin-7-yl)-5-(trifluoromethyl)-1H-pyrazole-4-carboxylate, 30a-2 |

Reaction run using 2-chloro-6,7-dihydro-5H-cyclopenta[b]pyridine **1o** (30.7 mg, 0.2 mmol, 1.0 equiv), ethyl 3-(trifluoromethyl)-1H-pyrazole-4-carboxylate **2a** (104.1 mg, 0.50 mmol, 2.5 equiv), and tetrabutylammonium chloride (5.6 mg, 0.02 mmol, 0.1 equiv) following the general procedure I (pressure tube) and two regioisomers were isolated.

30a-1: Yield = 14.0 mg (20%) of light-yellow liquid. TLC (pentane:EtOAc, 4:1 v/v): $R_f = 0.27$.

^1H NMR (CDCl_3 , 400 MHz): δ 7.89 (s, 1H), 7.34 (d, $J = 8.1$ Hz, 1H), 7.17 (d, $J = 8.1$ Hz, 1H), 6.09 (dd, $J = 8.4, 5.2$ Hz, 1H), 4.34 (q, $J = 7.1$ Hz, 2H), 3.41 (ddd, $J = 17.1, 9.3, 5.5$ Hz, 1H), 3.11 (ddd, $J = 17.3, 8.9, 6.1$ Hz, 1H), 2.77 (dtd, $J = 14.0, 8.7, 5.5$ Hz, 1H), 2.57 (ddt, $J = 14.3, 9.3, 5.7$ Hz, 1H), 1.36 (t, $J = 7.1$ Hz, 3H) ppm.

^{13}C NMR (CDCl_3 , 126 MHz): δ 165.6, 160.9, 152.5, 142.3, 135.1, 132.3, 131.7 (q, $J = 39.9$ Hz), 122.4, 119.7 (q, $J = 271.2$ Hz), 115.9, 63.7 (q, $J = 3.5$ Hz), 61.4, 32.4, 31.6, 14.2 ppm.

^{19}F NMR (377 MHz, CDCl_3): -55.6 ppm.

HRMS Calculated for $[\text{C}_{15}\text{H}_{13}\text{ClF}_3\text{N}_3\text{O}_2+\text{H}]^+$: 360.0721, Found: 360.0717.

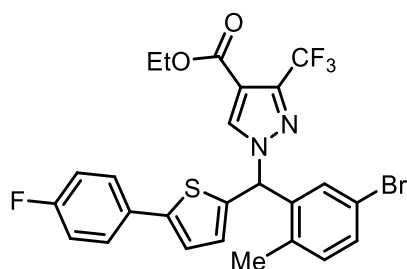
30a-2: Yield = 4.0 mg (6%) of light-yellow liquid. TLC (pentane:EtOAc, 9:1 v/v): $R_f = 0.16$.

^1H NMR (CDCl_3+DCM , 400 MHz): δ 7.89 (s, 1H), 7.62 (d, $J = 8.0$ Hz, 1H), 7.26 (d, $J = 8.3$ Hz, 3H), 6.05 (dd, $J = 8.6, 4.9$ Hz, 1H), 4.33 (qd, $J = 7.1, 1.7$ Hz, 2H), 3.24 (ddd, $J = 15.4, 9.0, 5.7$ Hz, 1H), 2.99 (ddd, $J = 16.3, 8.8, 5.2$ Hz, 1H), 2.77 (dtd, $J = 14.3, 8.7, 5.8$ Hz, 1H), 2.48 (ddt, $J = 14.1, 9.6, 5.1$ Hz, 1H), 1.35 (t, $J = 7.1$ Hz, 3H). ppm.

^{13}C NMR (CDCl_3 , 126 MHz): δ 161.1, 160.1, 150.7, 142.2, 136.4, 135.7, 131.7 (q, $J = 39.9$ Hz), 124.3, 119.7 (q, $J = 271.2$ Hz), 115.9, 65.52 (q, $J = 3.9$ Hz), 61.1, 31.7, 27.9, 14.1 ppm.

^{19}F NMR (377 MHz, CDCl_3): -55.7 ppm.

HRMS Calculated for $[\text{C}_{15}\text{H}_{13}\text{ClF}_3\text{N}_3\text{O}_2+\text{Na}]^+$: 382.0541, Found: 382.0538.



Ethyl 1-((5-bromo-2-methylphenyl)(5-(4-fluorophenyl)thiophen-2-yl)methyl)-3-(trifluoromethyl)-1H-pyrazole-4-carboxylate, **3pa'**

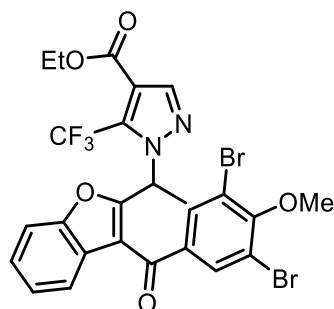
Reaction run using 2-(5-bromo-2-methylbenzyl)-5-(4-fluorophenyl)thiophene **1p** (68.6 mg, 0.2 mmol, 1.0 equiv), ethyl 3-(trifluoromethyl)-1H-pyrazole-4-carboxylate **2a** (104.1 mg, 0.50 mmol, 2.5 equiv), and tetrabutylammonium chloride (5.6 mg, 0.02 mmol, 0.1 equiv) following the general procedure II (glass vial) procedure. Yield = 101.6 mg (90%) of yellow solid. TLC (pentane:EtOAc, 9:1 v/v): R_f = 0.56. Mp: 115-118 °C.

^1H NMR (CDCl_3 , 500 MHz): 7.94 (s, 1H), 7.57 – 7.49 (m, 2H), 7.43 (dd, J = 8.1, 2.1 Hz, 1H), 7.15 (d, J = 3.7 Hz, 1H), 7.11 (d, J = 8.2 Hz, 1H), 7.08 (t, J = 8.6 Hz, 2H), 7.02 (s, 1H), 6.85 (d, J = 2.0 Hz, 1H), 6.80 (dd, J = 3.8, 0.9 Hz, 1H), 4.33 (q, J = 7.1 Hz, 2H), 2.23 (s, 3H), 1.35 (t, J = 7.1 Hz, 3H) ppm.

^{13}C NMR (CDCl_3 , 126 MHz): 162.7 (d, J = 248.6 Hz), 160.8, 146.0, 142.3 (q, J = 38.6 Hz), 138.2, 137.4, 135.5, 134.87, 132.8, 132.1, 130.0, 129.7 (d, J = 3.4 Hz), 128.7, 127.7 (d, J = 8.2 Hz), 123.1, 120.4, 120.2 (q, J = 270.0 Hz), 116.1 (d, J = 21.9 Hz), 113.6, 63.1, 61.2, 18.8, 14.1 ppm.

^{19}F NMR (CDCl_3 , 377 MHz): -62.0, -113.2 ppm.

HRMS Calculated for $[\text{C}_{25}\text{H}_{19}\text{BrF}_4\text{N}_2\text{O}_2\text{S}+\text{NH}_4]^+$: 584.0625, Found: 584.0617.



Ethyl 1-(1-(3-(3,5-dibromo-4-methoxybenzoyl)benzofuran-2-yl)ethyl)-5-(trifluoromethyl)-1H-pyrazole-4-carboxylate, **3qa**

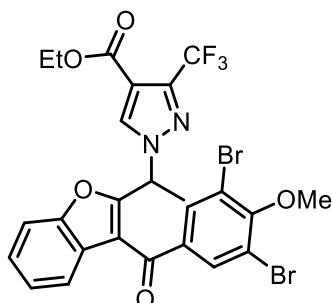
Reaction run using benzbromarone methyl ether **1q** (87.6 mg, 0.2 mmol, 1.0 equiv), ethyl 3-(trifluoromethyl)-1H-pyrazole-4-carboxylate **2a** (104.1 mg, 0.50 mmol, 2.5 equiv), and tetrabutylammonium chloride (5.6 mg, 0.02 mmol, 0.1 equiv) following the general procedure I (pressure tube). Yield = 99.0 mg (77%) of pale-yellow semisolid. TLC (pentane:EtOAc, 9:1 v/v): R_f = 0.42.

^1H NMR (CDCl_3 , 500 MHz): δ 7.99 (s, 1H), 7.94 (s, 2H), 7.60 (dt, J = 8.5, 0.9 Hz, 1H), 7.39 (ddd, J = 8.4, 7.0, 1.5 Hz, 1H), 7.27 (td, J = 7.5, 7.1, 0.8 Hz, 2H), 7.23 (dd, J = 8.0, 0.7 Hz, 1H), 6.37 (q, J = 6.9 Hz, 1H), 4.31 (qd, J = 7.2, 1.1 Hz, 2H), 3.98 (s, 3H), 2.08 (d, J = 6.9 Hz, 3H), 1.34 (t, J = 7.1 Hz, 3H) ppm.

^{13}C NMR (CDCl_3 , 126 MHz): δ 187.4, 160.9, 158.8, 158.3, 154.0, 141.9, 136.1, 133.7, 131.4 (q, $J = 40.0$ Hz), 126.0, 125.2, 124.4, 121.4, 119.4 (q, $J = 271.3$ Hz), 118.7, 117.1, 116.3 (q, $J = 1.3$ Hz), 112.2, 61.2, 60.9, 54.1 (q, $J = 3.6$ Hz), 19.5, 14.1 ppm.

^{19}F NMR (377 MHz, CDCl_3): -56.4 ppm.

HRMS Calculated for $[\text{C}_{25}\text{H}_{19}\text{Br}_2\text{F}_3\text{N}_2\text{O}_5+\text{H}]^+$: 642.9686, Found: 642.9687.



Ethyl 1-(1-(3-(3,5-dibromo-4-methoxybenzoyl)benzofuran-2-yl)ethyl)-3-(trifluoromethyl)-1H-pyrazole-4-carboxylate, **3qa'**

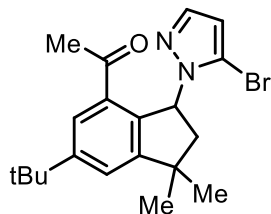
Reaction run using benzbromarone methyl ether **1q** (87.6 mg, 0.2 mmol, 1.0 equiv), ethyl 3-(trifluoromethyl)-1H-pyrazole-4-carboxylate **2a** (104.1 mg, 0.50 mmol, 2.5 equiv), and tetrabutylammonium chloride (5.6 mg, 0.02 mmol, 0.1 equiv) following the general procedure I (pressure tube). Yield = 58.0 mg (45%) of pale-yellow semisolid. TLC (pentane:EtOAc, 4:1 v/v): $R_f = 0.56$. Mp: 152-155 °C.

^1H NMR (CDCl_3 , 500 MHz): δ 8.31 (s, 1H), 8.01 (s, 2H), 7.59 (dt, $J = 8.4, 0.9$ Hz, 1H), 7.42 (ddd, $J = 8.5, 4.7, 3.8$ Hz, 1H), 7.30 (t, $J = 1.0$ Hz, 1H), 7.29 (d, $J = 0.8$ Hz, 1H), 6.06 (q, $J = 7.1$ Hz, 1H), 4.32 (q, $J = 7.1$ Hz, 2H), 4.00 (s, 3H), 2.06 (d, $J = 7.1$ Hz, 3H), 1.35 (t, $J = 7.1$ Hz, 3H) ppm.

^{13}C NMR (CDCl_3 , 126 MHz): δ 187.3, 160.8, 158.5, 158.2, 154.0, 141.7 (q, $J = 38.7$ Hz), 135.9, 134.8, 133.9, 126.3, 125.2, 124.6, 121.6, 120.3 (q, $J = 269.9$ Hz), 118.8, 117.7, 113.6, 112.2, 61.0, 60.9, 55.0, 18.8, 14.1 ppm.

^{19}F NMR (377 MHz, CDCl_3): -62.0 ppm.

HRMS Calculated for $[\text{C}_{25}\text{H}_{19}\text{Br}_2\text{F}_3\text{N}_2\text{O}_5+\text{H}]^+$: 642.9686, Found: 642.9687.



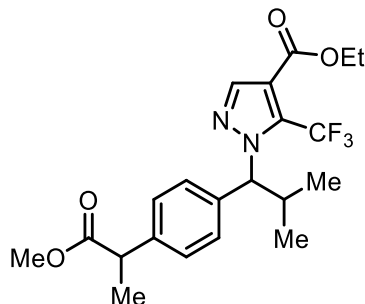
1-(3-(4-bromo-1H-pyrazol-1-yl)-6-(tert-butyl)-1,1-dimethyl-2,3-dihydro-1H-inden-4-yl)ethan-1-one, **3rb**

Reaction run using celestolide **1r** (48.9 mg, 0.2 mmol, 1.0 equiv), 3-bromopyrazole **2b** (73.5 mg, 0.50 mmol, 2.5 equiv), and tetrabutylammonium chloride (5.6 mg, 0.02 mmol, 0.1 equiv) following the general procedure I (pressure tube). Yield = 54.2 mg (70%) of white solid. TLC (pentane:EtOAc, 9:1 v/v): $R_f = 0.46$. Mp: 88-90 °C

$^1\text{H NMR}$ (CDCl_3 , 500 MHz): 7.63 (s, 1H), 7.42 (d, $J = 1.8$ Hz, 1H), 7.36 (d, $J = 1.9$ Hz, 1H), 6.40 (dd, $J = 8.2, 6.5$ Hz, 1H), 6.26 (d, 1H), 2.53 (dd, $J = 13.1, 8.3$ Hz, 1H), 2.35 (s, 3H), 2.09 (dd, $J = 13.1, 6.5$ Hz, 1H), 1.42 (s, 3H), 1.37 (s, 9H), 1.32 (s, 3H) ppm.

$^{13}\text{C NMR}$ (CDCl_3 , 126 MHz): 199.9, 154.2, 152.4, 139.6, 135.4, 135.1, 125.1, 123.0, 113.8, 107.6, 61.6, 49.3, 42.4, 34.9, 31.4, 30.3, 29.3, 27.6 ppm.

HRMS Calculated for $[\text{C}_{20}\text{H}_{25}\text{BrN}_2\text{O}+\text{H}]^+$: 389.1223, Found: 389.1220.



Ethyl 1-(1-(4-(1-methoxy-1-oxopropan-2-yl)phenyl)-2-methylpropyl)-5-(trifluoromethyl)-1H-pyrazole-4-carboxylate, **3sa**

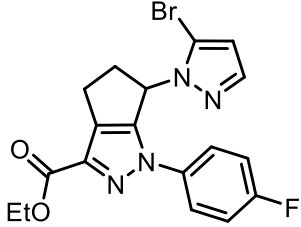
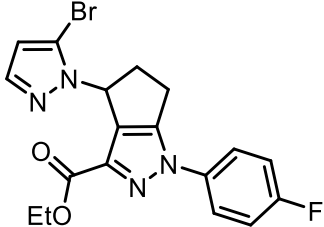
Reaction run using ibuprofen methyl ester **1s** (41.6 μL , 0.2 mmol, 1.0 equiv), ethyl 3-(trifluoromethyl)-1H-pyrazole-4-carboxylate **2a** (104.1 mg, 0.50 mmol, 2.5 equiv), and tetrabutylammonium chloride (5.6 mg, 0.02 mmol, 0.1 equiv) following the general procedure II (glass vial) procedure. Yield = 55.7 mg (65%) of white solid. TLC (pentane:EtOAc, 9:1 v/v): $R_f = 0.45$. Mp: 83-86 °C.

$^1\text{H NMR}$ (CDCl_3 , 500 MHz): 7.97 (s, 1H), 7.47 (d, $J = 8.3$ Hz, 2H), 7.25 (d, $J = 8.3$ Hz, 2H), 4.94 (d, $J = 10.6$ Hz, 1H), 4.29 (q, $J = 7.1$ Hz, 2H), 3.70 (q, $J = 7.2$ Hz, 1H), 3.65 (s, 3H), 2.97 – 2.86 (m, 1H), 1.47 (d, $J = 7.2$ Hz, 3H), 1.33 (t, $J = 7.1$ Hz, 3H), 0.81 (d, $J = 6.8$ Hz, 3H), 0.79 (d, $J = 6.4$ Hz, 3H) ppm.

$^{13}\text{C NMR}$ (CDCl_3 , 126 MHz): 174.8 (d, $J = 1.3$ Hz), 161.3, 141.7, 140.6 (d, $J = 1.0$ Hz), 136.9, 131.9 (q, $J = 39.8$ Hz), 128.5, 127.6, 119.7 (q, $J = 271.3$ Hz), 115.1 (q, $J = 1.5$ Hz), 72.3 (q, $J = 2.9$ Hz), 61.1, 52.1, 45.1, 33.6, 20.0, 19.7, 18.5, 14.1 ppm.

$^{19}\text{F NMR}$ (CDCl_3 , 377 MHz): -54.9 ppm.

HRMS Calculated for $[\text{C}_{21}\text{H}_{25}\text{F}_3\text{N}_2\text{O}_4+\text{NH}_4]^+$: 444.2105, Found: 444.2101.

| | |
|---|---|
|  |  |
| Ethyl 6-(5-bromo-1H-pyrazol-1-yl)-1-(4-fluorophenyl)-1,4,5,6-tetrahydrocyclopenta[<i>c</i>]pyrazole-3-carboxylate, 3tb-1 | Ethyl 4-(5-bromo-1H-pyrazol-1-yl)-1-(4-fluorophenyl)-1,4,5,6-tetrahydrocyclopenta[<i>c</i>]pyrazole-3-carboxylate, 3tb-2 |

Reaction run ethyl 1-(4-fluorophenyl)-1,4,5,6-tetrahydrocyclopenta[*c*]pyrazole-3-carboxylate **1t** (54.5 mg, 0.2 mmol, 1.0 equiv), ethyl 3-(trifluoromethyl)-1H-pyrazole-4-carboxylate **2a** (104.1 mg, 0.50 mmol, 2.5 equiv), and tetrabutylammonium chloride (5.6 mg, 0.02 mmol, 0.1 equiv) following the general procedure I (pressure tube) and two regioisomers were isolated.

3tb-1: Yield = 36.0 mg (43%) of light yellow amorphous solid. TLC (pentane:EtOAc, 4:1 v/v): R_f = 0.17.

^1H NMR (CDCl_3 , 500 MHz): 7.99 – 7.61 (m, 2H), 7.50 (d, J = 1.9 Hz, 1H), 7.22 – 7.10 (m, 2H), 6.30 (d, J = 1.9 Hz, 1H), 6.09 (dd, J = 8.4, 3.8 Hz, 1H), 4.23 (qt, J = 7.4, 3.8 Hz, 2H), 3.38 (dddd, J = 15.4, 8.9, 5.1, 1.3 Hz, 1H), 3.22 (dtd, J = 13.6, 8.6, 5.1 Hz, 1H), 3.03 (ddd, J = 15.4, 8.9, 4.4 Hz, 1H), 2.80 (ddt, J = 13.2, 8.6, 4.2 Hz, 1H), 1.18 (t, J = 7.1 Hz, 3H) ppm.

^{13}C NMR (CDCl_3 , 126 MHz): 161.5 (d, J = 247.6 Hz), 161.4, 151.3, 140.6, 138.3, 135.7 (d, J = 3.1 Hz), 129.2, 122.2 (d, J = 8.6 Hz), 116.3 (d, J = 23.0 Hz), 112.4, 108.0, 60.9, 55.8, 39.5, 25.1, 14.2 ppm.

^{19}F NMR (CDCl_3 , 377 MHz): -114.2 ppm.

HRMS Calculated for $[\text{C}_{18}\text{H}_{16}\text{BrFN}_4\text{O}_2+\text{H}]^+$: 419.0513, Found: 419.0508.

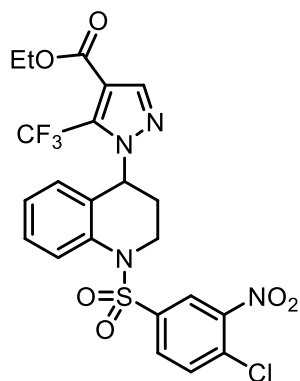
3tb-2: Yield = 5.1 mg (6%) of light-yellow semisolid. TLC (pentane:EtOAc, 4:1 v/v): R_f = 0.25.

^1H NMR (CDCl_3 , 500 MHz): 7.45 (d, J = 1.9 Hz, 1H), 7.21 – 7.14 (m, 2H), 6.97 (t, J = 8.6 Hz, 2H), 6.24 (d, J = 1.9 Hz, 1H), 6.07 (q, J = 4.4 Hz, 1H), 4.42 (qd, J = 7.1, 1.3 Hz, 2H), 3.21 (qd, J = 7.9, 3.8 Hz, 2H), 3.02 – 2.89 (m, 1H), 2.86 – 2.74 (m, 1H), 1.40 (t, J = 7.1 Hz, 3H) ppm.

^{13}C NMR (CDCl_3 , 126 MHz): 162.2, 161.8 (d, J = 248.1 Hz), 146.6, 141.4, 138.4, 135.1, 134.7, 123.5 (d, J = 8.7 Hz), 116.0 (d, J = 23.1 Hz), 112.2, 108.9, 61.0, 56.9, 40.1, 22.4, 14.4 ppm.

^{19}F NMR (CDCl_3 , 377 MHz): -113.6 ppm.

HRMS Calculated for $[\text{C}_{18}\text{H}_{16}\text{BrFN}_4\text{O}_2+\text{H}]^+$: 419.0513, Found: 419.0509.



ethyl 1-(1-((4-chloro-3-nitrophenyl)sulfonyl)-1,2,3,4-tetrahydroquinolin-4-yl)-5-(trifluoromethyl)-1H-pyrazole-4-carboxylate, **3ua**

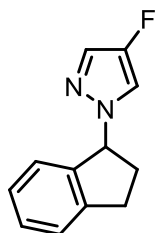
Reaction run using 1-(4-chloro-3-nitrobenzenesulfonyl)-1,2,3,4-tetrahydroquinoline **1u** (70.6 mg, 0.2 mmol, 1.0 equiv), ethyl 3-(trifluoromethyl)-1H-pyrazole-4-carboxylate **2a** (104.1 mg, 0.50 mmol, 2.5 equiv), and tetrabutylammonium chloride (5.6 mg, 0.02 mmol, 0.1 equiv) following the general procedure I (pressure tube). Yield = 47.0 mg (42%) of yellow semisolid. TLC (pentane:EtOAc, 4:1 v/v): $R_f = 0.40$.

^1H NMR (CDCl_3 , 500 MHz): 8.08 (d, $J = 2.2$ Hz, 1H), 7.90 (dd, $J = 8.4$, 1.1 Hz, 1H), 7.78 (dd, $J = 8.5$, 2.2 Hz, 1H), 7.71 (s, 1H), 7.63 (d, $J = 8.5$ Hz, 1H), 7.35 (ddd, $J = 8.5$, 7.2, 1.1 Hz, 2H), 7.14 (td, $J = 7.6$, 1.2 Hz, 1H), 6.68 (d, $J = 7.4$ Hz, 1H), 5.59 (t, $J = 7.2$ Hz, 1H), 4.33 (q, $J = 7.1$ Hz, 3H), 4.32 – 4.25 (m, 1H), 3.95 (ddd, $J = 13.9$, 9.3, 3.9 Hz, 1H), 2.22 – 2.09 (m, 2H), 1.35 (t, $J = 7.1$ Hz, 3H) ppm.

^{13}C NMR (CDCl_3 , 126 MHz) δ 160.7, 148.0, 142.1, 139.3, 136.2, 133.0, 132.1 (q, $J = 39.8$ Hz), 132.1, 131.2, 129.3, 128.5, 127.1, 126.5, 124.7, 124.7, 119.5 (q, $J = 271.4$ Hz), 115.7, 61.4, 56.9 (q, $J = 3.2$ Hz), 44.7, 28.5, 14.1 ppm.

^{19}F NMR (CDCl_3 , 377 MHz): -55.93 ppm.

HRMS Calculated for $[\text{C}_{22}\text{H}_{18}\text{ClF}_3\text{N}_4\text{O}_6\text{S}+\text{Na}]^+$: 581.0480, Found: 581.0478.



1-(2,3-dihydro-1H-inden-1-yl)-4-fluoro-1H-pyrazole, **3vc**

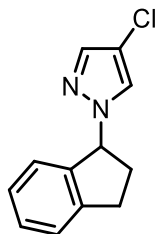
Reaction run using indane **1v** (24.5 μL , 0.2 mmol, 1.0 equiv), 4-fluoropyrazole **2c** (43.0 mg, 0.50 mmol, 2.5 equiv), and tetrabutylammonium chloride (5.6 mg, 0.02 mmol, 0.1 equiv) following the general procedure I (pressure tube) at 60°C. Yield = 33.4 mg (82%) of yellow liquid. TLC (pentane:EtOAc, 9:1 v/v): $R_f = 0.50$.

^1H NMR (CDCl_3 , 400 MHz): 7.36 (d, $J = 4.4$ Hz, 1H), 7.34 – 7.28 (m, 2H), 7.22 (td, $J = 7.0$, 6.3, 2.3 Hz, 1H), 7.16 (d, $J = 7.5$ Hz, 1H), 7.07 (d, $J = 4.7$ Hz, 1H), 5.76 (t, $J = 7.0$ Hz, 1H), 3.12 (ddd, $J = 16.0$, 8.7, 5.2 Hz, 1H), 2.96 (ddd, $J = 15.8$, 8.4, 6.6 Hz, 1H), 2.68 (dtd, $J = 13.5$, 8.2, 5.2 Hz, 1H), 2.30 (ddt, $J = 13.4$, 8.7, 6.2 Hz, 1H) ppm.

^{13}C NMR (CDCl_3 , 101 MHz): 149.6 (d, $J = 246.0$ Hz), 143.8, 140.6, 129.0, 127.1, 126.1 (d, $J = 13.5$ Hz), 125.2, 124.8, 113.6 (d, $J = 27.8$ Hz), 68.0, 33.7, 30.4 ppm.

^{19}F NMR (CDCl_3 , 377 MHz): -176.5 ppm.

HRMS Calculated for $[\text{C}_{12}\text{H}_{11}\text{FN}_2+\text{H}]^+$: 203.0979, Found: 203.0978.



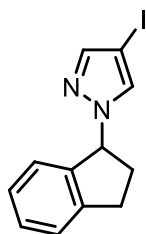
4-chloro-1-(2,3-dihydro-1H-inden-1-yl)-1H-pyrazole, **3vd**

Reaction run using indane **1v** (24.5 μL , 0.2 mmol, 1.0 equiv), 4-chloropyrazole **2d** (51.3 mg, 0.50 mmol, 2.5 equiv), and tetrabutylammonium chloride (5.6 mg, 0.02 mmol, 0.1 equiv) following the general procedure I (pressure tube) at 60°C. Yield = 28.8 mg (66%) of colorless liquid. TLC (pentane:EtOAc, 9:1 v/v): R_f = 0.57.

^1H NMR (CDCl_3 , 500 MHz): 7.45 (s, 1H), 7.32 (m, 2H), 7.23 (ddd, J = 8.0, 6.5, 2.1 Hz, 1H), 7.17 (m, 2H), 5.81 (dd, J = 7.9, 5.6 Hz, 1H), 3.13 (ddd, J = 14.4, 8.6, 5.6 Hz, 1H), 2.96 (ddd, J = 15.7, 8.2, 6.4 Hz, 1H), 2.68 (dtd, J = 13.6, 8.2, 5.6 Hz, 1H), 2.33 (ddt, J = 11.9, 8.6, 5.9 Hz, 1H) ppm.

^{13}C NMR (CDCl_3 , 126 MHz): 144.0, 140.4, 137.7, 129.0, 127.1, 125.6, 125.2, 124.9, 109.8, 67.7, 33.7, 30.4 ppm.

HRMS Calculated for $[\text{C}_{12}\text{H}_{11}\text{ClN}_2+\text{H}]^+$: 219.0684, Found: 219.0684.



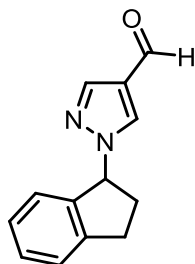
1-(2,3-dihydro-1H-inden-1-yl)-4-iodo-1H-pyrazole, **3ve**

Reaction run using indane **1v** (24.5 μL , 0.2 mmol, 1.0 equiv), 4-iodopyrazole **2e** (97.0 mg, 0.50 mmol, 2.5 equiv), and tetrabutylammonium chloride (5.6 mg, 0.02 mmol, 0.1 equiv) following the general procedure I (pressure tube) at 60°C. Yield = 37.5 mg (60%) of light-yellow liquid. TLC (pentane:EtOAc, 9:1 v/v): R_f = 0.60.

^1H NMR (CDCl_3 , 400 MHz): 7.54 (s, 1H), 7.37 – 7.28 (m, 2H), 7.27 – 7.19 (m, 2H), 7.17 (d, J = 7.6 Hz, 1H), 5.87 (dd, J = 7.9, 5.5 Hz, 1H), 3.13 (ddd, J = 16.0, 8.6, 5.6 Hz, 1H), 2.96 (ddd, J = 15.7, 8.4, 6.1 Hz, 1H), 2.68 (dtd, J = 13.7, 8.2, 5.6 Hz, 1H), 2.33 (ddt, J = 14.1, 8.6, 5.8 Hz, 1H) ppm.

^{13}C NMR (CDCl_3 , 101 MHz): 144.4, 144.0, 140.4, 132.1, 129.1, 127.2, 125.2, 125.0, 67.5, 56.1, 33.9, 30.4 ppm.

HRMS Calculated for $[\text{C}_{12}\text{H}_{11}\text{IN}_2+\text{H}]^+$: 311.0040, Found: 311.0036.



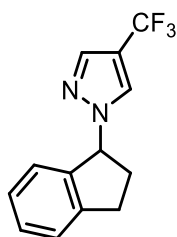
1-(2,3-dihydro-1H-inden-1-yl)-1H-pyrazole-4-carbaldehyde, **3vf**

Reaction run using indane **1v** (24.5 μ L, 0.2 mmol, 1.0 equiv), pyrazole-4-carboxaldehyde **2f** (48.0 mg, 0.50 mmol, 2.5 equiv), and tetrabutylammonium chloride (5.6 mg, 0.02 mmol, 0.1 equiv) following the general procedure I (pressure tube) at 60°C. Yield = 30.2 mg (71%) of light-yellow liquid. TLC (pentane:EtOAc, 9:1 v/v): R_f = 0.17.

^1H NMR (CDCl_3 , 400 MHz): 9.80 (s, 1H), 8.01 (s, 1H), 7.73 (s, 1H), 7.39 – 7.34 (m, 2H), 7.30 – 7.23 (m, 1H), 7.21 (d, J = 7.6 Hz, 1H), 5.90 (dd, J = 7.9, 4.9 Hz, 1H), 3.16 (ddd, J = 15.2, 8.5, 6.2 Hz, 1H), 3.00 (ddd, J = 16.1, 8.5, 5.4 Hz, 1H), 2.73 (dtd, J = 14.2, 8.2, 6.2 Hz, 1H), 2.41 (ddt, J = 13.7, 8.5, 5.2 Hz, 1H) ppm.

^{13}C NMR (CDCl_3 , 101 MHz): 184.1, 144.3, 141.0, 139.6, 131.1, 129.4, 127.3, 125.4, 125.0, 124.2, 67.5, 33.7, 30.4 ppm.

HRMS Calculated for $[\text{C}_{13}\text{H}_{12}\text{N}_2\text{O}+\text{H}]^+$: 213.1022, Found: 213.1021.



1-(2,3-dihydro-1H-inden-1-yl)-4-(trifluoromethyl)-1H-pyrazole, **3vg**

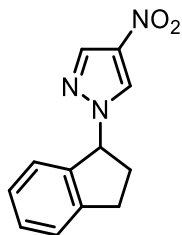
Reaction run using indane **1v** (24.5 μ L, 0.2 mmol, 1.0 equiv), 4-trifluoromethylpyrazole **2g** (68.0 mg, 0.50 mmol, 2.5 equiv), and tetrabutylammonium chloride (5.6 mg, 0.02 mmol, 0.1 equiv) following the general procedure I (pressure tube) at 60°C. Yield = 36.0 mg (71%) of colorless liquid. TLC (pentane:EtOAc, 9:1 v/v): R_f = 0.61.

^1H NMR (CDCl_3 , 500 MHz): 7.74 (s, 1H), 7.48 (s, 1H), 7.39 – 7.31 (m, 2H), 7.30 – 7.21 (m, 1H), 7.19 (d, J = 7.5 Hz, 1H), 5.89 (dd, J = 7.9, 5.3 Hz, 1H), 3.15 (ddd, J = 15.9, 8.6, 5.7 Hz, 1H), 2.99 (ddd, J = 15.9, 8.5, 5.9 Hz, 1H), 2.72 (dtd, J = 13.9, 8.2, 5.8 Hz, 1H), 2.38 (ddt, J = 13.9, 8.6, 5.6 Hz, 1H) ppm.

^{13}C NMR (CDCl_3 , 126 MHz): 144.1, 139.9, 137.1 (q, J = 2.8 Hz), 129.3, 127.3, 126.9 (q, J = 3.6 Hz), 125.3, 124.9, 122.7 (q, J = 265.9 Hz), 113.5 (q, J = 38.1 Hz), 67.5, 33.8, 30.4 ppm.

^{19}F NMR (CDCl_3 , 377 MHz): -56.3 ppm.

HRMS Calculated for $[\text{C}_{13}\text{H}_{11}\text{F}_3\text{N}_2+\text{H}]^+$: 253.0947, Found: 253.0944.



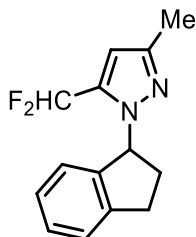
1-(2,3-dihydro-1*H*-inden-1-yl)-4-nitro-1*H*-pyrazole, **3vh**

Reaction run using indane **1v** (24.5 μ L, 0.2 mmol, 1.0 equiv), 4-nitropyrazole **2h** (56.5 mg, 0.50 mmol, 2.5 equiv), and tetrabutylammonium chloride (5.6 mg, 0.02 mmol, 0.1 equiv) following the general procedure I (pressure tube) at 60°C. Yield = 38.2 mg (83%) of dark yellow liquid. TLC (pentane:EtOAc, 9:1 v/v): R_f = 0.40.

^1H NMR (CDCl_3 , 400 MHz): 8.11 (s, 1H), 7.89 (s, 1H), 7.38 (d, J = 3.9 Hz, 2H), 7.29 (dt, J = 8.5, 4.2 Hz, 1H), 7.23 (d, J = 7.6 Hz, 1H), 5.87 (dd, J = 7.9, 4.6 Hz, 1H), 3.17 (ddd, J = 15.4, 8.5, 6.5 Hz, 1H), 3.02 (ddd, J = 16.2, 8.6, 5.1 Hz, 1H), 2.74 (dtd, J = 14.5, 8.2, 6.5 Hz, 1H), 2.41 (dtd, J = 13.5, 8.4, 4.9 Hz, 1H) ppm.

^{13}C NMR (CDCl_3 , 101 MHz): 144.4, 138.8, 136.0, 129.8, 127.5, 127.0, 125.5, 125.0, 68.3, 33.6, 30.3 ppm.

HRMS Calculated for $[\text{C}_{12}\text{H}_{11}\text{N}_3\text{O}_2+\text{Na}]^+$: 252.0743, Found: 252.0740.



5-(difluoromethyl)-1-(2,3-dihydro-1*H*-inden-1-yl)-3-methyl-1*H*-pyrazole, **3vi**

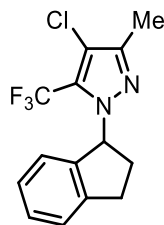
Reaction run using indane **1v** (24.5 μ L, 0.2 mmol, 1.0 equiv), 3-(difluoromethyl)-5-methyl-1*H*-pyrazole **2i** (66.0 mg, 0.50 mmol, 2.5 equiv), and tetrabutylammonium chloride (5.6 mg, 0.02 mmol, 0.1 equiv) following the general procedure I (pressure tube) in DCM. Yield = 25.7 mg (52%) of white solid. TLC (pentane:EtOAc, 9:1 v/v): R_f = 0.47. Mp: 75-77 °C.

^1H NMR (CDCl_3 , 500 MHz): 7.29 (d, J = 7.5 Hz, 1H), 7.25 (t, J = 7.3 Hz, 1H), 7.16 (t, J = 7.3 Hz, 1H), 6.99 (d, J = 7.6 Hz, 1H), 6.65 (t, J = 54.1 Hz, 1H), 6.28 (s, 1H), 5.93 (t, J = 7.9 Hz, 1H), 3.23 (ddd, J = 15.9, 9.1, 3.5 Hz, 1H), 2.97 (dt, J = 16.2, 8.3 Hz, 1H), 2.70 – 2.62 (m, 1H), 2.57 (dq, J = 13.1, 8.3 Hz, 1H), 2.22 (s, 3H) ppm.

^{13}C NMR (CDCl_3 , 126 MHz): 148.3, 143.3, 141.3, 136.1 (t, J = 26.0 Hz), 128.4, 126.8, 125.1, 124.1, 108.8 (t, J = 235.5 Hz), 106.4, 65.2, 32.9, 30.5, 13.6 ppm.

^{19}F NMR (CDCl_3 , 377 MHz): -109.1 (d, J = 307.2 Hz), -111.7 (d, J = 307.2 Hz) ppm.

HRMS Calculated for $[\text{C}_{14}\text{H}_{14}\text{F}_2\text{N}_2+\text{H}]^+$: 249.1198, Found: 249.1193.



4-chloro-1-(2,3-dihydro-1H-inden-1-yl)-3-methyl-5-(trifluoromethyl)-1H-pyrazole, **3vj**

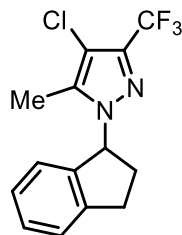
Reaction run using indane **1v** (24.5 μ L, 0.2 mmol, 1.0 equiv), 4-Chloro-3-trifluoromethyl-5-(methyl)pyrazole **2j** (92.3 mg, 0.50 mmol, 2.5 equiv), and tetrabutylammonium chloride (5.6 mg, 0.02 mmol, 0.1 equiv) following the general procedure I (pressure tube) in DCM. Yield = 32.7 mg (55%) of colorless liquid. TLC (pentane:Et₂O, 20:1 v/v): R_f = 0.56.

¹H NMR (CDCl₃, 500 MHz): 7.30 (d, *J* = 7.5 Hz, 1H), 7.30 – 7.25 (m, 1H), 7.18 (t, *J* = 7.3 Hz, 1H), 7.00 (d, *J* = 7.6 Hz, 1H), 5.89 (t, *J* = 7.4 Hz, 1H), 3.26 (ddd, *J* = 15.7, 9.0, 4.3 Hz, 1H), 2.97 (dt, *J* = 15.8, 7.9 Hz, 1H), 2.62 (dtt, *J* = 12.4, 8.5, 4.2 Hz, 1H), 2.54 (ddd, *J* = 13.1, 6.7, 1.7 Hz, 1H), 2.17 (s, 3H) ppm.

¹³C NMR (CDCl₃, 126 MHz): 146.9, 143.5, 140.6, 128.6, 127.8 (q, *J* = 37.6 Hz), 126.9, 125.1, 124.1, 120.0 (q, *J* = 270.2 Hz), 110.4, 65.7 (q, *J* = 2.3 Hz), 32.8, 30.6, 11.3 ppm.

¹⁹F NMR (CDCl₃, 377 MHz): -57.3 ppm.

HRMS Calculated for [C₁₄H₁₂ClF₃N₂+Na]⁺: 323.0533, Found: 323.0529.



4-chloro-1-(2,3-dihydro-1H-inden-1-yl)-5-methyl-3-(trifluoromethyl)-1H-pyrazole, **3vj'**

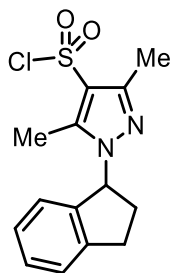
Reaction run using indane **1v** (24.5 μ L, 0.2 mmol, 1.0 equiv), 4-Chloro-3-trifluoromethyl-5-(methyl)pyrazole **2j** (92.3 mg, 0.50 mmol, 2.5 equiv), and BF₃•Et₂O (2.5 μ L, 0.02 mmol, 0.1 equiv) following the general procedure I (pressure tube) at 60°C. Yield = 27.9 mg (46%) of colorless liquid. TLC (pentane:EtOAc, 9:1 v/v): R_f = 0.63.

¹H NMR (CDCl₃, 500 MHz): 7.33 – 7.26 (m, 2H), 7.19 (td, *J* = 7.2, 1.6 Hz, 1H), 6.96 (d, *J* = 7.6 Hz, 1H), 5.90 (t, *J* = 7.9 Hz, 1H), 3.23 (ddd, *J* = 16.0, 9.2, 3.7 Hz, 1H), 3.01 (dt, *J* = 16.2, 8.2 Hz, 1H), 2.68 (dtd, *J* = 13.5, 8.5, 3.7 Hz, 1H), 2.50 (ddt, *J* = 13.4, 9.3, 7.8 Hz, 1H) ppm.

¹³C NMR (CDCl₃, 126 MHz): 143.4, 140.1, 137.7, 137.6 (q, *J* = 37.3 Hz), 129.0, 127.2, 125.4, 124.1, 120.9 (q, *J* = 269.3 Hz), 107.5, 66.6, 32.1, 30.7, 9.6 ppm.

¹⁹F NMR (CDCl₃, 377 MHz): -62.3 ppm.

HRMS Calculated for [C₁₄H₁₂ClF₃N₂+H]⁺: 301.0714, Found: 301.0710.



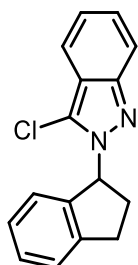
1-(2,3-dihydro-1H-inden-1-yl)-3,5-dimethyl-1H-pyrazole-4-sulfonyl chloride, **3vk**

Reaction run using indane **1v** (24.5 μ L, 0.2 mmol, 1.0 equiv), 3,5-dimethyl-1H-pyrazole-4-sulfonyl chloride **2k** (97.3 mg, 0.50 mmol, 2.5 equiv), and tetrabutylammonium chloride (5.6 mg, 0.02 mmol, 0.1 equiv) following the general procedure I (pressure tube) in DCM. Yield = 32.7 mg (53%) of white solid. TLC (pentane:EtOAc, 9:1 v/v): R_f = 0.37. Mp: 69-71 $^{\circ}$ C.

1 H NMR (CDCl_3 , 500 MHz): 7.33 (d, J = 7.5 Hz, 1H), 7.30 (t, J = 7.4 Hz, 1H), 7.20 (t, J = 7.3 Hz, 1H), 6.95 (d, J = 7.6 Hz, 1H), 5.83 (t, J = 7.7 Hz, 1H), 3.28 (ddd, J = 16.0, 9.0, 3.9 Hz, 1H), 3.02 (dt, J = 16.0, 8.1 Hz, 1H), 2.66 (m, 1H), 2.63 (s, 3H), 2.57 (dq, J = 13.2, 7.6 Hz, 1H), 2.42 (s, 3H) ppm.

13 C NMR (CDCl_3 , 126 MHz): 148.4, 143.4, 142.9, 139.9, 128.9, 127.1, 125.4, 123.8, 121.6, 64.2, 32.1, 30.7, 13.3, 10.9 ppm.

HRMS Calculated for $[\text{C}_{14}\text{H}_{15}\text{ClN}_2\text{O}_2\text{S}+\text{H}]^+$: 311.0616, Found: 311.0609.



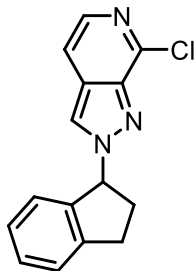
3-chloro-2-(2,3-dihydro-1H-inden-1-yl)-2H-indazole, **3vl**

Reaction run using indane **1v** (24.5 μ L, 0.2 mmol, 1.0 equiv), 3-chloroindazole **2l** (38.2 mg, 0.50 mmol, 2.5 equiv), and tetrabutylammonium chloride (5.6 mg, 0.02 mmol, 0.1 equiv) following the general procedure I (pressure tube) at 60 $^{\circ}$ C. Yield = 17.2 mg (32%) of colorless semisolid. TLC (pentane:EtOAc, 9:1 v/v): R_f = 0.71.

1 H NMR (CDCl_3 , 500 MHz): 7.68 (d, J = 8.1 Hz, 1H), 7.35 (d, J = 7.5 Hz, 1H), 7.31 (d, J = 7.3 Hz, 1H), 7.28 (d, J = 7.2 Hz, 1H), 7.18 (t, J = 7.5 Hz, 1H), 7.14 (t, J = 7.5 Hz, 1H), 7.07 (d, J = 8.5 Hz, 1H), 6.99 (d, J = 7.6 Hz, 1H), 6.22 (t, J = 7.9 Hz, 1H), 3.27 (ddd, J = 15.9, 9.1, 3.4 Hz, 2H), 3.06 (dt, J = 16.2, 8.3 Hz, 1H), 2.73 (ddt, J = 16.8, 8.4, 4.2 Hz, 2H), 2.56 (dq, J = 13.3, 8.2 Hz, 1H) ppm.

13 C NMR (CDCl_3 , 126 MHz): 143.3, 140.8, 140.3, 133.0, 128.6, 127.2, 126.9, 125.2, 124.4, 121.8, 121.2, 112.0, 110.1, 65.3, 32.1, 30.6 ppm.

HRMS Calculated for $[\text{C}_{16}\text{H}_{13}\text{ClN}_2+\text{H}]^+$: 269.0840, Found: 269.0838.



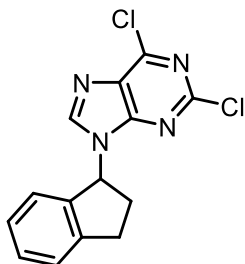
7-chloro-1-(2,3-dihydro-1H-inden-1-yl)-1H-pyrazolo[3,4-c]pyridine, **3vm**

Reaction run using indane **1v** (24.5 μ L, 0.2 mmol, 1.0 equiv), 7-Chloro-1H-pyrazolo[3,4-c]pyridine **2m** (76.8 mg, 0.50 mmol, 2.5 equiv), and tetrabutylammonium chloride (5.6 mg, 0.02 mmol, 0.1 equiv) following the general procedure I (pressure tube) at 60°C. Yield = 16.0 mg (30%) of yellow semisolid. TLC (DCM:MeOH, 19:1 v/v): R_f = 0.60.

^1H NMR (CDCl_3 , 500 MHz): 7.90 (d, J = 5.8 Hz, 1H), 7.70 (s, 1H), 7.44 – 7.37 (m, 2H), 7.36 (d, J = 6.0 Hz, 1H), 7.31 – 7.22 (m, 3H), 6.31 (dd, J = 8.1, 4.7 Hz, 1H), 3.21 (ddd, J = 15.3, 8.4, 6.4 Hz, 1H), 3.07 (ddd, J = 16.2, 8.6, 5.2 Hz, 1H), 2.90 (dtd, J = 14.5, 8.3, 6.3 Hz, 1H), 2.50 (dtd, J = 13.6, 8.6, 5.0 Hz, 1H) ppm.

^{13}C NMR (CDCl_3 , 126 MHz): 144.5, 142.9, 142.9, 139.5, 137.2, 129.7, 127.5, 125.6, 125.5, 125.3, 122.3, 113.6, 69.5, 34.7, 30.5 ppm.

HRMS Calculated for $[\text{C}_{15}\text{H}_{12}\text{ClN}_3+\text{Na}]^+$: 292.0612, Found: 292.0607.



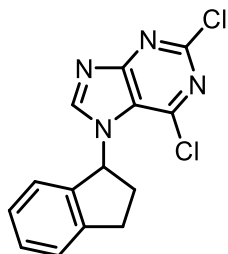
2,6-dichloro-9-(2,3-dihydro-1H-inden-1-yl)-9H-purine, **3vn-1**

Reaction run using indane **1v** (24.5 μ L, 0.2 mmol, 1.0 equiv), 2,6-dichloropurine **2n** (94.5 mg, 0.50 mmol, 2.5 equiv), and tetrabutylammonium chloride (5.6 mg, 0.02 mmol, 0.1 equiv) following the general procedure I (pressure tube) in DCM. Yield = 21.5 mg (35%) of white solid. TLC (pentane:EtOAc, 4:1 v/v): R_f = 0.26. Mp: 140-143 °C. **3vn-2** (13.9 mg, 23%) was also isolated in this reaction.

^1H NMR (CDCl_3 , 400 MHz): 7.79 (s, 1H), 7.46 – 7.35 (m, 2H), 7.27 (d, J = 7.7 Hz, 1H), 7.16 (d, J = 7.6 Hz, 1H), 6.25 (dd, J = 7.8, 5.5 Hz, 1H), 3.22 (ddd, J = 14.7, 8.5, 5.9 Hz, 1H), 3.10 (ddd, J = 16.0, 8.2, 6.4 Hz, 1H), 2.87 (dtd, J = 13.9, 8.1, 5.8 Hz, 1H), 2.28 (dtd, J = 14.0, 8.5, 5.7 Hz, 1H) ppm.

^{13}C NMR (CDCl_3 , 101 MHz): 153.2, 153.0, 151.8, 144.3, 144.1, 138.7, 131.0, 129.8, 127.7, 125.6, 124.6, 59.9, 34.1, 30.5 ppm.

HRMS Calculated for $[\text{C}_{14}\text{H}_{10}\text{Cl}_2\text{N}_4+\text{H}]^+$: 305.0355, Found: 305.0353.



2,6-dichloro-7-(2,3-dihydro-1H-inden-1-yl)-7H-purine, **3vn-2**

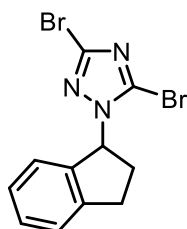
Reaction run using indane **1v** (24.5 μ L, 0.2 mmol, 1.0 equiv), 2,6-dichloropurine **2n** (94.5 mg, 0.50 mmol, 2.5 equiv), and $\text{BF}_3 \bullet \text{Et}_2\text{O}$ (2.5 μ L, 0.02 mmol, 0.1 equiv) following the general procedure I (pressure tube) at 60°C.

3vn-2: Yield = 38.5 mg (63%) of white solid. TLC (pentane:EtOAc, 4:1 v/v): R_f = 0.11. Mp: 167-170 °C.

^1H NMR (CDCl_3 , 400 MHz): 7.79 (s, 1H), 7.54 – 7.41 (m, 2H), 7.36 (dt, J = 8.3, 4.0 Hz, 1H), 7.31 (d, J = 7.7 Hz, 1H), 6.47 (dd, J = 7.6, 4.2 Hz, 1H), 3.36 – 3.00 (m, 2H), 2.87 (dq, J = 15.1, 7.7 Hz, 1H), 2.28 (ddt, J = 13.1, 8.4, 4.6 Hz, 1H) ppm.

^{13}C NMR (CDCl_3 , 101 MHz): 164.0, 157.9, 153.2, 148.4, 144.7, 143.8, 137.5, 130.3, 128.0, 125.9, 125.2, 62.8, 35.5, 30.1 ppm.

HRMS Calculated for $[\text{C}_{14}\text{H}_{10}\text{Cl}_2\text{N}_4+\text{Na}]^+$: 327.0175, Found: 327.0173.



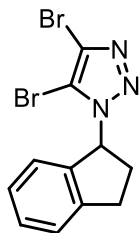
3,5-dibromo-1-(2,3-dihydro-1H-inden-1-yl)-1H-1,2,4-triazole, **3vo**

Reaction run using indane **1v** (24.5 μ L, 0.2 mmol, 1.0 equiv), 3,5-dibromo-1H-1,2,4-triazole **2o** (113.4 mg, 0.50 mmol, 2.5 equiv), and tetrabutylammonium chloride (5.6 mg, 0.02 mmol, 0.1 equiv) following the general procedure I (pressure tube) at 60°C. Yield = 53.1 mg (77%) of white solid. TLC (pentane:EtOAc, 9:1 v/v): R_f = 0.52. Mp: 83-86 °C.

^1H NMR (CDCl_3+DCM , 500 MHz): 7.37 – 7.28 (m, 2H), 7.24 – 7.16 (m, 1H), 7.08 (d, J = 7.6 Hz, 1H), 6.01 (dd, J = 8.2, 6.0 Hz, 1H), 3.32 (ddd, J = 15.9, 8.9, 4.9 Hz, 1H), 3.01 (ddd, J = 15.6, 8.5, 6.6 Hz, 1H), 2.67 (dtd, J = 13.4, 8.4, 5.0 Hz, 1H), 2.56 (ddt, J = 13.2, 8.9, 6.3 Hz, 1H) ppm.

^{13}C NMR (CDCl_3 , 126 MHz): 143.8, 140.4, 139.2, 129.3, 129.0, 127.1, 125.3, 124.1, 64.9, 31.9, 30.7 ppm.

HRMS Calculated for $[\text{C}_{11}\text{H}_9\text{Br}_2\text{N}_3+\text{H}]^+$: 341.9236, Found: 341.9233.



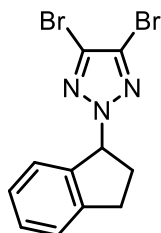
4,5-dibromo-1-(2,3-dihydro-1H-inden-1-yl)-1H-1,2,3-triazole, **3vp-1**

Reaction run using indane **1v** (24.5 μ L, 0.2 mmol, 1.0 equiv), 4,5-dibromo-1H-1,2,3-triazole **2p** (113.4 mg, 0.50 mmol, 2.5 equiv), and tetrabutylammonium chloride (5.6 mg, 0.02 mmol, 0.1 equiv) following the general procedure I (pressure tube) in DCM. Yield = 25.4 mg (37%) of colorless liquid. TLC (pentane:EtOAc, 9:1 v/v): R_f = 0.47. **3vp-2** (59 mg, 8%) was also isolated in this reaction.

^1H NMR (CDCl_3 , 500 MHz): 7.55 – 7.28 (m, 2H), 7.21 (t, J = 7.0 Hz, 1H), 7.11 (d, J = 7.7 Hz, 1H), 6.19 (dd, J = 8.4, 5.7 Hz, 1H), 3.38 (ddd, J = 15.8, 8.9, 5.3 Hz, 1H), 3.07 (ddd, J = 15.7, 8.6, 6.1 Hz, 1H), 2.77 (dtd, J = 13.9, 8.5, 5.4 Hz, 1H), 2.63 (ddt, J = 14.4, 8.8, 5.9 Hz, 1H) ppm.

^{13}C NMR (CDCl_3 , 126 MHz): 144.0, 138.9, 129.4, 127.2, 125.3, 124.4, 123.4, 111.7, 66.1, 32.2, 30.9 ppm.

HRMS Calculated for $[\text{C}_{11}\text{H}_9\text{Br}_2\text{N}_3+\text{Na}]^+$: 363.9055, Found: 363.9053.



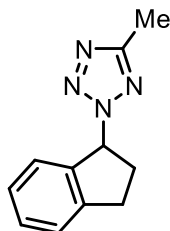
4,5-dibromo-2-(2,3-dihydro-1H-inden-1-yl)-2H-1,2,3-triazole, **3vp-2**

Reaction run using indane **1v** (24.5 μ L, 0.2 mmol, 1.0 equiv), 4,5-dibromo-1H-1,2,3-triazole **2p** (113.4 mg, 0.50 mmol, 2.5 equiv), and $\text{BF}_3 \bullet \text{Et}_2\text{O}$ (2.5 μ L, 0.02 mmol, 0.1 equiv) following the general procedure I (pressure tube) at 60°C in DCM. Yield = 5.9 mg (8%) of colorless liquid. TLC (pentane:EtOAc, 9:1 v/v): R_f = 0.73.

^1H NMR (CDCl_3 , 500 MHz): 7.34 – 7.30 (m, 1H), 7.24 – 7.18 (m, 1H), 6.10 (dd, J = 7.5, 5.9 Hz, 1H), 3.48 – 3.22 (m, 1H), 3.10 – 2.94 (m, 1H), 2.90 – 2.57 (m, 1H). ppm.

^{13}C NMR (CDCl_3 , 126 MHz): 144.0, 138.9, 129.4, 127.2, 125.3, 124.4, 123.4, 111.7, 66.1, 32.2, 30.9 ppm.

HRMS Calculated for $[\text{C}_{11}\text{H}_9\text{Br}_2\text{N}_3+\text{Na}]^+$: 363.9052, Found: 363.9055.



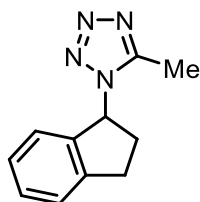
2-(2,3-dihydro-1H-inden-1-yl)-5-methyl-2H-tetrazole, **3vq-1**

Reaction run using indane **1v** (24.5 μ L, 0.2 mmol, 1.0 equiv), 5-methyl tetrazole **2q** (42.0 mg, 0.50 mmol, 2.5 equiv), and tetrabutylammonium chloride (5.6 mg, 0.02 mmol, 0.1 equiv) following the general procedure I (pressure tube) at 60°C in DCM. Yield = 20.0 mg (50%) of colorless liquid. TLC (pentane:Et₂O, 20:1 v/v): R_f = 0.30. **3vq-2** (3.6 mg, 18%) was also isolated in this reaction.

¹H NMR (CDCl₃, 400 MHz): 7.56 – 7.29 (m, 2H), 7.24 – 6.93 (m, 2H), 6.36 (dd, *J* = 8.1, 5.2 Hz, 1H), 3.37 (ddd, *J* = 15.3, 8.6, 6.1 Hz, 1H), 3.07 (ddd, *J* = 15.9, 8.4, 5.8 Hz, 1H), 2.88 – 2.64 (m, 2H), 2.50 (s, 3H) ppm.

¹³C NMR (CDCl₃, 101 MHz): 163.1, 144.0, 139.2, 129.4, 127.1, 125.2, 124.8, 68.0, 32.1, 30.8, 11.0 ppm.

HRMS Calculated for [C₁₁H₁₂N₄+H]⁺: 201.1135, Found: 201.1132.



1-(2,3-dihydro-1H-inden-1-yl)-5-methyl-1H-tetrazole, **3vq-2**

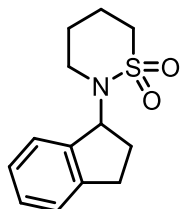
Reaction run using indane **1v** (24.5 μ L, 0.2 mmol, 1.0 equiv), 5-methyl tetrazole **2q** (42.0 mg, 0.50 mmol, 2.5 equiv), and BF₃•Et₂O (2.5 μ L, 0.02 mmol, 0.1 equiv) following the general procedure I (pressure tube) at 60°C. Yield = 16.7 mg (42%) of colorless liquid. TLC (pentane:Et₂O, 20:1 v/v): R_f = 0.30. **3vq-1** (15.2 mg, 37%) was also isolated in this reaction.

3vq-2: Yield = 14.4 mg (36%) of colorless liquid. TLC (pentane:EtOAc, 1:1 v/v): R_f = 0.23.

¹H NMR (CDCl₃, 600 MHz): 7.37 (d, *J* = 7.6 Hz, 1H), 7.34 (t, *J* = 7.3 Hz, 1H), 7.22 (t, *J* = 7.3 Hz, 0H), 6.99 (d, *J* = 7.7 Hz, 1H), 6.13 (dd, *J* = 8.4, 6.2 Hz, 1H), 3.33 (ddd, *J* = 16.2, 9.0, 4.8 Hz, 1H), 3.09 (ddd, *J* = 15.9, 8.8, 6.5 Hz, 1H), 2.81 (dtd, *J* = 13.5, 8.5, 4.8 Hz, 1H), 2.49 – 2.40 (m, 1H), 2.43 (s, 3H) ppm.

¹³C NMR (CDCl₃, 151 MHz): 150.9, 143.6, 138.5, 129.5, 127.4, 125.5, 124.1, 63.1, 32.6, 30.7, 9.5 ppm.

HRMS Calculated for [C₁₁H₁₂N₄+Na]⁺: 223.0954, Found: 223.0952.



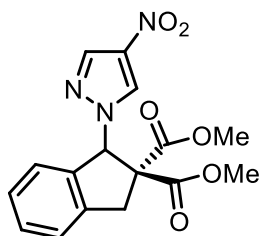
2-(2,3-dihydro-1H-inden-1-yl)-1,2-thiazinane 1,1-dioxide, **3vr**

Reaction run using indane **1v** (24.5 μ L, 0.2 mmol, 1.0 equiv), 1,4-propanesultam **2r** (67.5 mg, 0.50 mmol, 2.5 equiv), and tetrabutylammonium chloride (5.6 mg, 0.02 mmol, 0.1 equiv) following the general procedure I (pressure tube) in DCM. Yield = 23.5 mg (47%) of colorless liquid. TLC (pentane:EtOAc, 9:1 v/v): R_f = 0.13.

^1H NMR (CDCl_3 , 500 MHz): 7.40 – 7.30 (m, 1H), 7.28 – 7.19 (m, 3H), 5.67 (t, J = 8.0 Hz, 1H), 3.24 – 3.11 (m, 2H), 3.07 (ddd, J = 16.7, 8.8, 4.4 Hz, 1H), 3.03 – 2.90 (m, 2H), 2.85 (dt, J = 16.3, 8.4 Hz, 1H), 2.46 – 2.34 (m, 1H), 2.31 – 2.15 (m, 2H), 2.03 (dq, J = 13.3, 8.5 Hz, 1H), 1.64 (ddtq, J = 22.3, 13.6, 9.0, 4.1 Hz, 2H) ppm.

^{13}C NMR (CDCl_3 , 126 MHz): 143.6, 140.3, 128.1, 126.8, 124.9, 124.6, 59.7, 51.1, 43.8, 30.4, 29.3, 24.9, 24.2 ppm.

HRMS Calculated for $[\text{C}_{13}\text{H}_{17}\text{NO}_2\text{S}+\text{Na}]^+$: 274.0872, Found: 274.0868.



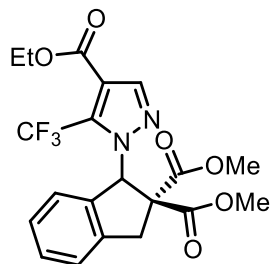
Dimethyl 1-(4-nitro-1H-pyrazol-1-yl)-1,3-dihydro-2H-indene-2,2-dicarboxylate, **3wh**

Reaction run using 2,2-dimethyl 1,3-dihydroindene-2,2-dicarboxylate **1w** (46.9 mg, 0.2 mmol, 1.0 equiv), 4-Nitropyrazole **2h** (56.0 mg, 0.50 mmol, 2.5 equiv), and tetrabutylammonium chloride (5.6 mg, 0.02 mmol, 0.1 equiv) following the general procedure I (pressure tube). Yield = 44.7 mg (65%) of yellow semisolid. TLC (pentane:EtOAc, 9:1 v/v): R_f = 0.10.

^1H NMR (CDCl_3 , 400 MHz): 8.03 (dd, J = 10.6, 0.6 Hz, 1H), 7.42 (td, J = 7.4, 1.2 Hz, 1H), 7.37 (d, J = 7.4 Hz, 1H), 7.32 (t, J = 7.6 Hz, 1H), 7.22 (d, J = 7.6 Hz, 1H), 6.60 (s, 1H), 4.09 (d, J = 16.8 Hz, 1H), 3.79 (s, 3H), 3.51 (s, 3H), 3.47 (d, J = 16.9 Hz, 1H) ppm.

^{13}C NMR (CDCl_3 , 101 MHz): 170.1, 167.6, 140.6, 136.3, 136.1, 135.9, 130.5, 129.4, 128.3, 125.23, 125.18, 71.3, 65.0, 53.6, 53.3, 38.8. ppm.

HRMS Calculated for $[\text{C}_{16}\text{H}_{15}\text{N}_3\text{O}_6\text{S}+\text{Na}]^+$: 368.0853, Found: 368.0846.



Dimethyl 1-(4-(ethoxycarbonyl)-5-(trifluoromethyl)-1*H*-pyrazol-1-yl)-1,3-dihydro-2*H*-indene-2,2-dicarboxylate, **3wa**

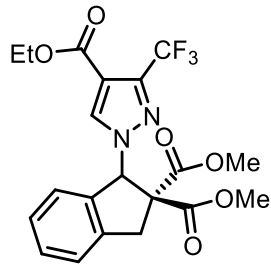
Reaction run using 2,2-dimethyl 1,3-dihydroindene-2,2-dicarboxylate **1w** (46.9 mg, 0.2 mmol, 1.0 equiv), ethyl 3-(trifluoromethyl)-1*H*-pyrazole-4-carboxylate **2a** (104.1 mg, 0.50 mmol, 2.5 equiv), and $\text{BF}_3 \cdot \text{Et}_2\text{O}$ (2.5 μL , 0.02 mmol, 0.1 equiv) following the general procedure I (pressure tube) at 60°C in DCM. Yield = 45.1 mg (51%) of yellow semisolid. TLC (pentane:EtOAc, 9:1 v/v): R_f = 0.20.

^1H NMR (CDCl_3 , 400 MHz): 7.79 (s, 1H), 7.41 – 7.29 (m, 2H), 7.25 – 7.16 (m, 2H), 6.82 (s, 1H), 4.39 (d, J = 16.8 Hz, 1H), 4.31 (q, J = 7.1 Hz, 2H), 3.76 (s, 3H), 3.51 (d, J = 16.8 Hz, 1H), 3.46 (s, 3H), 1.34 (t, J = 7.1 Hz, 3H) ppm.

^{13}C NMR (CDCl_3 , 101 MHz): 170.1, 167.4, 160.9, 142.6, 140.9, 138.4, 132.5 (q, J = 39.9 Hz), 129.9, 127.8, 125.0, 124.6, 119.6 (q, J = 271.8 Hz), 115.4, 68.4 (q, J = 4.3 Hz), 65.2, 61.2, 53.7, 53.0, 39.9, 14.1 ppm.

^{19}F NMR (CDCl_3 , 377 MHz): -56.6 ppm.

HRMS Calculated for $[\text{C}_{20}\text{H}_{19}\text{F}_3\text{N}_2\text{O}_6+\text{H}]^+$: 441.1268, Found: 441.1262.



Dimethyl 1-(4-(ethoxycarbonyl)-3-(trifluoromethyl)-1*H*-pyrazol-1-yl)-1,3-dihydro-2*H*-indene-2,2-dicarboxylate, **3wa'**

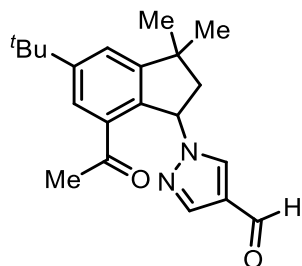
Reaction run using 2,2-dimethyl 1,3-dihydroindene-2,2-dicarboxylate **1w** (46.9 mg, 0.2 mmol, 1.0 equiv), ethyl 3-(trifluoromethyl)-1*H*-pyrazole-4-carboxylate **2a** (104.1 mg, 0.50 mmol, 2.5 equiv), and $\text{BF}_3 \cdot \text{Et}_2\text{O}$ (2.5 μL , 0.02 mmol, 0.1 equiv) following the general procedure I (pressure tube) at 60°C. Yield = 40.6 mg (46%) of white semisolid. TLC (pentane:EtOAc, 9:1 v/v): R_f = 0.13.

^1H NMR (CDCl_3 , 400 MHz): 7.79 (s, 1H), 7.41 – 7.29 (m, 2H), 7.25 – 7.16 (m, 2H), 6.82 (s, 1H), 4.39 (d, J = 16.8 Hz, 1H), 4.31 (q, J = 7.1 Hz, 2H), 3.76 (s, 3H), 3.51 (d, J = 16.8 Hz, 1H), 3.46 (s, 3H), 1.34 (t, J = 7.1 Hz, 3H) ppm.

^{13}C NMR (CDCl_3 , 101 MHz): 170.1, 167.4, 160.9, 142.6, 140.9, 138.4, 132.5 (q, J = 39.9 Hz), 129.9, 127.8, 125.0, 124.6, 119.6 (q, J = 271.8 Hz), 115.4, 68.4 (q, J = 4.3 Hz), 65.2, 61.2, 53.7, 53.0, 39.9, 14.1 ppm.

^{19}F NMR (CDCl_3 , 377 MHz): -56.6 ppm.

HRMS Calculated for $[\text{C}_{20}\text{H}_{19}\text{F}_3\text{N}_2\text{O}_6+\text{H}]^+$: 441.1268, Found: 441.1262.



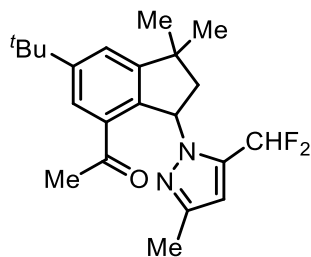
1-(7-acetyl-5-(tert-butyl)-3,3-dimethyl-2,3-dihydro-1H-inden-1-yl)-1H-pyrazole-4-carbaldehyde, **3rf**

Reaction run using celestolide **1r** (48.9 mg, 0.2 mmol, 1.0 equiv), pyrazole-4-carboxaldehyde **2f** (48.0 mg, 0.50 mmol, 2.5 equiv), and tetrabutylammonium chloride (5.6 mg, 0.02 mmol, 0.1 equiv) following the general procedure I (pressure tube) at 60°C. Yield = 61.0 mg (90%) of colorless semisolid. TLC (pentane:EtOAc, 4:1 v/v): $R_f = 0.29$.

^1H NMR (CDCl_3 , 500 MHz): 9.79 (s, 1H), 7.93 (s, 1H), 7.77 (d, $J = 1.8$ Hz, 1H), 7.74 (s, 1H), 7.48 (d, $J = 1.8$ Hz, 1H), 6.29 (dd, $J = 8.4, 3.9$ Hz, 1H), 2.54 (dd, $J = 13.8, 8.4$ Hz, 1H), 2.45 (s, 3H), 2.37 (dd, $J = 13.8, 3.9$ Hz, 1H), 1.40 (s, 10H), 1.34 (s, 3H), 1.30 (s, 3H) ppm.

^{13}C NMR (CDCl_3 , 126 MHz): 199.2, 184.3, 155.4, 153.8, 140.8, 134.4, 132.7, 126.2, 124.0, 123.1, 65.0, 49.0, 42.7, 35.1, 31.4, 30.3, 29.9, 27.8 ppm.

HRMS Calculated for $[\text{C}_{21}\text{H}_{26}\text{N}_2\text{O}_2 + \text{Na}]^+$: 361.1887, Found: 361.1880.



1-(6-(tert-butyl)-3-(5-(difluoromethyl)-3-methyl-1H-pyrazol-1-yl)-1,1-dimethyl-2,3-dihydro-1H-inden-4-yl)ethan-1-one, **3ri**

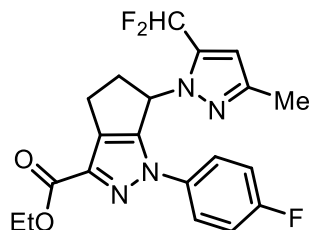
Reaction run using celestolide **1r** (48.9 mg, 0.2 mmol, 1.0 equiv), 3-(difluoromethyl)-5-methyl-1H-pyrazole **2i** (66.0 mg, 0.50 mmol, 2.5 equiv), and tetrabutylammonium chloride (5.6 mg, 0.02 mmol, 0.1 equiv) following the general procedure I (pressure tube) at 60°C in DCM. Yield = 38.7 mg (52%) of white solid. TLC (pentane:EtOAc, 9:1 v/v): $R_f = 0.56$. Mp: 113-116 °C.

^1H NMR (CDCl_3 , 400 MHz): 7.54 (d, $J = 1.8$ Hz, 1H), 7.39 (d, $J = 1.7$ Hz, 1H), 7.09 (dd, $J = 58.3, 53.1$ Hz, 1H), 6.19 (d, $J = 2.2$ Hz, 1H), 6.08 (t, $J = 7.9$ Hz, 1H), 2.51 (dd, $J = 12.9, 8.0$ Hz, 1H), 2.30 (s, 3H), 2.21 (dd, $J = 12.9, 7.9$ Hz, 1H), 2.14 (s, 3H), 1.47 (s, 3H), 1.36 (s, 9H), 1.27 (s, 3H) ppm.

^{13}C NMR (CDCl_3 , 101 MHz): 200.5, 153.8, 152.3, 147.4, 137.5 (dd, $J = 33.0, 24.4$ Hz), 135.7, 135.4, 124.4, 122.8, 109.8 (dd, $J = 235.3$ Hz, $J = 235.4$ Hz), 104.4 (dd, $J = 3.7, 2.4$ Hz), 61.9 (d, $J = 2.0$ Hz), 50.0, 42.1, 34.9, 31.5, 30.3, 28.8, 27.8, 13.6 ppm.

^{19}F NMR (CDCl_3 , 377 MHz): -106.96 (d, $J = 307.0$ Hz), -121.35 (d, $J = 307.0$ Hz) ppm.

HRMS Calculated for $[\text{C}_{22}\text{H}_{28}\text{F}_2\text{N}_2\text{O} + \text{Na}]^+$: 397.2062, Found: 297.2057.



Ethyl 6-(5-(difluoromethyl)-3-methyl-1H-pyrazol-1-yl)-1-(4-fluorophenyl)-1,4,5,6-tetrahydrocyclopenta[*c*]pyrazole-3-carboxylate, **3ti**

Reaction run using ethyl 1-(4-fluorophenyl)-1,4,5,6-tetrahydrocyclopenta[*c*]pyrazole-3-carboxylate **1t** (54.5 mg, 0.2 mmol, 1.0 equiv), 3-(difluoromethyl)-5-methyl-1H-pyrazole **2i** (66.0 mg, 0.50 mmol, 2.5 equiv), and tetrabutylammonium chloride (5.6 mg, 0.02 mmol, 0.1 equiv) following the general procedure I (pressure tube) at 50 °C in DCM. Yield = 33.6 mg (42%) of pale yellow amorphous solid. TLC (DCM:MeOH, 50:1 v/v): $R_f = 0.18$.

^1H NMR (CDCl_3 , 500 MHz): 7.72 – 7.65 (m, 2H), 7.20 – 7.13 (m, 2H), 6.99 (dd, $J = 56.5, 53.2$ Hz, 1H), 6.25 (d, $J = 1.9$ Hz, 1H), 5.86 (dd, $J = 8.6, 3.8$ Hz, 1H), 4.36 – 4.14 (m, 2H), 3.40 (dddd, $J = 15.1, 8.7, 5.1, 1.3$ Hz, 1H), 3.20 (dtd, $J = 13.6, 8.4, 5.0$ Hz, 1H), 2.99 (ddd, $J = 15.2, 8.6, 4.5$ Hz, 1H), 2.90 (ddt, $J = 13.2, 8.7, 4.2$ Hz, 1H), 2.21 (s, 3H), 1.19 (t, $J = 7.1$ Hz, 3H) ppm.

^{13}C NMR (CDCl_3 , 126 MHz): 161.7, 161.6 (d, $J = 247.6$ Hz), 151.5, 148.1, 138.2, 136.1 (dd, $J = 30.2, 25.0$ Hz), 135.7 (d, $J = 3.0$ Hz), 129.6, 122.3 (d, $J = 8.4$ Hz), 116.3 (d, $J = 23.1$ Hz), 109.2 (t, $J = 235.7$ Hz), 105.5 (t, $J = 3.8$ Hz), 61.0, 56.2 (d, $J = 2.4$ Hz), 39.8, 25.2, 14.1, 13.7 ppm.

^{19}F NMR (CDCl_3 , 377 MHz): -108.15 (d, $J = 307.6$ Hz), -114.20, -116.86 (d, $J = 307.8$ Hz) ppm. HRMS Calculated for $[\text{C}_{20}\text{H}_{19}\text{F}_3\text{N}_4\text{O}_2 + \text{H}]^+$: 405.1533, Found: 405.1529.

| | |
|--|--|
| | |
| Ethyl 4-(1,1-dioxidoisothiazolidin-2-yl)-1-(4-fluorophenyl)-1,4,5,6-tetrahydrocyclopenta[<i>c</i>]pyrazole-3-carboxylate, 3tt-1 | Ethyl 4-(1,1-dioxidoisothiazolidin-2-yl)-1-(4-fluorophenyl)-1,4,5,6-tetrahydrocyclopenta[<i>c</i>]pyrazole-3-carboxylate, 3tt-2 |

Reaction run using ethyl 1-(4-fluorophenyl)-1,4,5,6-tetrahydrocyclopenta[*c*]pyrazole-3-carboxylate **1t** (54.5 mg, 0.2 mmol, 1.0 equiv), 1,3-propanesultam **2t** (50.0 μL , 0.50 mmol, 2.5 equiv), and tetrabutylammonium chloride (5.6 mg, 0.02 mmol, 0.1 equiv) following the general procedure I (pressure tube) at 40 °C in DCM, and two regioisomers were isolated.

3ts-1: Yield = 39.0 mg (47%) of colorless semisolid. TLC (pentane:EtOAc, 1:2 v/v): $R_f = 0.33$.

^1H NMR (CDCl_3 , 500 MHz): 7.92 – 7.56 (m, 2H), 7.19 – 6.96 (m, 2H), 5.66 – 4.99 (m, 1H), 4.42 (qd, $J = 7.1, 3.0$ Hz, 2H), 3.36 – 3.11 (m, 5H), 3.03 – 2.89 (m, 2H), 2.85 (ddt, $J = 13.6, 5.2, 2.8$ Hz, 1H), 2.32 (dddd, $J = 13.3, 9.0, 6.4, 2.6$ Hz, 2H), 1.41 (t, $J = 7.1$ Hz, 3H). ppm.

^{13}C NMR (CDCl_3 , 126 MHz): 161.8, 161.6 (d, $J = 247.9$ Hz), 151.4, 139.0, 135.6 (d, $J = 3.0$ Hz),

128.4, 122.2 (d, $J = 8.5$ Hz), 116.4 (d, $J = 23.0$ Hz), 61.3, 51.3, 47.3, 42.7, 37.0, 25.2, 18.6, 14.4 ppm.

^{19}F NMR (CDCl_3 , 377 MHz): -113.9 ppm.

HRMS Calculated for $[\text{C}_{18}\text{H}_{20}\text{FN}_3\text{O}_4\text{S}+\text{H}]^+$: 394.1231, Found: 394.1226.

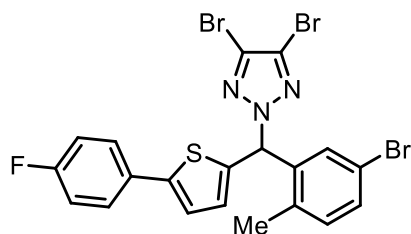
3ts-2: Yield = 4.0 mg (5%) of pale yellow amorphous solid. TLC (pentane:EtOAc, 1:1 v/v): $R_f = 0.33$.

^1H NMR (CDCl_3 , 500 MHz): 7.90 – 7.76 (m, 2H), 7.21 – 7.11 (m, 2H), 5.38 (dd, $J = 8.1, 3.2$ Hz, 1H), 4.42 (qd, $J = 7.1, 1.4$ Hz, 2H), 3.18 (dt, $J = 9.1, 7.3$ Hz, 1H), 3.11 (ddd, $J = 12.7, 8.2, 6.8$ Hz, 1H), 3.01 (dddd, $J = 24.5, 13.6, 9.0, 7.1$ Hz, 2H), 2.94 – 2.84 (m, 2H), 2.81 – 2.69 (m, 2H), 2.33 – 2.22 (m, 1H), 2.18 – 2.07 (m, 1H), 1.41 (t, $J = 7.1$ Hz, 3H) ppm.

^{13}C NMR (CDCl_3 , 126 MHz): 162.1, 161.7 (d, $J = 247.8$ Hz), 145.6, 138.2, 135.1 (d, $J = 3.0$ Hz), 134.6, 122.4 (d, $J = 8.4$ Hz), 116.2 (d, $J = 23.0$ Hz), 61.1, 51.1, 46.8, 40.7, 36.0, 22.8, 18.4, 14.1 ppm.

^{19}F NMR (CDCl_3 , 377 MHz): -114.1 ppm.

HRMS Calculated for $[\text{C}_{18}\text{H}_{20}\text{FN}_3\text{O}_4\text{S}+\text{H}]^+$: 394.1231, Found: 394.1229.



4,5-dibromo-2-((5-bromo-2-methylphenyl)(5-(4-fluorophenyl)thiophen-2-yl)methyl)-2H-1,2,3-triazole, **3pp'**

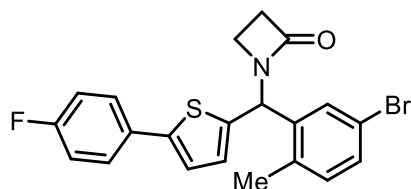
Reaction run using 2-(5-bromo-2-methylbenzyl)-5-(4-fluorophenyl)thiophene **1p** (68.6 mg, 0.2 mmol, 1.0 equiv), 4,5-Dibromo-1*H*-1,2,3-triazole **2p** (113.4 mg, 0.50 mmol, 2.5 equiv), and tetrabutylammonium chloride (5.6 mg, 0.02 mmol, 0.1 equiv) following the general procedure II (glass vial) procedure at 30 °C. Yield = 81.8 mg (70%) of colorless liquid. TLC (pentane:EtOAc, 9:1 v/v): $R_f = 0.51$.

^1H NMR (CDCl_3 , 500 MHz): 7.58 – 7.46 (m, 2H), 7.40 (d, $J = 7.4$ Hz, 2H), 7.20 (s, 1H), 7.09 (d, $J = 3.2$ Hz, 2H), 7.08 – 6.94 (m, 2 H), 6.84 (d, $J = 3.7$ Hz, 1H), 2.29 (s, 3H) ppm.

^{13}C NMR (CDCl_3 , 101 MHz): 162.6 (d, $J = 248.1$ Hz), 145.5, 137.6, 137.5, 134.6, 132.5, 132.1, 130.00, 129.95, 129.6, 127.6 (d, $J = 8.1$ Hz), 125.6, 122.8, 120.3, 116.0 (d, $J = 21.9$ Hz), 65.9, 18.9.

^{19}F NMR (CDCl_3 , 377 MHz): -113.6 ppm.

HRMS Calculated for $[\text{C}_{20}\text{H}_{13}\text{Br}_3\text{FN}_3\text{S}+\text{H}]^+$: 583.8437, Found: 583.8444.



4,5-dibromo-2-((5-bromo-2-methylphenyl)(5-(4-fluorophenyl)thiophen-2-yl)methyl)-2H-1,2,3-triazole, **3pr**

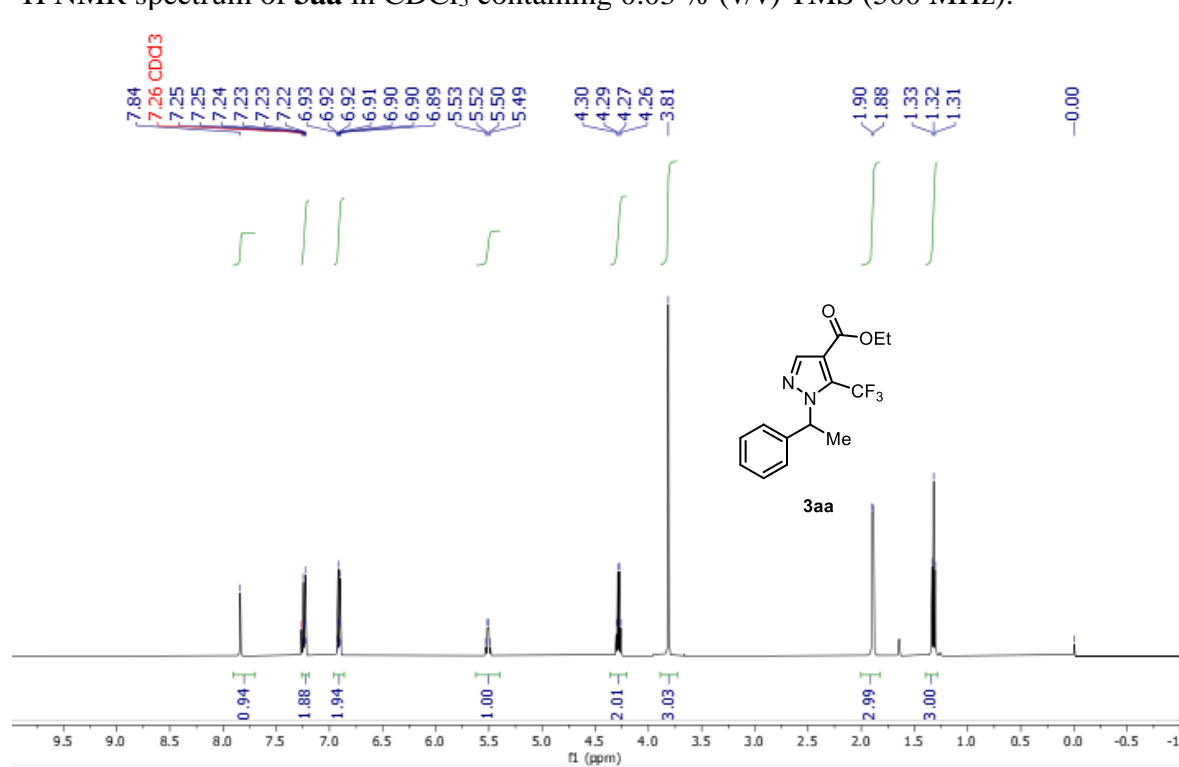
Reaction run using 2-(5-bromo-2-methylbenzyl)-5-(4-fluorophenyl)thiophene **1p** (68.6 mg, 0.2 mmol, 1.0 equiv), azetidin-2-one **2s** (35.0 mg, 0.50 mmol, 2.5 equiv), and tetrabutylammonium chloride (5.6 mg, 0.02 mmol, 0.1 equiv) following the general procedure II (glass vial) procedure at 30 °C. Yield = 68.5 mg (80%) of light-yellow liquid. TLC (pentane:EtOAc, 4:1 v/v): R_f = 0.10. ^1H NMR (CDCl_3 , 500 MHz): 7.57 – 7.48 (m, 2H), 7.41 (d, J = 2.1 Hz, 1H), 7.38 (dd, J = 8.1, 2.1 Hz, 1H), 7.15 – 7.06 (m, 2H), 7.06 (t, J = 8.6 Hz, 2H), 6.72 (d, J = 3.8 Hz, 1H), 6.43 (s, 1H), 3.38 (q, J = 5.1, 4.5 Hz, 1H), 3.24 (dt, J = 5.7, 4.0 Hz, 1H), 3.01 (t, J = 4.2 Hz, 2H), 2.29 (s, 3H) ppm. ^{13}C NMR (CDCl_3 , 101 MHz): 167.2, 162.5 (d, J = 247.7 Hz), 143.7, 140.7, 139.2, 135.1, 132.7, 131.3, 130.2 (d, J = 3.5 Hz), 129.9, 127.7, 127.4 (d, J = 8.1 Hz), 122.9, 119.8, 115.9 (d, J = 21.8 Hz), 53.8, 38.4, 36.1, 19.0 ppm. ^{19}F NMR (CDCl_3 , 471 MHz): -114.0 ppm. HRMS Calculated for $[\text{C}_{21}\text{H}_{17}\text{BrFNOS}+\text{H}]^+$: 452.0091, Found: 452.0089.

3B. XIII. Reference

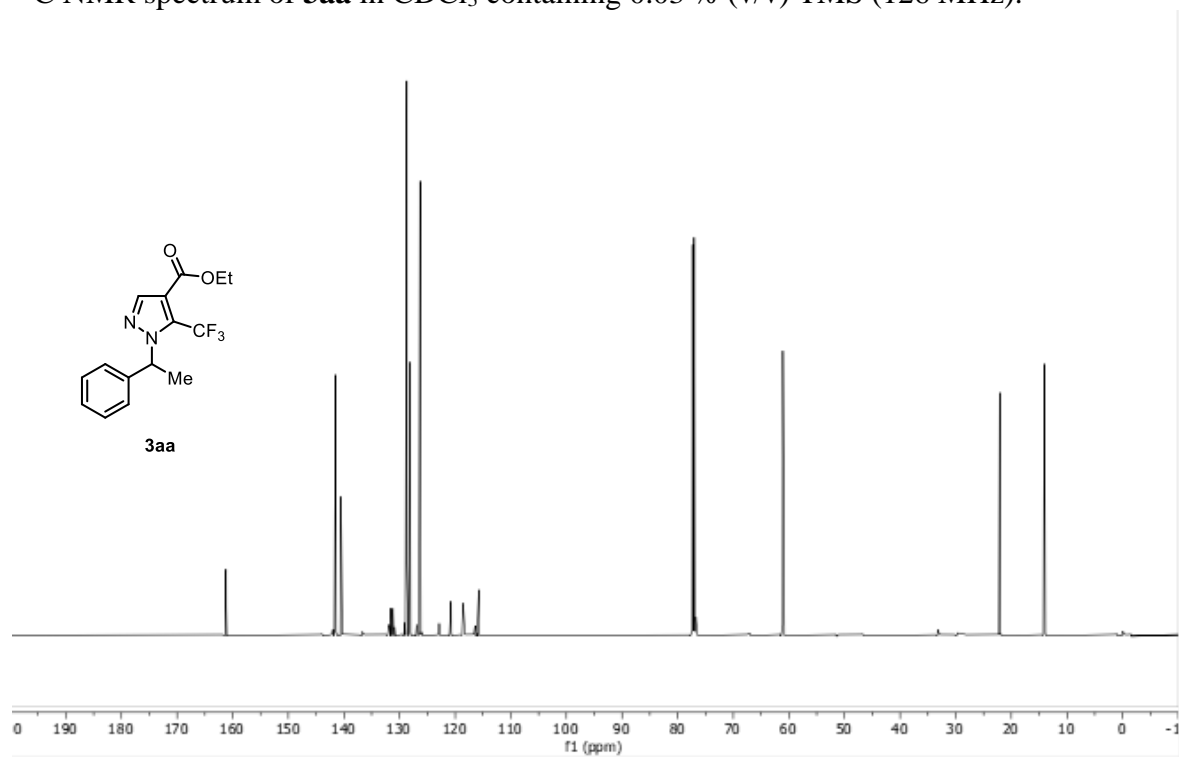
1. Hu, H.; Chen, S.-J.; Mandal, M.; Pratik, S. M.; Buss, J. A.; Krska, S. W.; Cramer, C. J.; Stahl, S. S. *Nat. Catal.* **2020**, *3*, 358–367.
2. Sun, H.-L.; Yang, F.; Ye, W.-T.; Wang, J.-J.; Zhu, R. *ACS Catal.* **2020**, *10*, 4983–4989.
3. Liu, W.; Sengupta, S.; Peterson, J. L.; Akhmedov, N. G.; Shi, X. *J. Org. Chem.* **2007**, *72*, 5012–5015.
4. Bruker-AXS (2016). *APEX3*. Version 2016.5-0. Madison, Wisconsin, USA.
5. Krause, L.; Herbst-Irmer, R.; Sheldrick, G. M.; Stalke, D. *J. Appl. Cryst.* **2015**, *48*, 3–10.
6. Sheldrick, G. M. (2013b). *XPREP*. Version 2013/1. Georg-August-Universität Göttingen, Göttingen, Germany.
7. Sheldrick, G. M. (2013a). The *SHELX* homepage, <http://shelx.uni-ac.gwdg.de/SHELX/>.
8. Sheldrick, G. M. *Acta Cryst.* **2015**, *A71*, 3–8.
9. Sheldrick, G. M. *Acta Cryst.* **2015**, *C71*, 3–8.
10. Dolomanov, O. V.; Bourhis, L. J.; Gildea, R. J.; Howard, J. A. K.; Puschmann, H. *J. Appl. Crystallogr.* **2009**, *42*, 339–341.
11. Guzei, I. A. (2007-2013). Programs *Gn*. University of Wisconsin-Madison, Madison, Wisconsin, USA.

3B.XIV. NMR Spectroscopic Data

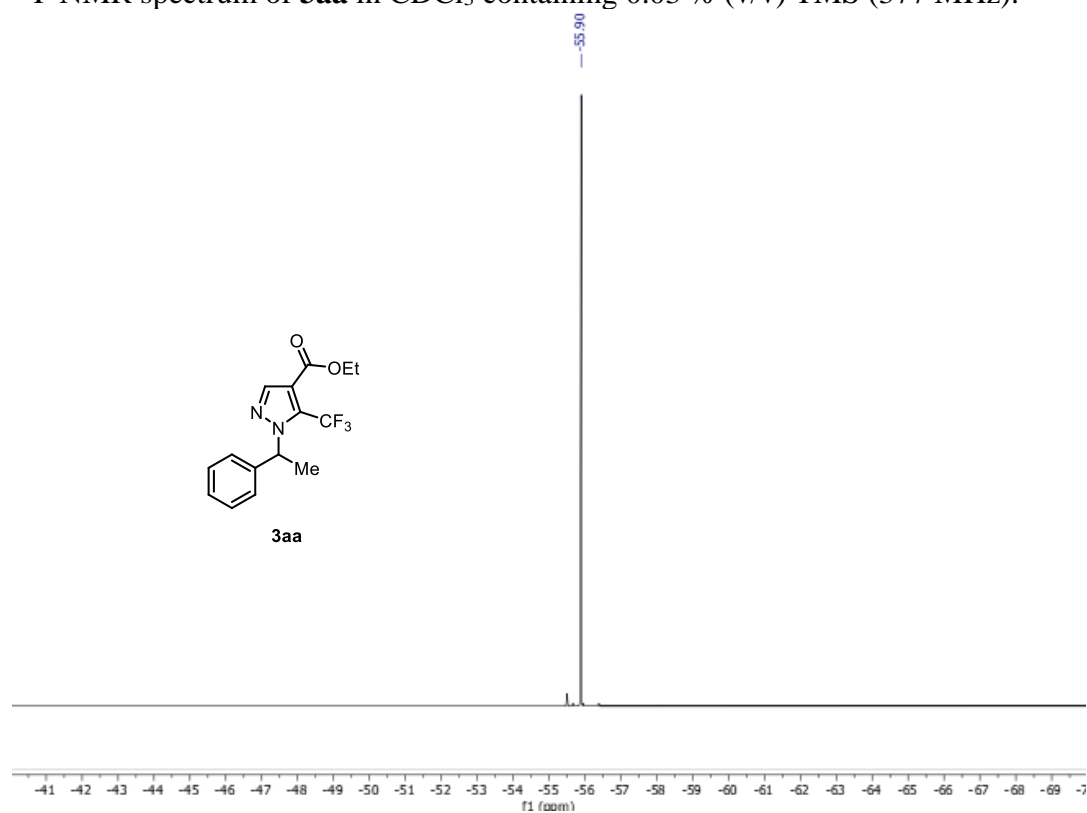
¹H NMR spectrum of **3aa** in CDCl₃ containing 0.03 % (v/v) TMS (500 MHz).



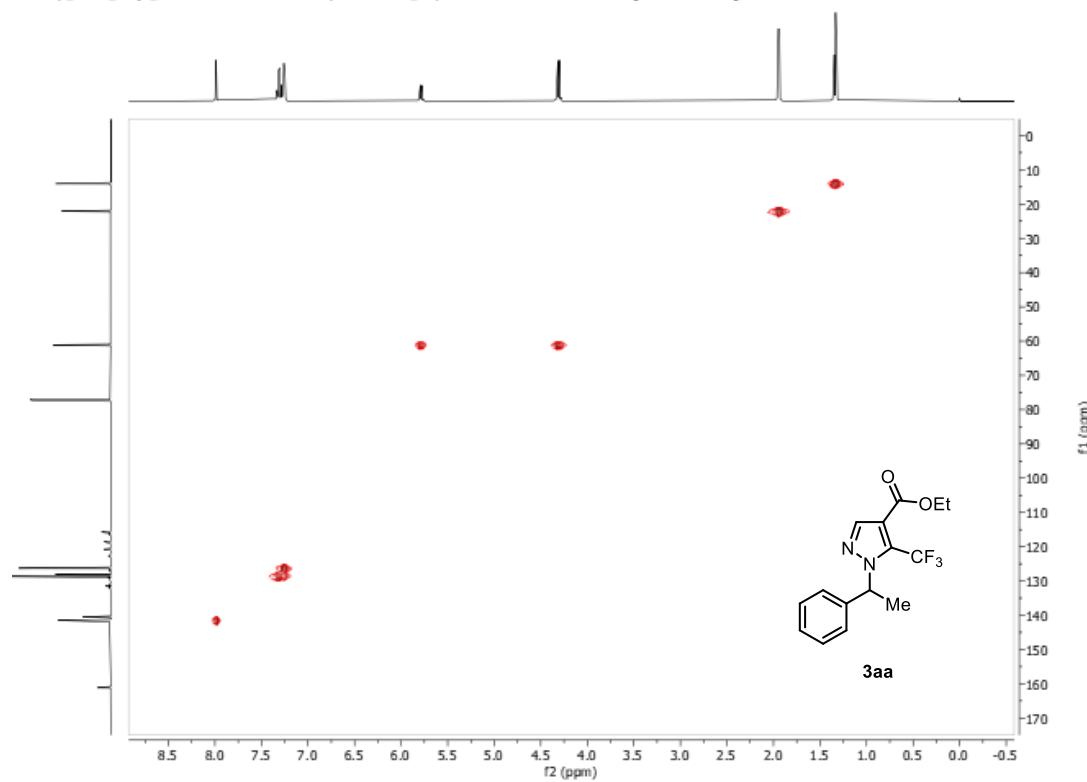
¹³C NMR spectrum of **3aa** in CDCl₃ containing 0.03 % (v/v) TMS (126 MHz).



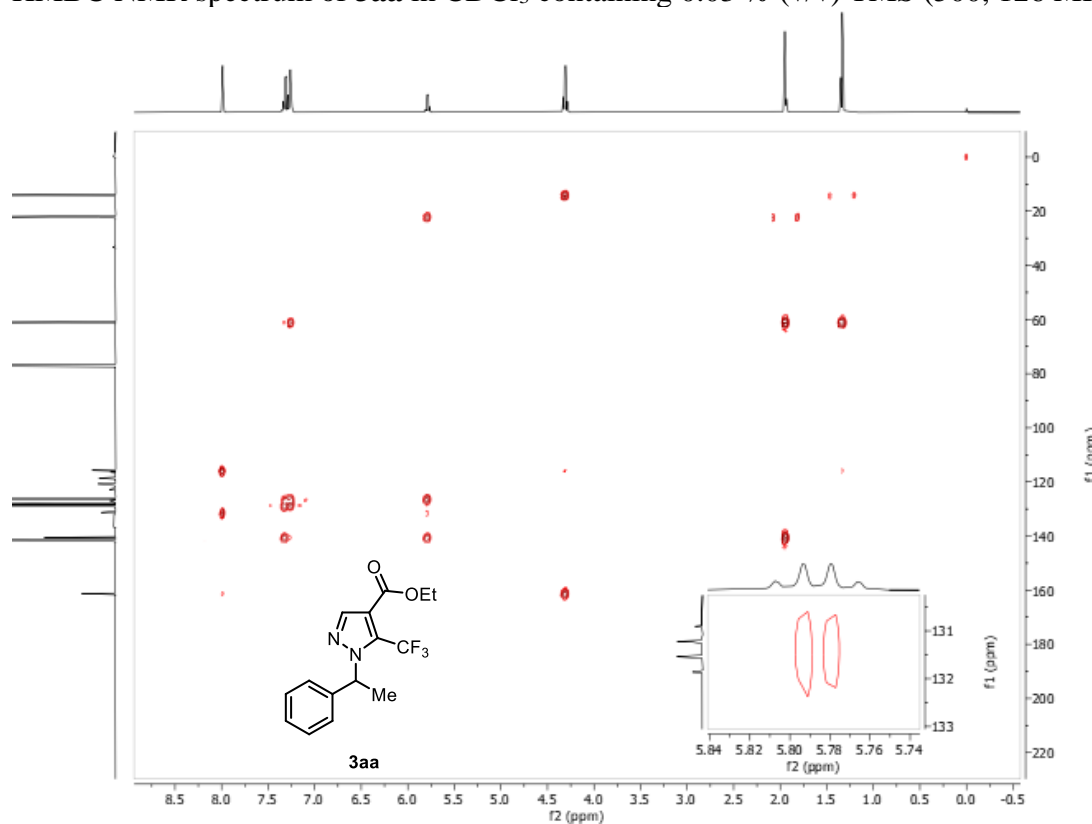
^{19}F NMR spectrum of **3aa** in CDCl_3 containing 0.03 % (v/v) TMS (377 MHz).



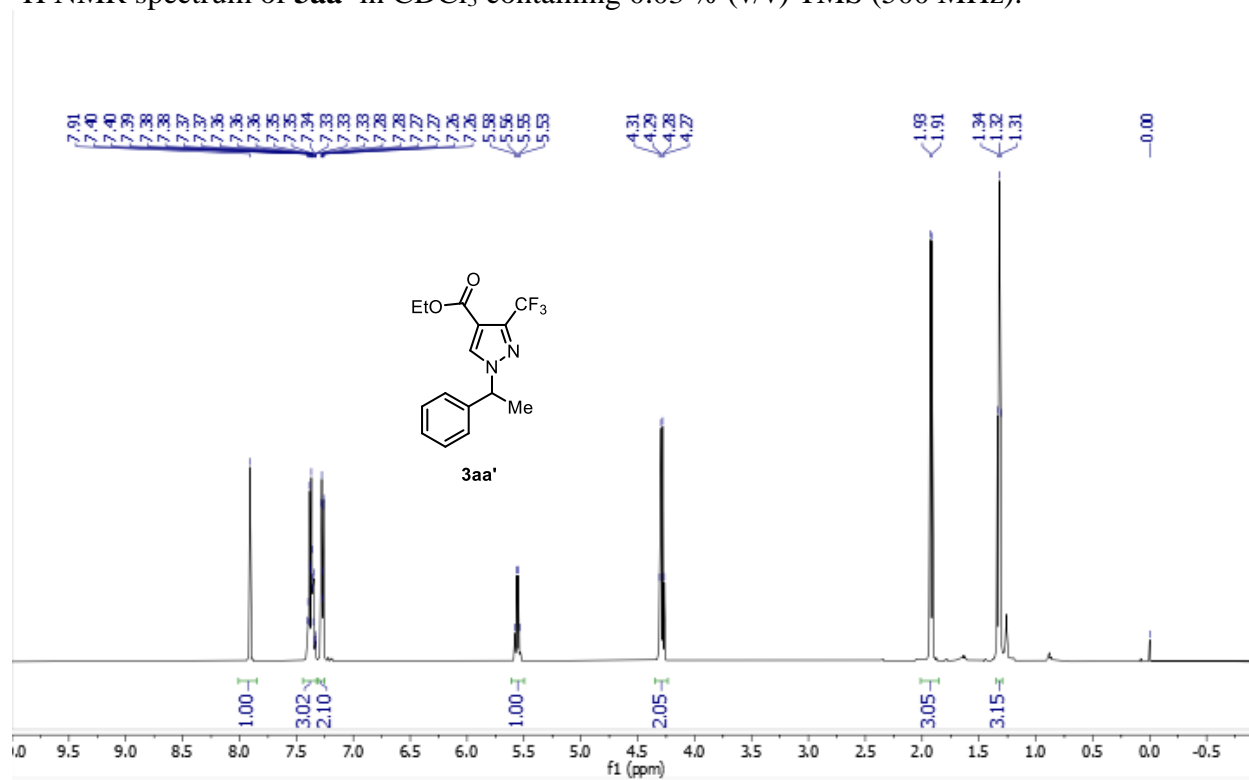
HSQC NMR spectrum of **3aa** in CDCl_3 containing 0.03 % (v/v) TMS (500, 126 MHz).



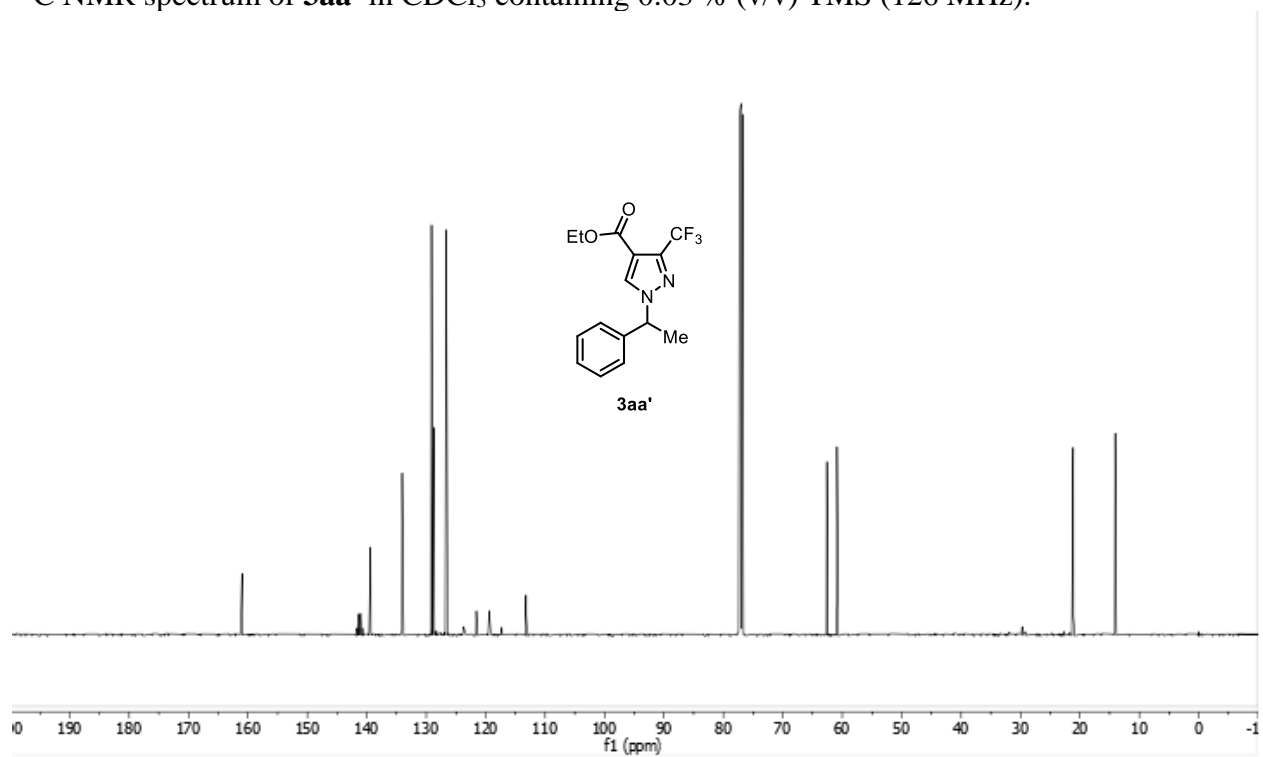
HMBC NMR spectrum of **3aa** in CDCl₃ containing 0.03 % (v/v) TMS (500, 126 MHz).



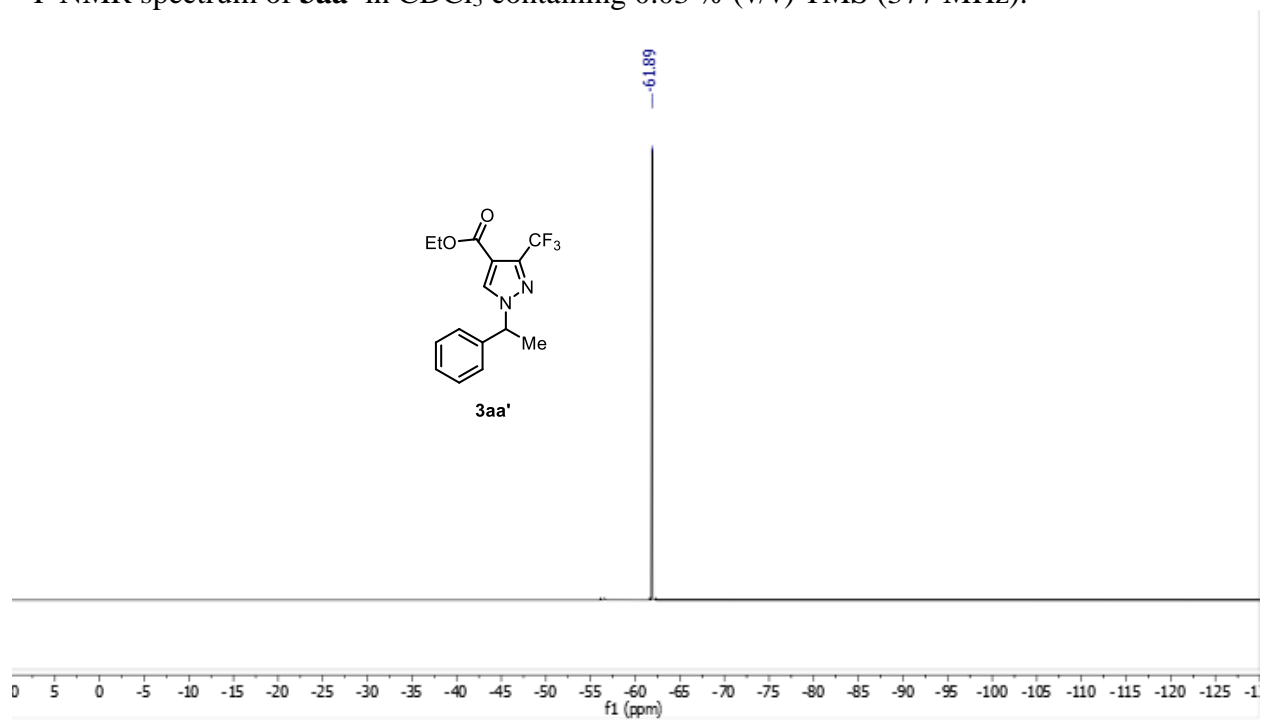
¹H NMR spectrum of **3aa'** in CDCl₃ containing 0.03 % (v/v) TMS (500 MHz).



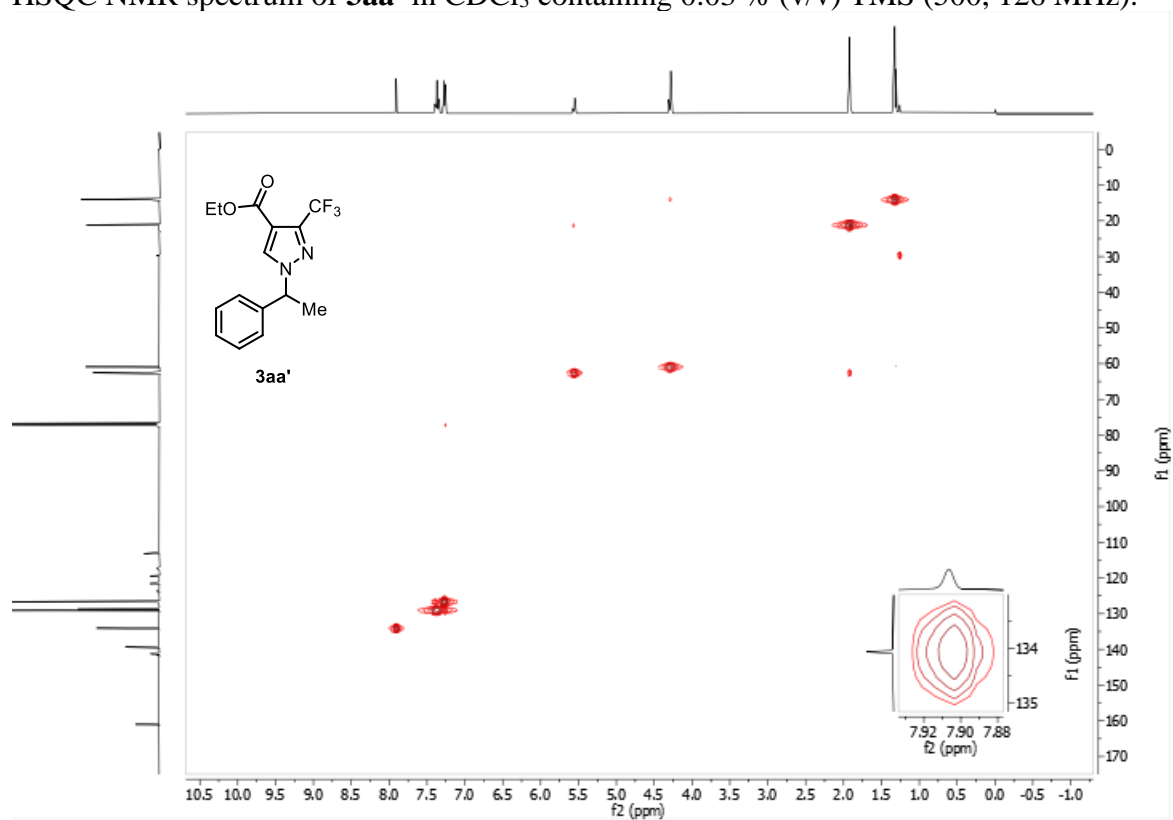
^{13}C NMR spectrum of **3aa'** in CDCl_3 containing 0.03 % (v/v) TMS (126 MHz).



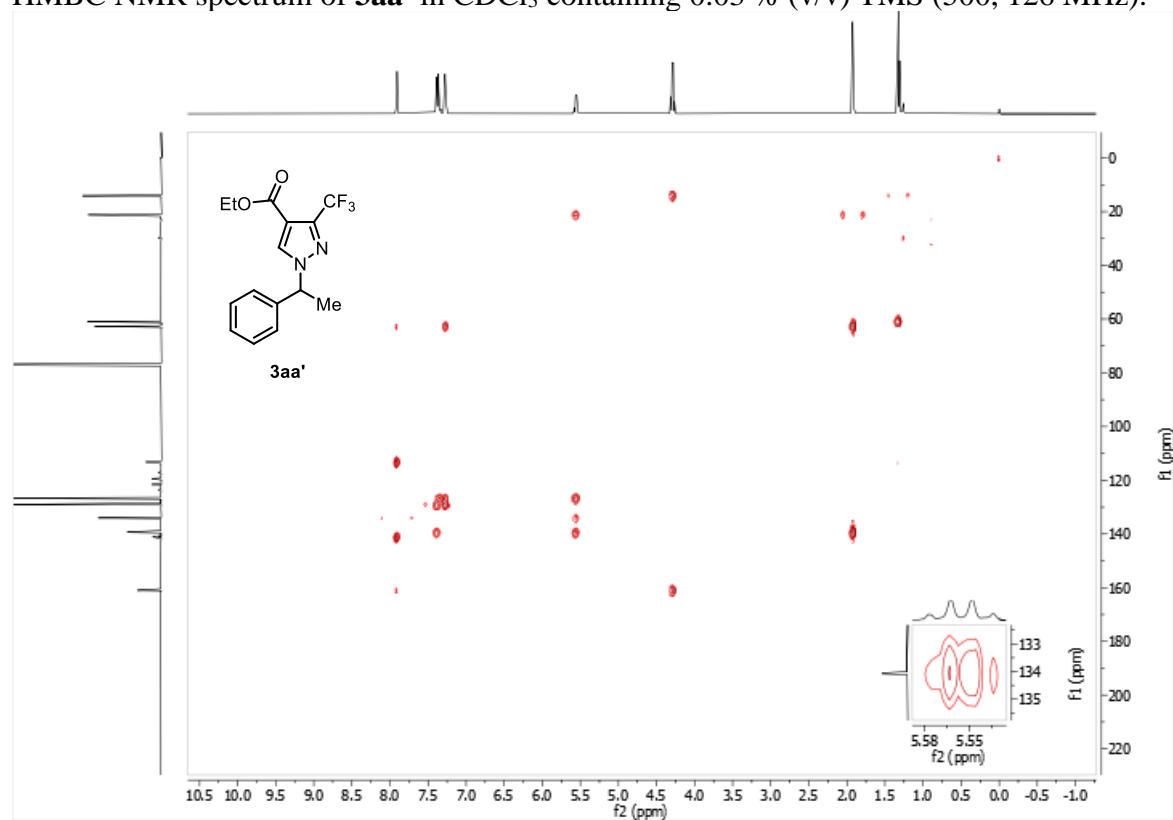
^{19}F NMR spectrum of **3aa'** in CDCl_3 containing 0.03 % (v/v) TMS (377 MHz).



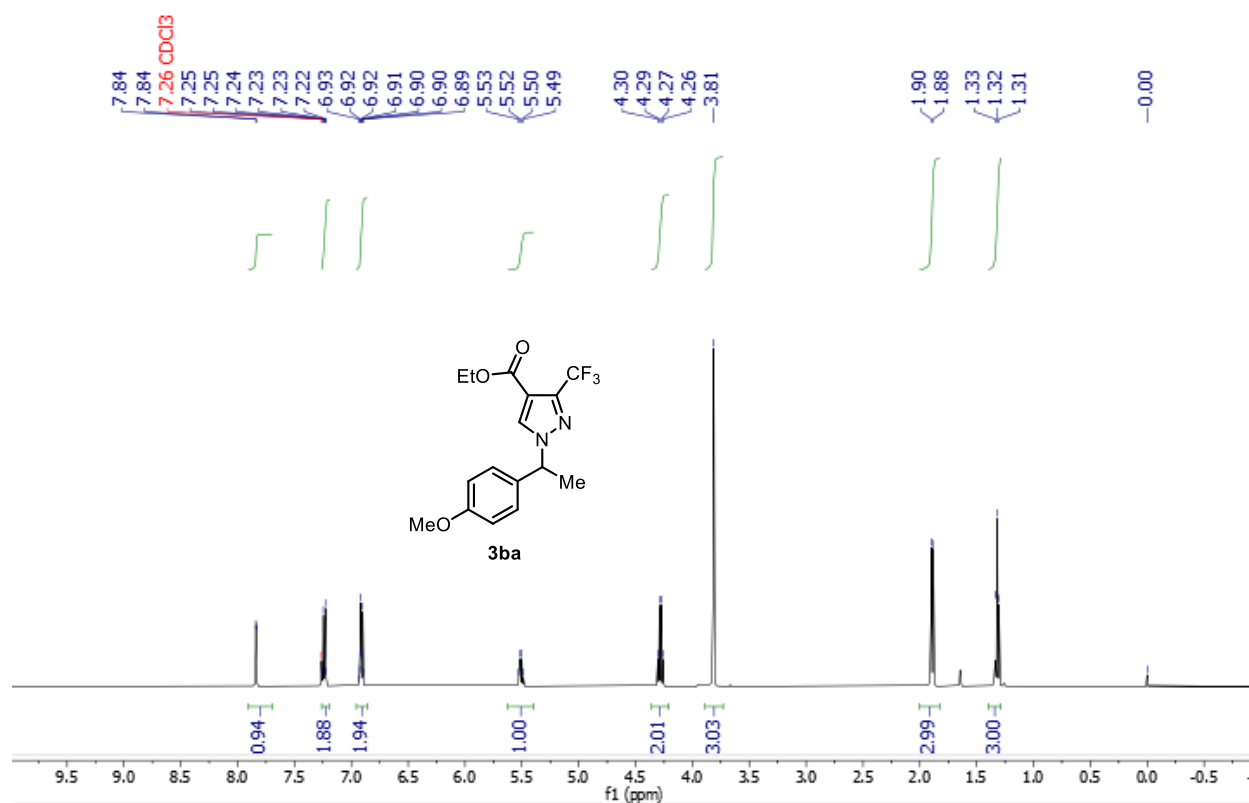
HSQC NMR spectrum of **3aa'** in CDCl₃ containing 0.03 % (v/v) TMS (500, 126 MHz).



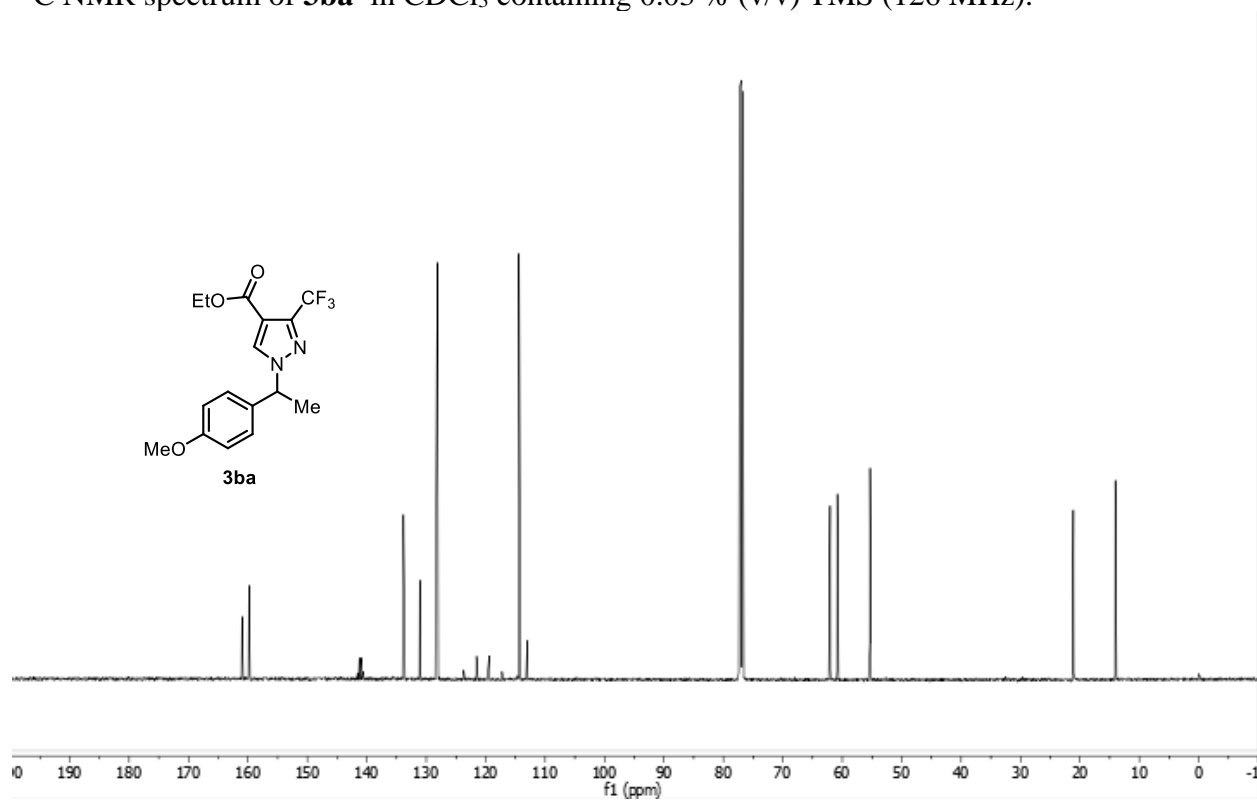
HMBC NMR spectrum of **3aa'** in CDCl₃ containing 0.03 % (v/v) TMS (500, 126 MHz).



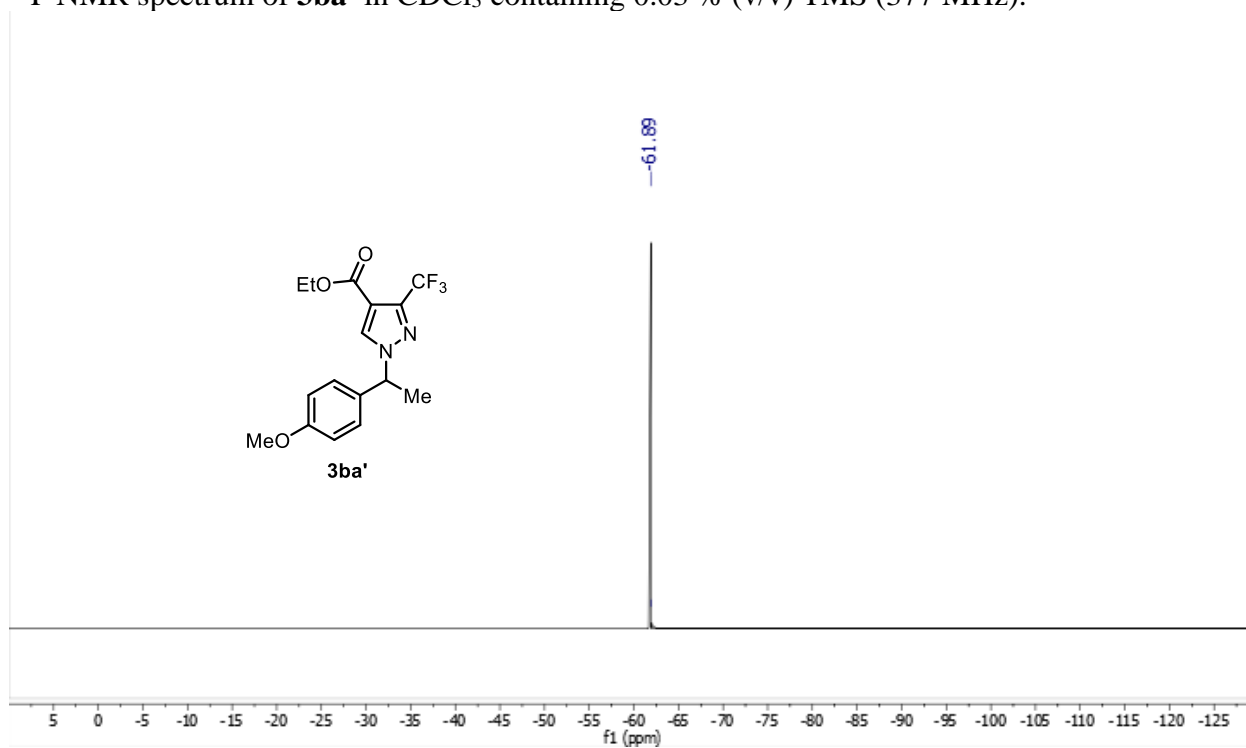
^1H NMR spectrum of **3ba'** in CDCl_3 containing 0.03 % (v/v) TMS (500 MHz).



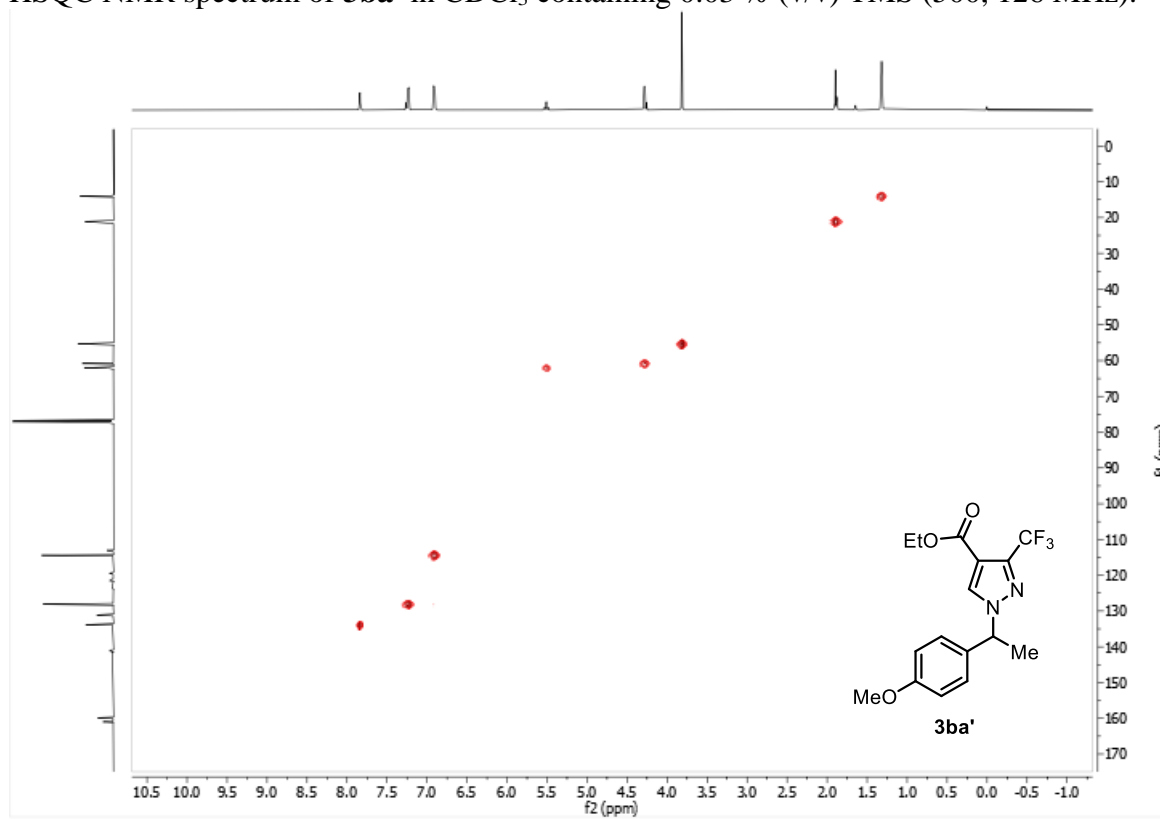
^{13}C NMR spectrum of **3ba'** in CDCl_3 containing 0.03 % (v/v) TMS (126 MHz).



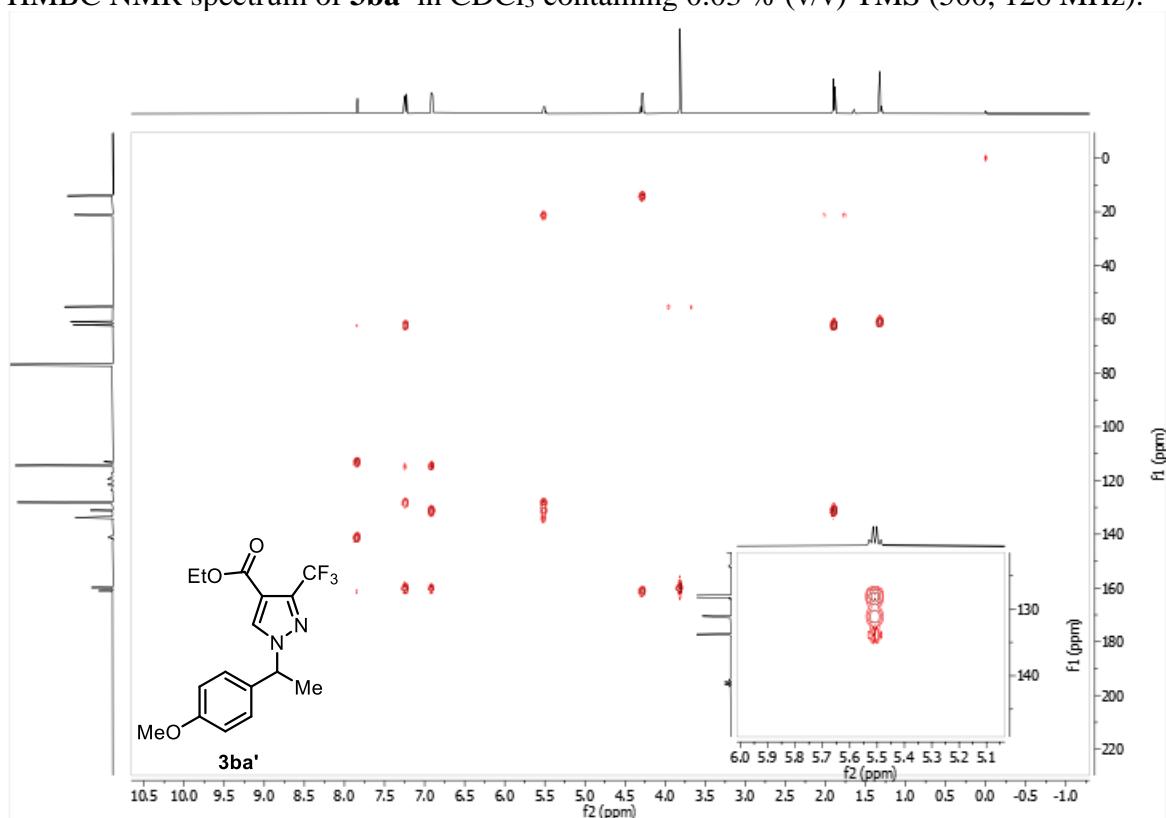
^{19}F NMR spectrum of **3ba'** in CDCl_3 containing 0.03 % (v/v) TMS (377 MHz).



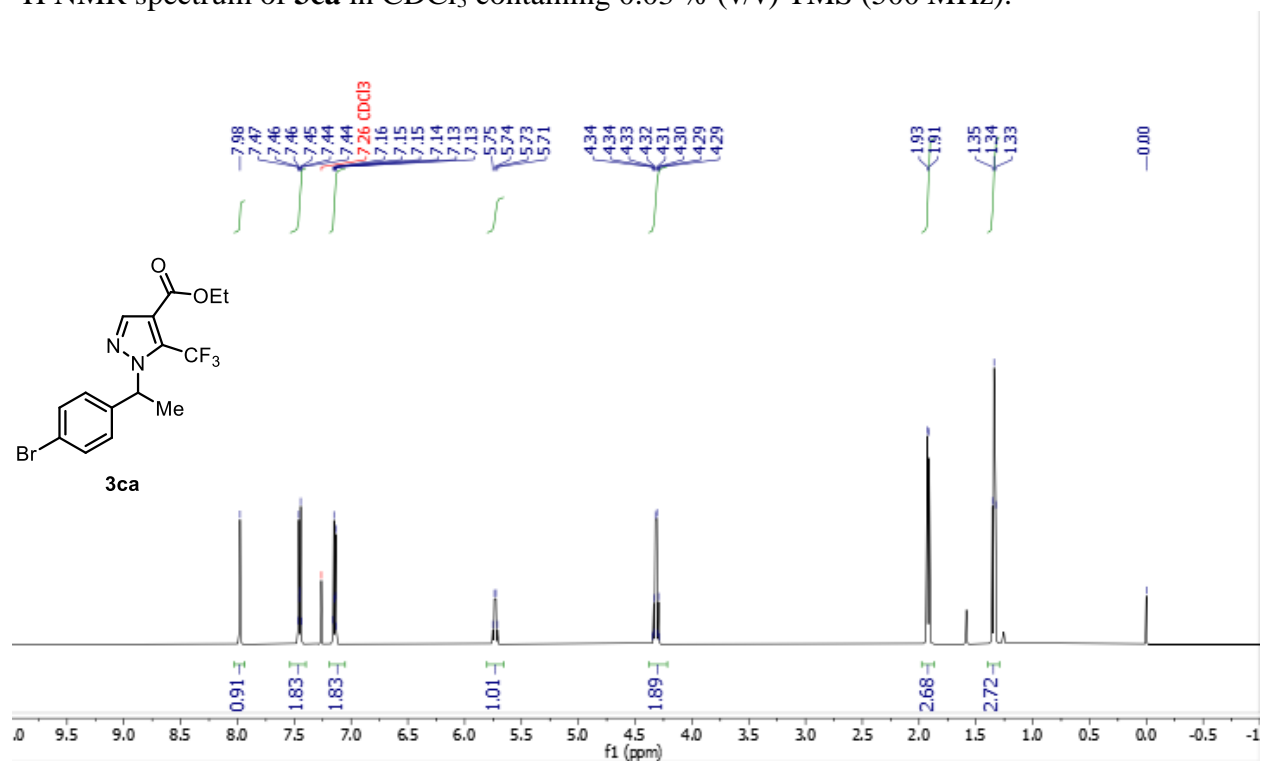
HSQC NMR spectrum of **3ba'** in CDCl_3 containing 0.03 % (v/v) TMS (500, 126 MHz).



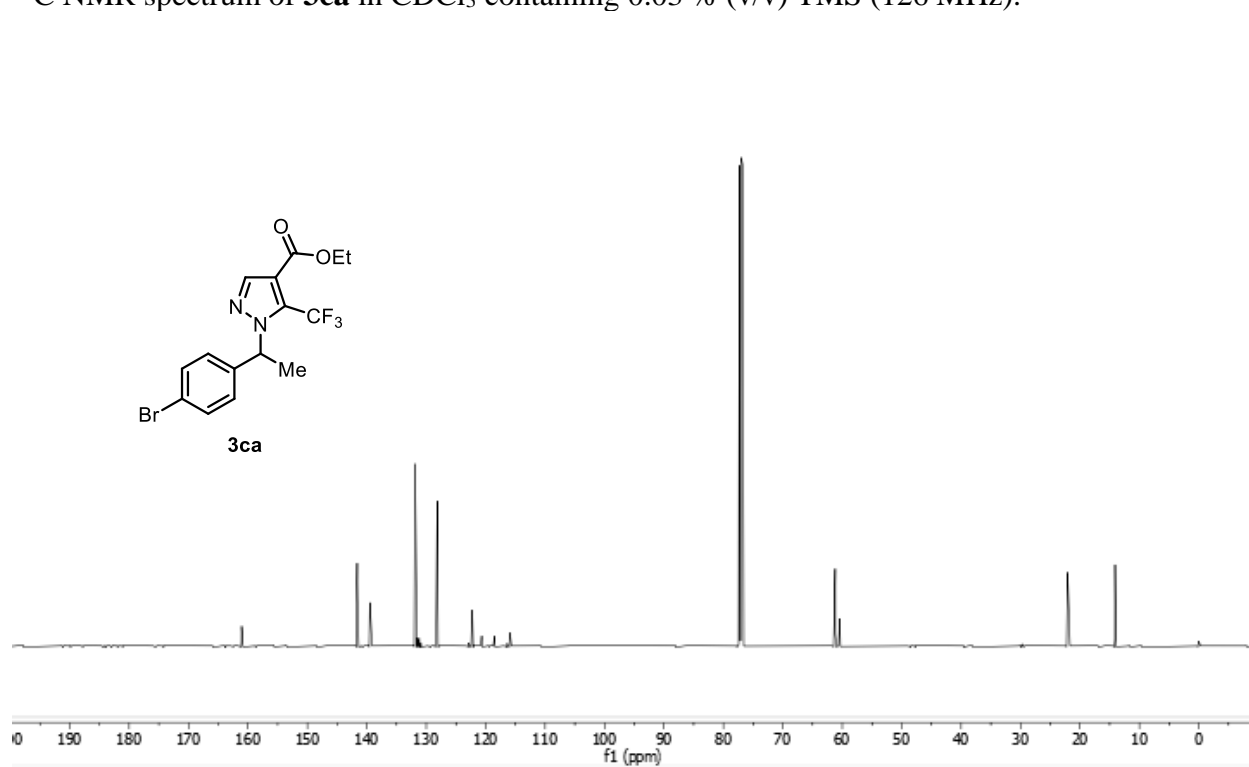
HMBC NMR spectrum of **3ba'** in CDCl₃ containing 0.03 % (v/v) TMS (500, 126 MHz).



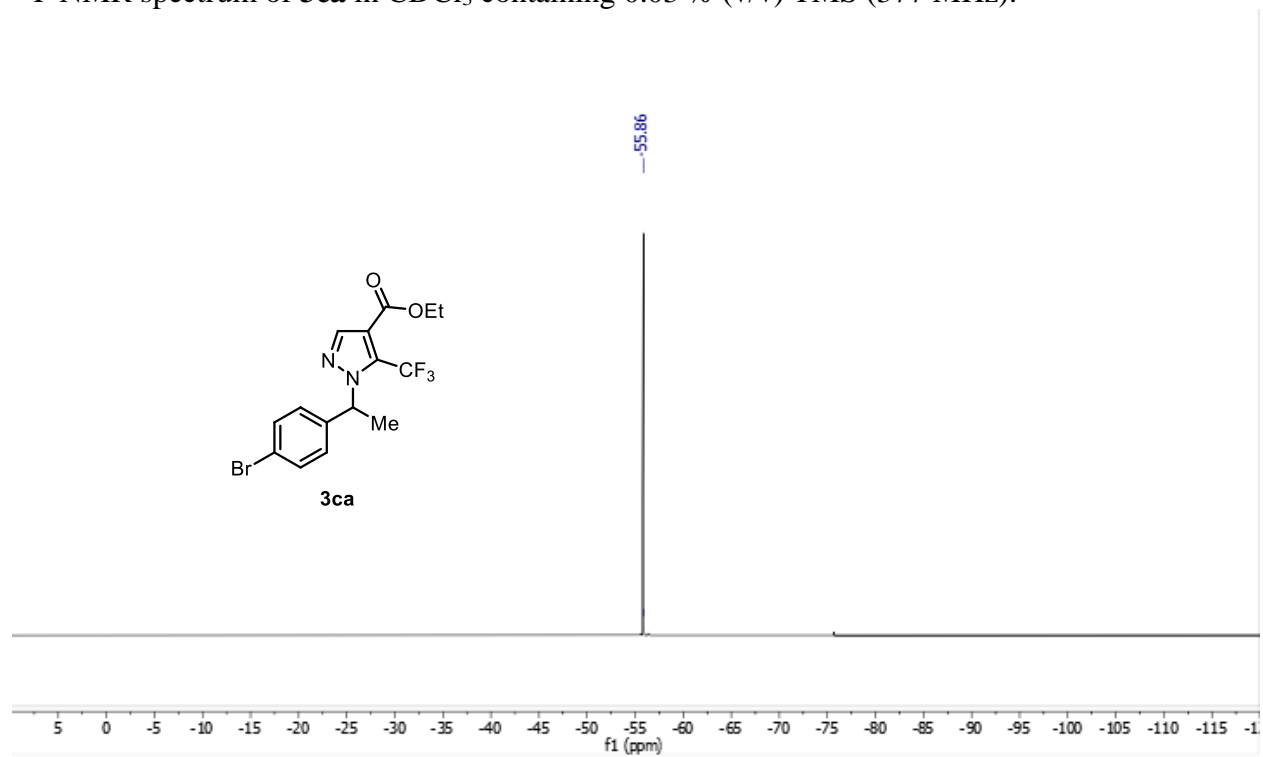
¹H NMR spectrum of **3ca** in CDCl₃ containing 0.03 % (v/v) TMS (500 MHz).



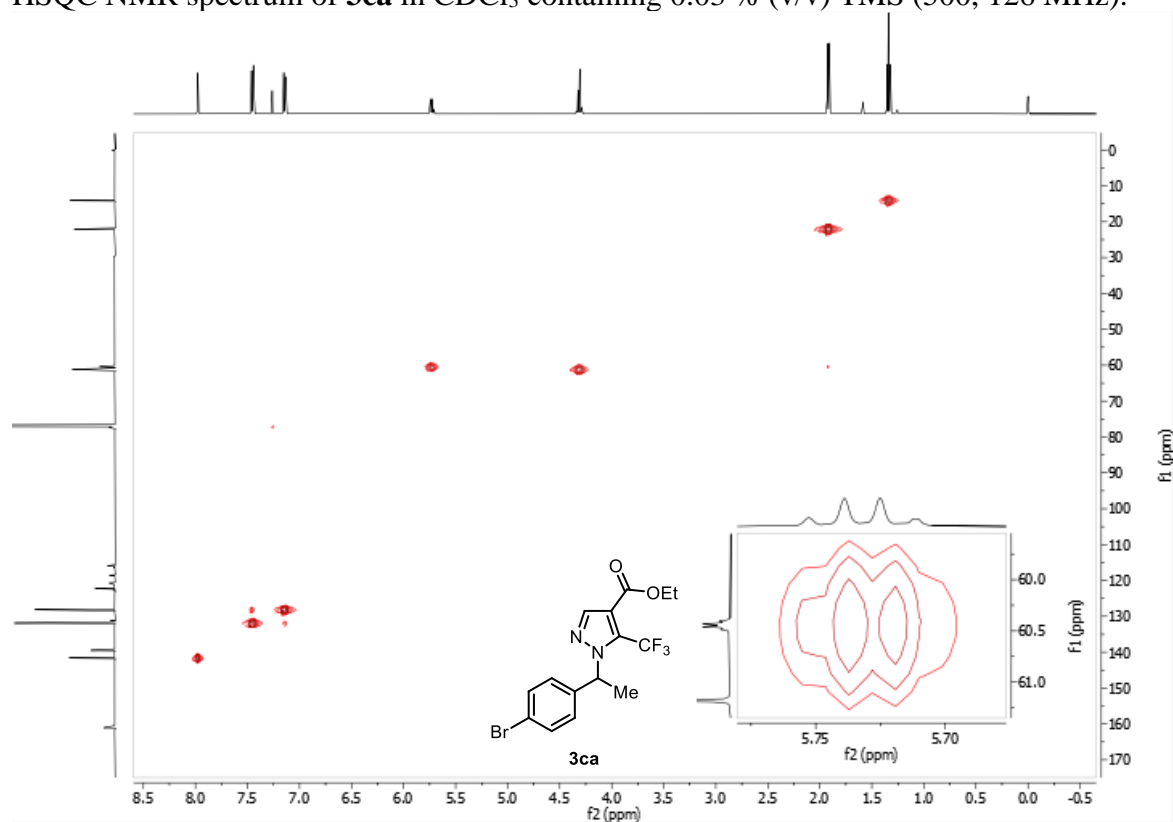
^{13}C NMR spectrum of **3ca** in CDCl_3 containing 0.03 % (v/v) TMS (126 MHz).



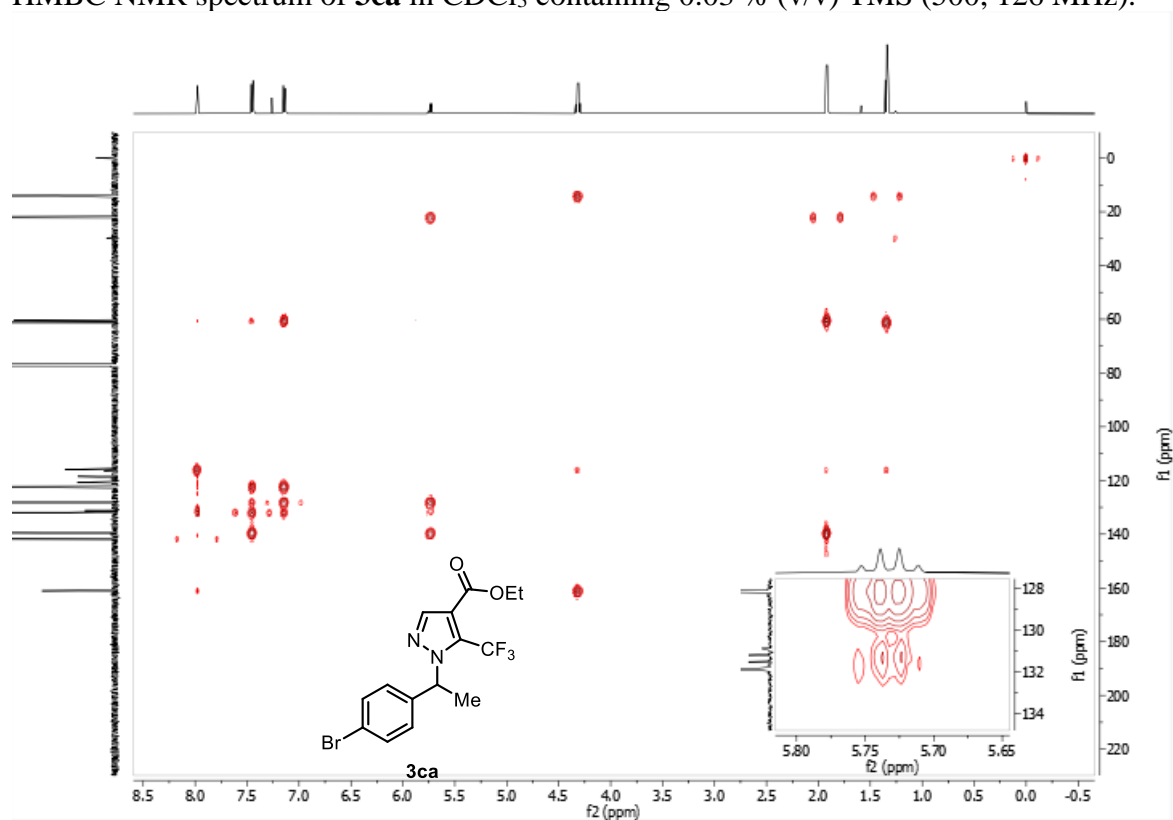
^{19}F NMR spectrum of **3ca** in CDCl_3 containing 0.03 % (v/v) TMS (377 MHz).



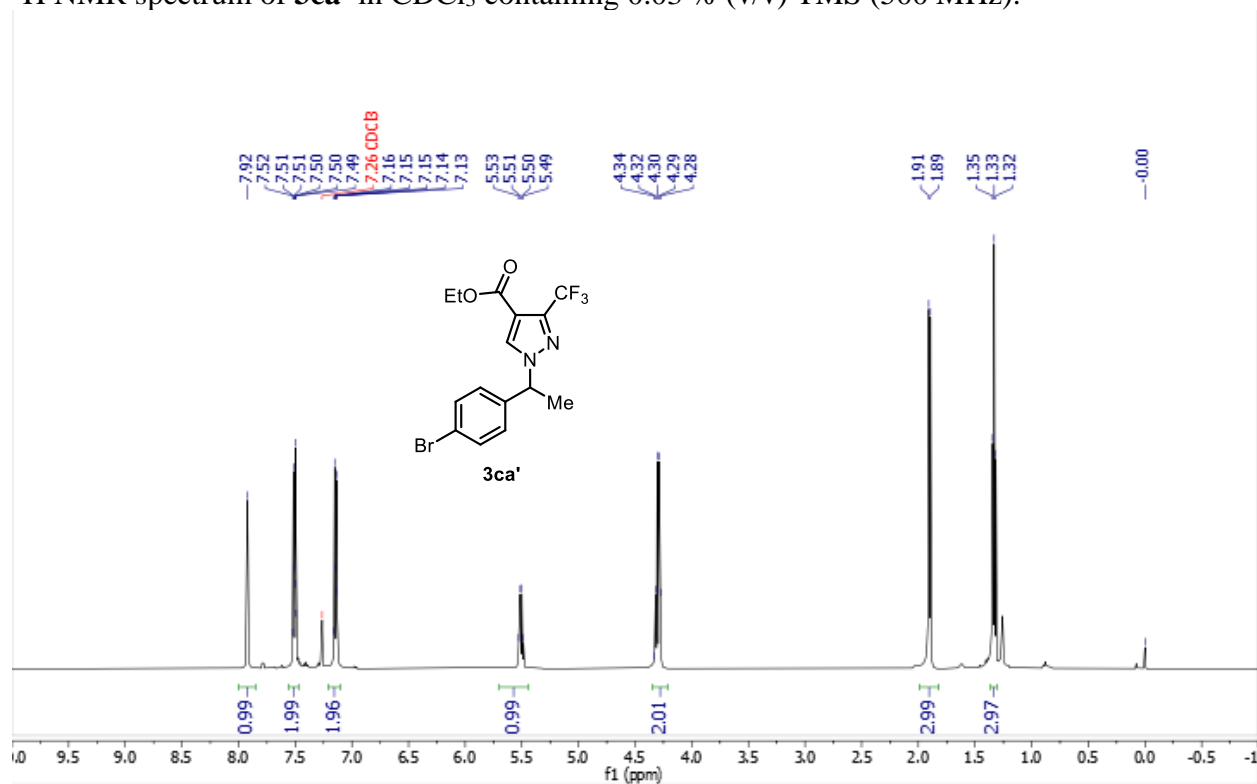
HSQC NMR spectrum of **3ca** in CDCl₃ containing 0.03 % (v/v) TMS (500, 126 MHz).



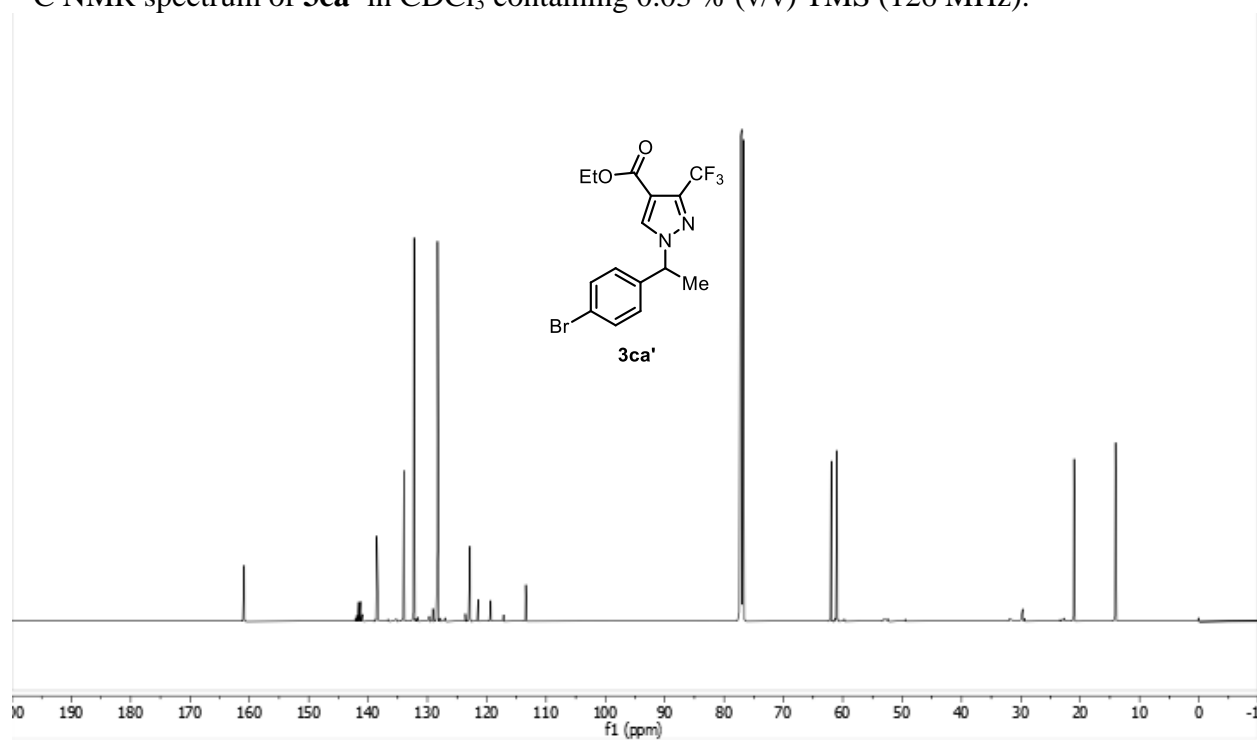
HMBC NMR spectrum of **3ca** in CDCl₃ containing 0.03 % (v/v) TMS (500, 126 MHz).



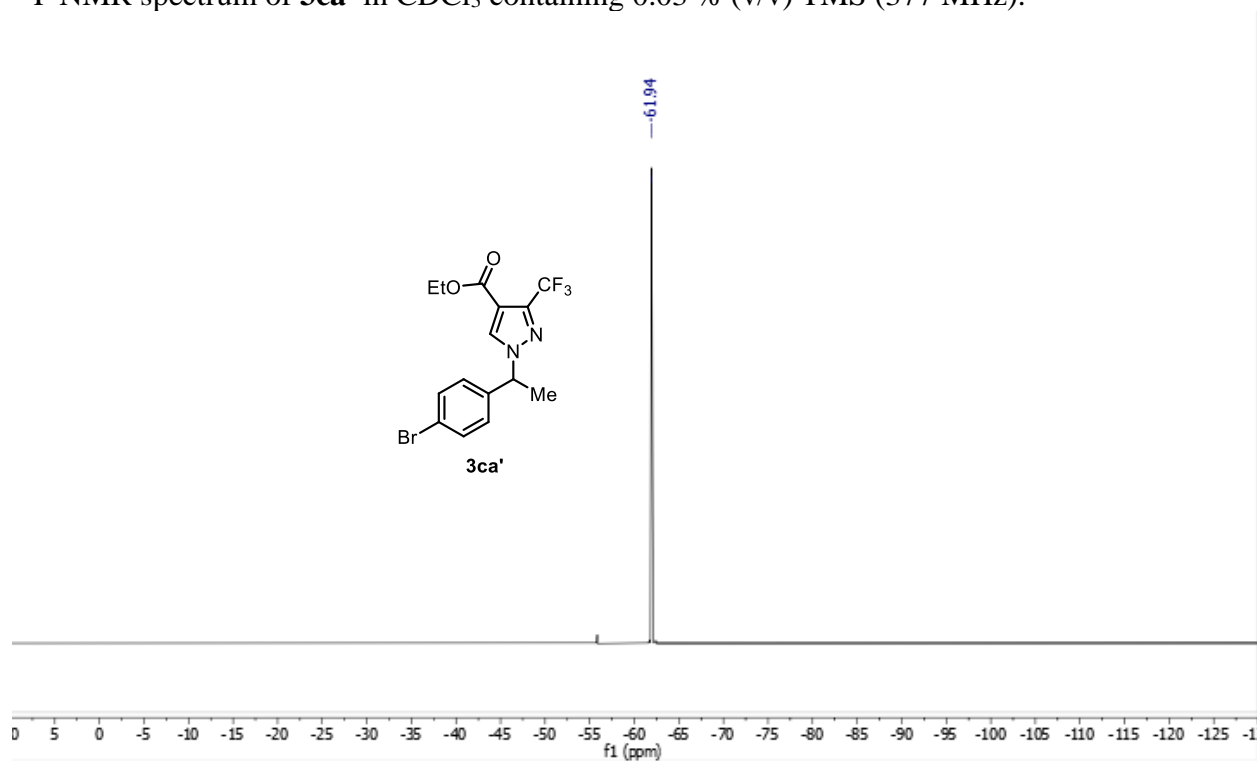
^1H NMR spectrum of **3ca'** in CDCl_3 containing 0.03 % (v/v) TMS (500 MHz).



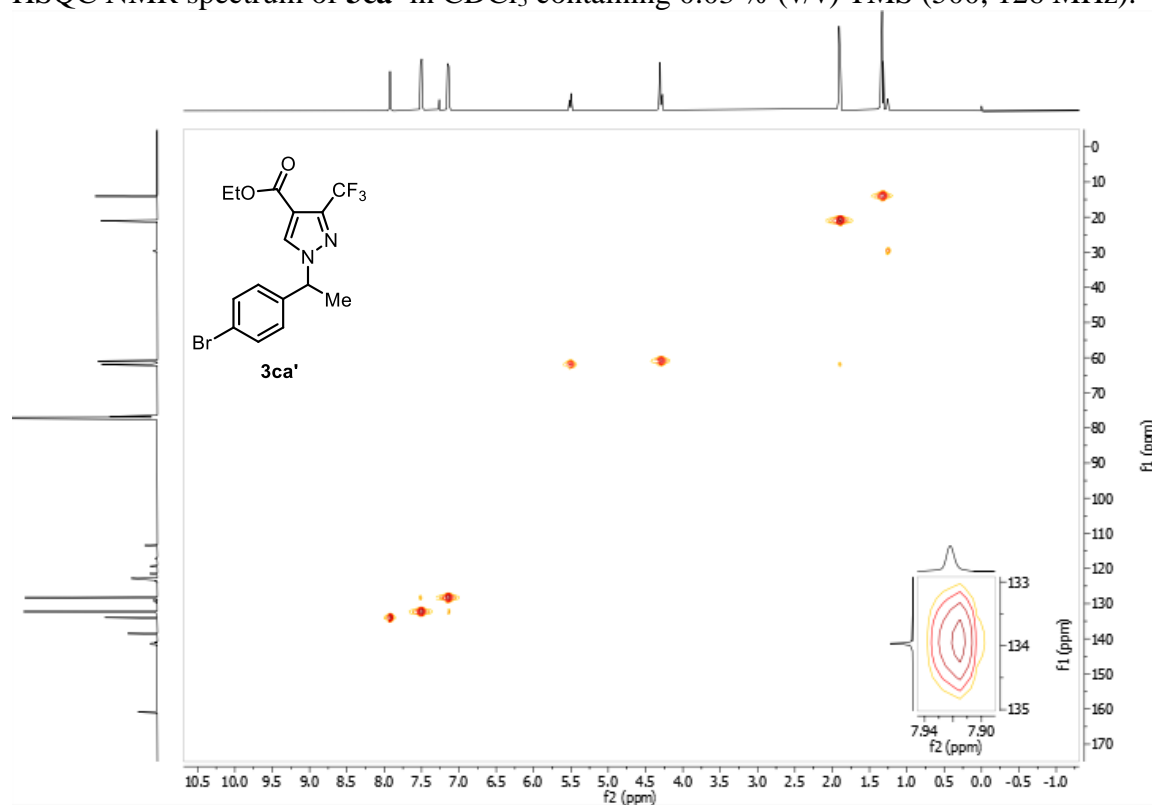
^{13}C NMR spectrum of **3ca'** in CDCl_3 containing 0.03 % (v/v) TMS (126 MHz).



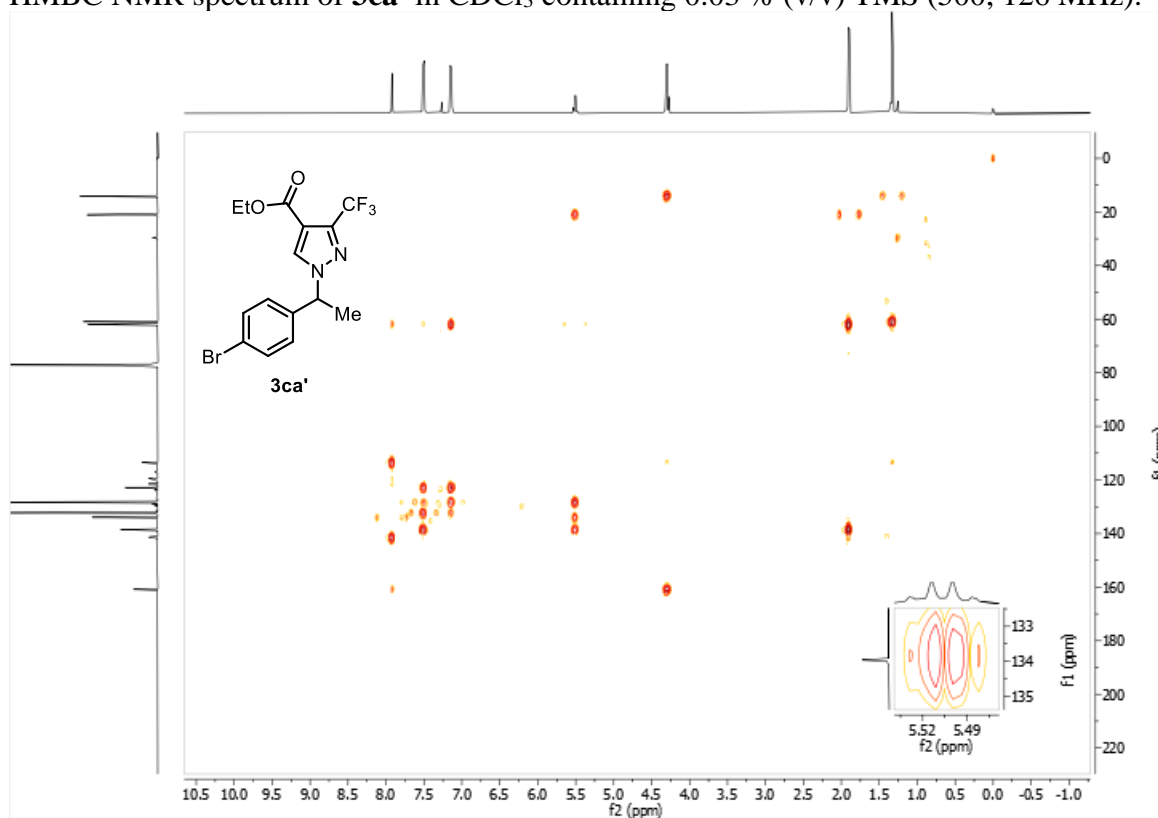
^{19}F NMR spectrum of **3ca'** in CDCl_3 containing 0.03 % (v/v) TMS (377 MHz).



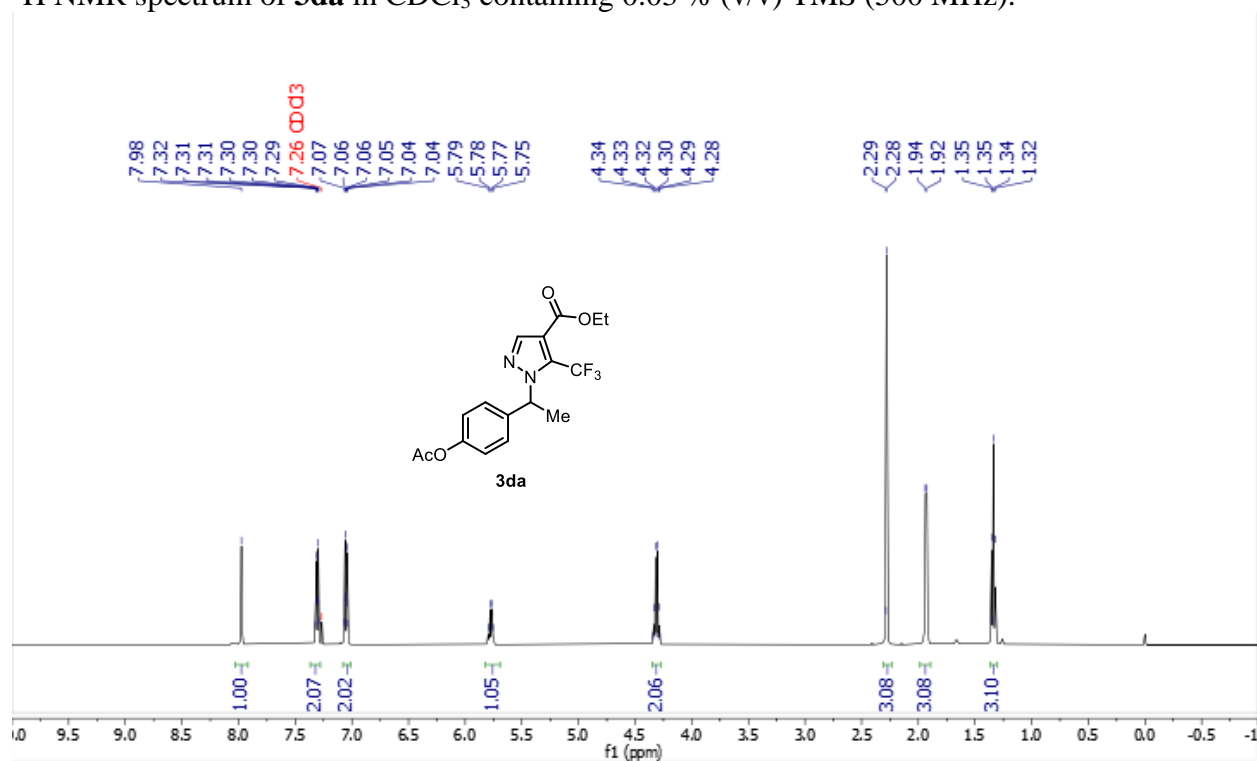
HSQC NMR spectrum of **3ca'** in CDCl_3 containing 0.03 % (v/v) TMS (500, 126 MHz).



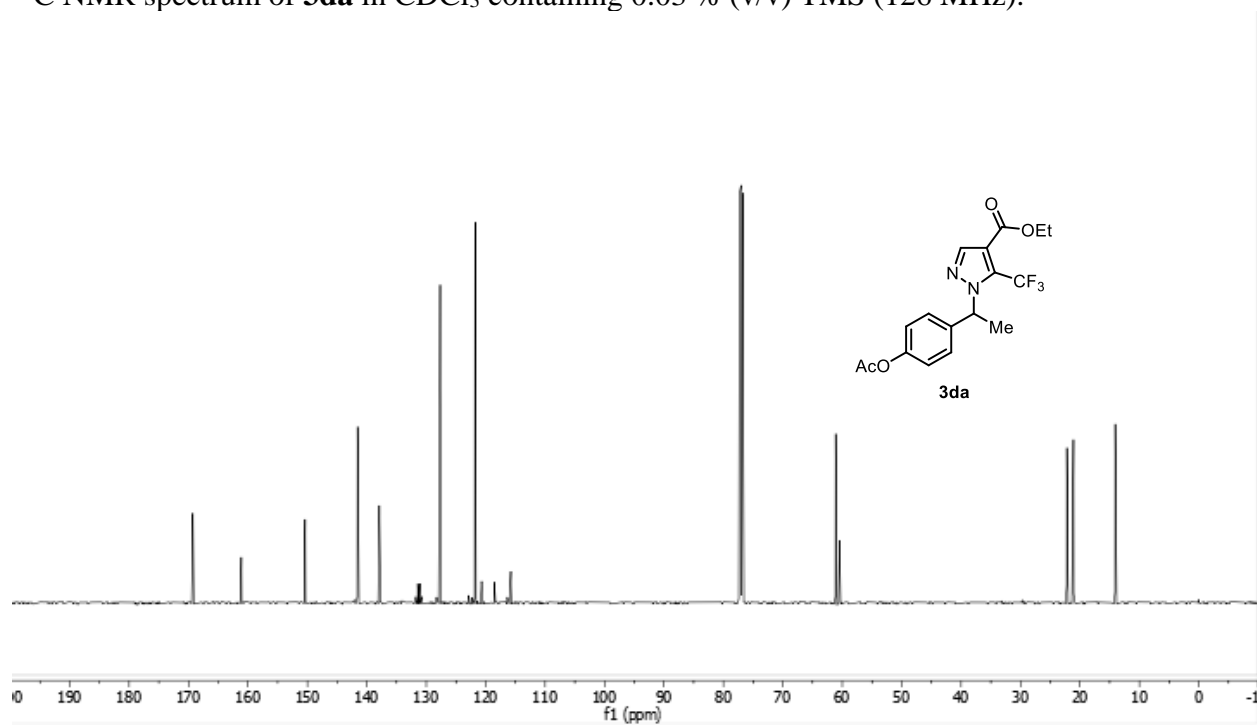
HMBC NMR spectrum of **3ca'** in CDCl₃ containing 0.03 % (v/v) TMS (500, 126 MHz).



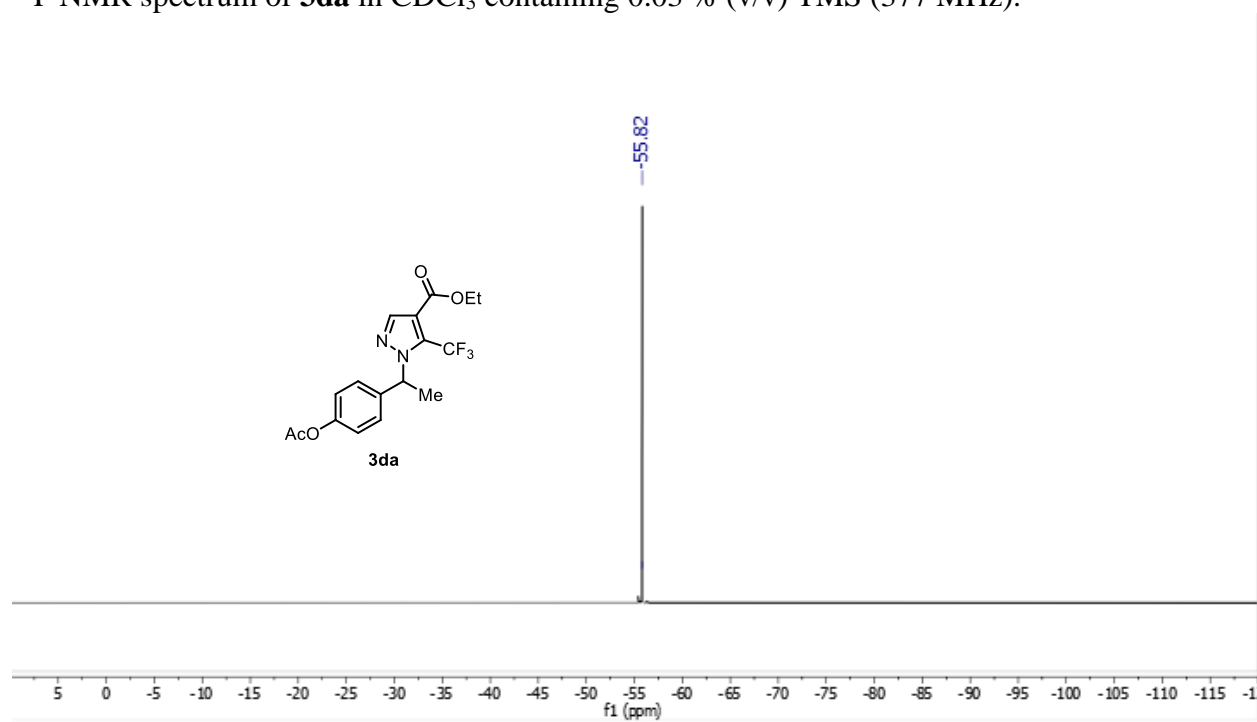
¹H NMR spectrum of **3da** in CDCl₃ containing 0.03 % (v/v) TMS (500 MHz).



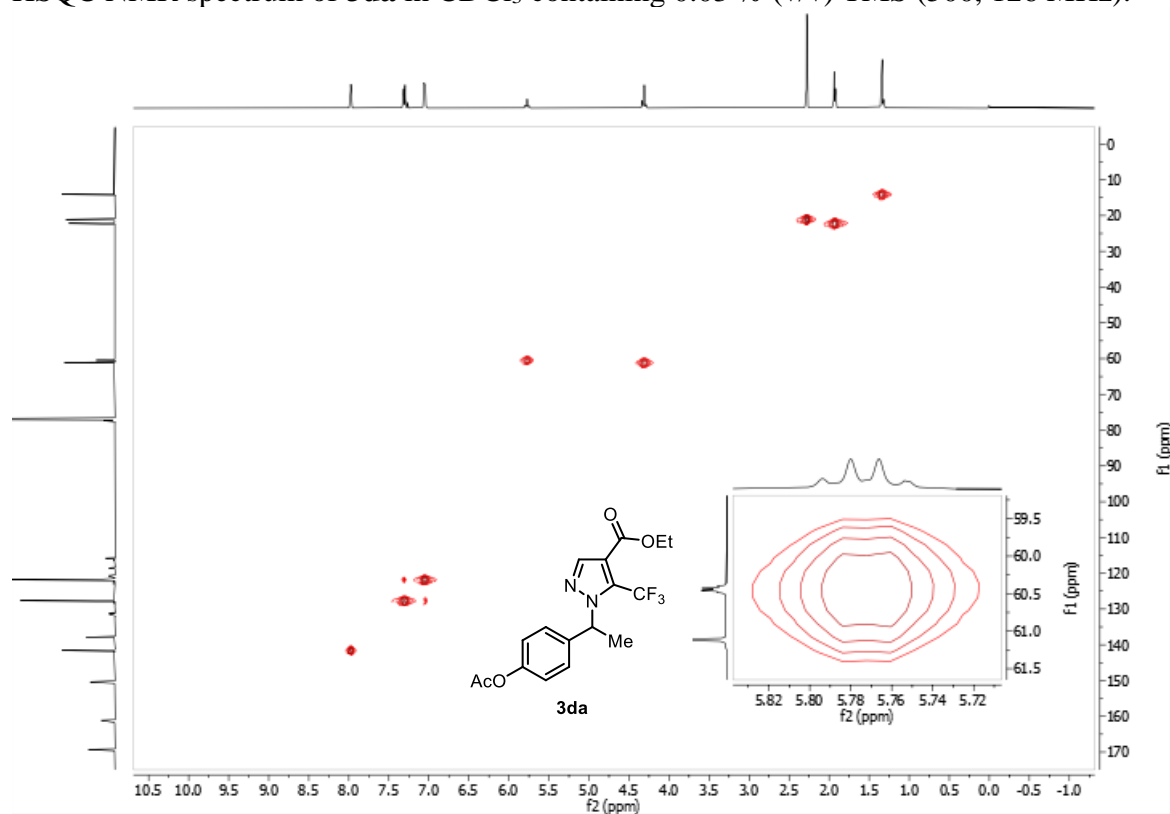
^{13}C NMR spectrum of **3da** in CDCl_3 containing 0.03 % (v/v) TMS (126 MHz).



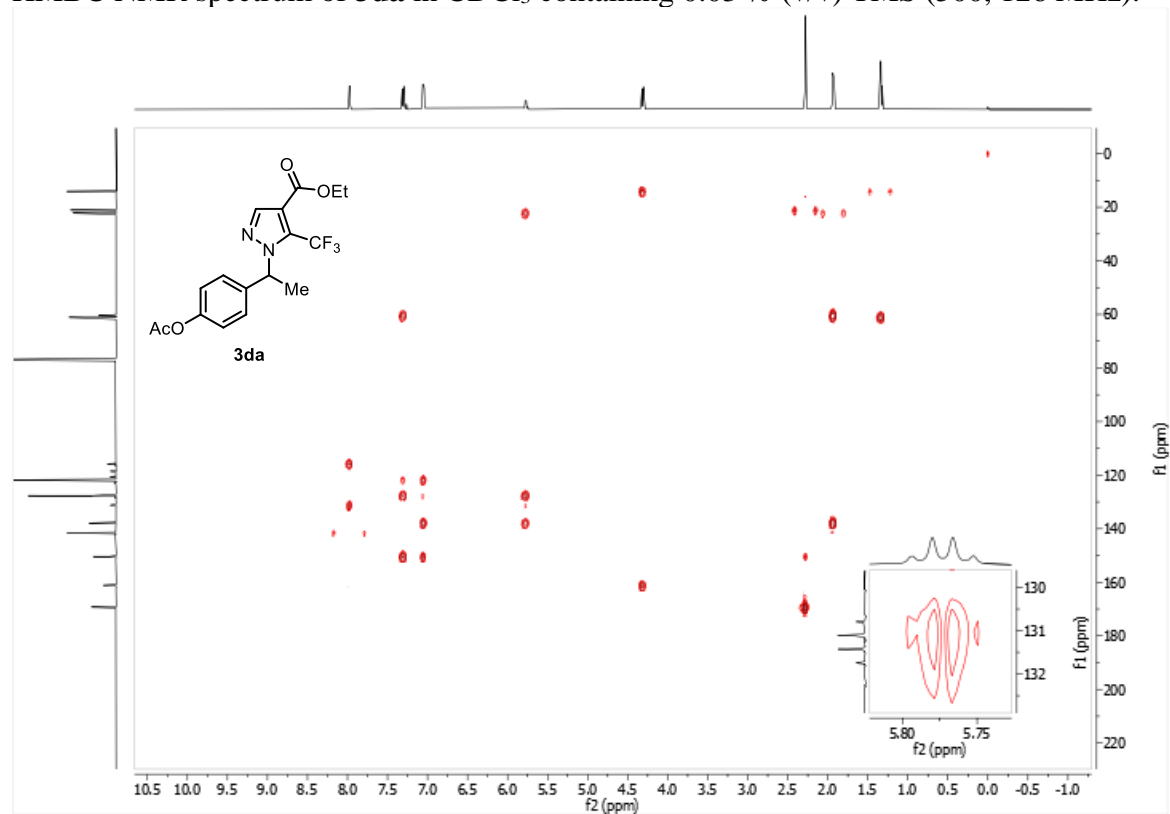
^{19}F NMR spectrum of **3da** in CDCl_3 containing 0.03 % (v/v) TMS (377 MHz).



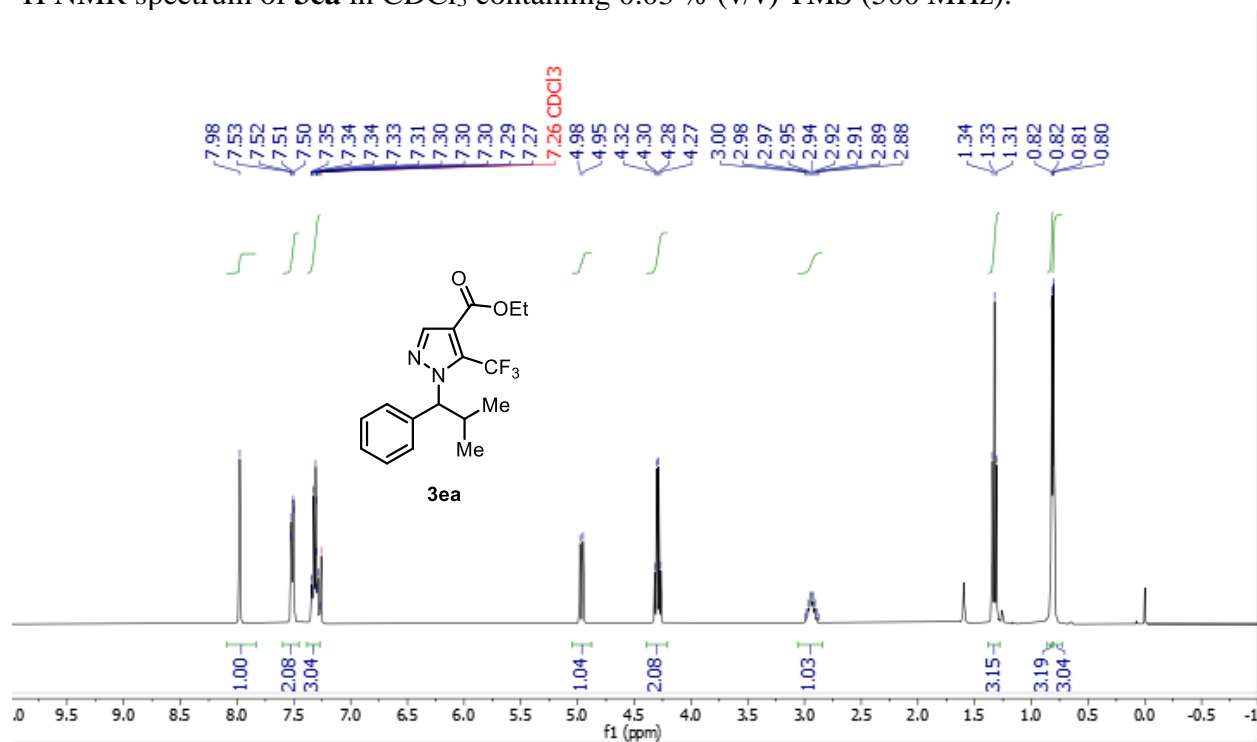
HSQC NMR spectrum of **3da** in CDCl₃ containing 0.03 % (v/v) TMS (500, 126 MHz).



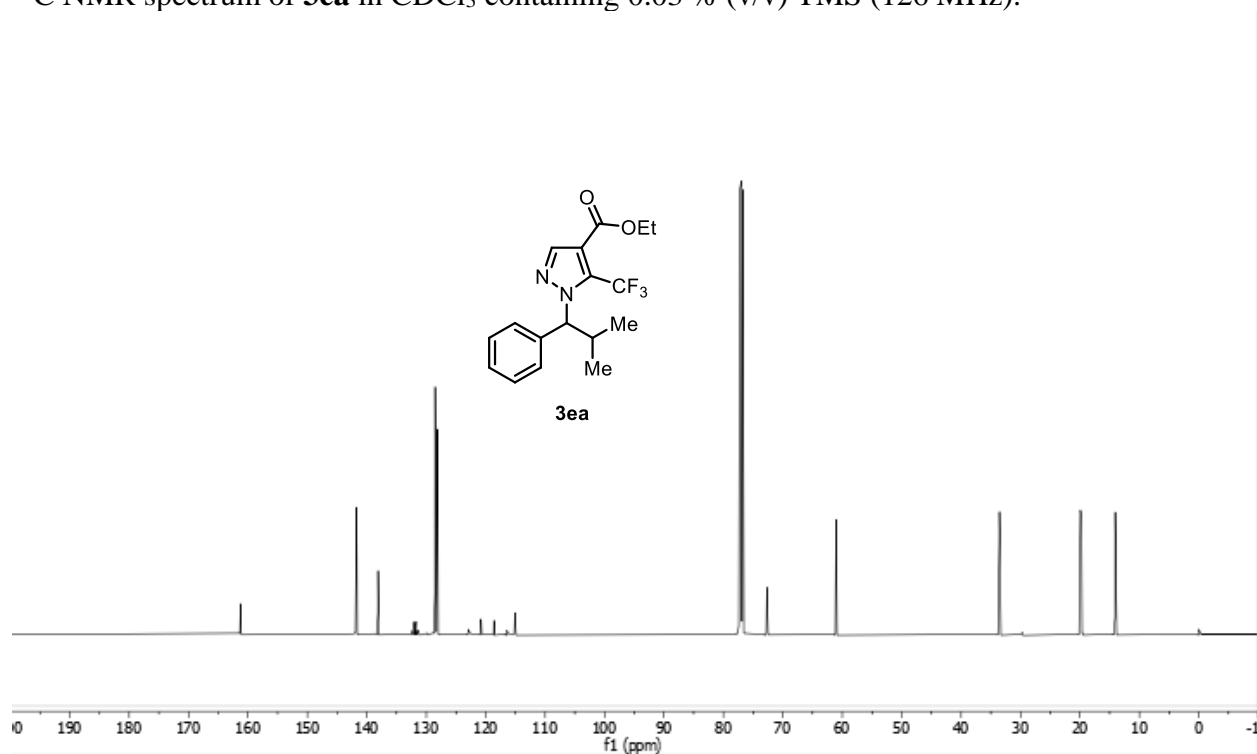
HMBC NMR spectrum of **3da** in CDCl₃ containing 0.03 % (v/v) TMS (500, 126 MHz).



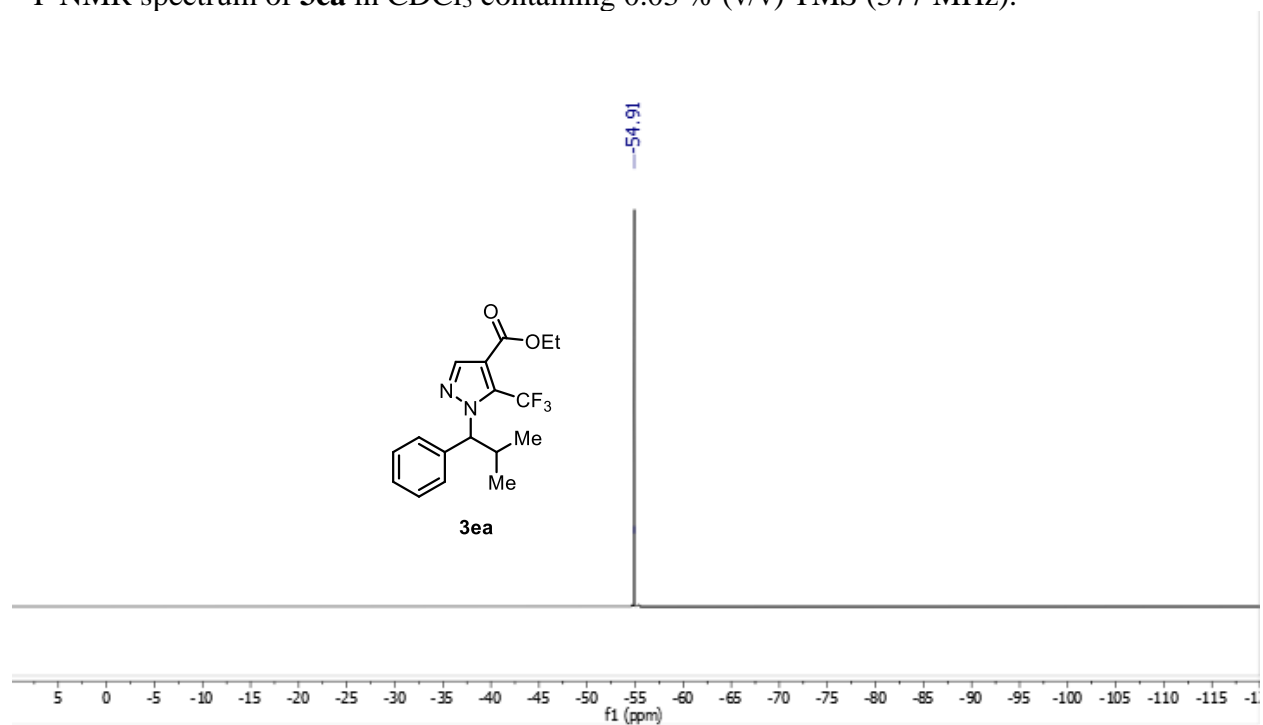
^1H NMR spectrum of **3ea** in CDCl_3 containing 0.03 % (v/v) TMS (500 MHz).



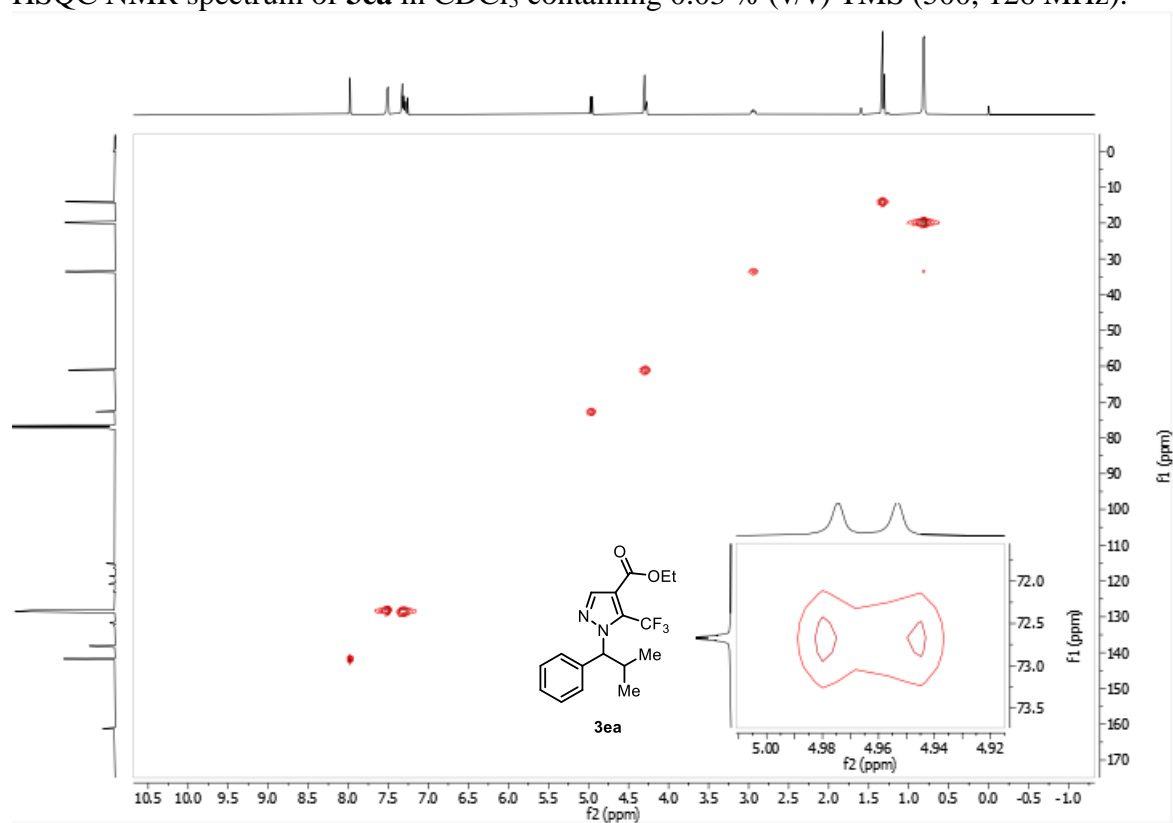
^{13}C NMR spectrum of **3ea** in CDCl_3 containing 0.03 % (v/v) TMS (126 MHz).



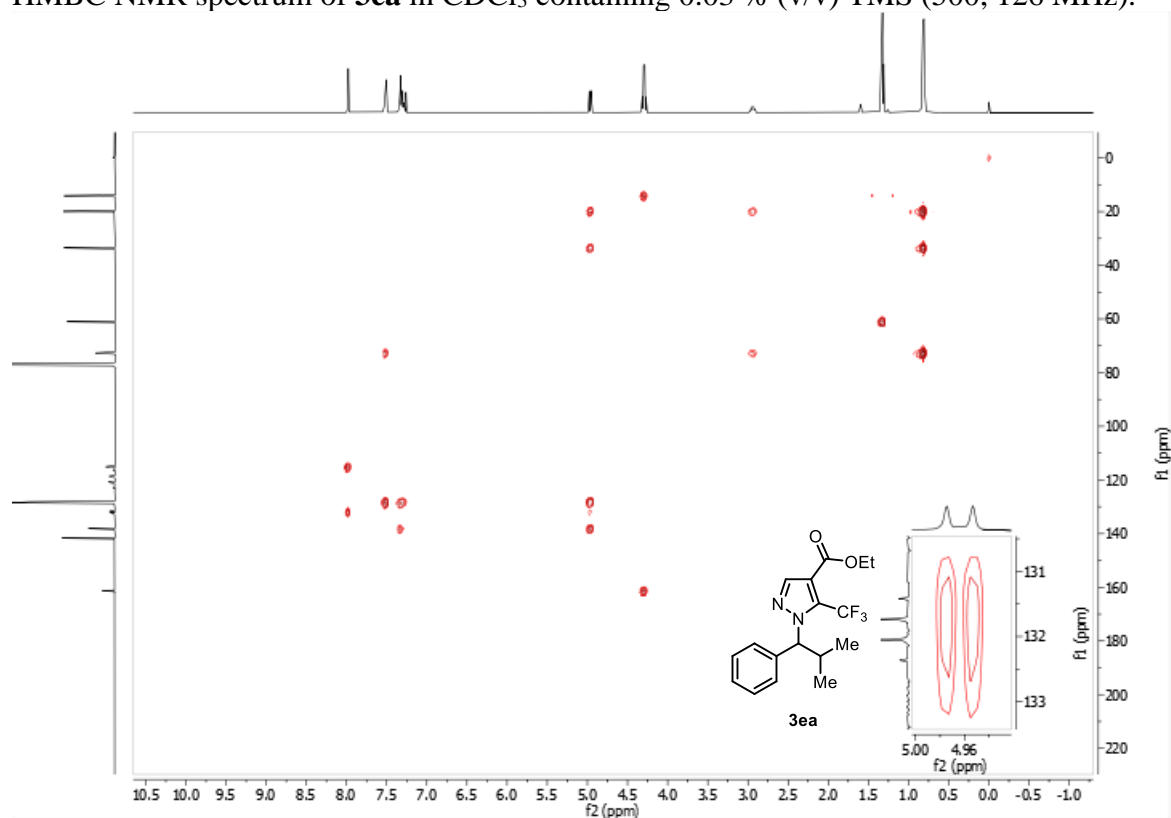
^{19}F NMR spectrum of **3ea** in CDCl_3 containing 0.03 % (v/v) TMS (377 MHz).



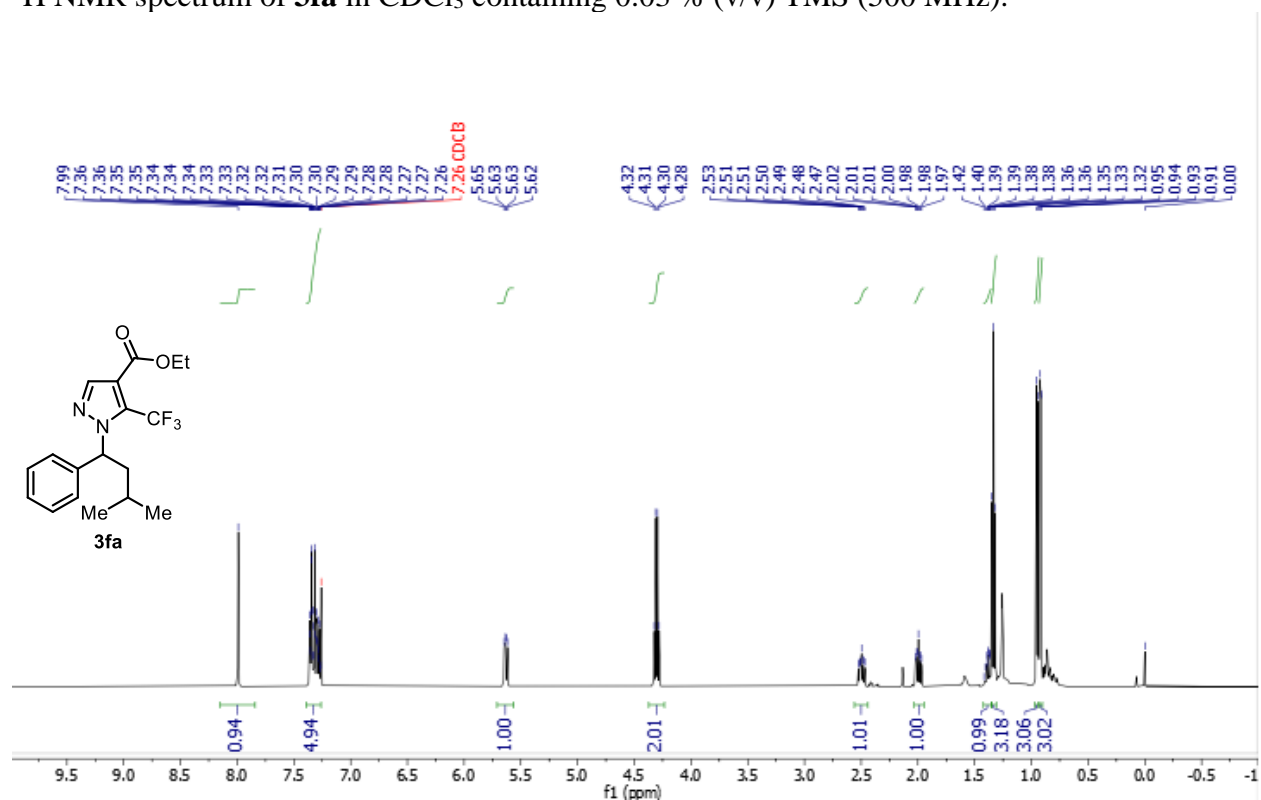
HSQC NMR spectrum of **3ea** in CDCl_3 containing 0.03 % (v/v) TMS (500, 126 MHz).



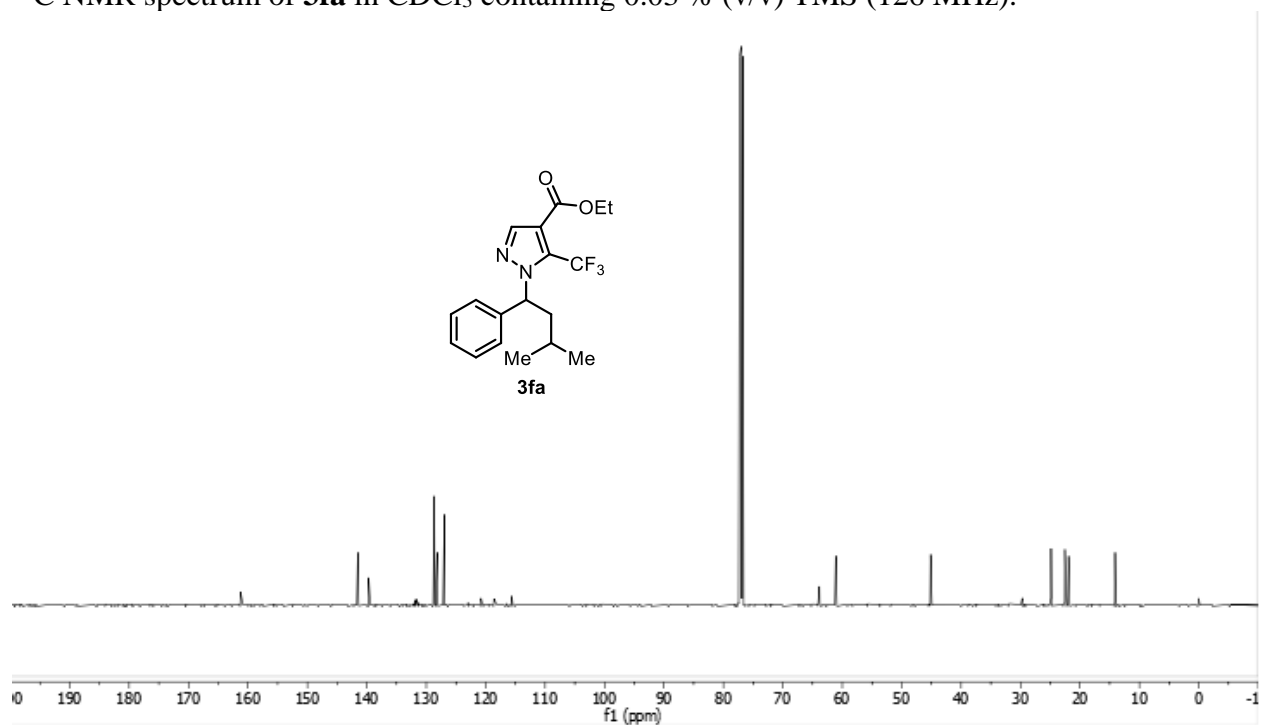
HMBC NMR spectrum of **3ea** in CDCl₃ containing 0.03 % (v/v) TMS (500, 126 MHz).



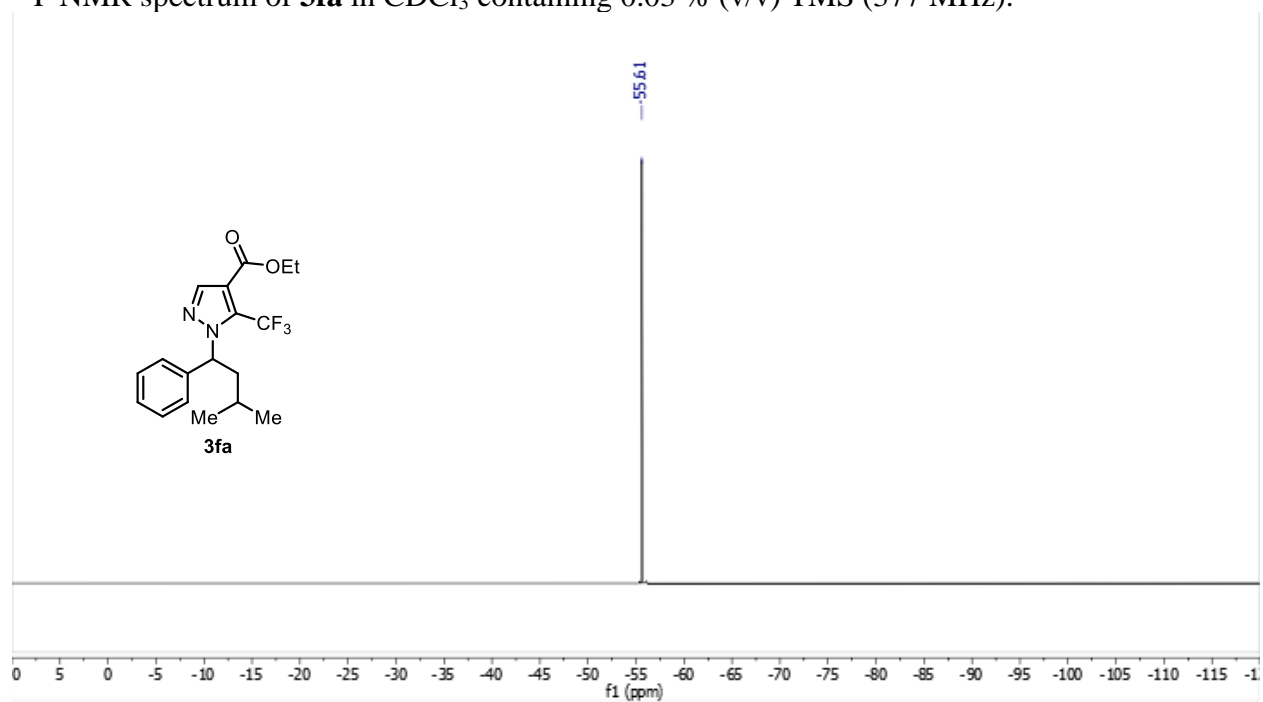
¹H NMR spectrum of **3fa** in CDCl₃ containing 0.03 % (v/v) TMS (500 MHz).



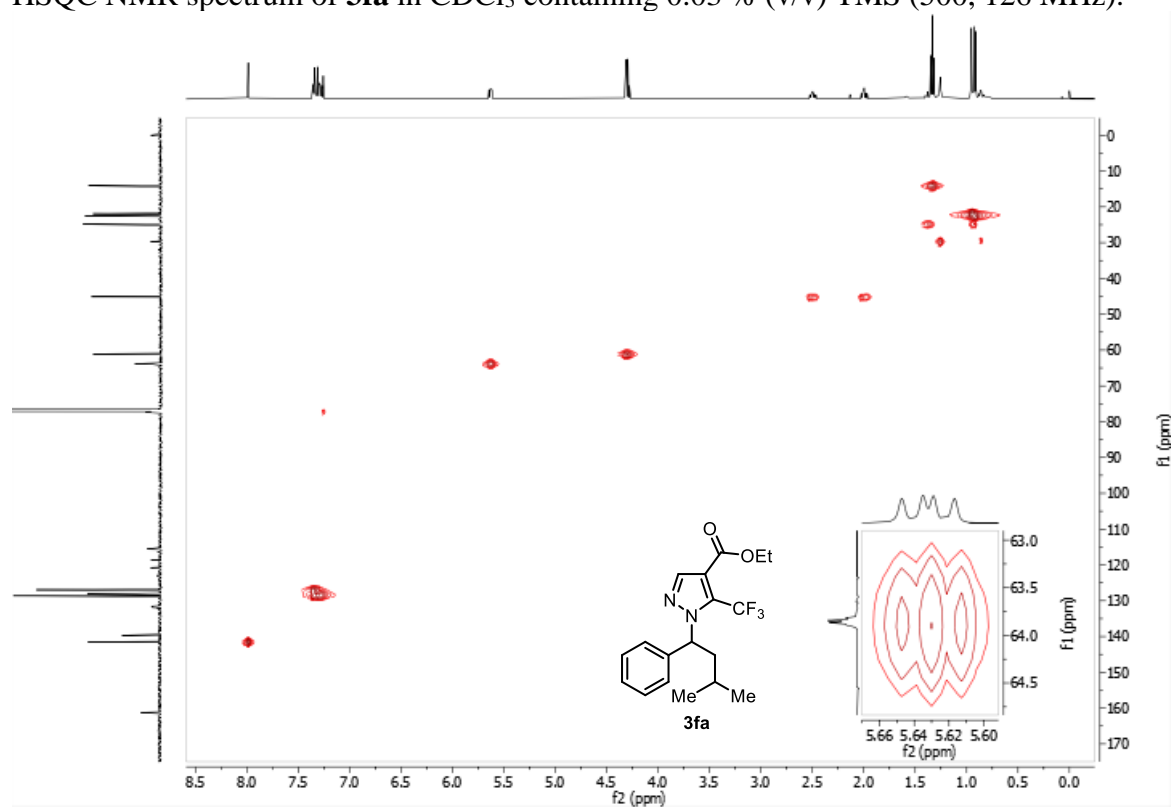
^{13}C NMR spectrum of **3fa** in CDCl_3 containing 0.03 % (v/v) TMS (126 MHz).



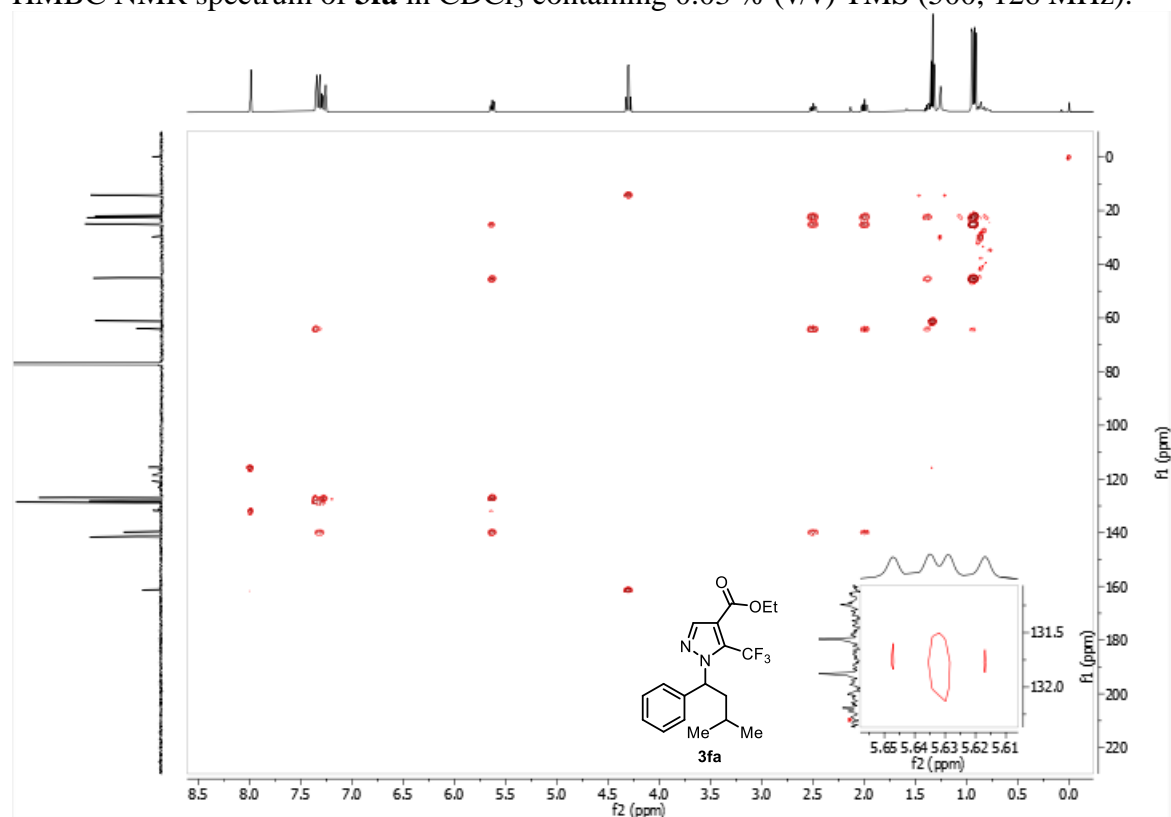
^{19}F NMR spectrum of **3fa** in CDCl_3 containing 0.03 % (v/v) TMS (377 MHz).



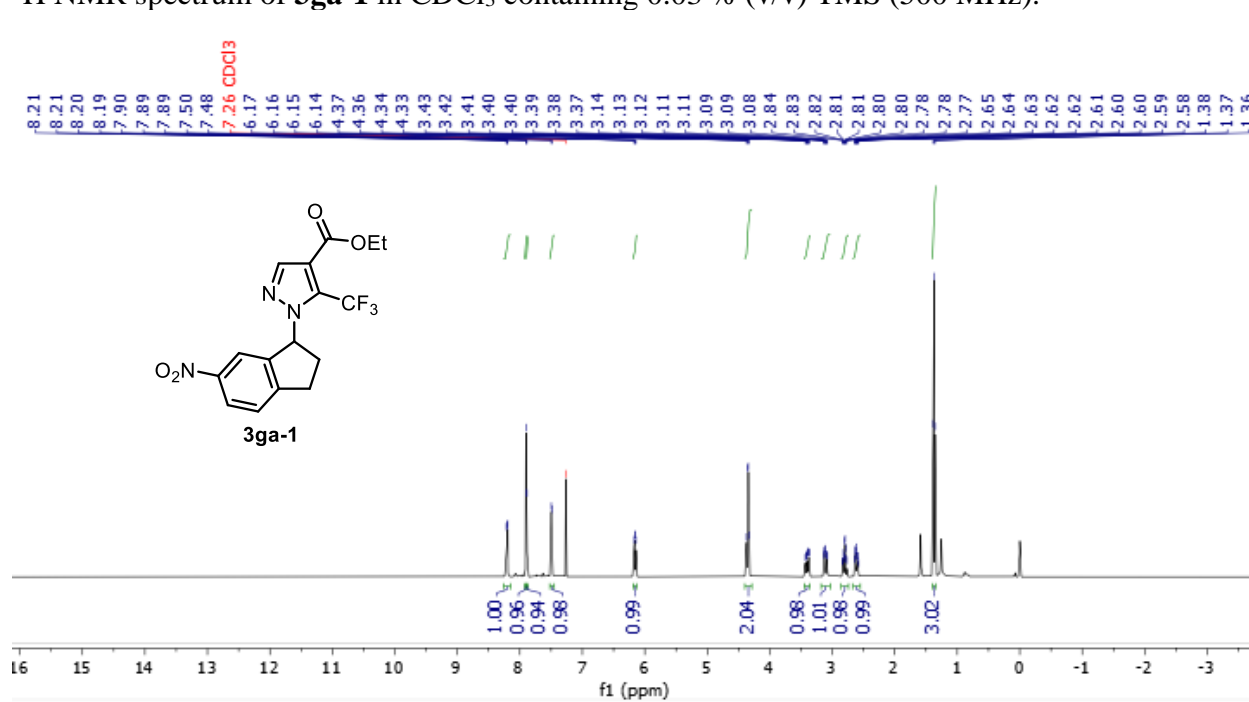
HSQC NMR spectrum of **3fa** in CDCl₃ containing 0.03 % (v/v) TMS (500, 126 MHz).



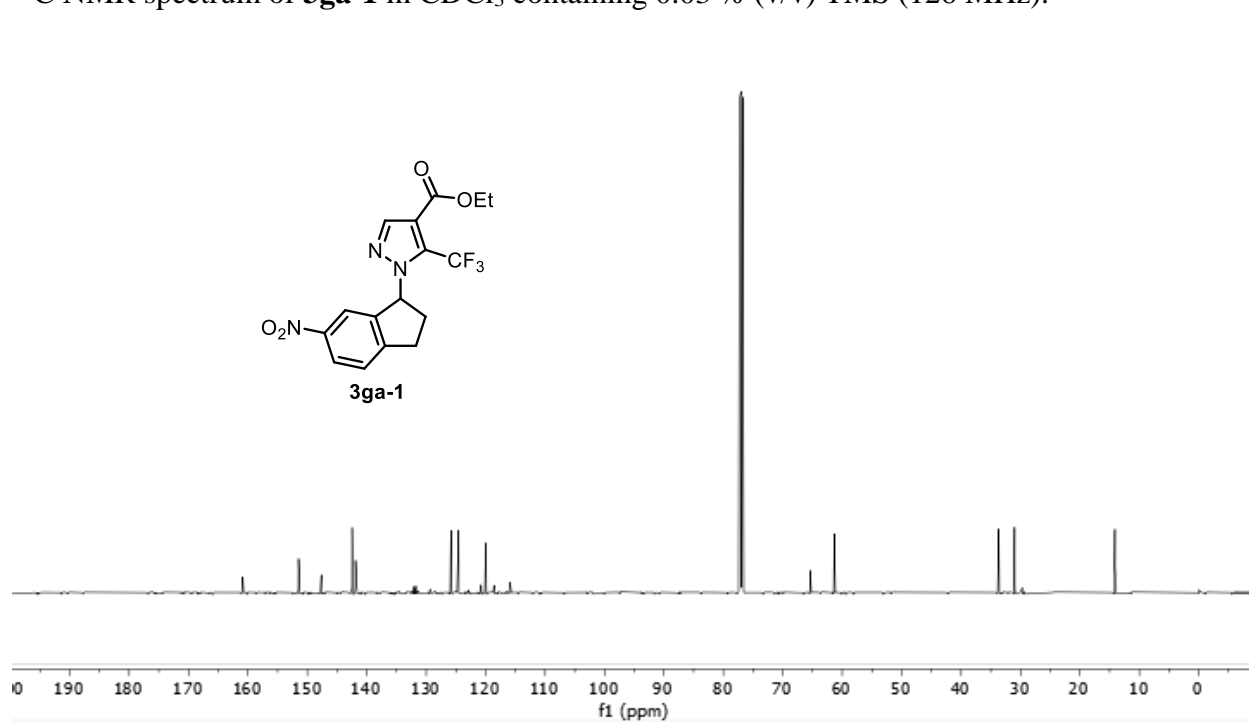
HMBC NMR spectrum of **3fa** in CDCl₃ containing 0.03 % (v/v) TMS (500, 126 MHz).



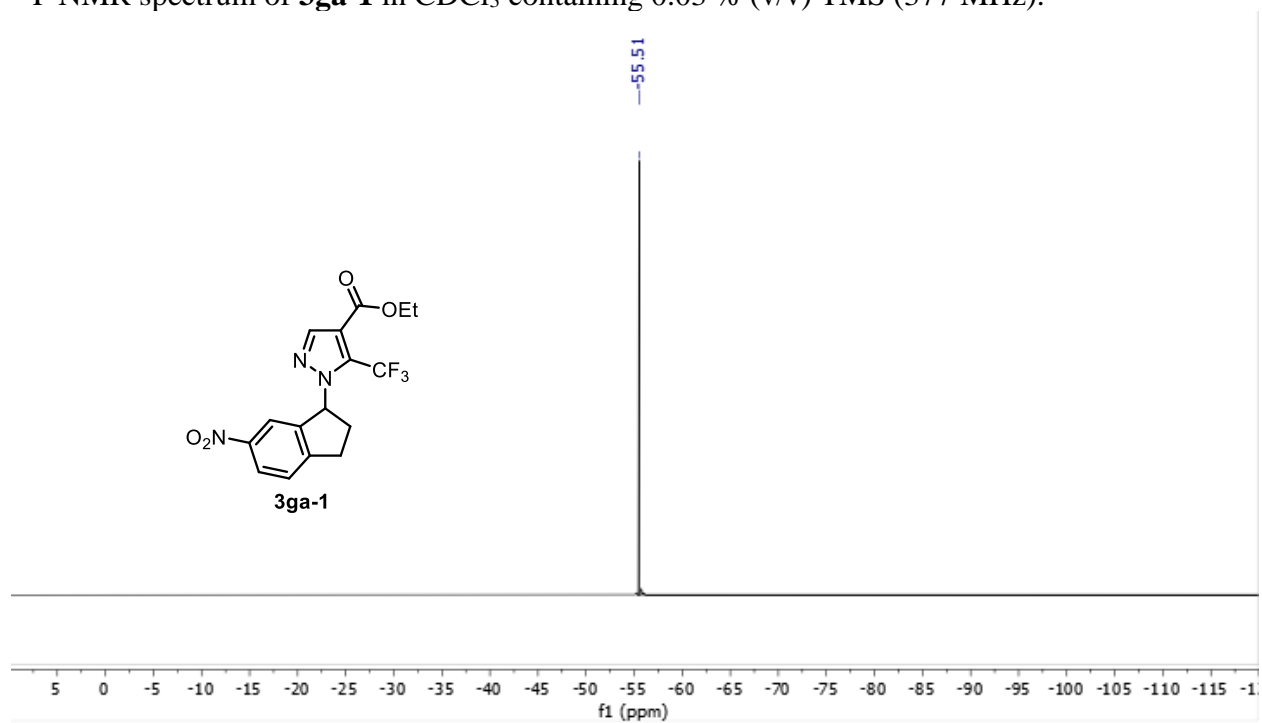
^1H NMR spectrum of **3ga-1** in CDCl_3 containing 0.03 % (v/v) TMS (500 MHz).



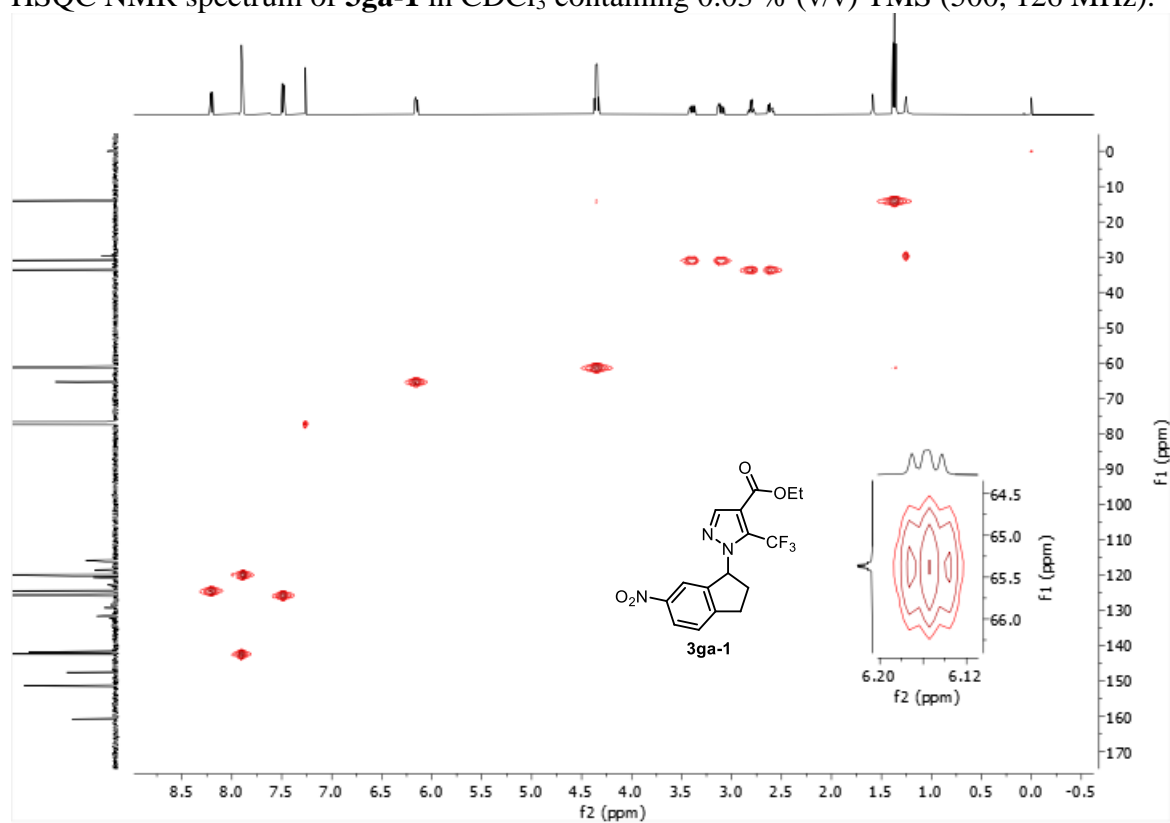
^{13}C NMR spectrum of **3ga-1** in CDCl_3 containing 0.03 % (v/v) TMS (126 MHz).



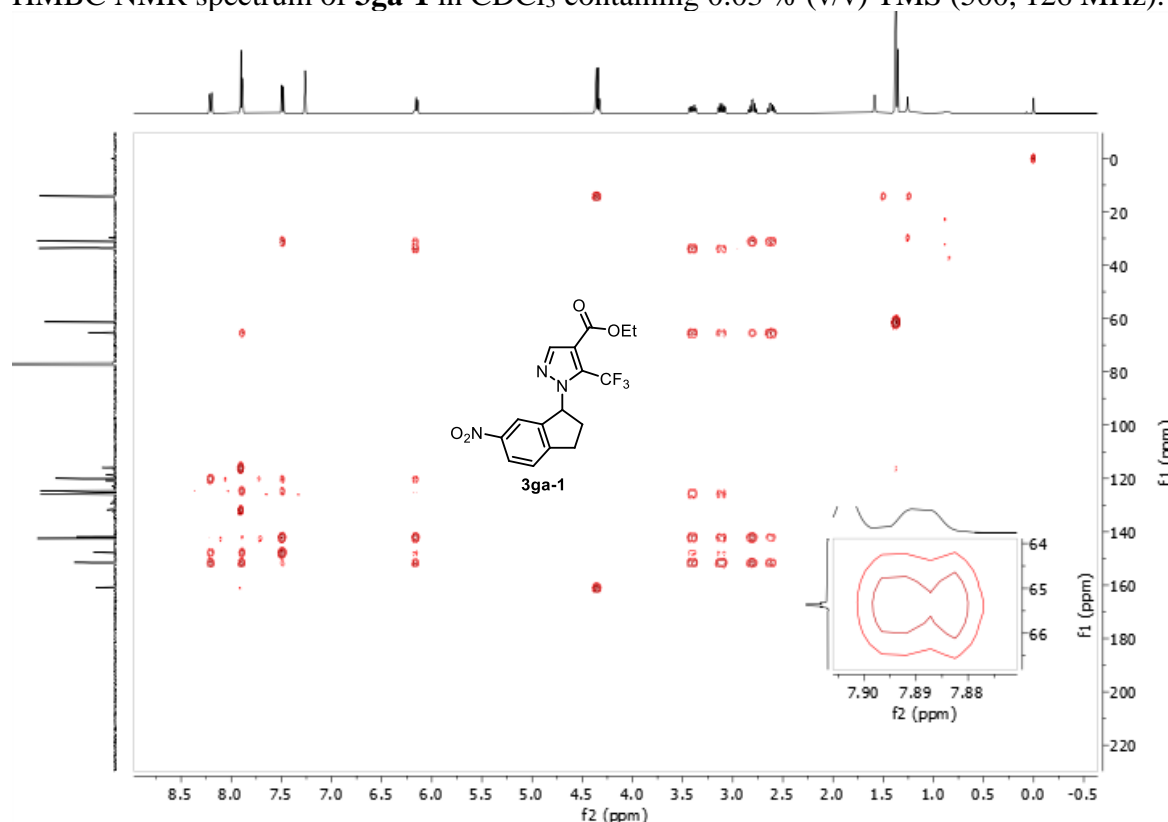
^{19}F NMR spectrum of **3ga-1** in CDCl_3 containing 0.03 % (v/v) TMS (377 MHz).



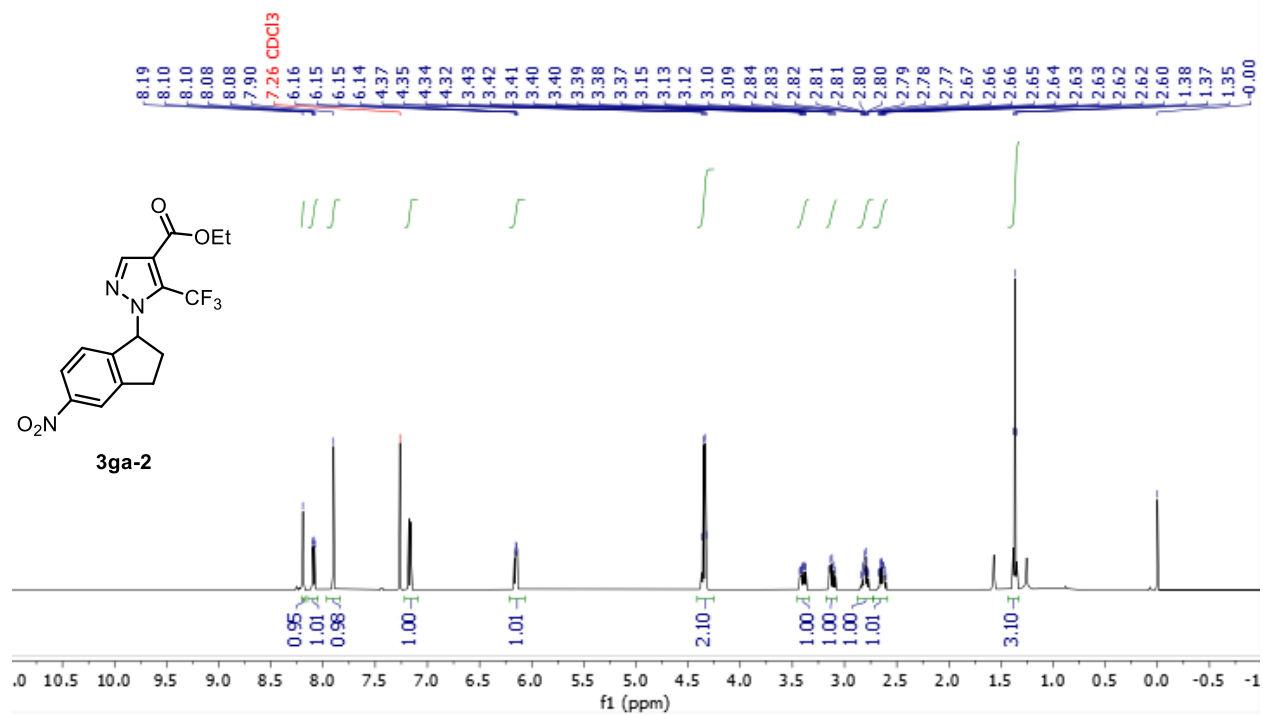
HSQC NMR spectrum of **3ga-1** in CDCl_3 containing 0.03 % (v/v) TMS (500, 126 MHz).



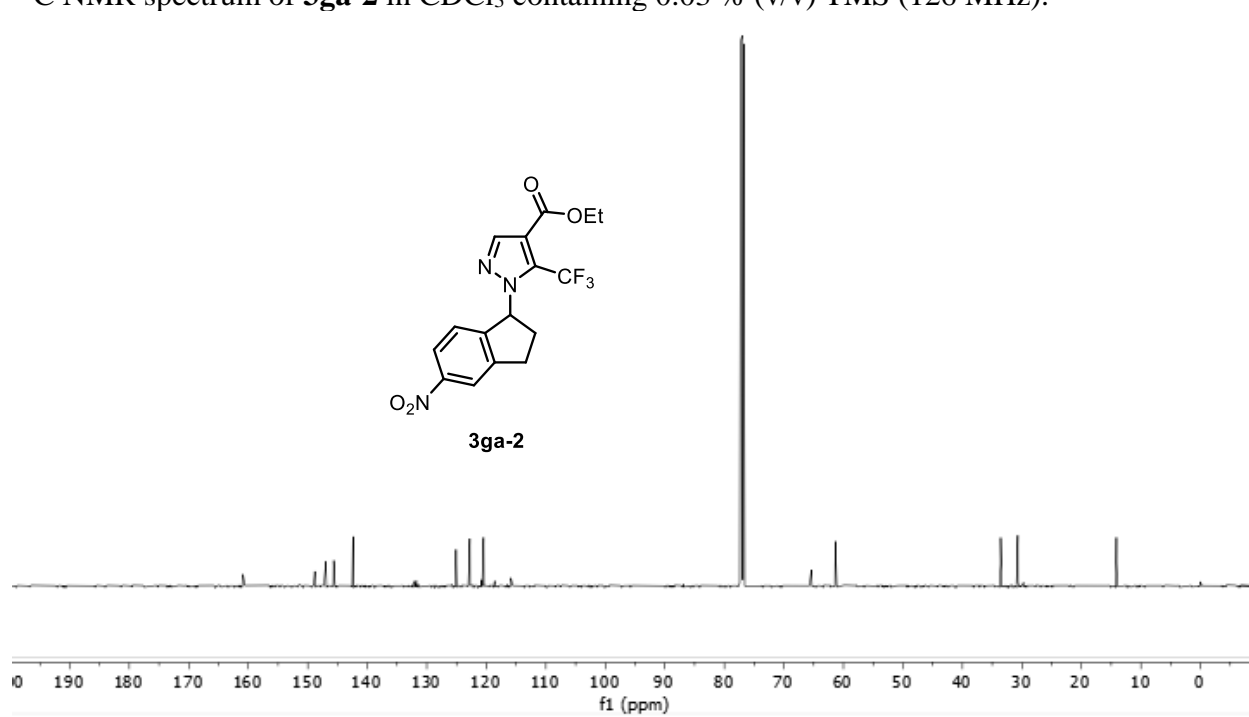
HMBC NMR spectrum of **3ga-1** in CDCl₃ containing 0.03 % (v/v) TMS (500, 126 MHz).



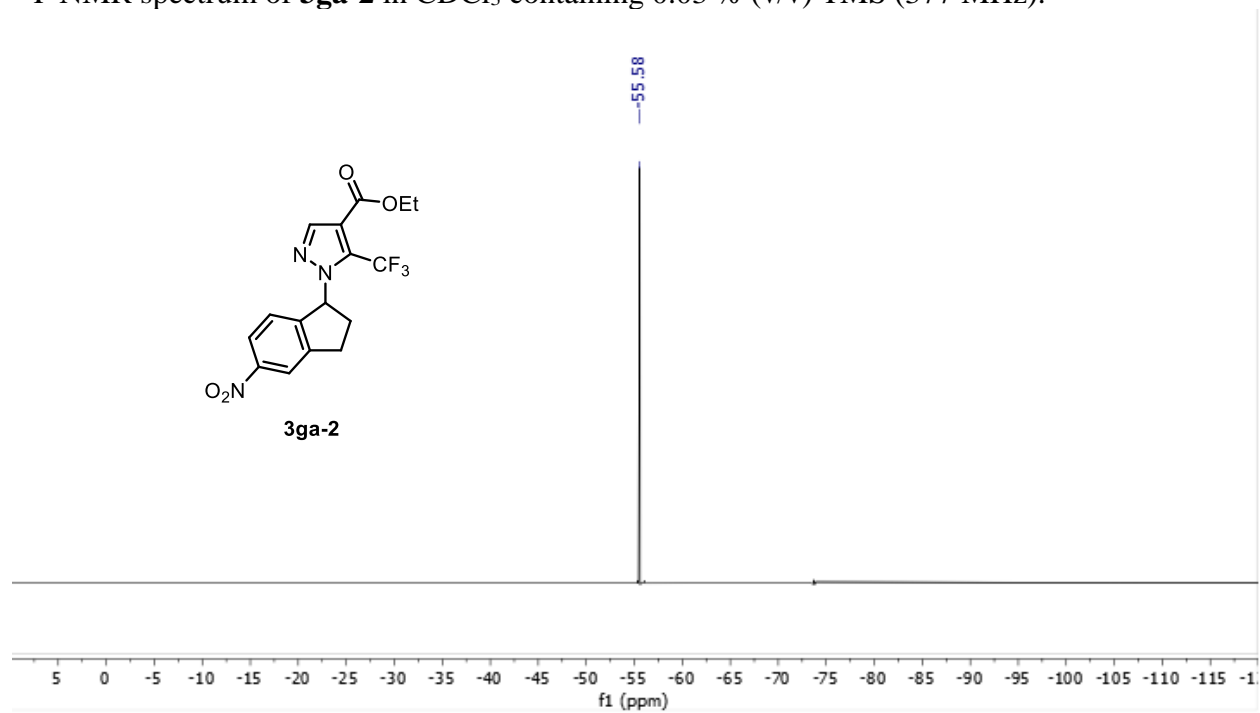
¹H NMR spectrum of **3ga-2** in CDCl₃ containing 0.03 % (v/v) TMS (500 MHz).



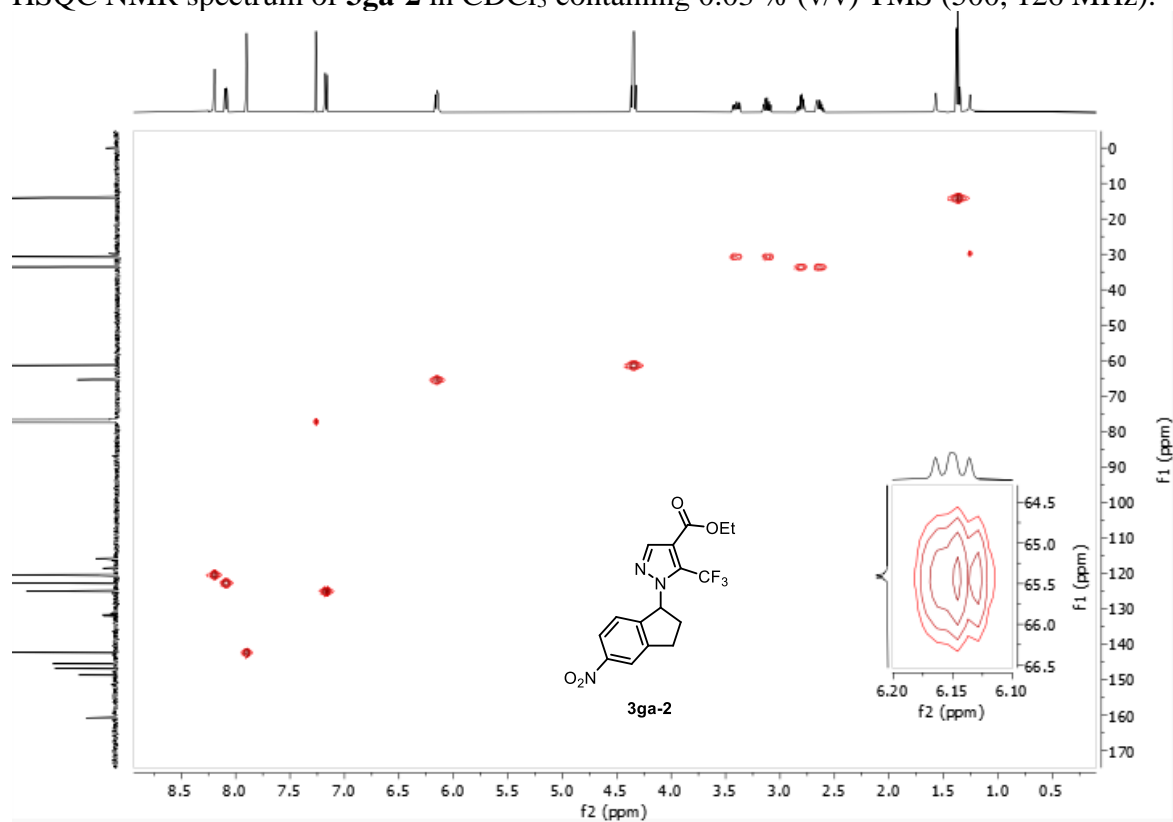
^{13}C NMR spectrum of **3ga-2** in CDCl_3 containing 0.03 % (v/v) TMS (126 MHz).



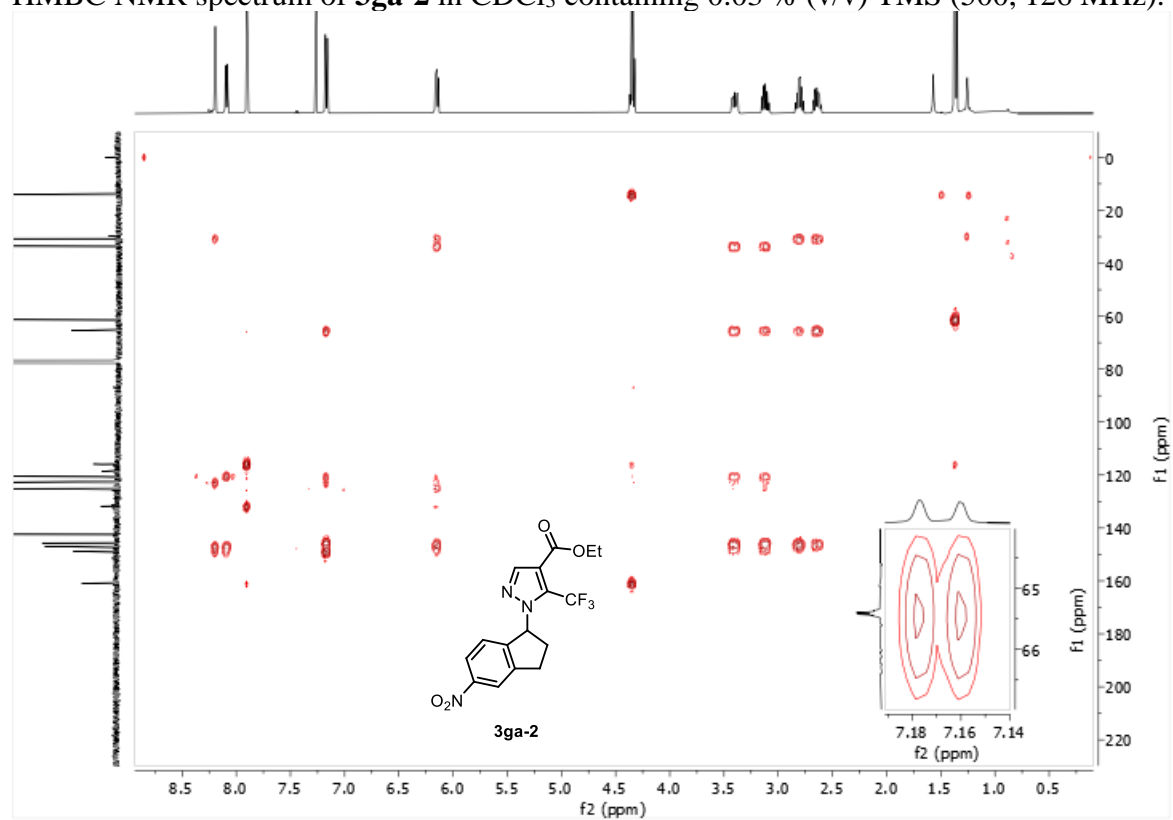
^{19}F NMR spectrum of **3ga-2** in CDCl_3 containing 0.03 % (v/v) TMS (377 MHz).



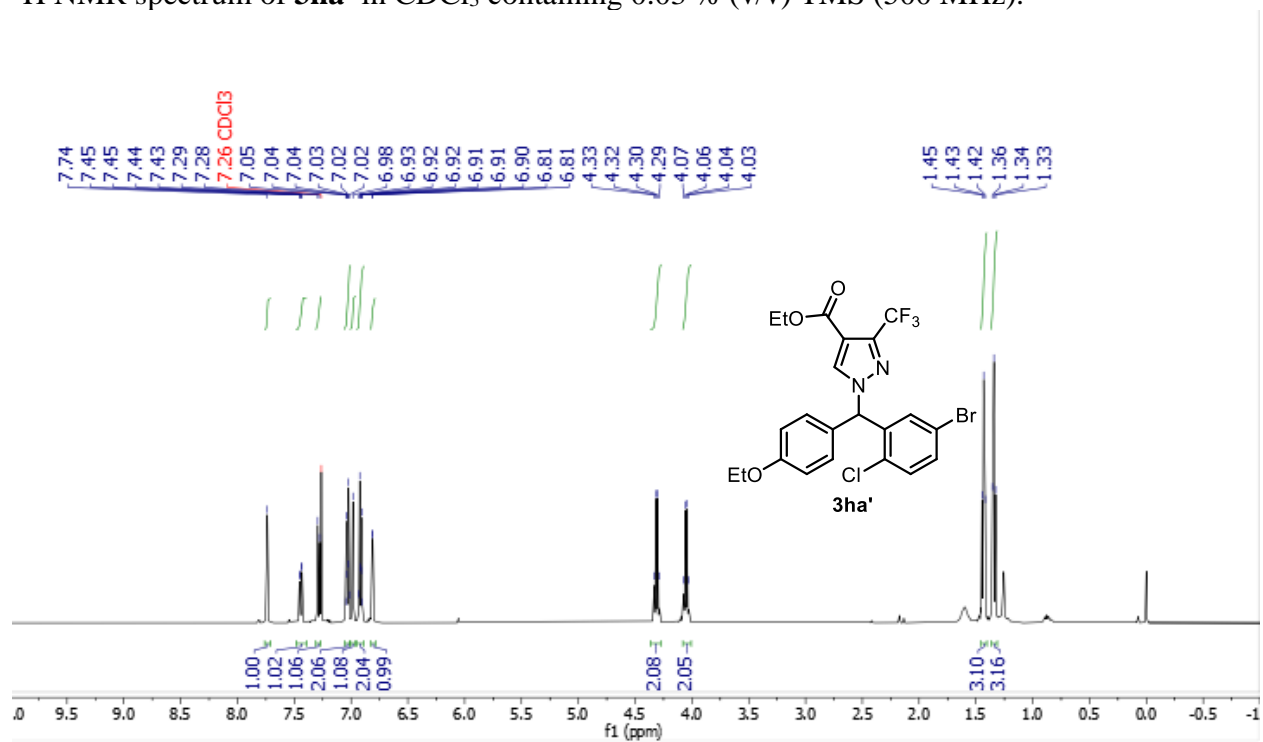
HSQC NMR spectrum of **3ga-2** in CDCl₃ containing 0.03 % (v/v) TMS (500, 126 MHz).



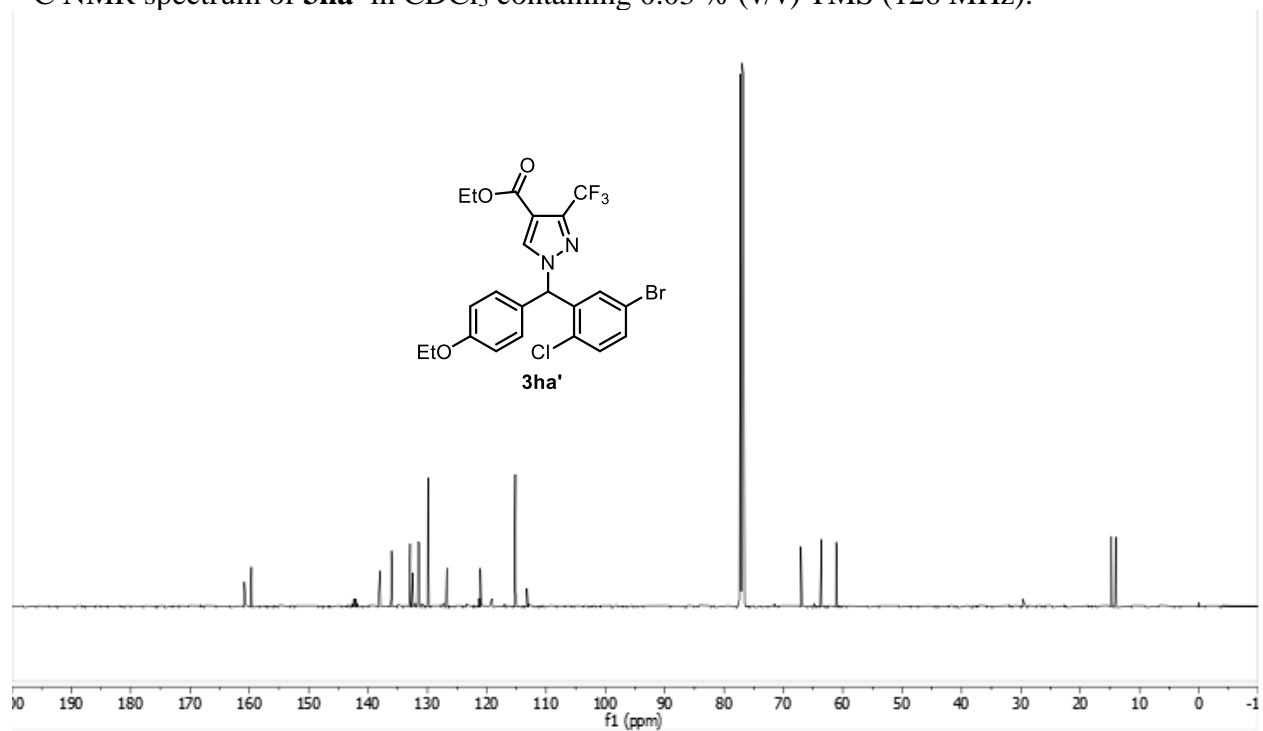
HMBC NMR spectrum of **3ga-2** in CDCl₃ containing 0.03 % (v/v) TMS (500, 126 MHz).



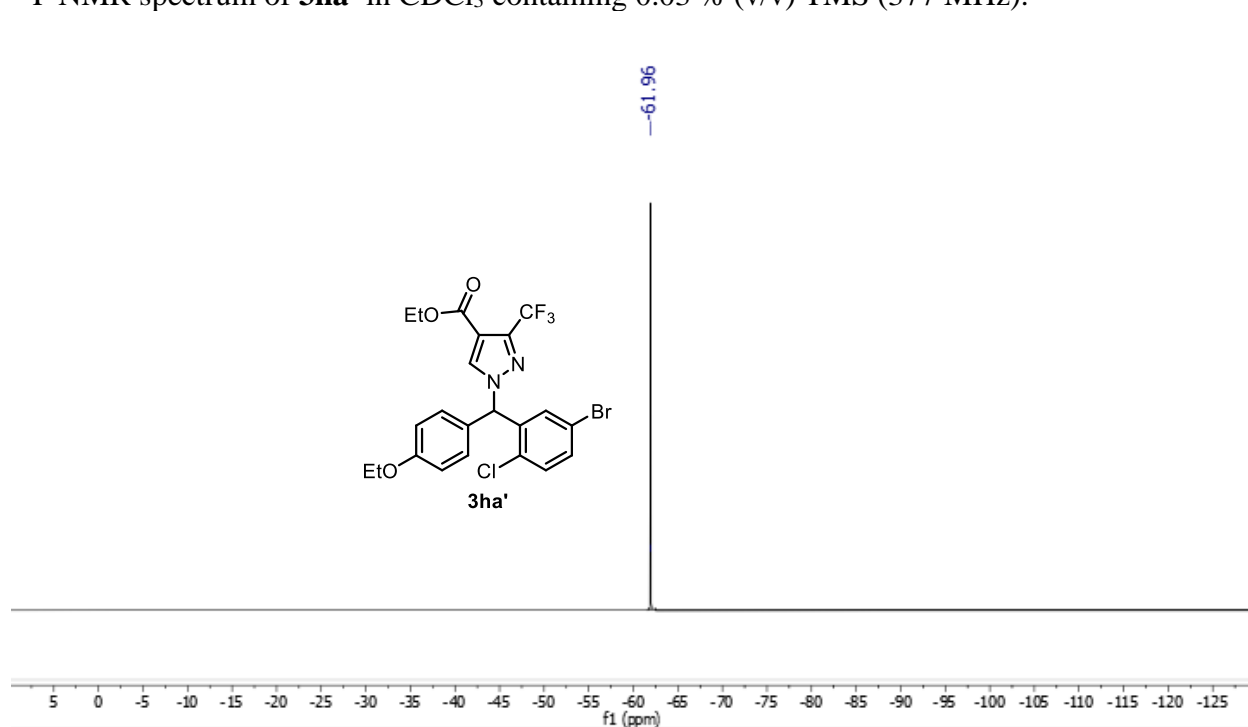
^1H NMR spectrum of **3ha'** in CDCl_3 containing 0.03 % (v/v) TMS (500 MHz).



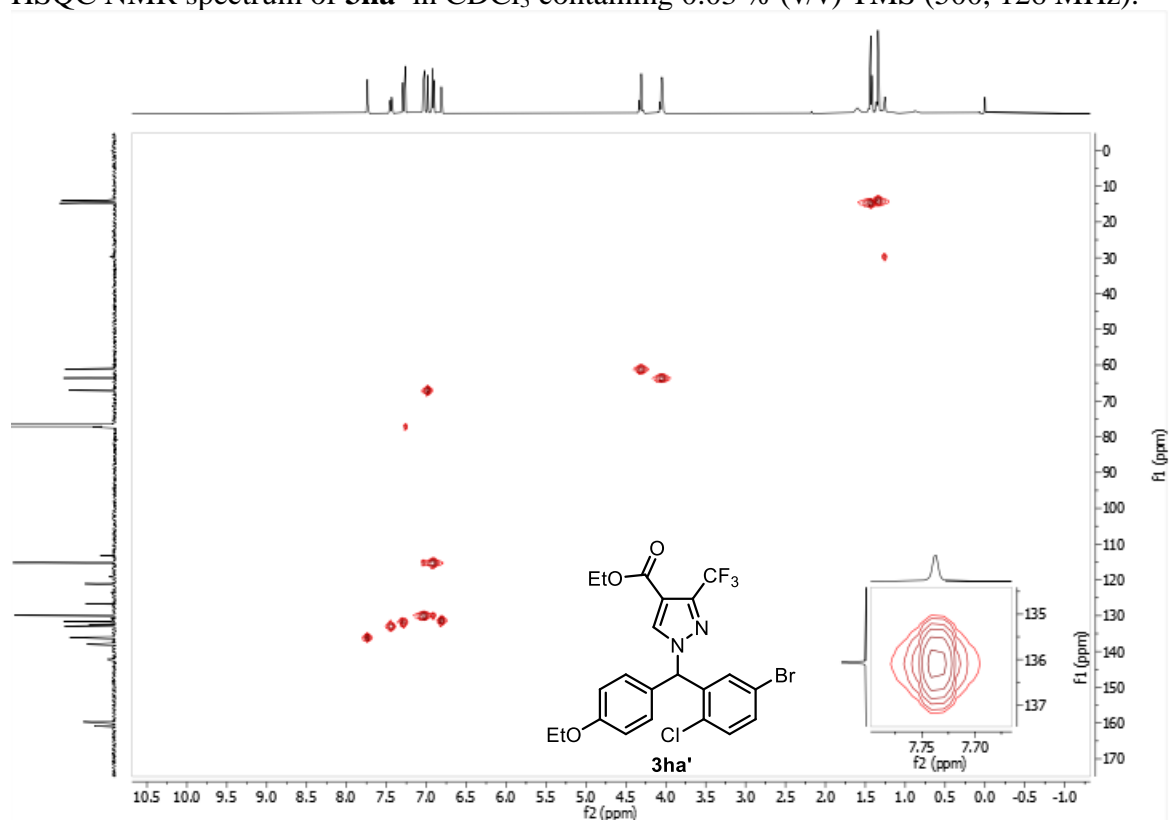
^{13}C NMR spectrum of **3ha'** in CDCl_3 containing 0.03 % (v/v) TMS (126 MHz).



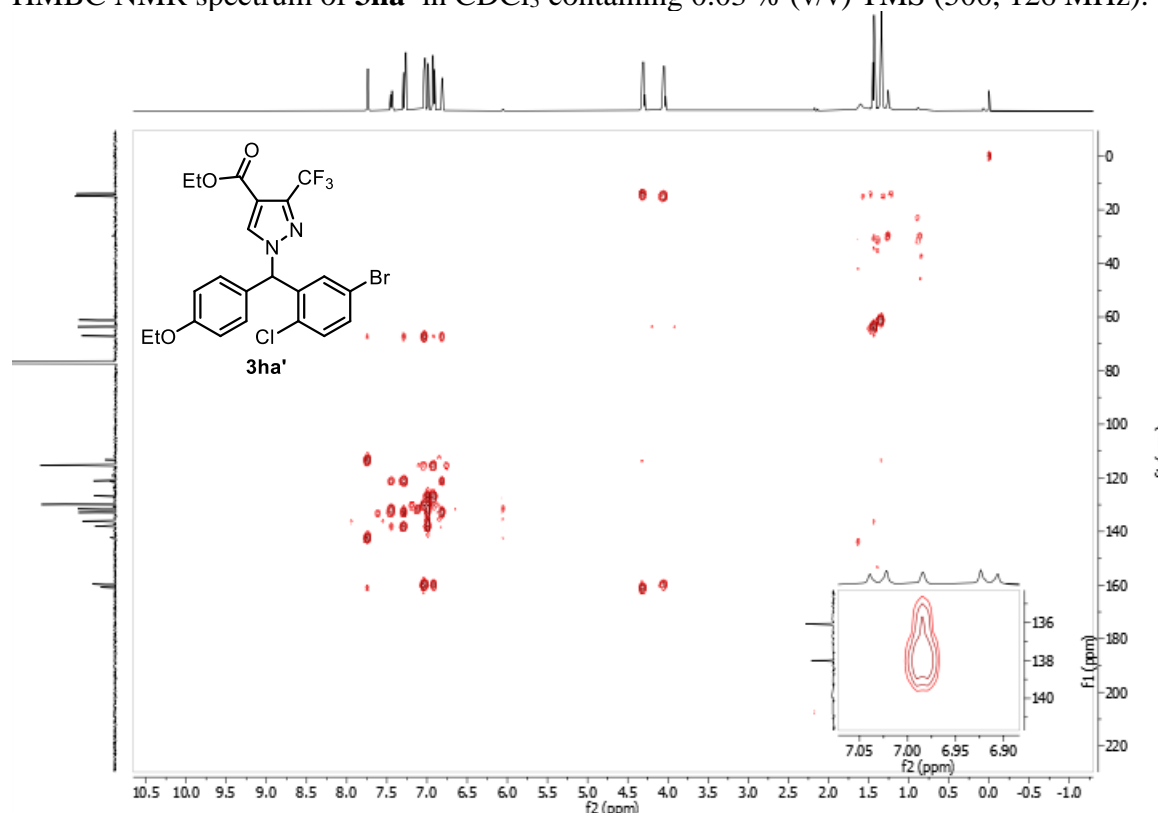
^{19}F NMR spectrum of **3ha'** in CDCl_3 containing 0.03 % (v/v) TMS (377 MHz).



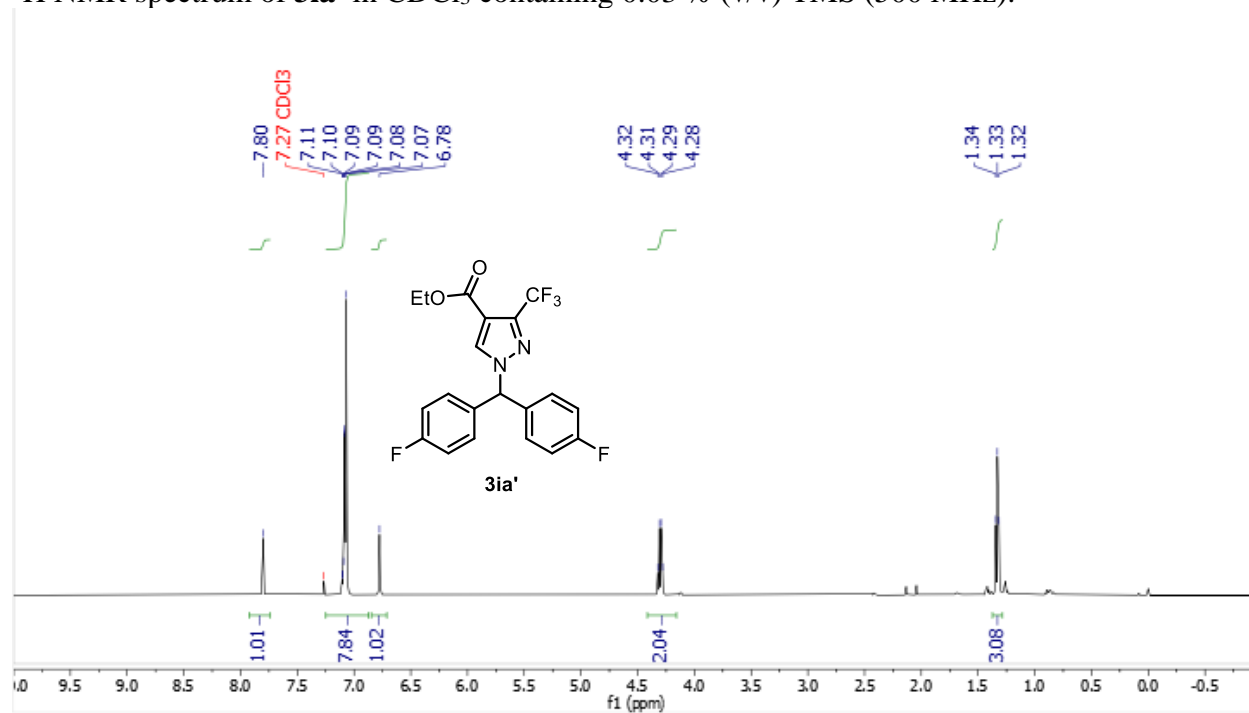
HSQC NMR spectrum of **3ha'** in CDCl_3 containing 0.03 % (v/v) TMS (500, 126 MHz).



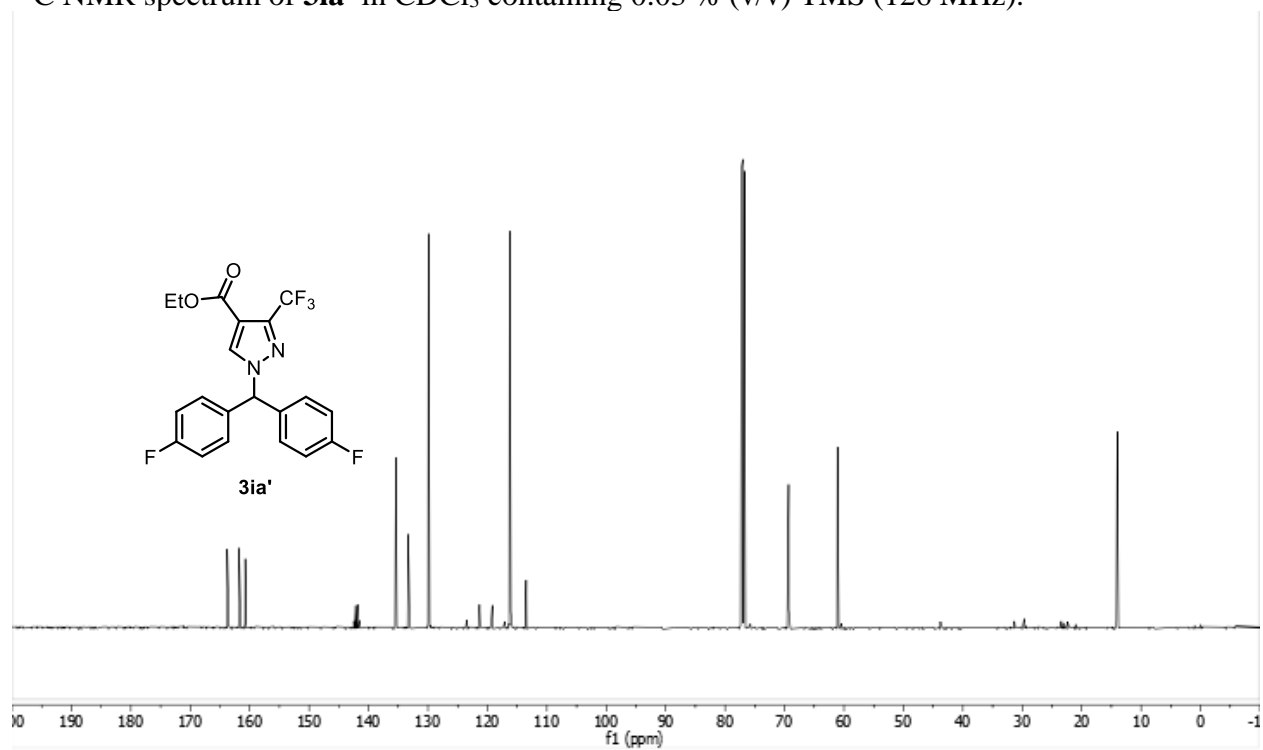
HMBC NMR spectrum of **3ha'** in CDCl₃ containing 0.03 % (v/v) TMS (500, 126 MHz).



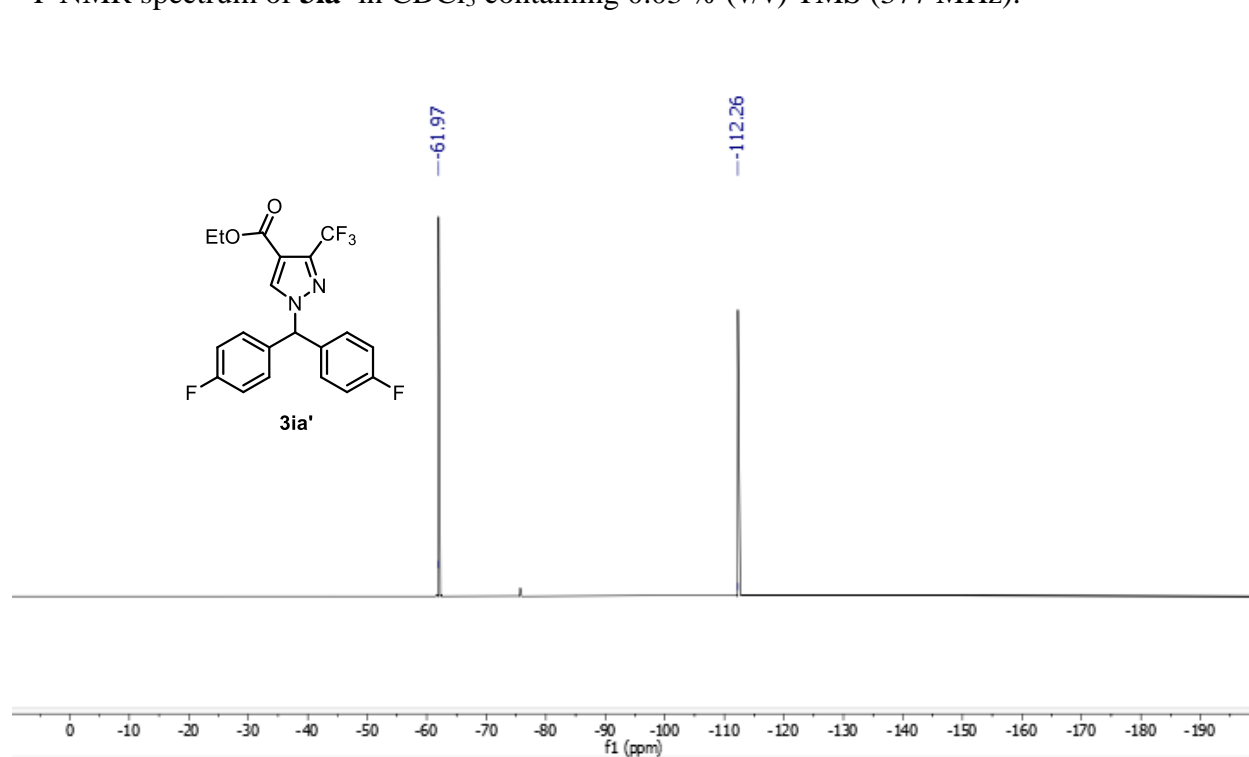
¹H NMR spectrum of **3ia'** in CDCl₃ containing 0.03 % (v/v) TMS (500 MHz).



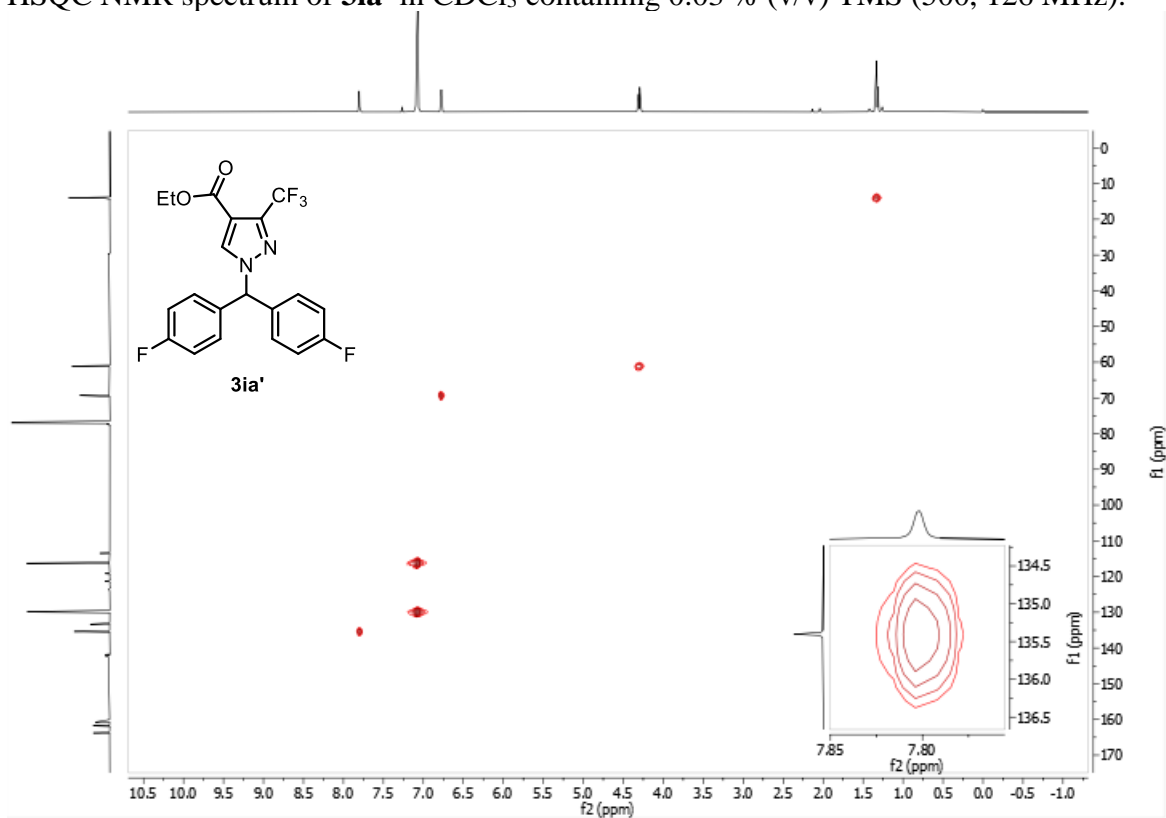
^{13}C NMR spectrum of **3ia'** in CDCl_3 containing 0.03 % (v/v) TMS (126 MHz).



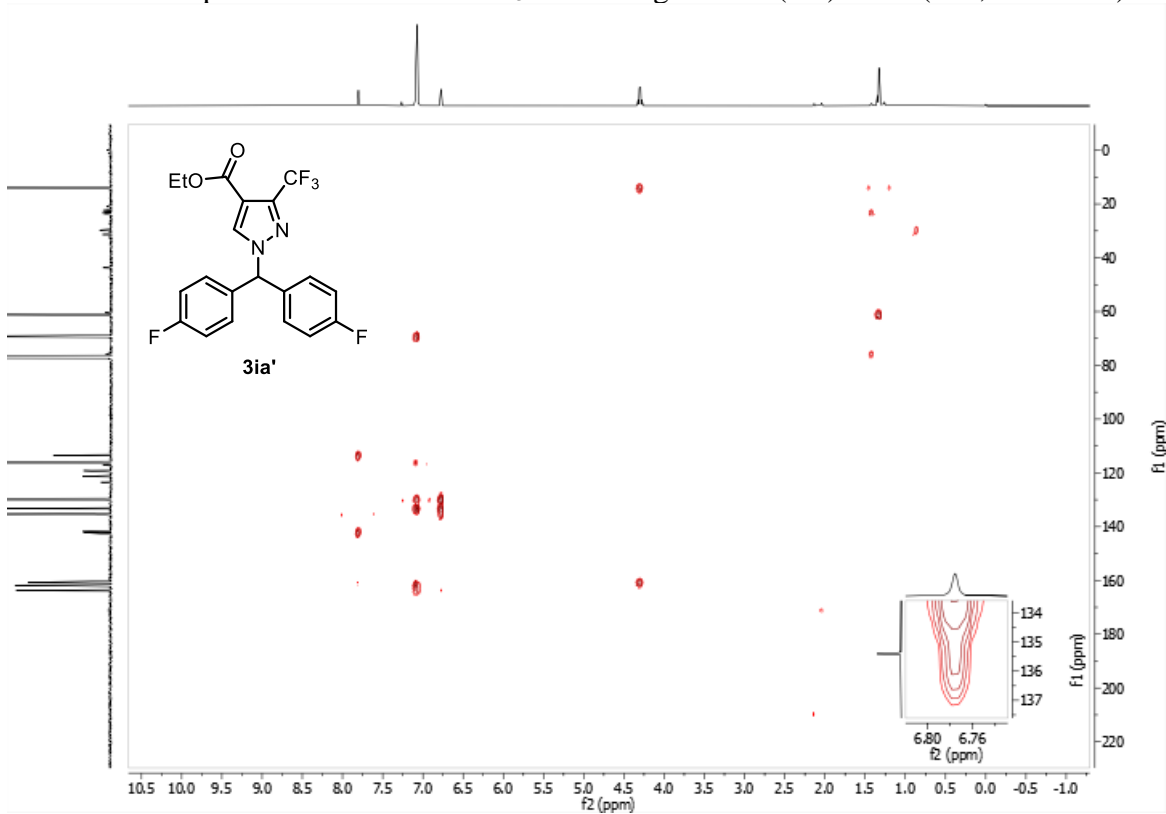
^{19}F NMR spectrum of **3ia'** in CDCl_3 containing 0.03 % (v/v) TMS (377 MHz).



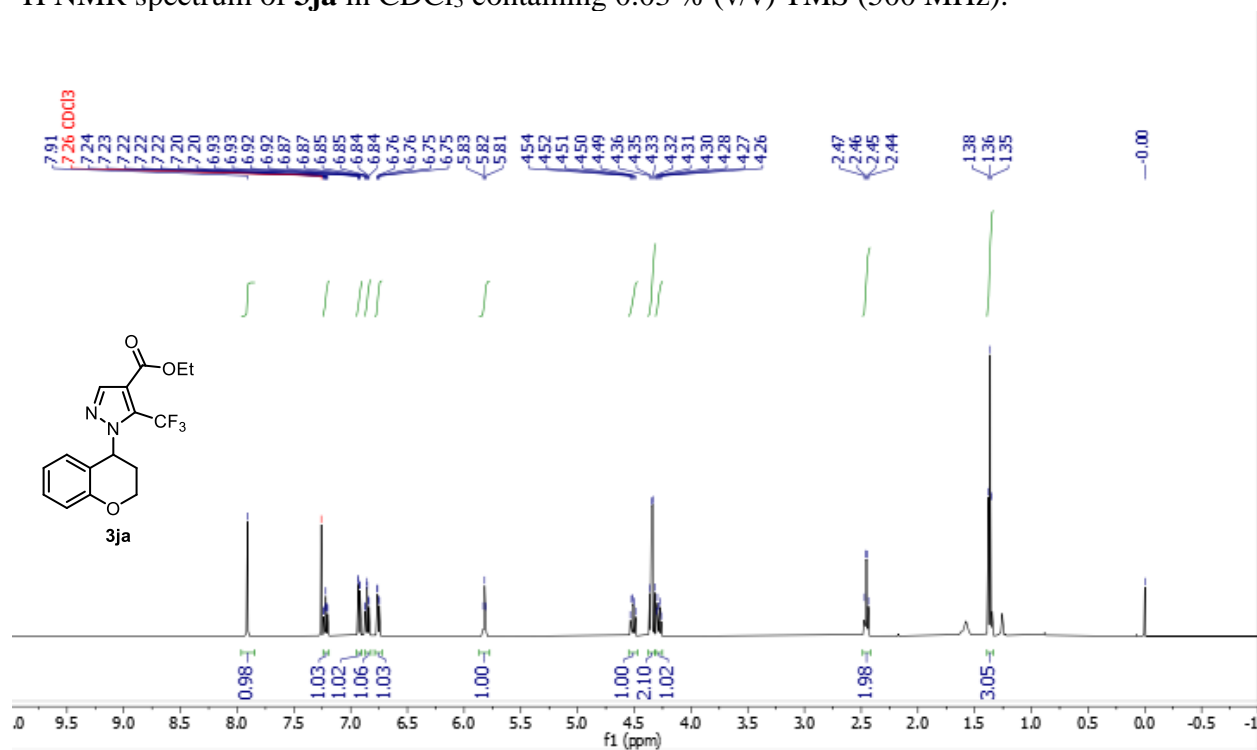
HSQC NMR spectrum of **3ia'** in CDCl₃ containing 0.03 % (v/v) TMS (500, 126 MHz).



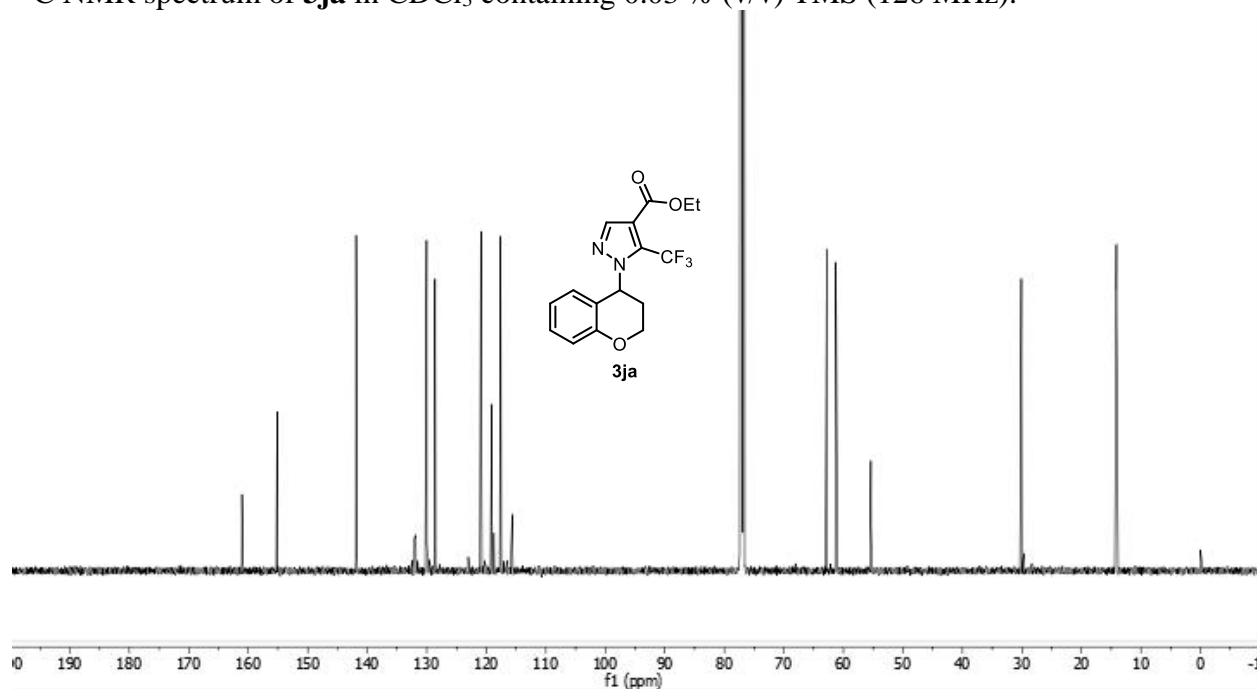
HMBC NMR spectrum of **3ia'** in CDCl₃ containing 0.03 % (v/v) TMS (500, 126 MHz).



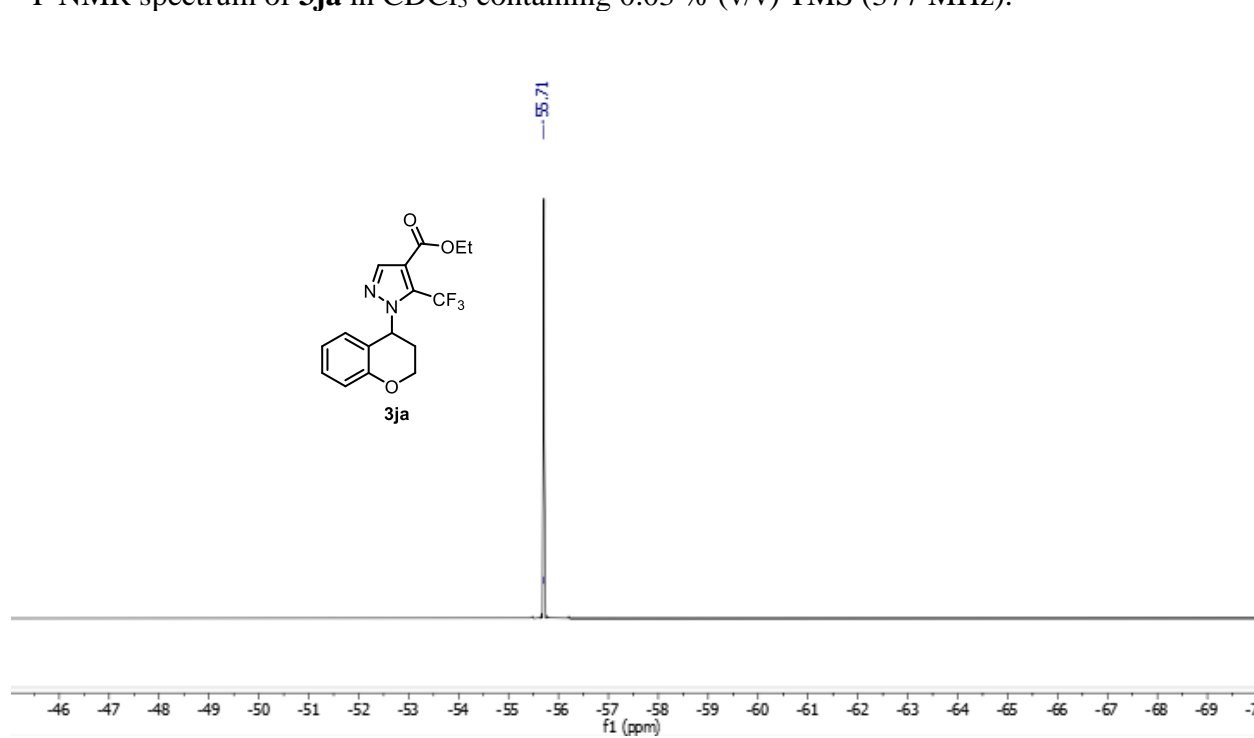
^1H NMR spectrum of **3ja** in CDCl_3 containing 0.03 % (v/v) TMS (500 MHz).



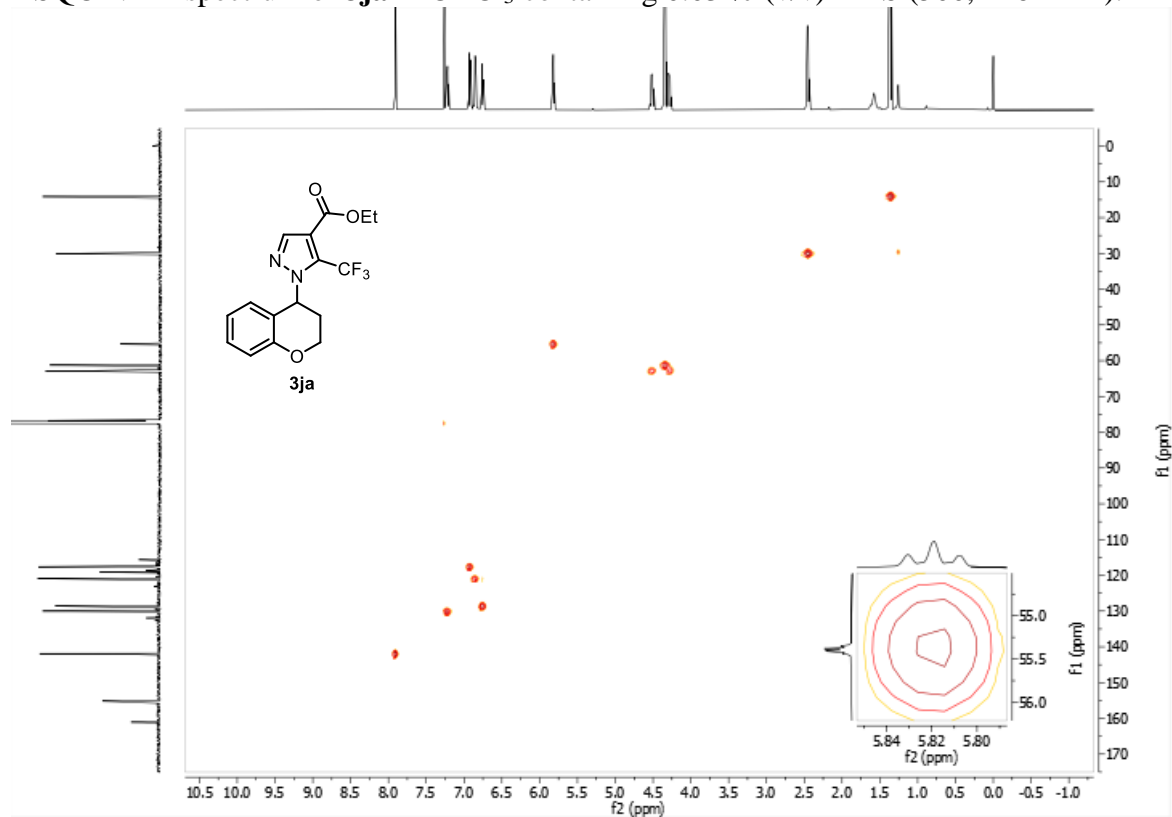
^{13}C NMR spectrum of **3ja** in CDCl_3 containing 0.03 % (v/v) TMS (126 MHz).



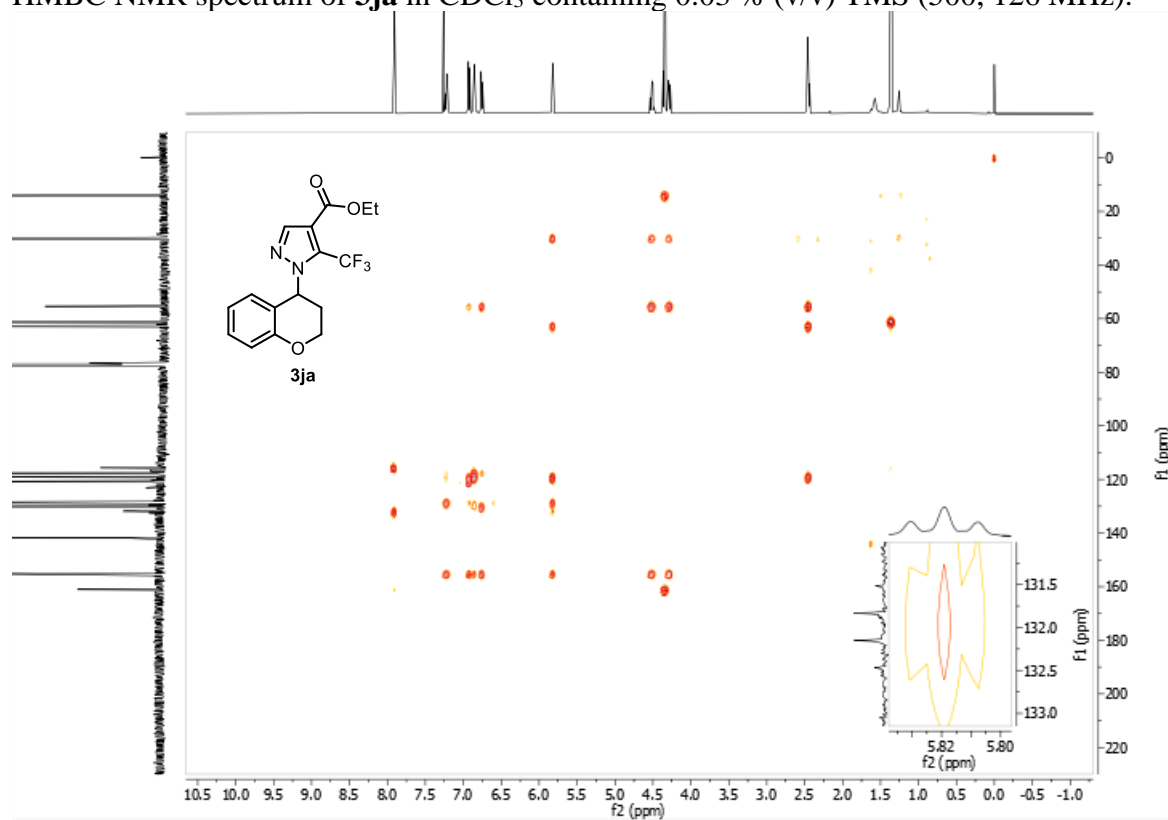
^{19}F NMR spectrum of **3ja** in CDCl_3 containing 0.03 % (v/v) TMS (377 MHz).



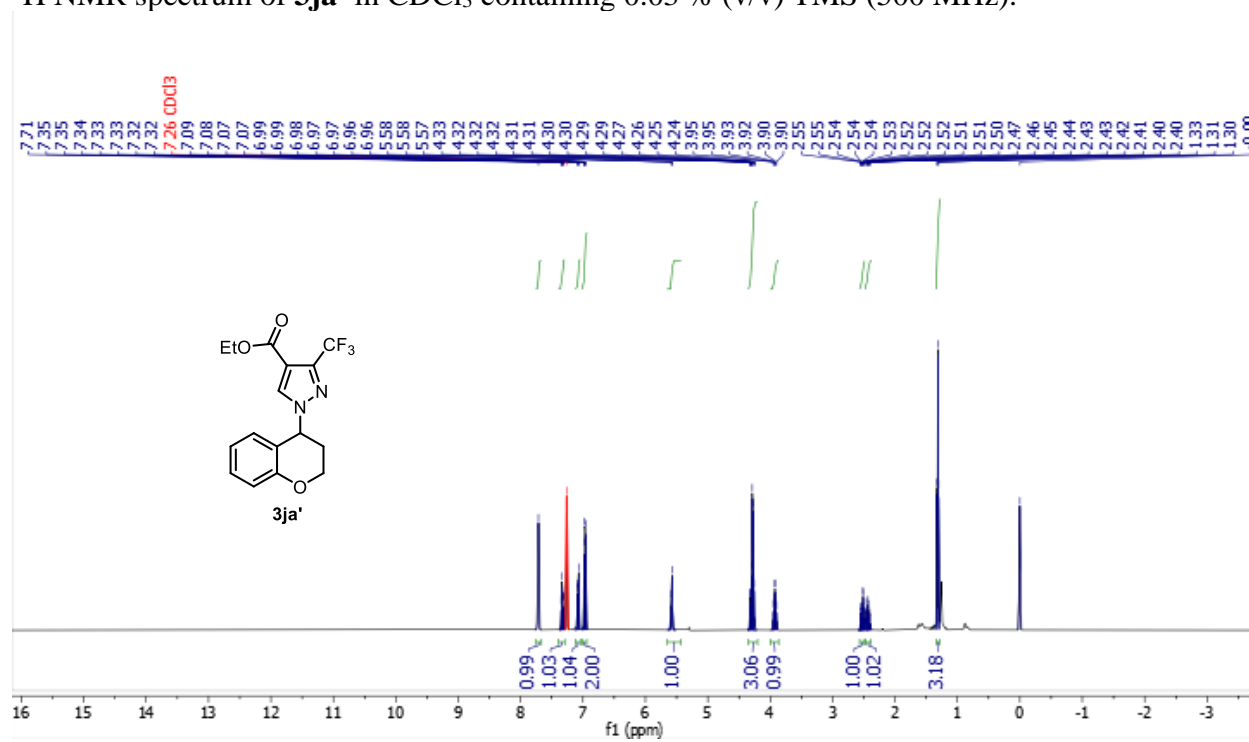
HSQC NMR spectrum of **3ja** in CDCl_3 containing 0.03 % (v/v) TMS (500, 126 MHz).



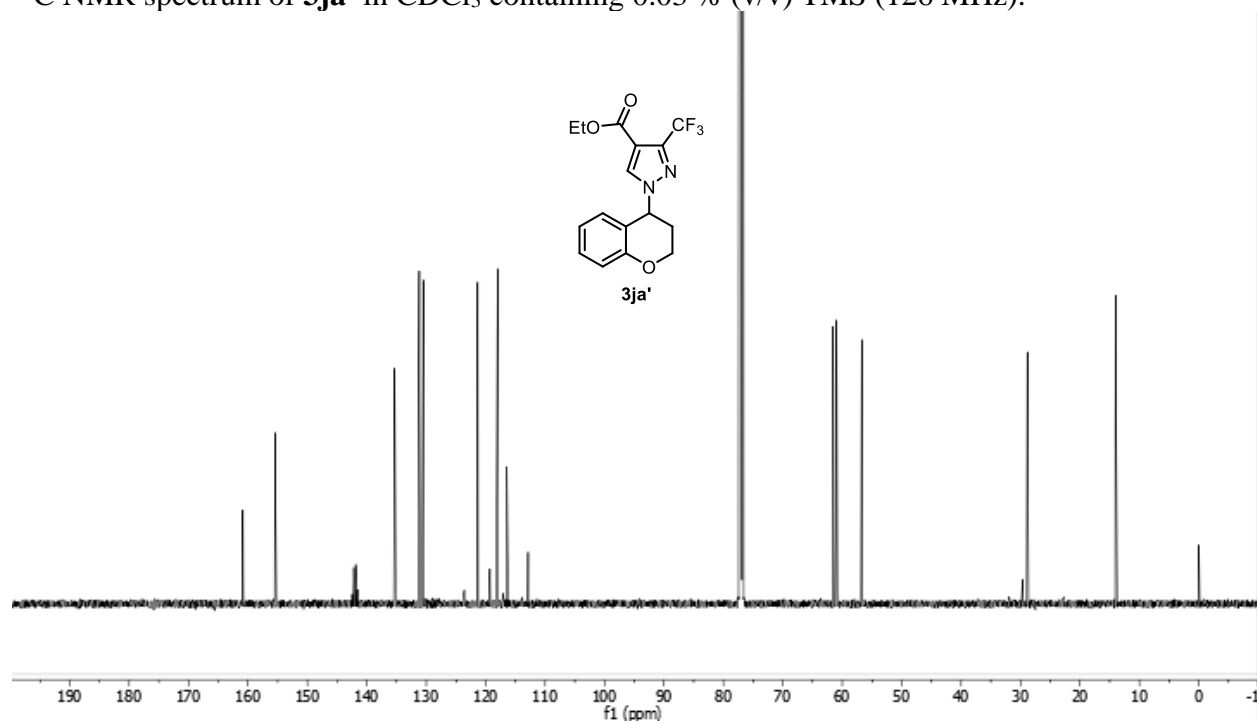
HMBC NMR spectrum of **3ja** in CDCl₃ containing 0.03 % (v/v) TMS (500, 126 MHz).



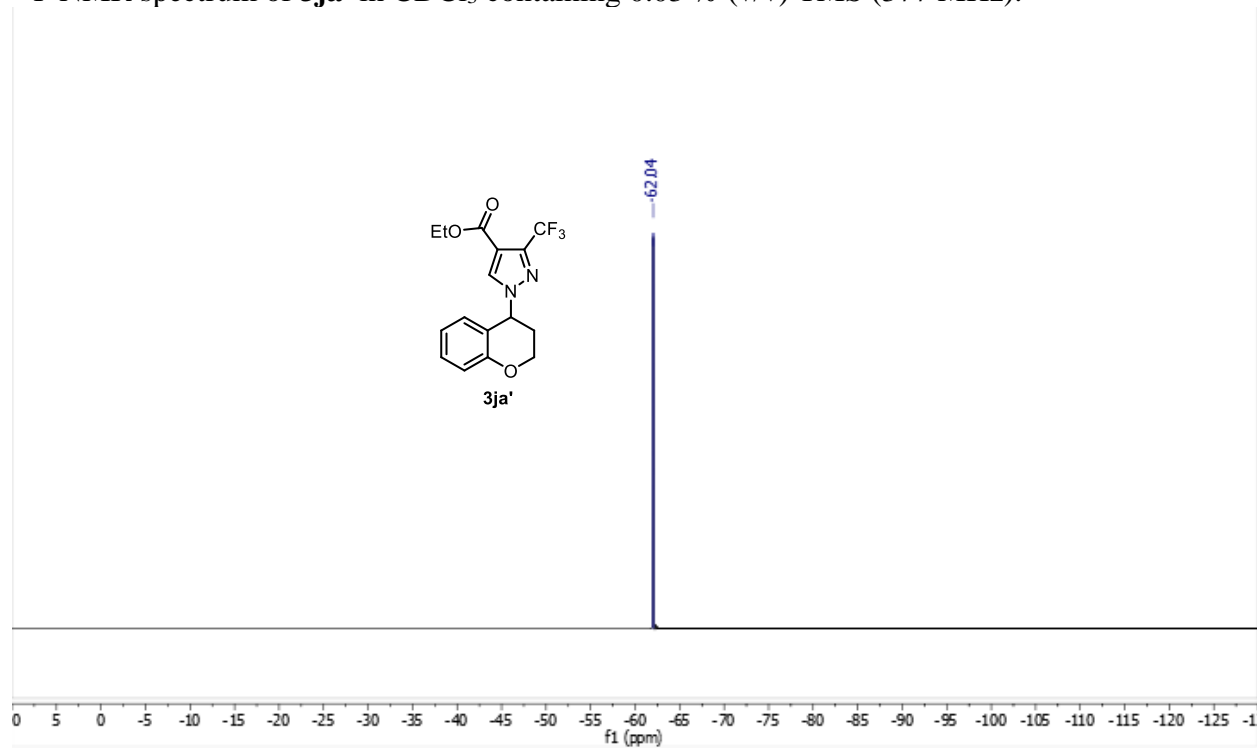
¹H NMR spectrum of **3ja'** in CDCl₃ containing 0.03 % (v/v) TMS (500 MHz).



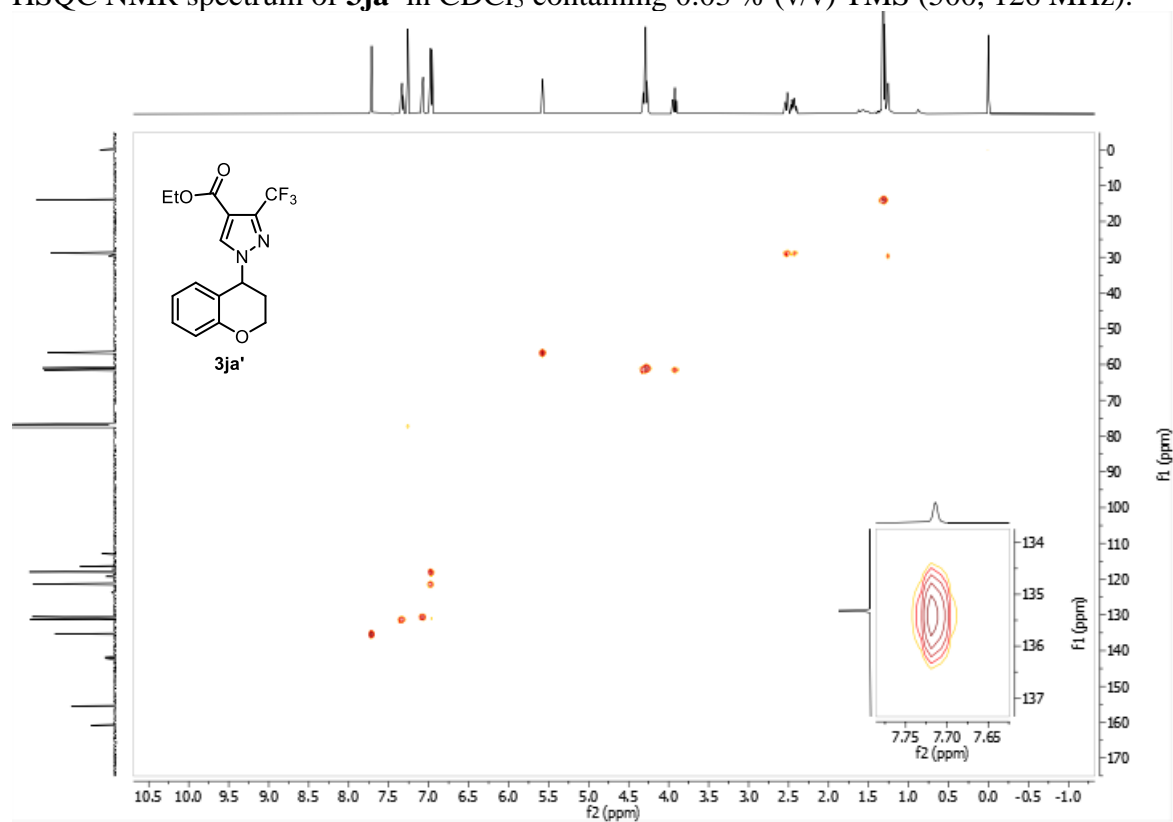
^{13}C NMR spectrum of **3ja'** in CDCl_3 containing 0.03 % (v/v) TMS (126 MHz).



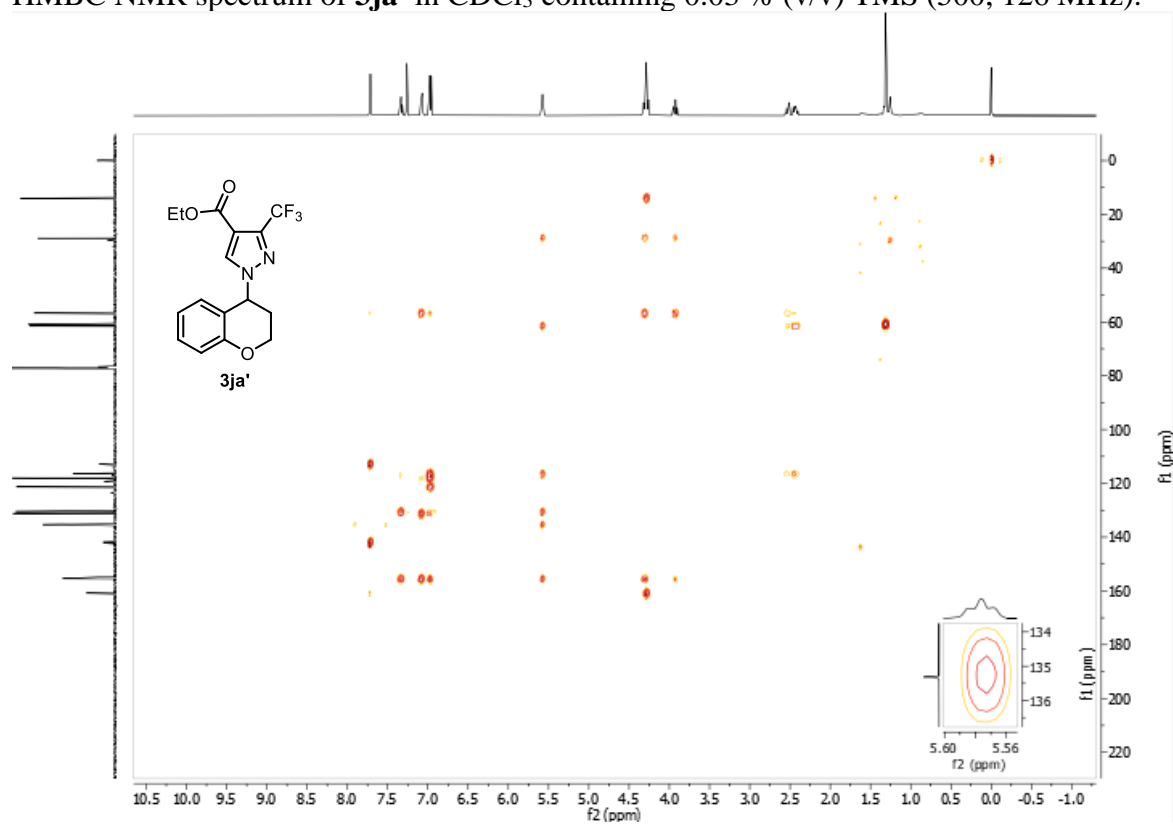
^{19}F NMR spectrum of **3ja'** in CDCl_3 containing 0.03 % (v/v) TMS (377 MHz).



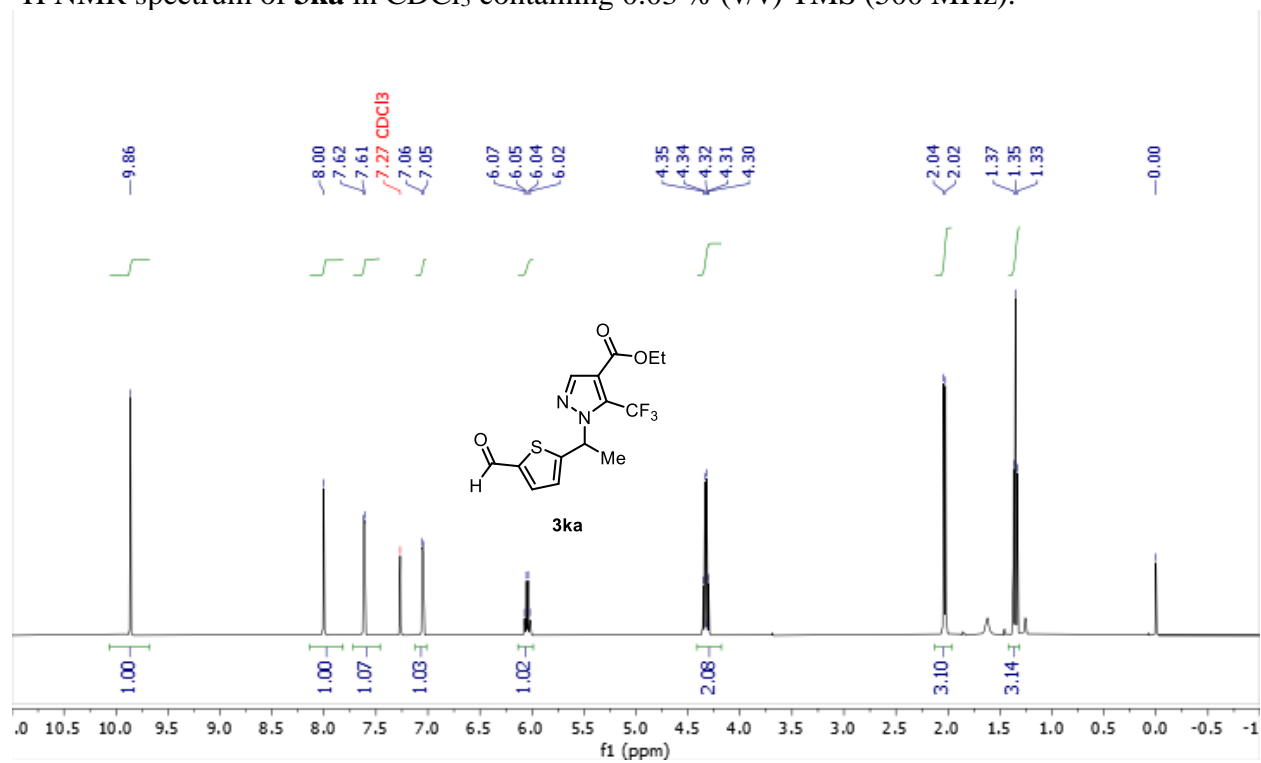
HSQC NMR spectrum of **3ja'** in CDCl₃ containing 0.03 % (v/v) TMS (500, 126 MHz).



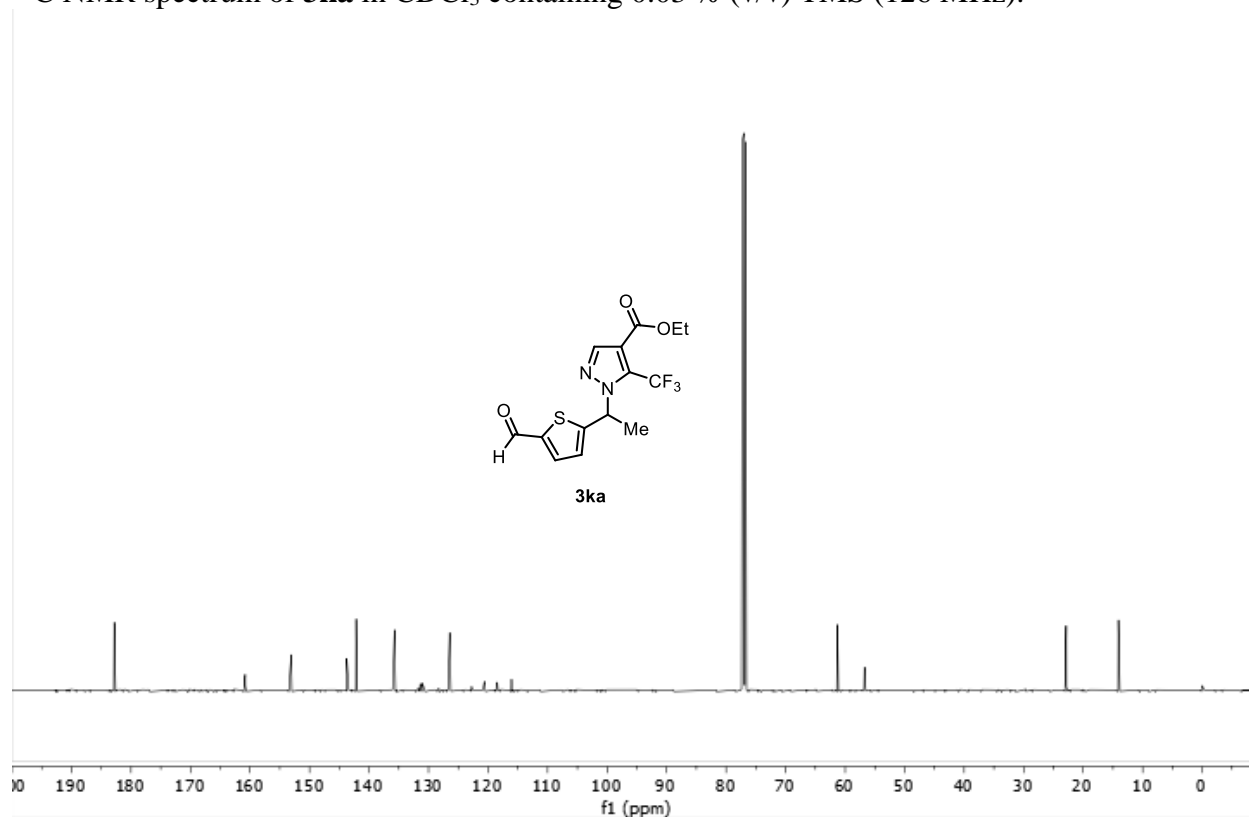
HMBC NMR spectrum of **3ja'** in CDCl₃ containing 0.03 % (v/v) TMS (500, 126 MHz).



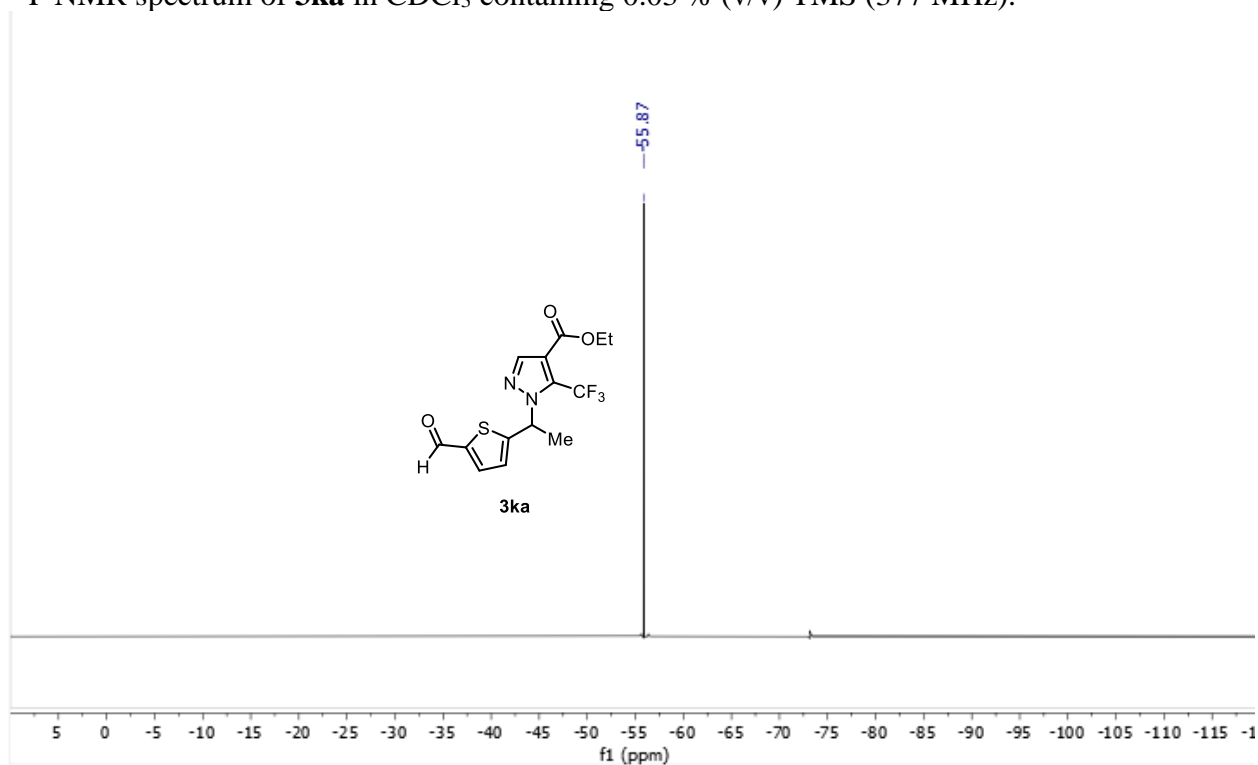
^1H NMR spectrum of **3ka** in CDCl_3 containing 0.03 % (v/v) TMS (500 MHz).



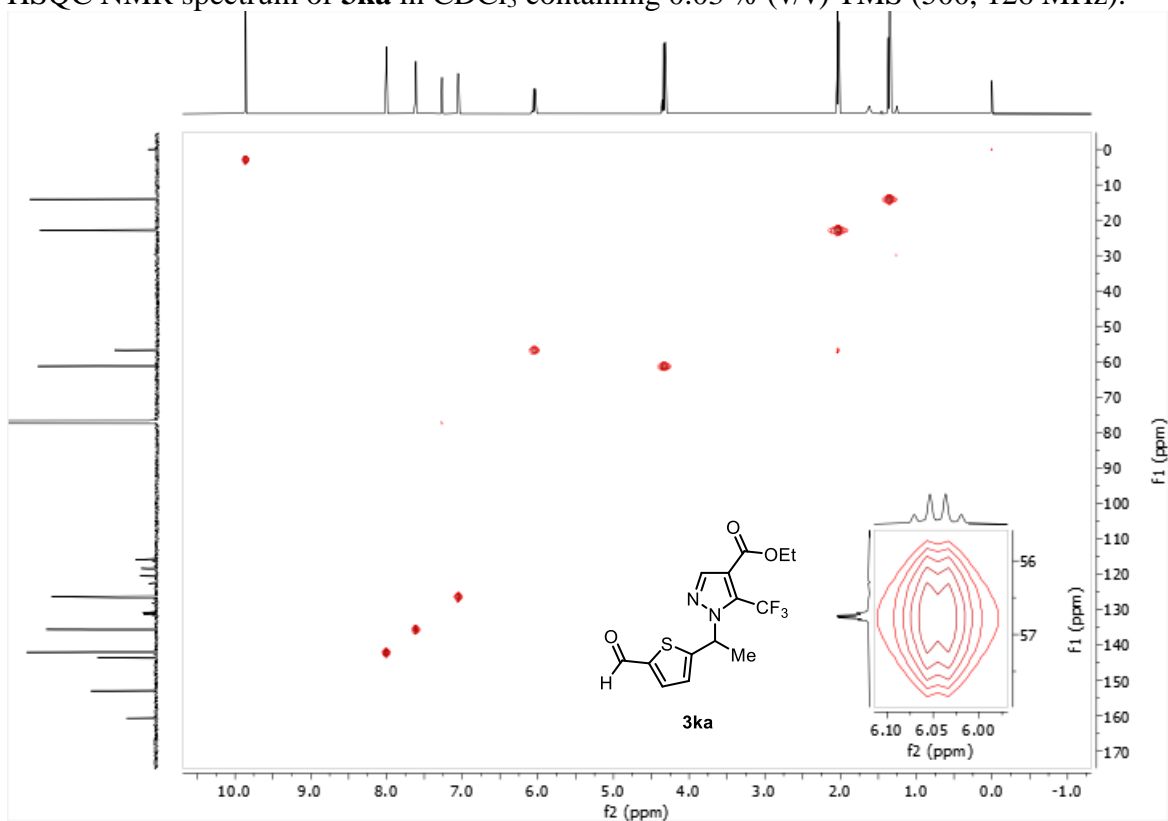
^{13}C NMR spectrum of **3ka** in CDCl_3 containing 0.03 % (v/v) TMS (126 MHz).



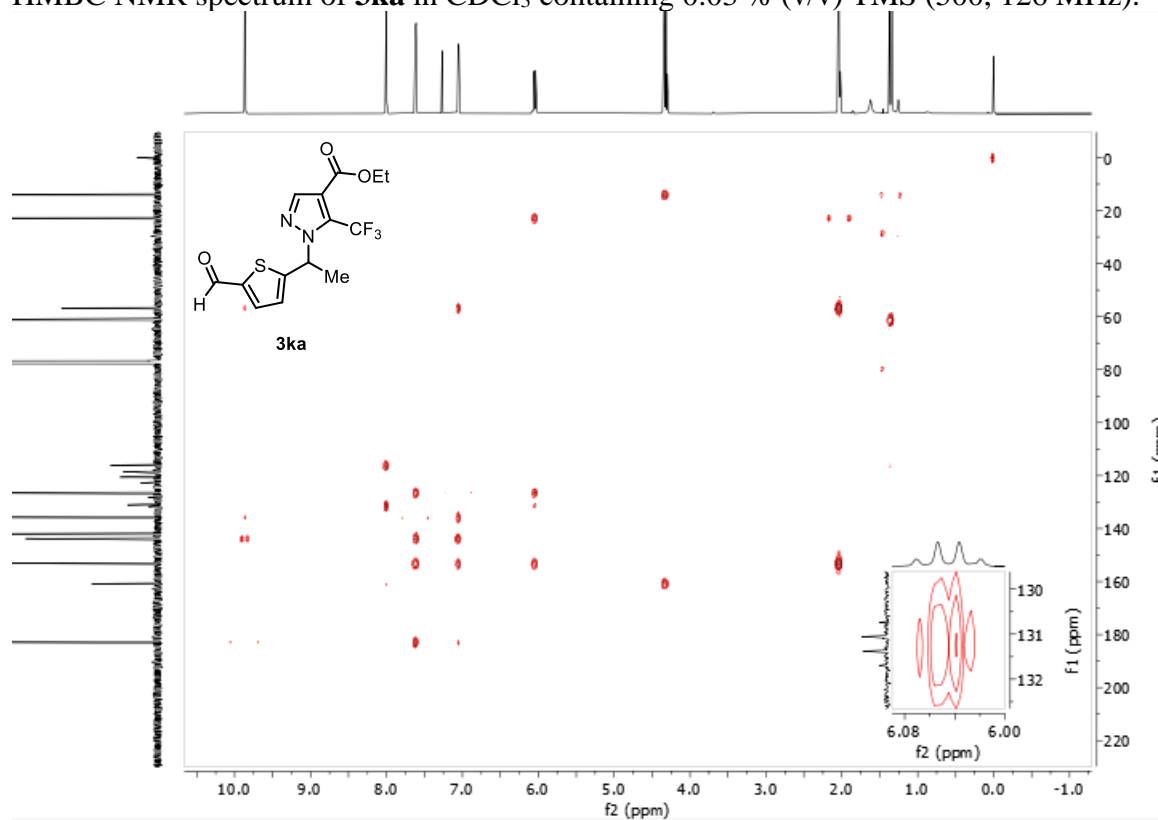
^{19}F NMR spectrum of **3ka** in CDCl_3 containing 0.03 % (v/v) TMS (377 MHz).



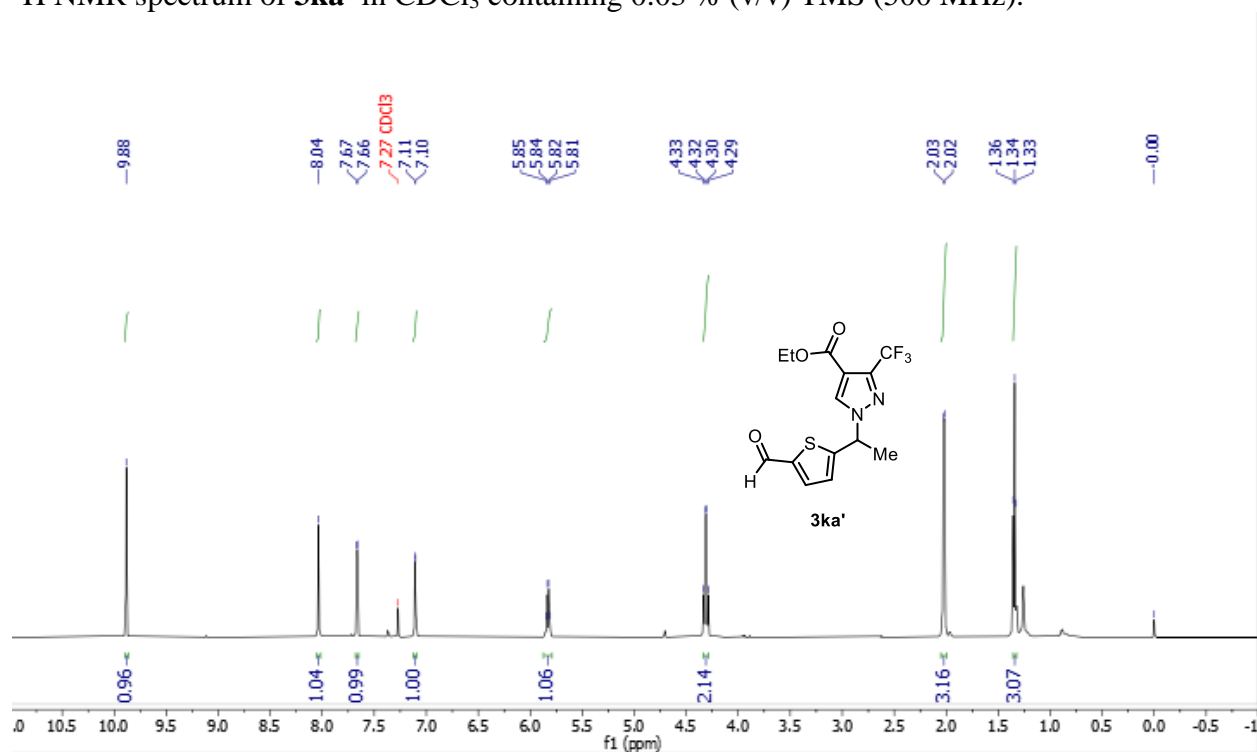
HSQC NMR spectrum of **3ka** in CDCl_3 containing 0.03 % (v/v) TMS (500, 126 MHz).



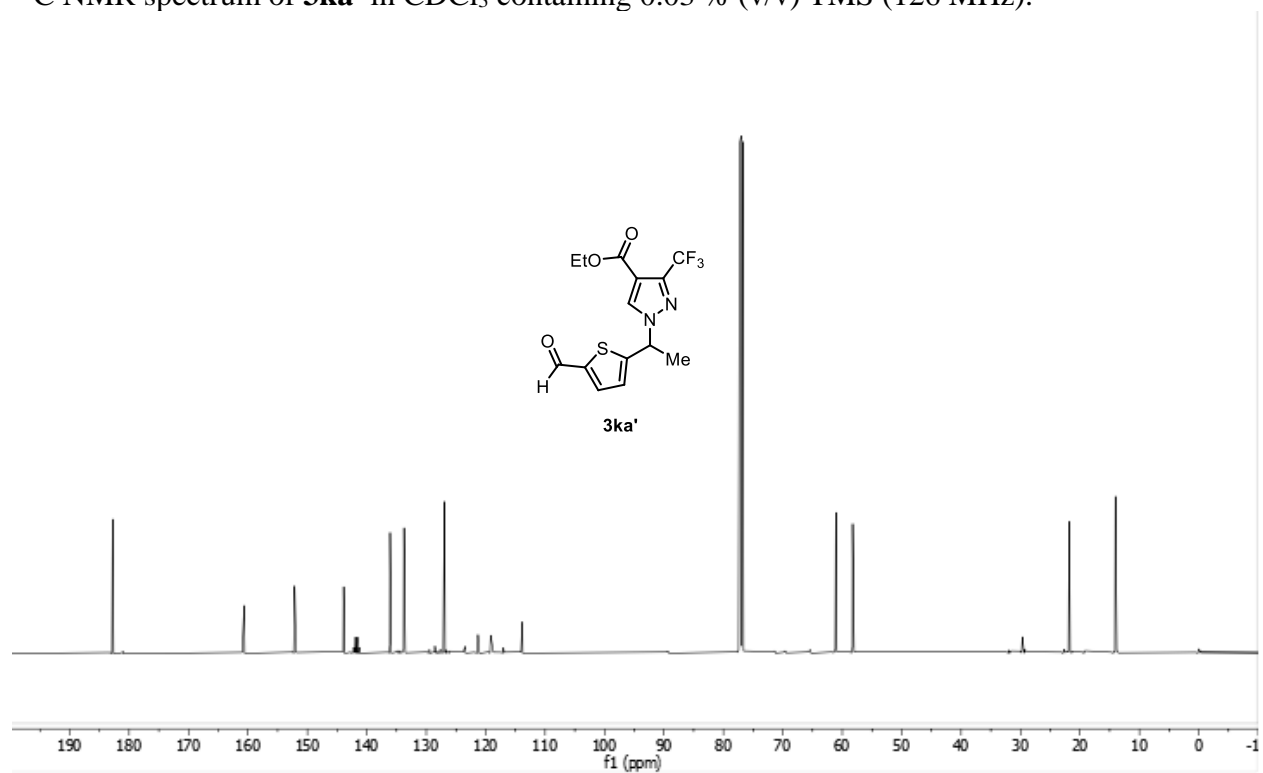
HMBC NMR spectrum of **3ka** in CDCl₃ containing 0.03 % (v/v) TMS (500, 126 MHz).



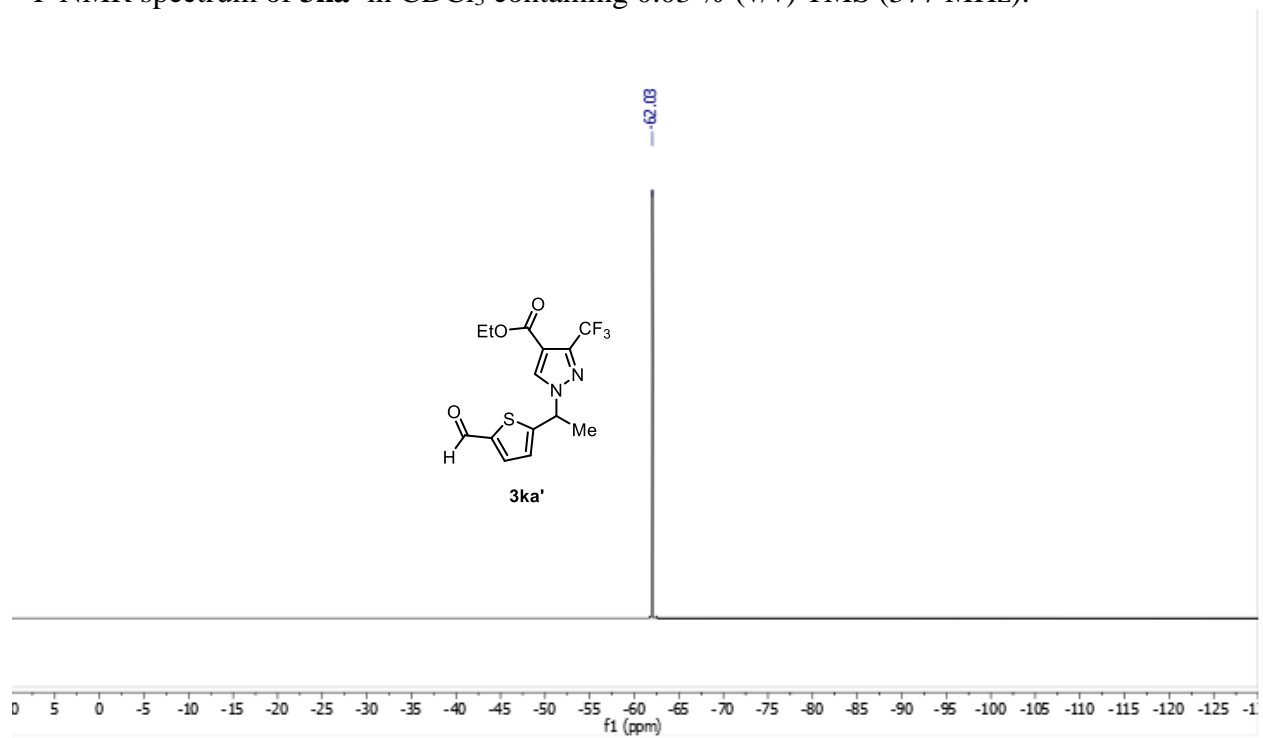
¹H NMR spectrum of **3ka'** in CDCl₃ containing 0.03 % (v/v) TMS (500 MHz).



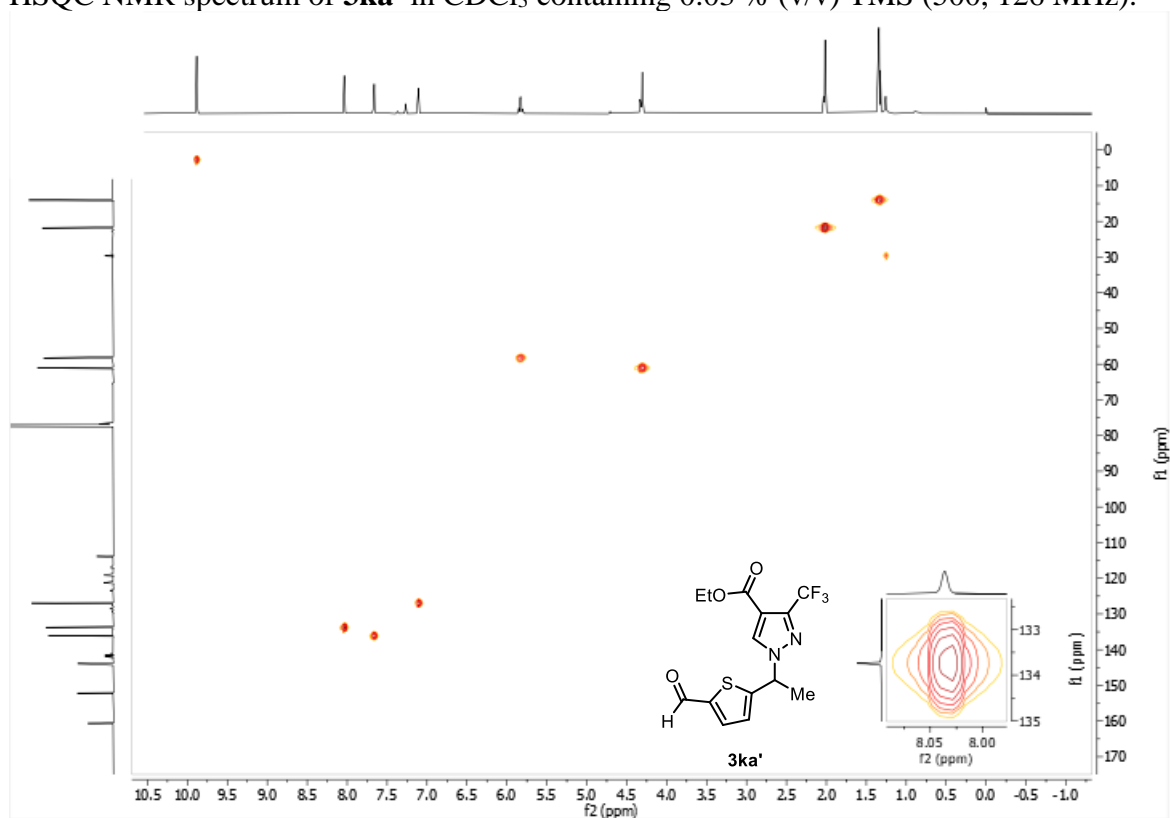
^{13}C NMR spectrum of **3ka'** in CDCl_3 containing 0.03 % (v/v) TMS (126 MHz).



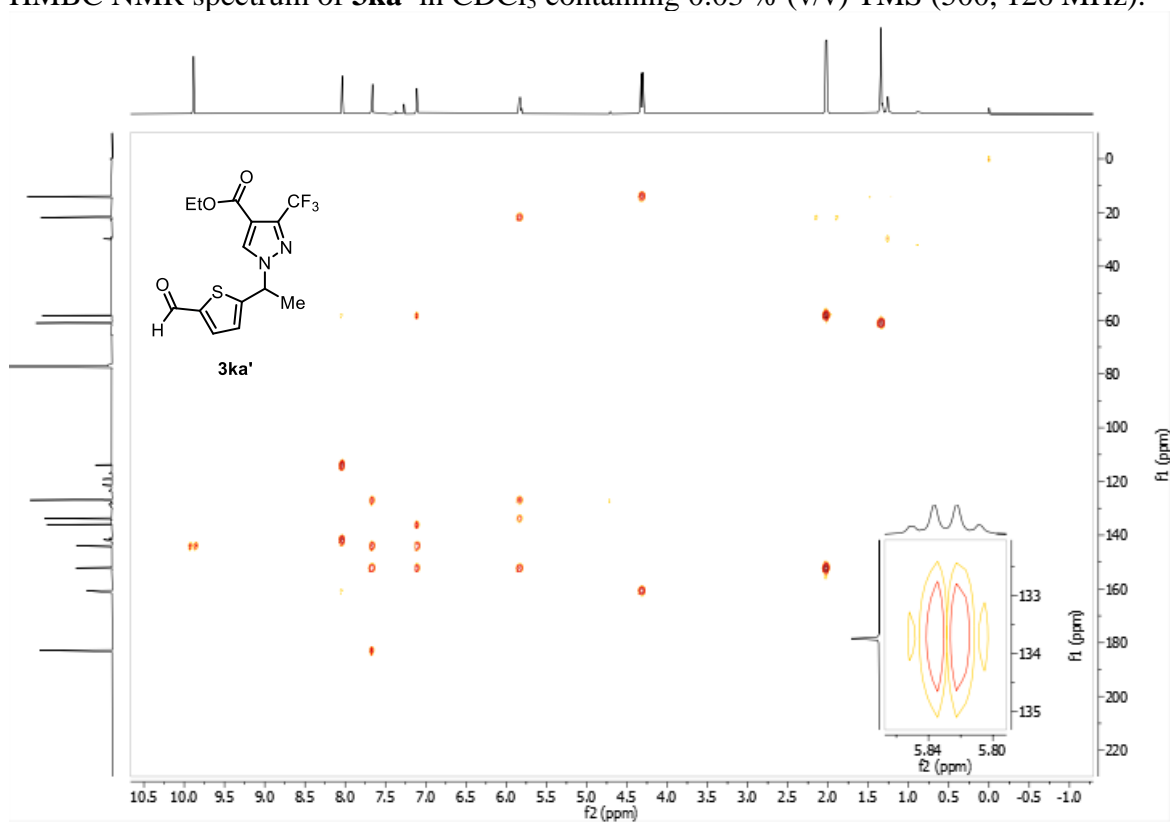
^{19}F NMR spectrum of **3ka'** in CDCl_3 containing 0.03 % (v/v) TMS (377 MHz).



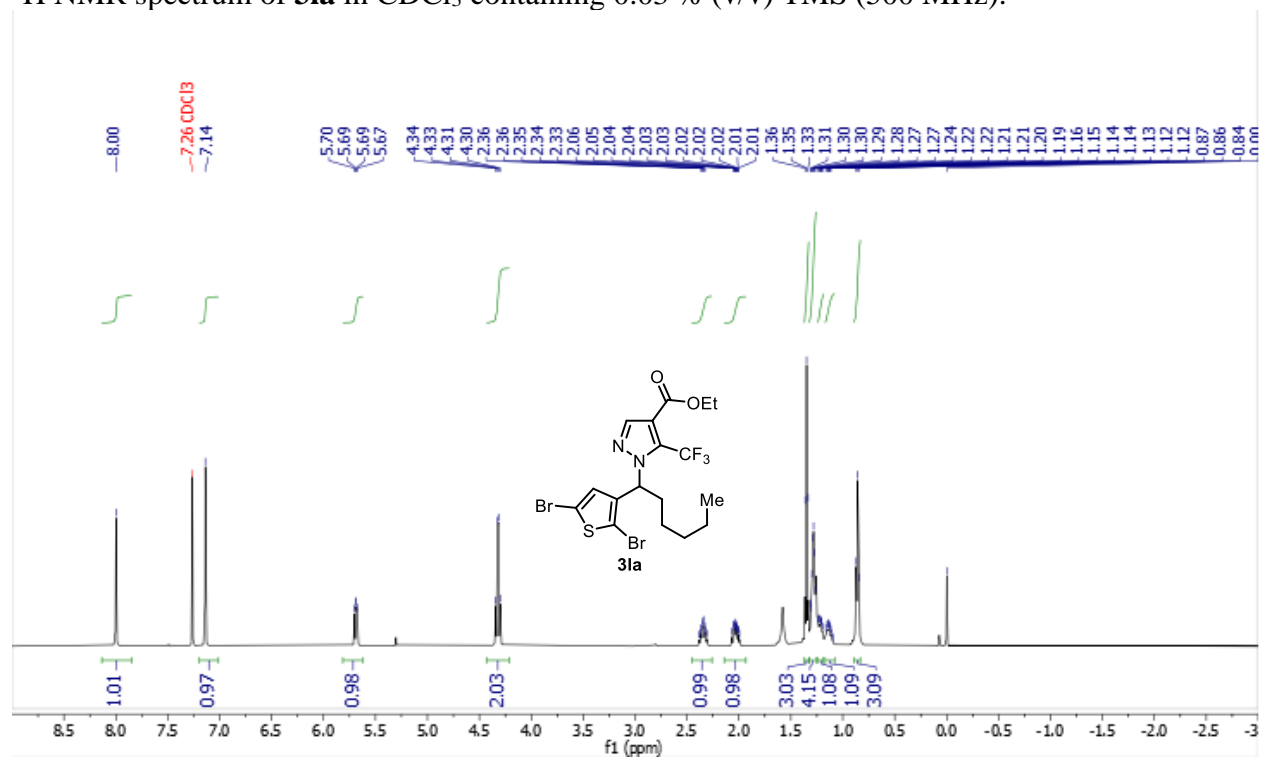
HSQC NMR spectrum of **3ka'** in CDCl₃ containing 0.03 % (v/v) TMS (500, 126 MHz).



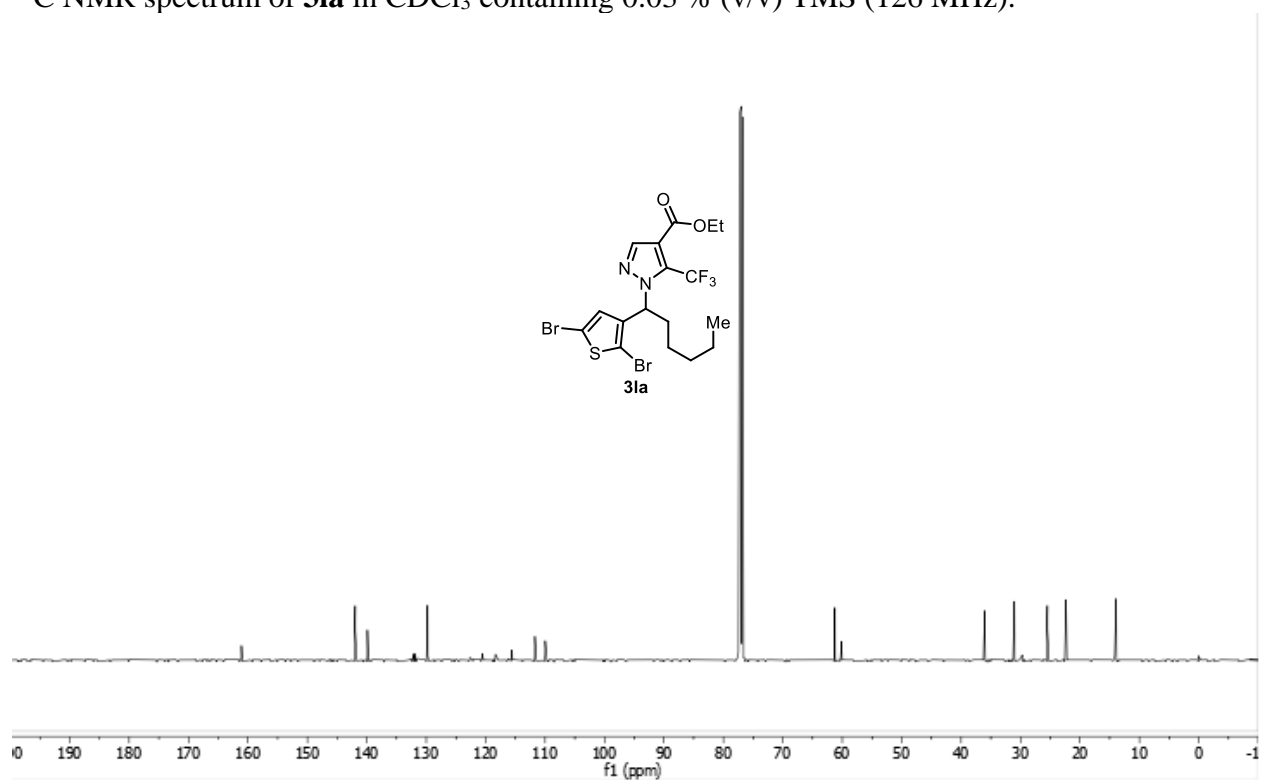
HMBC NMR spectrum of **3ka'** in CDCl₃ containing 0.03 % (v/v) TMS (500, 126 MHz).



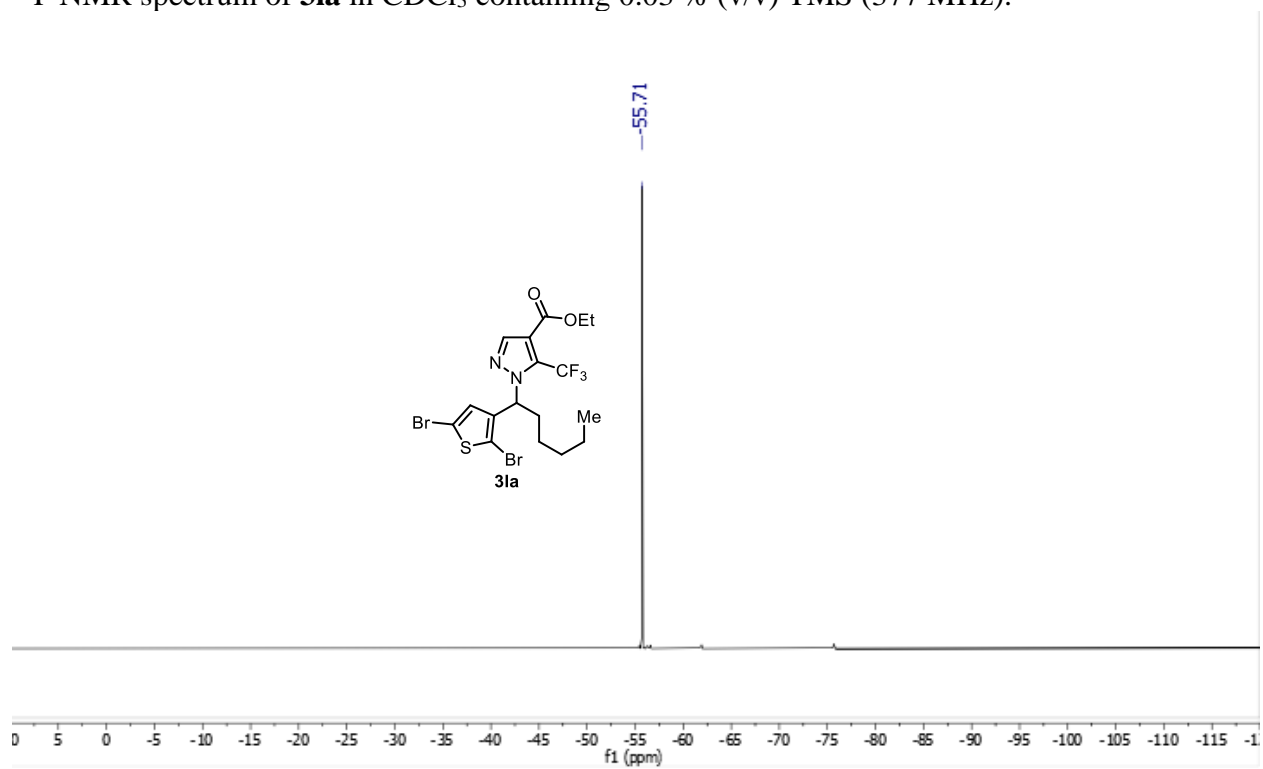
^1H NMR spectrum of **31a** in CDCl_3 containing 0.03 % (v/v) TMS (500 MHz).



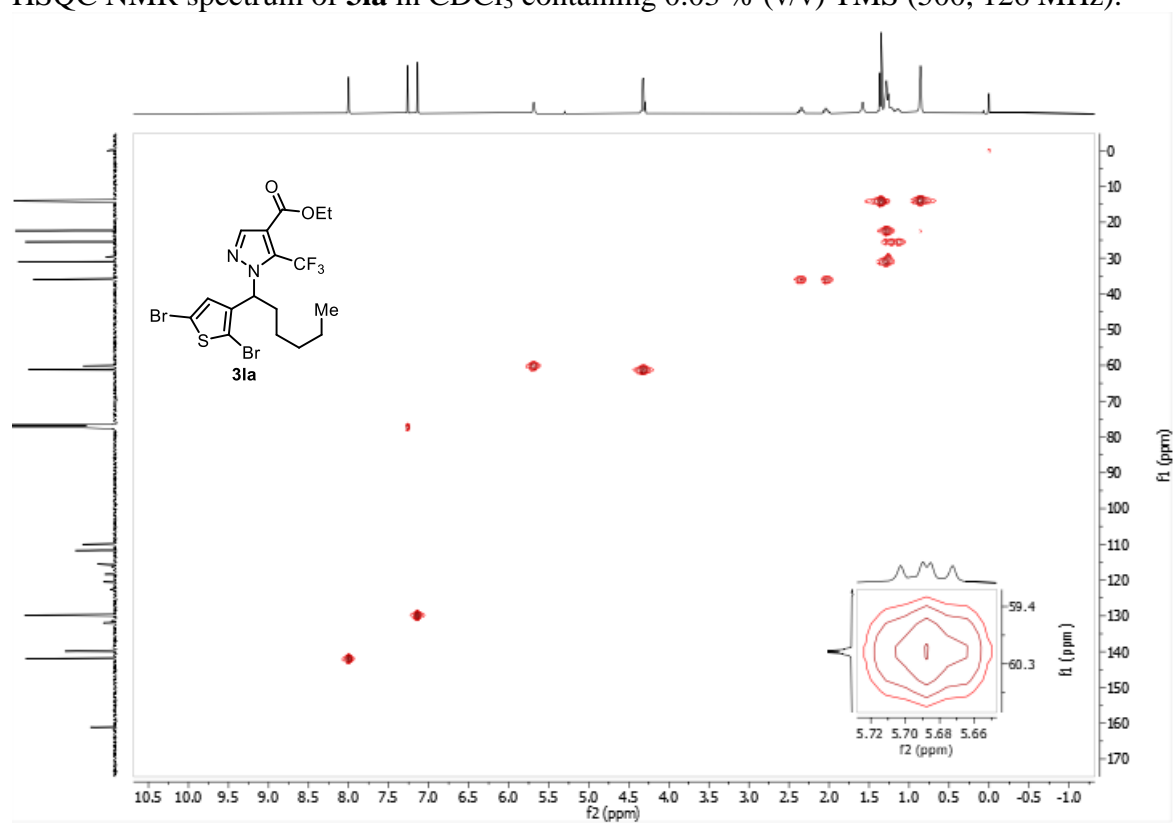
^{13}C NMR spectrum of **31a** in CDCl_3 containing 0.03 % (v/v) TMS (126 MHz).



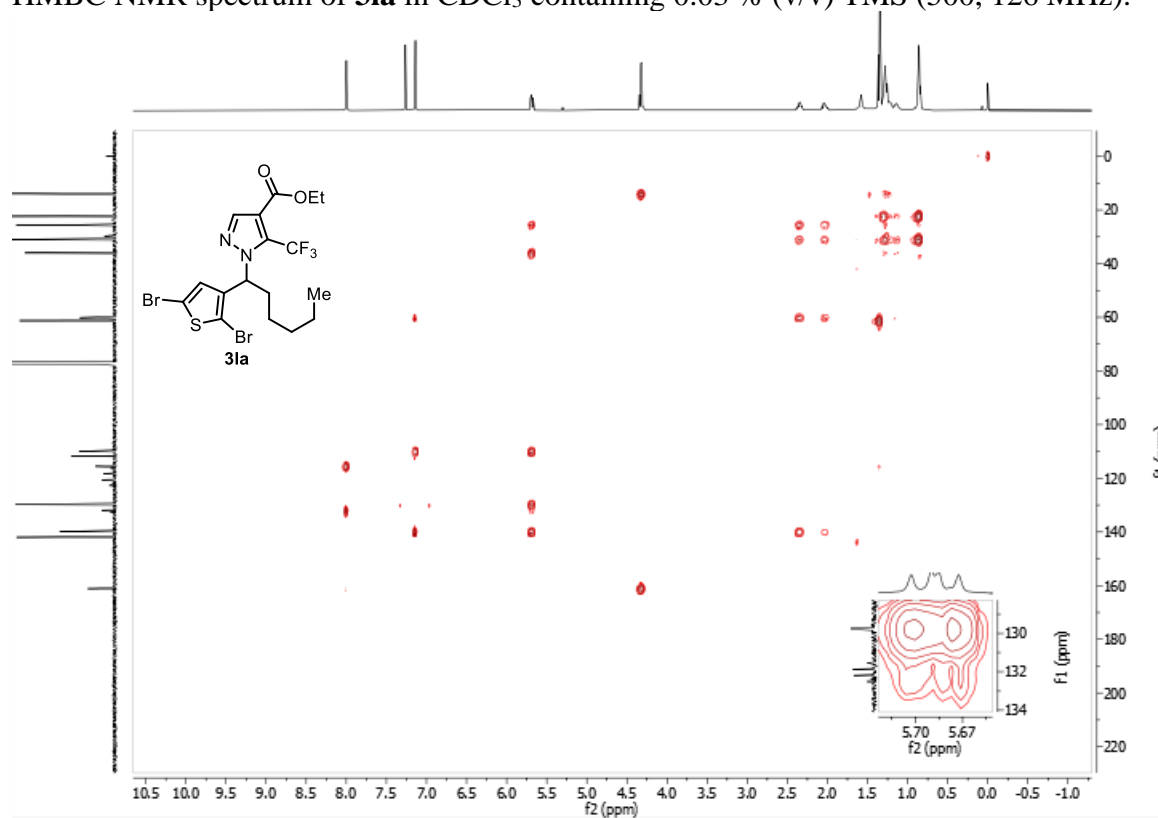
^{19}F NMR spectrum of **3la** in CDCl_3 containing 0.03 % (v/v) TMS (377 MHz).



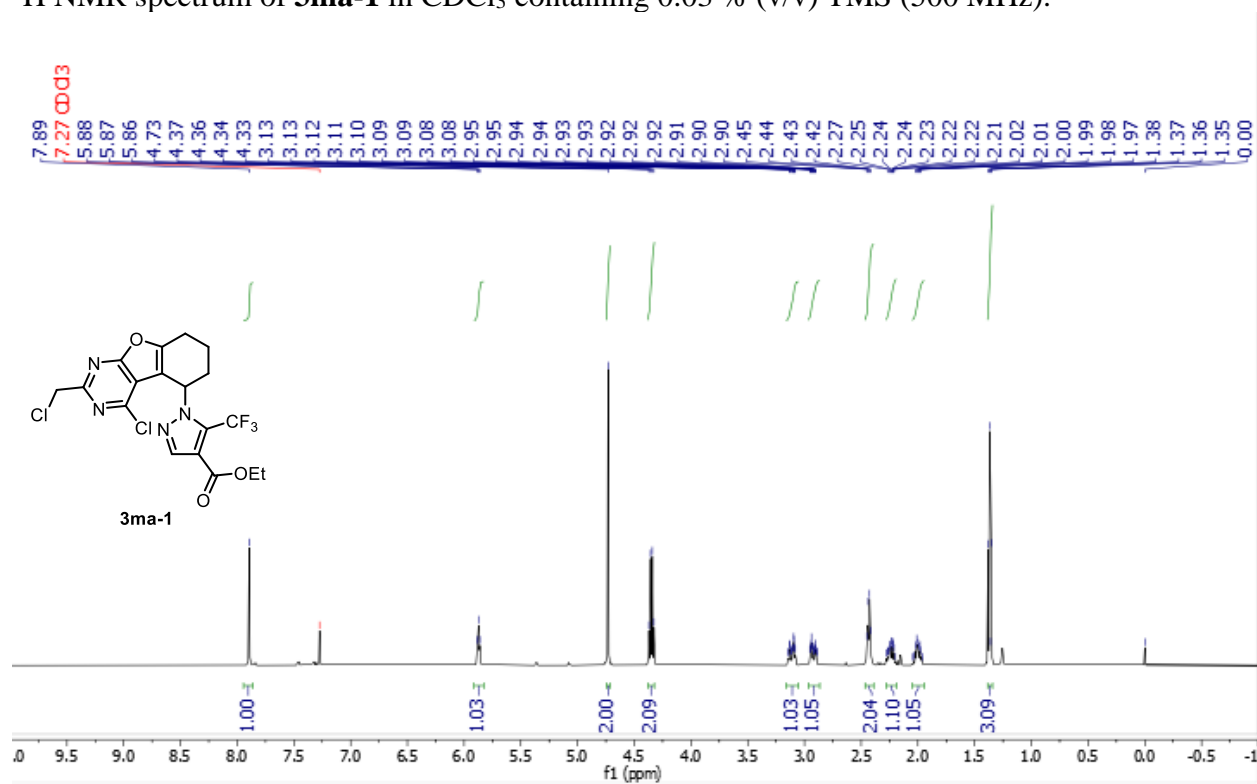
HSQC NMR spectrum of **3la** in CDCl_3 containing 0.03 % (v/v) TMS (500, 126 MHz).



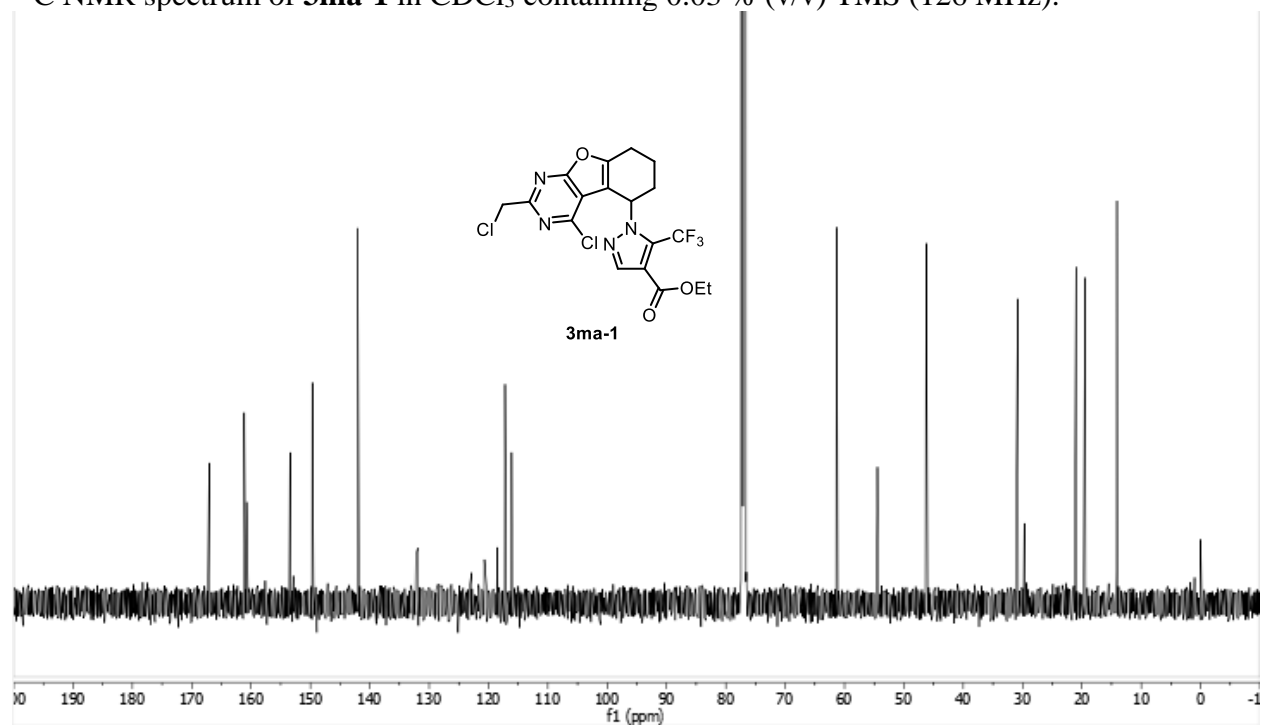
HMBC NMR spectrum of **3la** in CDCl₃ containing 0.03 % (v/v) TMS (500, 126 MHz).



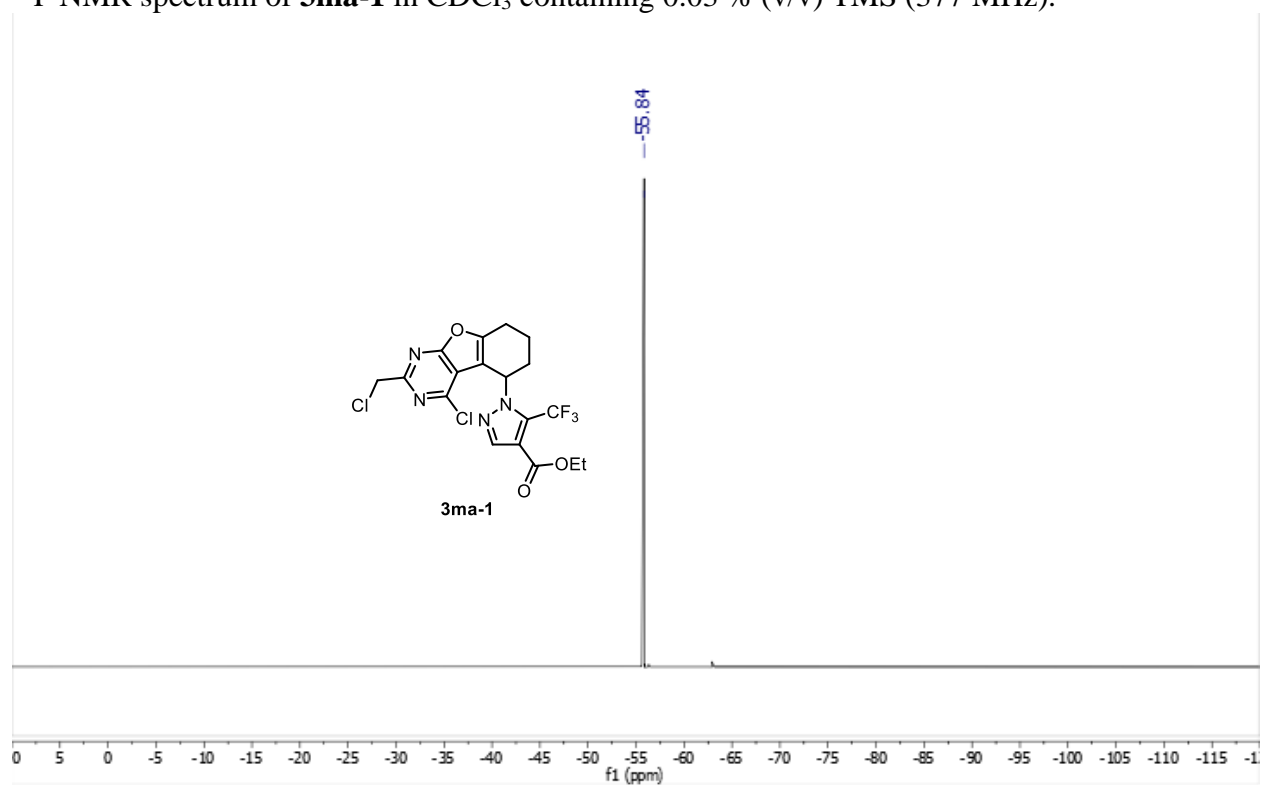
¹H NMR spectrum of **3ma-1** in CDCl₃ containing 0.03 % (v/v) TMS (500 MHz).



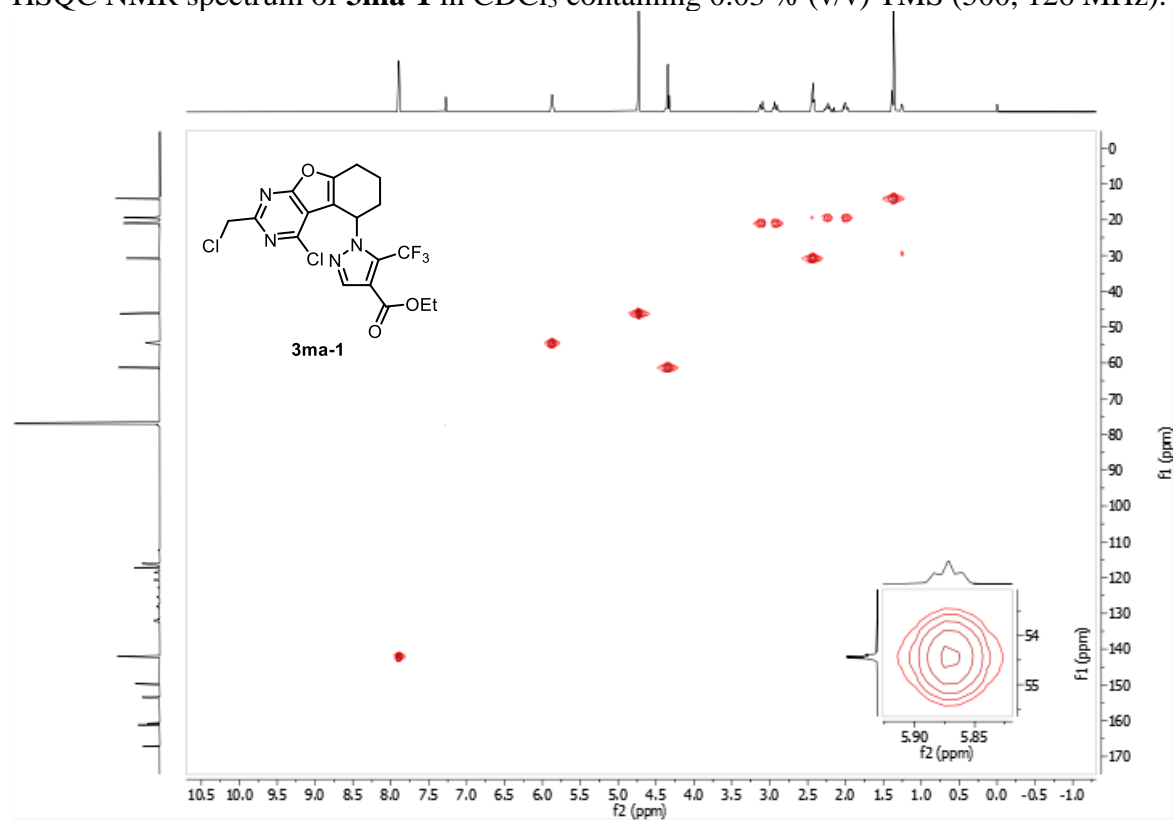
^{13}C NMR spectrum of **3ma-1** in CDCl_3 containing 0.03 % (v/v) TMS (126 MHz).



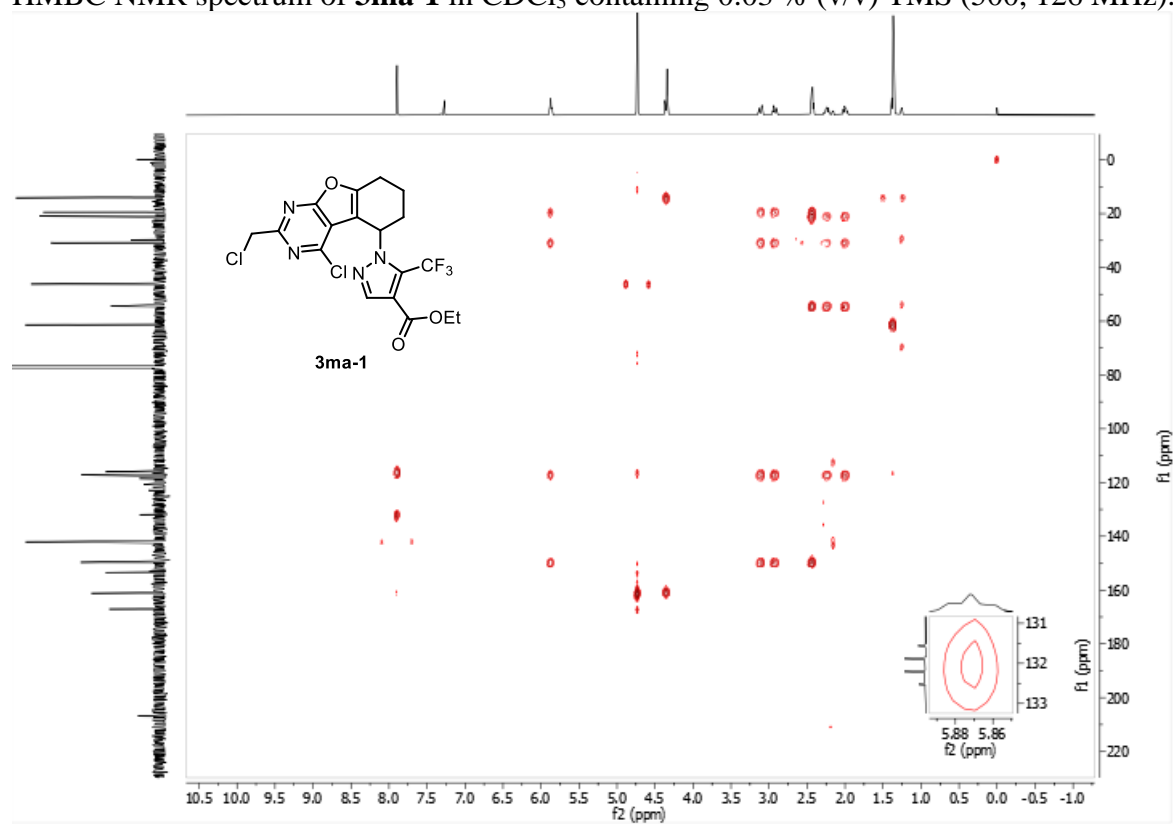
^{19}F NMR spectrum of **3ma-1** in CDCl_3 containing 0.03 % (v/v) TMS (377 MHz).



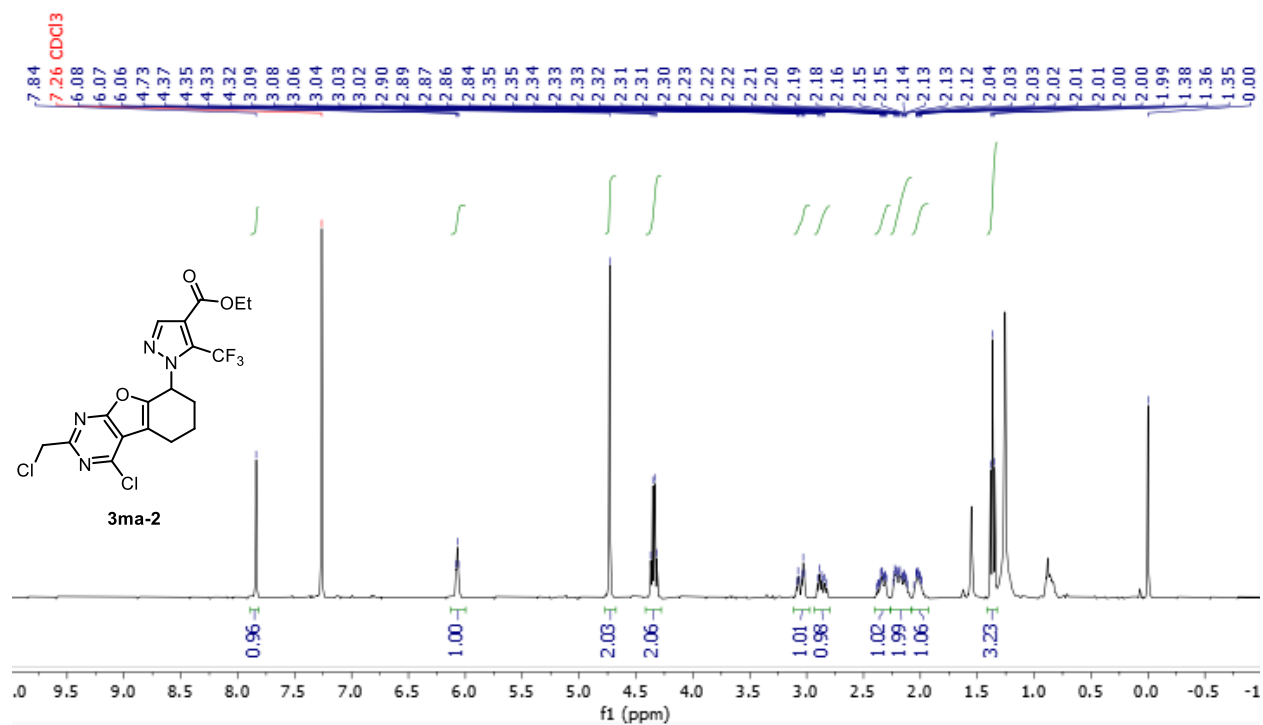
HSQC NMR spectrum of **3ma-1** in CDCl₃ containing 0.03 % (v/v) TMS (500, 126 MHz).



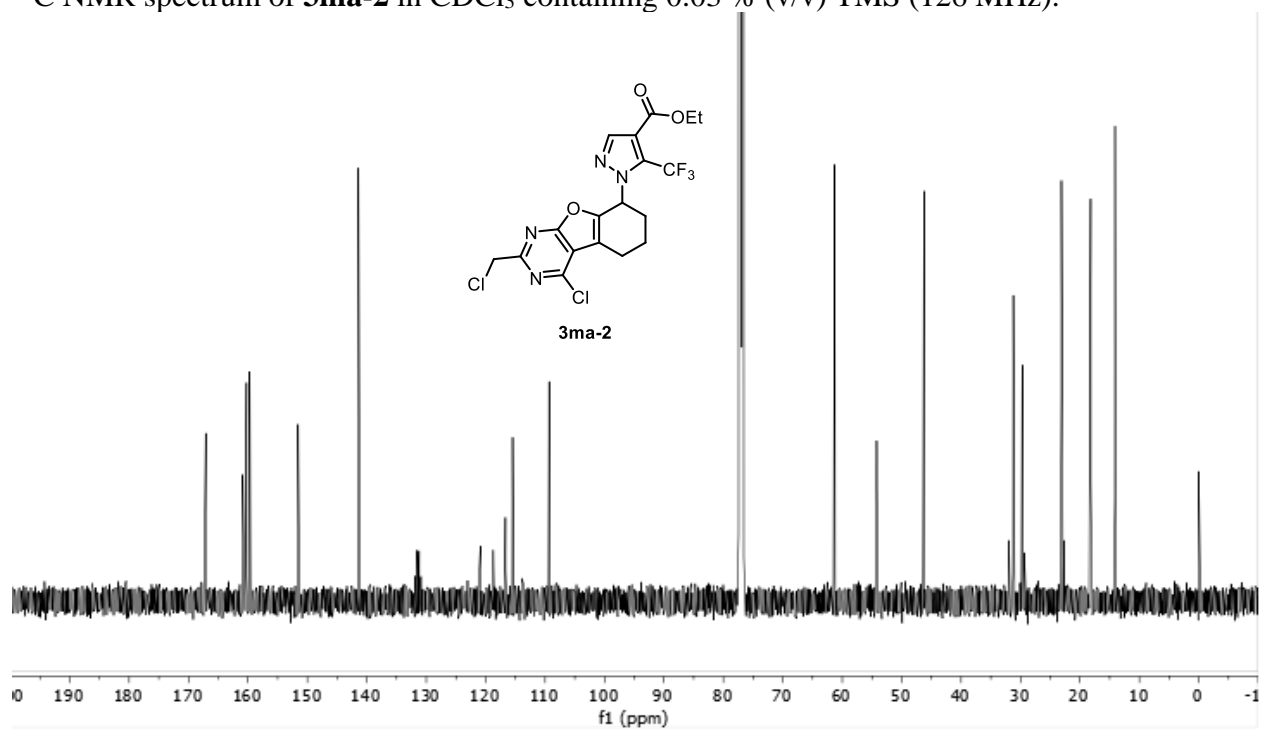
HMBC NMR spectrum of **3ma-1** in CDCl₃ containing 0.03 % (v/v) TMS (500, 126 MHz).



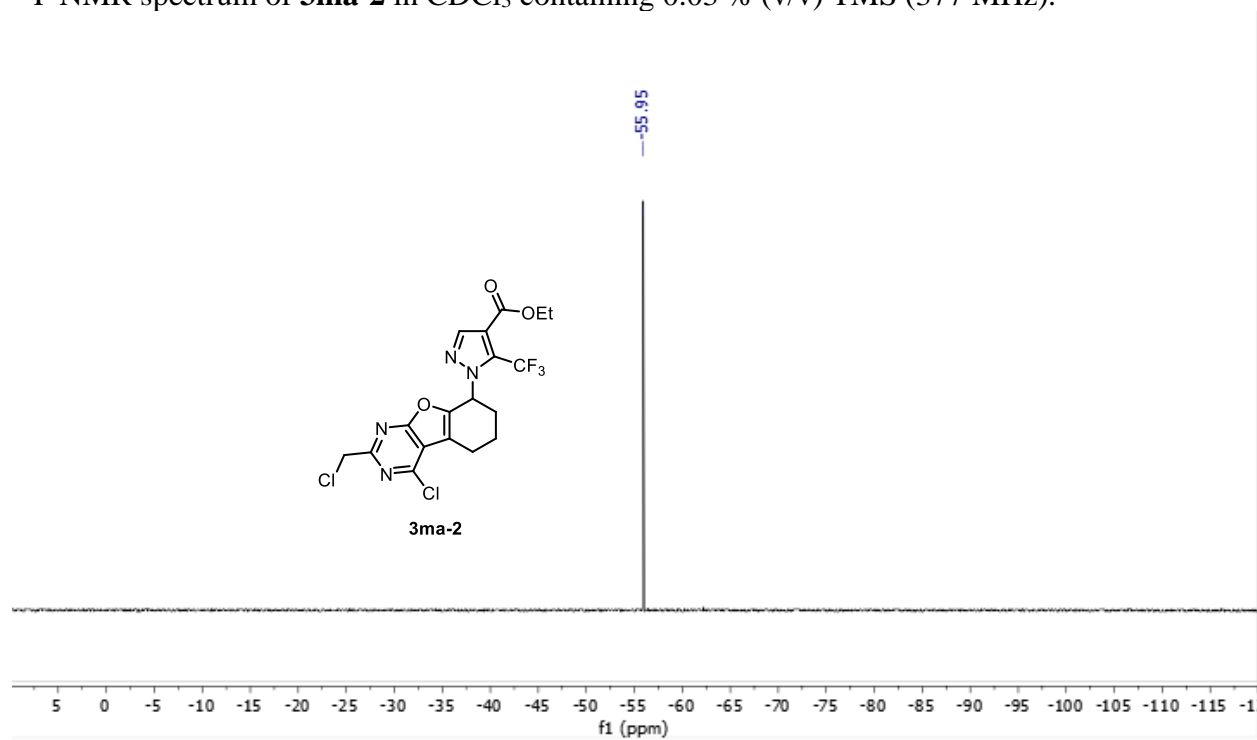
^1H NMR spectrum of **3ma-2** in CDCl_3 containing 0.03 % (v/v) TMS (500 MHz).



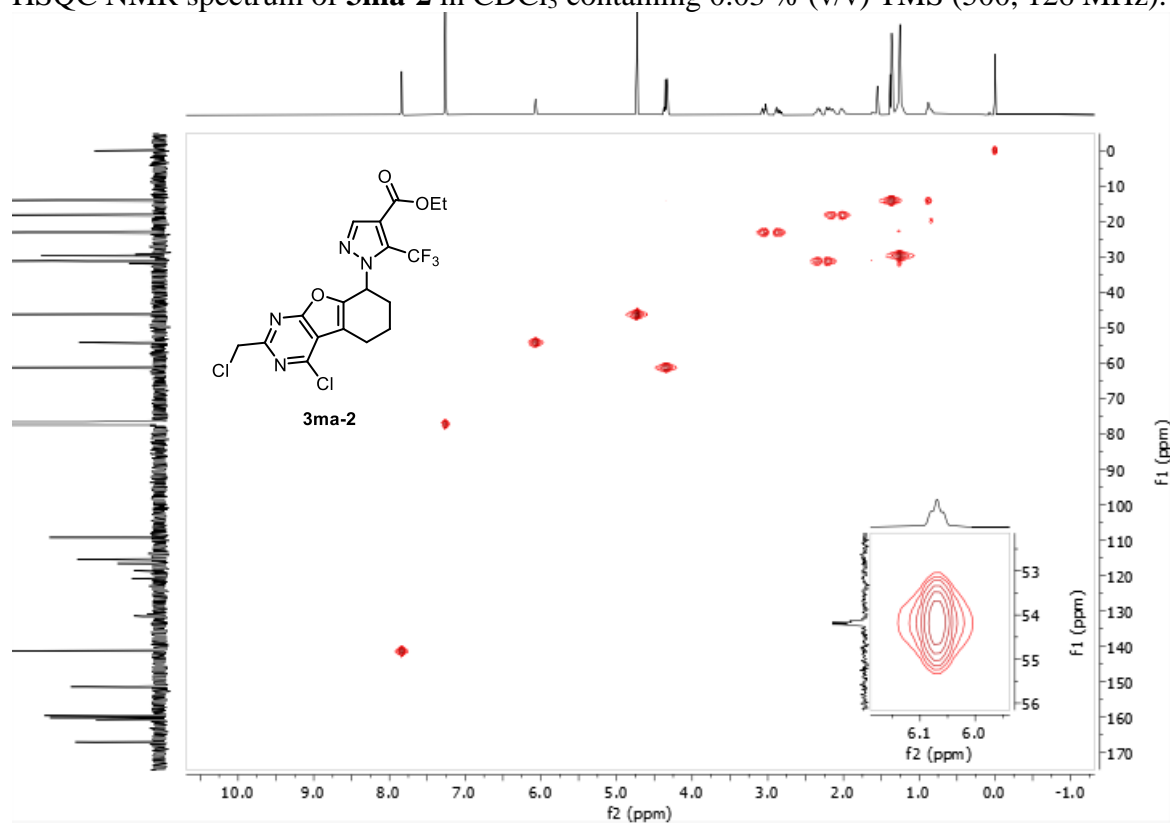
^{13}C NMR spectrum of **3ma-2** in CDCl_3 containing 0.03 % (v/v) TMS (126 MHz).



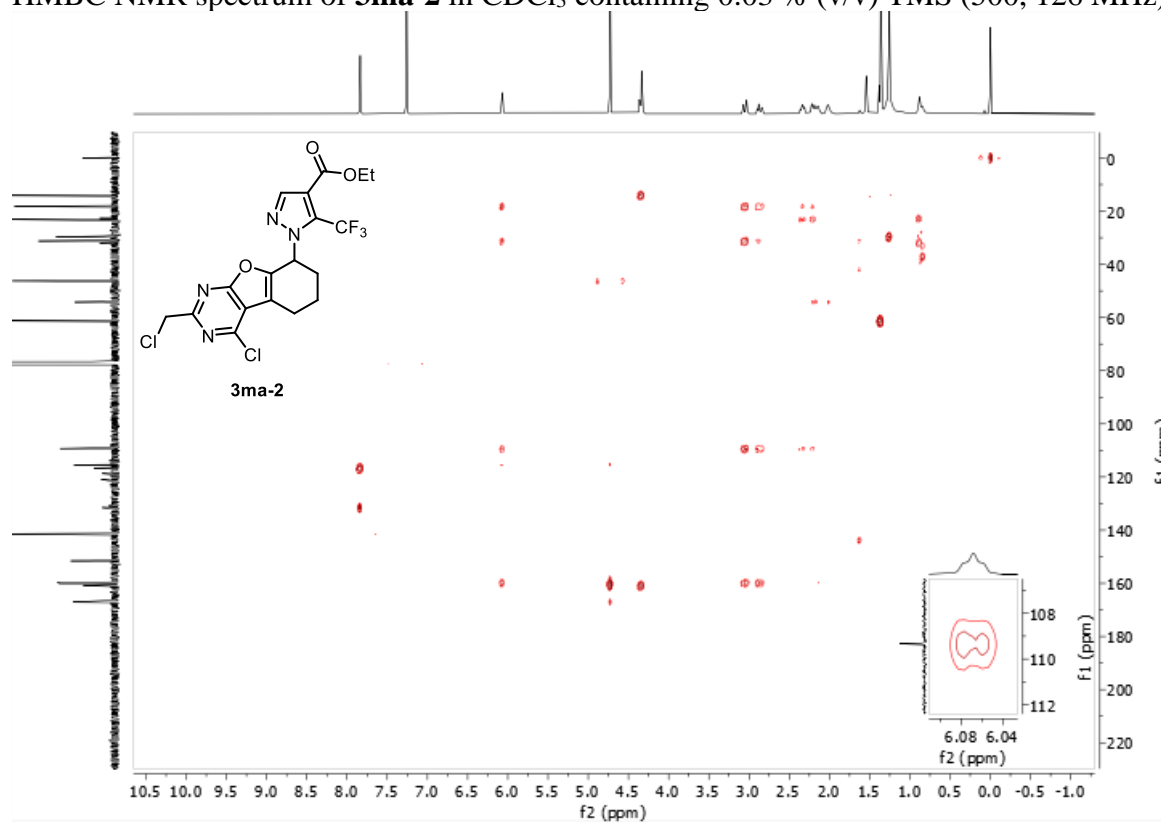
^{19}F NMR spectrum of **3ma-2** in CDCl_3 containing 0.03 % (v/v) TMS (377 MHz).



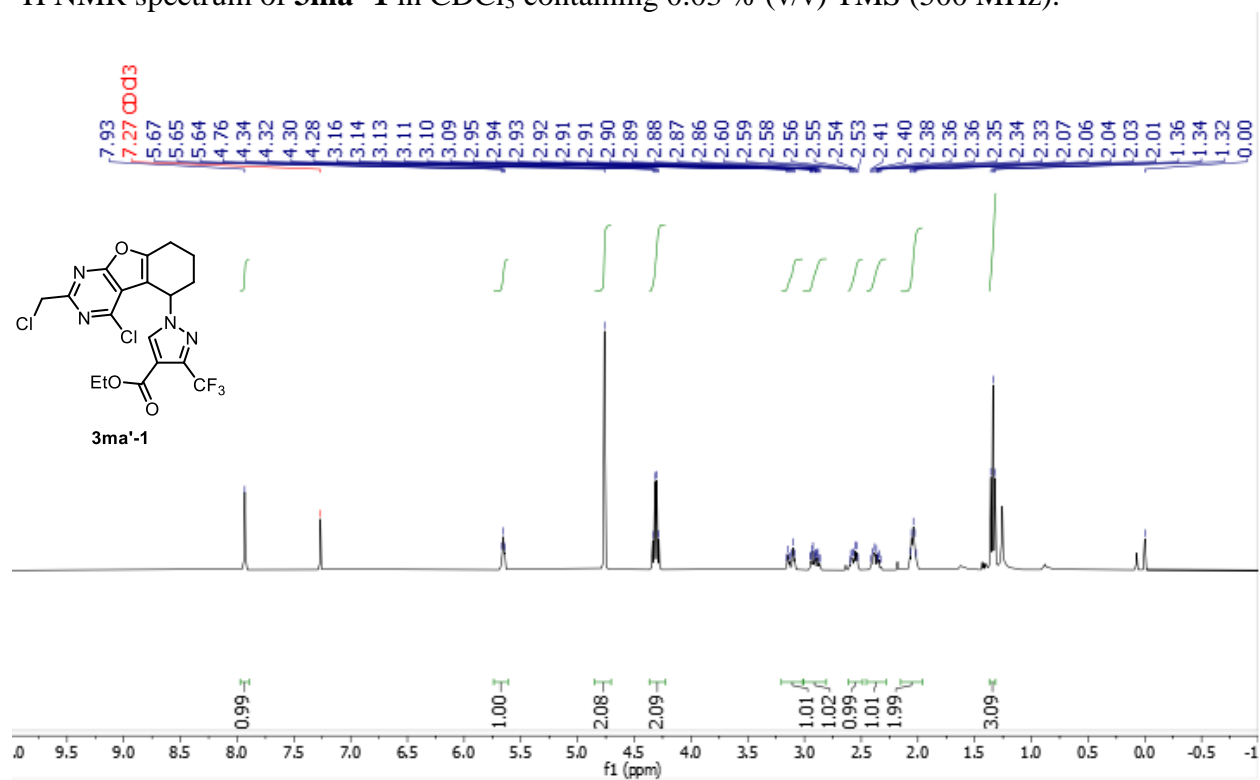
HSQC NMR spectrum of **3ma-2** in CDCl_3 containing 0.03 % (v/v) TMS (500, 126 MHz).



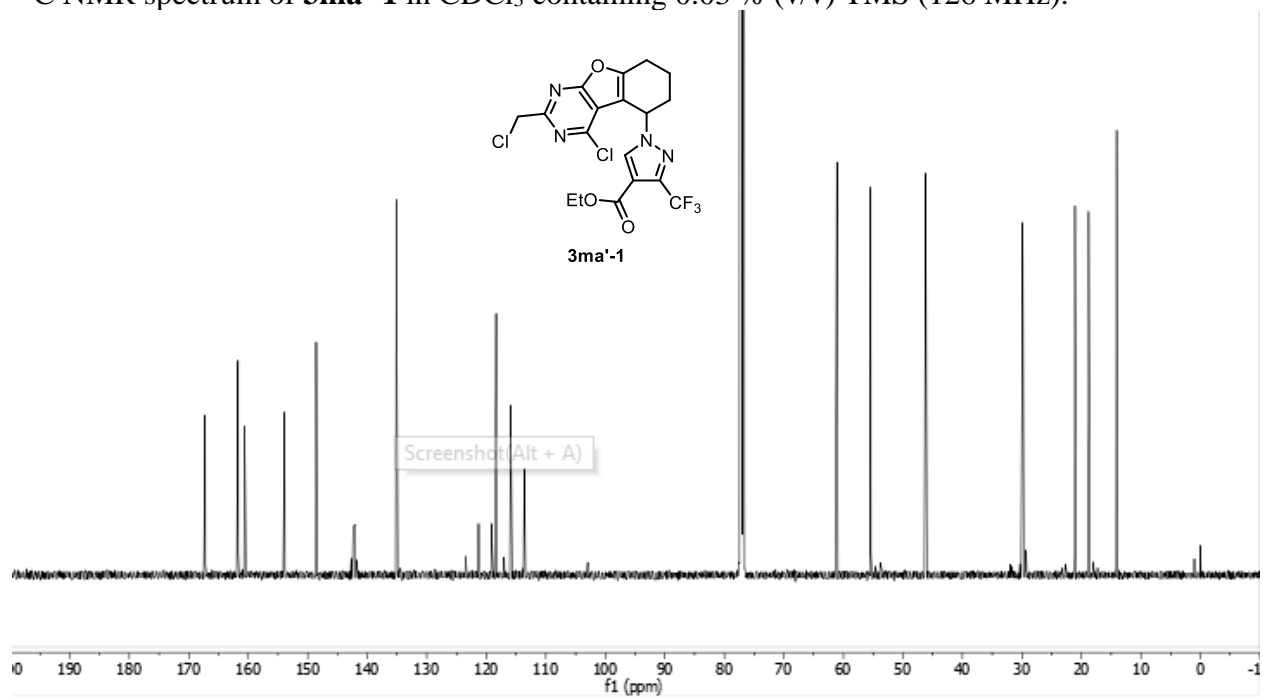
HMBC NMR spectrum of **3ma-2** in CDCl₃ containing 0.03 % (v/v) TMS (500, 126 MHz).



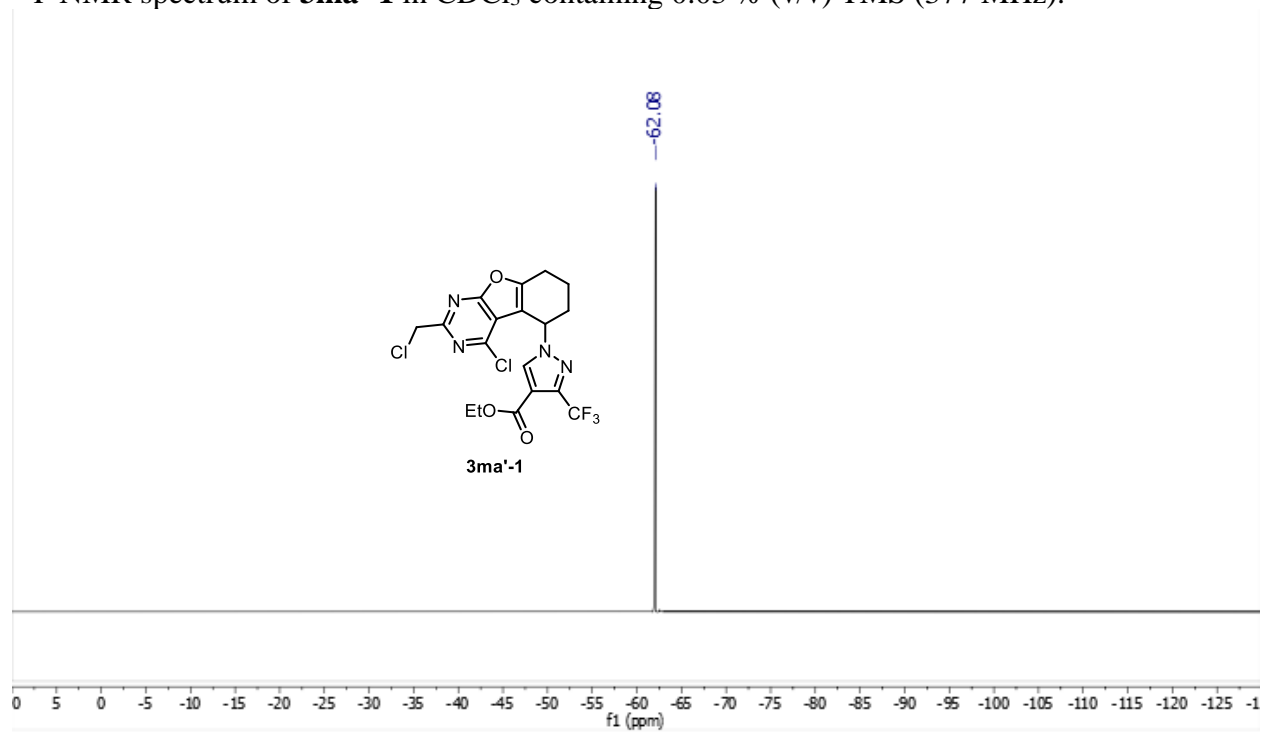
¹H NMR spectrum of **3ma'-1** in CDCl₃ containing 0.03 % (v/v) TMS (500 MHz).



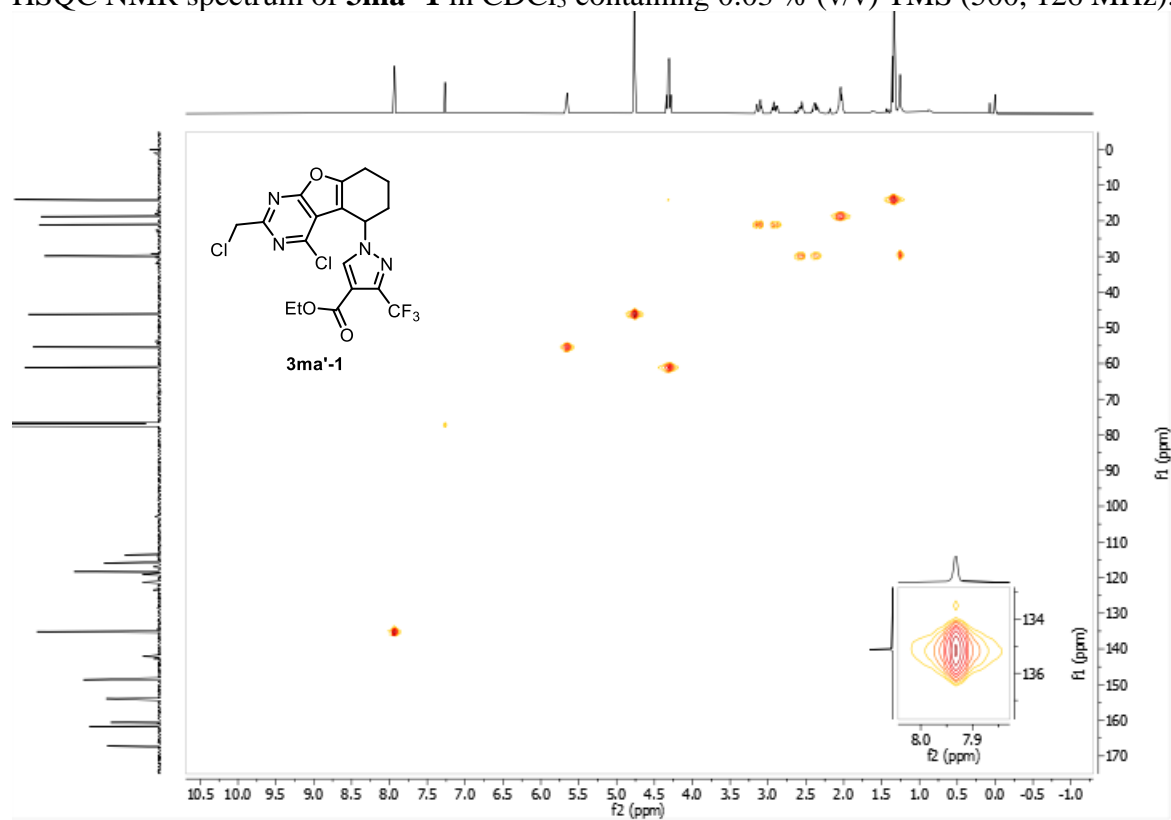
^{13}C NMR spectrum of **3ma'-1** in CDCl_3 containing 0.03 % (v/v) TMS (126 MHz).



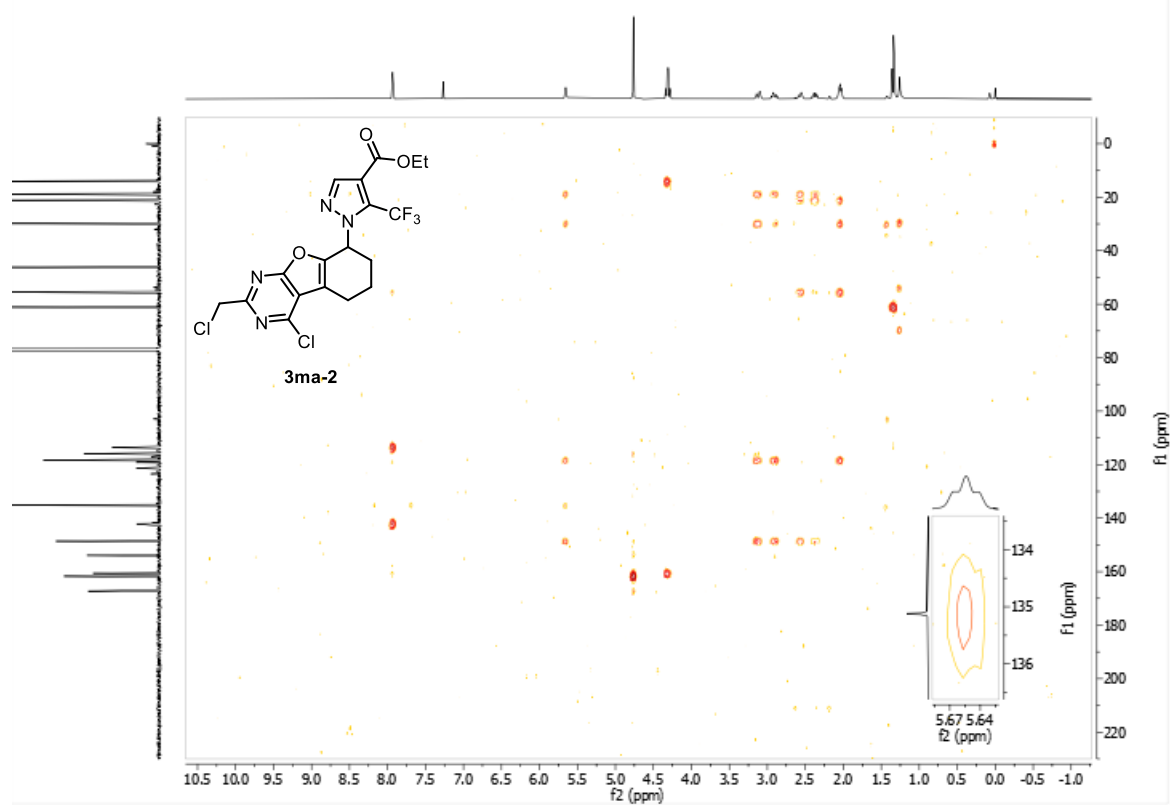
^{19}F NMR spectrum of **3ma'-1** in CDCl_3 containing 0.03 % (v/v) TMS (377 MHz).



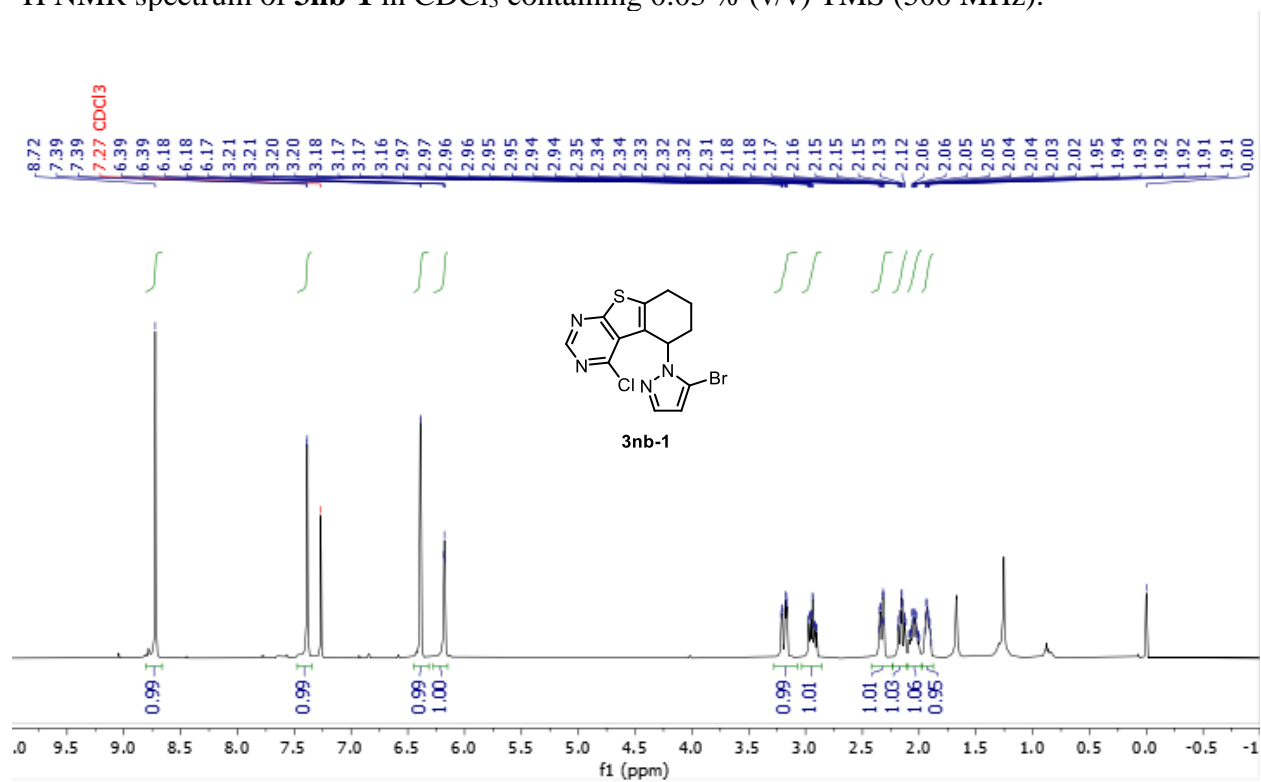
HSQC NMR spectrum of **3ma'-1** in CDCl₃ containing 0.03 % (v/v) TMS (500, 126 MHz).



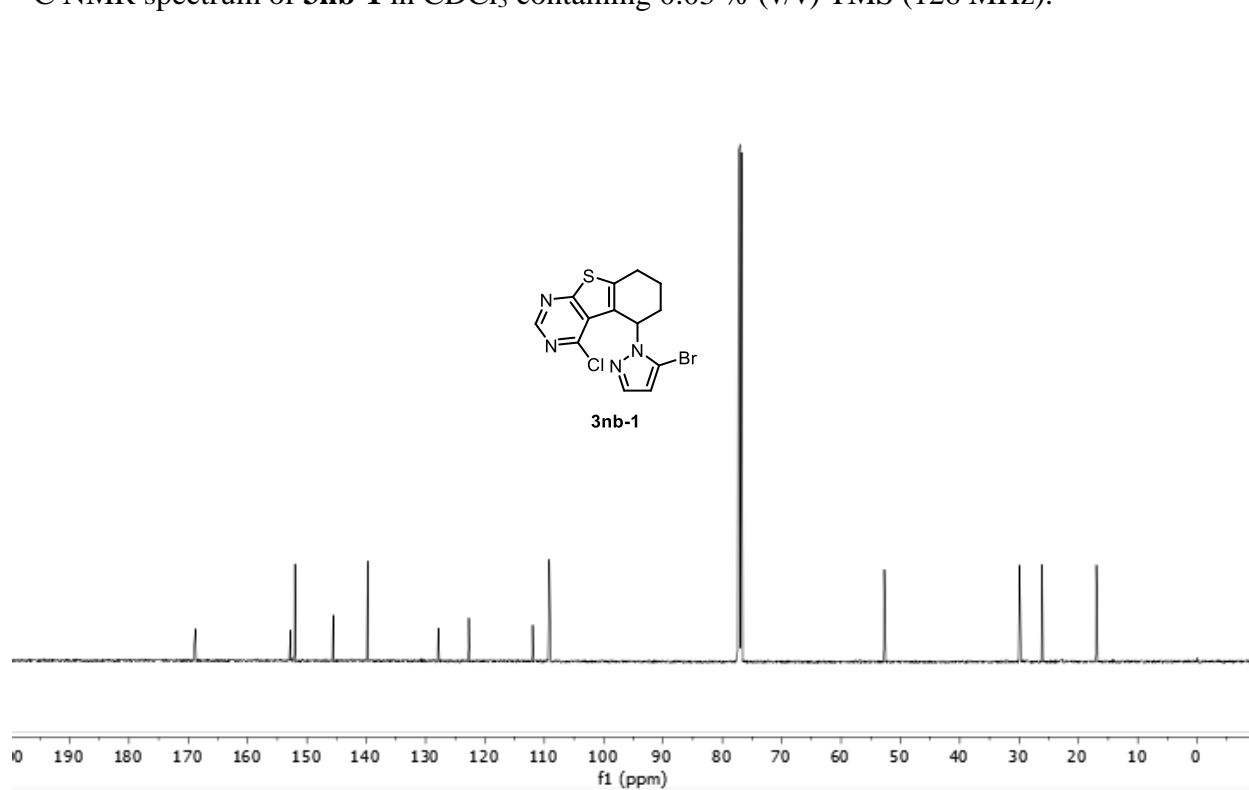
HMBC NMR spectrum of **3ma-1** in CDCl₃ containing 0.03 % (v/v) TMS (500, 126 MHz).



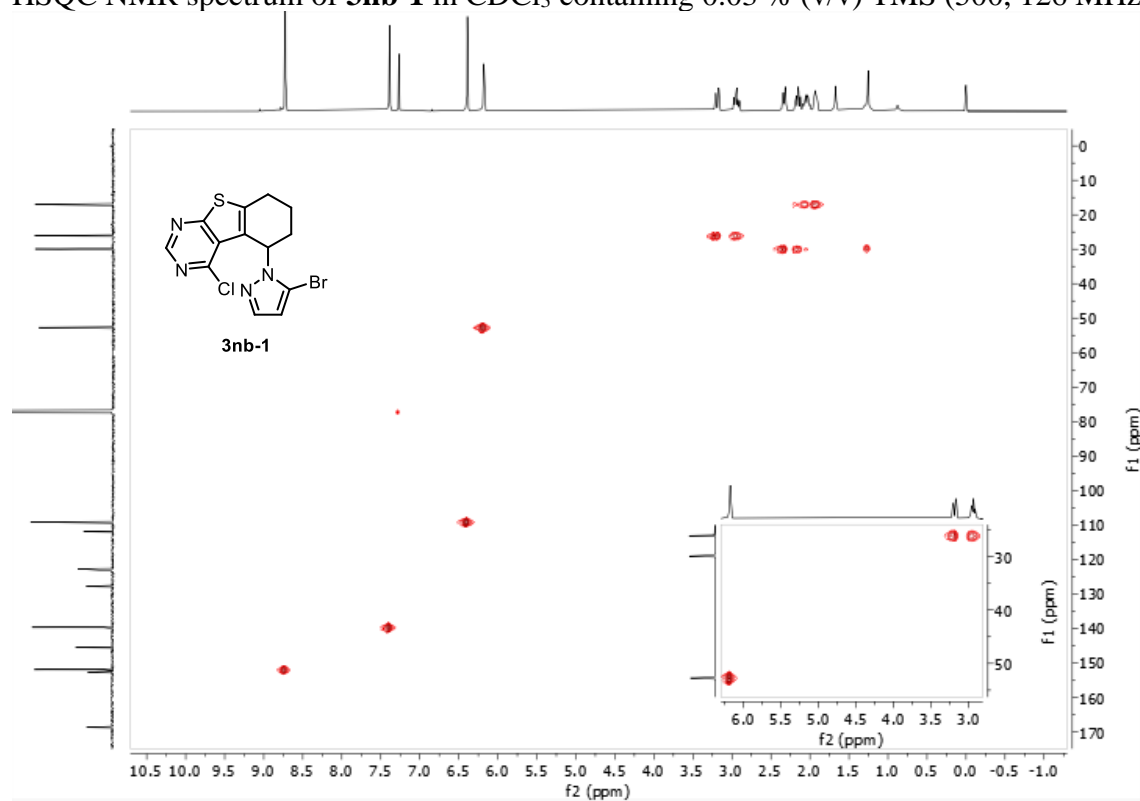
^1H NMR spectrum of **3nb-1** in CDCl_3 containing 0.03 % (v/v) TMS (500 MHz).



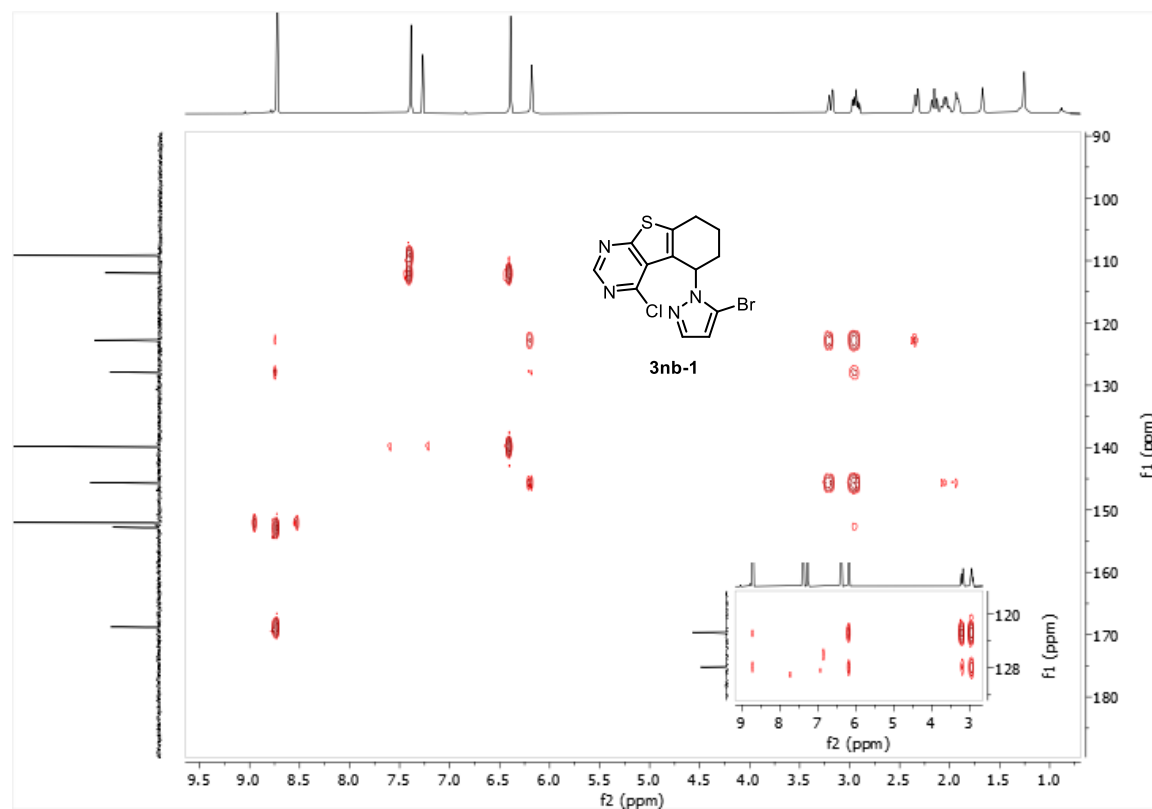
^{13}C NMR spectrum of **3nb-1** in CDCl_3 containing 0.03 % (v/v) TMS (126 MHz).



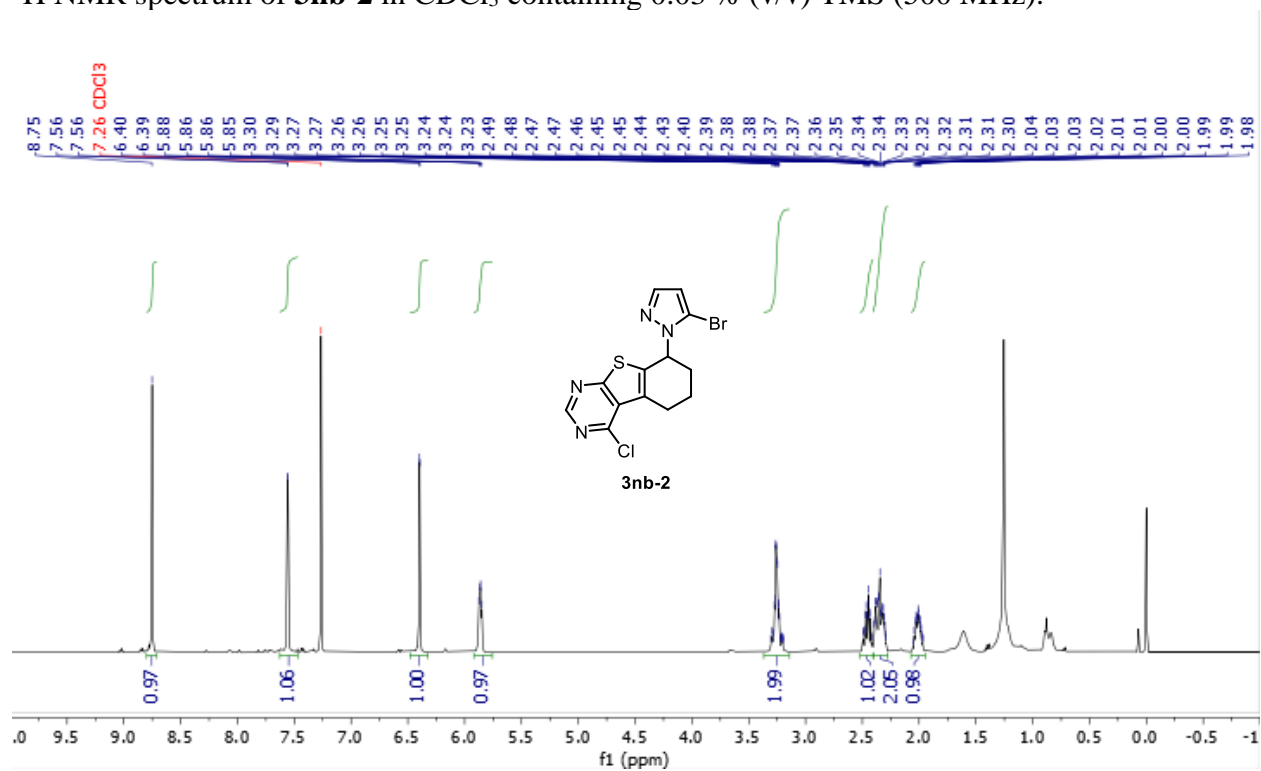
HSQC NMR spectrum of **3nb-1** in CDCl₃ containing 0.03 % (v/v) TMS (500, 126 MHz).



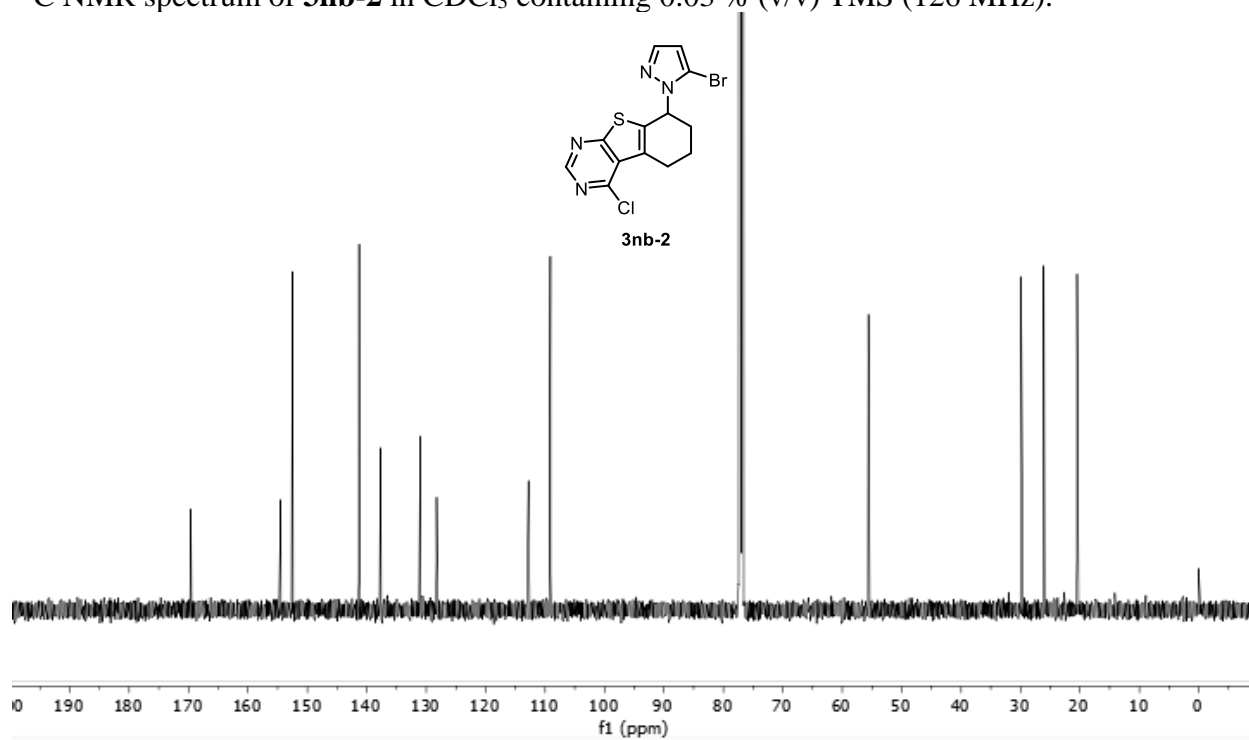
HMBC NMR spectrum of **3nb-1** in CDCl₃ containing 0.03 % (v/v) TMS (500, 126 MHz).



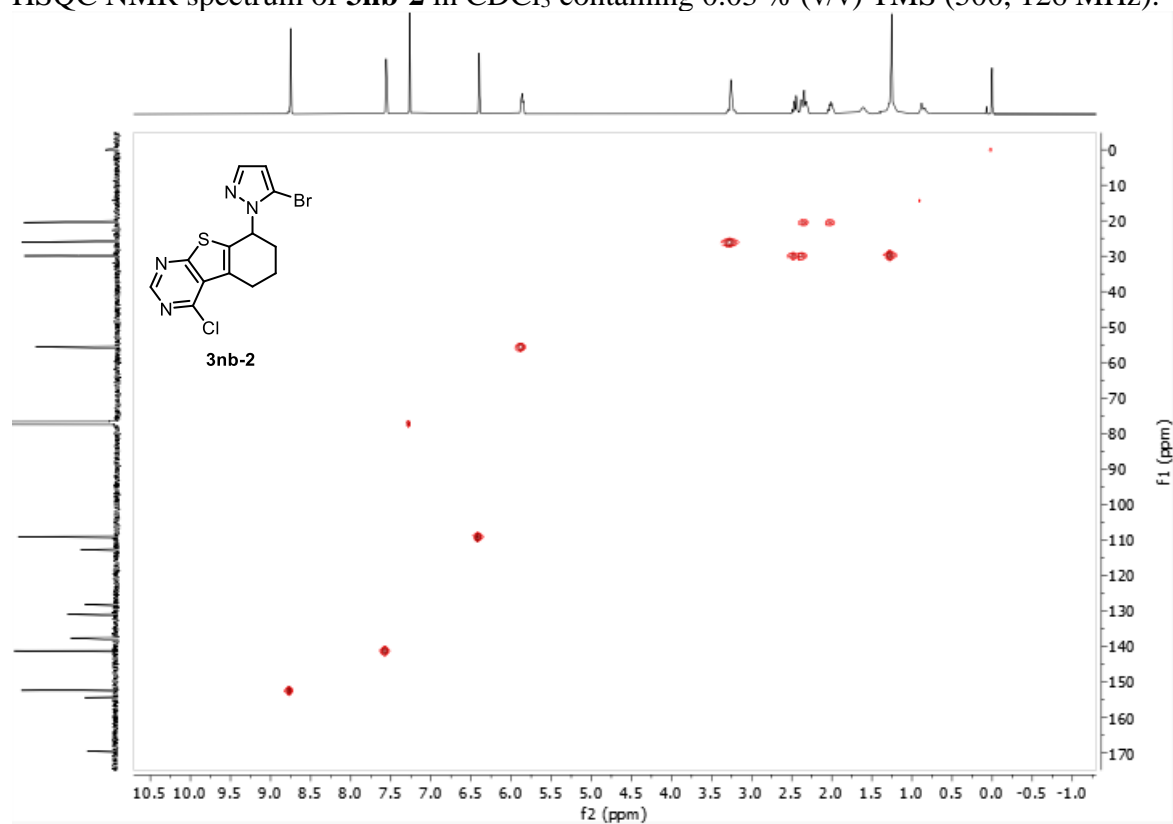
^1H NMR spectrum of **3nb-2** in CDCl_3 containing 0.03 % (v/v) TMS (500 MHz).



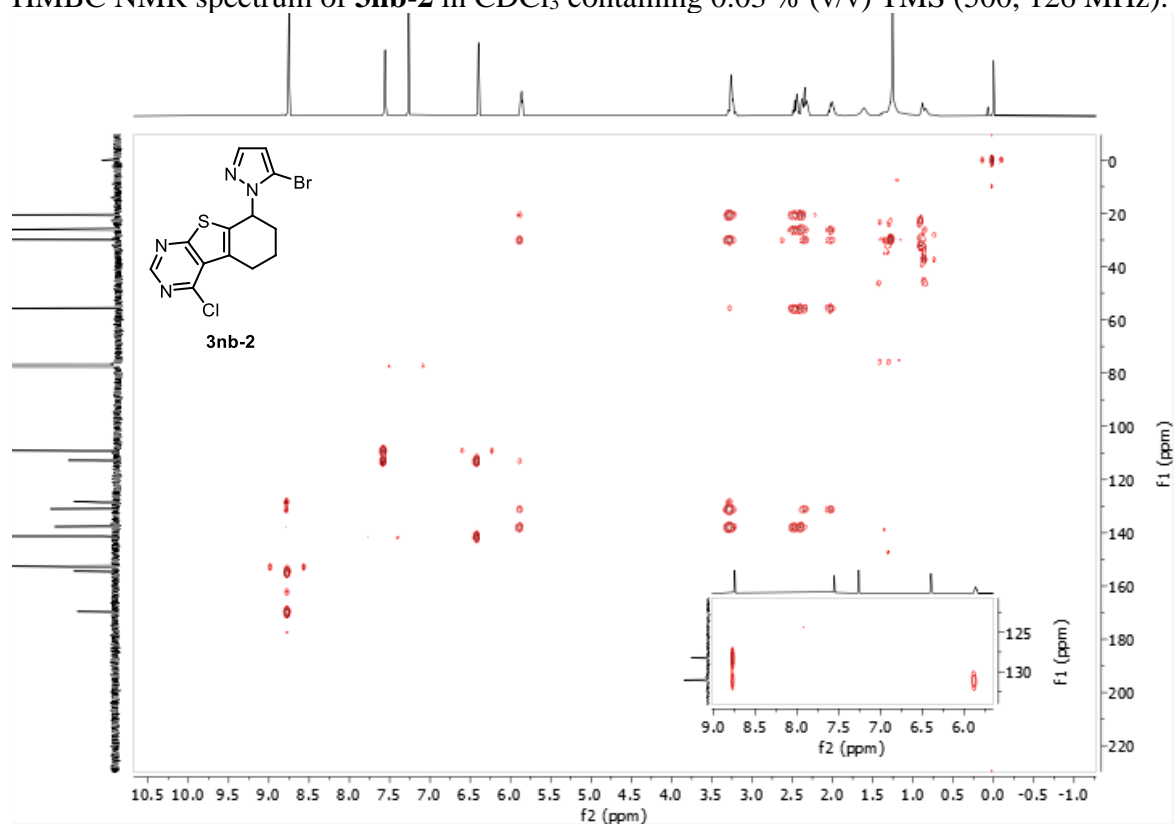
^{13}C NMR spectrum of **3nb-2** in CDCl_3 containing 0.03 % (v/v) TMS (126 MHz).



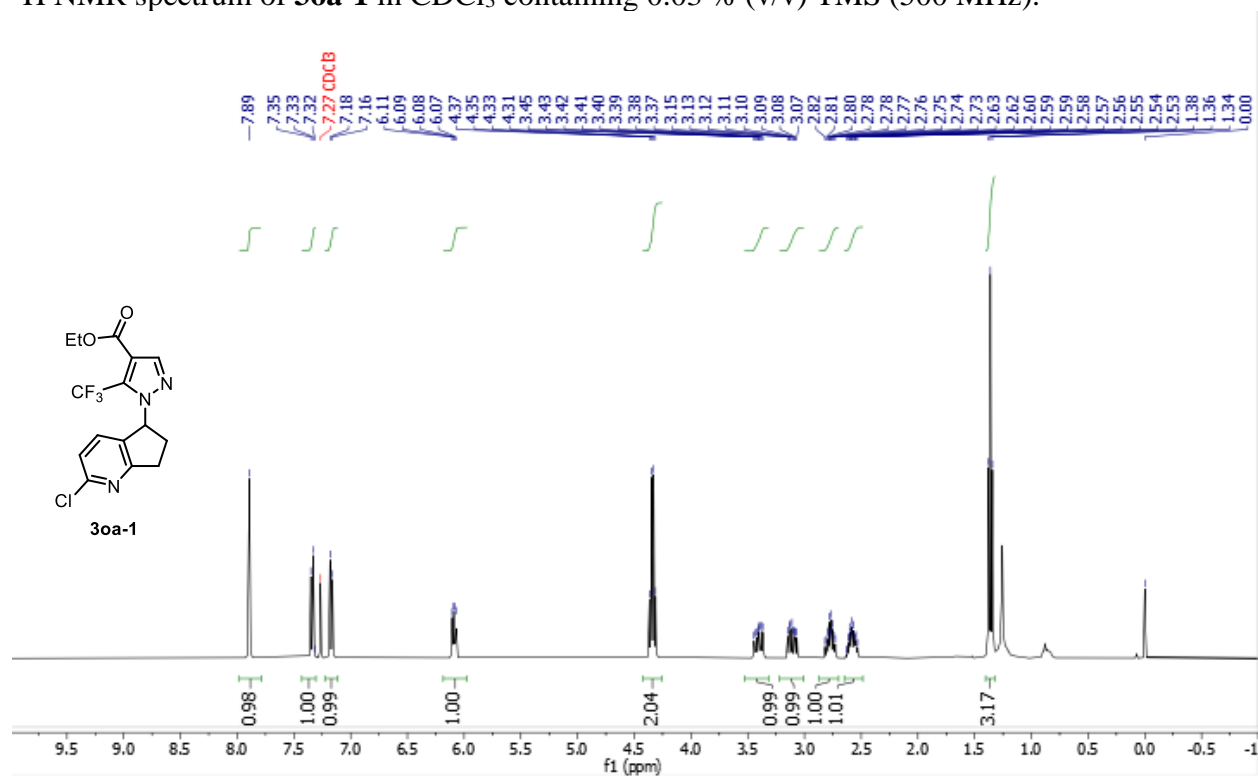
HSQC NMR spectrum of **3nb-2** in CDCl₃ containing 0.03 % (v/v) TMS (500, 126 MHz).



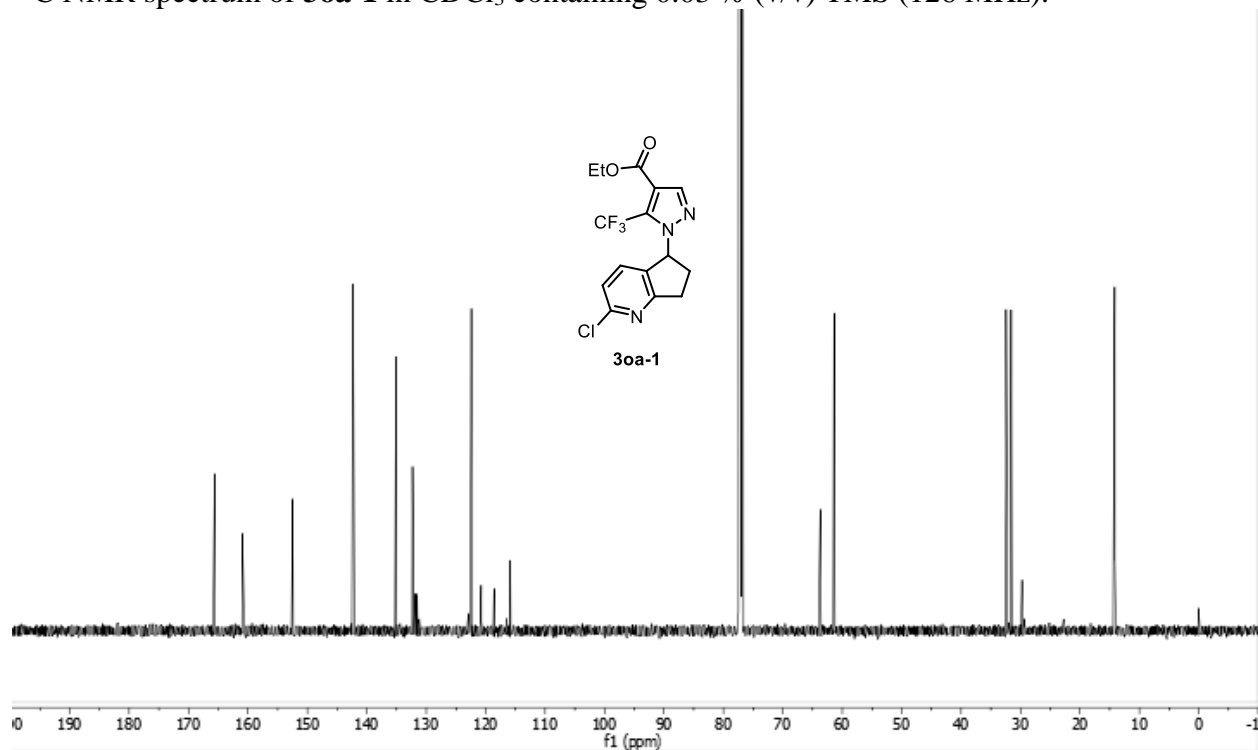
HMBC NMR spectrum of **3nb-2** in CDCl₃ containing 0.03 % (v/v) TMS (500, 126 MHz).



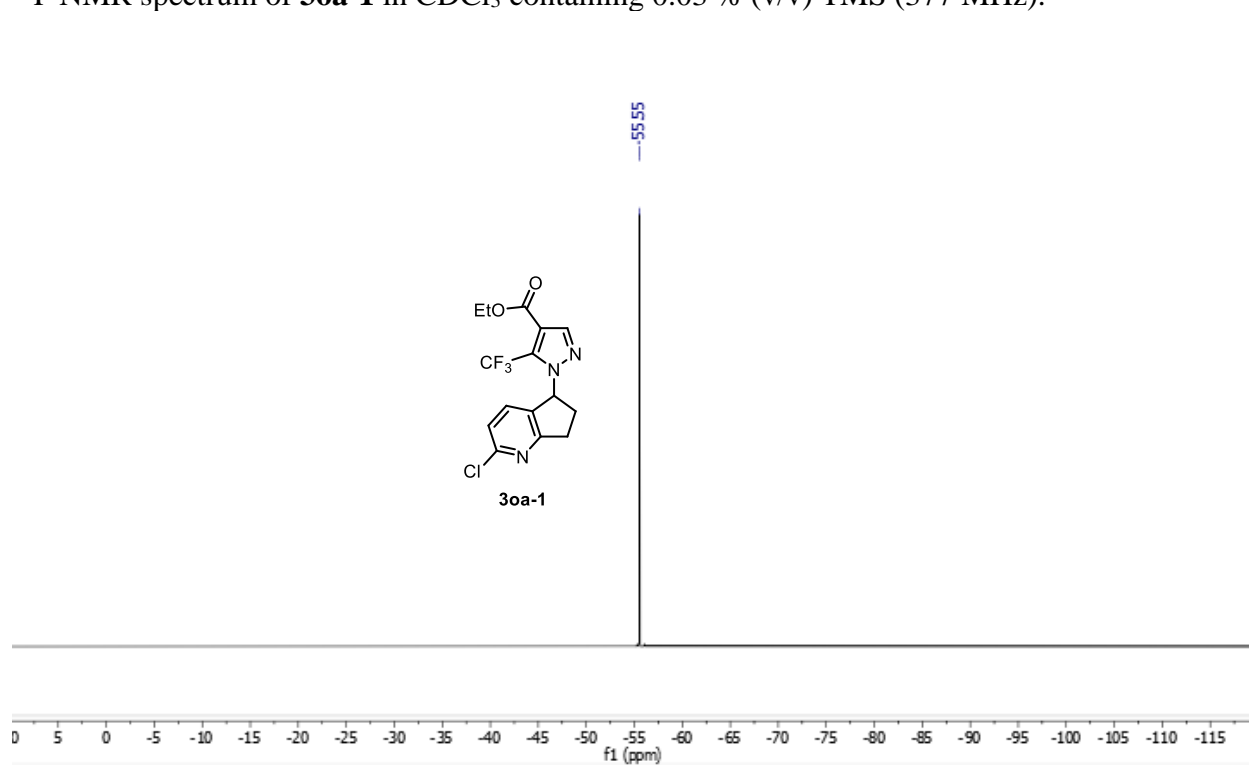
^1H NMR spectrum of **3oa-1** in CDCl_3 containing 0.03 % (v/v) TMS (500 MHz).



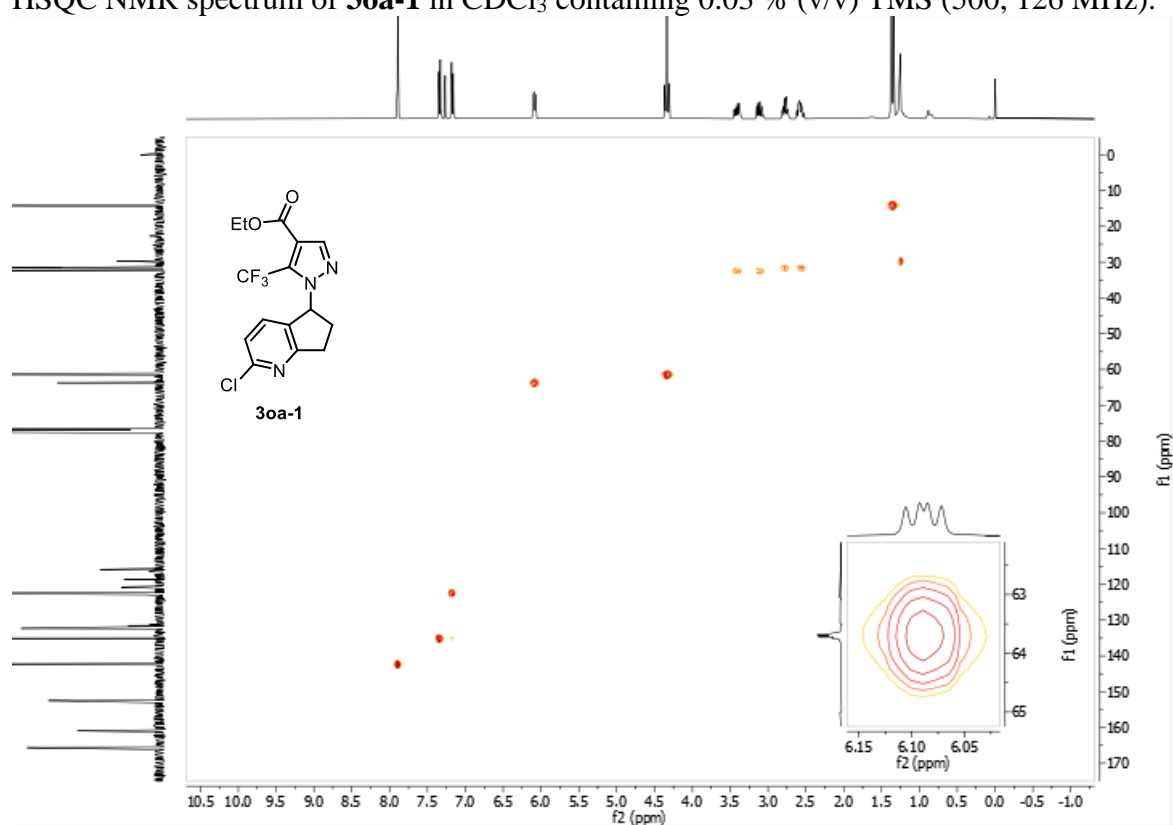
^{13}C NMR spectrum of **3oa-1** in CDCl_3 containing 0.03 % (v/v) TMS (126 MHz).



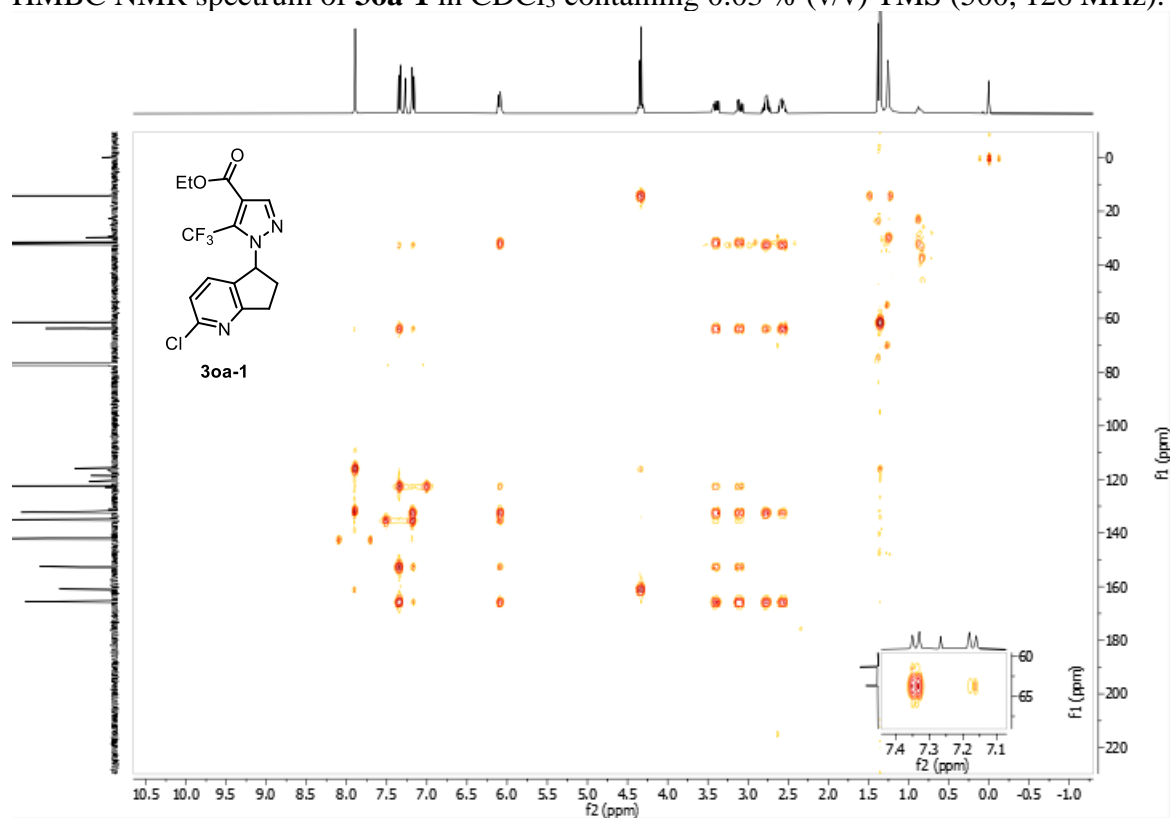
^{19}F NMR spectrum of **3oa-1** in CDCl_3 containing 0.03 % (v/v) TMS (377 MHz).



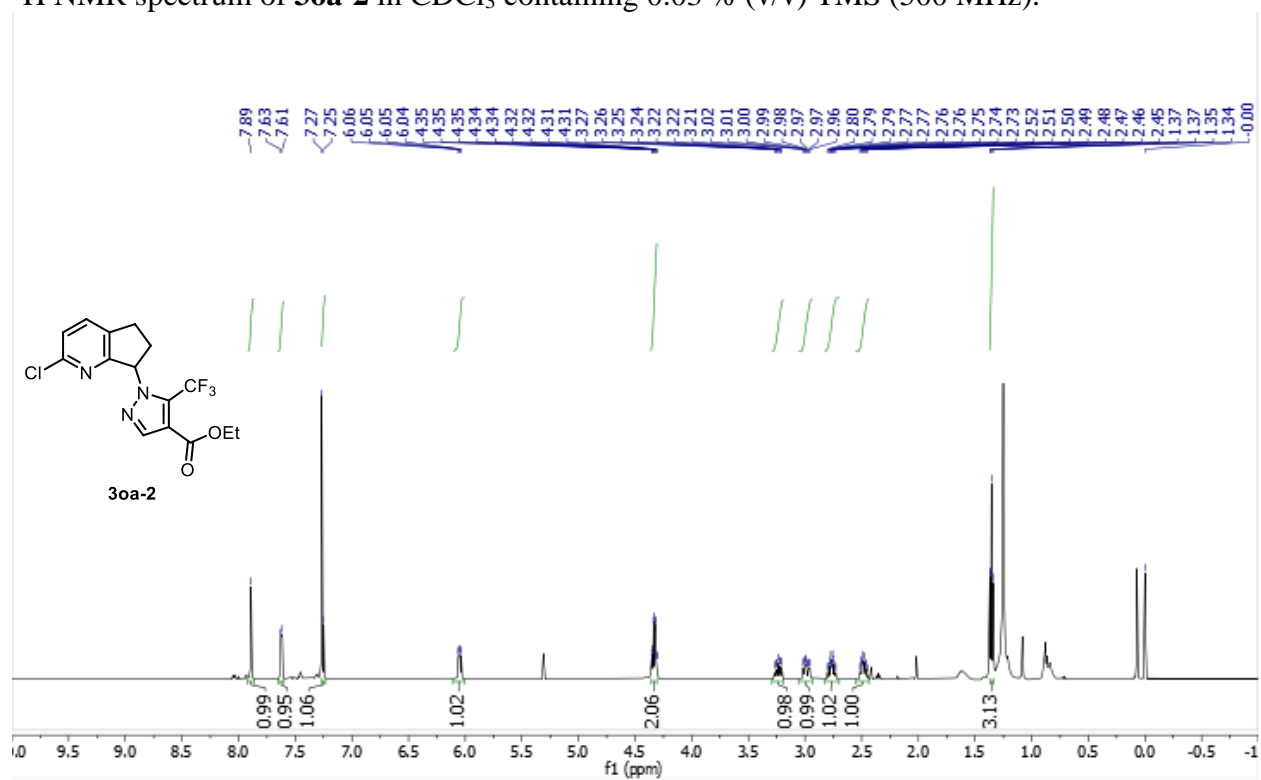
HSQC NMR spectrum of **3oa-1** in CDCl_3 containing 0.03 % (v/v) TMS (500, 126 MHz).



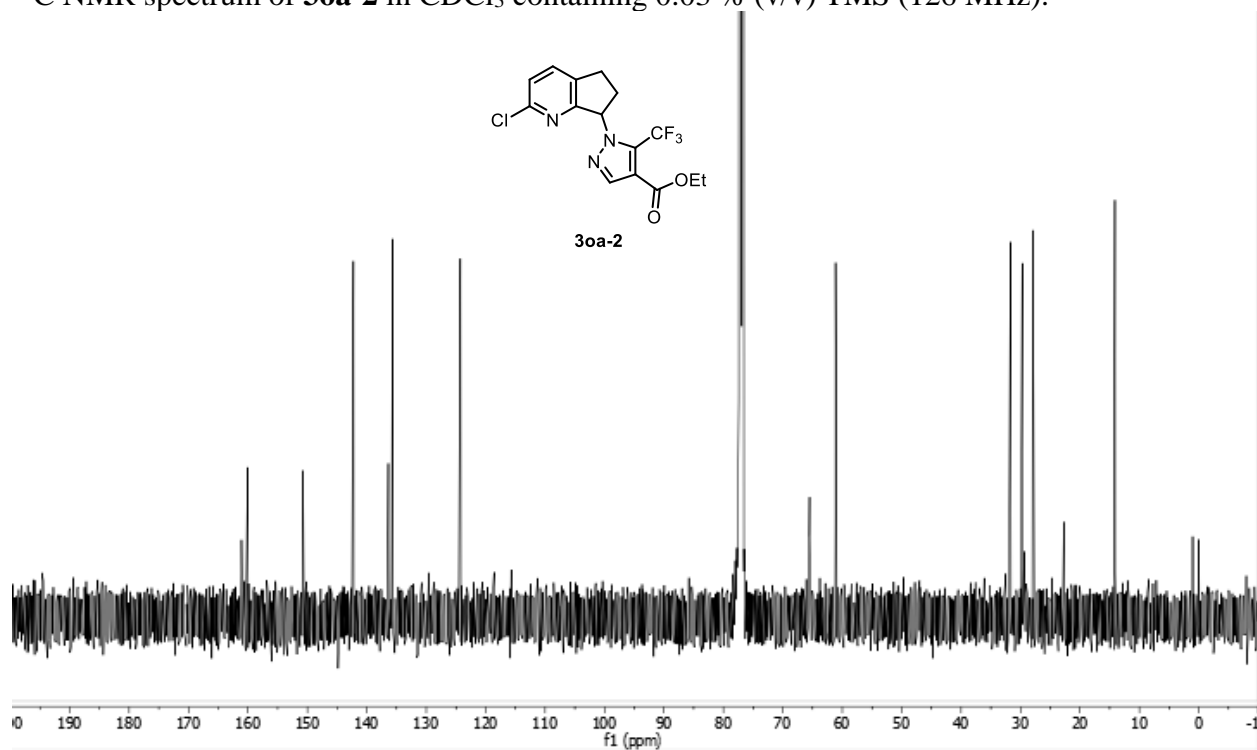
HMBC NMR spectrum of **3oa-1** in CDCl₃ containing 0.03 % (v/v) TMS (500, 126 MHz).



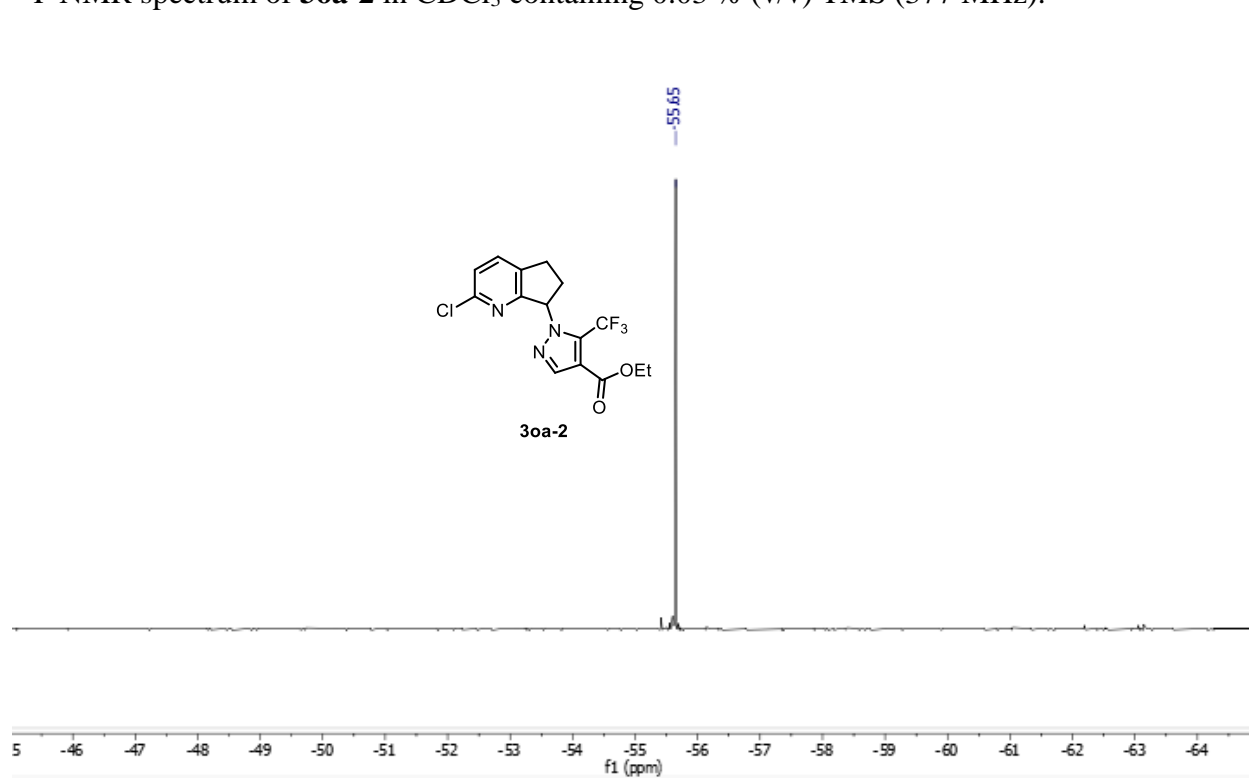
¹H NMR spectrum of **3oa-2** in CDCl₃ containing 0.03 % (v/v) TMS (500 MHz).



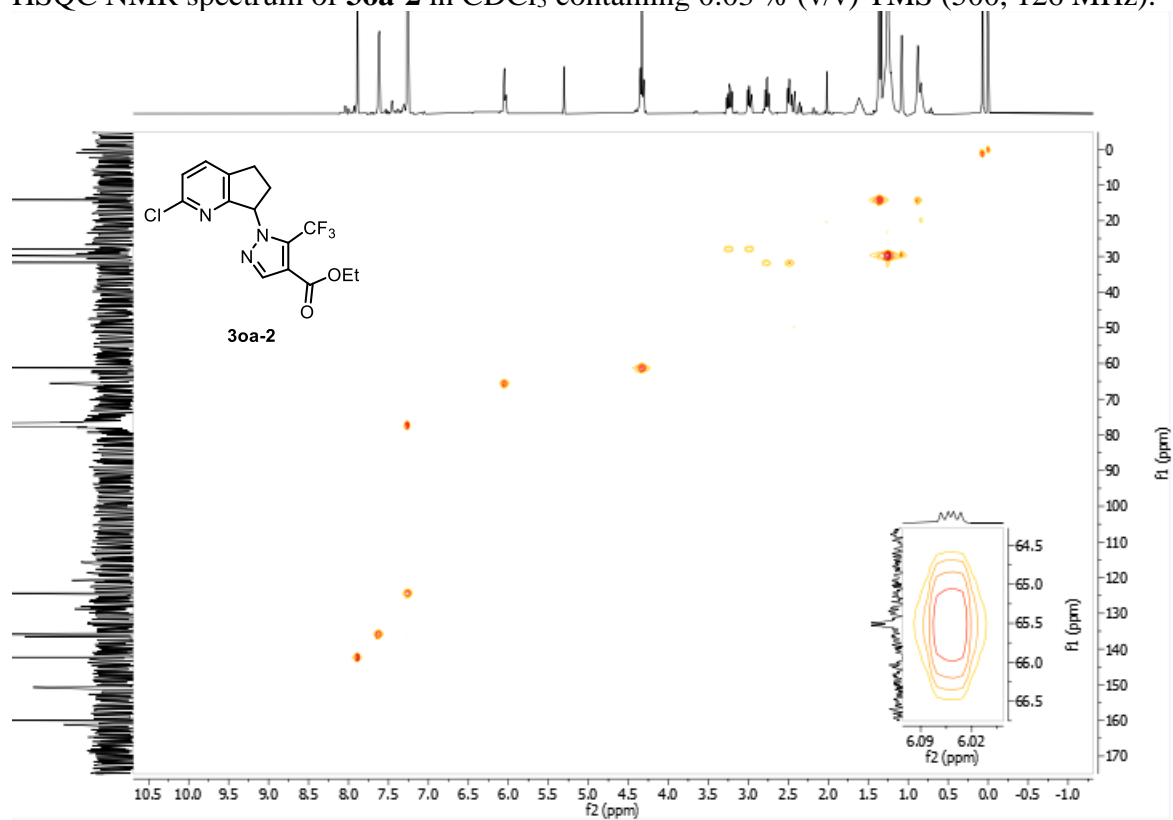
^{13}C NMR spectrum of **3oa-2** in CDCl_3 containing 0.03 % (v/v) TMS (126 MHz).



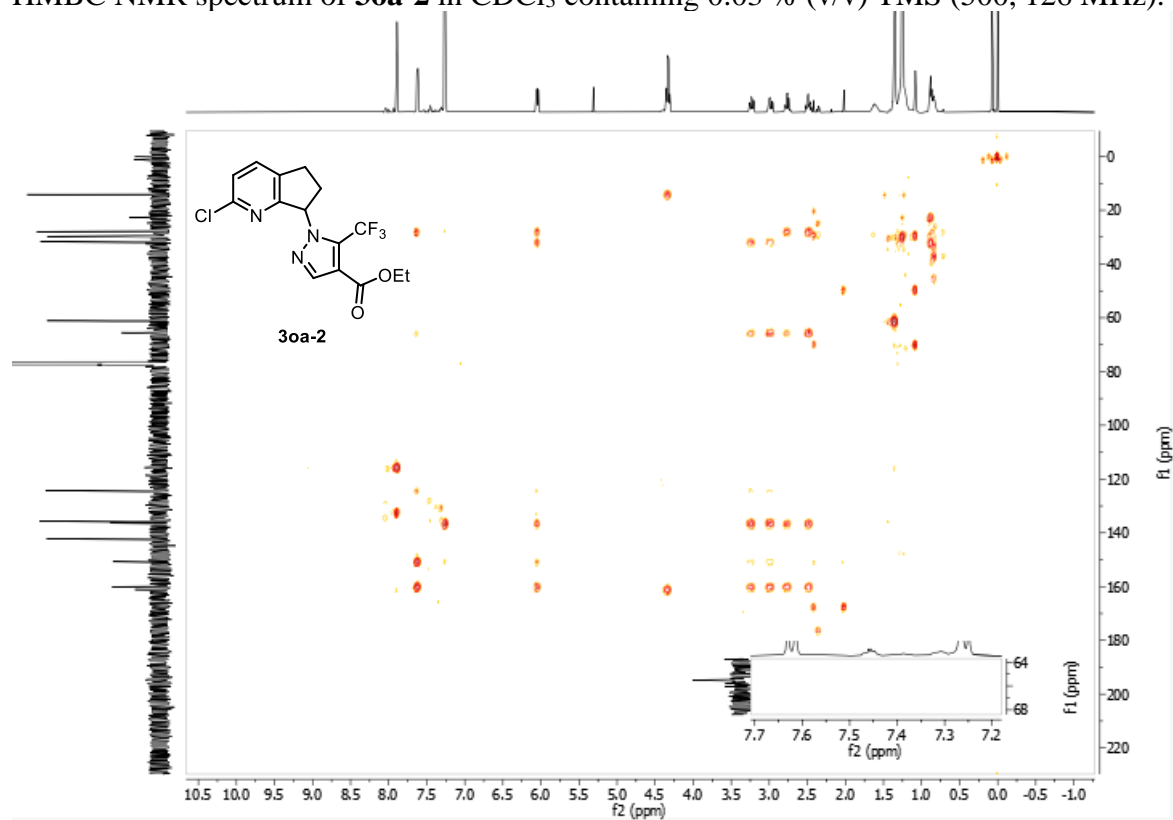
^{19}F NMR spectrum of **3oa-2** in CDCl_3 containing 0.03 % (v/v) TMS (377 MHz).



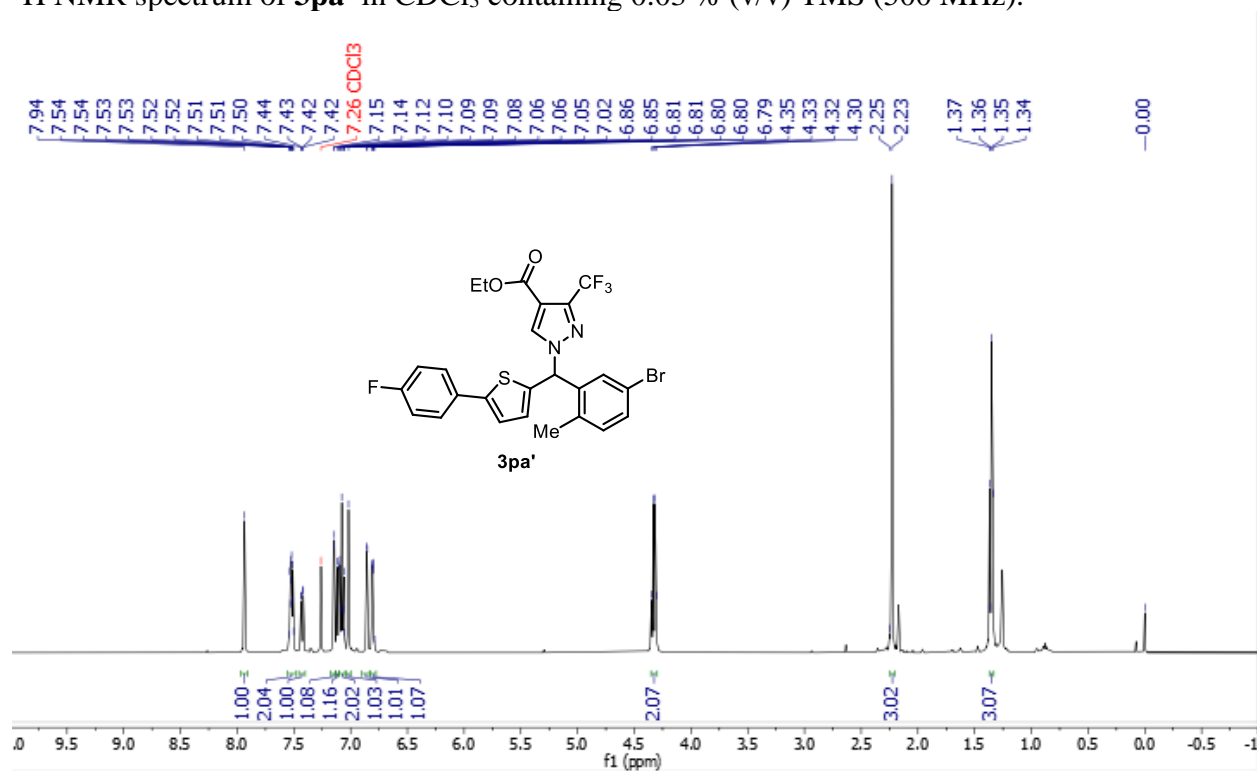
HSQC NMR spectrum of **3oa-2** in CDCl₃ containing 0.03 % (v/v) TMS (500, 126 MHz).



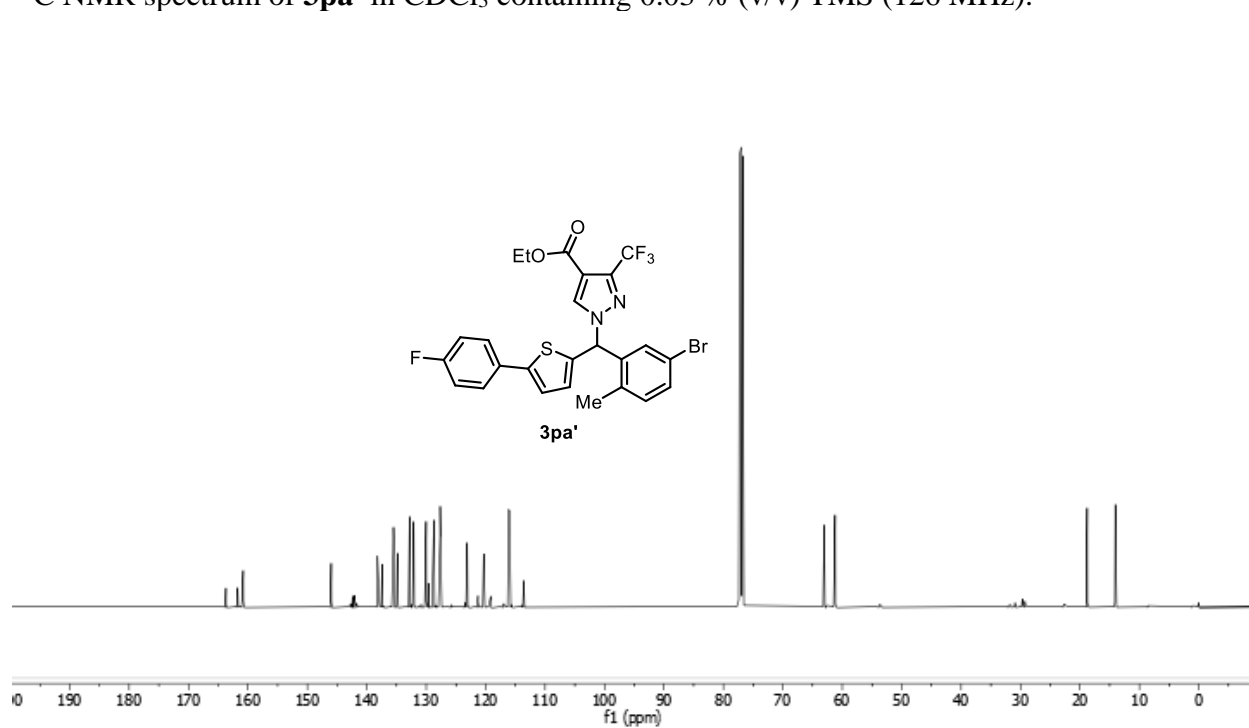
HMBC NMR spectrum of **3oa-2** in CDCl₃ containing 0.03 % (v/v) TMS (500, 126 MHz).



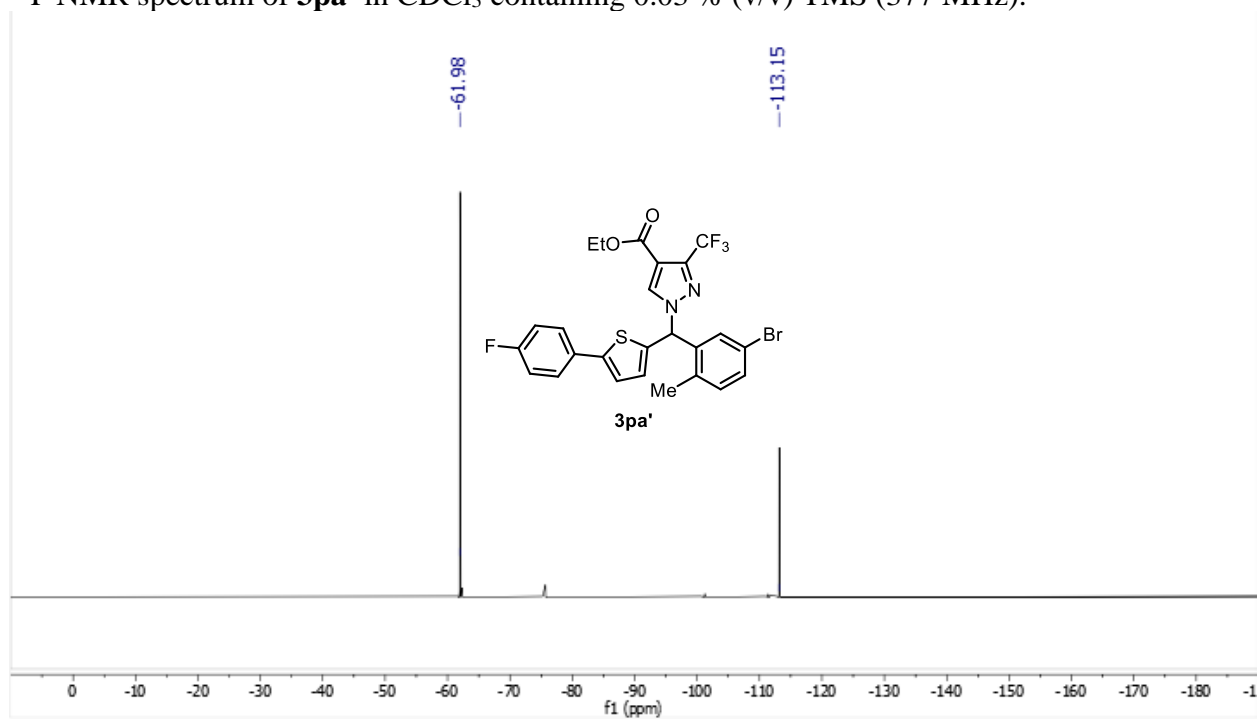
^1H NMR spectrum of **3pa'** in CDCl_3 containing 0.03 % (v/v) TMS (500 MHz).



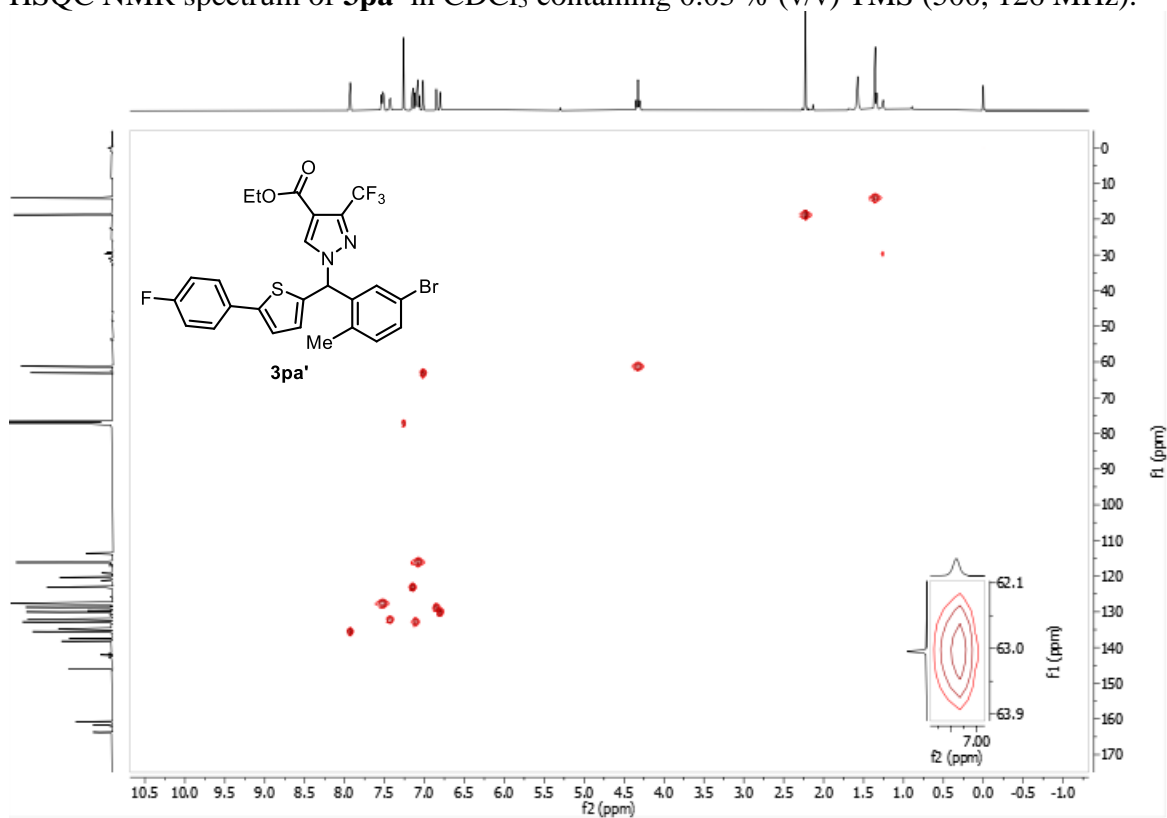
^{13}C NMR spectrum of **3pa'** in CDCl_3 containing 0.03 % (v/v) TMS (126 MHz).



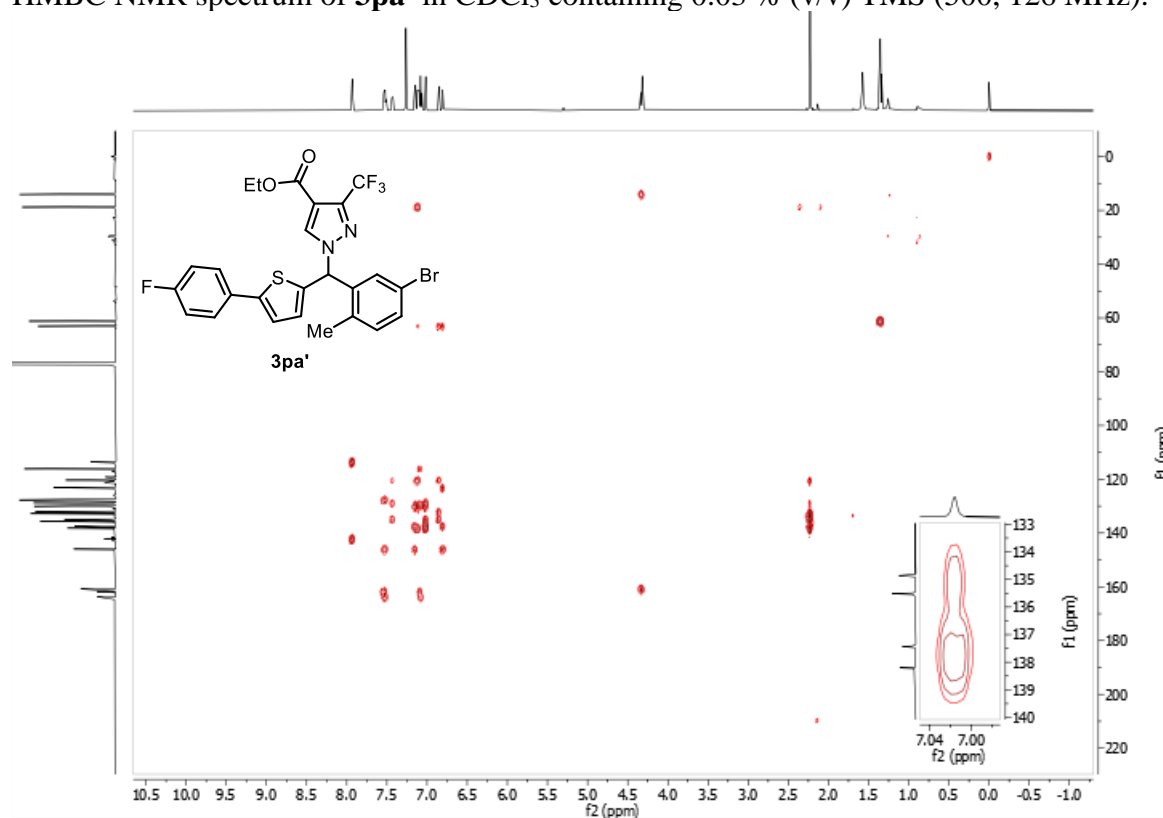
^{19}F NMR spectrum of **3pa'** in CDCl_3 containing 0.03 % (v/v) TMS (377 MHz).



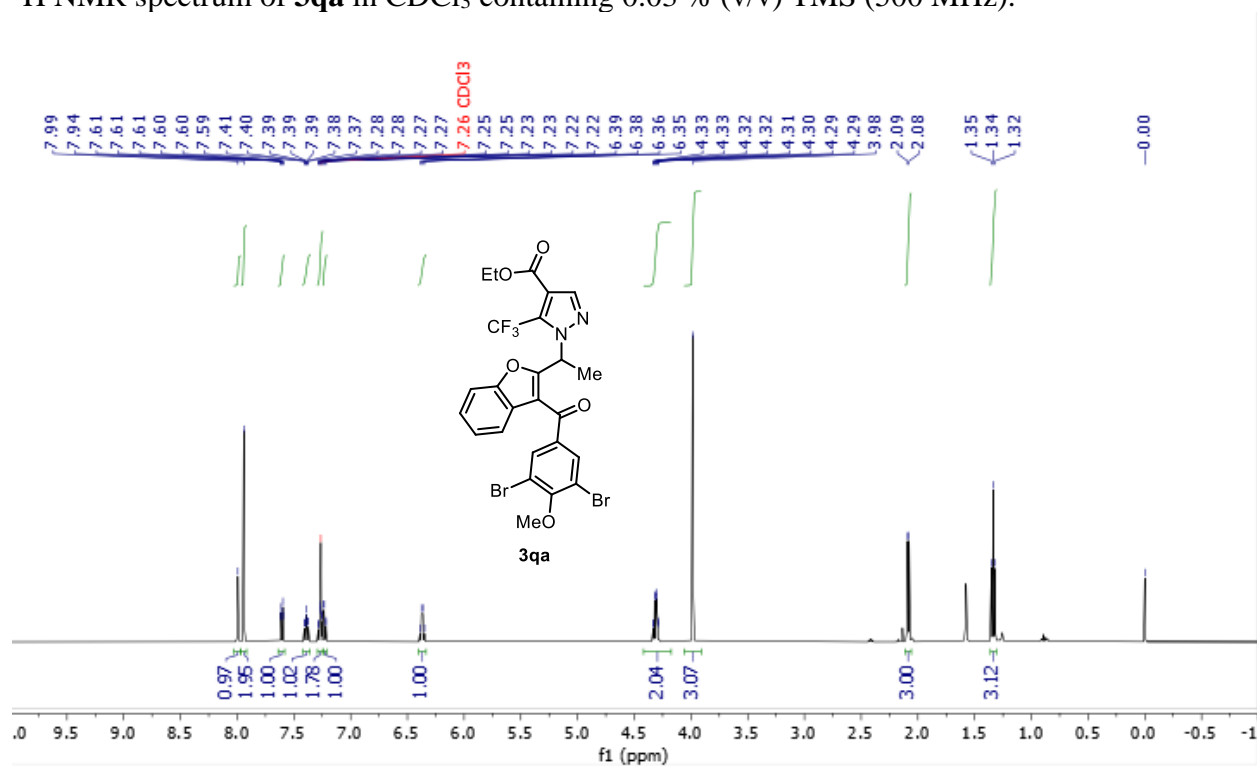
HSQC NMR spectrum of **3pa'** in CDCl_3 containing 0.03 % (v/v) TMS (500, 126 MHz).



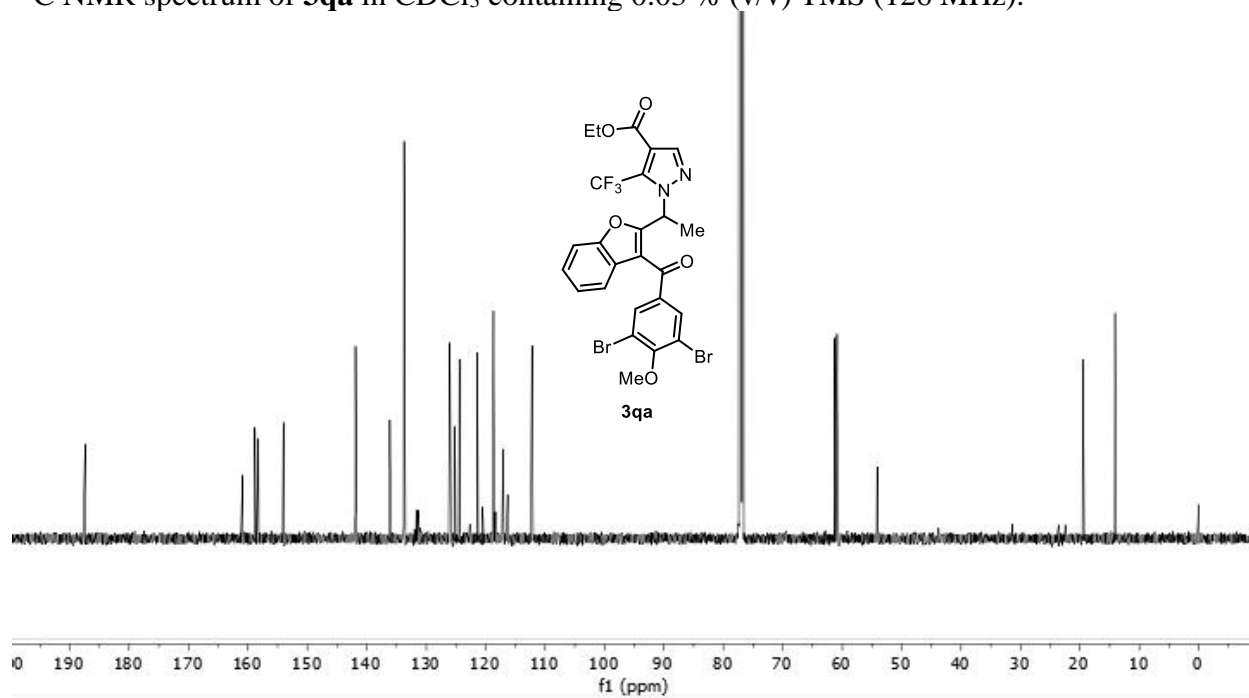
HMBC NMR spectrum of **3pa'** in CDCl₃ containing 0.03 % (v/v) TMS (500, 126 MHz).



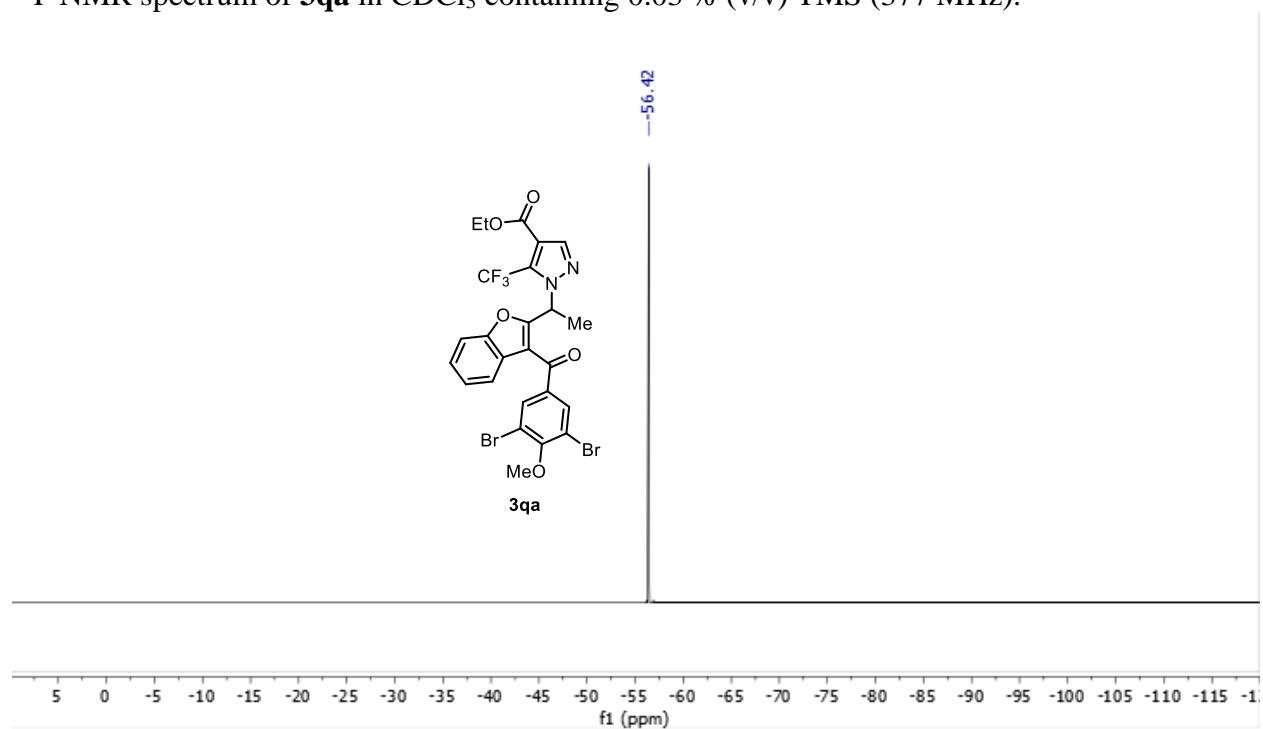
¹H NMR spectrum of **3qa** in CDCl₃ containing 0.03 % (v/v) TMS (500 MHz).



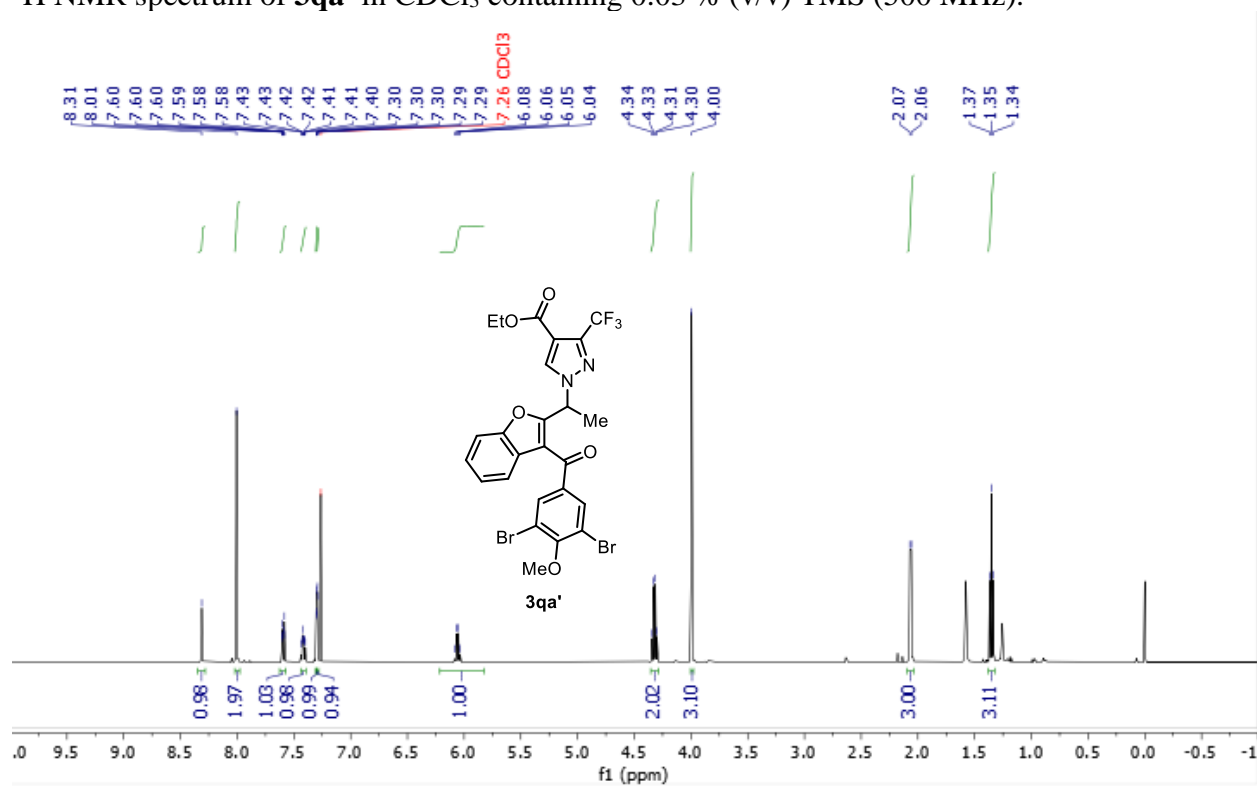
^{13}C NMR spectrum of **3qa** in CDCl_3 containing 0.03 % (v/v) TMS (126 MHz).



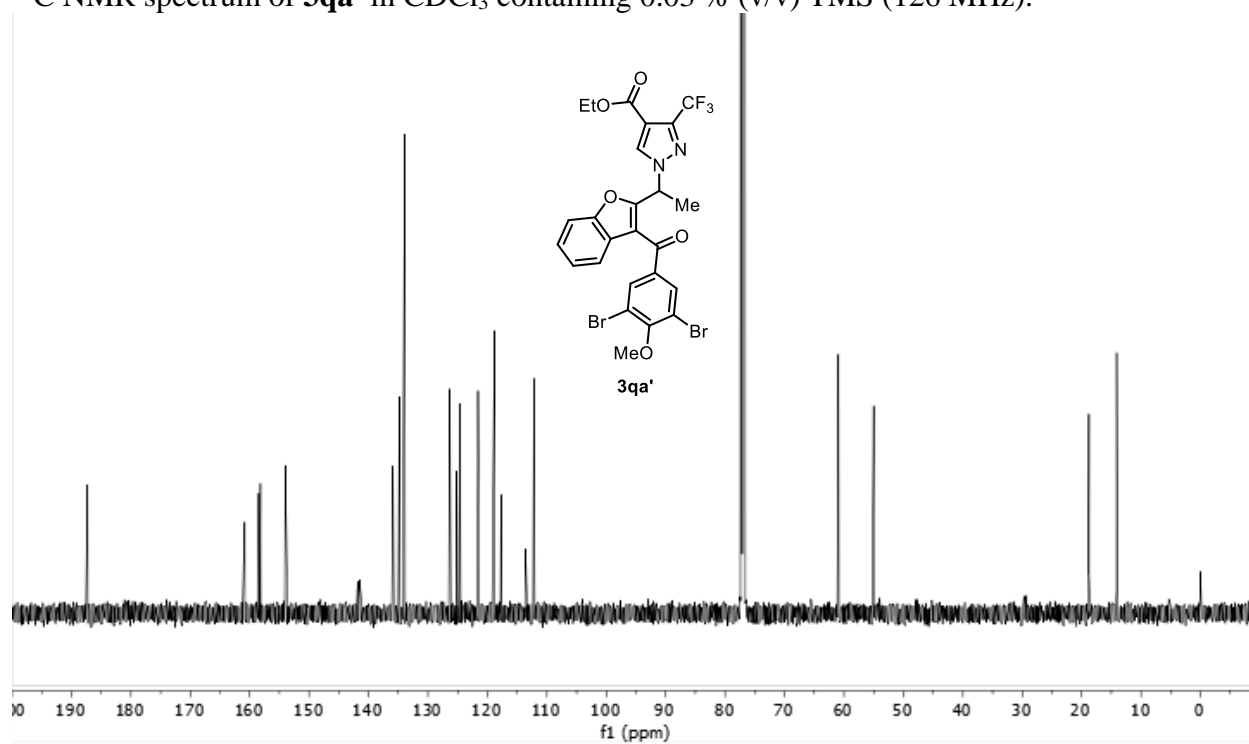
^{19}F NMR spectrum of **3qa** in CDCl_3 containing 0.03 % (v/v) TMS (377 MHz).



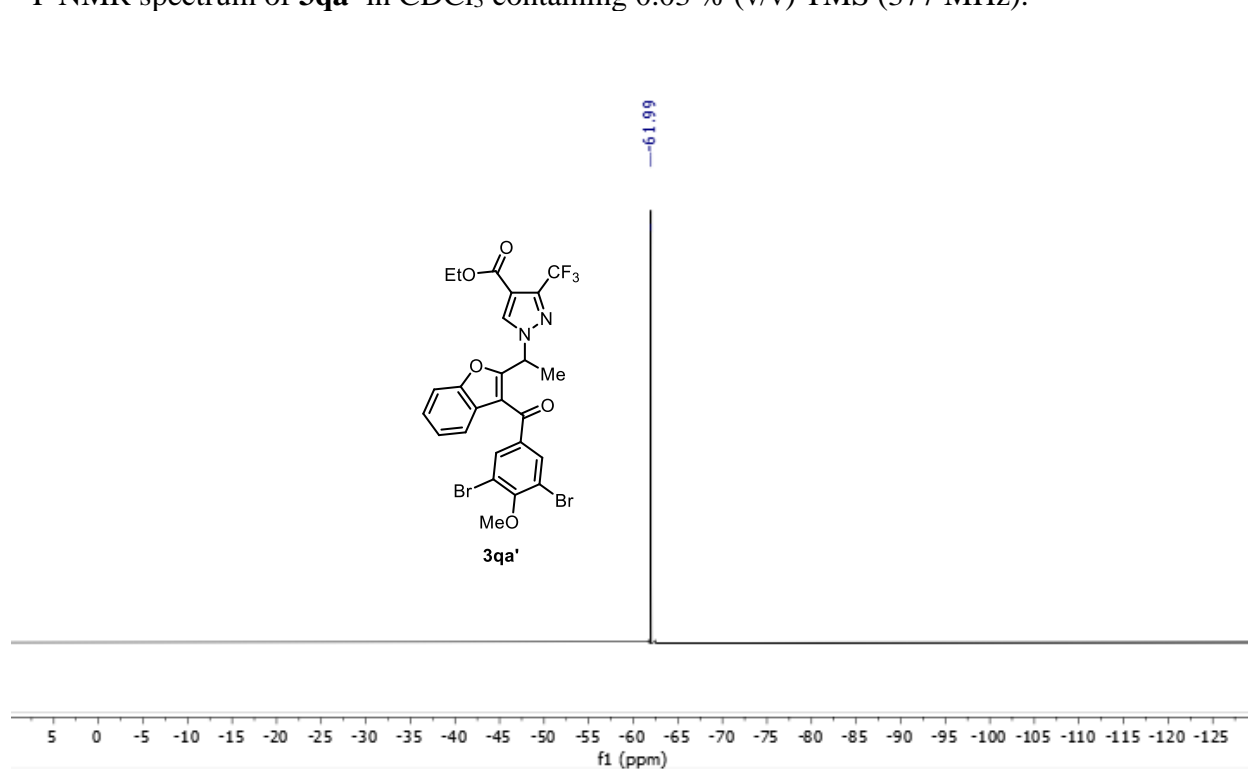
^1H NMR spectrum of **3qa'** in CDCl_3 containing 0.03 % (v/v) TMS (500 MHz).



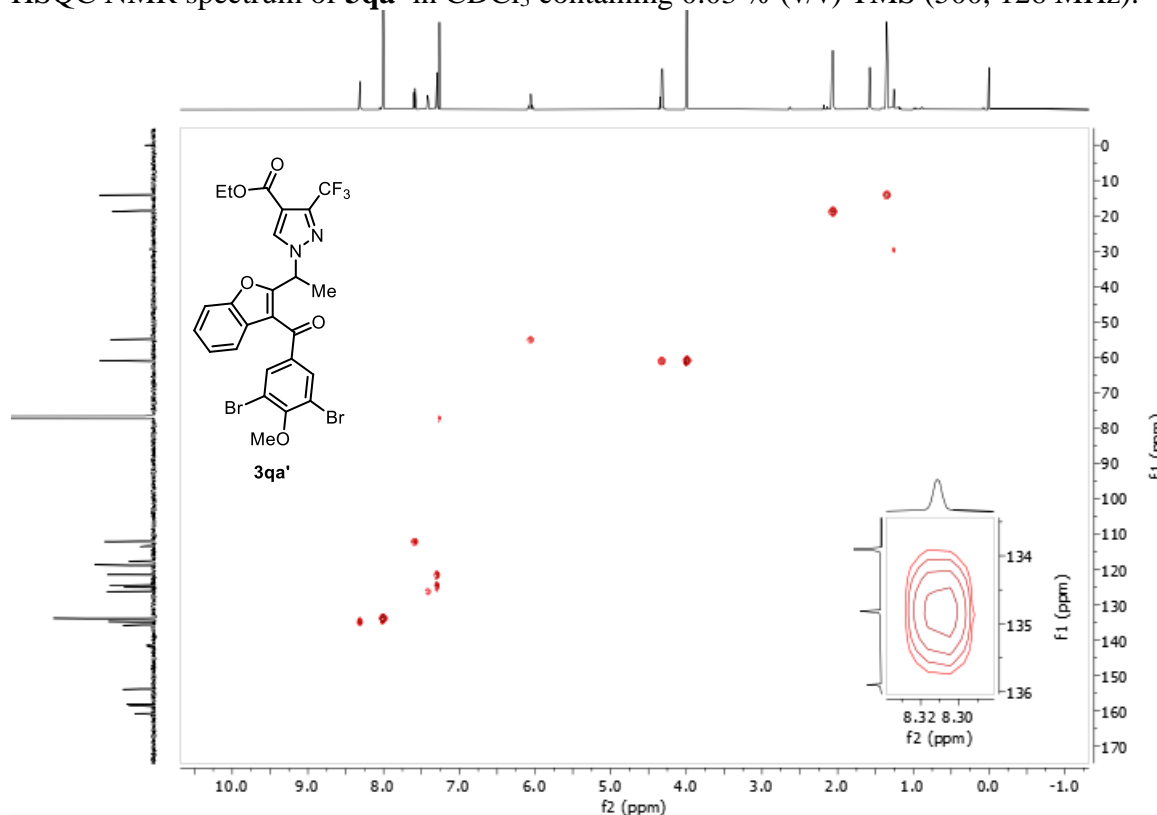
^{13}C NMR spectrum of **3qa'** in CDCl_3 containing 0.03 % (v/v) TMS (126 MHz).



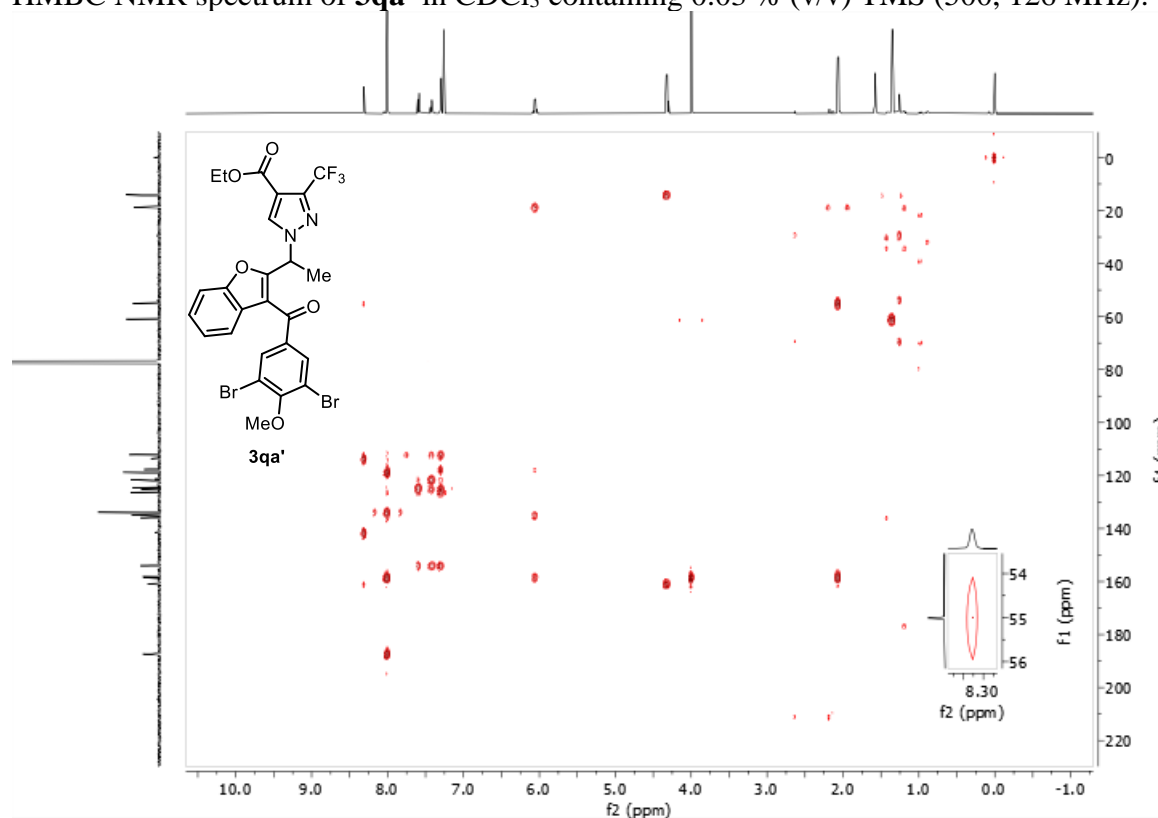
^{19}F NMR spectrum of **3qa'** in CDCl_3 containing 0.03 % (v/v) TMS (377 MHz).



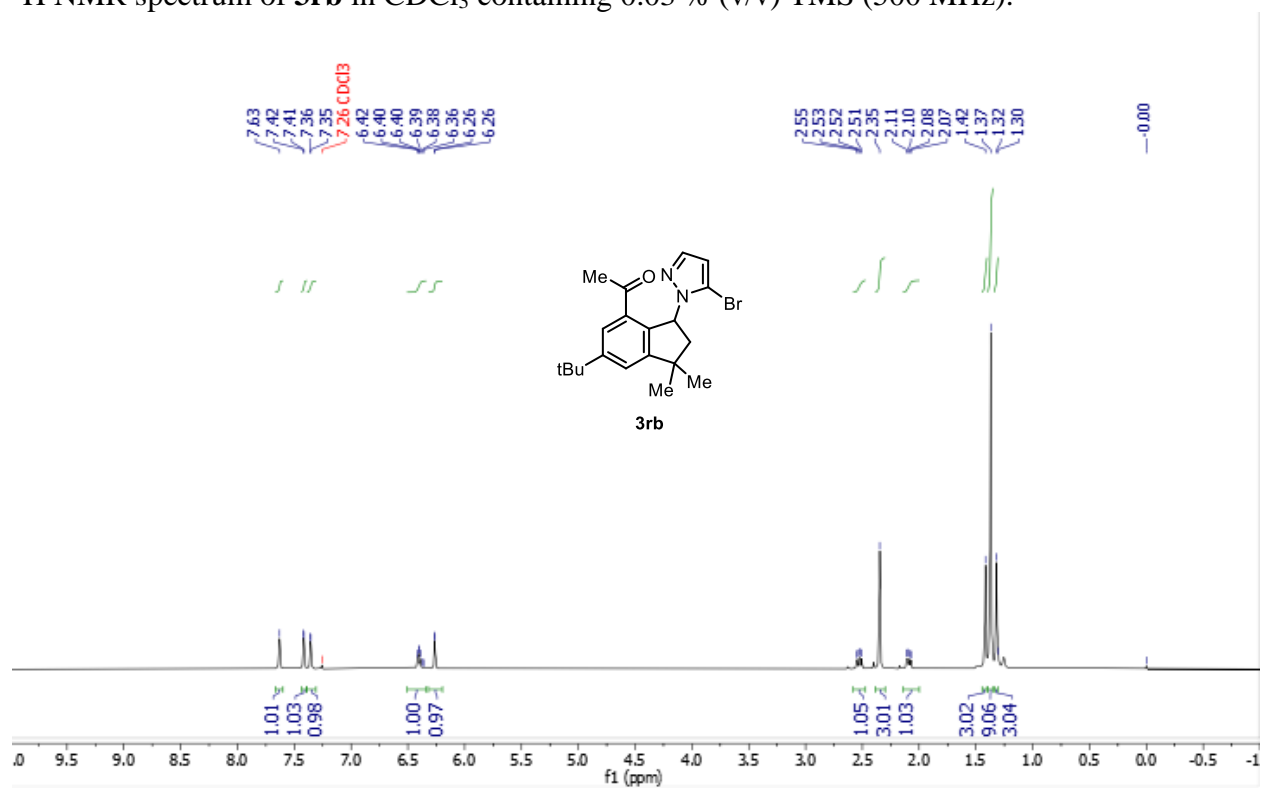
HSQC NMR spectrum of **3qa'** in CDCl_3 containing 0.03 % (v/v) TMS (500, 126 MHz).



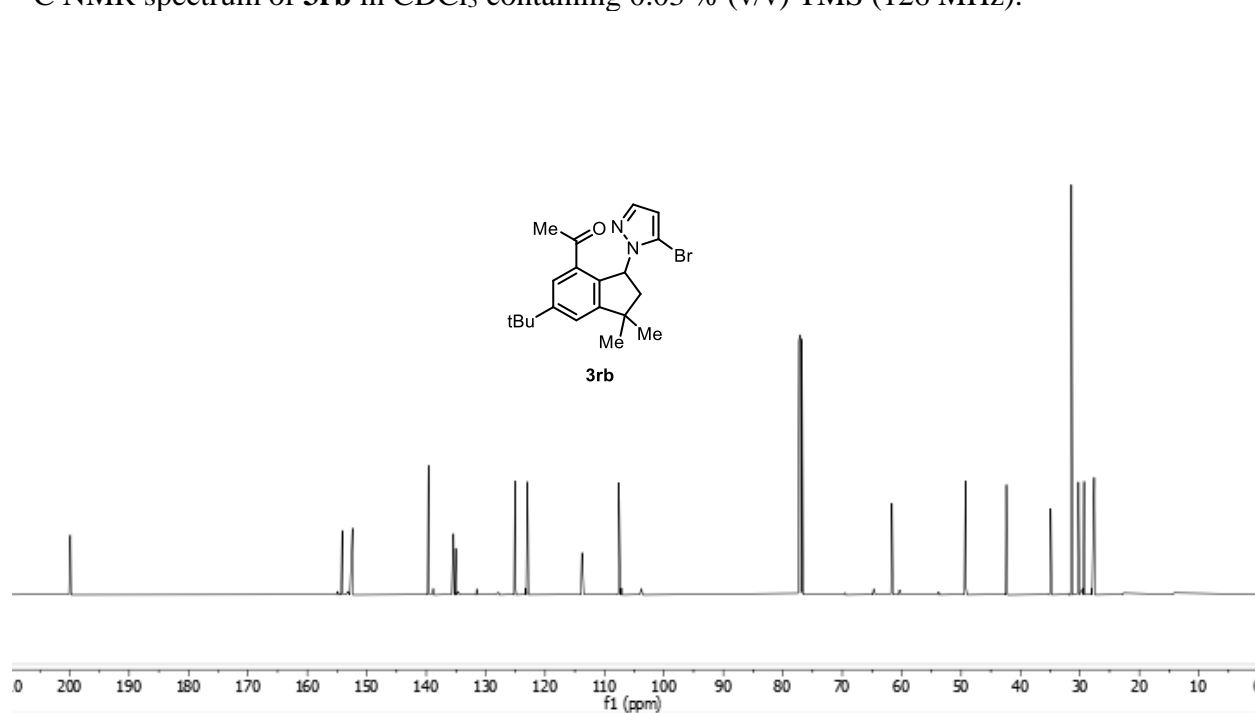
HMBC NMR spectrum of **3qa'** in CDCl₃ containing 0.03 % (v/v) TMS (500, 126 MHz).



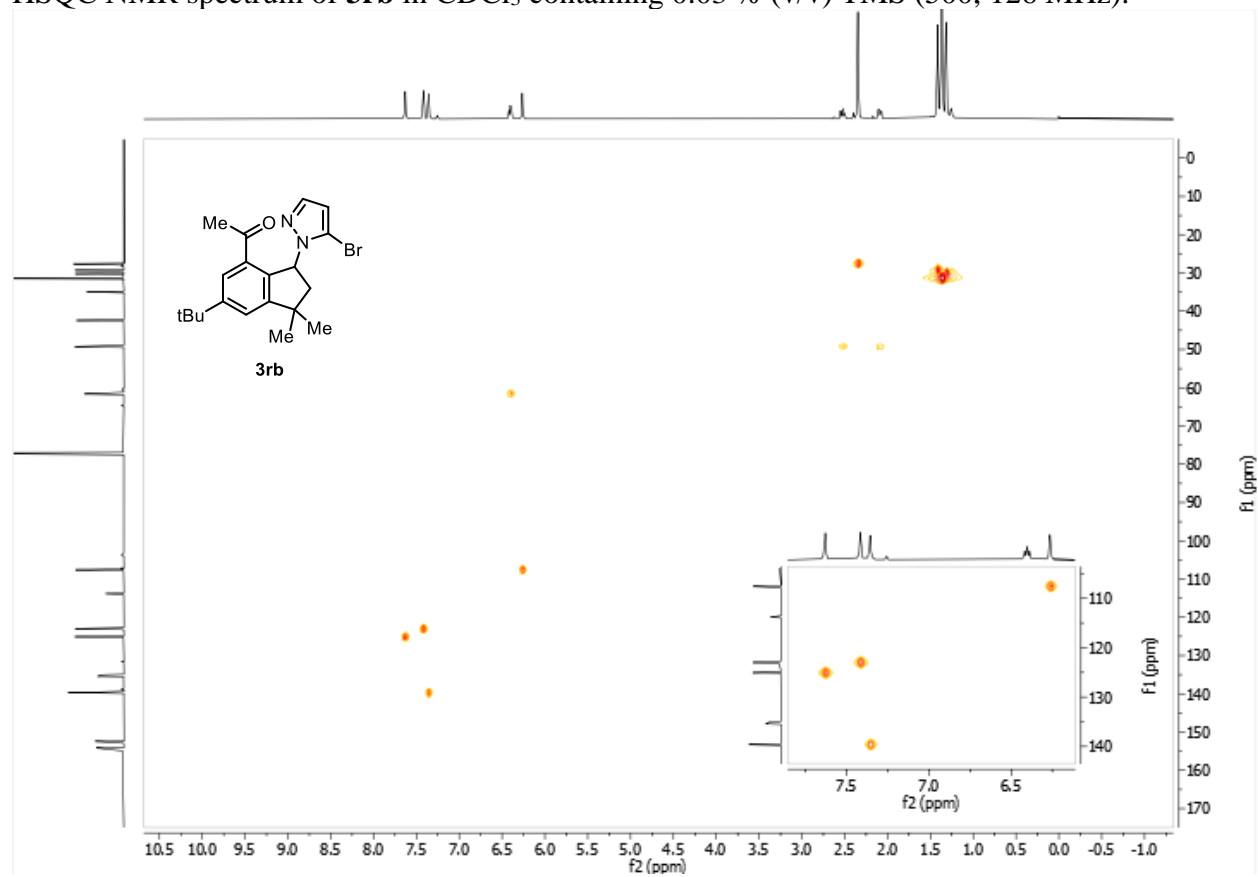
¹H NMR spectrum of **3rb** in CDCl₃ containing 0.03 % (v/v) TMS (500 MHz).



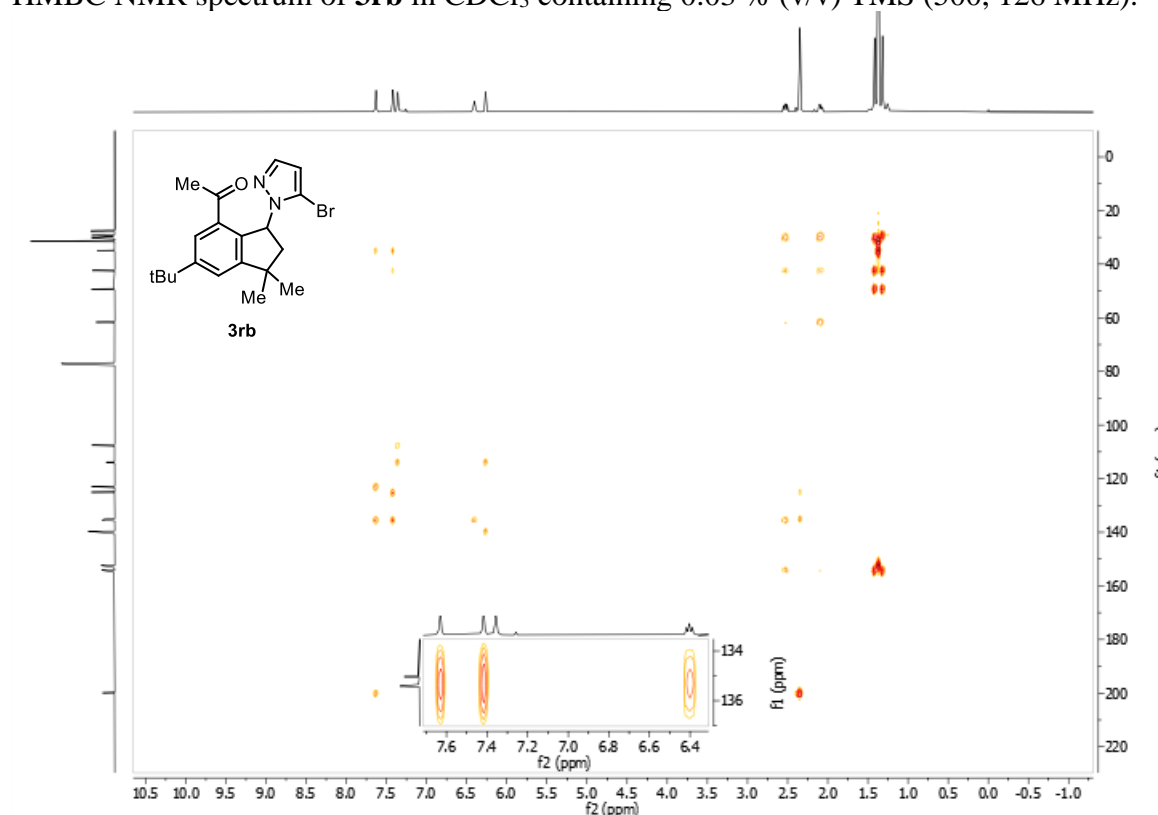
^{13}C NMR spectrum of **3rb** in CDCl_3 containing 0.03 % (v/v) TMS (126 MHz).



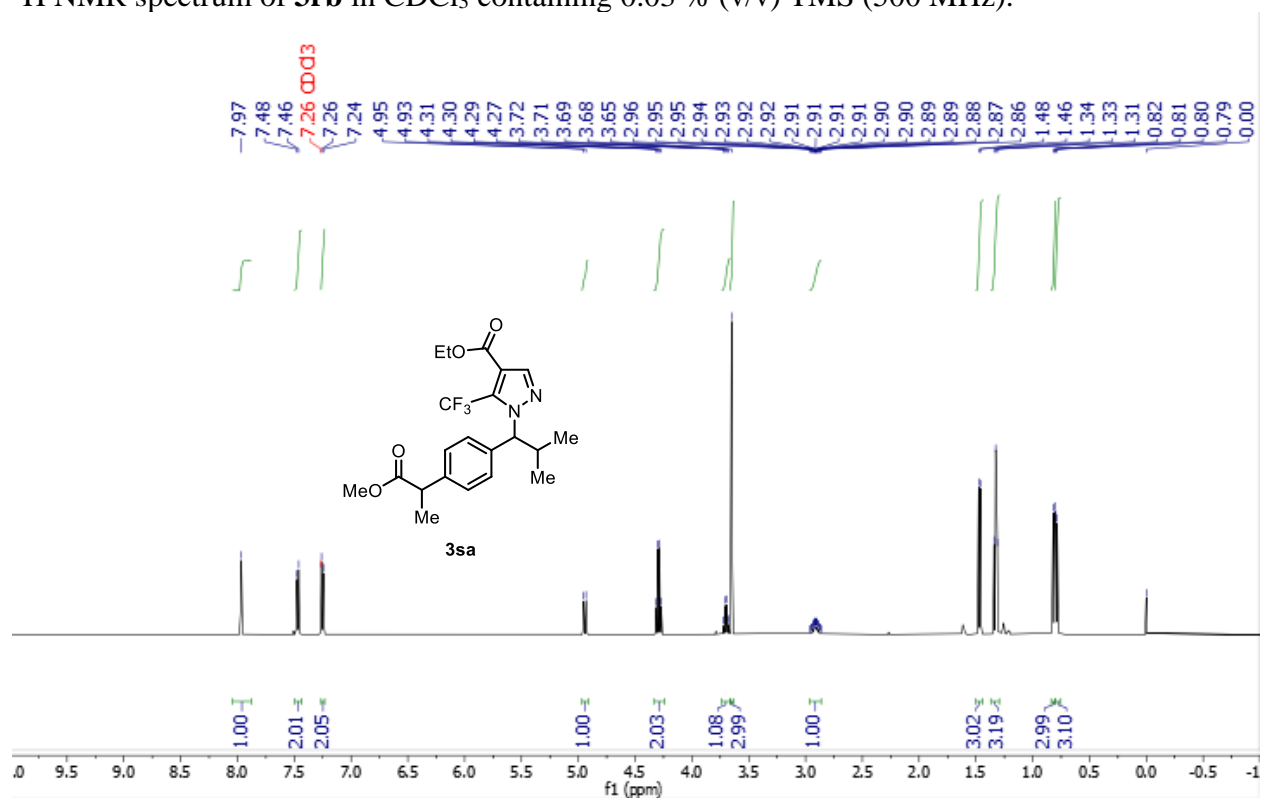
HSQC NMR spectrum of **3rb** in CDCl_3 containing 0.03 % (v/v) TMS (500, 126 MHz).



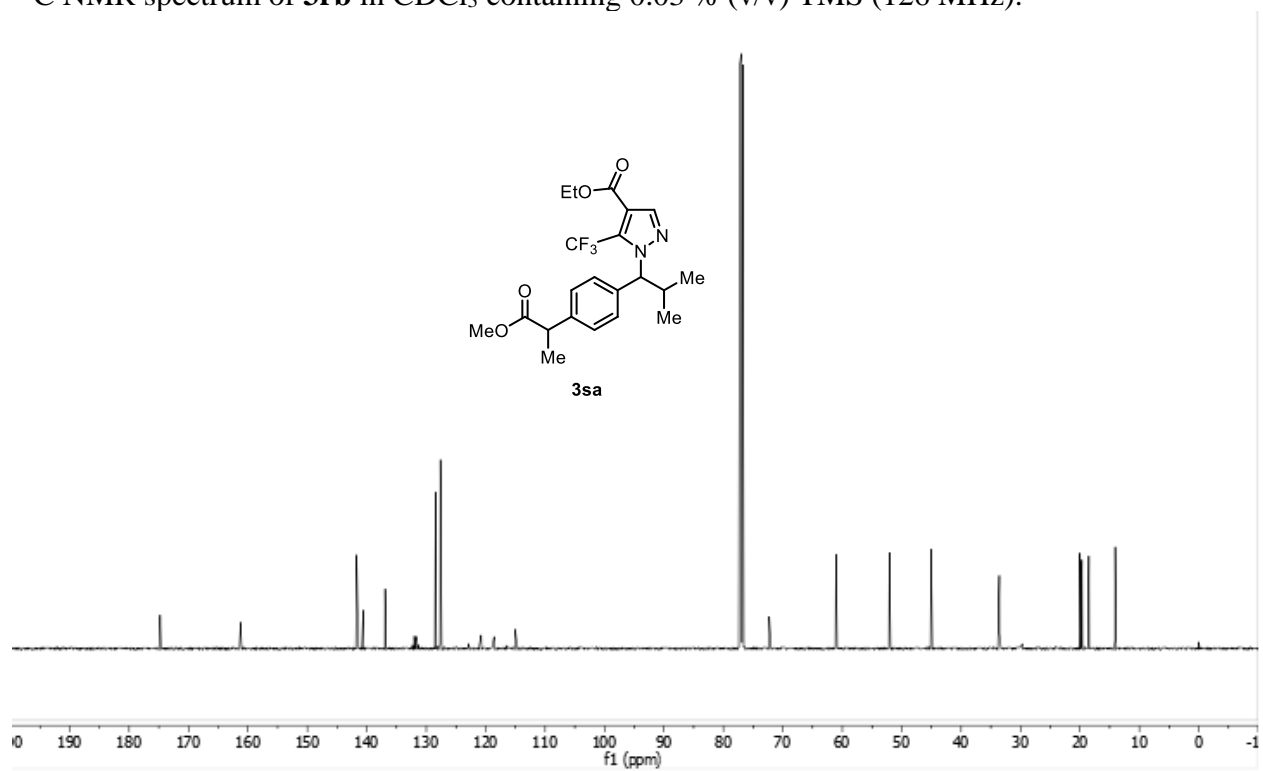
HMBC NMR spectrum of **3rb** in CDCl₃ containing 0.03 % (v/v) TMS (500, 126 MHz).



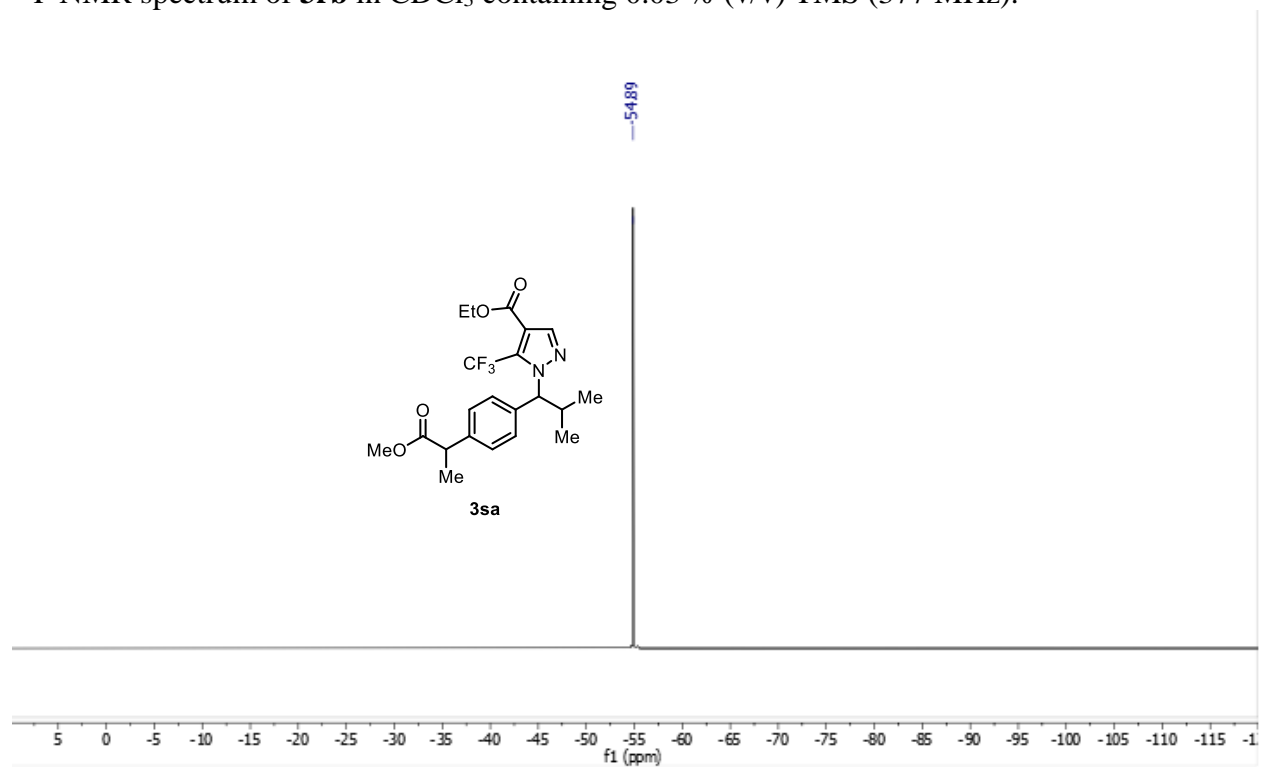
¹H NMR spectrum of **3rb** in CDCl₃ containing 0.03 % (v/v) TMS (500 MHz).



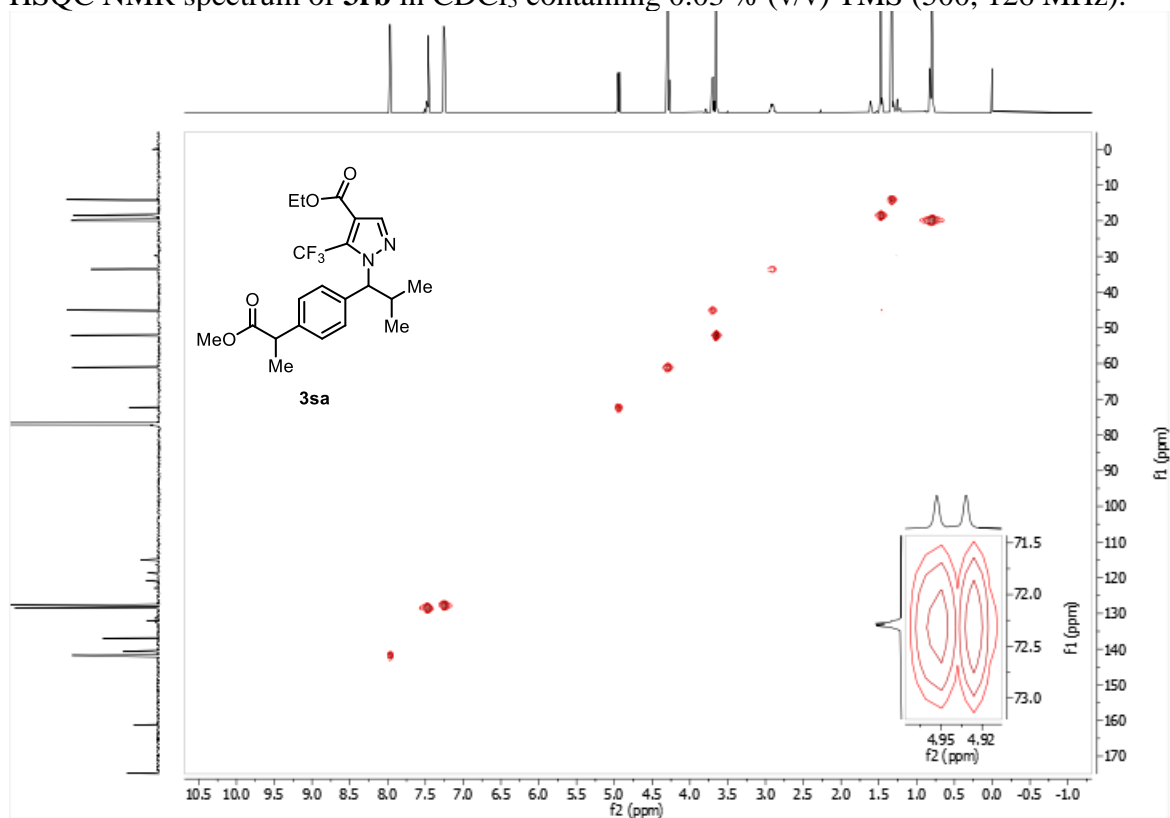
^{13}C NMR spectrum of **3rb** in CDCl_3 containing 0.03 % (v/v) TMS (126 MHz).



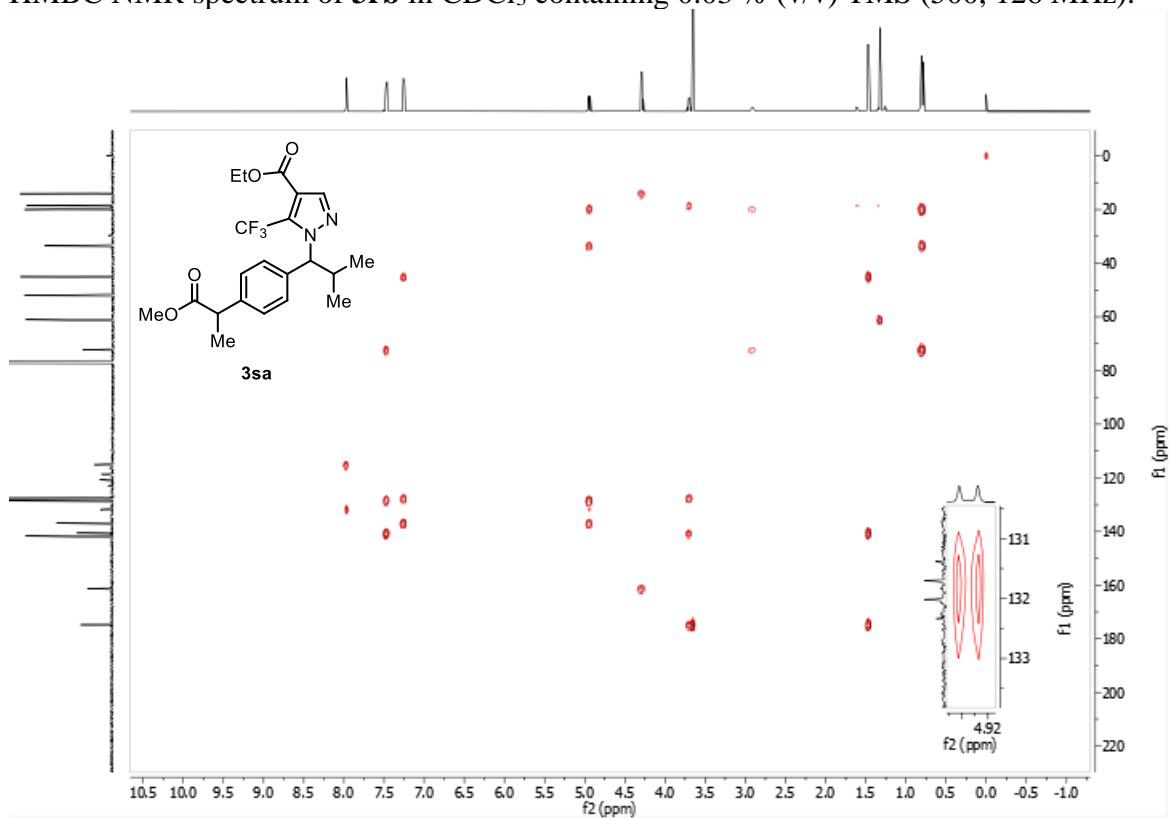
^{19}F NMR spectrum of **3rb** in CDCl_3 containing 0.03 % (v/v) TMS (377 MHz).



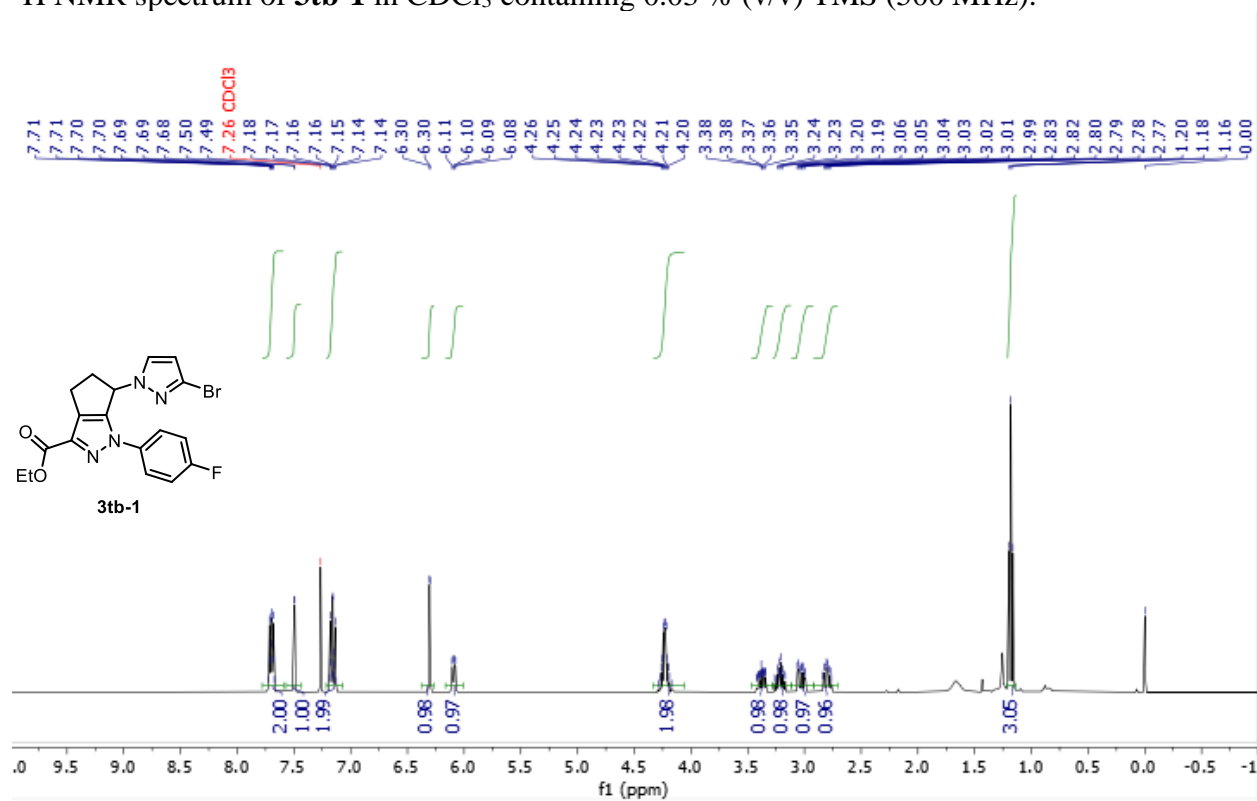
HSQC NMR spectrum of **3rb** in CDCl₃ containing 0.03 % (v/v) TMS (500, 126 MHz).



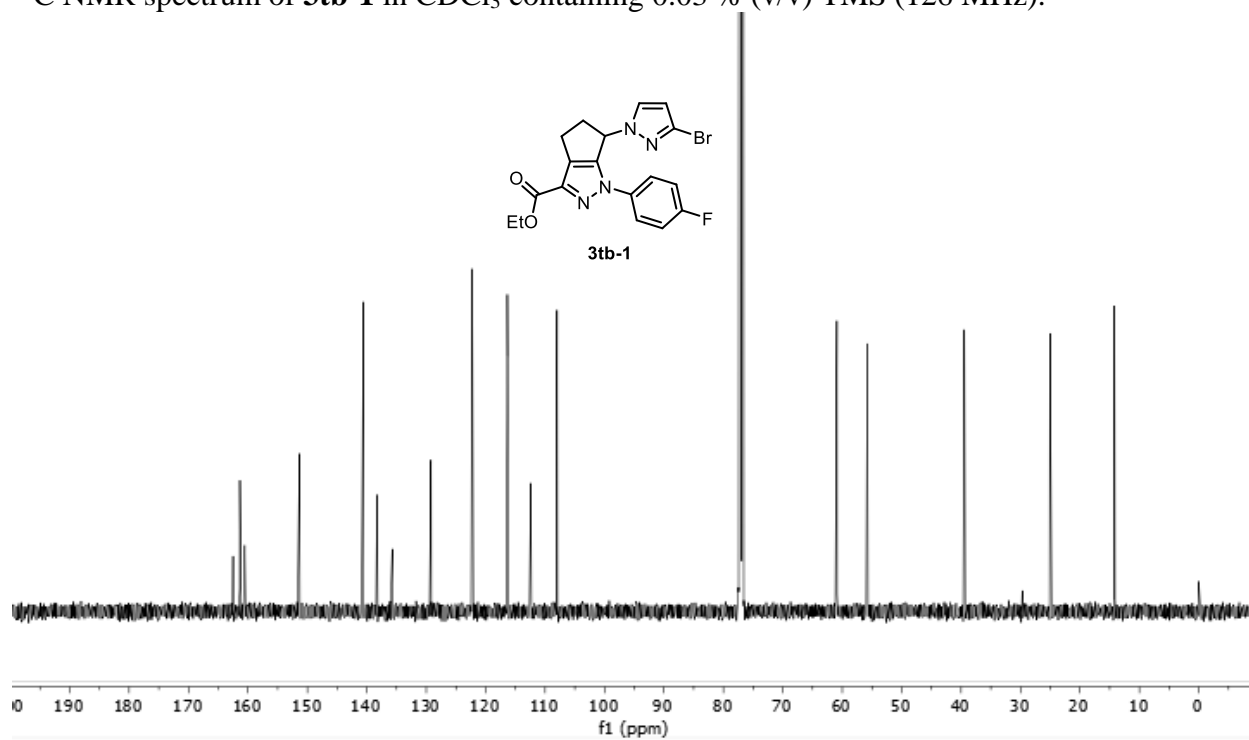
HMBC NMR spectrum of **3rb** in CDCl₃ containing 0.03 % (v/v) TMS (500, 126 MHz).



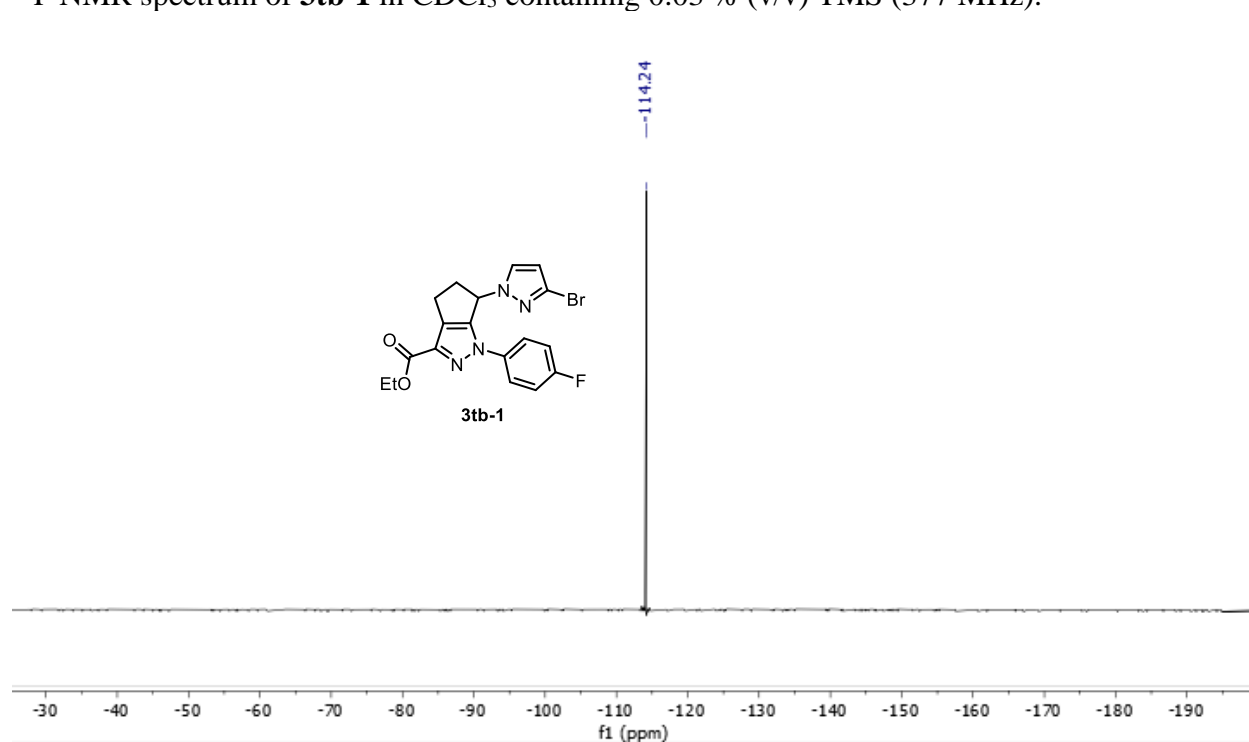
^1H NMR spectrum of **3tb-1** in CDCl_3 containing 0.03 % (v/v) TMS (500 MHz).



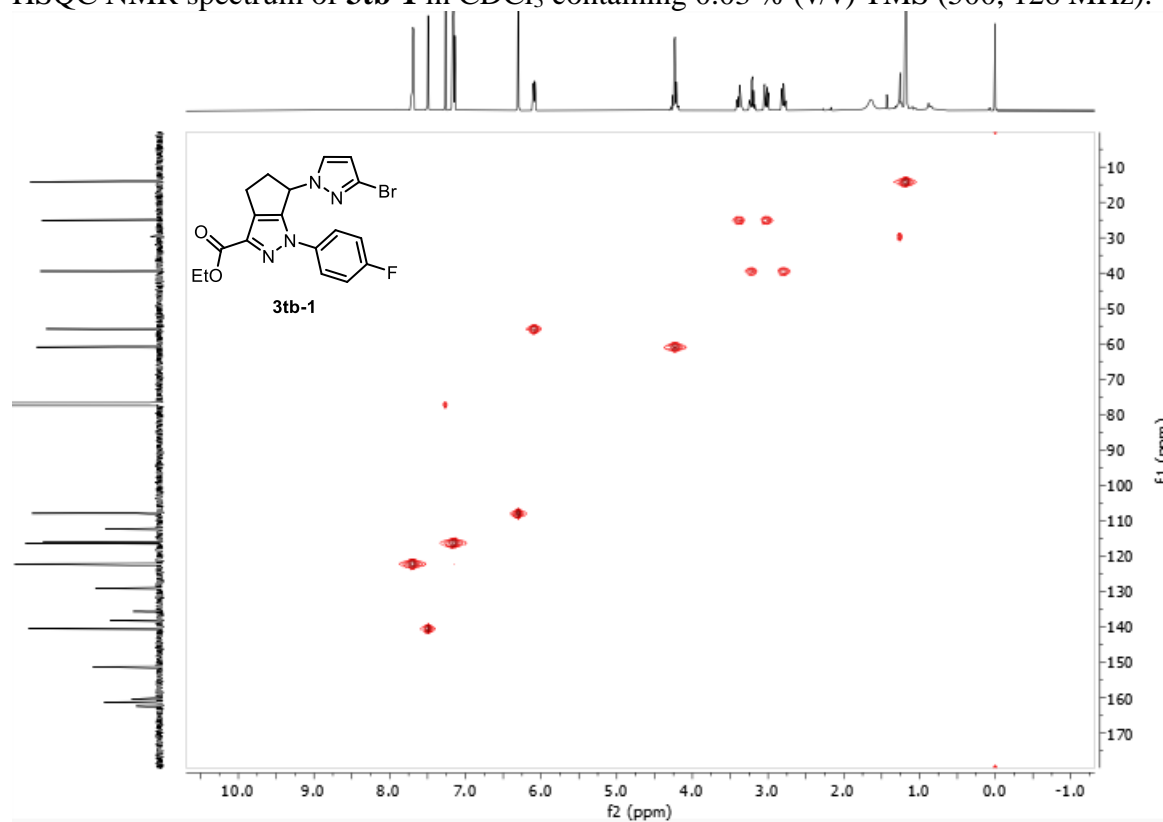
^{13}C NMR spectrum of **3tb-1** in CDCl_3 containing 0.03 % (v/v) TMS (126 MHz).



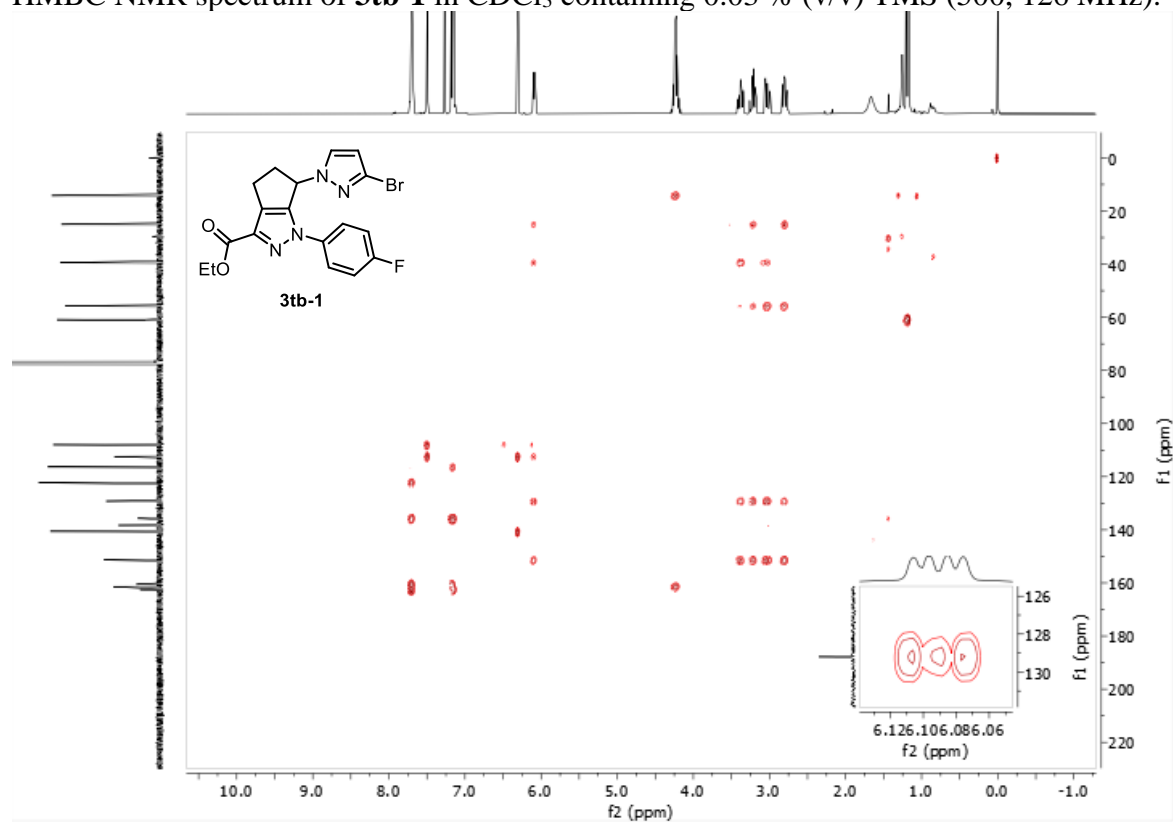
^{19}F NMR spectrum of **3tb-1** in CDCl_3 containing 0.03 % (v/v) TMS (377 MHz).



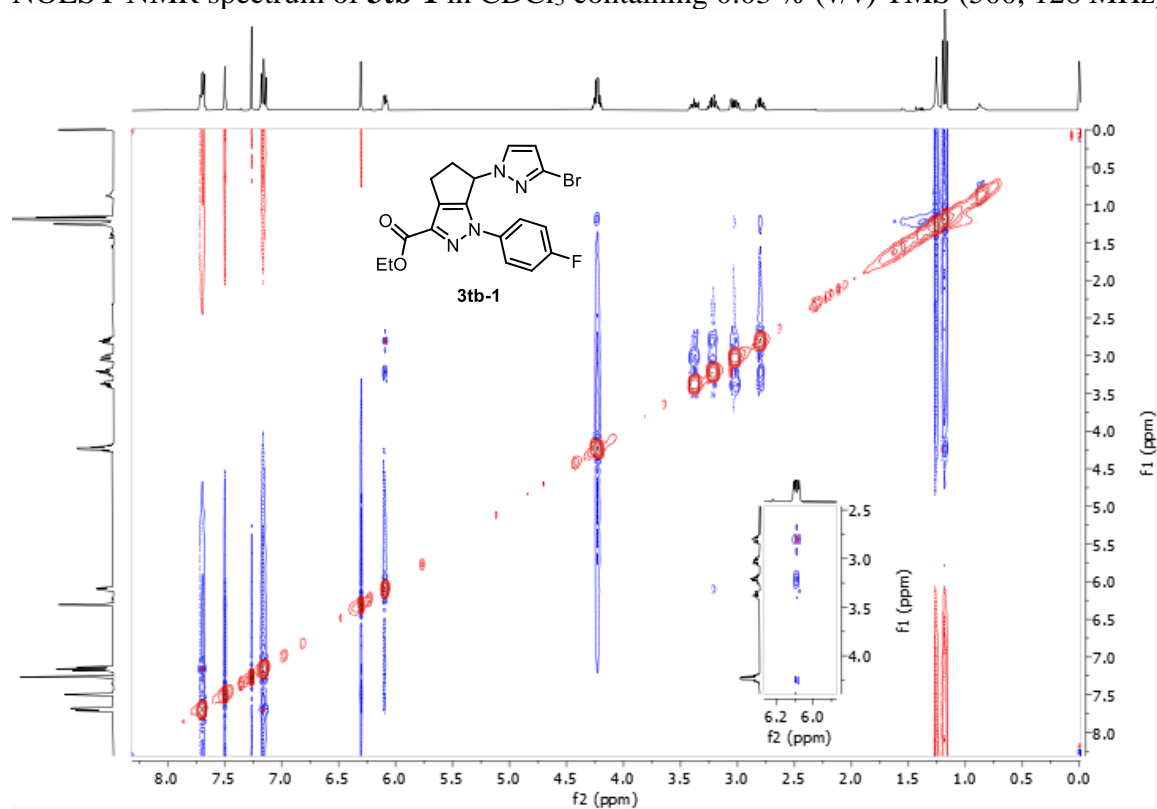
HSQC NMR spectrum of **3tb-1** in CDCl_3 containing 0.03 % (v/v) TMS (500, 126 MHz).



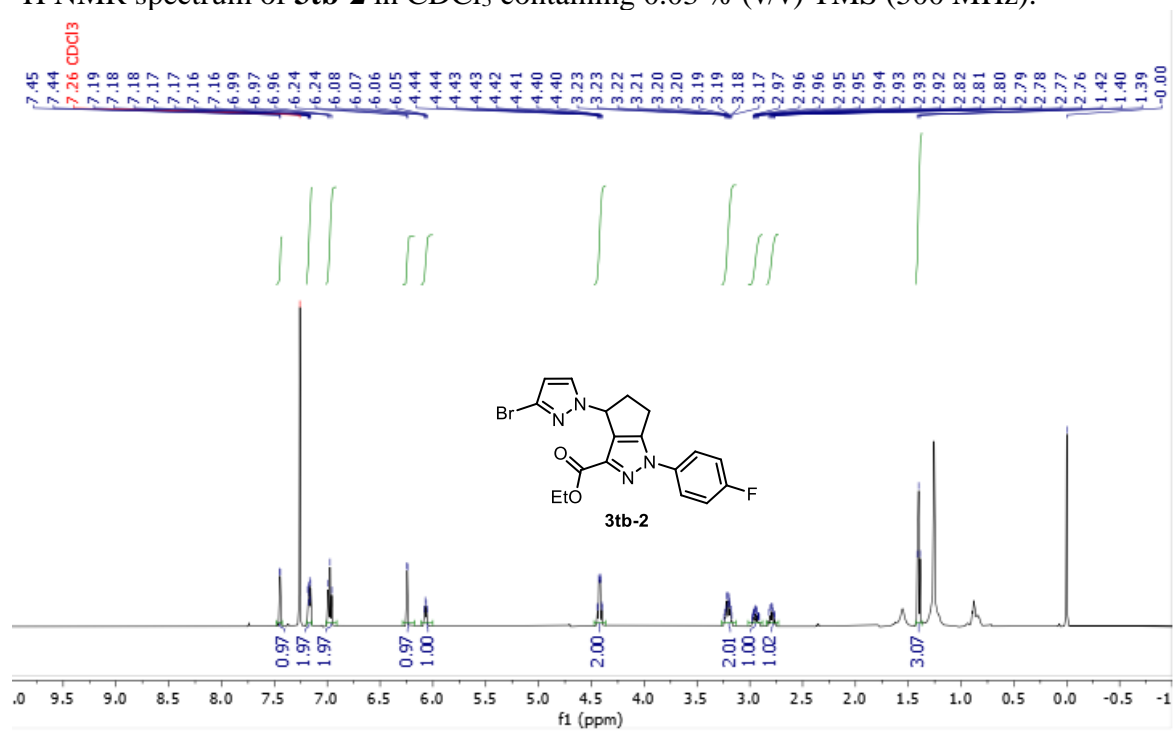
HMBC NMR spectrum of **3tb-1** in CDCl₃ containing 0.03 % (v/v) TMS (500, 126 MHz).



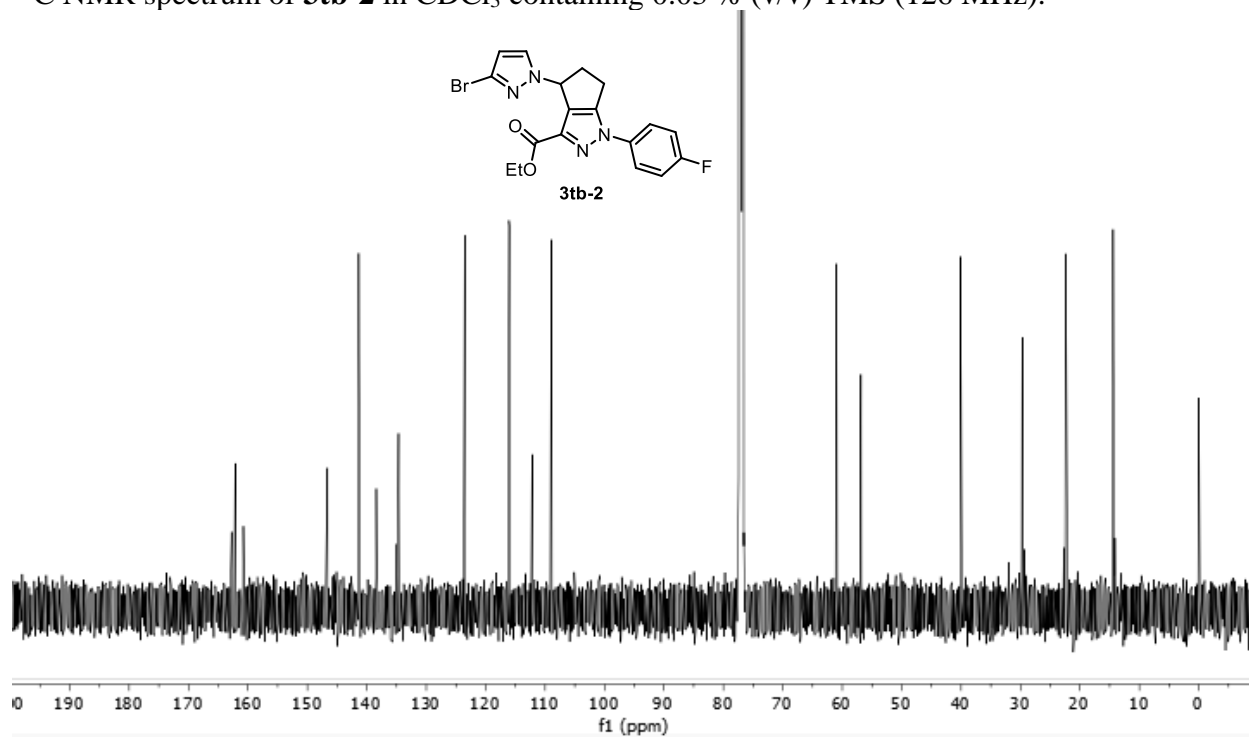
NOESY NMR spectrum of **3tb-1** in CDCl₃ containing 0.03 % (v/v) TMS (500, 126 MHz).



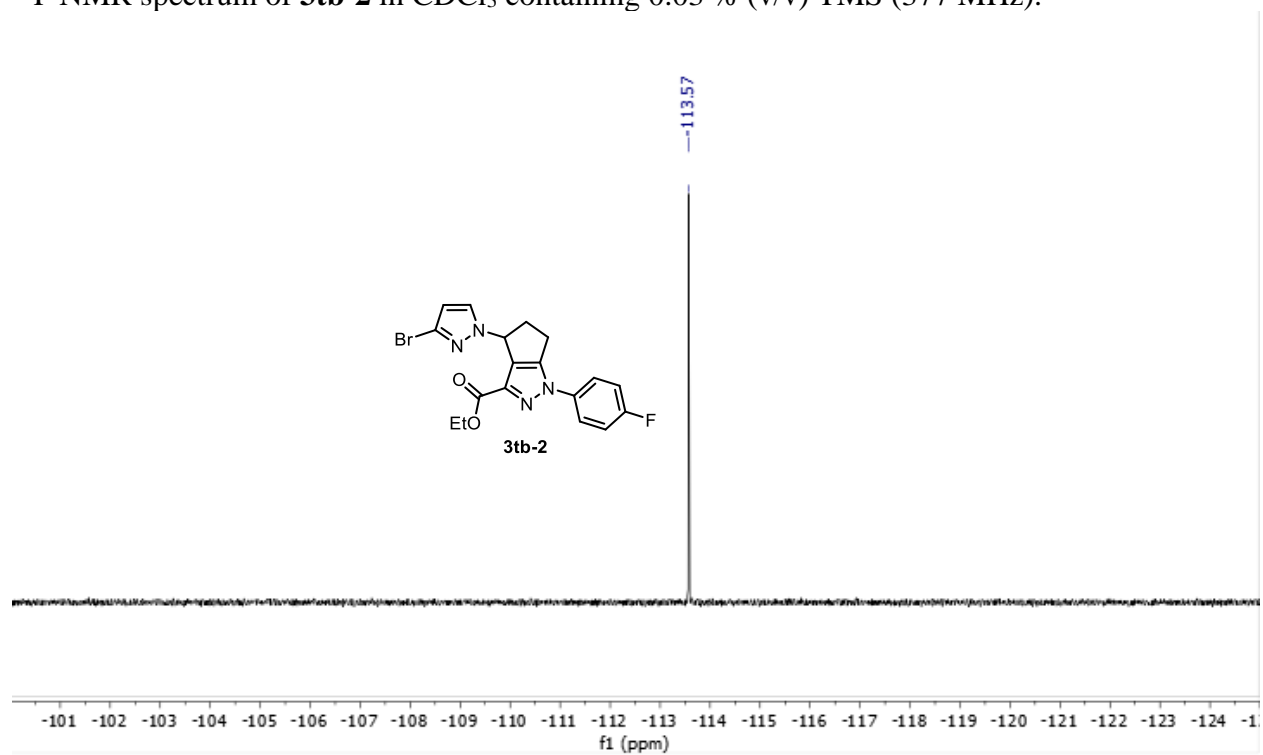
^1H NMR spectrum of **3tb-2** in CDCl_3 containing 0.03 % (v/v) TMS (500 MHz).



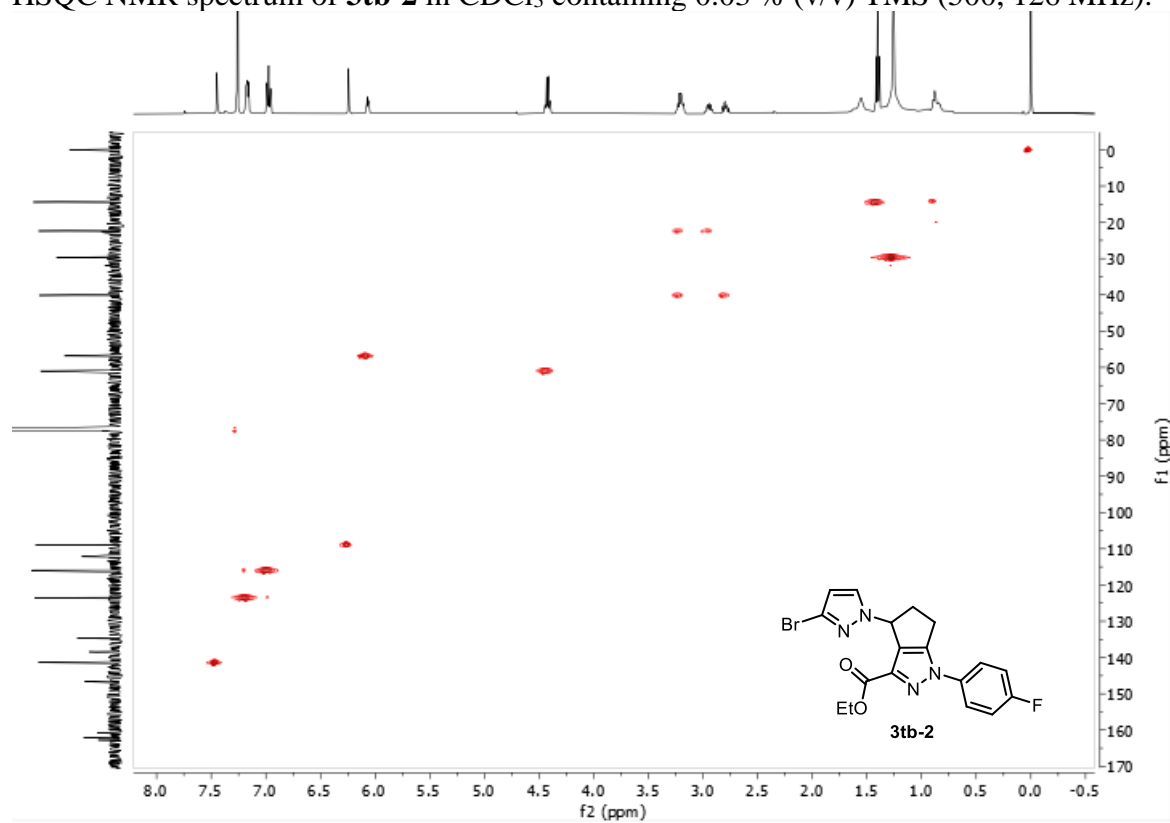
^{13}C NMR spectrum of **3tb-2** in CDCl_3 containing 0.03 % (v/v) TMS (126 MHz).



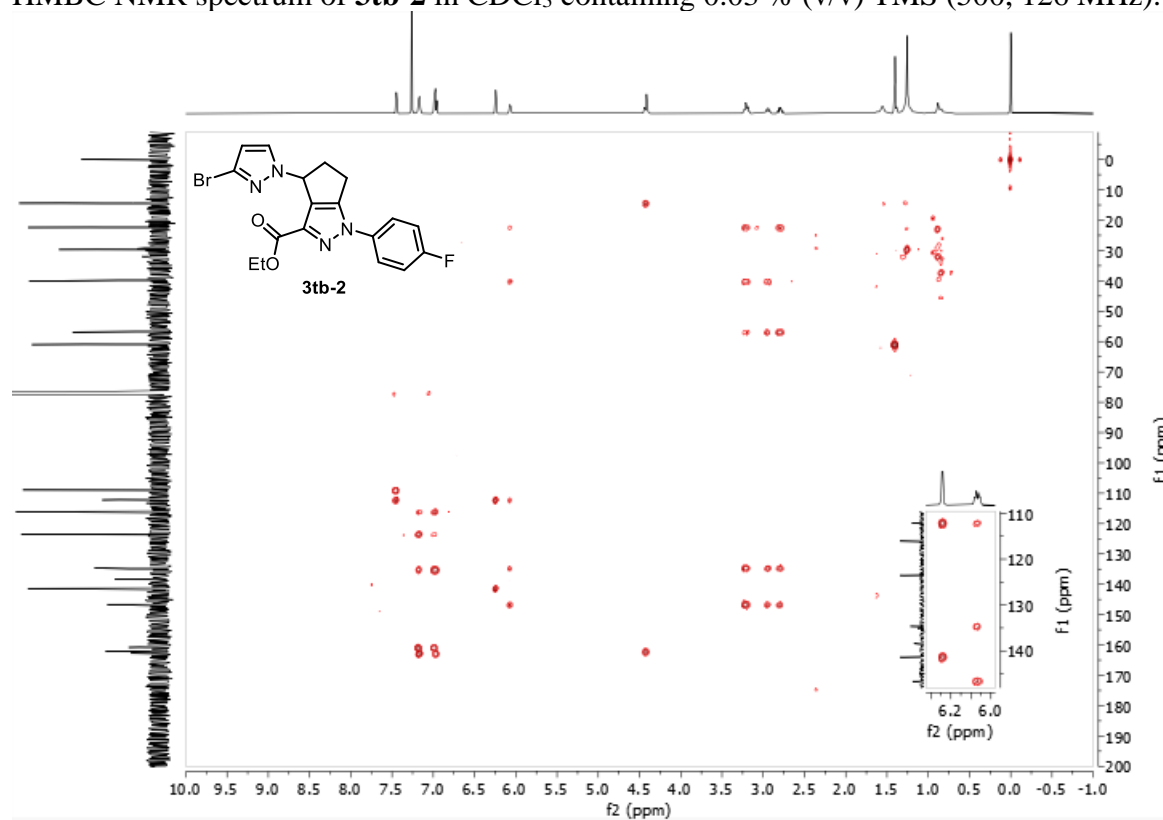
^{19}F NMR spectrum of **3tb-2** in CDCl_3 containing 0.03 % (v/v) TMS (377 MHz).



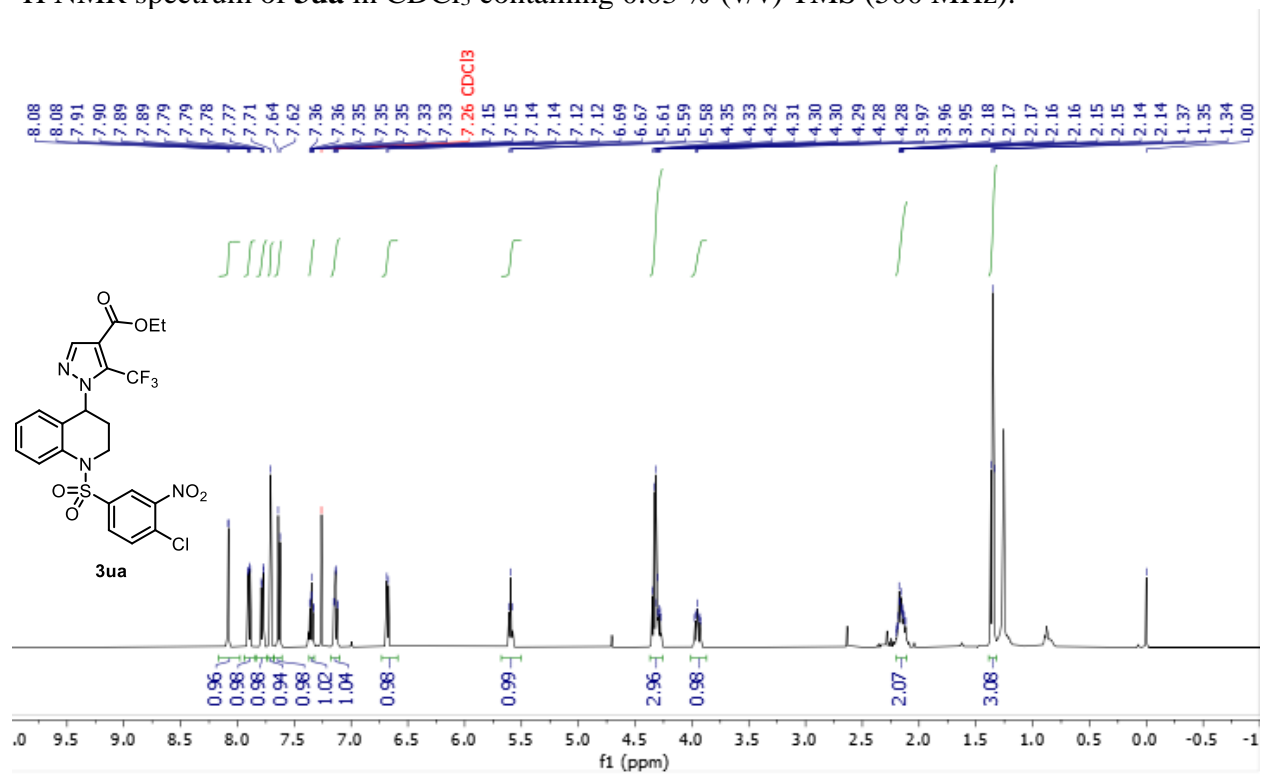
HSQC NMR spectrum of **3tb-2** in CDCl_3 containing 0.03 % (v/v) TMS (500, 126 MHz).



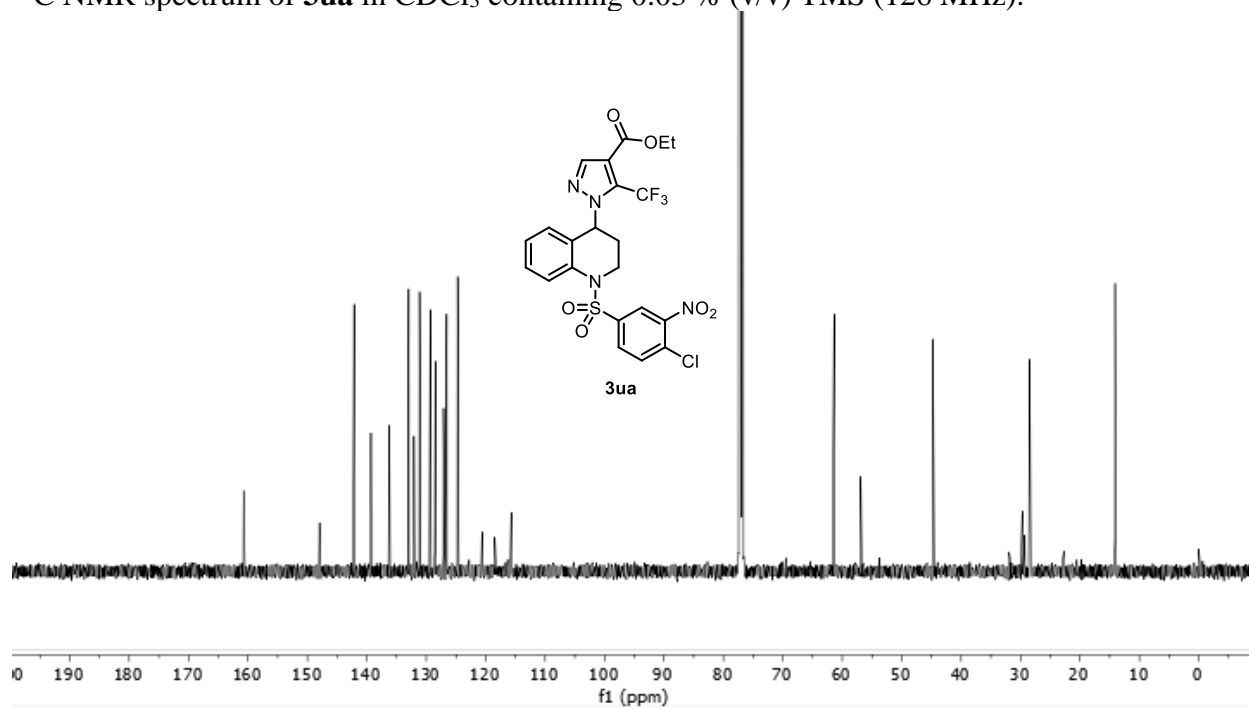
HMBC NMR spectrum of **3tb-2** in CDCl₃ containing 0.03 % (v/v) TMS (500, 126 MHz).



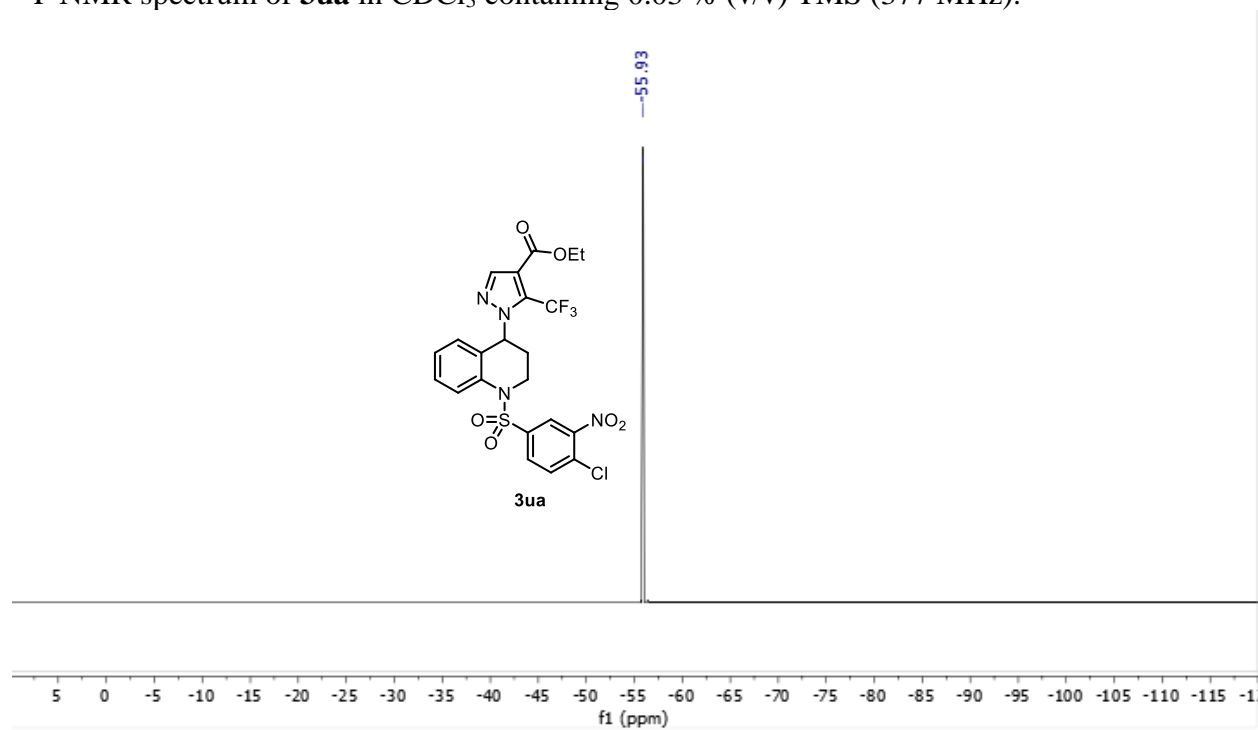
¹H NMR spectrum of **3ua** in CDCl₃ containing 0.03 % (v/v) TMS (500 MHz).



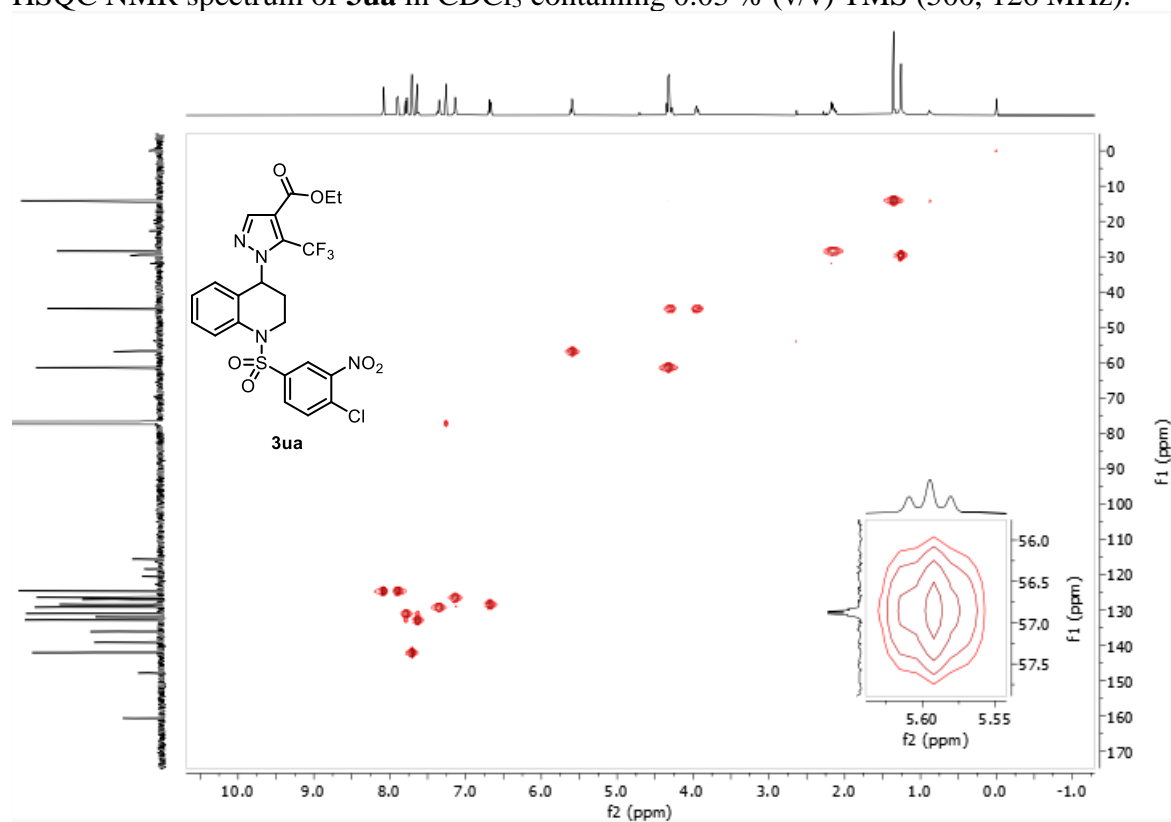
^{13}C NMR spectrum of **3ua** in CDCl_3 containing 0.03 % (v/v) TMS (126 MHz).



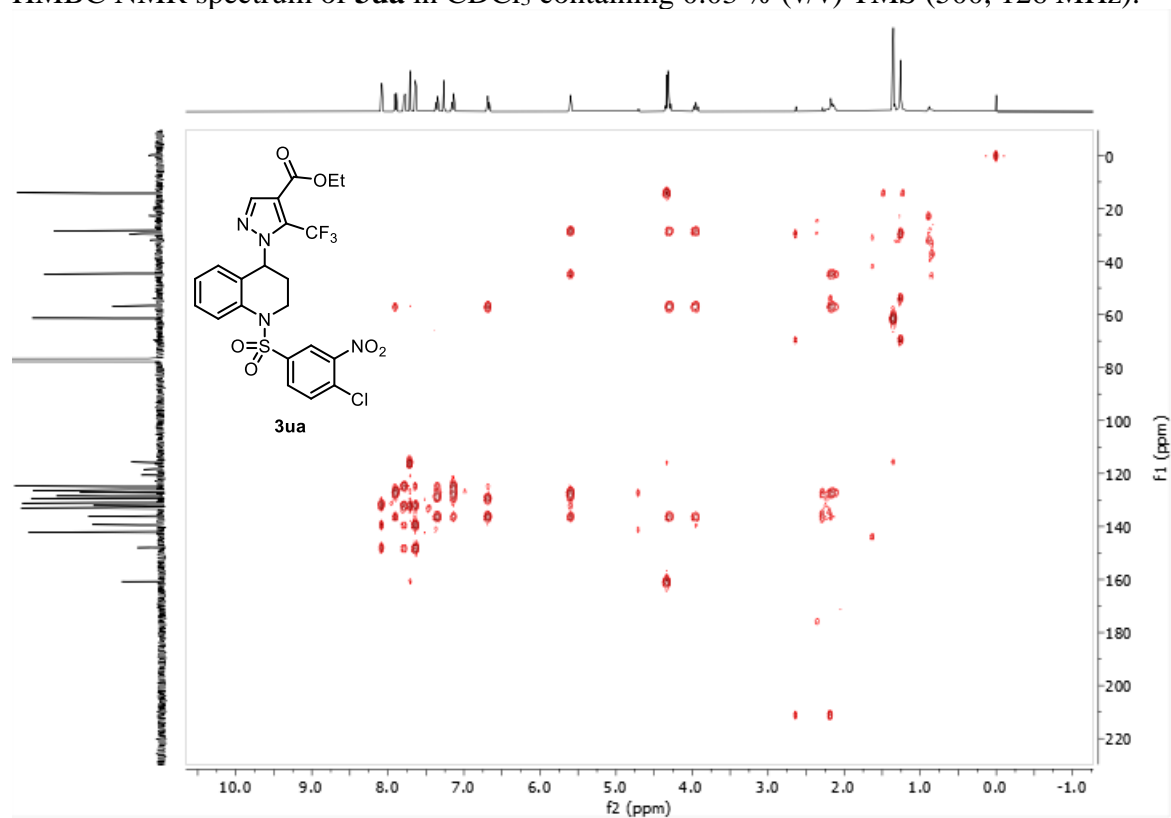
^{19}F NMR spectrum of **3ua** in CDCl_3 containing 0.03 % (v/v) TMS (377 MHz).



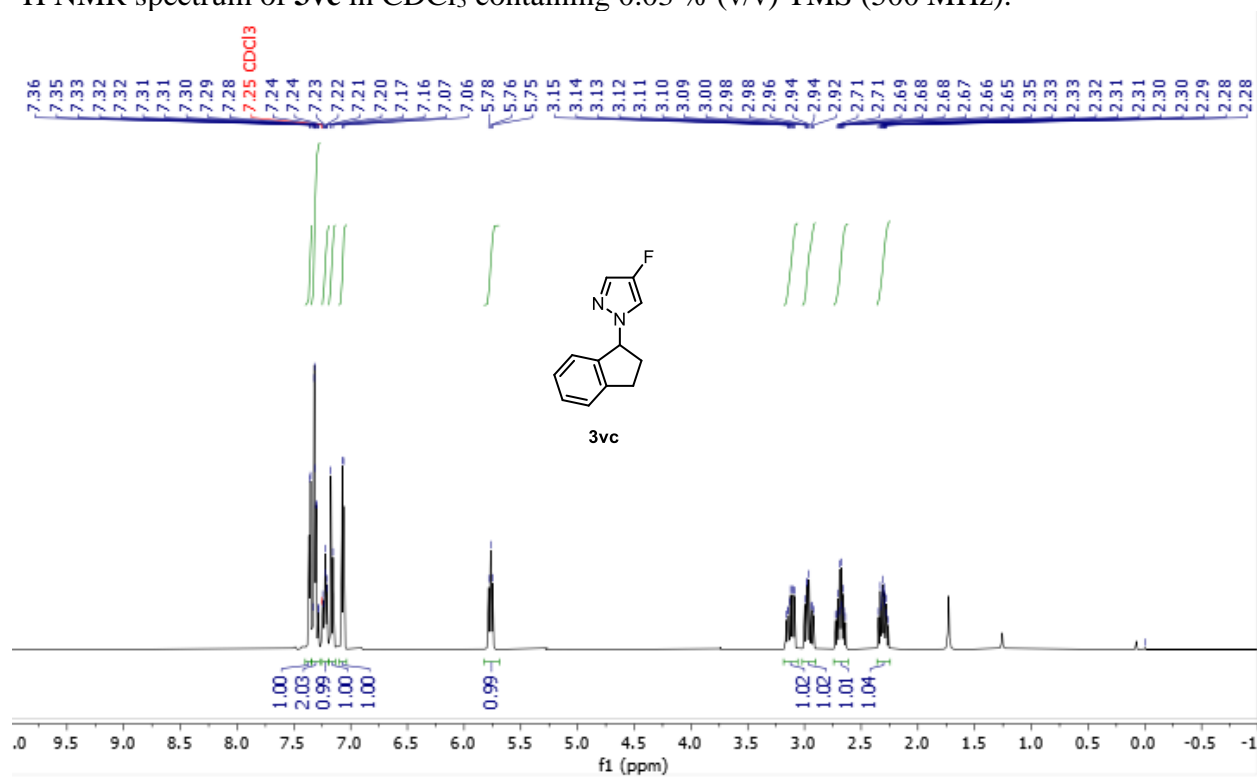
HSQC NMR spectrum of **3ua** in CDCl₃ containing 0.03 % (v/v) TMS (500, 126 MHz).



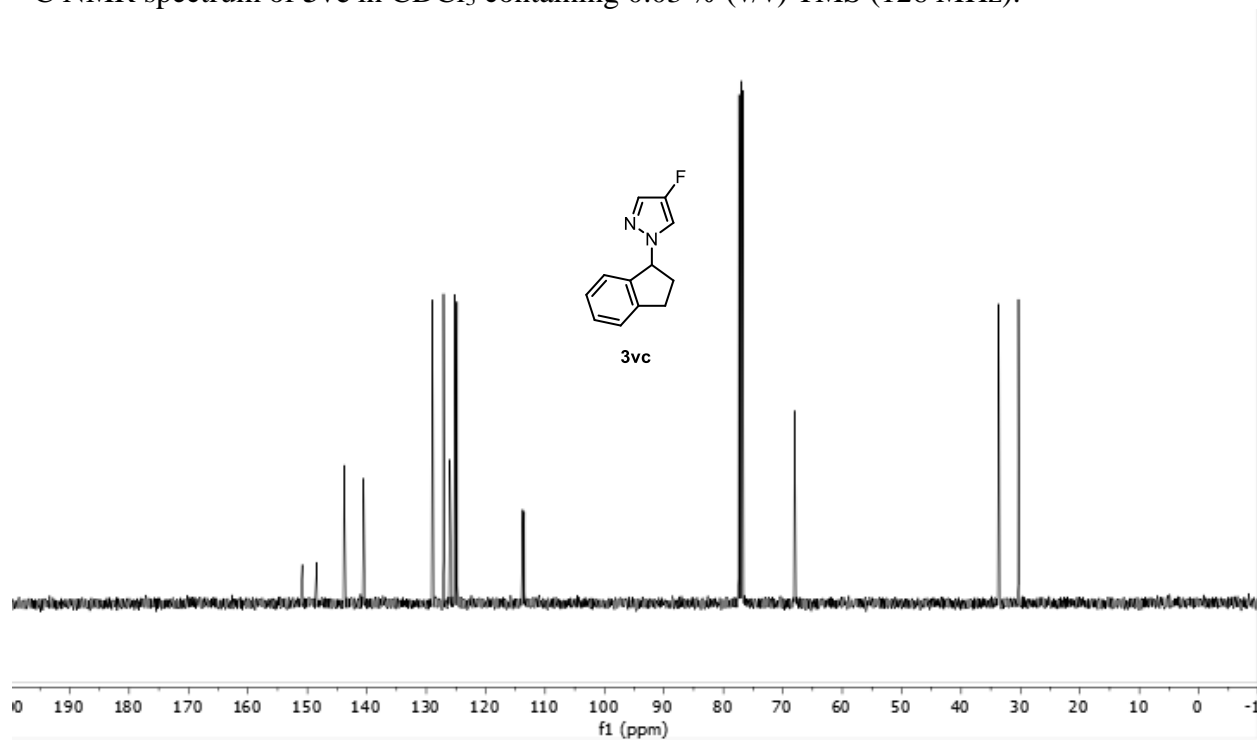
HMBC NMR spectrum of **3ua** in CDCl₃ containing 0.03 % (v/v) TMS (500, 126 MHz).



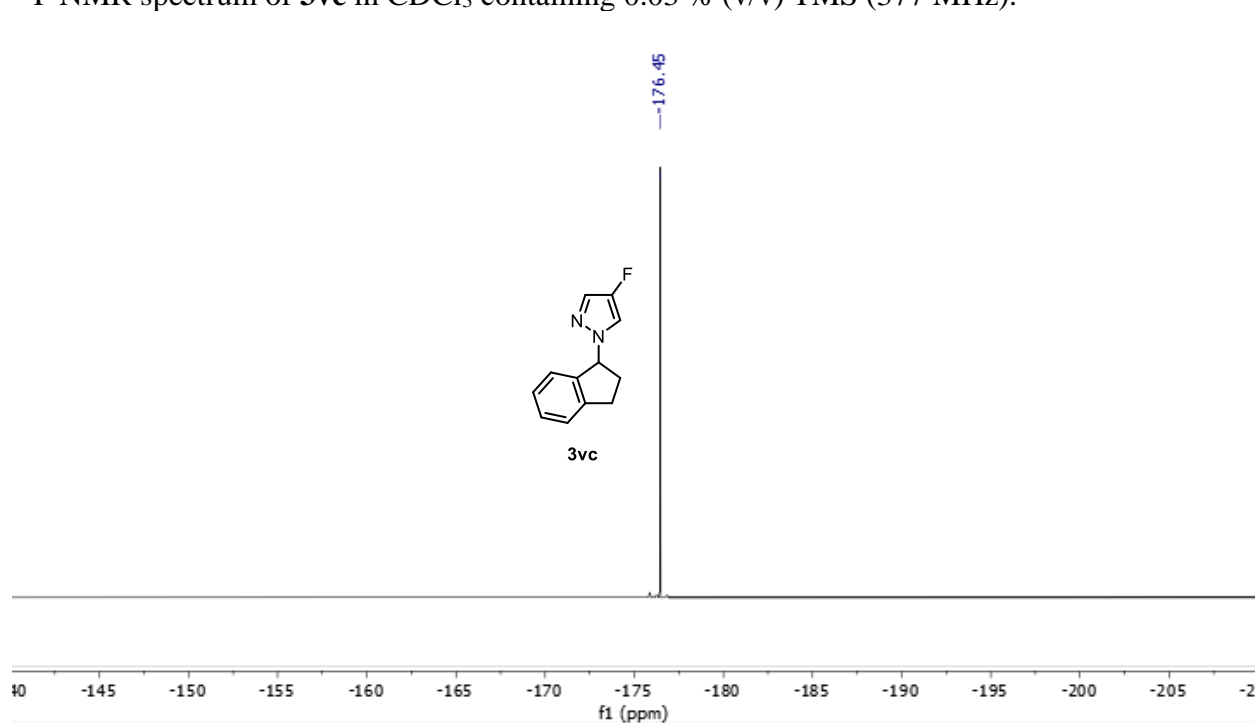
^1H NMR spectrum of **3vc** in CDCl_3 containing 0.03 % (v/v) TMS (500 MHz).



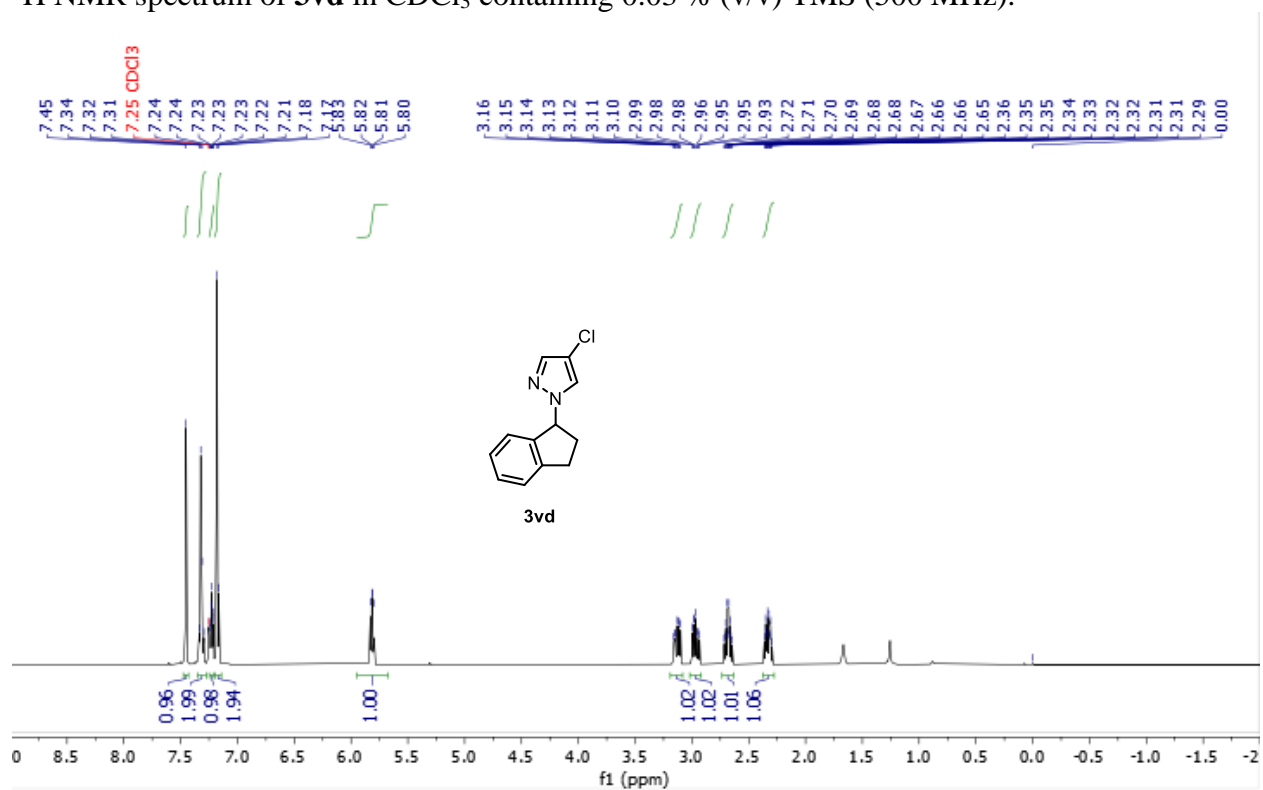
^{13}C NMR spectrum of **3vc** in CDCl_3 containing 0.03 % (v/v) TMS (126 MHz).



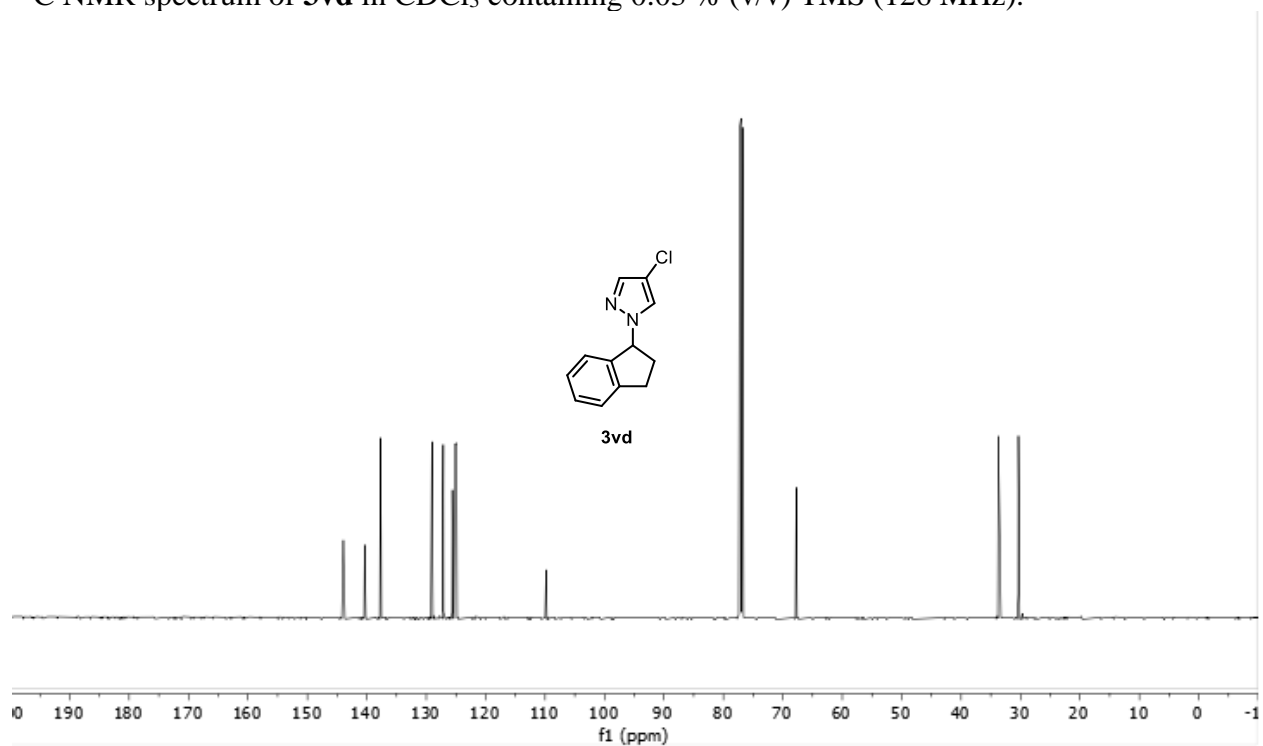
^{19}F NMR spectrum of **3vc** in CDCl_3 containing 0.03 % (v/v) TMS (377 MHz).



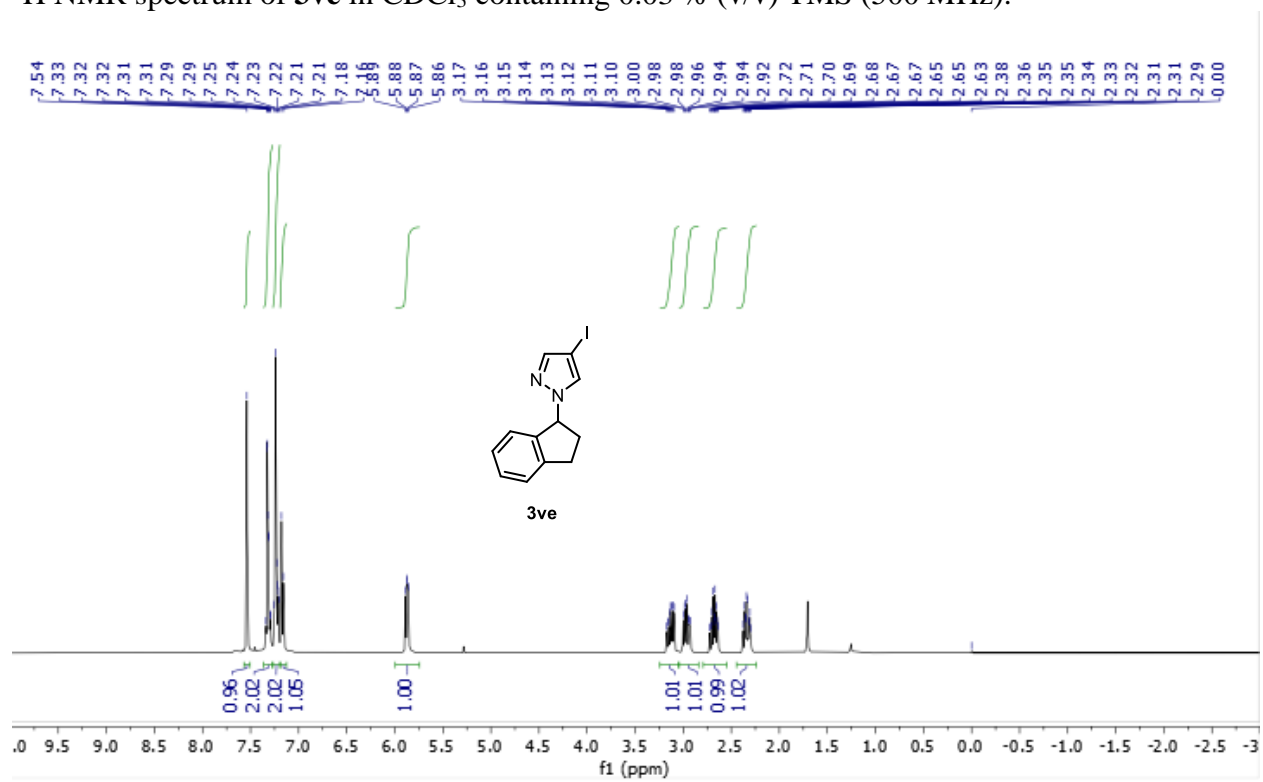
^1H NMR spectrum of **3vd** in CDCl_3 containing 0.03 % (v/v) TMS (500 MHz).



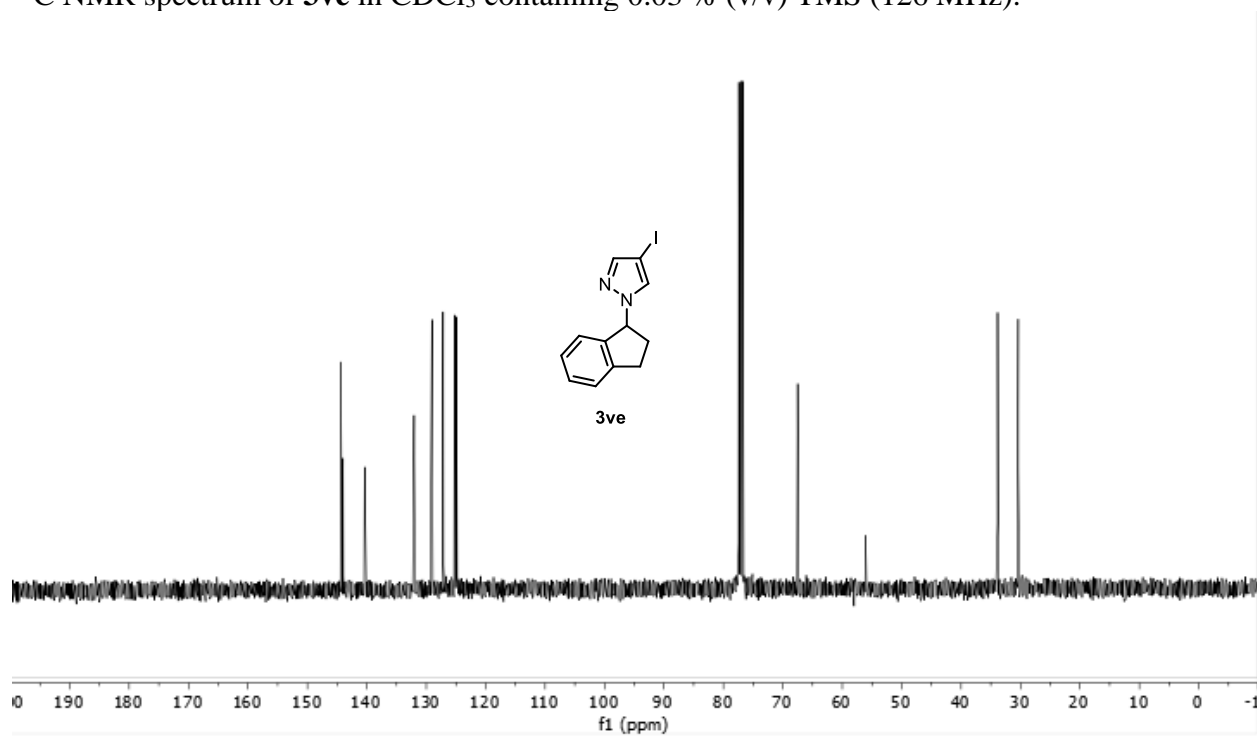
^{13}C NMR spectrum of **3vd** in CDCl_3 containing 0.03 % (v/v) TMS (126 MHz).



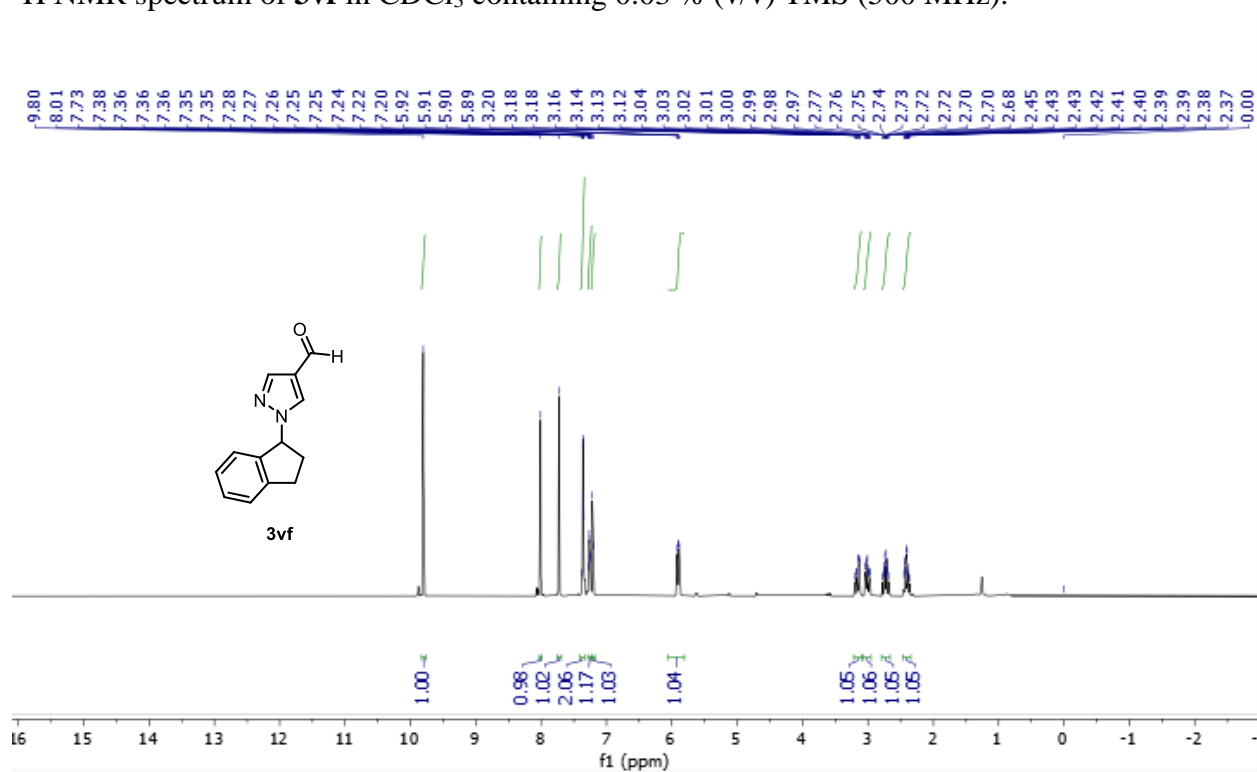
^1H NMR spectrum of **3ve** in CDCl_3 containing 0.03 % (v/v) TMS (500 MHz).



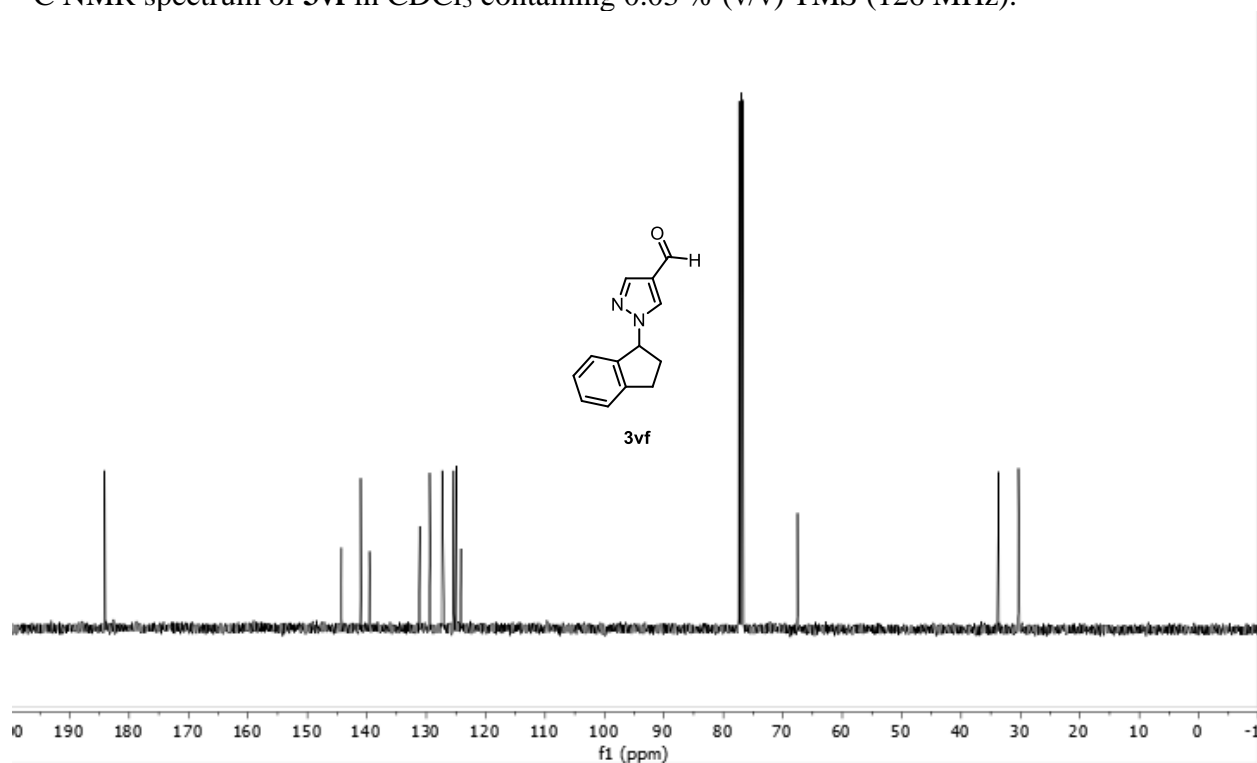
^{13}C NMR spectrum of **3ve** in CDCl_3 containing 0.03 % (v/v) TMS (126 MHz).



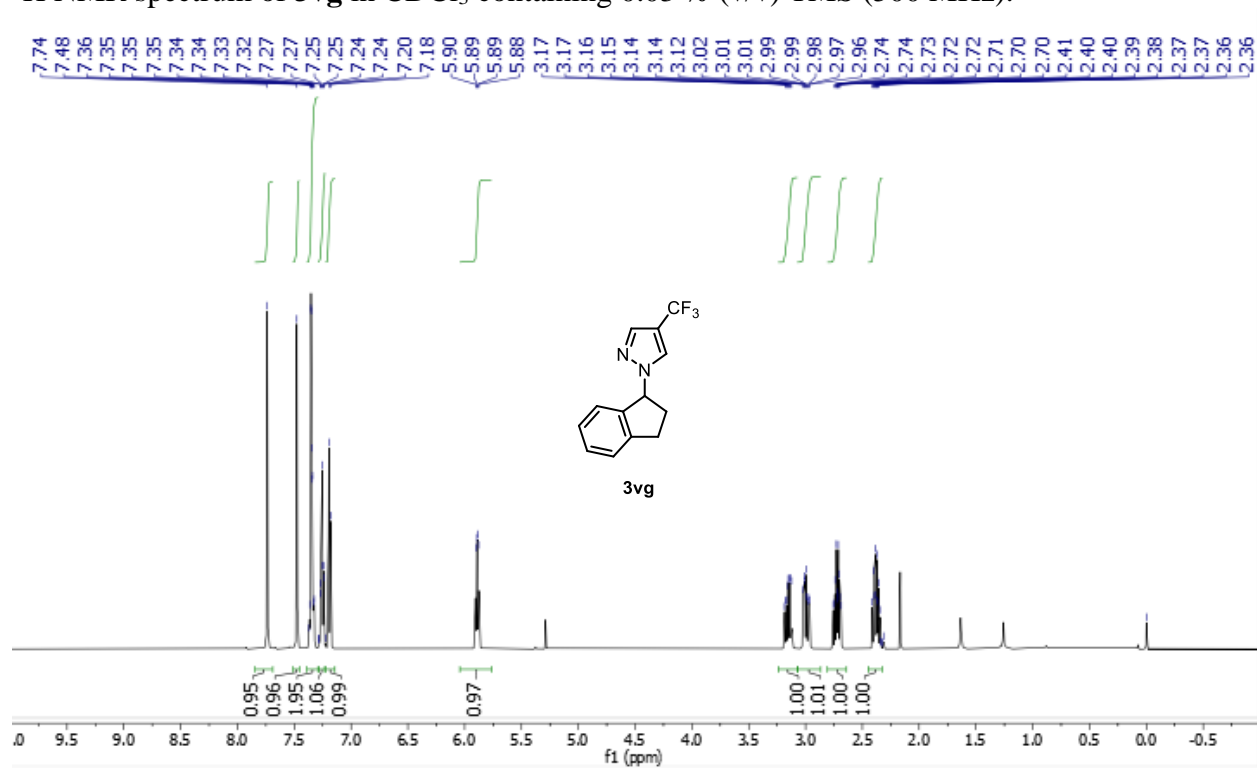
^1H NMR spectrum of **3vf** in CDCl_3 containing 0.03 % (v/v) TMS (500 MHz).



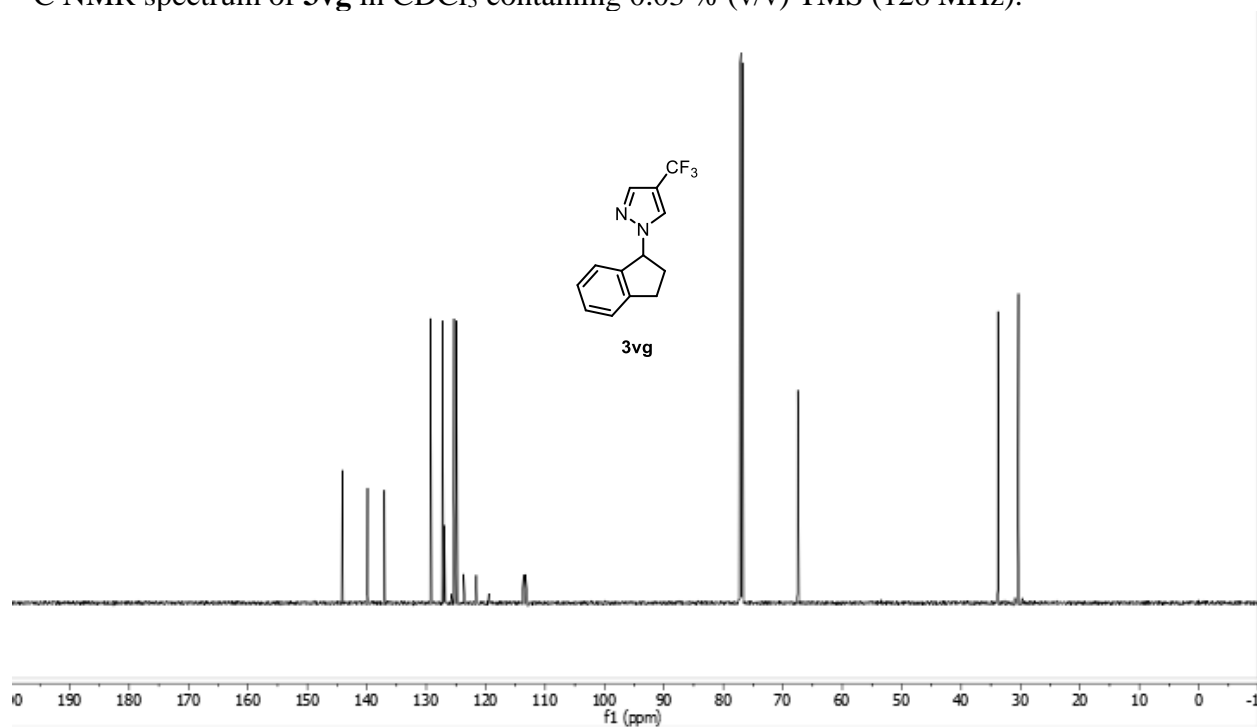
^{13}C NMR spectrum of **3vf** in CDCl_3 containing 0.03 % (v/v) TMS (126 MHz).



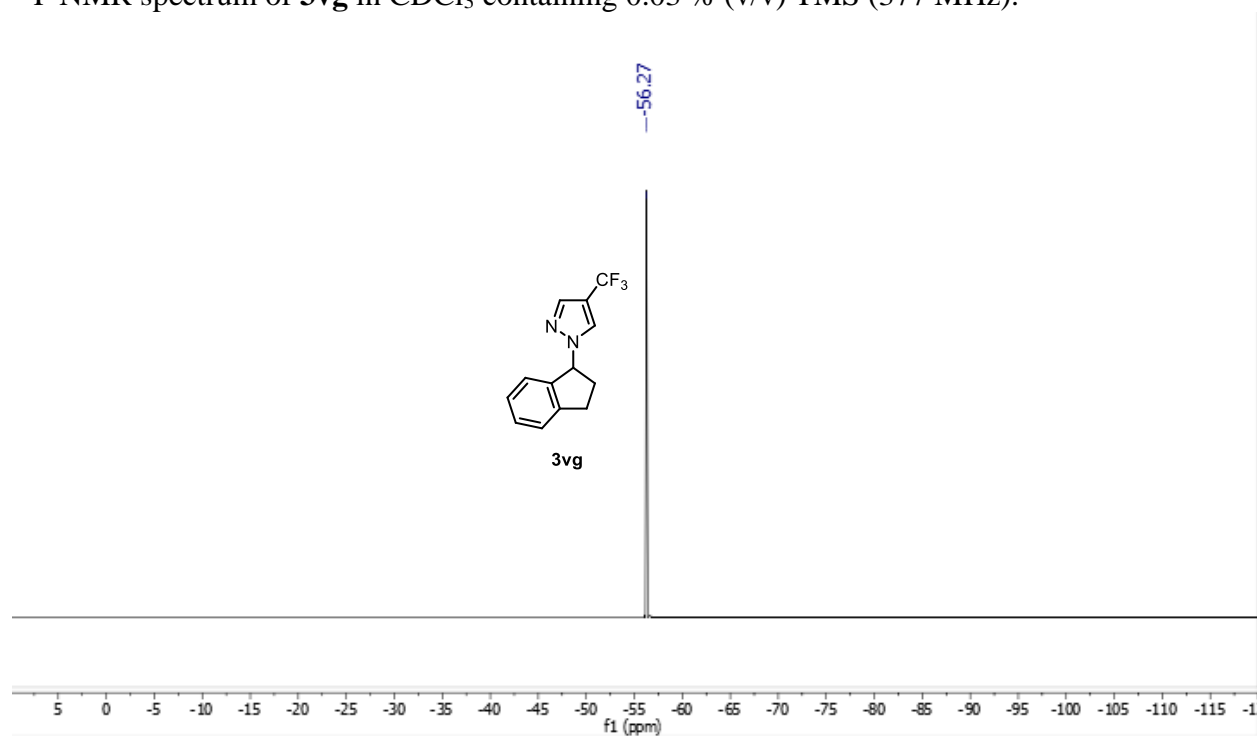
^1H NMR spectrum of **3vg** in CDCl_3 containing 0.03 % (v/v) TMS (500 MHz).



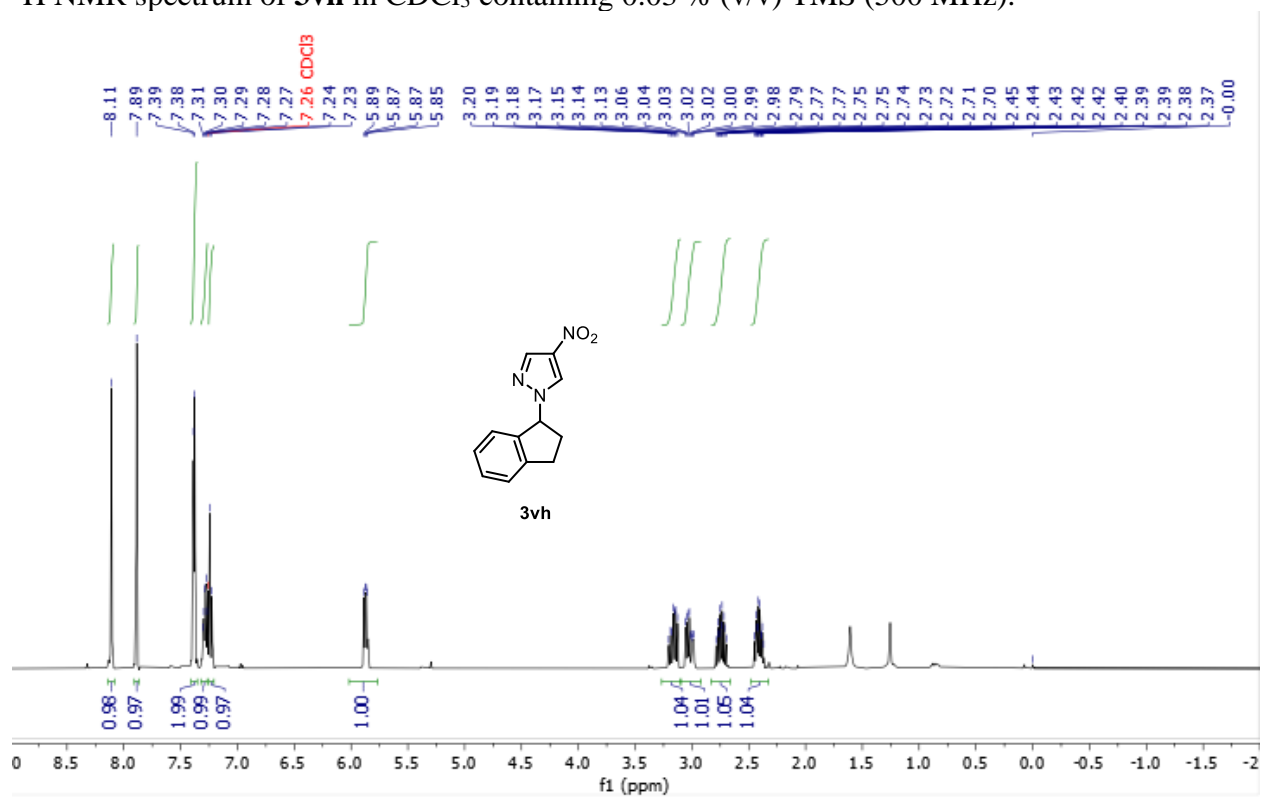
^{13}C NMR spectrum of **3vg** in CDCl_3 containing 0.03 % (v/v) TMS (126 MHz).



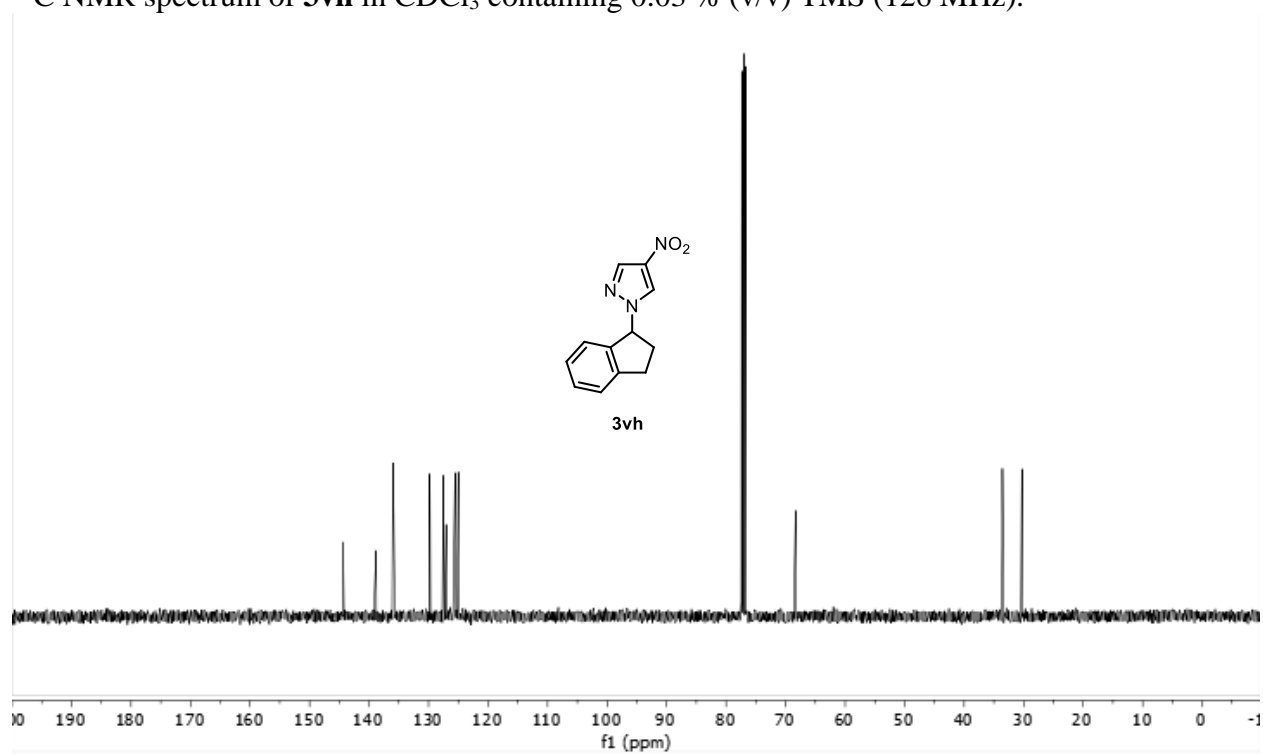
^{19}F NMR spectrum of **3vg** in CDCl_3 containing 0.03 % (v/v) TMS (377 MHz).



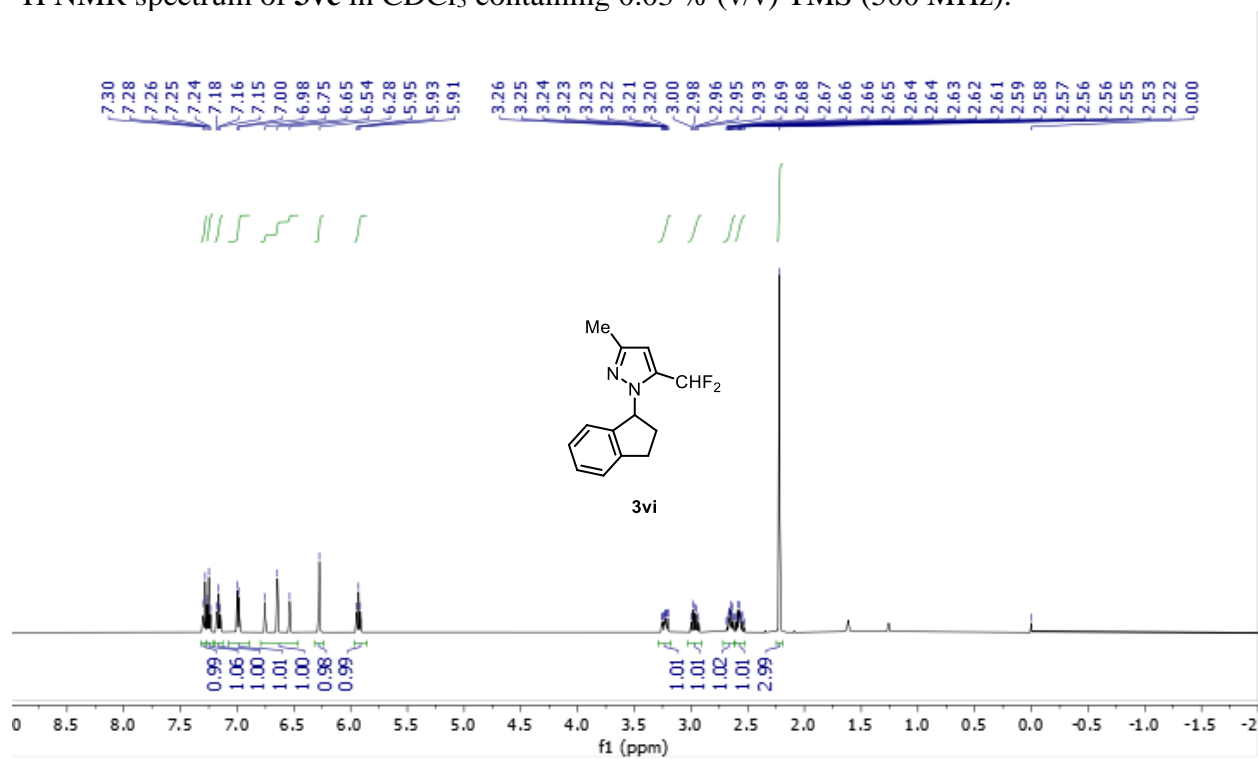
^1H NMR spectrum of **3vh** in CDCl_3 containing 0.03 % (v/v) TMS (500 MHz).



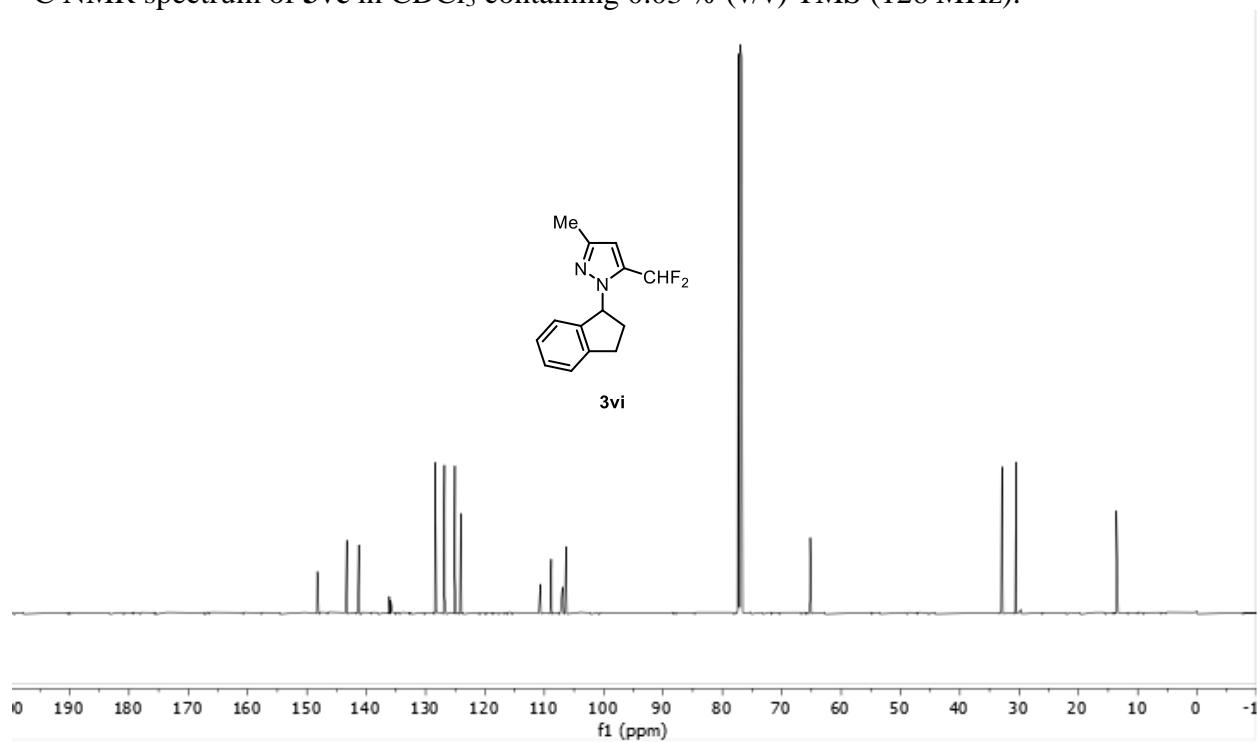
^{13}C NMR spectrum of **3vh** in CDCl_3 containing 0.03 % (v/v) TMS (126 MHz).



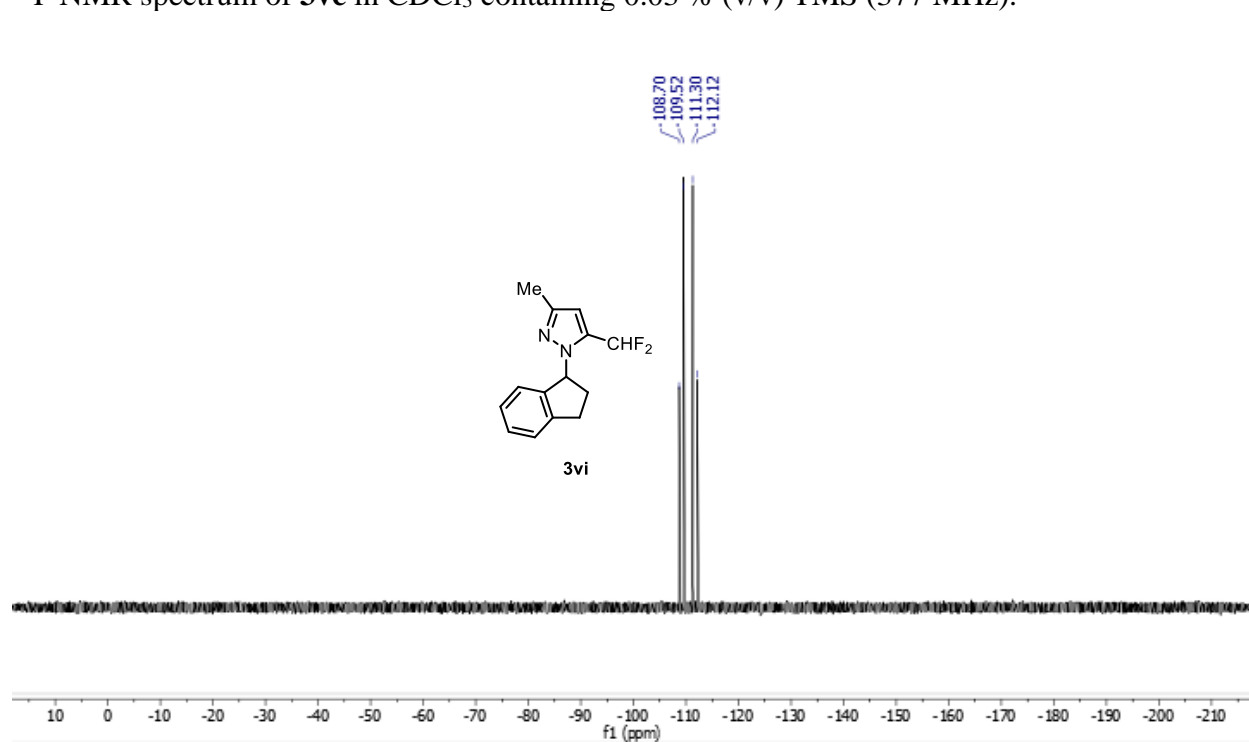
^1H NMR spectrum of **3ve** in CDCl_3 containing 0.03 % (v/v) TMS (500 MHz).



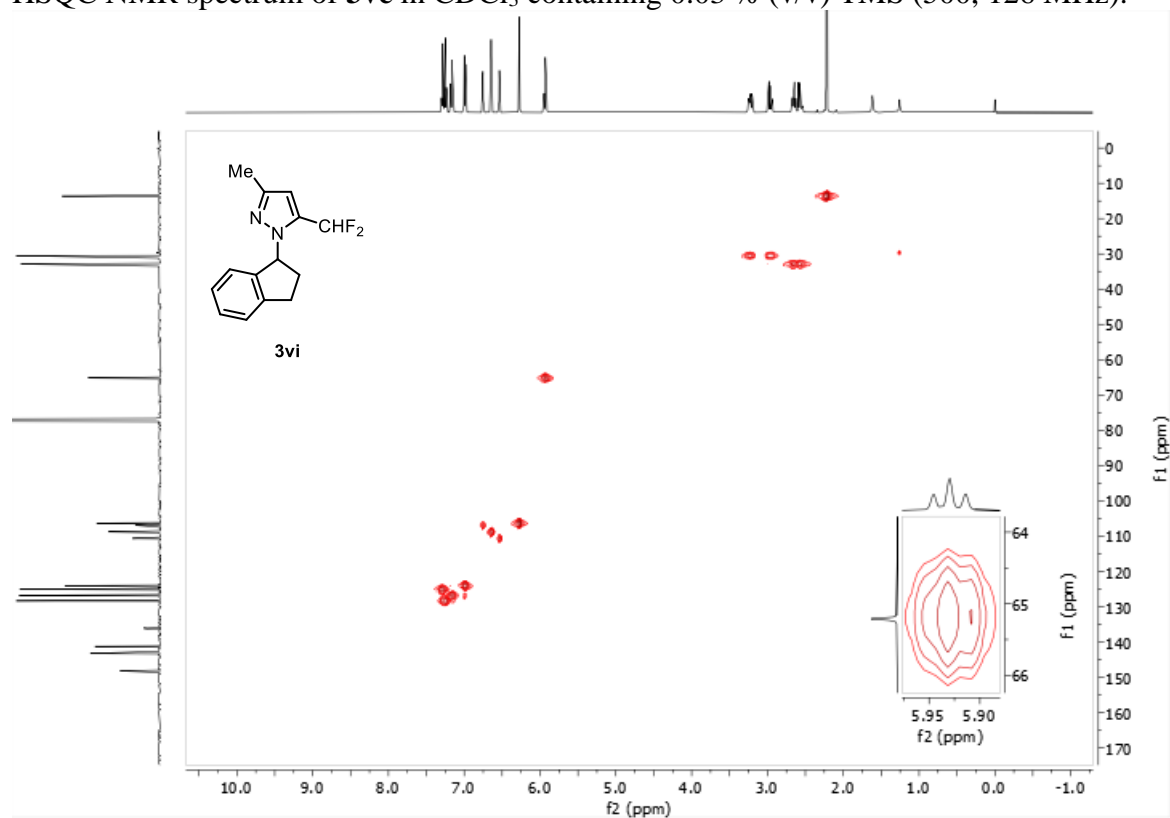
^{13}C NMR spectrum of **3ve** in CDCl_3 containing 0.03 % (v/v) TMS (126 MHz).



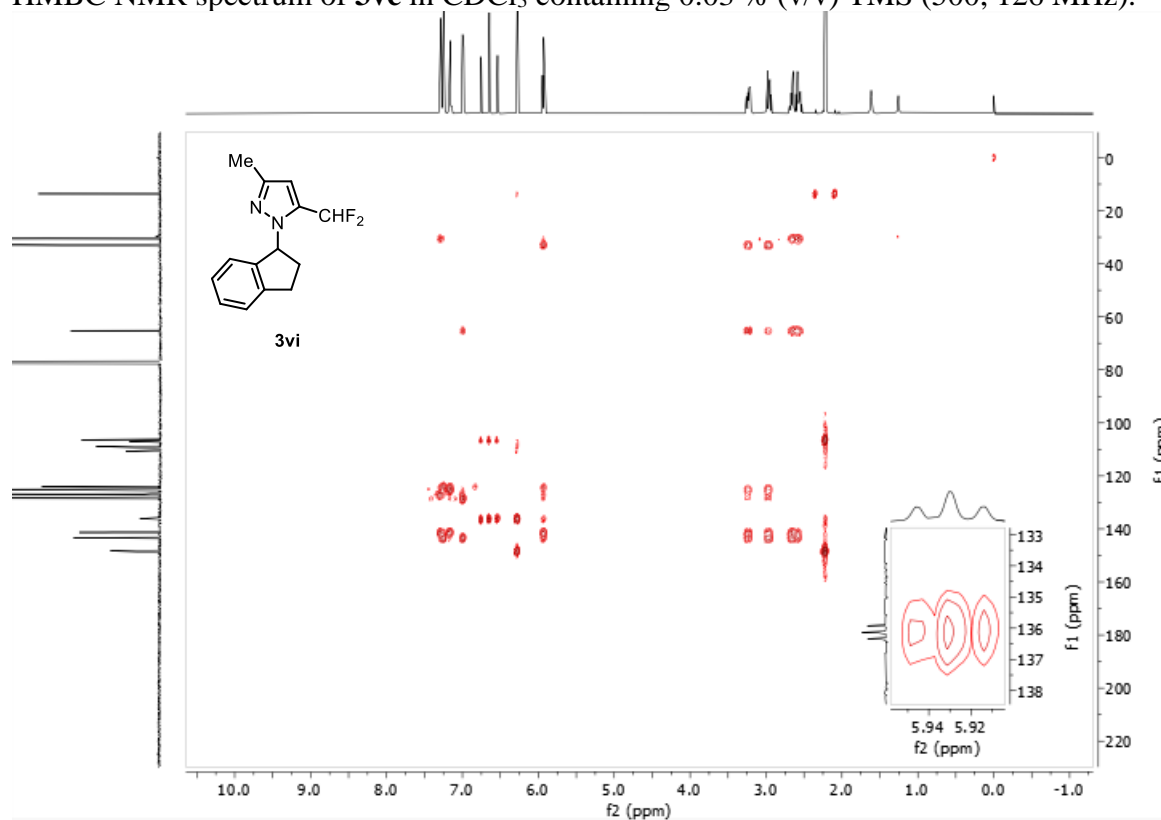
^{19}F NMR spectrum of **3vc** in CDCl_3 containing 0.03 % (v/v) TMS (377 MHz).



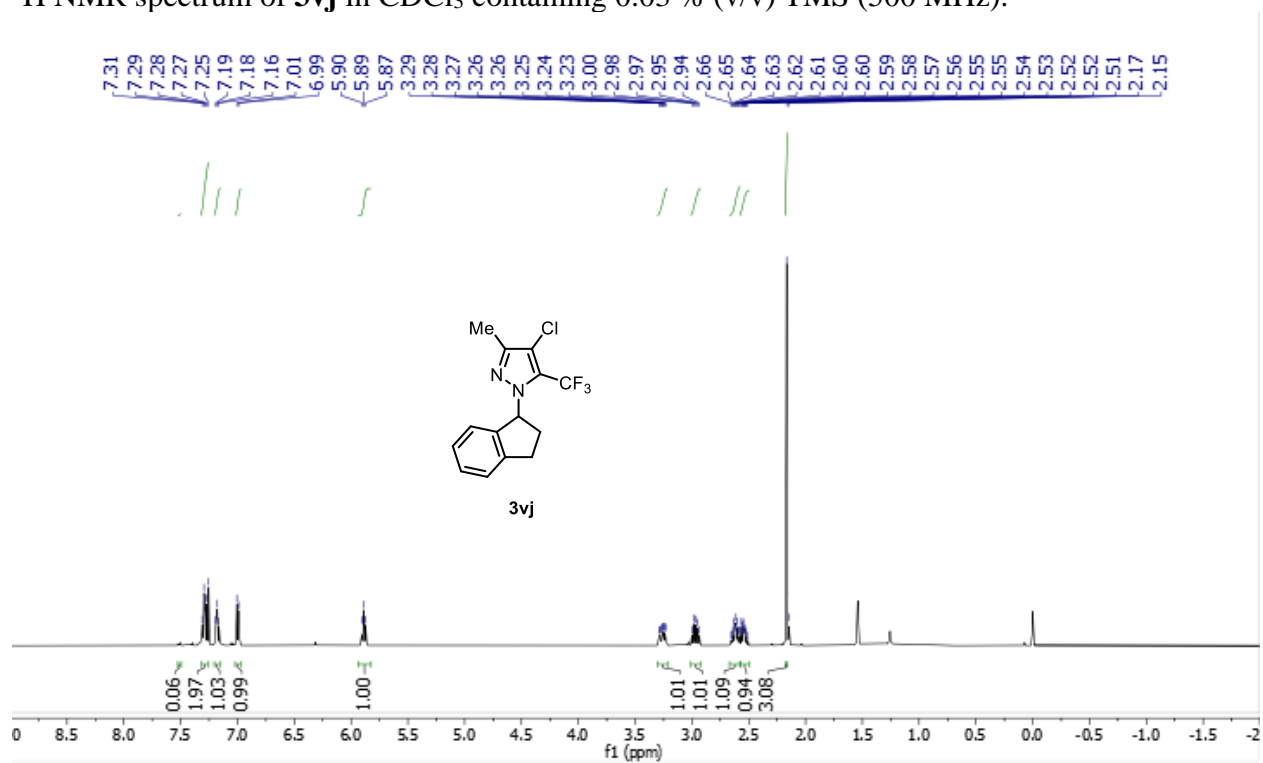
HSQC NMR spectrum of **3vc** in CDCl_3 containing 0.03 % (v/v) TMS (500, 126 MHz).



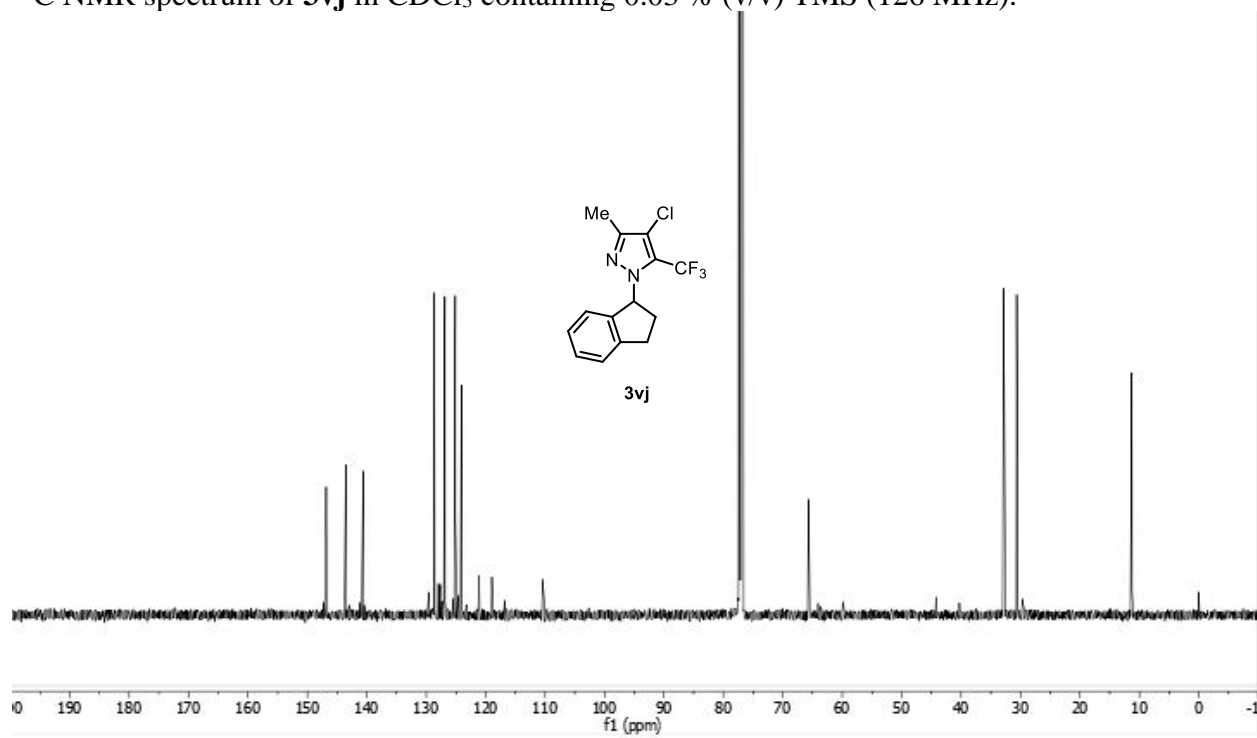
HMBC NMR spectrum of **3vc** in CDCl₃ containing 0.03 % (v/v) TMS (500, 126 MHz).



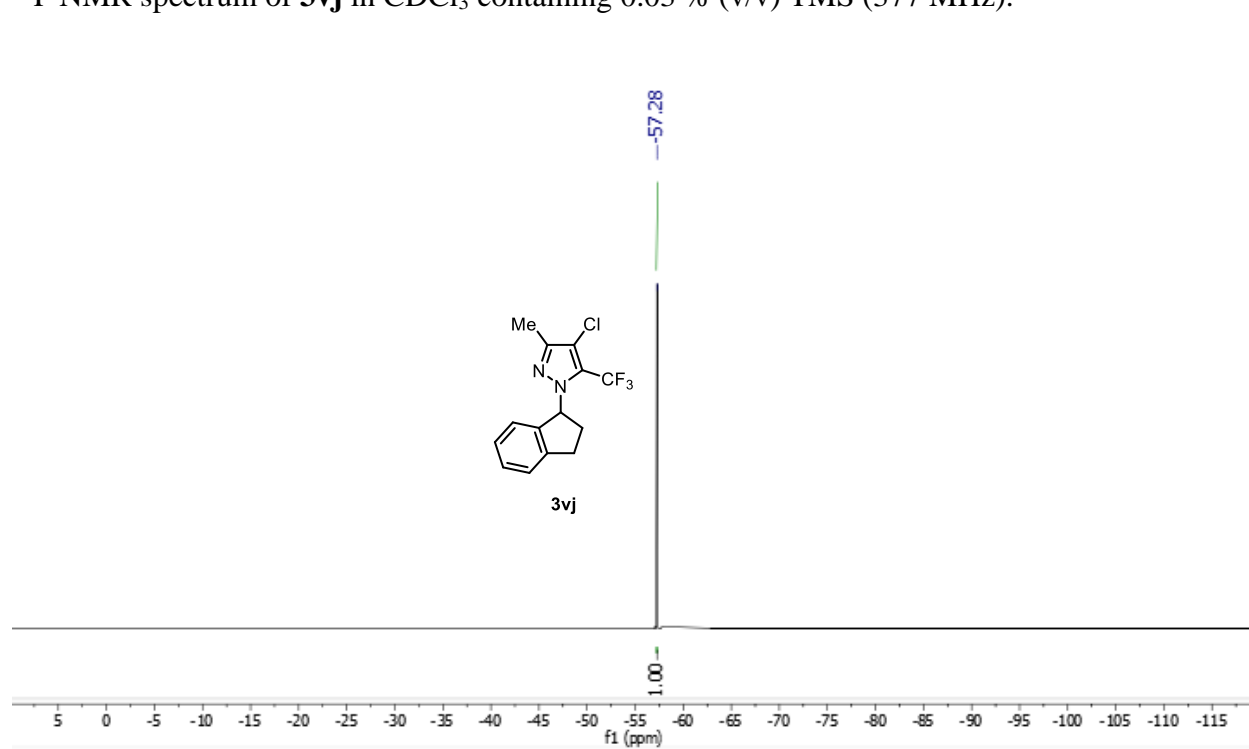
¹H NMR spectrum of **3vj** in CDCl₃ containing 0.03 % (v/v) TMS (500 MHz).



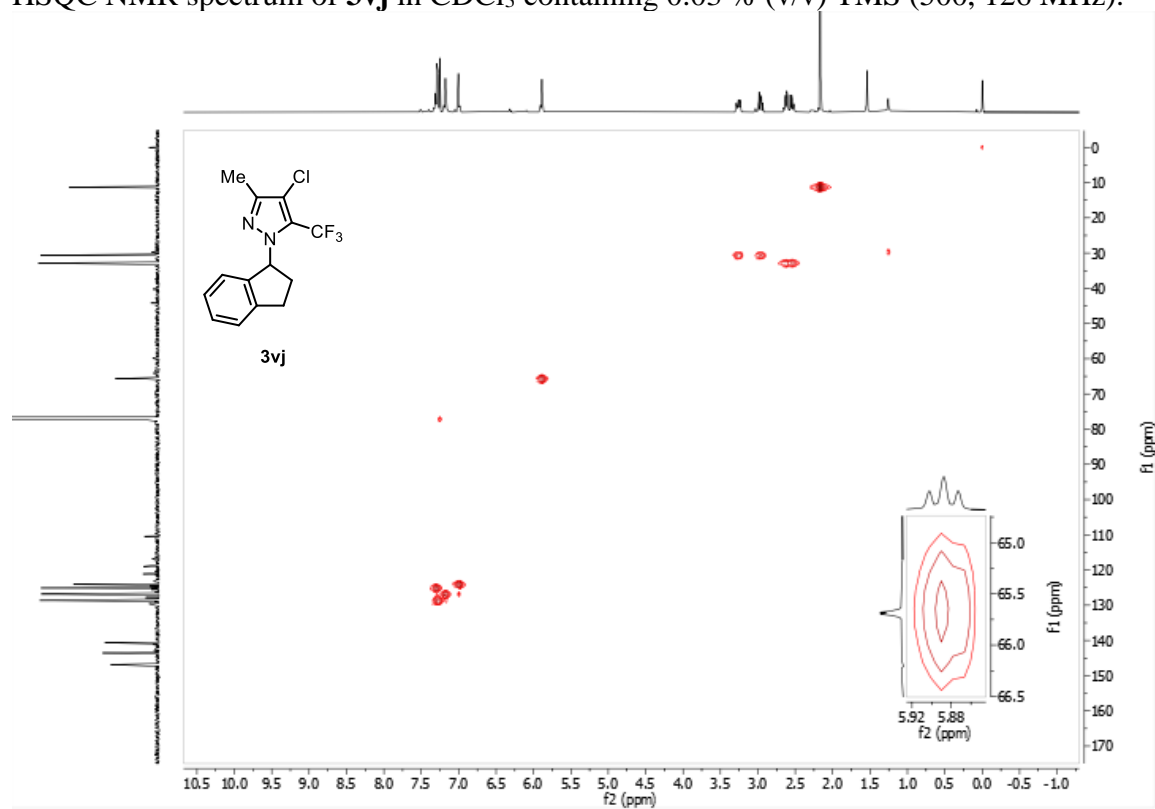
^{13}C NMR spectrum of **3vj** in CDCl_3 containing 0.03 % (v/v) TMS (126 MHz).



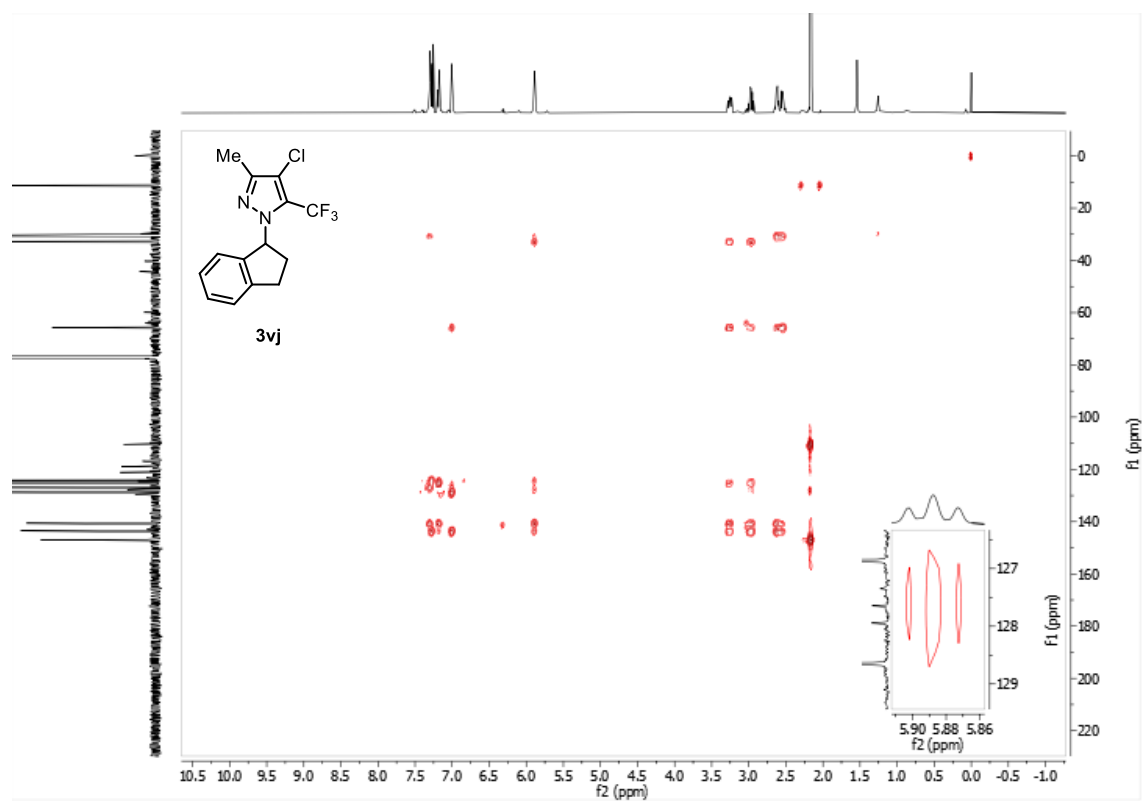
^{19}F NMR spectrum of **3vj** in CDCl_3 containing 0.03 % (v/v) TMS (377 MHz).



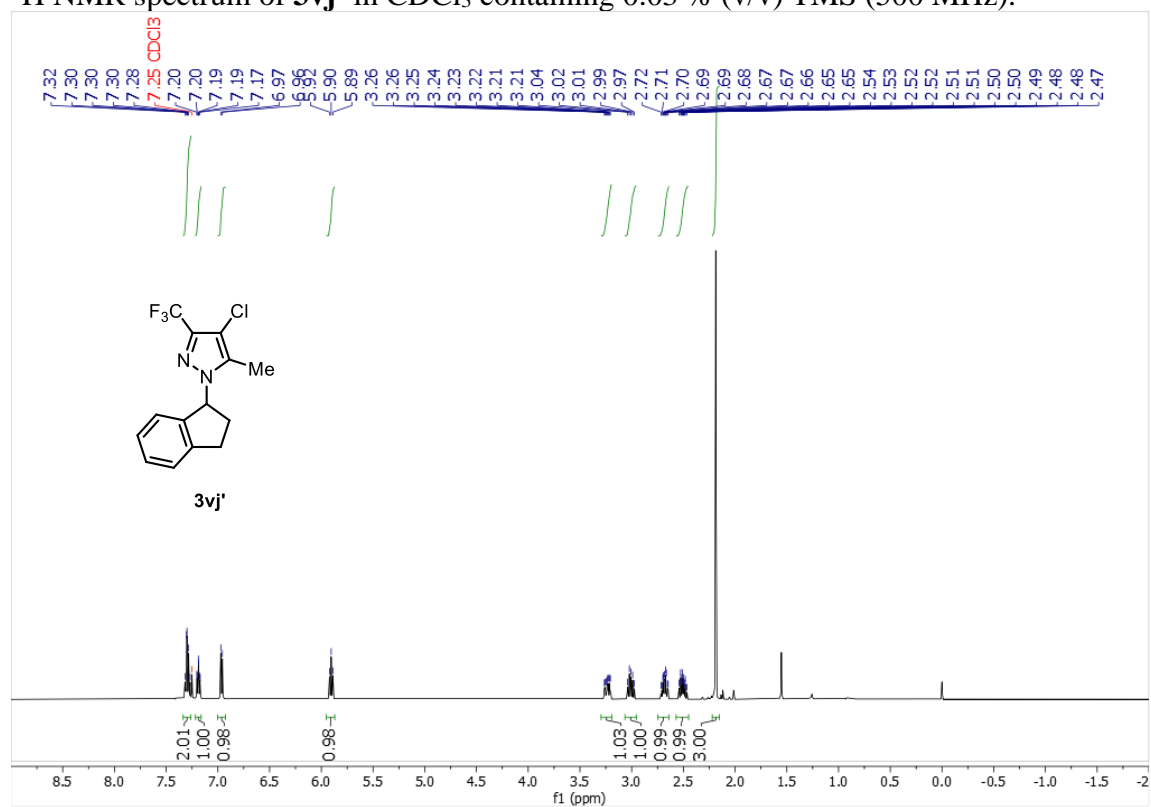
HSQC NMR spectrum of **3vj** in CDCl₃ containing 0.03 % (v/v) TMS (500, 126 MHz).



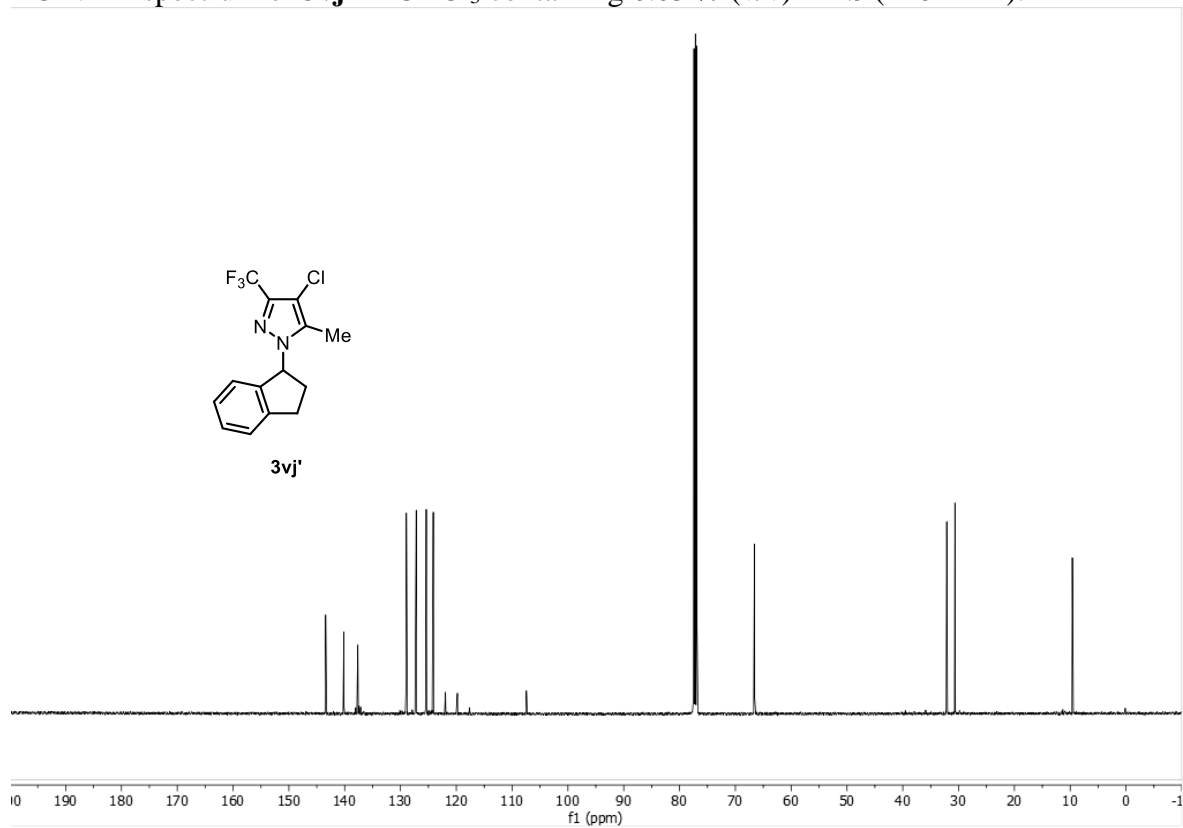
HMBC NMR spectrum of **3vj** in CDCl₃ containing 0.03 % (v/v) TMS (500, 126 MHz).



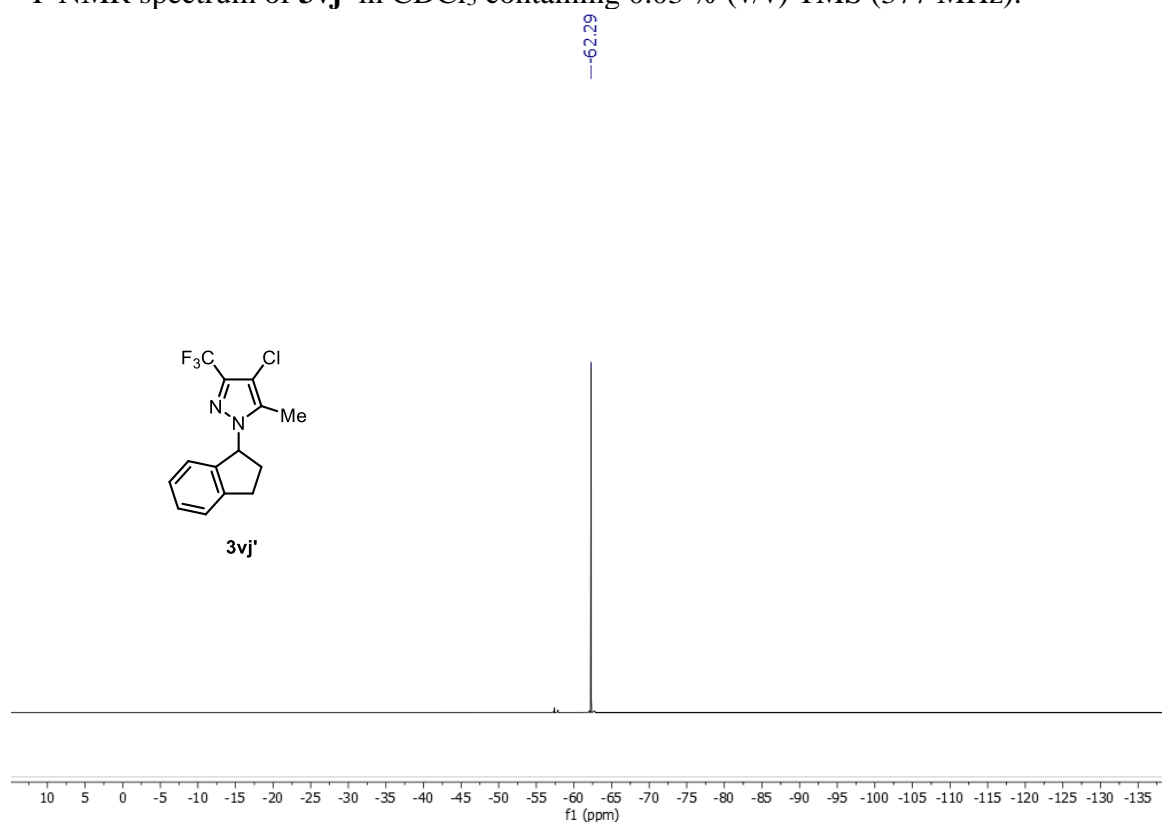
^1H NMR spectrum of **3vj'** in CDCl_3 containing 0.03 % (v/v) TMS (500 MHz).



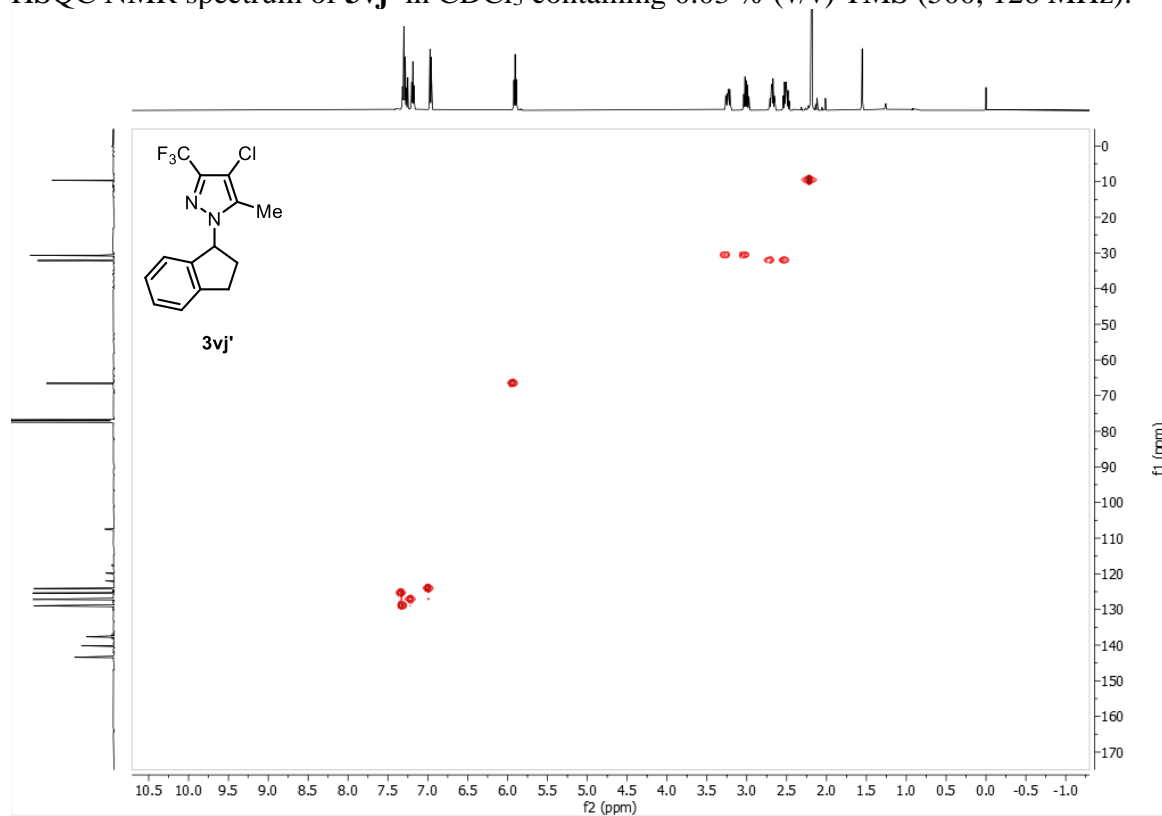
^{13}C NMR spectrum of **3vj'** in CDCl_3 containing 0.03 % (v/v) TMS (126 MHz).



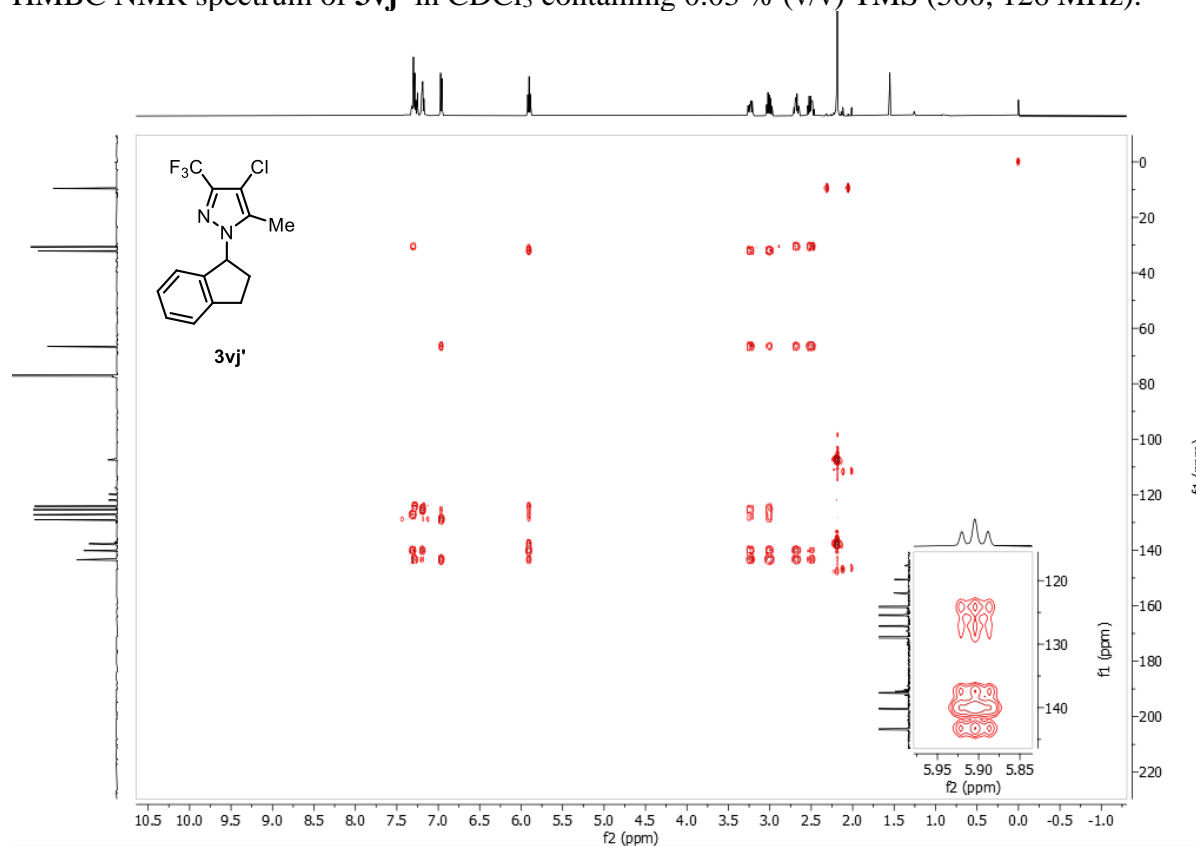
^{19}F NMR spectrum of **3vj'** in CDCl_3 containing 0.03 % (v/v) TMS (377 MHz).



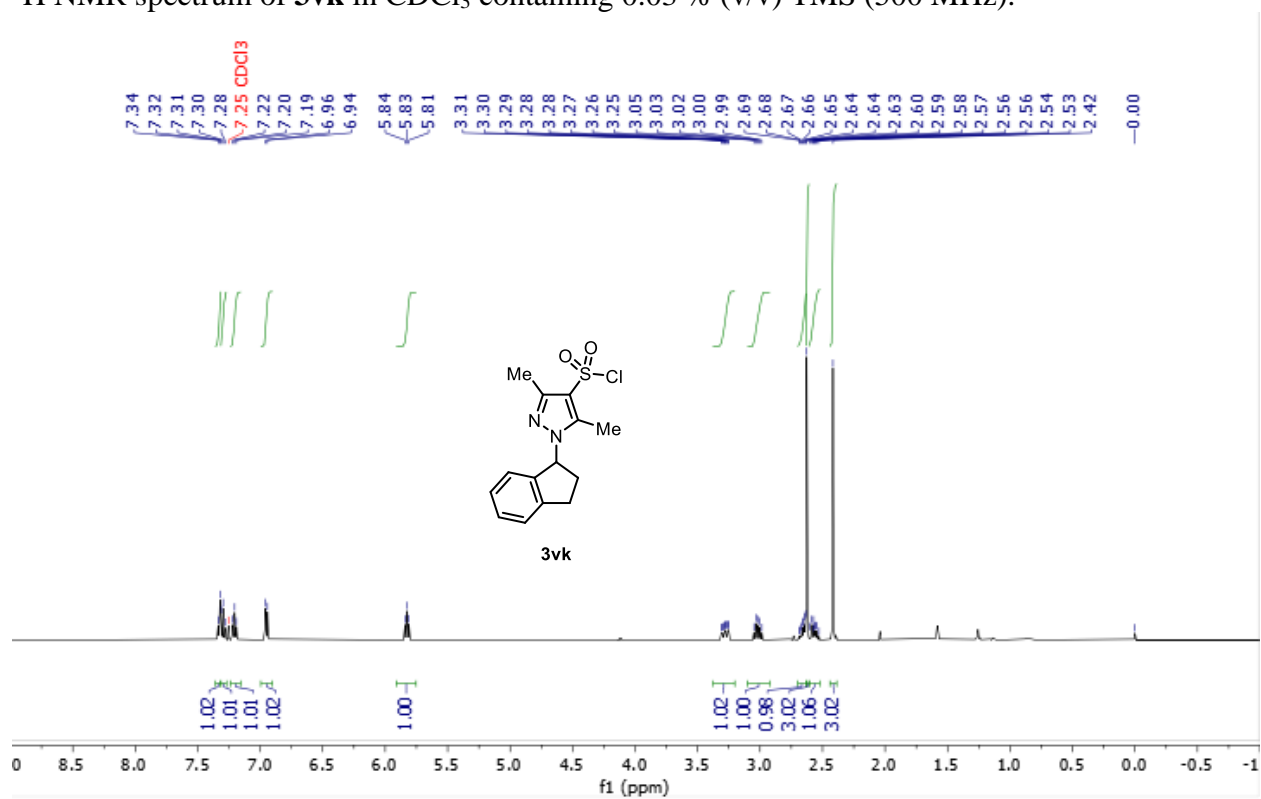
HSQC NMR spectrum of **3vj'** in CDCl_3 containing 0.03 % (v/v) TMS (500, 126 MHz).



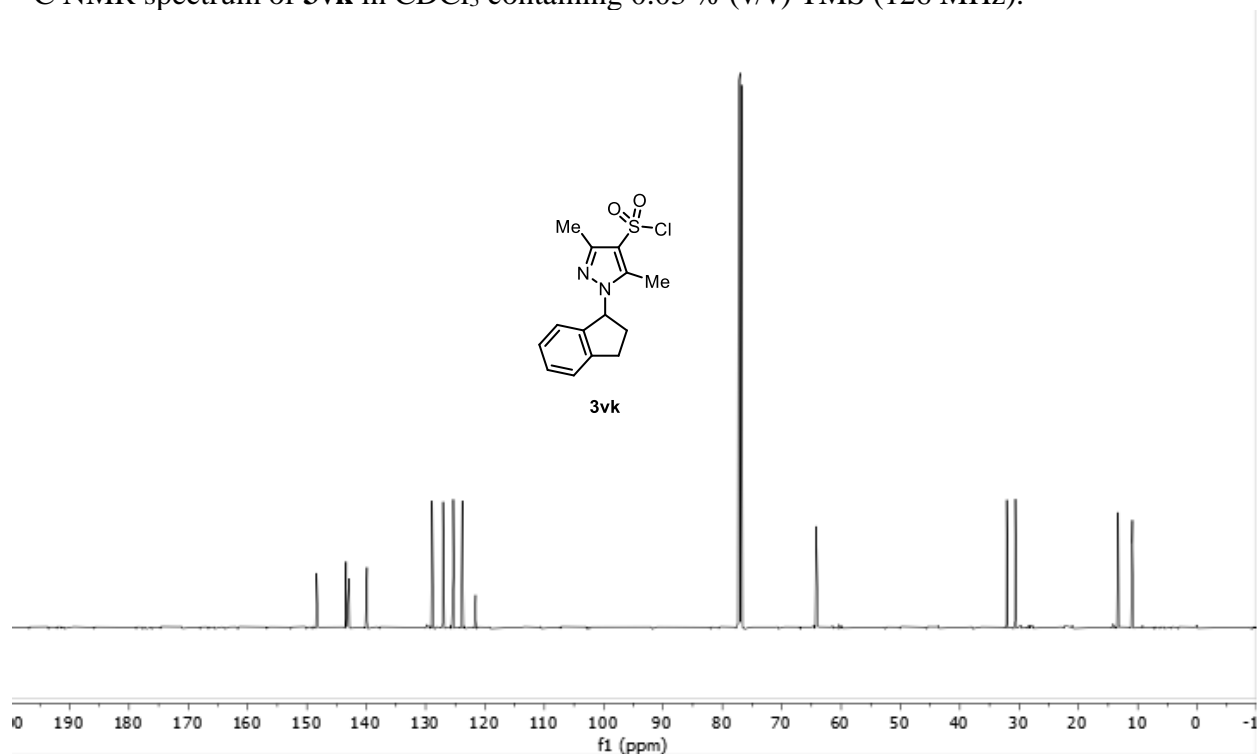
HMBC NMR spectrum of **3vj'** in CDCl₃ containing 0.03 % (v/v) TMS (500, 126 MHz).



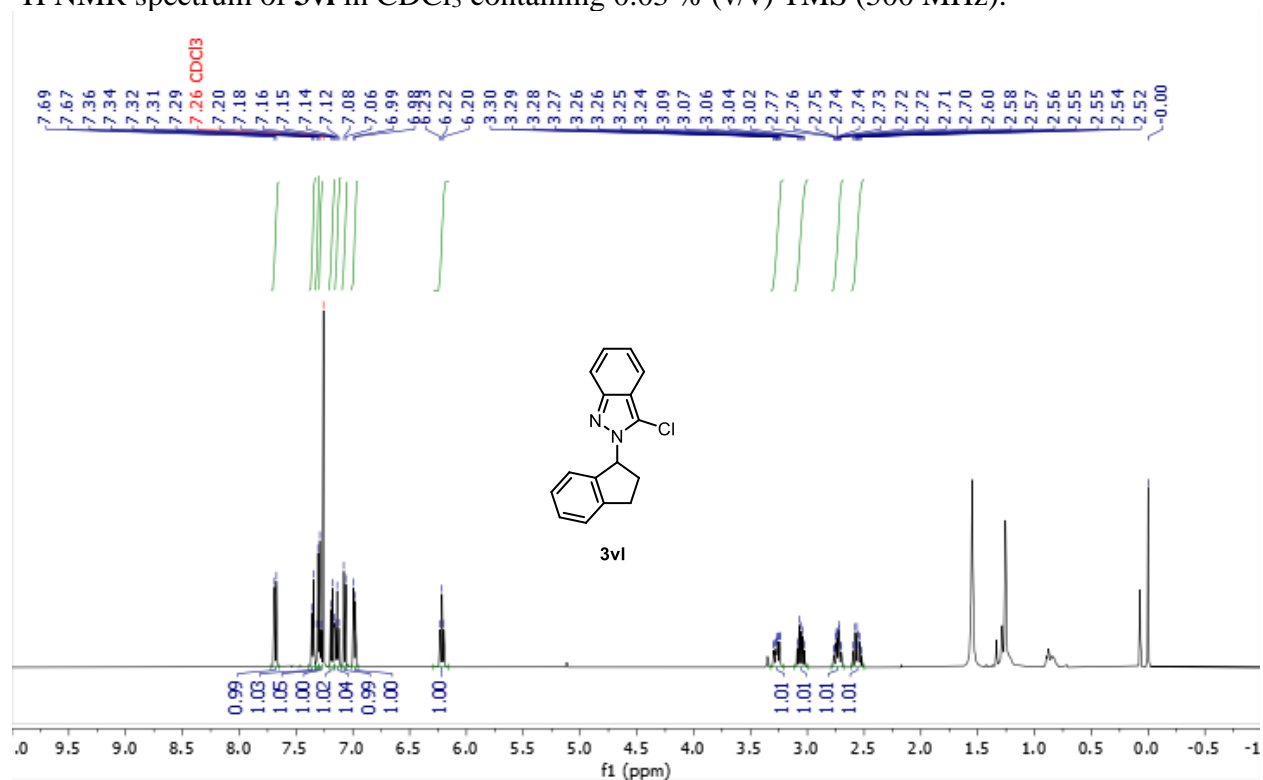
¹H NMR spectrum of **3vk** in CDCl₃ containing 0.03 % (v/v) TMS (500 MHz).



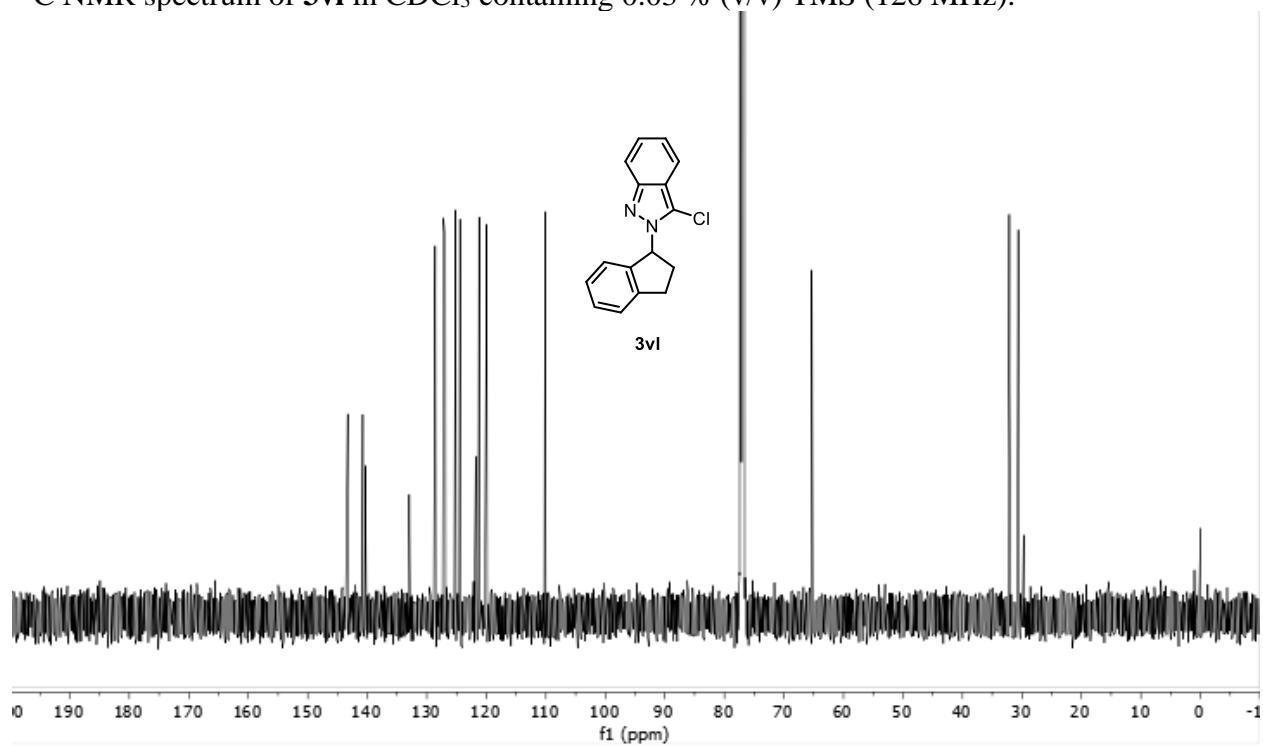
^{13}C NMR spectrum of **3vk** in CDCl_3 containing 0.03 % (v/v) TMS (126 MHz).



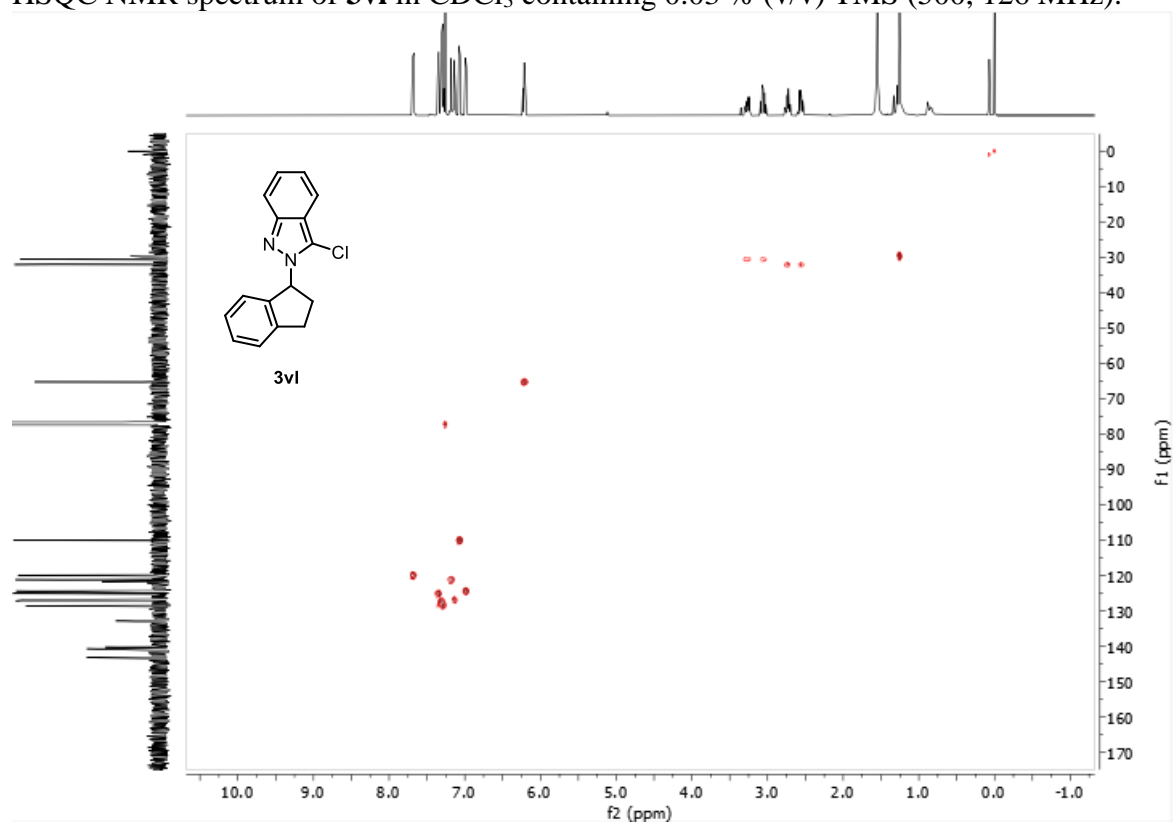
^1H NMR spectrum of **3vl** in CDCl_3 containing 0.03 % (v/v) TMS (500 MHz).



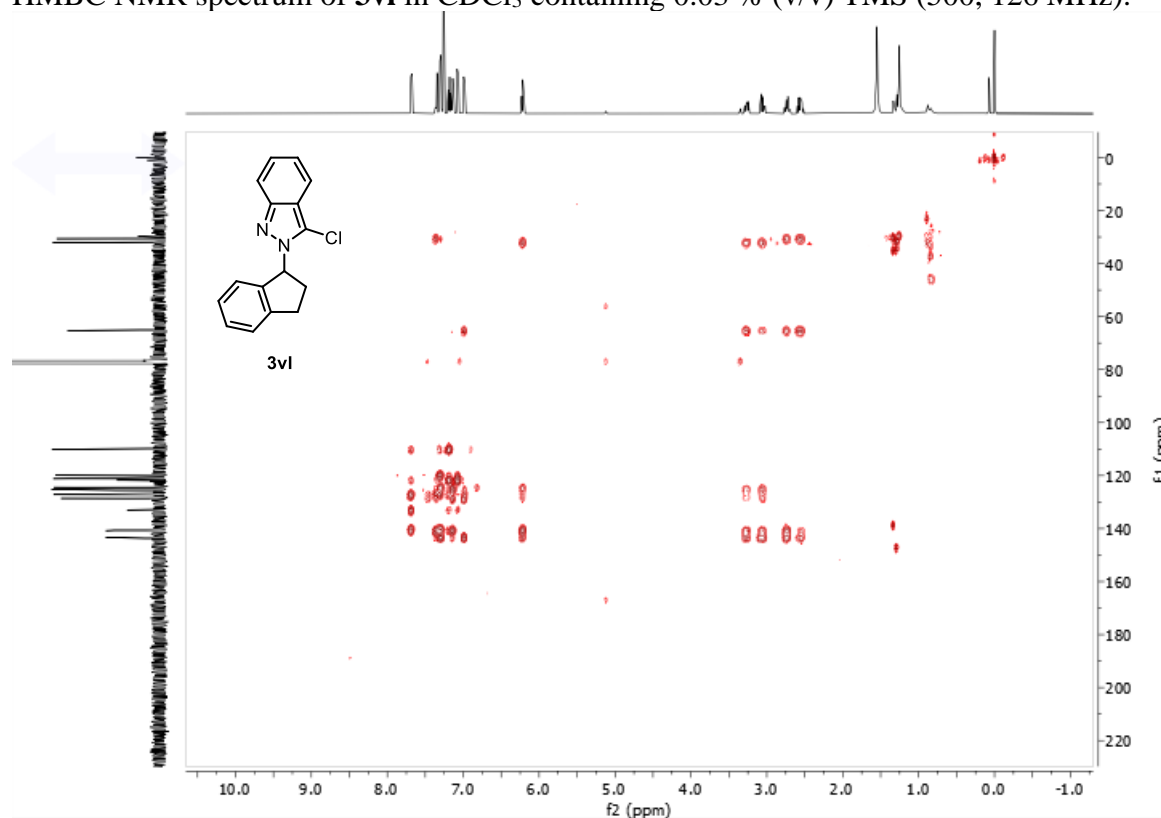
^{13}C NMR spectrum of **3vl** in CDCl_3 containing 0.03 % (v/v) TMS (126 MHz).



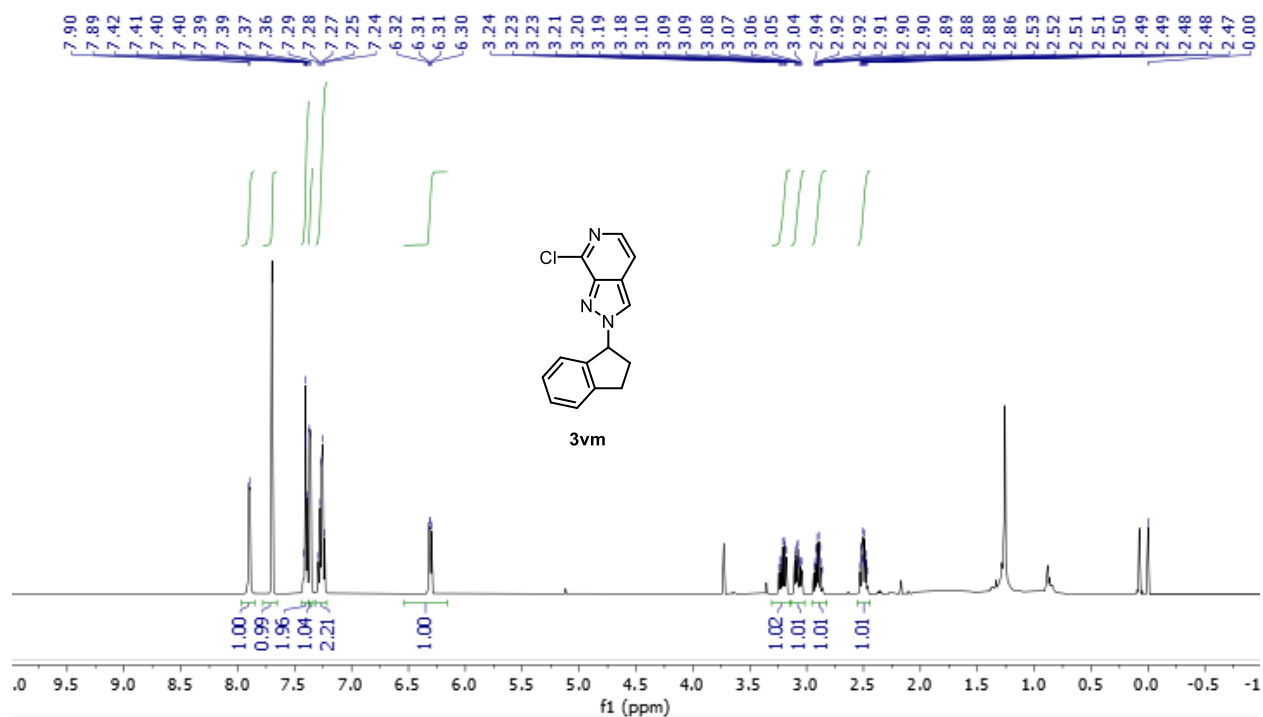
HSQC NMR spectrum of **3vl** in CDCl_3 containing 0.03 % (v/v) TMS (500, 126 MHz).



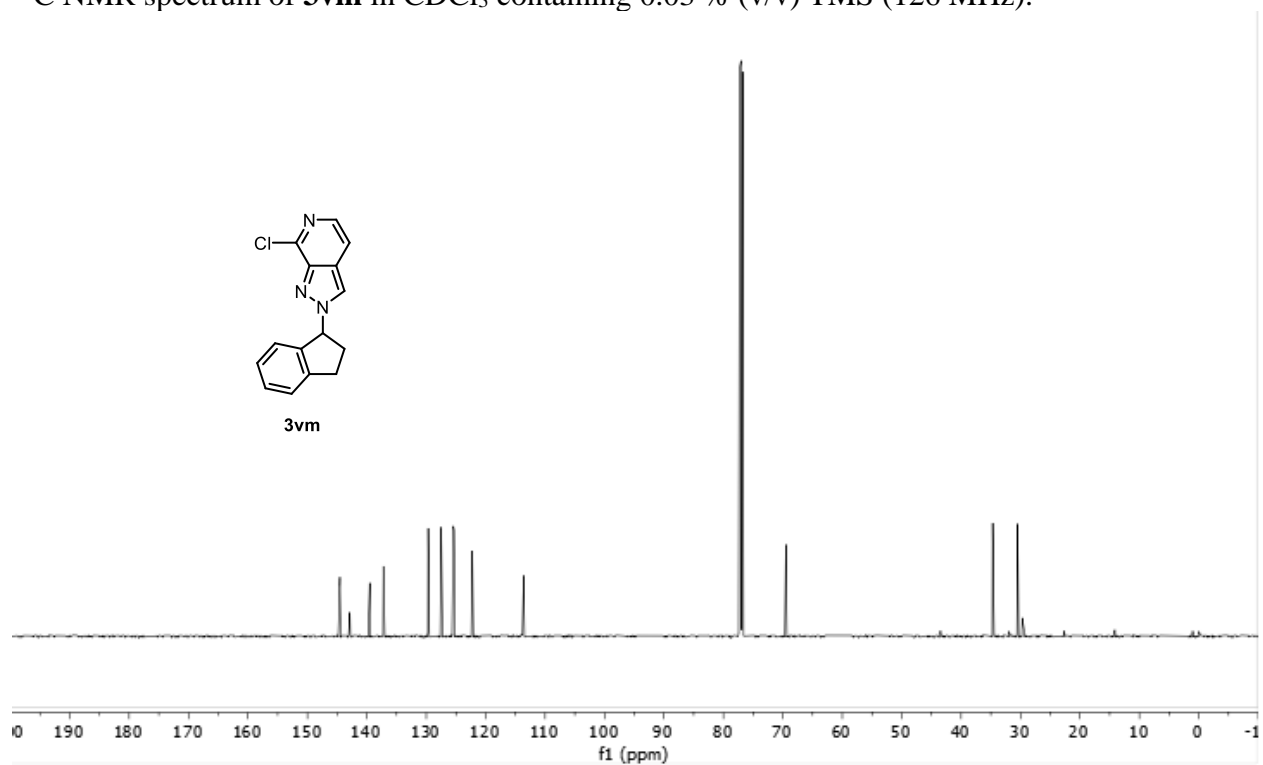
HMBC NMR spectrum of **3vl** in CDCl₃ containing 0.03 % (v/v) TMS (500, 126 MHz).



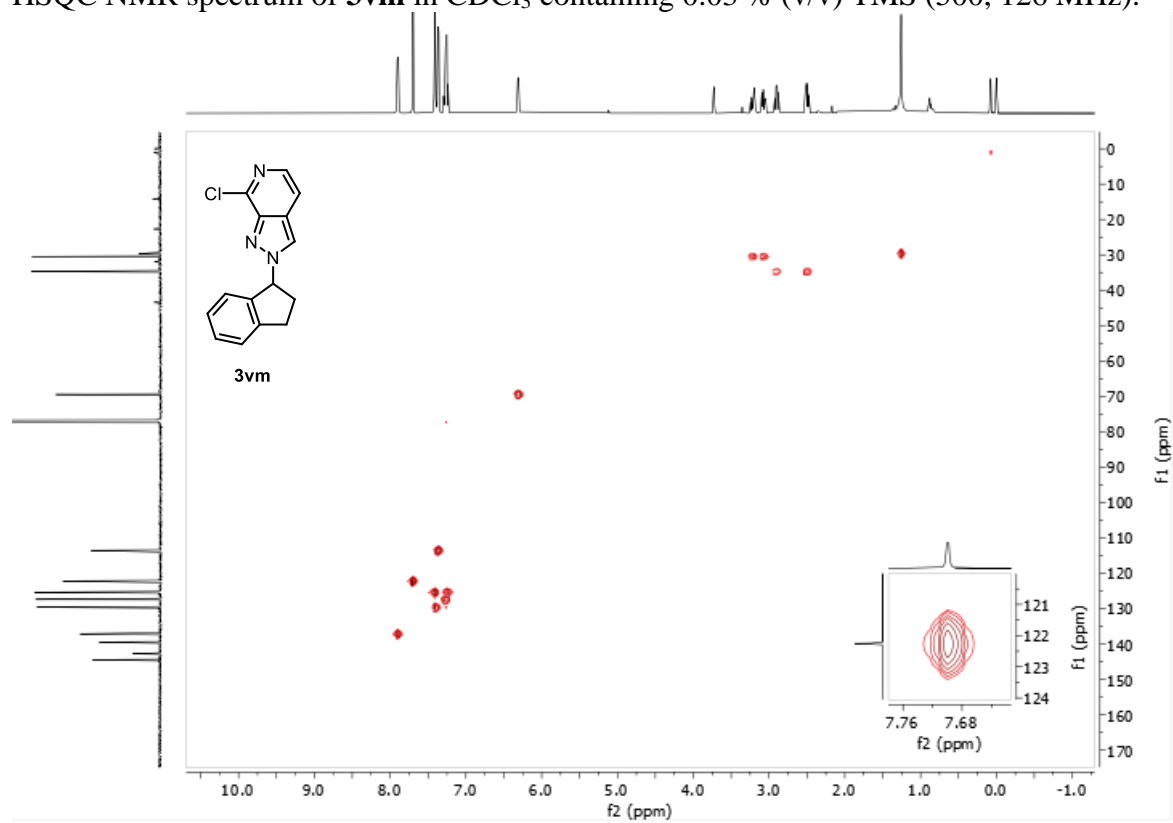
¹H NMR spectrum of **3vm** in CDCl₃ containing 0.03 % (v/v) TMS (500 MHz).



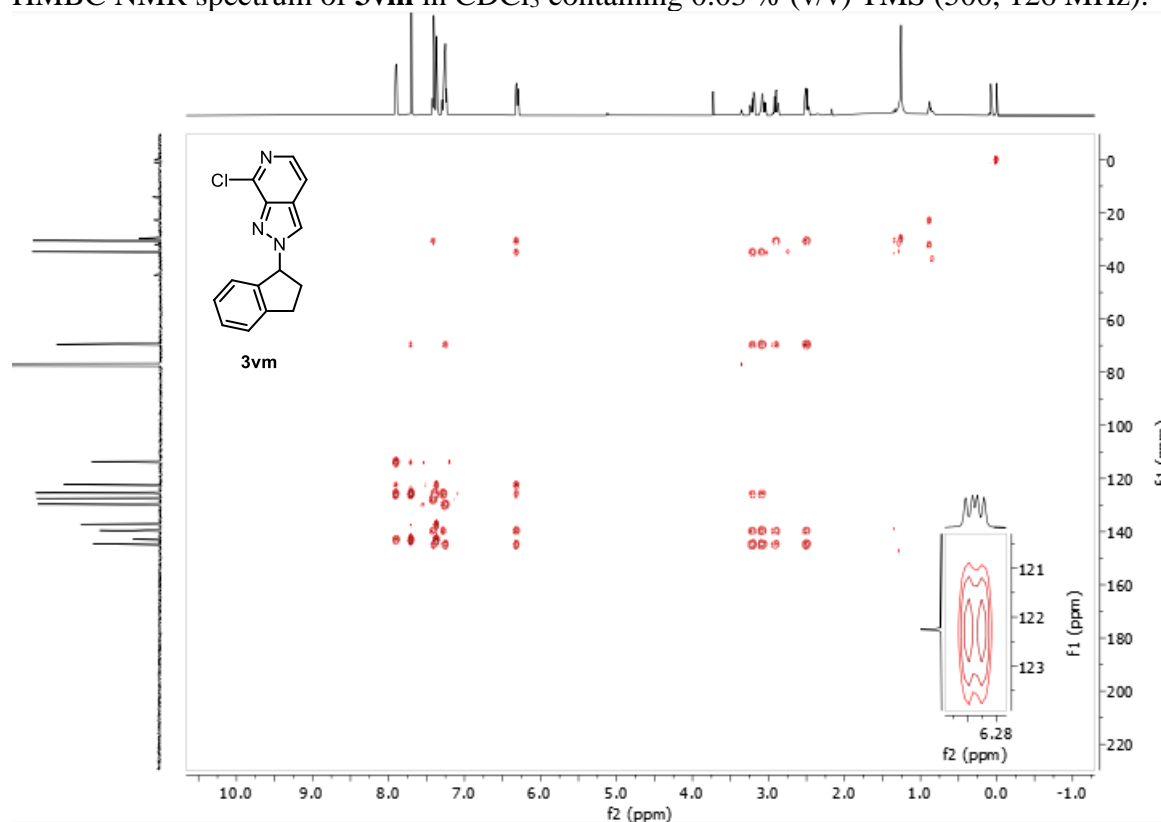
^{13}C NMR spectrum of **3vm** in CDCl_3 containing 0.03 % (v/v) TMS (126 MHz).



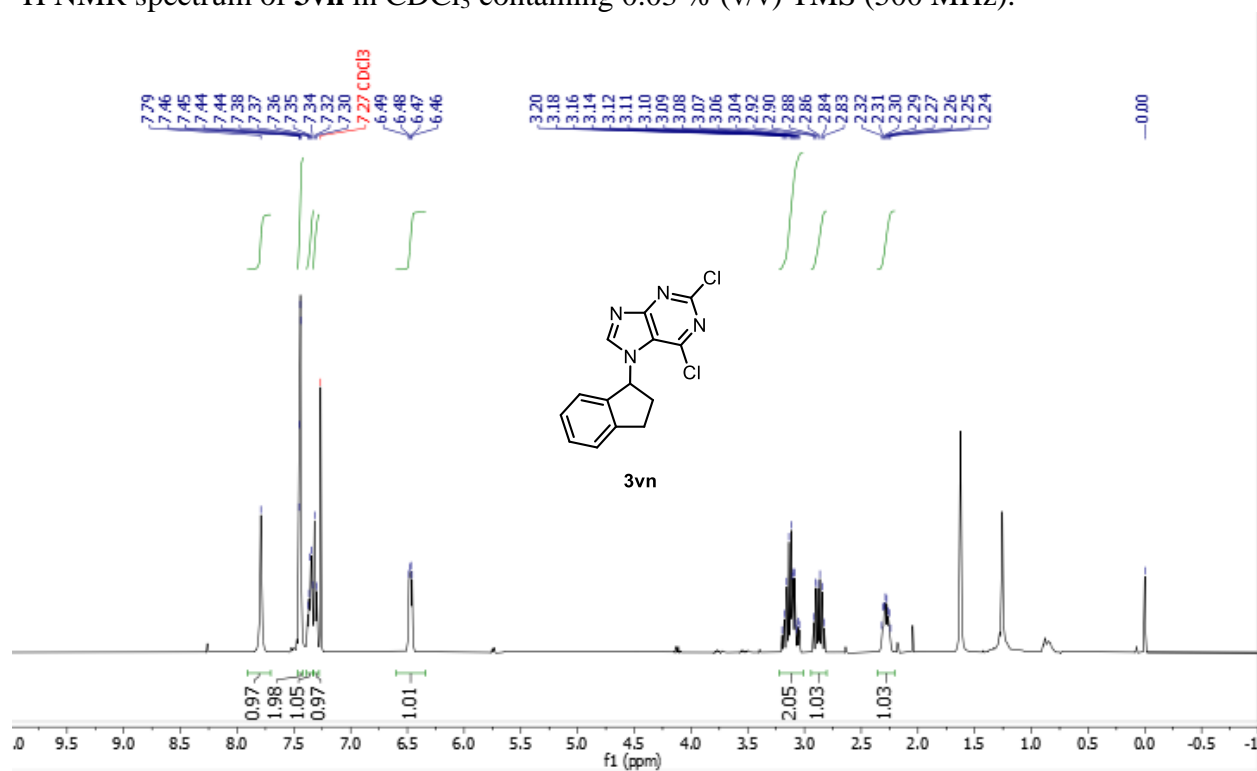
HSQC NMR spectrum of **3vm** in CDCl_3 containing 0.03 % (v/v) TMS (500, 126 MHz).



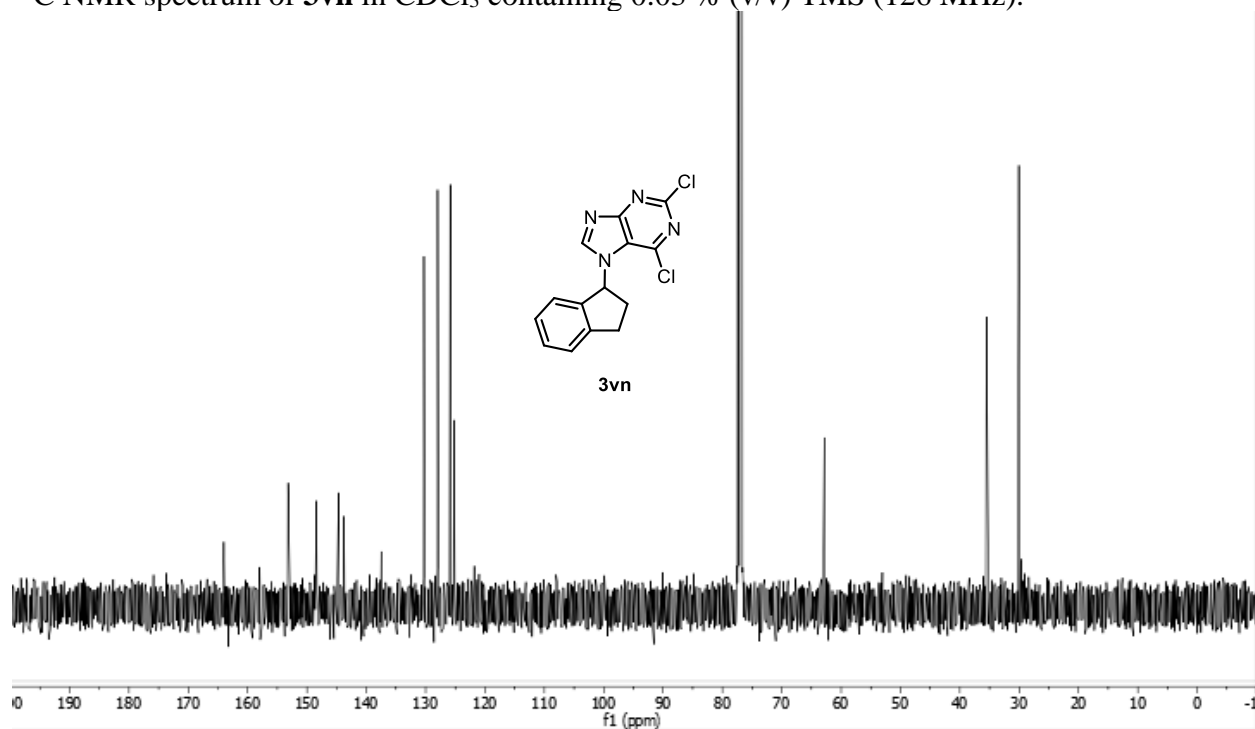
HMBC NMR spectrum of **3vm** in CDCl₃ containing 0.03 % (v/v) TMS (500, 126 MHz).



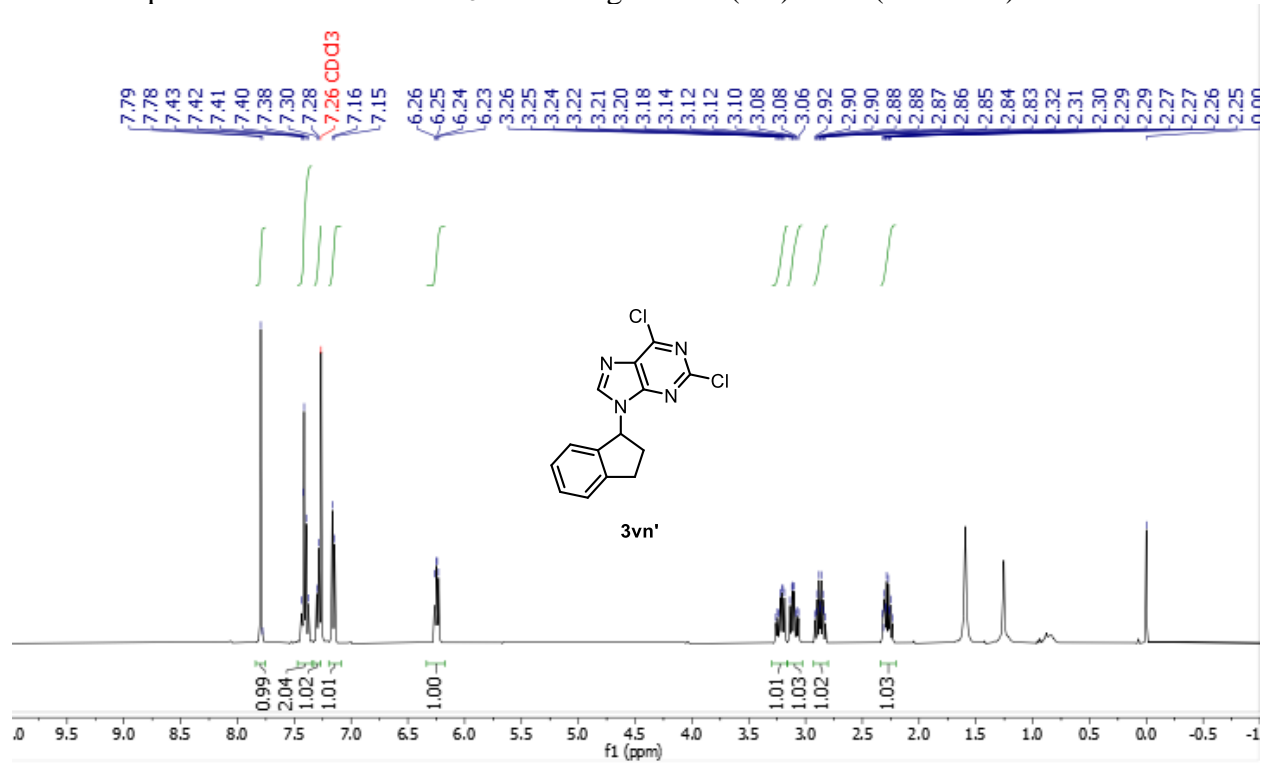
¹H NMR spectrum of **3vn** in CDCl₃ containing 0.03 % (v/v) TMS (500 MHz).



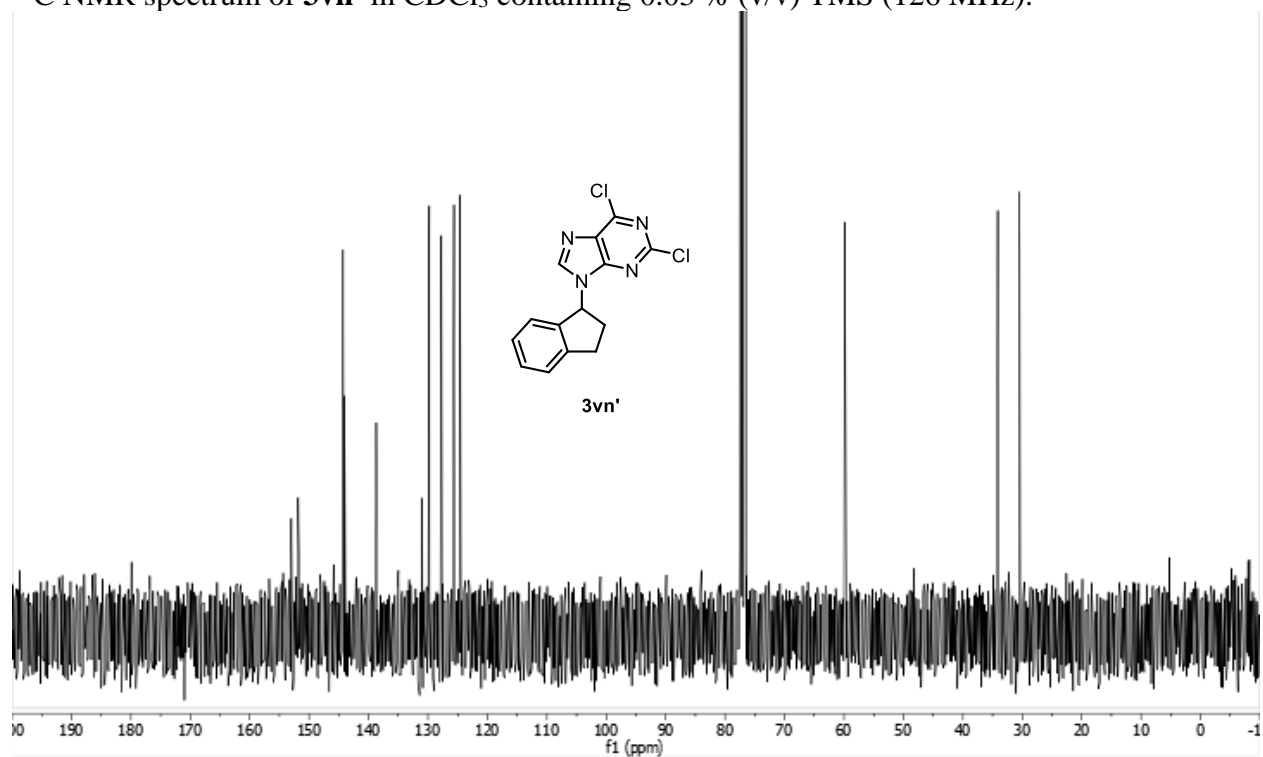
^{13}C NMR spectrum of **3vn** in CDCl_3 containing 0.03 % (v/v) TMS (126 MHz).



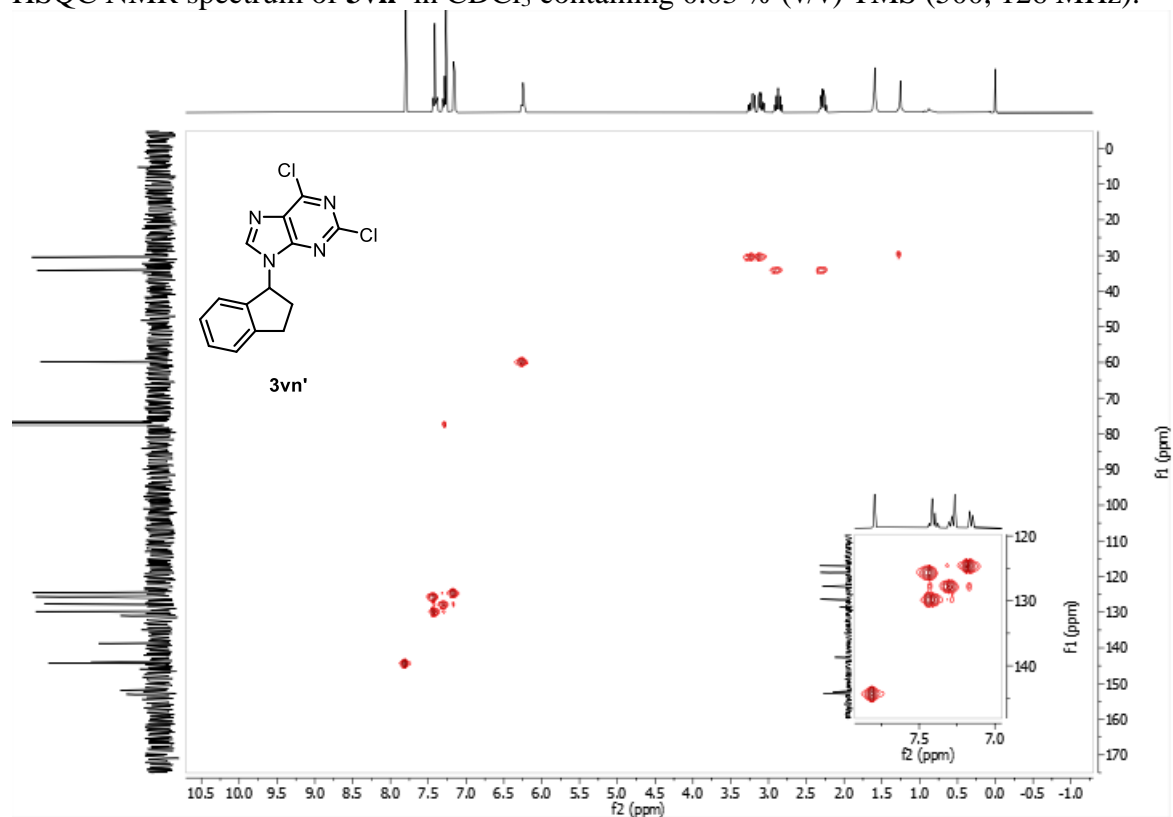
^1H NMR spectrum of **3vn'** in CDCl_3 containing 0.03 % (v/v) TMS (500 MHz).



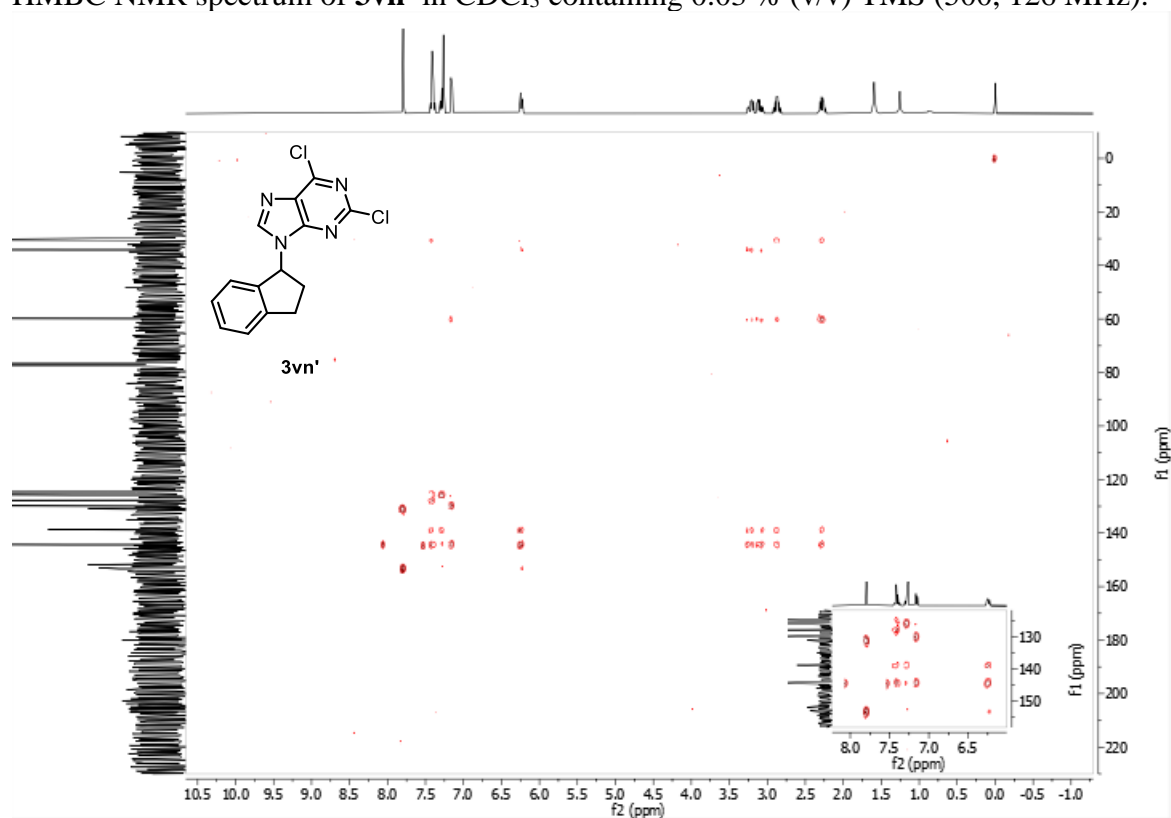
^{13}C NMR spectrum of **3vn'** in CDCl_3 containing 0.03 % (v/v) TMS (126 MHz).



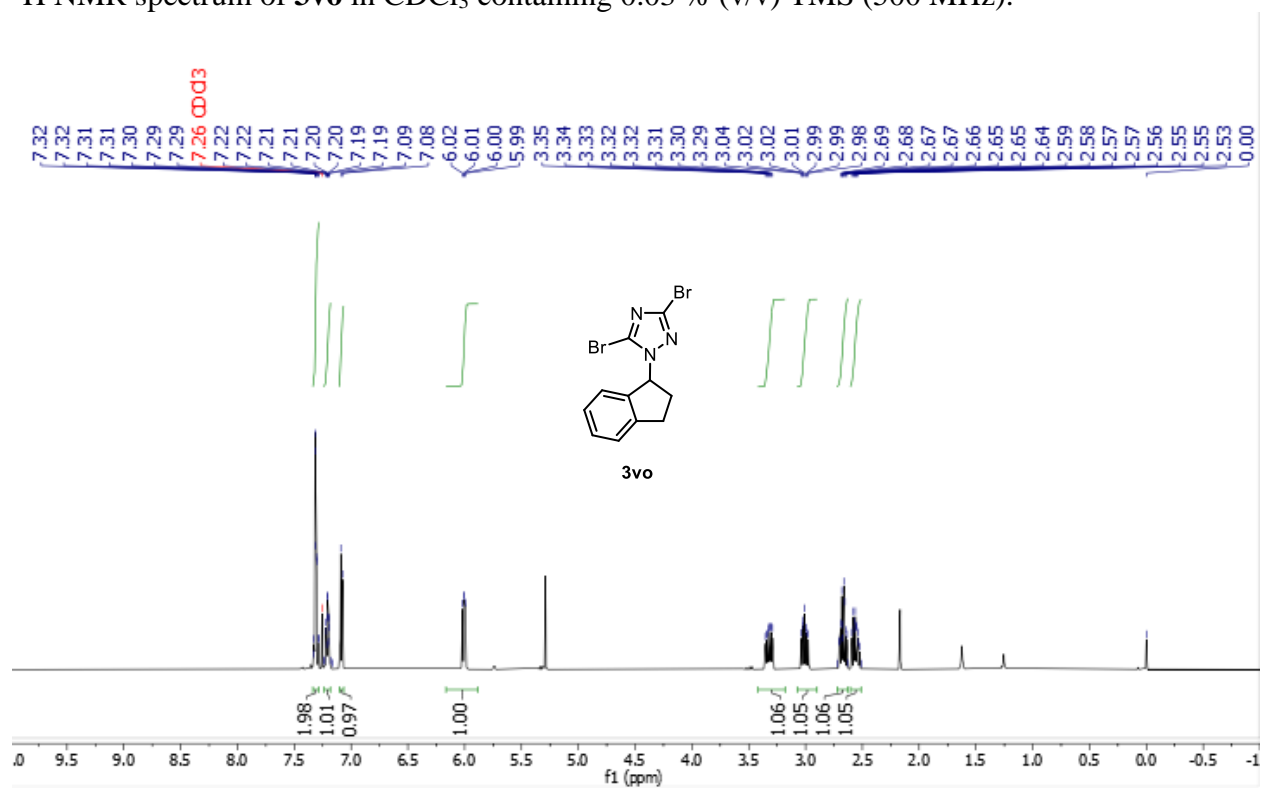
HSQC NMR spectrum of **3vn'** in CDCl_3 containing 0.03 % (v/v) TMS (500, 126 MHz).



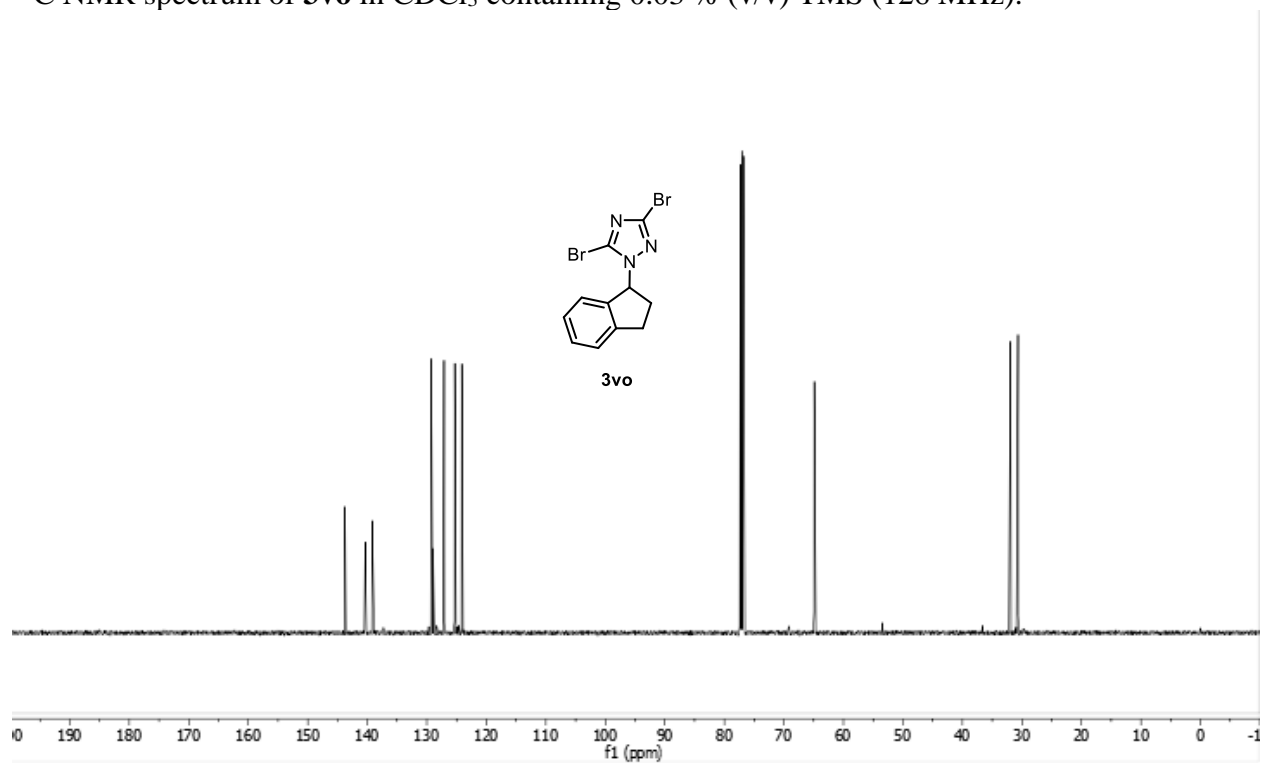
HMBC NMR spectrum of **3vn'** in CDCl₃ containing 0.03 % (v/v) TMS (500, 126 MHz).



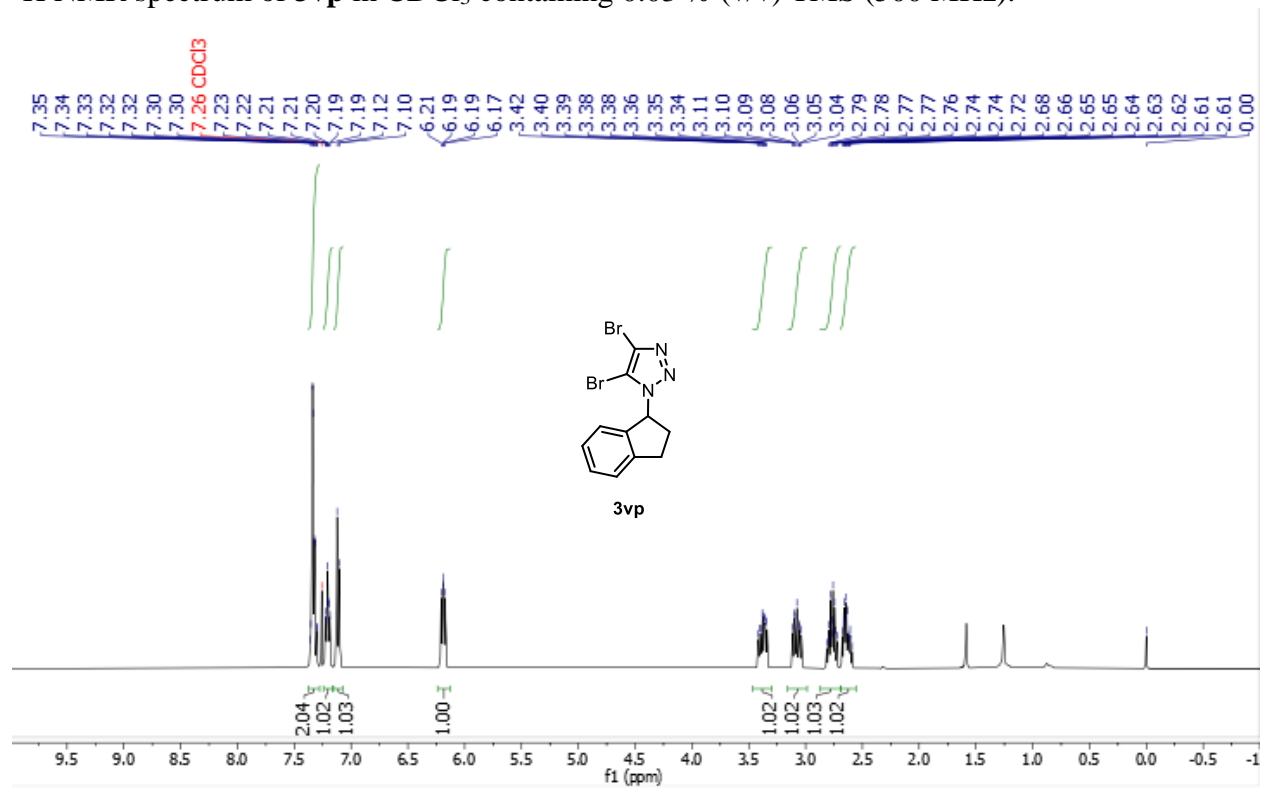
¹H NMR spectrum of **3vo** in CDCl₃ containing 0.03 % (v/v) TMS (500 MHz).



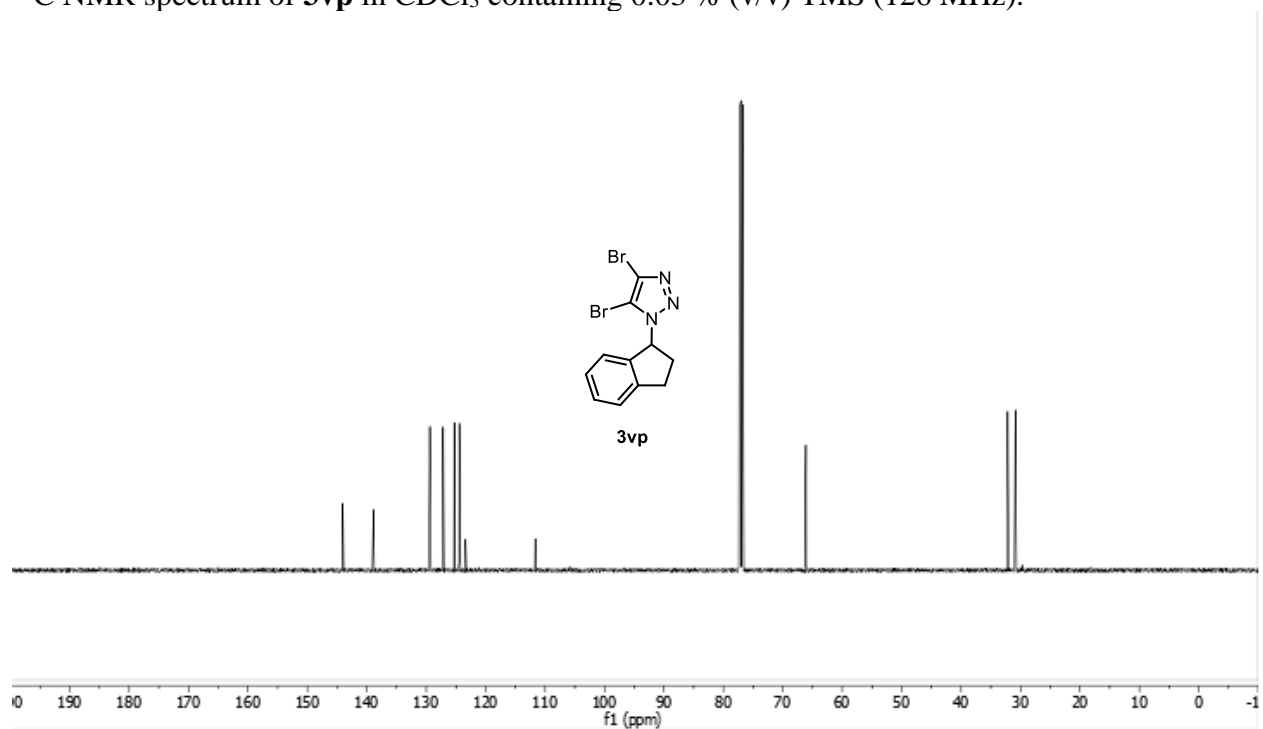
^{13}C NMR spectrum of **3vo** in CDCl_3 containing 0.03 % (v/v) TMS (126 MHz).



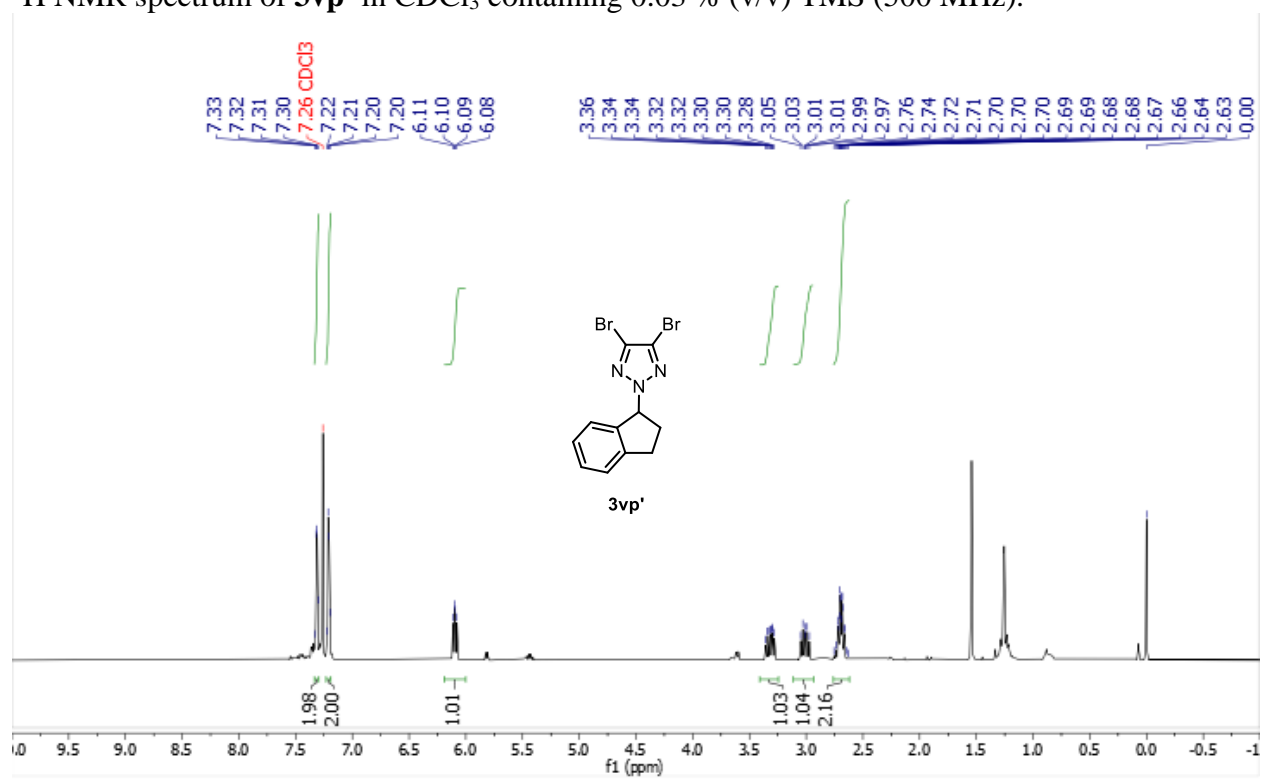
^1H NMR spectrum of **3vp** in CDCl_3 containing 0.03 % (v/v) TMS (500 MHz).



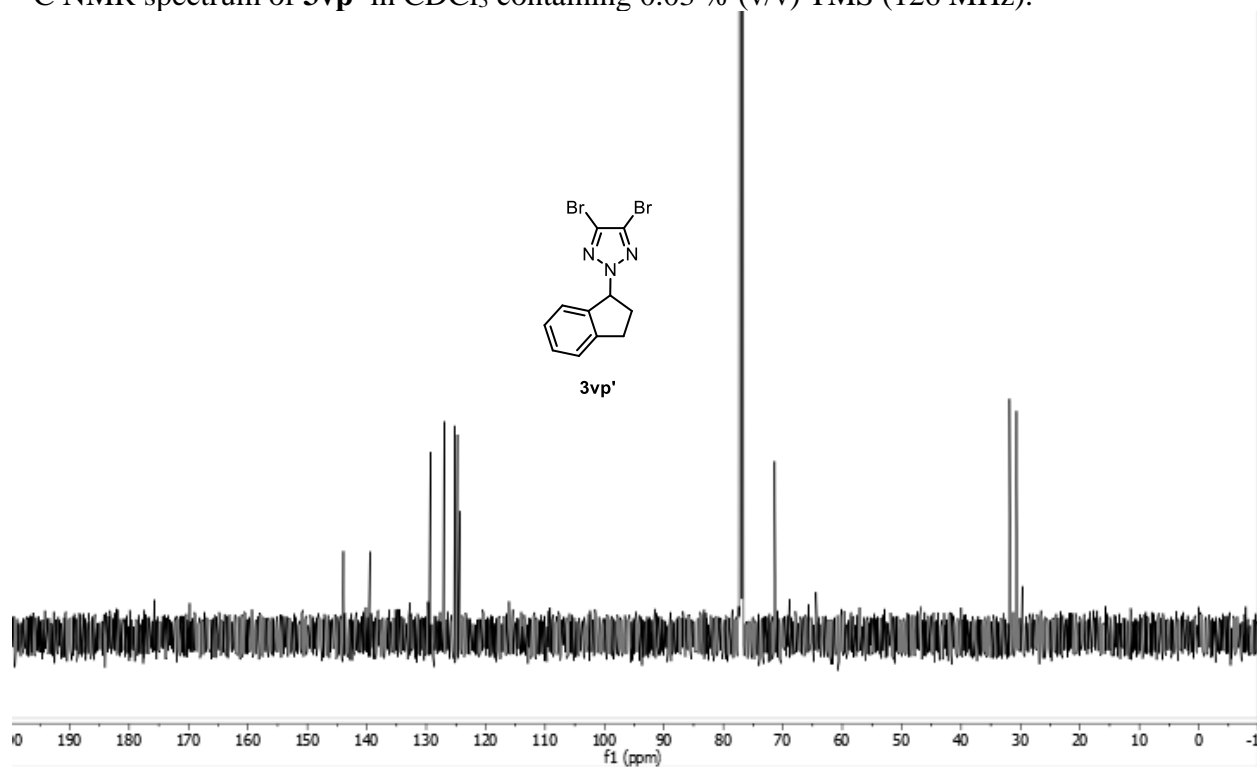
^{13}C NMR spectrum of **3vp** in CDCl_3 containing 0.03 % (v/v) TMS (126 MHz).



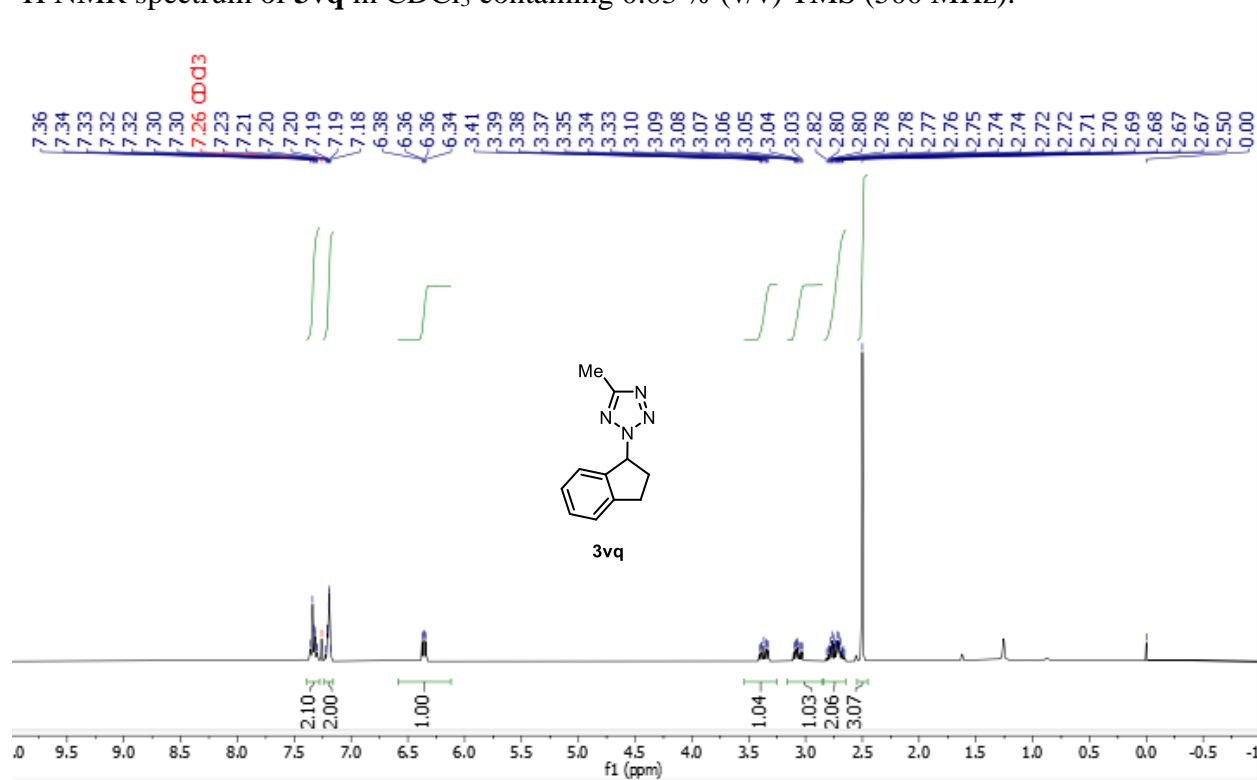
^1H NMR spectrum of **3vp'** in CDCl_3 containing 0.03 % (v/v) TMS (500 MHz).



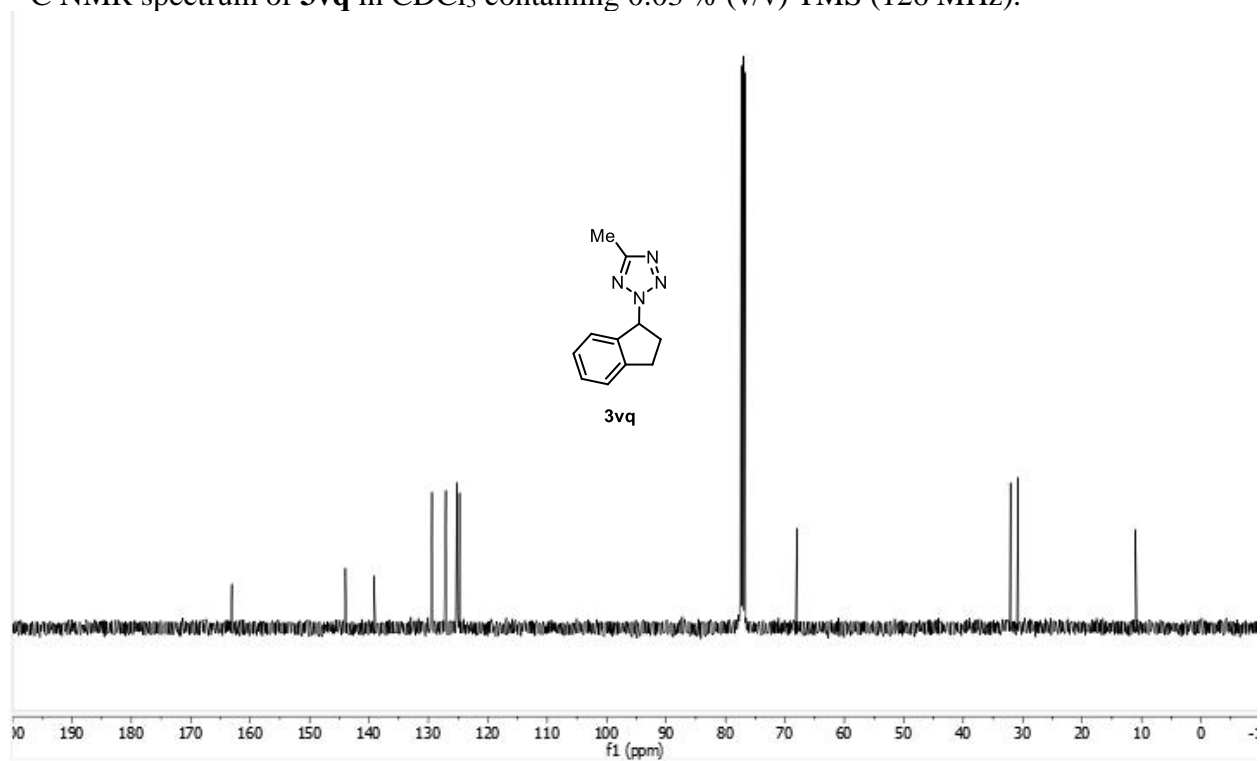
^{13}C NMR spectrum of **3vp'** in CDCl_3 containing 0.03 % (v/v) TMS (126 MHz).



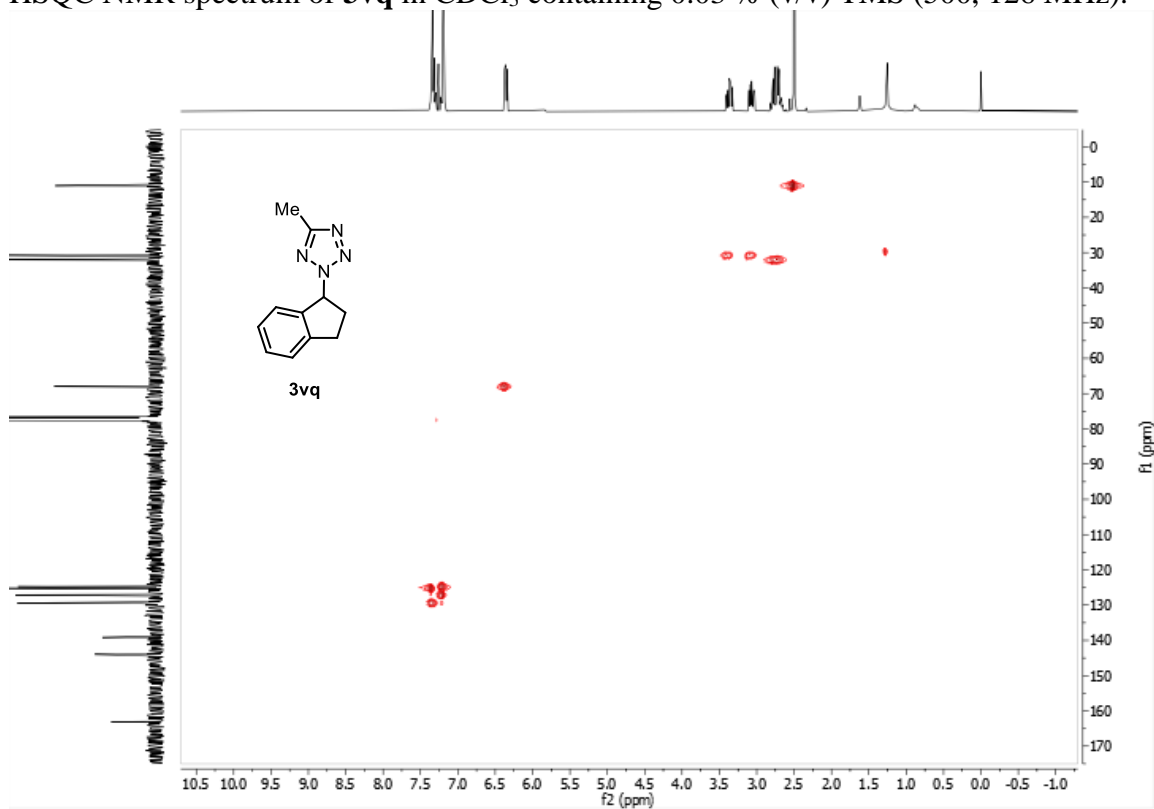
^1H NMR spectrum of **3vq** in CDCl_3 containing 0.03 % (v/v) TMS (500 MHz).



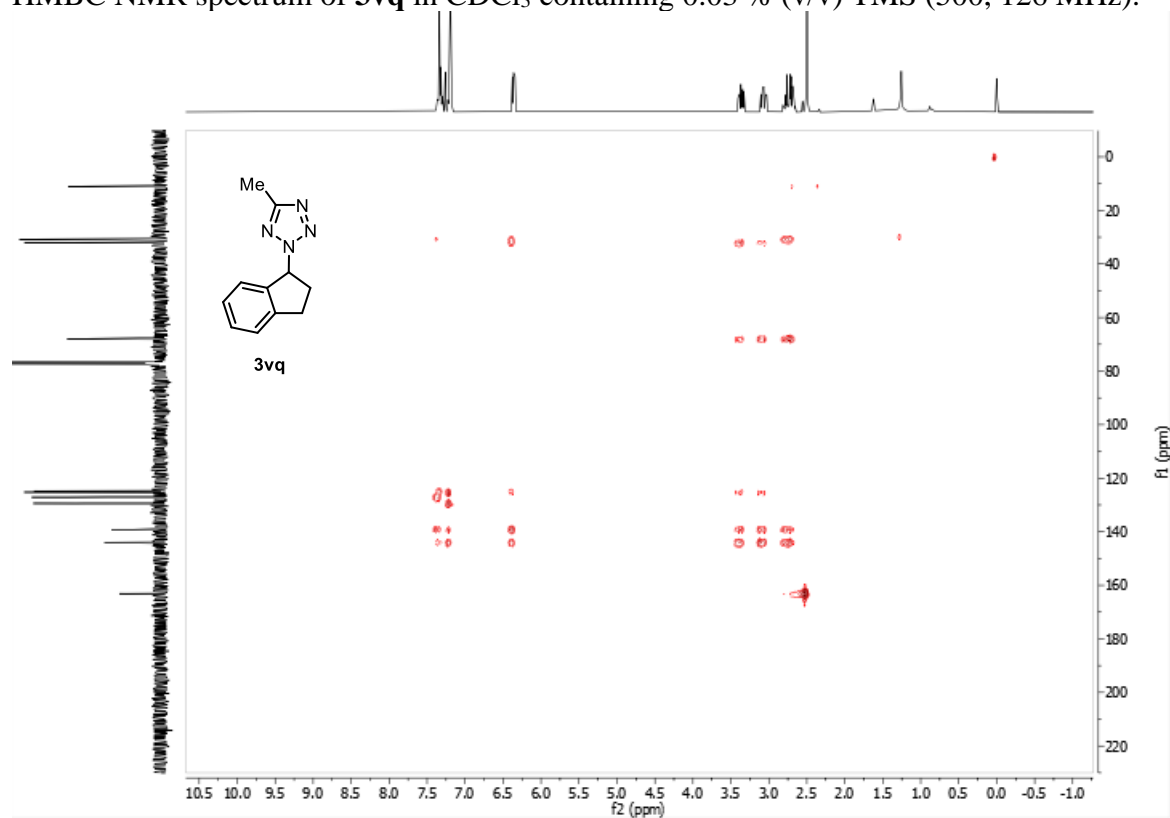
^{13}C NMR spectrum of **3vq** in CDCl_3 containing 0.03 % (v/v) TMS (126 MHz).



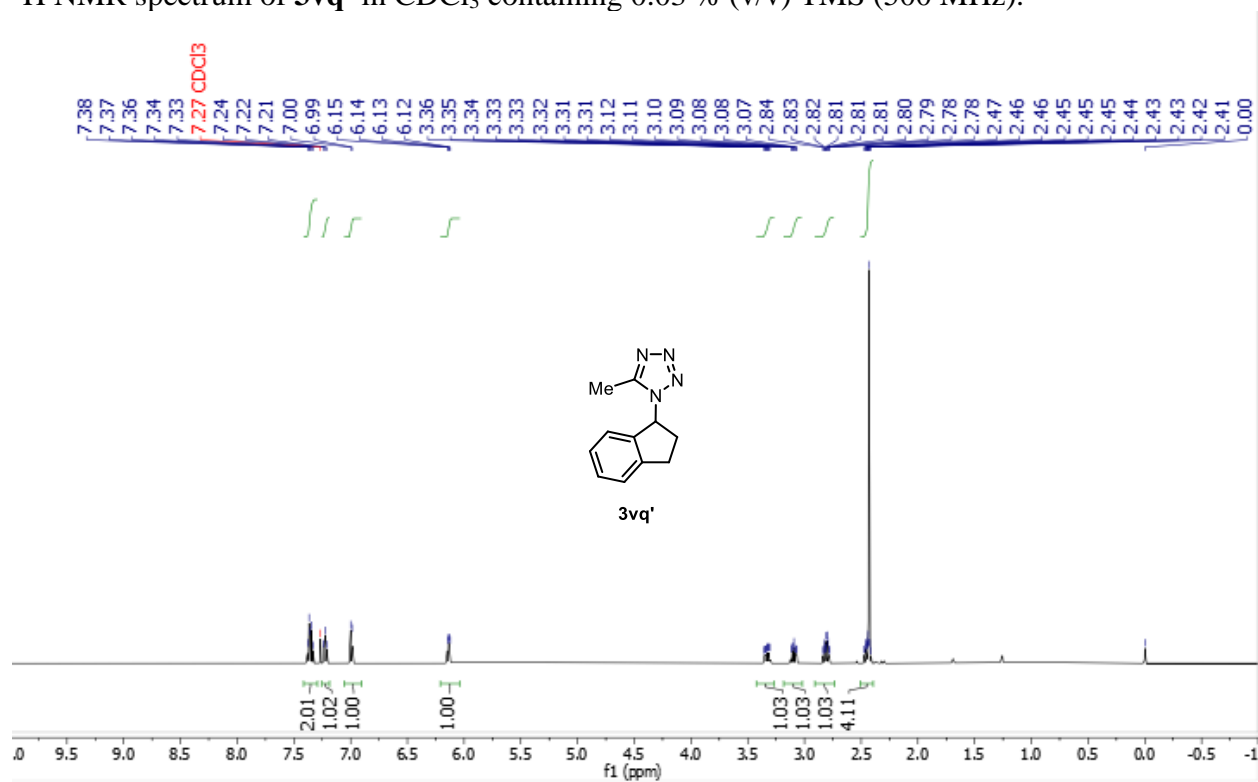
HSQC NMR spectrum of **3vq** in CDCl_3 containing 0.03 % (v/v) TMS (500, 126 MHz).



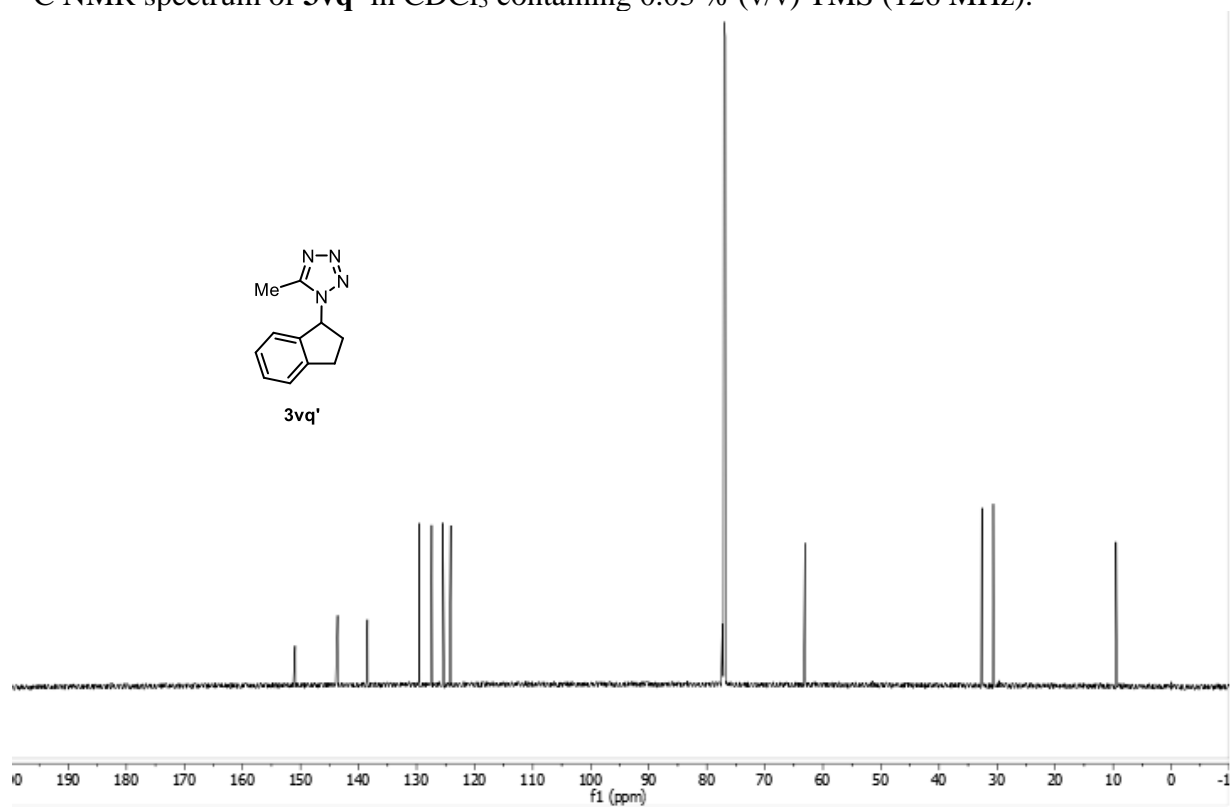
HMBC NMR spectrum of **3vq** in CDCl₃ containing 0.03 % (v/v) TMS (500, 126 MHz).



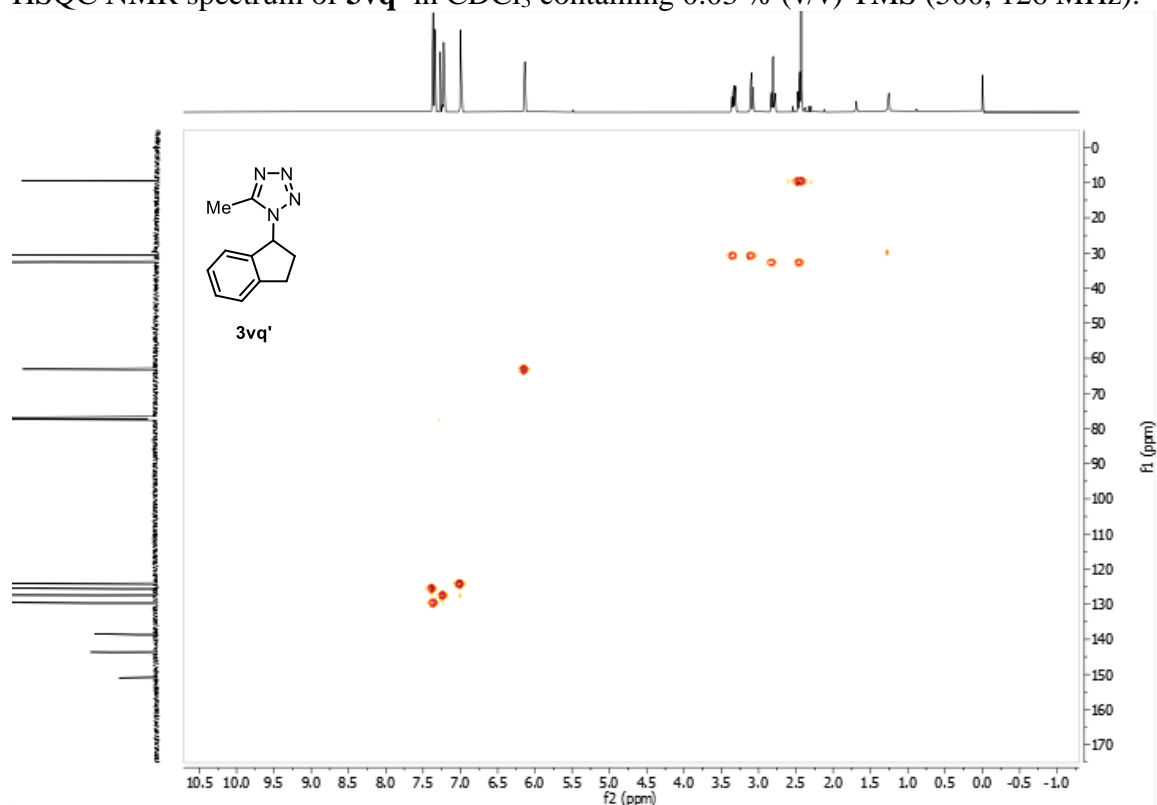
¹H NMR spectrum of **3vq'** in CDCl₃ containing 0.03 % (v/v) TMS (500 MHz).



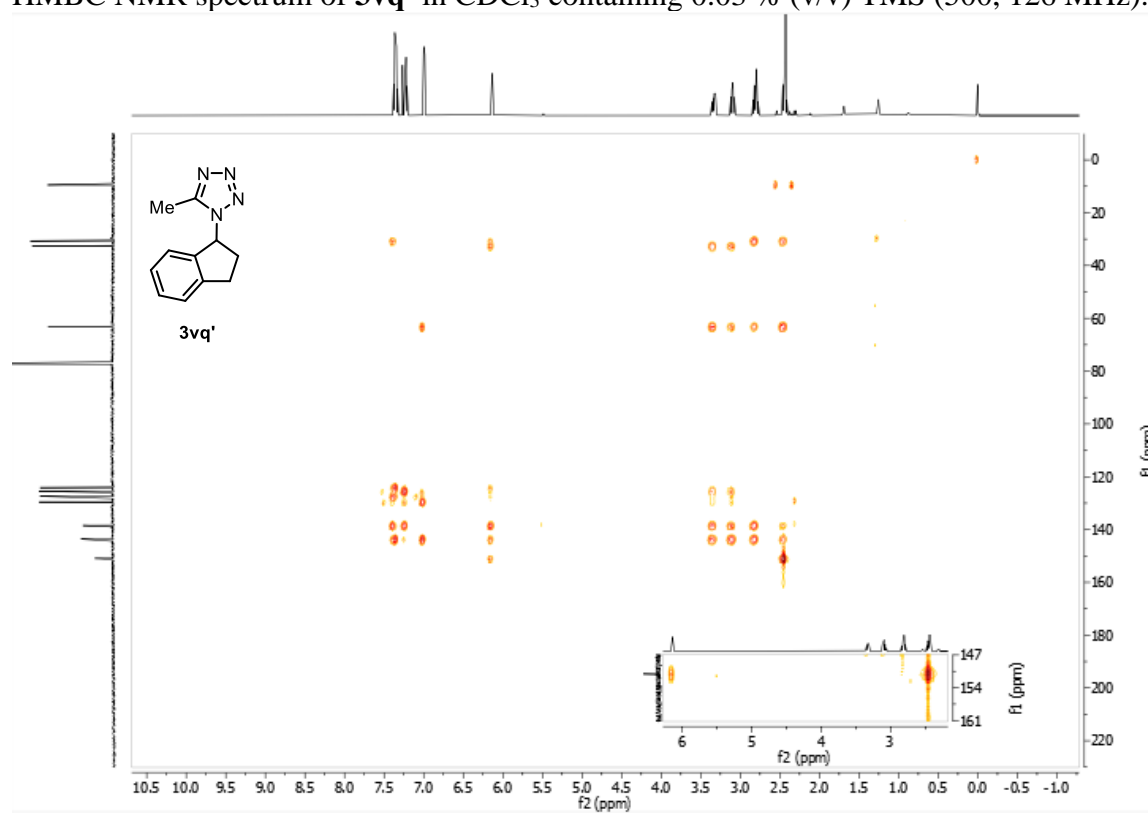
^{13}C NMR spectrum of **3vq'** in CDCl_3 containing 0.03 % (v/v) TMS (126 MHz).



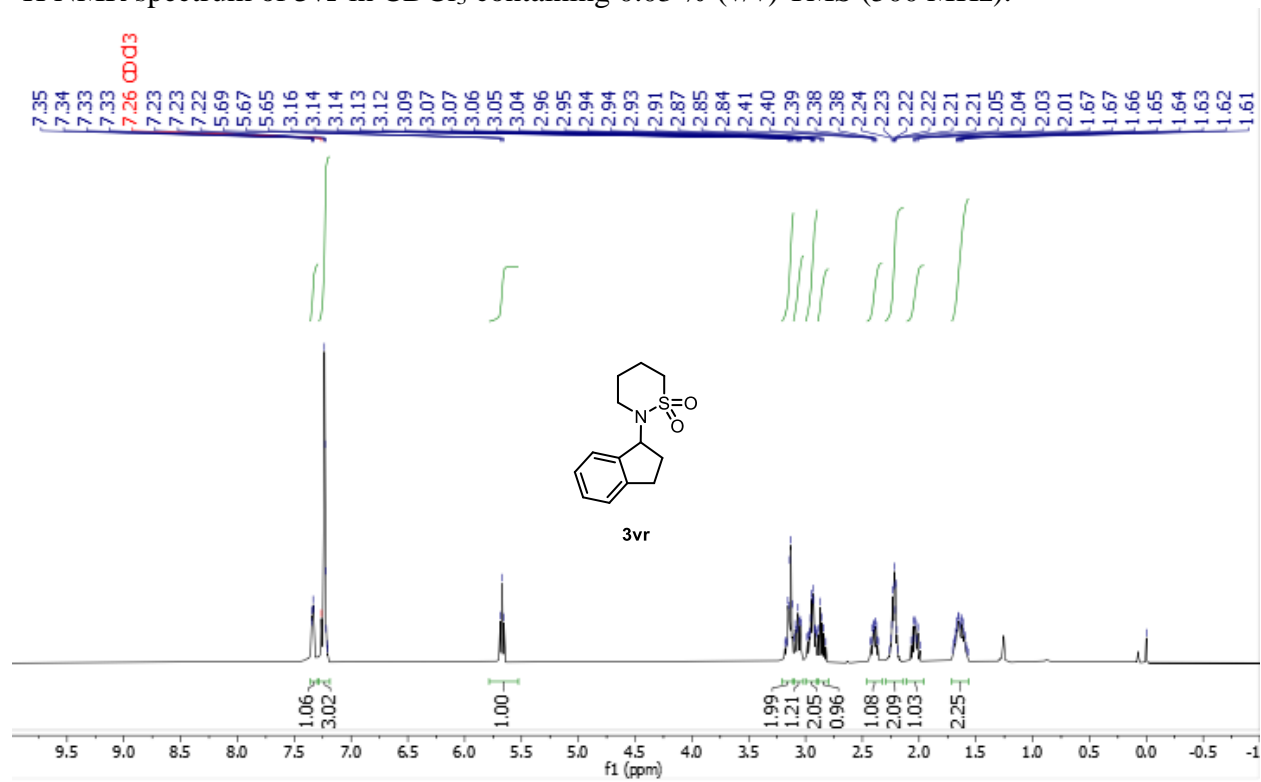
HSQC NMR spectrum of **3vq'** in CDCl_3 containing 0.03 % (v/v) TMS (500, 126 MHz).



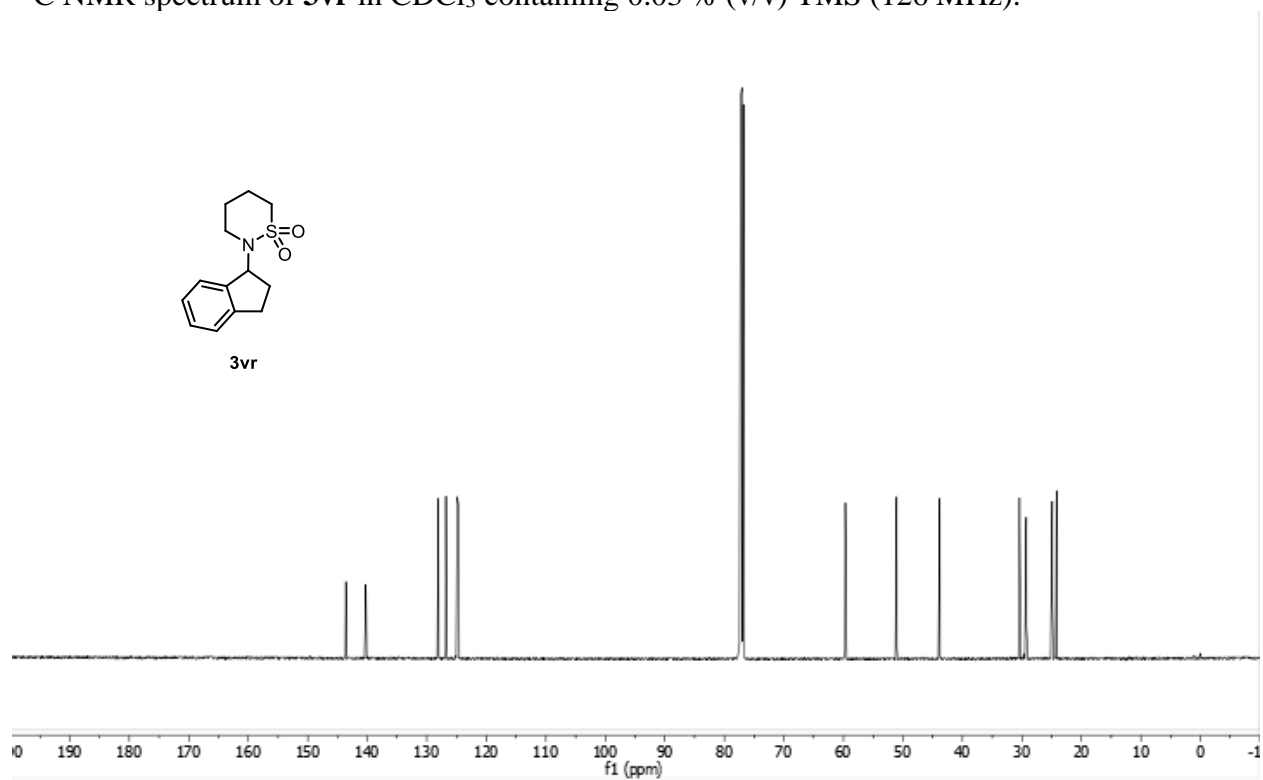
HMBC NMR spectrum of **3vq'** in CDCl₃ containing 0.03 % (v/v) TMS (500, 126 MHz).



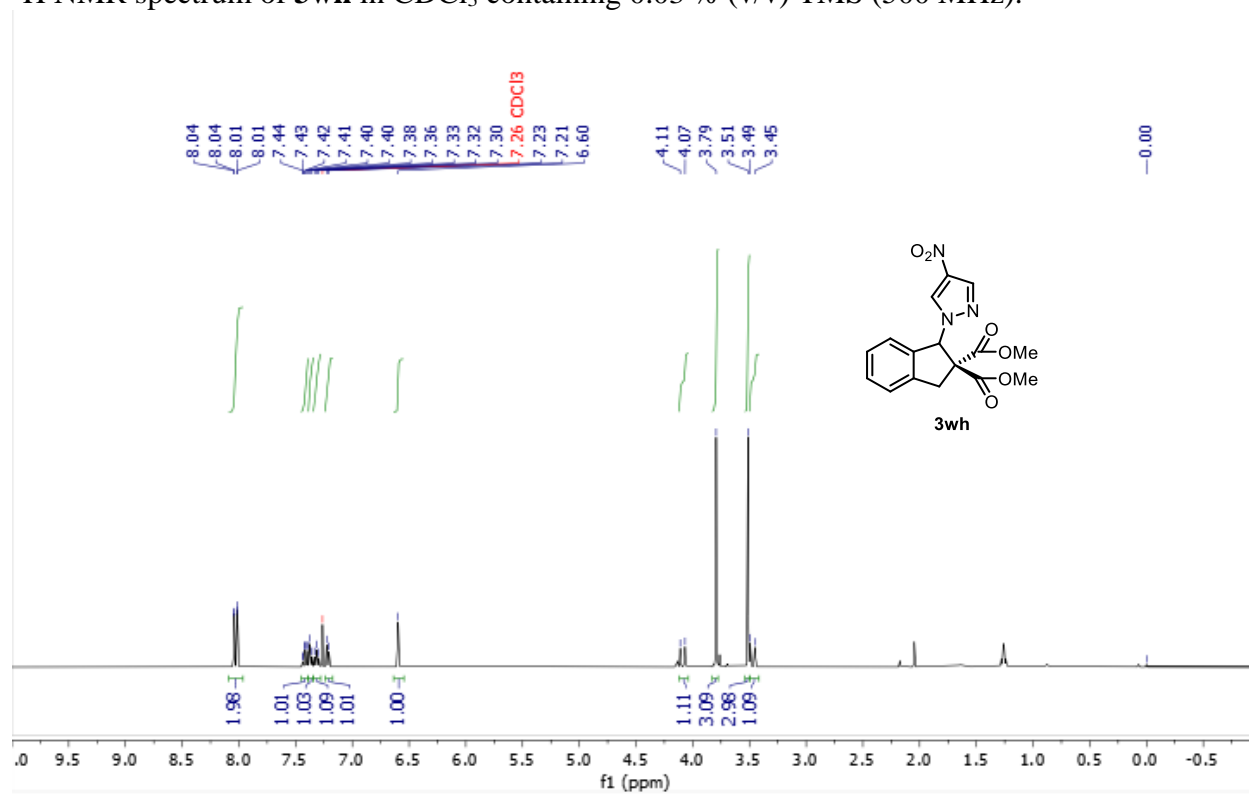
¹H NMR spectrum of **3vr** in CDCl₃ containing 0.03 % (v/v) TMS (500 MHz).



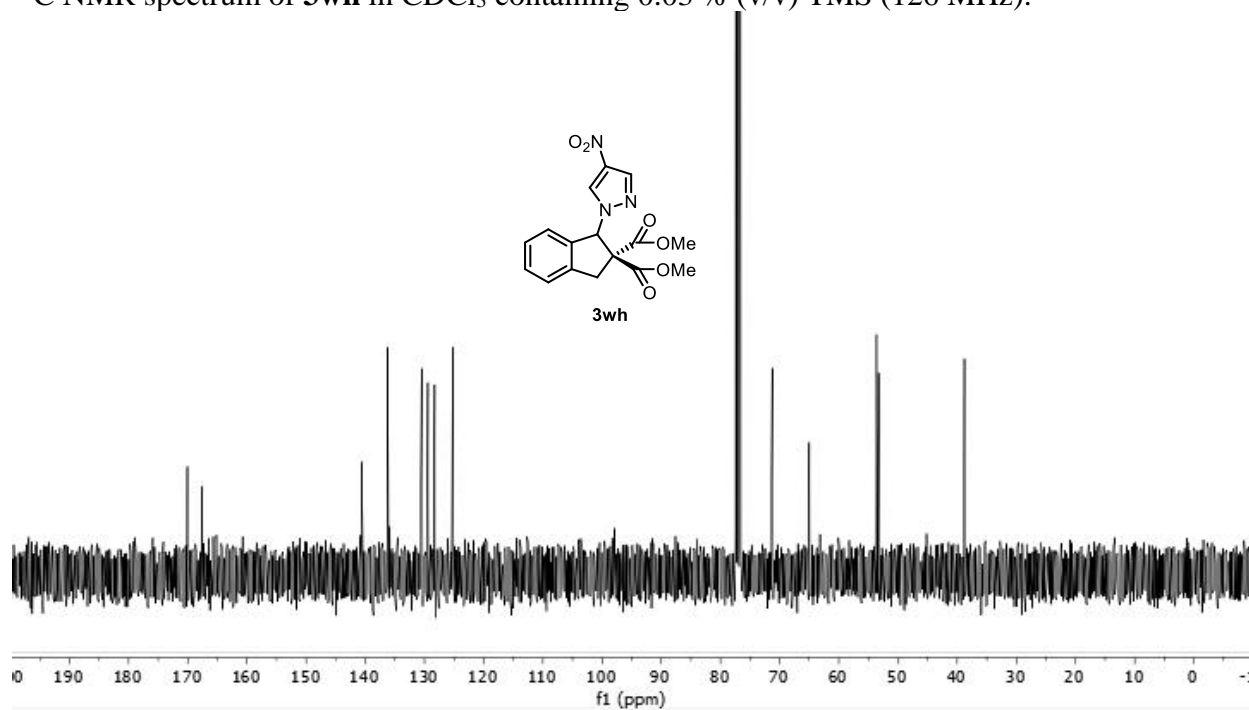
^{13}C NMR spectrum of **3vr** in CDCl_3 containing 0.03 % (v/v) TMS (126 MHz).



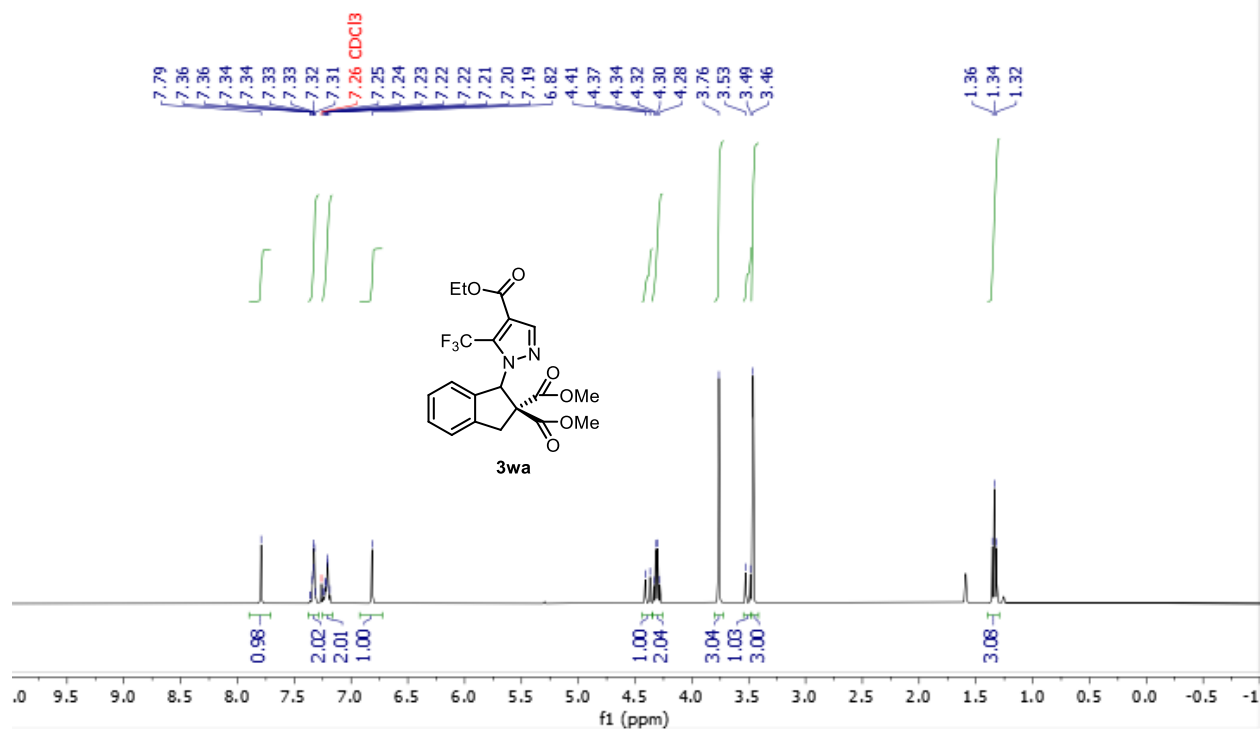
^1H NMR spectrum of **3wh** in CDCl_3 containing 0.03 % (v/v) TMS (500 MHz).



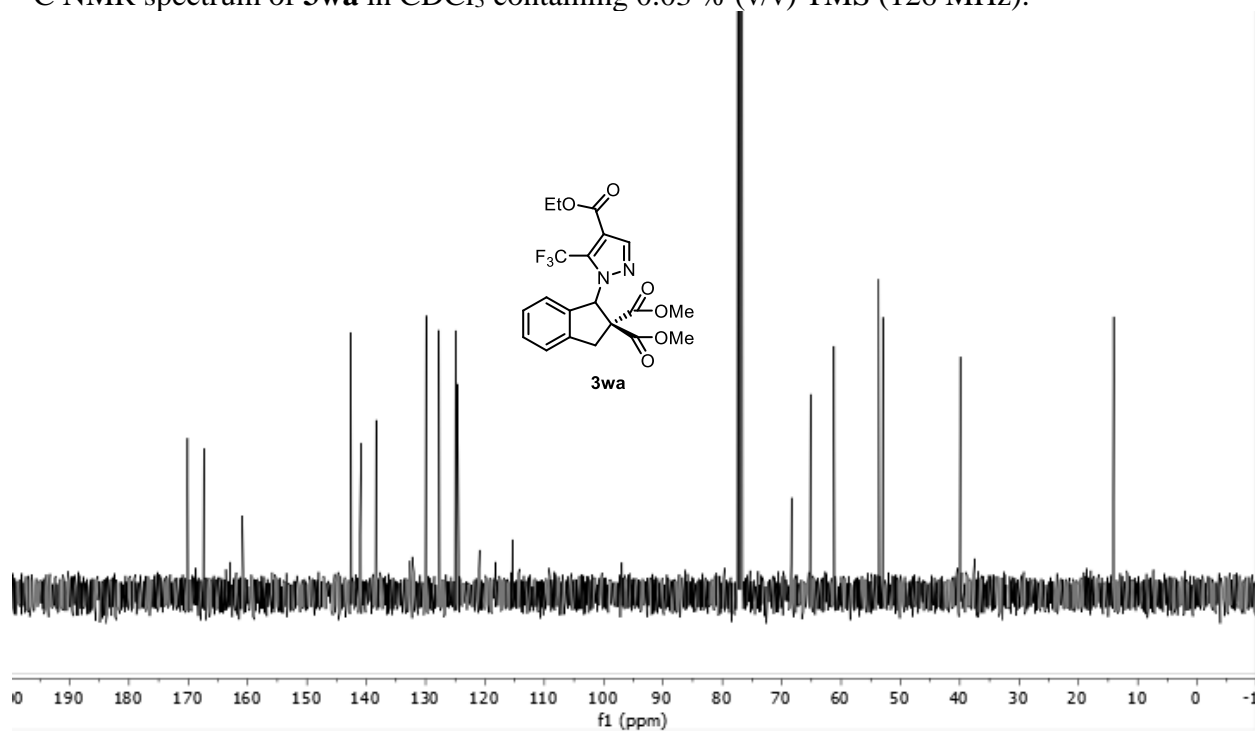
^{13}C NMR spectrum of **3wh** in CDCl_3 containing 0.03 % (v/v) TMS (126 MHz).



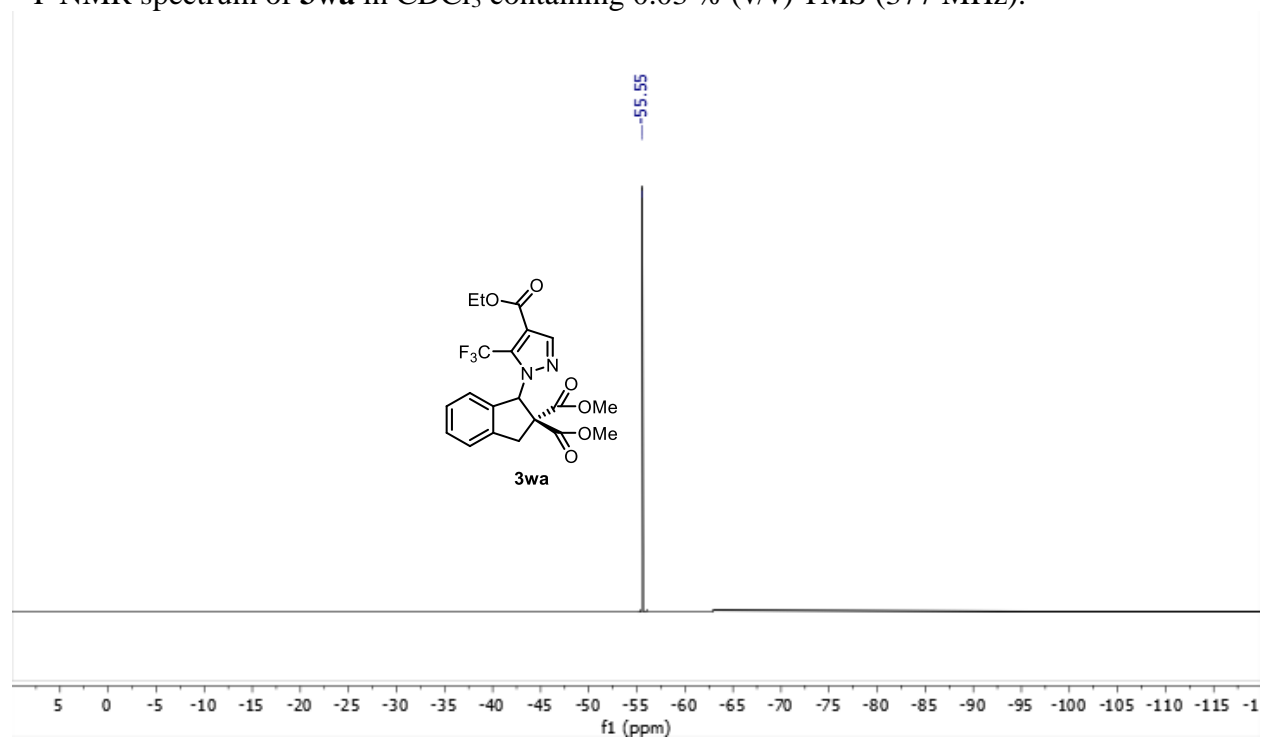
^1H NMR spectrum of **3wa** in CDCl_3 containing 0.03 % (v/v) TMS (500 MHz).



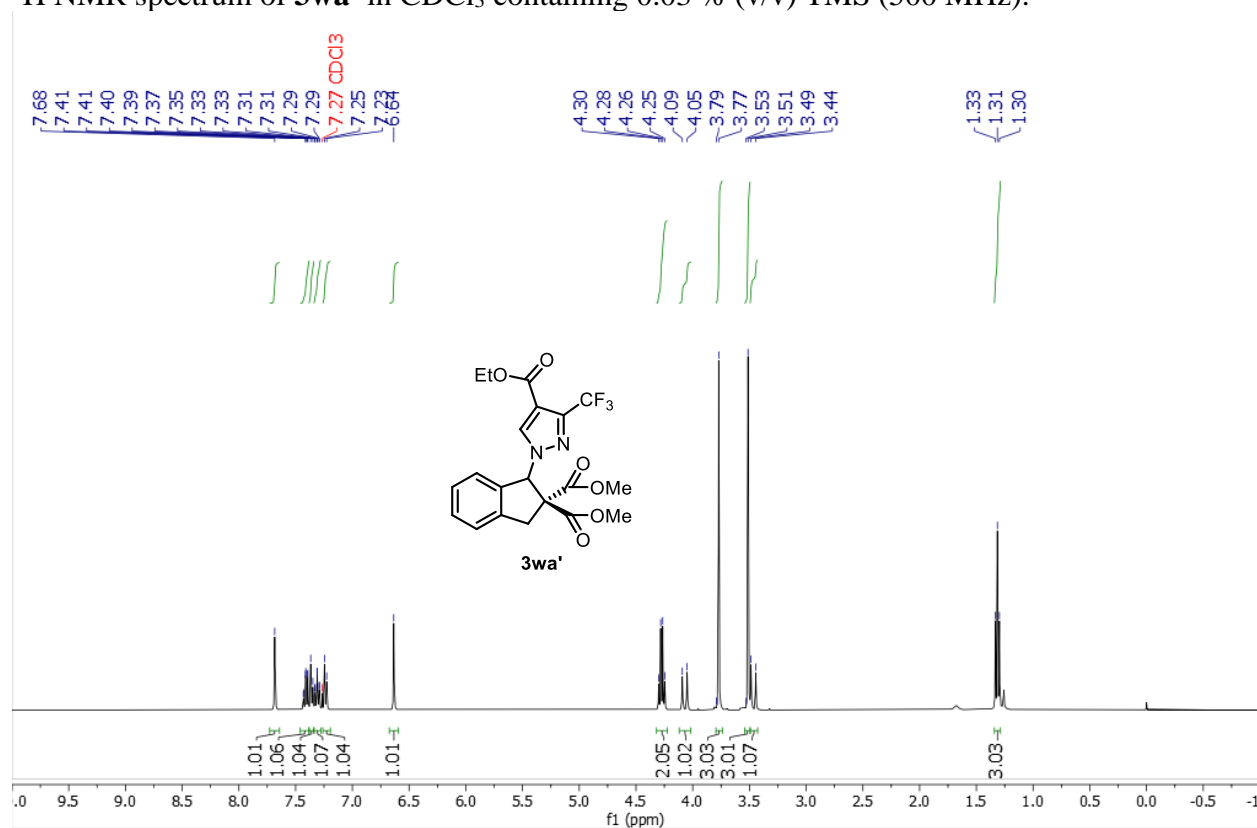
^{13}C NMR spectrum of **3wa** in CDCl_3 containing 0.03 % (v/v) TMS (126 MHz).



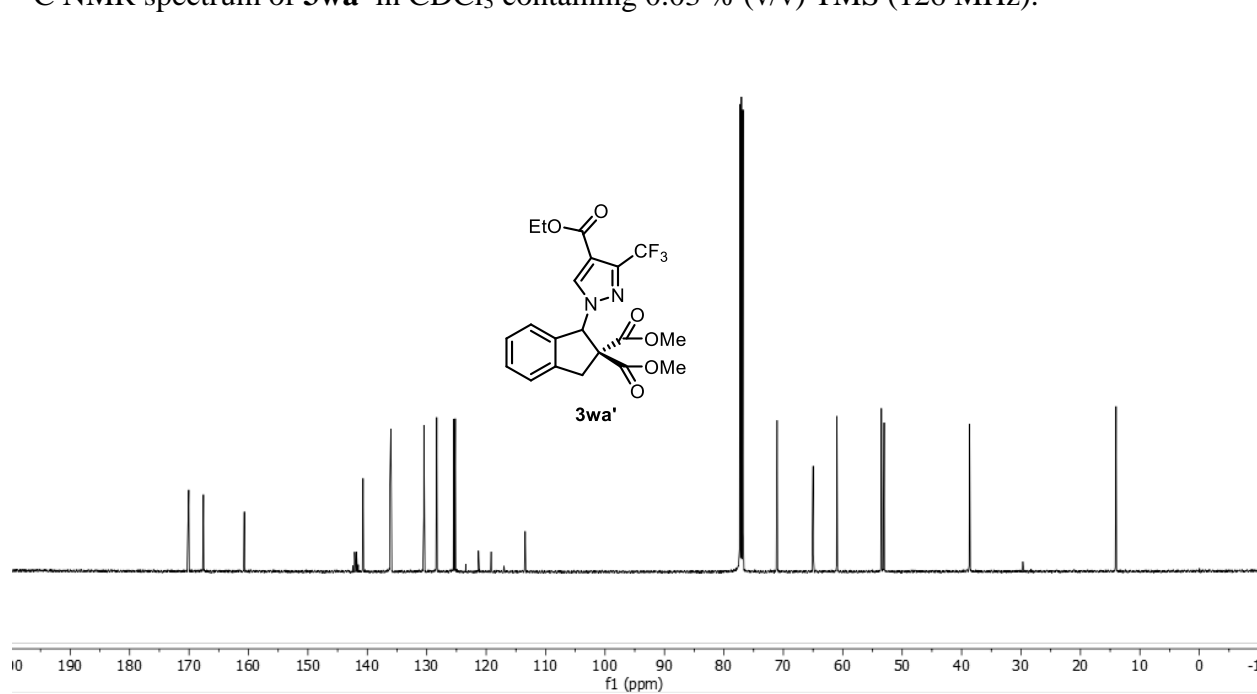
^{19}F NMR spectrum of **3wa** in CDCl_3 containing 0.03 % (v/v) TMS (377 MHz).



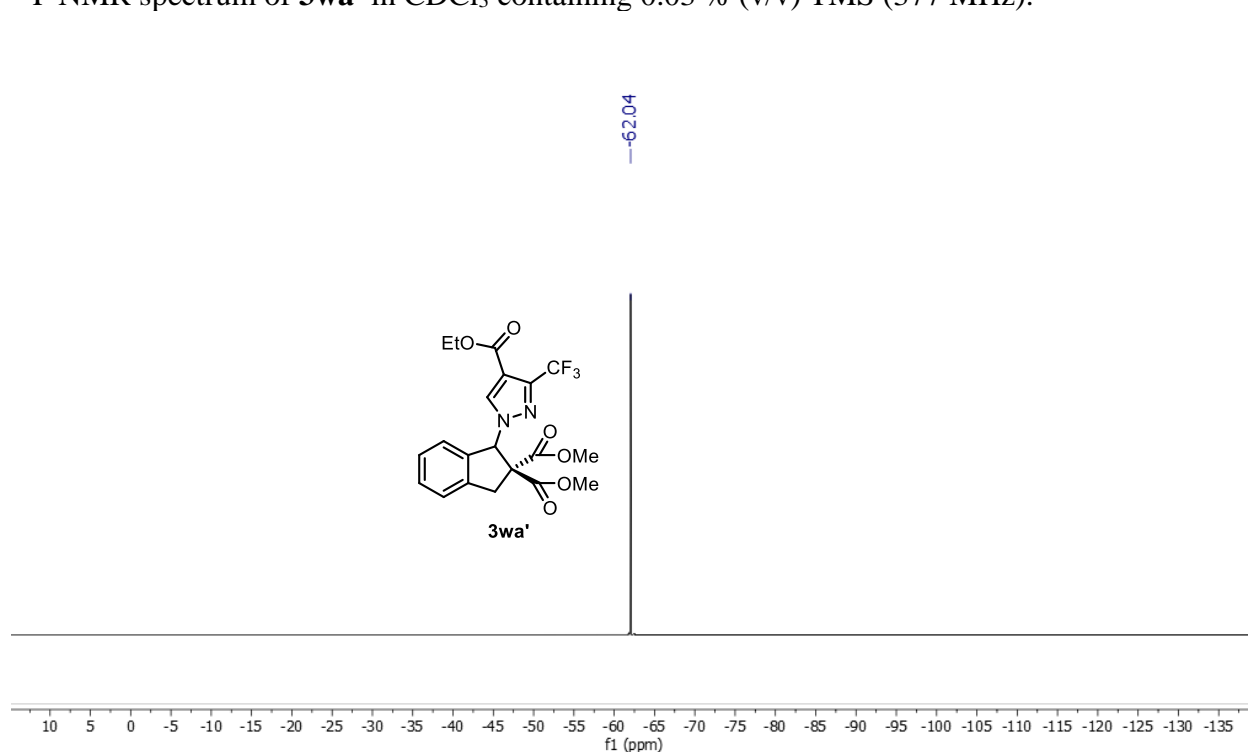
^1H NMR spectrum of **3wa'** in CDCl_3 containing 0.03 % (v/v) TMS (500 MHz).



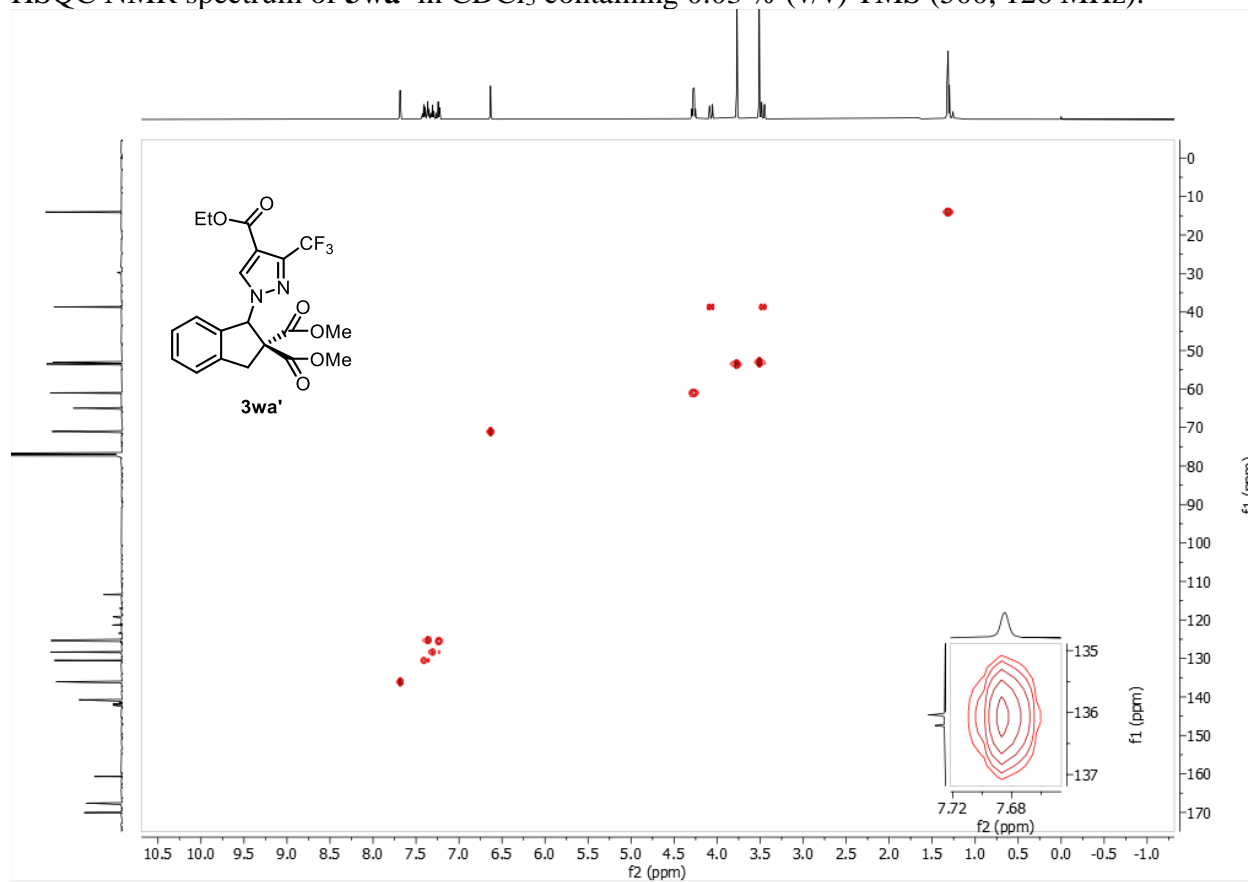
^{13}C NMR spectrum of **3wa'** in CDCl_3 containing 0.03 % (v/v) TMS (126 MHz).



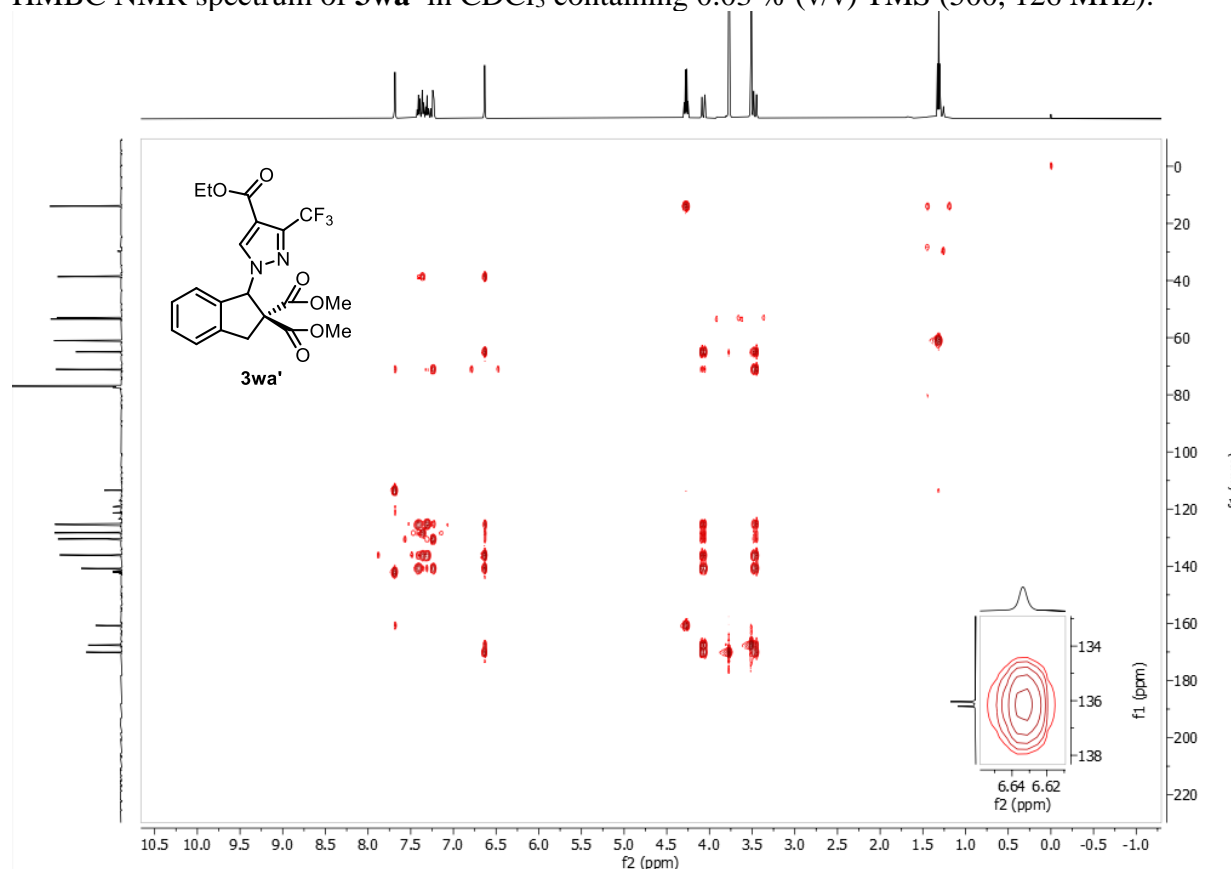
^{19}F NMR spectrum of **3wa'** in CDCl_3 containing 0.03 % (v/v) TMS (377 MHz).



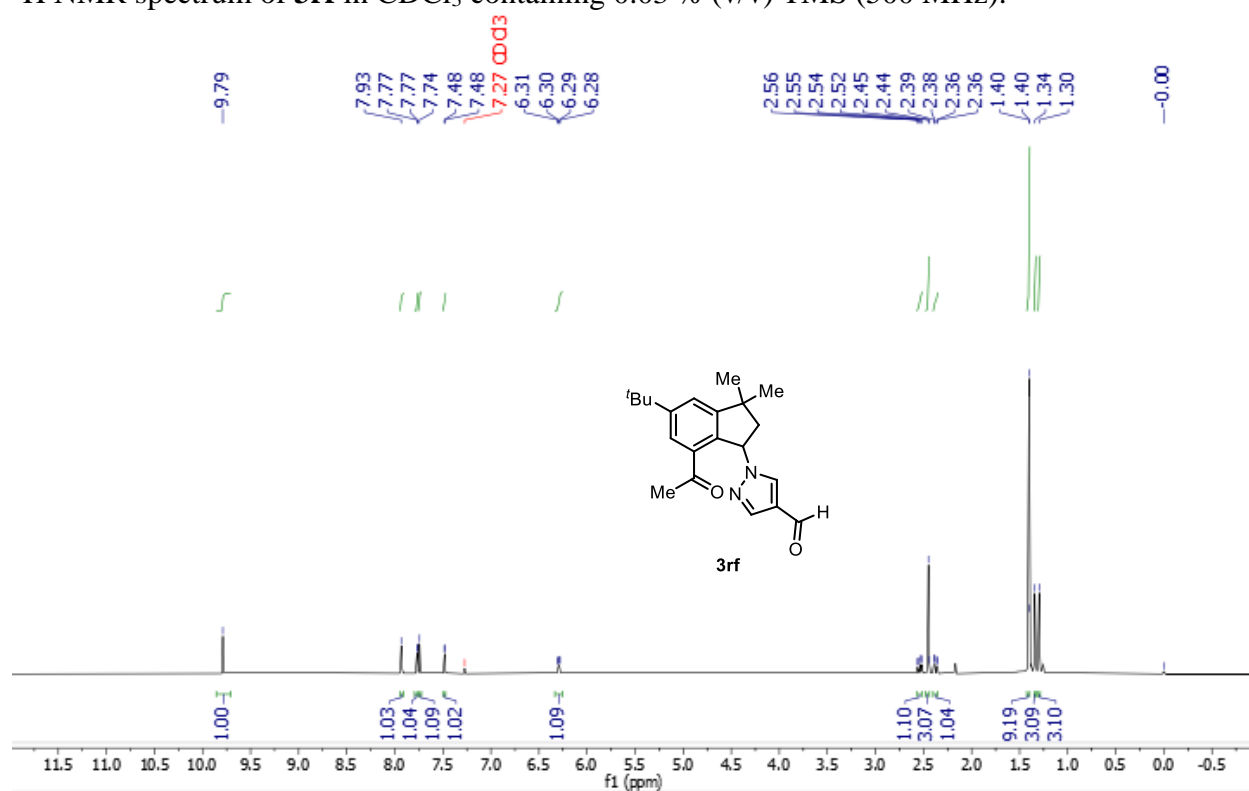
HSQC NMR spectrum of **3wa'** in CDCl_3 containing 0.03 % (v/v) TMS (500, 126 MHz).



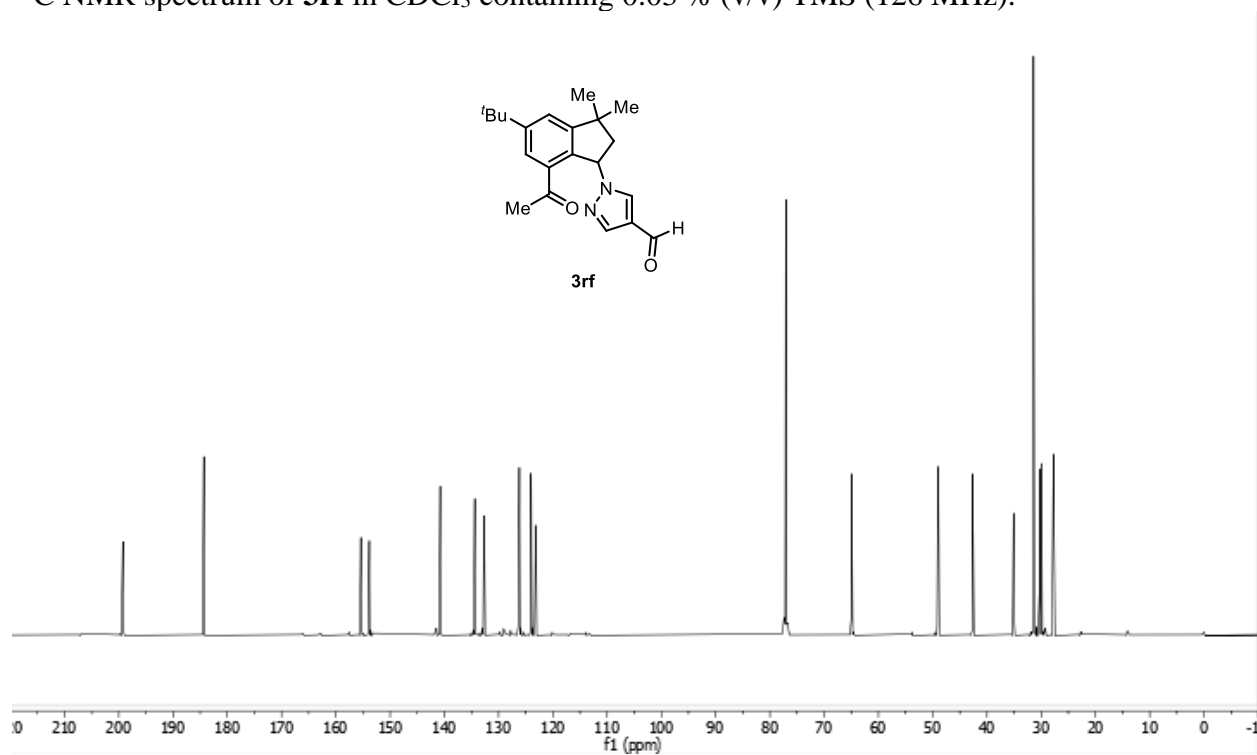
HMBC NMR spectrum of **3wa'** in CDCl₃ containing 0.03 % (v/v) TMS (500, 126 MHz).



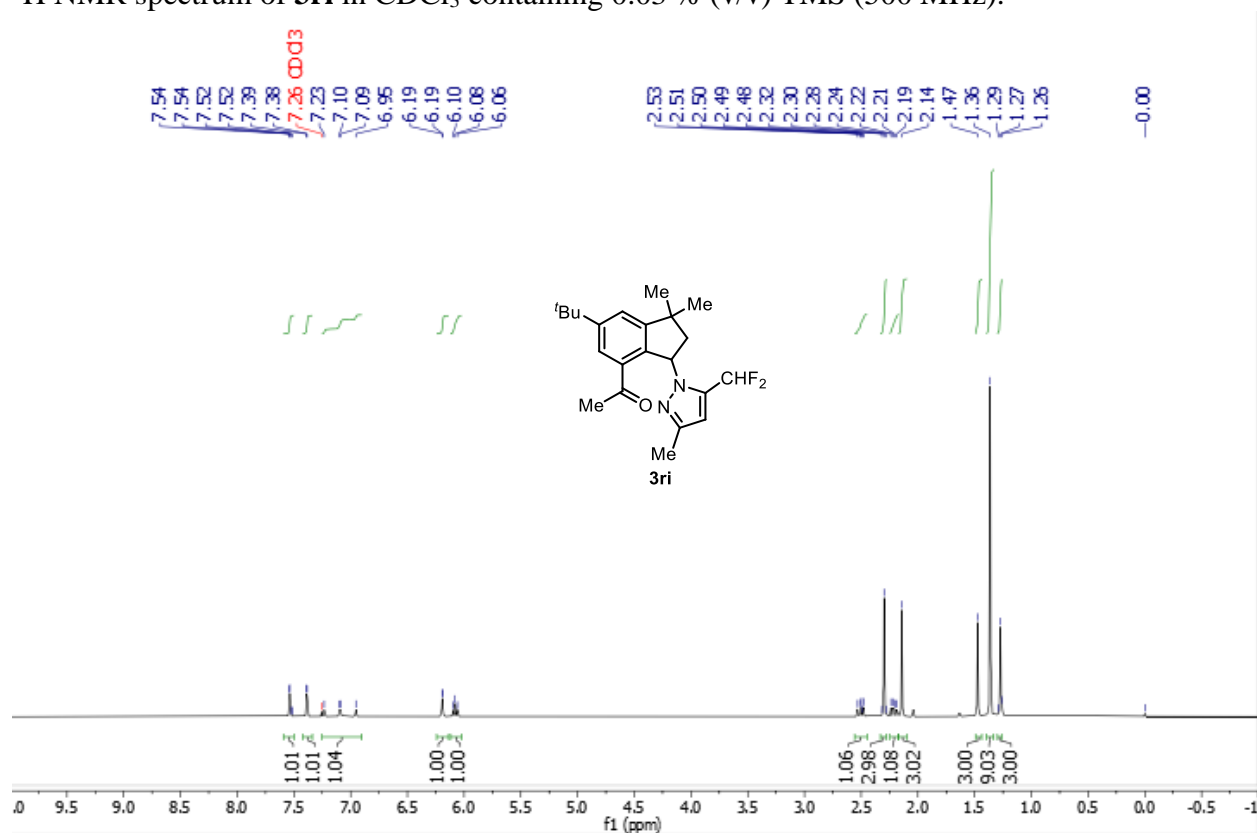
¹H NMR spectrum of **3rf** in CDCl₃ containing 0.03 % (v/v) TMS (500 MHz).



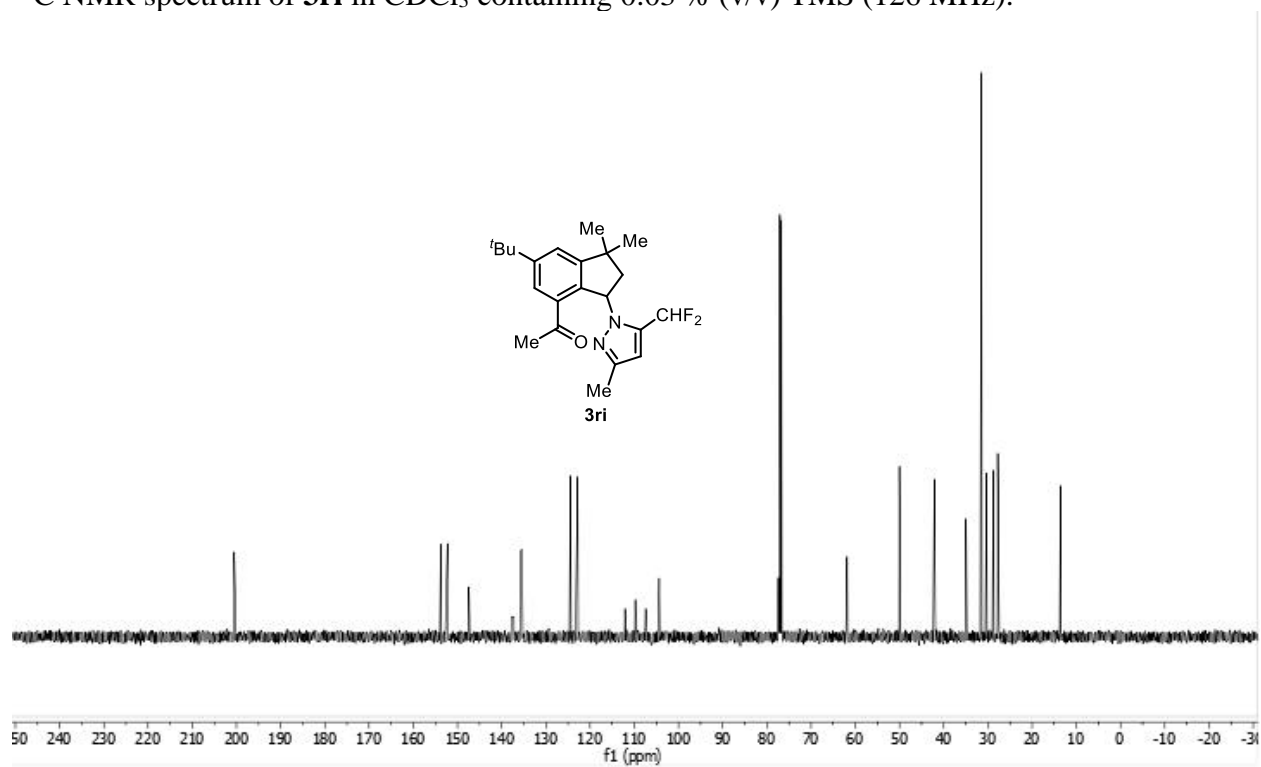
^{13}C NMR spectrum of **3rf** in CDCl_3 containing 0.03 % (v/v) TMS (126 MHz).



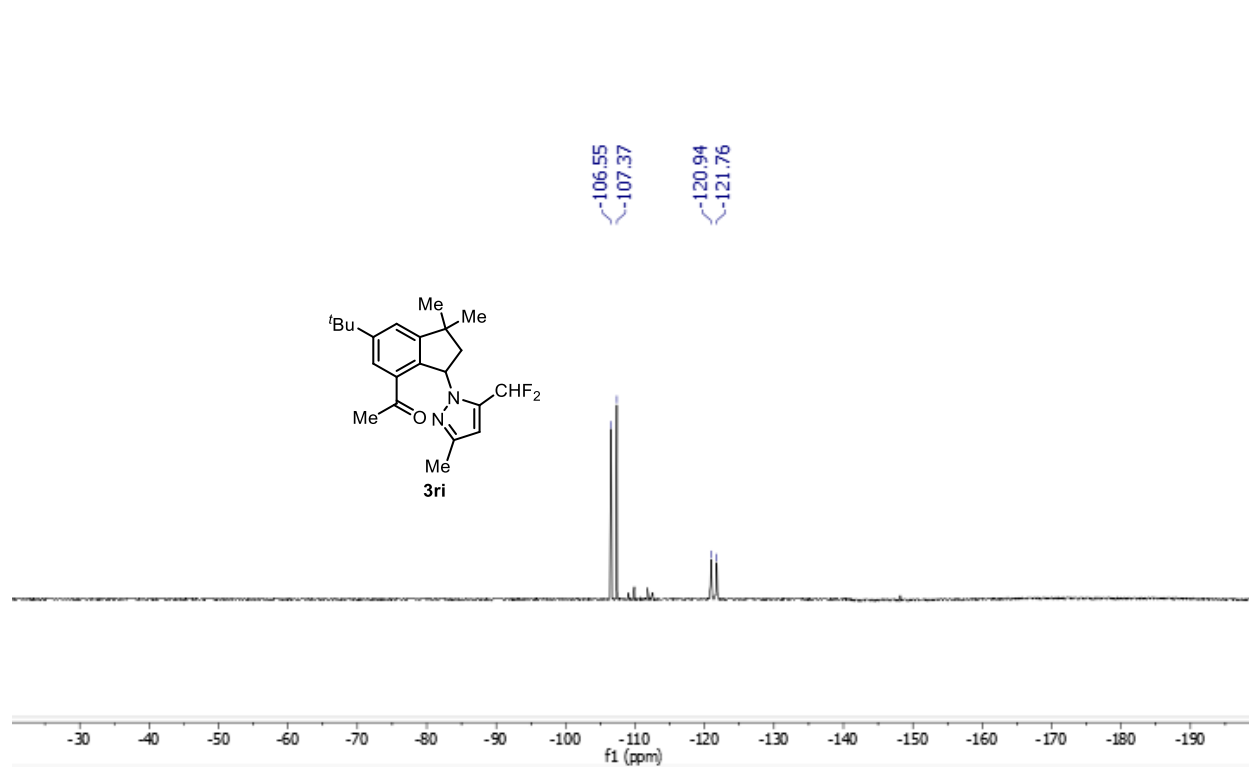
^1H NMR spectrum of **3ri** in CDCl_3 containing 0.03 % (v/v) TMS (500 MHz).



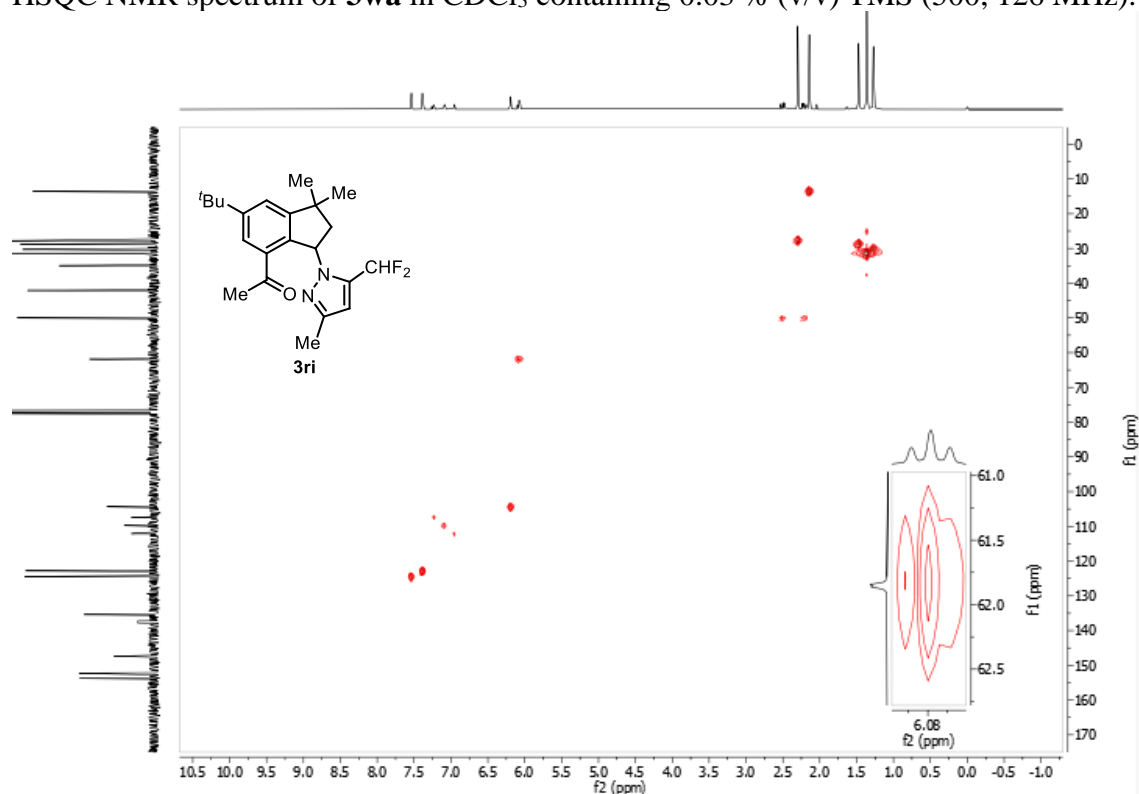
^{13}C NMR spectrum of **3ri** in CDCl_3 containing 0.03 % (v/v) TMS (126 MHz).



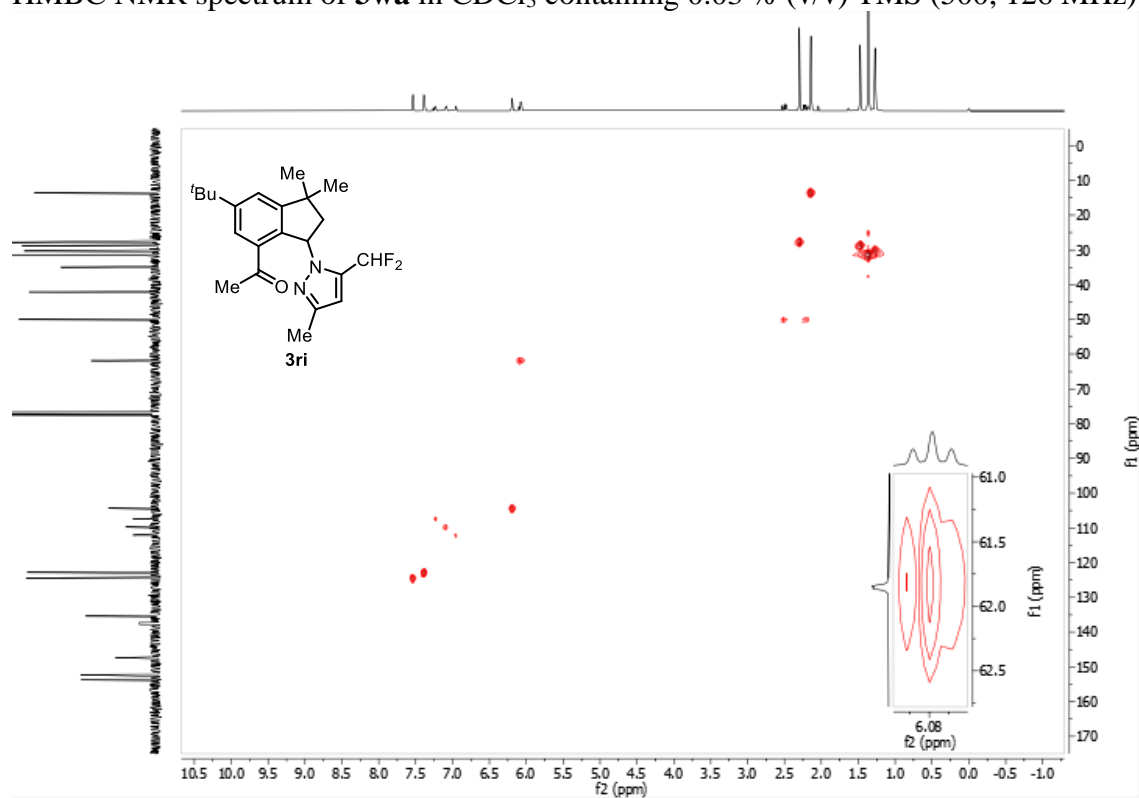
^{19}F NMR spectrum of **3ri** in CDCl_3 containing 0.03 % (v/v) TMS (377 MHz).



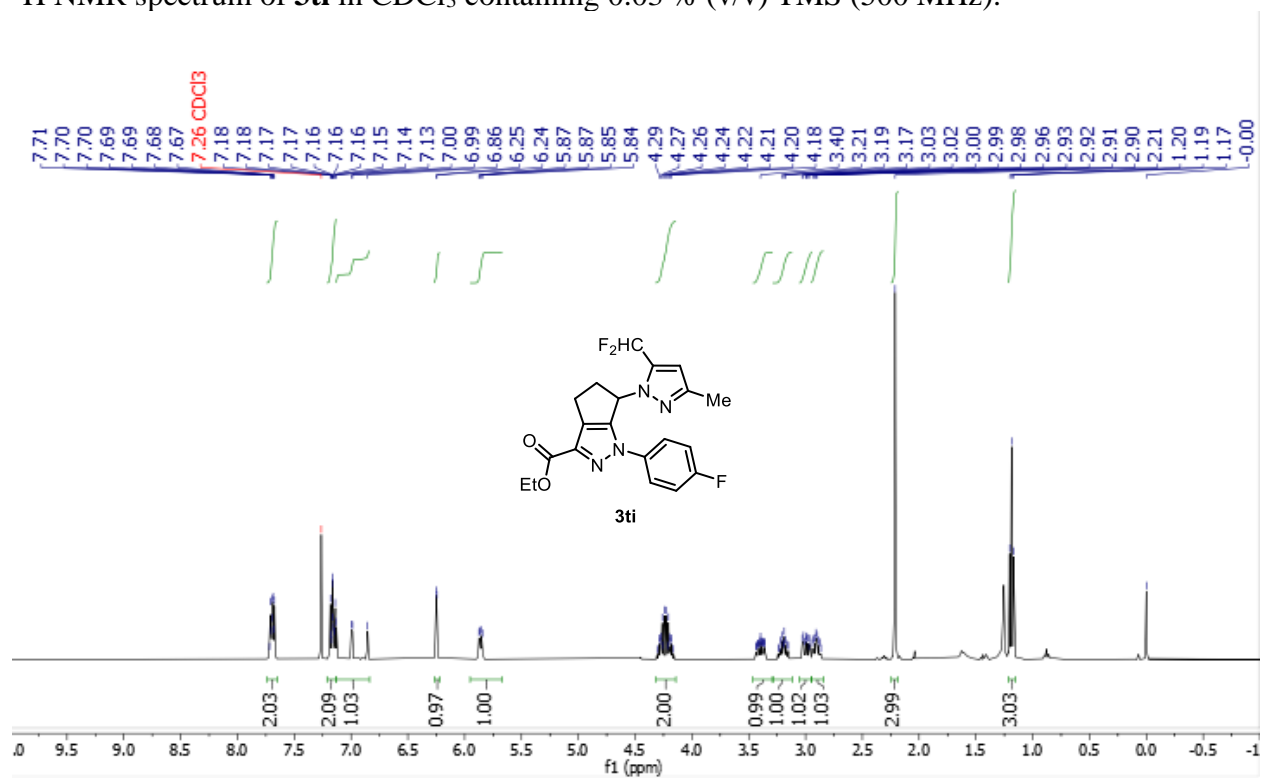
HSQC NMR spectrum of **3wa** in CDCl₃ containing 0.03 % (v/v) TMS (500, 126 MHz).



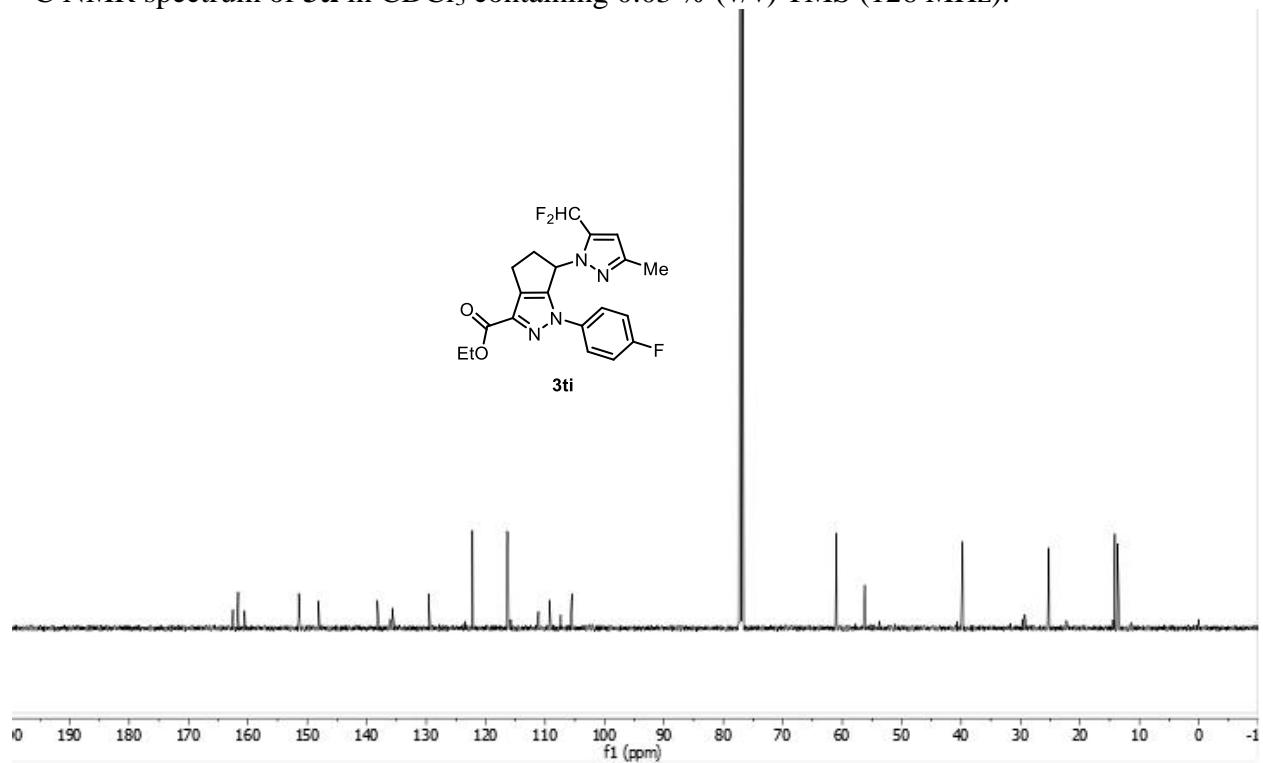
HMBC NMR spectrum of **3wa** in CDCl₃ containing 0.03 % (v/v) TMS (500, 126 MHz).



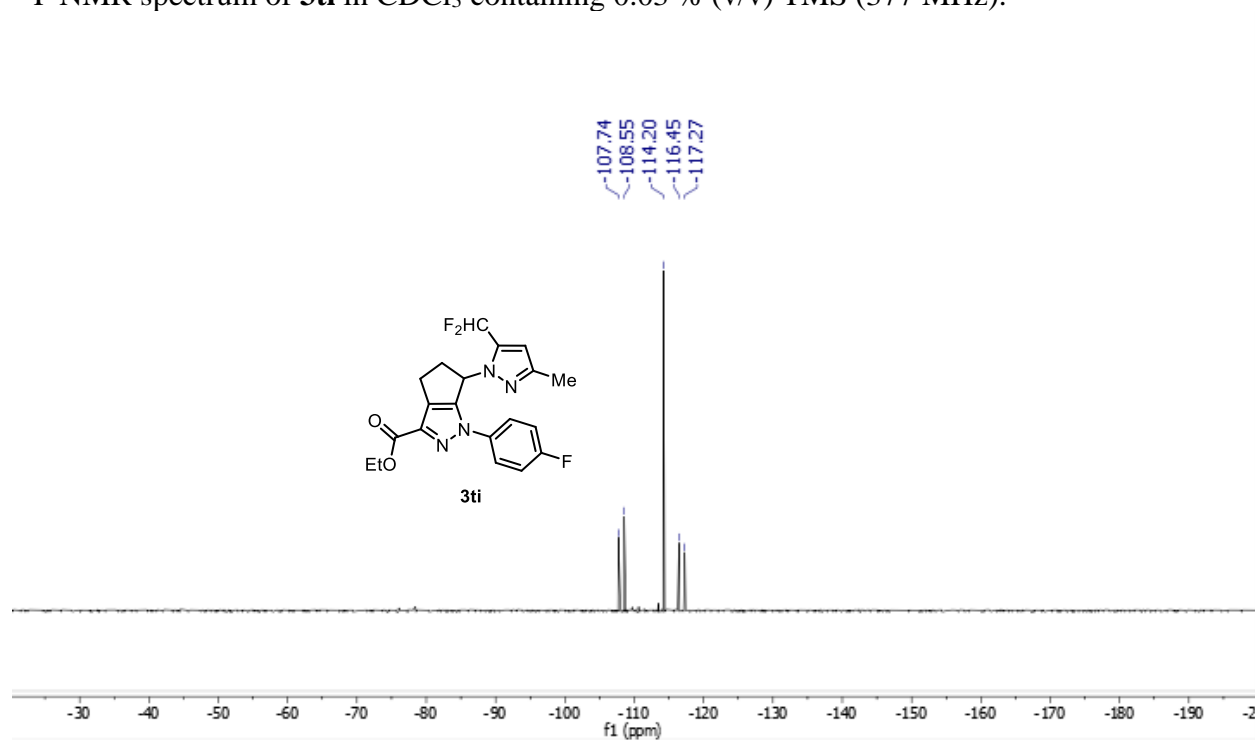
^1H NMR spectrum of **3ti** in CDCl_3 containing 0.03 % (v/v) TMS (500 MHz).



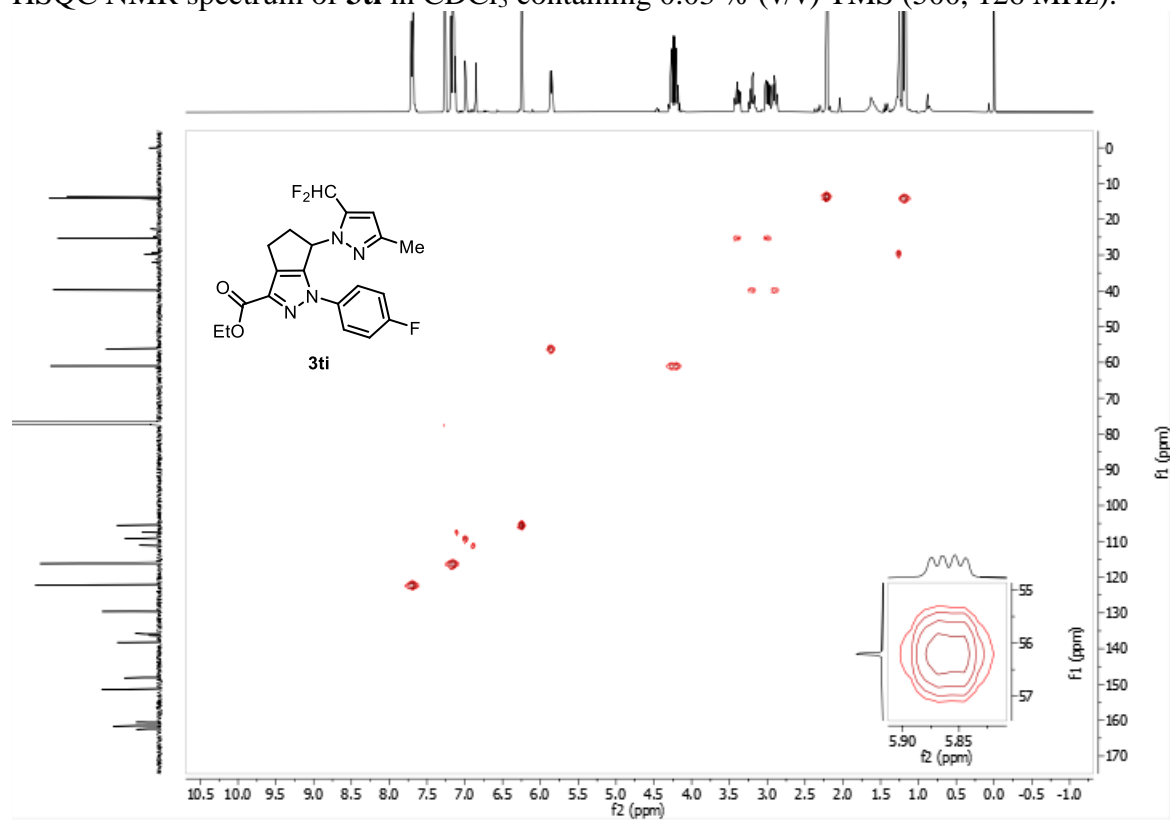
^{13}C NMR spectrum of **3ti** in CDCl_3 containing 0.03 % (v/v) TMS (126 MHz).



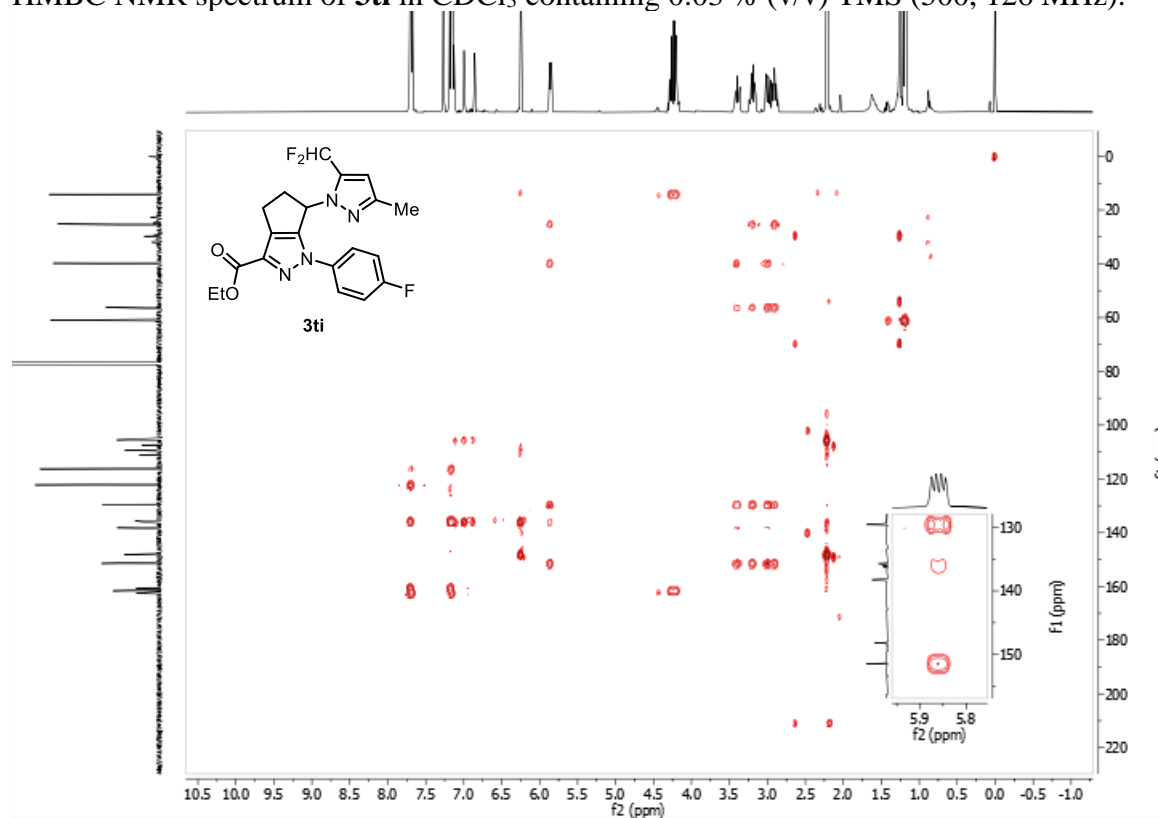
^{19}F NMR spectrum of **3ti** in CDCl_3 containing 0.03 % (v/v) TMS (377 MHz).



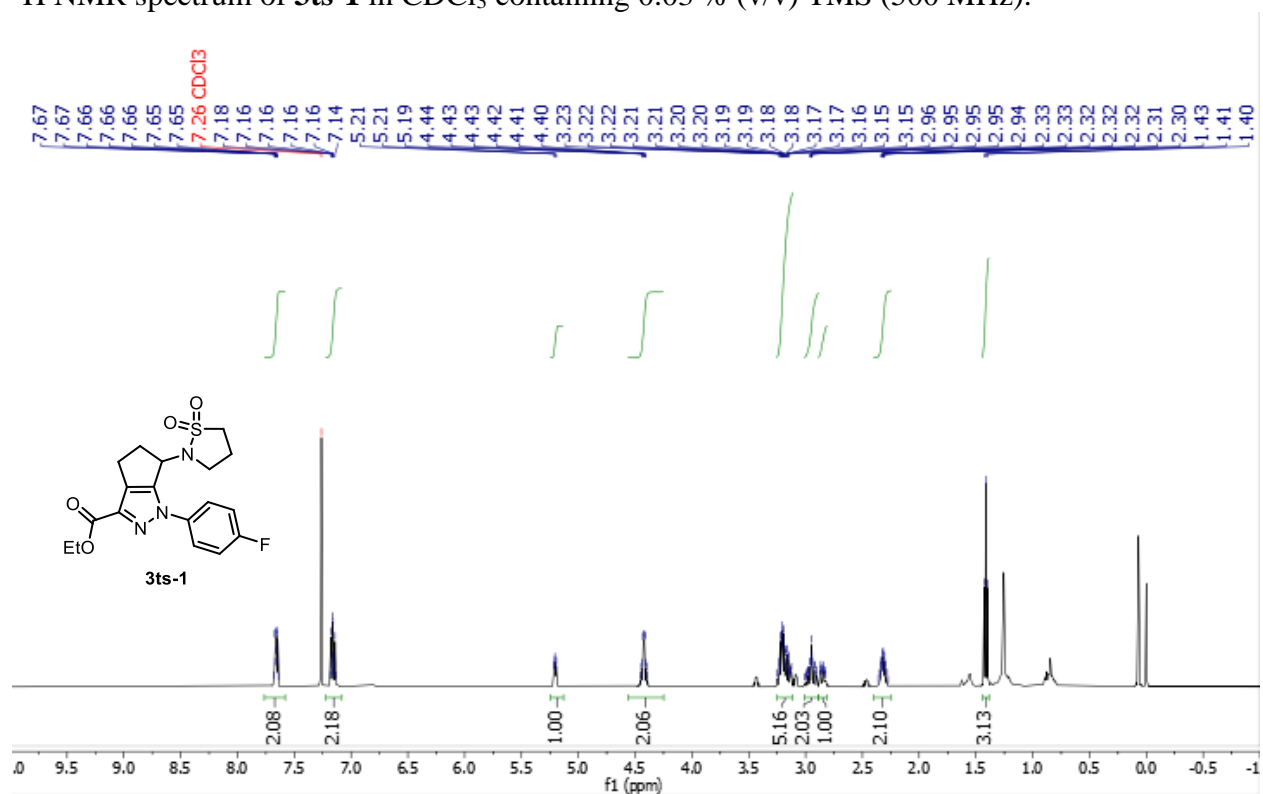
HSQC NMR spectrum of **3ti** in CDCl_3 containing 0.03 % (v/v) TMS (500, 126 MHz).



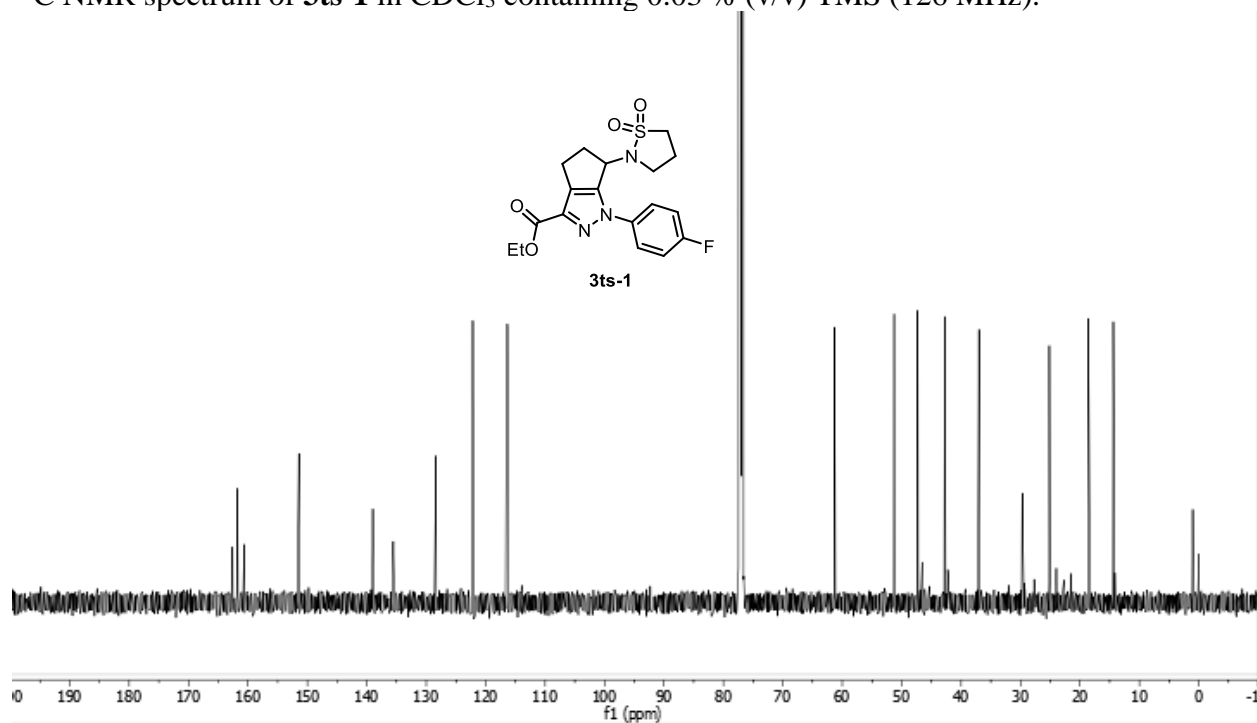
HMBC NMR spectrum of **3ti** in CDCl₃ containing 0.03 % (v/v) TMS (500, 126 MHz).



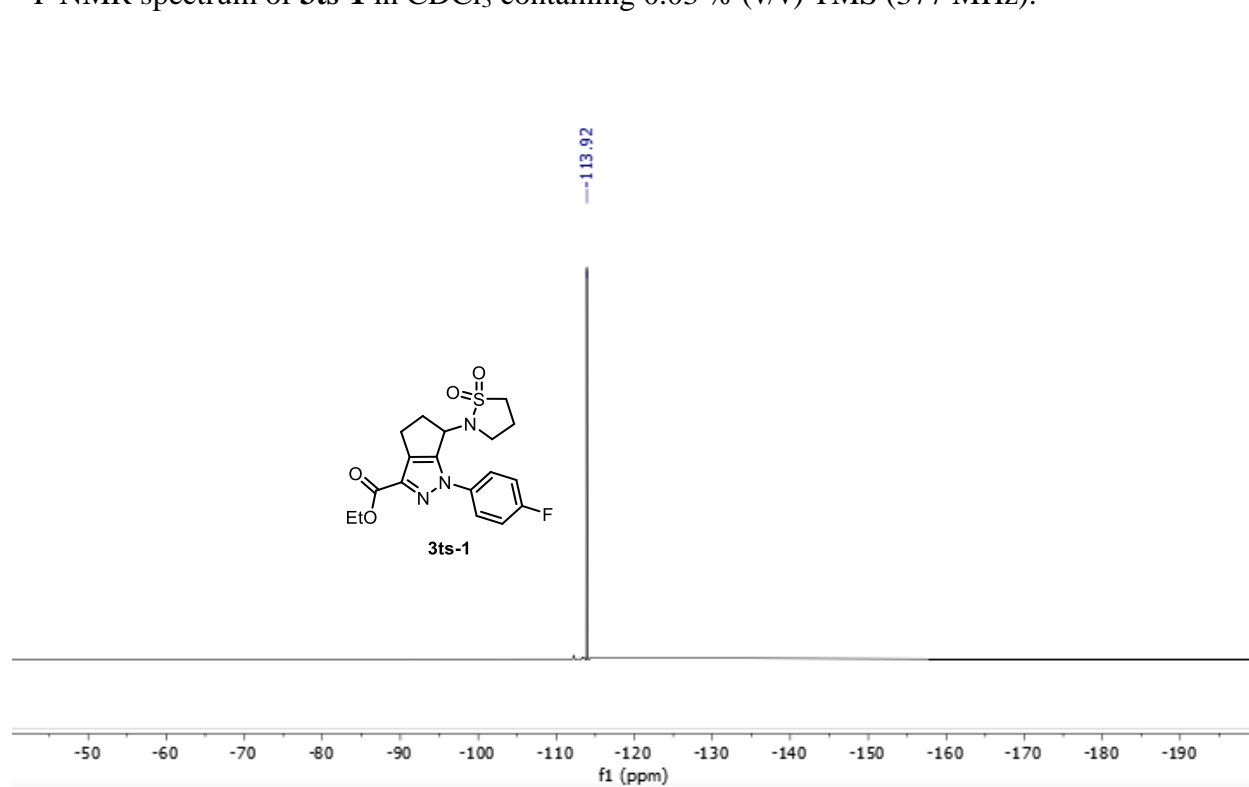
¹H NMR spectrum of **3ts-1** in CDCl₃ containing 0.03 % (v/v) TMS (500 MHz).



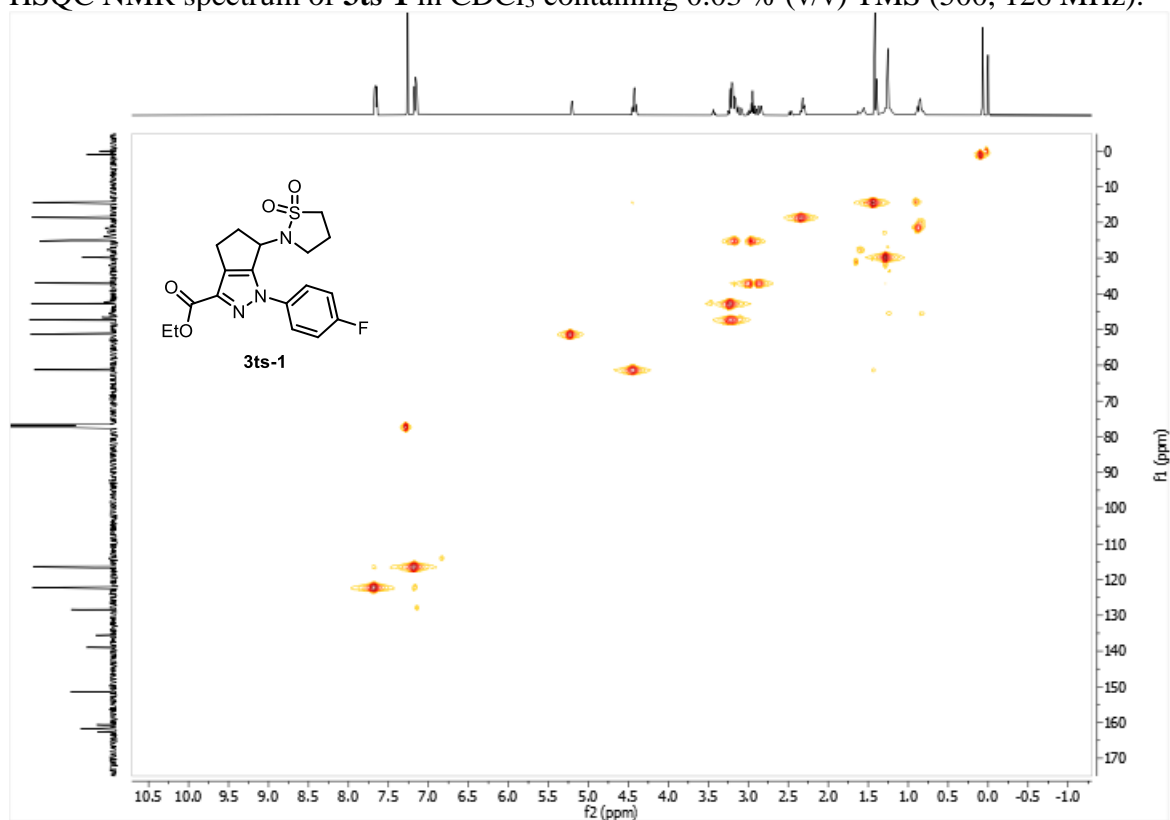
^{13}C NMR spectrum of **3ts-1** in CDCl_3 containing 0.03 % (v/v) TMS (126 MHz).



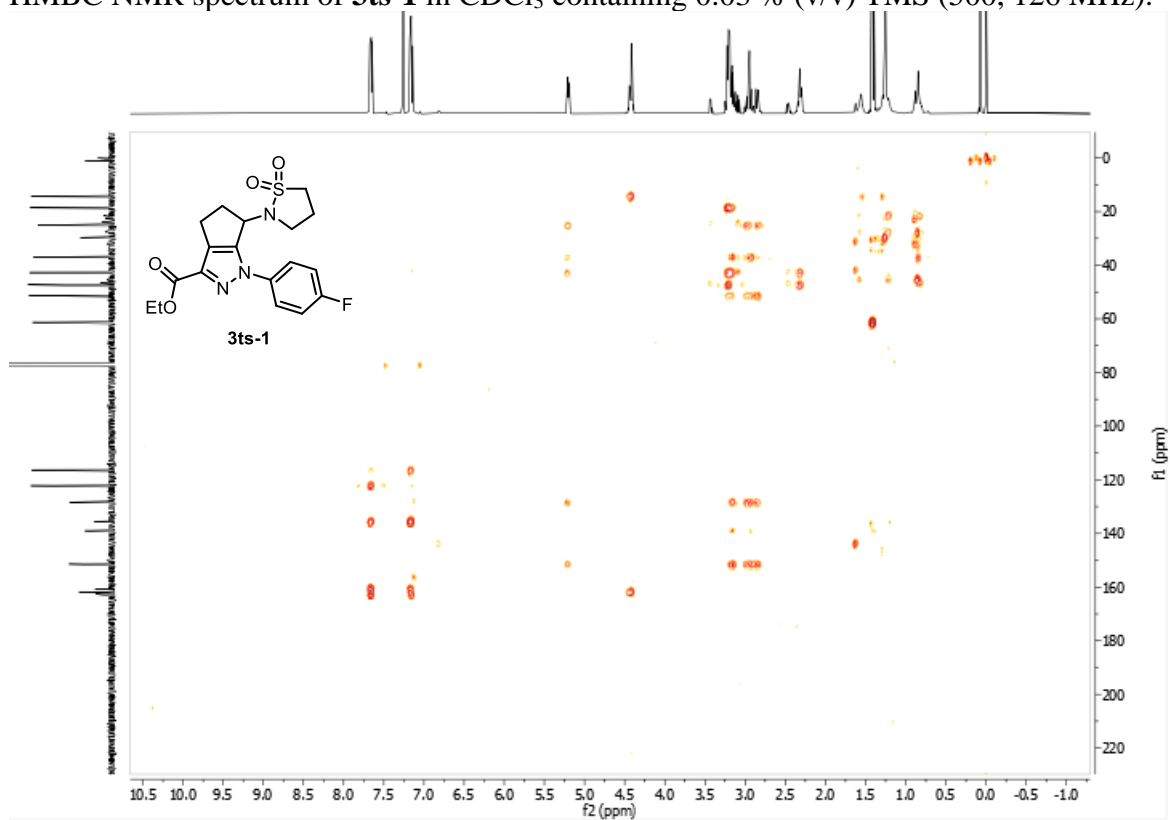
^{19}F NMR spectrum of **3ts-1** in CDCl_3 containing 0.03 % (v/v) TMS (377 MHz).



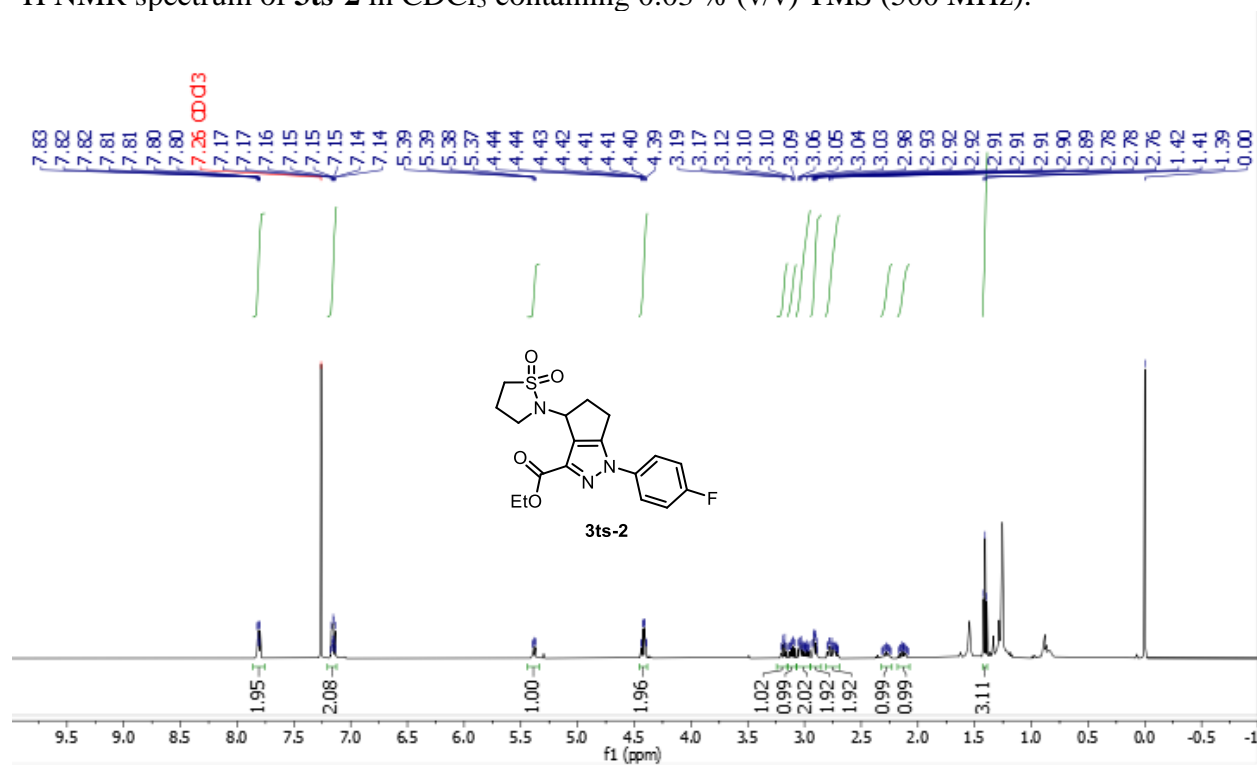
HSQC NMR spectrum of **3ts-1** in CDCl₃ containing 0.03 % (v/v) TMS (500, 126 MHz).



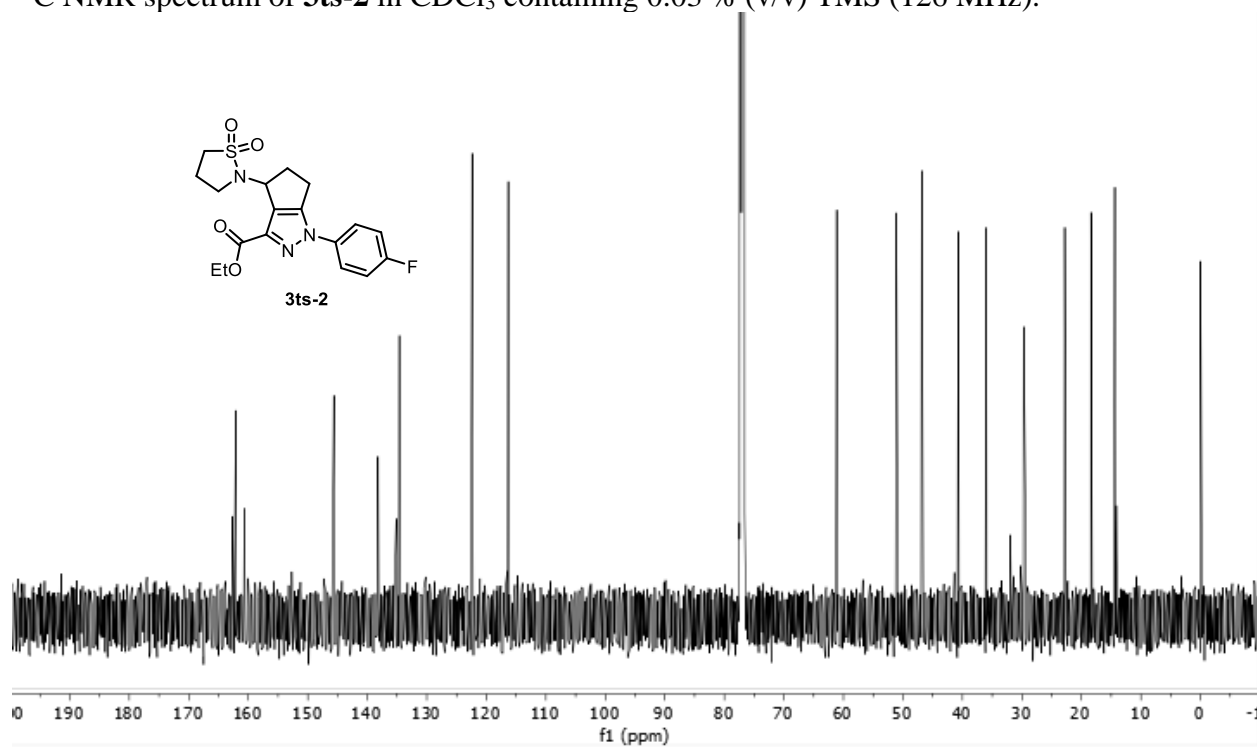
HMBC NMR spectrum of **3ts-1** in CDCl₃ containing 0.03 % (v/v) TMS (500, 126 MHz).



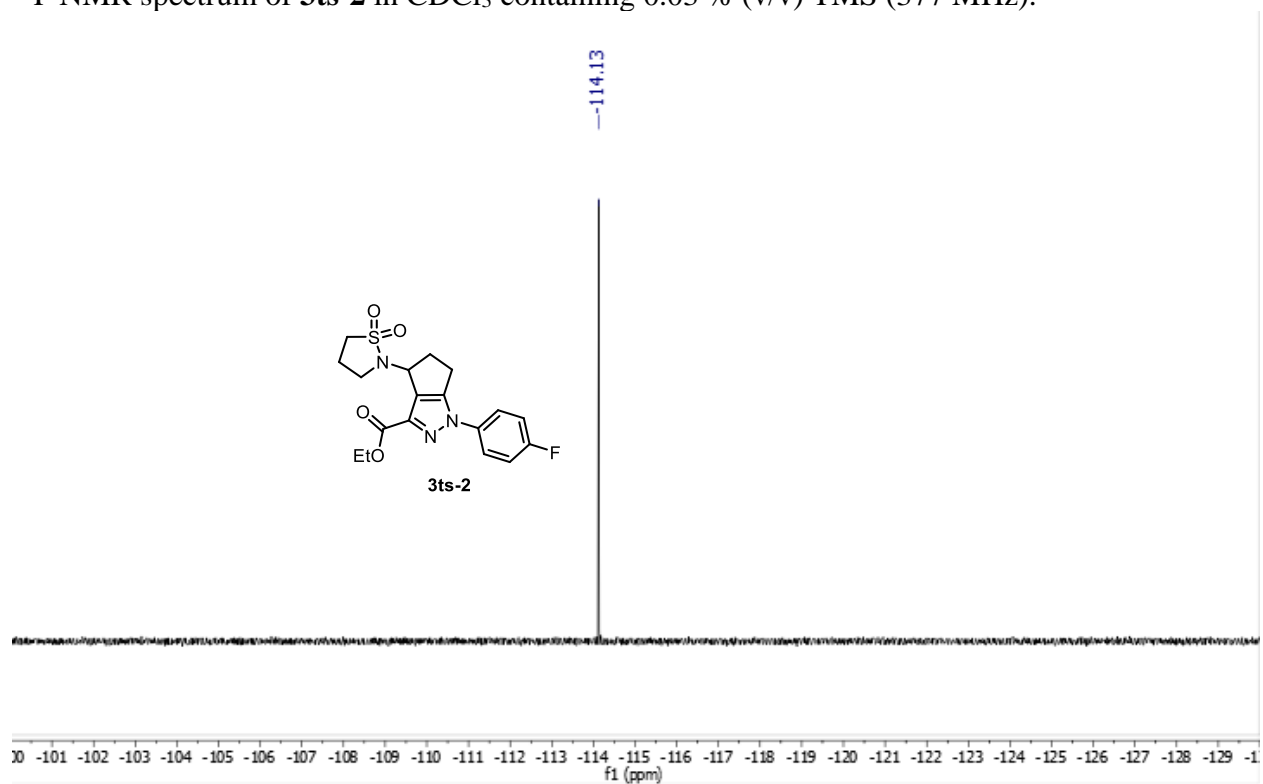
^1H NMR spectrum of **3ts-2** in CDCl_3 containing 0.03 % (v/v) TMS (500 MHz).



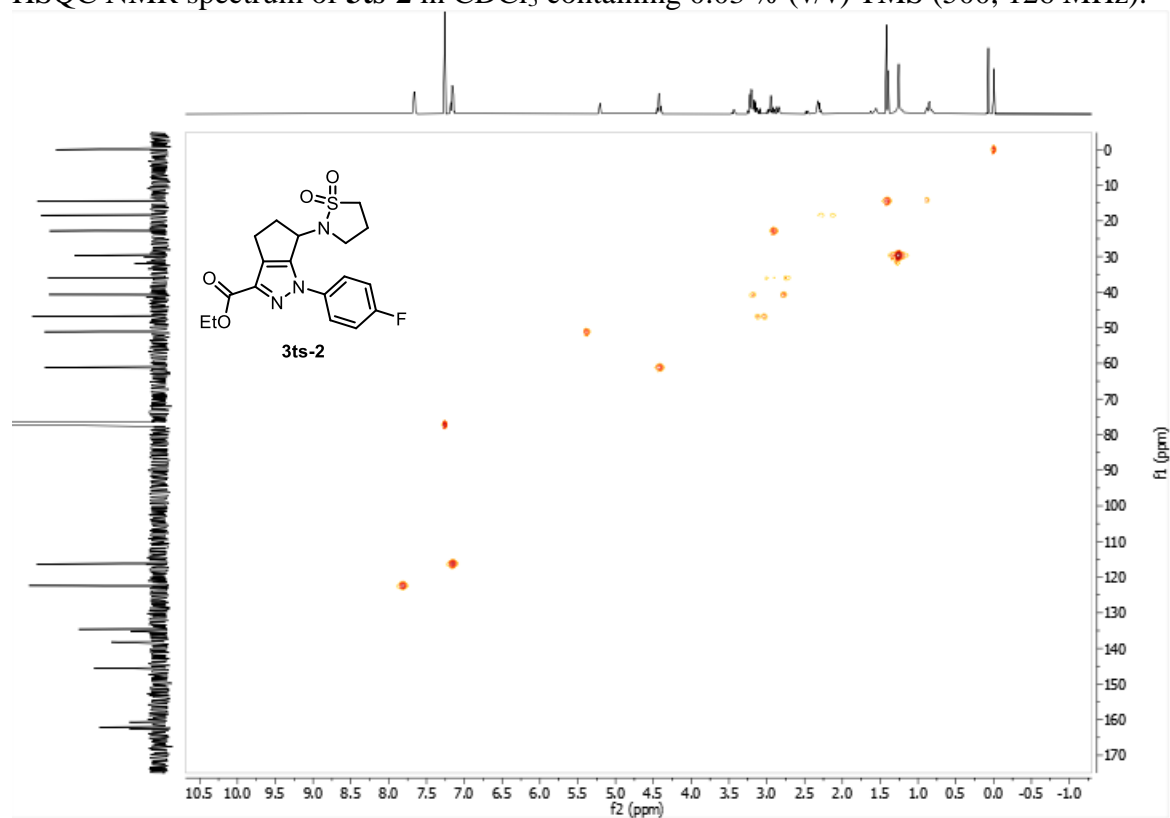
^{13}C NMR spectrum of **3ts-2** in CDCl_3 containing 0.03 % (v/v) TMS (126 MHz).



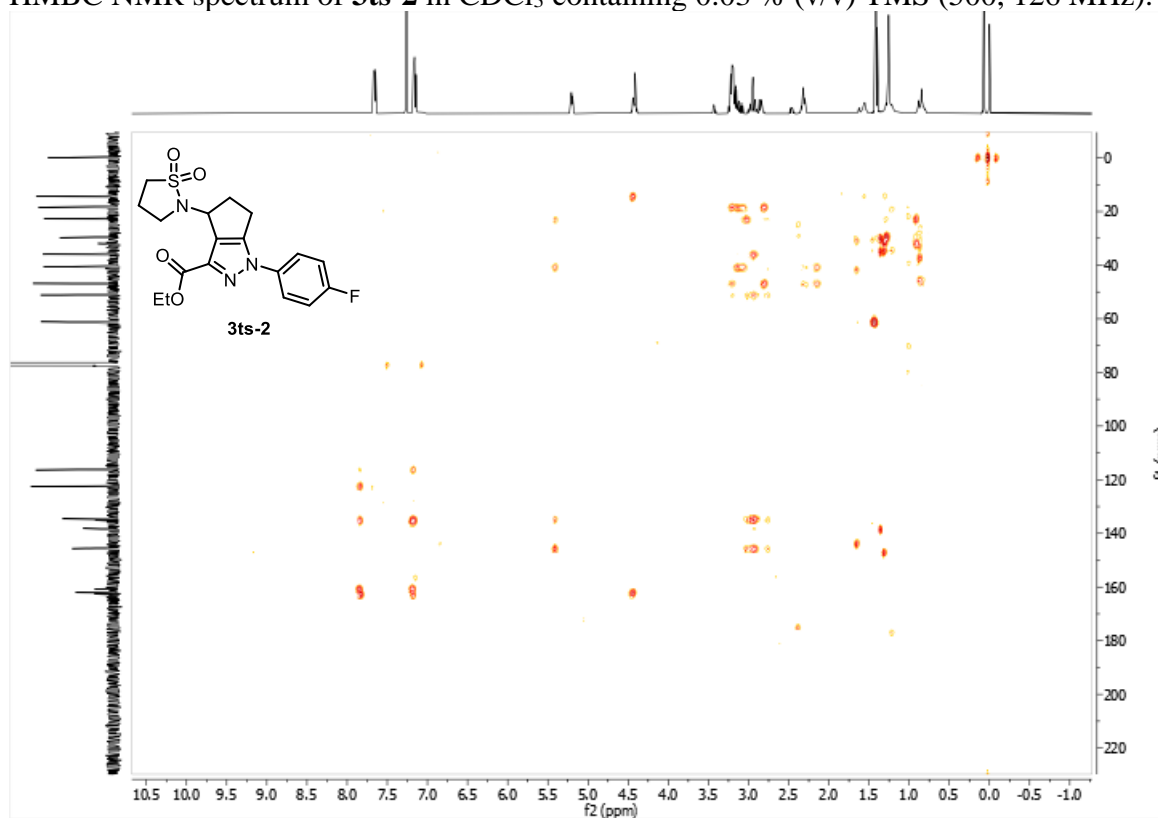
^{19}F NMR spectrum of **3ts-2** in CDCl_3 containing 0.03 % (v/v) TMS (377 MHz).



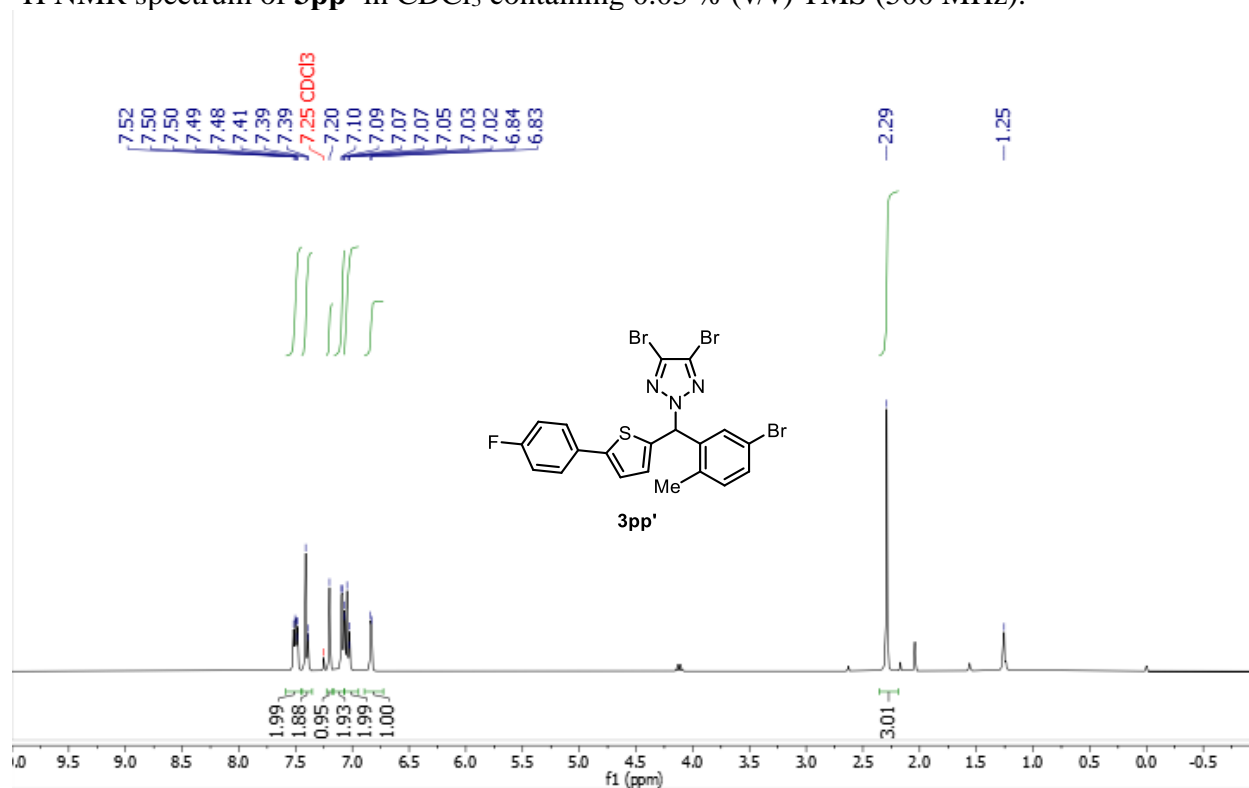
HSQC NMR spectrum of **3ts-2** in CDCl_3 containing 0.03 % (v/v) TMS (500, 126 MHz).



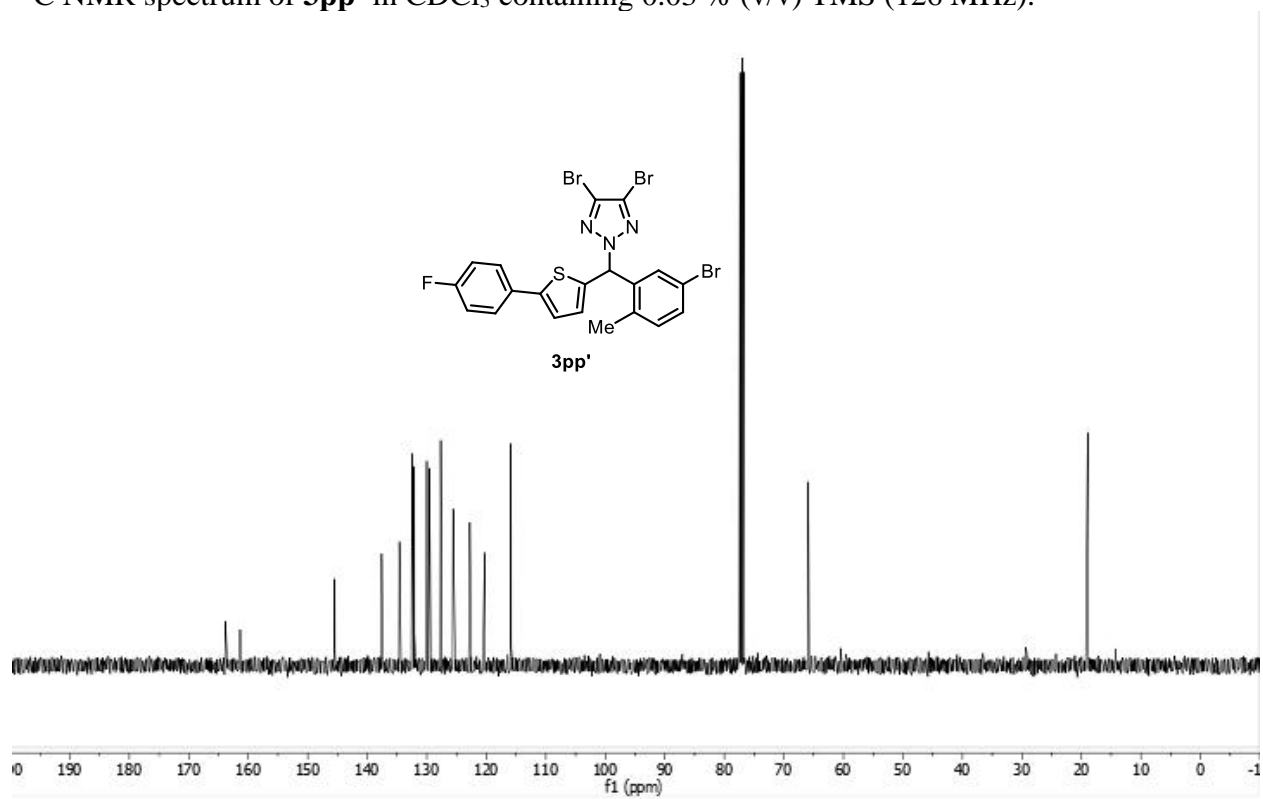
HMBC NMR spectrum of **3ts-2** in CDCl₃ containing 0.03 % (v/v) TMS (500, 126 MHz).



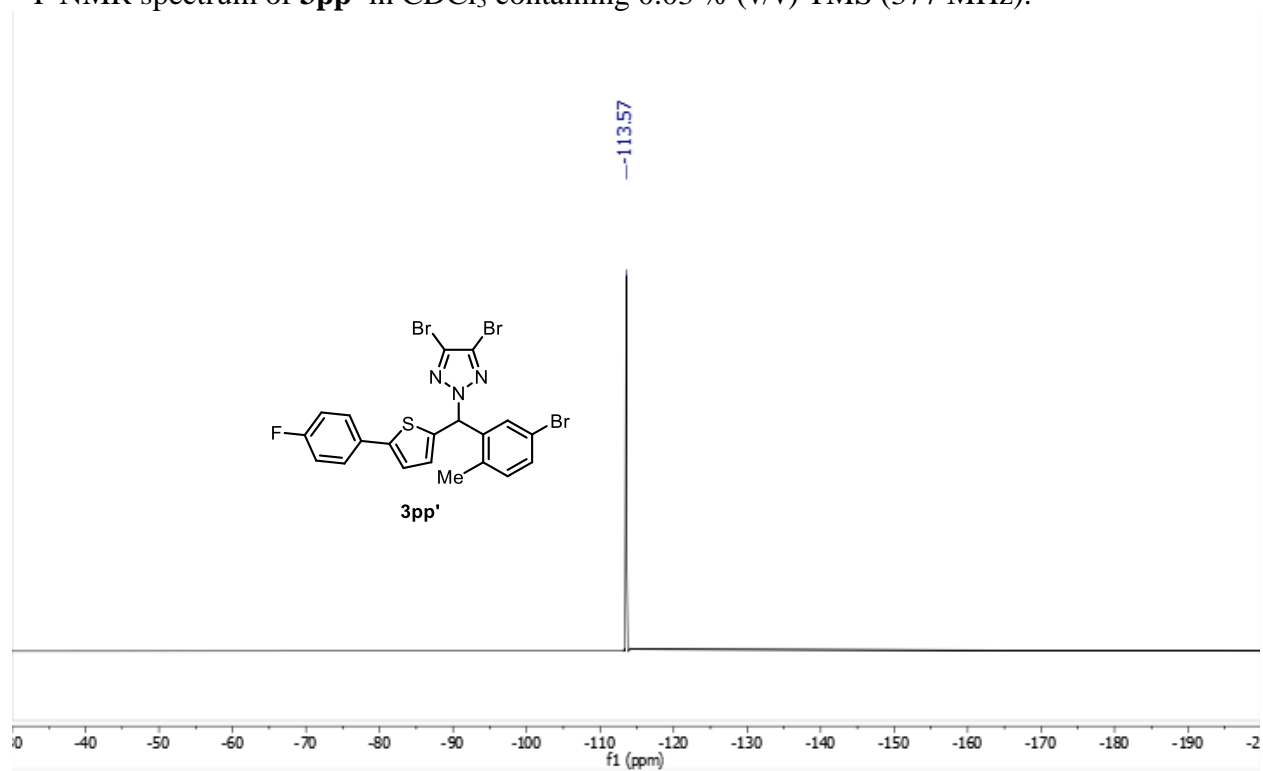
¹H NMR spectrum of **3pp'** in CDCl₃ containing 0.03 % (v/v) TMS (500 MHz).



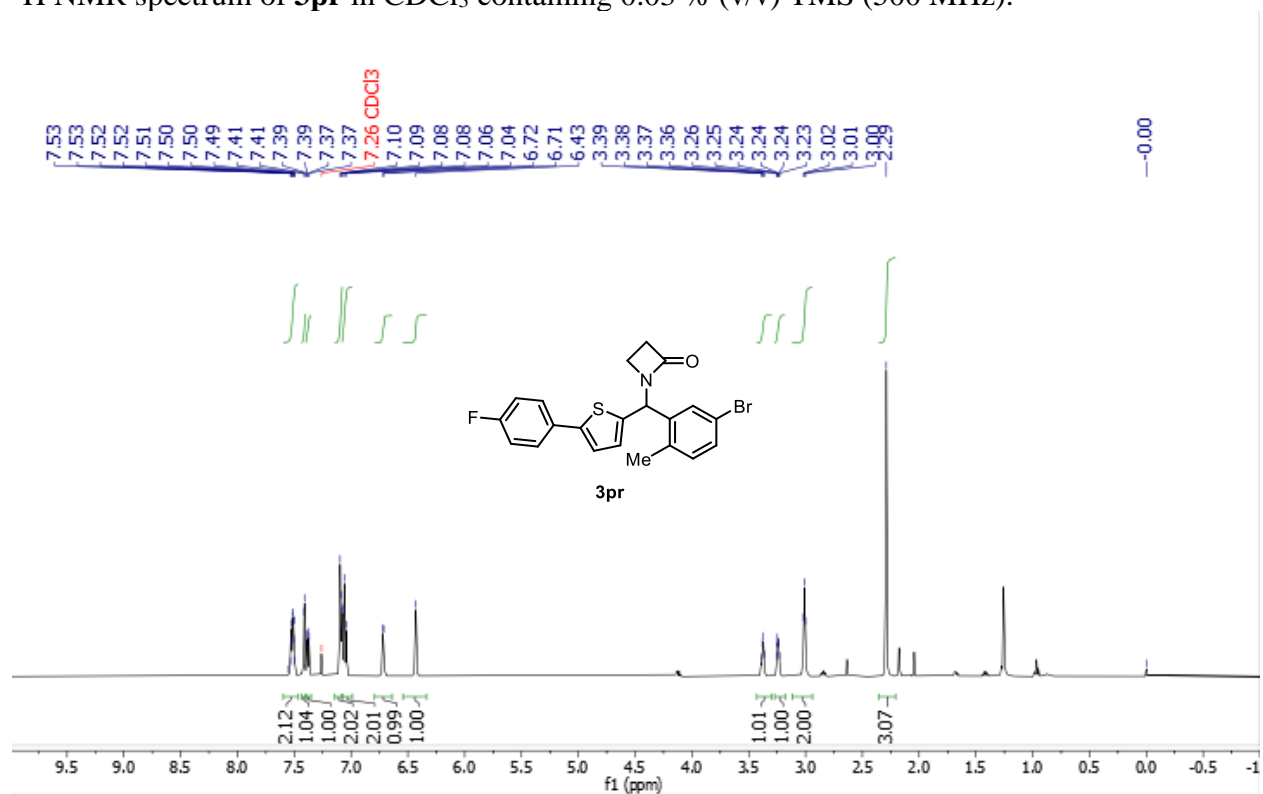
^{13}C NMR spectrum of **3pp'** in CDCl_3 containing 0.03 % (v/v) TMS (126 MHz).



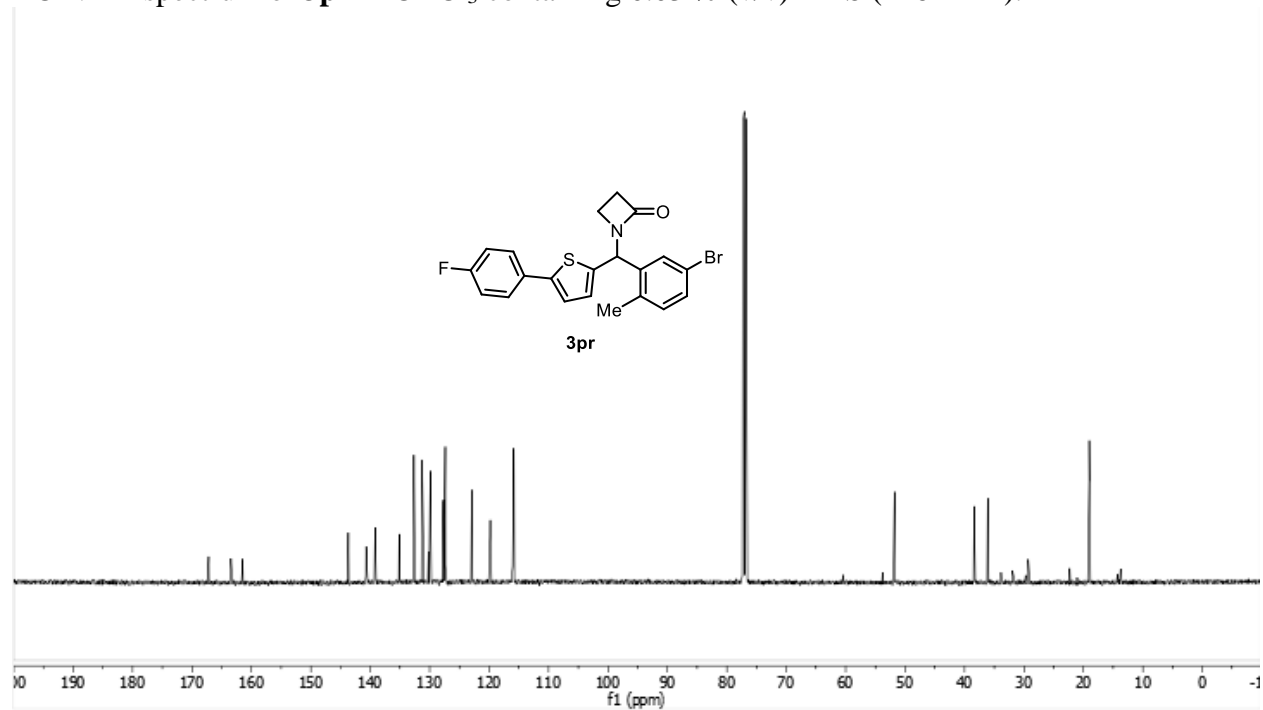
^{19}F NMR spectrum of **3pp'** in CDCl_3 containing 0.03 % (v/v) TMS (377 MHz).



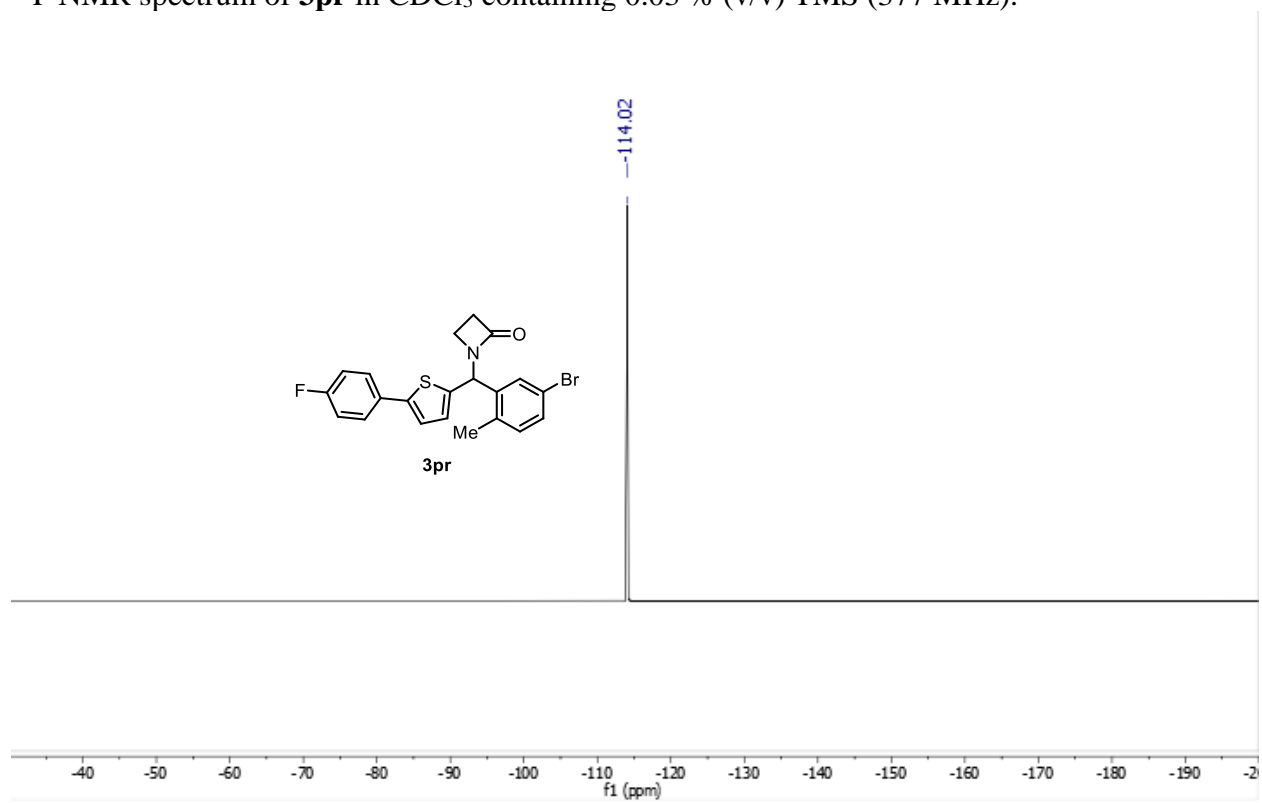
^1H NMR spectrum of **3pr** in CDCl_3 containing 0.03 % (v/v) TMS (500 MHz).



^{13}C NMR spectrum of **3pr** in CDCl_3 containing 0.03 % (v/v) TMS (126 MHz).



^{19}F NMR spectrum of **3pr** in CDCl_3 containing 0.03 % (v/v) TMS (377 MHz).



Appendix C: Supporting Information Chapter 4

4C.I. General Considerations

All reagents were purchased and used as received unless otherwise noted. Cu salts were purchased from Millipore Sigma. 2,2'-bisoxazoline was purchased from Combi-Blocks. Benzylic C–H scaffolds monomers were ordered from commercial sources. N-Fluorobenzenesulfonimide (NFSI) was purchased from Ark Pharm. Diisopropyl phosphites were purchased from Alfa Aesar. Trimethylsilyl isocyanate was purchased from TCI America. Acetonitrile was dried with activated 3 Å molecular sieves.

¹H and ¹³C NMR spectra were recorded on Bruker 400 MHz, 500 MHz or 600 MHz spectrometers and chemical shifts are reported in parts per million (ppm). ¹H NMR spectra were referenced to tetramethylsilane at 0.00 ppm, CD₂Cl₂ at 5.32 ppm or DMSO-d₆ at 2.50 ppm. ¹³C NMR spectra were referenced to CDCl₃ at 77.16 ppm, CD₂Cl₂ at 53.84 ppm or DMSO-d₆ at 39.52 ppm. Column chromatography was performed using a Biotage Isolera One® 40 g or 80 g SiliaSep® cartridges for normal phase chromatography, or with reusable 60 g or 120 g SNAP Ultra® C18 cartridges for reverse phase chromatography. Benzylic ethers were purified with normal phase column chromatography and ureas were purified with reverse phase column chromatography unless otherwise noted. Further purification of impure samples was conducted with preparative thin-layer chromatography plates purchased from Analtech® Glass-Backed Silica G UNIPLATES®. High-resolution mass spectra were obtained using a Thermo Q Exactive™ Plus (ESI or ASAP-MS) by the mass spectrometry facility at the University of Wisconsin (funded by NIH grant: 1S10OD020022-1). Melting points were determined using a DigiMelt MPA160 SRS melting point apparatus.

4C.II. Experimental Procedures for Preparations of Compounds

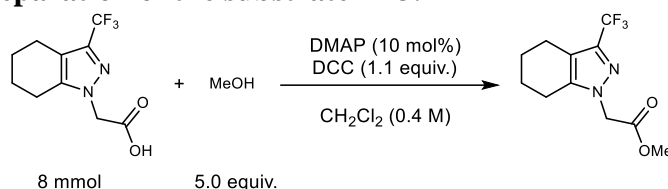
General Procedure for Cross Coupling of Benzylic C–H Substrates and Alcohols.

Copper(I) chloride (2.0 mg, 0.020 mmol, 10 mol%), 2, 2'-bisoxazoline (2.8 mg, 0.020 mmol, 10 mol%), NFSI (126.1 mg, 0.40 mmol, 2.0 equiv.), N–H nucleophiles (0.30 mmol, 3.0 equiv.) and benzylic substrate (if solid, 0.20 mmol, 1.0 equiv.) were added under air to a 4 ml borosilicate glass vial containing a magnetic stir bar. Then the vial was capped with a pierceable Teflon cap. A needle was pierced through the cap to facilitate exchange of the vial headspace with the atmosphere. Then the vial was moved into a glove box, through three vacuum-nitrogen-backfill cycles. The needle was removed, and the vial was taken out of the glove box (now sealed under an inert gas). Solvent (1.0 mL), benzylic substrate (if liquid, 0.20 mmol, 1.0 equiv.), and diisopropyl phosphite (16.3 μL, 0.10 mmol, 0.5 equiv.) were added into the vial by injection through the cap. The sealed vial was heated at 40 °C and stirred for 18 h. When the reaction finished, the mixture was cooled down to room temperature. Then the mixture was evaporated under vacuum and the crude mixture was purified by column chromatography (silica gel, eluted by pentane:ethyl acetate = 20:1 to 4:1).

General Procedure for Benzylic C–H Isocyanation/Urea Synthesis.

Copper(I) acetate (2.9 mg, 0.024 mmol, 6.0 mol%), 2, 2'-bisoxazoline (3.4 mg, 0.024 mmol, 6.0 mol%), NFSI (315 mg, 1.0 mmol, 2.5 equiv.) and benzylic substrate (if solid, 0.40 mmol, 1.0 equiv.) were added under air to an 8 ml borosilicate glass vial containing a magnetic stir bar. Then the vial was capped with a pierceable Teflon cap. A needle was pierced through the cap to facilitate exchange of the vial headspace with the atmosphere. Then the vial was moved into a glove box, through three vacuum-nitrogen-backfill cycles. The needle was removed in the glove box. Acetonitrile (1.0 mL), benzylic substrate (if liquid, 0.20 mmol, 1.0 equiv.), diisopropyl phosphite (33 μ L, 0.10 mmol, 0.5 equiv.) and trimethylsilyl isocyanate (160 μ L, 1.2 mmol, 3.0 equiv.) were added into the vial. The vial was capped, removed from the glove box, heated at 30 °C and stirred for 2 h. When the reaction finished, the vial was uncapped, and an amine (1.4 mmol, 3.5 equiv.) was added into the reaction mixture. Then the mixture was heated at 50 °C and stirred for 20 h. When finished, the reaction mixture was purified by reverse phase column chromatography (H₂O/MeCN = 80:20 to 40:60) without further workup.

Procedure for the preparation of the substrate **A13**.



A 50 mL round-bottom flask was charged with 2-(3-(trifluoromethyl)-4,5,6,7-tetrahydro-1H-indazol-1-yl)acetic acid (8.0 mmol, 2.0 g, 1.0 equiv.), 4-Dimethylaminopyridine (DMAP, 0.8 mmol, 98 mg, 0.1 equiv.), MeOH (40 mmol, 1.6 mL, 5.0 equiv.) and CH₂Cl₂ (10 mL). The reaction mixture was stirred at room temperature for 30 min. N, N'-dicyclohexylcarbodiimide (DCC, 8.8 mmol, 1.1 equiv.) was dissolved in CH₂Cl₂ (10 mL) and the solution was added to the reaction mixture at 0 °C in a dropwise manner. When finished, the reaction was stirred and allowed to be warmed to room temperature over 12 h. 1.7g (81% yield) of **A13** was isolated. Characterization data are consistent with literature report¹.

4C.III. Procedure for Cheminformatic Study

Data set of known bioactive molecules.

To obtain a collection of relevant drug molecules, 2,470 FDA approved drugs were downloaded from Drugbank (accessed May 25th, 2020, <https://go.drugbank.com/releases/latest#structures>), 4,288 drugs approved not by FDA but by other countries were downloaded from ZINC database (accessed November 20th, 2020, <https://zinc.docking.org/substances/subsets/world-not-fda/>) and 6,778 SARS-CoV-2 relevant compounds were downloaded from ChEMBL (accessed November 18th, 2020, https://www.ebi.ac.uk/chembl/g/#browse/compounds/filter/_metadata.compound_records.src_id%3A52). These compounds were combined, filtered (molecular weight ≤ 1000 , carbon count ≥ 5 , $-12 \leq \text{AlogP} \leq 12$, polar surface area ≤ 500 and metal atom count = 0) and duplicates were removed from the collection. Finally, 2,014 compounds Drugbank, 4,175 compounds from ZINC and 6,422 compounds from ChEMBL amounted to 12,611 compounds in the collection.

Enumeration of benzylic C–H cross coupling products.

Benzylic C–H scaffolds and monomers were selected and ordered from commercial sources. Certain monomers were intentionally excluded due to interfering (e.g. carboxylic acids) or no reactivity (e.g. tertiary amines and anilines, which do not react with isocyanates to afford ureas). The "Enumerate Combinatorial Reaction" component in Pipeline Pilot (version 18.1.100.11) was used to enumerate benzylic C–H cross coupling products. All the output products were hydrolyzed to retreat more drug-relevant physicochemical properties (simple alkyl carbamates to amines, simple alkyl esters to carboxylic acids and simple alkyl phosphates to phosphoric acids; simple alkyl defined as Me, Et, ^tPr or ^tBu). Duplicated molecules were removed after hydrolysis.

Molecular properties.

21 common physical chemical and topological properties were used a molecular descriptors to probe the medicinal relevance of the enumerated compounds by comparison with bioactive compounds: molecular weight, number of positive atoms, number of negative atoms, number of rings, number of ring assemblies, number of aromatic rings, number of stereo atoms, number of N atoms, number of O atoms, number of hydrogen bond donors, number of hydrogen bond acceptors, AlogP, molecular volume, molecular polar surface area, fractional molecular polar surface area, dipole magnitude, quantitative estimate of drug-likeness (QED) (ref), fraction of sp³ carbon atoms (Fsp³), 3D scores and plane of best fit scores (PBF). All the properties but 3D scores and PBF scores were directly calculated with Pipeline Pilot (version 18.1.100.11) from Dassault Systèmes (Vélizy-Villacoublay, France).

3D scores were calculated as $3D \text{ score} = npr1 + npr2$, where $npr1 = I_1/I_3$, and $npr2 = I_2/I_3$ and I_1 , I_2 and I_3 are the three calculated principal moments of inertia in an ascending order ($I_1 \leq I_2 \leq I_3$). I_1 , I_2 and I_3 were directly measured with Pipeline Pilot and then calculated to obtain 3D scores.

PBF scores were calculated with RDKit package for Python. 3D conformation for each of enumerated compounds and bioactive compounds were computed with Pipeline Pilot and exported as SD files, which were then loaded into Jupyter Notebook with RDKit and PBF values were calculated for each of the conformer.

PCA.

The principal components were calculated with R programming language and the procedure was adopted from literature². Prior to PCA calculation, all the physical chemical and topological properties calculated were centered (subtract mean) and scaled (divide by variance). The cumulative total variance explained by the principal components were as follows: 35% (PC1), 51% (PC2), 63% (PC3) and 71% (PC4). Density plots were created with Python to avoid significant overlap of spot markers due to the large number of compounds. The loadings of all the properties were tabulated to assist the interpretation of the PCA.

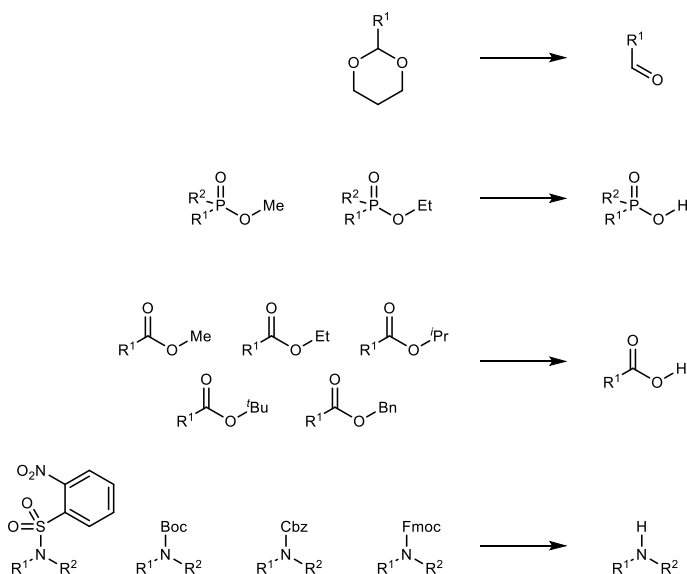


Figure 4C.3. Hydrolysis of P01-20 compounds.

4C.IV. Selection and Analysis of the 160-compound subset of P01-20

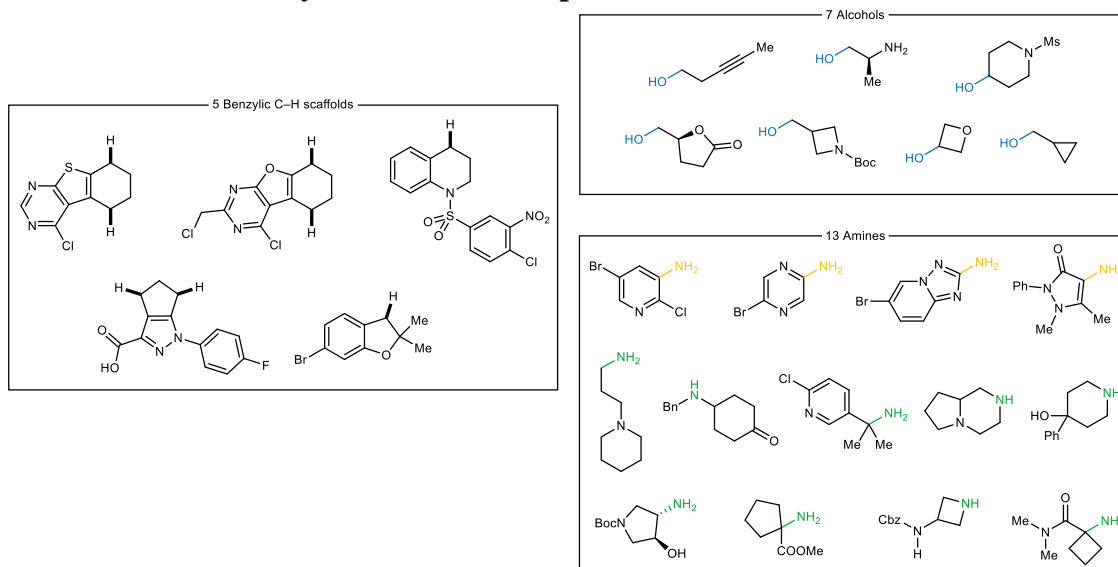


Figure 4C.2. Scaffolds and monomers selected to assemble the 160-compound subset of P01-20 library.

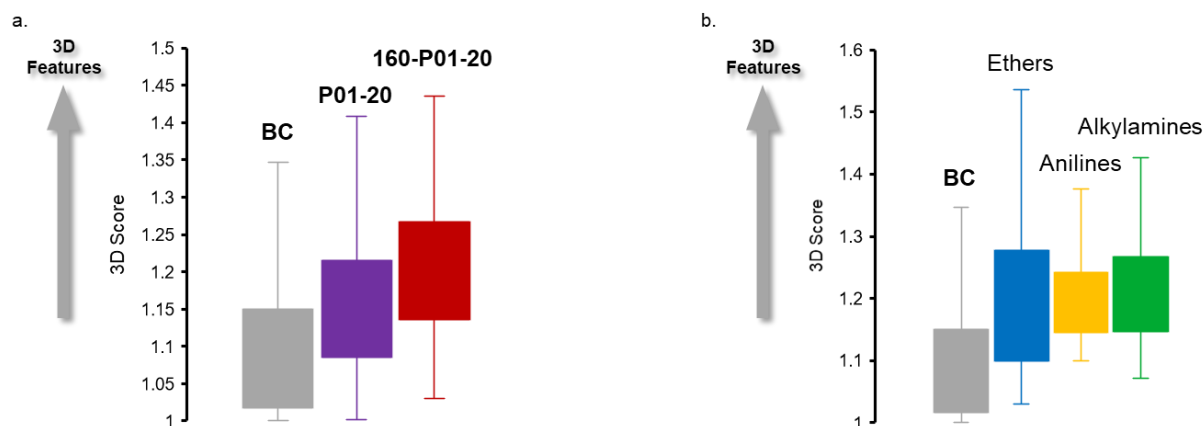


Figure 4C.3. Analysis of 3D scores of the 160-compound subset of P01-20 library. **a**, Comparison of 3D scores between BC molecules, P01-20 molecules and the 160-compound subset of P01-20. **b**, Comparison of 3D scores between BC molecules and the 160-compound subset of P01-20 (160-P01-20) by monomer categories.

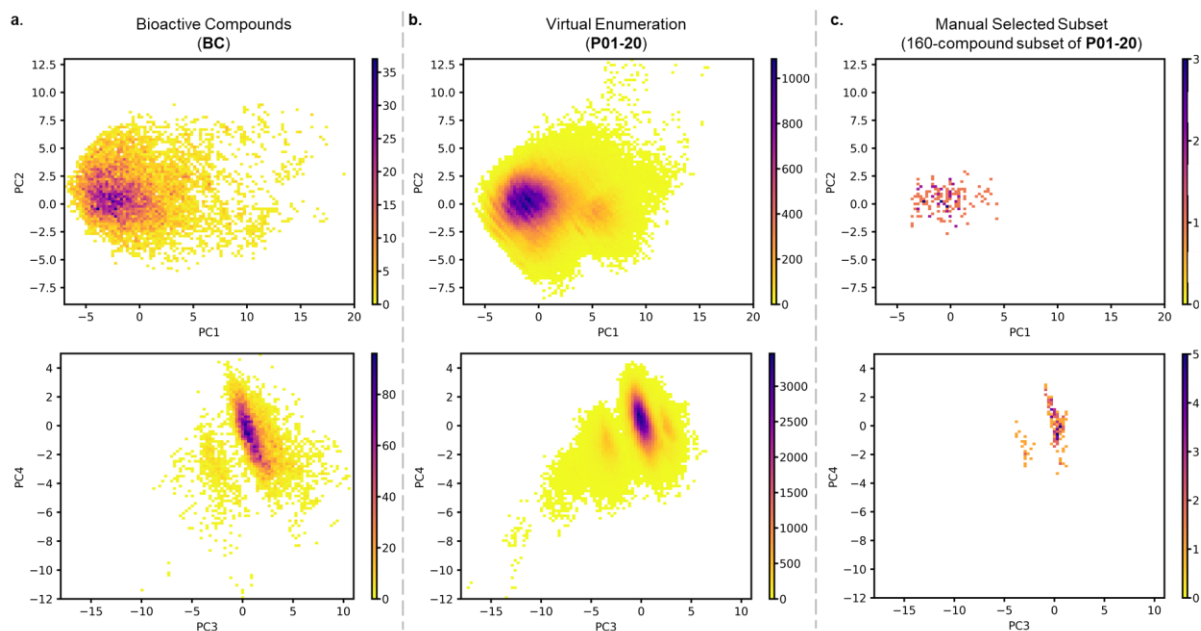


Figure 4C.4. Comparison of PCA between BC, P01-20 and the 160-compound subset of P01-20. PCA depicted for **a**, BC; **b**, P01-20 and **c**, a 160-compound subset of P01-20. Libraries are visualized in density heatmaps, where BC ($n = 12,611$), P01-20 ($n = 368,948$) and a subset of P01-20 ($n = 160$) compounds were analyzed by 100×100 bins and the color of each bin was determined by the number of compounds in it.

4C.V. Comparison of sp^2 and sp^3 functionalization product derived from A10

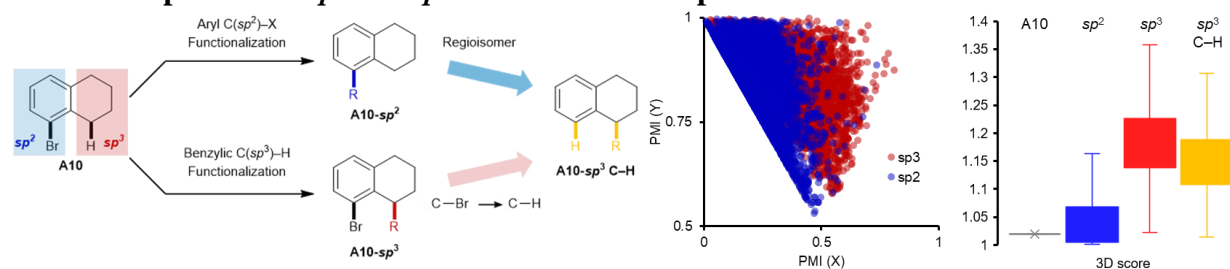


Figure 4C.5. Comparison of PMI and 3D scores (Box-Whisker plot) between sp^2 and sp^3 functionalization products derived from A10.

4C.VI. Loading Coefficients for PCA Plots

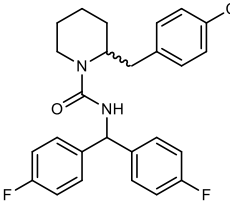
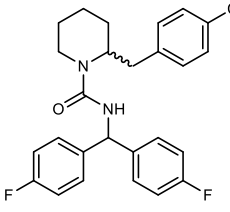
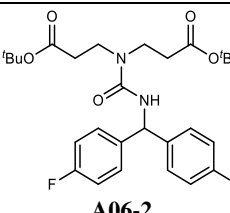
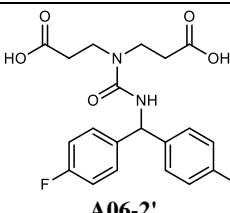
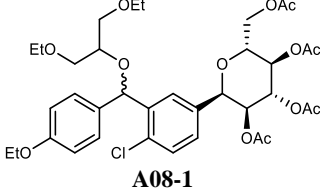
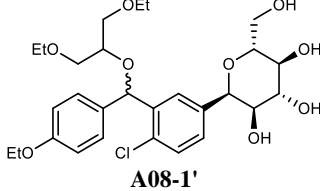
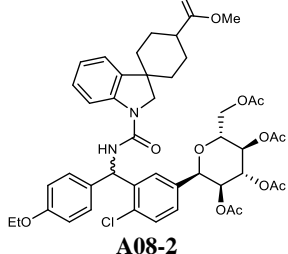
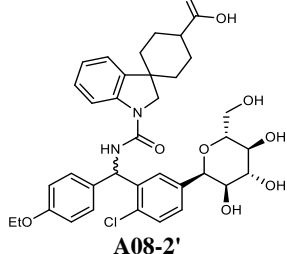
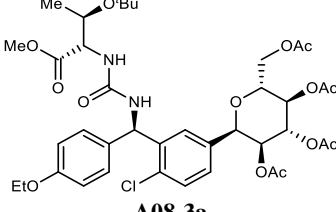
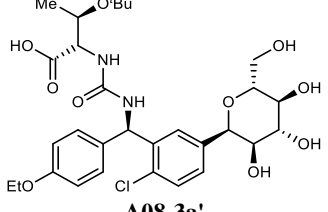
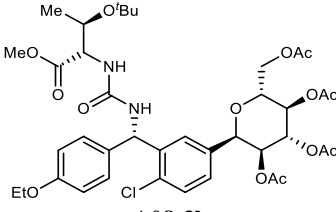
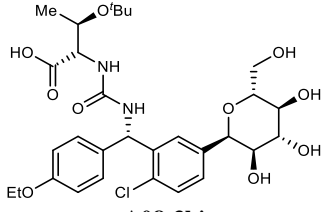
Table 4C.1. Loading coefficients for PC1-PC4 in PCA plots.

| | PC1 | PC2 | PC3 | PC4 |
|-------------------------------|----------|----------|----------|----------|
| Molecular Weight | 0.32151 | -0.19728 | -0.04531 | 0.0158 |
| No. Positive Atoms | 0.13738 | 0.149388 | -0.49229 | -0.30437 |
| No. Negative Atoms | 0.138031 | 0.149726 | -0.49297 | -0.3002 |
| No. Rotatable Bonds | 0.232608 | -0.13278 | 0.16723 | -0.27264 |
| No. Rings | 0.182456 | -0.22396 | -0.18909 | 0.313868 |
| No. Aromatic Rings | 0.057912 | -0.09161 | -0.09973 | 0.166042 |
| No. Ring Assemblies | 0.232323 | -0.27042 | -0.05797 | 0.180158 |
| No. Stereo Atoms | 0.24058 | -0.03516 | 0.313007 | -0.10463 |
| No. H Acceptors | 0.31875 | 0.153016 | 0.151316 | -0.00887 |
| No. H Donors | 0.249158 | 0.187331 | 0.252213 | 0.147264 |
| ALogP | -0.04243 | -0.46037 | -0.13104 | 0.039292 |
| Molecular Volume | 0.320278 | -0.22232 | 0.028481 | -0.06186 |
| Polar Surface Area | 0.314713 | 0.257877 | 0.001367 | 0.115412 |
| Fractional Polar Surface Area | 0.168917 | 0.432067 | 0.000673 | 0.201208 |
| No. N Atom | 0.117602 | 0.247419 | -0.17041 | 0.447764 |
| No. O Atom | 0.311064 | 0.051463 | 0.165388 | -0.22502 |
| Dipole moment magnitude | 0.122632 | 0.16314 | -0.26601 | -0.21945 |
| QED | -0.30227 | 0.142378 | 0.088633 | -0.05025 |
| 3D_score | 0.004498 | -0.15471 | -0.11668 | -0.14668 |
| fsp3 | -0.02819 | 0.089571 | 0.290612 | -0.40977 |
| PBF | 0.206521 | -0.2237 | 0.001024 | -0.03151 |

4C.VII. Analysis of Benzylic Cross Coupling Products in PCA and PMI Plots

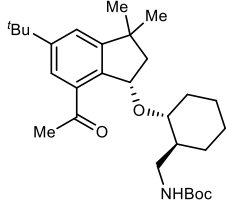
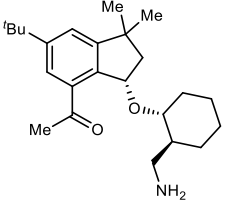
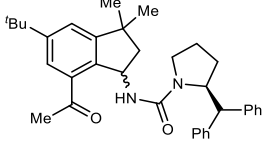
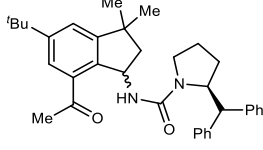
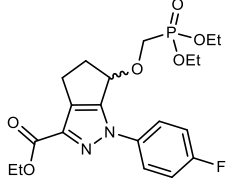
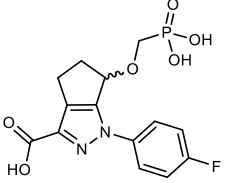
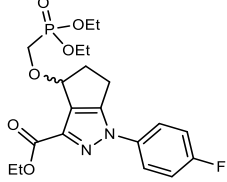
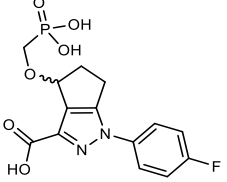
All the benzylic cross coupling products were hydrolyzed before analysis, when applicable.

Table 4C.2. Compounds synthesized and compounds enumerated and analyzed in cheminformatic study.

| Entry | Compound Synthesized | Compound in Analysis |
|-------|--|--|
| 1 |  <p>A06-1</p> |  <p>A06-1</p> |
| 2 |  <p>A06-2</p> |  <p>A06-2'</p> |
| 3 |  <p>A08-1</p> |  <p>A08-1'</p> |
| 4 |  <p>A08-2</p> |  <p>A08-2'</p> |
| 5 |  <p>A08-3a</p> |  <p>A08-3a'</p> |
| 6 |  <p>A08-3b</p> |  <p>A08-3b'</p> |

| | | |
|----|----------------------|----------------------|
| 7 | <p>A11-1a</p> | <p>A11-1a</p> |
| 8 | <p>A11-1b</p> | <p>A11-1b</p> |
| 9 | <p>A12-1a</p> | <p>A12-1a</p> |
| 10 | <p>A12-1b</p> | <p>A12-1b</p> |
| 11 | <p>A12-2a</p> | <p>A12-2a</p> |
| 12 | <p>A12-2b</p> | <p>A12-2b</p> |
| 13 | <p>A12-3a</p> | <p>A12-3a</p> |

| | | |
|----|----------------------|-----------------------|
| 14 | <p>A12-3b</p> | <p>A12-3b</p> |
| 15 | <p>A13-1</p> | <p>A13-1'</p> |
| 16 | <p>A15-1</p> | <p>A15-1</p> |
| 17 | <p>A15-2</p> | <p>A15-2</p> |
| 18 | <p>A15-3</p> | <p>A15-3</p> |
| 19 | <p>A16-1a</p> | <p>A16-1a'</p> |

| | | |
|----|---|--|
| 20 |  <p>A16-1b</p> |  <p>A16-1b'</p> |
| 21 |  <p>A16-2</p> |  <p>A16-2</p> |
| 22 |  <p>A18-1a</p> |  <p>A18-1a'</p> |
| 23 |  <p>A18-1b</p> |  <p>A18-1b'</p> |

4C.VIII. Crystallographic Data for A16-1a

Data Collection

A colorless crystal with approximate dimensions 0.037 x 0.010 x 0.008 mm³ was selected under oil under ambient conditions and attached to the tip of a MiTeGen MicroMount©. The crystal was mounted in a stream of cold nitrogen at 100(1) K and centered in the X-ray beam by using a video camera.

The crystal evaluation and data collection were performed on a Bruker D8 VENTURE PhotonIII four-circle diffractometer with Cu K α ($\lambda = 1.54178 \text{ \AA}$) radiation and the detector to crystal distance of 4.0 cm³.

The initial cell constants were obtained from a 180° ϕ scan conducted at a $2\theta = 50^\circ$ angle with an exposure time of 1 second per frame. The reflections were successfully indexed by an automated indexing routine built into the APEX3 program. The final cell constants were calculated from a set of 7344 strong reflections from the actual data collection.

The data were collected by using a full sphere data collection routine to survey reciprocal space to the extent of a full sphere to a resolution of 0.81 \AA . A total of 97290 data were harvested by collecting 32 sets of frames with 0.85° scans in ω and ϕ with exposure times of 10-20 sec per frame. These highly redundant datasets were corrected for Lorentz and polarization effects. The absorption correction was based on fitting a function to the empirical transmission surface as sampled by multiple equivalent measurements⁴.

Structure Solution and Refinement

The diffraction data were consistent with the space groups $P\bar{1}$ and $P1$. The E -statistics strongly suggested the centrosymmetric space group $P\bar{1}$ which yielded chemically reasonable and computationally stable results of refinement⁵⁻¹⁰.

A successful solution by intrinsic phasing provided most non-hydrogen atoms from the E -map. The remaining non-hydrogen atoms were located with an alternating series of least-squares cycles and difference Fourier maps. All non-hydrogen atoms were refined with anisotropic displacement coefficients. All hydrogen atoms (except the one bound to a N atom) were included in the structure factor calculation at idealized positions and were allowed to ride on the neighboring atoms with relative isotropic displacement coefficients.

The structure contains two molecules with identical compositions and inverted stereochemistry at C7, C12, and C13. The structure crystallizes as a racemate and the (R, S, R) enantiomer shown in the diagrams below was chosen arbitrarily.

The tertbutyl group attached to atom C24 is disordered over two positions with the major disorder component occupancy equal to 51.7(4)%. C24–C26 and C24–C26A distances were refined with one geometric restraint.

The final least-squares refinement of 360 parameters against 5507 data resulted in residuals R (based on F^2 for $I \geq 2\sigma$) and wR (based on F^2 for all data) of 0.0486 and 0.1275, respectively. The final difference Fourier map was featureless.

Summary

Crystal Data for $C_{29}H_{45}NO_4$ ($M = 471.66$ g/mol): triclinic, space group $P\bar{1}$ (no. 2), $a = 8.546(5)$ Å, $b = 11.859(6)$ Å, $c = 14.215(6)$ Å, $\alpha = 87.70(2)^\circ$, $\beta = 75.00(2)^\circ$, $\gamma = 88.33(3)^\circ$, $V = 1390.2(11)$ Å³, $Z = 2$, $T = 100.0$ K, $\mu(\text{Cu K}\alpha) = 0.579$ mm⁻¹, $D_{\text{calc}} = 1.127$ g/cm³, 48831 reflections measured ($6.44^\circ \leq 2\theta \leq 145.004^\circ$), 5507 unique ($R_{\text{int}} = 0.0831$, $R_{\text{sigma}} = 0.0391$) which were used in all calculations. The final R_1 was 0.0486 ($I > 2\sigma(I)$) and wR_2 was 0.1275 (all data).

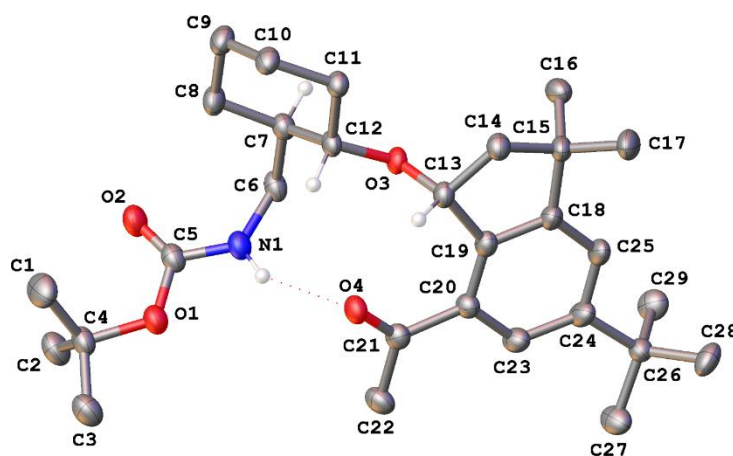


Figure 4C.6. A molecular drawing of the molecule in **A16-1** shown with 50% probability ellipsoids. All minor disorder components and H atoms (except for those bound to chiral centers or the N atom) are omitted. The conformations of the chiral atoms C7, C12, and C13 are R, S, and R but the crystal contains a racemate.

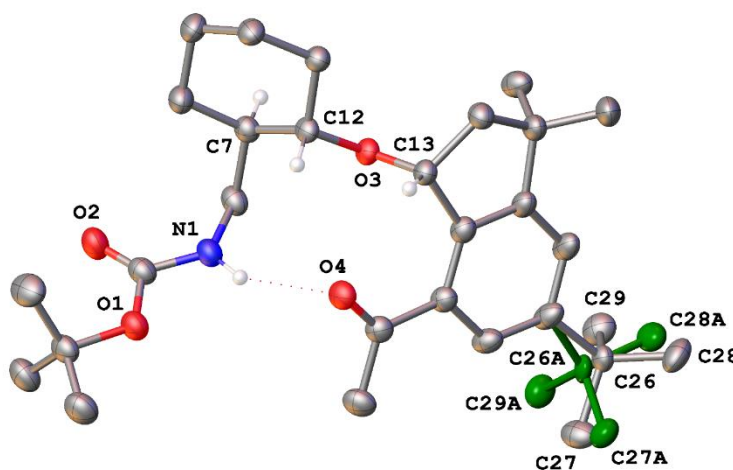


Figure 4C.7. A molecular drawing highlighting the disordered tertbutyl group in **A16-1** shown with select atom labels and 50% probability ellipsoids. All H atoms are omitted except for those bound to chiral centers or a N atom. The conformations of the chiral atoms C7, C12, and C13 are R, S, and R but the crystal contains a racemate.

Table 4C.3. Crystal data and structure refinement for **A16-1**.

| | |
|--|--|
| Identification code | A16-1 |
| Empirical formula | C ₂₉ H ₄₅ NO ₄ |
| Formula weight | 471.66 |
| Temperature/K | 100.0 |
| Crystal system | triclinic |
| Space group | <i>P</i> $\bar{1}$ |
| <i>a</i> /Å | 8.546(5) |
| <i>b</i> /Å | 11.859(6) |
| <i>c</i> /Å | 14.215(6) |
| α /° | 87.70(2) |
| β /° | 75.00(2) |
| γ /° | 88.33(3) |
| Volume/Å ³ | 1390.2(11) |
| <i>Z</i> | 2 |
| ρ_{calc} /cm ³ | 1.127 |
| μ /mm ⁻¹ | 0.579 |
| <i>F</i> (000) | 516.0 |
| Crystal size/mm ³ | 0.037 × 0.01 × 0.008 |
| Radiation | Cu K α (λ = 1.54178) |
| 2 Θ range for data collection/° | 6.44 to 145.004 |
| Index ranges | -10 ≤ <i>h</i> ≤ 10, -14 ≤ <i>k</i> ≤ 14, -17 ≤ <i>l</i> ≤ 17 |
| Reflections collected | 48831 |
| Independent reflections | 5507 [<i>R</i> _{int} = 0.0831, <i>R</i> _{sigma} = 0.0391] |
| Data/restraints/parameters | 5507/1/360 |
| Goodness-of-fit on <i>F</i> ² | 1.058 |
| Final <i>R</i> indexes [<i>I</i> ≥ 2 σ (<i>I</i>)] | <i>R</i> ₁ = 0.0486, <i>wR</i> ₂ = 0.1111 |
| Final <i>R</i> indexes [all data] | <i>R</i> ₁ = 0.0778, <i>wR</i> ₂ = 0.1275 |
| Largest diff. peak/hole / e Å ⁻³ | 0.29/-0.19 |

Table 4C.4. Fractional Atomic Coordinates (×10⁴) and Equivalent Isotropic Displacement Parameters (Å²×10³) for A16-1. *U*_{eq} is defined as 1/3 of the trace of the orthogonalized *U*_{ij} tensor.

| Atom | <i>x</i> | <i>y</i> | <i>z</i> | <i>U</i> (eq) |
|------|------------|------------|------------|---------------|
| O1 | 5764.5(16) | 5615.6(11) | 6947.0(9) | 35.2(3) |
| O2 | 3329.1(18) | 4908.1(12) | 6901.3(10) | 38.8(3) |
| O3 | 3775.6(15) | 8350.7(10) | 4075.2(8) | 27.0(3) |
| O4 | 6906.6(16) | 7879.5(11) | 4672.9(9) | 33.2(3) |
| N1 | 4619(2) | 6248.9(14) | 5801.8(11) | 32.3(4) |
| C1 | 4400(3) | 5522(2) | 8675.0(15) | 50.5(6) |
| C2 | 5697(3) | 3777.5(18) | 7820.0(15) | 43.7(5) |
| C3 | 7405(3) | 5374(2) | 8011.3(16) | 45.3(5) |

| Atom | <i>x</i> | <i>y</i> | <i>z</i> | U(eq) |
|------|----------|-------------|------------|----------|
| C4 | 5775(2) | 5042.7(17) | 7879.5(13) | 34.6(4) |
| C5 | 4456(2) | 5538.0(16) | 6579.0(13) | 32.3(4) |
| C6 | 3491(2) | 6262.0(16) | 5189.7(13) | 32.4(4) |
| C7 | 2235(2) | 7223.4(15) | 5388.4(12) | 28.9(4) |
| C8 | 1207(2) | 7187.2(17) | 6447.8(13) | 34.7(4) |
| C9 | -55(2) | 8141.3(17) | 6645.0(14) | 37.2(5) |
| C10 | 766(2) | 9272.2(16) | 6394.5(13) | 33.5(4) |
| C11 | 1736(2) | 9322.3(16) | 5330.1(12) | 29.0(4) |
| C12 | 2991(2) | 8372.3(15) | 5102.1(12) | 26.4(4) |
| C13 | 4904(2) | 9237.7(15) | 3713.5(12) | 27.1(4) |
| C14 | 4204(2) | 10216.9(16) | 3194.2(13) | 31.7(4) |
| C15 | 4620(2) | 9956.8(17) | 2100.0(13) | 33.0(4) |
| C16 | 3240(2) | 9332.3(19) | 1847.2(14) | 38.6(5) |
| C17 | 5007(3) | 11029(2) | 1462.4(15) | 46.3(6) |
| C18 | 6080(2) | 9166.8(17) | 2002.8(13) | 30.9(4) |
| C19 | 6256(2) | 8773.6(16) | 2903.7(12) | 28.5(4) |
| C20 | 7515(2) | 8001.8(16) | 2950.0(12) | 29.0(4) |
| C21 | 7753(2) | 7550.3(16) | 3899.8(13) | 29.4(4) |
| C22 | 9055(3) | 6670.1(18) | 3894.1(14) | 37.7(5) |
| C23 | 8568(2) | 7669.2(18) | 2078.5(13) | 33.9(4) |
| C24 | 8407(2) | 8055.2(19) | 1166.1(13) | 36.8(5) |
| C25 | 7142(2) | 8815.4(19) | 1143.0(13) | 37.3(5) |
| C26 | 9550(14) | 7797(8) | 162(5) | 29.1(17) |
| C27 | 10968(7) | 7073(5) | 341(3) | 44.3(12) |
| C28 | 10254(5) | 8836(4) | -463(3) | 44.1(12) |
| C29 | 8570(5) | 7117(4) | -340(3) | 42.3(11) |
| C26A | 9598(15) | 7457(8) | 306(5) | 29.4(19) |
| C27A | 11321(6) | 7702(5) | 313(3) | 34.9(11) |
| C28A | 9336(5) | 7963(4) | -671(3) | 38.6(12) |
| C29A | 9395(6) | 6161(3) | 272(3) | 38.7(11) |

Table 4C.5 Anisotropic Displacement Parameters ($\text{\AA}^2 \times 10^3$) for A16-1. The Anisotropic displacement factor exponent takes the form: $-2\pi^2[h^2a^{*2}U_{11}+2hka^*b^*U_{12}+\dots]$.

| Atom | U ₁₁ | U ₂₂ | U ₃₃ | U ₂₃ | U ₁₃ | U ₁₂ |
|------|-----------------|-----------------|-----------------|-----------------|-----------------|-----------------|
| O1 | 40.0(8) | 38.2(8) | 28.5(7) | 2.7(6) | -11.9(6) | 3.7(6) |
| O2 | 45.7(9) | 38.3(8) | 34.2(7) | 7.8(6) | -14.9(6) | -2.0(7) |
| O3 | 30.9(7) | 32.1(7) | 17.2(6) | -1.3(5) | -4.6(5) | 0.5(5) |
| O4 | 38.5(8) | 40.1(8) | 21.6(6) | -1.8(5) | -9.4(6) | 3.9(6) |
| N1 | 36.9(9) | 33.4(9) | 26.7(8) | 3.2(7) | -9.7(7) | 3.1(7) |
| C1 | 55.3(14) | 64.2(15) | 29.8(11) | -8.4(10) | -8.1(10) | 15.7(12) |

| Atom | U ₁₁ | U ₂₂ | U ₃₃ | U ₂₃ | U ₁₃ | U ₁₂ |
|------|-----------------|-----------------|-----------------|-----------------|-----------------|-----------------|
| C2 | 56.9(14) | 39.3(12) | 38.3(11) | 5.3(9) | -20.3(10) | 5.2(10) |
| C3 | 48.9(13) | 50.9(13) | 41.3(12) | 0.3(10) | -21.8(10) | 4.8(10) |
| C4 | 41.4(11) | 39.9(11) | 23.8(9) | -0.2(8) | -12.0(8) | 7.5(9) |
| C5 | 39.2(11) | 32.4(10) | 26.8(9) | -1.7(8) | -11.9(8) | 6.6(9) |
| C6 | 44.1(11) | 29.6(10) | 24.1(9) | -0.8(7) | -10.8(8) | 4.5(8) |
| C7 | 32.3(10) | 32.0(10) | 23.6(9) | -0.7(7) | -9.8(7) | 1.9(8) |
| C8 | 37.3(11) | 34.6(11) | 29.0(10) | 4.8(8) | -4.1(8) | 2.3(8) |
| C9 | 34.5(11) | 42.3(11) | 29.4(10) | 4.0(8) | 0.0(8) | 2.3(9) |
| C10 | 35.0(11) | 35.8(10) | 26.5(9) | -1.6(8) | -3.2(8) | 7.7(8) |
| C11 | 30.6(10) | 31.9(10) | 23.5(9) | -0.3(7) | -5.7(7) | 3.0(8) |
| C12 | 31.1(10) | 30.3(9) | 16.8(8) | -1.8(7) | -4.7(7) | 4.1(7) |
| C13 | 29.7(9) | 30.4(10) | 20.4(8) | -0.1(7) | -5.6(7) | 0.9(7) |
| C14 | 34.1(10) | 32.9(10) | 26.9(9) | 0.8(8) | -6.6(8) | 4.8(8) |
| C15 | 31.1(10) | 43.0(11) | 23.7(9) | 6.5(8) | -6.1(8) | 3.1(8) |
| C16 | 31.9(11) | 57.1(13) | 27.0(10) | -1.9(9) | -9.1(8) | 7.9(9) |
| C17 | 39.7(12) | 56.9(14) | 37.0(11) | 19.6(10) | -3.9(9) | 5.1(10) |
| C18 | 27.1(10) | 41.9(11) | 23.1(9) | 2.5(8) | -6.1(7) | -0.7(8) |
| C19 | 28.8(9) | 34.5(10) | 22.5(9) | -1.7(7) | -6.8(7) | -0.6(8) |
| C20 | 29.1(10) | 37.0(10) | 21.8(9) | -3.4(7) | -8.3(7) | 1.6(8) |
| C21 | 31.7(10) | 32.6(10) | 25.9(9) | -4.1(8) | -10.8(8) | -0.4(8) |
| C22 | 39.8(11) | 44.6(12) | 33.6(10) | -5.8(9) | -18.6(9) | 7.7(9) |
| C23 | 27.5(10) | 48.6(12) | 26.6(9) | -7.2(8) | -8.3(8) | 5.9(8) |
| C24 | 27.5(10) | 59.7(13) | 22.6(9) | -5.2(9) | -4.8(8) | 1.5(9) |
| C25 | 30.5(10) | 61.2(14) | 19.8(9) | 2.3(9) | -6.4(8) | 0.7(9) |
| C26 | 29(2) | 40(5) | 19(3) | 4(2) | -8(2) | 4(3) |
| C27 | 44(3) | 56(3) | 32(2) | -12(2) | -11(2) | 17(3) |
| C28 | 41(2) | 46(3) | 35(2) | 0.1(18) | 8.3(18) | -3.9(19) |
| C29 | 43(2) | 52(3) | 31(2) | -10.3(19) | -7.4(18) | 2(2) |
| C26A | 32(3) | 42(5) | 13(2) | 7(3) | -4(2) | 1(4) |
| C27A | 30(2) | 46(3) | 25(2) | -5(2) | 0.2(17) | -2(2) |
| C28A | 39(2) | 48(3) | 25(2) | -4.1(18) | -3.2(17) | 8(2) |
| C29A | 45(3) | 33(2) | 36(2) | -7.4(17) | -5.1(19) | -3.6(18) |

Table 4C.6. Bond Lengths for A16-1.

| Atom | Atom | Length/Å | Atom | Atom | Length/Å |
|------|------|----------|------|------|----------|
| O1 | C4 | 1.467(2) | C14 | C15 | 1.545(3) |
| O1 | C5 | 1.359(2) | C15 | C16 | 1.536(3) |
| O2 | C5 | 1.217(2) | C15 | C17 | 1.524(3) |
| O3 | C12 | 1.441(2) | C15 | C18 | 1.518(3) |
| O3 | C13 | 1.435(2) | C18 | C19 | 1.388(2) |

| Atom Atom Length/Å | | | Atom Atom Length/Å | | |
|--------------------|-----|----------|--------------------|------|-----------|
| O4 | C21 | 1.221(2) | C18 | C25 | 1.392(3) |
| N1 | C5 | 1.343(2) | C19 | C20 | 1.405(3) |
| N1 | C6 | 1.455(2) | C20 | C21 | 1.493(2) |
| C1 | C4 | 1.519(3) | C20 | C23 | 1.393(3) |
| C2 | C4 | 1.511(3) | C21 | C22 | 1.502(3) |
| C3 | C4 | 1.517(3) | C23 | C24 | 1.397(3) |
| C6 | C7 | 1.526(3) | C24 | C25 | 1.393(3) |
| C7 | C8 | 1.534(3) | C24 | C26 | 1.543(6) |
| C7 | C12 | 1.520(3) | C24 | C26A | 1.555(6) |
| C8 | C9 | 1.523(3) | C26 | C27 | 1.534(10) |
| C9 | C10 | 1.518(3) | C26 | C28 | 1.533(9) |
| C10 | C11 | 1.525(3) | C26 | C29 | 1.501(14) |
| C11 | C12 | 1.518(2) | C26A | C27A | 1.512(16) |
| C13 | C14 | 1.540(2) | C26A | C28A | 1.557(9) |
| C13 | C19 | 1.513(3) | C26A | C29A | 1.555(11) |

Table 4C.7. Bond Angles for **A16-1**.

| Atom Atom Atom Angle/° | | | | Atom Atom Atom Angle/° | | | |
|------------------------|-----|-----|------------|------------------------|-----|------|------------|
| C5 | O1 | C4 | 119.92(16) | C18 | C15 | C17 | 112.72(17) |
| C13 | O3 | C12 | 115.05(13) | C19 | C18 | C15 | 111.98(16) |
| C5 | N1 | C6 | 121.83(18) | C19 | C18 | C25 | 120.95(18) |
| O1 | C4 | C1 | 108.97(16) | C25 | C18 | C15 | 127.05(16) |
| O1 | C4 | C2 | 111.36(15) | C18 | C19 | C13 | 110.35(16) |
| O1 | C4 | C3 | 101.95(16) | C18 | C19 | C20 | 119.66(17) |
| C2 | C4 | C1 | 112.67(19) | C20 | C19 | C13 | 129.89(16) |
| C2 | C4 | C3 | 110.58(17) | C19 | C20 | C21 | 121.76(16) |
| C3 | C4 | C1 | 110.81(18) | C23 | C20 | C19 | 118.24(16) |
| O2 | C5 | O1 | 124.84(17) | C23 | C20 | C21 | 120.00(17) |
| O2 | C5 | N1 | 125.82(18) | O4 | C21 | C20 | 121.19(17) |
| N1 | C5 | O1 | 109.34(18) | O4 | C21 | C22 | 119.93(16) |
| N1 | C6 | C7 | 114.05(15) | C20 | C21 | C22 | 118.87(16) |
| C6 | C7 | C8 | 112.01(15) | C20 | C23 | C24 | 122.83(18) |
| C12 | C7 | C6 | 112.35(16) | C23 | C24 | C26 | 127.2(4) |
| C12 | C7 | C8 | 111.31(15) | C23 | C24 | C26A | 113.1(4) |
| C9 | C8 | C7 | 112.06(15) | C25 | C24 | C23 | 117.63(17) |
| C10 | C9 | C8 | 109.98(17) | C25 | C24 | C26 | 115.1(4) |
| C9 | C10 | C11 | 110.22(16) | C25 | C24 | C26A | 128.9(4) |
| C12 | C11 | C10 | 111.93(15) | C18 | C25 | C24 | 120.69(17) |
| O3 | C12 | C7 | 106.57(14) | C27 | C26 | C24 | 107.5(5) |
| O3 | C12 | C11 | 111.55(13) | C28 | C26 | C24 | 115.0(6) |

| Atom | Atom | Atom | Angle/° | Atom | Atom | Atom | Angle/° |
|------|------|------|------------|------|------|------|----------|
| C11 | C12 | C7 | 111.78(16) | C28 | C26 | C27 | 107.9(8) |
| O3 | C13 | C14 | 113.43(15) | C29 | C26 | C24 | 105.4(7) |
| O3 | C13 | C19 | 107.94(14) | C29 | C26 | C27 | 109.7(6) |
| C19 | C13 | C14 | 102.69(14) | C29 | C26 | C28 | 111.2(6) |
| C13 | C14 | C15 | 107.21(15) | C24 | C26A | C28A | 108.8(5) |
| C16 | C15 | C14 | 111.31(16) | C27A | C26A | C24 | 109.4(8) |
| C17 | C15 | C14 | 111.45(18) | C27A | C26A | C28A | 107.0(6) |
| C17 | C15 | C16 | 110.02(17) | C27A | C26A | C29A | 109.6(6) |
| C18 | C15 | C14 | 101.61(14) | C29A | C26A | C24 | 115.7(7) |
| C18 | C15 | C16 | 109.49(17) | C29A | C26A | C28A | 105.8(8) |

Table 4C.7. Hydrogen Bonds for **A16-1**.

| D | H | A | d(D-H)/Å | d(H-A)/Å | d(D-A)/Å | D-H-A/° |
|----|----|----|----------|----------|----------|-----------|
| N1 | H1 | O4 | 0.92(2) | 2.09(2) | 2.913(3) | 148.3(18) |

Table 4C.8. Torsion Angles for **A16-1**.

| A | B | C | D | Angle/° | A | B | C | D | Angle/° |
|-----|-----|-----|-----|-------------|-----|-----|-----|------|-------------|
| O3 | C13 | C14 | C15 | -91.92(18) | C15 | C18 | C19 | C13 | 1.3(2) |
| O3 | C13 | C19 | C18 | 104.19(17) | C15 | C18 | C19 | C20 | 177.88(17) |
| O3 | C13 | C19 | C20 | -72.0(2) | C15 | C18 | C25 | C24 | -177.9(2) |
| N1 | C6 | C7 | C8 | -58.8(2) | C16 | C15 | C18 | C19 | -103.94(19) |
| N1 | C6 | C7 | C12 | 67.4(2) | C16 | C15 | C18 | C25 | 74.4(2) |
| C4 | O1 | C5 | O2 | -9.5(3) | C17 | C15 | C18 | C19 | 133.25(19) |
| C4 | O1 | C5 | N1 | 171.40(15) | C17 | C15 | C18 | C25 | -48.4(3) |
| C5 | O1 | C4 | C1 | -61.6(2) | C18 | C19 | C20 | C21 | -179.78(18) |
| C5 | O1 | C4 | C2 | 63.3(2) | C18 | C19 | C20 | C23 | 1.0(3) |
| C5 | O1 | C4 | C3 | -178.76(16) | C19 | C13 | C14 | C15 | 24.30(19) |
| C5 | N1 | C6 | C7 | 101.4(2) | C19 | C18 | C25 | C24 | 0.3(3) |
| C6 | N1 | C5 | O1 | 173.07(15) | C19 | C20 | C21 | O4 | -3.6(3) |
| C6 | N1 | C5 | O2 | -6.0(3) | C19 | C20 | C21 | C22 | 175.97(18) |
| C6 | C7 | C8 | C9 | -179.57(17) | C19 | C20 | C23 | C24 | -1.1(3) |
| C6 | C7 | C12 | O3 | 59.50(18) | C20 | C23 | C24 | C25 | 0.8(3) |
| C6 | C7 | C12 | C11 | -178.38(14) | C20 | C23 | C24 | C26 | 176.3(6) |
| C7 | C8 | C9 | C10 | -56.9(2) | C20 | C23 | C24 | C26A | -173.2(6) |
| C8 | C7 | C12 | O3 | -173.96(14) | C21 | C20 | C23 | C24 | 179.62(19) |
| C8 | C7 | C12 | C11 | -51.84(19) | C23 | C20 | C21 | O4 | 175.62(18) |
| C8 | C9 | C10 | C11 | 58.0(2) | C23 | C20 | C21 | C22 | -4.8(3) |
| C9 | C10 | C11 | C12 | -57.4(2) | C23 | C24 | C25 | C18 | -0.4(3) |
| C10 | C11 | C12 | O3 | 173.58(15) | C23 | C24 | C26 | C27 | -2.6(11) |
| C10 | C11 | C12 | C7 | 54.4(2) | C23 | C24 | C26 | C28 | -122.8(5) |

| | | | | | | | | | |
|----------|----------|----------|----------|----------------|----------|----------|----------|----------|----------------|
| A | B | C | D | Angle/° | A | B | C | D | Angle/° |
| C12 | O3 | C13 | C14 | -100.20(16) | C23 | C24 | C26 | C29 | 114.3(5) |
| C12 | O3 | C13 | C19 | 146.72(13) | C23 | C24 | C26A | C27A | -62.4(6) |
| C12 | C7 | C8 | C9 | 53.7(2) | C23 | C24 | C26A | C28A | -179.0(6) |
| C13 | O3 | C12 | C7 | -164.71(13) | C23 | C24 | C26A | C29A | 62.1(10) |
| C13 | O3 | C12 | C11 | 73.03(19) | C25 | C18 | C19 | C13 | -177.21(18) |
| C13 | C14 | C15 | C16 | 93.15(19) | C25 | C18 | C19 | C20 | -0.6(3) |
| C13 | C14 | C15 | C17 | -143.62(17) | C25 | C24 | C26 | C27 | 173.0(5) |
| C13 | C14 | C15 | C18 | -23.3(2) | C25 | C24 | C26 | C28 | 52.8(10) |
| C13 | C19 | C20 | C21 | -3.9(3) | C25 | C24 | C26 | C29 | -70.1(5) |
| C13 | C19 | C20 | C23 | 176.85(18) | C25 | C24 | C26A | C27A | 124.5(5) |
| C14 | C13 | C19 | C18 | -15.9(2) | C25 | C24 | C26A | C28A | 7.8(12) |
| C14 | C13 | C19 | C20 | 167.92(19) | C25 | C24 | C26A | C29A | -111.1(6) |
| C14 | C15 | C18 | C19 | 13.9(2) | C26 | C24 | C25 | C18 | -176.4(6) |
| C14 | C15 | C18 | C25 | -167.8(2) | C26A | C24 | C25 | C18 | 172.5(7) |

Table 4C.9. Hydrogen Atom Coordinates ($\text{\AA}\times 10^4$) and Isotropic Displacement Parameters ($\text{\AA}^2\times 10^3$) for **A16-1**.

| Atom | x | y | z | U(eq) |
|-------------|----------|----------|----------|--------------|
| H1 | 5520(30) | 6699(19) | 5639(15) | 39 |
| H1A | 4492.72 | 6344.21 | 8674.49 | 76 |
| H1B | 4460.54 | 5195.56 | 9309.11 | 76 |
| H1C | 3360.37 | 5337.05 | 8554.55 | 76 |
| H2A | 4624.86 | 3577.24 | 7756.69 | 65 |
| H2B | 5884.96 | 3412.77 | 8412.91 | 65 |
| H2C | 6529.18 | 3521.72 | 7251.72 | 65 |
| H3A | 8271.74 | 5078.32 | 7478.87 | 68 |
| H3B | 7534.11 | 5057.97 | 8635.17 | 68 |
| H3C | 7461.12 | 6198.1 | 8005.18 | 68 |
| H6A | 2918.97 | 5535.51 | 5289.55 | 39 |
| H6B | 4114.44 | 6321.64 | 4498.44 | 39 |
| H7 | 1482.12 | 7112.13 | 4967.68 | 35 |
| H8A | 653.36 | 6454.51 | 6591.24 | 42 |
| H8B | 1925.3 | 7242.17 | 6889.23 | 42 |
| H9A | -836.65 | 8053.24 | 6247.57 | 45 |
| H9B | -660.5 | 8109.45 | 7340.65 | 45 |
| H10A | 1498.56 | 9379.5 | 6819.97 | 40 |
| H10B | -61.41 | 9887.83 | 6510.25 | 40 |
| H11A | 985.67 | 9274.56 | 4907.01 | 35 |
| H11B | 2286.66 | 10055.69 | 5183.08 | 35 |
| H12 | 3826.86 | 8480.81 | 5467.52 | 32 |

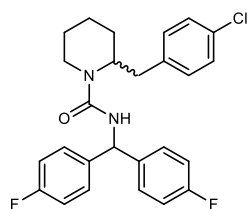
| Atom | x | y | z | U(eq) |
|-------------|----------|----------|----------|--------------|
| H13 | 5340.56 | 9521.82 | 4246.11 | 32 |
| H14A | 4687.03 | 10938.86 | 3288.8 | 38 |
| H14B | 3014.92 | 10278.76 | 3461.19 | 38 |
| H16A | 2932.85 | 8682.53 | 2299.3 | 58 |
| H16B | 3603.87 | 9070.8 | 1178.96 | 58 |
| H16C | 2303.03 | 9845.15 | 1902.26 | 58 |
| H17A | 4054.24 | 11535.16 | 1591.91 | 69 |
| H17B | 5299.31 | 10833.29 | 774.57 | 69 |
| H17C | 5915.17 | 11406.21 | 1610.81 | 69 |
| H22A | 8861.18 | 6014.02 | 3544.61 | 57 |
| H22B | 9038.68 | 6438.32 | 4565.96 | 57 |
| H22C | 10113.39 | 6983.51 | 3567.87 | 57 |
| H23 | 9433.14 | 7158.01 | 2105.92 | 41 |
| H25 | 7003.86 | 9096.87 | 533.96 | 45 |
| H27A | 11544.89 | 7493.63 | 722.87 | 66 |
| H27B | 11712.79 | 6886.59 | -284.84 | 66 |
| H27C | 10553.31 | 6375.11 | 700.78 | 66 |
| H28A | 9368.95 | 9320.65 | -577.94 | 66 |
| H28B | 10946.83 | 8595.05 | -1088.02 | 66 |
| H28C | 10897.43 | 9258.13 | -121.84 | 66 |
| H29A | 8103.77 | 6474.54 | 84.29 | 63 |
| H29B | 9270.51 | 6841.36 | -950.24 | 63 |
| H29C | 7696.71 | 7593.01 | -482.04 | 63 |
| H27D | 11442.95 | 8518.13 | 341.35 | 52 |
| H27E | 12065.86 | 7423.81 | -282.2 | 52 |
| H27F | 11572.23 | 7323.09 | 882.99 | 52 |
| H28D | 8257.73 | 7768.1 | -725.71 | 58 |
| H28E | 10161.79 | 7652.85 | -1217.35 | 58 |
| H28F | 9425.11 | 8785.54 | -683.96 | 58 |
| H29D | 9604.14 | 5791.14 | 857.86 | 58 |
| H29E | 10166.09 | 5870.52 | -307.27 | 58 |
| H29F | 8288.17 | 6006.4 | 245.16 | 58 |

Table 4C.10. Atomic Occupancy for **A16-1**.

| | | |
|-----------------------|-----------------------|-----------------------|
| Atom Occupancy | Atom Occupancy | Atom Occupancy |
| C26 0.517(4) | C27 0.517(4) | H27A 0.517(4) |
| H27B 0.517(4) | H27C 0.517(4) | C28 0.517(4) |
| H28A 0.517(4) | H28B 0.517(4) | H28C 0.517(4) |
| C29 0.517(4) | H29A 0.517(4) | H29B 0.517(4) |
| H29C 0.517(4) | C26A 0.483(4) | C27A 0.483(4) |

| Atom Occupancy | Atom Occupancy | Atom Occupancy |
|-----------------------|-----------------------|-----------------------|
| H27D 0.483(4) | H27E 0.483(4) | H27F 0.483(4) |
| C28A 0.483(4) | H28D 0.483(4) | H28E 0.483(4) |
| H28F 0.483(4) | C29A 0.483(4) | H29D 0.483(4) |
| H29E 0.483(4) | H29F 0.483(4) | |

4C.IX. Characterization of Compounds



N-(bis(4-fluorophenyl)methyl)-2-(4-chlorobenzyl)piperidine-1-carboxamide, **A06-1**

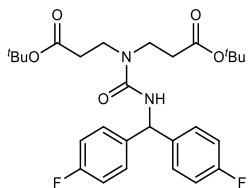
Reaction run using 4,4'-difluorodiphenylmethane **A06** (70.4 μ L, 0.40 mmol, 1.0 equiv.) and 2-[(4-chlorophenyl)methyl]piperidine (293.6 mg, 1.4 mmol, 3.5 equiv.) and two rotamers were isolated as a mixture. Yield = 105.8 mg (58%) of white solid isolated.

^1H NMR (CD_2Cl_2 , 500 MHz) (mixture of rotamers: 50:50): 7.28 – 7.16 (m, 2H), 7.15 – 7.06 (m, 4H), 7.04 – 6.95 (m, 6H), 5.82 (d, $J = 6.1$ Hz, 1H), 4.46 (d, $J = 6.2$ Hz, 1H), 4.24 (t, $J = 8.4$ Hz, 1H), 4.01 – 3.83 (m, 1H), 3.11 – 2.94 (m, 2H), 2.70 (dd, $J = 13.5, 6.3$ Hz, 1H), 1.77 – 1.60 (m, 5H), 1.53 – 1.39 (m, 1H) ppm.

^{13}C NMR (CD_2Cl_2 , 101 MHz) (mixture of rotamers: 50:50): 162.27 (d, $J = 245.0$ Hz), 162.25 (d, $J = 245.0$ Hz), 156.67, 139.14 (d, $J = 3.2$ Hz), 139.01 (d, $J = 3.1$ Hz), 138.53, 132.42, 130.89, 129.21 (d, $J = 7.9$ Hz), 129.15 (d, $J = 7.9$ Hz), 128.99, 115.64 (d, $J = 21.5$ Hz), 115.60 (d, $J = 21.5$ Hz), 57.63, 53.77, 39.43, 35.71, 28.77, 25.97, 19.48 ppm.

^{19}F NMR (CD_2Cl_2 , 377 MHz) (mixture of rotamers: 50:50): -116.12, -116.27.

HRMS Calculated for $[\text{C}_{26}\text{H}_{25}\text{ClF}_2\text{N}_2\text{O}+\text{Na}]^+$: 477.1516, Found: 477.1511.



di-*tert*-butyl 3,3'-(((bis(4-fluorophenyl)methyl)carbamoyl)azanediyl)dipropionate, **A06-2**

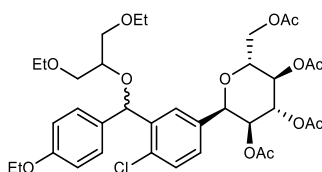
Reaction run using 4,4'-difluorodiphenylmethane **A06** (70.4 μ L, 0.40 mmol, 1.0 equiv.) and *N*-Bis(*tert*-butylpropionate)amine (264.9 mg, 1.4 mmol, 3.5 equiv.) and two diastereomers were isolated as a mixture. Yield = 106.0 mg (51%) of white solid isolated.

^1H NMR (CD_2Cl_2 , 500 MHz): 7.35 – 7.21 (m, 4H), 7.01 (t, $J = 8.8$ Hz, 4H), 6.97 (d, $J = 7.9$ Hz, 1H), 6.00 (d, $J = 7.7$ Hz, 1H), 3.45 (t, $J = 6.3$ Hz, 4H), 2.51 (t, $J = 6.3$ Hz, 4H), 1.41 (d, $J = 1.5$ Hz, 18H) ppm.

^{13}C NMR (CD_2Cl_2 , 126 MHz): 172.9, 162.3 (d, $J = 244.6$ Hz), 158.0, 139.7 (d, $J = 3.2$ Hz), 129.4 (d, $J = 8.1$ Hz), 115.5 (d, $J = 21.5$ Hz), 81.5, 57.6, 43.4, 34.9, 28.2 ppm.

^{19}F NMR (CD_2Cl_2 , 377 MHz): –117.6 ppm.

HRMS Calculated for $[\text{C}_{28}\text{H}_{36}\text{F}_2\text{N}_2\text{O}_5+\text{Na}]^+$: 541.2485, Found: 541.2479.



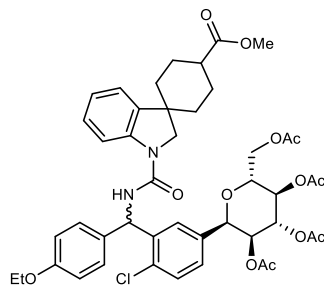
(2*R*,3*R*,4*R*,5*S*,6*R*)-2-(acetoxymethyl)-6-(4-chloro-3-(((1,3-diethoxypropan-2-yl)oxy)(4-ethoxyphenyl)methyl)phenyl)tetrahydro-2*H*-pyran-3,4,5-triyl triacetate, **A08-1**

Reaction run using dapagliflozin tetraacetate **A08** (115.4 mg, 0.20 mmol, 1.0 equiv.) and 1,3-diethoxypropan-2-ol (93.5 μ L, 0.60 mmol, 5.0 equiv.) and two diastereomers were isolated as a mixture. Yield = 50.0 mg (35%) of white amorphous solid isolated.

^1H NMR (CD_2Cl_2 , 500 MHz)(mixture of diastereomers: 50:50): 7.66 (d, $J = 2.2$ Hz, $0.5 \times 1\text{H}$), 7.59 (d, $J = 2.1$ Hz, $0.5 \times 1\text{H}$), 7.32 (d, $J = 8.3$ Hz, $0.5 \times 1\text{H}$), 7.28 (dd, $J = 8.3, 1.3$ Hz, $0.5 \times 3\text{H}$), 7.26 (d, $J = 2.8$ Hz, $0.5 \times 1\text{H}$), 7.22 (dd, $J = 8.5, 2.1$ Hz, $0.5 \times 3\text{H}$), 6.83 – 6.80 (m, 1H), 6.80 – 6.76 (m, 1H), 6.12 (s, $0.5 \times 1\text{H}$), 6.09 (s, $0.5 \times 1\text{H}$), 5.31 (dt, $J = 18.8, 9.4$ Hz, 1H), 5.22 (q, $J = 9.4$ Hz, 1H), 5.12 (t, $J = 9.6$ Hz, $0.5 \times 1\text{H}$), 5.03 (t, $J = 9.6$ Hz, $0.5 \times 1\text{H}$), 4.40 (dd, $J = 9.8, 4.1$ Hz, 1H), 4.28 (ddd, $J = 12.4, 4.9, 1.4$ Hz, 1H), 4.16 (ddd, $J = 12.4, 10.1, 2.3$ Hz, 1H), 3.98 (dq, $J = 11.7, 7.0$ Hz, 2H), 3.82 (dddd, $J = 11.0, 9.9, 4.9, 2.3$ Hz, 1H), 3.72 (dp, $J = 18.8, 5.2$ Hz, 1H), 3.57 (dd, $J = 5.2, 3.6$ Hz, 1H), 3.55 – 3.47 (m, 4H), 3.44 (qd, $J = 7.1, 2.0$ Hz, 3H), 2.09 (s, $0.5 \times 3\text{H}$), 2.08 (s, $0.5 \times 3\text{H}$), 2.06 (s, $0.5 \times 3\text{H}$), 2.06 (s, $0.5 \times 3\text{H}$), 2.01 (s, $0.5 \times 3\text{H}$), 1.98 (s, $0.5 \times 3\text{H}$), 1.86 (s, $0.5 \times 3\text{H}$), 1.57 (s, $0.5 \times 3\text{H}$), 1.37 (q, $J = 6.8$ Hz, 3H), 1.24 – 1.12 (m, 6H) ppm.

^{13}C NMR (CD_2Cl_2 , 126 MHz) (mixture of diastereomers: 50:50):: 170.83, 170.49, 170.45, 169.63, 169.12, 168.95, 158.58, 158.48, 140.57, 140.12, 135.55, 135.22, 133.33, 133.20, 133.08, 132.63, 129.93, 129.79, 129.36, 128.63, 128.17, 127.57, 126.72, 126.46, 114.31, 114.28, 79.84, 79.78, 77.84, 76.30, 76.29, 75.69, 75.05, 74.32, 74.31, 72.83, 72.61, 71.15 (d, $J = 1.6$ Hz), 70.97, 70.86, 68.73, 68.72, 66.88, 66.84, 66.82, 66.77, 63.51, 63.48, 62.50, 20.89, 20.88, 20.79, 20.76, 20.57, 20.29, 15.33, 15.31, 14.96, 14.93 ppm.

HRMS Calculated for $[\text{C}_{36}\text{H}_{47}\text{ClO}_{13}+\text{Na}]^+$: 745.2597, Found: 745.2591.



(2*R*,3*R*,4*R*,5*S*,6*R*)-2-(acetoxymethyl)-6-(4-chloro-3-((4-ethoxyphenyl)(4-(methoxycarbonyl)spiro[cyclohexane-1,3'-indoline]-1'-carboxamido)methyl)phenyl)tetrahydro-2*H*-pyran-3,4,5-triyl triacetate, **A08-2**

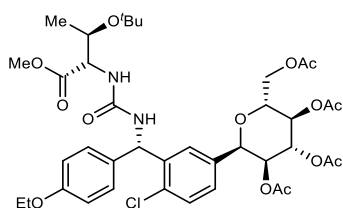
Reaction run using dapagliflozin tetraacetate **A08** (230.8 mg, 0.40 mmol, 1.0 equiv.) and methyl spiro[cyclohexane-1,3'-indoline]-4-carboxylate (490.6 mg, 2.0 mmol, 5.0 equiv.) and two diastereomers were isolated as a mixture.

A08-2: Yield = 79.1 mg (23%) of white solid isolated.

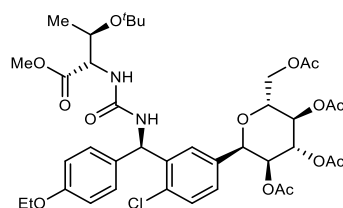
^1H NMR (CD_2Cl_2 , 600 MHz) (mixture of diastereomers: 53:47): 7.90 (d, $J = 8.0$ Hz, $0.53 \times 1\text{H}$), 7.86 (d, $J = 8.1$ Hz, $0.47 \times 1\text{H}$), 7.50 (d, $J = 2.2$ Hz, $0.47 \times 1\text{H}$), 7.41 (d, $J = 8.2$ Hz, $0.53 \times 1\text{H}$), 7.38 (dd, $J = 5.2, 3.0$ Hz, 1H), 7.29 (td, $J = 7.9, 2.2$ Hz, 1H), 7.18 (d, $J = 8.7$ Hz, 1H), 7.14 (t, $J = 8.3$ Hz, 2H), 7.12 – 7.04 (m, 1H), 6.94 (tdd, $J = 7.5, 3.2, 1.1$ Hz, 1H), 6.86 (d, $J = 8.6$ Hz, 2H), 6.45 (d, $J = 6.3$ Hz, $0.53 \times 1\text{H}$), 6.37 (d, $J = 6.2$ Hz, $0.47 \times 1\text{H}$), 5.31 (t, $J = 9.5$ Hz, 1H), 5.28 (dd, $J = 6.4, 1.8$ Hz, 1H), 5.21 – 5.14 (m, $1 + 0.53 \times 1\text{H}$), 5.09 (t, $J = 9.7$ Hz, $0.47 \times 1\text{H}$), 4.47 (d, $J = 9.8$ Hz, $0.47 \times 1\text{H}$), 4.43 (d, $J = 9.9$ Hz, $0.53 \times 1\text{H}$), 4.23 – 4.11 (m, 2H), 4.01 (qd, $J = 7.0, 4.4$ Hz, 2H), 3.90 – 3.83 (m, 2H), 3.79 (d, $J = 9.3$ Hz, $0.53 \times 1\text{H}$), 3.74 (d, $J = 9.3$ Hz, $0.47 \times 1\text{H}$), 3.66 (s, $0.47 \times 3\text{H}$), 3.64 (s, $0.53 \times 3\text{H}$), 2.49 – 2.37 (m, 1H), 2.07 – 2.01 (m, 6H), 1.99 – 1.94 (m, 3H), 1.88 – 1.80 (m, 2H), 1.80 – 1.74 (m, 1H), 1.73 (d, $J = 1.9$ Hz, 3H), 1.72 – 1.66 (m, 1H), 1.66 – 1.52 (m, 3H), 1.38 (td, $J = 6.9, 2.6$ Hz, 3H) ppm.

^{13}C NMR (CD_2Cl_2 , 151 MHz) (mixture of diastereomers: 53:47): 176.22, 176.17, 170.84, 170.83, 170.44, 170.40, 169.89, 169.87, 169.41, 169.31, 159.07, 158.93, 154.13, 154.07, 143.30, 143.11, 140.33, 140.32, 139.05, 136.04, 135.96, 134.12, 133.88, 132.90, 132.32, 130.66, 129.58, 128.73, 128.51, 128.40, 128.28, 127.63, 127.44, 122.57, 122.54, 122.42, 122.31, 115.32, 115.31, 114.99, 114.97, 79.79, 79.76, 76.66, 76.64, 74.33, 74.26, 72.84, 72.63, 69.06, 69.00, 63.95, 62.78, 62.74, 57.67, 57.57, 56.04, 55.41, 51.90, 51.85, 44.45 (d, $J = 3.8$ Hz), 42.50, 36.96, 36.92, 36.89, 36.85, 26.04, 20.90, 20.85, 20.81, 20.77, 20.60, 20.57, 15.00 ppm.

HRMS Calculated for $[\text{C}_{45}\text{H}_{51}\text{ClN}_2\text{O}_{13}+\text{H}]^+$: 863.3152, Found: 863.3156.



(2*R*,3*R*,4*R*,5*S*,6*R*)-2-(acetoxymethyl)-6-(3-((*S*)-(3-((2*S*,3*R*)-3-(*tert*-butoxy)-1-methoxy-1-oxobutan-2-yl)ureido)(4-ethoxyphenyl)methyl)-4-chlorophenyl)tetrahydro-2*H*-pyran-3,4,5-triyl triacetate, **A08-3a**



(2*R*,3*R*,4*R*,5*S*,6*R*)-2-(acetoxymethyl)-6-(3-((*R*)-(3-((2*S*,3*R*)-3-(*tert*-butoxy)-1-methoxy-1-oxobutan-2-yl)ureido)(4-ethoxyphenyl)methyl)-4-chlorophenyl)tetrahydro-2*H*-pyran-3,4,5-triyl triacetate, **A08-3b**

Reaction run using dapagliflozin tetraacetate **A08** (230.8 mg, 0.40 mmol, 1.0 equiv.) and methyl (2*S*,3*R*)-2-amino-3-(*tert*-butoxy)butanoate (265.0 mg, 1.4 mmol, 3.5 equiv.) and two diastereomers were isolated.

A08-3a: Yield = 59.7 mg (19%) of white solid isolated.

¹H NMR (CD₂Cl₂, 500 MHz): 7.46 (d, *J* = 2.1 Hz, 1H), 7.35 (d, *J* = 8.2 Hz, 1H), 7.26 (dd, *J* = 8.3, 2.1 Hz, 1H), 7.13 – 7.07 (m, 2H), 6.85 – 6.79 (m, 2H), 6.21 (d, *J* = 6.8 Hz, 1H), 5.36 – 5.28 (m, 3H), 5.28 – 5.18 (m, 2H), 5.10 (t, *J* = 9.7 Hz, 1H), 4.46 (d, *J* = 9.8 Hz, 1H), 4.34 – 4.29 (m, 1H), 4.28 (dd, *J* = 3.7, 1.9 Hz, 1H), 4.20 (qd, *J* = 6.2, 1.8 Hz, 1H), 4.14 (dd, *J* = 12.3, 2.3 Hz, 1H), 3.99 (q, *J* = 6.9 Hz, 2H), 3.87 (ddd, *J* = 9.9, 5.6, 2.4 Hz, 1H), 3.68 (s, 3H), 2.04 (s, 3H), 2.03 (s, 4H), 1.96 (s, 4H), 1.77 (s, 3H), 1.37 (t, *J* = 7.0 Hz, 3H), 1.18 (d, *J* = 6.2 Hz, 3H), 1.09 (s, 8H) ppm.

¹³C NMR (CD₂Cl₂, 101 MHz): 172.8, 171.0 (d, *J* = 3.2 Hz), 170.4, 169.9, 169.4, 158.9, 157.3, 140.4, 136.3, 133.7, 133.0, 130.4, 128.9, 127.8, 127.4, 114.9, 79.5, 76.5, 74.5, 74.2, 73.0, 69.1, 68.0, 63.9, 63.0, 59.4 (d, *J* = 4.1 Hz), 55.6, 52.3, 28.5, 21.2, 21.0, 20.9, 20.8, 20.7, 15.0 ppm.

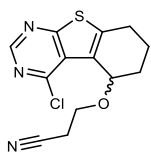
HRMS Calculated for [C₃₉H₅₁ClN₂O₁₄+H]⁺: 807.3102, Found: 807.3097.

A08-3b: Yield = 56.1 mg (17%) of white solid isolated.

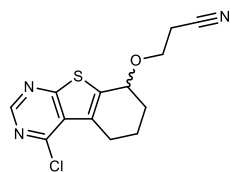
¹H NMR (CD₂Cl₂, 500 MHz): 7.49 (d, *J* = 2.1 Hz, 1H), 7.33 (d, *J* = 8.2 Hz, 1H), 7.23 (dd, *J* = 8.2, 2.2 Hz, 1H), 7.16 – 7.06 (m, 2H), 6.86 – 6.77 (m, 2H), 6.22 (d, *J* = 6.8 Hz, 1H), 5.33 (t, *J* = 9.5 Hz, 1H), 5.26 (dd, *J* = 11.3, 8.2 Hz, 2H), 5.18 (t, *J* = 9.7 Hz, 1H), 5.11 (t, *J* = 9.7 Hz, 1H), 4.44 (d, *J* = 9.9 Hz, 1H), 4.25 (dd, *J* = 9.6, 1.8 Hz, 1H), 4.23 – 4.15 (m, 3H), 4.00 (q, *J* = 7.0 Hz, 2H), 3.88 (ddd, *J* = 10.1, 4.6, 3.2 Hz, 1H), 3.68 (s, 3H), 2.06 (s, 3H), 2.04 (s, 3H), 1.97 (s, 3H), 1.80 (s, 3H), 1.37 (t, *J* = 7.0 Hz, 3H), 1.17 (d, *J* = 6.2 Hz, 3H), 1.08 (s, 9H) ppm.

¹³C NMR (CD₂Cl₂, 101 MHz): 172.76, 171.00, 170.41, 169.92, 169.27, 158.88, 157.24, 140.77, 136.06, 133.80, 132.93, 130.38, 129.28, 127.66, 127.27, 114.89, 79.81, 76.69, 74.33, 74.31, 72.85, 69.15, 67.91, 63.92, 62.97, 59.40, 55.61, 52.32, 28.47, 21.32, 21.02, 20.87, 20.84, 20.62, 15.01 ppm.

HRMS Calculated for [C₃₉H₅₁ClN₂O₁₄+H]⁺: 807.3102, Found: 807.3103.



3-((4-chloro-5,6,7,8-tetrahydrobenzo[4,5]thieno[2,3-d]pyrimidin-5-yl)oxy)propanenitrile, **A11-1a**



3-((4-chloro-5,6,7,8-tetrahydrobenzo[4,5]thieno[2,3-d]pyrimidin-8-yl)oxy)propanenitrile, **A11-1b**

Reaction run using 4-chloro-5,6,7,8-tetrahydro[1]benzothieno[2,3-*d*]pyrimidine **A11** (44.8 mg, 0.20 mmol, 1.0 equiv.) and 3-Hydroxypropionitrile (68.3 μ L, 0.60 mmol, 3.0 equiv.) and two regioisomers were isolated.

A11-1a: Yield = 18.3 mg (31%) of brownish semisolid. TLC (Pentane:EtOAc, 1:1 v/v): R_f = 0.56. ^1H NMR (CDCl_3 , 500 MHz): 8.77 (s, 1H), 5.10 (t, J = 2.9 Hz, 1H), 3.97 – 3.87 (m, 2H), 3.05 (ddd, J = 17.7, 5.4, 1.2 Hz, 1H), 2.85 (ddd, J = 17.8, 11.8, 6.0 Hz, 1H), 2.71 – 2.59 (m, 2H), 2.40 (ddt, J = 14.4, 4.8, 2.9 Hz, 1H), 2.17 (tddd, J = 14.0, 11.8, 5.5, 2.7 Hz, 1H), 2.04 – 1.89 (m, 1H), 1.73 (tt, J = 14.2, 3.1 Hz, 1H) ppm.

^{13}C NMR (CDCl_3 , 126 MHz): 169.1, 152.8, 151.9, 145.3, 128.1, 126.0, 117.7, 69.9, 63.1, 26.2, 25.4, 19.3, 17.1 ppm.

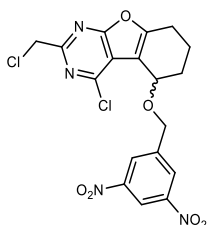
HRMS Calculated for $[\text{C}_{13}\text{H}_{12}\text{ClN}_3\text{OS}+\text{Na}]^+$: 316.0282, Found: 316.0276.

A11-2: Yield = 5.0 mg (9%) of white semisolid isolated. TLC (CH_2Cl_2 :MeOH = 50:1 v/v): R_f = 0.31.

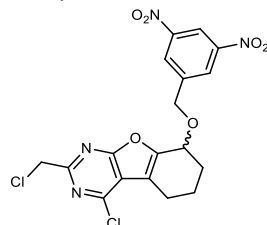
^1H NMR (CDCl_3 , 500 MHz): 8.78 (s, 1H), 4.71 (td, J = 4.8, 2.1 Hz, 1H), 3.93 (dt, J = 9.1, 6.4 Hz, 1H), 3.86 (dt, J = 9.1, 6.3 Hz, 1H), 3.43 – 3.07 (m, 2H), 2.69 (t, J = 6.3 Hz, 2H), 2.44 – 2.11 (m, 2H), 2.06 – 1.96 (m, 1H), 1.95 – 1.84 (m, 1H) ppm.

^{13}C NMR (CDCl_3 , 126 MHz): 169.7, 154.6, 152.5, 139.2, 130.1, 128.2, 117.5, 73.8, 63.7, 28.3, 26.3, 19.4, 19.3 ppm.

HRMS Calculated for $[\text{C}_{13}\text{H}_{12}\text{ClN}_3\text{OS}+\text{H}]^+$: 294.0462, Found: 294.0458.



4-chloro-2-(chloromethyl)-5-((3,5-dinitrobenzyl)oxy)-5,6,7,8-tetrahydrobenzofuro[2,3-d]pyrimidine, **A12-1a**



4-chloro-2-(chloromethyl)-8-((3,5-dinitrobenzyl)oxy)-5,6,7,8-tetrahydrobenzofuro[2,3-d]pyrimidine, **A12-1b**

Reaction run using 3-chloro-5-(chloromethyl)-8-oxa-4,6-diazatricyclo[7.4.0.0{2,7}]trideca-1(9),2,4,6-tetraene **A12** (51.4 mg, 0.2 mmol, 1.0 equiv.) and 3,5-dinitrobenzyl alcohol (118.6 mg, 0.60 mmol, 3.0 equiv.) and two regioisomers were isolated.

A12-1a: Yield = 37.0 mg (41%) of yellow semisolid isolated. TLC (pentane:EtOAc = 4:1): R_f = 0.27.

^1H NMR (CDCl_3 , 500 MHz): 8.96 (t, J = 2.1 Hz, 1H), 8.56 (d, J = 2.1 Hz, 2H), 5.08 (d, J = 13.0 Hz, 1H), 4.99 (d, J = 13.2 Hz, 1H), 4.77 (s, 2H), 4.74 (t, J = 3.7 Hz, 1H), 3.05 (dt, J = 16.9, 4.2 Hz, 1H), 2.79 (ddd, J = 16.8, 9.2, 5.5 Hz, 1H), 2.44 – 2.26 (m, 1H), 2.14 – 1.95 (m, 3H) ppm.

^{13}C NMR (CDCl_3 , 126 MHz): 167.1, 161.0, 153.6, 148.6, 142.8, 128.8, 127.0, 126.4, 118.0, 116.2, 116.1, 69.8, 46.3, 29.7 (d, J = 5.2 Hz), 29.4, 21.4, 18.4 ppm.

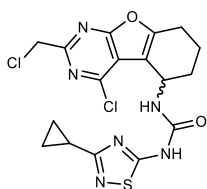
HRMS Calculated for $[\text{C}_{18}\text{H}_{14}\text{Cl}_2\text{N}_4\text{O}_6+\text{Na}]^+$: 475.0183, Found: 475.0177.

A12-1b: Yield = 15.5 mg (17%) of yellow semisolid isolated. TLC (pentane:EtOAc = 4:1): R_f = 0.15.

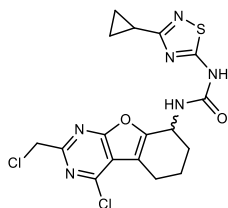
^1H NMR (CDCl_3 , 500 MHz): 8.96 (t, J = 2.1 Hz, 1H), 8.56 (d, J = 2.1 Hz, 2H), 5.07 (t, J = 3.0 Hz, 1H), 4.98 (d, J = 12.5 Hz, 1H), 4.93 (d, J = 12.3 Hz, 1H), 4.77 (s, 2H), 2.98 (ddd, J = 18.2, 5.8, 2.2 Hz, 1H), 2.81 (ddd, J = 18.0, 11.1, 6.3 Hz, 1H), 2.37 (ddt, J = 14.5, 5.3, 2.9 Hz, 1H), 2.20 (ttdd, J = 13.7, 11.4, 5.8, 2.7 Hz, 1H), 2.15 – 2.05 (m, 1H), 1.86 (tt, J = 13.9, 3.5 Hz, 1H) ppm.

^{13}C NMR (CDCl_3 , 126 MHz): 167.2, 160.1, 159.7, 151.3, 148.6, 142.8, 129.2, 127.2, 126.4, 118.0, 116.0, 111.6, 69.6, 69.1, 46.3, 26.8, 23.4, 17.2 ppm.

HRMS Calculated for $[\text{C}_{18}\text{H}_{14}\text{Cl}_2\text{N}_4\text{O}_6+\text{Na}]^+$: 475.0183, Found: 475.0178.



1-(4-chloro-2-(chloromethyl)-5,6,7,8-tetrahydrobenzofuro[2,3-d]pyrimidin-5-yl)-3-(3-cyclopropyl-1,2,4-thiadiazol-5-yl)urea,
A12-2a



1-(4-chloro-2-(chloromethyl)-5,6,7,8-tetrahydrobenzofuro[2,3-d]pyrimidin-8-yl)-3-(3-cyclopropyl-1,2,4-thiadiazol-5-yl)urea,
A12-2b

Reaction run using 3-chloro-5-(chloromethyl)-8-oxa-4,6-diazatricyclo[7.4.0.0{2,7}]trideca-1(9),2,4,6-tetraene **A12** (102.8 mg, 0.40 mmol, 1.0 equiv.) and 3-cyclopropyl-1,2,4-thiadiazol-5-amine (282.4 mg, 2.0 mmol, 5.0 equiv.) and two regioisomers were isolated.

A12-2a: Yield = 55.0 mg (31%) of yellow semisolid isolated.

^1H NMR ($\text{DMSO}-d_6$, 500 MHz): 11.34 (s, 1H), 7.43 (d, J = 8.3 Hz, 1H), 5.10 (q, J = 7.1, 6.2 Hz, 1H), 4.87 (s, 2H), 2.89 – 2.71 (m, 2H), 2.19 – 2.09 (m, 1H), 2.11 – 2.04 (m, 1H), 1.97 – 1.83 (m, 3H), 0.94 (dt, J = 8.2, 2.8 Hz, 2H), 0.92 – 0.85 (m, 2H) ppm.

^{13}C NMR ($\text{DMSO}-d_6$, 126 MHz): 176.2, 172.1, 166.4, 159.9, 154.2, 153.7, 151.4, 115.9, 113.9, 46.4, 43.6, 29.5, 20.6, 19.6, 13.3, 8.4 ppm.

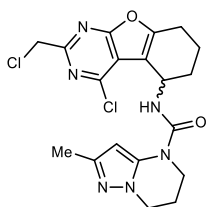
HRMS Calculated for $[\text{C}_{17}\text{H}_{16}\text{Cl}_2\text{N}_6\text{O}_2\text{S}+\text{H}]^+$: 439.0505, Found: 439.0502.

A12-2b: Yield = 28.6 mg (16%) of yellow semisolid isolated.

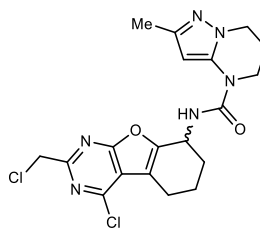
^1H NMR (DMSO- d_6 , 500 MHz): 11.04 (s, 1H), 7.33 (d, J = 7.8 Hz, 1H), 5.18 (d, J = 5.1 Hz, 1H), 4.88 (s, 2H), 2.97 – 2.84 (m, 1H), 2.84 – 2.73 (m, 1H), 2.11 – 2.02 (m, 1H), 1.99 – 1.92 (m, 2H), 1.92 – 1.71 (m, 2H), 1.03 – 0.91 (m, 2H), 0.91 – 0.75 (m, 2H) ppm.

^{13}C NMR (DMSO- d_6 , 126 MHz): 176.24, 172.06, 166.48, 159.51, 159.35, 153.14, 150.37, 115.70, 110.80, 46.42, 41.63, 29.11, 22.60, 17.32, 13.26, 8.42, 8.35 ppm.

HRMS Calculated for $[\text{C}_{17}\text{H}_{16}\text{Cl}_2\text{N}_6\text{O}_2\text{S}+\text{H}]^+$: 439.0505, Found: 439.0504.



N-(4-chloro-2-(chloromethyl)-5,6,7,8-tetrahydrobenzofuro[2,3-*d*]pyrimidin-5-yl)-2-methyl-6,7-dihydropyrazolo[1,5-*a*]pyrimidine-4(5H)-carboxamide, **A12-3a**



N-(4-chloro-2-(chloromethyl)-5,6,7,8-tetrahydrobenzofuro[2,3-*d*]pyrimidin-8-yl)-2-methyl-6,7-dihydropyrazolo[1,5-*a*]pyrimidine-4(5H)-carboxamide, **A12-3b**

Reaction run using 3-chloro-5-(chloromethyl)-8-oxa-4,6-diazatricyclo[7.4.0.0{2,7}]trideca-1(9),2,4,6-tetraene **A12** (102.8 mg, 0.40 mmol, 1.0 equiv.) and 4,5,6,7-Tetrahydro-2-methylpyrazolo[1,5-*a*]pyrimidine (274.4 mg, 2.0 mmol, 5.0 equiv.) and two regioisomers were isolated.

A12-3a: Yield = 34.0 mg (20%) of light yellow solid isolated.

^1H NMR (CD_2Cl_2 , 500 MHz): 5.77 (s, 1H), 5.73 (d, J = 8.2 Hz, 1H), 5.29 – 5.21 (m, 1H), 4.74 (s, 2H), 4.17 – 4.03 (m, 2H), 3.82 (td, J = 5.2, 4.0 Hz, 2H), 2.96 – 2.80 (m, 2H), 2.30 – 2.21 (m, 1H), 2.19 – 2.10 (m, 5H), 1.99 – 1.91 (m, 3H) ppm.

^{13}C NMR (CD_2Cl_2 , 126 MHz): 167.5, 160.8, 154.5, 153.6, 153.0, 116.8, 115.6, 47.0, 46.3, 45.0, 41.6, 30.9, 22.8, 21.6, 20.5, 14.0 ppm.

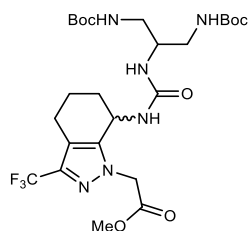
HRMS Calculated for $[\text{C}_{19}\text{H}_{20}\text{Cl}_2\text{N}_6\text{O}_2+\text{H}]^+$: 435.1098, Found: 435.1087.

A12-3b: Yield = 20.6 mg (12%) of light yellow solid isolated.

^1H NMR (CD_2Cl_2 , 500 MHz): 5.67 (d, J = 7.7 Hz, 1H), 5.60 (s, 1H), 5.38 (dt, J = 6.5, 3.1 Hz, 1H), 4.75 (s, 2H), 4.05 (t, J = 6.3 Hz, 2H), 3.88 – 3.74 (m, 2H), 2.89 (ddd, J = 17.5, 4.7, 2.4 Hz, 1H), 2.76 (dddd, J = 20.0, 10.7, 5.9, 1.8 Hz, 1H), 2.17 – 2.07 (m, 3H), 2.06 (s, 3H), 2.04 (dd, J = 8.4, 4.5 Hz, 1H), 1.97 – 1.85 (m, 2H).

^{13}C NMR (CD_2Cl_2 , 126 MHz): 167.63, 160.45, 159.91, 153.16, 151.92, 148.03, 139.66, 116.28, 111.89, 93.18, 47.02, 46.28, 42.91, 41.53, 29.94, 23.69, 22.95, 18.3, 14.0 ppm.

HRMS Calculated for $[\text{C}_{19}\text{H}_{20}\text{Cl}_2\text{N}_6\text{O}_2+\text{H}]^+$: 435.1098, Found: 435.1091.



methyl 2-(7-(3-(2,2,12,12-tetramethyl-4,10-dioxo-3,11-dioxo-5,9-diazatridecan-7-yl)ureido)-3-(trifluoromethyl)-4,5,6,7-tetrahydro-1*H*-indazol-1-yl)acetate, **A13-1**

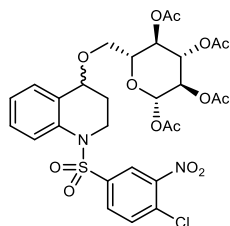
Reaction run using methyl 2-(3-(trifluoromethyl)-4,5,6,7-tetrahydro-1*H*-indazol-1-yl)acetate **A15** (104.9 mg, 0.40 mmol, 1.0 equiv.) and 4-(*tert*-butyl)-2-chloroaniline (405.1 mg, 1.4 mmol, 3.5 equiv.). Yield = 76.5 mg (32%) of white solid isolated.

^1H NMR (CD_2Cl_2 , 400 MHz): 5.87 (s, 1H), 5.61 (t, $J = 6.4$ Hz, 1H), 5.55 (t, $J = 6.5$ Hz, 1H), 5.47 – 5.12 (m, 1H), 5.11 – 4.91 (m, 1H), 4.86 (d, $J = 17.5$ Hz, 1H), 4.79 (d, $J = 17.7$ Hz, 1H), 3.76 (s, 3H), 3.54 (s, 1H), 3.23 – 3.11 (m, 4H), 2.63 – 2.54 (m, 1H), 2.44 (dt, $J = 15.9, 7.6$ Hz, 1H), 1.98 – 1.82 (m, 3 H), 1.82 – 1.71 (m, 1H), 1.40 (s, 9H), 1.39 (s, 9H) ppm.

^{13}C NMR (CD_2Cl_2 , 126 MHz): 167.8, 157.7, 157.6, 157.5, 143.6, 139.5 (q, $J = 37.3$ Hz), 123.1 (q, $J = 269.2$ Hz), 116.3, 79.8, 53.2, 52.7, 51.0, 42.1, 42.0, 41.9, 30.5, 28.5, 28.4, 21.4, 18.2 ppm.

^{19}F NMR (CD_2Cl_2 , 377 MHz): –61.8 ppm.

HRMS Calculated for $[\text{C}_{25}\text{H}_{39}\text{F}_3\text{N}_6\text{O}_7+\text{H}]^+$: 593.2905, Found: 593.2906.



(2*S*,3*R*,4*S*,5*R*,6*R*)-6-(((1-((4-chloro-3-nitrophenyl)sulfonyl)-1,2,3,4-tetrahydroquinolin-4-yl)oxy)methyl)tetrahydro-2*H*-pyran-2,3,4,5-tetra-yl tetraacetate, **A15-1**

Reaction run using 1-(4-chloro-3-nitrobenzenesulfonyl)-1,2,3,4-tetrahydroquinoline **A15** (70.6 mg, 0.20 mmol, 1.0 equiv.) and 1,2,3,4-tetra-*O*-acetyl- β -*D*-glucopyranose (209 mg, 0.60 mmol, 3.0 equiv.) and two diastereomers were isolated as a mixture.

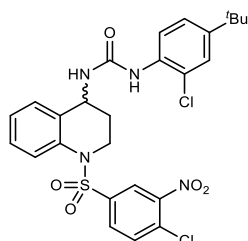
Yield = 45.9 mg (33%) of white semisolid isolated. TLC (100% Et_2O): $R_f = 0.52$.

^1H NMR (CDCl_3 , 500 MHz)(mixture of diastereomers: 55:45): 8.16 (dd, $J = 11.9, 2.1$ Hz, 1H), 7.83 (dd, $J = 8.4, 1.1$ Hz, 1×0.55 H), 7.77 (dd, $J = 8.4, 1.1$ Hz, 1×0.45 H), 7.73 (dd, $J = 8.5, 2.2$ Hz, 1×0.45 H), 7.71 (dd, $J = 8.4, 2.1$ Hz, 1×0.45 H), 7.61 (d, $J = 8.5$ Hz, 1×0.45 H), 7.59 (d, $J = 8.5$ Hz, 1×0.55 H), 7.30 (dddd, $J = 8.5, 7.3, 3.4, 1.7$ Hz, 1H), 7.25 (dd, $J = 7.7, 1.8$ Hz, 1×0.45 H), 7.20 (dd, $J = 7.6, 1.7$ Hz, 1×0.55 H), 7.14 (tdd, $J = 7.5, 3.8, 1.1$ Hz, 1H), 5.66 (dd, $J = 9.5, 8.3$ Hz, 1H), 5.22 (q, $J = 9.7$ Hz, 1H), 5.13 – 5.05 (m, 1H + 1×0.45 H), 4.27 (t, $J = 3.8$ Hz, 1×0.45 H), 4.23 (t, $J = 3.8$ Hz, 1×0.55 H), 4.13 (dt, $J = 12.9, 4.4$ Hz, 1×0.45 H), 4.05 (dt, $J = 12.6, 4.5$ Hz, 1×0.55 H), 3.78 (tt, $J = 12.4, 3.6$ Hz, 1H), 3.69 (ddd, $J = 10.0, 4.6, 2.7$ Hz, 1×0.45 H), 3.61 (ddd, $J = 10.0, 5.2, 2.9$ Hz, 1×0.55 H), 3.55 (dd, $J = 11.3, 2.7$ Hz, 1×0.45 H), 3.47 – 3.36 (m, 2×0.55 H), 3.33 (dd, $J = 11.3, 4.6$ Hz, 1×0.45 H), 2.10 (s, 3×0.55 H), 2.10 (s, 3×0.45 H),

2.04 (s, 3 × 0.55 H), 2.03 (s, 3 × 0.45 H), 2.01 (d, $J = 1.6$ Hz, 3H), 1.97 (s, 3 × 0.55 H), 1.82 (s, 3 × 0.45 H) ppm.

^{13}C NMR (CDCl_3 , 126 MHz): 170.13, 170.04, 169.51, 169.29, 169.26, 169.05, 169.01, 147.72, 139.38, 138.91, 135.63, 135.54, 132.74, 132.71, 131.62, 131.09, 130.96, 130.80, 130.34, 129.53, 129.41, 128.35, 127.65, 124.97, 124.76, 124.61, 124.45, 122.76, 122.46, 91.82, 91.71, 74.32, 74.05, 73.00, 72.85, 72.56, 70.22 (d, $J = 5.4$ Hz), 68.64, 68.36, 66.88, 65.90, 42.59, 27.15, 20.79, 20.78, 20.60, 20.57, 20.36 ppm.

HRMS Calculated for $[\text{C}_{29}\text{H}_{31}\text{ClN}_2\text{O}_{14}\text{S}+\text{Na}]^+$: 721.1077, Found: 721.1078.



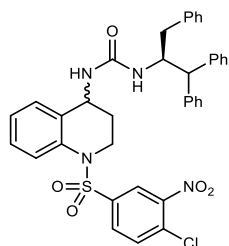
1-(4-(*tert*-butyl)-2-chlorophenyl)-3-(1-((4-chloro-3-nitrophenyl)sulfonyl)-1,2,3,4-tetrahydroquinolin-4-yl)urea, **A15-2**

Reaction run using 1-(4-chloro-3-nitrobenzenesulfonyl)-1,2,3,4-tetrahydroquinoline **A15** (70.6 mg, 0.40 mmol, 1.0 equiv.) and 4-(*tert*-butyl)-2-chloroaniline (367.0 mg, 2.0 mmol, 5.0 equiv.). Yield = 33.6 mg (15%) of off-white solid isolated.

^1H NMR (CD_2Cl_2 , 500 MHz): 8.12 (d, $J = 2.2$ Hz, 1H), 7.89 (d, $J = 8.6$ Hz, 1H), 7.76 (td, $J = 8.6$, 1.7 Hz, 2H), 7.66 (d, $J = 8.4$ Hz, 1H), 7.42 – 7.33 (m, 2H), 7.30 (td, $J = 8.3$, 7.8, 1.7 Hz, 1H), 7.25 (dd, $J = 8.6$, 2.3 Hz, 1H), 7.19 (td, $J = 7.5$, 1.2 Hz, 1H), 6.64 (s, 1H), 5.12 (d, $J = 7.6$ Hz, 1H), 4.79 (q, $J = 6.4$ Hz, 1H), 4.03 (ddd, $J = 14.0$, 7.4, 3.8 Hz, 1H), 3.83 (ddd, $J = 14.0$, 8.7, 3.5 Hz, 1H), 1.96 – 1.88 (m, 1H), 1.82 (dtd, $J = 13.8$, 6.9, 3.5 Hz, 1H), 1.28 (s, 9H) ppm.

^{13}C NMR (CD_2Cl_2 , 126 MHz): 154.3, 148.2, 148.0, 140.1, 136.4, 133.7, 133.1, 132.4, 131.4, 130.4, 129.8, 128.9, 126.6, 126.4, 125.2, 124.7, 123.9, 123.4, 121.8, 46.3, 44.8, 34.7, 31.3, 29.3 ppm.

HRMS Calculated for $[\text{C}_{26}\text{H}_{26}\text{Cl}_2\text{N}_4\text{O}_5\text{S}+\text{H}]^+$: 577.1073, Found: 577.1068.



1-((S)-1-((4-chloro-3-nitrophenyl)sulfonyl)-1,2,3,4-tetrahydroquinolin-4-yl)-3-((S)-1,1,3-triphenylpropan-2-yl)urea, **A15-3**

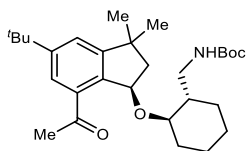
Reaction run using 1-(4-chloro-3-nitrobenzenesulfonyl)-1,2,3,4-tetrahydroquinoline **A15** (70.6 mg, 0.40 mmol, 1.0 equiv.) and (*S*)-(-)-1-benzyl-2,2-diphenylethylamine (402.37 mg, 1.4 mmol, 3.5 equiv.) and two diastereomers were isolated as a mixture.

A15-1: Yield = 70.8 mg (26%) of light yellow solid isolated.

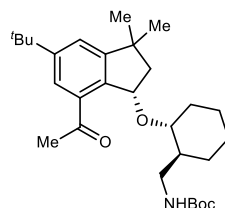
^1H NMR (CD_2Cl_2 , 600 MHz) (mixture of diastereomers: 50:50): 8.07 (d, $J = 2.2$ Hz, $0.5 \times 1\text{H}$), 8.04 (d, $J = 2.2$ Hz, $0.5 \times 1\text{H}$), 7.73 – 7.65 (m, 2H), 7.63 (d, $J = 8.7$ Hz, $0.5 \times 1\text{H}$), 7.61 (d, $J = 8.6$ Hz, $0.5 \times 1\text{H}$), 7.44 – 7.40 (m, 1H), 7.43 – 7.38 (m, 1H), 7.35 (td, $J = 7.8, 2.6$ Hz, 2H), 7.35 – 7.30 (m, 1H), 7.32 – 7.28 (m, 1H), 7.30 – 7.15 (m, 8H), 7.12 (m, $2 + 0.5 \times 1\text{H}$), 7.06 (td, $J = 7.5, 1.2$ Hz, $0.5 \times 1\text{H}$), 6.95 (dd, $J = 7.8, 1.6$ Hz, $0.5 \times 1\text{H}$), 6.80 (d, $J = 7.7$ Hz, $0.5 \times 1\text{H}$), 4.87 (s, 1H), 4.46 (p, $J = 6.2$ Hz, 1H), 4.07 (d, $J = 8.6$ Hz, 1H), 4.05 (d, $J = 8.0$ Hz, 1H), 3.96 (d, $J = 6.6$ Hz, $0.5 \times 1\text{H}$), 3.94 (d, $J = 6.6$ Hz, $0.5 \times 1\text{H}$), 3.86 (dddd, $J = 14.2, 10.9, 7.5, 3.6$ Hz, 1H), 3.66 (ddd, $J = 13.9, 8.5, 3.4$ Hz, $0.5 \times 1\text{H}$), 3.53 (ddd, $J = 13.8, 8.8, 3.4$ Hz, $0.5 \times 1\text{H}$), 2.92 (dd, $J = 5.6, 4.0$ Hz, $0.5 \times 1\text{H}$), 2.92 – 2.88 (m, $0.5 \times 1\text{H}$), 2.60 (dd, $J = 8.6, 1.9$ Hz, $0.5 \times 1\text{H}$), 2.58 (dd, $J = 8.7, 1.9$ Hz, $0.5 \times 1\text{H}$), 1.72 – 1.55 (m, 1H), 1.51 – 1.38 (m, 1H) ppm.

^{13}C NMR (CD_2Cl_2 , 151 MHz) (mixture of diastereomers: 50:50): 156.38, 156.36, 148.12, 143.15, 143.13, 142.91, 142.85, 139.96, 139.95, 138.92, 138.80, 136.02, 135.97, 133.54, 133.52, 132.25, 132.23, 131.02, 130.96, 130.00, 129.99, 129.73, 129.57, 129.29, 128.84, 128.81, 128.72, 128.70, 128.59, 128.57, 128.55, 128.51, 128.50, 127.14, 126.88, 126.68, 126.15 (d, $J = 2.1$ Hz), 124.63, 124.58, 123.53, 123.49, 57.48, 57.33, 45.84, 45.82, 44.84, 44.70, 40.23, 40.22, 40.16, 29.14, 29.02 ppm.

HRMS Calculated for $[\text{C}_{37}\text{H}_{33}\text{ClN}_4\text{O}_5\text{S}+\text{Na}]^+$: 703.1752, Found: 703.1757.



tert-butyl (((1*S*,2*R*)-2-(((*R*)-7-acetyl-5-(tert-butyl)-3,3-dimethyl-2,3-dihydro-1*H*-inden-1-yl)oxy)cyclohexyl)methyl)carbamate, **A16-1a**



tert-butyl (((1*S*,2*R*)-2-(((*S*)-7-acetyl-5-(tert-butyl)-3,3-dimethyl-2,3-dihydro-1*H*-inden-1-yl)oxy)cyclohexyl)methyl)carbamate, **A16-1b**

Reaction run using celestolide **A16** (48.9 mg, 0.20 mmol, 1.0 equiv.) and *tert*-butyl *N*-{[(1*S*,2*R*)-2-hydroxycyclohexyl]methyl}carbamate (137.6 mg, 0.60 mmol, 3.0 equiv.) and two diastereomers were isolated.

A16-1a: Yield = 11.3 mg (12%) of white solid isolated. TLC (pentane:Et₂O = 4:1): $R_f = 0.14$.

^1H NMR (CDCl_3 , 500 MHz): 7.68 (d, $J = 1.7$ Hz, 1H), 7.37 (d, $J = 1.7$ Hz, 1H), 5.40 (dd, $J = 7.1, 2.7$ Hz, 2H), 3.57 (td, $J = 10.1, 4.0$ Hz, 1H), 3.07 (ddd, $J = 13.4, 6.8, 3.5$ Hz, 1H), 2.97 (dt, $J = 12.9, 5.9$ Hz, 1H), 2.61 (s, 3H), 2.25 (dd, $J = 12.0, 3.5$ Hz, 1H), 2.19 (dd, $J = 13.4, 6.9$ Hz, 1H), 2.00 (dd, $J = 13.5, 2.6$ Hz, 1H), 1.75 (dq, $J = 12.6, 2.8$ Hz, 1H), 1.71 – 1.61 (m, 2H), 1.46 – 1.39 (m, 1H), 1.36 (s, 9H), 1.35 (br, 12H), 1.25 (s, 3H), 1.23 (m, 1H), 1.22 – 1.11 (m, 3H) ppm.

^{13}C NMR (CDCl_3 , 126 MHz): 201.2, 156.3, 154.7, 152.2, 139.3, 134.4, 125.5, 123.5, 83.4, 78.7, 78.0, 51.2, 44.0, 43.8, 42.6, 34.9, 33.7, 31.5, 31.2, 29.8, 29.0, 28.5, 28.2, 25.3, 24.6 ppm.

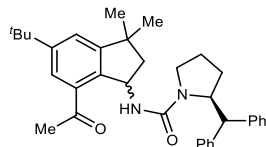
HRMS Calculated for $[\text{C}_{29}\text{H}_{45}\text{NO}_4+\text{H}]^+$: 472.3421, Found: 472.3416.

A16-1b: Yield = 9.0 mg (10%) of colorless semisolid isolated. TLC (pentane:Et₂O = 4:1): R_f = 0.18.

¹H NMR (CDCl₃, 500 MHz): 7.52 (d, *J* = 1.7 Hz, 1H), 7.31 (d, *J* = 1.8 Hz, 1H), 5.55 (dd, *J* = 6.6, 2.9 Hz, 1H), 4.83 (s, 1H), 3.34 – 3.04 (m, 3H), 2.59 (s, 3H), 2.38 (d, *J* = 10.5 Hz, 1H), 2.11 (dd, *J* = 13.4, 6.5 Hz, 1H), 1.97 (dd, *J* = 13.5, 2.9 Hz, 1H), 1.87 – 1.73 (m, 2H), 1.69 – 1.61 (m, 1H), 1.47 – 1.40 (m, 2H), 1.37 (s, 3H), 1.35 (s, 9H), 1.34 (s, 9H), 1.28 (s, 3H), 1.25 – 1.10 (m, 4H), 1.03 (qd, *J* = 12.4, 3.9 Hz, 1H) ppm.

¹³C NMR (CDCl₃, 126 MHz): 201.7, 156.0, 154.3, 152.2, 137.6, 136.4, 124.0, 122.3, 78.6, 78.5, 75.2, 46.9, 44.5, 43.8, 42.7, 34.9, 31.4, 31.1, 30.1, 30.0, 29.4, 29.3, 28.4, 25.3, 24.6 ppm.

HRMS Calculated for [C₂₉H₄₅NO₄+H]⁺: 472.3421, Found: 472.3418.



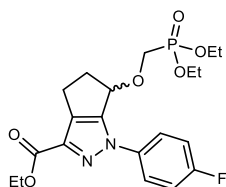
(2*S*)-*N*-(7-acetyl-5-(*tert*-butyl)-3,3-dimethyl-2,3-dihydro-1H-inden-1-yl)-2-benzhydrylpyrrolidine-1-carboxamide, **A16-2**

Reaction run using celestolide **A16** (97.8 mg, 0.40 mmol, 1.0 equiv.) and (*S*)-(-)-2-(diphenylmethyl)pyrrolidine (332.3 mg, 1.4 mmol, 3.5 equiv.) and two diastereomers were isolated as a mixture. Yield = 107.7 mg (52%) of off-white solid isolated.

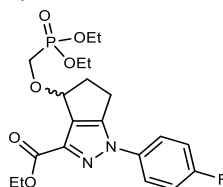
¹H NMR (CD₂Cl₂, 500 MHz)(mixture of diastereomers: 54:46): 7.56 (d, *J* = 1.8 Hz, 0.54 × 1H), 7.49 (d, *J* = 1.8 Hz, 0.46 × 1H), 7.40 (d, *J* = 1.8 Hz, 0.54 × 1H), 7.35 (d, *J* = 1.8 Hz, 0.46 × 1H), 7.33 – 7.14 (m, 9H), 7.13 – 7.05 (m, 1H), 5.43 (td, *J* = 7.3, 4.4 Hz, 0.54 × 1H), 5.37 – 5.29 (m, 0.46 × 1H), 4.82 (ddd, *J* = 8.2, 6.1, 1.9 Hz, 0.54 × 1H), 4.58 (t, *J* = 6.2 Hz, 0.46 × 1H), 4.44 (d, *J* = 6.1 Hz, 0.54 × 1H), 4.36 (d, *J* = 7.1 Hz, 0.46 × 1H), 4.31 (s, 0.54 × 1H), 4.05 (s, 0.46 × 1H), 3.41 (s, 0.46 × 1H), 3.16 (q, *J* = 8.6 Hz, 0.54 × 1H), 3.05 (td, *J* = 9.3, 2.9 Hz, 0.46 × 1H), 2.93 (td, *J* = 8.9, 3.1 Hz, 0.54 × 1H), 2.54 (s, 0.46 × 3H), 2.53 (s, 0.54 × 3H), 2.34 (t, *J* = 7.2 Hz, 0.46 × 1H), 2.31 (t, *J* = 7.4 Hz, 0.54 × 1H), 2.03 (m, 1H), 1.95 – 1.81 (m, 2H), 1.69 (m, 1H), 1.40 (s, 0.54 × 3H), 1.38 (s, 0.46 × 9H), 1.37 (s, 0.54 × 9H), 1.33 (s, 0.46 × 3H), 1.30 (s, 0.54 × 3H), 1.22 (s, 0.46 × 3H) ppm.

¹³C NMR (CDCl₃, 126 MHz): 203.25, 201.99, 157.64, 156.91, 154.97, 154.41, 152.56, 152.43, 143.17, 143.08, 142.83, 142.71, 138.34, 137.93, 137.34, 136.59, 129.90, 129.73, 129.30, 129.28, 128.71, 128.71, 128.51, 128.40, 126.88, 126.83, 126.78, 126.52, 124.80, 124.06, 123.20, 122.59, 62.06, 60.66, 54.62, 54.19, 53.90, 53.86, 50.85, 50.57, 46.41, 46.32, 42.73, 42.72, 35.24, 35.23, 31.60, 31.03, 30.27, 30.06, 29.98, 29.85, 29.51, 28.78, 23.97, 23.60 ppm.

HRMS Calculated for [C₃₅H₄₂N₂O₂+H]⁺: 523.3319, Found: 523.3314.



ethyl 6-((diethoxyphosphoryl)methoxy)-1-(4-fluorophenyl)-1,4,5,6-tetrahydrocyclopenta[*c*]pyrazole-3-carboxylate, **A18-1a**



ethyl 4-((diethoxyphosphoryl)methoxy)-1-(4-fluorophenyl)-1,4,5,6-tetrahydrocyclopenta[*c*]pyrazole-3-carboxylate, **A18-1b**

Reaction run ethyl 1-(4-fluorophenyl)-1,4,5,6-tetrahydrocyclopenta[*c*]pyrazole-3-carboxylate **A18** (54.5 mg, 0.2 mmol, 1.0 equiv.) and diethyl (hydroxymethyl)phosphonate (64.6 μ L, 0.60 mmol, 3.0 equiv.) and two regioisomers were isolated.

A18-1a: Yield = 14.2 mg (16%) of colorless liquid isolated.

^1H NMR (CDCl_3 , 500 MHz): 7.71 – 7.60 (m, 2H), 7.20 – 7.12 (m, 2H), 5.03 (d, $J = 6.0$ Hz, 1H), 4.43 (q, $J = 7.1$ Hz, 2H), 4.15 (dq, $J = 8.1, 7.1$ Hz, 4H), 3.99 (dd, $J = 13.6, 9.4$ Hz, 1H), 3.93 (dd, $J = 13.6, 9.2$ Hz, 1H), 3.23 (dt, $J = 15.0, 7.2$ Hz, 1H), 2.88 (ddt, $J = 13.2, 8.8, 6.5$ Hz, 1H), 2.80 (ddd, $J = 15.4, 8.8, 1.4$ Hz, 1H), 2.75 – 2.66 (m, 1H), 1.42 (t, $J = 7.1$ Hz, 3H), 1.32 (t, $J = 7.1$ Hz, 6H) ppm.

^{13}C NMR (CDCl_3 , 126 MHz): 162.2, 161.8 (d, $J = 248.0$ Hz), 152.8, 138.9, 135.8 (d, $J = 3.0$ Hz), 130.7, 122.5 (d, $J = 8.5$ Hz), 116.5 (d, $J = 23.1$ Hz), 77.3, 63.2 (d, $J = 156.0$ Hz), 62.5 (dd, $J = 7.3, 5.5$ Hz), 61.4, 39.6, 24.7, 16.6 (d, $J = 5.8$ Hz), 14.5 ppm.

^{19}F NMR (CDCl_3 , 377 MHz): –114.0 ppm.

^{31}P NMR (CDCl_3 , 162 MHz): 22.0 ppm.

HRMS Calculated for $[\text{C}_{20}\text{H}_{26}\text{FN}_2\text{O}_6\text{P}+\text{Na}]^+$: 463.1405, Found: 463.1399.

A18-1b: Yield = 7.6 mg (9%) of colorless liquid isolated.

^1H NMR (400 MHz, CDCl_3) δ 7.93 – 7.83 (m, 2H), 7.19 – 7.10 (m, 2H), 5.23 – 5.15 (m, 1H), 4.42 (q, $J = 7.1$ Hz, 2H), 4.18 – 4.05 (m, 4H), 3.78 – 3.62 (m, 2H), 3.08 – 2.93 (m, 1H), 2.92 – 2.79 (m, 2H), 2.74 – 2.59 (m, 1H), 1.40 (t, $J = 7.1$ Hz, 3H), 1.28 (td, $J = 7.1, 3.7$ Hz, 6H) ppm.

^{13}C NMR (CDCl_3 , 126 MHz): 162.33, 161.85 (d, $J = 247.4$ Hz), 147.52, 138.24, 135.87 (d, $J = 2.9$ Hz), 135.45, 122.93 (d, $J = 8.4$ Hz), 116.33 (d, $J = 23.0$ Hz), 76.51 (d, $J = 14.3$ Hz), 62.69 (t, $J = 7.0$ Hz), 61.18, 60.78 (d, $J = 170.0$ Hz), 36.97, 22.47, 16.58 (dd, $J = 5.7, 3.0$ Hz), 14.54 ppm.

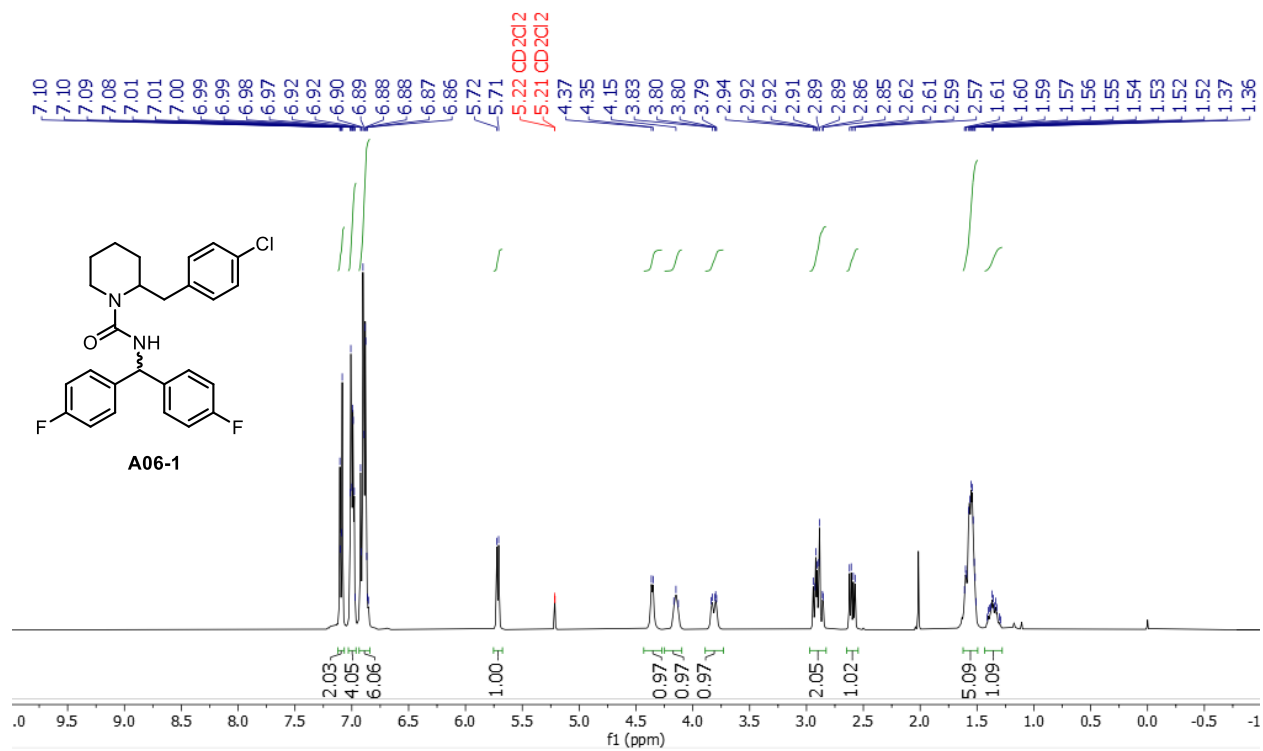
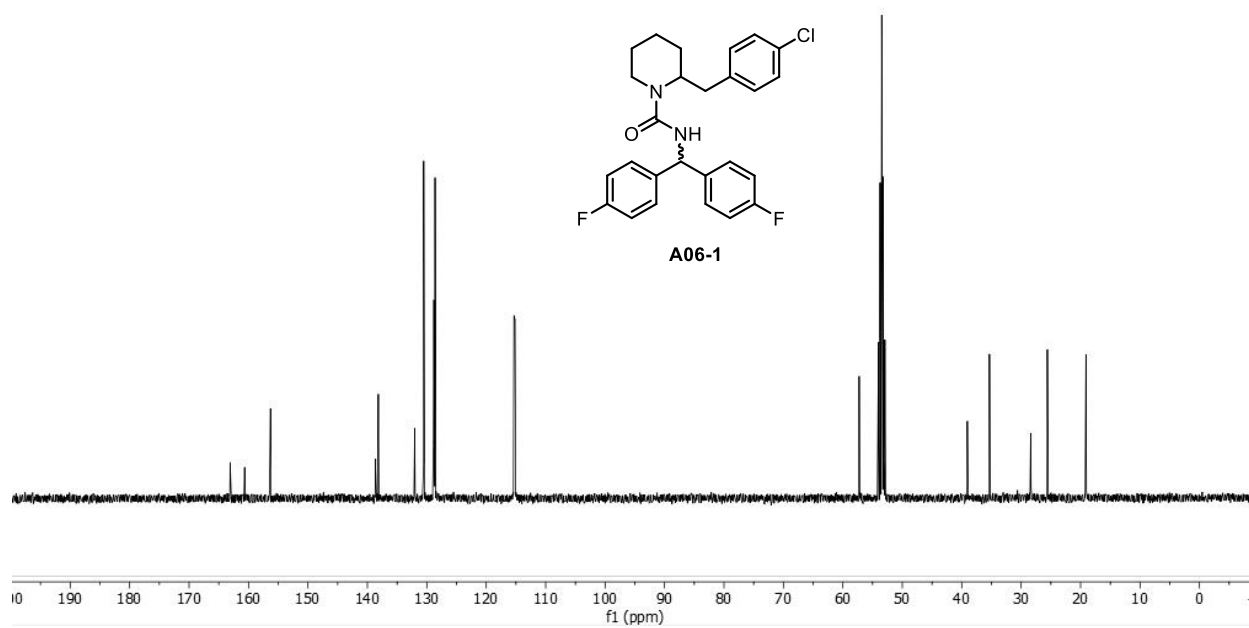
^{19}F NMR (CD_2Cl_2 , 377 MHz): –114.4 ppm.

^{31}P NMR (CDCl_3 , 162 MHz): 20.8 ppm.

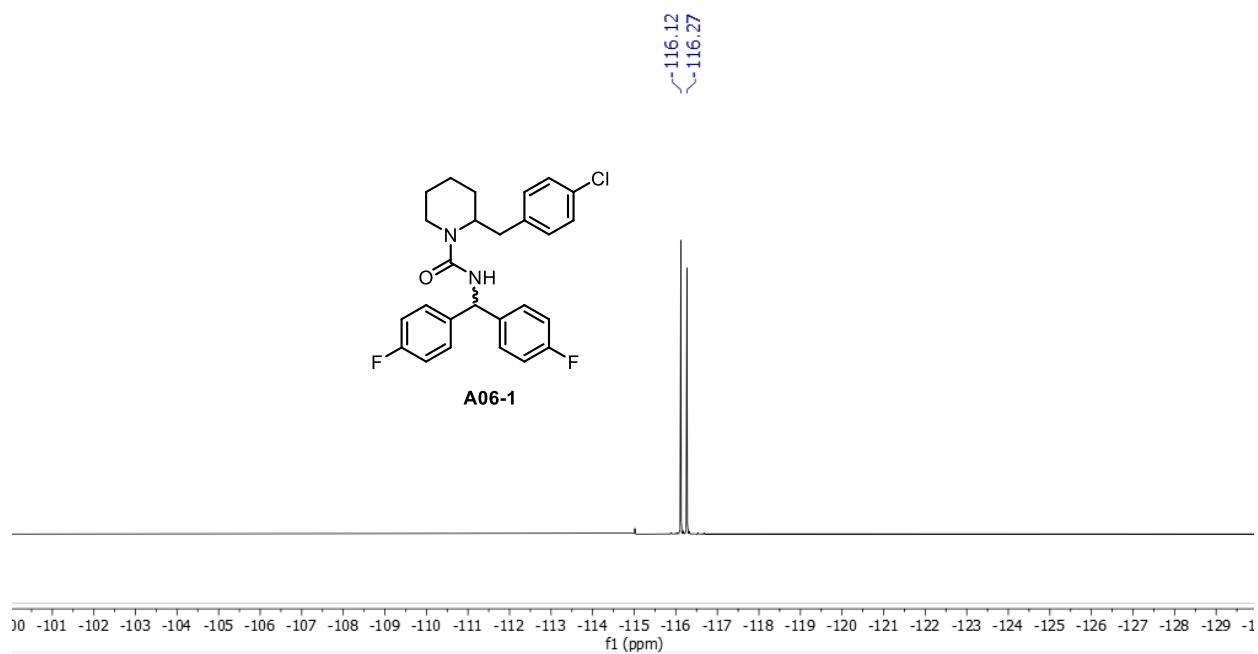
HRMS Calculated for $[\text{C}_{20}\text{H}_{26}\text{FN}_2\text{O}_6\text{P}+\text{H}]^+$: 441.1585, Found: 441.1581.

4C.X. Reference

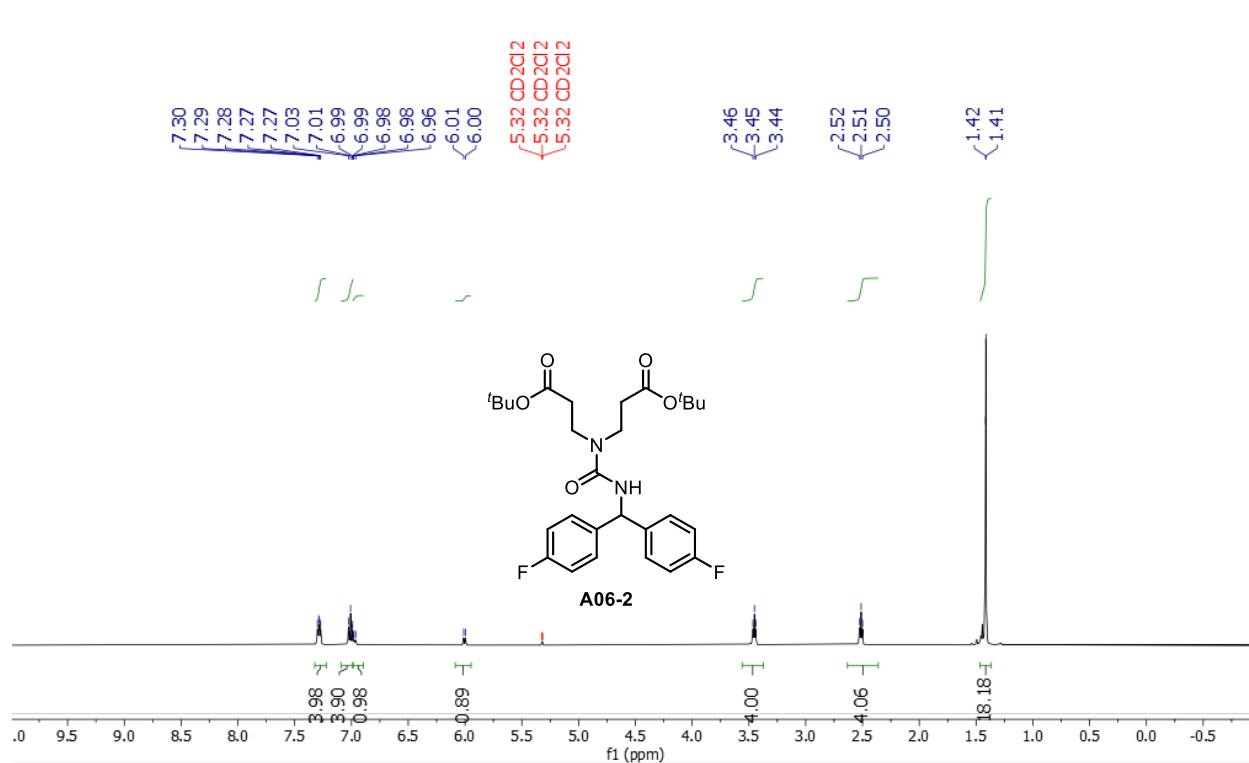
1. Hu, H. *et al.* Copper-catalysed benzylic C–H coupling with alcohols via radical relay enabled by redox buffering. *Nat Catal* **3**, 358–367 (2020).
2. Wenderski, T. A., Stratton, C. F., Bauer, R. A., Kopp, F. & Tan, D. S. Principal Component Analysis as a Tool for Library Design: A Case Study Investigating Natural Products, Brand-Name Drugs, Natural Product-Like Libraries, and Drug-Like Libraries. in *Chemical Biology: Methods and Protocols* (eds. Hempel, J. E., Williams, C. H. & Hong, C. C.) 225–242 (Springer New York, 2015). doi:10.1007/978-1-4939-2269-7_18.
3. Bruker-AXS. *APEX3*. Version 2018.1-0. Madison, Wisconsin, USA (2018)
4. Krause, L., Herbst-Irmer, R., Sheldrick, G. M. & Stalke, D. Comparison of silver and molybdenum microfocus X-ray sources for single-crystal structure determination. *J. Appl. Crystallogr.* **48**, 3–10 (2015).
5. Sheldrick, G. M. *XPREP*. Version 2013/1. Georg-August-Universität Göttingen, Göttingen, Germany (2013b).
6. Sheldrick, G. M. The *SHELX* homepage, <http://shelx.uni-ac.gwdg.de/SHELX/> (2013a)
7. Sheldrick, G. M. *SHELXT* – Integrated space-group and crystal-structure determination. *Acta Crystallogr. A Found. Adv.* **71**, 3–8 (2015).
8. Sheldrick, G. M. Crystal structure refinement with *SHELXL*. *Acta Crystallogr. C Struct. Chem.* **71**, 3–8 (2015).
9. Dolomanov, O. V., Bourhis, L. J., Gildea, R. J., Howard, J. A. K. & Puschmann, H. *OLEX2*: a complete structure solution, refinement and analysis program. *J. Appl. Crystallogr.* **42**, 339–341 (2009).
10. Guzei, I. A. Programs *Gn*. University of Wisconsin-Madison, Madison, Wisconsin, USA (2007-2013).

4C.XI. NMR Spectroscopic Data¹H NMR spectrum of **A06-1** in CD₂Cl₂ (500 MHz).¹³C NMR spectrum of **A06-1** in CD₂Cl₂ (126 MHz).

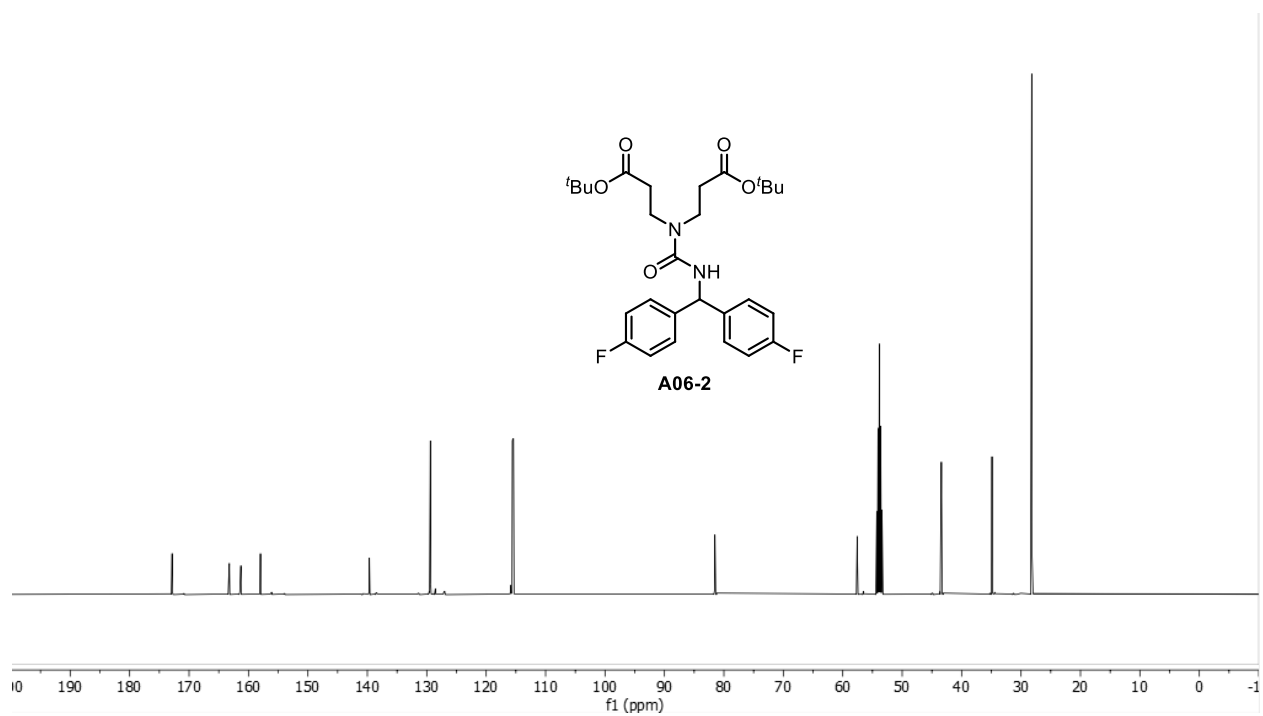
^{19}F NMR spectrum of **A06-1** in CD_2Cl_2 (377 MHz).



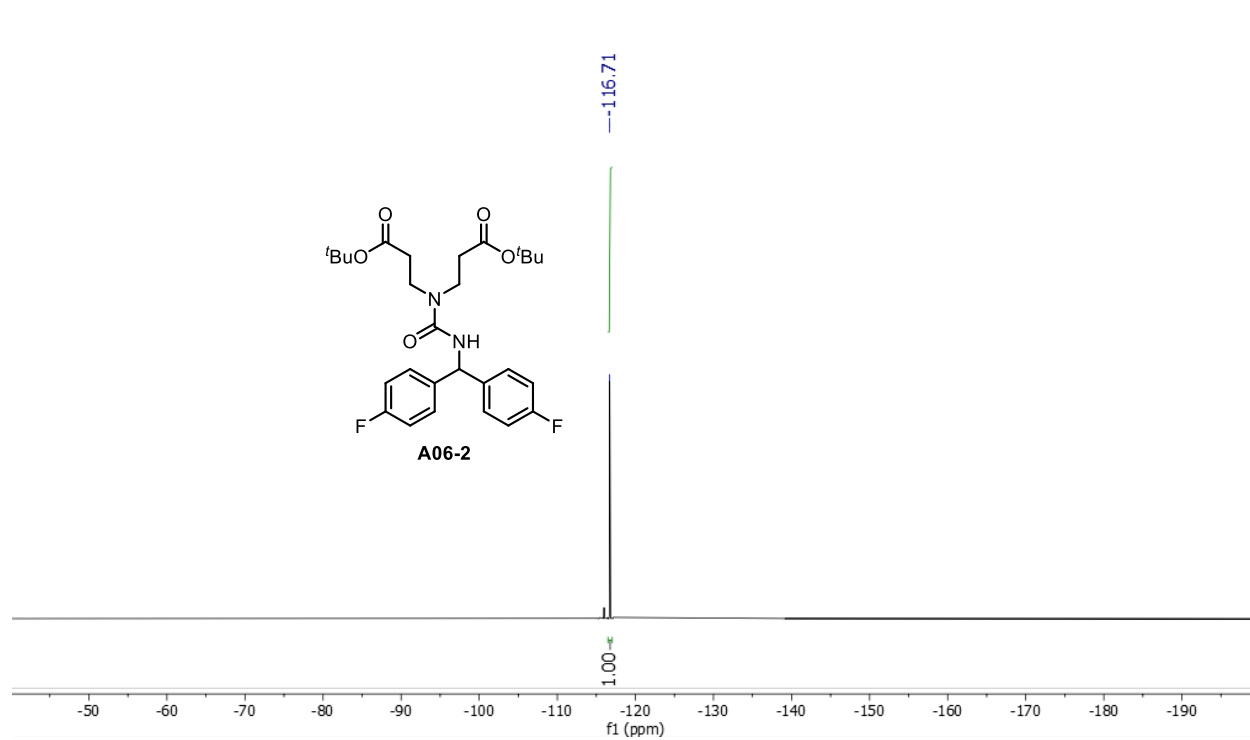
^1H NMR spectrum of **A06-2** in CD_2Cl_2 (500 MHz).



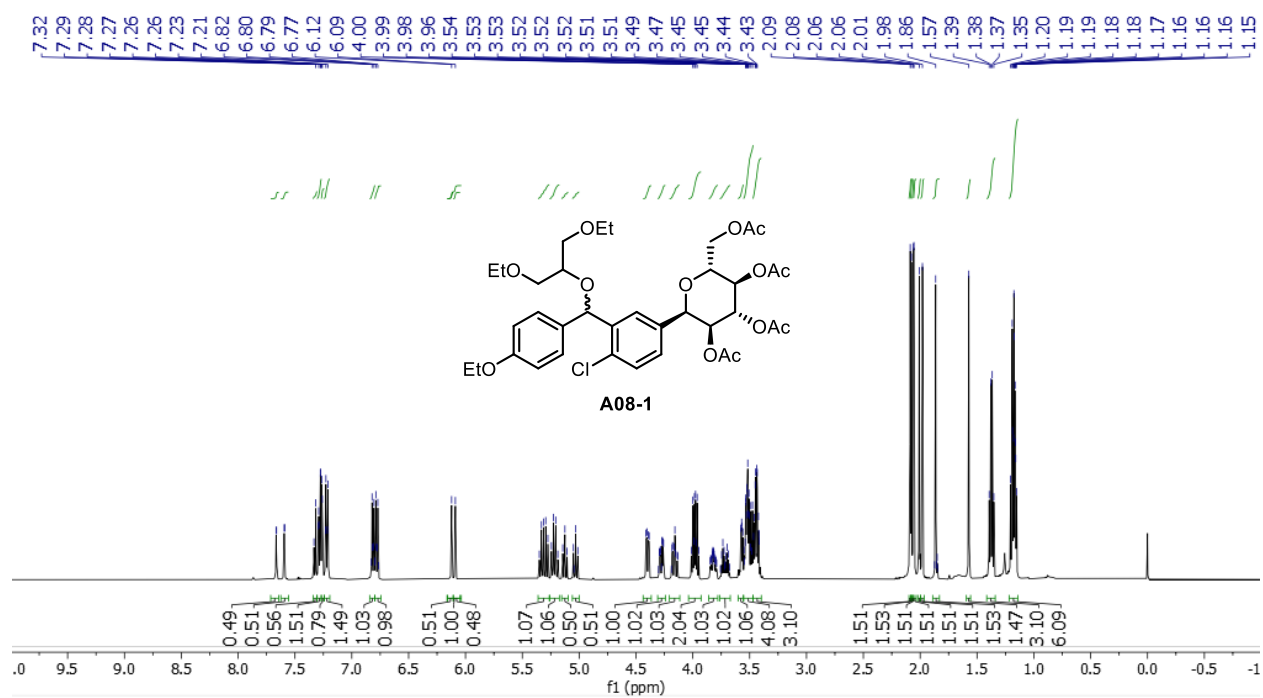
^{13}C NMR spectrum of **A06-2** in CD_2Cl_2 (126 MHz).



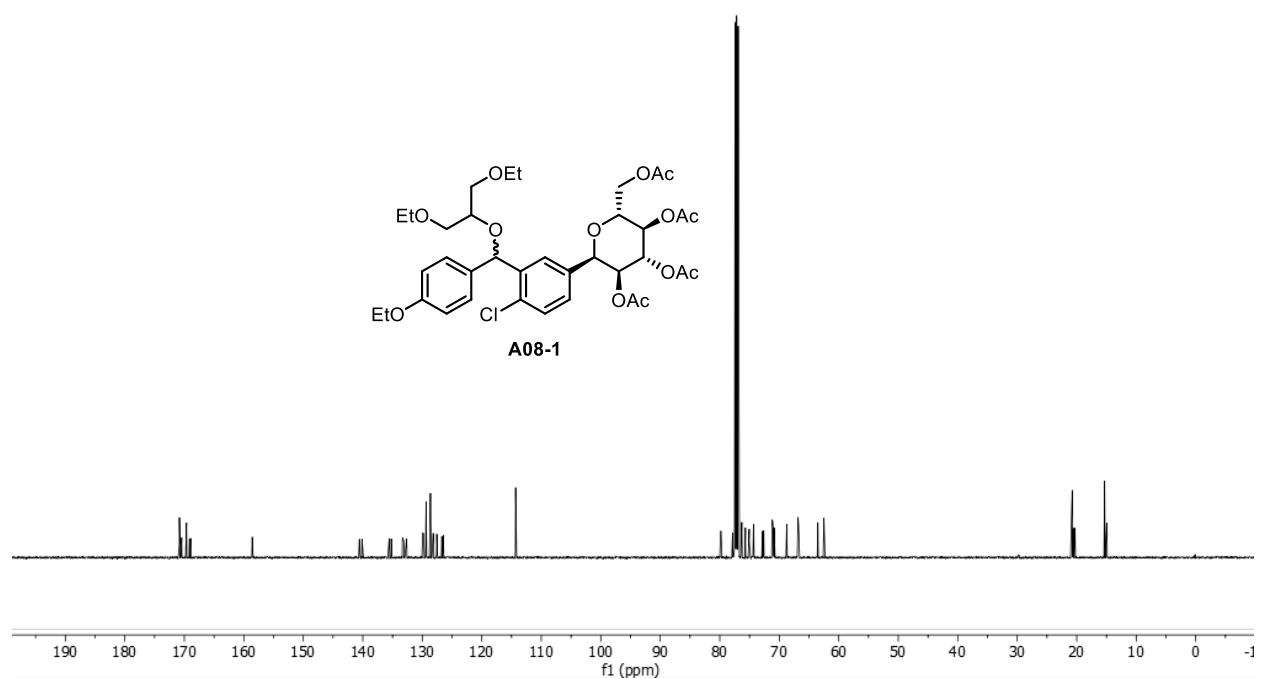
^{19}F NMR spectrum of **A06-2** in CD_2Cl_2 (377 MHz).



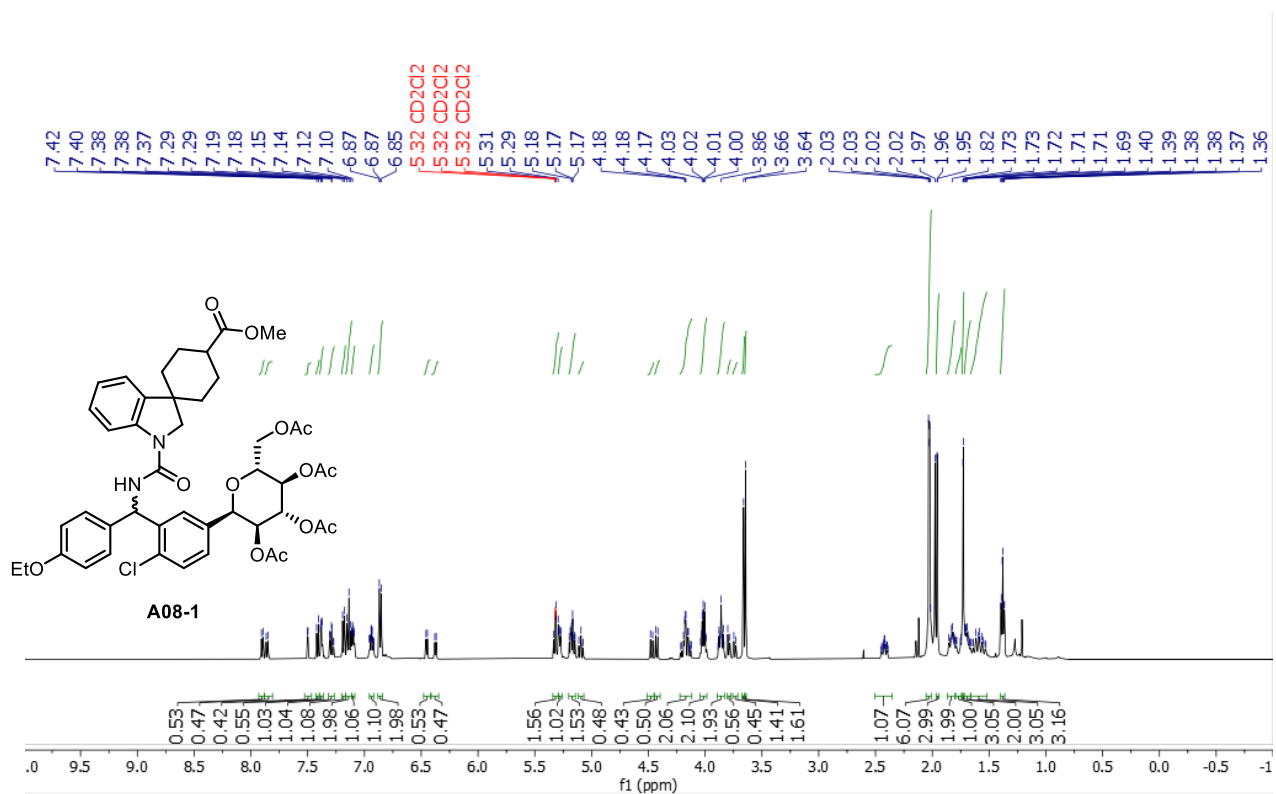
^1H NMR spectrum of **A08-1** in CDCl_3 containing 0.03 % (v/v) TMS (500 MHz).



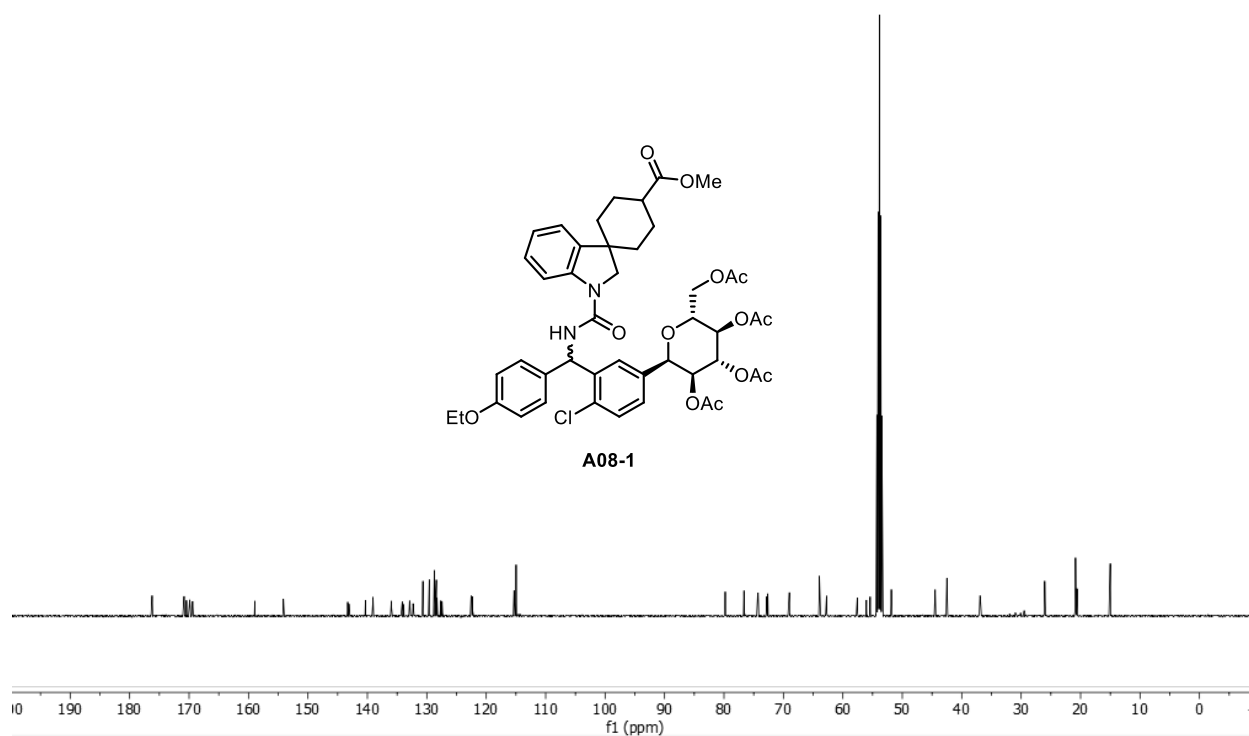
^{13}C NMR spectrum of **A08-1** in CDCl_3 containing 0.03 % (v/v) TMS (126 MHz).



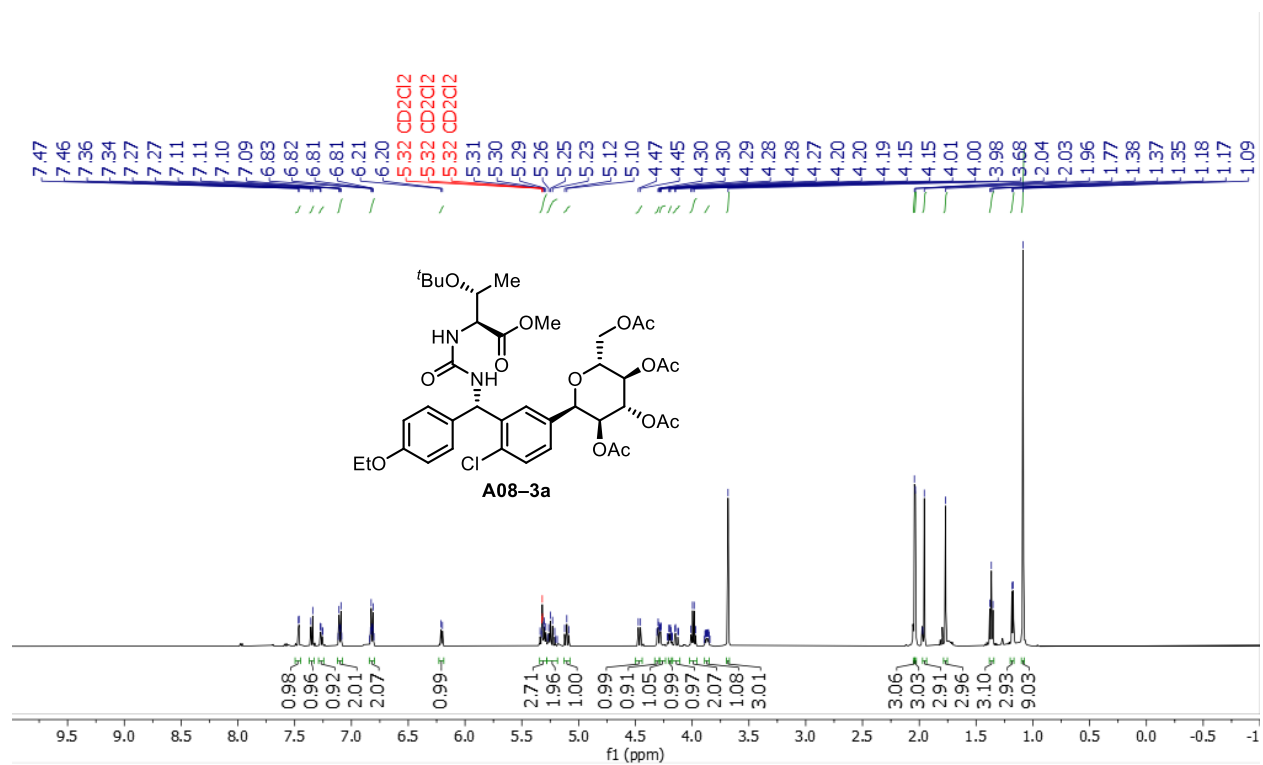
^1H NMR spectrum of **A08-2** in CD_2Cl_2 (500 MHz).



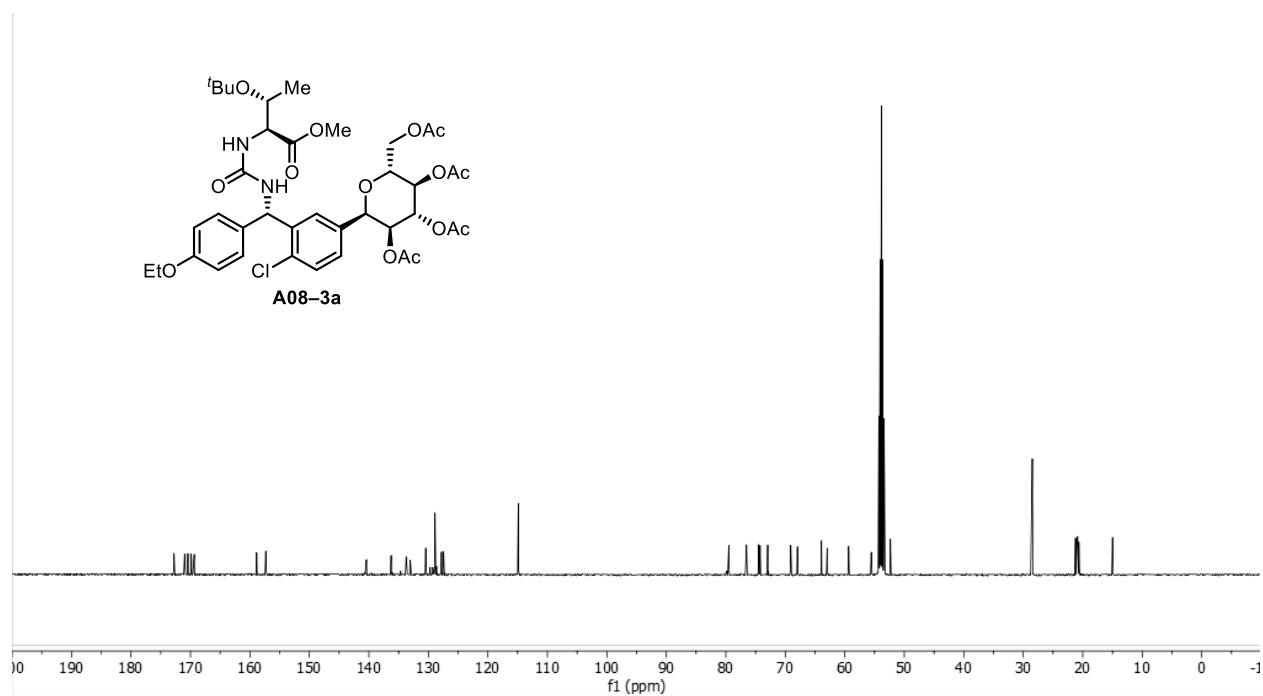
^{13}C NMR spectrum of **A08-2** in CD_2Cl_2 (126 MHz).



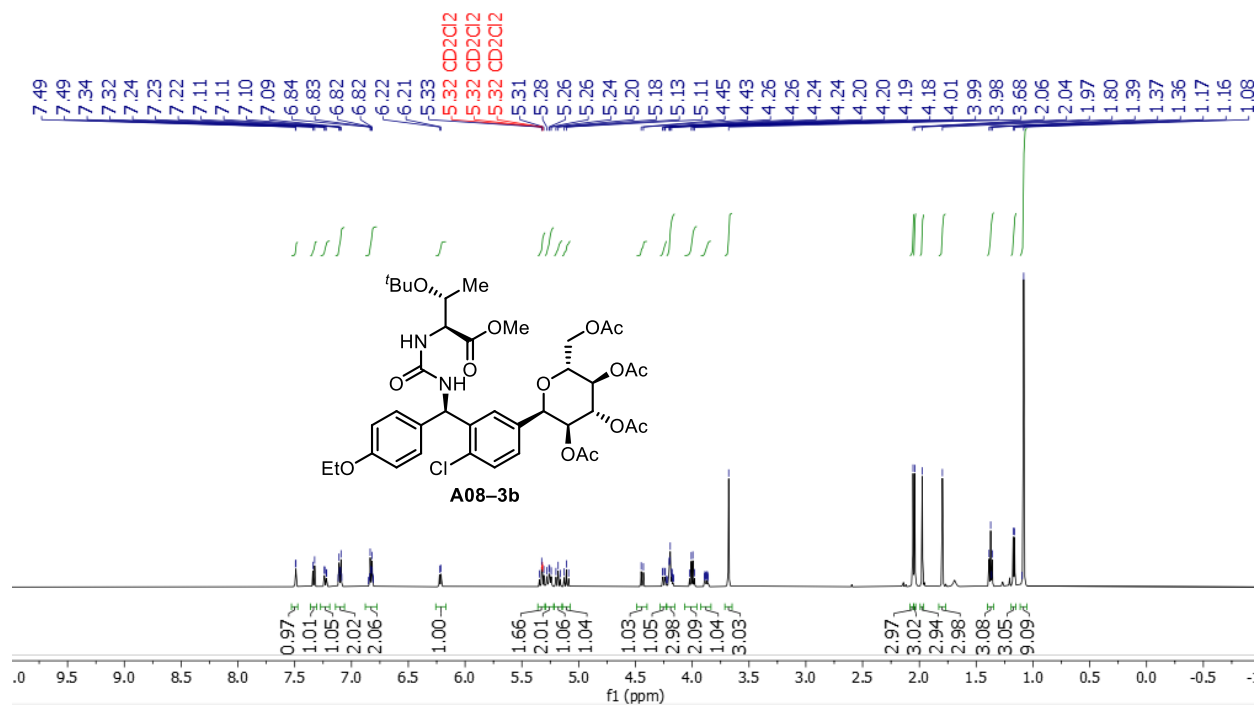
^1H NMR spectrum of **A08-3a** in CD_2Cl_2 (500 MHz).



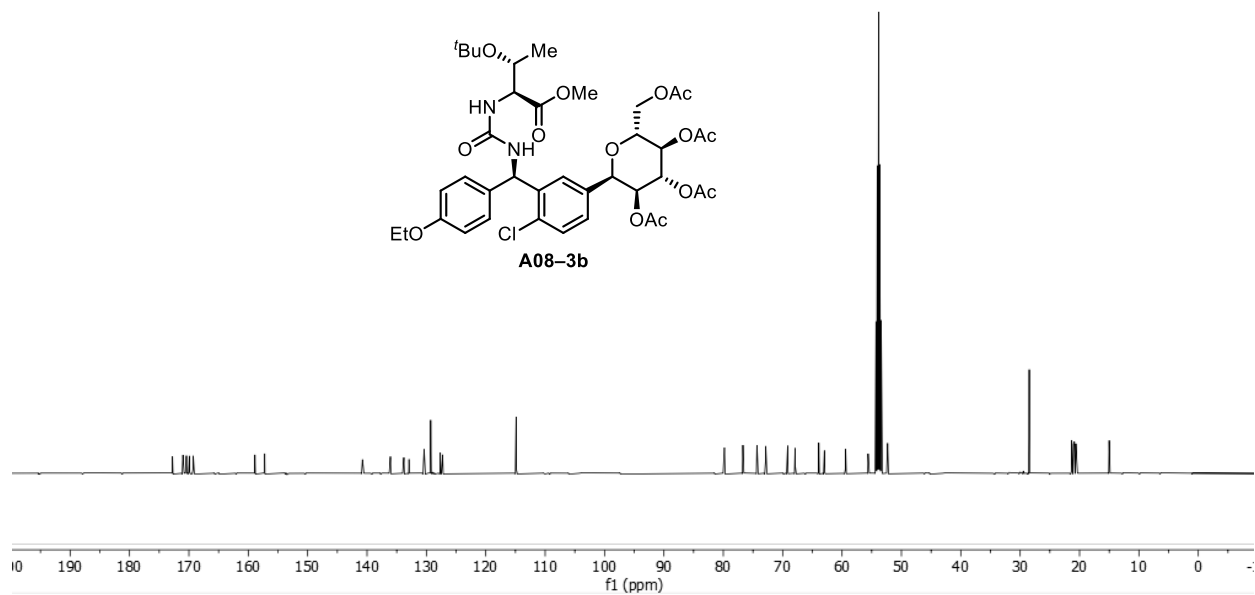
^{13}C NMR spectrum of **A08-3a** in CD_2Cl_2 (126 MHz).



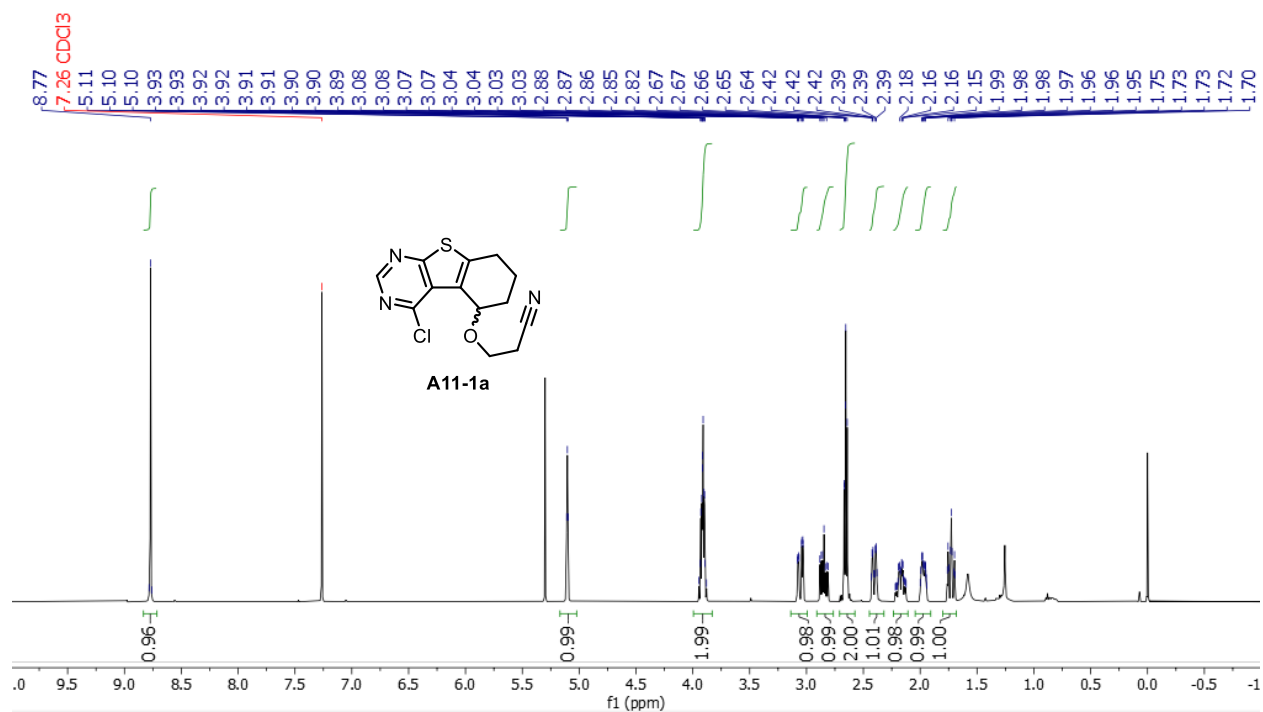
^1H NMR spectrum of **A08-3b** in CD_2Cl_2 (500 MHz).



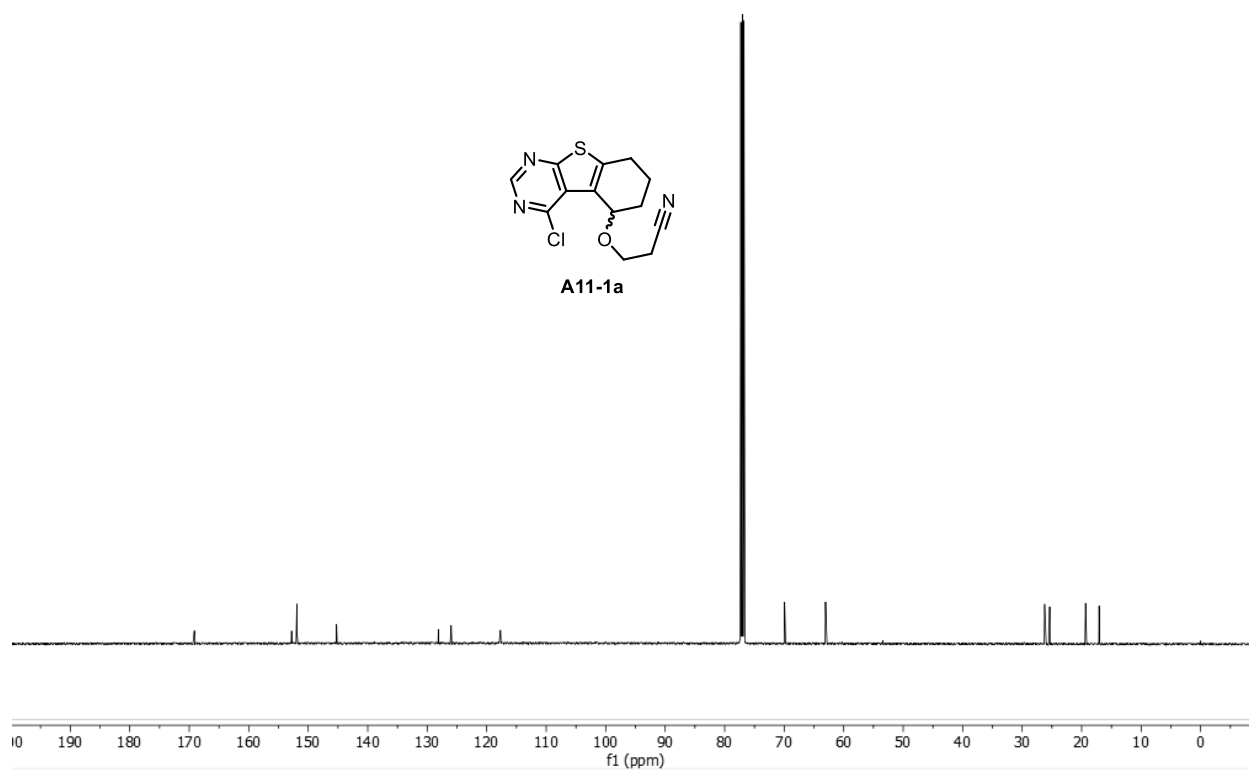
^{13}C NMR spectrum of **A08-3b** in CD_2Cl_2 (126 MHz).



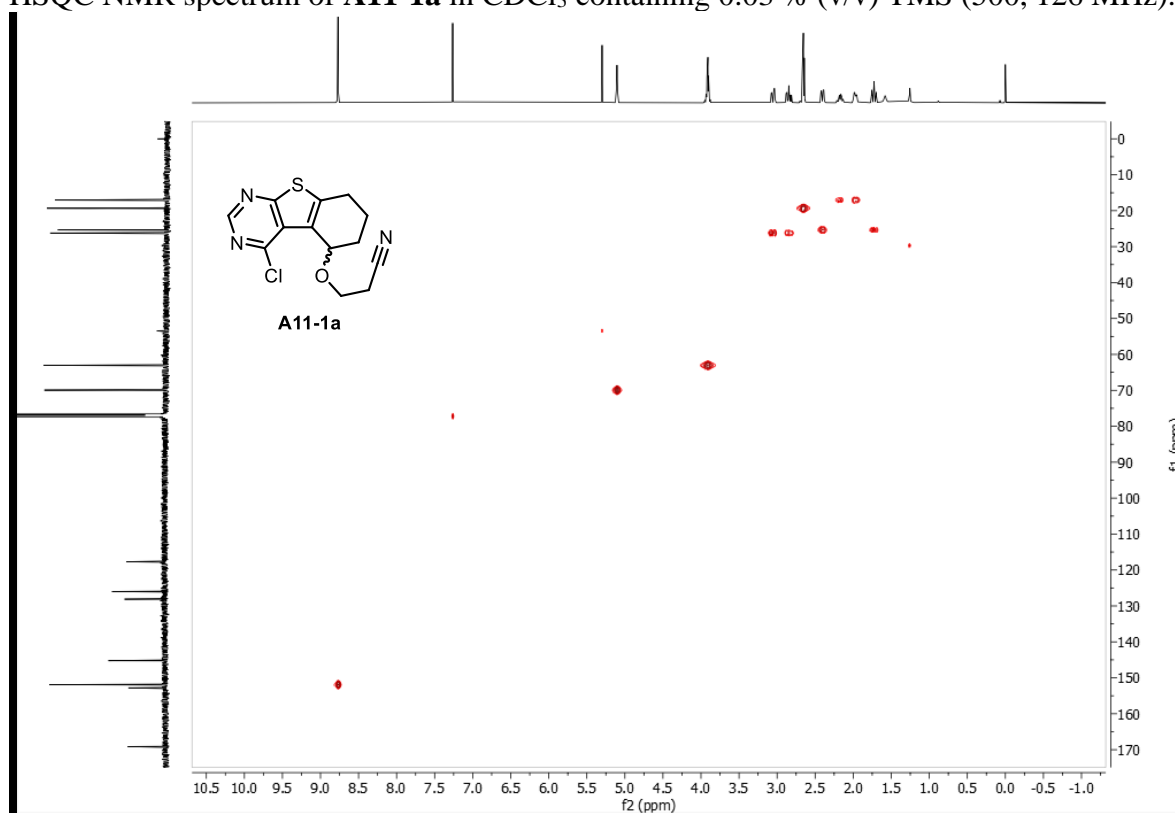
^1H NMR spectrum of **A11-1a** in CDCl_3 containing 0.03 % (v/v) TMS (500 MHz).



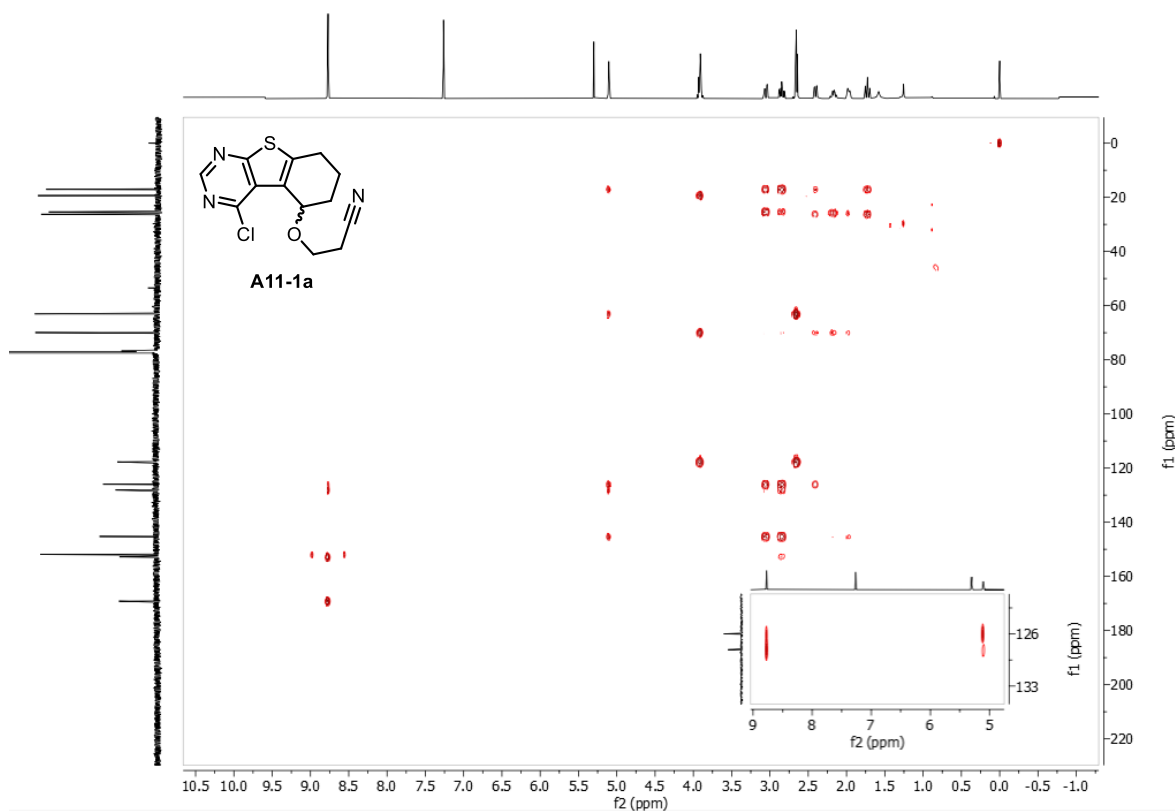
^{13}C NMR spectrum of **A11-1a** in CDCl_3 containing 0.03 % (v/v) TMS (126 MHz).



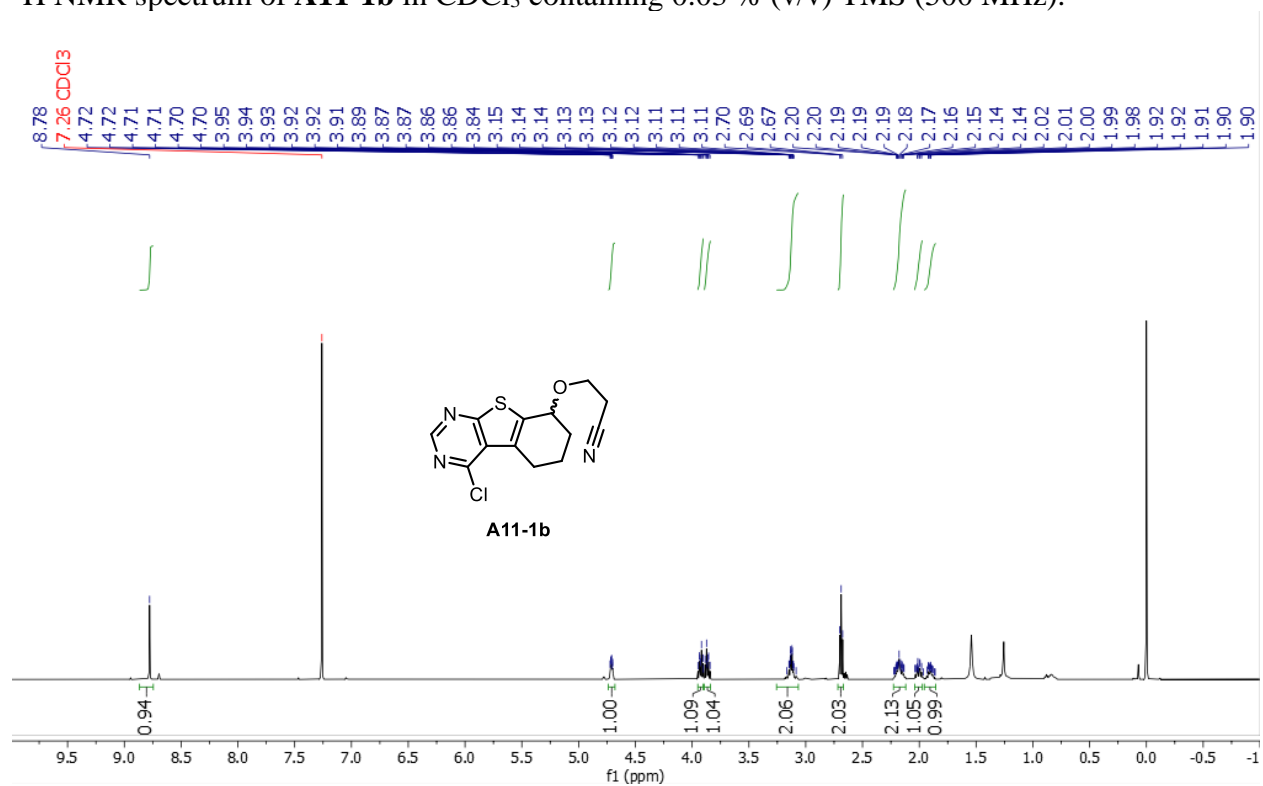
HSQC NMR spectrum of **A11-1a** in CDCl₃ containing 0.03 % (v/v) TMS (500, 126 MHz).



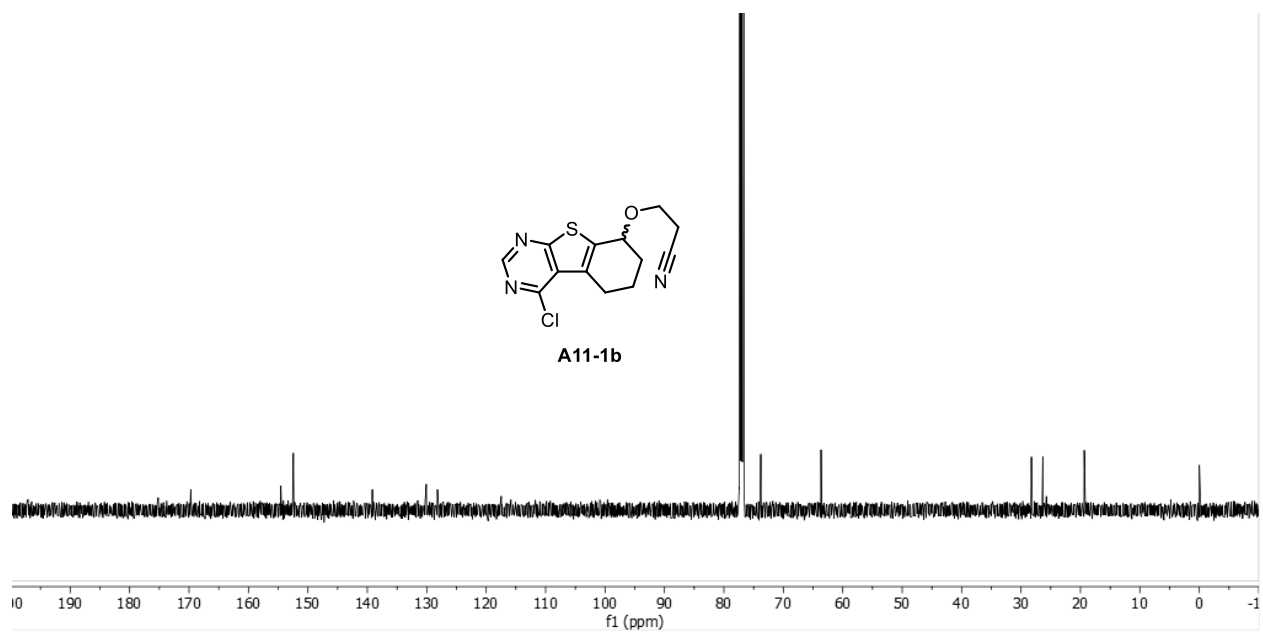
HMBC NMR spectrum of **A11-1a** in CDCl₃ containing 0.03 % (v/v) TMS (500, 126 MHz).



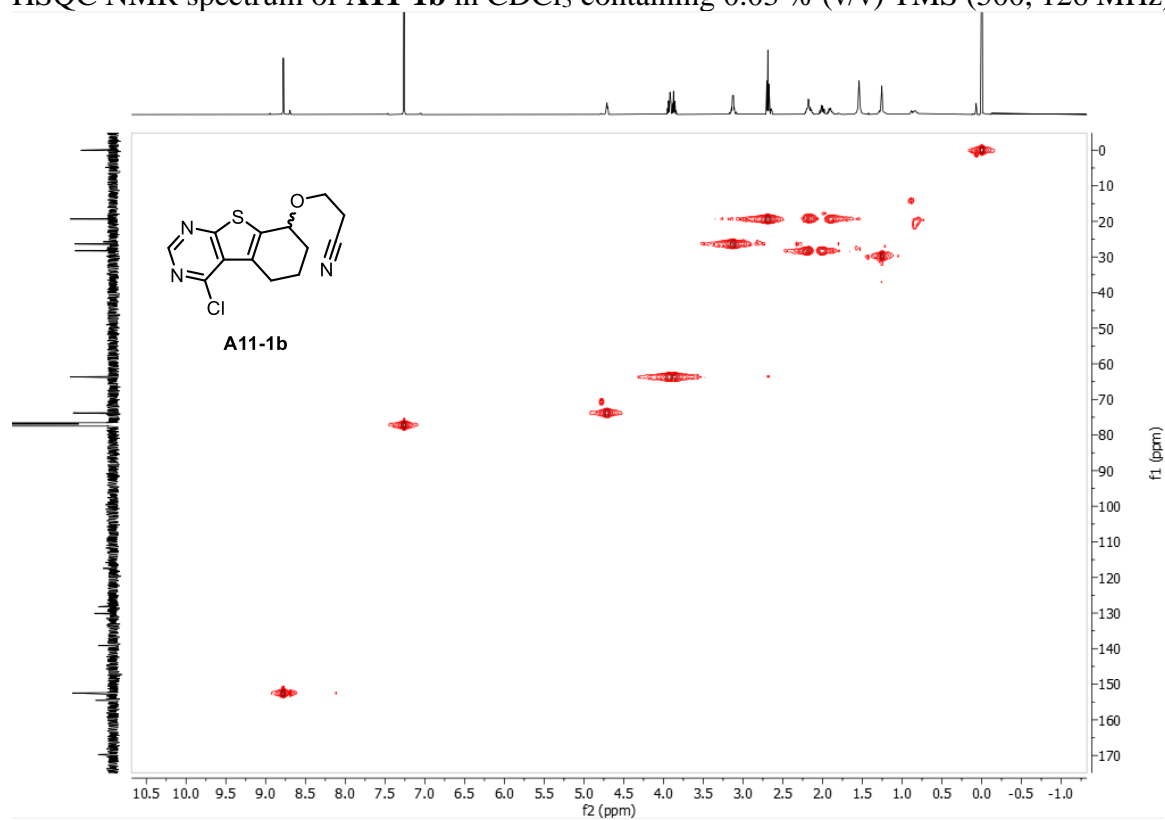
^1H NMR spectrum of **A11-1b** in CDCl_3 containing 0.03 % (v/v) TMS (500 MHz).



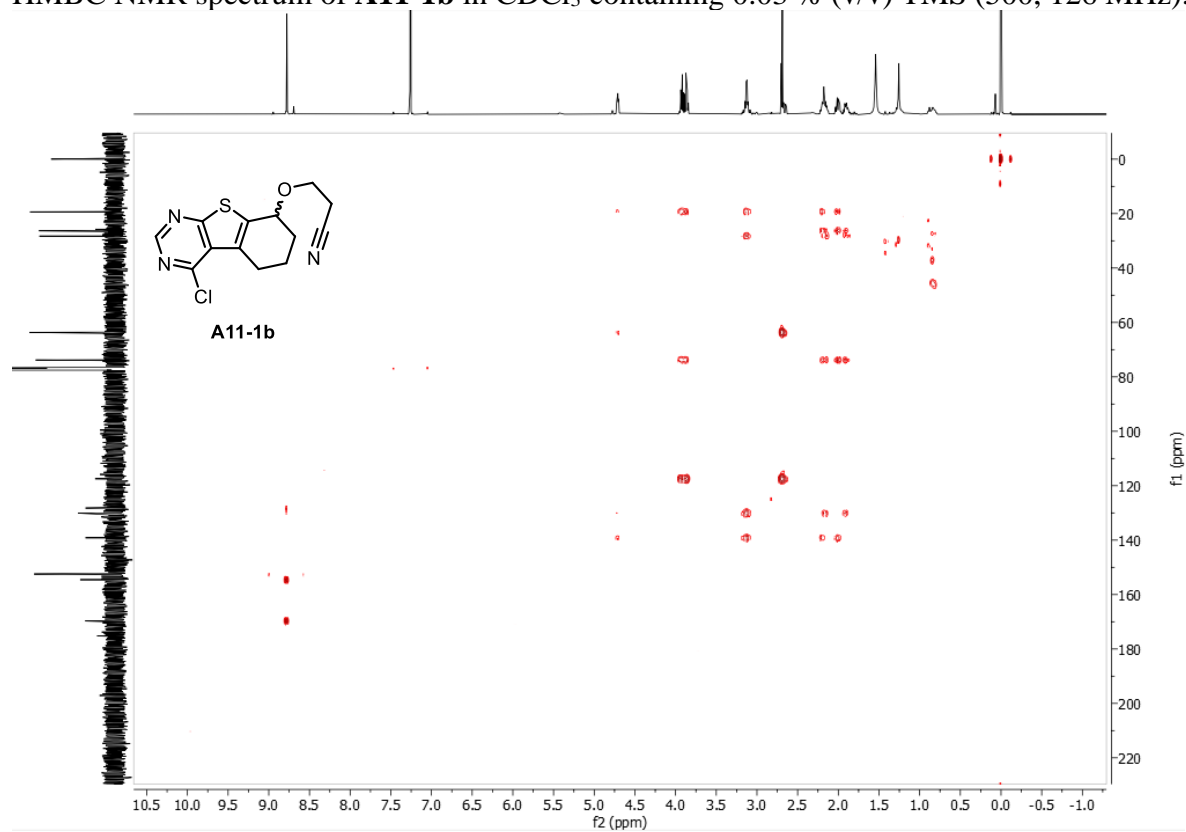
^{13}C NMR spectrum of **A11-1b** in CDCl_3 containing 0.03 % (v/v) TMS (126 MHz).



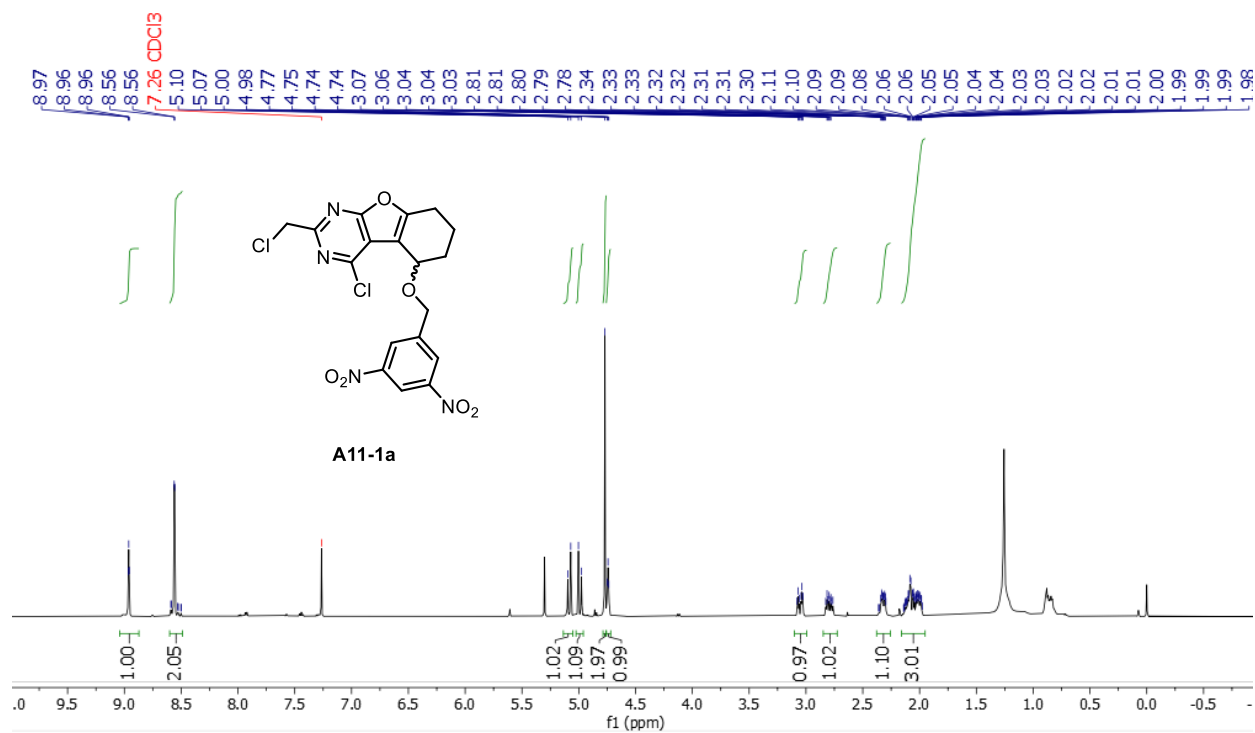
HSQC NMR spectrum of **A11-1b** in CDCl₃ containing 0.03 % (v/v) TMS (500, 126 MHz).



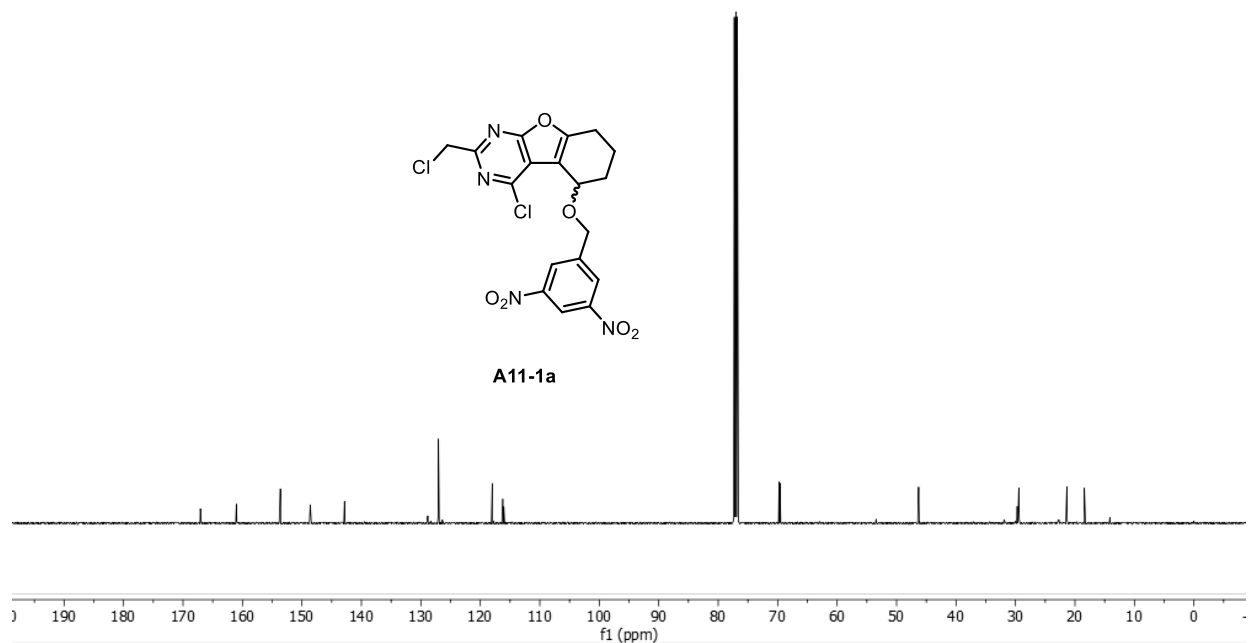
HMBC NMR spectrum of **A11-1b** in CDCl₃ containing 0.03 % (v/v) TMS (500, 126 MHz).



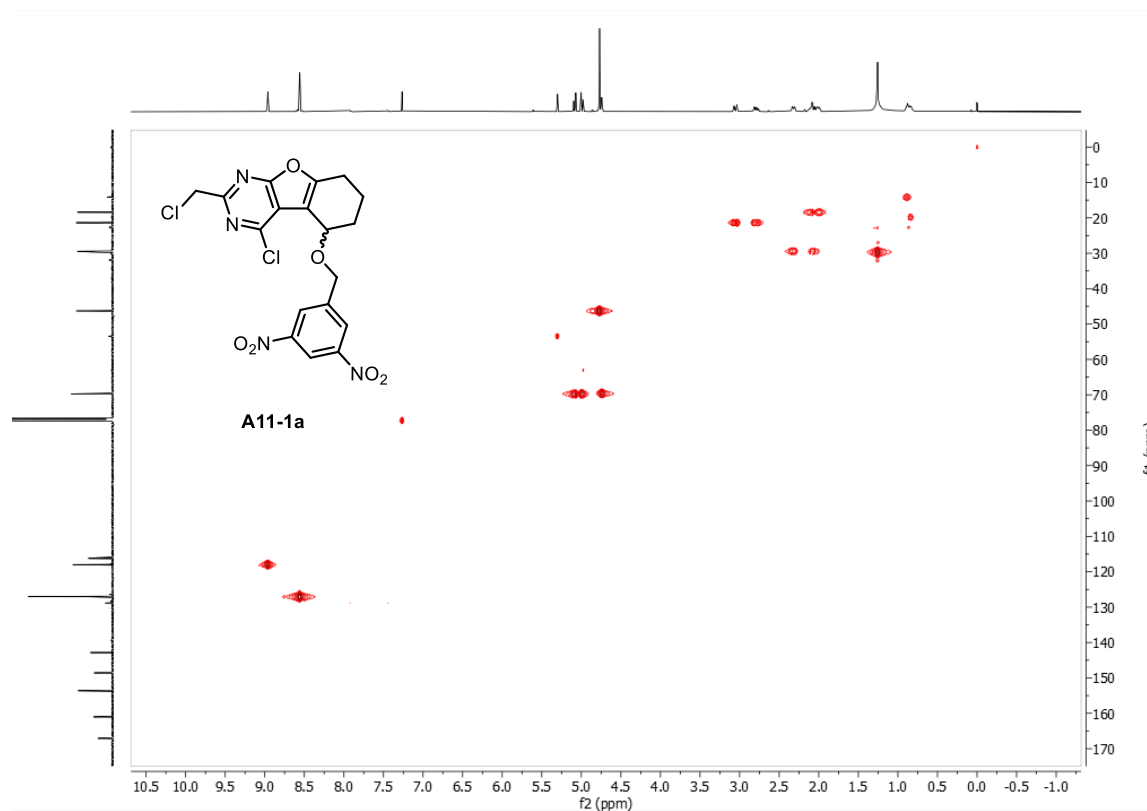
^1H NMR spectrum of **A12-1a** in CDCl_3 containing 0.03 % (v/v) TMS (500 MHz).



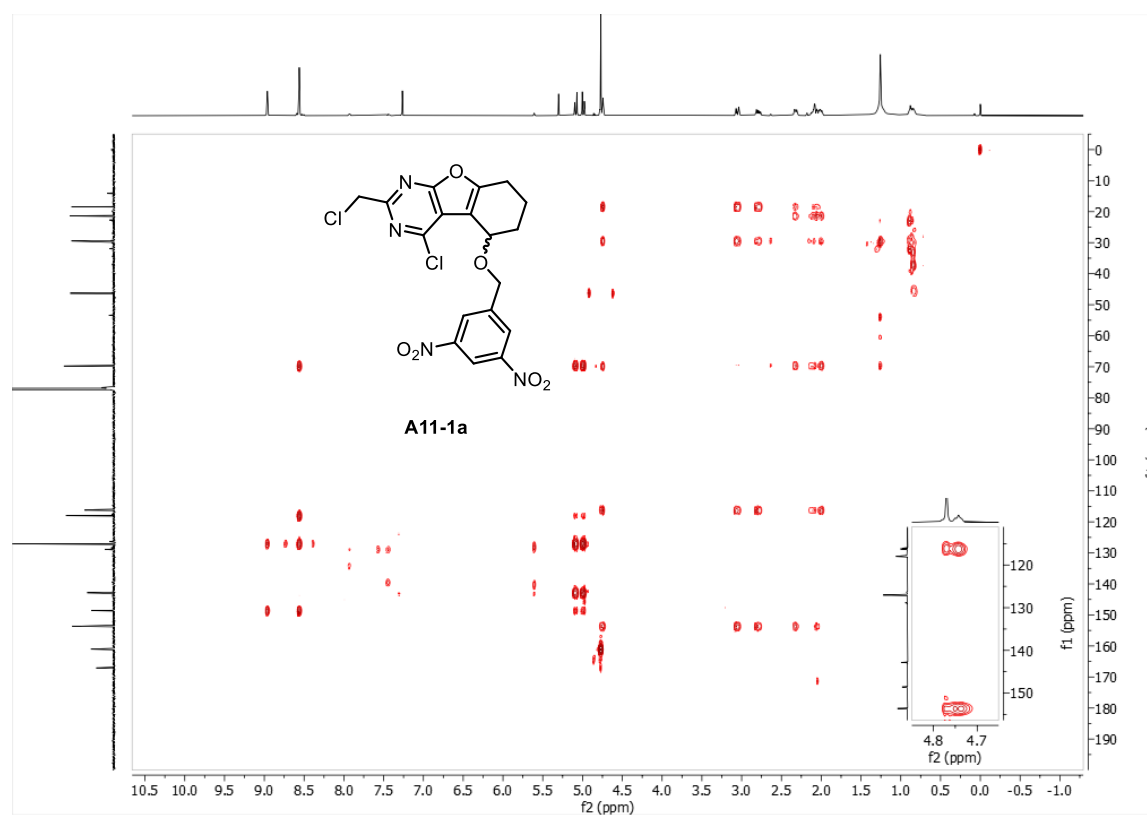
^{13}C NMR spectrum of **A12-1a** in CDCl_3 containing 0.03 % (v/v) TMS (126 MHz).



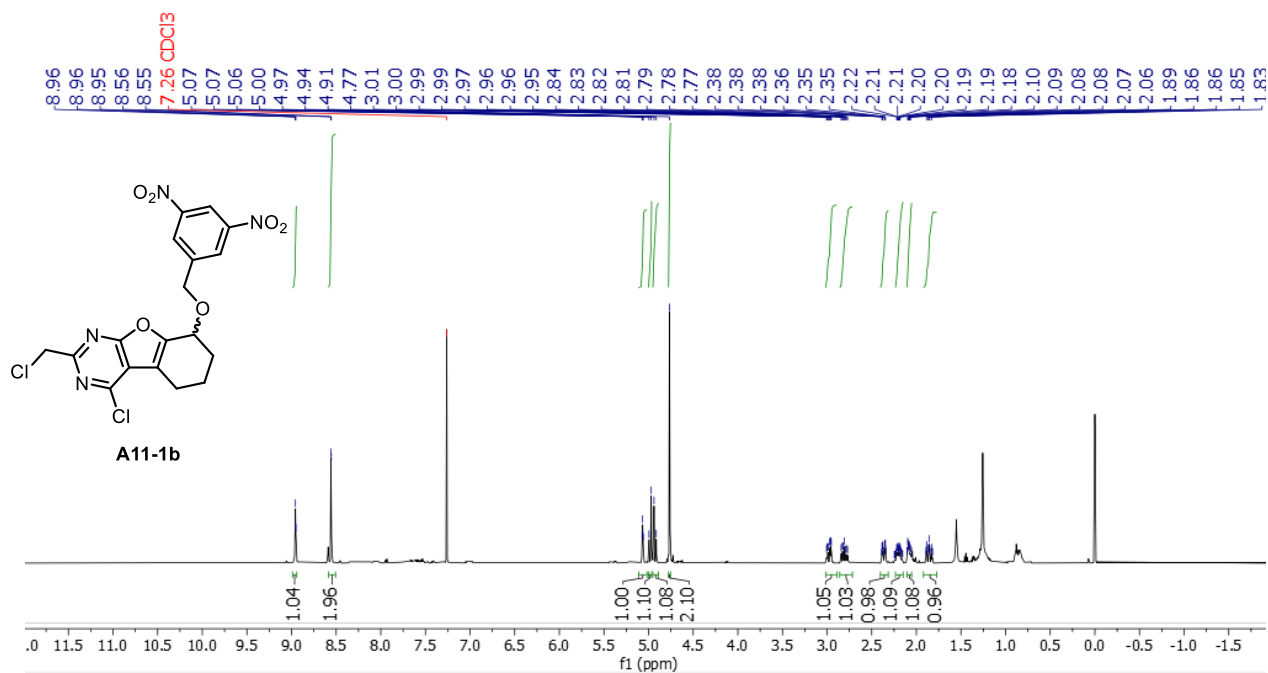
HSQC NMR spectrum of **A12-1a** in CDCl₃ containing 0.03 % (v/v) TMS (500, 126 MHz).



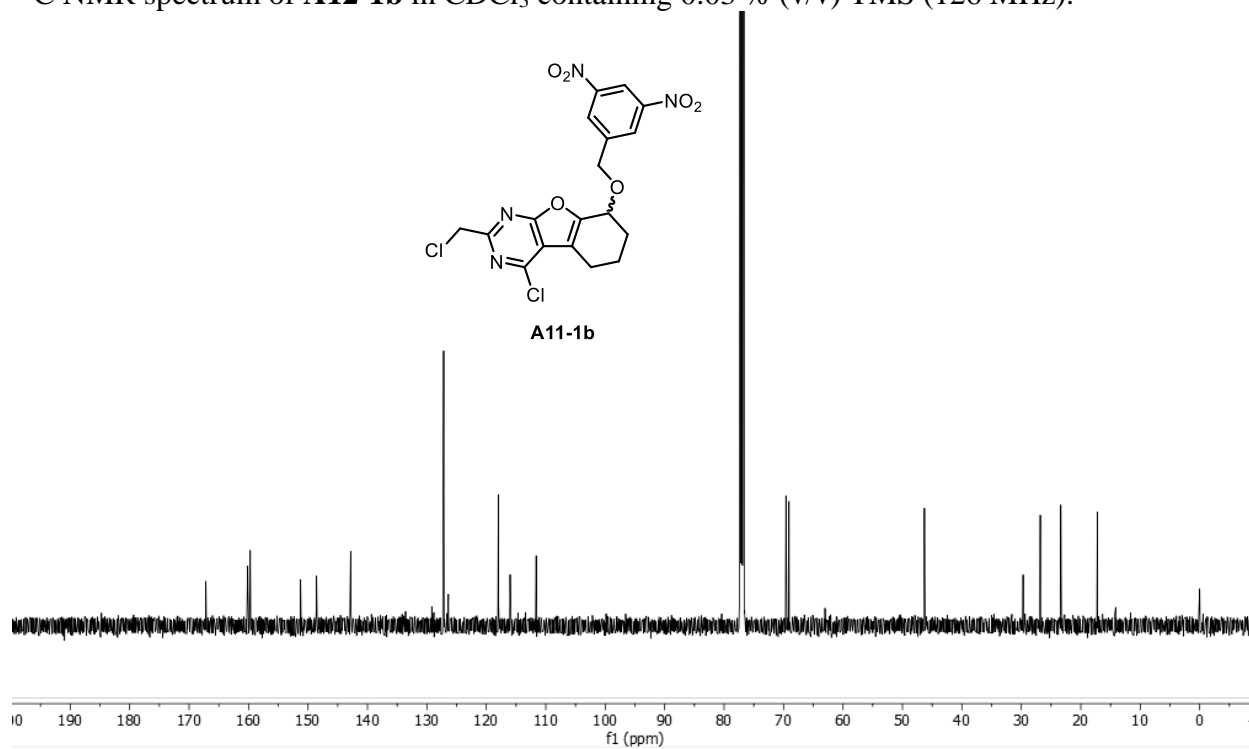
HMBC NMR spectrum of **A12-1a** in CDCl₃ containing 0.03 % (v/v) TMS (500, 126 MHz).



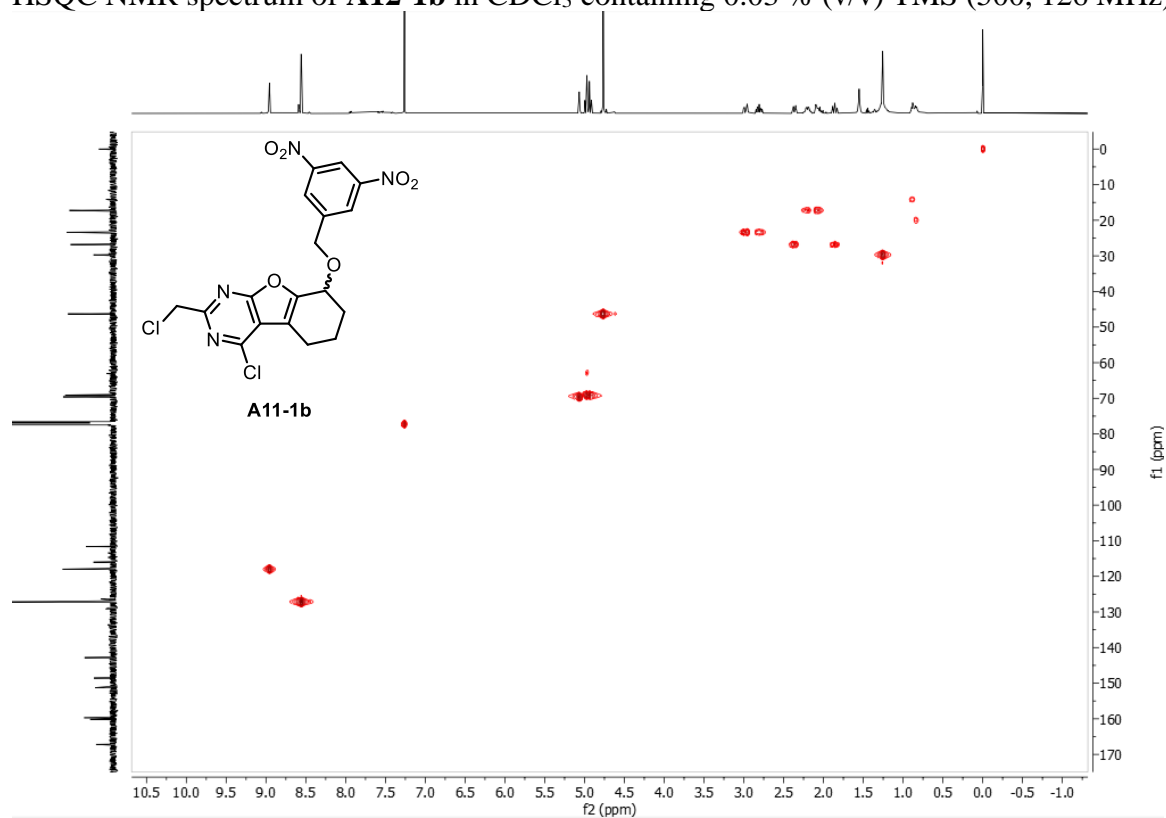
^1H NMR spectrum of **A12-1b** in CDCl_3 containing 0.03 % (v/v) TMS (500 MHz).



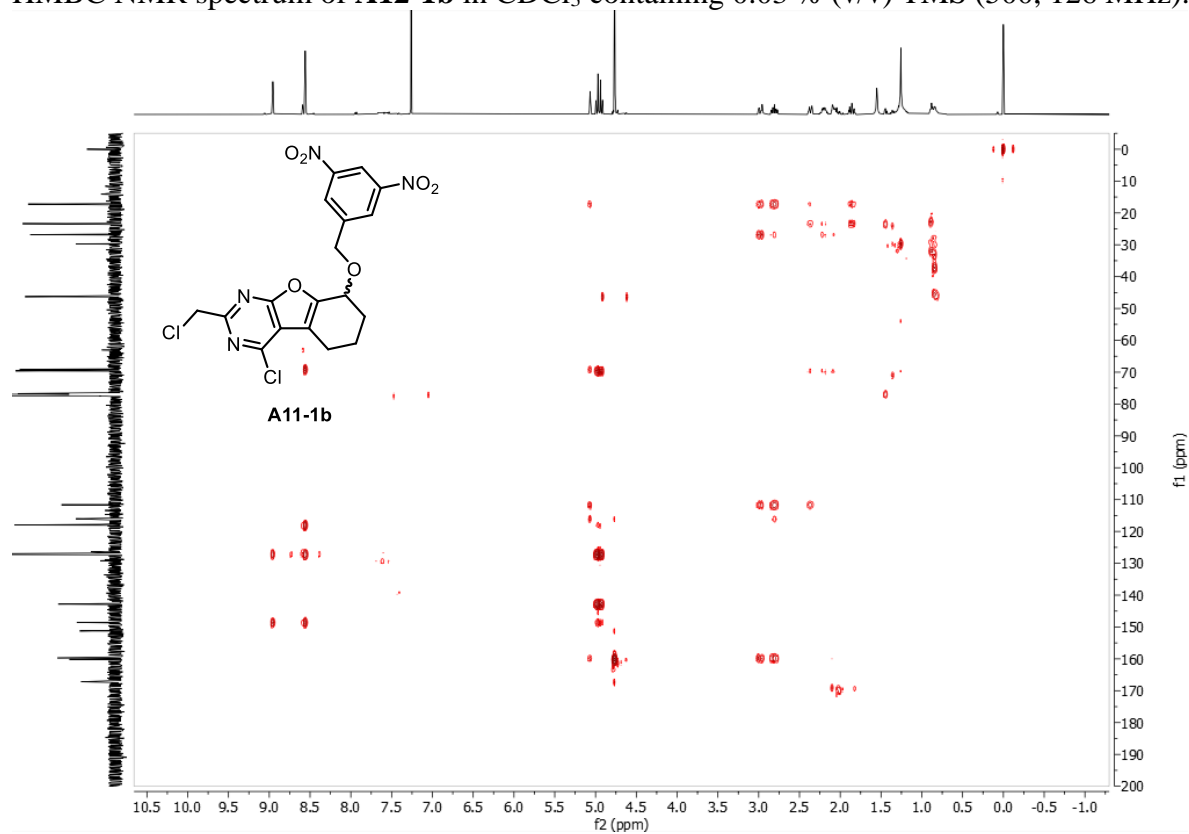
^{13}C NMR spectrum of **A12-1b** in CDCl_3 containing 0.03 % (v/v) TMS (126 MHz).



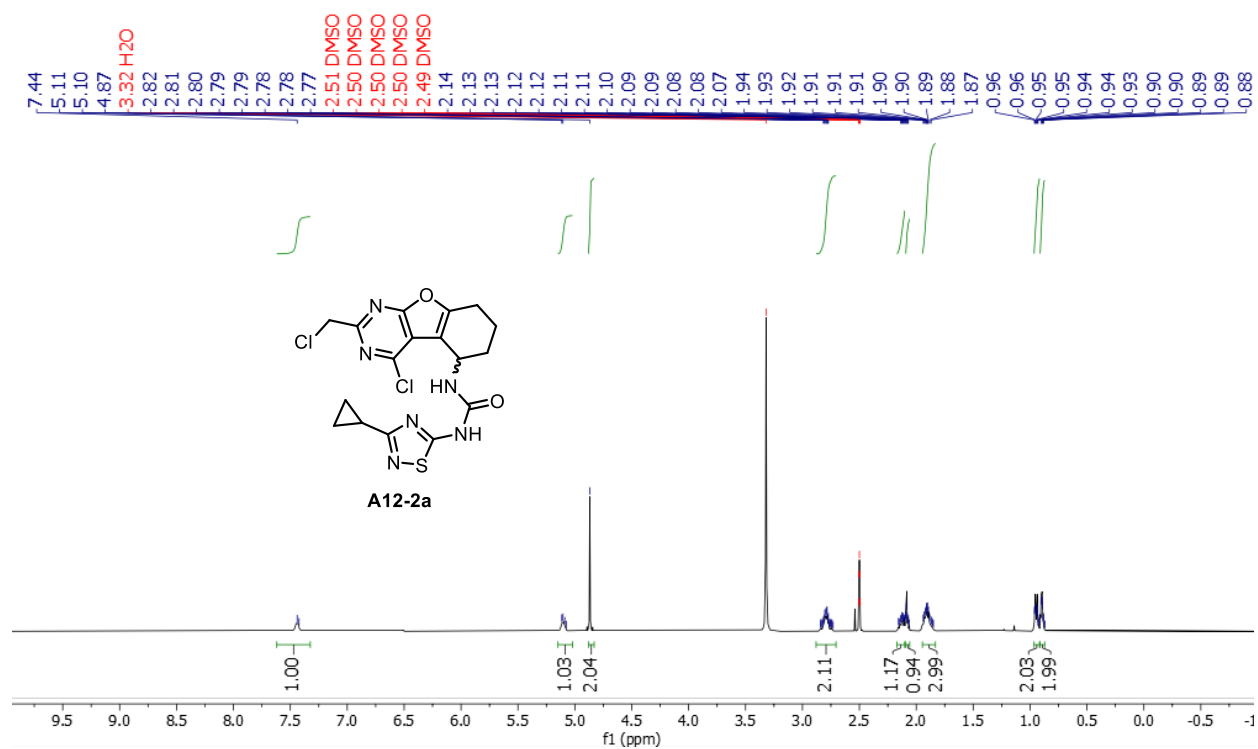
HSQC NMR spectrum of **A12-1b** in CDCl₃ containing 0.03 % (v/v) TMS (500, 126 MHz).



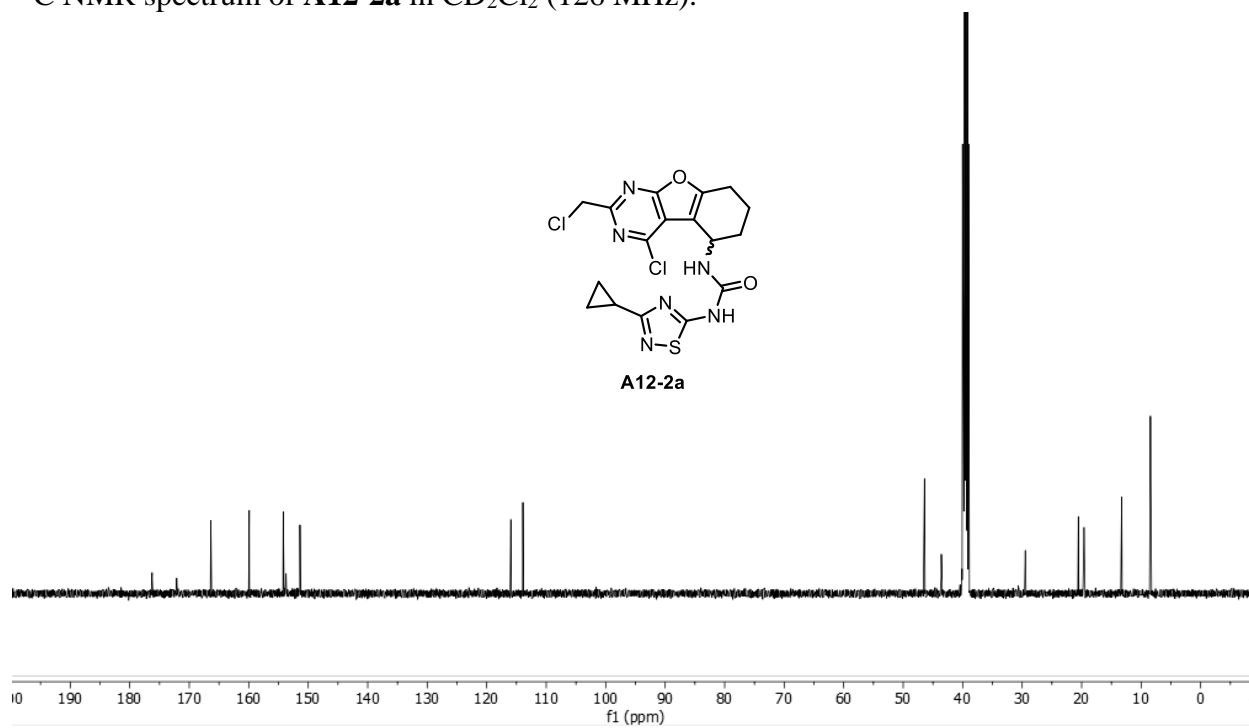
HMBC NMR spectrum of **A12-1b** in CDCl₃ containing 0.03 % (v/v) TMS (500, 126 MHz).

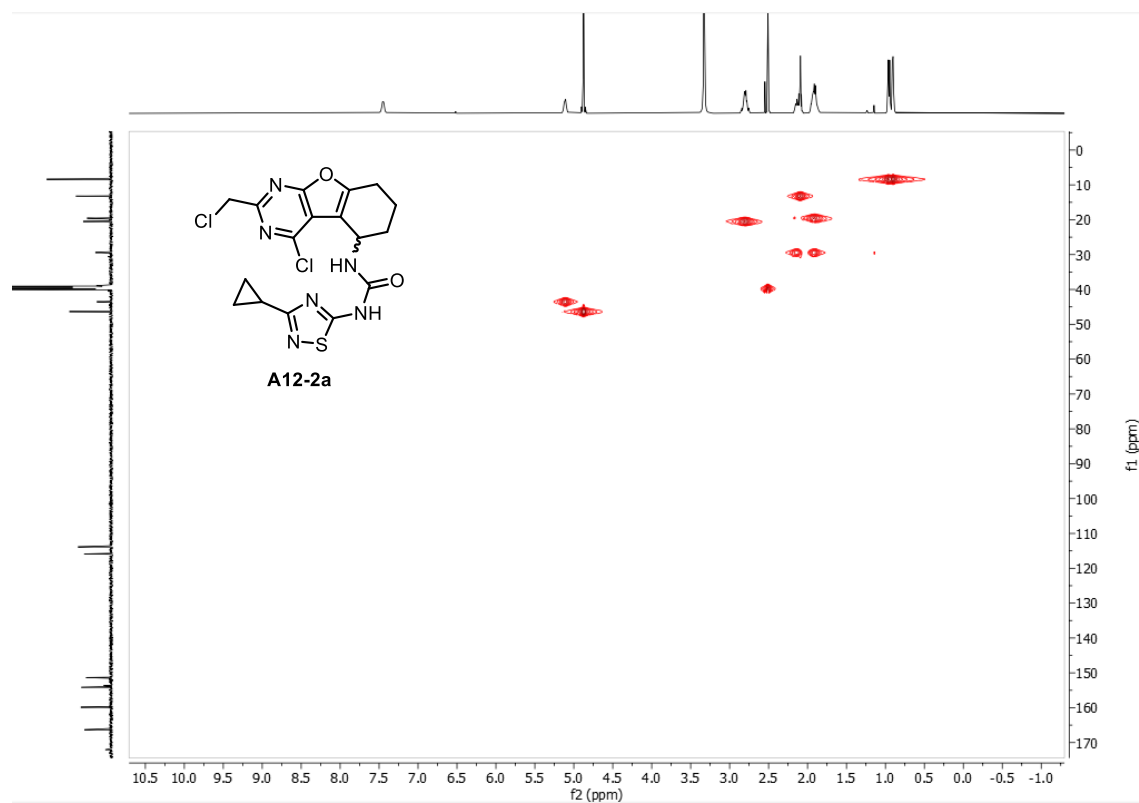
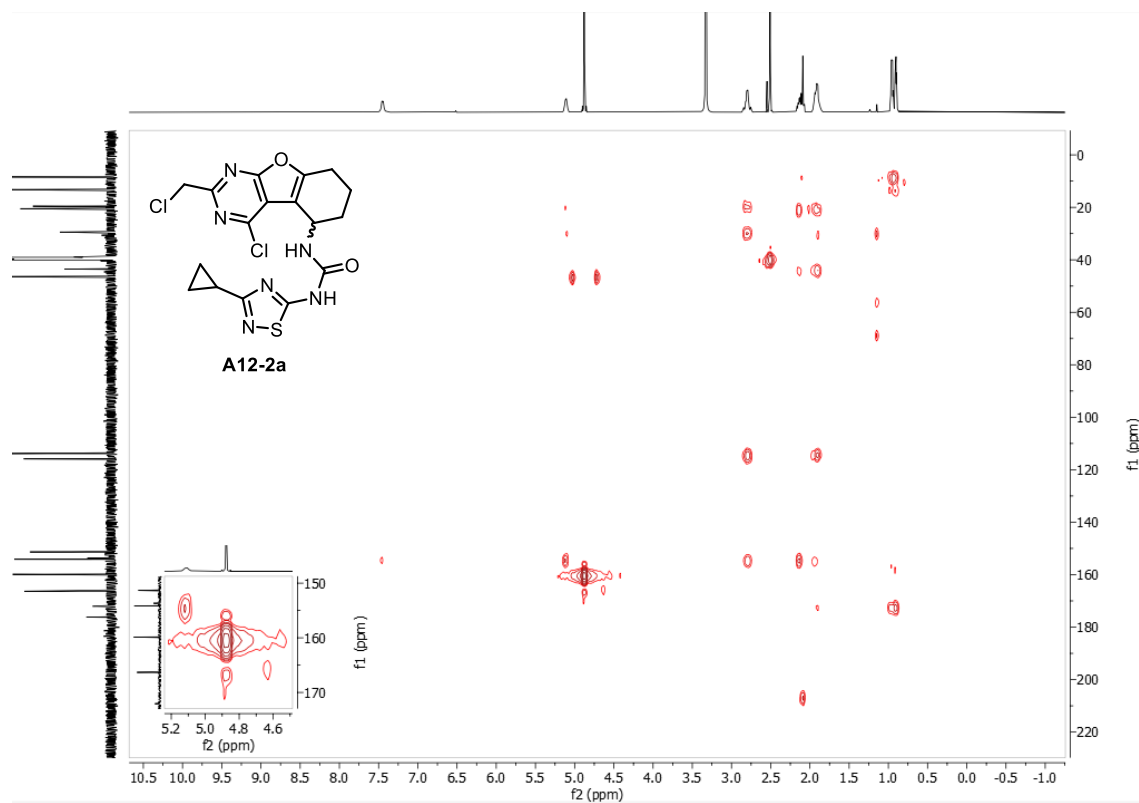


^1H NMR spectrum of **A12-2a** in CD_2Cl_2 (500 MHz).

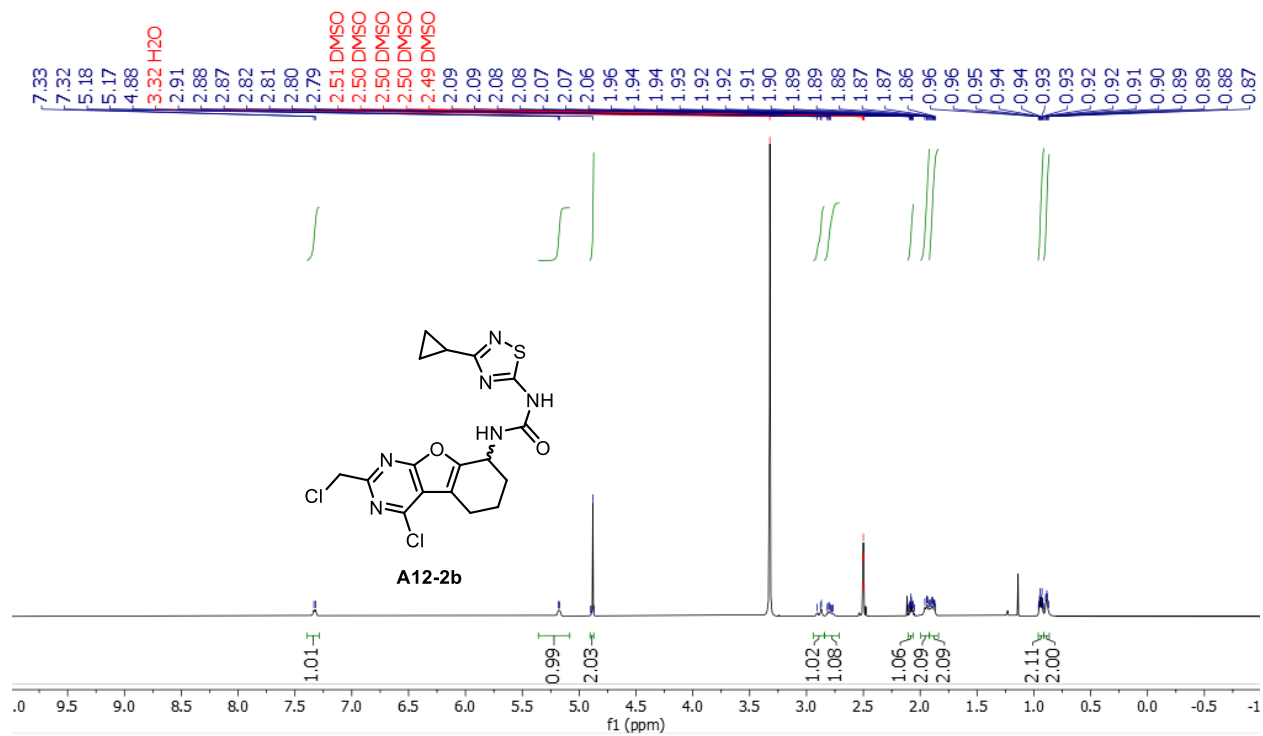


^{13}C NMR spectrum of **A12-2a** in CD_2Cl_2 (126 MHz).

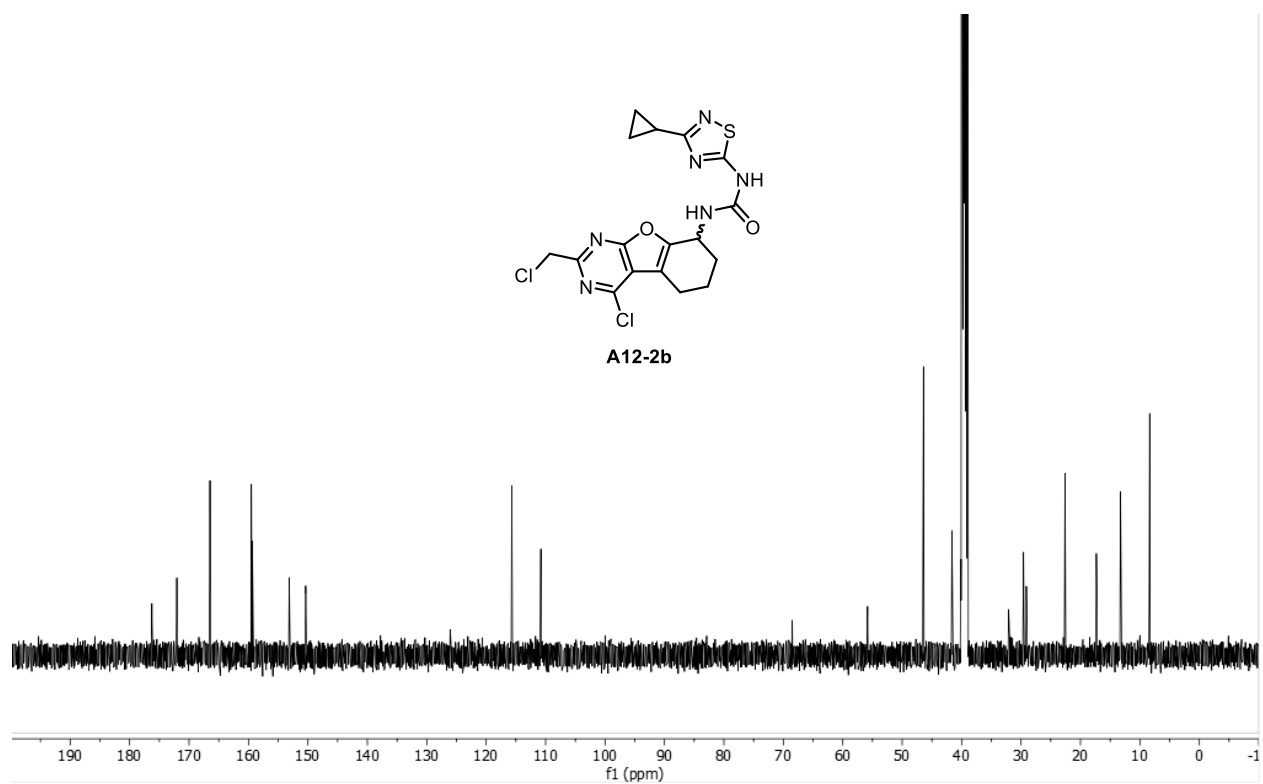


HSQC NMR spectrum of **A12-2a** in CD₂Cl₂ (500, 126 MHz).HMBC NMR spectrum of **A12-2a** in CD₂Cl₂ (500, 126 MHz).

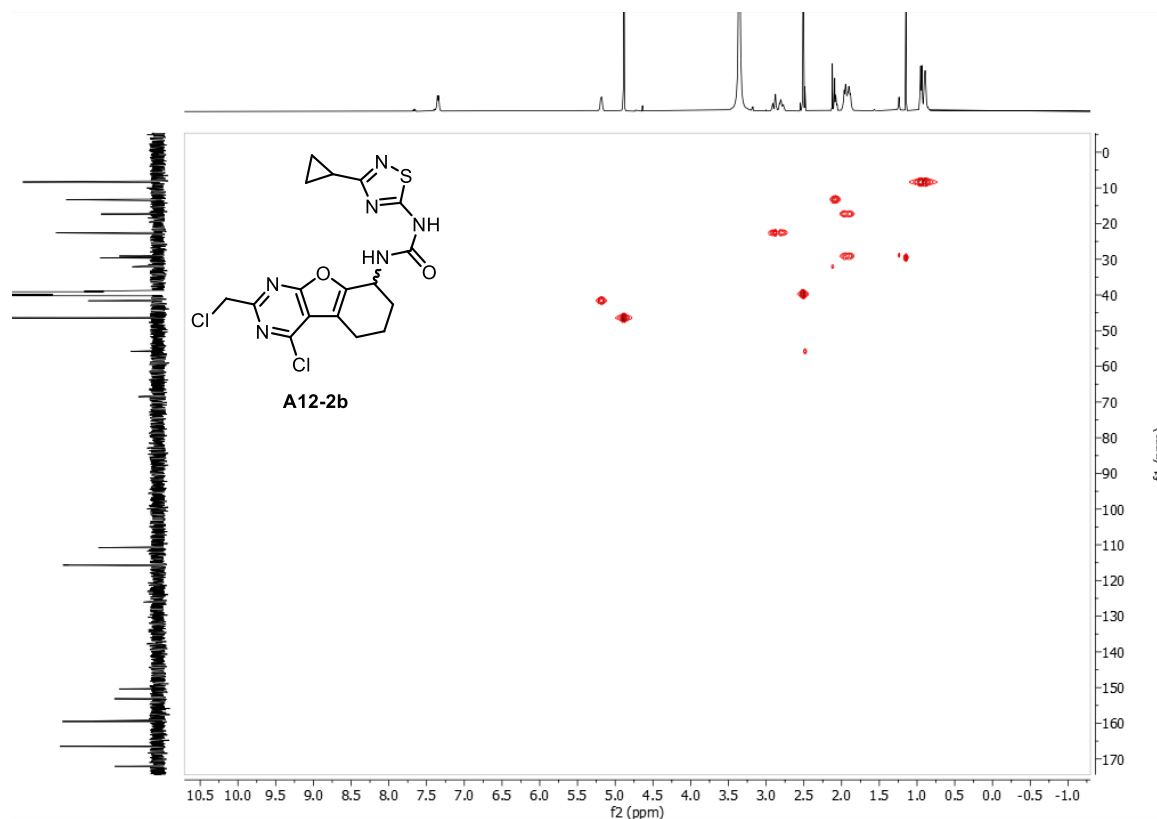
^1H NMR spectrum of **A12-2b** in CD_2Cl_2 (500 MHz).



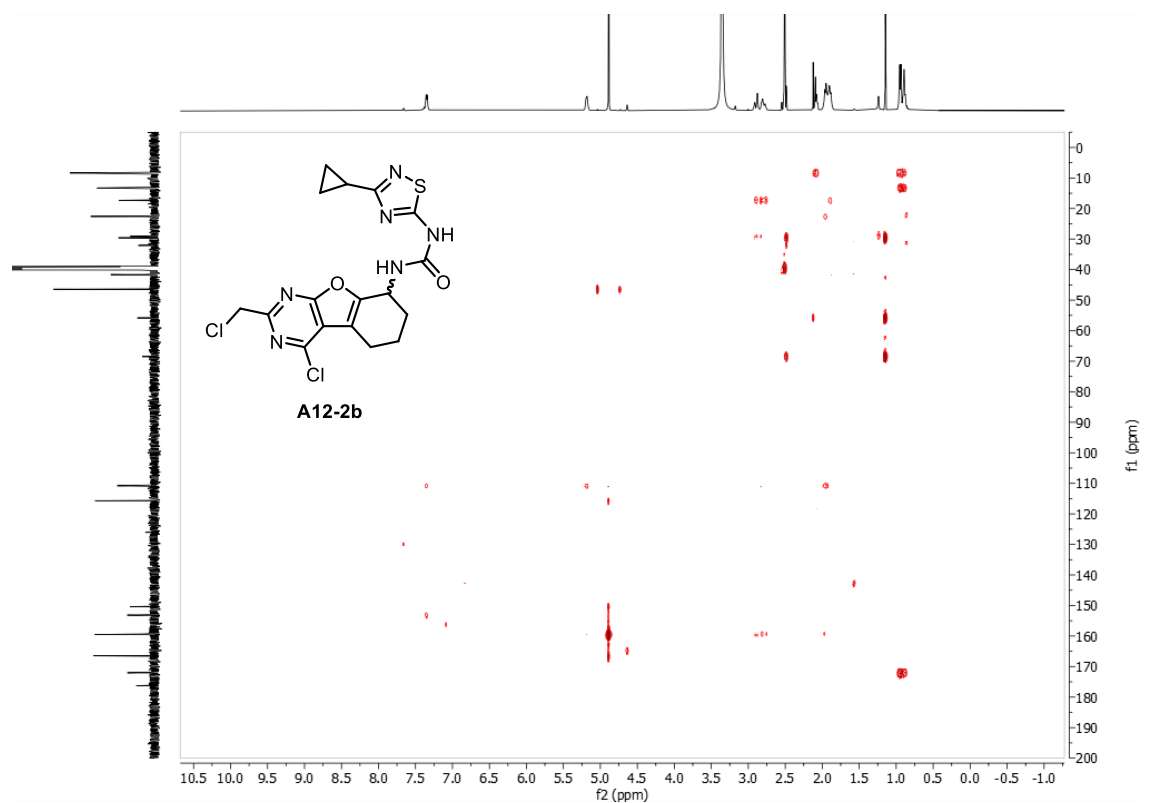
^{13}C NMR spectrum of **A12-2b** in CD_2Cl_2 (126 MHz).



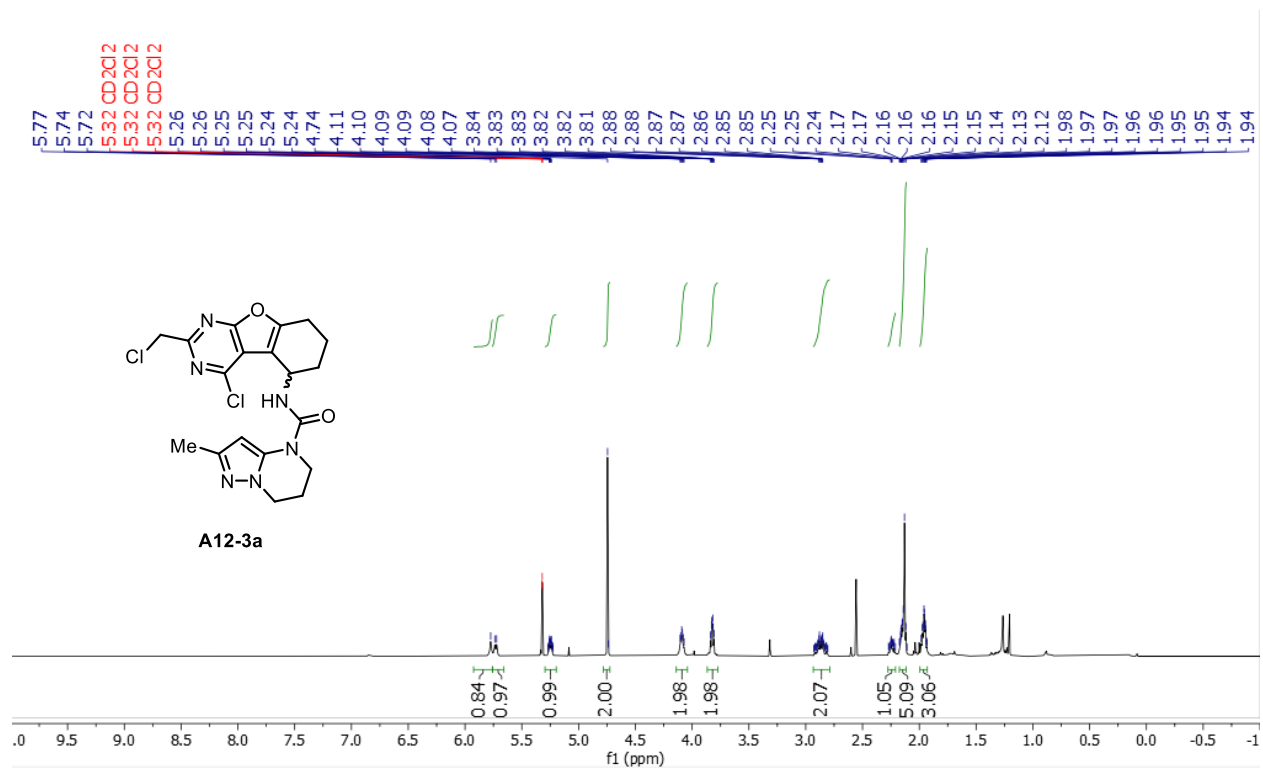
HSQC NMR spectrum of **A12-2b** in CD₂Cl₂ (500, 126 MHz).



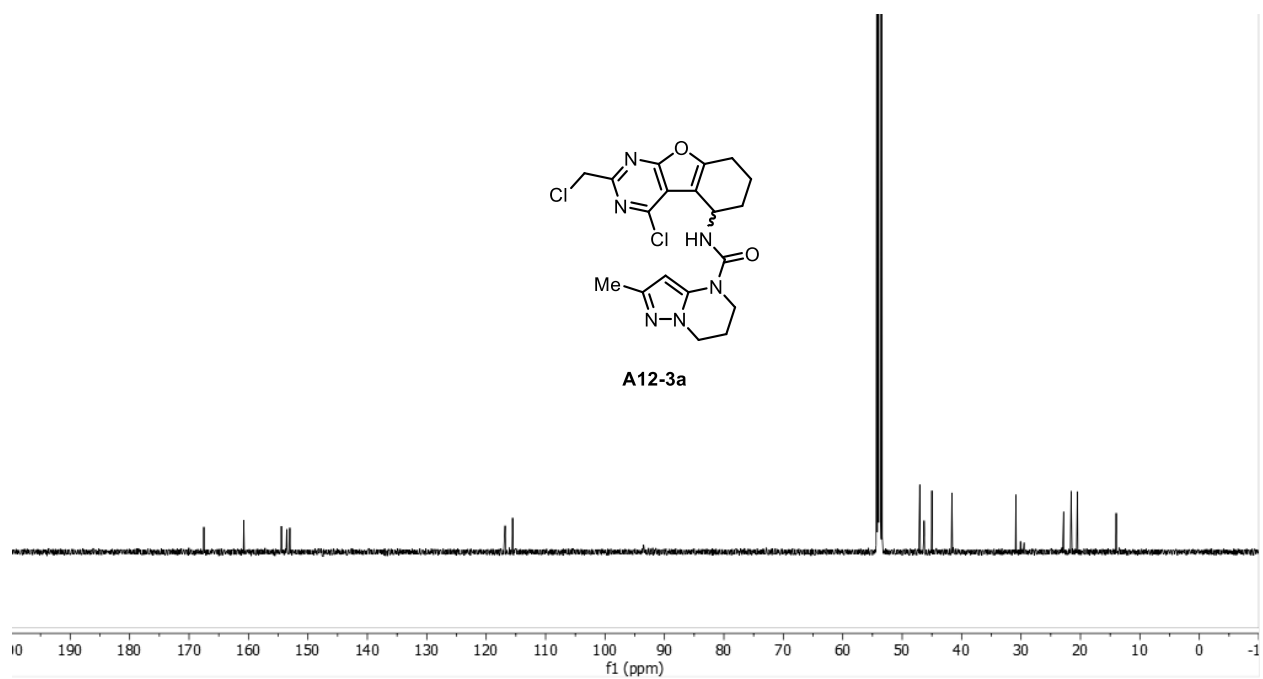
HMBC NMR spectrum of **A12-2a** in CD₂Cl₂ (500, 126 MHz).

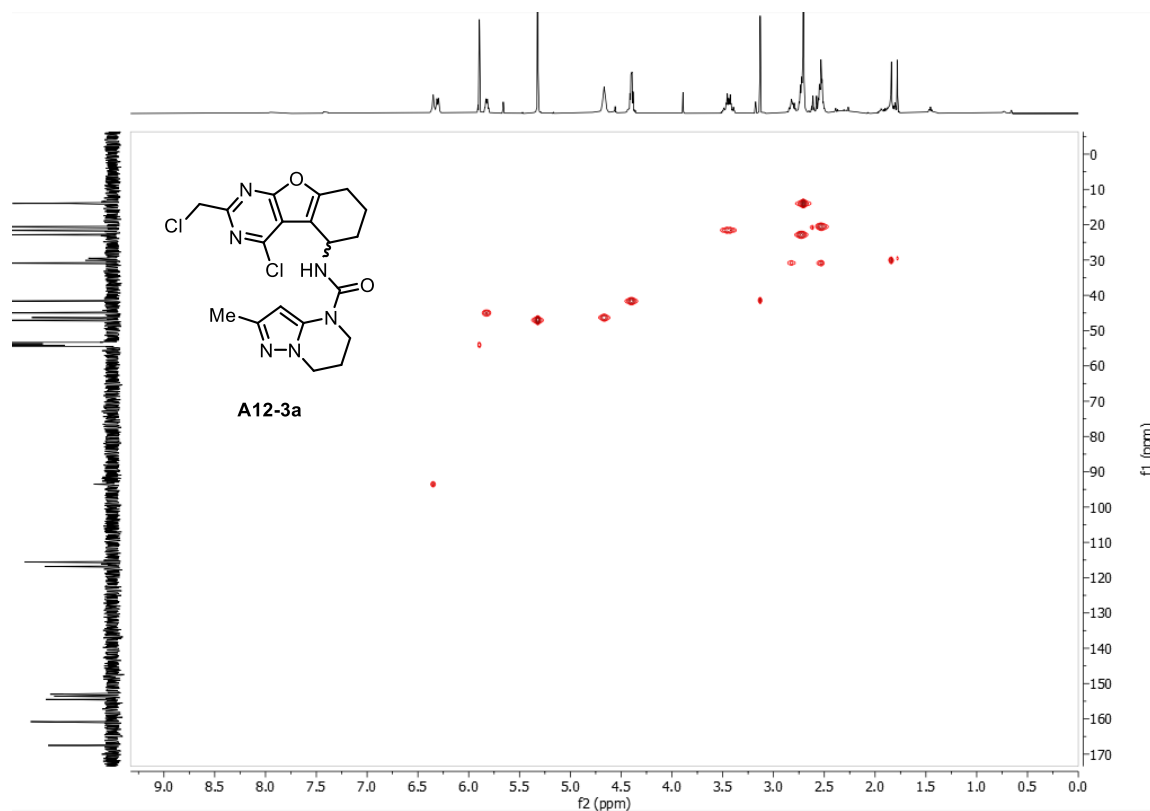
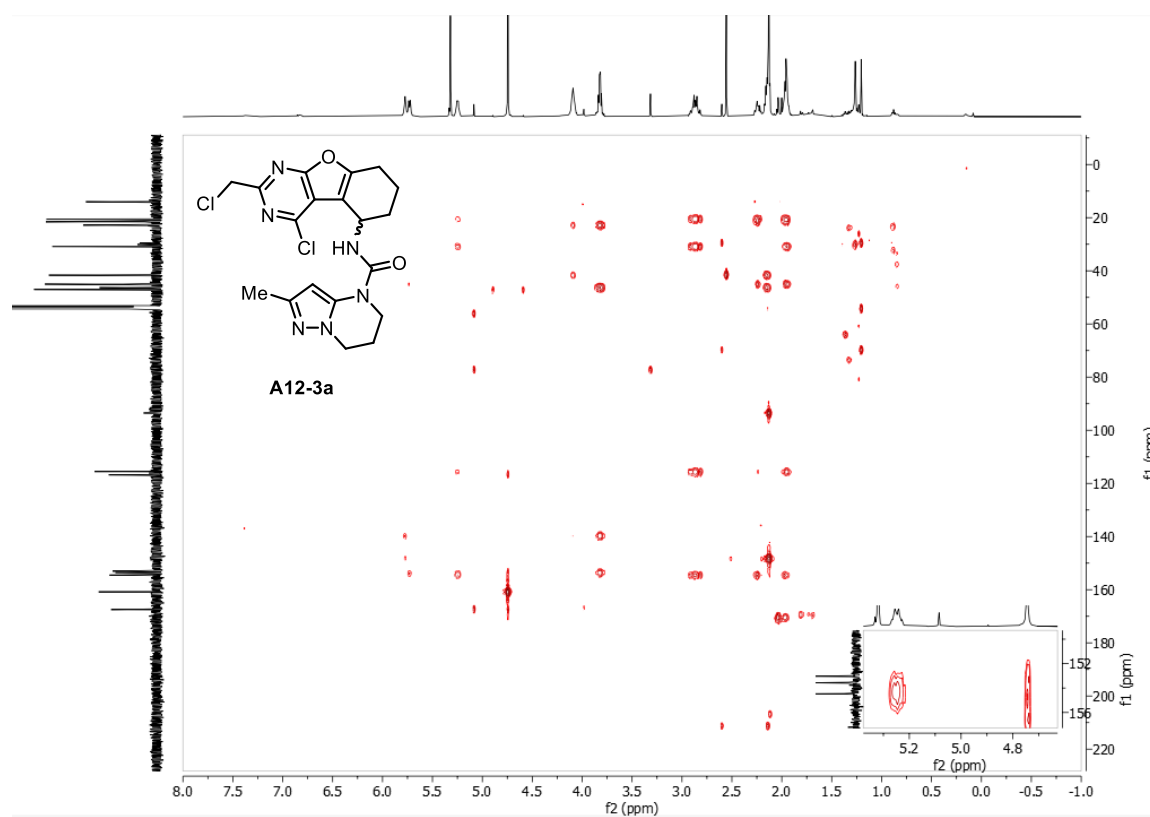


^1H NMR spectrum of **A12-3a** in CD_2Cl_2 (500 MHz).

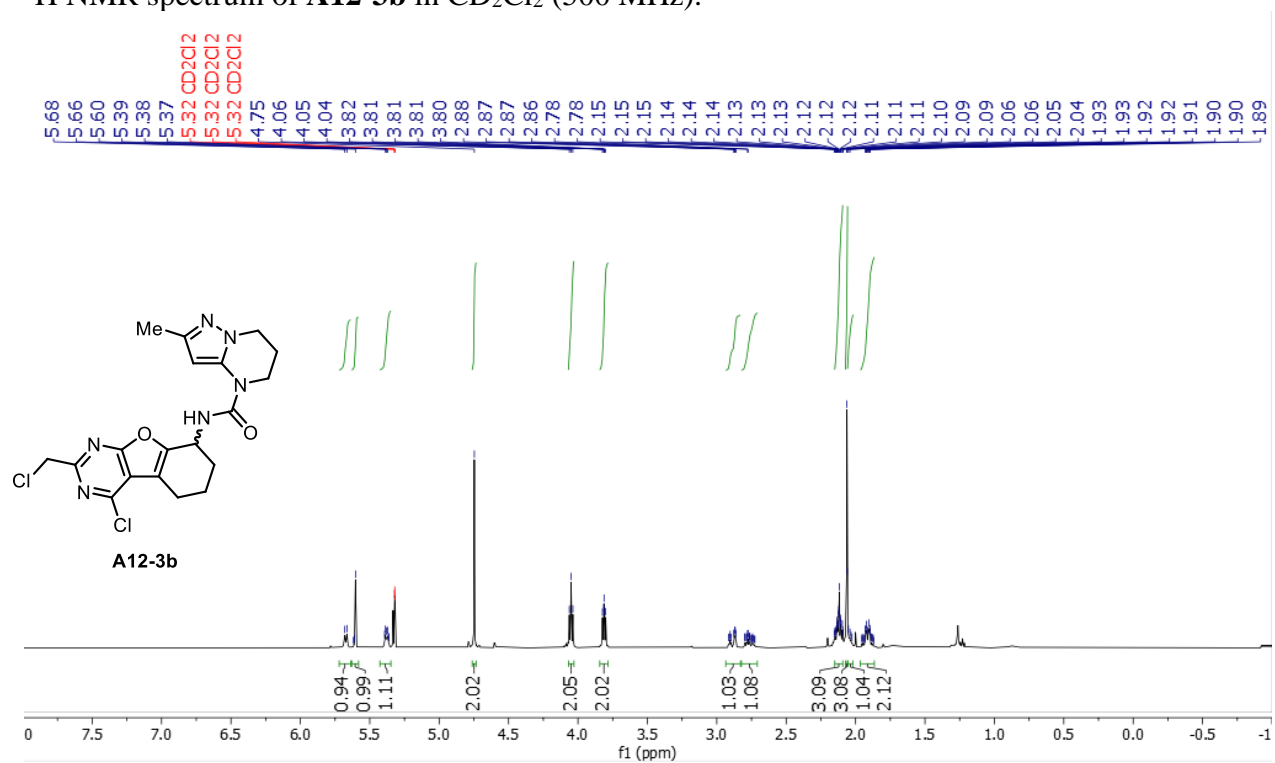


^{13}C NMR spectrum of **A12-3a** in CD_2Cl_2 (126 MHz).

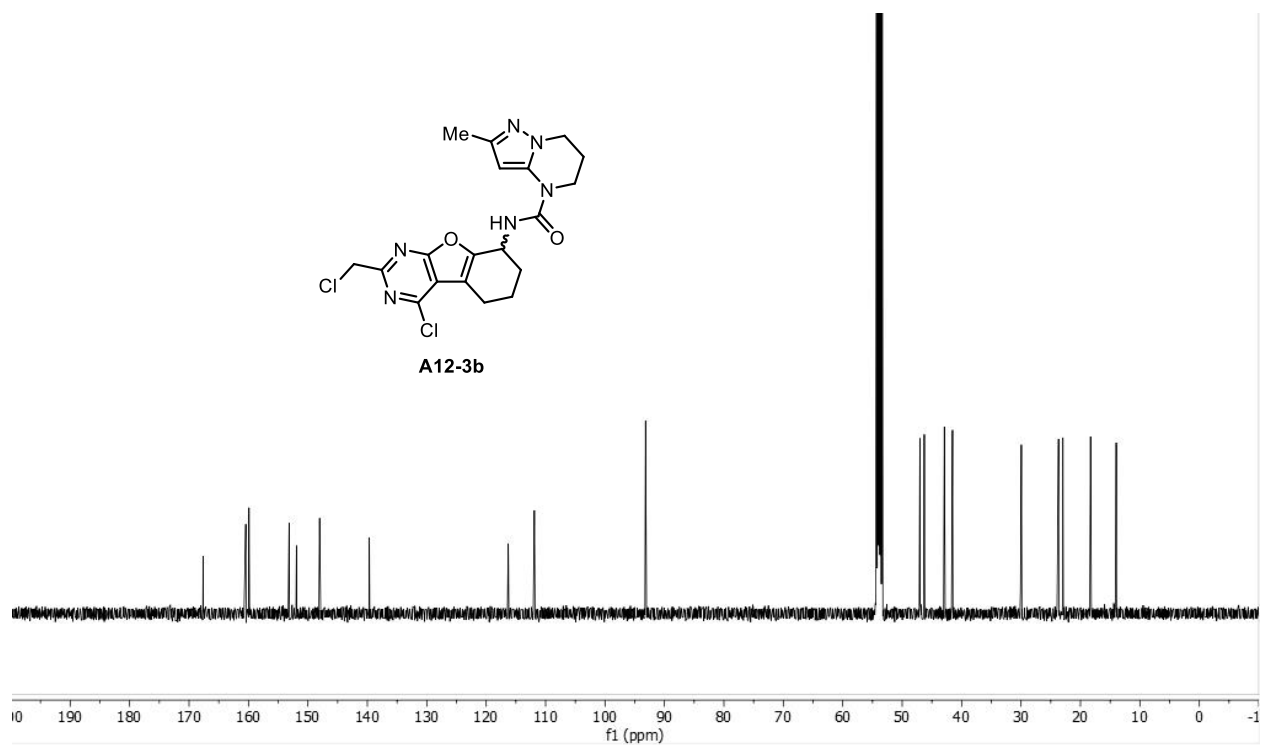


HSQC NMR spectrum of **A12-3a** in CD₂Cl₂ (500, 126 MHz).HMBC NMR spectrum of **A12-3a** in CD₂Cl₂ (500, 126 MHz).

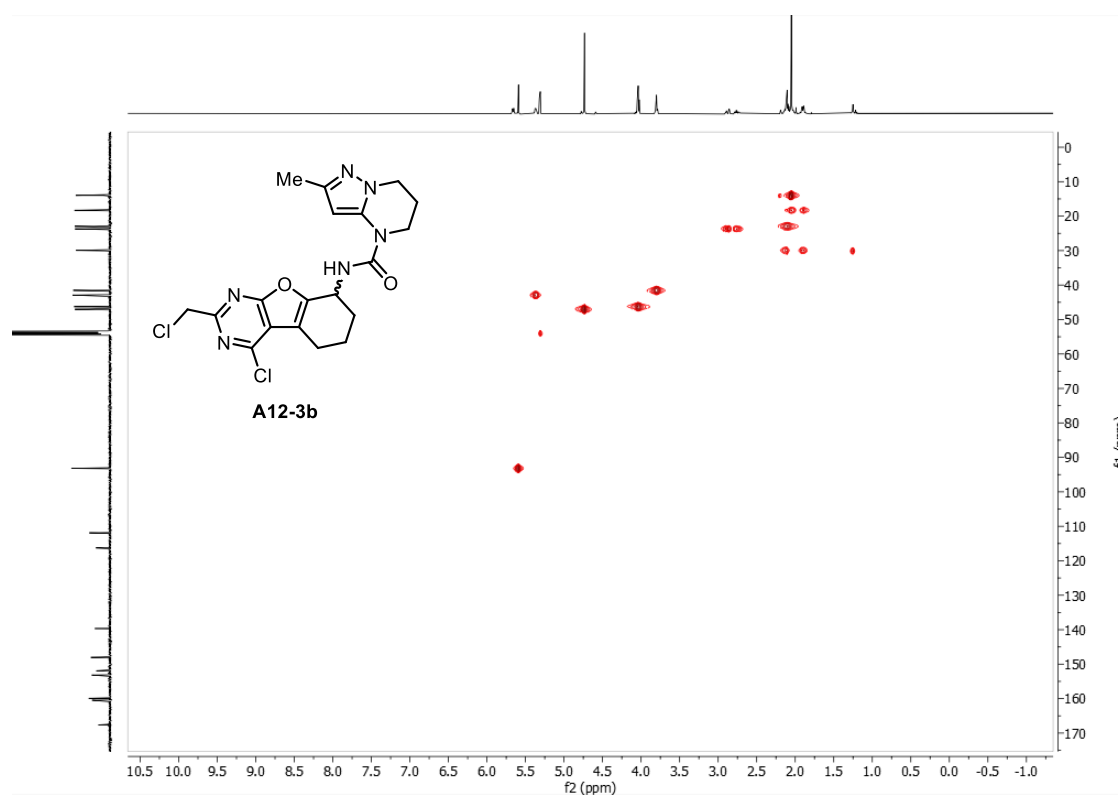
^1H NMR spectrum of **A12-3b** in CD_2Cl_2 (500 MHz).



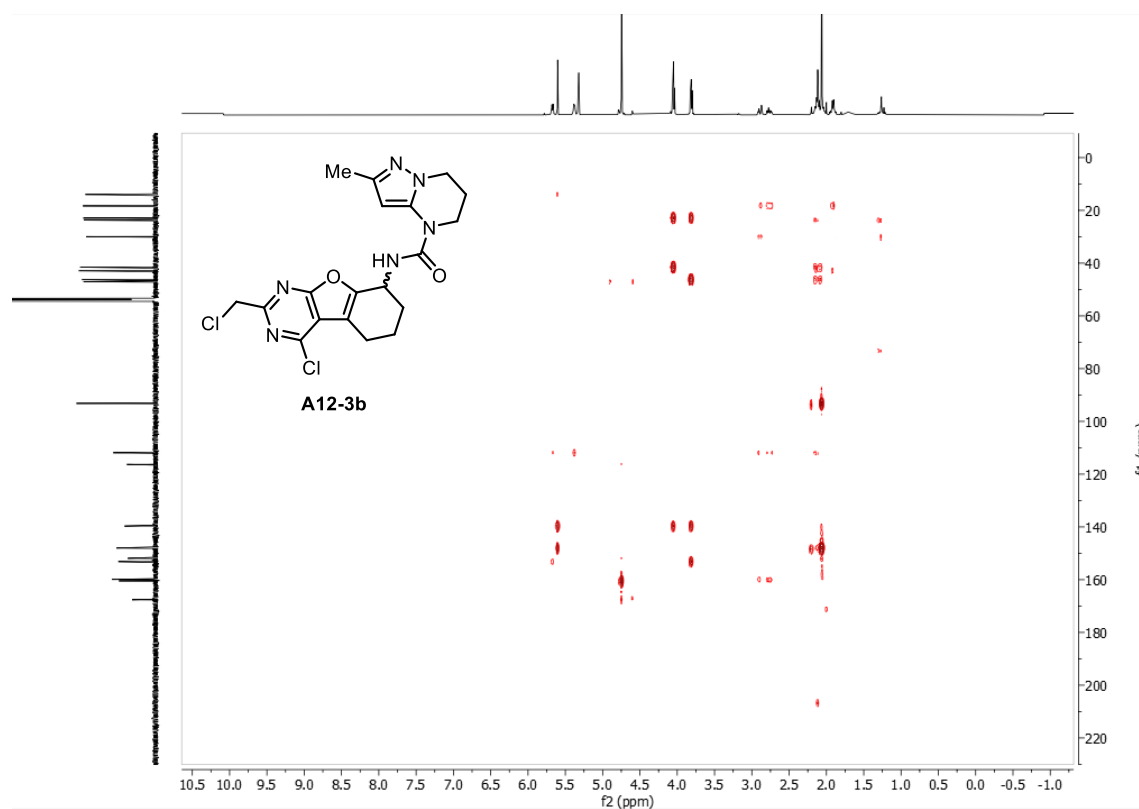
^{13}C NMR spectrum of **A12-3b** in CD_2Cl_2 (126 MHz).



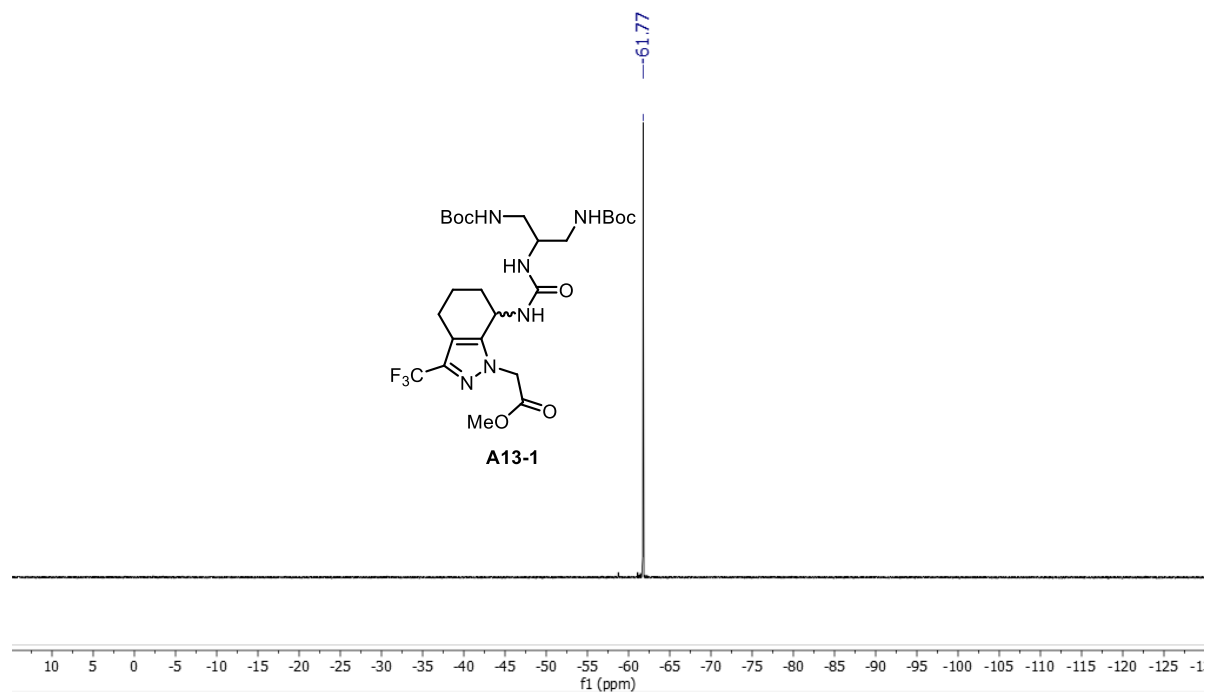
HSQC NMR spectrum of **A12-3b** in CD₂Cl₂ (500, 126 MHz).



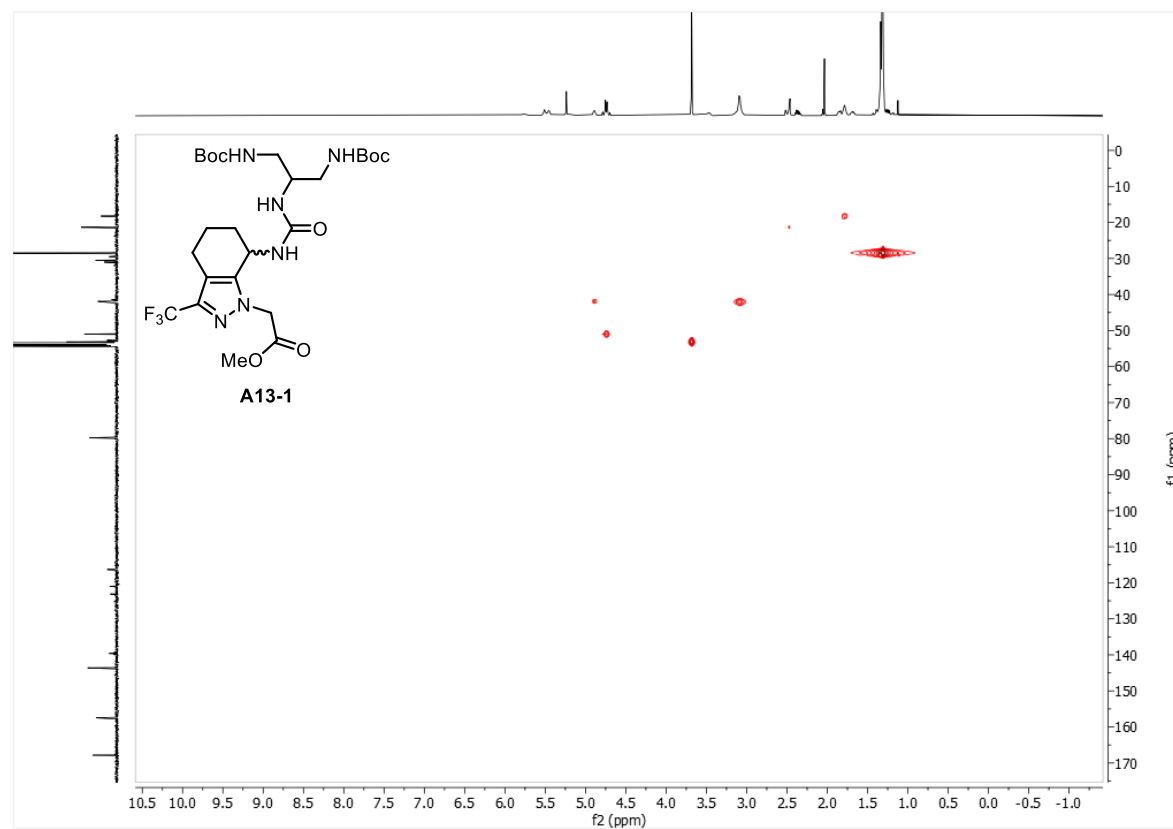
HMBC NMR spectrum of **A12-3b** in CD₂Cl₂ (500, 126 MHz).



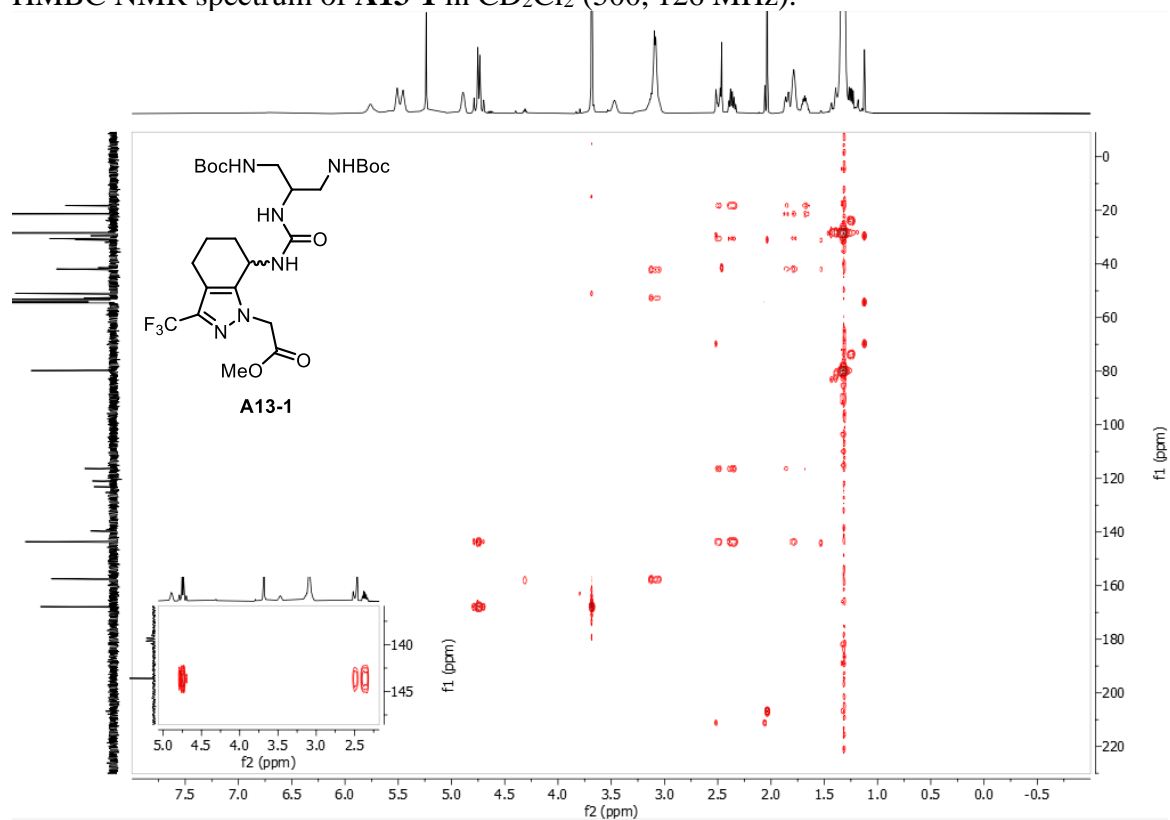
^{19}F NMR spectrum of **A13-1** in CD_2Cl_2 (377 MHz).



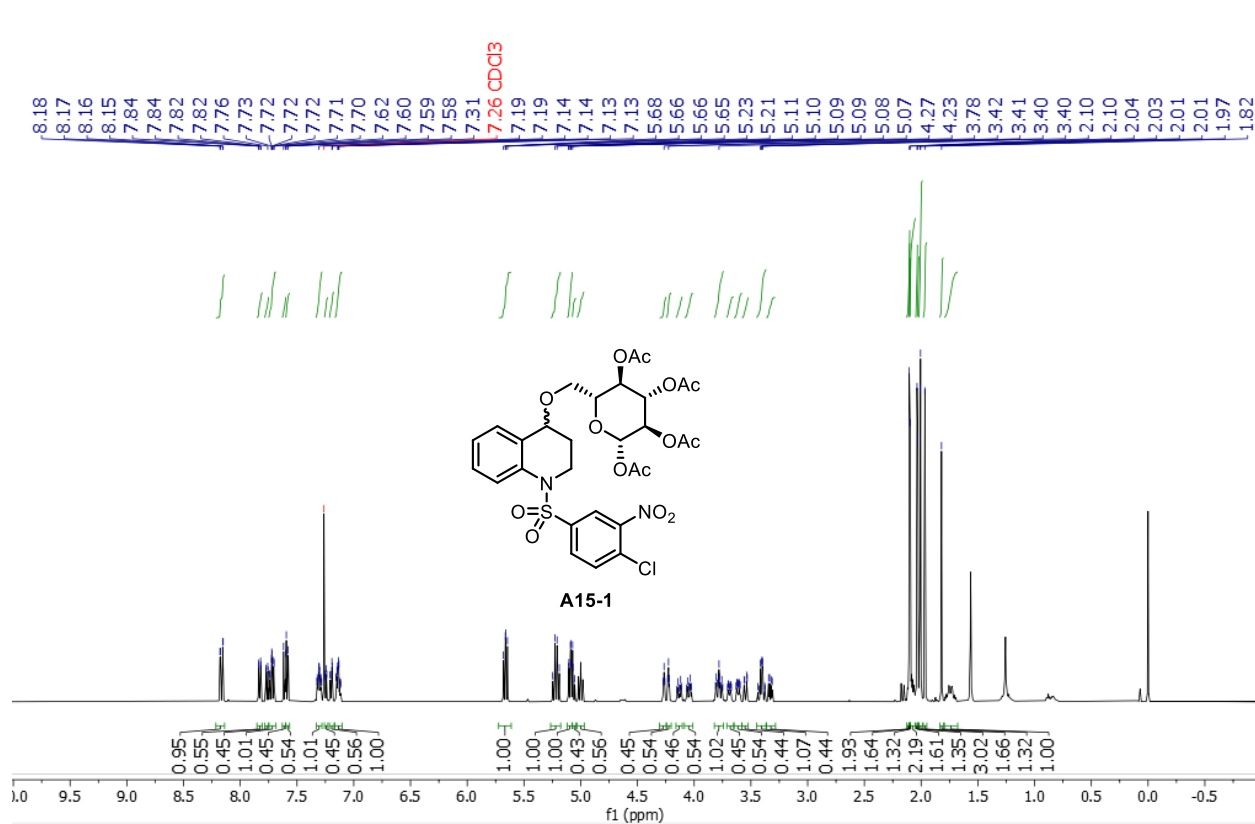
HSQC NMR spectrum of **A13-1** in CD_2Cl_2 (500, 126 MHz).



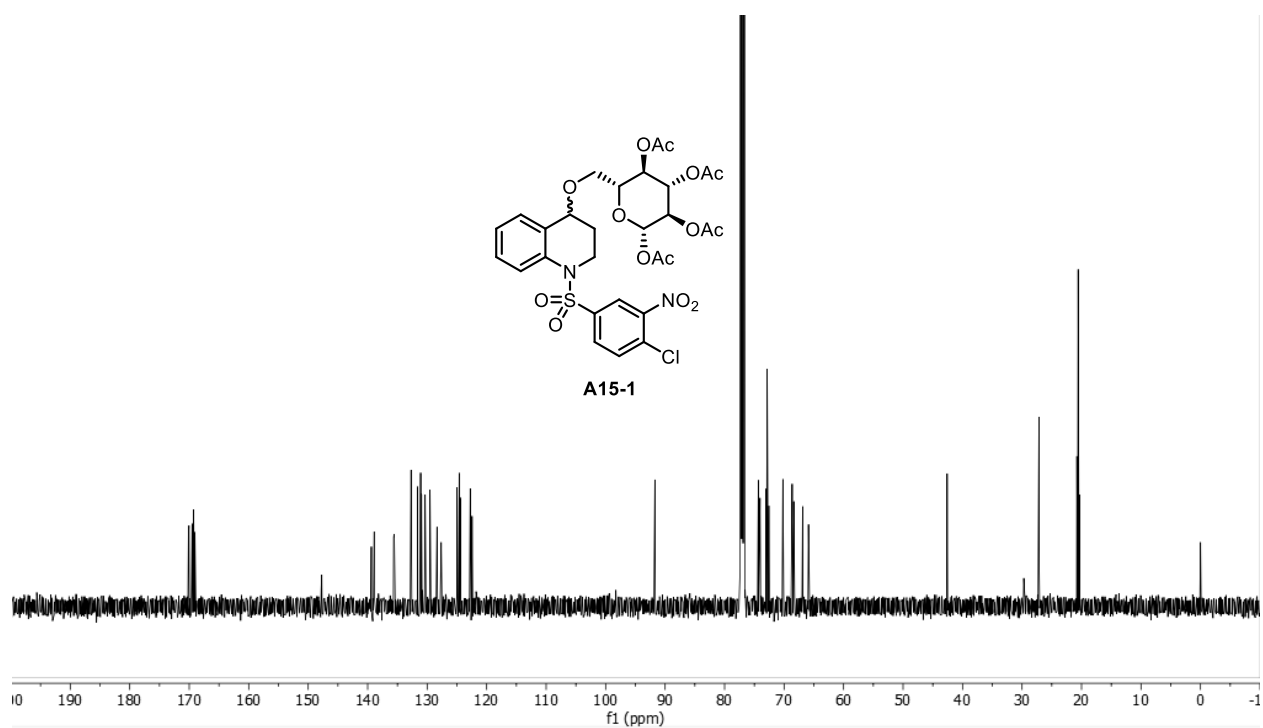
HMBC NMR spectrum of **A13-1** in CD_2Cl_2 (500, 126 MHz).



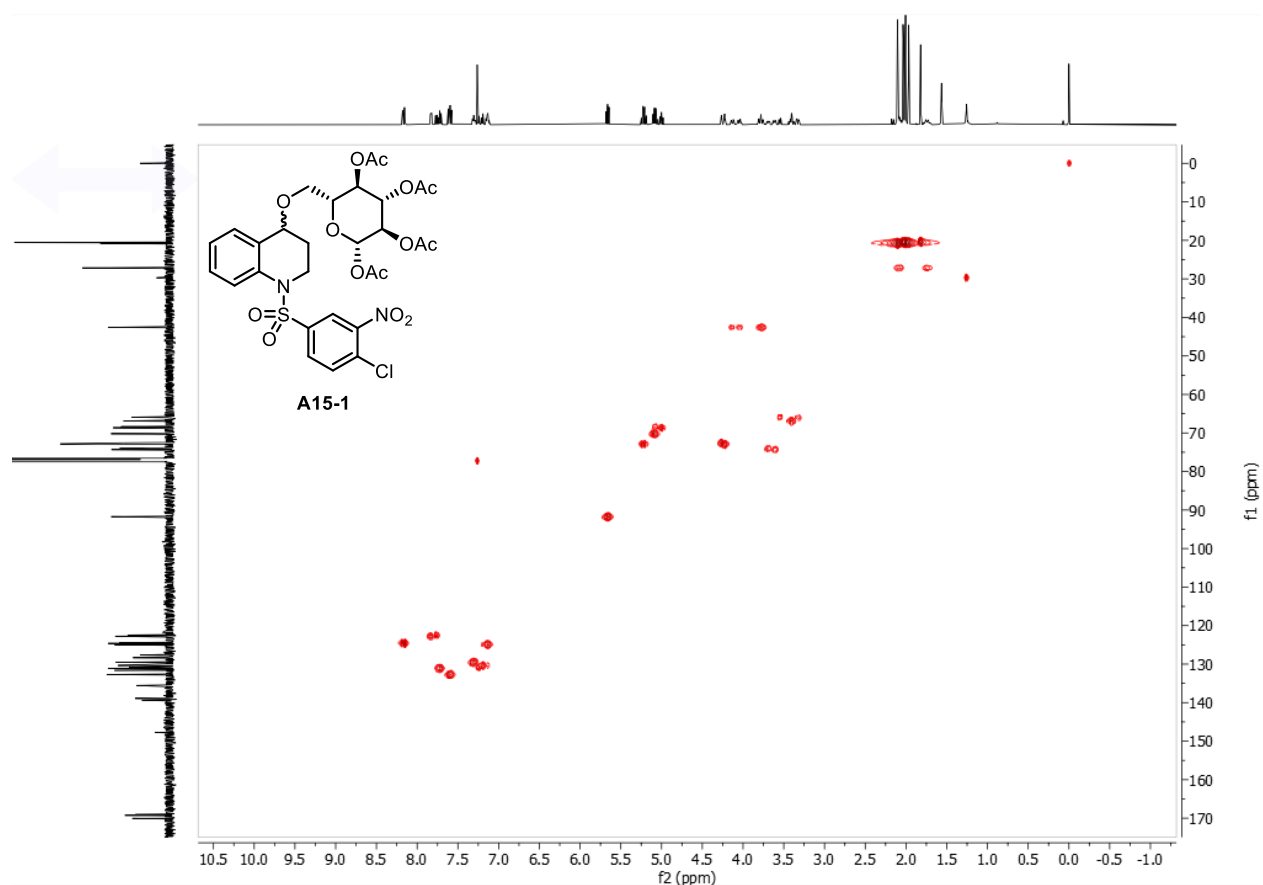
^1H NMR spectrum of **A15-1** in CDCl_3 containing 0.03 % (v/v) TMS (500 MHz).



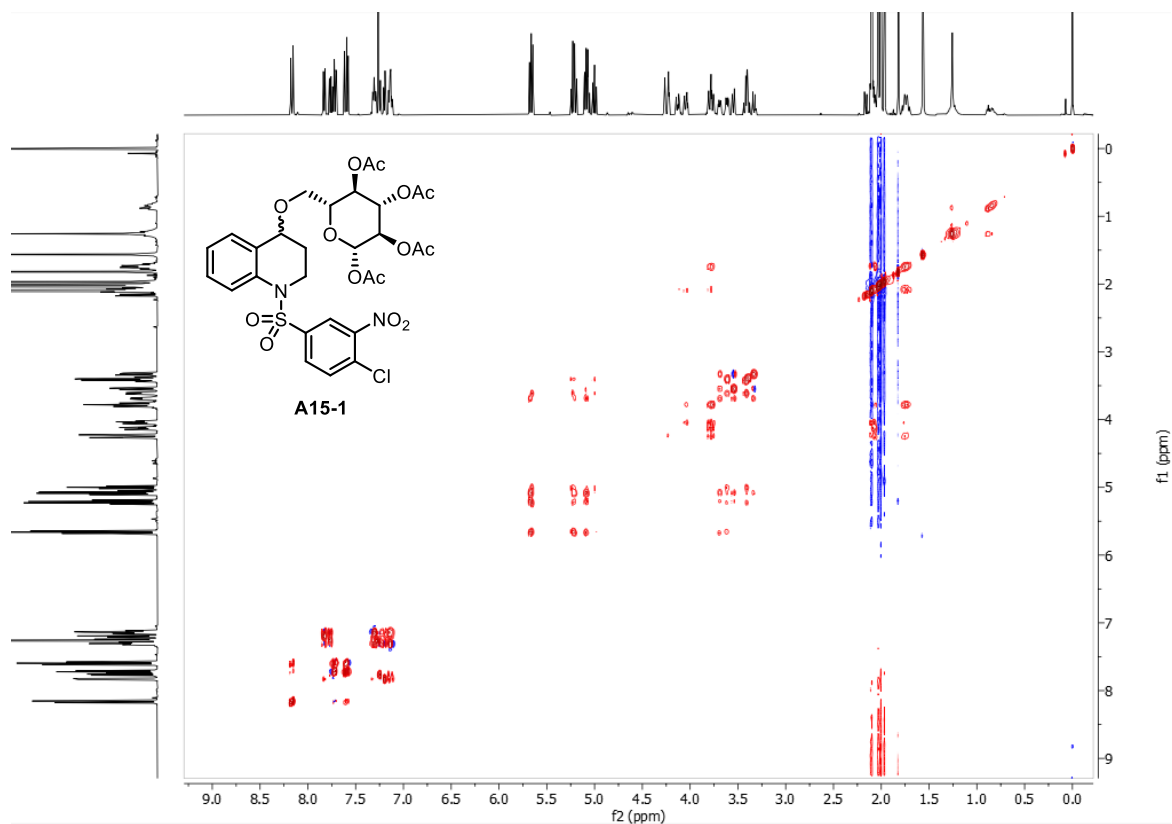
^{13}C NMR spectrum of **A15-1** in CDCl_3 containing 0.03 % (v/v) TMS (126 MHz).



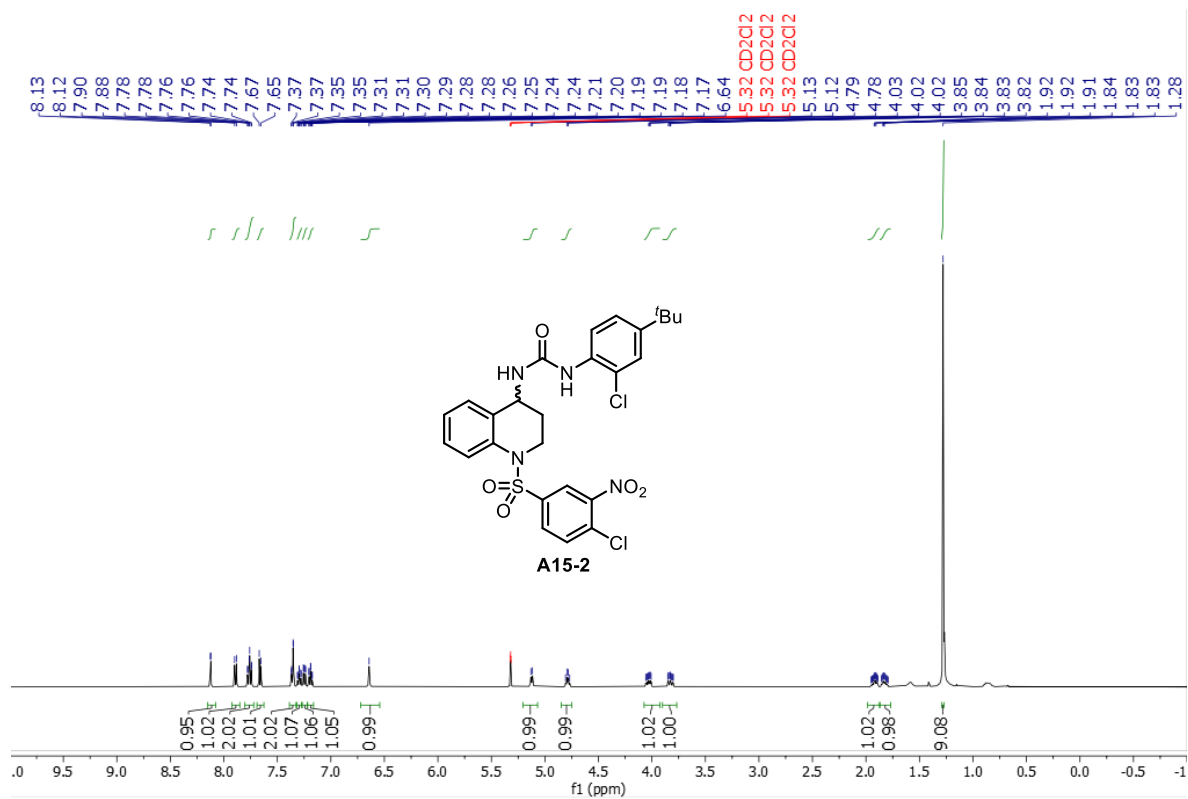
HSQC NMR spectrum of **A15-1** in CDCl_3 containing 0.03 % (v/v) TMS (500, 126 MHz).



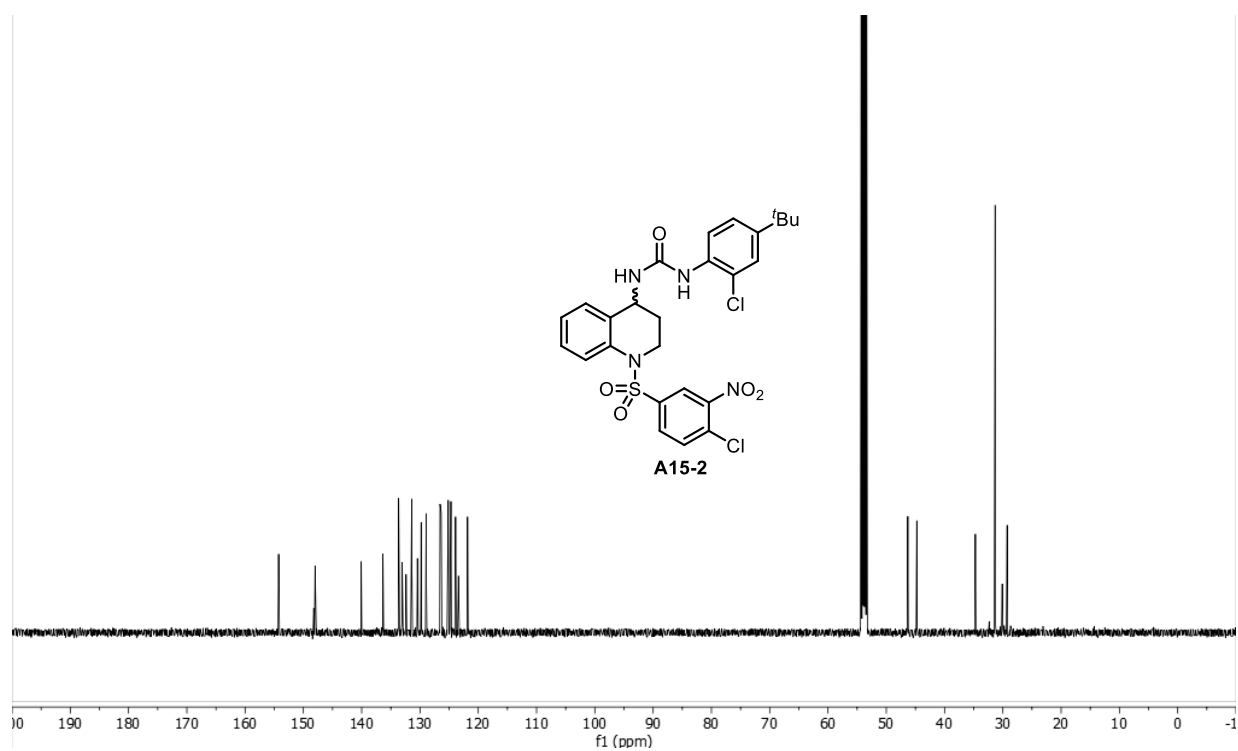
COSY NMR spectrum of **A15-1** in CDCl_3 containing 0.03 % (v/v) TMS (500, 500 MHz).



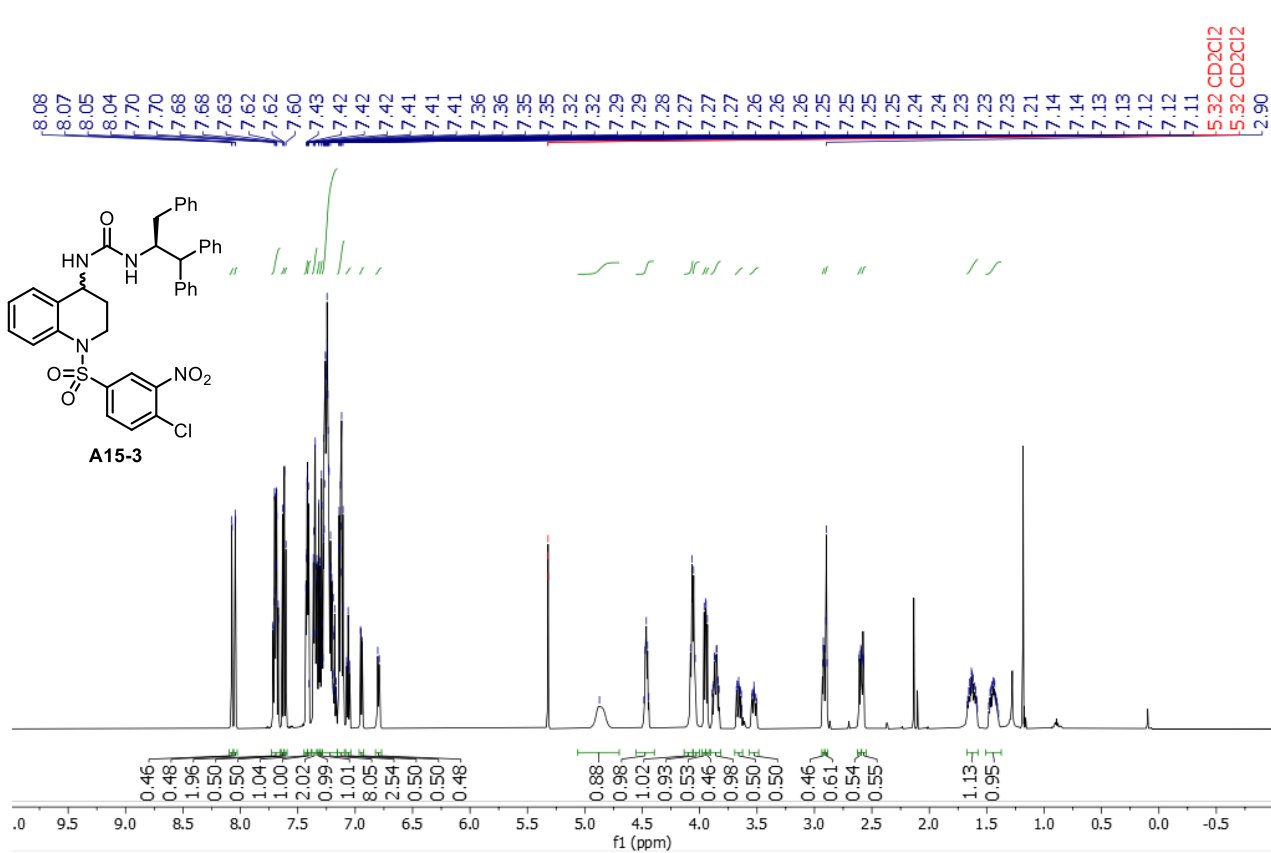
¹H NMR spectrum of **A15-2** in CD_2Cl_2 (500 MHz).



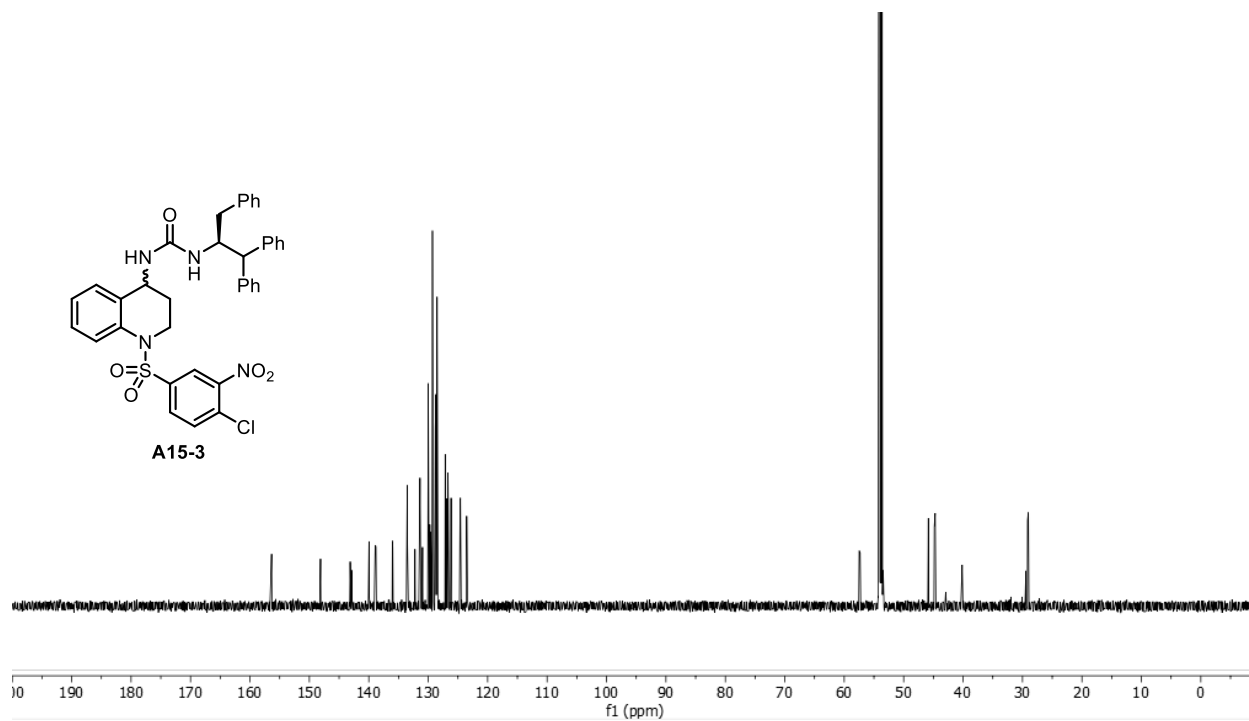
^{13}C NMR spectrum of **A15-2** in CD_2Cl_2 (126 MHz).



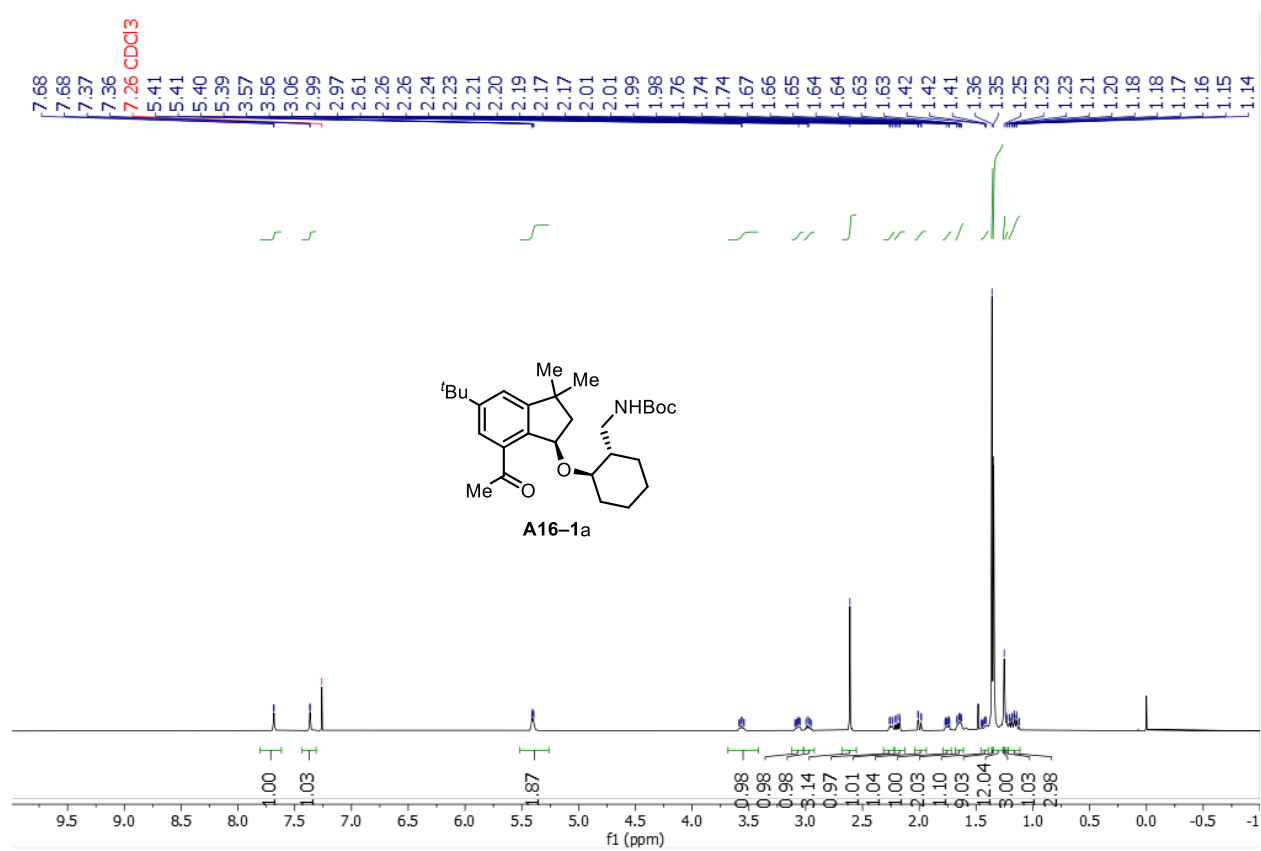
^1H NMR spectrum of **A15-3** in CD_2Cl_2 (600 MHz).



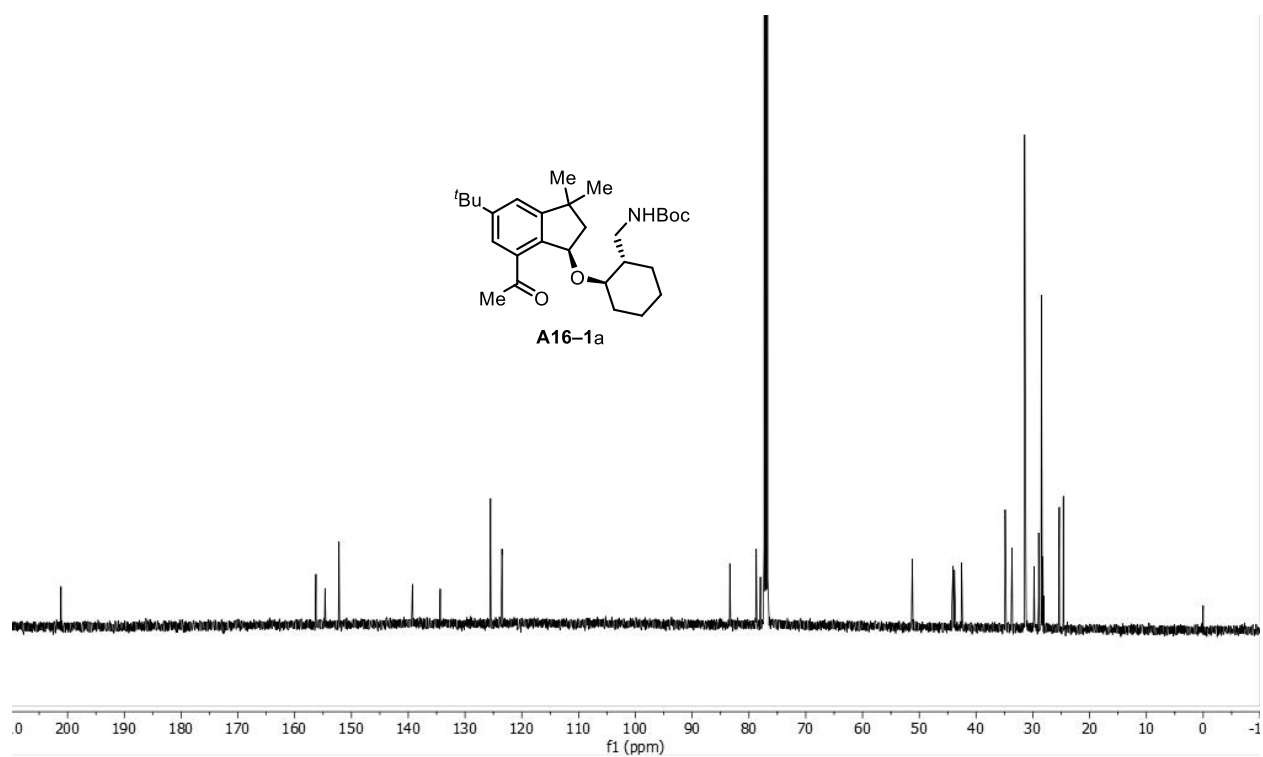
^{13}C NMR spectrum of **A15-3** in CD_2Cl_2 (151 MHz).



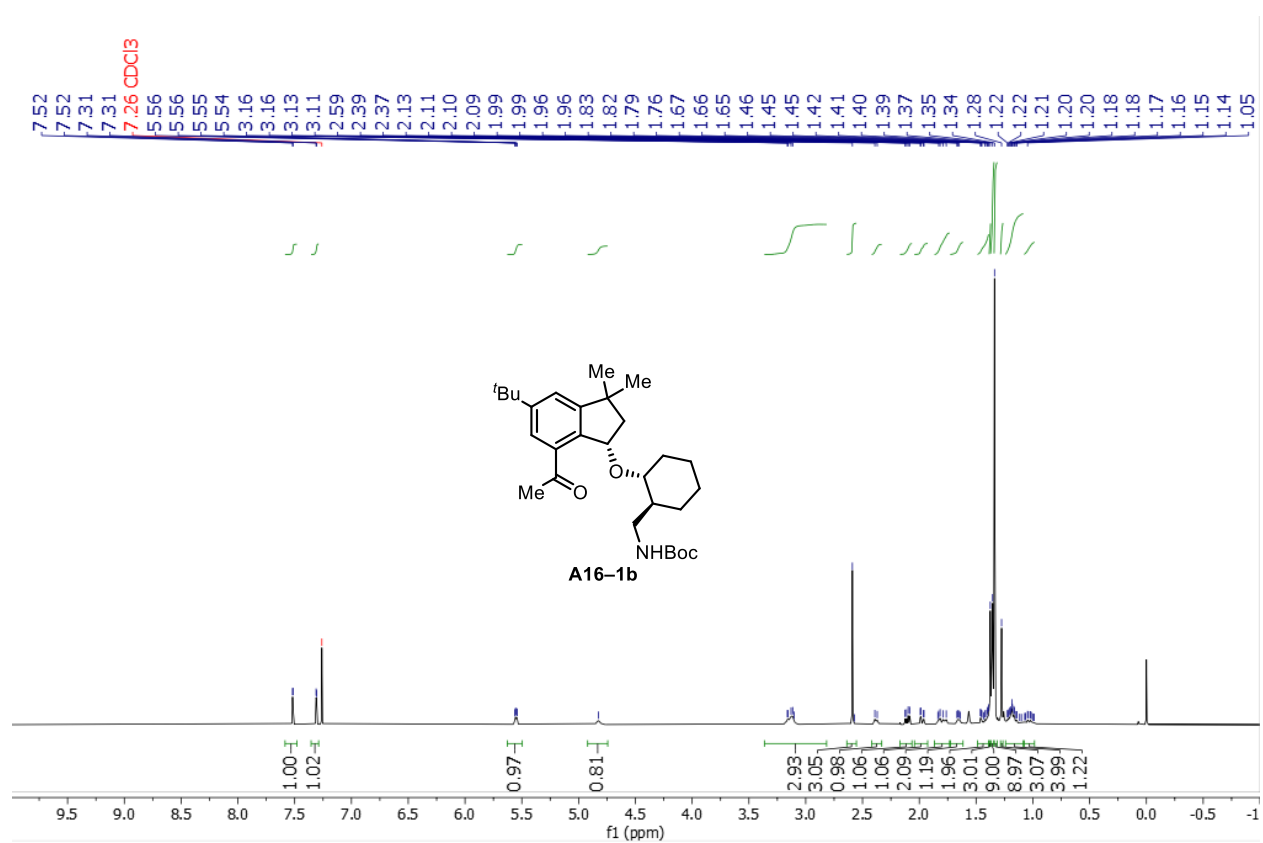
^1H NMR spectrum of **A16-1a** in CDCl_3 containing 0.03 % (v/v) TMS (500 MHz).



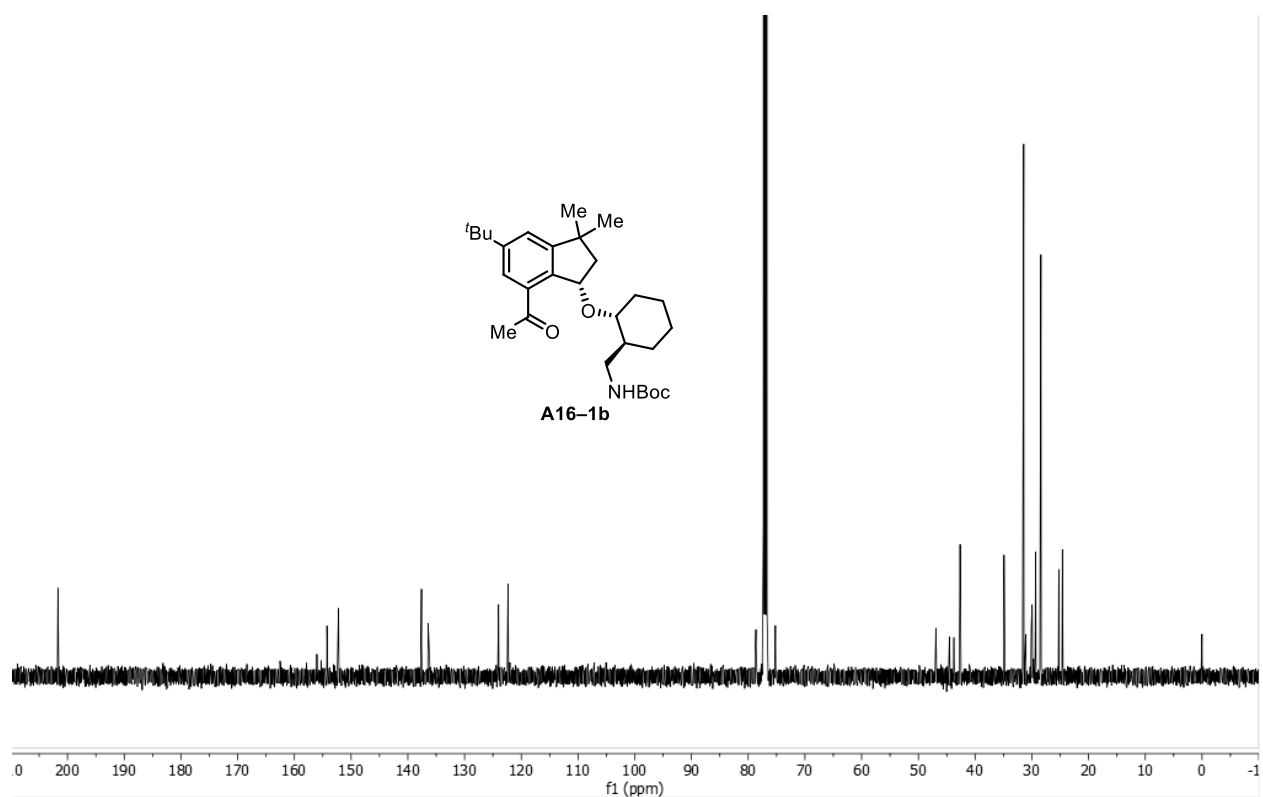
^{13}C NMR spectrum of **A16-1a** in CDCl_3 containing 0.03 % (v/v) TMS (126 MHz).



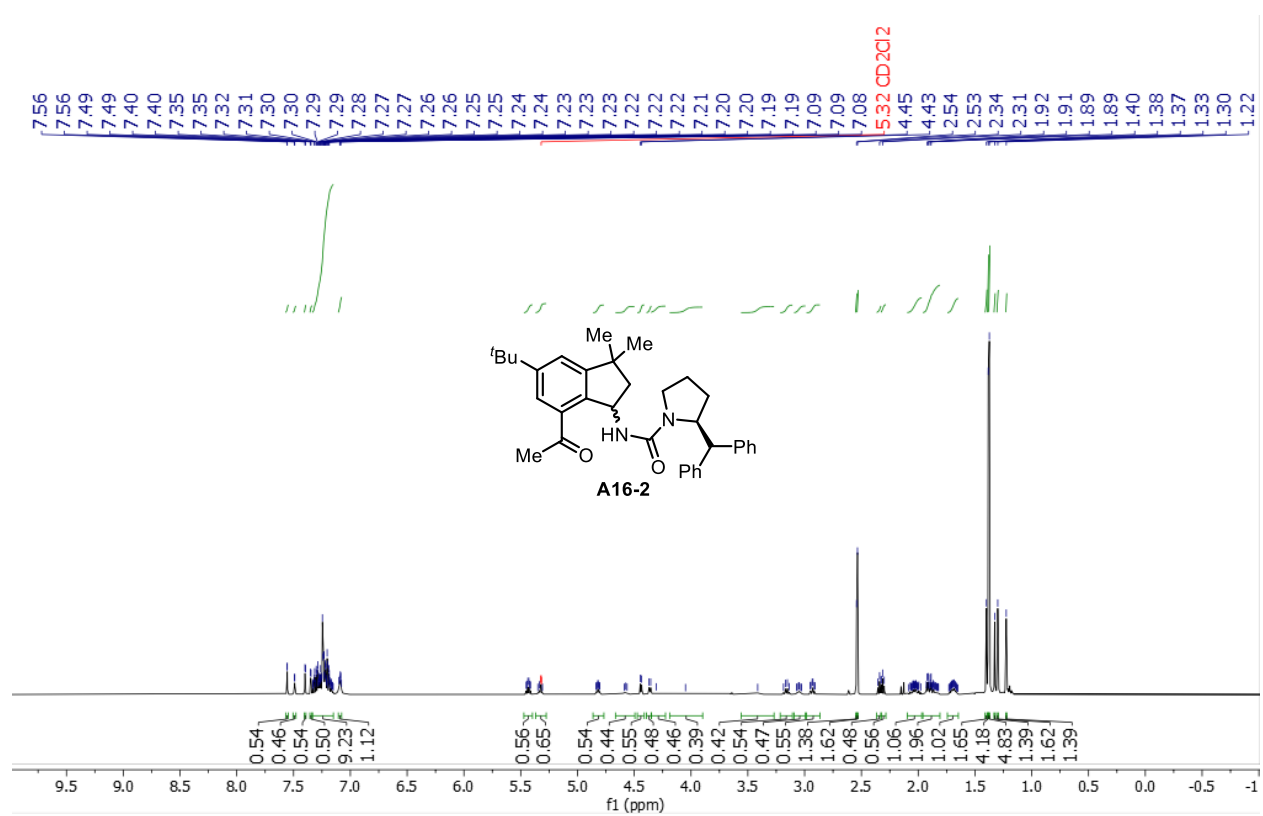
^1H NMR spectrum of **A16-1b** in CDCl_3 containing 0.03 % (v/v) TMS (500 MHz).



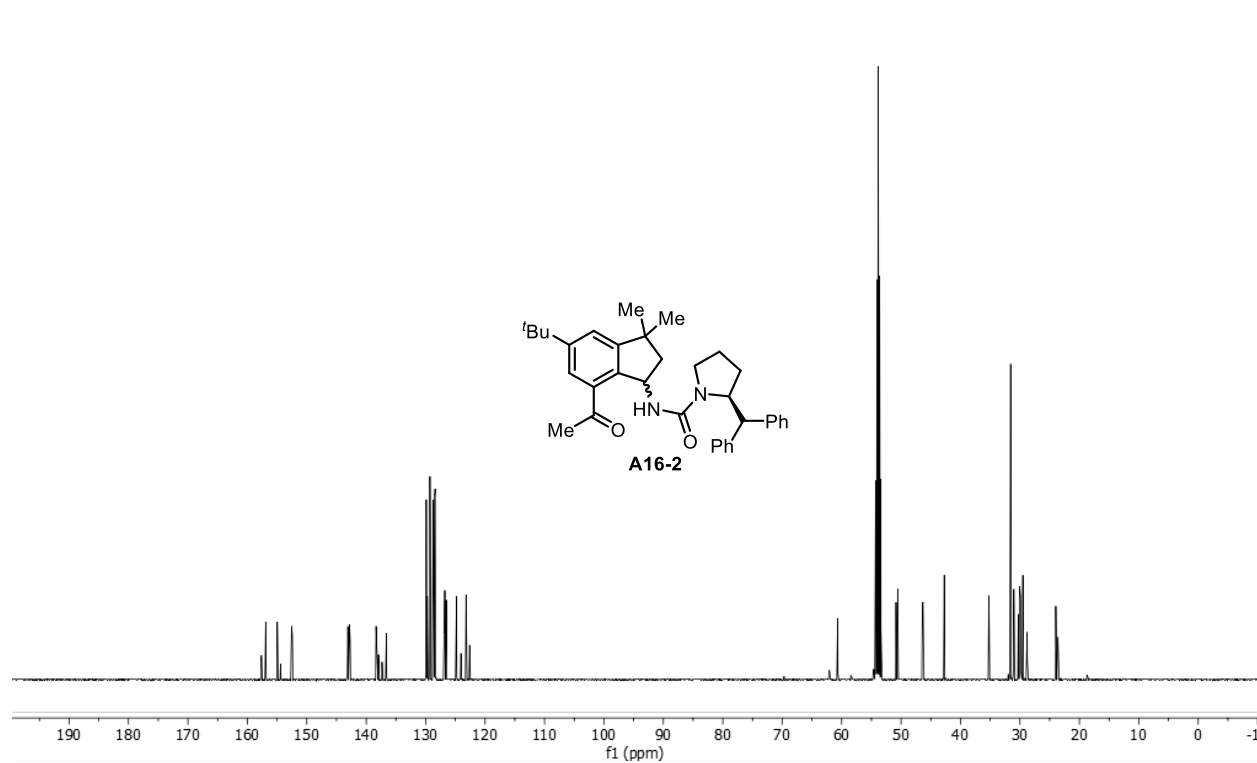
^{13}C NMR spectrum of **A16-1b** in CDCl_3 containing 0.03 % (v/v) TMS (126 MHz).



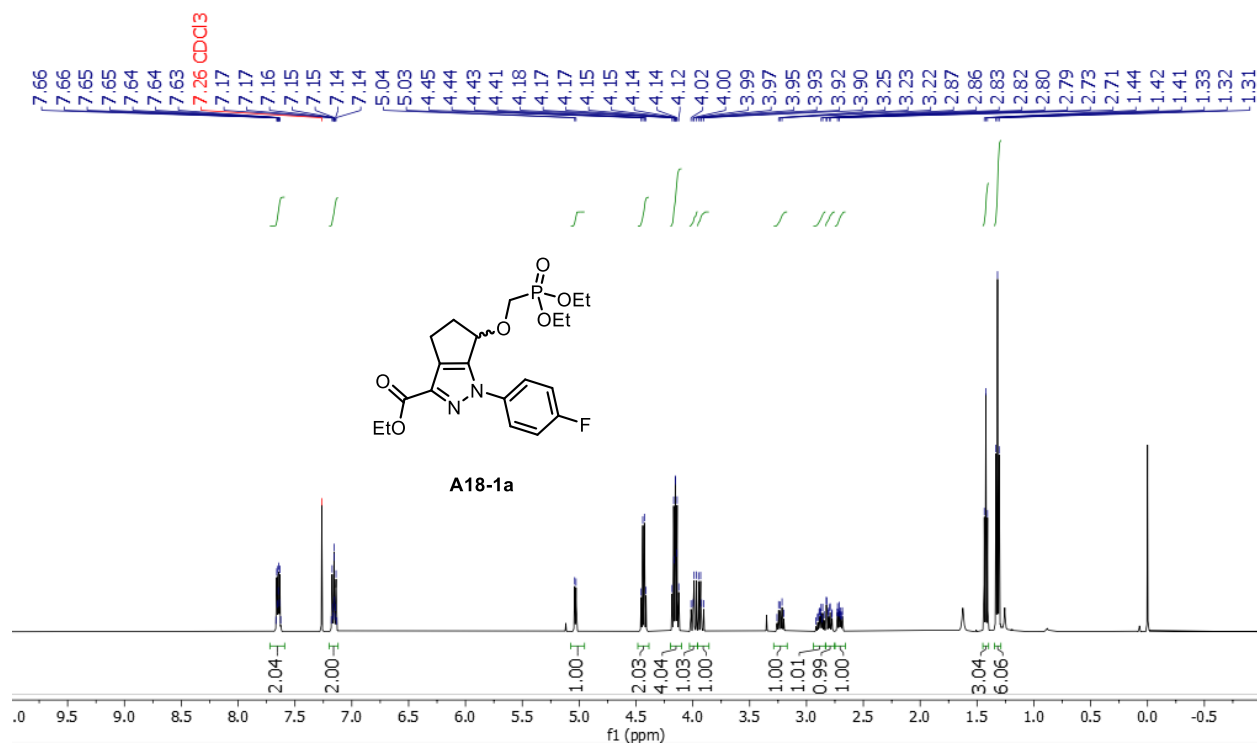
^1H NMR spectrum of **A16-2** in CD_2Cl_2 (500 MHz).



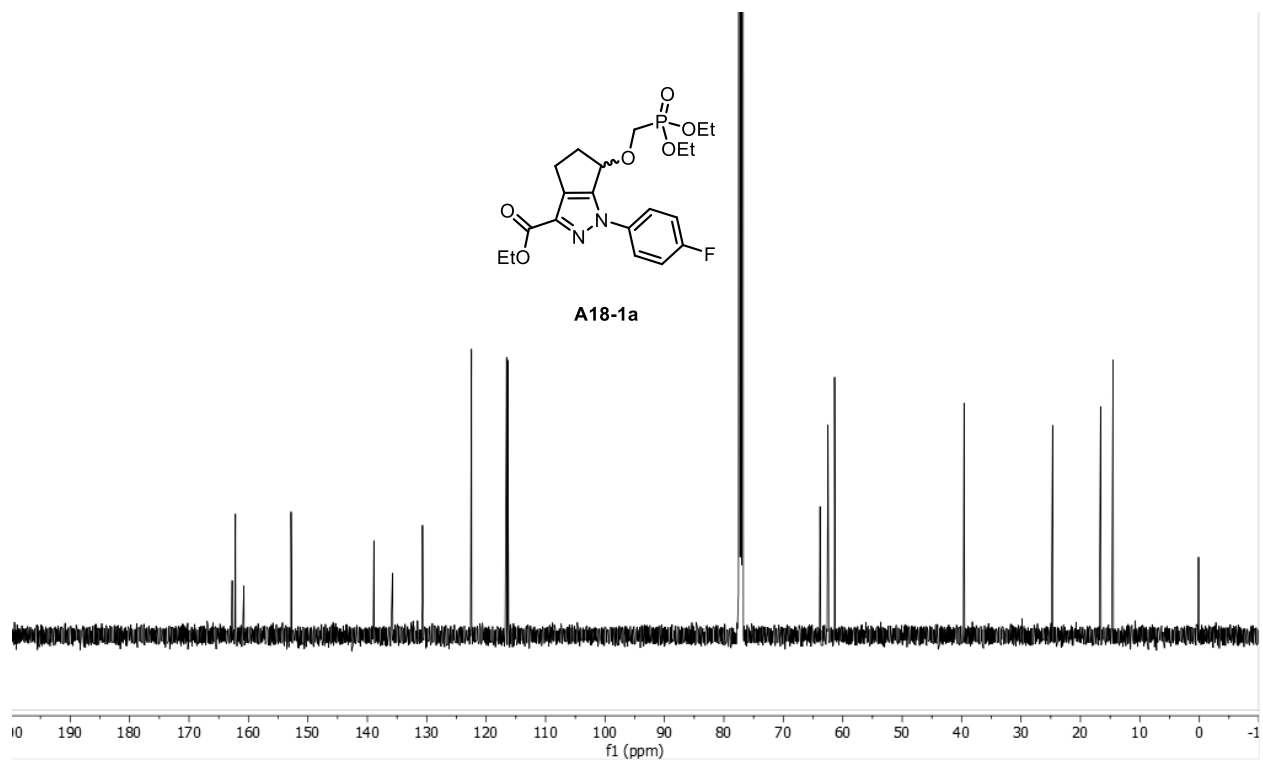
^{13}C NMR spectrum of **A16-2** in CD_2Cl_2 (126 MHz).



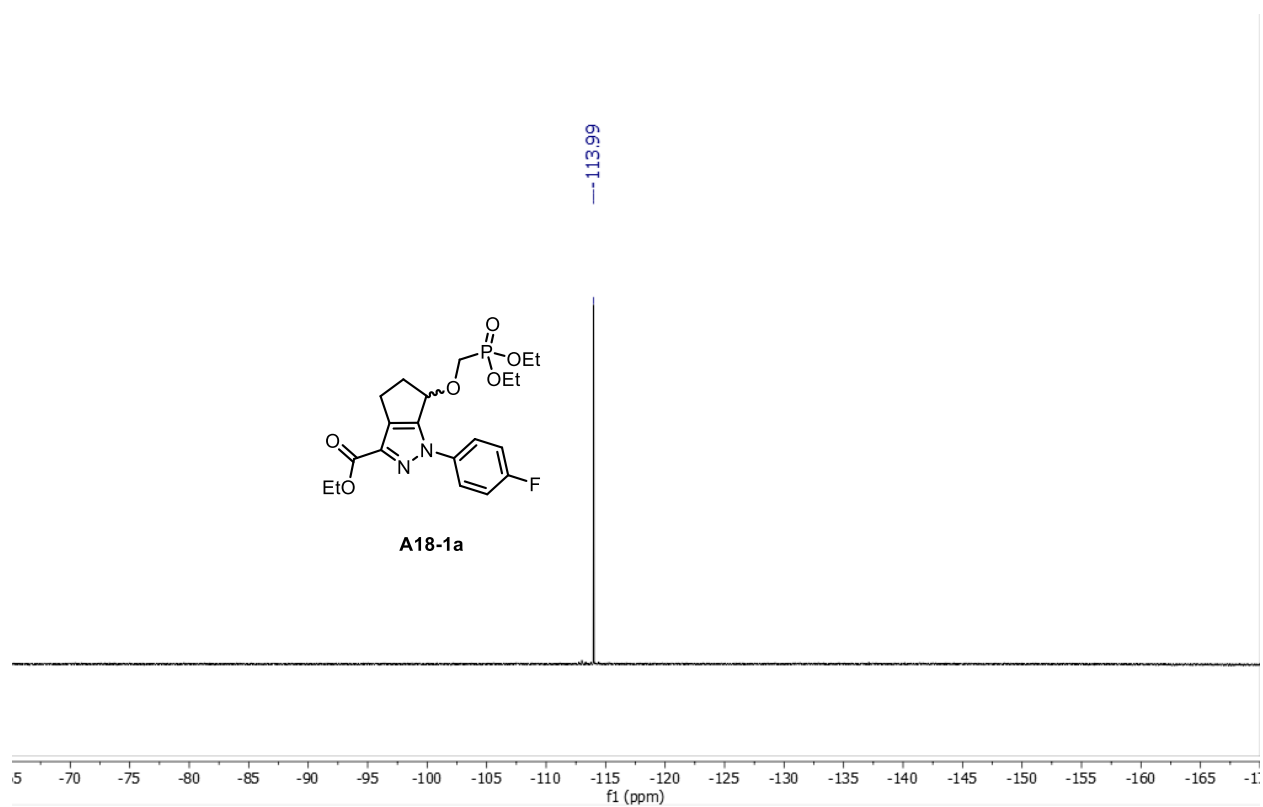
^1H NMR spectrum of **A18-1a** in CDCl_3 containing 0.03 % (v/v) TMS (500 MHz).



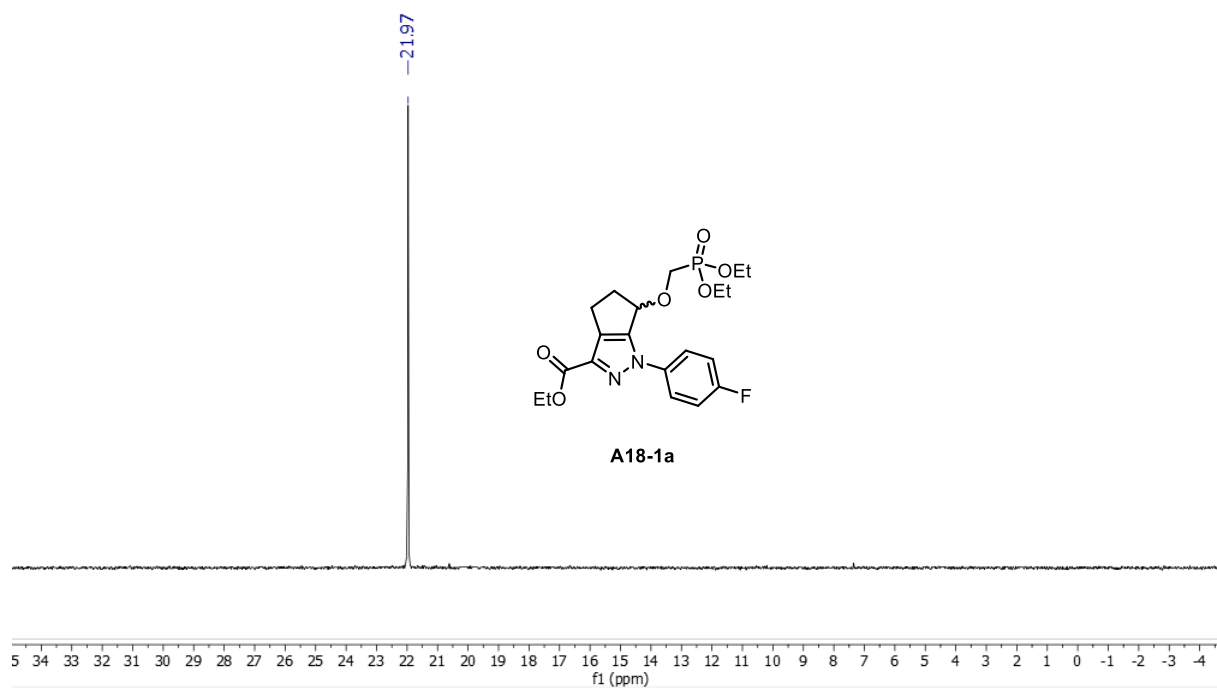
^{13}C NMR spectrum of **A18-1a** in CDCl_3 containing 0.03 % (v/v) TMS (126 MHz).



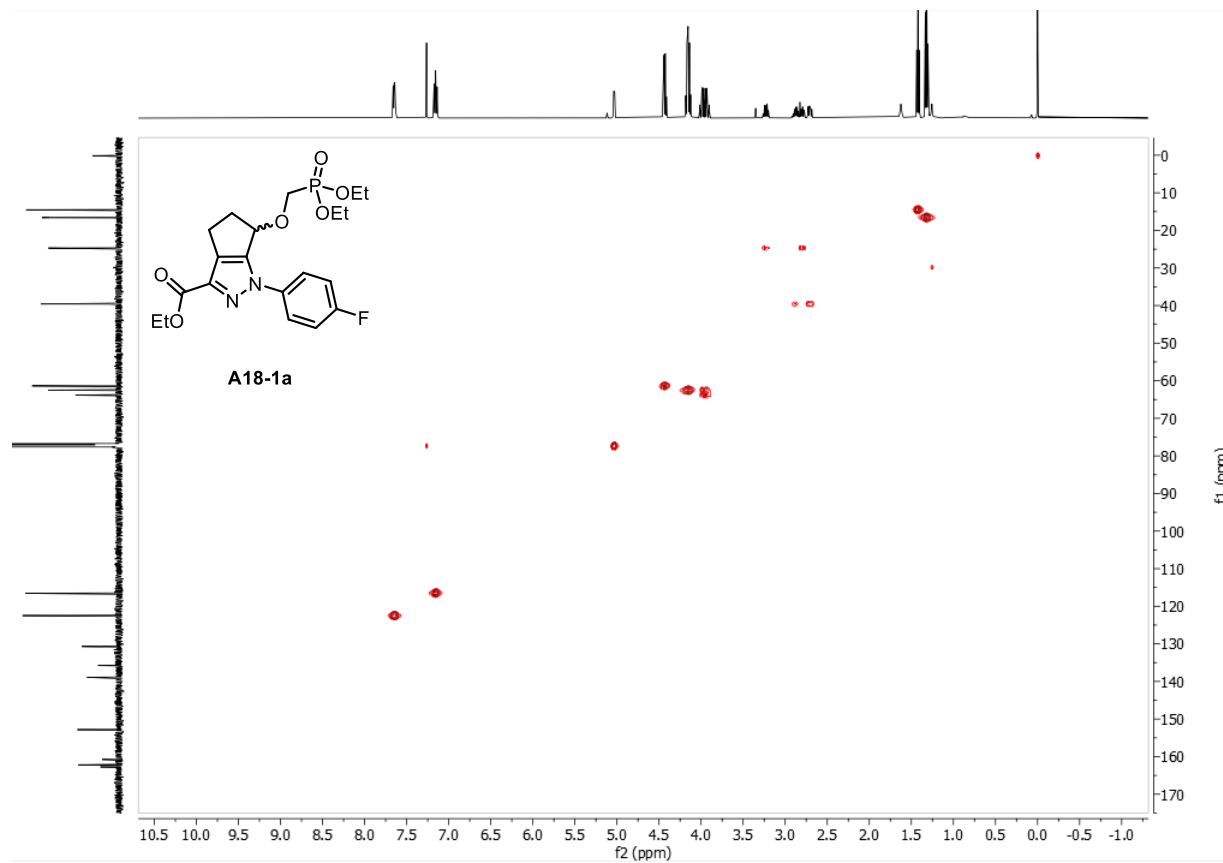
^{19}F NMR spectrum of **A18-1a** in CDCl_3 containing 0.03 % (v/v) TMS (377 MHz).



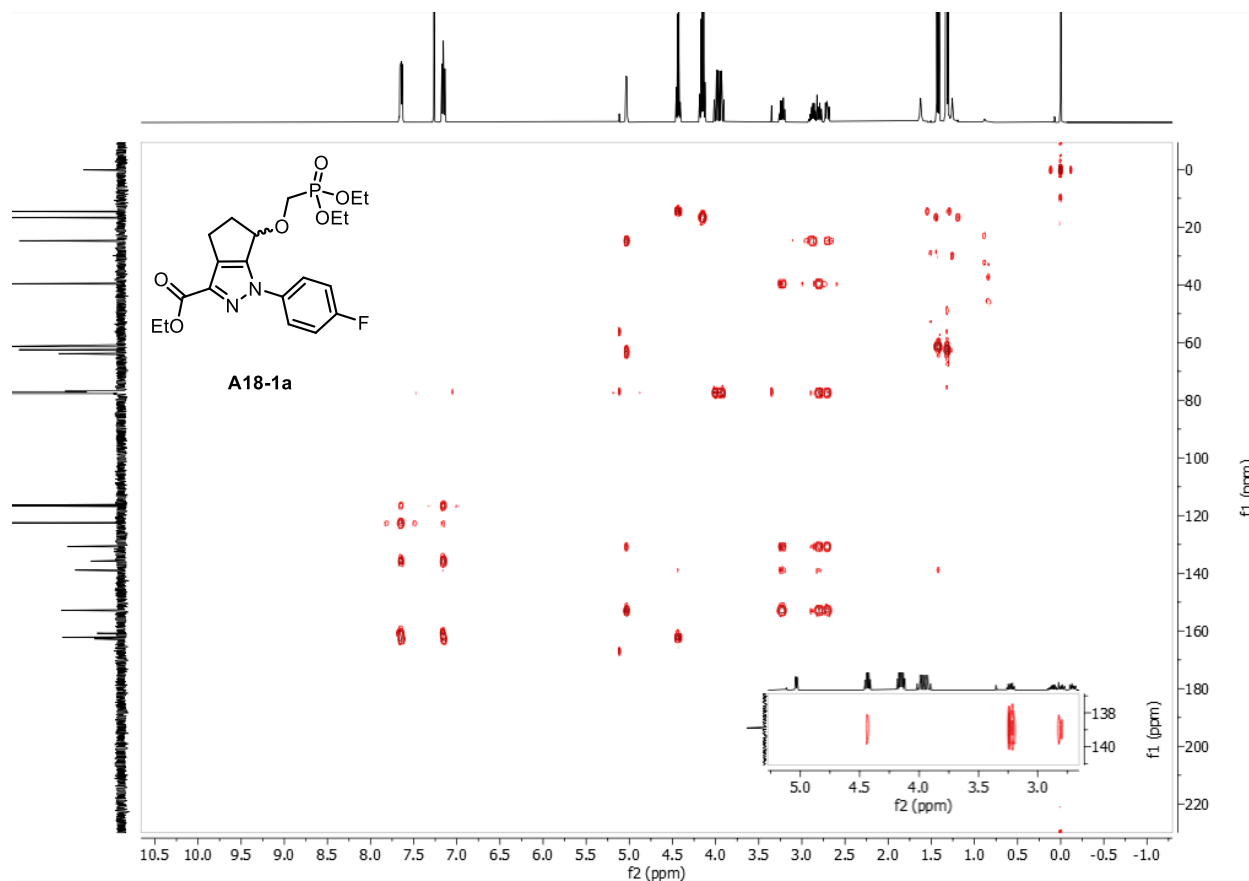
^{31}P NMR spectrum of **A18-1a** in CDCl_3 containing 0.03 % (v/v) TMS (162 MHz).



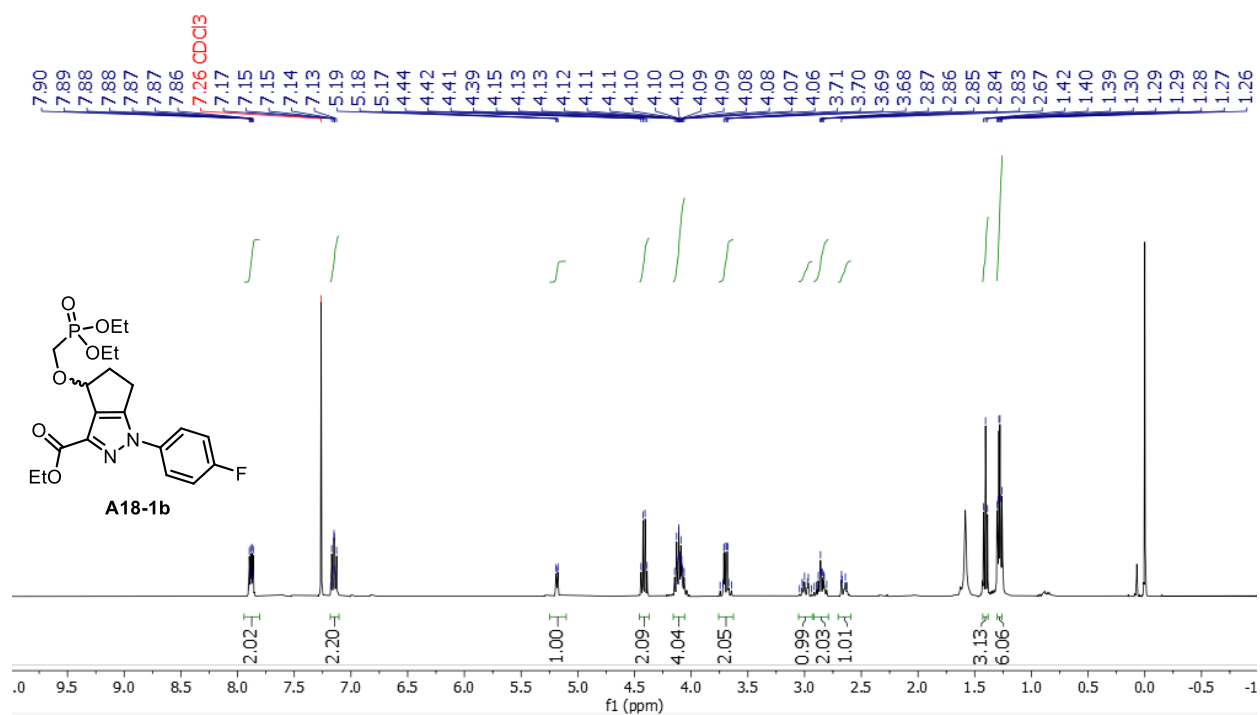
HSQC NMR spectrum of **A18-1a** in CDCl_3 containing 0.03 % (v/v) TMS (500, 126 MHz).



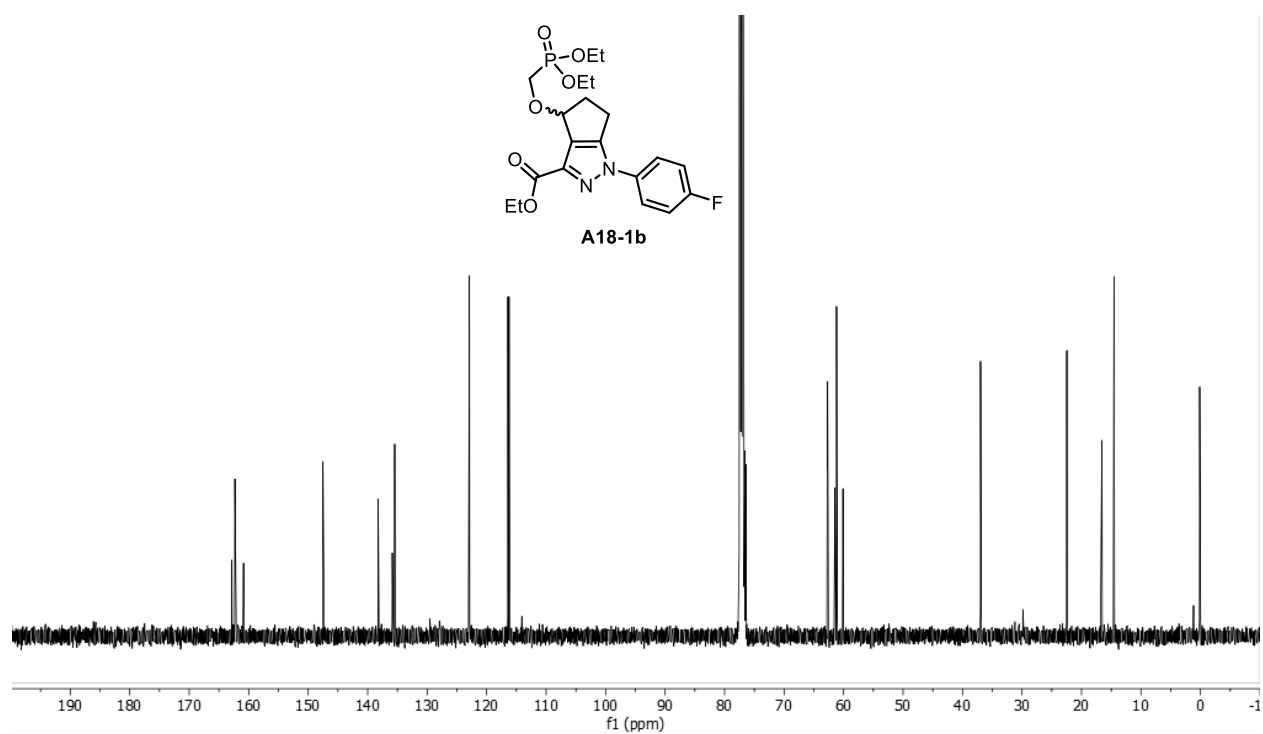
HMBC NMR spectrum of **A18-1a** in CDCl₃ containing 0.03 % (v/v) TMS (500, 126 MHz).



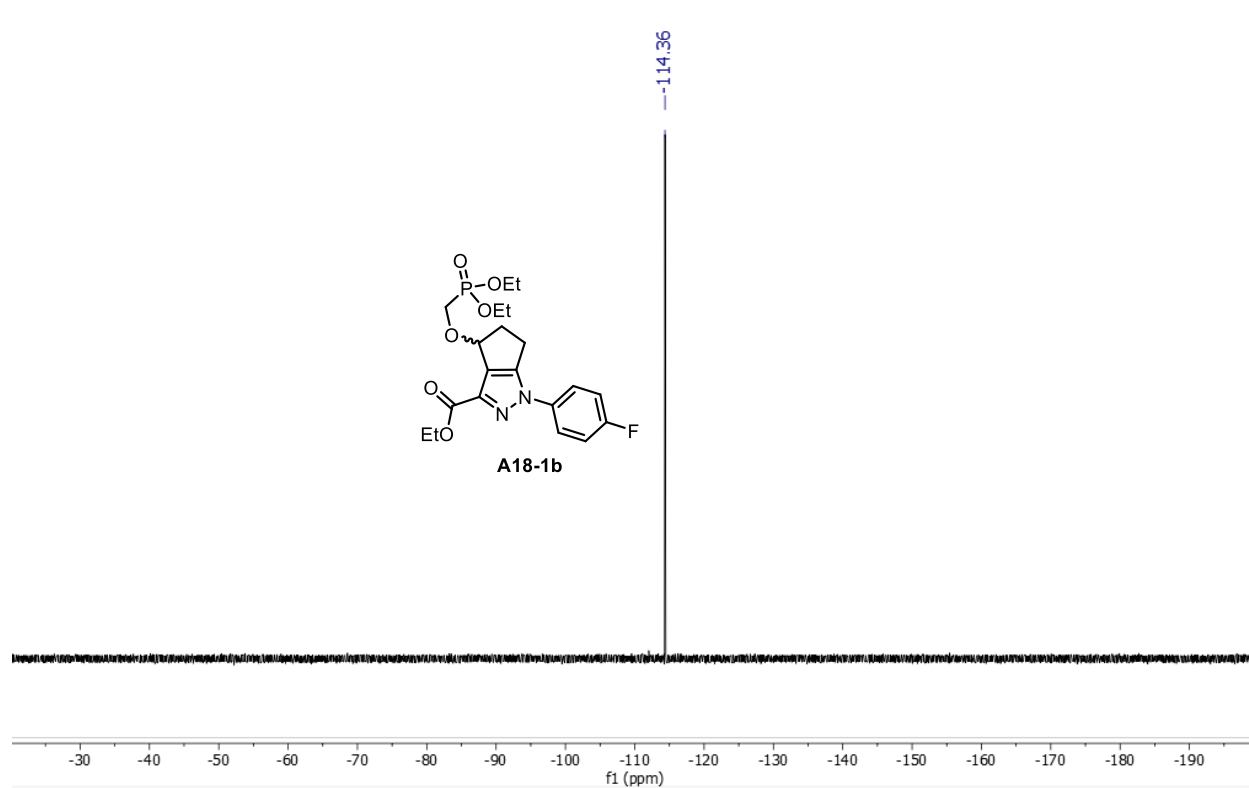
¹H NMR spectrum of **A18-1b** in CDCl₃ containing 0.03 % (v/v) TMS (500 MHz).



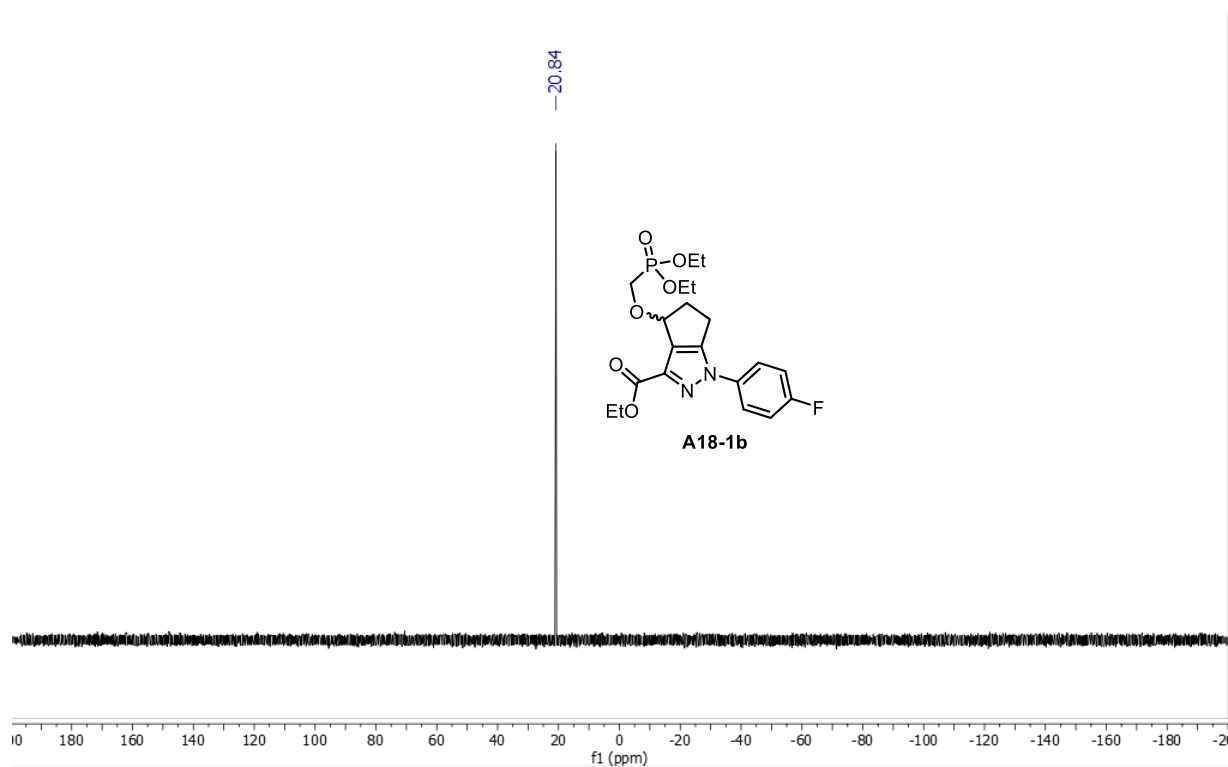
^{13}C NMR spectrum of **A18-1b** in CDCl_3 containing 0.03 % (v/v) TMS (126 MHz).



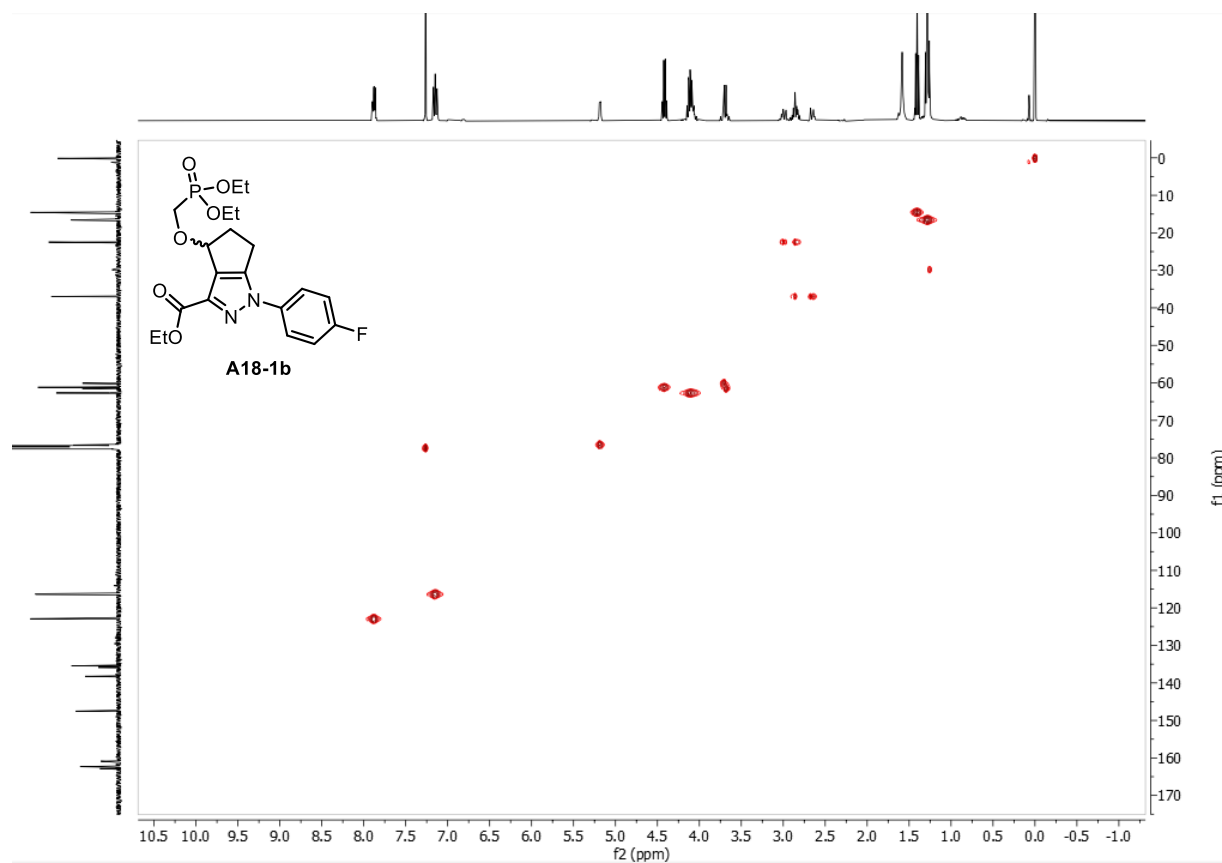
^{19}F NMR spectrum of **A18-1b** in CDCl_3 containing 0.03 % (v/v) TMS (377 MHz).



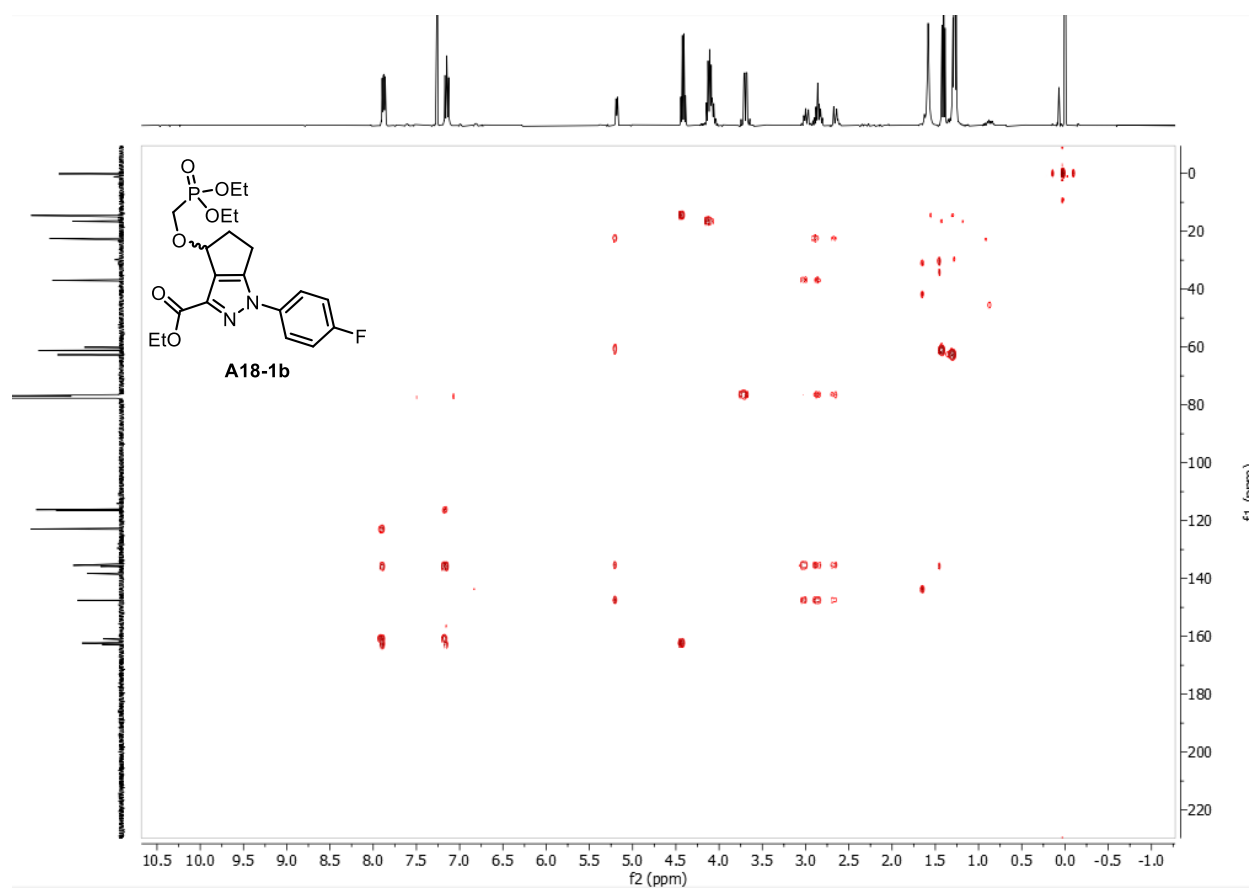
^{31}P NMR spectrum of **A18-1b** in CDCl_3 containing 0.03 % (v/v) TMS (162 MHz).

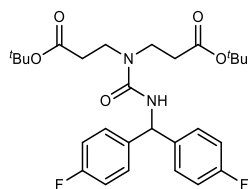


HSQC NMR spectrum of **A18-1b** in CDCl_3 containing 0.03 % (v/v) TMS (500, 126 MHz).



HMBC NMR spectrum of **A18-1b** in CDCl₃ containing 0.03 % (v/v) TMS (500, 126 MHz).





di-*tert*-butyl 3,3'-(((bis(4-fluorophenyl)methyl)carbamoyl)azanediyl)dipropionate, **A06-2**

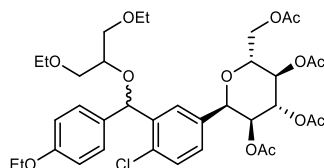
Reaction run using 4,4'-difluorodiphenylmethane **A06** (70.4 μ L, 0.40 mmol, 1.0 equiv.) and *N*-Bis(tert-butylpropionate)amine (264.9 mg, 1.4 mmol, 3.5 equiv.) and two diastereomers were isolated as a mixture. Yield = 106.0 mg (51%) of white solid isolated.

^1H NMR (CD_2Cl_2 , 500 MHz): 7.35 – 7.21 (m, 4H), 7.01 (t, J = 8.8 Hz, 4H), 6.97 (d, J = 7.9 Hz, 1H), 6.00 (d, J = 7.7 Hz, 1H), 3.45 (t, J = 6.3 Hz, 4H), 2.51 (t, J = 6.3 Hz, 4H), 1.41 (d, J = 1.5 Hz, 18H) ppm.

^{13}C NMR (CD_2Cl_2 , 126 MHz): 172.9, 162.3 (d, J = 244.6 Hz), 158.0, 139.7 (d, J = 3.2 Hz), 129.4 (d, J = 8.1 Hz), 115.5 (d, J = 21.5 Hz), 81.5, 57.6, 43.4, 34.9, 28.2 ppm.

^{19}F NMR (CD_2Cl_2 , 377 MHz): –117.6 ppm.

HRMS Calculated for $[\text{C}_{28}\text{H}_{36}\text{F}_2\text{N}_2\text{O}_5+\text{Na}]^+$: 541.2485, Found: 541.2479.



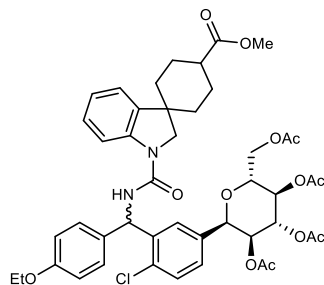
(2*R*,3*R*,4*R*,5*S*,6*R*)-2-(acetoxymethyl)-6-(4-chloro-3-(((1,3-diethoxypropan-2-yl)oxy)(4-ethoxyphenyl)methyl)phenyl)tetrahydro-2*H*-pyran-3,4,5-triyl triacetate, **A08-1**

Reaction run using dapagliflozin tetraacetate **A08** (115.4 mg, 0.20 mmol, 1.0 equiv.) and 1,3-diethoxypropan-2-ol (93.5 μ L, 0.60 mmol, 5.0 equiv.) and two diastereomers were isolated as a mixture. Yield = 50.0 mg (35%) of white amorphous solid isolated.

^1H NMR (CD_2Cl_2 , 500 MHz)(mixture of diastereomers: 50:50): 7.66 (d, J = 2.2 Hz, $0.5 \times 1\text{H}$), 7.59 (d, J = 2.1 Hz, $0.5 \times 1\text{H}$), 7.32 (d, J = 8.3 Hz, $0.5 \times 1\text{H}$), 7.28 (dd, J = 8.3, 1.3 Hz, $0.5 \times 3\text{H}$), 7.26 (d, J = 2.8 Hz, $0.5 \times 1\text{H}$), 7.22 (dd, J = 8.5, 2.1 Hz, $0.5 \times 3\text{H}$), 6.83 – 6.80 (m, 1H), 6.80 – 6.76 (m, 1H), 6.12 (s, $0.5 \times 1\text{H}$), 6.09 (s, $0.5 \times 1\text{H}$), 5.31 (dt, J = 18.8, 9.4 Hz, 1H), 5.22 (q, J = 9.4 Hz, 1H), 5.12 (t, J = 9.6 Hz, $0.5 \times 1\text{H}$), 5.03 (t, J = 9.6 Hz, $0.5 \times 1\text{H}$), 4.40 (dd, J = 9.8, 4.1 Hz, 1H), 4.28 (ddd, J = 12.4, 4.9, 1.4 Hz, 1H), 4.16 (ddd, J = 12.4, 10.1, 2.3 Hz, 1H), 3.98 (dq, J = 11.7, 7.0 Hz, 2H), 3.82 (dddd, J = 11.0, 9.9, 4.9, 2.3 Hz, 1H), 3.72 (dp, J = 18.8, 5.2 Hz, 1H), 3.57 (dd, J = 5.2, 3.6 Hz, 1H), 3.55 – 3.47 (m, 4H), 3.44 (qd, J = 7.1, 2.0 Hz, 3H), 2.09 (s, $0.5 \times 3\text{H}$), 2.08 (s, $0.5 \times 3\text{H}$), 2.06 (s, $0.5 \times 3\text{H}$), 2.06 (s, $0.5 \times 3\text{H}$), 2.01 (s, $0.5 \times 3\text{H}$), 1.98 (s, $0.5 \times 3\text{H}$), 1.86 (s, $0.5 \times 3\text{H}$), 1.57 (s, $0.5 \times 3\text{H}$), 1.37 (q, J = 6.8 Hz, 3H), 1.24 – 1.12 (m, 6H) ppm.

^{13}C NMR (CD_2Cl_2 , 126 MHz) (mixture of diastereomers: 50:50):: 170.83, 170.49, 170.45, 169.63, 169.12, 168.95, 158.58, 158.48, 140.57, 140.12, 135.55, 135.22, 133.33, 133.20, 133.08, 132.63, 129.93, 129.79, 129.36, 128.63, 128.17, 127.57, 126.72, 126.46, 114.31, 114.28, 79.84, 79.78, 77.84, 76.30, 76.29, 75.69, 75.05, 74.32, 74.31, 72.83, 72.61, 71.15 (d, J = 1.6 Hz), 70.97, 70.86, 68.73, 68.72, 66.88, 66.84, 66.82, 66.77, 63.51, 63.48, 62.50, 20.89, 20.88, 20.79, 20.76, 20.57, 20.29, 15.33, 15.31, 14.96, 14.93 ppm.

HRMS Calculated for $[\text{C}_{36}\text{H}_{47}\text{ClO}_{13}+\text{Na}]^+$: 745.2597, Found: 745.2591.



(2*R*,3*R*,4*R*,5*S*,6*R*)-2-(acetoxymethyl)-6-(4-chloro-3-((4-ethoxyphenyl)(4-methoxycarbonyl)spiro[cyclohexane-1,3'-indoline]-1'-carboxamido)methyl)phenyl)tetrahydro-2*H*-pyran-3,4,5-triyl triacetate, **A08-2**

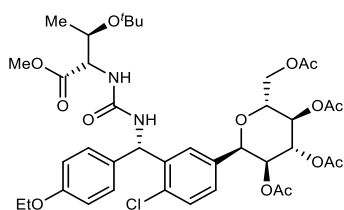
Reaction run using dapagliflozin tetraacetate **A08** (230.8 mg, 0.40 mmol, 1.0 equiv.) and methyl spiro[cyclohexane-1,3'-indoline]-4-carboxylate (490.6 mg, 2.0 mmol, 5.0 equiv.) and two diastereomers were isolated as a mixture.

A08-2: Yield = 79.1 mg (23%) of white solid isolated.

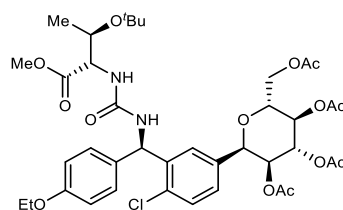
¹H NMR (CD₂Cl₂, 600 MHz) (mixture of diastereomers: 53:47): 7.90 (d, *J* = 8.0 Hz, 0.53 × 1H), 7.86 (d, *J* = 8.1 Hz, 0.47 × 1H), 7.50 (d, *J* = 2.2 Hz, 0.47 × 1H), 7.41 (d, *J* = 8.2 Hz, 0.53 × 1H), 7.38 (dd, *J* = 5.2, 3.0 Hz, 1H), 7.29 (td, *J* = 7.9, 2.2 Hz, 1H), 7.18 (d, *J* = 8.7 Hz, 1H), 7.14 (t, *J* = 8.3 Hz, 2H), 7.12 – 7.04 (m, 1H), 6.94 (tdd, *J* = 7.5, 3.2, 1.1 Hz, 1H), 6.86 (d, *J* = 8.6 Hz, 2H), 6.45 (d, *J* = 6.3 Hz, 0.53 × 1H), 6.37 (d, *J* = 6.2 Hz, 0.47 × 1H), 5.31 (t, *J* = 9.5 Hz, 1H), 5.28 (dd, *J* = 6.4, 1.8 Hz, 1H), 5.21 – 5.14 (m, 1 + 0.53 × 1H), 5.09 (t, *J* = 9.7 Hz, 0.47 × 1H), 4.47 (d, *J* = 9.8 Hz, 0.47 × 1H), 4.43 (d, *J* = 9.9 Hz, 0.53 × 1H), 4.23 – 4.11 (m, 2H), 4.01 (qd, *J* = 7.0, 4.4 Hz, 2H), 3.90 – 3.83 (m, 2H), 3.79 (d, *J* = 9.3 Hz, 0.53 × 1H), 3.74 (d, *J* = 9.3 Hz, 0.47 × 1H), 3.66 (s, 0.47 × 3H), 3.64 (s, 0.53 × 3H), 2.49 – 2.37 (m, 1H), 2.07 – 2.01 (m, 6H), 1.99 – 1.94 (m, 3H), 1.88 – 1.80 (m, 2H), 1.80 – 1.74 (m, 1H), 1.73 (d, *J* = 1.9 Hz, 3H), 1.72 – 1.66 (m, 1H), 1.66 – 1.52 (m, 3H), 1.38 (td, *J* = 6.9, 2.6 Hz, 3H) ppm.

¹³C NMR (CD₂Cl₂, 151 MHz) (mixture of diastereomers: 53:47): 176.22, 176.17, 170.84, 170.83, 170.44, 170.40, 169.89, 169.87, 169.41, 169.31, 159.07, 158.93, 154.13, 154.07, 143.30, 143.11, 140.33, 140.32, 139.05, 136.04, 135.96, 134.12, 133.88, 132.90, 132.32, 130.66, 129.58, 128.73, 128.51, 128.40, 128.28, 127.63, 127.44, 122.57, 122.54, 122.42, 122.31, 115.32, 115.31, 114.99, 114.97, 79.79, 79.76, 76.66, 76.64, 74.33, 74.26, 72.84, 72.63, 69.06, 69.00, 63.95, 62.78, 62.74, 57.67, 57.57, 56.04, 55.41, 51.90, 51.85, 44.45 (d, *J* = 3.8 Hz), 42.50, 36.96, 36.92, 36.89, 36.85, 26.04, 20.90, 20.85, 20.81, 20.77, 20.60, 20.57, 15.00 ppm.

HRMS Calculated for [C₄₅H₅₁ClN₂O₁₃+H]⁺: 863.3152, Found: 863.3156.



(2*R*,3*R*,4*R*,5*S*,6*R*)-2-(acetoxymethyl)-6-(3-((*S*)-(3-((2*S*,3*R*)-3-(*tert*-butoxy)-1-methoxy-1-oxobutan-2-yl)ureido)(4-ethoxyphenyl)methyl)-4-chlorophenyl)tetrahydro-2*H*-pyran-3,4,5-triyl triacetate, **A08-3a**



(2*R*,3*R*,4*R*,5*S*,6*R*)-2-(acetoxymethyl)-6-(3-((*R*)-(3-((2*S*,3*R*)-3-(*tert*-butoxy)-1-methoxy-1-oxobutan-2-yl)ureido)(4-ethoxyphenyl)methyl)-4-chlorophenyl)tetrahydro-2*H*-pyran-3,4,5-triyl triacetate, **A08-3b**

Reaction run using dapagliflozin tetraacetate **A08** (230.8 mg, 0.40 mmol, 1.0 equiv.) and methyl (2*S*,3*R*)-2-amino-3-(*tert*-butoxy)butanoate (265.0 mg, 1.4 mmol, 3.5 equiv.) and two diastereomers were isolated.

A08-3a: Yield = 59.7 mg (19%) of white solid isolated.

¹H NMR (CD₂Cl₂, 500 MHz): 7.46 (d, *J* = 2.1 Hz, 1H), 7.35 (d, *J* = 8.2 Hz, 1H), 7.26 (dd, *J* = 8.3, 2.1 Hz, 1H), 7.13 – 7.07 (m, 2H), 6.85 – 6.79 (m, 2H), 6.21 (d, *J* = 6.8 Hz, 1H), 5.36 – 5.28 (m, 3H), 5.28 – 5.18 (m, 2H), 5.10 (t, *J* = 9.7 Hz, 1H), 4.46 (d, *J* = 9.8 Hz, 1H), 4.34 – 4.29 (m, 1H), 4.28 (dd, *J* = 3.7, 1.9 Hz, 1H), 4.20 (qd, *J* = 6.2, 1.8 Hz, 1H), 4.14 (dd, *J* = 12.3, 2.3 Hz, 1H), 3.99 (q, *J* = 6.9 Hz, 2H), 3.87 (ddd, *J* = 9.9, 5.6, 2.4 Hz, 1H), 3.68 (s, 3H), 2.04 (s, 3H), 2.03 (s, 4H), 1.96 (s, 4H), 1.77 (s, 3H), 1.37 (t, *J* = 7.0 Hz, 3H), 1.18 (d, *J* = 6.2 Hz, 3H), 1.09 (s, 8H) ppm.

¹³C NMR (CD₂Cl₂, 101 MHz): 172.8, 171.0 (d, *J* = 3.2 Hz), 170.4, 169.9, 169.4, 158.9, 157.3, 140.4, 136.3, 133.7, 133.0, 130.4, 128.9, 127.8, 127.4, 114.9, 79.5, 76.5, 74.5, 74.2, 73.0, 69.1, 68.0, 63.9, 63.0, 59.4 (d, *J* = 4.1 Hz), 55.6, 52.3, 28.5, 21.2, 21.0, 20.9, 20.8, 20.7, 15.0 ppm.

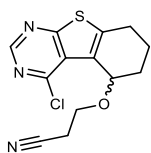
HRMS Calculated for [C₃₉H₅₁ClN₂O₁₄+H]⁺: 807.3102, Found: 807.3097.

A08-3b: Yield = 56.1 mg (17%) of white solid isolated.

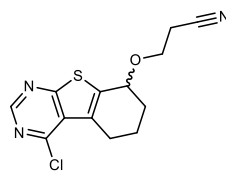
¹H NMR (CD₂Cl₂, 500 MHz): 7.49 (d, *J* = 2.1 Hz, 1H), 7.33 (d, *J* = 8.2 Hz, 1H), 7.23 (dd, *J* = 8.2, 2.2 Hz, 1H), 7.16 – 7.06 (m, 2H), 6.86 – 6.77 (m, 2H), 6.22 (d, *J* = 6.8 Hz, 1H), 5.33 (t, *J* = 9.5 Hz, 1H), 5.26 (dd, *J* = 11.3, 8.2 Hz, 2H), 5.18 (t, *J* = 9.7 Hz, 1H), 5.11 (t, *J* = 9.7 Hz, 1H), 4.44 (d, *J* = 9.9 Hz, 1H), 4.25 (dd, *J* = 9.6, 1.8 Hz, 1H), 4.23 – 4.15 (m, 3H), 4.00 (q, *J* = 7.0 Hz, 2H), 3.88 (ddd, *J* = 10.1, 4.6, 3.2 Hz, 1H), 3.68 (s, 3H), 2.06 (s, 3H), 2.04 (s, 3H), 1.97 (s, 3H), 1.80 (s, 3H), 1.37 (t, *J* = 7.0 Hz, 3H), 1.17 (d, *J* = 6.2 Hz, 3H), 1.08 (s, 9H) ppm.

¹³C NMR (CD₂Cl₂, 101 MHz): 172.76, 171.00, 170.41, 169.92, 169.27, 158.88, 157.24, 140.77, 136.06, 133.80, 132.93, 130.38, 129.28, 127.66, 127.27, 114.89, 79.81, 76.69, 74.33, 74.31, 72.85, 69.15, 67.91, 63.92, 62.97, 59.40, 55.61, 52.32, 28.47, 21.32, 21.02, 20.87, 20.84, 20.62, 15.01 ppm.

HRMS Calculated for [C₃₉H₅₁ClN₂O₁₄+H]⁺: 807.3102, Found: 807.3103.



3-((4-chloro-5,6,7,8-tetrahydrobenzo[4,5]thieno[2,3-d]pyrimidin-5-yl)oxy)propanenitrile, **A11-1a**



3-((4-chloro-5,6,7,8-tetrahydrobenzo[4,5]thieno[2,3-d]pyrimidin-8-yl)oxy)propanenitrile, **A11-1b**

Reaction run using 4-chloro-5,6,7,8-tetrahydro[1]benzothieno[2,3-*d*]pyrimidine **A11** (44.8 mg, 0.20 mmol, 1.0 equiv.) and 3-Hydroxypropionitrile (68.3 μ L, 0.60 mmol, 3.0 equiv.) and two regioisomers were isolated.

A11-1a: Yield = 18.3 mg (31%) of brownish semisolid. TLC (Pentane:EtOAc, 1:1 v/v): R_f = 0.56. $^1\text{H NMR}$ (CDCl_3 , 500 MHz): 8.77 (s, 1H), 5.10 (t, J = 2.9 Hz, 1H), 3.97 – 3.87 (m, 2H), 3.05 (ddd, J = 17.7, 5.4, 1.2 Hz, 1H), 2.85 (ddd, J = 17.8, 11.8, 6.0 Hz, 1H), 2.71 – 2.59 (m, 2H), 2.40 (ddt, J = 14.4, 4.8, 2.9 Hz, 1H), 2.17 (tddd, J = 14.0, 11.8, 5.5, 2.7 Hz, 1H), 2.04 – 1.89 (m, 1H), 1.73 (tt, J = 14.2, 3.1 Hz, 1H) ppm.

$^{13}\text{C NMR}$ (CDCl_3 , 126 MHz): 169.1, 152.8, 151.9, 145.3, 128.1, 126.0, 117.7, 69.9, 63.1, 26.2, 25.4, 19.3, 17.1 ppm.

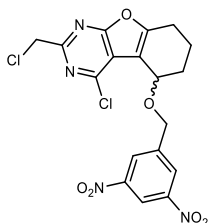
HRMS Calculated for $[\text{C}_{13}\text{H}_{12}\text{ClN}_3\text{OS}+\text{Na}]^+$: 316.0282, Found: 316.0276.

A11-2: Yield = 5.0 mg (9%) of white semisolid isolated. TLC (CH_2Cl_2 :MeOH = 50:1 v/v): R_f = 0.31.

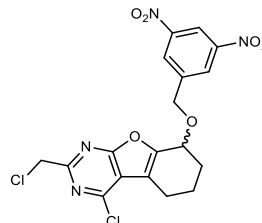
$^1\text{H NMR}$ (CDCl_3 , 500 MHz): 8.78 (s, 1H), 4.71 (td, J = 4.8, 2.1 Hz, 1H), 3.93 (dt, J = 9.1, 6.4 Hz, 1H), 3.86 (dt, J = 9.1, 6.3 Hz, 1H), 3.43 – 3.07 (m, 2H), 2.69 (t, J = 6.3 Hz, 2H), 2.44 – 2.11 (m, 2H), 2.06 – 1.96 (m, 1H), 1.95 – 1.84 (m, 1H) ppm.

$^{13}\text{C NMR}$ (CDCl_3 , 126 MHz): 169.7, 154.6, 152.5, 139.2, 130.1, 128.2, 117.5, 73.8, 63.7, 28.3, 26.3, 19.4, 19.3 ppm.

HRMS Calculated for $[\text{C}_{13}\text{H}_{12}\text{ClN}_3\text{OS}+\text{H}]^+$: 294.0462, Found: 294.0458.



4-chloro-2-(chloromethyl)-5-((3,5-dinitrobenzyl)oxy)-5,6,7,8-tetrahydrobenzofuro[2,3-d]pyrimidine, **A12-1a**



4-chloro-2-(chloromethyl)-8-((3,5-dinitrobenzyl)oxy)-5,6,7,8-tetrahydrobenzofuro[2,3-d]pyrimidine, **A12-1b**

Reaction run using 3-chloro-5-(chloromethyl)-8-oxa-4,6-diazatricyclo[7.4.0.0{2,7}]trideca-1(9),2,4,6-tetraene **A12** (51.4 mg, 0.2 mmol, 1.0 equiv.) and 3,5-dinitrobenzyl alcohol (118.6 mg, 0.60 mmol, 3.0 equiv.) and two regioisomers were isolated.

A12-1a: Yield = 37.0 mg (41%) of yellow semisolid isolated. TLC (pentane:EtOAc = 4:1): R_f = 0.27.

^1H NMR (CDCl_3 , 500 MHz): 8.96 (t, J = 2.1 Hz, 1H), 8.56 (d, J = 2.1 Hz, 2H), 5.08 (d, J = 13.0 Hz, 1H), 4.99 (d, J = 13.2 Hz, 1H), 4.77 (s, 2H), 4.74 (t, J = 3.7 Hz, 1H), 3.05 (dt, J = 16.9, 4.2 Hz, 1H), 2.79 (ddd, J = 16.8, 9.2, 5.5 Hz, 1H), 2.44 – 2.26 (m, 1H), 2.14 – 1.95 (m, 3H) ppm.

^{13}C NMR (CDCl_3 , 126 MHz): 167.1, 161.0, 153.6, 148.6, 142.8, 128.8, 127.0, 126.4, 118.0, 116.2, 116.1, 69.8, 46.3, 29.7 (d, J = 5.2 Hz), 29.4, 21.4, 18.4 ppm.

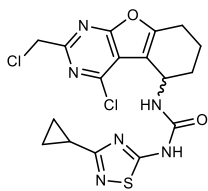
HRMS Calculated for $[\text{C}_{18}\text{H}_{14}\text{Cl}_2\text{N}_4\text{O}_6+\text{Na}]^+$: 475.0183, Found: 475.0177.

A12-1b: Yield = 15.5 mg (17%) of yellow semisolid isolated. TLC (pentane:EtOAc = 4:1): R_f = 0.15.

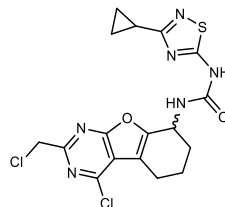
^1H NMR (CDCl_3 , 500 MHz): 8.96 (t, J = 2.1 Hz, 1H), 8.56 (d, J = 2.1 Hz, 2H), 5.07 (t, J = 3.0 Hz, 1H), 4.98 (d, J = 12.5 Hz, 1H), 4.93 (d, J = 12.3 Hz, 1H), 4.77 (s, 2H), 2.98 (ddd, J = 18.2, 5.8, 2.2 Hz, 1H), 2.81 (ddd, J = 18.0, 11.1, 6.3 Hz, 1H), 2.37 (ddt, J = 14.5, 5.3, 2.9 Hz, 1H), 2.20 (tddd, J = 13.7, 11.4, 5.8, 2.7 Hz, 1H), 2.15 – 2.05 (m, 1H), 1.86 (tt, J = 13.9, 3.5 Hz, 1H) ppm.

^{13}C NMR (CDCl_3 , 126 MHz): 167.2, 160.1, 159.7, 151.3, 148.6, 142.8, 129.2, 127.2, 126.4, 118.0, 116.0, 111.6, 69.6, 69.1, 46.3, 26.8, 23.4, 17.2 ppm.

HRMS Calculated for $[\text{C}_{18}\text{H}_{14}\text{Cl}_2\text{N}_4\text{O}_6+\text{Na}]^+$: 475.0183, Found: 475.0178.



1-(4-chloro-2-(chloromethyl)-5,6,7,8-tetrahydrobenzofuro[2,3-d]pyrimidin-5-yl)-3-(3-cyclopropyl-1,2,4-thiadiazol-5-yl)urea,
A12-2a



1-(4-chloro-2-(chloromethyl)-5,6,7,8-tetrahydrobenzofuro[2,3-d]pyrimidin-8-yl)-3-(3-cyclopropyl-1,2,4-thiadiazol-5-yl)urea,
A12-2b

Reaction run using 3-chloro-5-(chloromethyl)-8-oxa-4,6-diazatricyclo[7.4.0.0{2,7}]trideca-1(9),2,4,6-tetraene **A12** (102.8 mg, 0.40 mmol, 1.0 equiv.) and 3-cyclopropyl-1,2,4-thiadiazol-5-amine (282.4 mg, 2.0 mmol, 5.0 equiv.) and two regioisomers were isolated.

A12-2a: Yield = 55.0 mg (31%) of yellow semisolid isolated.

^1H NMR ($\text{DMSO}-d_6$, 500 MHz): 11.34 (s, 1H), 7.43 (d, J = 8.3 Hz, 1H), 5.10 (q, J = 7.1, 6.2 Hz, 1H), 4.87 (s, 2H), 2.89 – 2.71 (m, 2H), 2.19 – 2.09 (m, 1H), 2.11 – 2.04 (m, 1H), 1.97 – 1.83 (m, 3H), 0.94 (dt, J = 8.2, 2.8 Hz, 2H), 0.92 – 0.85 (m, 2H) ppm.

^{13}C NMR ($\text{DMSO}-d_6$, 126 MHz): 176.2, 172.1, 166.4, 159.9, 154.2, 153.7, 151.4, 115.9, 113.9, 46.4, 43.6, 29.5, 20.6, 19.6, 13.3, 8.4 ppm.

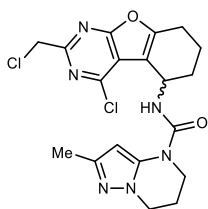
HRMS Calculated for $[\text{C}_{17}\text{H}_{16}\text{Cl}_2\text{N}_6\text{O}_2\text{S}+\text{H}]^+$: 439.0505, Found: 439.0502.

A12-2b: Yield = 28.6 mg (16%) of yellow semisolid isolated.

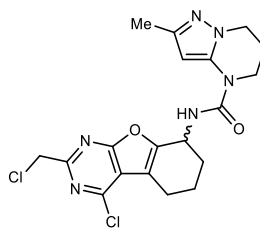
^1H NMR (DMSO- d_6 , 500 MHz): 11.04 (s, 1H), 7.33 (d, $J = 7.8$ Hz, 1H), 5.18 (d, $J = 5.1$ Hz, 1H), 4.88 (s, 2H), 2.97 – 2.84 (m, 1H), 2.84 – 2.73 (m, 1H), 2.11 – 2.02 (m, 1H), 1.99 – 1.92 (m, 2H), 1.92 – 1.71 (m, 2H), 1.03 – 0.91 (m, 2H), 0.91 – 0.75 (m, 2H) ppm.

^{13}C NMR (DMSO- d_6 , 126 MHz): 176.24, 172.06, 166.48, 159.51, 159.35, 153.14, 150.37, 115.70, 110.80, 46.42, 41.63, 29.11, 22.60, 17.32, 13.26, 8.42, 8.35 ppm.

HRMS Calculated for $[\text{C}_{17}\text{H}_{16}\text{Cl}_2\text{N}_6\text{O}_2\text{S}+\text{H}]^+$: 439.0505, Found: 439.0504.



N-(4-chloro-2-(chloromethyl)-5,6,7,8-tetrahydrobenzofuro[2,3-*d*]pyrimidin-5-yl)-2-methyl-6,7-dihydropyrazolo[1,5-*a*]pyrimidine-4(5H)-carboxamide, **A12-3a**



N-(4-chloro-2-(chloromethyl)-5,6,7,8-tetrahydrobenzofuro[2,3-*d*]pyrimidin-8-yl)-2-methyl-6,7-dihydropyrazolo[1,5-*a*]pyrimidine-4(5H)-carboxamide, **A12-3b**

Reaction run using 3-chloro-5-(chloromethyl)-8-oxa-4,6-diazatricyclo[7.4.0.0{2,7}]trideca-1(9),2,4,6-tetraene **A12** (102.8 mg, 0.40 mmol, 1.0 equiv.) and 4,5,6,7-Tetrahydro-2-methylpyrazolo[1,5-*a*]pyrimidine (274.4 mg, 2.0 mmol, 5.0 equiv.) and two regioisomers were isolated.

A12-3a: Yield = 34.0 mg (20%) of light yellow solid isolated.

^1H NMR (CD_2Cl_2 , 500 MHz): 5.77 (s, 1H), 5.73 (d, $J = 8.2$ Hz, 1H), 5.29 – 5.21 (m, 1H), 4.74 (s, 2H), 4.17 – 4.03 (m, 2H), 3.82 (td, $J = 5.2, 4.0$ Hz, 2H), 2.96 – 2.80 (m, 2H), 2.30 – 2.21 (m, 1H), 2.19 – 2.10 (m, 5H), 1.99 – 1.91 (m, 3H) ppm.

^{13}C NMR (CD_2Cl_2 , 126 MHz): 167.5, 160.8, 154.5, 153.6, 153.0, 116.8, 115.6, 47.0, 46.3, 45.0, 41.6, 30.9, 22.8, 21.6, 20.5, 14.0 ppm.

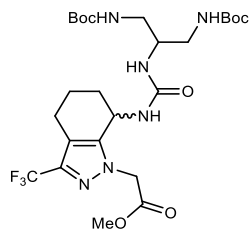
HRMS Calculated for $[\text{C}_{19}\text{H}_{20}\text{Cl}_2\text{N}_6\text{O}_2+\text{H}]^+$: 435.1098, Found: 435.1087.

A12-3b: Yield = 20.6 mg (12%) of light yellow solid isolated.

^1H NMR (CD_2Cl_2 , 500 MHz): 5.67 (d, $J = 7.7$ Hz, 1H), 5.60 (s, 1H), 5.38 (dt, $J = 6.5, 3.1$ Hz, 1H), 4.75 (s, 2H), 4.05 (t, $J = 6.3$ Hz, 2H), 3.88 – 3.74 (m, 2H), 2.89 (ddd, $J = 17.5, 4.7, 2.4$ Hz, 1H), 2.76 (dddd, $J = 20.0, 10.7, 5.9, 1.8$ Hz, 1H), 2.17 – 2.07 (m, 3H), 2.06 (s, 3H), 2.04 (dd, $J = 8.4, 4.5$ Hz, 1H), 1.97 – 1.85 (m, 2H).

^{13}C NMR (CD_2Cl_2 , 126 MHz): 167.63, 160.45, 159.91, 153.16, 151.92, 148.03, 139.66, 116.28, 111.89, 93.18, 47.02, 46.28, 42.91, 41.53, 29.94, 23.69, 22.95, 18.3, 14.0 ppm.

HRMS Calculated for $[\text{C}_{19}\text{H}_{20}\text{Cl}_2\text{N}_6\text{O}_2+\text{H}]^+$: 435.1098, Found: 435.1091.



methyl 2-(7-(3-(2,2,12,12-tetramethyl-4,10-dioxo-3,11-dioxo-5,9-diazatridecan-7-yl)ureido)-3-(trifluoromethyl)-4,5,6,7-tetrahydro-1*H*-indazol-1-yl)acetate, **A13-1**

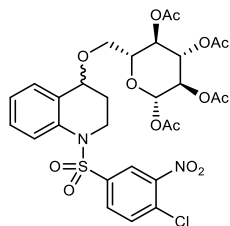
Reaction run using methyl 2-(3-(trifluoromethyl)-4,5,6,7-tetrahydro-1*H*-indazol-1-yl)acetate **A15** (104.9 mg, 0.40 mmol, 1.0 equiv.) and 4-(*tert*-butyl)-2-chloroaniline (405.1 mg, 1.4 mmol, 3.5 equiv.). Yield = 76.5 mg (32%) of white solid isolated.

^1H NMR (CD_2Cl_2 , 400 MHz): 5.87 (s, 1H), 5.61 (t, $J = 6.4$ Hz, 1H), 5.55 (t, $J = 6.5$ Hz, 1H), 5.47 – 5.12 (m, 1H), 5.11 – 4.91 (m, 1H), 4.86 (d, $J = 17.5$ Hz, 1H), 4.79 (d, $J = 17.7$ Hz, 1H), 3.76 (s, 3H), 3.54 (s, 1H), 3.23 – 3.11 (m, 4H), 2.63 – 2.54 (m, 1H), 2.44 (dt, $J = 15.9, 7.6$ Hz, 1H), 1.98 – 1.82 (m, 3 H), 1.82 – 1.71 (m, 1H), 1.40 (s, 9H), 1.39 (s, 9H) ppm.

^{13}C NMR (CD_2Cl_2 , 126 MHz): 167.8, 157.7, 157.6, 157.5, 143.6, 139.5 (q, $J = 37.3$ Hz), 123.1 (q, $J = 269.2$ Hz), 116.3, 79.8, 53.2, 52.7, 51.0, 42.1, 42.0, 41.9, 30.5, 28.5, 28.4, 21.4, 18.2 ppm.

^{19}F NMR (CD_2Cl_2 , 377 MHz): –61.8 ppm.

HRMS Calculated for $[\text{C}_{25}\text{H}_{39}\text{F}_3\text{N}_6\text{O}_7+\text{H}]^+$: 593.2905, Found: 593.2906.



(2*S*,3*R*,4*S*,5*R*,6*R*)-6-(((1-((4-chloro-3-nitrophenyl)sulfonyl)-1,2,3,4-tetrahydroquinolin-4-yl)oxy)methyl)tetrahydro-2*H*-pyran-2,3,4,5-tetrayl tetraacetate, **A15-1**

Reaction run using 1-(4-chloro-3-nitrobenzenesulfonyl)-1,2,3,4-tetrahydroquinoline **A15** (70.6 mg, 0.20 mmol, 1.0 equiv.) and 1,2,3,4-tetra-*O*-acetyl- β -*D*-glucopyranose (209 mg, 0.60 mmol, 3.0 equiv.) and two diastereomers were isolated as a mixture.

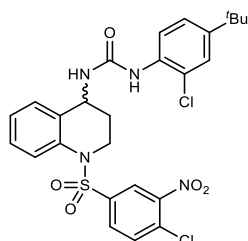
Yield = 45.9 mg (33%) of white semisolid isolated. TLC (100% Et_2O): $R_f = 0.52$.

^1H NMR (CDCl_3 , 500 MHz)(mixture of diastereomers: 55:45): 8.16 (dd, $J = 11.9, 2.1$ Hz, 1H), 7.83 (dd, $J = 8.4, 1.1$ Hz, 1×0.55 H), 7.77 (dd, $J = 8.4, 1.1$ Hz, 1×0.45 H), 7.73 (dd, $J = 8.5, 2.2$ Hz, 1×0.45 H), 7.71 (dd, $J = 8.4, 2.1$ Hz, 1×0.45 H), 7.61 (d, $J = 8.5$ Hz, 1×0.45 H), 7.59 (d, $J = 8.5$ Hz, 1×0.55 H), 7.30 (dddd, $J = 8.5, 7.3, 3.4, 1.7$ Hz, 1H), 7.25 (dd, $J = 7.7, 1.8$ Hz, 1×0.45 H), 7.20 (dd, $J = 7.6, 1.7$ Hz, 1×0.55 H), 7.14 (tdd, $J = 7.5, 3.8, 1.1$ Hz, 1H), 5.66 (dd, $J = 9.5, 8.3$ Hz, 1H), 5.22 (q, $J = 9.7$ Hz, 1H), 5.13 – 5.05 (m, 1H + 1×0.45 H), 4.27 (t, $J = 3.8$ Hz, 1×0.45 H), 4.23 (t, $J = 3.8$ Hz, 1×0.55 H), 4.13 (dt, $J = 12.9, 4.4$ Hz, 1×0.45 H), 4.05 (dt, $J = 12.6, 4.5$ Hz, 1×0.55 H), 3.78 (tt, $J = 12.4, 3.6$ Hz, 1H), 3.69 (ddd, $J = 10.0, 4.6, 2.7$ Hz, 1×0.45 H), 3.61 (ddd, $J = 10.0, 5.2, 2.9$ Hz, 1×0.55 H), 3.55 (dd, $J = 11.3, 2.7$ Hz, 1×0.45 H), 3.47 – 3.36 (m, 2×0.55 H), 3.33 (dd, $J = 11.3, 4.6$ Hz, 1×0.45 H), 2.10 (s, 3×0.55 H), 2.10 (s, 3×0.45 H),

2.04 (s, 3 × 0.55 H), 2.03 (s, 3 × 0.45 H), 2.01 (d, $J = 1.6$ Hz, 3H), 1.97 (s, 3 × 0.55 H), 1.82 (s, 3 × 0.45 H) ppm.

^{13}C NMR (CDCl_3 , 126 MHz): 170.13, 170.04, 169.51, 169.29, 169.26, 169.05, 169.01, 147.72, 139.38, 138.91, 135.63, 135.54, 132.74, 132.71, 131.62, 131.09, 130.96, 130.80, 130.34, 129.53, 129.41, 128.35, 127.65, 124.97, 124.76, 124.61, 124.45, 122.76, 122.46, 91.82, 91.71, 74.32, 74.05, 73.00, 72.85, 72.56, 70.22 (d, $J = 5.4$ Hz), 68.64, 68.36, 66.88, 65.90, 42.59, 27.15, 20.79, 20.78, 20.60, 20.57, 20.36 ppm.

HRMS Calculated for $[\text{C}_{29}\text{H}_{31}\text{ClN}_2\text{O}_{14}\text{S}+\text{Na}]^+$: 721.1077, Found: 721.1078.



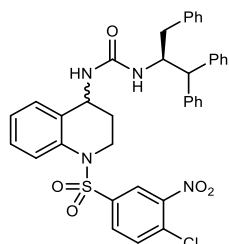
1-(4-(*tert*-butyl)-2-chlorophenyl)-3-(1-((4-chloro-3-nitrophenyl)sulfonyl)-1,2,3,4-tetrahydroquinolin-4-yl)urea, **A15-2**

Reaction run using 1-(4-chloro-3-nitrobenzenesulfonyl)-1,2,3,4-tetrahydroquinoline **A15** (70.6 mg, 0.40 mmol, 1.0 equiv.) and 4-(*tert*-butyl)-2-chloroaniline (367.0 mg, 2.0 mmol, 5.0 equiv.). Yield = 33.6 mg (15%) of off-white solid isolated.

^1H NMR (CD_2Cl_2 , 500 MHz): 8.12 (d, $J = 2.2$ Hz, 1H), 7.89 (d, $J = 8.6$ Hz, 1H), 7.76 (td, $J = 8.6$, 1.7 Hz, 2H), 7.66 (d, $J = 8.4$ Hz, 1H), 7.42 – 7.33 (m, 2H), 7.30 (td, $J = 8.3$, 7.8, 1.7 Hz, 1H), 7.25 (dd, $J = 8.6$, 2.3 Hz, 1H), 7.19 (td, $J = 7.5$, 1.2 Hz, 1H), 6.64 (s, 1H), 5.12 (d, $J = 7.6$ Hz, 1H), 4.79 (q, $J = 6.4$ Hz, 1H), 4.03 (ddd, $J = 14.0$, 7.4, 3.8 Hz, 1H), 3.83 (ddd, $J = 14.0$, 8.7, 3.5 Hz, 1H), 1.96 – 1.88 (m, 1H), 1.82 (dtd, $J = 13.8$, 6.9, 3.5 Hz, 1H), 1.28 (s, 9H) ppm.

^{13}C NMR (CD_2Cl_2 , 126 MHz): 154.3, 148.2, 148.0, 140.1, 136.4, 133.7, 133.1, 132.4, 131.4, 130.4, 129.8, 128.9, 126.6, 126.4, 125.2, 124.7, 123.9, 123.4, 121.8, 46.3, 44.8, 34.7, 31.3, 29.3 ppm.

HRMS Calculated for $[\text{C}_{26}\text{H}_{26}\text{Cl}_2\text{N}_4\text{O}_5\text{S}+\text{H}]^+$: 577.1073, Found: 577.1068.



1-((S)-1-((4-chloro-3-nitrophenyl)sulfonyl)-1,2,3,4-tetrahydroquinolin-4-yl)-3-((S)-1,1,3-triphenylpropan-2-yl)urea, **A15-3**

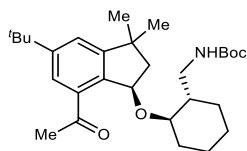
Reaction run using 1-(4-chloro-3-nitrobenzenesulfonyl)-1,2,3,4-tetrahydroquinoline **A15** (70.6 mg, 0.40 mmol, 1.0 equiv.) and (*S*)-(-)-1-benzyl-2,2-diphenylethylamine (402.37 mg, 1.4 mmol, 3.5 equiv.) and two diastereomers were isolated as a mixture.

A15-1: Yield = 70.8 mg (26%) of light yellow solid isolated.

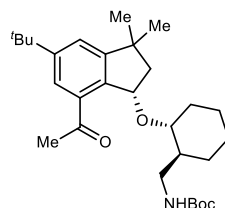
^1H NMR (CD_2Cl_2 , 600 MHz) (mixture of diastereomers: 50:50): 8.07 (d, $J = 2.2$ Hz, $0.5 \times 1\text{H}$), 8.04 (d, $J = 2.2$ Hz, $0.5 \times 1\text{H}$), 7.73 – 7.65 (m, 2H), 7.63 (d, $J = 8.7$ Hz, $0.5 \times 1\text{H}$), 7.61 (d, $J = 8.6$ Hz, $0.5 \times 1\text{H}$), 7.44 – 7.40 (m, 1H), 7.43 – 7.38 (m, 1H), 7.35 (td, $J = 7.8, 2.6$ Hz, 2H), 7.35 – 7.30 (m, 1H), 7.32 – 7.28 (m, 1H), 7.30 – 7.15 (m, 8H), 7.12 (m, $2 + 0.5 \times 1\text{H}$), 7.06 (td, $J = 7.5, 1.2$ Hz, $0.5 \times 1\text{H}$), 6.95 (dd, $J = 7.8, 1.6$ Hz, $0.5 \times 1\text{H}$), 6.80 (d, $J = 7.7$ Hz, $0.5 \times 1\text{H}$), 4.87 (s, 1H), 4.46 (p, $J = 6.2$ Hz, 1H), 4.07 (d, $J = 8.6$ Hz, 1H), 4.05 (d, $J = 8.0$ Hz, 1H), 3.96 (d, $J = 6.6$ Hz, $0.5 \times 1\text{H}$), 3.94 (d, $J = 6.6$ Hz, $0.5 \times 1\text{H}$), 3.86 (dddd, $J = 14.2, 10.9, 7.5, 3.6$ Hz, 1H), 3.66 (ddd, $J = 13.9, 8.5, 3.4$ Hz, $0.5 \times 1\text{H}$), 3.53 (ddd, $J = 13.8, 8.8, 3.4$ Hz, $0.5 \times 1\text{H}$), 2.92 (dd, $J = 5.6, 4.0$ Hz, $0.5 \times 1\text{H}$), 2.92 – 2.88 (m, $0.5 \times 1\text{H}$), 2.60 (dd, $J = 8.6, 1.9$ Hz, $0.5 \times 1\text{H}$), 2.58 (dd, $J = 8.7, 1.9$ Hz, $0.5 \times 1\text{H}$), 1.72 – 1.55 (m, 1H), 1.51 – 1.38 (m, 1H) ppm.

^{13}C NMR (CD_2Cl_2 , 151 MHz) (mixture of diastereomers: 50:50): 156.38, 156.36, 148.12, 143.15, 143.13, 142.91, 142.85, 139.96, 139.95, 138.92, 138.80, 136.02, 135.97, 133.54, 133.52, 132.25, 132.23, 131.02, 130.96, 130.00, 129.99, 129.73, 129.57, 129.29, 128.84, 128.81, 128.72, 128.70, 128.59, 128.57, 128.55, 128.51, 128.50, 127.14, 126.88, 126.68, 126.15 (d, $J = 2.1$ Hz), 124.63, 124.58, 123.53, 123.49, 57.48, 57.33, 45.84, 45.82, 44.84, 44.70, 40.23, 40.22, 40.16, 29.14, 29.02 ppm.

HRMS Calculated for $[\text{C}_{37}\text{H}_{33}\text{ClN}_4\text{O}_5\text{S}+\text{Na}]^+$: 703.1752, Found: 703.1757.



tert-butyl (((1*S*,2*R*)-2-(((*R*)-7-acetyl-5-(tert-butyl)-3,3-dimethyl-2,3-dihydro-1*H*-inden-1-yl)oxy)cyclohexyl)methyl)carbamate, **A16-1a**



tert-butyl (((1*S*,2*R*)-2-(((*S*)-7-acetyl-5-(tert-butyl)-3,3-dimethyl-2,3-dihydro-1*H*-inden-1-yl)oxy)cyclohexyl)methyl)carbamate, **A16-1b**

Reaction run using celestolide **A16** (48.9 mg, 0.20 mmol, 1.0 equiv.) and *tert*-butyl *N*-{[(1*S*,2*R*)-2-hydroxycyclohexyl]methyl}carbamate (137.6 mg, 0.60 mmol, 3.0 equiv.) and two diastereomers were isolated.

A16-1a: Yield = 11.3 mg (12%) of white solid isolated. TLC (pentane:Et₂O = 4:1): $R_f = 0.14$.

^1H NMR (CDCl_3 , 500 MHz): 7.68 (d, $J = 1.7$ Hz, 1H), 7.37 (d, $J = 1.7$ Hz, 1H), 5.40 (dd, $J = 7.1, 2.7$ Hz, 2H), 3.57 (td, $J = 10.1, 4.0$ Hz, 1H), 3.07 (ddd, $J = 13.4, 6.8, 3.5$ Hz, 1H), 2.97 (dt, $J = 12.9, 5.9$ Hz, 1H), 2.61 (s, 3H), 2.25 (dd, $J = 12.0, 3.5$ Hz, 1H), 2.19 (dd, $J = 13.4, 6.9$ Hz, 1H), 2.00 (dd, $J = 13.5, 2.6$ Hz, 1H), 1.75 (dq, $J = 12.6, 2.8$ Hz, 1H), 1.71 – 1.61 (m, 2H), 1.46 – 1.39 (m, 1H), 1.36 (s, 9H), 1.35 (br, 12H), 1.25 (s, 3H), 1.23 (m, 1H), 1.22 – 1.11 (m, 3H) ppm.

^{13}C NMR (CDCl_3 , 126 MHz): 201.2, 156.3, 154.7, 152.2, 139.3, 134.4, 125.5, 123.5, 83.4, 78.7, 78.0, 51.2, 44.0, 43.8, 42.6, 34.9, 33.7, 31.5, 31.2, 29.8, 29.0, 28.5, 28.2, 25.3, 24.6 ppm.

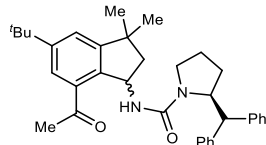
HRMS Calculated for $[\text{C}_{29}\text{H}_{45}\text{NO}_4+\text{H}]^+$: 472.3421, Found: 472.3416.

A16-1b: Yield = 9.0 mg (10%) of colorless semisolid isolated. TLC (pentane:Et₂O = 4:1): R_f = 0.18.

¹H NMR (CDCl₃, 500 MHz): 7.52 (d, *J* = 1.7 Hz, 1H), 7.31 (d, *J* = 1.8 Hz, 1H), 5.55 (dd, *J* = 6.6, 2.9 Hz, 1H), 4.83 (s, 1H), 3.34 – 3.04 (m, 3H), 2.59 (s, 3H), 2.38 (d, *J* = 10.5 Hz, 1H), 2.11 (dd, *J* = 13.4, 6.5 Hz, 1H), 1.97 (dd, *J* = 13.5, 2.9 Hz, 1H), 1.87 – 1.73 (m, 2H), 1.69 – 1.61 (m, 1H), 1.47 – 1.40 (m, 2H), 1.37 (s, 3H), 1.35 (s, 9H), 1.34 (s, 9H), 1.28 (s, 3H), 1.25 – 1.10 (m, 4H), 1.03 (qd, *J* = 12.4, 3.9 Hz, 1H) ppm.

¹³C NMR (CDCl₃, 126 MHz): 201.7, 156.0, 154.3, 152.2, 137.6, 136.4, 124.0, 122.3, 78.6, 78.5, 75.2, 46.9, 44.5, 43.8, 42.7, 34.9, 31.4, 31.1, 30.1, 30.0, 29.4, 29.3, 28.4, 25.3, 24.6 ppm.

HRMS Calculated for [C₂₉H₄₅NO₄+H]⁺: 472.3421, Found: 472.3418.



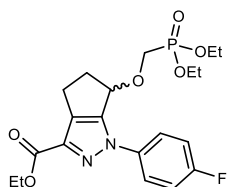
(2*S*)-*N*-(7-acetyl-5-(*tert*-butyl)-3,3-dimethyl-2,3-dihydro-1H-inden-1-yl)-2-benzhydrylpyrrolidine-1-carboxamide, **A16-2**

Reaction run using celestolide **A16** (97.8 mg, 0.40 mmol, 1.0 equiv.) and (*S*)-(-)-2-(diphenylmethyl)pyrrolidine (332.3 mg, 1.4 mmol, 3.5 equiv.) and two diastereomers were isolated as a mixture. Yield = 107.7 mg (52%) of off-white solid isolated.

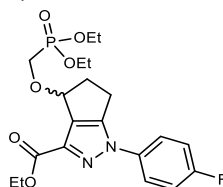
¹H NMR (CD₂Cl₂, 500 MHz)(mixture of diastereomers: 54:46): 7.56 (d, *J* = 1.8 Hz, 0.54 × 1H), 7.49 (d, *J* = 1.8 Hz, 0.46 × 1H), 7.40 (d, *J* = 1.8 Hz, 0.54 × 1H), 7.35 (d, *J* = 1.8 Hz, 0.46 × 1H), 7.33 – 7.14 (m, 9H), 7.13 – 7.05 (m, 1H), 5.43 (td, *J* = 7.3, 4.4 Hz, 0.54 × 1H), 5.37 – 5.29 (m, 0.46 × 1H), 4.82 (ddd, *J* = 8.2, 6.1, 1.9 Hz, 0.54 × 1H), 4.58 (t, *J* = 6.2 Hz, 0.46 × 1H), 4.44 (d, *J* = 6.1 Hz, 0.54 × 1H), 4.36 (d, *J* = 7.1 Hz, 0.46 × 1H), 4.31 (s, 0.54 × 1H), 4.05 (s, 0.46 × 1H), 3.41 (s, 0.46 × 1H), 3.16 (q, *J* = 8.6 Hz, 0.54 × 1H), 3.05 (td, *J* = 9.3, 2.9 Hz, 0.46 × 1H), 2.93 (td, *J* = 8.9, 3.1 Hz, 0.54 × 1H), 2.54 (s, 0.46 × 3H), 2.53 (s, 0.54 × 3H), 2.34 (t, *J* = 7.2 Hz, 0.46 × 1H), 2.31 (t, *J* = 7.4 Hz, 0.54 × 1H), 2.03 (m, 1H), 1.95 – 1.81 (m, 2H), 1.69 (m, 1H), 1.40 (s, 0.54 × 3H), 1.38 (s, 0.46 × 9H), 1.37 (s, 0.54 × 9H), 1.33 (s, 0.46 × 3H), 1.30 (s, 0.54 × 3H), 1.22 (s, 0.46 × 3H) ppm.

¹³C NMR (CDCl₃, 126 MHz): 203.25, 201.99, 157.64, 156.91, 154.97, 154.41, 152.56, 152.43, 143.17, 143.08, 142.83, 142.71, 138.34, 137.93, 137.34, 136.59, 129.90, 129.73, 129.30, 129.28, 128.71, 128.71, 128.51, 128.40, 126.88, 126.83, 126.78, 126.52, 124.80, 124.06, 123.20, 122.59, 62.06, 60.66, 54.62, 54.19, 53.90, 53.86, 50.85, 50.57, 46.41, 46.32, 42.73, 42.72, 35.24, 35.23, 31.60, 31.03, 30.27, 30.06, 29.98, 29.85, 29.51, 28.78, 23.97, 23.60 ppm.

HRMS Calculated for [C₃₅H₄₂N₂O₂+H]⁺: 523.3319, Found: 523.3314.



ethyl 6-((diethoxyphosphoryl)methoxy)-1-(4-fluorophenyl)-1,4,5,6-tetrahydrocyclopenta[*c*]pyrazole-3-carboxylate, **A18-1a**



ethyl 4-((diethoxyphosphoryl)methoxy)-1-(4-fluorophenyl)-1,4,5,6-tetrahydrocyclopenta[*c*]pyrazole-3-carboxylate, **A18-1b**

Reaction run ethyl 1-(4-fluorophenyl)-1,4,5,6-tetrahydrocyclopenta[*c*]pyrazole-3-carboxylate **A18** (54.5 mg, 0.2 mmol, 1.0 equiv.) and diethyl (hydroxymethyl)phosphonate (64.6 μ L, 0.60 mmol, 3.0 equiv.) and two regioisomers were isolated.

A18-1a: Yield = 14.2 mg (16%) of colorless liquid isolated.

^1H NMR (CDCl_3 , 500 MHz): 7.71 – 7.60 (m, 2H), 7.20 – 7.12 (m, 2H), 5.03 (d, $J = 6.0$ Hz, 1H), 4.43 (q, $J = 7.1$ Hz, 2H), 4.15 (dq, $J = 8.1, 7.1$ Hz, 4H), 3.99 (dd, $J = 13.6, 9.4$ Hz, 1H), 3.93 (dd, $J = 13.6, 9.2$ Hz, 1H), 3.23 (dt, $J = 15.0, 7.2$ Hz, 1H), 2.88 (ddt, $J = 13.2, 8.8, 6.5$ Hz, 1H), 2.80 (ddd, $J = 15.4, 8.8, 1.4$ Hz, 1H), 2.75 – 2.66 (m, 1H), 1.42 (t, $J = 7.1$ Hz, 3H), 1.32 (t, $J = 7.1$ Hz, 6H) ppm.

^{13}C NMR (CDCl_3 , 126 MHz): 162.2, 161.8 (d, $J = 248.0$ Hz), 152.8, 138.9, 135.8 (d, $J = 3.0$ Hz), 130.7, 122.5 (d, $J = 8.5$ Hz), 116.5 (d, $J = 23.1$ Hz), 77.3, 63.2 (d, $J = 156.0$ Hz), 62.5 (dd, $J = 7.3, 5.5$ Hz), 61.4, 39.6, 24.7, 16.6 (d, $J = 5.8$ Hz), 14.5 ppm.

^{19}F NMR (CDCl_3 , 377 MHz): –114.0 ppm.

^{31}P NMR (CDCl_3 , 162 MHz): 22.0 ppm.

HRMS Calculated for $[\text{C}_{20}\text{H}_{26}\text{FN}_2\text{O}_6\text{P}+\text{Na}]^+$: 463.1405, Found: 463.1399.

A18-1b: Yield = 7.6 mg (9%) of colorless liquid isolated.

^1H NMR (400 MHz, CDCl_3) δ 7.93 – 7.83 (m, 2H), 7.19 – 7.10 (m, 2H), 5.23 – 5.15 (m, 1H), 4.42 (q, $J = 7.1$ Hz, 2H), 4.18 – 4.05 (m, 4H), 3.78 – 3.62 (m, 2H), 3.08 – 2.93 (m, 1H), 2.92 – 2.79 (m, 2H), 2.74 – 2.59 (m, 1H), 1.40 (t, $J = 7.1$ Hz, 3H), 1.28 (td, $J = 7.1, 3.7$ Hz, 6H) ppm.

^{13}C NMR (CDCl_3 , 126 MHz): 162.33, 161.85 (d, $J = 247.4$ Hz), 147.52, 138.24, 135.87 (d, $J = 2.9$ Hz), 135.45, 122.93 (d, $J = 8.4$ Hz), 116.33 (d, $J = 23.0$ Hz), 76.51 (d, $J = 14.3$ Hz), 62.69 (t, $J = 7.0$ Hz), 61.18, 60.78 (d, $J = 170.0$ Hz), 36.97, 22.47, 16.58 (dd, $J = 5.7, 3.0$ Hz), 14.54 ppm.

^{19}F NMR (CD_2Cl_2 , 377 MHz): –114.4 ppm.

^{31}P NMR (CDCl_3 , 162 MHz): 20.8 ppm.

HRMS Calculated for $[\text{C}_{20}\text{H}_{26}\text{FN}_2\text{O}_6\text{P}+\text{H}]^+$: 441.1585, Found: 441.1581.

Appendix D: Supporting Information Chapter 5

5D.I. General Considerations

Materials and spectroscopic methods. Cu salts were purchased from Sigma Aldrich. Benzylic C–H substrates and the reagents for the syntheses were purchased from Oakwood Chemicals, Combi-Blocks, Chem-Impex, Alfa Aesar, TCI America, Ark Pharm, Enamine, AstaTech or Sigma Aldrich, and were used without further purification. TMS-N₃ was purchased from Sigma Aldrich. Ligands were purchased from Aldrich or TCI America. *N*-Fluorobenzenesulfonimide (NFSI) was purchased from Ark Pharm. The solvents were purchased from Fisher Scientific or Sigma Aldrich. The silica gel (particle size 40–63 μm, 230–400 mesh) that was used for flash column chromatography and thin layer chromatography plates (250 μm thickness) were purchased from SiliCycle. The photoreactions were carried out with two Par38 LED lamps supplying blue light ($\lambda = 440\text{--}460\text{ nm}$). The ¹H NMR, ¹³C NMR, and ¹⁹F NMR spectra were recorded on either a Bruker 400 MHz spectrometer or a Bruker 500 MHz spectrometer. High-resolution mass spectra were obtained using a Thermo Q Exactive™ Plus by the mass spectrometry facility at the University of Wisconsin-Madison. IR spectra were recorded on a Bruker Platinum-ATR ALPHA spectrometer. Melting points were determined using a DigiMelt MPA160 SRS melting point apparatus. Optical rotation was obtained using a Rudolph Research Autopol III polarimeter at room temperature. Elemental analysis was performed by Midwest Microlab, LLC. Enantioselectivities were determined by SFC/MS analyses on a Waters TharInvestigator equipped with a Daicel CHIRALCEL® OD-H HPLC analytical column (particle size 5 μm, ID 4.6 mm x L 250 mm).

Safety Consideration for Organic Azides^{1,2}

Azides are potentially explosive chemicals (PECs) that can decompose under the impact from external sources (heat, light, pressure, and shock). They should be stored in locations away from light, pressure, and shock at below room temperature. A blast shield should be placed around the reaction vessels containing the azides. The total number of nitrogen atoms in organic azide compounds should not surpass that of carbon. Azide compounds with a ratio of $(N_{\text{Carbon}} + N_{\text{Oxygen}}) / N_{\text{Nitrogen}} \geq 3$ are generally stable. Azide compounds with $(N_{\text{Carbon}} + N_{\text{Oxygen}}) / N_{\text{Nitrogen}}$ ratio between 1 and 3 can be synthesized and isolated but should be stored below room temperature with $\leq 1\text{ M}$ concentration and at a maximum of 5 grams of material. Isolation of azides with $(N_{\text{Carbon}} + N_{\text{Oxygen}}) / N_{\text{Nitrogen}}$ ratio < 1 are not allowed. Azide and acidic wastes should not be mingled as highly toxic and explosive hydrazoic acid can be generated. Azide waste should be stored in a container designated only for azide waste.

Computational Methods

For all computed structures, density functional theory (DFT) calculations are performed with the Gaussian 16 (rev. C.01) electronic structure program suite.³ Geometries of all stationary points are optimized in the *gas phase* at the B3LYP-D3(BJ)/basis-I level of theory,^{4,5} where *basis-I* comprises the 6-31G(d,p) basis⁶ for non-metals and the Stuttgart/Dresden effective core potential with its associated basis set (SDD) for Cu.⁷ For numerical integration in DFT, “ultrafine” grid is chosen together with the default integral accuracy set at 10⁻¹². Vibrational frequency calculations were performed at the same level of theory to ensure natures of all stationary points. Frequencies below 50 cm⁻¹ were replaced by a value of 50 cm⁻¹ in the vibrational partition function when

computing thermal contributions to free energies (1 atm pressure, T = 298.15K). For better estimate to Gibbs free energies, single point electronic energies were recomputed using M06-L/basis-II level of theory⁸ where *basis-II* consists of the def2-TZVP basis⁹ for non-metals and def2-TZVP basis/SDD pseudo potential for Cu. Solvation effects were included employing the SMD continuum solvation model¹⁰ with solvent parameters for nitromethane ($\epsilon = 36.562$). For the series of reactions (Figure 5D.10; Path-II) of the doublet benzylic radical with the triplet [LCu^{II}(N₃)₂]₂ dimer, yielding a benzylic azide product and the LCu^I(N₃) species, both having closed shell singlet electronic structures, along with the doublet [LCu^{II}(N₃)₂] monomer species, the corresponding transition-state (TS) structures were located on the broken-symmetry (BS) surface. In those cases, the spin-projection scheme of Yamaguchi et al.¹¹ was used for obtaining approximate spin-projected electronic energies of the lower-spin states using equation (S1). Redox potentials of various species were also computed (at 298.15 K) using the above-mentioned protocol. For the redox transformation: O(sol) + $ne^-(g) \rightarrow R(sol)$, standard reduction potential has been computed using equation (S2).

$$E_{AP}^{LS} = E^{HS} + (E_{BS}^{LS} - E^{HS}) \times \frac{\langle \hat{S}^2 \rangle_{\text{exact}}^{HS} - \langle \hat{S}^2 \rangle_{\text{exact}}^{LS}}{\langle \hat{S}^2 \rangle^{HS} - \langle \hat{S}^2 \rangle_{BS}^{LS}} \quad (\text{S1})$$

Where, E = electronic energy, BS = broken (spin) symmetry, AP = approximate (spin) projection, LS = low-spin, HS = high-spin.

$$E_{O|R}^0 = \frac{G^0(O,\text{sol}) - G^0(R,\text{sol})}{n_e F} - E_{\text{reference}}^0 \quad (\text{S2})$$

Where, $n_e = 1$, F is the Faraday constant. We first report *absolute* reduction potentials of various species setting $E_{\text{reference}}^0$ at 0 V. Corresponding values vs. the Fc^{0/+} reference were then calculated using an empirical correction factor accounting for experimentally available redox data, as detailed in Section S9 (Computed Reduction Potentials).

Cartesian Coordinates of Structures

Cartesian coordinates of all DFT-optimized structures can be accessed from the coordinate file (.xyz).

5D.II. General Procedure for Cu-Catalyzed Benzylic C-H Azidation

Procedure A: A 4 mL borosilicate glass vial was charged with benzylic substrate (0.4 mmol), 2.0 mol% of copper(II) acetate (1.5 mg, 8.0 μmol), 4.0 mol% of 2,2'-bis[(4*S*)-4-benzyl-2-oxazoline] (5.1 mg, 16 μmol), 2.5 equivalents of *N*-fluorobenzenesulfonimide (315 mg, 1.00 mmol), and a magnetic stir bar outside a glovebox. The vial was capped with an open-top cap installed with a TFE lined silicone SURE-LINK™ septum. The septum cap was pierced by a needle (22 gauge - 1 1/2", 0.7 mm x 40 mm) and the vial was moved into the glovebox and underwent four cycles of vacuum-nitrogen-backfill over 40 minutes. After removal of the needle, the vial was removed from the glovebox. The vial was charged with nitromethane (2.0 mL, 0.20 M) and 3.6 equivalents of azidotrimethylsilane (190 μL , 1.44 mmol) sequentially, stirred, and heated to 30 °C (inner temperature) in a heating block on a hot plate. After 24 hours, the vial was cooled to room temperature (25 °C), charged with 3.0 equivalents of Li_2CO_3 (89 mg, 1.2 mmol), opened to air, and stirred for 30 minutes. The reaction mixture was then filtered through a pipette-silica plug with dichloromethane (1.0 mL x 3 times). After evaporation of solvent on a rotary evaporator at 30 °C, flash column chromatography was performed. The isolated compound was dried to give the desired azido product.

Procedure B: Adopting Procedure A, the reaction was performed at 50 °C for 16 hours.

Procedure C: Adopting Procedure A, the reaction was performed for 48 hours.

Procedure D: Adopting Procedure A, the reaction was conducted in 0.2 mmol scale based on benzylic substrate. Deviation from Procedure A was 6.0 mol% of copper(II) acetate (2.2 mg, 12 μmol), 12 mol% of 2,2'-bis[(4*S*)-4-benzyl-2-oxazoline] (7.7 mg, 24 μmol), 2.5 equivalents of *N*-fluorobenzenesulfonimide (158 mg, 0.5 mmol), nitromethane (1.0 mL, 0.20 M), and 3.6 equivalents of azidotrimethylsilane (96 μL , 0.72 mmol). 3.0 equivalents of Li_2CO_3 (44 mg, 0.60 mmol) was used for workup process.

Procedure E: Adopting Procedure A, the reaction was conducted in 0.2 mmol scale based on benzylic substrate. Deviation from Procedure A was 1.0 mol% of copper(II) acetate (0.40 mg, 2.0 μmol), 2.0 mol% of 2,2'-bis[(4*S*)-4-benzyl-2-oxazoline] (1.3 mg, 4.0 μmol), 2.5 equivalents of *N*-fluorobenzenesulfonimide (158 mg, 0.5 mmol), nitromethane (1.0 mL, 0.20 M), and 3.6 equivalents of azidotrimethylsilane (96 μL , 0.72 mmol). 3.0 equivalents of Li_2CO_3 (44 mg, 0.60 mmol) was used for workup process.

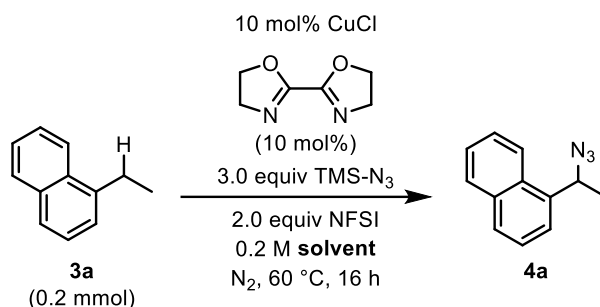
Notes:

- (1) For safety, all reaction should be performed with the use of blast shield.
- (2) Calibration of hot plate is highly recommended to maintain inner reaction temperature because performance of this reaction is sensitive to temperature (especially for reactions conducted at 30 °C; Procedure A and B).
- (3) Liquid benzylic C–H substrates were added between addition of nitromethane and azidomethylsilane.
- (4) Both dichloromethane (1.0 mL x 3 times) and nitromethane (1.0 mL x 3 times) were used for filtration with a pipette-silica plug.
- (5) Evaporation of solvent from compound **4a** or **4b** on the rotary evaporator should be carefully conducted at low temperature due to their high volatility.
- (6) Li_2CO_3 was not used for the crude mixture of compound **4t** to minimize keto-enol tautomerization.

5D.III. Screening Tables for Reaction Optimization

Note: Reaction conditions for screening were adopted from General Procedure A.

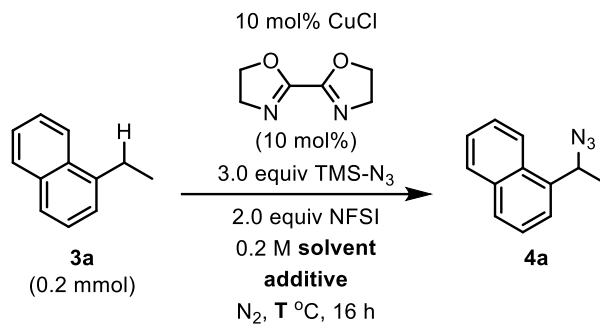
Table 5D.1. Optimization of the Reaction Conditions with Various Solvents^a



| entry | solvent | conv. of 3a (%) | yield of 4a (%) |
|----------|-------------------------|------------------------|------------------------|
| 1 | MeNO₂ | 100 | 57 |
| 2 | DCE | 18 | 7.0 |
| 3 | ACN | 100 | 49 |
| 4 | PhCl | 94 | 39 |
| 5 | PhCF ₃ | 9.0 | - |
| 6 | PhNO ₂ | 100 | 51 |
| 7 | PhH | 74 | 37 |
| 8 | Ph ₂ O | 11 | - |
| 9 | DME | 39 | 32 |
| 10 | 1,4-Dioxane | 8.0 | 22 |
| 11 | THF | 21 | 12 |
| 12 | CHCl ₃ | 86 | 47 |
| 13 | Acetone | 57 | 32 |
| 14 | EtOAc | 37 | 20 |
| 15 | DMF | 30 | 12 |
| 16 | DMAc | 23 | 8.0 |

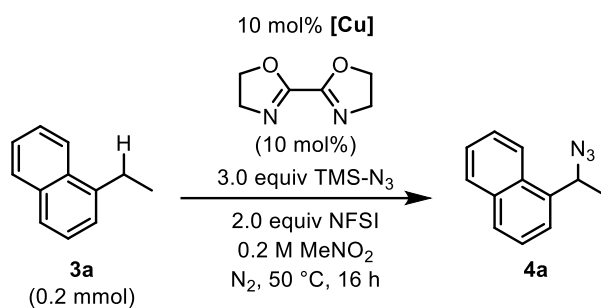
^aReaction yields monitored by ¹H NMR spectroscopy with 0.2 mmol mesitylene as the external standard. DCE, 1,2-dichloroethane; ACN, acetonitrile; DME, 1,2-dimethoxyethane; THF, tetrahydrofuran; EtOAc, ethyl acetate; DMF, *N,N*-dimethylformamide; DMAc, *N,N*-dimethylacetamide.

To summarize the results above, the reaction in nitromethane proceeds in the highest yield, but other polar solvents including acetonitrile, nitrobenzene, and acetone also led to a high conversion. Exceptions include the polar aprotic solvents *N,N*-dimethylformamide and *N,N*-dimethylacetamide. Etheral solvents such as 1,2-dimethoxyethane, tetrahydrofuran, 1,4-dioxane, and diphenyl ether afforded poor to no yield with low conversion.

Table 5D.2. Optimization of Reaction Conditions with Various Temperatures and Additives^a

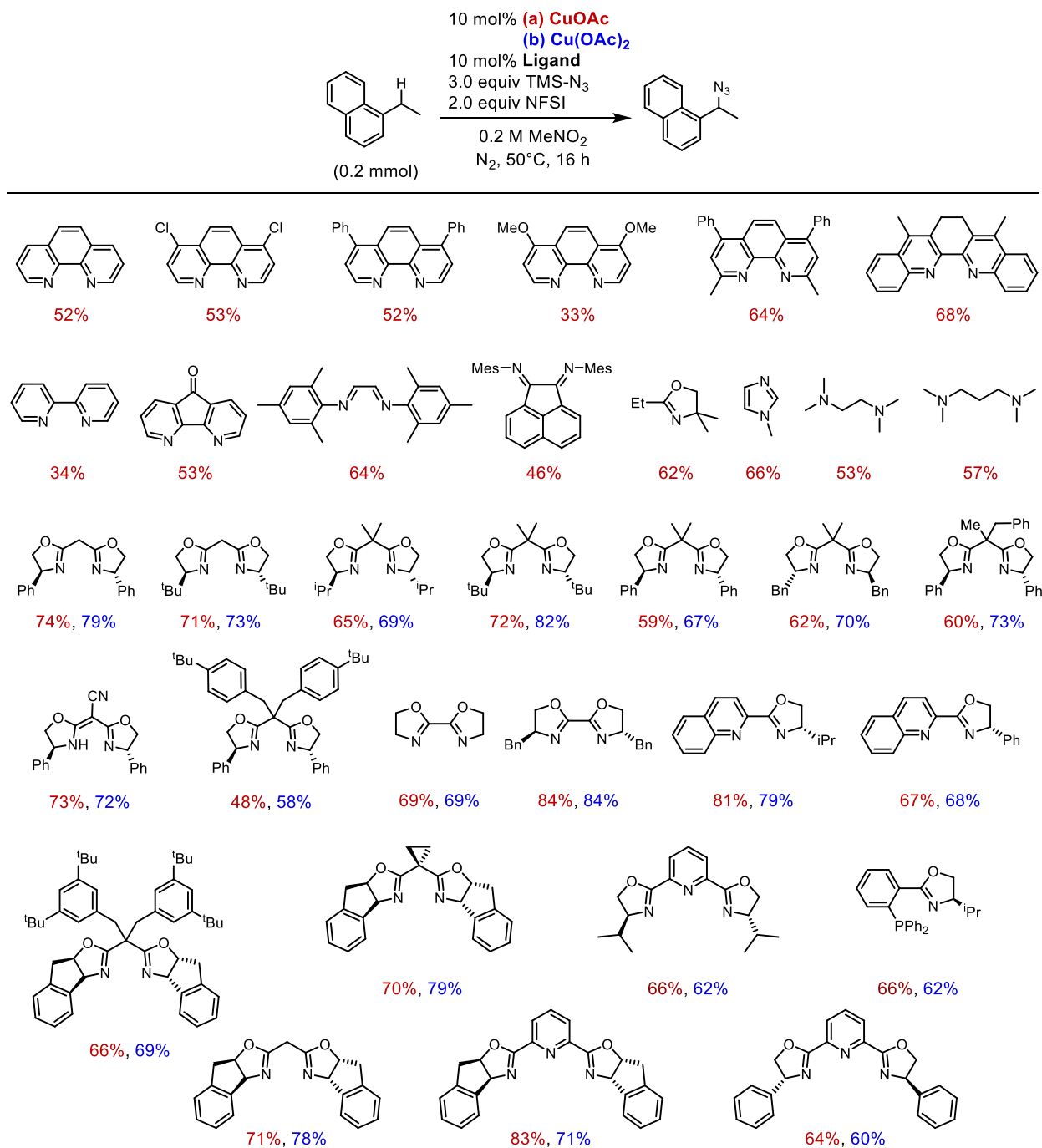
| entry | solvent | additive | temp (T) | conv. of 3a (%) | yield of 4a (%) |
|----------|-------------------------------|--|-----------|------------------------|------------------------|
| 1 | MeNO ₂ | - | 24 | 3.0 | - |
| 2 | MeNO ₂ | - | 40 | 37 | 29 |
| 3 | MeNO₂ | - | 50 | 88 | 63 |
| 4 | MeNO ₂ | - | 60 | 100 | 54 |
| 5 | MeNO ₂ :HFIP (4:1) | - | 50 | 86 | 65 |
| 6 | MeNO ₂ :HFIP (4:1) | 50 mol% (ⁱ PrO) ₂ P(O)H | 50 | 77 | 37 |
| 7 | MeNO ₂ | 50 mol% (ⁱ PrO) ₂ P(O)H | 50 | 64 | 51 |
| 8 | MeNO ₂ :HFIP (4:1) | - | 24 | 9.0 | 3.0 |
| 9 | MeNO ₂ :HFIP (4:1) | 50 mol% (ⁱ PrO) ₂ P(O)H | 24 | 3.0 | 3.0 |
| 10 | MeNO ₂ | 50 mol% (ⁱ PrO) ₂ P(O)H | 24 | 7.0 | - |

^aReaction yields monitored by ¹H NMR spectroscopy with 0.2 mmol mesitylene as the external standard.

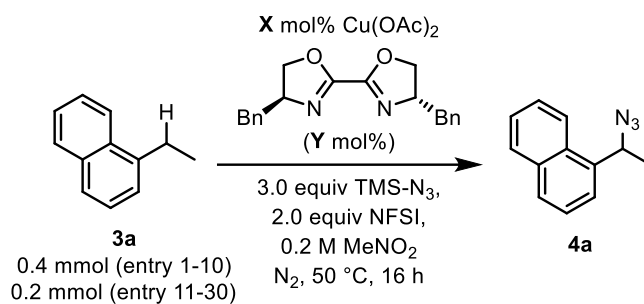
Table 5D.3. Optimization of Reaction Conditions with Various Copper Salts^a

| entry | [Cu] | conv. of 3a (%) | yield of 4a (%) |
|----------|--|------------------------|------------------------|
| 1 | CuCl | 90 | 63 |
| 2 | CuBr | 82 | 60 |
| 3 | CuI | 70 | 48 |
| 4 | CuOAc | 89 | 69 |
| 5 | Cu(ACN) ₄ PF ₆ | 83 | 39 |
| 6 | CuBr·SMe ₂ | 58 | 29 |
| 7 | Cu ₂ O | 1.0 | - |
| 8 | CuCl ₂ | 88 | 63 |
| 9 | Cu(OAc)₂ | 88 | 69 |
| 10 | Cu(acac) ₂ | 71 | 55 |
| 11 | Cu(OTf) ₂ ·PhH | 84 | 66 |
| 12 | Cu(OTf) ₂ ·PhMe | 64 | 51 |
| 13 | Cu(NO ₃) ₂ ·2.5H ₂ O | 56 | 42 |
| 14 | CuSO ₄ | 72 | 57 |
| 15 | CuPc | 17 | 9.0 |
| 16 | (<i>i</i> -Pr)CuCl | 91 | 67 |

^aReaction yields monitored by ¹H NMR spectroscopy with 0.2 mmol mesitylene as the external standard. acac, acetylacetonate; Pc, phthalocyanine

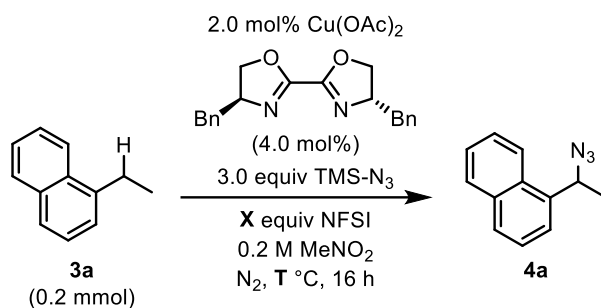
Table 5D.4. Optimization of Reaction Conditions with Various Ligands and Copper Salts^a

^aReaction yields monitored by ¹H NMR spectroscopy with 0.2 mmol mesitylene as the external standard.

Table 5D.5. Investigation of various radical initiators/oxidants

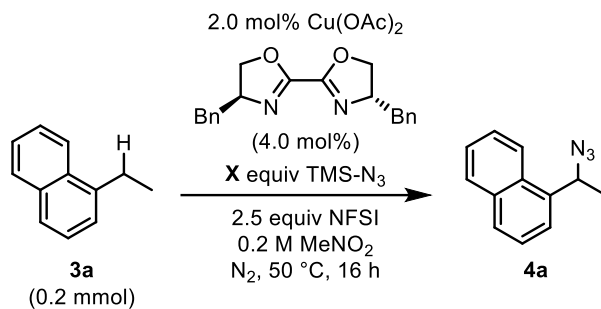
| entry | $\text{Cu}(\text{OAc})_2$ [X] | ligand [Y] | conv. of 3a (%) | yield of 4a (%) |
|----------|--|---------------------|------------------------|------------------------|
| 1 | 1.0 | 0.5 | 78 | 68 |
| 2 | 1.0 | 1.0 | 71 | 64 |
| 3 | 1.0 | 1.5 | 95 | 85 |
| 4 | 1.0 | 2.0 | 93 | 82 |
| 5 | 1.0 | 3.0 | 73 | 63 |
| 6 | 2.0 | 1.0 | 87 | 77 |
| 7 | 2.0 | 2.0 | 96 | 83 |
| 8 | 2.0 | 3.0 | 100 | 88 |
| 9 | 2.0 | 4.0 | 100 | 89 |
| 10 | 2.0 | 6.0 | 98 | 86 |
| 11 | 5.0 | 2.5 | 97 | 83 |
| 12 | 5.0 | 5.0 | 100 | 85 |
| 13 | 5.0 | 7.5 | 100 | 87 |
| 14 | 5.0 | 10 | 100 | 81 |
| 15 | 5.0 | 15 | 100 | 76 |
| 16 | 10 | 5.0 | 98 | 75 |
| 17 | 10 | 10 | 100 | 84 |
| 18 | 10 | 15 | 100 | 86 |
| 19 | 10 | 20 | 100 | 74 |
| 20 | 10 | 30 | 100 | 74 |
| 21 | 15 | 7.5 | 99 | 79 |
| 22 | 15 | 15 | 100 | 79 |
| 23 | 15 | 24 | 100 | 75 |
| 24 | 15 | 30 | 99 | 74 |
| 25 | 15 | 45 | 98 | 74 |
| 26 | 20 | 10 | 99 | 79 |
| 27 | 20 | 20 | 100 | 79 |
| 28 | 20 | 30 | 100 | 77 |
| 29 | 20 | 40 | 100 | 75 |
| 30 | 20 | 60 | 100 | 74 |

^aReaction yields monitored by ¹H NMR spectroscopy with 0.2 mmol mesitylene as the external standard

Table 5D.6. Optimization of Reaction Conditions with Various Equivalents of NFSI/Temperature^a

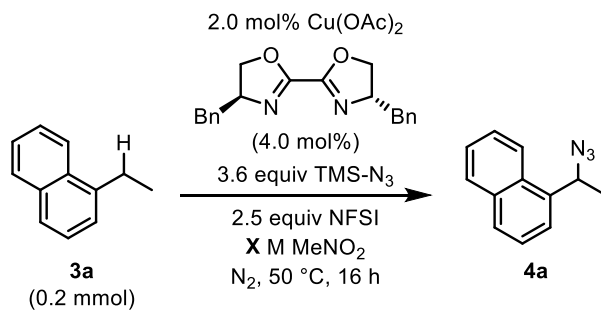
| entry | NFSI [X] | temp [T] | conv. of 3a (%) | yield of 4a (%) |
|-----------|------------|-----------|------------------------|------------------------|
| 1 | - | 30 | - | - |
| 2 | 0.5 | 30 | 26 | 24 |
| 3 | 1.0 | 30 | 39 | 32 |
| 4 | 1.5 | 30 | 47 | 36 |
| 5 | 2.0 | 30 | 53 | 40 |
| 6 | 2.5 | 30 | 58 | 42 |
| 7 | 3.0 | 30 | 59 | 50 |
| 8 | 4.0 | 30 | 70 | 51 |
| 9 | - | 40 | - | - |
| 10 | 0.5 | 40 | 40 | 37 |
| 11 | 1.0 | 40 | 65 | 56 |
| 12 | 1.5 | 40 | 76 | 64 |
| 13 | 2.0 | 40 | 82 | 70 |
| 14 | 2.5 | 40 | 92 | 74 |
| 15 | 3.0 | 40 | 95 | 74 |
| 16 | 4.0 | 40 | 97 | 76 |
| 17 | - | 50 | - | - |
| 18 | 0.5 | 50 | 42 | 40 |
| 19 | 1.0 | 50 | 72 | 70 |
| 20 | 1.5 | 50 | 98 | 87 |
| 21 | 2.0 | 50 | 100 | 89 |
| 22 | 2.5 | 50 | 100 | 91 |
| 23 | 3.0 | 50 | 100 | 86 |
| 24 | 4.0 | 50 | 100 | 86 |

^aReaction yields monitored by ¹H NMR spectroscopy with 0.2 mmol mesitylene as the external standard.

Table 5D.7. Optimization of Reaction Conditions with Various Equivalents of TMS-N₃^a

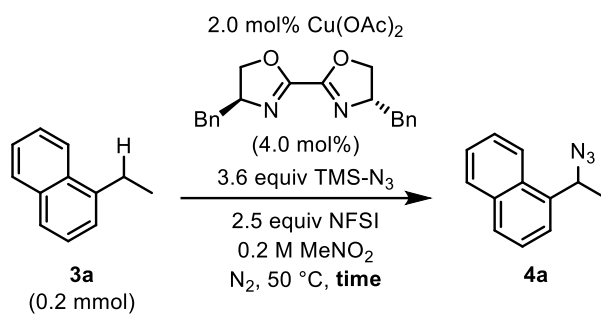
| entry | TMS-N ₃ [X] | conv. of 3a (%) | yield of 4a (%) |
|-----------|------------------------|------------------------|------------------------|
| 1 | 1.0 | 93 | 47 |
| 2 | 1.2 | 97 | 55 |
| 3 | 1.4 | 99 | 58 |
| 4 | 1.6 | 100 | 63 |
| 5 | 1.8 | 100 | 67 |
| 6 | 2.0 | 100 | 69 |
| 7 | 2.2 | 100 | 75 |
| 8 | 2.4 | 100 | 81 |
| 9 | 2.6 | 100 | 83 |
| 10 | 2.8 | 100 | 85 |
| 11 | 3.0 | 100 | 91 |
| 12 | 3.2 | 100 | 92 |
| 13 | 3.4 | 100 | 92 |
| 14 | 3.6 | 100 | 93 |
| 15 | 3.8 | 100 | 88 |
| 16 | 4.0 | 100 | 89 |
| 17 | 5.0 | 100 | 89 |
| 18 | 6.0 | 100 | 86 |
| 19 | 8.0 | 100 | 86 |

^aReaction yields monitored by ¹H NMR spectroscopy with 0.2 mmol mesitylene as the external standard.

Table 5D.8. Optimization of Reaction Conditions with Various Concentration^a

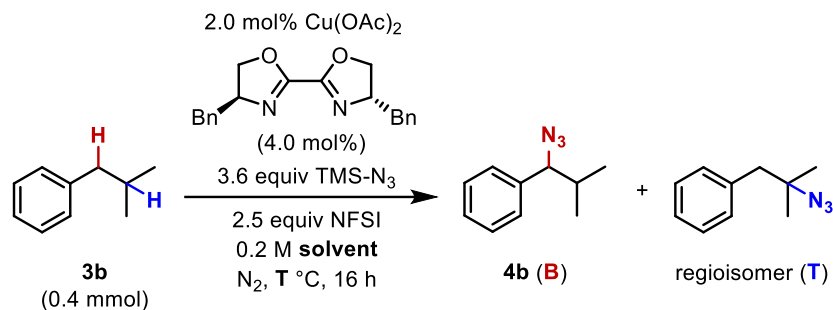
| entry | MeNO ₂ [X] | conv. of 3a (%) | yield of 4a (%) |
|----------|-----------------------|------------------------|------------------------|
| 1 | 2.00 | 100 | 82 |
| 2 | 1.00 | 100 | 83 |
| 3 | 0.50 | 100 | 86 |
| 4 | 0.40 | 100 | 87 |
| 5 | 0.30 | 100 | 90 |
| 6 | 0.25 | 100 | 91 |
| 7 | 0.22 | 100 | 92 |
| 8 | 0.20 | 100 | 93 |
| 9 | 0.18 | 100 | 91 |
| 10 | 0.15 | 100 | 85 |
| 11 | 0.13 | 100 | 86 |

^aReaction yields monitored by ¹H NMR spectroscopy with 0.2 mmol mesitylene as the external standard.

Table 5D.9. Optimization of Reaction Conditions with Various Reaction Time^a

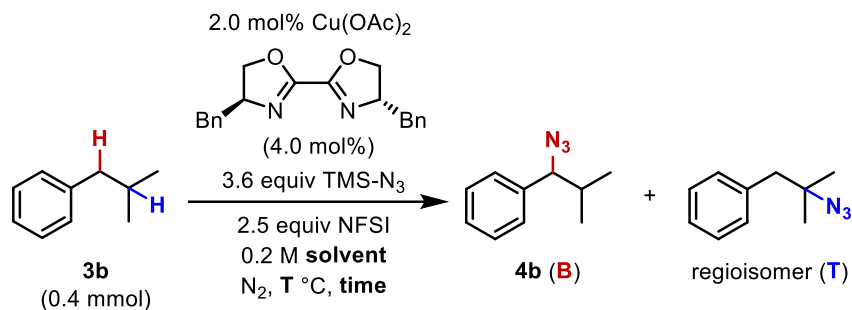
| entry | time | conv. of 3a (%) | yield of 4a (%) |
|-----------|-------------|------------------------|------------------------|
| 1 | 0.5 min | - | - |
| 2 | 1.0 min | - | - |
| 3 | 2.5 min | 1.0 | 1.0 |
| 4 | 5.0 min | 3.0 | 3.0 |
| 5 | 10 min | 8.0 | 7.0 |
| 6 | 15 min | 12 | 9.0 |
| 7 | 20 min | 12 | 12 |
| 8 | 30 min | 18 | 17 |
| 9 | 40 min | 21 | 20 |
| 10 | 50 min | 25 | 24 |
| 11 | 1.0 h | 32 | 31 |
| 12 | 1.5 h | 54 | 40 |
| 13 | 2.0 h | 56 | 47 |
| 14 | 2.5 h | 61 | 52 |
| 15 | 3.0 h | 69 | 59 |
| 16 | 4.0 h | 78 | 67 |
| 17 | 5.0 h | 84 | 75 |
| 18 | 6.0 h | 86 | 80 |
| 19 | 8.0 h | 99 | 89 |
| 20 | 12 h | 100 | 91 |
| 21 | 16 h | 100 | 93 |
| 22 | 24 h | 100 | 90 |
| 23 | 32 h | 100 | 89 |
| 24 | 48 h | 100 | 85 |
| 25 | 72 h | 100 | 80 |

^aReaction yields monitored by ¹H NMR spectroscopy with 0.2 mmol mesitylene as the external standard

Table 5D.10. Optimization of Benzylic C–H Site-Selectivity with Various Solvents and Temperatures^a

| entry | solvent | temp [T] | conv. of 3b (%) | product (B+T) (%) | ratio (B : T) |
|----------|-------------------------------|-----------|------------------------|----------------------------|-------------------------------|
| 1 | MeNO ₂ | 25 | 3 | 3 | Only B |
| 2 | MeNO₂ | 30 | 50 | 40 | 12 : 1.0 |
| 3 | MeNO ₂ | 40 | 90 | 50 | 6.0 : 1.0 |
| 4 | MeNO ₂ | 50 | 97 | 46 | 4.6 : 1.0 |
| 5 | C ₆ H ₆ | 25 | 8 | 7.9 | 9.5 : 1.0 |
| 6 | C ₆ H ₆ | 30 | 45 | 32 | 8.8 : 1.0 |
| 7 | C ₆ H ₆ | 40 | 70 | 38 | 7.8 : 1.0 |
| 8 | C ₆ H ₆ | 50 | 85 | 33 | 5.1 : 1.0 |
| 9 | PhCl | 25 | 28 | 23 | 8.7 : 1.0 |
| 10 | PhCl | 30 | 57 | 37 | 11 : 1.0 |
| 11 | PhCl | 40 | 83 | 36 | 6.0 : 1.0 |
| 12 | PhCl | 50 | 93 | 26 | 3.4 : 1.0 |

^aReaction yields monitored by ¹H NMR spectroscopy with 0.2 mmol mesitylene as the external standard.

Table 5D.11. Optimization of Benzylic C–H Site-Selectivity with Various Length of Reaction Time^a

| entry | solvent | temp [T] | time (h) | conv. of 3b (%) | product (B + T) (%) | ratio (B : T) |
|-----------|-------------------------------|-----------|-----------|------------------------|-------------------------------------|-------------------------------|
| 1 | PhCl | 25 | 16 | 28 | 23 | 8.7 : 1.0 |
| 2 | PhCl | 25 | 24 | 45 | 31 | 12 : 1.0 |
| 3 | PhCl | 25 | 40 | 69 | 40 | 10 : 1.0 |
| 4 | PhCl | 25 | 64 | 85 | 34 | 7.1 : 1.0 |
| 5 | PhCl | 25 | 88 | 89 | 32 | 6.6 : 1.0 |
| 6 | PhCl | 25 | 112 | 91 | 28 | 7.2 : 1.0 |
| 7 | PhCl | 30 | 16 | 57 | 37 | 11 : 1.0 |
| 8 | PhCl | 30 | 24 | 75 | 40 | 9.2 : 1.0 |
| 9 | PhCl | 30 | 40 | 85 | 36 | 7.8 : 1.0 |
| 10 | PhCl | 30 | 64 | 85 | 29 | 6.9 : 1.0 |
| 11 | PhCl | 30 | 88 | 93 | 25 | 4.6 : 1.0 |
| 12 | PhCl | 30 | 112 | 96 | 21 | 3.8 : 1.0 |
| 13 | C ₆ H ₆ | 30 | 16 | 45 | 32 | 8.8 : 1.0 |
| 14 | C ₆ H ₆ | 30 | 24 | 59 | 38 | 7.5 : 1.0 |
| 15 | C ₆ H ₆ | 30 | 40 | 73 | 39 | 8.0 : 1.0 |
| 16 | C ₆ H ₆ | 30 | 64 | 84 | 36 | 4.8 : 1.0 |
| 17 | C ₆ H ₆ | 30 | 88 | 87 | 31 | 7.0 : 1.0 |
| 18 | C ₆ H ₆ | 30 | 112 | 89 | 29 | 5.4 : 1.0 |
| 19 | MeNO ₂ | 30 | 16 | 50 | 40 | 12 : 1.0 |
| 20 | MeNO₂ | 30 | 24 | 60 | 48 | 11 : 1.0 |
| 21 | MeNO ₂ | 30 | 40 | 80 | 51 | 9.7 : 1.0 |
| 22 | MeNO ₂ | 30 | 64 | 91 | 56 | 8.1 : 1.0 |
| 23 | MeNO ₂ | 30 | 88 | 95 | 51 | 7.5 : 1.0 |
| 24 | MeNO ₂ | 30 | 112 | 97 | 48 | 7.2 : 1.0 |

^aReaction yields monitored by ¹H NMR spectroscopy with 0.2 mmol mesitylene as the external standard.

5D.IV. Racemization Experiments

Yields, conversion, and enantioselectivities of azide products were determined by ^1H NMR spectroscopy and supercritical fluid chromatography (SFC) analysis respectively. SFC/MS analyses were performed on a Waters TherInvestigator equipped with a Daicel CHIRALCEL[®] OD-H HPLC analytical column (particle size 5 μm , ID 4.6 mm x L 250 mm) was used for separations of enantiomers. The sample was eluted with MeOH 20% with CO_2 at a flow rate of 3 mL/min at 35 $^\circ\text{C}$ with an automated backpressure regulator at 100 bar. Injection volume for each sample was 5.0 μL of a 10-30 μM solution in acetonitrile and the detection wavelength was 273 nm.

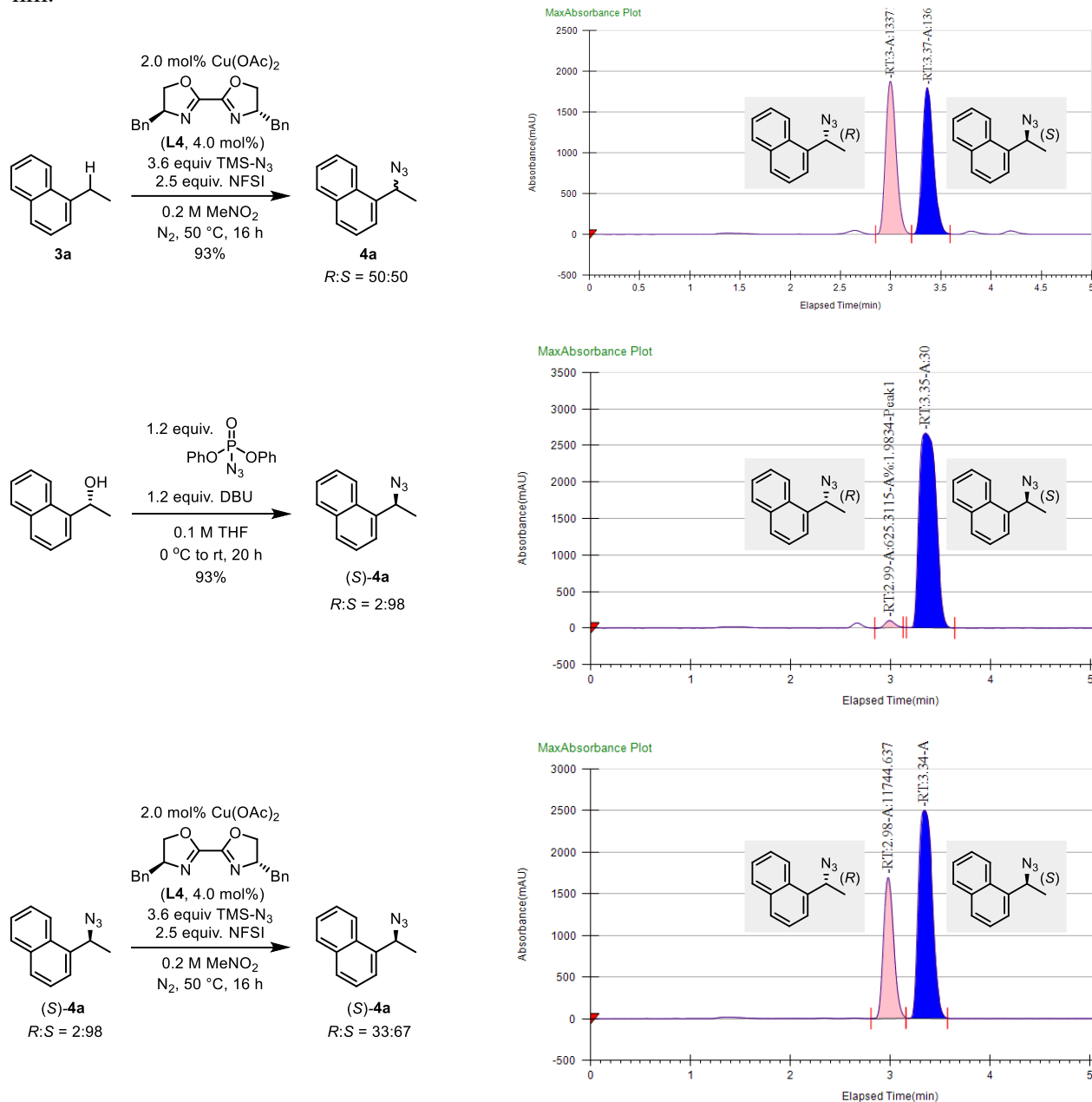


Figure 5D. 1. Supercritical fluid chromatography data.

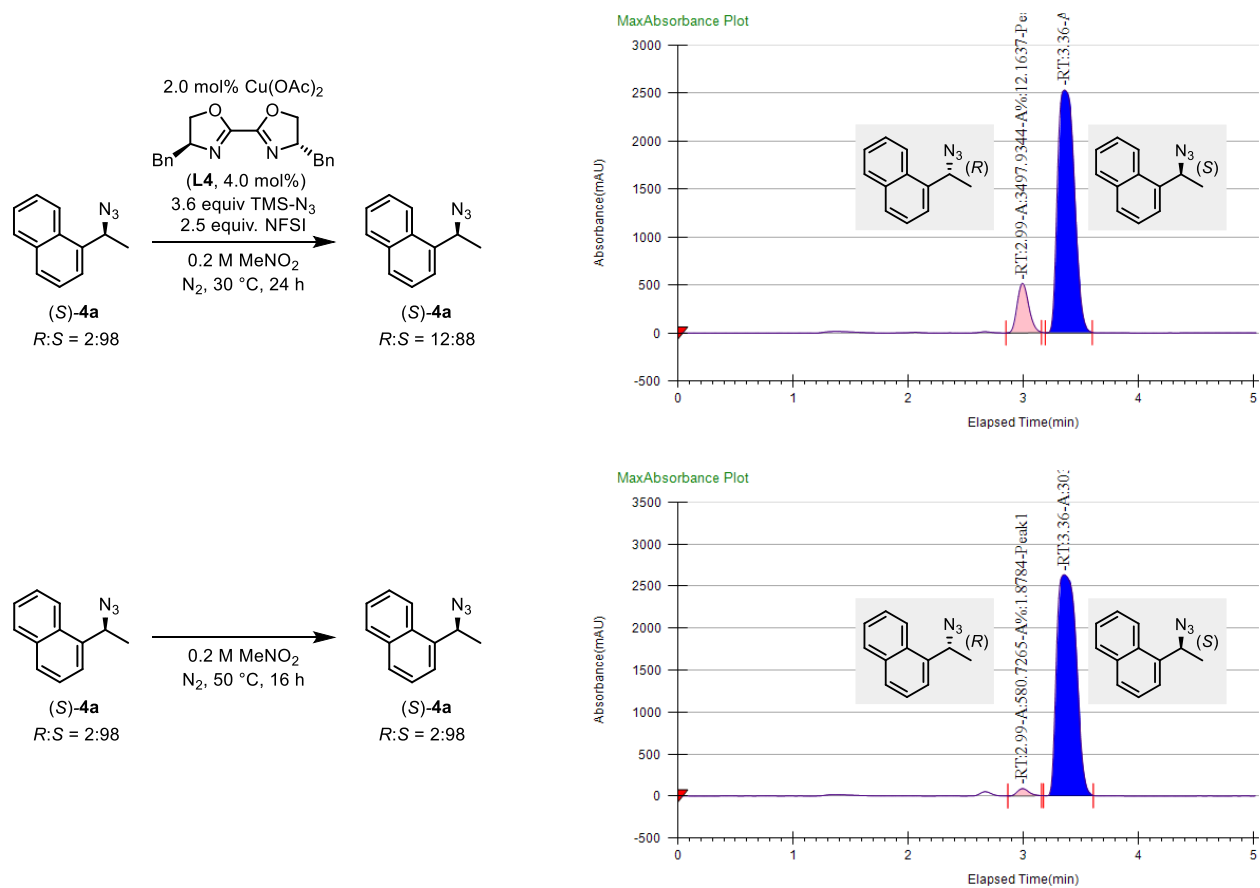
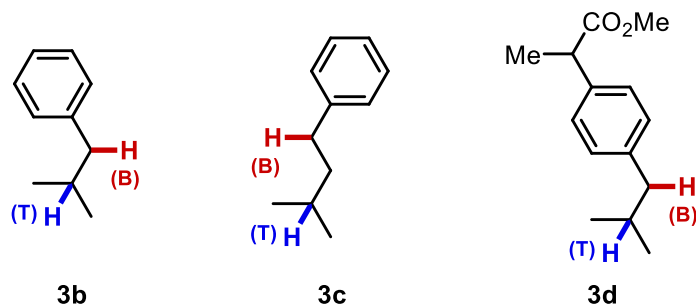


Figure 5D. 1. (Continued) Supercritical fluid chromatography data.

5D.V. Comparative Experiments and Results with Known C-H Azidation Methods

Table 5D.12. Tabulated Summary of Yield of Benzylic and Tertiary Azido Products^a

| catalyst | Benzylic | Tertiary | Benzylic | Tertiary | Benzylic | Tertiary |
|--|-------------------|-------------------|-------------|------------|-------------------|-------------------|
| Mes-Acr ^b | 17.4 ^e | 22.6 ^e | none | 34.0 | 27.0 ^e | 30.0 ^e |
| Mn(salen)Cl ^c | 19.5 | 4.2 | 23.4 | 5.1 | 43.0 | 3.3 |
| Fe(OAc) ₂ ·PyBOX ^d | 19.4 | 20.6 | 27.8 | 19.9 | 18.0 | 7.0 |
| This work | 44.0 | 4.0 | 68.0 | 2.7 | 60.0 | 2.0 |

^aReaction yields were monitored by ¹H NMR spectroscopy with 0.2 mmol mesitylene as the external standard. ^bMethod II. ^cMethod III. ^dMethod IV. ^eYields and ratios were obtained from the literature.¹²

Method II: General Procedure for Mes-Acr System. According to the literature,¹² a 4 mL borosilicate glass vial was charged with a magnetic stir bar, 5.0 mol% of 9-mesityl-3,6-di-*tert*-butyl-10-phenylacridinium tetrafluoroborate (Mes-Acr, 2.9 mg, 5.0 μmol), 1.1 equivalents of K₃PO₄ (23.3 mg, 0.11 mmol), 3.0 equivalents of 4-(trifluoromethyl)benzenesulfonyl azide **S7** (75.4 mg, 0.3 mmol), hexafluoroisopropanol (HFIP, 1.0 mL), 0.1 mmol of substrate **3b** or **3c** sequentially in a glovebox. The vial was taken out of the glovebox and positioned on a stir plate with a gap of 2 cm between two Par38 LED lamps (blue light, λ = 440-460 nm). After stirring with irradiation for 20 hours, the crude solution was filtered through a pipette-silica plug with dichloromethane (1.0 mL x 3 times). Ratios of benzylic (**4b** or **4c**)^{13,14} and tertiary product^{15,16} were determined by ¹H NMR analysis of crude mixture with 0.2 mmol mesitylene as an external standard.

Note: (1) The azidation reagent (**S7**) was synthesized according to literature procedure.¹⁷ (2) The yield and ratio of benzylic:tertiary products from **3c** was not reported by using the MES-Acr system in the literature.¹² (3) **3b** was used as a literature substrate to reproduce the reported yield (40%, isolated yield) and the ratio of regioisomers (benzylic:tertiary = 1.0:1.3) prior to the comparative experiments with the targeted substrate **3c**. Our experiment gave reproducible results: 45% NMR yield and the 1.0:1.3 ratio of tertiary benzylic to primary benzylic. This reaction condition was applied to C-H azidation of **3c**.

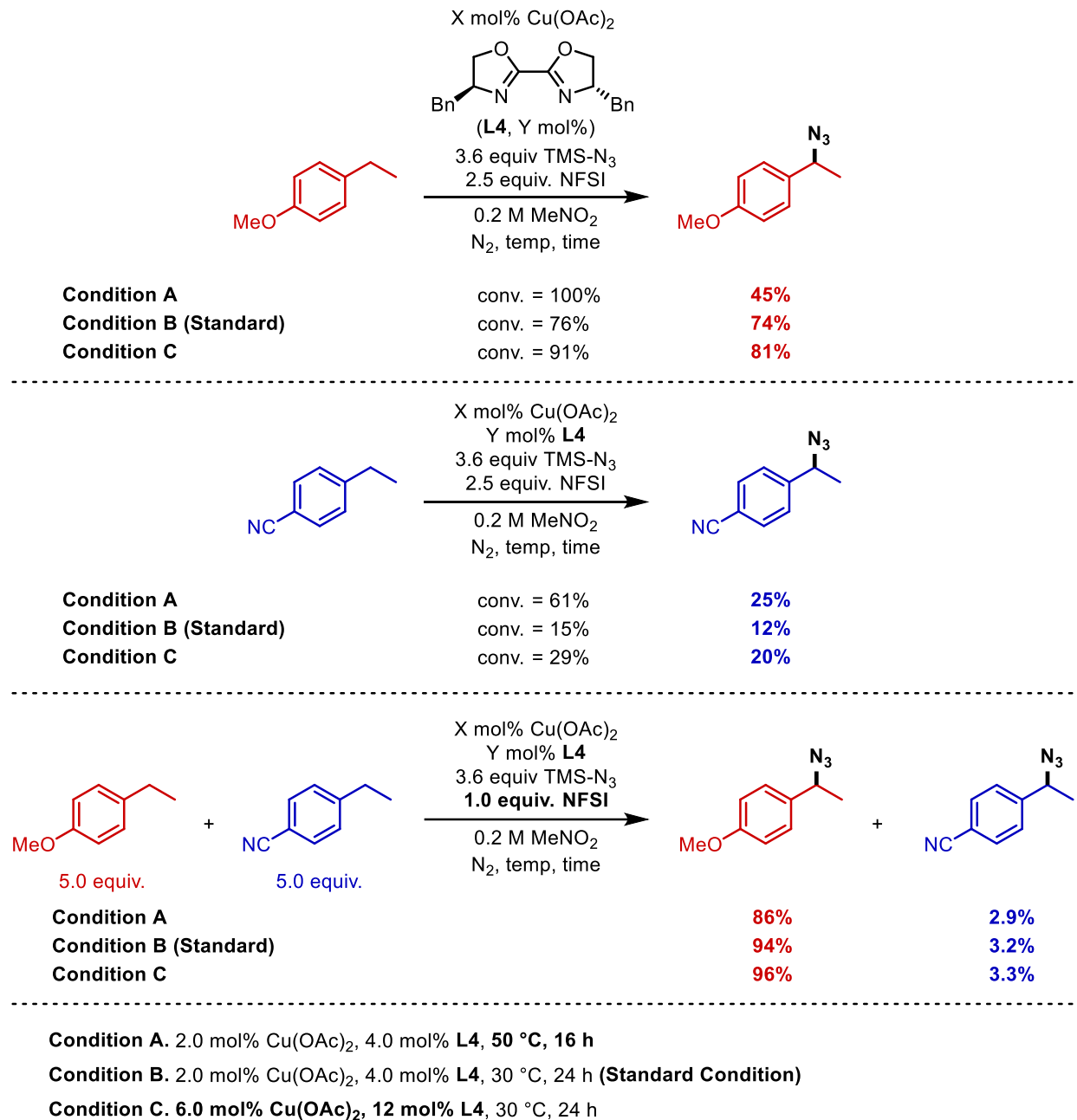
Method III: General Procedure for Mn(salen)Cl System. According to the literature procedure,¹⁸ a 6 mL borosilicate glass vial was charged with a magnetic stir bar, 0.6 mmol of substrate (**3b**, **3c**, or **3d**), 0.8 equivalents of iodosylbenzene (110 mg, 0.48 mmol) and 3.0 mol% Mn(salen)Cl (11 mg, 18 μ mol). To the vial was added 1.0 mL of 1.5 M sodium azide solution (aq., 1.5 mmol) and ethyl acetate (1.0 mL) sequentially. The capped vial was stirred at room temperature (25 °C) until the complete consumption of iodosylbenzene. Additional 1.0 mol% Mn(salen)Cl (3.5 mg, 6.0 μ mol), 1.5 M sodium azide solution (0.10 mL, 0.15 mmol), and iodosylbenzene (110 mg, 0.48 mmol) were added sequentially. The vial was recapped and stirred at room temperature (25 °C). After the consumption of iodosylbenzene, this step was repeated 6 times. The reaction was quenched with brine solution (10 mL) and the organic layer was separated from the extraction with ethyl acetate (15 mL) three times and concentrated. Regioselectivity of benzylic (**4b**, **4c**, or **4d**)^{13,14,18} and tertiary product^{12,15,16} was determined by ¹H NMR analysis of crude mixture with 0.6 mmol mesitylene as an external standard.

Note: (1) Salen ligand (**S1**) and manganese salen catalyst (**S2**) were synthesized according to literature procedure.^{19,20} (2) Iodosylbenzene (**S3**) was synthesized according to the literature method.²¹ (3) There are no literature reports for the synthesis of **4b** and **4c** using the Mn(salen)Cl system.¹⁸ The yield of **4d** was reported but the tertiary regioisomer of **4d** was not reported.¹⁸ (4) Since a specific procedure for each C–H substrate was not reported and the provided general procedure has a wide range of reaction time (i.e. 3-12 hours) and equivalents of reagents [i.e. repeating the addition of Mn(salen)Cl (3.5 mg, 1.0 mol%), 1.5 M sodium azide solution (0.1 mL), and iodosylbenzene (110 mg) 4-8 times] in the literature procedure, we performed the optimization of the reaction conditions for **3d** to reproduce the yield of **4d**. We obtained consistent result four times (41-46% yield, B:T = 13:1), but the reported literature yield was not achieved. Our optimal reaction condition was applied to C–H azidation of **3b–3d**.

Method IV: General Procedure for Fe(OAc)₂·PyBOX System. According to literature procedure,^{22,23} a 20 mL borosilicate glass vial was charged with a magnetic stir bar, 1.0 equivalent of Fe(OAc)₂ (41.7 mg, 0.24 mmol), 1.1 equivalents of 2,6-bis[(4*S*)-(–)-isopropyl-2-oxazolin-2-yl]pyridine (PyBOX, 79.6 g, 0.26 mmol), and acetonitrile (12.0 mL) sequentially in a glovebox. The resulting solution was stirred for 16 hours at room temperature (25 °C). A 4 mL vial was charged with a magnetic stir bar, 0.2 mmol of substrate (*p*-cymene, **3a**, **3b**, or **3c**), and 3.0 equivalents of the azidation reagent **S6** (173 mg, 0.6 mmol), and the prepared 0.02 M stock solution of Fe(OAc)₂·PyBOX catalyst (1.0 mL). The vial was capped and taken out of the glovebox. After stirring at 50 °C for 48 hours, ethyl acetate (2 mL) was added to the crude solution. The solution was filtered through a basic alumina plug for ¹H NMR analysis.

Note: (1) **S6** was prepared in three-step synthesis including syntheses of intermediates (**S4** and **S5**) according to the literature method,²⁴ and stored in a glovebox. (2) The synthesis of **4b**, **4c**, and **4d** has not been previously attempted using the Fe(OAc)₂·PyBOX system.^{22,23} (3) *p*-Cymene was chosen as the substrate to reproduce the reported yield (70%, isolated yield)²³ and the ratio of regioisomers (tertiary benzylic:primary benzylic = 14:1)²³ prior to the comparative experiments with the targeted substrates **3b–3d**. Our experiment gave the reproducible result (82% NMR yield and the 14.1:1.0 ratio of tertiary to primary by ¹H NMR analysis). This reaction condition was applied to the C–H azidation of **3b–3d**.

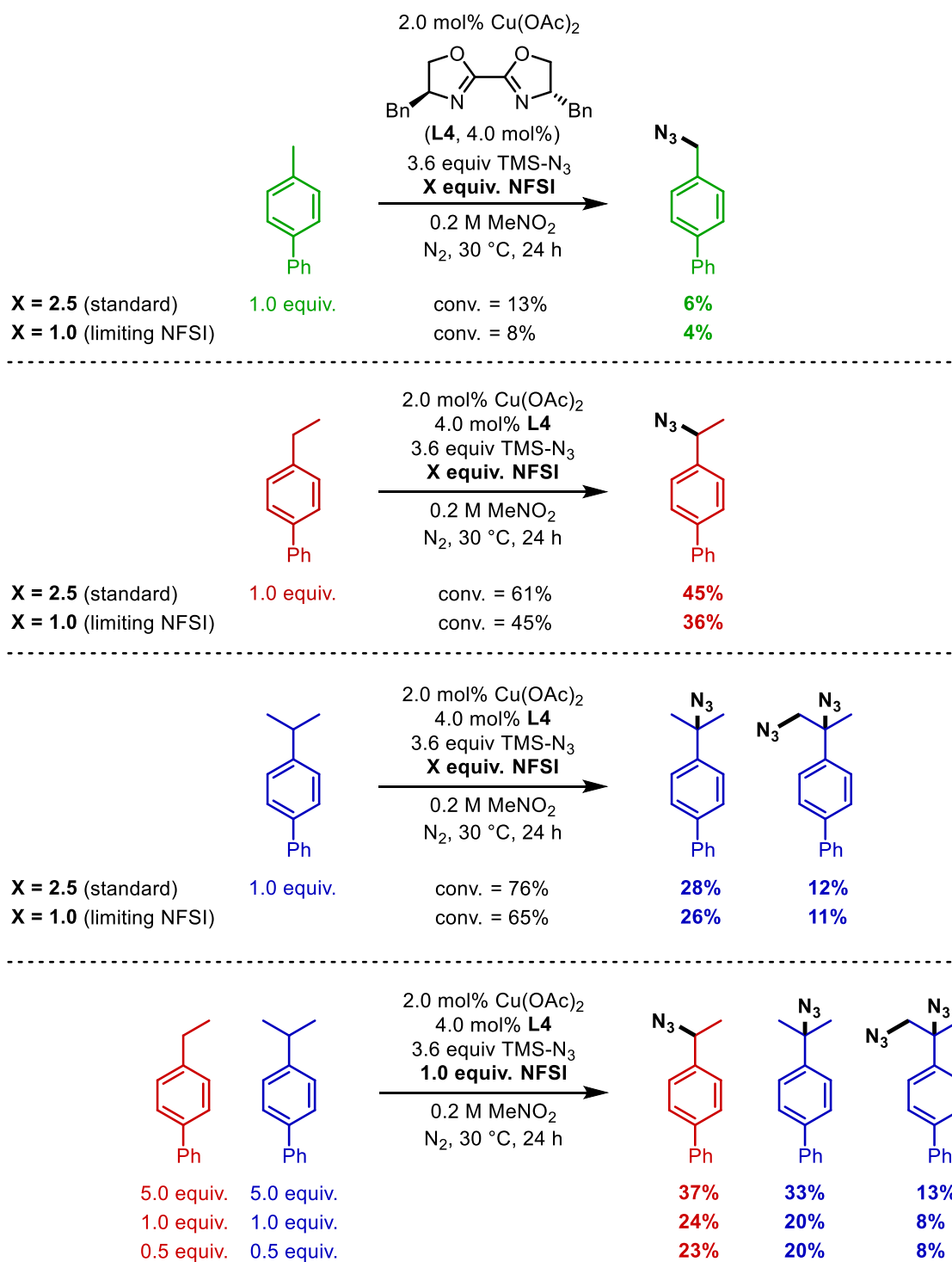
5D.VI. Reactivity Assessment



* NFSI was the limiting reagent.

* Yield (%) was based on the mole of NFSI.

Figure 5D. 2. Independent comparison and competition experiments of *p*-methoxy and *p*-cyanoethylbenzene. Reaction conditions for screening were adopted from General Procedure A.



* NFSI was the limiting reagent.

* Yield (%) was based on mole of NFSI.

Figure 5D. 3. Independent comparison and competition experiments of primary, secondary, and tertiary benzylic C–H substrate. Reaction conditions for screening were adopted from General Procedure A.

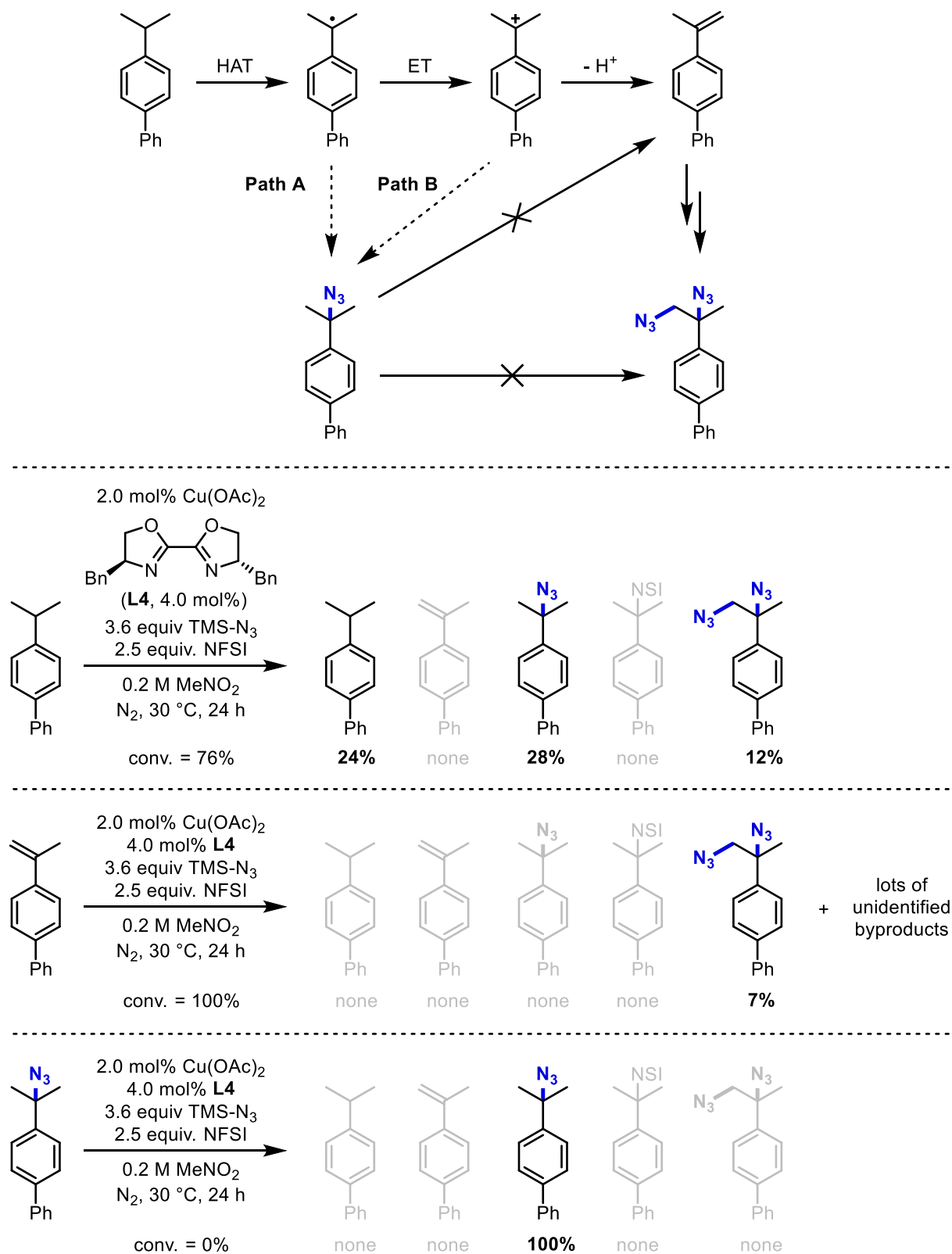
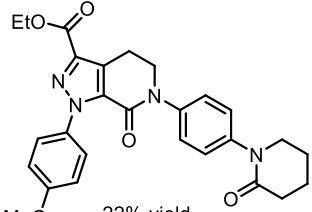
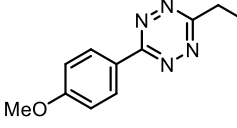
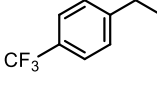
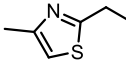
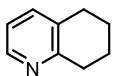
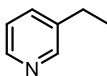
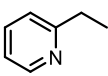
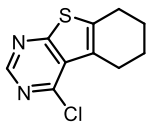
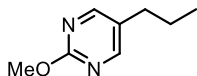
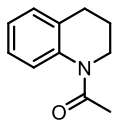
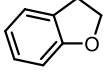
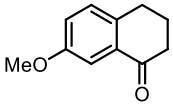
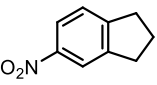
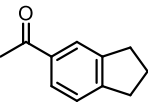
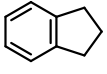
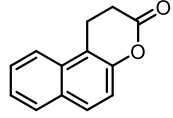


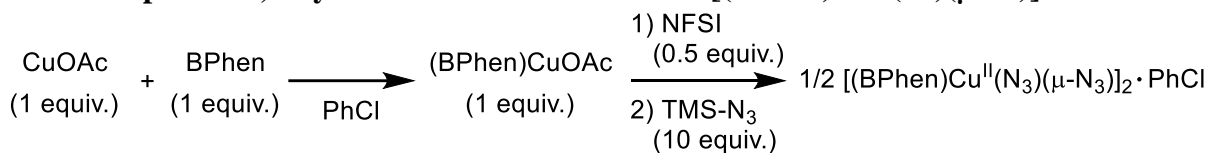
Figure 5D. 4. Investigation of vicinal diazide formation. Reaction conditions for screening were adopted from General Procedure A.

Table 5D.13. Unsuccessful C–H Substrates

| | | | | | | |
|---|---|--|---|--|---|---|
| A | | | | | | |
|  |  |  | | | | |
| 22% yield 35% conv. | 3% yield 20% conv. | 28% yield 59% conv. | | | | |
| B | | | | | | |
|  |  |  |  |  |  | |
| not found 100% conv. | not found 100% conv. | not found 82% conv. | not found 63% conv. | 9% yield 100% conv. | 9% yield 84% conv. | |
| C | | | | | | |
|  |  |  |  |  |  |  |
| 21% yield 100% conv. | 31% yield 100% conv. | 9% yield 83% conv. | 18% yield 100% conv. | 6% yield 100% conv. | 12% yield 100% conv. | Splitomicin 24% yield 100% conv. |

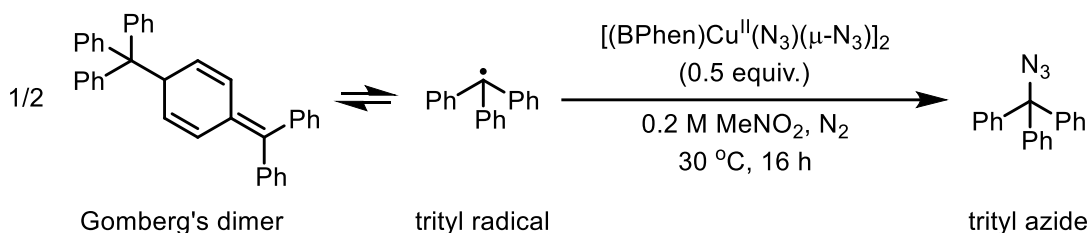
Some substrates were not successful for azidation. Electron-deficient heterobenzylic and benzylic substrates gave poor conversion (Table 5D.13A). Despite of good to excellent conversion, thiazole, pyridine, purimidine derivatives gave low-to-negligible yield (Table 5D.13B). In Table 5D.13C, *N*-acetyl protected 1,2,3,4-tetrahydroquinoline gave lower yield in comparison to *N*-sulfonyl protected compound (42%, **4ac** in Table 5.2 in the manuscript). Dihydrobenzofuran, dihydronaphthalenone, and indane derivatives showed high conversion but low yield. More than 50% yield of elimination product was observed in the reaction of splitomicin.

5D.VII. Preparation, Crystallization and Reaction of [(BPhen)Cu^{II}(N₃)(μ-N₃)₂]



Preparation and Crystallization of [(BPhen)Cu^{II}(N₃)(μ-N₃)₂]: A 4 mL borosilicate glass vial was charged with copper(I) acetate (7.4 mg, 60 μmol) and 1.0 equivalent of bathophenanthroline (20 mg, 60 μmol), and a magnetic stir bar outside a glovebox. The vial was capped with an open-top cap installed with a TFE lined silicone SURE-LINKTM septum. The septum cap was pierced by a needle (22 gauge - 1 1/2", 0.7 mm x 40 mm) and the vial was moved into the glovebox and underwent four cycles of vacuum-nitrogen-backfill over 40 minutes. After removal of the needle, the vial was taken out of the glovebox. Chlorobenzene (3.0 mL, 20 μM) was then added to the vial through the cap and the reaction mixture was stirred at room temperature (25 °C) for 30 minutes, the solution was cannulated into the vial charged with 0.50 equivalents of *N*-fluorobenzenesulfonimide (9.5 mg, 30 μmol) and a magnetic stir bar. After stirring, 10 equivalents of azidotrimethylsilane (80 μL, 0.60 mmol) was added to the solution. The resulting solution was stirred for 10 minutes and left with no agitation for 24 hours. Resulting dark green crystals were washed with pentane (5 mL x 12 times) to afford 21 mg of 1/2 [(BPhen)Cu^{II}(N₃)(μ-N₃)₂] · PhCl in 65% yield. Elemental analysis (E.A.) and X-ray crystallography were performed for characterization of [(BPhen)Cu^{II}(N₃)(μ-N₃)₂] · PhCl.

E.A. (%): Calcd. For [(BPhen)Cu^{II}(N₃)(μ-N₃)₂] · PhCl (C₅₄H₃₇ClCu₂N₁₆, 1072.52 g/mol) C, 60.47; H, 3.48; N, 20.90; Found. C, 59.67; H, 3.59; N, 20.67.



Reaction of [(BPhen)Cu^{II}(N₃)(μ-N₃)₂] · PhCl with 3-triphenylmethyl-6-diphenylmethylidene-1,4-cyclohexadiene (Gomberg's dimer): A 4 mL borosilicate glass vial was charged with 3-triphenylmethyl-6-diphenylmethylidene-1,4-cyclohexadiene (7.3 mg, 15 μmol; 30 μmol of trityl radical), 0.5 equivalent of [(BPhen)Cu^{II}(N₃)(μ-N₃)₂] · PhCl (16 mg, 15 μmol), and a magnetic stir bar inside a glovebox. The vial was capped with an open-top cap installed with a TFE lined silicone SURE-LINKTM septum and taken out of the glovebox. Nitromethane (0.15 mL, 0.20 M) was then added into the vial through the cap and the reaction mixture was stirred and heated to 30 °C (inner temperature) in a heating block on a hot plate. After 16 hours, the reaction mixture was cooled to room temperature (25 °C). All precipitates and catalysts were filtered out through a pipette-silica plug with dichloromethane (1.0 mL x 3 times). The yield (91%) of trityl azide was determined by ¹H NMR analysis of crude mixture with 0.2 mmol mesitylene as an external standard. After evaporation of solvent on a rotary evaporator at 30 °C, flash column chromatography was performed. The isolated compound was dried to give 7.4 mg (86% isolated yield) of trityl azide. The ¹H and ¹³C NMR spectra of trityl azide match the literature report.^{25,26}

5D.VIII. Crystallographic Data for [(BPhen)Cu^{II}(N₃)(μ-N₃)₂·PhCl.

Data Collection

A green crystal with approximate dimensions 0.09 x 0.05 x 0.01 mm³ was selected under oil under ambient conditions and attached to the tip of a MiTeGen MicroMount[®]. The crystal was mounted in a stream of cold nitrogen at 100(1) K and centered in the X-ray beam by using a video camera.

The crystal evaluation and data collection were performed on a Bruker Quazar SMART APEXII diffractometer with Mo K_α (λ = 0.71073 Å) radiation and the diffractometer to crystal distance of 4.96 cm.²⁷

The initial cell constants were obtained from three series of ω scans at different starting angles. Each series consisted of 12 frames collected at intervals of 0.5° in a 6° range about ω with the exposure time of 20 seconds per frame. The reflections were successfully indexed by an automated indexing routine built in the APEXII program suite. The final cell constants were calculated from a set of 5489 strong reflections from the actual data collection.

The data were collected by using the full sphere data collection routine to survey the reciprocal space to the extent of a full sphere to a resolution of 0.70 Å. A total of 22580 data were harvested by collecting 4 sets of frames with 0.5° scans in ω and φ with exposure times of 70 sec per frame. These highly redundant datasets were corrected for Lorentz and polarization effects. The absorption correction was based on fitting a function to the empirical transmission surface as sampled by multiple equivalent measurements.²⁸

Structure Solution and Refinement

The diffraction data were consistent with the space groups $P\bar{1}$ and $P1$. The *E*-statistics strongly suggested the centrosymmetric space group $P\bar{1}$ that yielded chemically reasonable and computationally stable results of refinement.²⁹⁻³⁴

A successful solution by the direct methods provided most non-hydrogen atoms from the *E*-map. The remaining non-hydrogen atoms were located in an alternating series of least-squares cycles and difference Fourier maps. All non-hydrogen atoms were refined with anisotropic displacement coefficients. All hydrogen atoms were included in the structure factor calculation at idealized positions and were allowed to ride on the neighboring atoms with relative isotropic displacement coefficients.

The dinuclear Cu complex occupies a crystallographic inversion center, thus only one half of the complex is symmetry independent.

There is also one solvent molecule of chlorobenzene per dinuclear complex. The solvent molecule is disordered over a crystallographic inversion center. The refinement of the solvent molecule was problematic: whereas it was possible to locate all carbon atoms, the chlorine atom was refined with a total occupancy of 71.8(6)% (or 35.9(3) % in the asymmetric unit). This result is believed to be due to the solvent molecule disorder but it was not possible to locate alternative Cl atom positions. The solvent molecule composition is consistent with the synthetic procedure and a possible benzene/chlorobenzene compositional disorder was ruled out. The solvent molecule was refined with an idealized geometry³⁵ and thermal displacement parameter restraints.³⁰

The final least-squares refinement of 347 parameters against 6999 data resulted in residuals *R* (based on *F*² for *I* ≥ 2σ) and *wR* (based on *F*² for all data) of 0.0420 and 0.1075, respectively. The final difference Fourier map was featureless.

Summary

Crystal Data for $C_{54}H_{37}ClCu_2N_{16}$ ($M = 1072.52$ g/mol): triclinic, space group P-1 (no. 2), $a = 6.452(2)$ Å, $b = 12.895(4)$ Å, $c = 14.135(5)$ Å, $\alpha = 88.073(16)^\circ$, $\beta = 80.255(12)^\circ$, $\gamma = 81.571(17)^\circ$, $V = 1146.4(7)$ Å³, $Z = 1$, $T = 100.01$ K, $\mu(\text{MoK}\alpha) = 1.046$ mm⁻¹, $D_{\text{calc}} = 1.554$ g/cm³, 22580 reflections measured ($2.924^\circ \leq 2\Theta \leq 61.16^\circ$), 6999 unique ($R_{\text{int}} = 0.0424$, $R_{\text{sigma}} = 0.0515$) which were used in all calculations. The final R_1 was 0.0420 ($I > 2\sigma(I)$) and wR_2 was 0.1075 (all data).

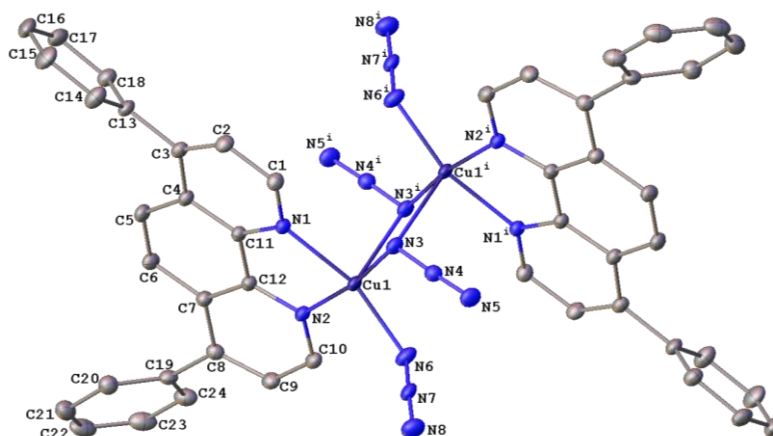


Figure 5D.5. A molecular drawing of the entire complex in $[(\text{BPhen})\text{Cu}^{\text{II}}(\text{N}_3)(\mu\text{-N}_3)]_2 \cdot \text{PhCl}$ shown with 50% probability ellipsoids. All H atoms and solvent molecule are omitted. [Symmetry code: (i) $2-x, 2-y, 1-z$.]

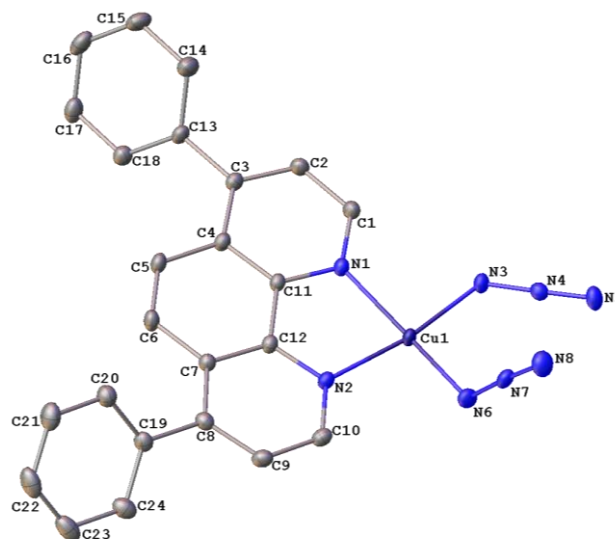


Figure 5D.6. A molecular drawing of the symmetry independent portion of the complex in $[(\text{BPhen})\text{Cu}^{\text{II}}(\text{N}_3)(\mu\text{-N}_3)]_2 \cdot \text{PhCl}$ shown with 50% probability ellipsoids. All H atoms and solvent molecule are omitted.

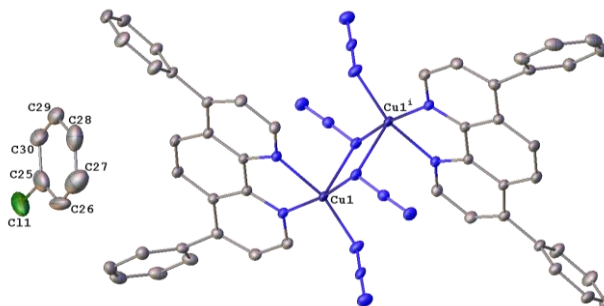


Figure 5D.7. A molecular drawing of $[(\text{BPhen})\text{Cu}^{\text{II}}(\text{N}_3)(\mu\text{-N}_3)]_2 \cdot \text{PhCl}$ shown with 50% probability ellipsoids. All H atoms are omitted. [Symmetry code: (i) $2-x, 2-y, 1-z$.]

Table 5D.14. Crystal Data and Structure Refinement for $[(\text{BPhen})\text{Cu}^{\text{II}}(\text{N}_3)(\mu\text{-N}_3)]_2 \cdot \text{PhCl}$.

| | |
|---|--|
| Empirical formula | $\text{C}_{48}\text{H}_{32}\text{Cu}_2\text{N}_{16} \cdot \text{C}_6\text{H}_5\text{Cl}$ |
| Formula weight | 1072.52 |
| Temperature/K | 100.0 |
| Crystal system | triclinic |
| Space group | $P\bar{1}$ |
| $a/\text{\AA}$ | 6.452(2) |
| $b/\text{\AA}$ | 12.895(4) |
| $c/\text{\AA}$ | 14.135(5) |
| $\alpha/^\circ$ | 88.073(16) |
| $\beta/^\circ$ | 80.255(12) |
| $\gamma/^\circ$ | 81.571(17) |
| Volume/ \AA^3 | 1146.4(7) |
| Z | 1 |
| $\rho_{\text{calc}}/\text{cm}^3$ | 1.554 |
| μ/mm^{-1} | 1.046 |
| F(000) | 548.0 |
| Crystal size/ mm^3 | $0.09 \times 0.05 \times 0.01$ |
| Radiation | $\text{MoK}\alpha$ ($\lambda = 0.71073$) |
| 2θ range for data collection/ $^\circ$ | 2.924 to 61.16 |
| Index ranges | $-9 \leq h \leq 9, -18 \leq k \leq 18, -15 \leq l \leq 20$ |
| Reflections collected | 22580 |
| Independent reflections | 6999 [$R_{\text{int}} = 0.0424, R_{\text{sigma}} = 0.0515$] |
| Data/restraints/parameters | 6999/36/347 |
| Goodness-of-fit on F^2 | 1.042 |
| Final R indexes [$I \geq 2\sigma(I)$] | $R_1 = 0.0420, wR_2 = 0.1004$ |
| Final R indexes [all data] | $R_1 = 0.0605, wR_2 = 0.1075$ |
| Largest diff. peak/hole / $e \text{\AA}^{-3}$ | 0.69/-0.48 |

5D.IX. Experimental and Computational Redox Potentials and Reaction Energetics

Cyclic Voltammetry (CV) of [(BPhen)Cu^{II}(N₃)(μ-N₃)₂]: CV experiments were performed with BASi potentiostat and cell stand at room temperature under nitrogen gas. A glassy carbon (1.5 mm diameter) as working electrode was polished with alumina before each experiment. An Ag/AgNO₃ reference electrode and Pt wire counter electrode were used. The Ag/AgNO₃ was calibrated with ferrocene in the same concentration (0.23 mM in nitromethane) as analyte. The supporting electrolyte for all electrochemical experiments was 0.1 M tetrabutylammonium hexafluorophosphate (TBAHFP). The solution of 0.23 mM Cu complex and 0.1 M TBAHFP in nitromethane was used to measure the half-wave potentials $E^{\circ}_{1/2}(\text{Cu}^{\text{II/I}})$ with 50 mV/s scan rate.

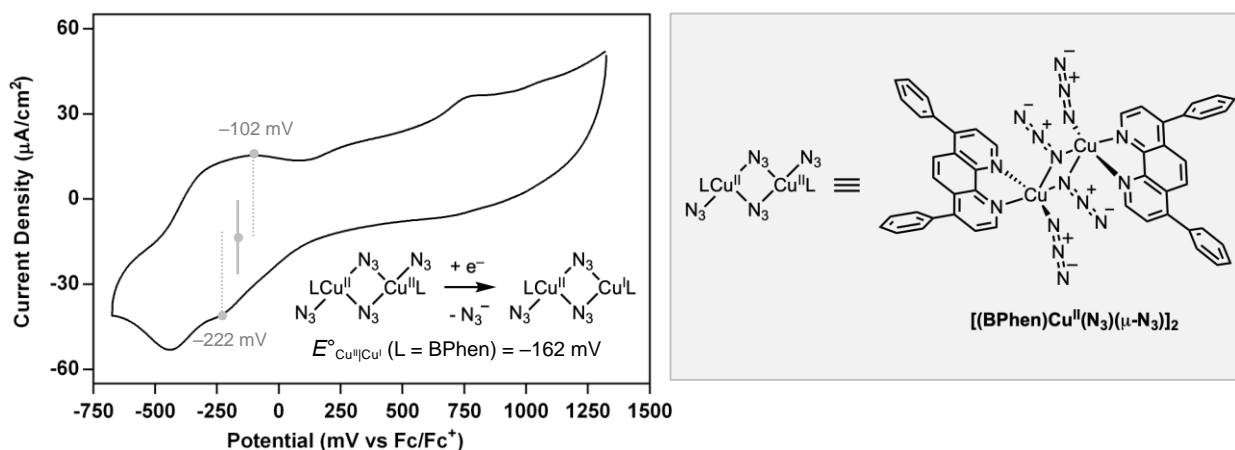


Figure 5D.8. Cyclic voltammogram of [(BPhen)Cu^{II}(N₃)(μ-N₃)₂].

Electronic Structure of the $[\text{LCu}^{\text{II}}(\text{N}_3)_2]_2$ Dimer and Analysis of the Dimer/Monomer Equilibrium.

Electronic structure of the experimentally isolated $[\text{LCu}^{\text{II}}(\text{N}_3)_2]_2$ dimer ($L = \text{BPhen}$ experimentally and $L = \text{Phen}$ computationally) was probed at the DFT level. Dimerization in the triplet electronic state was found to be energetically most favorable, the triplet dimer being ~ 7.7 kcal/mol lower in free energy relative to the corresponding infinitely separated monomers. When the ligand is switched to the chiral BiOx^* (**L4**) ligand, however, the dimer stabilization is reduced to only ~ 2.0 kcal/mol.

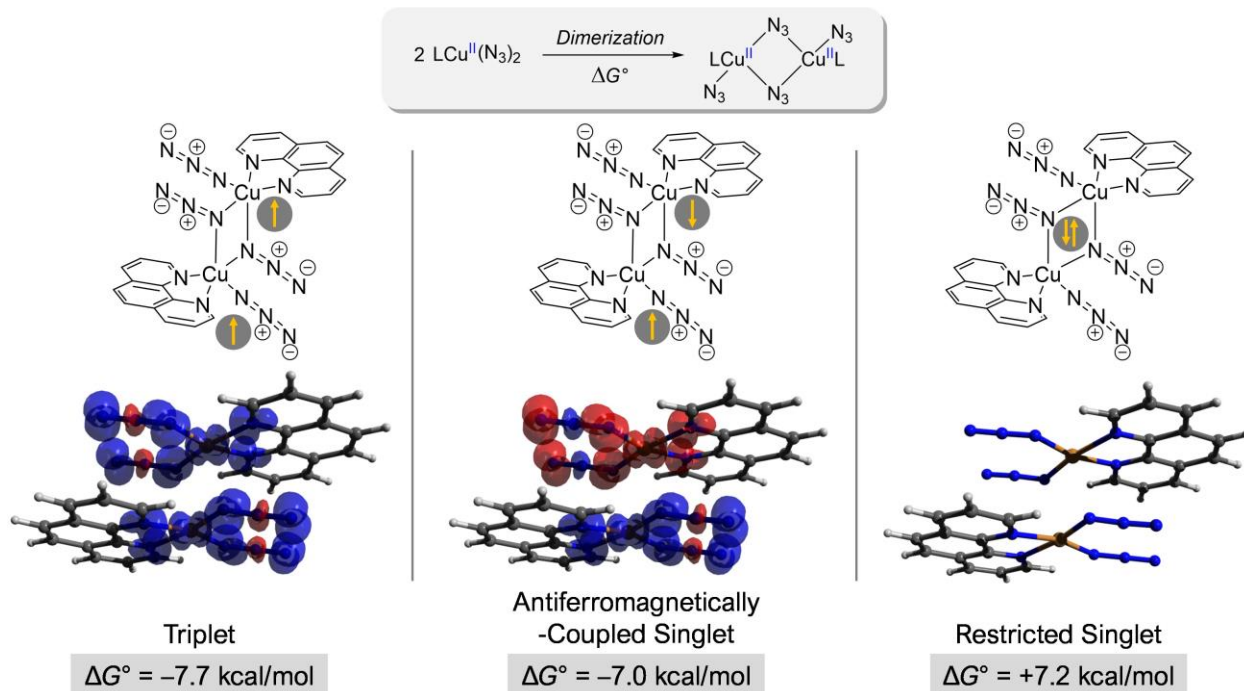


Figure 5D.9. Gibbs free energy change (kcal/mol) due to dimerization. Calculations done at 298.15 K at M06-L/basis-II/SMD(MeNO₂)/B3LYP-D3(BJ)/basis-I level of theory.

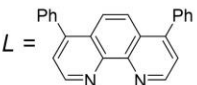
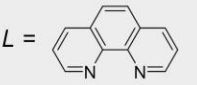
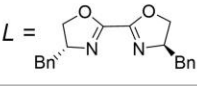
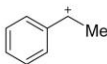
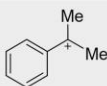
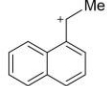
Energetics for Reactivity and Redox Potential Calculations

Table 5D.15. Solution phase electronic energies, E(sol)/hartree, spin-projected electronic energies, E'(sol)/hartree, thermal contribution to Gibbs free energy/hartree and absolute solution-phase Gibbs free energies, G(sol)/hartree (at 298.15 K) computed at M06-L/basis-II/SMD(nitromethane)//B3LYP-D3(BJ)/basis-I level of theory.

| File Description | E(sol)/a.u. | E'(sol)/a.u. (Spin-projected) | Thermal Contribution to G/a.u. | G(sol)/a.u. (T=298.15K) |
|---|------------------|----------------------------------|--------------------------------|----------------------------|
| Phen-[Cu(i)(N3)]-Singlet | - 932.0027411 | | 0.142544 | - 931.8571771 |
| Phen-[Cu(ii)(N3)2]-Doublet | - 1096.264552 | | 0.151653 | - 1096.109879 |
| Phen-[Cu(ii)(N3)2]2-Triplet | - 2192.566919 | | 0.331833 | - 2192.232066 |
| Phen-[Cu(ii)(N3)2]2-afc-singlet | - 2192.566875 | -2192.566876 | 0.332864 | - 2192.230992 |
| Phen-[Cu(ii)(N3)2]2-restricted-singlet | - 2192.541209 | | 0.329961 | - 2192.208228 |
| Phen-[Cu(ii)(N3)2][Cu(i)(N3)]-Doublet | - 2028.300921 | | 0.320247 | - 2027.977654 |
| BPhen-[Cu(i)(N3)]-Singlet | -1394.21454 | | 0.292941 | - 1393.918579 |
| BPhen-[Cu(ii)(N3)2]-Doublet | - 1558.478141 | | 0.301591 | - -1558.17353 |
| BPhen-[Cu(ii)(N3)2]2-Triplet | - 3116.994757 | | 0.633514 | - 3116.358223 |
| BPhen-[Cu(ii)(N3)2][Cu(i)(N3)]-Doublet | - 2952.734291 | | 0.626283 | - 2952.104988 |
| BioxBn-[Cu(i)(N3)]-Singlet | - 1394.613896 | | 0.322542 | - 1394.288334 |
| BioxBn-[Cu(ii)(N3)2]-Doublet | - 1558.869798 | | 0.331684 | - 1558.535094 |
| BioxBn-[Cu(ii)(N3)2]2-Triplet | - -3117.76763 | | 0.691206 | - 3117.073404 |
| BioxBn-[Cu(ii)(N3)2][Cu(i)(N3)]-Doublet | - 2953.507024 | | 0.680222 | - 2952.823782 |
| N3(-)Anion | -164.381172 | | -0.005329 | -164.383481 |
| PhCH(+)Me | -310.141482 | | 0.113942 | -310.02452 |
| PhCH(.)Me | - 310.3025969 | | 0.11053 | - 310.1890469 |
| PhC(+)Me2 | - 349.4749839 | | 0.138991 | - 349.3329729 |
| PhC(.)Me2 | - 349.6287683 | | 0.13643 | - 349.4893183 |

| | | | | |
|---|------------------|--------------|----------|------------------|
| 1-Naph-CH(+) Me | - 463.8239193 | | 0.157228 | - 463.6636713 |
| 1-Naph-CH(-) Me | - 463.9820586 | | 0.154009 | - 463.8250296 |
| INT-R-formal- Cu(iii)(N3)2(Naph) | - 2022.866549 | | 0.518644 | - 2022.344885 |
| INT-S-formal- Cu(iii)(N3)2(Naph) | - 2022.871457 | | 0.517816 | - 2022.350621 |
| RE-TS1-R- Cu(iii)(N3)2(Naph) | - 2022.857459 | | 0.516226 | - 2022.338213 |
| RE-TS1-S-Cu(iii)(N3)2(Naph) | - 2022.859985 | | 0.51711 | - 2022.339855 |
| TS2-b3-R-BioxDimer-Naph- RAL | - 3581.769096 | -3581.770596 | 0.873308 | - 3580.894268 |
| TS2-b3-S-BioxDimer-Naph- RAL | - 3581.764865 | -3581.766271 | 0.873066 | - 3580.890185 |
| TS2-b1-R-BioxDimer-Naph- RAL | - 3581.758769 | -3581.758602 | 0.873644 | - 3580.881938 |
| TS2-b1-S-BioxDimer-Naph- RAL | - 3581.756309 | -3581.756889 | 0.872568 | - 3580.881301 |
| TS2-t3-R-BioxDimer-Naph- RAL | - 3581.762928 | -3581.764806 | 0.870997 | - 3580.890789 |
| TS2-t3-S-BioxDimer-Naph- RAL | - 3581.767102 | -3581.7689 | 0.871279 | - 3580.894601 |
| TS2-t1-R-BioxDimer-Naph- RAL | - 3581.766474 | -3581.767069 | 0.871371 | - 3580.892678 |
| TS2-t1-S-BioxDimer-Naph- RAL | - 3581.768039 | -3581.76929 | 0.872504 | - 3580.893766 |

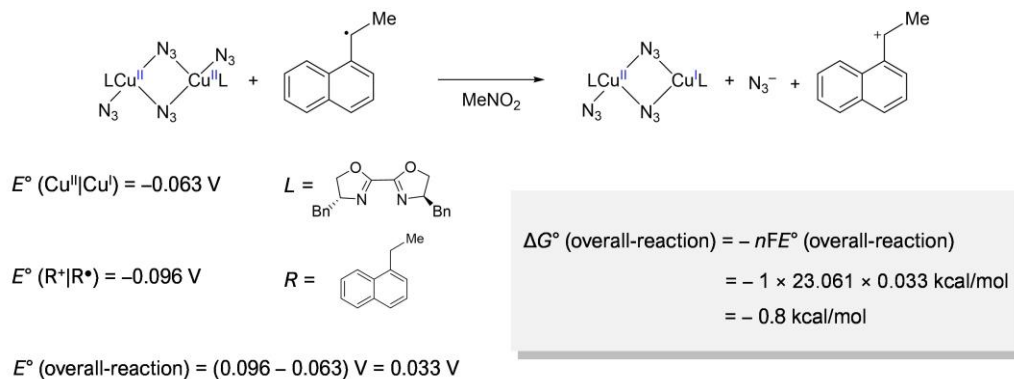
Table 5D.16. Calculated (vs $\text{Fc}^{0/+}$), and experimental (vs $\text{Fc}^{0/+}$) reduction potentials (V) of various species at 298.15 K using reaction schemes (eqs S3 and S4).

| $f(\text{Cu}) = 3.706 \text{ V}$ | | | |
|--|---|--|--|
| [LCu ^{II} (N ₃) ₂] ₂ Species | $E^\circ (\text{Cu}^{\text{II}} \text{Cu}^{\text{I}})^a$ absolute, V | $E^\circ (\text{Cu}^{\text{II}} \text{Cu}^{\text{I}})$ vs $\text{Fc}^{0/+}$, V | $E^\circ (\text{Cu}^{\text{II}} \text{Cu}^{\text{I}})$ [exp] vs $\text{Fc}^{0/+}$, V |
| $L = $  | 3.544 | -0.162 | -0.162 ^b |
| $L = $  | 3.482 | -0.223 | N.A. |
| $L = $  | 3.642 | -0.063 | N.A. |
| $f(\text{Org}) = 4.487 \text{ V}$ | | | |
| R^+ Species | $E^\circ (R^+ R^\bullet)^a$ absolute, V | $E^\circ (R^+ R^\bullet)$ vs $\text{Fc}^{0/+}$, V | $E^\circ (R^+ R^\bullet)$ [exp] vs $\text{Fc}^{0/+}$, V |
|  | 4.477 | -0.01 | -0.01 ^c |
|  | 4.254 | -0.233 | -0.22 ^c |
|  | 4.391 | -0.096 | N.A. |

^aComputed at 298.15 K at M06-L/basis-II/SMD(nitromethane)//B3LYP-D3(BJ)/basis-I level of theory. ^bHalf-wave potentials $E^\circ_{1/2}(\text{Cu}^{\text{II}})$ was measured; Glassy carbon (W.E.), Pt wire (C.E.), Ag/AgNO₃ (R.E.), 50 mV/s scan rate, 0.23 mM [(BPhen)Cu^{II}(N₃)(μ-N₃)₂], 0.1 M TBAHFP (electrolyte), rt, N₂. ^cRef. 37.

Thermodynamics of Radical Polar Crossover Pathway

Using the reduction potentials presented in Table 5D.16, Gibbs free energy change (ΔG°) for the oxidation of the R^\bullet radical ($R = 1\text{-Naph}(\text{CH})\text{Me}$) by the Cu^{II} dimer yielding the R^+ cation can be calculated as follows:



Scheme 5D.1. Derivation of Gibbs free energy change (ΔG°) for the oxidation of the 1-Naph-CH(\bullet)Me radical by the Cu^{II} -dimer yielding the corresponding benzylic cation. Reduction potentials were obtained from Table 5D.16.

Comparison of Product Forming Pathways

As discussed in the text, starting from the 1-Naph-CH(•)Me and [LCu^{II}(N₃)₂]₂ (L = **L4**) dimer, we have considered three possible pathways leading to the product [1-Naph-CH(N₃)Me] formation. These pathways are detailed in Figure 5D.10, and their corresponding energetics are shown in Figure 5D.11.

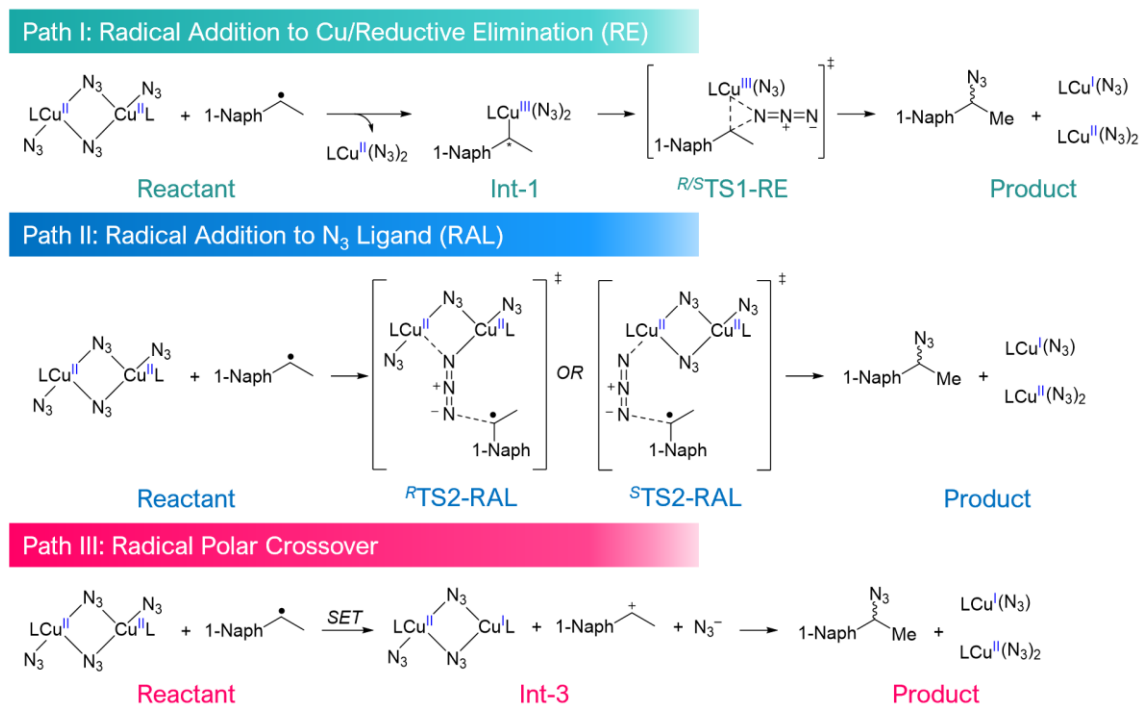


Figure 5D.10. Possible pathways leading to the benzylic azide formation.

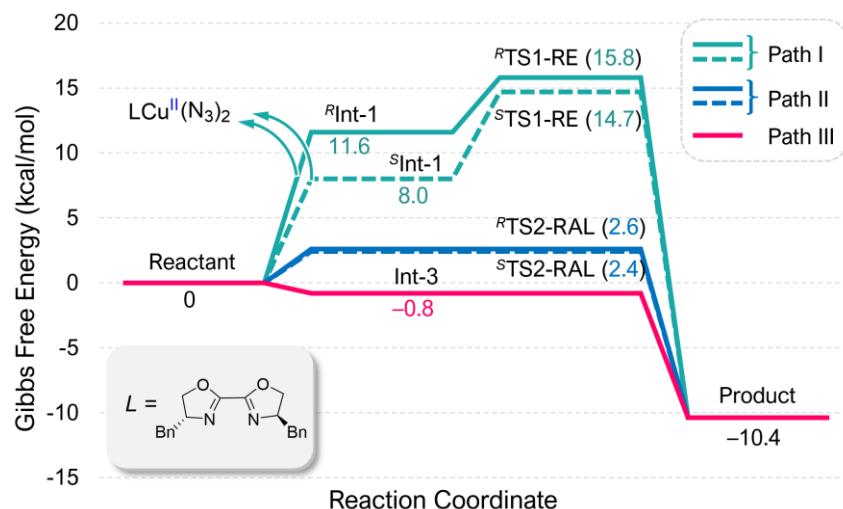


Figure 5D.11. Energetics of pathways leading to the benzylic azide formation using the BiOx (**L4**) ligand. Gibbs free energies are in kcal/mol computed at 298.15 K at M06-L/basis-II/SMD(MeNO₂)/B3LYP-D3(BJ)/basis-I level of theory. Free energy of **Int-3** was determined according to Scheme 5D.1.

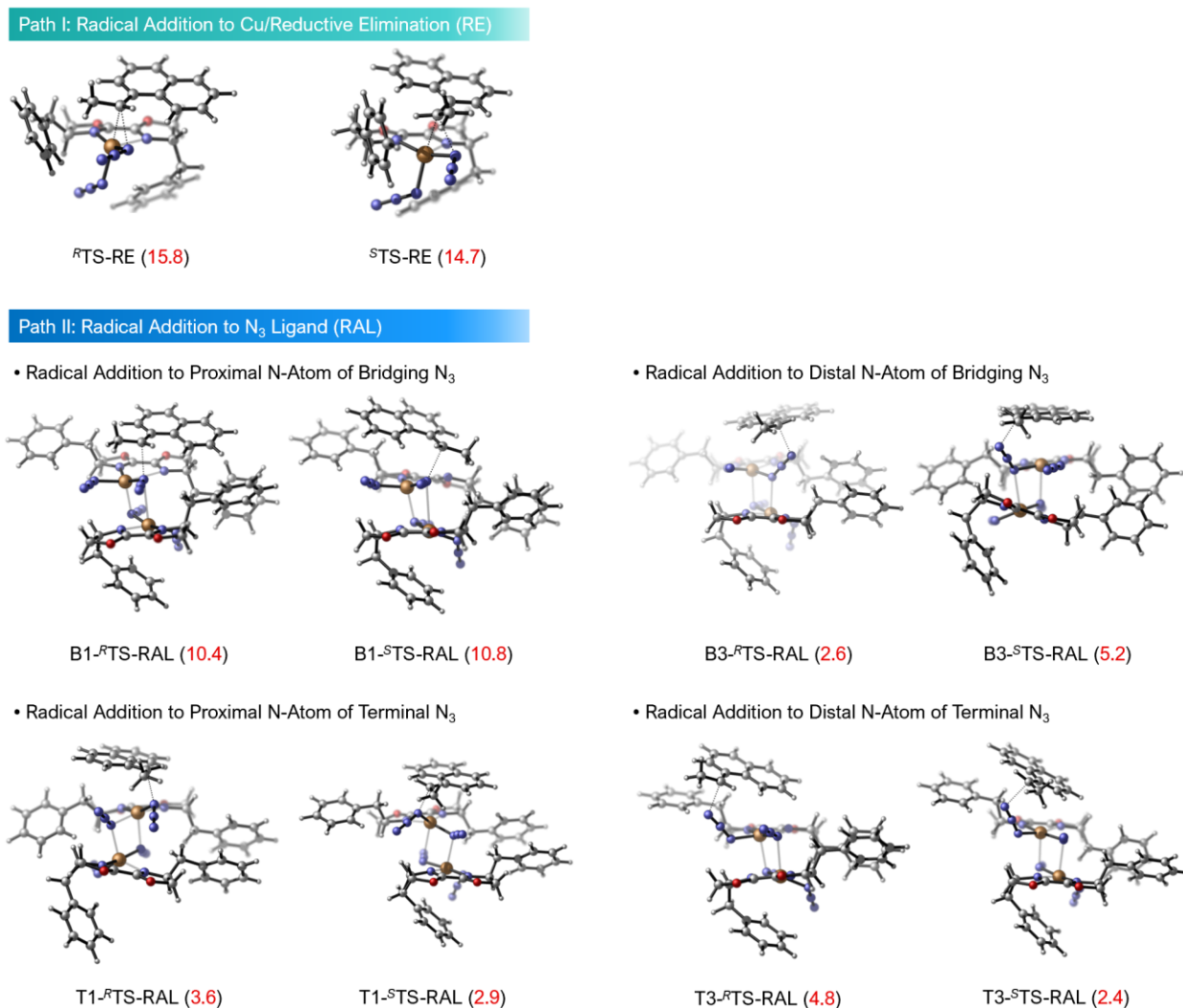
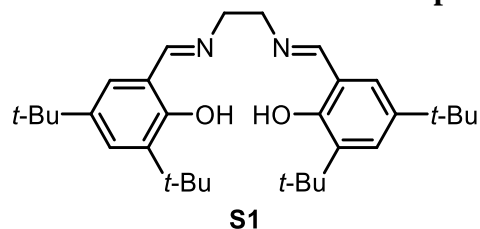


Figure 5D.12. Optimized transition-state (TS) structures leading to product formation via reductive elimination (RE) and direct radical addition to the azide ligand (RAL) for both pro-R and pro-S faces of the benzylic radical derived from 1-ethylnaphthalene. Gibbs free energies of activation (ΔG^\ddagger ; kcal/mol) of the respective TS structures are included in parenthesis. Gibbs free energies are reported at 298.15 K calculated at M06-L/basis-II/SMD(MeNO₂)/B3LYP-D3(BJ)/basis-I level of theory. “RE” implies reductive elimination (Path-I). The prefix “B3–” implies that the reaction is happening at the distal N-atom of the bridging azide group. Similarly, “T1–” prefix means that it is the proximal N-atom of the terminal azide group.

5D.X. Characterization of Compounds

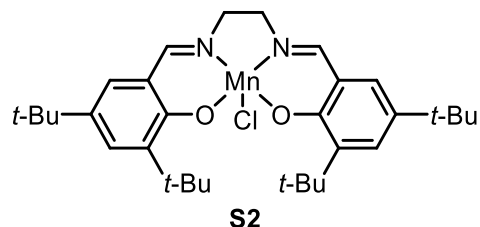


6,6'-((1E,1'E)-(ethane-1,2-diylbis(azanylylidene))bis(methanylylidene))bis(2,4-di-tert-butylphenol) (S1): Prepared according to the literature procedure. A 250 mL round-bottle flask was charged with a magnetic stir bar, 2.3 equivalents of 3,5-di-*t*-butylsalicylaldehyde (2.1 g, 9.0 mmol) and ethanol (80 mL). To the solution, 1,2-diaminoethane (0.27 mL, 4.0 mmol) was added dropwise. The resulting solution was heated under reflux for 12 hours and cooled to 0 °C for 2 hours. The yellow precipitate was filtered and washed with cold ethanol (30 mL) to afford 1.72 g of **S1**. ¹H NMR spectrum of **S1** was matched with the literature.¹⁹

Isolated Yield: 87%

Physical Property: Yellow solid.

¹H NMR (400 MHz, CDCl₃ containing 1 % (v/v) TMS) δ 13.64 (s, 2H), 8.38 (s, 2H), 7.36 (d, 2H, *J* = 2.5 Hz), 7.06 (d, 2H, *J* = 2.5 Hz), 3.92 (s, 4H), 1.43 (s, 18H), 1.28 (s, 18H).

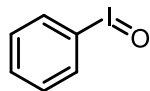


Manganese salen catalyst (S2): Prepared from **S1** according to the literature procedure.²⁰ A 250 mL three-neck round-bottle flask was charged with a magnetic stir bar, 3.0 equivalents of manganese(II) acetate tetrahydrate (9.0 mmol, 2.2 g) and ethanol (60 mL) under nitrogen gas and heated under reflux. To the solution, a solution of **S1** (3.0 mmol, 1.5 g) in toluene (45 mL) was added dropwise. After 2 hours, air bubbling to the solution through a needle was performed for 1 hour. Brine solution (80 mL) was added and the resulting solution was cooled to room temperature (25 °C). The needle was detached and toluene (25 mL) was added to the reaction mixture. The solution was washed with water (120 mL) three times and brine solution (100 mL) three times sequentially. The organic layer was dried and concentrated to afford 1.6 g of **S2**. HRMS analysis was performed for characterization of **S2**.

Isolated Yield: 92%

Physical Property: Brown solid.

HRMS (ESI) calculated for C₃₂H₄₆ClMnN₂O₂⁻ [M]⁻ 580.2634, found 580.2636.

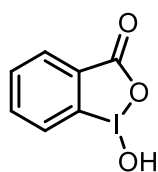
**S3**

iodobenzene (S3): Prepared according to the literature procedure.²¹ 3.0 M aqueous sodium hydroxide solution (55 mL) was added dropwise to (diacetoxyiodo)benzene (10 g, 31 mmol) over 10 minutes. After stirring 2 hours at room temperature (25 °C), the resulting solid was washed with water (100 mL) twice and chloroform (125 mL) twice sequentially and dried *in vacuo* to afford 5.1 g of **S3**. ¹H NMR spectrum of **S3** was matched with the literature.²¹

Isolated Yield: 75%

Physical Property: Colorless solid.

¹H NMR (400 MHz, CD₃OD) δ 8.08 – 8.02 (m, 2H), 7.64 – 7.55 (m, 2H).

**S4**

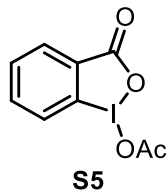
1-hydroxy-1,2-benziodoxol-3(1H)-one (S4): Prepared according to the literature procedure.²⁴ A 100 mL round-bottom flask was charged with a magnetic stir bar, 1.00 equivalents of 2-iodobenzoic acid (6.40 g, 260 mmol) and 30% v/v aqueous acetic acid (50 mL). 1.15 equivalents of NaIO₄ (6.40 g, 300 mmol) was added to the solution at room temperature (25 °C) and the reaction mixture was heated to 120 °C. After 4 hours, the solution was cooled to room temperature (25 °C) and quenched with water (180 mL). The precipitate was filtered, washed with water (20 mL) three times and cold acetone (20 mL) three times sequentially, and dried *in vacuo* to give 6.1 g of **S4**. ¹H NMR spectrum of **S4** was matched with the literature.²⁴

Isolated Yield: 90%

Physical Property: Colorless crystal.

¹H NMR (400 MHz, DMSO-*d*₆) δ 8.04 (s, 1H), 8.02 (dd, *J* = 7.6, 1.5 Hz, 1H), 7.97 (ddd, *J* = 8.6, 7.2, 1.5 Hz, 1H), 7.85 (dd, *J* = 8.2, 1.0 Hz, 1H), 7.71 (td, *J* = 7.2, 1.0 Hz, 1H).

Note: Residual NaIO₄ should be washed thoroughly with additional water/cold acetone until ¹H NMR analysis proves nearly 100% purity of **S4** with external standard.

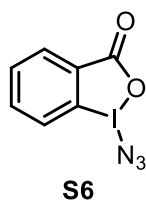


1-(acetyloxy)-1,2-benziodoxol-3(1H)-one (S5): Prepared from **S4** according to the literature procedure.²⁴ To a 50 mL round-bottom flask charged with a magnetic stir bar, **S4** (3.0 g, 11 mmol) was added acetic anhydride (11 mL) at room temperature (25 °C). The cloudy solution was heated to 135 °C and stirred until the solution becomes clear. The reaction mixture was cooled to -20 °C and stayed for 1 hour. The grown crystals were filtered, washed with pentane three times, and dried in vacuo to afford 3.3 g of **S5**. ¹H NMR spectrum of **S5** was matched with the literature.²⁴

Isolated Yield: 98%

Physical Property: Colorless crystal.

¹H NMR (400 MHz, CDCl₃ containing 1 % (v/v) TMS) δ 8.25 (dd, *J* = 7.6, 1.6 Hz, 1H), 8.02 (dd, *J* = 8.4, 1.0 Hz, 1H), 7.94 (ddd, *J* = 8.4, 7.1, 1.6 Hz, 1H), 7.73 (td, *J* = 7.4, 1.0 Hz, 1H), 2.27 (s, 3H).

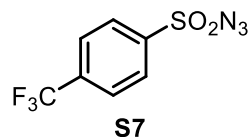


1-azido-1,2-benziodoxol-3(1H)-one (S6): Prepared from **S5** according to the literature procedure.²⁴ A 20 mL vial was charged with a magnetic stir bar, **S5** (2.3 g, 7.5 mmol) and anhydrous methylene chloride (7.0 mL). 1.5 equivalents of azidotrimethylsilane (5.9 mL, 11 mmol) and 0.50 mol% trimethylsilyl trifluoromethanesulfonate (6.8 μL, 38 μmol) was added to the solution sequentially at room temperature (25 °C). After 1 hour, the precipitate was filtered, washed with pentane (10 mL) twice and methylene chloride (10 mL) twice sequentially, and dried in vacuo to afford 1.8 g of **S6**. ¹H NMR spectrum of **S6** was matched with the literature.²⁴

Isolated Yield: 83%

Physical Property: Yellow solid.

¹H NMR (400 MHz, CDCl₃ containing 1 % (v/v) TMS) δ 8.35 – 8.29 (m, 1H), 8.04 – 7.95 (m, 2H), 7.79 (ddd, *J* = 7.5, 6.0, 2.1 Hz, 1H).



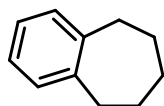
4-(trifluoromethyl)benzenesulfonyl azide (S7): Prepared according to the literature procedure.¹⁷ A 100 mL round-bottom flask was charged with a magnetic stir bar, 4-(trifluoromethyl)benzene-1-sulfonyl chloride (122 mg, 5.00 mmol) and acetone (25 mL). A solution of 1.20 equivalents of sodium azide (390 mg, 6.00 mmol) in DI water (25 mL) was added dropwise at 0 °C. The reaction was slowly warmed up to room temperature (25 °C) and stirred for 5 hours. Acetone was evaporated *in vacuo* at room temperature (25 °C) and extracted with methylene chloride three times. The resulting solution was dried over MgSO₄ and concentrated *in vacuo*. The crude mixture was purified through a short silica gel plug with methylene chloride to afford 119 mg of **S7**. ¹H and ¹⁹F NMR spectrum of **S7** was matched with the literature.³⁸

Isolated Yield: 95%

Physical Property: White solid.

¹H NMR (400 MHz, CDCl₃ containing 1 % (v/v) TMS) δ 8.11 (d, *J* = 8.0 Hz, 2H), 7.90 (d, *J* = 8.0 Hz, 2H).

¹⁹F NMR (377 MHz, CDCl₃ containing 1 % (v/v) TMS) δ -63.4.



3n

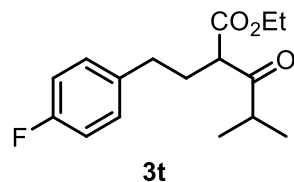
6,7,8,9-tetrahydro-5H-benzo[7]annulene (3n): Prepared according to the literature procedure.³⁹ A 20 mL vial was charged with a magnetic stir bar, 6,7,8,9-tetrahydro-5H-benzo[7]annulen-5-one (1.00 g, 6.16 mmol) and trifluoroacetic acid (10 mL). 1.50 equivalents of triethylsilane (1.48 mL, 9.24 mmol) was added to the solution at room temperature (25 °C) and the solution was heated to 60 °C. After 24 hours, the resulting mixture was cooled down to room temperature (25 °C) and concentrated *in vacuo*. The crude solution was treated with cold water (100 mL) and extracted with ethyl acetate (100 mL) three times. The organic layer was washed with brine solution (100 mL), dried over MgSO₄, filtered, and concentrated. The crude mixture was purified by flash chromatography (straight pentane) to afford 620 mg of **3n**. ¹H NMR spectrum of **3n** was matched with the literature.⁴⁰

Isolated Yield: 69%

Physical Property: Colorless oil.

¹H NMR (400 MHz, CDCl₃ containing 1 % (v/v) TMS) δ 7.09 (s, 4H), 2.85 – 2.73 (m, 4H), 1.84 (p, *J* = 5.9 Hz, 2H), 1.64 (p, *J* = 5.4 Hz, 4H).

Note: Overlapped fraction between **3n** and triethylsilane was collected and re-purified by flash column chromatography (pentane).



ethyl 2-(4-fluorophenethyl)-4-methyl-3-oxopentanoate (3t): A 100 mL round-bottom flask was charged with a magnetic stir bar, 3.0 equivalents of dry NaH (90%; 1.6 g, 60 mmol) and anhydrous THF (10 mL). To the suspension of NaH was added a solution of 1.0 equivalents of ethyl isobutyrylacetate (3.2 mL, 20 mmol) in anhydrous THF (10 mL) dropwise at 0 °C at under a nitrogen atmosphere. The solution was warmed to room temperature (25 °C) and stirred for 30 minutes. To the resulting mixture was added a solution of 1.5 equivalents of 4-fluorobenzyl bromide (3.7 mL, 30 mmol) in THF (10 mL) dropwise and stirred for 24 hours under reflux. The reaction mixture was cooled to 0 °C, quenched with water (10 mL), and extracted with ethyl acetate (50 mL) three times. The organic layer was washed with brine (50 mL), dried over Na₂SO₄, filtered, and concentrated. The crude mixture was purified by column chromatography (methylene chloride:pentane = 1:1 to 2:1) to afford 4.06 g of **3t**.

Isolated Yield: 72%

Physical Property: Colorless oil.

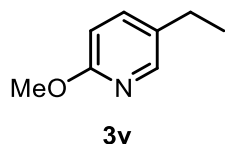
¹H NMR (400 MHz, CDCl₃ containing 1 % (v/v) TMS) δ 7.15 – 7.10 (m, 2H), 7.00 – 6.94 (m, 2H), 4.18 (q, *J* = 7.1 Hz, 2H), 3.59 (t, *J* = 7.1 Hz, 1H), 2.77 (hept, *J* = 6.9 Hz, 1H), 2.65 – 2.50 (m, 2H), 2.20 – 2.06 (m, 2H), 1.26 (t, *J* = 7.1 Hz, 2H), 1.10 (d, *J* = 6.9 Hz, 3H), 1.07 (d, *J* = 6.9 Hz, 3H).

¹⁹F NMR (377 MHz, CDCl₃ containing 1 % (v/v) TMS) δ -117.2.

¹³C NMR (126 MHz, CDCl₃ containing 1 % (v/v) TMS) δ 208.8, 169.6, 161.4 (d, *J* = 244.0 Hz), 136.5 (d, *J* = 3.2 Hz), 129.8 (d, *J* = 7.8 Hz), 115.2 (d, *J* = 21.2 Hz), 61.4, 56.1, 40.5, 32.7, 29.8 (d, *J* = 1.1 Hz), 18.5, 18.1, 14.1.

IR (neat): 2973, 2935, 2874, 1739, 1711, 1509, 1219, 1155, 831 cm⁻¹.

HRMS (ESI) calculated for C₁₆H₂₂FO₃⁺ [M+H]⁺ 281.1547, found 281.1544.



5-ethyl-2-methoxypyridine (3v): A 250 mL round-bottom flask was charged with a magnetic stir bar, 5-bromo-2-methoxypyridine (1.0 mL, 8.0 mmol) and anhydrous THF (16 mL). To the diluted solution was added a solution of 2.3 equivalents of 1.7 M *tert*-butyllithium (11 mL, 18 mmol) in THF dropwise at $-78\text{ }^{\circ}\text{C}$ at under a nitrogen atmosphere. After stirring for 1 hour, 10 equivalents of iodoethane (6.4 mL, 80 mmol) in 80 mL was added dropwise to the solution followed by stirring for additional 3 hours at $-78\text{ }^{\circ}\text{C}$. The solution was warmed up to $25\text{ }^{\circ}\text{C}$, stirred for 5 hours, quenched with 20 mL of water and extracted with 20 mL of diethyl ether twice. The organic layer was washed with brine (50 mL), dried over Na_2SO_4 , filtered, and concentrated. The crude mixture was purified by column chromatography (diethyl ether:pentane = 1:3) to afford 0.6 g of **3v**.

Isolated Yield: 55%

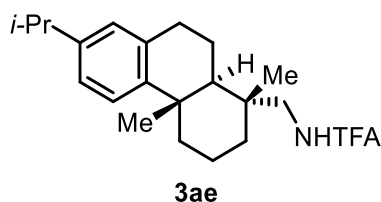
Physical Property: Colorless oil.

^1H NMR (500 MHz, CDCl_3 containing 1 % (v/v) TMS) δ 7.98 (d, $J = 2.4$ Hz, 1H), 7.41 (dd, $J = 8.4, 2.4$ Hz, 1H), 6.67 (d, $J = 8.4$ Hz, 1H), 3.91 (s, 3H), 2.56 (q, $J = 7.6$ Hz, 2H), 1.21 (t, $J = 7.6$ Hz, 3H).

^{13}C NMR (126 MHz, CDCl_3 containing 1 % (v/v) TMS) δ 162.7, 145.6, 138.6, 132.1, 110.5, 53.4, 25.3, 15.8.

IR (neat): 2963, 2873, 2361, 1606, 1492, 1286, 1026 cm^{-1} .

HRMS (ESI) calculated for $\text{C}_8\text{H}_{12}\text{NO}^+$ $[\text{M}+\text{H}]^+$ 138.0913, found 138.0913.



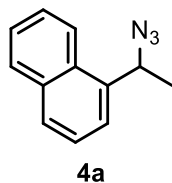
2,2,2-trifluoro-N-(((1R,4aS,10aR)-7-isopropyl-1,4a-dimethyl-1,2,3,4,4a,9,10,10a-octahydrophenanthren-1-yl)methyl)acetamide (3ae): Prepared adopting the literature procedure.⁴¹ A 100 mL round-bottom flask was charged with a magnetic stir bar, ((1R,4aS,10aR)-7-isopropyl-1,4a-dimethyl-1,2,3,4,4a,9,10,10a-octahydrophenanthren-1-yl)methanamine (90% purity, 6.23 mmol, 1.98 g) and tetrahydrofuran (30 mL). 2.00 equivalents of triethylamine (12.5 mmol, 1.70 mL) and 1.10 equivalents of ethyl trifluoroacetate (6.85 mmol, 0.800 mL) was added to the solution sequentially at $0\text{ }^{\circ}\text{C}$. The reaction mixture was heated under reflux. After 4 hours, the resulting solution was quenched with 1.0 M HCl (aq, 50 mL), washed with water and dried over Na_2SO_4 . After evaporation of solvent, the crude mixture was purified by flash column chromatography (ethyl acetate:pentane = 1:8 to 1:4) to afford 1.52 g of **3ae**. ^1H NMR spectrum of **3ae** was matched with the literature.⁴²

Isolated Yield: 64%

Physical Property: Amorphous solid.

^1H NMR (400 MHz, CDCl_3 containing 1 % (v/v) TMS) δ 7.17 (d, $J = 8.2$ Hz, 1H), 7.01 (dd, $J = 8.2, 2.0$ Hz, 1H), 6.90 (s, 1H), 6.20 (s, 1H), 3.34 – 3.22 (m, 2H), 2.99 – 2.73 (m, 3H), 2.36 – 2.25 (m, 1H), 1.91 – 1.62 (m, 4H), 1.52 – 1.33 (m, 3H), 1.29 – 1.22 (m, 10H), 0.98 (s, 3H).

Note: Due to the hygroscopic nature of **3ae**, it should be dried in a vacuum desiccator for 24 hours and stored in a glovebox for the next step.

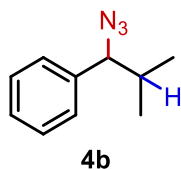


1-(1-azidoethyl)naphthalene (4a): Prepared from 1-ethylnaphthalene (**3a**) according to Procedure B. The reaction mixture was purified by flash column chromatography (ethyl acetate:pentane = 1:30) to afford 73.2 mg of **4a**. ^1H NMR spectrum of **4a** was matched with the literature.¹⁸

Isolated Yield: 93%

Physical Property: Colorless oil.

^1H NMR (400 MHz, CDCl_3) δ 8.12 (d, $J = 8.4$ Hz, 1H), 7.95 – 7.89 (m, 1H), 7.86 (d, $J = 8.2$ Hz, 1H), 7.63 – 7.49 (m, 4H), 5.38 (q, $J = 6.8$ Hz, 1H), 1.75 (d, $J = 6.8$ Hz, 3H).



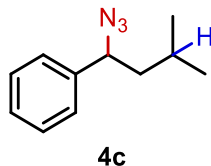
(1-azido-2-methylpropyl)benzene (4b): Prepared from isobutylbenzene (**3b**) according to Procedure A. The reaction mixture was purified by flash column chromatography (ethyl acetate:pentane = 1:50) to afford 28.3 mg of **4b**. Regioselectivity of benzylic (**4b**)¹³ and tertiary product¹⁵ was determined by ^1H NMR analysis of crude mixture.

Yield and Site-Selectivity (^1H NMR): 44%, benzylic to tertiary product = 11:1.

Isolated Yield: 40% for only benzylic product (**4b**).

Physical Property: Colorless oil.

^1H NMR (500 MHz, CDCl_3 containing 1 % (v/v) TMS) δ 7.40 – 7.34 (m, 2H), 7.34 – 7.29 (m, 1H), 7.28 – 7.24 (m, 2H), 4.13 (d, $J = 8.0$ Hz, 1H), 1.98 (dh, $J = 8.0, 6.7$ Hz, 1H), 1.02 (d, $J = 6.7$ Hz, 3H), 0.79 (d, $J = 6.7$ Hz, 3H).



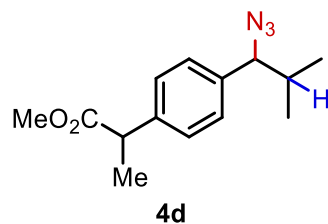
(1-azido-3-methylbutyl)benzene (4c): Prepared from isopentylbenzene (**3c**) according to Procedure C. The reaction mixture was purified by flash column chromatography (ethyl acetate:pentane = 1:50) to afford 49.1 mg of **4c**. Regioselectivity of benzylic (**4c**)¹⁴ and tertiary product¹⁶ was determined by ^1H NMR analysis of crude mixture.

Yield and Site-Selectivity (^1H NMR): 71%, benzylic to tertiary product = 25:1.

Isolated Yield: 65% for only benzylic product (**4c**).

Physical Property: Colorless oil.

^1H NMR (500 MHz, CDCl_3 containing 1 % (v/v) TMS) δ 7.38 (tt, $J = 7.0, 1.1$ Hz, 2H), 7.35 – 7.28 (m, 3H), 4.46 (dd, $J = 8.6, 6.4$ Hz, 1H), 1.76 (ddd, $J = 13.4, 8.6, 6.1$ Hz, 1H), 1.65 (dp, $J = 12.9, 6.4$ Hz, 1H), 1.57 (ddd, $J = 13.7, 7.3, 6.4$ Hz, 1H), 0.94 (d, $J = 6.4$ Hz, 6H).



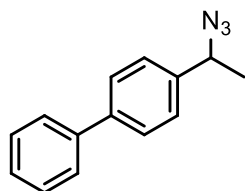
methyl 2-(4-(1-azido-2-methylpropyl)phenyl)propanoate (4d): Prepared from ibuprofen methyl ester (**3c**) according to Procedure C. The reaction mixture was purified by flash column chromatography (ethyl acetate:pentane = 1:25) to afford 61.8 mg of **4d**. Regioselectivity of benzylic (**4d**)¹⁸ and tertiary product was determined by ¹H NMR analysis of crude mixture.

Yield and Site-Selectivity (¹H NMR): 62%, benzylic to tertiary product = 30:1.

Isolated Yield: 59%, for only benzylic product (**4d**).

Physical Property: Colorless oil.

¹H NMR (500 MHz, CDCl₃ containing 1 % (v/v) TMS) δ 7.32 – 7.27 (m, 2H), 7.24 – 7.18 (m, 2H), 4.12 (d, J = 7.9 Hz, 1H), 3.73 (q, J = 7.2 Hz, 1H), 3.67 (s, 3H), 1.97 (dp, J = 7.9, 6.6 Hz, 1H), 1.50 (d, J = 7.2 Hz, 3H), 1.01 (d, J = 6.6 Hz, 3H), 0.80 (d, J = 6.7 Hz, 3H).

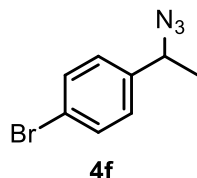


4-(1-azidoethyl)-1,1'-biphenyl (4e): Prepared from 4-ethyl-1,1'-biphenyl (**3e**) according to Procedure B. The reaction mixture was purified by flash column chromatography (ethyl acetate:pentane = 1:40) to afford 40.5 mg of **4e**. ¹H NMR spectrum of **4e** was matched with the literature.⁴³

Isolated Yield: 45%

Physical Property: White solid.

¹H NMR (500 MHz, CDCl₃ containing 1 % (v/v) TMS) δ 7.63 – 7.55 (m, 4H), 7.44 (dd, J = 8.4, 6.9 Hz, 2H), 7.42 – 7.37 (m, 2H), 7.37 – 7.33 (m, 1H), 4.66 (q, J = 6.8 Hz, 1H), 1.56 (d, J = 6.8 Hz, 3H).

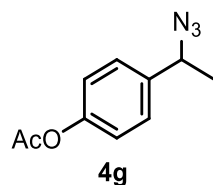


1-(1-azidoethyl)-4-bromobenzene (4f): Prepared from 1-bromo-4-ethylbenzene (**3f**) according to Procedure C. The reaction mixture was purified by flash column chromatography (ethyl acetate:pentane = 1:40) to afford 55.0 mg of **4f**. ¹H NMR spectrum of **4f** was matched with the literature.⁴⁴

Isolated Yield: 61%

Physical Property: Colorless oil.

¹H NMR (400 MHz, CDCl₃ containing 1 % (v/v) TMS) δ 7.53 – 7.47 (m, 2H), 7.23 – 7.17 (m, 2H), 4.59 (q, J = 6.8 Hz, 1H), 1.51 (d, J = 6.8 Hz, 3H).

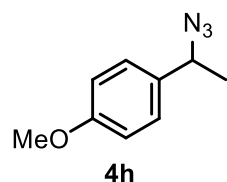


4-(1-azidoethyl)phenyl acetate (4g): Prepared from 4-ethylphenyl acetate (**3g**) according to Procedure A. The reaction mixture was purified by flash column chromatography (ethyl acetate:pentane = 1:15) to afford 46.0 mg of **4g**. ^1H NMR spectrum of **4g** was matched with the literature.¹⁸

Isolated Yield: 56%

Physical Property: Colorless oil.

^1H NMR (400 MHz, CDCl_3 containing 1 % (v/v) TMS) δ 7.37 – 7.31 (m, 2H), 7.13 – 7.07 (m, 2H), 4.62 (q, $J = 6.8$ Hz, 1H), 2.30 (s, 3H), 1.52 (d, $J = 6.8$ Hz, 3H).

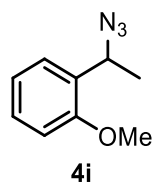


1-(1-azidoethyl)-4-methoxybenzene (4h): Prepared from 1-ethyl-4-methoxybenzene (**3h**) according to Procedure D. The reaction mixture was purified by flash column chromatography (ethyl acetate:pentane = 1:12) to afford 28.7 mg of **4h**. ^1H NMR spectrum of **4h** was matched with the literature.⁴⁴

Isolated Yield: 81%

Physical Property: Colorless oil.

^1H NMR (500 MHz, CDCl_3 containing 1 % (v/v) TMS) δ 7.29 – 7.23 (m, 2H), 6.94 – 6.88 (m, 2H), 4.57 (q, $J = 6.8$ Hz, 1H), 3.81 (s, 3H), 1.51 (d, $J = 6.8$ Hz, 3H).

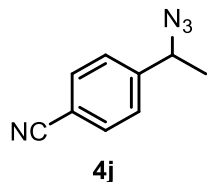


1-(1-azidoethyl)-2-methoxybenzene (4i): Prepared from 1-ethyl-2-methoxybenzene (**3i**) according to Procedure A. The reaction mixture was purified by flash column chromatography (ethyl acetate:pentane = 1:12) to afford 40.5 mg of **4i**. ^1H NMR spectrum of **4i** was matched with the literature.⁴⁵

Isolated Yield: 57%

Physical Property: Colorless oil.

^1H NMR (500 MHz, CDCl_3 containing 1 % (v/v) TMS) δ 7.35 (dd, $J = 7.6, 1.7$ Hz, 1H), 7.28 (ddd, $J = 8.2, 7.4, 1.7$ Hz, 1H), 6.99 (td, $J = 7.5, 1.1$ Hz, 1H), 6.90 (dd, $J = 8.2, 1.1$ Hz, 1H), 5.06 (q, $J = 6.9$ Hz, 1H), 3.85 (s, 3H), 1.50 (d, $J = 6.9$ Hz, 3H).

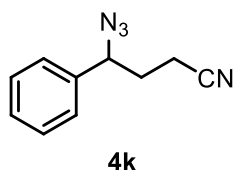


4-(1-azidoethyl)benzonitrile (4j): Prepared from 4-ethylbenzonitrile (**3j**) according to Procedure B. The reaction mixture was purified by flash column chromatography (ethyl acetate:pentane = 1:25) to afford 17.4 mg of **4j**. ^1H NMR spectrum of **4j** was matched with the literature.¹³

Isolated Yield: 25%

Physical Property: Colorless oil.

^1H NMR (400 MHz, CDCl_3 containing 1 % (v/v) TMS) δ 7.74 – 7.62 (m, 2H), 7.49 – 7.40 (m, 2H), 4.69 (q, J = 6.8 Hz, 1H), 1.55 (d, J = 6.9 Hz, 3H).

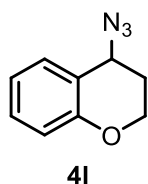


4-azido-4-phenylbutanenitrile (4k): Prepared from 4-phenylbutanenitrile (**3k**) according to Procedure B. The reaction mixture was purified by flash column chromatography (ethyl acetate:pentane = 1:30) to afford 38.0 mg of **4k**. ^1H NMR spectrum of **4k** was matched with the literature.⁴⁶

Isolated Yield: 51%

Physical Property: Colorless oil.

^1H NMR (500 MHz, CDCl_3 containing 1 % (v/v) TMS) δ 7.45 – 7.40 (m, 2H), 7.40 – 7.36 (m, 1H), 7.34 – 7.31 (m, 2H), 4.63 (dd, J = 8.7, 5.7 Hz, 1H), 2.53 – 2.33 (m, 2H), 2.15 – 1.98 (m, 2H).

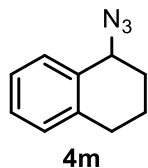


4-azidochroman (4l): Prepared from chroman (**3l**) according to Procedure A. The reaction mixture was purified by flash column chromatography (ethyl acetate:pentane = 1:30) to afford 42.2 mg of **4l**. ^1H NMR spectrum of **4l** was matched with the literature.¹³

Isolated Yield: 60%

Physical Property: Colorless oil.

^1H NMR (400 MHz, CDCl_3 containing 1 % (v/v) TMS) δ 7.28 – 7.19 (m, 2H), 6.95 (td, J = 7.4, 1.2 Hz, 1H), 6.91 – 6.85 (m, 1H), 4.60 (t, J = 4.0 Hz, 1H), 4.29 (dtd, J = 11.3, 4.0, 1.1 Hz, 1H), 4.22 (td, J = 11.2, 2.5 Hz, 1H), 2.18 (ddt, J = 14.2, 11.1, 4.3 Hz, 1H), 2.03 (dtd, J = 14.2, 3.7, 2.5 Hz, 1H).



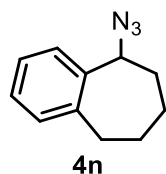
1-azido-1,2,3,4-tetrahydronaphthalene (4m): Prepared from 1,2,3,4-tetrahydronaphthalene (**3m**) according to Procedure A. The reaction mixture was purified by flash column chromatography (ethyl acetate:pentane = 1:30) to afford 62.6 mg of **4m**. ^1H NMR spectrum of **4m** was matched with the literature.¹³

Isolated Yield: 90%

Physical Property: Colorless oil.

^1H NMR (500 MHz, CDCl_3 containing 1 % (v/v) TMS)

δ 7.32 – 7.28 (m, 1H), 7.26 – 7.19 (m, 2H), 7.14 (dd, $J = 7.1, 1.8$ Hz, 1H), 4.57 (t, $J = 4.5$ Hz, 1H), 2.85 (dt, $J = 16.3, 5.0$ Hz, 1H), 2.75 (dt, $J = 17.2, 7.1$ Hz, 1H), 2.06 – 1.93 (m, 3H), 1.88 – 1.77 (m, 1H).

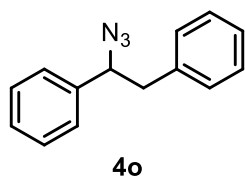


5-azido-6,7,8,9-tetrahydro-5H-benzo[7]annulene (4n): Prepared from 6,7,8,9-tetrahydro-5H-benzo[7]annulene (**3n**) according to Procedure A. The reaction mixture was purified by flash column chromatography (ethyl acetate:pentane = 1:30) to afford 63.8 mg of **4n**. ^1H NMR spectrum of **4n** was matched with the literature.¹³

Isolated Yield: 85%

Physical Property: Colorless oil.

^1H NMR (500 MHz, CDCl_3 containing 1 % (v/v) TMS) δ 7.30 – 7.26 (m, 1H), 7.22 – 7.16 (m, 2H), 7.15 – 7.12 (m, 1H), 4.80 – 4.75 (m, 1H), 3.00 (ddd, $J = 14.5, 9.9, 2.0$ Hz, 1H), 2.72 (ddd, $J = 14.4, 8.6, 1.8$ Hz, 1H), 2.13 – 2.01 (m, 1H), 1.98 – 1.86 (m, 2H), 1.81 (dtt, $J = 14.0, 7.2, 3.5$ Hz, 1H), 1.75 – 1.66 (m, 1H), 1.65 – 1.55 (m, 1H).

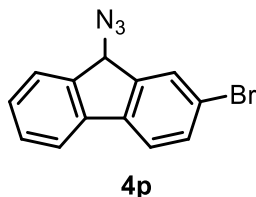


(1-azidoethane-1,2-diyl)dibenzene (4o): Prepared from 1,2-diphenylethane (**3o**) according to Procedure D. The reaction mixture was purified by flash column chromatography (ethyl acetate:pentane = 1:40) to afford 32.1 mg of **4o**. ^1H NMR spectrum of **4o** was matched with the literature.¹⁸

Isolated Yield: 72%

Physical Property: Colorless oil.

^1H NMR (500 MHz, CDCl_3 containing 1 % (v/v) TMS) δ 7.39 – 7.30 (m, 3H), 7.29 – 7.20 (m, 5H), 7.17 – 7.11 (m, 2H), 4.66 (dd, $J = 8.4, 6.1$ Hz, 1H), 3.12 – 2.98 (m, 2H).



9-azido-2-bromo-9H-fluorene (4p): Prepared from 2-bromo-9H-fluorene (**3p**) according to Procedure D. The reaction mixture was purified by flash column chromatography (ethyl acetate:pentane = 1:20) to afford 27.6 mg of **4p**.

Isolated Yield: 48%

Physical Property: White solid.

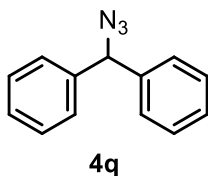
Melting Point: 82-84 °C

¹H NMR (500 MHz, CDCl₃ containing 1 % (v/v) TMS) δ 7.76 (q, *J* = 1.1 Hz, 1H), 7.68 (d, *J* = 7.5 Hz, 1H), 7.63 (dd, *J* = 7.4, 1.0 Hz, 1H), 7.57 (d, *J* = 1.1 Hz, 2H), 7.48 – 7.43 (m, 0H), 7.39 (td, *J* = 7.5, 1.2 Hz, 1H), 5.18 (s, 1H).

¹³C NMR (126 MHz, CDCl₃ containing 1 % (v/v) TMS) δ 143.7, 141.3, 139.7, 139.7, 132.6, 129.7, 128.6, 128.4, 125.3, 121.64, 121.57, 120.4, 63.9.

IR (neat): 2925, 2092, 1447, 765, 741, 427 cm⁻¹.

HRMS (ESI) calculated for C₁₃H₈BrN₃⁺ [M]⁺ 284.9896, found 284.9890.

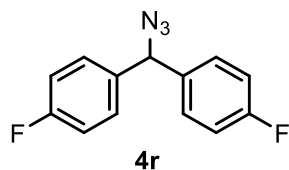


(azidomethylene)dibenzene (4q): According to Procedure A in 10 mmol scale, a 250 mL round-bottom flask was charged with diphenylmethane (**3q**, 1.68 g, 10.0 mmol), 2.00 mol% of copper(II) acetate (36 mg, 0.2 mmol), 4.0 mol% of 2,2'-bis[(4*S*)-4-benzyl-2-oxazoline] (128 mg, 0.400 mmol), 2.50 equivalents of *N*-fluorobenzenesulfonimide (7.88 g, 25.0 mmol), and a magnetic stir bar outside a glovebox. The flask was capped with serrated natural rubber septum. The septum was pierced by a needle (22 gauge - 1 1/2", 0.7 mm x 40 mm) and the flask was moved into the glovebox and underwent four cycles of vacuum-nitrogen-backfill over 40 minutes. After removal of the needle, the flask was taken out of the glovebox and equipped with a balloon filled with nitrogen gas. The flask was charged with nitromethane (50 mL, 0.2 M) and 3.60 equivalents of azidotrimethylsilane (4.78 mL, 1.44 mmol) sequentially, stirred, and heated to 30 °C (inner temperature) in a heating block on a hot plate. After 24 hours, the flask was cooled to room temperature (25 °C), charged with 3.00 equivalents of lithium(I) carbonate (2.21 g, 30.0 mmol), stirred for 30 minutes, and stayed in air for 30 minutes. All precipitates and catalysts were filtered out through a silica plug (glass Buchner funnel with frit) with dichloromethane (50 mL x 3 times). After evaporation of solvent on a rotary evaporator at 30 °C, flash column chromatography (ethyl acetate:pentane = 1:30) was performed. The isolated compound was dried to give 1.7 g of **4q**. ¹H NMR spectrum of **4q** was matched with the literature.⁴⁷

Isolated Yield: 81%

Physical Property: Colorless oil.

¹H NMR (400 MHz, CDCl₃ containing 1 % (v/v) TMS) δ 7.40 – 7.27 (m, 10H), 5.71 (s, 1H).

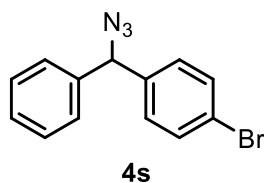


4,4'-(azidomethylene)bis(fluorobenzene) (4r): Prepared from bis(4-fluorophenyl)methane (**3r**) according to Procedure C. The reaction mixture was purified by flash column chromatography (ethyl acetate:pentane = 1:30) to afford 58.5 mg of **4r**. ^1H NMR spectrum of **4r** was matched with the literature.⁴⁷

Isolated Yield: 60%

Physical Property: Colorless oil.

^1H NMR (400 MHz, CDCl_3 containing 1 % (v/v) TMS) δ 7.29 – 7.23 (m, 4H), 7.09 – 7.02 (m, 4H), 5.68 (s, 1H).



1-(azido(phenyl)methyl)-4-bromobenzene (4s): Prepared from 1-benzyl-4-bromobenzene (**3s**) according to Procedure D. The reaction mixture was purified by flash column chromatography (ethyl acetate:pentane = 1:30) to afford 29.2 mg of **4s**.

Isolated Yield: 51%

Physical Property: Colorless oil.

^1H NMR (400 MHz, CDCl_3 containing 1 % (v/v) TMS)

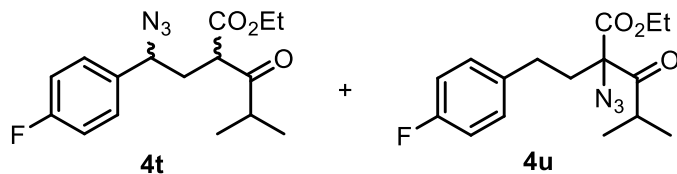
δ 7.51 – 7.45 (m, 2H), 7.39 – 7.26 (m, 5H), 7.22 – 7.16 (m, 2H), 5.66 (s, 1H).

^{13}C NMR (126 MHz, CDCl_3 containing 1 % (v/v) TMS)

δ 139.0, 138.7, 131.8, 129.0, 128.8, 128.3, 127.4, 122.0, 67.9.

IR (neat): 3029, 2096, 1486, 1239, 1071, 1010, 698, 480 cm^{-1} .

HRMS (ESI) calculated for $\text{C}_{13}\text{H}_{10}\text{Br}^+$ $[\text{M}-\text{N}_3]^+$ 244.9960, found 244.9962.



ethyl 2-(2-azido-2-(4-fluorophenyl)ethyl)-4-methyl-3-oxopentanoate (4t) and **ethyl 2-azido-2-(4-fluorophenethyl)-4-methyl-3-oxopentanoate (4u)**: Prepared from ethyl 2-(4-fluorophenethyl)-4-methyl-3-oxopentanoate (**3t**) according to Procedure E. The reaction mixture was purified by flash column chromatography (ethyl acetate:pentane = 1:30) to afford 16.8 mg of **4t** (d.r. = 1.1:1.0) along with 16.5 mg of the regioisomer **4u**. ^1H NMR spectrum of **4t** was matched with the literature.⁴⁸

ethyl 2-(2-azido-2-(4-fluorophenyl)ethyl)-4-methyl-3-oxopentanoate (4t):

Isolated Yield: 26%

Physical Property: Colorless oil.

^1H NMR (400 MHz, CDCl_3 containing 1 % (v/v) TMS) for inseparable diastereomers; d.r = 1.1:1.0 based on ^1H NMR analysis of the crude reaction mixture. A and B represents each diastereomer. δ 7.33 – 7.27 (m, 4H, A and B), 7.13 – 7.03 (m, 4H, A and B), 4.53 (dd, $J = 9.8, 5.0$ Hz, 1H, CHN_3 of A), 4.40 (dd, $J = 9.7, 5.2$ Hz, 1H, CHN_3 of B), 4.25 – 4.15 (m, 4H, A and B), 3.86 – 3.77 (m, 2H, A and B), 2.89 – 2.75 (m, 2H, A and B), 2.31 – 2.08 (m, 4H, A and B), 1.32 – 1.24 (m, 6H, A and B), 1.16 – 1.06 (m, 12H, A and B).

^1H NMR (400 MHz, CDCl_3 containing 1 % (v/v) TMS) for **4t-A**; ^1H NMR spectrum includes 13% of **4t-B** (diastereomer) but the peaks of **4t-B** was distinguished and ignored for characterization of a single diastereomer **4t-A**. δ 7.33 – 7.27 (m, 2H), 7.13 – 7.03 (m, 2H), 4.53 (dd, $J = 9.8, 5.0$ Hz, 1H), 4.20 (qd, $J = 7.2, 1.3$ Hz, 2H), 3.82 (dd, $J = 8.6, 5.3$ Hz, 1H), 2.82 (dq, $J = 13.8, 7.0$ Hz, 1H), 2.25 (ddd, $J = 13.8, 8.6, 5.0$ Hz, 1H), 2.14 (ddd, $J = 14.5, 9.7, 5.3$ Hz, 1H), 1.28 (t, $J = 7.2$ Hz, 3H), 1.12 (d, $J = 7.0$ Hz, 3H), 1.10 (d, $J = 7.0$ Hz, 3H).

ethyl 2-azido-2-(4-fluorophenethyl)-4-methyl-3-oxopentanoate (4u):

Isolated Yield: 26%

Physical Property: Colorless oil.

^1H NMR (500 MHz, CDCl_3 containing 1 % (v/v) TMS) δ 7.17 – 7.12 (m, 2H), 7.00 – 6.94 (m, 2H), 4.34 – 4.22 (m, 2H), 3.04 (hept, $J = 6.7$ Hz, 1H), 2.67 – 2.50 (m, 2H), 2.32 – 2.19 (m, 2H), 1.32 (t, $J = 7.1$ Hz, 3H), 1.13 (d, $J = 6.7$ Hz, 3H), 1.11 (d, $J = 6.7$ Hz, 3H).

^{13}C NMR (126 MHz, CDCl_3 containing 1 % (v/v) TMS) δ 161.5 (d, $J = 244.2$ Hz), 136.1 (d, $J = 3.3$ Hz), 129.8 (d, $J = 7.9$ Hz), 115.3 (d, $J = 21.2$ Hz), 35.2 (d, $J = 1.2$ Hz).

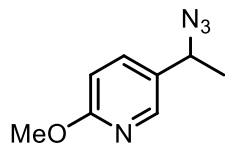
^{19}F NMR (377 MHz, CDCl_3 containing 1 % (v/v) TMS) δ – 116.86.

DEPT-135 NMR (126 MHz, CDCl_3 containing 1 % (v/v) TMS)

δ 129.8 (d, $J = 7.9$ Hz, positive), 115.3 (d, $J = 21.2$ Hz, positive), 62.9 (negative), 36.4 (positive), 35.2 (negative), 29.5 (negative), 19.6 (positive), 19.4 (positive), 14.1 (positive).

IR (neat): 2977, 2937, 2875, 2111, 1723, 1509, 1221, 1014, 829 cm^{-1} .

HRMS (ESI) calculated for $\text{C}_{16}\text{H}_{21}\text{FN}_3\text{O}_3^+$ $[\text{M}+\text{H}]^+$ 322.1561, found 322.1560.

**4v**

5-(1-azidoethyl)-2-methoxypyridine (4v): Prepared from 5-ethyl-2-methoxypyridine (**3v**) according to Procedure A in 0.2 mmol scale. The reaction mixture was purified by flash column chromatography (diethyl ether:pentane = 1:3) to afford 10.8 mg of **4v**.

Isolated Yield: 30%

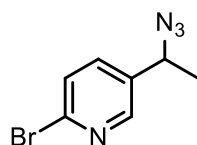
Physical Property: Colorless oil.

¹H NMR (500 MHz, CDCl₃ containing 1 % (v/v) TMS) δ 8.11 (d, *J* = 2.5 Hz, 1H), 7.57 (dd, *J* = 8.5, 2.5 Hz, 1H), 6.77 (d, *J* = 8.5 Hz, 1H), 4.60 (q, *J* = 6.9 Hz, 1H), 3.94 (s, 3H), 1.52 (d, *J* = 6.9 Hz, 3H).

¹³C NMR (126 MHz, CDCl₃ containing 1 % (v/v) TMS) δ 164.3, 145.2, 136.9, 129.2, 111.4, 58.5, 53.7, 21.4.

IR (neat): 2976, 2941, 2098, 1604, 1491, 1316, 1281, 1020 cm⁻¹.

HRMS (ESI) calculated for C₈H₁₁N₄O⁺ [M]⁺ 179.0927, found 179.0926.

**4w**

5-(1-azidoethyl)-2-bromopyridine (4w): Prepared from 2-bromo-5-ethylpyridine (**3w**) according to Procedure B in 0.2 mmol scale. The reaction mixture was purified by flash column chromatography (diethyl ether:pentane = 1:3) to afford 13.8 mg of **4w**.

Isolated Yield: 30%

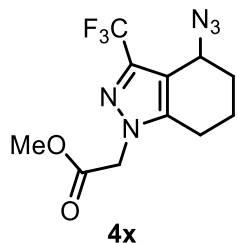
Physical Property: Colorless oil.

¹H NMR (500 MHz, CDCl₃ containing 1 % (v/v) TMS) δ 8.34 (d, *J* = 2.4 Hz, 1H), 7.57 – 7.48 (m, 2H), 4.66 (q, *J* = 6.8 Hz, 1H), 1.56 (d, *J* = 6.8 Hz, 3H).

¹³C NMR (126 MHz, CDCl₃ containing 1 % (v/v) TMS) δ 148.5, 141.9, 136.6, 136.1, 128.4, 58.1, 21.6.

IR (neat): 2978, 2925, 2101, 1572, 1454, 1248, 1090 cm⁻¹.

HRMS (ESI) calculated for C₇H₈BrN₄⁺ [M]⁺ 226.9927, found 226.9924.



methyl 2-(4-azido-3-(trifluoromethyl)-4,5,6,7-tetrahydro-1H-indazol-1-yl)acetate (4x): Prepared from methyl 2-(3-(trifluoromethyl)-4,5,6,7-tetrahydro-1H-indazol-1-yl)acetate (**3x**) according to Procedure D in 0.2 mmol scale. The reaction mixture was purified by flash column chromatography (diethyl ether:pentane = 1:1) to afford 39.6 mg of **4x**.

Isolated Yield: 65%

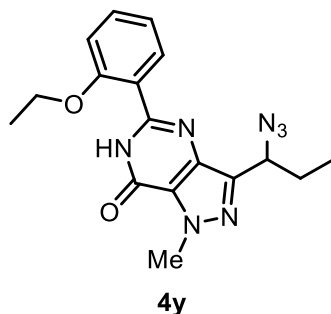
Physical Property: Colorless oil.

¹H NMR (500 MHz, CDCl₃ containing 1 % (v/v) TMS) δ 4.91 (d, *J* = 17.6 Hz, 1H), 4.81 (d, *J* = 17.6 Hz, 1H), 4.72 – 4.66 (m, 1H), 3.78 (s, 3H), 2.65 (ddd, *J* = 16.5, 5.4, 3.4 Hz, 1H), 2.51 (ddd, *J* = 16.5, 10.0, 7.0 Hz, 1H), 2.14 – 2.05 (m, 1H), 2.03 – 1.91 (m, 2H), 1.84 (ddt, *J* = 13.8, 11.3, 4.2 Hz, 1H).

¹³C NMR (126 MHz, CDCl₃ containing 1 % (v/v) TMS) δ 167.2, 143.1, 140.1 (q, *J* = 37.6 Hz), 121.4 (q, *J* = 269.5 Hz), 113.4, 53.0, 52.0, 50.9, 29.3, 21.0, 17.6.

IR (neat): 2954, 2861, 2098, 1755, 1213, 1127 cm⁻¹.

HRMS (ESI) calculated for C₁₁H₁₃F₃N₅O₂⁺ [M+H]⁺ 304.1016, found 304.1011.



3-(1-azidopropyl)-5-(2-ethoxyphenyl)-1-methyl-1H-pyrazolo[4,3-d]pyrimidin-7(6H)-one (4y): Prepared from 5-(2-ethoxyphenyl)-1-methyl-3-propyl-1H-pyrazolo[4,3-d]pyrimidin-7(6H)-one (**3y**) according to Procedure D. The reaction mixture was purified by flash column chromatography (ethyl acetate:pentane = 2:1) to afford 21.5 mg of **4y**.

Isolated Yield: 30%

Physical Property: White solid.

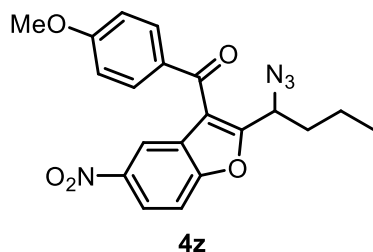
Melting Point: 111-113 °C

¹H NMR (500 MHz, CDCl₃ containing 1 % (v/v) TMS) δ 11.26 (s, 1H), 8.50 (dd, *J* = 7.9, 1.9 Hz, 1H), 7.47 (ddd, *J* = 8.8, 7.4, 1.9 Hz, 1H), 7.18 – 7.13 (m, 1H), 7.05 (dd, *J* = 8.4, 0.9 Hz, 1H), 4.77 (t, *J* = 7.4 Hz, 1H), 4.34 – 4.28 (m, 5H), 2.23 (p, *J* = 7.4 Hz, 2H), 1.62 (t, *J* = 7.0 Hz, 3H), 1.06 (t, *J* = 7.4 Hz, 3H).

¹³C NMR (126 MHz, CDCl₃ containing 1 % (v/v) TMS) δ 156.6, 153.6, 149.4, 143.5, 138.5, 132.7, 131.3, 125.0, 121.9, 119.7, 112.9, 65.4, 59.6, 38.7, 26.6, 14.7, 11.0.

IR (neat): 3296, 2975, 2935, 2095, 1696, 1588, 1484, 1234, 1033, 763 cm⁻¹.

HRMS (ESI) calculated for C₁₇H₂₀N₇O₂⁺ [M+H]⁺ 354.1673, found 354.1671.



(2-(1-azidobutyl)-5-nitrobenzofuran-3-yl)(4-methoxyphenyl)methanone (4z): Prepared from (2-butyl-5-nitrobenzofuran-3-yl)(4-methoxyphenyl)methanone (**3z**) according to Procedure B. The reaction mixture was purified by flash column chromatography (methylene chloride:pentane = 2:3) to afford 86.5 mg of **4z**.

Isolated Yield: 55%

Physical Property: White solid.

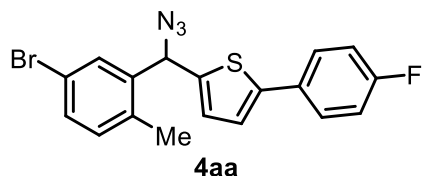
Melting Point: 64-66 °C

¹H NMR (500 MHz, CDCl₃ containing 1 % (v/v) TMS) δ 8.36 – 8.27 (m, 2H), 7.90 – 7.84 (m, 2H), 7.68 (d, *J* = 9.0 Hz, 1H), 7.05 – 6.99 (m, 2H), 4.80 (t, *J* = 7.6 Hz, 1H), 3.93 (s, 3H), 2.11 – 1.96 (m, 2H), 1.53 – 1.42 (m, 1H), 1.40 – 1.28 (m, 1H), 0.94 (t, *J* = 7.3 Hz, 3H).

¹³C NMR (126 MHz, CDCl₃ containing 1 % (v/v) TMS) δ 187.8, 164.5, 161.6, 156.5, 144.9, 132.0, 130.3, 126.8, 121.4, 119.4, 118.4, 114.3, 112.3, 56.8, 55.7, 34.5, 19.3, 13.5.

IR (neat): 3103, 2961, 2934, 2099, 1598, 1527, 1344, 1252, 1168, 900, 837 cm⁻¹.

HRMS (ESI) calculated for C₂₀H₁₉N₄O₅⁺ [M+H]⁺ 395.1350, found 395.1346.



2-(azido(5-bromo-2-methylphenyl)methyl)-5-(4-fluorophenyl)thiophene (4aa): Prepared from 2-(5-bromo-2-methylbenzyl)-5-(4-fluorophenyl)thiophene (**3aa**) according to Procedure C. The reaction mixture was purified by flash column chromatography (ethyl acetate:pentane = 1:10) to afford 29.2 mg of **4aa**.

Isolated Yield: 36%

Physical Property: Yellow oil.

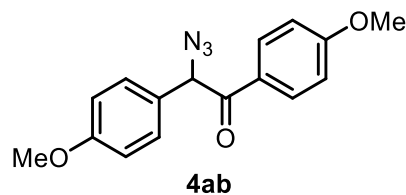
¹H NMR (500 MHz, CDCl₃ containing 1 % (v/v) TMS) δ 7.70 (d, *J* = 2.1 Hz, 1H), 7.53 – 7.47 (m, 2H), 7.39 (dd, *J* = 8.1, 2.1 Hz, 1H), 7.09 (d, *J* = 3.7 Hz, 1H), 7.08 – 7.02 (m, 3H), 6.89 (dd, *J* = 3.7, 0.8 Hz, 1H), 5.99 (s, 1H), 2.23 (s, 3H).

¹⁹F NMR (377 MHz, CDCl₃ containing 1 % (v/v) TMS) δ -113.9.

¹³C NMR (126 MHz, CDCl₃ containing 1 % (v/v) TMS) δ 162.5 (d, *J* = 247.9 Hz), 140.6, 139.1, 134.4, 132.4, 131.4, 130.1 (d, *J* = 3.4 Hz), 129.6, 127.7, 127.5 (d, *J* = 8.1 Hz), 122.64, 122.63, 120.1, 115.9 (d, *J* = 22.0 Hz), 61.1, 18.9.

IR (neat): 2922, 2852, 2097, 1546, 1233, 808 cm⁻¹.

HRMS (ESI) calculated for C₁₈H₁₃BrFS⁺ [M-N₃]⁺ 358.9900, found 358.9897.

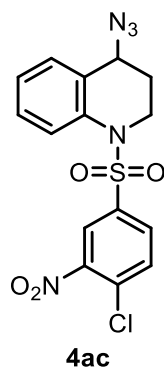


2-azido-1,2-bis(4-methoxyphenyl)ethanone (4ab): Prepared from 1,2-bis(4-methoxyphenyl)ethanone (**3ab**) according to Procedure A. The reaction mixture was purified by flash column chromatography (ethyl acetate:pentane = 1:8) to afford 72.9 mg of **4ab**. $^1\text{H NMR}$ spectrum of **4ab** was matched with the literature.⁴⁹

Isolated Yield: 62%

Physical Property: Colorless oil.

$^1\text{H NMR}$ (500 MHz, CDCl_3 containing 1 % (v/v) TMS) δ 7.88 – 7.84 (m, 2H), 7.33 – 7.28 (m, 2H), 6.93 – 6.89 (m, 2H), 6.88 – 6.84 (m, 2H), 5.63 (s, 1H), 3.82 (s, 3H), 3.78 (s, 3H).



4-azido-1-((4-chloro-3-nitrophenyl)sulfonyl)-1,2,3,4-tetrahydroquinoline (4ac): Prepared from 1-((4-chloro-3-nitrophenyl)sulfonyl)-1,2,3,4-tetrahydroquinoline (**3ac**) according to Procedure C. The reaction mixture was purified by flash column chromatography (ethyl acetate:pentane = 1:10) to afford 33.2 mg of **4ac**.

Isolated Yield: 42%

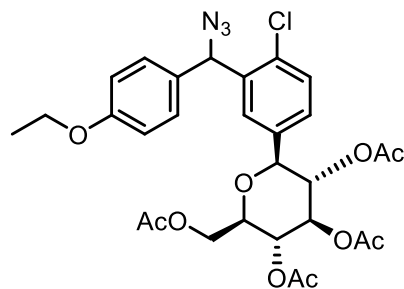
Physical Property: Colorless oil.

$^1\text{H NMR}$ (500 MHz, CDCl_3 containing 1 % (v/v) TMS) δ 8.13 (d, $J = 2.1$ Hz, 1H), 7.93 (d, $J = 7.9$ Hz, 1H), 7.67 (dd, $J = 8.5, 2.1$ Hz, 1H), 7.60 (d, $J = 8.5$ Hz, 1H), 7.40 (ddd, $J = 8.6, 6.3, 2.7$ Hz, 1H), 7.26 – 7.20 (m, 2H), 4.46 (t, $J = 4.1$ Hz, 1H), 4.12 – 4.04 (m, 1H), 3.74 (ddd, $J = 13.1, 11.4, 4.1$ Hz, 1H), 1.98 (dq, $J = 14.1, 4.1$ Hz, 1H), 1.91 – 1.80 (m, 1H).

$^{13}\text{C NMR}$ (126 MHz, CDCl_3 containing 1 % (v/v) TMS) δ 147.6, 138.4, 135.3, 132.9, 132.2, 130.8, 130.0, 129.6, 126.9, 125.7, 124.4, 124.0, 56.6, 42.9, 27.5.

IR (neat): 3092, 2929, 2097, 1537, 1349, 1174, 887, 762 cm^{-1} .

HRMS (ESI) calculated for $\text{C}_{15}\text{H}_{12}\text{ClN}_5\text{NaO}_4\text{S}^+$ $[\text{M}+\text{Na}]^+$ 416.0191, found 416.0188.

**4ad**

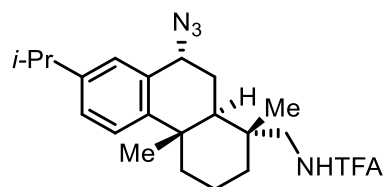
(2R,3R,4R,5S,6S)-2-(acetoxymethyl)-6-(3-(azido(4-ethoxyphenyl)methyl)-4-chlorophenyl)tetrahydr-o-2H-pyran-3,4,5-triyl triacetate (4ad): Prepared from dapagliflozin tetraacetate (**3ad**) according to Procedure C. The reaction mixture was purified by flash column chromatography (ethyl acetate:pentane = 1:4) to afford an inseparable mixture of **3ad** and **4ad** (d.r. = 1.4:1.0).

Note: The yield of **3ad** and **4ad**, and the diastereomeric ratio of **4ad** were measured after filtration through a silica pad.

Yield (¹H NMR): 34%

Physical Property: White solid.

HRMS (ESI) calculated for C₂₉H₃₂ClN₃NaO₁₀⁺ [M+Na]⁺ 640.1668, found 640.1661.

**(-)-4ae**

N-(((1R,4aS,9R,10aR)-9-azido-7-isopropyl-1,4a-dimethyl-1,2,3,4,4a,9,10,10a-octahydrophenanthre-n-1-yl)methyl)-2,2,2-trifluoroacetamide ((-)-4ae): Prepared from **3ae** in 0.2 mmol scale according to Procedure A. The major diastereomer (47.0 mg of (-)-**4ae**) was separated from the minor diastereomer via flash column chromatography (ethyl acetate:pentane = 1:20). The relative configuration (d.r. = 6.0:1.0) was determined by ¹H, ¹³C, DEPT-135, HSQC, HMBC, and TOCSY NMR analysis and then confirmed with the literature⁵⁰ after reduction of azide to primary amine group.

For 2.0 mmol reaction scale, a 50 mL round-bottom flask was charged with 2.00 mol% of copper(II) acetate (7.30 mg, 20.0 μmol), 4.0 mol% of 2,2'-bis[(4S)-4-benzyl-2-oxazoline] (25.6 mg, 40.0 μmol), 2.50 equivalents of *N*-fluorobenzenesulfonimide (1.58 g, 5.00 mmol), and a magnetic stir bar outside a glovebox. The flask was capped with serrated natural rubber septum. The septum was pierced by a needle (22 gauge - 1 1/2", 0.7 mm x 40 mm) and the flask was moved into the glovebox and underwent four cycles of vacuum-nitrogen-backfill over 40 minutes. After removal of the needle, the flask was taken out of the glovebox and equipped with a balloon filled with nitrogen gas. The flask was charged with the solution of **3ae** (763 mg, 2.00 mmol) in 50 mL of nitromethane (0.20 M) and 3.60 equivalents of azidotrimethylsilane (956 μL, 7.20 mmol) sequentially, stirred, and heated to 30 °C (inner temperature) in an oil bath on a hot plate. After 24 hours, the flask was cooled to room temperature (25 °C), charged with 3.00 equivalents of lithium(I) carbonate (222 mg, 6.00 mmol), stirred for 30 minutes, and stayed in air for 30 minutes.

All precipitates and catalysts were filtered out through a silica plug (glass Buchner funnel with frit) with dichloromethane (10 mL x 3 times) and nitromethane (10 mL x 3 times). After evaporation of solvent on a rotary evaporator at 30 °C, flash column chromatography (ethyl acetate:pentane = 1:20) was performed. The isolated compound was dried to give 450.0 mg of (–)-**4ae** (d.r. = 5.8:1.0).

Yield (¹H NMR): Total 63% for both diastereomers in 0.2 mmol scale and total 62% in 2.0 mmol scale.

Isolated Yield: 56% and 53% of (–)-**4ae** in 0.2 mmol scale and 2.0 mmol scale respectively.

Physical Property: Amorphous solid.

Melting Point: 122-124 °C

¹H NMR (500 MHz, CDCl₃ containing 1 % (v/v) TMS) δ 7.30 – 7.19 (m, 2H), 6.99 (d, *J* = 1.9 Hz, 1H), 4.76 (dd, *J* = 3.7, 2.2 Hz, 1H), 3.54 (dd, *J* = 14.1, 9.9 Hz, 1H), 3.00 – 2.85 (m, 2H), 2.26 (dd, *J* = 13.1, 3.6 Hz, 1H), 1.94 (ddd, *J* = 13.8, 12.1, 3.7 Hz, 1H), 1.85 – 1.64 (m, 4H), 1.45 – 1.28 (m, 3H), 1.27 (s, 3H), 1.25 (s, 3H), 1.21 (s, 3H), 0.95 (s, 3H).

¹⁹F NMR (377 MHz, CDCl₃ containing 1 % (v/v) TMS) δ -76.0.

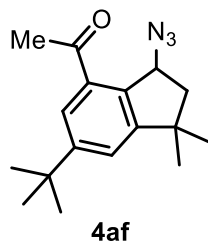
¹³C NMR (126 MHz, CDCl₃ containing 1 % (v/v) TMS) δ 157.9 (q, *J* = 36.7 Hz), 147.0, 146.7, 131.1, 127.8, 127.5, 126.0, 116.2 (q, *J* = 288.1 Hz), 61.9, 48.6, 40.3, 38.32, 38.29, 37.4, 35.3, 33.6, 25.6, 24.7, 24.1, 23.8, 19.4, 18.6.

DEPT-135 NMR (126 MHz, CDCl₃ containing 1 % (v/v) TMS) δ 127.8 (positive), 127.5 (positive), 126.0 (positive), 61.9 (positive), 48.6 (negative), 40.3 (positive), 38.3 (negative), 35.3 (negative), 33.6 (positive), 25.6 (negative), 24.7 (positive), 24.1 (positive), 23.8 (positive), 19.4 (positive), 18.6 (negative).

IR (neat): 3336, 2958, 2930, 2870, 2102, 1725, 1207, 1162, 830, 609 cm⁻¹.

HRMS (ESI) calculated for C₂₂H₂₉F₃N₄NaO⁺ [M+Na]⁺ 445.2186, found 445.2183.

[α]_D²⁴ = -20° (c = 0.40, CHCl₃)



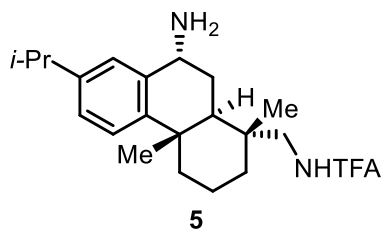
1-(3-azido-6-(tert-butyl)-1,1-dimethyl-2,3-dihydro-1H-inden-4-yl)ethanone (4af): According to Procedure A, a 100 mL round-bottom flask was charged with celestolide (**3af**, 1.22 g, 5.00 mmol) 2.00 mol% of copper(II) acetate (18.0 mg, 0.100 mmol), 4.00 mol% of 2,2'-bis[(4S)-4-benzyl-2-oxazoline] (64.0 mg, 0.200 mmol), 2.50 equivalents of *N*-fluorobenzenesulfonimide (3.94 g, 12.5 mmol), and a magnetic stir bar outside a glovebox. The flask was capped with serrated natural rubber septum. The septum was pierced by a needle (22 gauge - 1 1/2", 0.7 mm x 40 mm) and the flask was moved into the glovebox and underwent four cycles of vacuum-nitrogen-backfill over 40 minutes. After removal of the needle, the flask was taken out of the glovebox and equipped with a balloon filled with nitrogen gas. The flask was charged with nitromethane (25 mL, 0.2 M) and 3.60 equivalents of azidotrimethylsilane (2.40 mL, 18.0 mmol) sequentially, stirred, and heated to 30 °C (inner temperature) in an oil bath on a hot plate. After 24 hours, the flask was cooled to room temperature (25 °C), charged with 3.00 equivalents of lithium(I) carbonate (1.10 g, 15.0 mmol), stirred for 30 minutes, and stayed in air for 30 minutes. All precipitates and catalysts

were filtered out through a silica plug (glass Buchner funnel with frit) with dichloromethane (25 mL x 3 times). After evaporation of solvent on a rotary evaporator at 30 °C, flash column chromatography (ethyl acetate:pentane = 1:40) was performed. The isolated compound was dried to give 1.25 g of **4af**. ¹H NMR spectrum of **4af** was matched with the literature.¹⁸

Isolated Yield: 92%

Physical Property: Yellow oil.

¹H NMR (500 MHz, CDCl₃ containing 1 % (v/v) TMS) δ 7.76 (d, *J* = 1.8 Hz, 1H), 7.40 (d, *J* = 1.8 Hz, 1H), 5.59 (dd, *J* = 7.4, 1.8 Hz, 1H), 2.65 (s, 3H), 2.19 (dd, *J* = 13.7, 7.4 Hz, 1H), 2.08 (dd, *J* = 13.7, 1.8 Hz, 1H), 1.38 (s, 9H), 1.34 (s, 3H), 1.32 (s, 3H).



***N*-(((1*R*,4*aS*,9*R*,10*aR*)-9-amino-7-isopropyl-1,4*a*-dimethyl-1,2,3,4,4*a*,9,10,10*a*-octahydrophenanthrene-1-yl)methyl)-2,2,2-trifluoroacetamide ((-)-**5**):**

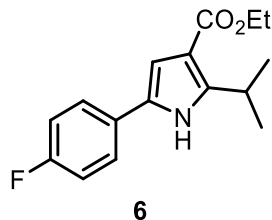
For 69 μmol scale, a 4 mL vial was charged with a magnetic stir bar, 2.0 equivalents of resin-bound triphenylphosphine (3 mmol/g grade, 23 mg, 0.14 mmol) and the resin was washed with THF (1.0 mL) three times and dried *in vacuo*. (-)-**4ae** (69 μmol, 23 mg), 0.1 M THF (0.7 mL), and 0.1 M DI water (0.7 mL) were added to the vial at room temperature (25 °C). After vigorous stirring for 6 hours, the solution was filtered, concentrated, and purified by flash column chromatography (methanol:methylene chloride = 1:19) to afford 25.0 mg of (-)-**5**. ¹H NMR spectrum of (-)-**5** was matched with the literature.⁵⁰

For 0.2 mmol scale, a 20 mL borosilicate glass vial was charged with 2.00 equivalents of resin-bound triphenylphosphine (3 mmol/g grade, 133 mg, 0.400 mmol) and the resin was washed with THF (3.0 mL) three times and dried *in vacuo*. (-)-**4ae** (0.200 mmol, 76.0 mg), 0.1 M THF (2 mL), and 0.1 M DI water (2 mL) were added to the vial at room temperature (25 °C). After vigorous stirring for 9 hours, the solution was filtered, concentrated, and purified by flash column chromatography (methanol:methylene chloride = 1:19) to afford 84.7 mg of (-)-**5**.

Isolated Yield: 91% for 69 μmol scale, 85% for 0.2 mmol scale.

Physical Property: Hygroscopic pale-yellow solid.

¹H NMR (500 MHz, CDCl₃ containing 1 % (v/v) TMS) δ 8.68 (s, 1H), 7.19 (d, *J* = 8.2 Hz, 1H), 7.11 (dd, *J* = 8.2, 2.0 Hz, 1H), 7.04 (d, *J* = 2.0 Hz, 1H), 4.24 (dd, *J* = 3.8, 2.0 Hz, 1H), 3.57 (dd, *J* = 13.9, 8.6 Hz, 1H), 2.99 (d, *J* = 13.9 Hz, 1H), 2.87 (hept, *J* = 6.9 Hz, 1H), 2.73 – 2.08 (m, 3H), 1.99 (d, *J* = 11.9 Hz, 1H), 1.87 – 1.72 (m, 2H), 1.65 (dp, *J* = 14.2, 3.6 Hz, 1H), 1.58 (d, *J* = 12.8 Hz, 1H), 1.43 – 1.36 (m, 1H), 1.31 (ddd, *J* = 13.3, 6.1, 4.1 Hz, 2H), 1.24 (dd, *J* = 6.9, 1.2 Hz, 6H), 1.22 (s, 3H), 0.96 (s, 3H).

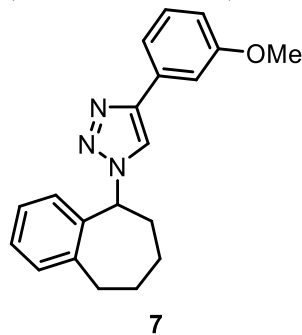


ethyl 5-(4-fluorophenyl)-2-isopropyl-1H-pyrrole-3-carboxylate (6): Prepared modifying to the literature procedure.⁴⁸ A 4 mL borosilicate glass vial was charged with a magnetic stir bar, 10.0 μmol of **4t** (3.20 mg), 12.5 μM of anhydrous THF (800 μL), 3.0 equivalents of triphenylphosphine (7.9 mg, 30 μmol) sequentially and stirred under N_2 gas for 24 hours at room temperature (25 $^\circ\text{C}$). After the removal of solvent, 10 wt% Pd/C (1.40 mg) and 300 μL of *o*-xylene was added to the vial. The resulting mixture was sonicated for 30 minutes and stirred at 145 $^\circ\text{C}$ for 10 hours. The solution was filtered through a silica plug, concentrated, and purified by flash column chromatography (diethyl ether:pentane = 1:2) to afford **6**. After purification, the exact yield (1.65 mg) was determined by ^1H NMR analysis with mesitylene as an external standard. ^1H NMR spectrum of **6** was matched with the literature.⁴⁸

Isolated Yield: 60%

Physical Property: Colorless oil.

^1H NMR (400 MHz, CDCl_3 containing 1 % (v/v) TMS) δ 8.28 (bs, 1H), 7.47-7.37 (m, 2H), 7.12-7.05 (m, 2H), 6.77 (d, $J = 2.9$ Hz, 1H), 4.29 (q, $J = 7.2$ Hz, 2H), 3.86 (sept, $J = 7.1$ Hz, 1H), 1.36 (t, $J = 7.2$ Hz, 3H), 1.33 (d, $J = 7.1$ Hz, 6H).



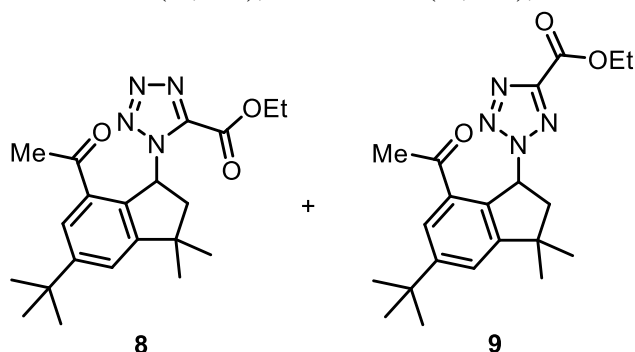
4-(3-methoxyphenyl)-1-(6,7,8,9-tetrahydro-5H-benzo[7]annulen-5-yl)-1H-1,2,3-triazole (7): Prepared modifying to the literature procedure.⁵¹ A 4 mL borosilicate glass vial was charged with a magnetic stir bar, **4n** (0.120 mmol, 22.5 mg), 1.10 equivalents of 1-ethynyl-3-methoxybenzene (0.132 mmol, 17.0 μL), and 0.4 M THF (0.3 mL). To the solution was added 20.0 mol% $\text{CuSO}_4 \cdot 5\text{H}_2\text{O}$ (24.0 μmol , 50.0 mg), 20.0 mol% sodium ascorbate (24.0 μmol , 4.80 mg), and 0.4 M DI water (0.3 mL) sequentially at room temperature (25 $^\circ\text{C}$). After vigorous stirring under nitrogen gas for 12 hours, 10 mL of water was added to the reaction mixture and organic layer was separated from extraction with ethyl acetate (20 mL) three times. The crude mixture was purified by flash column chromatography (ethyl acetate:pentane = 1:8) to afford 32.7 mg of **7**. ^1H NMR spectrum of **7** was matched with the literature.⁵¹

Isolated Yield: 85%

Physical Property: White solid.

^1H NMR (500 MHz, CDCl_3 containing 1 % (v/v) TMS) δ 7.70 (s, 1H), 7.49 (dd, $J = 2.6, 1.5$ Hz, 1H), 7.38 (dt, $J = 7.6, 1.2$ Hz, 1H), 7.32 (t, $J = 7.9$ Hz, 1H), 7.24 – 7.16 (m, 2H), 7.09 (td, $J = 7.2, 2.2$ Hz, 1H), 6.89 (ddd, $J = 8.2, 2.6, 1.1$ Hz, 1H), 6.41 (d, $J = 7.8$ Hz, 1H), 5.90 (d, $J = 9.5$ Hz, 1H),

3.87 (s, 3H), 2.85 (dddd, $J = 42.9, 14.8, 9.2, 1.9$ Hz, 2H), 2.60 – 2.47 (m, 1H), 2.44 – 2.35 (m, 1H), 2.13 – 2.05 (m, 1H), 2.00 – 1.85 (m, 2H), 1.64 – 1.52 (m, 1H).



ethyl 1-(7-acetyl-5-(*tert*-butyl)-3,3-dimethyl-2,3-dihydro-1*H*-inden-1-yl)-1*H*-tetrazole-5-carboxylate (8) and **ethyl 2-(7-acetyl-5-(*tert*-butyl)-3,3-dimethyl-2,3-dihydro-1*H*-inden-1-yl)-2*H*-tetrazole-5-carboxylate (9)**: A 4 mL borosilicate glass vial was charged with a magnetic stir bar, **4af** (0.10 mmol, 27 mg), 13 equivalents of ethyl carbonocyanidate (1.3 mmol, 0.13 g), and 1.0 equivalents of ZnBr_2 (0.10 mmol 23 mg) at room temperature (25 °C). After vigorous stirring for 45 hours, the crude mixture was directly purified flash column chromatography (ethyl acetate:pentane = 1:4) to afford 17.0 mg of **8** and 21.2 mg of **9**.

ethyl 1-(7-acetyl-5-(*tert*-butyl)-3,3-dimethyl-2,3-dihydro-1*H*-inden-1-yl)-1*H*-tetrazole-5-carboxylate (8):

Isolated Yield: 44%

Physical Property: White solid.

Melting Point: 117-119 °C

^1H NMR (500 MHz, CDCl_3 containing 1 % (v/v) TMS) δ 7.79 (d, $J = 1.8$ Hz, 1H), 7.51 (d, $J = 1.8$ Hz, 1H), 7.12 (dd, $J = 8.9, 4.3$ Hz, 1H), 4.62 (qt, $J = 7.1, 3.6$ Hz, 2H), 2.75 (dd, $J = 14.1, 8.9$ Hz, 1H), 2.21 (dd, $J = 14.1, 4.3$ Hz, 1H), 1.54 (t, $J = 7.1$ Hz, 3H), 1.43 (s, 3H), 1.40 (s, 9H), 1.37 (s, 3H).

^{13}C NMR (126 MHz, CDCl_3 containing 1 % (v/v) TMS) δ 199.0, 157.2, 155.0, 154.0, 146.2, 134.0, 133.0, 126.8, 124.1, 63.3, 62.9, 49.0, 43.0, 35.1, 31.4, 30.4, 29.9, 27.4, 14.1.

IR (neat): 2959, 2868, 1736, 1680, 1465, 1426, 1362, 1258, 1238, 1180, 1131, 1066 cm^{-1} .

HRMS (ESI) calculated for $\text{C}_{21}\text{H}_{29}\text{N}_4\text{O}_3^+$ $[\text{M}+\text{H}]^+$ 385.2234, found 385.2229.

ethyl 2-(7-acetyl-5-(*tert*-butyl)-3,3-dimethyl-2,3-dihydro-1*H*-inden-1-yl)-2*H*-tetrazole-5-carboxylate (9):

Isolated Yield: 55%

Physical Property: White solid.

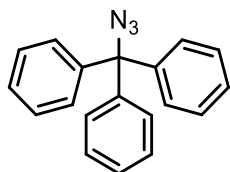
Melting Point: 149-151 °C

^1H NMR (500 MHz, CDCl_3 containing 1 % (v/v) TMS) δ 7.82 (d, $J = 1.8$ Hz, 1H), 7.50 (d, $J = 1.8$ Hz, 1H), 6.85 (dd, $J = 8.7, 3.7$ Hz, 1H), 4.50 (q, $J = 7.1$ Hz, 2H), 2.70 (dd, $J = 14.1, 8.7$ Hz, 1H), 2.49 (s, 3H), 2.34 (dd, $J = 14.1, 3.7$ Hz, 1H), 1.44 (t, $J = 7.1$ Hz, 3H), 1.41 (s, 8H), 1.38 (s, 3H), 1.26 (s, 3H).

^{13}C NMR (126 MHz, CDCl_3 containing 1 % (v/v) TMS) δ 199.3, 158.2, 157.1, 155.4, 154.4, 134.2, 132.0, 126.5, 123.9, 67.2, 62.4, 48.8, 43.0, 35.1, 31.4, 29.9, 29.69, 27.5, 14.2.

IR (neat): 2960, 2869, 1743, 1683, 1466, 1361, 1233, 1203, 1065 cm^{-1} .

HRMS (ESI) calculated for $\text{C}_{21}\text{H}_{29}\text{N}_4\text{O}_3^+$ $[\text{M}+\text{H}]^+$ 385.2234, found 385.2227.



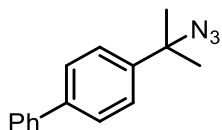
(azidomethanetriyl)tribenzene: According to Procedure A, a 4 mL borosilicate glass vial was charged with triphenylmethane (97.7 g, 0.40 mmol) 2.00 mol% of copper(II) acetate (1.50 mg, 8.00 μ mol), 2.00 mol% of bathophenanthroline (2.70 mg, 8.00 μ mol), 2.50 equivalents of *N*-fluorobenzenesulfonimide (315 mg, 1.00 mmol), and a magnetic stir bar outside a glovebox. The flask was capped with an open-top cap installed with a TFE lined silicone SURE-LINKTM septum. The septum cap was pierced by a needle (22 gauge - 1 1/2", 0.7 mm x 40 mm) and the vial was moved into the glovebox and underwent four cycles of vacuum-nitrogen-backfill over 40 minutes. After removal of the needle, the vial was removed from the glovebox. The vial was charged with nitromethane (2.0 mL, 0.20 M) and 3.6 equivalents of azidotrimethylsilane (190 μ L, 1.44 mmol) sequentially, stirred, and heated to 30 °C (inner temperature) in a heating block on a hot plate. After 16 hours, the vial was cooled to room temperature (25 °C). All precipitates and catalysts were filtered out through a pipette-silica plug with dichloromethane (1.0 mL x 3 times). After evaporation of solvent on a rotary evaporator at 30 °C, flash column chromatography (pentane) was performed. The isolated compound was dried to give 16 mg of trityl azide. ¹H and ¹³C NMR spectrum of trityl azide was matched with the literature.^{25,26}

Isolated Yield: 14%

Physical Property: Colorless oil.

¹H NMR (500 MHz, CDCl₃ containing 1 % (v/v) TMS) δ 7.37 – 7.26 (m, 15H).

¹³C NMR (126 MHz, CDCl₃ containing 1 % (v/v) TMS) δ 143.1, 128.5, 128.2, 127.7, 77.1.



4-(2-azidopropan-2-yl)-1,1'-biphenyl: Prepared from 4-isopropyl-1,1'-biphenyl according to Procedure A. The reaction mixture was purified by flash column chromatography (diethyl ether:pentane = 1:30) to afford 26.7 mg of **4ab**.

Isolated Yield: 28%

Physical Property: White solid.

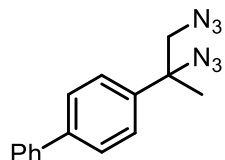
Melting Point: 45-47 °C.

¹H NMR (500 MHz, CDCl₃ containing 1 % (v/v) TMS) δ 7.64 – 7.55 (m, 4H), 7.55 – 7.48 (m, 2H), 7.48 – 7.41 (m, 2H), 7.39 – 7.31 (m, 1H), 1.68 (s, 6H).

¹³C NMR (126 MHz, CDCl₃ containing 1 % (v/v) TMS) δ 143.8, 140.7, 140.4, 128.9, 127.5, 127.4, 127.2, 125.7, 63.8, 28.5.

IR (neat): 2974, 2103, 1487, 1247, 763 cm⁻¹.

HRMS (ESI) calculated for C₁₅H₁₅⁺ [M-N₃]⁺ 195.1168, found 195.1168.



4-(1,2-diazidopropan-2-yl)-1,1'-biphenyl: Prepared from 4-isopropyl-1,1'-biphenyl according to Procedure A. The reaction mixture was purified by flash column chromatography (diethyl ether:pentane = 1:30) to afford 13.5 mg of **4ab**.

Isolated Yield: 12%

Physical Property: Colorless oil.

¹H NMR (500 MHz, CDCl₃ containing 1 % (v/v) TMS) δ 7.67 – 7.56 (m, 4H), 7.55 – 7.41 (m, 4H), 7.40 – 7.32 (m, 1H), 3.54 (d, J = 12.5 Hz, 1H), 3.44 (d, J = 12.5 Hz, 1H), 1.80 (s, 3H).

¹³C NMR (126 MHz, CDCl₃ containing 1 % (v/v) TMS) δ 141.3, 140.4, 139.7, 129.0, 127.8, 127.7, 127.3, 126.4, 66.6, 61.1, 22.5.

IR (neat): 2981, 2101, 1294, 1249, 833 cm⁻¹.

HRMS (ESI) calculated for C₁₄H₁₃⁺ [M-N₃-CH₂N₃+H]⁺ 181.1012, found 181.1011.

5D.XI. Reference

1. Kolb, H. C.; Sharpless, K. B. The Growing Impact of Click Chemistry on Drug Discovery. *Drug Discov. Today* **2003**, *8*, 1128–1137.
2. Kolb, H. C.; Finn, M. G.; Sharpless, K. B. Click Chemistry: Diverse Chemical Function from a Few Good Reactions. *Angew. Chem. Int. Ed.* **2001**, *40*, 2004–2021.
3. Gaussian 16, Revision C.01, Frisch, M. J.; Trucks, G. W.; Schlegel, H. B.; Scuseria, G. E.; Robb, M. A.; Cheeseman, J. R.; Scalmani, G.; Barone, V.; Petersson, G. A.; Nakatsuji, H.; Li, X.; Caricato, M.; Marenich, A. V.; Bloino, J.; Janesko, B. G.; Gomperts, R.; Mennucci, B.; Hratchian, H. P.; Ortiz, J. V.; Izmaylov, A. F.; Sonnenberg, J. L.; Williams-Young, D.; Ding, F.; Lipparini, F.; Egidi, F.; Goings, J.; Peng, B.; Petrone, A.; Henderson, T.; Ranasinghe, D.; Zakrzewski, V. G.; Gao, J.; Rega, N.; Zheng, G.; Liang, W.; Hada, M.; Ehara, M.; Toyota, K.; Fukuda, R.; Hasegawa, J.; Ishida, M.; Nakajima, T.; Honda, Y.; Kitao, O.; Nakai, H.; Vreven, T.; Throssell, K.; Montgomery, J. A., Jr.; Peralta, J. E.; Ogliaro, F.; Bearpark, M. J.; Heyd, J. J.; Brothers, E. N.; Kudin, K. N.; Staroverov, V. N.; Keith, T. A.; Kobayashi, R.; Normand, J.; Raghavachari, K.; Rendell, A. P.; Burant, J. C.; Iyengar, S. S.; Tomasi, J.; Cossi, M.; Millam, J. M.; Klene, M.; Adamo, C.; Cammi, R.; Ochterski, J. W.; Martin, R. L.; Morokuma, K.; Farkas, O.; Foresman, J. B.; Fox, D. J. Gaussian, Inc., Wallingford CT, 2016.
4. (a) Becke, A. D. Density-Functional Thermochemistry. III. The Role of Exact Exchange. *J. Chem. Phys.* **1993**, *98*, 5648. (b) Becke, A. D. Density-functional Thermochemistry. IV. A New Dynamical Correlation Functional and Implications for Exact-exchange Mixing. *J. Chem. Phys.* **1996**, *104*, 1040.
5. (a) Grimme, S.; Ehrlich, S.; Goerigk, L. Effect of the Damping Function in Dispersion Corrected Density Functional Theory. *J. Comput. Chem.* **2011**, *32*, 1456–1465. (b) Johnson, E. R.; Becke, A. D. A Post-Hartree-Fock Model of Intermolecular Interactions: Inclusion of Higher-Order Corrections. *J. Chem. Phys.* **2006**, *124*, 174104.
6. Hehre, W. J.; Ditchfield, R.; Pople, J. A. Self—Consistent Molecular Orbital Methods. XII. Further Extensions of Gaussian—Type Basis Sets for Use in Molecular Orbital Studies of Organic Molecules. *J. Chem. Phys.* **1972**, *56*, 2257–2261.
7. Dolg, M.; Wedig, U.; Stoll, H.; Preuss, H. Energy-adjusted Ab Initio Pseudopotentials for the First Row Transition Elements. *J. Chem. Phys.* **1987**, *86*, 866–872.
8. Zhao, Y.; Truhlar, D. G. A New Local Density Functional for Main-Group Thermochemistry, Transition Metal Bonding, Thermochemical Kinetics, and Noncovalent Interactions. *J. Chem. Phys.* **2006**, *125*, 194101.
9. Weigend, F.; Ahlrichs, R. Balanced Basis Sets of Split Valence, Triple Zeta Valence and Quadruple Zeta Valence Quality for H to Rn: Design and Assessment of Accuracy. *Phys. Chem. Chem. Phys.* **2005**, *7*, 3297.
10. Marenich, A. V.; Cramer, C. J.; Truhlar, D. G. Universal Solvation Model Based on Solute Electron Density and on a Continuum Model of the Solvent Defined by the Bulk Dielectric Constant and Atomic Surface Tensions. *J. Phys. Chem. B* **2009**, *113*, 6378–6396.
11. (a) Yamaguchi, K.; Takahara, Y.; Fueno, T.; Houk, K. N. Extended Hartree-Fock (EHF) Theory of Chemical Reactions. *Theor. Chim. Acta* **1988**, *73*, 337–364. (b) Kitagawa, Y.; Saito, K.; Yamaguchi, K. Approximate Spin Projection for Broken-Symmetry Method and Its

- Application in *Symmetry (Group Theory) and Mathematical Treatment in Chemistry*; IntechOpen: Rijeka, 2018; Chapter 7, p. 121-139. (c) Mandal, M.; Elwell, C. E.; Bouchey, C. J.; Zerk, T. J.; Tolman, W. B.; Cramer, C. J. Mechanisms for Hydrogen Atom Abstraction by Mononuclear Copper(III) Cores: Hydrogen Atom Transfer or Concerted Proton-Coupled Electron Transfer? *J. Am. Chem. Soc.* **2019**, *141*, 17236–17244.
- Margrey, K. A.; Czaplyski, W. L.; Nicewicz, D. A.; Alexanian, E. J. A General Strategy for Aliphatic C–H Functionalization Enabled by Organic Photoredox Catalysis. *J. Am. Chem. Soc.* **2018**, *140*, 4213–4217.
 - Han, J.; Jeon, M.; Pak, H. K.; Rhee, Y. H.; Park, J. Exploiting the Nucleophilicity of N–H Imines: Synthesis of Enamides from Alkyl Azides and Acid Anhydrides. *Adv. Synth. Catal.* **2014**, *356*, 2769–2774.
 - Li, W.-Y.; Wang, Q.-Q.; Yang, L. Fe-Catalyzed Radical-Type Difunctionalization of Styrenes with Aliphatic Aldehydes and Trimethylsilyl Azide Via a Decarbonylative Alkylation-Azidation Cascade. *Org. Biomol. Chem.* **2017**, *15*, 9987–9991.
 - Dryzhakov, M.; Hellal, M.; Wolf, E.; Falk, F. C.; Moran, J. Nitro-Assisted Brønsted Acid Catalysis: Application to a Challenging Catalytic Azidation. *J. Am. Chem. Soc.* **2015**, *137*, 9555–9558.
 - Kuroda, K.; Hayashi, Y.; Mukaiyama, T. Conversion of Tertiary Alcohols to Tert-Alkyl Azides by Way of Quinone-Mediated Oxidation-Reduction Condensation Using Alkyl Diphenylphosphinites. *Tetrahedron* **2007**, *63*, 6358–6364.
 - Kim, H.; Choi, T.-L. Preparation of a Library of Poly(*N*-Sulfonylimidates) by Cu-Catalyzed Multicomponent Polymerization. *ACS Macro Lett.* **2014**, *3*, 791–794.
 - Huang, X.; Bergsten, T. M.; Groves, J. T. Manganese-Catalyzed Late-Stage Aliphatic C–H Azidation. *J. Am. Chem. Soc.* **2015**, *137*, 5300–5303.
 - Fallis, I. A.; Murphy, D. M.; Willock, D. J.; Tucker, R. J.; Farley, R. D.; Jenkins, R.; Stevens, R. R. Direct Observation of Enantiomer Discrimination of Epoxides by Chiral Salen Complexes Using Endor. *J. Am. Chem. Soc.* **2004**, *126*, 15660–15661.
 - Lee, Y. E.; Cao, T.; Torruellas, C.; Kozlowski, M. C. Selective Oxidative Homo- and Cross-Coupling of Phenols with Aerobic Catalysts. *J. Am. Chem. Soc.* **2014**, *136*, 6782–6785.
 - Matos, P. M.; Lewis, W.; Moore, J. C.; Stockman, R. A. Sulfonimidates: Useful Synthetic Intermediates for Sulfoximine Synthesis Via C–S Bond Formation. *Org. Lett.* **2018**, *20*, 3674–3677.
 - Karimov, R. R.; Sharma, A.; Hartwig, J. F. Late Stage Azidation of Complex Molecules. *ACS Cent. Sci.* **2016**, *2*, 715–724.
 - Sharma, A.; Hartwig, J. F. Metal-Catalysed Azidation of Tertiary C–H Bonds Suitable for Late-Stage Functionalization. *Nature* **2015**, *517*, 600–604.
 - Hendrick, C. E.; Bitting, K. J.; Cho, S.; Wang, Q. Site-Selective Copper-Catalyzed Amination and Azidation of Arenes and Heteroarenes Via Deprotonative Zincation. *J. Am. Chem. Soc.* **2017**, *139*, 11622–11628.
 - Roy, H. N.; Pitchaiah, A.; Kim, M.; Hwang, I. T.; Lee, K.-I. Protective Group-Free Synthesis of New Chiral Diamines Via Direct Azidation of 1,1-Diaryl-2-Aminoethanols. *RSC Adv.* **2013**, *3*, 3526–3530.
 - Kitamura, M.; Kato, S.; Yano, M.; Tashiro, N.; Shiratake, Y.; Sando, M.; Okauchi, T. A Reagent for Safe and Efficient Diazo-Transfer to Primary Amines: 2-Azido-1,3-Dimethylimidazolium Hexafluorophosphate. *Org. Biomol. Chem.* **2014**, *12*, 4397–4406.
 - Bruker-Axis (2016). APEX3, Version 2016.2015-2010. Madison, Wisconsin, USA.

28. Krause, L.; Herbst-Irmer, R.; Sheldrick, G. M.; Stalke, D. Comparison of Silver and Molybdenum Microfocus X-Ray Sources for Single-Crystal Structure Determination. *J. Appl. Cryst.* **2015**, *48*, 3-10.
29. Sheldrick, G. M. (2013b). XPREP, Version 2013/2011. Georg-August-Universität Göttingen, Göttingen, Germany.
30. Sheldrick, G. M. (2013a). The *SHELX* Homepage, <http://Shelx.Uni-Ac.Gwdg.De/SHELX/>.
31. Sheldrick, G. M. SHELXT – Integrated Space-Group and Crystal-Structure Determination. *Acta Cryst.* **2015**, *A71*, 3–8.
32. Sheldrick, G. M. Crystal Structure Refinement with SHELXL. *Acta Cryst.* **2015**, *C71*, 3–8.
33. Dolomanov, O. V.; Bourhis, L. J.; Gildea, R. J.; Howard, J. A. K.; Puschmann, H. OLEX2: A Complete Structure Solution, Refinement and Analysis Program. *J. Appl. Crystallogr.* **2009**, *42*, 339–341.
34. Guzei, I. A. (2007-2013) Programs. *Gn*, University of Wisconsin-Madison, Madison, Wisconsin, USA.
35. Guzei, I. A. An Idealized Molecular Geometry Library for Refinement of Poorly Behaved Molecular Fragments with Constraints. *J. Appl. Cryst.* **2014**, *47*, 806–809.
36. Dereli, B.; Ortuño, M. A.; Cramer, C. J. Accurate Ionization Energies for Mononuclear Copper Complexes Remain a Challenge for Density Functional Theory. *ChemPhysChem* **2018**, *19*, 959–966.
37. (a) Wayner, D. D. M.; McPhee, D. J.; Griller, D. Oxidation and Reduction Potentials of Transient Free Radicals. *J. Am. Chem. Soc.* **1988**, *110*, 132–137. (b) Pavlishchuk, V. V.; Addison, A. W. Conversion Constants for Redox Potentials Measured versus Different Reference Electrodes in Acetonitrile Solutions at 25°C. *Inorganica Chim. Acta* **2000**, *298*, 97–102.
38. Ryu, T.; Min, J.; Choi, W.; Jeon, W. H.; Lee, P. H. Synthesis of 2-Aryl-2H-Benzotriazoles from Azobenzenes and N-Sulfonyl Azides through Sequential Rhodium-Catalyzed Amidation and Oxidation in One Pot. *Org. Lett.* **2014**, *16*, 2810–2813.
39. Wang, Y.; Di, H.; Chen, F.; Xu, Y.; Xiao, Q.; Wang, X.; Wei, H.; Lu, Y.; Zhang, L.; Zhu, J.; Lan, L.; Li, J. Discovery of Benzocycloalkane Derivatives Efficiently Blocking Bacterial Virulence for the Treatment of Methicillin-Resistant *S. Aureus* (MRSA) Infections by Targeting Diapophytoene Desaturase (CrtN). *J. Med. Chem.* **2016**, *59*, 4831–4848.
40. Kasai, S.; Kamaura, M.; Kamata, M.; Aso, K.; Ogino, H.; Nakano, Y.; Watanabe, K.; Kaisho, T.; Tawada, M.; Nagisa, Y.; Takekawa, S.; Kato, K.; Suzuki, N.; Ishihara, Y. Melanin-Concentrating Hormone Receptor 1 Antagonists: Synthesis, Structure–Activity Relationship, Docking Studies, and Biological Evaluation of 2,3,4,5-Tetrahydro-1H-3-Benzazepine Derivatives. *Bioorg. Med. Chem.* **2011**, *19*, 6261–6273.
41. Bume, D. D.; Harry, S. A.; Pitts, C. R.; Lectka, T. Sensitized Aliphatic Fluorination Directed by Terpenoidal Enones: A “Visible Light” Approach. *J. Org. Chem.* **2018**, *83*, 1565–1575.
42. Piszal, P. E.; Vasilopoulos, A.; Stahl, S. S. Oxidative Amide Coupling from Functionally Diverse Alcohols and Amines Using Aerobic Copper/Nitroxyl Catalysis. *Angew. Chem. Int. Ed.* **2019**, *58*, 12211–12215.
43. Rokade, B. V.; Gadde, K.; Prabhu, K. R. Copper-Catalyzed Direct Transformation of Secondary Allylic and Benzylic Alcohols into Azides and Amides: An Efficient Utility of Azide as a Nitrogen Source. *Eur. J. Org. Chem.* **2015**, 2706–2717.

44. Murali, A.; Puppala, M.; Varghese, B.; Baskaran, S. A Lewis Acid Mediated Schmidt Reaction of Benzylic Azide: Synthesis of Sterically Crowded Aromatic Tertiary Amines. *Eur. J. Org. Chem.* **2011**, 5297–5302.
45. Kamble, S.; More, S.; Rode, C. Highly Selective Direct Azidation of Alcohols over a Heterogeneous Povidone-Phosphotungstic Solid Acid Catalyst. *New J. Chem.* **2016**, *40*, 10240–10245.
46. Tukhtaev, H. B.; Ivanov, K. L.; Bezzubov, S. I.; Cheshkov, D. A.; Melnikov, M. Y.; Budynina, E. M. Aza-Wittig Reaction with Nitriles: How Carbonyl Function Switches from Reacting to Activating. *Org. Lett.* **2019**, *21*, 1087–1092.
47. Tandiyar, M. A.; Masui, Y.; Onaka, M. A Combination of Trimethylsilyl Chloride and Hydrous Natural Montmorillonite Clay: An Efficient Solid Acid Catalyst for the Azidation of Benzylic and Allylic Alcohols with Trimethylsilyl Azide. *RSC Adv.* **2015**, *5*, 15736–15739.
48. Ivanov, K. L.; Villemson, E. V.; Budynina, E. M.; Ivanova, O. A.; Trushkov, I. V.; Melnikov, M. Y. Ring Opening of Donor–Acceptor Cyclopropanes with the Azide Ion: A Tool for Construction of N-Heterocycles. *Chem. Eur. J.* **2015**, *21*, 4975–4987.
49. Chiba, S.; Zhang, L.; Ang, G. Y.; Hui, B. W.-Q. Generation of Iminyl Copper Species from A-Azido Carbonyl Compounds and Their Catalytic C–C Bond Cleavage under an Oxygen Atmosphere. *Org. Lett.* **2010**, *12*, 2052–2055.
50. Clark, J. R.; Feng, K.; Sookezian, A.; White, M. C. Manganese-Catalysed Benzylic C(sp³)–H Amination for Late-Stage Functionalization. *Nat. Chem.* **2018**, *10*, 583–591.
51. Sajja, Y.; Vanguru, S.; Jilla, L.; Vulupala, H. R.; Bantu, R.; Yogeswari, P.; Sriram, D.; Nagarapu, L. A Convenient Synthesis and Screening of Benzosuberone Bearing 1,2,3-Triazoles against Mycobacterium Tuberculosis. *Bioorg. Med. Chem. Lett.* **2016**, *26*, 4292–4295.

